Attachment 5C.D

Water Clarity—
Suspended Sediment Concentration and Turbidity

Contents

14

Tables

Figures

25

26

Acronyms and Abbreviations

2	µm	micrometers
3	BDCP	Bay Delta Conservation Plan
4	CDOM	colored dissolved organic material
5	cfs	cubic feet per second
6	cm	centimeters
7	DCC	Delta Cross Channel
8	Delta	Sacramento–San Joaquin River Delta
9	DRERIP	Delta Regional Ecosystem Restoration Implementation Plan
10	EBC	existing biological conditions
11	EC	salinity
12	ESO	Evaluated Starting Operations
13	EXP	Delta export pumping
14	HOS	higher outflow scenario
15	IAV	Invasive aquatic vegetation
16	LLT	late long-term
17	LOS	lower outflow scenario
18	m/s	meters per second
19	mg/L	milligrams per liter
20	MLLW	mean low-low-water
21	mm	millimeters
22	mm/yr	millimeters per year
23	OMR	Old and Middle River
24	ORH	head of Old River
25	Pa	Pascals
26	ROAs	restoration opportunity areas
27	SAV	submerged aquatic vegetation
28	SSC	suspended sediment concentration
29	SWAN	Simulation WAves Nearshore
30	USGS	U.S. Geological Survey
31	X2	The location of the 2 parts-per-thousand contour for bottom salinity
32		

Water Clarity—
Suspended Sediment Concentration and Turbidity

5C.D.1 Introduction

This analysis explores the physical influences on water clarity in the Bay Delta Conservation Plan (BDCP) Plan Area for existing conditions as well as potential factors that could influence water clarity in the late long-term (LLT) timeframe for a scenario including possible changes proposed by the BDCP as well as for a scenario without those changes. The analysis begins with a general discussion of the prevailing theory of water clarity and sediment transport through the Plan Area. The mechanisms addressed include sediment source locations and seasonal timing, tidal transport, and wind-wave resuspension. The effects of specific, Plan Area-wide, future changes are then addressed, including changing water export conditions, climate change and sea level rise, and changing salinity conditions. Individual restoration areas are examined to assess their potential to decrease local water clarity through increased wind-wave sediment resuspension. While the main focus is on the physical factors contributing to water clarity changes, consideration is also given to the potential for newly opened restoration areas to become colonized by submerged aquatic vegetation, which may have large consequences for clarity (the analysis of submerged aquatic vegetation habitat suitability is presented in Appendix 5.F, *Biological Stressors on Covered Fish* (Section 5F.4). The analysis closes by individually reviewing potential clarity changes for seven geographical subregions of the Plan Area as well as the cumulative effect of future planned changes on Plan Area-wide clarity. A thorough discussion of biological influences on water clarity, although potentially important, is not included. The emphasis in the analysis is on differences between the existing biological conditions and the evaluated starting operations scenarios, with information related to the high-outflow and low-outflow scenarios being introduced as necessary.

5C.D.2 Background

5C.D.2.1 Measurement Types for Water Clarity

Turbidity is an easily measured indicator of water clarity, and automated devices have been installed in many Plan Area locations since 2009. Governing equations for mass conservation and force balance for suspended sediment concentration (SSC) can be solved by a numerical model of suspended sediment transport, and these results can be used to estimate turbidity by establishing empirical relationships between the suspended sediment measurements and turbidity measurements at a given location.[1] The data requirements for developing suspended sediment model boundary conditions and model parameters are numerous and adequate data are not yet available in the Plan Area. A simpler approach is to assume a linear relationship between SSC and turbidity and approximate the effect of deposition on turbidity. This form of turbidity model has

---

[1] <http://www.deltacouncil.ca.gov/sites/default/files/documents/files/workshop_OCAP_2010_presentation_16_Wright_Shoellhamer.pdf>.

1   been developed and applied (RMA 2010c). In order to represent the additional processes discussed
2   below a full suspended sediment model is required.

3   In the following sections, the Delta Regional Ecosystem Restoration Implementation Plan (DRERIP)
4   Ecosystem Conceptual Model for Sedimentation (Schoellhamer et al. 2007) is used as a resource to
5   guide the summary of factors influencing water clarity, and to evaluate the potential changes to the
6   Plan Area in the LLT timeframe which includes sea level rise (45 centimeters [cm]) and Evaluated
7   Starting Operations (ESO) operations, in comparison to current conditions which are assumed
8   comparable to Existing Biological Conditions (EBC2). We focus on these bookend changes although
9   it is acknowledged that conclusions may be different when considering an interim timeframe.

10 It is assumed in what follows that an increase in SSC is linearly related to an increase in turbidity,
11 although the relationship will likely differ by location. The range of sediment sizes available in the
12 water column influences water clarity, with fine sediment (less than 63 micrometers [µm] diameter)
13 being the most easily mobilized in comparison to coarse sediment. SSC is the dominant contributor
14 to turbidity. Colored dissolved organic material (CDOM) and phytoplankton are important in some
15 systems but are probably negligible contributions in the Plan Area (Kimmerer 2004). In measuring
16 the sources contributing to reduction of light available for algal growth, Kimmerer et al. (2012)
17 found chlorophyll contributed only about 1–3% of total light extinction, implying the remainder was
18 due to inorganic particles in the time periods that were studied.

5C.D.2.2   Sediment Supply and Water Clarity: Existing Conditions and General Background on Transport, Remobilization, and Local Conditions in the Plan Area

22 Water clarity in the Plan Area is determined primarily by the amount of suspended sediment
23 transported in the water column (Kimmerer 2004). As rivers enter estuaries, sediment eroded from
24 upstream areas is deposited in the estuary in varying degrees depending on factors such as flow
25 rate, tidal forcing and local conditions such as bathymetry and the presence of vegetation. The
26 patterns of geomorphic change occur on time scales varying from episodic, as storm flows can
27 transport large volumes of sediment, to decadal, for example due to changes in climate patterns, the
28 damming of rivers and land usage.

29 The major source of sediment to the Plan Area is the Sacramento River plus the Yolo Bypass, which
30 accounted for up to 85% of the sediment supply over the period 1999–2002 (Wright and
31 Schoellhamer 2005). The San Joaquin River accounted for about 13%, with the eastside inflows
32 (Cosumnes, Calaveras and Mokelumne) accounting for the remaining 2% over the same period.
33 Although in recent history (since 1957) sediment supply to the Plan Area has been decreasing, the
34 Plan Area remains depositional (Wright and Schoellhamer 2005; Schoellhamer et al. 2007), with
35 approximately two thirds of sediment entering the Plan Area remaining in the Plan Area during the
36 period 1999–2002. Suisun Bay and Grizzly Bay were both calculated to be erosional in the period
37 1867–1990 (Cappiela et al. 1999), with both areas sustaining losses to tidal flats. However, Wright
38 and Schoellhamer (2004) state that the Sacramento–San Joaquin River Delta (Delta) is likely to
39 remain net depositional independent of decreases in sediment supply, due to tidal influences (slack
40 tide deposition) and the availability of large depositional areas, although depositional pattern will
41 vary with sediment supply (Ganju and Schoellhamer 2010).

1 The great majority of Sacramento River sediment (more than 80%) enters the Plan Area episodically
2 during high flow events in the wet periods, with sediment concentrations that are generally higher
3 during first flush events (Schoellhamer et al. 2007). Wright and Schoellhamer (2005) estimated that
4 during the four year period 1999–2002, this accounted for about 31% of the total time. In
5 comparing the proportion of the available sediment actually deposited, about 69% of the available
6 sediment was deposited during wet periods, in comparison with about 56% of the available
7 sediment deposited during dry periods. In other words, conditions are more conducive to sediment
8 deposition during the wet season than during the dry season.

9 The decreasing trend in sediment supply from the Sacramento River since 1957 (Wright and
10 Schoellhamer 2004) is due to a variety of factors. The construction of reservoirs has resulted in an
11 upstream accumulation of sediment within the reservoirs. In addition, previous stores of hydraulic
12 mining-derived sediments have been depleted, and there have been various changes associated with
13 channel adjustments downstream of dams and bank protection measures that decrease sediment
14 supply. However, other factors such as land use changes (e.g., logging and grazing) and urbanization
15 can increase sediment supply.

16 The current balance between the factors regulating sediment supply to the Sacramento River is
17 unknown (Wright and Schoellhamer 2004), so it is not possible to predict the evolution of sediment
18 supply in the coming decades with certainty. Thus, it is hard to predict whether sufficient sediment
19 will enter the Plan Area to be available for all BDCP restoration opportunity areas (ROAs). In
20 addition, sea level rise requires sediment deposition to maintain the elevation of current wetlands
21 above tidal water levels. Given these uncertainties, potential consequences for sediment deposition
22 and water clarity due to sea level rise and the development of ROAs are discussed in greater detail
23 below.

24 The range of sediment size available in the water column influences water clarity. Fine sediment
25 (less than 63 μm diameter) is the primary component of suspended sediment in the San Francisco
26 estuary (Schoellhamer et al. 2007). Turbidity and SSC are well correlated in the San Francisco
27 estuary, as suspended sediment is predominantly fine sediment and flocculated sediment sizes are
28 relatively homogeneous in the estuary (Schoellhamer et al. 2007; Ganju et al. 2007). Sand and coarse
29 sediment (greater than 63 μm diameter) can be transported both as suspended load (in the water
30 column) or bed load (rolling along the bed). Bed load is a small fraction of sediment load in the Plan
31 Area, estimated as two orders of magnitude less than total suspended sediment load (Schoellhamer
32 et al. 2007). Coarse sediment is found primarily in deeper channels with high flows, such as along
33 the Sacramento River or the deeper channels in Suisun Bay.

34 Sediment is a critical resource in habitat creation. Tidal marsh and floodplain restoration efforts
35 may require a sediment source as the substrate for the restoration effort, so knowledge of sediment
36 transport patterns can enable the optimal siting of restoration areas for maximum sediment
37 trapping from local waterborne sources (Ganju et al. 2004). Sediments are advected downstream
38 into transitional areas where tidal forcing can mobilize the mass of fine sediments in an oscillation,
39 the net direction of which (landward or seaward) is dictated by a variety of factors such as net
40 outflow, tidal strength (e.g., timing in the spring-neap cycle), and timing within the diurnal tidal
41 cycle (Ganju et al. 2004). Deposition typically occurs at slack water after ebb and flood tides. More
42 generally, deposition occurs as flow velocity decreases, as coarser, heavier sediments settle out of
43 the water column.

1   On a local scale, erosion increases SSC and reduces water clarity and deposition decreases SSC and
2   increases water clarity (Schoellhamer et al. 2007). Several factors can stabilize or resuspend the
3   sediments in place in the beds of rivers and estuaries. Wind waves can resuspend bed sediment, and
4   the magnitude of decrease in water clarity (i.e., increase in turbidity) is affected by depth and areal
5   extent of the open water (fetch length), which influence the magnitude of the wind-waves and the
6   resulting turbidity. Benthic creatures can increase water clarity both by filtering the water column
7   and by stabilizing bed sediments when populations become locally dense. Macrophytes are
8   generally associated with sediment deposition and increased water clarity, as they reduce water
9   velocity, attenuate waves, reduce vertical mixing in the water column and reduce bed shear stress
10 (Schoellhamer et al. 2007).

11 Water depth is another factor in the regulation of water clarity, both in regulating the local
12 hydrodynamics and as a determinant in the ability of vegetation to colonize a given location. As
13 discussed in Schoellhamer et al. (2007), brackish vegetation can colonize locations where elevation
14 is greater than mean tide level, while freshwater emergent vegetation colonizes in water depths up
15 to up to 0.2 meter (0.66 feet). Brazilian waterweed (*Egeria densa*), an invasive waterweed that has
16 colonized many areas of the Delta, roots in a water depth range of approximately 0–3 meters
17 (California Department of Boating and Waterways 2001).

18 Accretion of sediment to the bed removes sediment from the erodible pool of sediment, thereby
19 increasing water clarity. Strong accretion of sediment, in the range of 10 millimeters (mm) per year
20 at Browns Island, 30 mm per year at Donlon Island, and even higher local rates of deposition, have
21 been observed in the Delta (Reed 2002). In contrast, several open water regions, including Franks
22 Tract, appear to be at open-water equilibrium (Simenstad et al. 2000). These different results are
23 attributable to the influence of wind waves on sediment resuspension.

24 Wind resuspension of fine sediments increases turbidity both episodically during winter storms and
25 seasonally in the spring and summer due to diurnal westerly winds (Ganju et al. 2006). Newly
26 deposited sediment (unconsolidated) is more easily brought into suspension (Ganju et al. 2006), so
27 spring winds may increase turbidity locally more than summer winds of the same velocity. However,
28 peak wind strength occurs in the summer Plan Area-wide, although the average strength varies by
29 location. In the spring and summer, winds are typically westerly from approximately 250 degrees,
30 with a maximum velocity in the afternoon. Figure 5C.D–1 illustrates hourly wind direction data at
31 the Twitchell Island station.

32 Wind blowing over an open water area will result in wind waves, which can affect turbidity. The
33 wave height is dependent primarily on the wind speed, fetch and water depth with larger waves
34 generally developing in deeper areas. These waves may then propagate into shallow areas and
35 possibly steepen, further increasing wave height. Wind waves in channel areas are typically small
36 due to limited fetch. However, larger wind waves can occur in open water areas, which could include
37 proposed restoration within the ROAs. Wave heights and period depend primarily on water depth
38 and fetch, and approximate relationships have been developed to describe this variation (Coastal
39 Engineering Research Center 1984). Example wave height dependence plots for wind speeds of 4
40 and 10 meters per second (m/s) are shown in Figure 5C.D–2 and Figure 5C.D–3.

41 Wind waves induce water particles to move in orbital paths with excursion distances decreasing
42 downward through the water column (Dean and Dalrymple 2002). In addition, breaking wind waves
43 cause turbulence at the water surface. In shallow water, this turbulence can extend down to the bed
44 (Jones and Monismith 2008). Wind waves affect turbidity in several ways. The most direct is

1   through the local resuspension of sediment resulting from bed shear stress. Sediment is eroded from
2   the bed when shear stress exceeds a critical shear stress, where the critical shear stress is primarily
3   dependent on sediment size for noncohesive sediment and additional bed properties for cohesive
4   sediment. The bed shear stress associated with wind waves is proportional to the square of the
5   orbital velocities at the bed. The orbital velocities decrease with depth. Therefore, deep water
6   columns experience less bed shear stress than shallow water columns for a given wind wave. In
7   places where the turbulent kinetic energy associated with whitecapping waves extends down to the
8   bed, this can cause sediment resuspension. This typically occurs in shallow regions with large fetch,
9   such as Grizzly Bay (Jones and Monismith 2008). Wind waves also have less direct effects on
10   sediment. For example wind waves can break or remove biofilms that bind sediment to the bed,
11   thereby increasing the erodibility of the bed.

12   Through these multiple mechanisms, wind waves can strongly influence the morphology of coastal
13   lagoons observed in many locations. For example, in Venice Lagoon wind waves cause a bimodal
14   distribution of depth in which most regions of Venice Lagoon are either at marsh elevations or
15   subtidal elevations (Fagherazzi et al. 2007). Relatively little intertidal area is present in Venice
16   Lagoon. As discussed above, this distribution occurs because the shear stress associated with wind
17   waves peaks at a certain depth, very roughly 1 meter with the exact "critical depth" depending on
18   fetch and wind climate (Fagherazzi et al. 2007). If deposition decreases at water depths below this
19   critical value a positive feedback loop results in smaller waves and reduced bed shear stress which
20   further decreases deposition, allowing the region to evolve to marsh elevation. In deeper regions,
21   wind waves are larger and wind wave resuspension slows deposition and may cause net erosion
22   leading to gradual deepening.

23   The linear wave relationships used by Fagherazzi et al. (2007) to relate shear stress to wind speed,
24   fetch length and water depth can be applied for a range of a parameters representative of present
25   Plan Area conditions. Figure 5C.D–4 and Figure 5C.D–5 show the estimated bed shear stress as a
26   function of depth for multiple fetch lengths for a wind speed of 4 m/s and 10 m/s, respectively. The
27   friction coefficient associated with wave-induced bed shear stress (f_w) in the formulation of Madsen
28   and Wikramanayake (1991) was set to a value of 0.05, following Bricker (2003). Wind waves will
29   result in sediment resuspenson when the critical shear stress of erosion is exceeded. A weak critical
30   shear stress of erosion value of 0.1 Pascals (Pa) and a strong critical shear stress of erosion value
31   (1.0 Pa), used by Ganju and Schoellhamer (2007) to represent two different size classes in their
32   sediment transport modeling in Suisun Bay, are labeled on the figures. Plan Area sediments
33   consisting largely of sand (Ganju and Schoellhamer 2006) correspond to the strong critical shear
34   stress of erosion (i.e., 1.0 Pa). Therefore, at the lower wind speed of 4 m/s, resuspension would only
35   be expected in shallow regions of unconsolidated silt and clay while at the higher wind speed of
36   10 m/s, all shallow regions that are not sheltered from the wind are likely to experience significant
37   wind wave driven resuspension of sediment. More specifically, for long fetch distances, the
38   predicted bottom shear stress exceeds the strong critical shear stress of erosion for depths greater
39   than 0.1 meter and less than 2 meters. This corresponds roughly with the observed depths in
40   Sherman Lake and other large open water areas. Deeper than 2 meters, the critical shear stress of
41   erosion decreases below the strong critical shear stress of erosion for all fetch lengths.

42   These figures largely explain the open water geomorphology observations discussed by Simenstad
43   et al. (2000). High rates of sediment accumulation have been observed in Mildred Island (47–
44   51 millimeters per year [mm/yr]) and Rhode Island (44 mm/yr) because those deeply subsided
45   areas are too deep for wind wave driven sediment resuspension to be effective. Similarly, high rates
46   of sediment accumulation have been observed in upstream portions of the Yolo Bypass and other

1   bypasses (Singer et al. 2008) due to the combination of high sediment load and deep water. Some
2   areas such as Sherman Lake, Big Break and possibly Franks Tract appear to have reached open-
3   water equilibrium with associated slow accretion rates (Simenstad et al. 2000). In Franks Tract,
4   resuspension from wind waves is understood to result in bed elevations remaining more than
5   2 meters below mean low-low-water (MLLW) (Simenstad et al. 2000).

6   The Suisun Bay region is particularly important as habitat because it typically contains the low
7   salinity zone which is associated with peak observed abundance of several species of plankton and
8   epibenthos, as well as larval and juvenile fish (Kimmerer et al. 2002). The important habitat
9   indicator X2 (the location of the 2 parts-per-thousand contour for bottom salinity) is frequently
10   located in Suisun Bay. Suisun Bay has extensive areas of shallow water (less than 2 meters deep)
11   with predominance of fine suspended and bed sediment, as well as channels 9–11 meters deep with
12   sandy bed sediment (Ganju et al. 2006). A large volume of sediment was deposited historically in
13   Suisun Bay from hydraulic mining activities, but Suisun Bay has been consistently erosional for
14   more than a century and experienced major loss of tidal flat area (Cappiela et al. 1999). However,
15   the last bathymetric survey used in the analysis of Cappiela et al. (1999) was performed in 1990.
16   Because the overall sediment supply to the Plan Area was decreasing (Wright and Schoellhamer
17   2004) from 1957 through 2001, it is likely that Suisun Bay will continue to be erosional. However, as
18   Suisun Bay deepens and intertidal regions are lost, wind waves will become less effective at
19   suspending sediment, so erosion rates may slow even in the presence of reduced sediment supply.

20   Water clarity has been increasing in the Plan Area for decades. As illustrated in Figure 5C.D–6 using
21   Secchi disk data gathered from monitoring programs (B. J. Miller pers. comm., based on the regions
22   shown in Figure 5C.D–7), this trend in increasing transparency is most pronounced in the central,
23   and particularly, the south Delta. The trend in the south Delta appears to have accelerated in the
24   most recent decade. Nobriga et al. (2008) noted the trend in central and south Delta transparency
25   and associated it with the decline of the early summer abundance of juvenile delta smelt in this
26   region. An increase in water clarity corresponds to a decrease in turbidity and in SSC. In a recent
27   publication (Cloern et al. 2011), the authors investigated the future consequences of changes in
28   sediment supply to the Delta and found that when they assumed future sediment supply remained
29   at current levels, SSC only changed slightly, while a 1.6% per year decrease in sediment supply
30   resulted in a rapid fall in SSC (average of 2.8 milligrams per liter decade [mg/L decade]).

31   While some of the historical decrease in turbidity could be due to a decrease in sediment supply, the
32   role of submerged aquatic vegetation (SAV) has also been considered (Kimmerer 2004). The SAV
33   *Egeria* has been mentioned, in particular, as its presence is known to slow water velocity which can
34   induce sediment deposition. Although *Egeria* beds can trap fine sediment, neither the geographic
35   distribution of *Egeria* nor the seasonal timing of *Egeria* growth (late summer and fall) closely match
36   the historical changes in Secchi depth (Kimmerer 2004). However, the relationship between
37   increases in water clarity and the presence of *Egeria* has been well-established in other systems
38   (Yarrow et al. 2009).

39   In summary, aside from some localized regions, the Plan Area is understood to be a depositional
40   environment and is likely to remain that way into the future (Simenstad et al. 2000). However, the
41   rate of accretion is spatially variable. High rates have been observed in marsh regions and deep
42   open water areas while much lower accretion rates are associated with shallow subtidal open water
43   areas, such as Sherman Lake. Therefore, marshes and deep open water areas reduce turbidity by
44   accreting sediment while shallow open water areas can temporarily increase turbidity during strong

1 wind periods. Due to the strong influence of fetch on wind wave growth, resuspension could be
2 reduced by design features such as wind wave-break islands in ROAs.
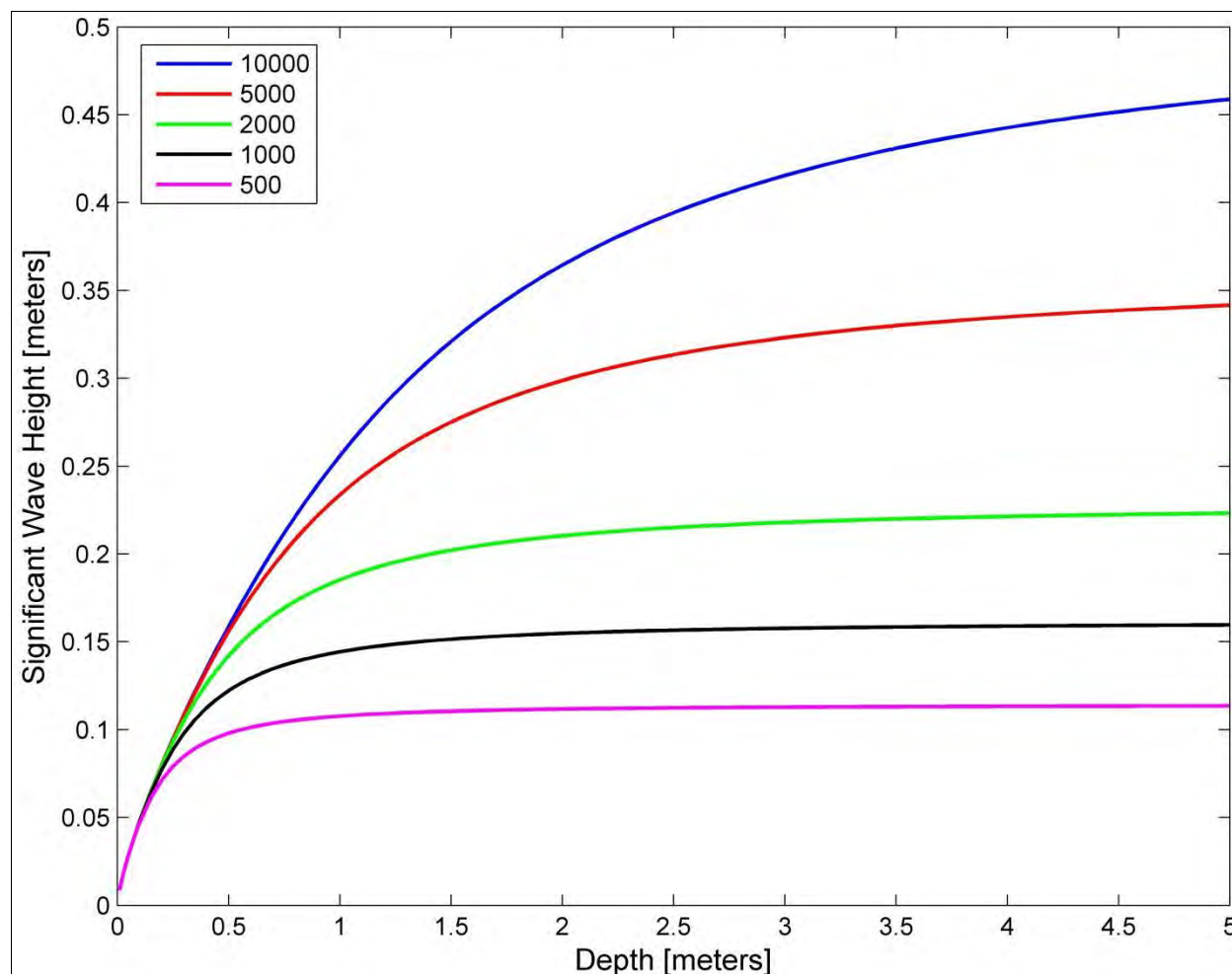
3 Several factors that are known to affect sediment resuspension and transport, and thus water
4 clarity, have not been addressed in this document which focuses on physical considerations and only
5 briefly touches on biological considerations with the potential influence of SAV. Because there is a
6 high level of uncertainty in the major driver of sediment supply, factors such as wetting and drying
7 of sediments at the outer ranges of tidal inundation (sediment hardening), and the role of
8 bioturbation and contributions from organic matter (Ganju et al. 2009), although important, are not
9 considered here. However, it should be noted that the critical shear stress of erosion has been
10 observed to vary substantially with changes in benthic algae and macrofauna (Ysebaert et al. 2005).
11 Changes to the community of benthic organisms in the estuary could lead to substantial and
12 unpredictable changes in water clarity; for example, increases in benthic filter feeders can
13 potentially result in decreases in seasonal and regional water clarity.

14
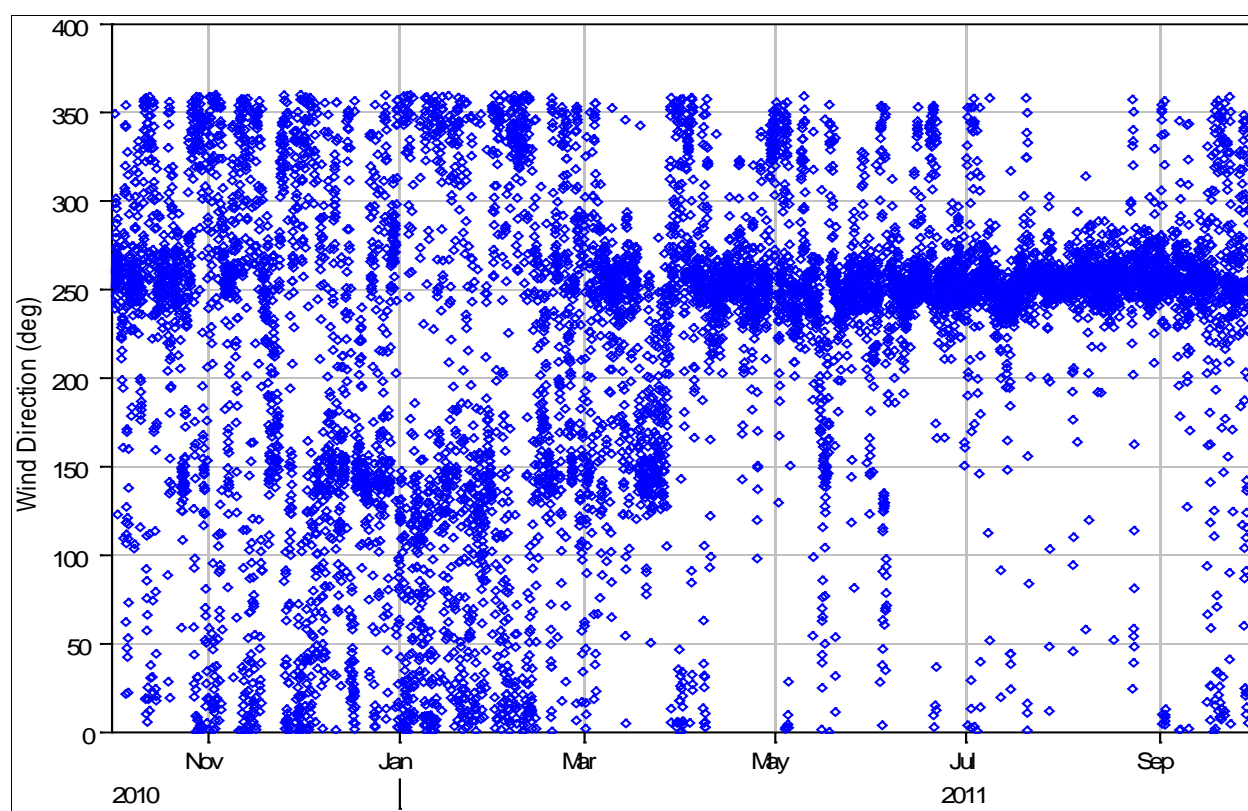
15 **Figure 5C.D–1. Hourly Wind Direction at Twitchell Island CIMIS Station from October 2010 to**
16 **September 2011**
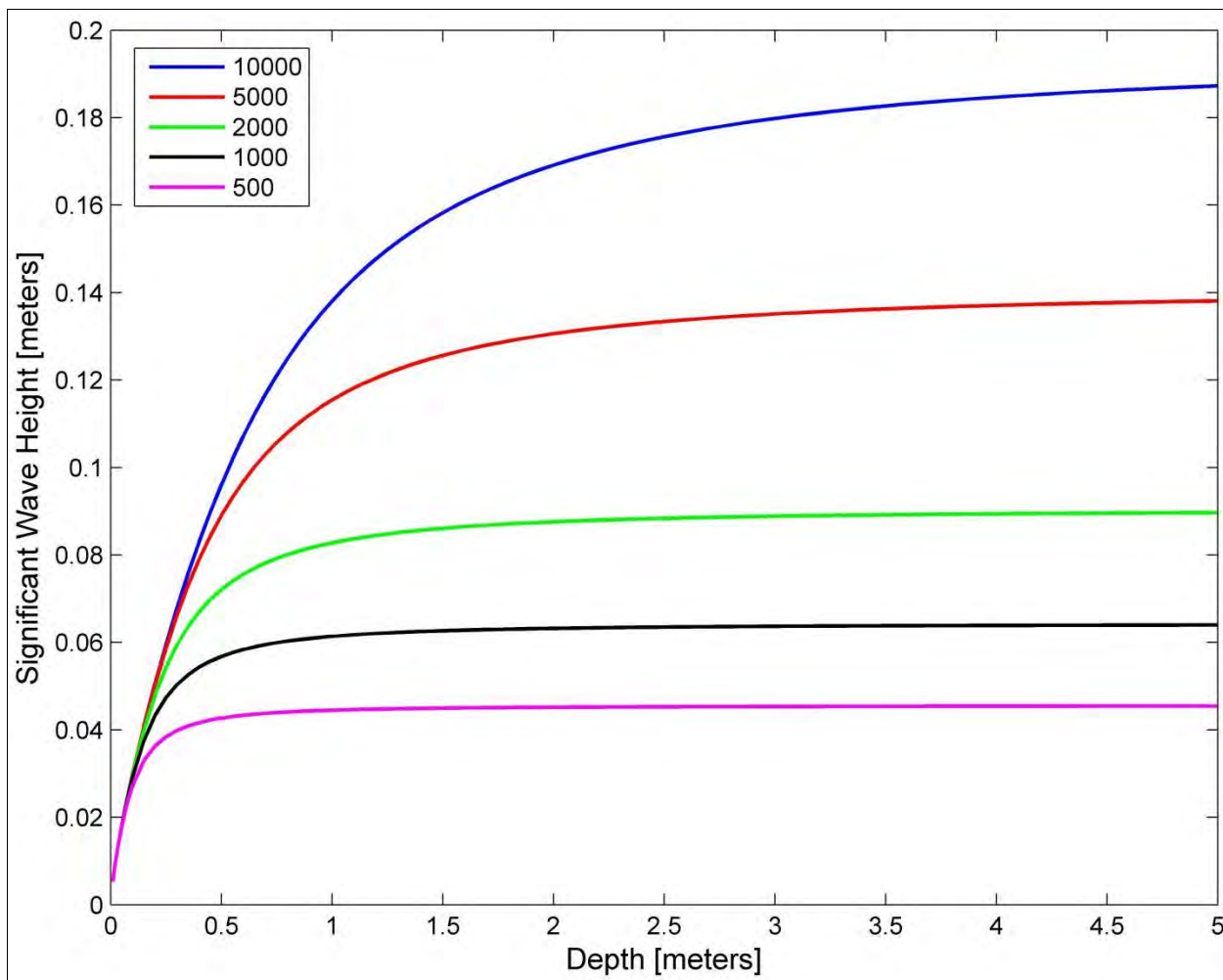
Figure 5C.D–2. Estimated Significant Wave Height for Wind Speed of 4 m/s and Multiple Fetch Lengths (Meters)

Figure 5C.D–3. Estimated Significant Wave Height for Wind Speed of 10 m/s and Multiple Fetch Lengths (Meters)
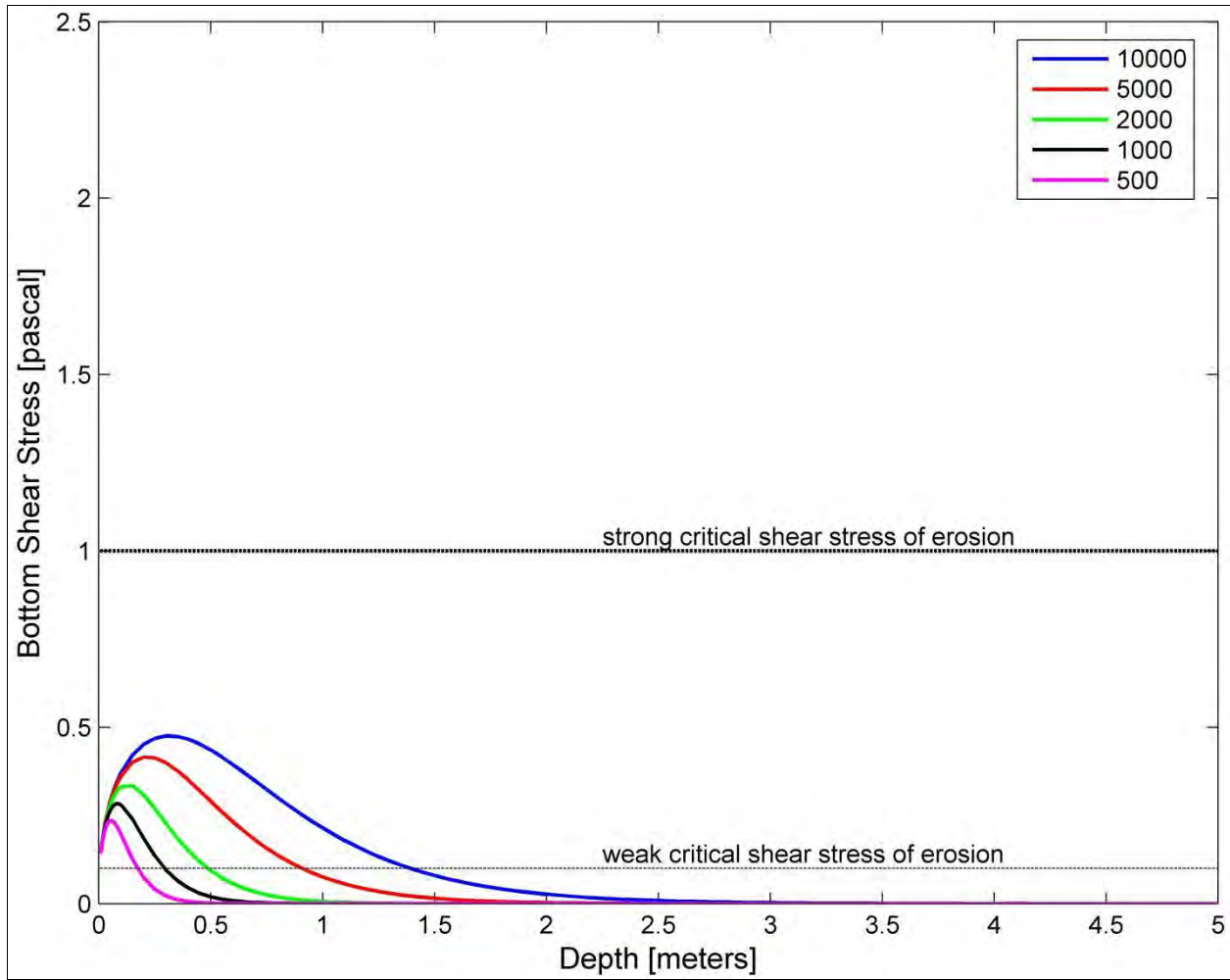
1
2　　　　**Figure 5C.D–4. Estimated Bed Shear Stress for Wind Speed of 4 m/s and Multiple Fetch Lengths**
3　　　　　　　　　　　　　　　　　　　　　**(Meters)**
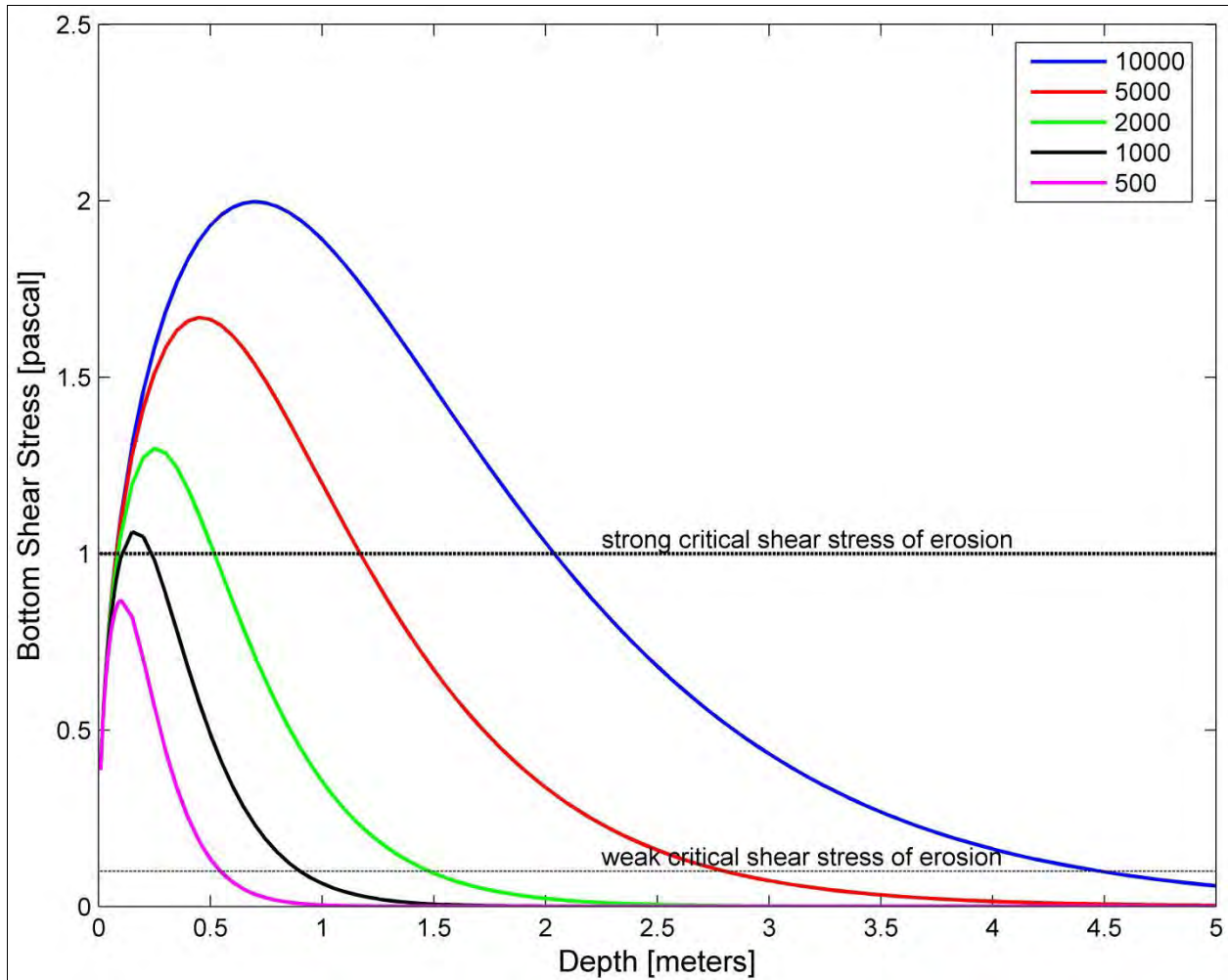
Figure 5C.D–5. Estimated Bed Shear Stress for Wind Speed of 10 m/s and Multiple Fetch Lengths (Meters)
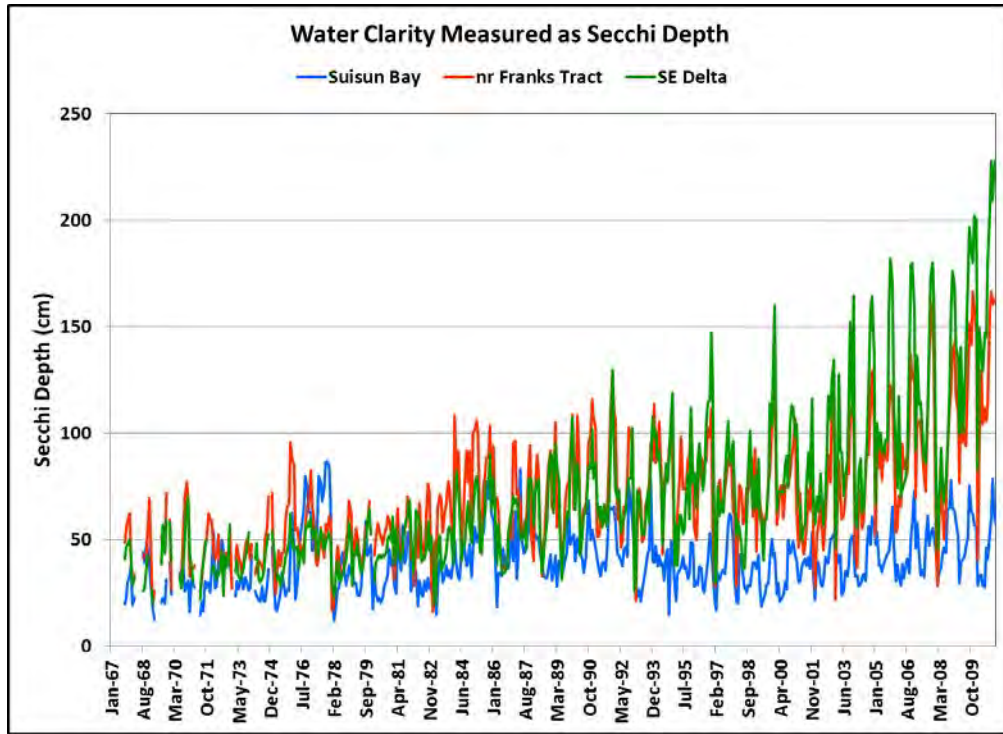
Data taken from B.J. Miller analysis (Miller pers. comm.).

Figure 5C.D–6. Secchi Depth Measured during Regular Monitoring and Fish Surveys—Monthly Averaged Data Averaged Regionally
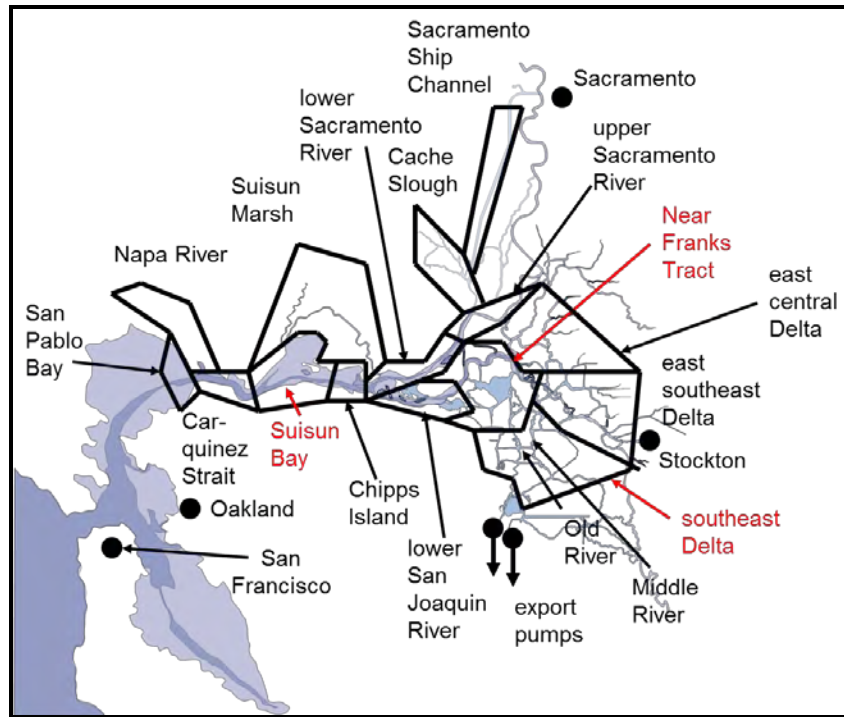
Taken from B.J. Miller analysis (Miller pers. comm.).

Figure 5C.D–7. The Regions Used in Averaging Secchi Data (Red Font) Illustrated in Figure 5C.D–6

5C.D.3   Factors Affecting Sediment Supply Because of BDCP Implementation of Dual Conveyance

5C.D.3.1   Methods

In the ESO_LLT scenario, water is exported from the Sacramento River near Freeport and diversions from the south Delta are less than for the EBC2_LLT scenario, which only exports water from the south Delta. Export levels for both scenarios are shown in Figure 5C.D–8. In the east Delta subregion, less Sacramento River flow due to the shift in export location means that less flow is directed though Georgiana Slough and through the Delta Cross Channel (DCC), the latter in part due to operation of the DCC.

The present analysis assessed whether exporting more water near the major source of sediment supply will significantly affect depositional characteristics of the Plan Area; i.e., whether this change will cause enough reduction in sediment deposition that in the long term the Plan Area will cease to be depositional and therefore turbidity and water clarity would be affected. Wright and Schoellhamer (2005) estimate the Sacramento watershed supplies about 85% of the total Plan Area sediment budget. For areas where sediment supply would be affected by South Delta exports, the question is how the change in export volume and timing will affect depositional characteristics there, as this area receives sediment from both the Sacramento and San Joaquin watersheds. In order to calculate the magnitude of the overall effect of changes in export location and volume, a sediment transport model would need to be developed for the Plan Area and applied to ESO_LLT and EBC2_LLT scenarios; such a model is not currently available.

Because a sediment transport model for the Plan Area is not yet available, coarse estimates of the difference in suspended sediment loads delivered to the Plan Area between the EBC2_LLT and the ESO_LLT scenarios were made using output from the CALSIM and DSM2 simulations and U.S. Geological Survey (USGS) sediment data. As Wright and Schoellhamer (2004) noted, several factors have contributed to a reduction in sediment supply to the Plan Area in recent decades and the future supply of sediment is uncertain. As the BDCP model simulations represent hypothetical future conditions, several assumptions have been made concerning the historical suspended sediment data used for the analysis and the relationships between flow and suspended sediment load.

The analysis was also conducted for the HOS_LLT scenario to provide an indication of differences from the EBC2_LLT. There is little difference between the ESO_LLT and LOS_LLT in terms of north Delta exports during the main period of sediment delivery to the Plan Area (i.e., winter-spring), so the conclusions for the ESO_LLT also apply to the LOS_LLT. [HOS = higher outflow scenario; LOS = lower outflow scenario.]

5C.D.3.1.1   Analysis for the North Delta and Yolo Bypass Subregions

The USGS has data quantifying daily suspended sediment concentration and suspended sediment load in tons/day at Freeport on the Sacramento River. For the purposes of this analysis, the USGS data for suspended sediment load was used for the time period January 1991 through December 2002 which represents a recent time period with full calendar years overlapping with the BDCP CALSIM output for the EBC2_LLT and ESO_LLT simulations which run from October 1921 through September 2003. The BDCP simulations represent hypothetical future conditions and there are no explicit assumptions about future conditions that might affect sediment supply from the watersheds,

1   such as changes in upstream land use. Although USGS sediment data is available over a longer time
2   span, the most recent period was chosen as more indicative of reductions in sediment supply over
3   the period 1957–2001 noted by Wright and Schoellhamer (2004).

4   Because explicit knowledge of important factors, such as future sediment supply and the
5   distribution of sediment across the channel in the Sacramento River, is not available, many
6   simplifying assumptions were made about the relationship between suspended sediment load in the
7   Sacramento River and flow. These assumptions were (see also Table 5C.D-1):

8   1. Suspended sediment load is distributed uniformly in Sacramento River flow.

9   2. USGS historical suspended sediment load at Freeport during the period January 1991–December
10   2002 is representative of sediment load at Freeport for both EBC2_LLT and ESO_LLT scenarios.

11   3. Suspended sediment load at Freeport is representative of suspended sediment load in the
12   Sacramento River approaching Fremont and Sacramento Weirs.

13   4. Yolo flow from the Sacramento and Fremont weirs in the EBC2_LLT and ESO_LLT scenarios
14   removes sediment load from the Sacramento River in proportion to the relative flow. As a
15   consequence, suspended sediment load on the Sacramento River above these weirs is assumed
16   equal to the load at Freeport plus load delivered to the Yolo Bypass region over the weirs.

17   5. Exports in the ESO_LLT scenario remove suspended sediment load in proportion to export flow
18   from the Sacramento River at Freeport.

19   6. The portion of the Yolo Bypass flow originating from sources other than the Sacramento River is
20   not included in this sediment load analysis. Although sources such as Cache Creek and Putah
21   Creek can cause localized flooding even when the Fremont Weir does not spill, information
22   about suspended sediment load from these sources is not available from the USGS data set.

23   These assumptions allowed calculation of coarse estimates of the suspended sediment load available
24   to the Plan Area in the EBC2_LLT and ESO_LLT scenarios using historical USGS suspended sediment
25   concentration data and modeled time series available from the CALSIM output. Monthly time series
26   were used in the analysis. For the USGS sediment data, the daily suspended sediment load data was
27   accumulated on a monthly basis, and the monthly accumulated load (in tons) was used in the
28   calculations shown in Table 5C.D-1.

29   Total suspended sediment load from the Sacramento River was assumed equal to the load available
30   at Freeport plus the load available to the Yolo Bypass in the analysis. Total suspended sediment load
31   available to the Plan Area is then equal to the total suspended sediment load from the Sacramento
32   River at Freeport plus the load to the Yolo Bypass from the Sacramento River minus the amount
33   removed by the proposed north Delta intakes downstream of Freeport. Changes in suspended
34   sediment because of changes in water velocity and resulting potential effects on deposition were not
35   included in this analysis. While the ESO_LLT scenario exports water from the Plan Area at this
36   location, the EBC2_LLT scenario has no exports there. Table 5C.D-1 details the calculations made to
37   estimate suspended sediment loads. The postulated sediment load above Freeport, S_A, is calculated
38   based on downstream flow and sediment concentration data.

39   Monthly cumulative loads were calculated at Freeport, above Freeport, in the Yolo Bypass and
40   exported, and then the simulation period was partitioned by month to obtain a total load for each
41   month. For example, the cumulative load available for January in the Yolo Bypass was the sum over

1   all January loads to the Yolo from 1991 through 2002. These values were then used to estimate
2   differences between the EBC2_LLT and ESO_LLT scenarios.

5C.D.3.1.2   Analysis for the East Delta and South Delta Subregions

4   Analyses for potential changes in sediment supply to the East Delta and South Delta were conducted
5   qualitatively by examining modeled differences between scenarios for important flow channels and
6   available information for sediment supply.

5C.D.3.2 Results

5C.D.3.2.1   North Delta and Yolo Bypass Subregions

9   There is only a small difference in the cumulative flow down the Sacramento River plus Yolo flow
10   between the EBC2_LLT and ESO_LLT scenarios, but in the ESO_LLT scenario more flow is directed
11   down the Yolo Bypass than in the EBC2_LLT scenario. Figure 5C.D–9 illustrates that these
12   differences between the ESO_LLT and EBC2_LLT scenarios result in small differences to the assumed
13   suspended sediment load available from the Sacramento River above Freeport (under
14   Assumption 2, above). Figure 5C.D–10 illustrates the percentage of total load available to the Yolo
15   Bypass for both ESO_LLT and EBC2_LLT scenarios; percentages are given as these numbers are
16   relative to the loads from the individual scenarios. Figure 5C.D–11 illustrates the proportion of
17   suspended sediment load available at Freeport that was exported (for the ESO_LLT scenario). Figure
18   5C.D–12 illustrates the differences in suspended sediment load available to the Delta.

19   Estimates over the simulation period, 1991–2002, show that of the total load available to the Yolo
20   Bypass in the two LLT scenarios, approximately 24% more suspended sediment load is available in
21   the ESO_LLT scenario. Table 5C.D-2 illustrates these load calculations. Although the percent
22   difference in sediment load available above Freeport to the two scenarios is small (3%), since more
23   of the flow, and by assumption also more sediment, is available to the Yolo Bypass, the percent
24   difference is much greater. Of the total suspended sediment load estimated to reach Freeport in the
25   ESO_LLT scenario, about 12% was estimated to be exported on an average annual basis. Viewed
26   cumulatively over the Delta, there would be about 9% less sediment load for the Delta in the
27   ESO_LLT scenario than in the EBC2_LLT scenario (note that, based on the definition of S_D [Sediment
28   load to Delta] in Table 5C.D-1, sediment inputs to the Yolo Bypass subregion are counted as load to
29   the Delta; it is uncertain the extent to which such sediments would leave the Yolo Bypass subregion
30   and enter the other subregions).

31   The results for the HOS_LLT scenario suggested that around 8% less sediment would be available to
32   the Delta (Plan Area) on an average annual basis.

33   These results must be considered coarse estimates due to the large number of assumptions made in
34   the calculations. There are a number of factors that are challenging to capture with these coarse
35   estimates.

36   ● Most of the sediment supply is episodic in nature during the wet period, while the assumptions
37   on load were computed on a monthly basis to smooth out shorter term variations due the
38   assumption that historical load is representative of future load on the Sacramento River.

39   ● Sediment concentrations are generally higher during "first flush" events annually, which occur
40   over a period of days to weeks or sometimes not at all during low flow years. Ramping down of

1   north Delta diversions for pulse protection during such periods would affect the quantity of
2   sediment exported and calculations using the methodology above might not be captured in the
3   monthly estimates.

4   ● More water will be directed down the Yolo Bypass in the ESO as a result of the notching of
5   Fremont Weir under *CM2 Yolo Bypass Fisheries Enhancements*, and the sediment in this water
6   would not be subject to export at the north Delta intakes, but it is uncertain the extent to which
7   the sediment would be deposited in the bypass and therefore would not be available to
8   downstream ROAs. A full sediment model would be required to assess the extent to which such
9   deposition may occur.

10   Note that removal of sediment at the north Delta exports would result in less sediment available to
11   downstream areas (West Delta, Suisun Bay, and East Delta subregions). This is discussed further
12   below.

5C.D.3.2.2   East Delta Subregion

14   Sacramento River water flows to the East Delta subregion via Georgiana Slough, and when open,
15   through the DCC to the Mokelumne River system. The DCC is typically open from June into
16   November/December and closed December/January through May/June, with gate opening also
17   contingent upon the absence of excessive Sacramento River flow (<25,000 cubic feet per second
18   [cfs]). Thus the DCC is typically closed for times when the Sacramento River sediment load is high,
19   leaving Georgiana Slough as the primary wet season conduit for transferring sediment from the
20   Sacramento River to the east Delta.

21   Several factors associated with the ESO_LLT result in lower flow to the East Delta subregion as
22   observed in both the DSM2 and RMA2 model results.

23   1. Overall reduced Sacramento River flow downstream of the north Delta exports.

24   2. Reduction in the tidal range for the Sacramento River at Georgiana Slough and the DCC.

25   3. Connection of Miner Slough to the Sacramento Ship Channel through the restoration of Prospect
26   Island.

27   The analysis used DSM2 model results for the ESO_LLT and EBC2_LLT scenarios. Factors 2 and 3
28   reflect the change to the overall north Delta hydrodynamics with the development of the ROAs. The
29   DSM2 model results were scanned to find periods where north Delta exports for the ESO_LLT were
30   zero and flow for the Sacramento River at Freeport were about equal for the ESO_LLT and the
31   EBC2_LLT scenarios. Figure 5C.D–13 compares the flow split for the Sutter Slough+Steamboat
32   Slough channels and the Sacramento River downstream of the slough junctions. The plot illustrates
33   that with the ESO_LLT less water is carried downstream on the Sacramento River and less is
34   available to the DCC and Georgiana Slough. Figure 5C.D–14 shows the overall reduction in the
35   eastside flow transfer (Georgiana Slough+DCC) with the ESO_LLT relative to the EBC2_LLT. Figure
36   5C.D–14 also includes Sacramento River flow downstream of the DCC and Georgiana Slough. The
37   plot suggests for the ESO_LLT, a relatively smaller fraction of the available Sacramento River flow is
38   transferred to Georgiana Slough and to the DCC.

39   The primary factor affecting the change in flow through Georgiana Slough and the DCC with the
40   ESO_LLT is the degree of the north Delta exports which reduce the overall available Sacramento
41   River flow downstream of the intake locations. As Figure 5C.D–8 shows, the north Delta exports are
42   highest in the winter months when the Sacramento River sediment load is expected to be high.

1   Comparisons of the ESO_LLT and ECB2_LLT monthly flows for Georgiana Slough+DCC and for the
2   DCC alone are presented in Figure 5C.D–15 and Figure 5C.D–16 respectively.

3   Under the HOS_LLT scenario, average north Delta exports are lower than under the ESO_LLT and
4   LOS_LLT scenarios, mostly in the months of March–May to achieve higher spring outflow for longfin
5   smelt. The difference is ~1,000–3,000 cfs lower in wet, above normal, and below normal years, and
6   ~500 cfs in dry years (see Appendix 5.B, *Entrainment*). Less north Delta exports under the HOS_LLT
7   would result in somewhat more sediment reaching the East Delta subregion than under the
8   ESO_LLT/LOS_LLT scenarios, although note that the differences in north Delta exports occur outside
9   of the main winter period when most sediment is delivered to the Plan Area. Therefore the
10   differences are unlikely to be substantial.

5C.D.3.2.3   South Delta Subregion

12   San Joaquin River inflow remains essentially the same in the EBC2_LLT and ESO_LLT scenarios,
13   although less water is exported from San Joaquin River inflow in the ESO_LLT alternative as exports
14   in the south Delta are diminished. As exports decrease in the south Delta, the portion of the
15   sediment supply that was previously exported is available for deposition in the south and central
16   Delta. Wright and Schoellhamer (2005) found that there is a significant diminution of sediment
17   supply downstream of Vernalis before Stockton, indicating that deposition is occurring along the San
18   Joaquin River and thus potentially also along Old River and Middle River.

19   In the ESO_LLT scenario, total exports (North and South Delta) are lower than EBC2_LLT in the fall
20   and summer and increase in the winter and spring. South Delta exports are lower for the ESO_LLT
21   versus EBC2_LLT for all months. On a percentage basis, the south Delta reductions are the least for
22   July, August and December. South Delta exports are lower under the HOS_LLT scenario than the
23   ESO_LLT scenario, which would result in less sediment removal under the HOS_LLT. As noted for the
24   north Delta intakes above, the differences occur in the spring, during which delivery of sediment is
25   lower than winter. The differences occur primarily in above normal, below normal, and dry years.

26   Wright and Schoellhamer (2005) estimate the south Delta exports consume about 1.2% of the
27   current total Delta sediment budget. Under the ESO_LLT scenario, less Delta sediment would be
28   removed with the decrease in south Delta pumping. In addition to the change in overall south Delta
29   export flow, the factors affecting the degree of sediment loss for the ESO_LLT scenario are as follows.

5C.D.3.2.3.1 The Seasonality of the South Delta Export Flows

31   South Delta turbidity is higher in winter and spring (the wet season). Reducing south Delta pumping
32   in the winter and spring months should proportionally further reduce the sediment loss on an
33   annual basis. Wet season (January–June) south Delta exports are reduced with the ESO_LLT by 50%
34   versus the 12-month 44% reduction. Less export flow in the winter and spring months suggest a
35   further reduction in sediment removal by the ESO_LLT.

5C.D.3.2.3.2 Export Flows Relative to San Joaquin River Flows

37   The most direct path for wet season San Joaquin River flow to the SWP and CVP intakes is from the
38   junction at the head of Old River into Old River and into the Grant Line Canal upstream of Clifton
39   Court. When this flow is not sufficient to fill the export needs, additional water is drawn to the
40   exports from the central Delta along the Old and Middle River (OMR) corridors resulting in a net
41   negative OMR (Old + Middle River) flow condition. The examination of observed data (CDEC

1   database) shows that typically the wet season San Joaquin River water coming from the head of Old
2   River junction is higher in turbidity than central Delta water. DSM2 model flows for the EBC2_LLT
3   and ESO_LLT scenarios were evaluated to examine the San Joaquin River flow split at the head of Old
4   River (ORH) relative to south Delta export pumping (EXP). The ESO includes an operable barrier or
5   gate controlling flow between the San Joaquin River and the head of Old River. In the DSM2
6   simulations, the barrier limits flow to Old River for the winter and spring months for San Joaquin
7   River flows at Vernalis flows <10,000 cfs. Figure 5C.D–17 compares the DSM2 model ESO_LLT and
8   EBC2_LLT head of Old River flow available for export. That is the minimum of the head of Old River
9   flow and the south Delta Export flow. During very wet months (San Joaquin River >10,000 cfs) south
10   Delta exports are greatly reduced for the ESO_LLT versus the EBC2_LLT, and the commensurate
11   ORH flow exported is reduced for the ESO_LLT case. For lower San Joaquin River flow conditions
12   during the winter and spring months, ORH flow is reduced for the ESO_LLT by the Head of Old River
13   operable barrier.

5C.D.3.2.3.3 Direct Effects of the South Delta ROA on South Delta Turbidity

15   Sediment deposition in the south Delta ROA would lower south Delta SSC and likely further reduce
16   the removal of Delta sediment with SWP and CVP exports under the ESO_LLT scenario. Effects of the
17   ROAs on water clarity are discussed further below.

5C.D.3.3   Summary of Changes to Sediment Supply in the Plan Area Due to BDCP Shift in Export Location and Volume

20   The analysis estimated that 12% of the suspended sediment load from the Sacramento River near
21   Freeport would be removed due to the north Delta intakes under the ESO_LLT. Due to increases in
22   Yolo Bypass flow and sediment deposition there, this corresponds to a 9% reduction in Sacramento
23   watershed suspended sediment load to the Plan Area in relation to EBC2_LLT. The ESO_LLT flow
24   export from the north Delta would include a commensurate reduction in the south Delta export flow
25   of 44% relative to EBC2_LLT levels, implying a reduction in sediment load exported from the south
26   Delta.

27   While the change in south Delta export flow can be assessed for the ESO_LLT versus ECB2_LLT, the
28   changes in SSC near the south Delta SWP and CVP intakes at the time of export pumping are more
29   uncertain. A coarse estimate for the reduction in sediment export with the reduced south Delta
30   export under the ESO_LLT scenario is 50%. Wright and Schoellhamer (2005) estimate current south
31   Delta exports remove about 1.2% of the Delta inflowing sediments. Reducing the exported sediment
32   by half would increase sediment to the Delta by about 0.6%. This estimate is uncertain but is small
33   relative to the estimated 9% of Delta sediment load removed by the proposed north Delta intake in
34   the ESO_LLT scenario.

1   **Table 5C.D-1. Monthly Variables and Calculations for Suspended Sediment Load**

Monthly Flow Variables and Calculations	CALSIM Variable or Calculation[1,2]
Q_F = Sacramento R. flow at Freeport	C169_D168B_D168C
Flow to the Yolo Bypass from the Fremont Weir	D160
Flow to the Yolo Bypass from the Sacramento Weir	D166A
Q_A =Sacramento R. flow at Freeport plus flow to Yolo	Q_F + D160 + D166A
q_Y = Proportion Sacramento R. flow to Yolo Bypass	(D160 + D166A) / Q_A
q_E = Proportion Sacramento R. flow exported	NDD_ADJ / Q_A
Monthly Suspended Sediment Load (in tons) Variables and Calculations	
S_F = Sediment load at Freeport	USGS data (tons)
S_Y = Sediment load in Yolo	$q_Y * S_F$
S_A = Sediment load above Freeport	$S_A = q_Y * S_F + S_F$
S_E = Sediment load exported in the ESO_LLT scenario in the N Delta	$q_E * S_F$
S_D = Sediment load to Delta	$S_D = S_A - S_E$
[1] The CALSIM variable D160 is the flow to the Yolo Bypass from the Fremont weir; D166A is the flow to the Yolo Bypass from the Sacramento weir. [2] The CALSIM variable C169_D168B_D168C represents Sacramento River flow at Freeport and NDD_ADJ is the total diversion flow from the "isolated facility" export location.	

2
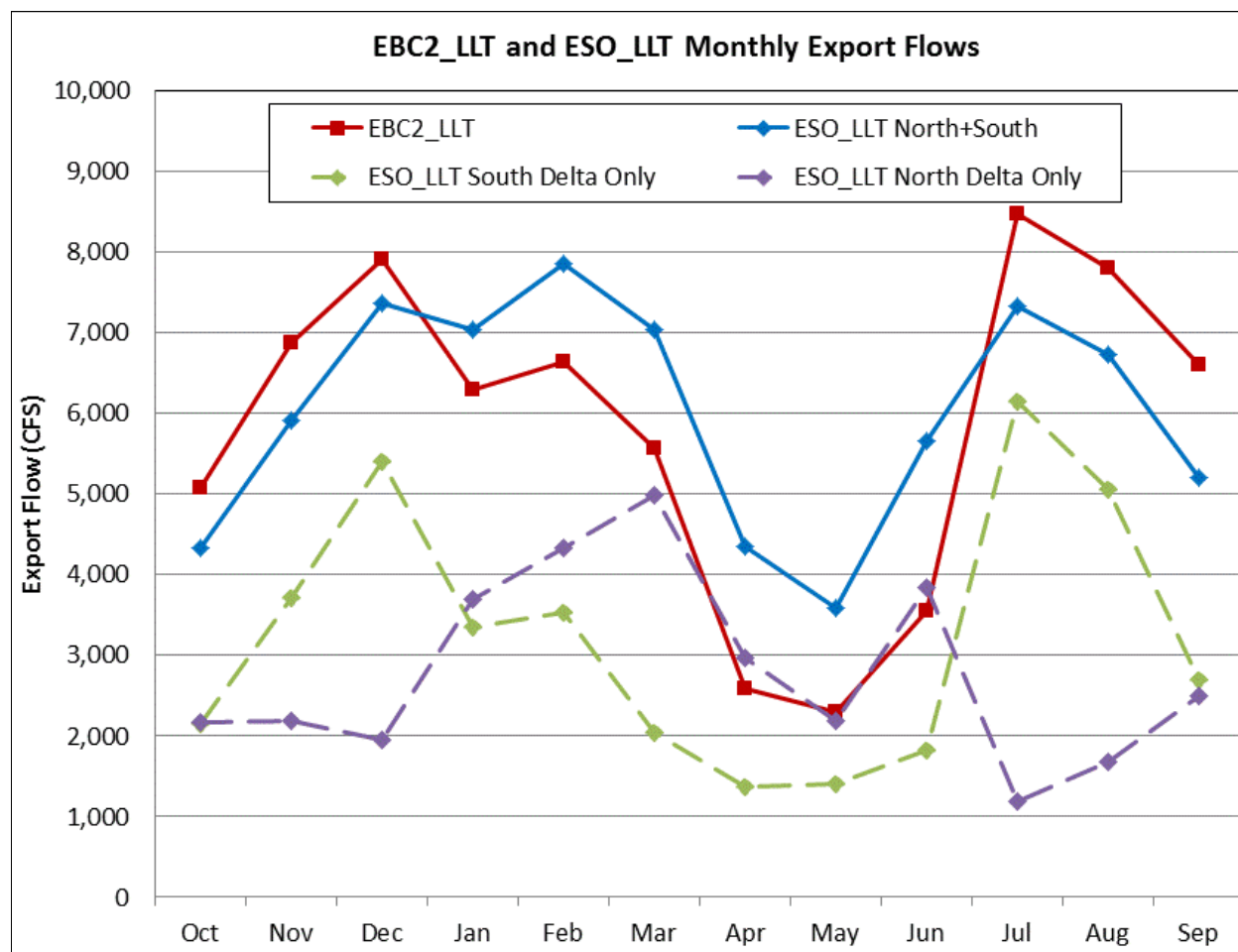
Figure 5C.D–8. Comparison of Monthly Average Exports for EBC2_LLT and ESO_LLT Scenarios, Based on CALSIM Modeling for Water Years 1922–2003

APPROXIMATE SUSPENDED SEDIMENT LOAD AVAILABLE FROM THE SACRAMENTO RIVER
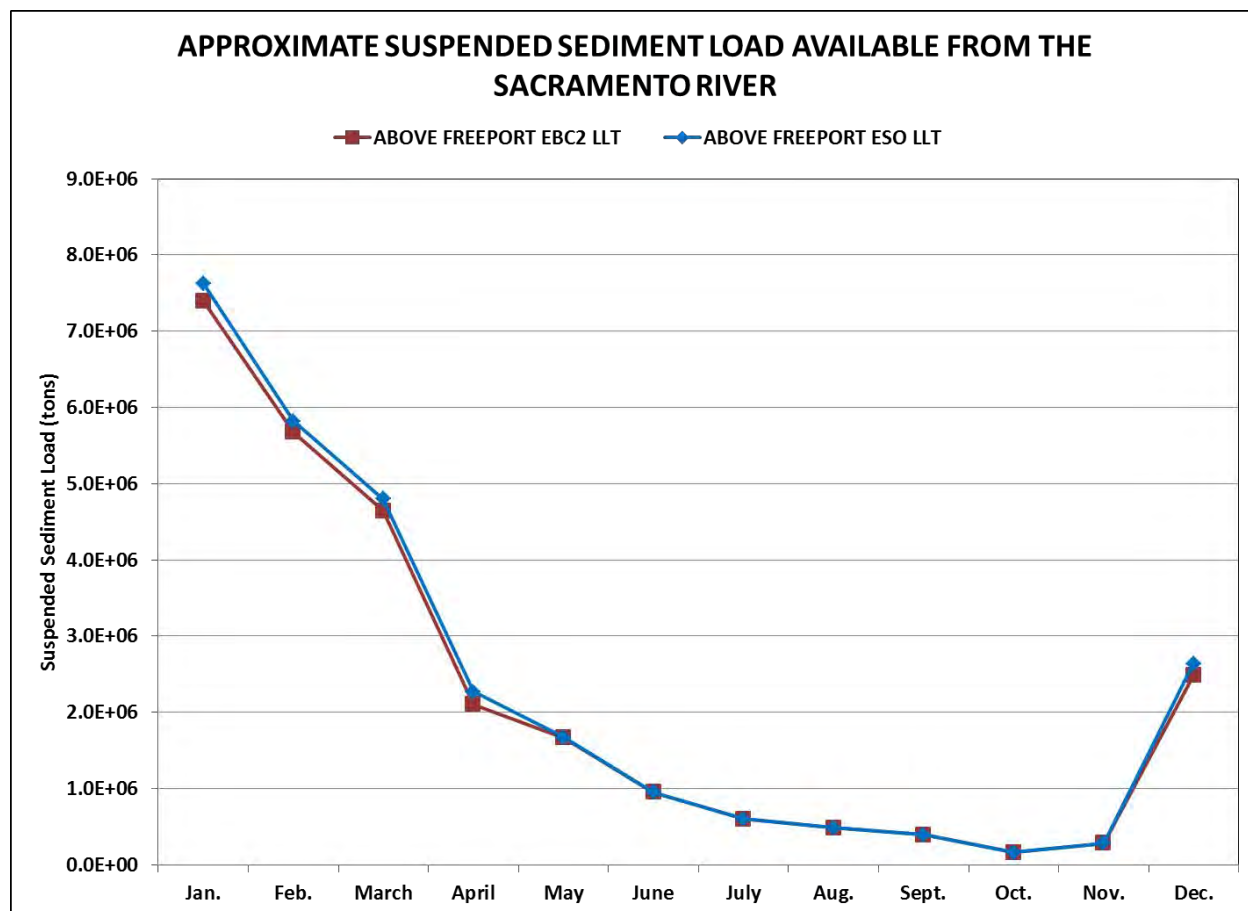
1

2   This calculation uses variable S_A in Table 5C.D-1 which includes sediment load available to the Yolo Bypass.

3   **Figure 5C.D–9. Comparison of Cumulative Suspended Sediment Load Available from the Sacramento**
4   **River in the EBC2_LLT and ESO_LLT Scenarios, for 1991–2002**

APPROXIMATE PERCENTAGE OF SUSPENDED SEDIMENT LOAD AVAILABLE TO YOLO BYPASS FROM SACRAMENTO RIVER

1
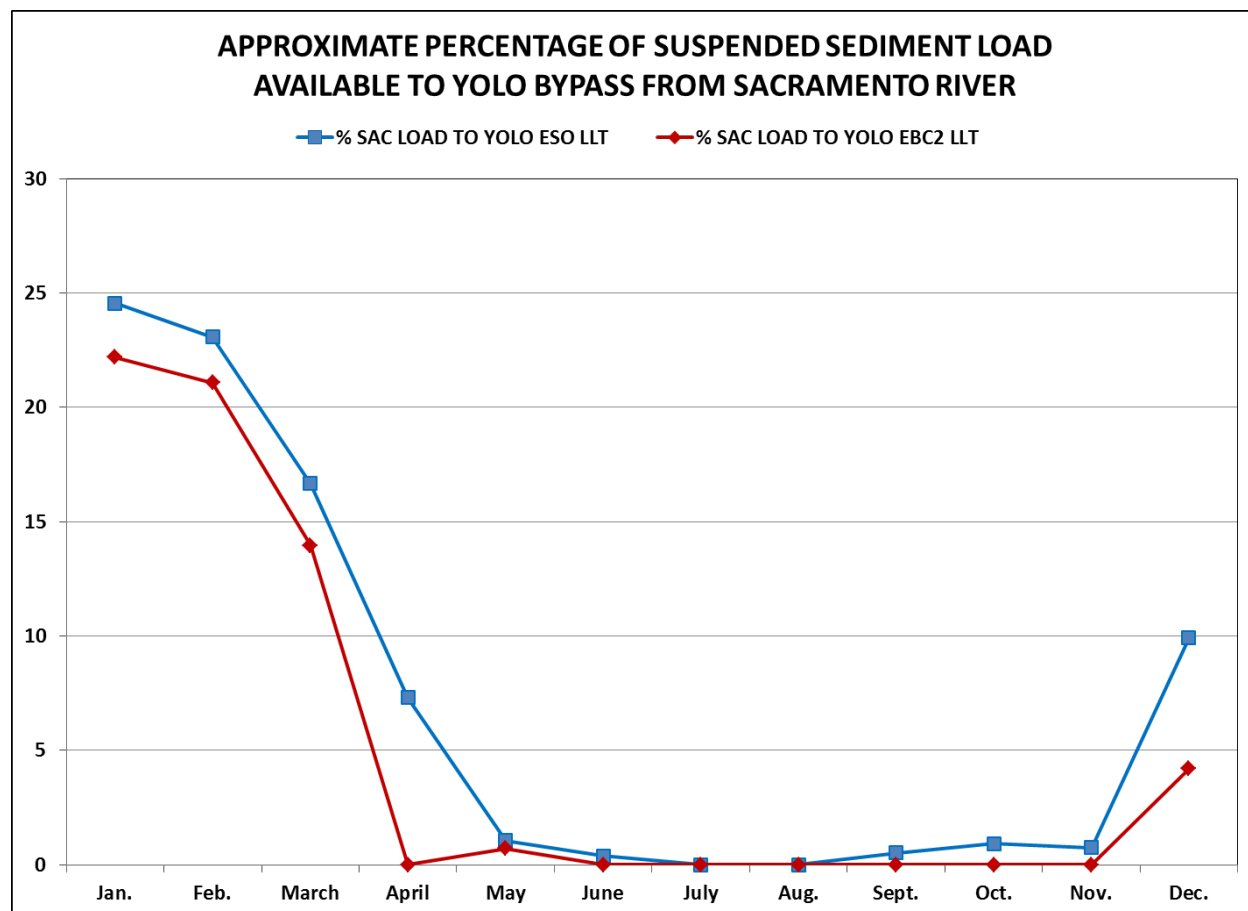
2 **Figure 5C.D–10. Comparison of Percentage of Sacramento River Suspended Sediment Load Available**
3 **to the Yolo Bypass in EBC2_LLT and ESO_LLT Scenarios, 1991–2002**

Table 5C.D-2. Cumulative Load Calculations for Total Load Available above Freeport and Load Available to the Yolo Bypass for the EBC2_LLT and ESO_LLT Scenarios

Month	Above Freeport			Yolo Bypass		
	EBC2_LLT	ESO_LLT	Difference (ESO–EBC2)_LLT	EBC2_LLT	ESO_LLT	Difference (ESO–EBC2)_LLT
January	7,395,182	7,626,338	231,155	1,641,770	1,872,926	231,155
February	5,672,703	5,819,007	146,304	1,196,288	1,342,592	146,304
March	4,646,942	4,797,691	150,749	648,962	799,711	150,749
April	2,105,491	2,271,640	166,149	58	166,207	166,149
May	1,664,882	1,670,688	5,806	11,747	17,553	5,806
June	949,920	953,658	3,738	0	3,738	3,738
July	602,043	602,043	0	0	0	0
August	483,863	483,863	0	0	0	0
September	390,364	392,421	2,507	0	2,057	2,057
October	161,935	163,431	1,496	0	1,496	1,496
November	281,735	283,872	2,137	0	2,137	2,137
December	2,482,731	2,639,863	157,132	104,549	261,681	157,132
Cumulative load	26,837,792	27,704,514	866,722	3,603,375	4,470,097	866,722
Percent difference (ESO–EBC2)_LLT			3%			24%

% SACRAMENTO RIVER LOAD EXPORTED ESO LLT
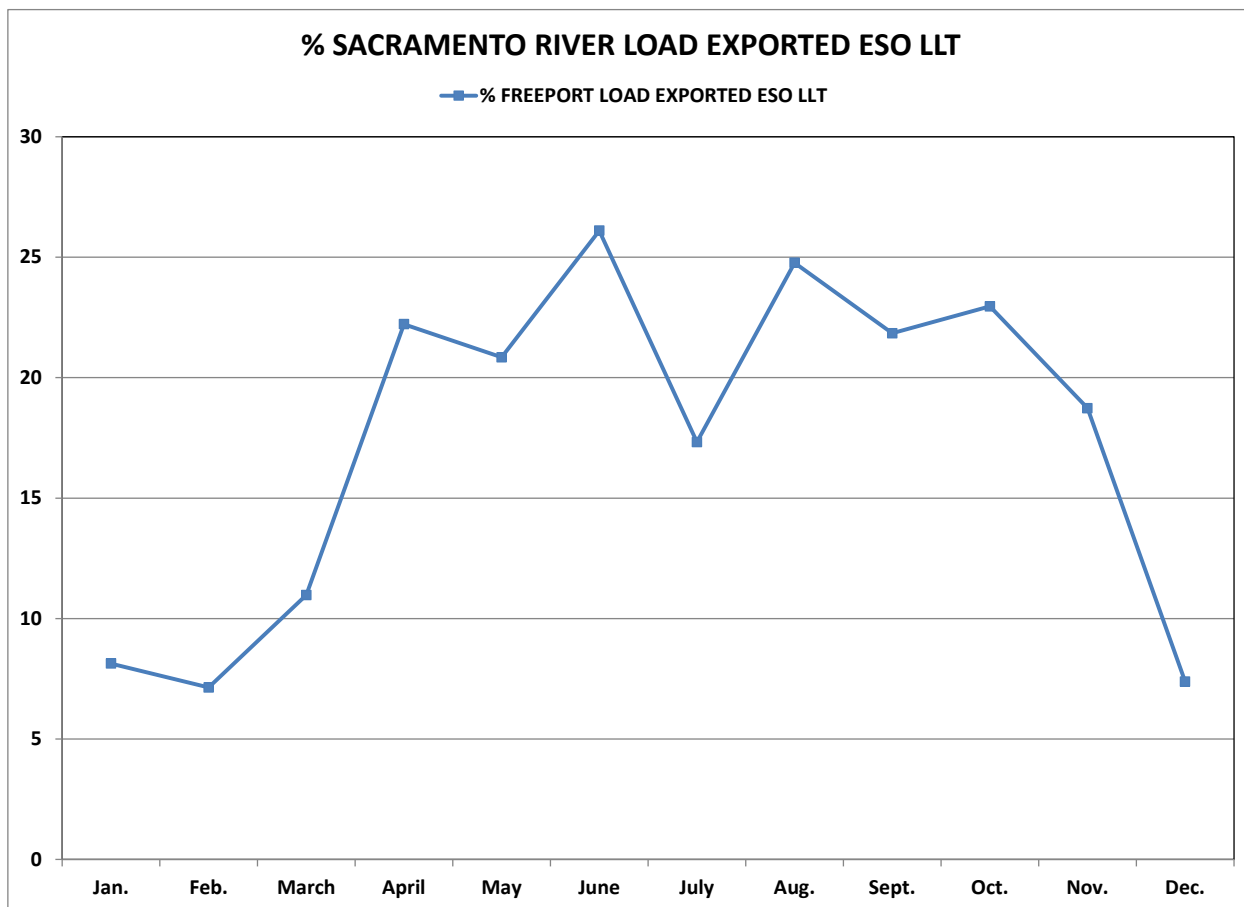
Figure 5C.D–11. Percentage of Sacramento River Suspended Sediment Load Exported in the ESO_LLT Scenario
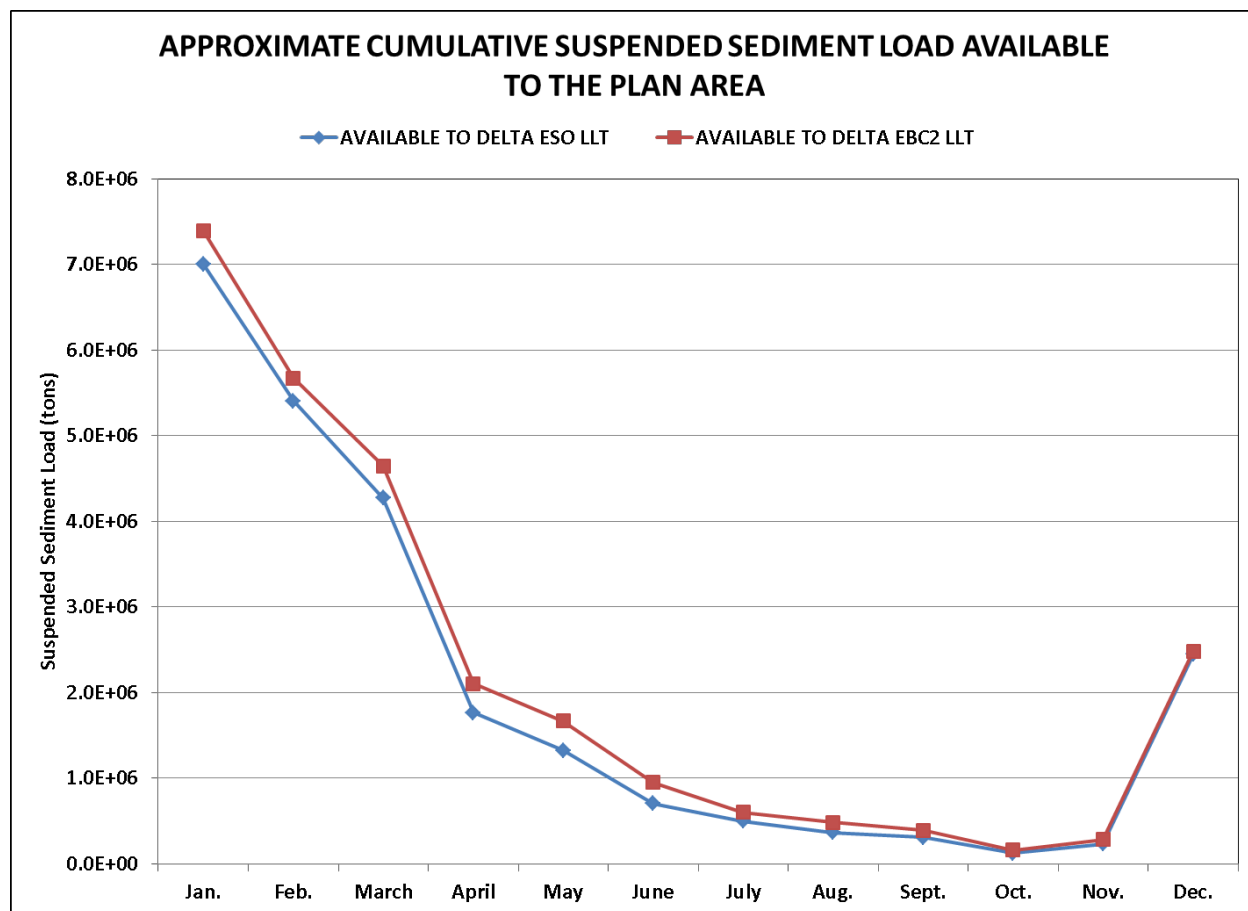
Note that the Yolo Bypass is included in this estimate, and that exports removed sediment in the ESO_LLT scenario.

Figure 5C.D–12. Comparison of Cumulative Suspended Sediment Load Available to the Plan Area in the EBC2_LLT and ESO_LLT Scenarios
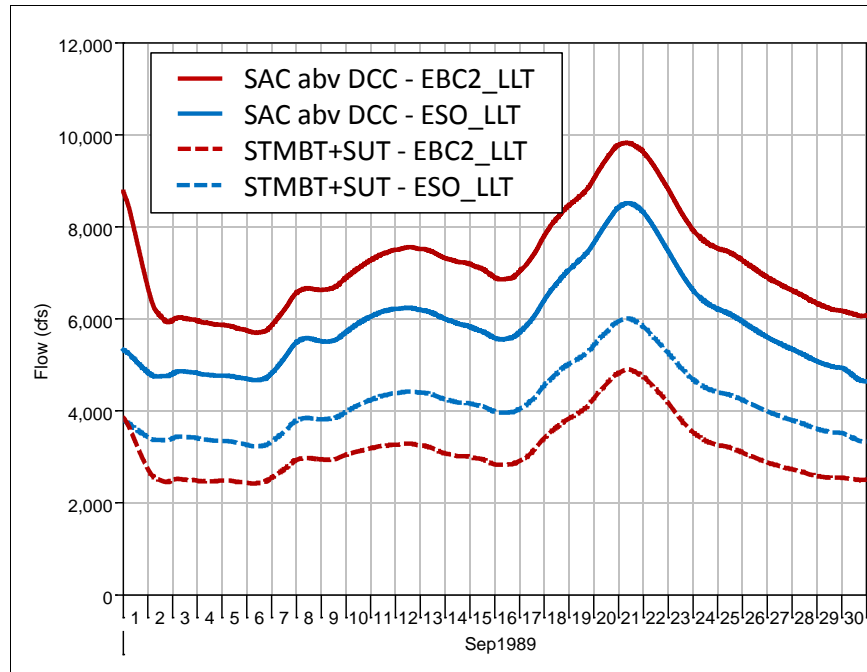
1

2 The plot shows a greater flow split to Steamboat Slough and Sutter Slough with the ESO_LLT in comparison to
3   the EBC2_LLT

4 **Figure 5C.D–13. Tidally-Averaged DSM2 Model Channel Flows for a Period with No North Delta Export**
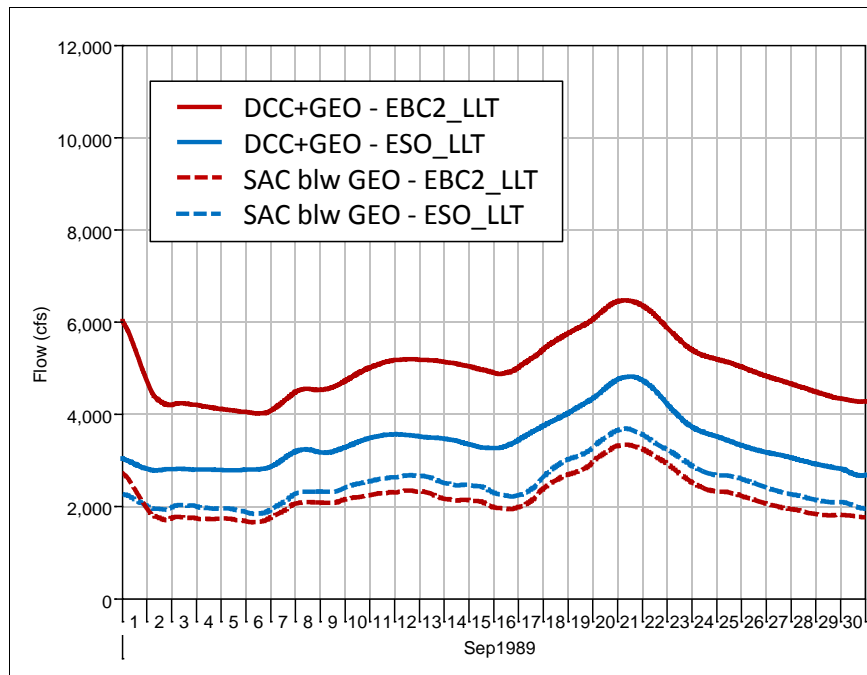
5

6   The plot shows the reduction in DCC+Georgiana Slough flow with the ESO_LLT in comparison to the
7   EBC2_LLT.

8 **Figure 5C.D–14. Tidally-Averaged DSM2 Model Channel Flows for a Period with No North Delta Export**

Month	Flow (cfs)	
	EBC2_LLT	ESO_LLT
January	5115	4074
February	5482	4327
March	5609	4324
April	3864	2944
May	2730	1995
June	5093	3434
July	7032	4463
August	6005	3329
September	5051	3665
October	4557	2553
November	4053	2743
December	4918	4017
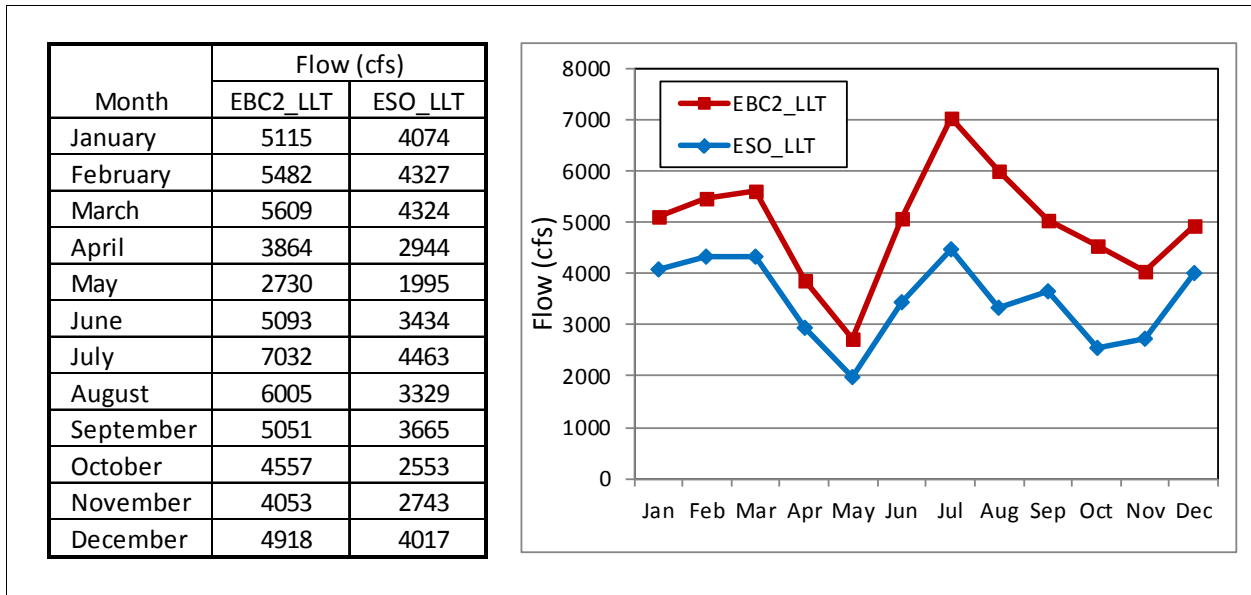
Figure 5C.D–15. Monthly Average Flows for Georgiana Slough+DCC Computed from 1976–1991 DSM2 Simulations for the ESO_LLT and EBC2_LLT Scenarios

Month	Flow (cfs)	
	EBC2_LLT	ESO_LLT
January	0	0
February	0	0
March	0	0
April	0	0
May	0	0
June	2719	1712
July	3992	2283
August	3694	1852
September	2464	2097
October	2379	1193
November	1028	669
December	687	480
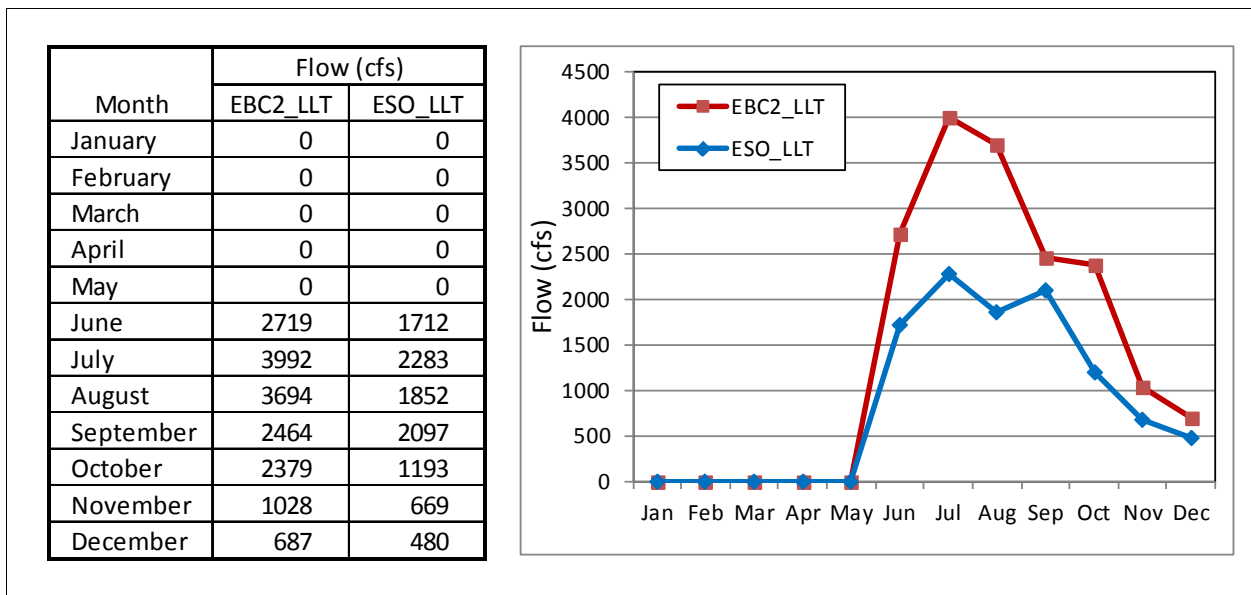
Figure 5C.D–16. Monthly Average Flows for the DCC Computed from 1976–1991 DSM2 Simulations for the ESO_LLT and EBC2_LLT Scenarios
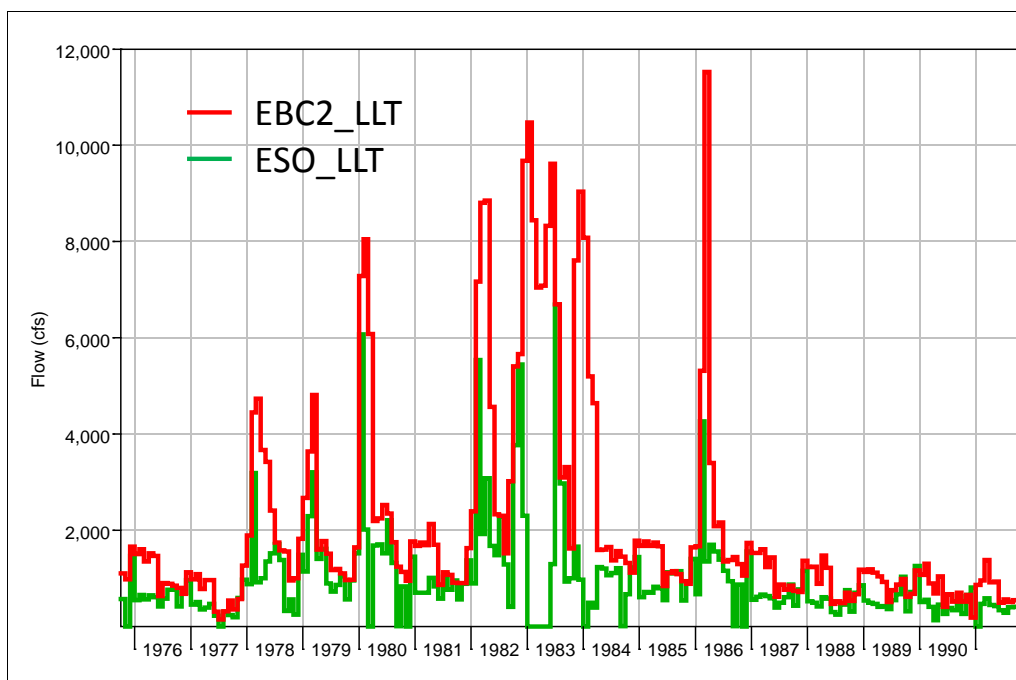
Time series of monthly averaged min (ORH,EXP) flow for the EBC2_LTT and ESO_LLT.

Month	Flow (cfs)	
	EBC2_LLT	ESO_LLT
January	2882	879
February	3416	1435
March	3688	789
April	2504	948
May	2209	890
June	1708	784
July	1475	1284
August	1165	959
September	1267	596
October	1199	738
November	1567	967
December	2415	1310
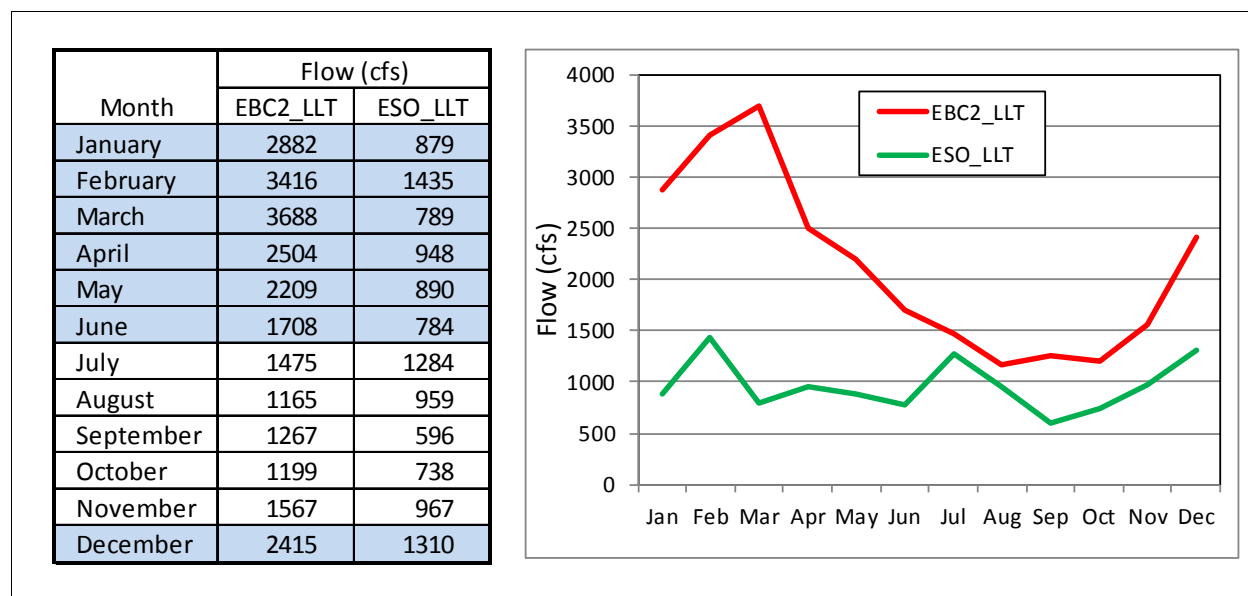
Monthly values of the minimum (ORH,EXP) flow.

Figure 5C.D–17. Old River at Head Flow Available for South Delta Export (Minimum of ORH Flow and South Delta Export Flow) from DSM2 Modeling

5C.D.4 Factors Affecting Sediment Supply and Water Clarity in the EBC2_LLT and ESO_LLT Models due to Climate Change and Sea Level Rise

Although the current trend is for decreasing sediment supply to the Plan Area, the uncertainty in change in sediment supply in coming decades, as discussed above, is high (Wright and Schoellhamer 2004; Cloern et al. 2011). Change in the timing and volume of flow patterns due to climate change has the potential to alter sediment supply and the timing of the supply, as spring snowmelt sediment concentrations are lower than first flush events at the same flow rates (Schoellhamer et al. 2007). The timing of the bulk of sediment deposition may affect resuspension during the seasonal period of high winds. Since newly deposited sediment is more easily resuspended, earlier deposition of sediment due to earlier snowmelt may result in less resuspension in the summer and a seasonal increase in water clarity (Ganju and Schoellhamer 2010).

Sediment supply could increase due to climate-change induced changes in land use patterns from urbanization, shifts in agriculture, grazing, and logging. Sediment supply to the Plan Area could decrease with upstream removal of levees or replacement of armored levees with set-back levees, as deposition would then occur along upstream reaches. Overall, Schoellhamer et al. (2007) have concluded that those factors that modify the flow regime alone, such as climate change, are less likely to affect sediment supply to the Plan Area than factors that change both flow regime and upstream supply.

Ganju and Schoellhamer (2010) conducted a series of modeling exercises to evaluate the effects of sea level rise (6 cm sea level rise at the seaward boundary), climate change (effects of increased air temperature) and changes in sediment supply in Suisun Bay for several 2030 scenarios. In Suisun Bay, the authors found that increases of water depth due to sea level rise reduced sediment resuspension, thereby increasing water clarity. Sediment deposition actually showed a net increase in areas with depths of 0–2 meters, although this was not quite enough to keep pace with sea level rise, so the shallowest areas deepened despite this deposition. All other areas showed net erosion. When assuming a reduced sediment supply of 34%, the authors found that the shallowest areas still experienced an increase in deposition with all other areas showing a net loss. In dry years, landward transport of existing unconsolidated sediment supply in San Pablo Bay was more predominant, favoring an increase in deposition on the seaward end of Suisun Bay. Increased tributary flows in wet years overall resulted in greater sediment export from the Plan Area, although off channel shoals were still depositional from this upstream sediment supply.

Although assumptions differ from some of those in the BDCP models, many of the observations of Ganju and Schoellhamer (2010) are general enough to inform discussion about the Plan Area as a whole as applied to the EBC2 LLT scenario (45 cm sea level rise, no development of ROAs) in comparison with the ESO_LLT scenario (45 cm sea level rise, with ROA development). Much of the discussion of sediment transport in Suisun Bay under sea level rise scenarios in Ganju and Schoellhamer (2010) informs expected effects of the EBC2_LLT and ESO_LLT scenarios on turbidity. If sediment supplies are reduced in the future, there will be a net decrease in deposition in the estuary, which is likely to be linear with distance from the sediment source or weakly nonlinear. An increase in mean water depth due to sea level rise will result in a reduction in shear stress due to wind waves, and potentially lead to a (local) increase in water clarity as sediment resuspension is decreased. On the other hand, an increase in tidal prism, as would occur with the increase in the

1　　mean volume of the Plan Area in the ESO_LLT scenario with the development of the ROAs, could
2　　result in increased tidal velocity and increased shear stresses, and potentially a (local) decrease in
3　　water clarity due to increased resuspension. However, the complex geometry of the Plan Area
4　　precludes an overly simplistic interpretation of these generalizations (Ganju and Schoellhamer
5　　2010).

5C.D.5　Effects of Tidal Currents, Net Flows and Stratification on Water Clarity

6
7

5C.D.5.1　Background

9　　For Suisun Bay and the western Delta, suspended sediment (and, as a result, measured turbidity)
10　　varies on annual, seasonal, spring-neap cycle and tidal time scales. Sediment loading into the Plan
11　　Area has been previously examined, and the focus of this section is the resuspension, transport and
12　　re-deposition of the bed sediment deposited during the wet season loading. Mechanisms that were
13　　examined include tidal circulation, net channel flow, gravitational circulation and stratification. The
14　　potential interactions of the ESO_LLT alternative with these processes is discussed below. A short
15　　discussion related to the HOS_LLT and LOS_LLT scenarios is provided following the detailed
16　　examination for the ESO_LLT potential effects.

17　　As discussed in previous sections, the existing conceptual model (Ganju et al. 2006) is that the
18　　majority of suspended sediment is delivered through the Plan Area with the large wet season flows,
19　　creating a large reservoir of erodible sediments within the channels and shallows. Persistent winds
20　　in the spring and summer months allow wind-wave resuspension of sediments in the shallows. The
21　　sediment deposited in channels may be resuspended and transported by tidal currents. Sediments
22　　are most likely transported away from high energy (high current velocities and/or wind
23　　resuspension) areas and deposited in low energy zones. As summer progresses, the erodible pool is
24　　reduced and suspended sediment concentration falls.

25　　On a tidal time scale, sediments are resuspended with strong ebb or flood tide currents, while there
26　　is increasing deposition near or during slack tide (Schoellhamer et al. 2007). Flood tides transport
27　　sediment from Suisun Bay into the Delta and the process reverses on ebb. The spring-neap cycle
28　　may have a significant effect on the resuspension, transport and deposition of suspended sediments.
29　　This can be further complicated by salinity stratification, gravitational circulation and bottom
30　　topography (Schoellhamer 2001).

31　　Tidally averaged historical (not modeled) turbidity and salinity (EC) for five locations (Figure 5C.D–
32　　18) in Suisun Bay and the western Delta are illustrated for the months May-December for 2010
33　　(Figure 5C.D–19) and 2011 (Figure 5C.D–20). The plots illustrate several of the processes discussed
34　　above. The Water Year Hydrologic classification for WY2010 is below normal for the Sacramento
35　　River region and above normal for the San Joaquin River region. For WY2011, both the Sacramento
36　　River and San Joaquin River regions are classified as wet. Turbidity is usually highest in western
37　　Suisun Bay and generally decreases going inland, although summer turbidities for the Sacramento
38　　River at Decker Island station are often close to Mallard Island values.

39　　Most notable in the turbidity plots are the large variations in the tidally averaged turbidity for
40　　Martinez. Schoellhamer (2001) has shown SSC for Benicia and the western Suisun Bay increases as

1   near bottom currents increase with spring tide conditions, while with the neap tide bottom currents
2   decrease and deposition is enhanced. Furthermore, salinity stratification is greatest during neap
3   tides due to reduced vertical mixing, further increasing deposition and decreasing SSC. Generally
4   SSC concentrations are greater at Benicia and the western Suisun Bay than locations further to the
5   east. However, during neap tides, tidally averaged surface SSC at Benicia is occasionally less than at
6   Mallard Island (Schoellhamer 2001). Similar effects may be observed in the tidally averaged
7   turbidities for Martinez and Mallard Island in Figure 5C.D–19 and Figure 5C.D–20. Gravitational
8   circulation is important in transporting higher SSC that are near the bed in the landward direction
9   (Ganju and Schoellhamer 2006).

10   Ganju and Schoellhamer (2007) have computed the components of SSC transport (advective,
11   dispersive and Stokes drift) at Benicia. Advective sediment flux (contributions from mean discharge
12   and mean concentration) was predominantly seaward while dispersive flux (correlation between
13   velocity and concentration variations) was landward, except for a period of sustained freshwater
14   flow. Advection during high flow periods leads to the net transport of sediment seaward out of
15   Suisun Bay. During low flow periods, dispersive flux leads to net transport of sediment into Suisun
16   Bay, and the SSC source is understood to be San Pablo Bay (Ganju et al. 2006).

17   For eastern Suisun Bay (Mallard Island), advective suspended sediment transport is typically
18   seaward. During low flow periods, dispersive flux moves suspended sediment landward as
19   suspended sediment concentration in Suisun Bay is typically higher relative to the lower
20   Sacramento River and due to flood tide/ebb tide asymmetries (McKee et al. 2006). Still, McKee et al.
21   (2006) determined the net advective+dispersive flux to be seaward. Numerical modeling results
22   (Ganju and Schoellhamer 2006) indicate net seaward sediment transport in the upper water column
23   and a landward flux in the lower water column, so that for low flow periods the redistribution of
24   Suisun Bay sediments is landward.

25   The plots in Figure 5C.D–19 and Figure 5C.D–20 show increasing salinity for the western Delta in
26   early summer with some increase in turbidity. With late summer and early fall, salinity continues to
27   increase while western Delta turbidity decreases. Early summer salinity intrusion, particularly for
28   the lower San Joaquin River, can be seen to coincide with reduced or negative net channel flows.
29   South Delta exports increase beginning in June for both years, affecting both net Delta outflow and
30   net flow on the lower San Joaquin. Net channel flows also vary with the spring-neap tidal cycle, as
31   the average Suisun Bay and Delta water surface elevations increase on the spring tide and decreases
32   on the neap tide. The Delta thus fills approaching the peak spring tide and drains on approaching the
33   peak neap cycle (Oltmann and Simpson 1997). The net channel flow and net advection for the lower
34   San Joaquin River flows can be upstream. Tidal excursion is also at a maximum during spring tides
35   and may carry salinity and turbidity further upstream on the peak flood tide for dispersive mixing.

36   Figure 5C.D–21 shows the tidally averaged turbidities for the Sacramento River at Rio Vista and the
37   Sacramento River at Decker Island, along the tidally averaged lower Sacramento River flow
38   (Sacramento River at Rio Vista less Threemile Slough). The plot suggests that above 20,000 cfs lower
39   Sacramento River flow, Rio Vista and Decker Island turbidities are strongly coupled. At lesser flows,
40   turbidity at Decker Island is noticeably greater.

41   Figure 5C.D–22 and Figure 5C.D–23 illustrate the variation in turbidity and EC on an inter-tidal
42   scale. Fifteen-minute turbidity and EC time series are plotted for the western Delta locations
43   Sacramento River at Decker Island and the San Joaquin River at Antioch. Figure 5C.D–22 shows peak
44   EC and peak turbidity occurring with the peak flood tide. However the characteristics of the

1   turbidity time series differ from the EC time series. Peak EC occurs at or just before the slack after
2   flood. However, turbidity drops near slack tide as suspended material settles out. Turbidity rises
3   later on the following ebb tide as current velocities increase and resuspend the sediment deposited
4   upstream of the station. The resuspended sediment (and sediment that remained in suspension) is
5   then advected past the Decker Island location on the continuing ebb (Ganju et al. 2004). Figure
6   5C.D–23 provides the turbidity and EC time series for the SJR at Antioch location. The turbidity time
7   series for the Antioch station includes an additional feature from that described for the Decker
8   Island record. A sharp turbidity peak occurs just at the beginning of ebb with the initial local
9   resuspension of sediments (Ganju et al. 2004). The source of the EC peaks seen at peak flood is
10 clearly from the west (Suisun Bay). The source of turbidity at both stations is more complex because
11 in addition to advection and dispersion of turbidity, the sediment bed is both a source and sink for
12 suspended sediment.

5C.D.5.2   ESO_LLT Effects

14 The above discussion outlined the role of tidal currents, net channel flows and stratification to SSC
15 in Suisun Bay and the western Delta in the late spring to fall after the initial delivery of sediments to
16 the region with the high flow period. Possible effects of ESO_LLT on these processes were examined
17 to assess potential effects on water clarity. The processes reviewed include the effects of ESO_LLT on
18 tidal currents, salinity intrusion in early summer, and net flow. The salinity intrusion and net flows
19 are viewed as a measure of exchange of higher turbidity water from Suisun Bay with the western
20 Delta over the tidal cycle. The analysis is performed comparing DSM2 model results for the
21 EBC2_LLT and ESO_LLT scenarios - both simulations include 45 cm of sea level rise. Table 5C.D-3
22 summarizes the effects on turbidity for the processes on an individual basis for western Suisun Bay,
23 eastern Suisun Bay, the lower Sacramento River and the lower San Joaquin River.

24 Higher velocity tidal currents should increase resuspension of the erodible pool of sediments that
25 are deposited during the high flow period. Furthermore higher tidal current velocities should
26 increase vertical mixing and may reflect greater tidal excursion and tidal mixing. Ganju and
27 Schoellhamer (2006) performed a model sensitivity analysis (historical configuration) that
28 indicated decreases in tidal velocity lead to increased deposition due to reduced shear stress in
29 Suisun Bay. The changes in the tidal currents (ESO_LLT versus ECB2_LLT) after the high flow period
30 are illustrated in Figure 5C.D–24 which shows the RMS velocity times series (see Schoellhamer
31 2001) during May–December 1979 (after the high flow period, with 1979 a representative year) for
32 western Suisun Bay at Martinez, eastern Suisun Bay at Mallard Island, the lower Sacramento River at
33 Emmaton and the lower San Joaquin River at Antioch. The cumulative effect of all the ROAs is to
34 slightly increase the overall tidal prism at Martinez, while the presence of the Suisun Marsh ROA
35 tends to decrease tidal flow in eastern Suisun Bay at Mallard Island (RMA 2010a). The base
36 condition tidal flow at Mallard Island is partly redirected into Montezuma Slough (near Collinsville)
37 for the ESO_LLT. The development of the Cache Slough ROA increases the tidal currents for the
38 lower Sacramento River at Emmaton. The lower San Joaquin River at Antioch shows a notable
39 decrease in tidal current velocity. Table 5C.D-3 lists the inferred increase or decrease in turbidity
40 based upon the changes in modeled tidal currents.

41 The introductory discussion examined the relation of late-spring and early-summer salinity
42 intrusion to turbidity in the western Delta. The proposition is that EC intrusion may be viewed as an
43 indicator of the advection and tidal mixing processes that may transport or exchange turbidity
44 between Suisun Bay and the western Delta. This is illustrated in Figure 5C.D–25 which presents

1 monthly modeled EC for Suisun Bay and western Delta stations for Dry and Below Normal/Above
2 Normal water-year types (these year types give average, representative results). The EBC2_LLT and
3 ESO_LLT results show similar EC values for June, but ESO_LLT has notably higher EC values for July.
4 Exclusive of the effects of all other mechanisms, the higher EC suggest more transport of turbidity to
5 the western Delta from Suisun Bay.

6 Figure 5C.D–26 presents the modeled net monthly flows for Suisun Bay and western Delta stations
7 for Dry and Below Normal/Above Normal water-year types. The net flow provides an assessment of
8 the advection of suspended sediment in Suisun Bay and western Delta. Decreased positive advection
9 increases the importance of the dispersive transport term (McKee et al. 2006). Negative net flow will
10 increase the advective transport of sediment into the western Delta. The net outflows for eastern
11 Suisun Bay (Mallard Island) and Emmaton with ESO_LLT are primarily unchanged for June, but are
12 notably lower for July. The flow reductions are less in August, but are reduced from a smaller base
13 flow. The reductions in outflow for the Mallard Island and Emmaton locations are reflected by the
14 increases in EC (Figure 5C.D–25) in July and August. With ESO_LLT, the net flows are slightly more
15 negative (200–to 600 cfs) for July and August for the lower San Joaquin River at Antioch and
16 increase the advective transport of suspended sediment from Suisun Bay to the lower San Joaquin
17 River.

18 **Table 5C.D-3. Estimated Changes in Low Flow Season Turbidity in Suisun Bay and the Western Delta**
19 **for Implementation of ESO_LLT In Response to Tidal Currents, Salinity Intrusion, and Net Flow**

Process/Indicator	Potential Changes in Turbidity with ESO_LLT Relative to EBC2_LLT			
	Western Suisun Bay	Eastern Suisun Bay	Lower Sacramento River	Lower San Joaquin River
Tidal currents	Higher	Lower	Higher	Lower
Salinity Intrusion (late Spring-early Summer)	Uncertain	Higher	Higher	Higher
Net flow	Uncertain	Higher	Higher	Slightly Higher

20

21 5C.D.5.3 HOS_LLT/LOS_LLT Effects

22 During the late-spring/early summer period discussed above, there is very little difference in Delta
23 outflow between the ESO_LLT and LOS_LLT. Therefore the potential effects described above for the
24 ESO_LLT also apply to the LOS_LLT. Delta outflow under the HOS_LLT in April and May is similar to
25 or slightly higher than the EBC2_LLT scenario in above normal and below normal years, which may
26 make turbidity similar to or slightly less than EBC2_LLT. However, the differences are not great and
27 are limited to the spring (April/May) months that have higher outflows for longfin smelt benefits.
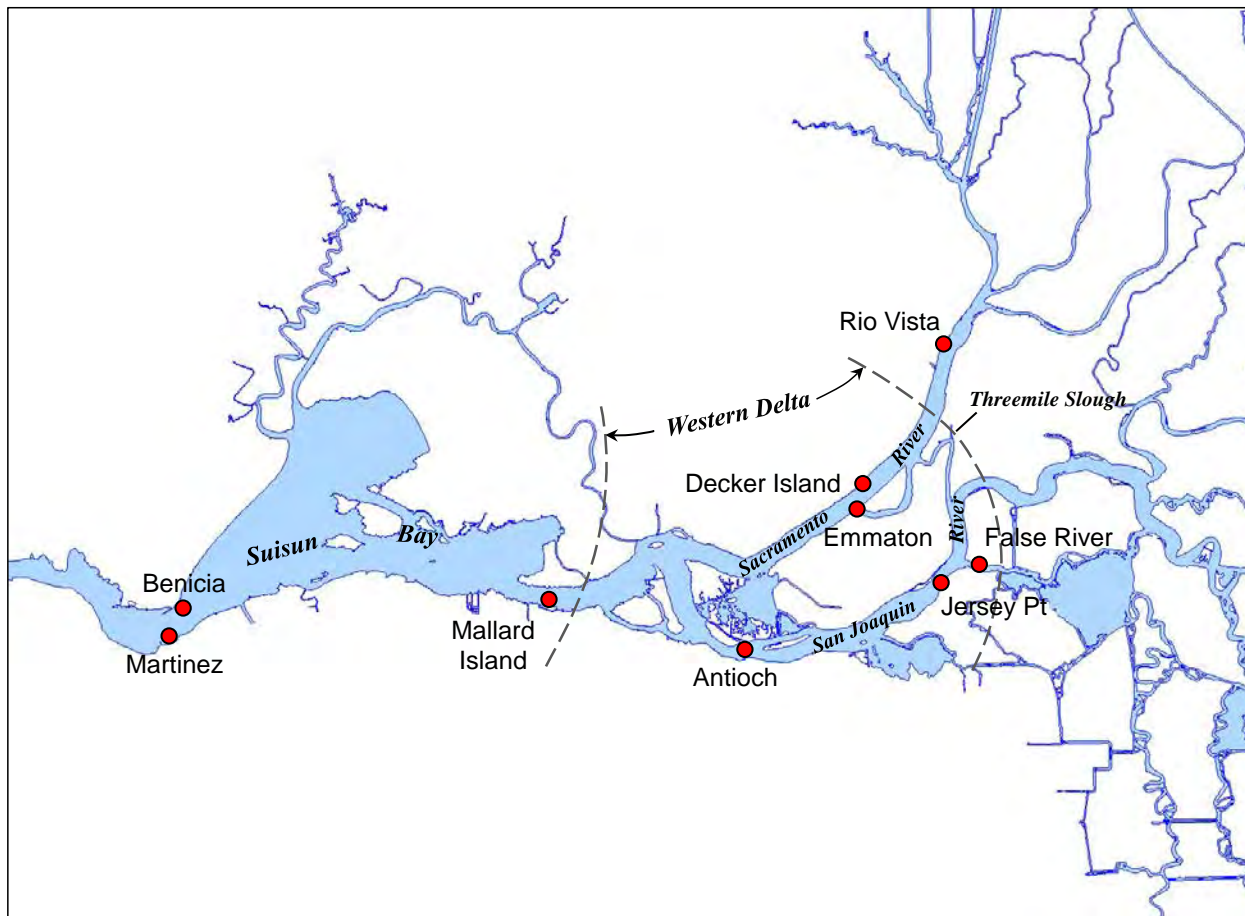
Figure 5C.D–18. Referenced Measurement and Model Output Locations for Suisun Bay and the Western Delta
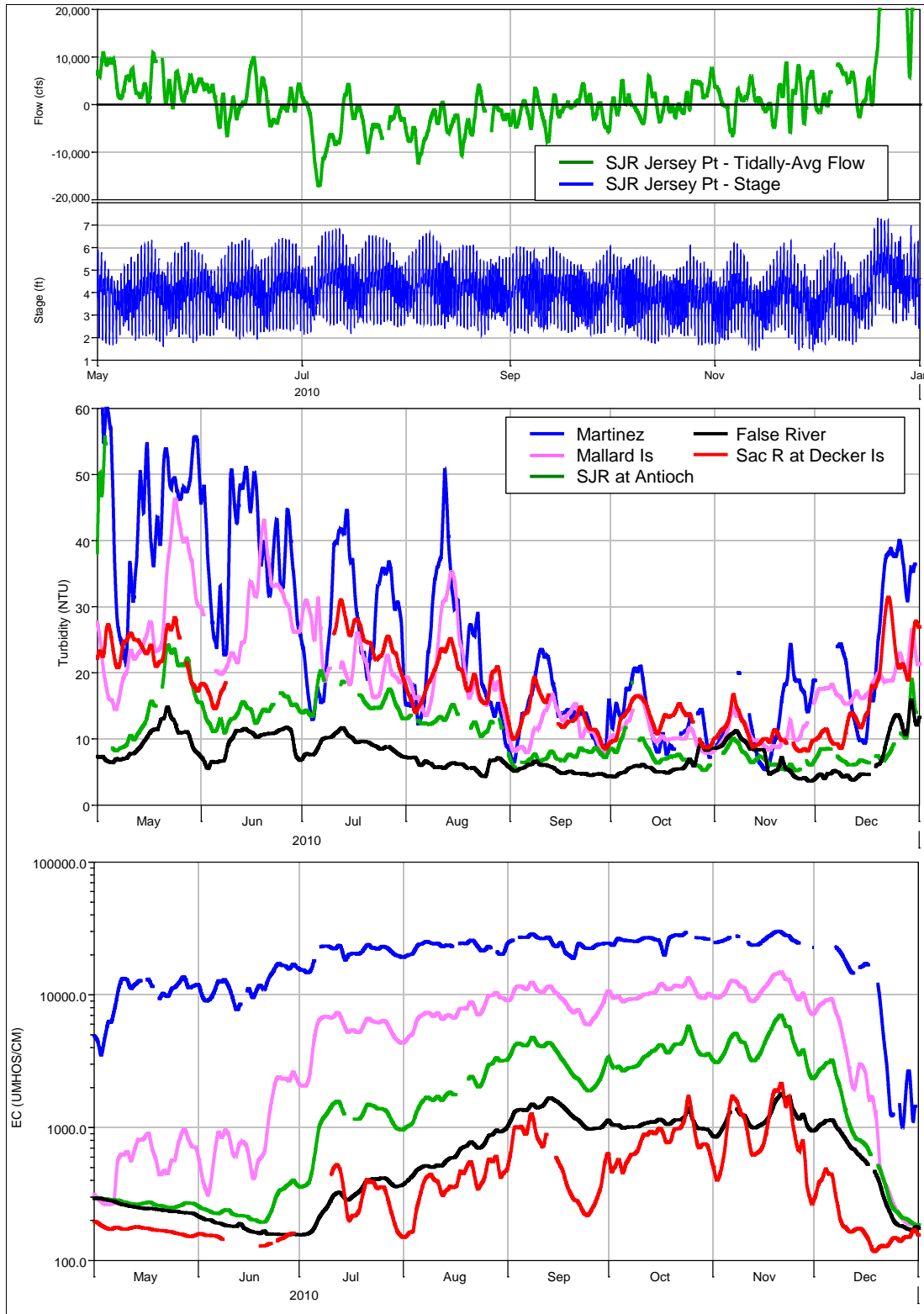
Stage and tidally averaged flow for the San Joaquin River at Jersey Point are plotted at the top.

Figure 5C.D–19. Observed Tidally Averaged Turbidity and EC Plotted for Suisun Bay and the Western Delta Locations May 1 to December 31, 2010
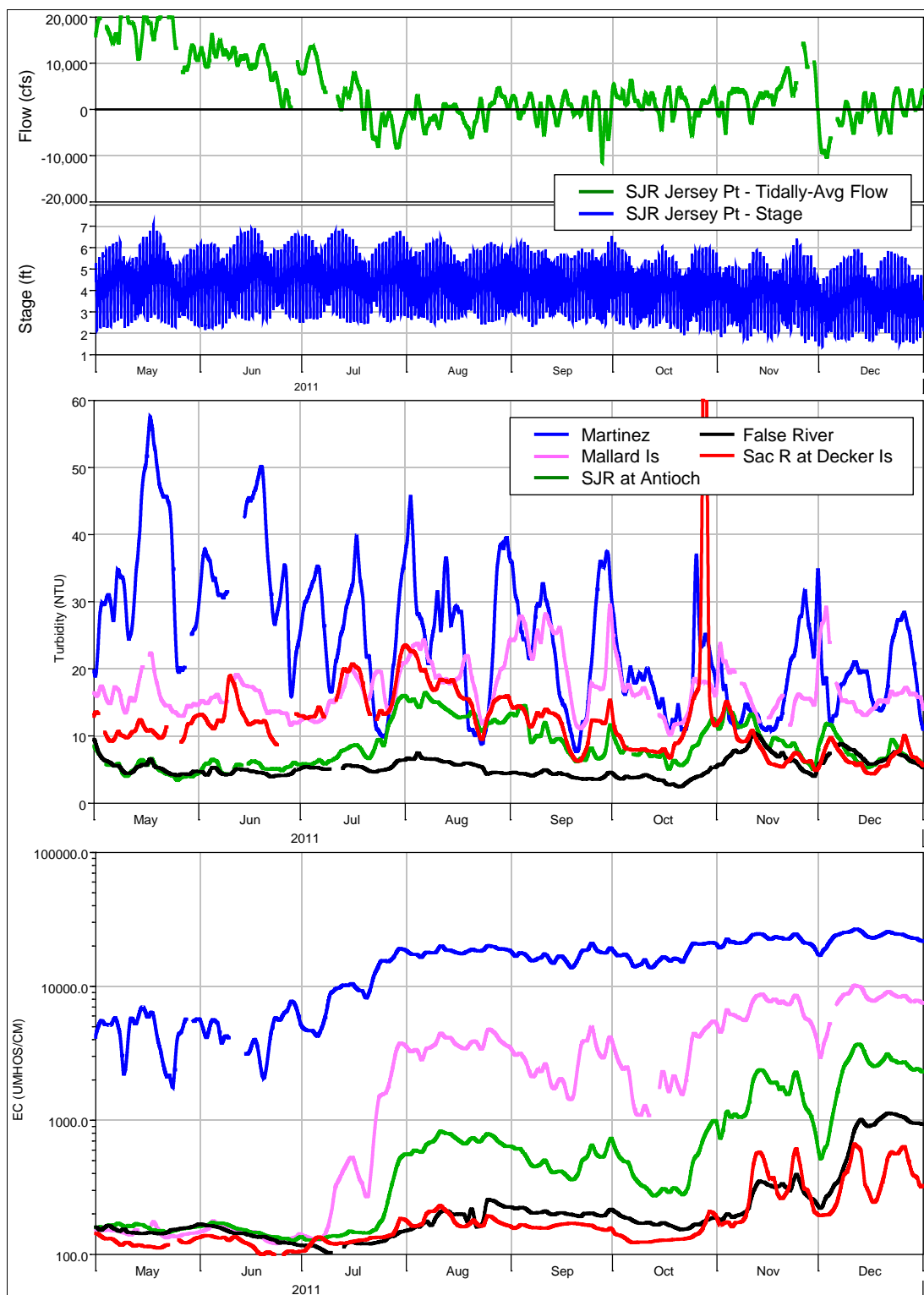
1
2   Stage and tidally averaged flow for the San Joaquin River at Jersey Point are plotted at the top.
3   **Figure 5C.D–20. Observed Tidally Averaged Turbidity and EC Plotted for Suisun Bay and the Western**
4   **Delta Locations May 1 to December 31, 2011**

1
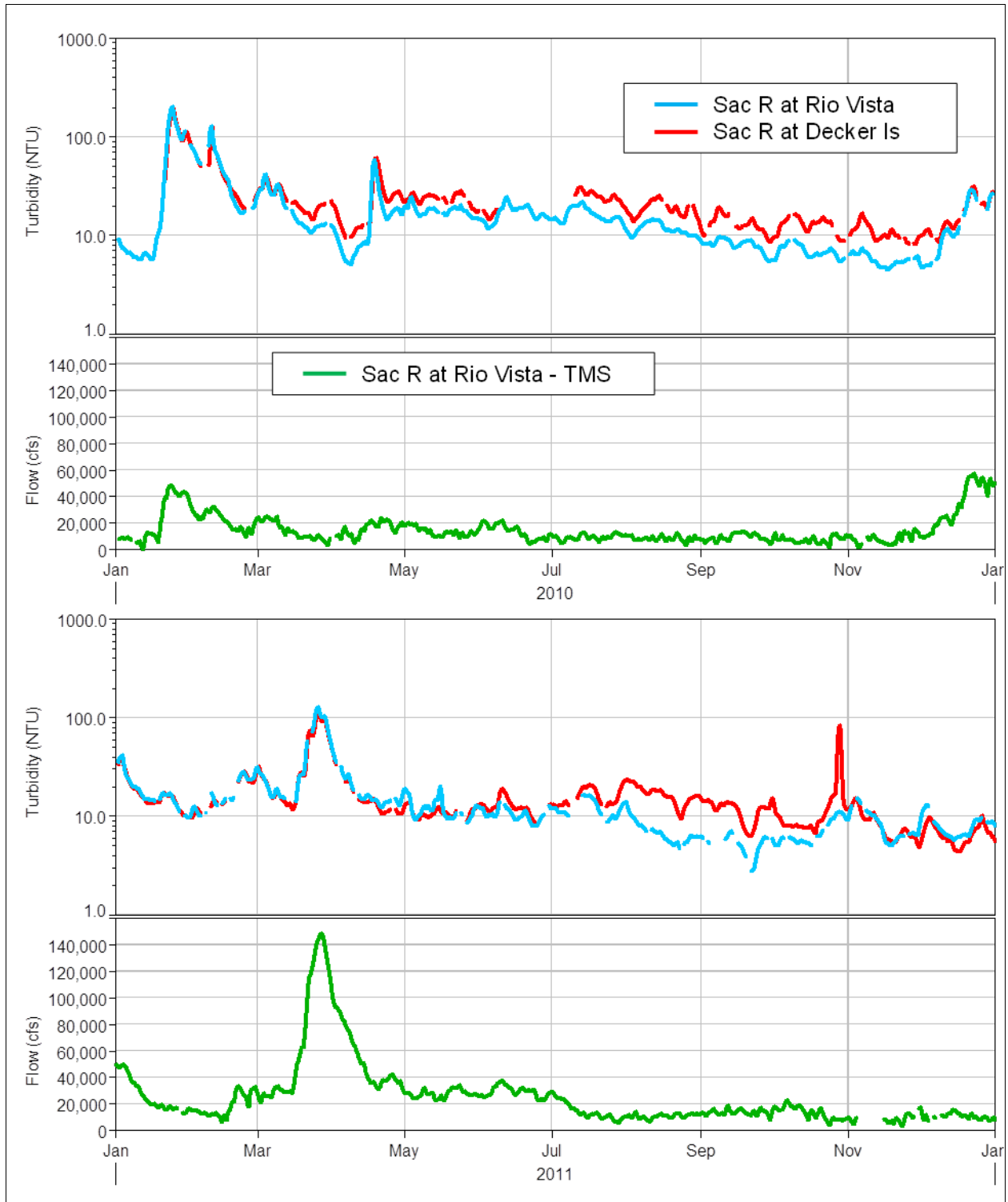
2   **Figure 5C.D–21. Observed Tidally Averaged Turbidity for the Sacramento River at Rio Vista and Decker**
3   **Island, and Tidally Averaged Flow for the Sacramento River at Rio Vista Minus Threemile Slough**
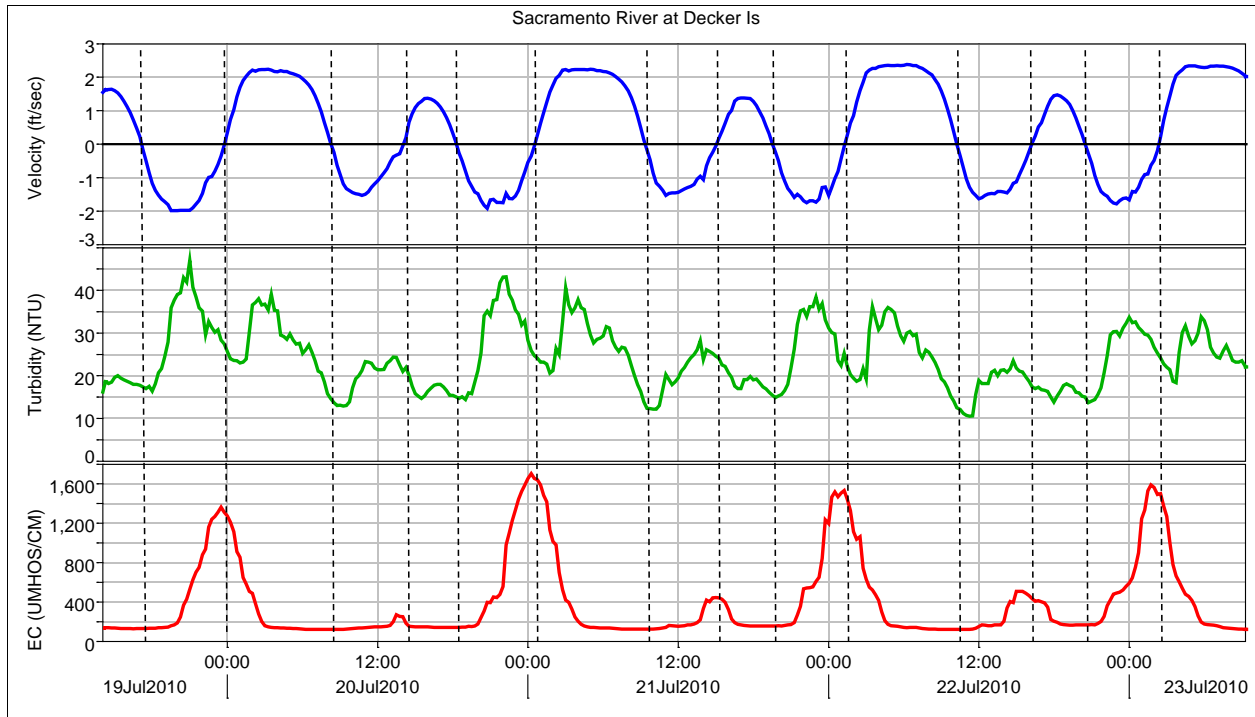
Vertical dashed lines indicate time of slack tide.

Figure 5C.D–22. Observed Velocity, Turbidity and EC Plotted for the Sacramento River at Decker Island, July 19–23, 2010
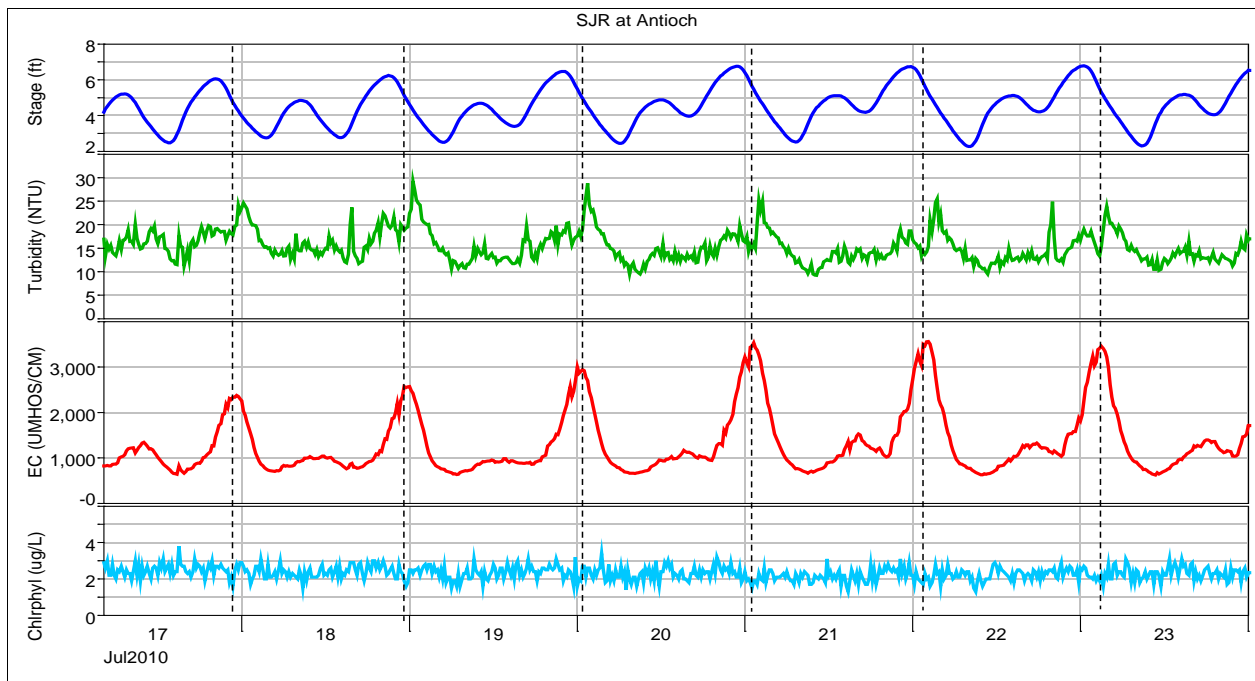
Vertical dashed lines indicate time of slack after flood inferred from peak EC.

Figure 5C.D–23. Observed Stage, Turbidity, EC and Chlorophyll Plotted for the San Joaquin River at Antioch July 17–23, 2010

1
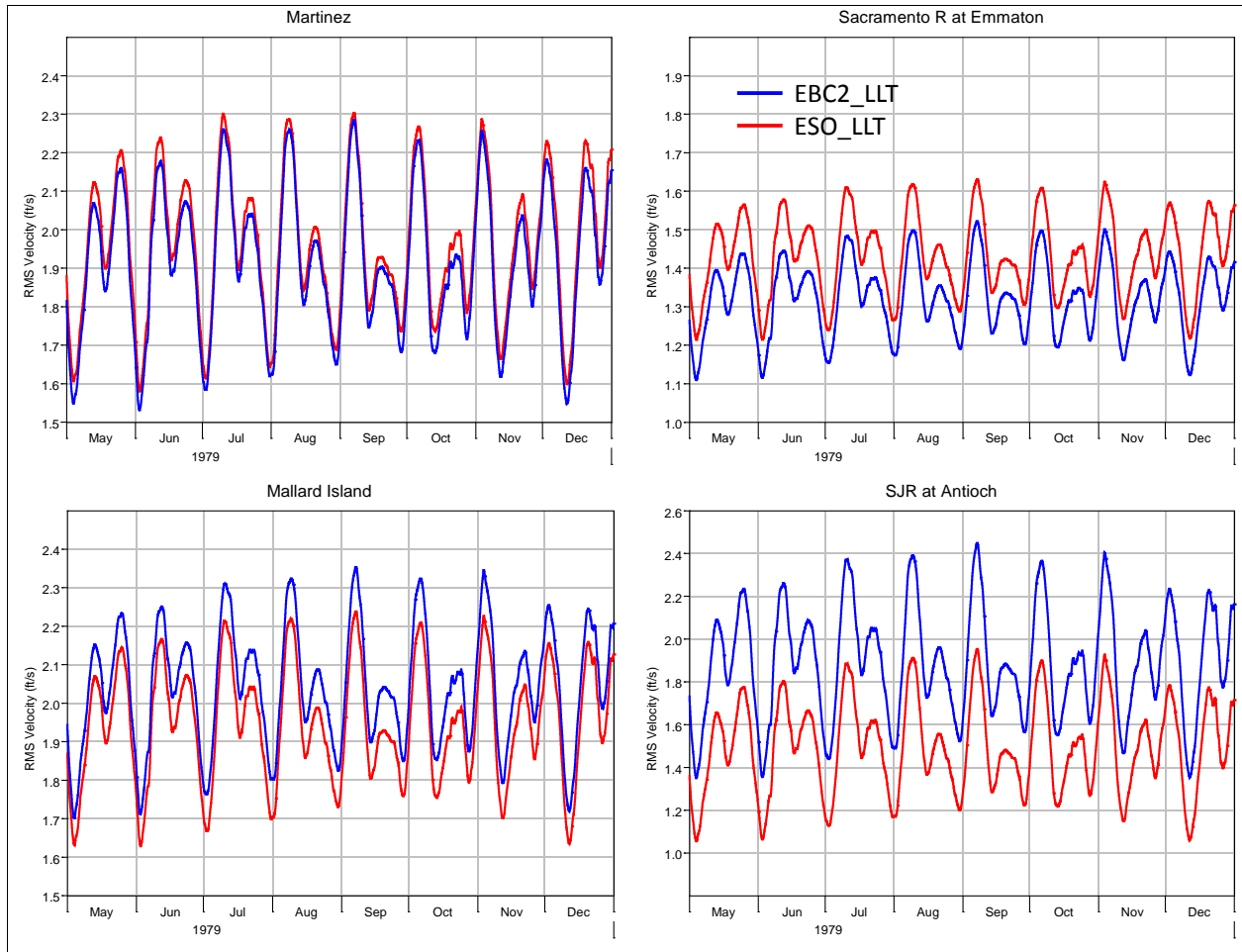
2
3   **Figure 5C.D–24. DSM2 RMS Velocity (DSM2) for the EBC2_LLT and the ESO_LLT, May–December 1979**

1
2   Results for "BN" (below normal) and "AN" (above normal) are combined.
3   **Figure 5C.D–25. DSM2 Average Monthly EC by Water-Year Type for EBC2_LLT and the ESO_LLT**
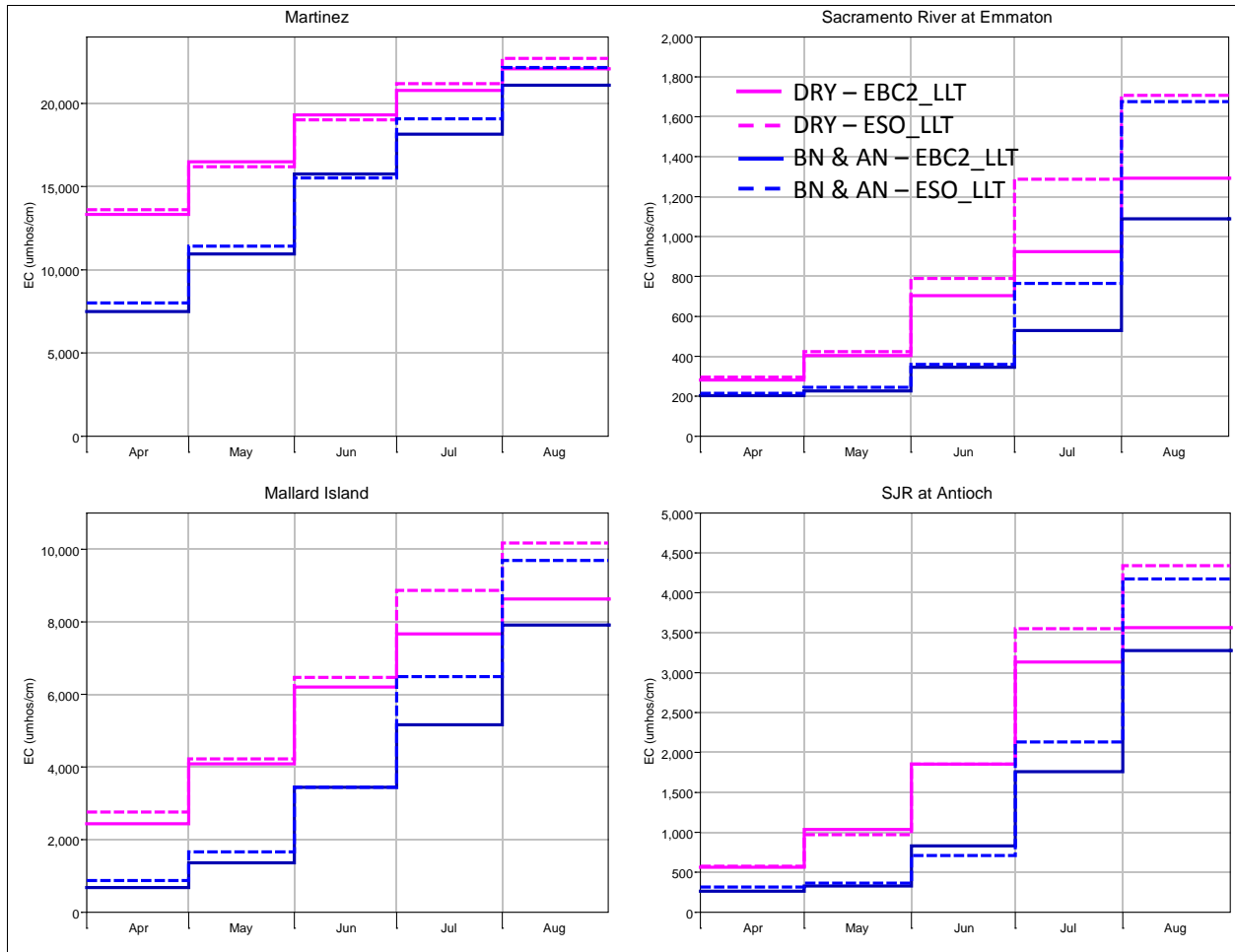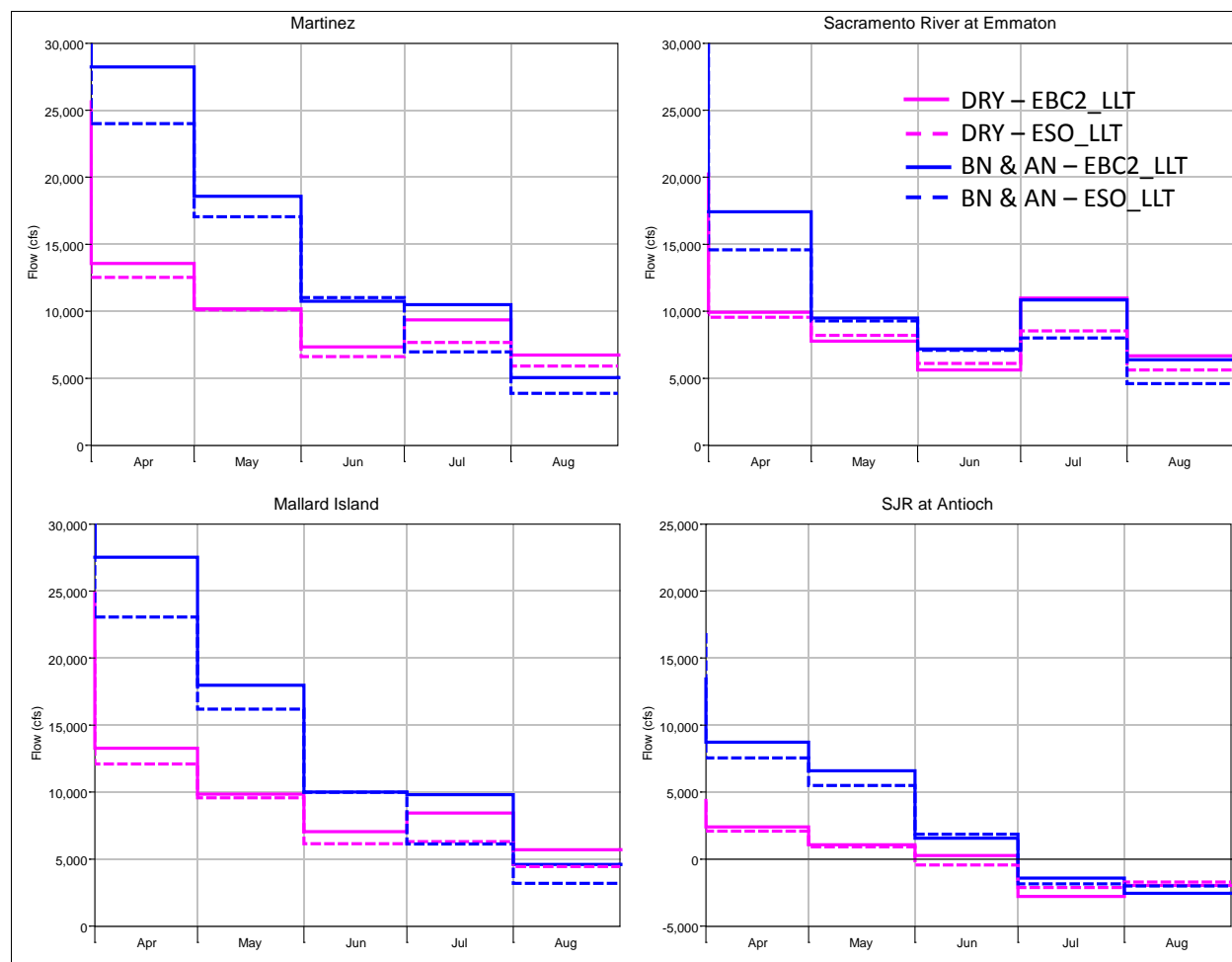
Results for "BN" (below normal) and "AN" (above normal) are combined.

Figure 5C.D–26. DSM2 Averaged Monthly Net Flow by Water-Year Type for EBC2_LLT and the ESO_LLT

5C.D.6 Invasive Aquatic Vegetation Influences on Water Clarity in ROAs and Existing Channels of the Plan Area

Invasive aquatic vegetation (IAV) and in particular submerged aquatic vegetation (SAV) has the potential to influence water clarity within the ROAs and existing channels of the Plan Area. In general, the presence of SAV will decrease local turbidity. By providing structural impedance to water flow, SAV decreases currents and wind wave-induced, orbital velocities. This dampening of velocities decreases shear stresses at the bed and thereby decreases sediment resuspension and increases deposition. Thus, local turbidity is typically lower in areas having higher SAV cover (Hestir 2010).

An analysis described in Appendix 5.F, *Biological Stressors on Covered Fish*, focused on the physical factors (water depth, channel velocity, and salinity) in the ROAs that may limit the area available for colonization by the SAV species *Egeria*. An additional analysis described in Appendix 5.F examined potential changes in maximum annual channel velocity in the existing channels of the Plan Area. The

1   main results from these analyses are found in Section 5F.4 of Appendix 5.F; the summary of results
2   in relation to turbidity considers the main findings of the analysis.

5C.D.7 Analysis of Wind-Wave Sediment Resuspension Potential Within the BDCP Restoration Opportunity Areas

5C.D.7.1 Background

7   Wind blowing over open water areas will result in wind waves, which can resuspend sediment.
8   Wind wave heights and periods are dependent on wind speed, fetch, and water depth (see Figure
9   5C.D–2 and Figure 5C.D–3), with larger waves generally developing in deeper areas. Wind waves
10   induce water particles to move in orbital paths, and the resulting bed shear stress is proportional to
11   the square of the orbital velocities at the bed (Figure 5C.D–4 and Figure 5C.D–5). Because the orbital
12   velocities decrease with depth, deep water columns experience less bed shear stress than shallow
13   water columns for a given wind wave. Sediment is resuspended from the bed when shear stress
14   exceeds a critical shear stress.

5C.D.7.2 Methodology

16   To assess the potential for wind-wave sediment resuspension in the ROAs, historical wind data from
17   CIMIS locations throughout the Plan Area were used. For each ROA, a single CIMIS station was
18   assumed to be representative of the wind speeds and directions experienced by the entire ROA. The
19   particular CIMIS station chosen to represent each ROA was generally the closest station. These
20   stations, along with their period of record, are given in Table 5C.D-4. An exception to the closest
21   distance requirement was made for the Cosumnes/Mokelumne ROA, where the Bryte station was
22   used instead of the closer Lodi West station. This substitution was made in order to better represent
23   the wind directions experienced in that part of the North Delta, which are known to be
24   predominantly out of the south during the spring and summer[2].

25   The calendar year 2006 was chosen as a representative period for the wind resuspension analysis,
26   although it is noted that climate change effects are assumed to have occurred during the LLT time
27   period, they are not considered here for wind direction or speed. 2006 was the most recent year
28   without any significant periods of time where one or more of the wind station sensors recorded bad
29   data or was missing data. Wind speed and direction are shown for each of the five CIMIS stations in
30   Figure 5C.D–27 through Figure 5C.D–31. The late spring and summer seasonal wind pattern is
31   clearly visible in the consistent wind direction data during this period at each location. For this
32   reason, the potential for wind-wave sediment resuspension was analyzed during two periods: the
33   spring-summer period and the fall-winter period. The two periods were delimited by examining the
34   standard deviation of the observed wind direction, which is substantially lower in the spring-
35   summer period (Figure 5C.D–32). Using this method, the dates used for analysis were: 18 Apr 2006–
36   15 Sep 2006 (spring-summer period); 1 Jan 2006–17 Apr 2006 and 16 Sep 2006–31 Dec 2006 (fall-
37   winter period). Average spring-summer wind speed is higher than average fall-winter wind speed in

---

[2] Based on unpublished wind data collected 2003–2005 at the Cosumnes River Preserve by the UC Davis Cosumnes
Research Group (http://watershed.ucdavis.edu/doc/cosumnes-research-group/project-overview).

1 the Cache Slough, West Delta, and Suisun Marsh ROAs. There is some small difference between
2 seasons in the Cosumnes/Mokelumne and South Delta ROAs (Figure 5C.D–33). The average
3 direction of the relatively constant spring-summer wind direction pattern is shown graphically in
4 Figure 5C.D–34. The fall-winter period does not experience the same consistency in wind direction.

5 The potential for wind resuspension was calculated using the relationships for estimating bed shear
6 stress from wind speed, fetch, and water depth given in the U.S. Army Corps of Engineers *Shore*
7 *Protection Manual* (Coastal Engineering Research Center 1984) and Fagherazzi et al. (2007).

8 To apply these equations, the CIMIS station wind speed, recorded in m/s at a height 2 meters above
9 ground level (U_{2m}) is first converted to wind speed at 10 meters above ground level (U_{10m}).

10
$$U_{10m} = U_{2m} \left(\frac{10\ m}{2\ m} \right)^{\frac{1}{7}}$$

11 The wind stress factor, U_A, can then be calculated

12
$$U_A = 0.71\ U_{10m}^{1.23}$$

13 and used to calculate the wave height, *h*, and period, *T*:

14
15
$$h = 0.283\ \frac{U_A^2}{g}\ \tanh\left(0.530 \left(\frac{gd}{U_A^2} \right)^{\frac{3}{4}} \right) \tanh\left(\frac{0.0056 \left(\frac{gf}{U_A^2} \right)^{\frac{1}{2}}}{\tanh\left(0.530 \left(\frac{gd}{U_A^2} \right)^{\frac{3}{4}} \right)} \right)$$

$$T = 7.54\ \frac{U_A^2}{g}\ \tanh\left(0.833 \left(\frac{gd}{U_A^2} \right)^{\frac{3}{8}} \right) \tanh\left(\frac{0.0379 \left(\frac{gf}{U_A^2} \right)^{\frac{1}{3}}}{\tanh\left(0.833 \left(\frac{gd}{U_A^2} \right)^{\frac{3}{8}} \right)} \right)$$

16
17 where *g* is gravitational acceleration (m/s²), *d* is the water depth (m), and *f* is the fetch length
18 (m). Values for wave height and period are then used to estimate wind wave lengths, λ, bottom
19 orbital velocities, u_b, and, ultimately, the bottom shear stresses, τ_b.

20
$$\lambda = \frac{2\pi d}{\left\{ C \left[C + \frac{1}{(1 + C\{0.6522 + C[0.4622 + C^2\ (0.0864 + 0.0675\ C)]\})} \right] \right\}^{\frac{1}{2}}}$$

21
22
$$C = 4\pi^2 \frac{d}{g\ T^2}$$

23

$$u_b = \frac{\pi\, h}{T\, \sinh\left(2\,\pi\, \frac{d}{\lambda}\right)}$$

1

2

$$\tau_b = \left(\frac{0.05\,\rho}{2}\right) u_b^2$$

3

4

5        $\rho = 1000$ kg/m^3 is the density of water.

6   These equations have previously been applied to produce successful estimates in the San Francisco
7   Estuary (e.g., Ganju and Schoellhamer 2007). Although they neglect effects of wave shoaling,
8   refraction, whitecapping, and other processes that are represented by more sophisticated
9   approaches, such as the Simulation WAves Nearshore (SWAN) model (SWAN team 2009), Bricker
10   (2003) compared predictions made with the two approaches in South San Francisco Bay and found
11   them to match closely at some locations. The simpler approach, however, tended to underestimate
12   amplitude and large fetch due to neglect of energy loss associated with wave breaking.

13   Wind fetch was calculated as the linear distance from a point within the ROA to the shoreline
14   location at mean tidal level, in the upwind direction of the wind. Wind speeds were adjusted from
15   their 2-meter measurement height to a height of 10 meters (needed for the empirical equations)
16   using the methods described in the U.S. Army Corps of Engineers *Shore Protection Manual* (Coastal
17   Engineering Research Center 1984). Water depths for points within each ROA were calculated from
18   the ROA bathymetry and RMA2 model results for ESO_LLT conditions obtained for calendar year
19   2003. This year did not correspond to the year used for wind data because predicted water depths
20   were not available during 2006. Most of the variability in water level is due to tidal forcing, so using
21   water level predictions from a different year than wind forcing is not expected to be a major source
22   of uncertainty in this analysis.

23   Sediment resuspended by wind waves typically settles out slowly over a period of hours to days
24   (see, for example, the attenuation of peak turbidities associated with ebb tide velocities in Figure
25   5C.D–23) Therefore the frequency of days with resuspension events is used as a metric of expected
26   turbidity in ROAs.

27   For a grid of points within each ROA, daily maximum bed shear stresses were calculated from CIMIS
28   hourly average wind data and model-predicted hourly average water depths. The daily maximum
29   shear values were then compared to the weak critical shear stress of erosion, $\tau_{cr,weak}$, and the strong
30   critical shear stress of erosion, $\tau_{cr,strong}$. Whether a particular point in the ROA would be likely to
31   consistently resuspend sediment was determined by placing it into one of four resuspension
32   likelihood categories, based on the percent of days it exceeded either of the critical stresses during
33   each seasonal period. Therefore the categories take into account both the certainty and the expected
34   frequency of resuspension events over the seasonal period. For example, if a point in an ROA had a
35   daily maximum shear stress below $\tau_{cr,weak}$ for greater than 80% of days, it was placed in the "rare or
36   none" resuspension frequency category. If the daily max shear stress was above $\tau_{cr,strong}$ for greater
37   than 80% of the days, it was placed in the "frequent" category. These categories are summarized in
38   Table 5C.D-5. A weak critical shear stress of erosion value of 0.1 Pa and a strong critical shear stress
39   of erosion value of 1.0 Pa were used, following Ganju and Schoellhamer (2007).

5C.D.7.3 Results

In much of the Cache Slough ROA, turbid conditions were estimated to be common during the entire year due to wind wave resuspension. Specifically, Egbert Tract, Hastings Tract, and Cache Hass were all estimated to have frequent resuspension in substantial regions during the spring-summer period and somewhat less prevalent but still widespread common resuspension and elevated turbidity in the fall-winter period. The resuspended sediment is expected to mix through these tracts to a large extent. The wind wave-driven resuspension is likely to reduce sediment accretion rates in these regions. In contrast, in Little Egbert Tract and Prospect Island, due to greater water depth, wind wave-driven resuspension was not estimated to occur regularly.

In most of the West Delta ROA, resuspension was estimated to be common to frequent in spring-summer and common in fall-winter. In most of the ROA bordering Dutch Slough resuspension was estimated to be rare.

In most of the Suisun Marsh ROA, resuspension was estimated to be rare. This is largely due to lower wind velocities at the Suisun Valley CIMIS station relative to the CIMIS stations used for the Cache Slough ROA and the West Delta ROA. Limited fetch is also a factor in the Suisun Marsh ROA. In some shallow regions in the northern portion of the ROA bordering Duck Slough, frequent resuspension was estimated to occur. Similarly in some of the marsh bordering Nurse Slough, frequent resuspension was estimated to occur. Though the resuspension was estimated to occur in a relatively small portion of these individual regions, the sediment is likely to mix horizontally to increase turbidity over a broader area.

Through most of the Cosumnes/Mokelumne ROA, resuspension events were estimated to be rare. In the east portion of the ROA occasional resuspension was estimated to occur. The predicted frequency of resuspension was similar for the two periods because the peak daily winds are of similar magnitude for the two periods, as shown in Figure 5C.D–34. Given the limited regions of expected recurrent resuspension, this ROA can be expected to typically have low turbidity and be a strongly depositional environment.

In much of the South Delta ROA resuspension was estimated to be rare or sporadic. Resuspension events were estimated to be more likely to occur more frequently near the eastern boundary of the ROA due to shallower depths in that region. Overall this ROA is likely to be a depositional environment. The seasonal differences in likelihood of resuspension are small for this ROA, because the peak daily winds are of similar magnitude for the two periods (Figure 5C.D–33).

Large flow events in the Plan Area will bring in fresh unconsolidated sediment which will be relatively easily resuspended. Therefore even in regions where turbid conditions would not typically be expected based on the above analysis, they may be present following large flow events.

Substantial uncertainty is associated with these predictions. Perhaps the largest sources of uncertainty are the critical shear stress of erosion values. In order to span a range of values, the analysis used two values, a weak critical shear stress of erosion (0.1 Pa), which is representative of unconsolidated sediment, and a strong critical shear stress of erosion (1 Pa), which is representative of sediment that is consolidated or of larger grain size (Ganju and Schoellhamer 2007). The actual shear stress at which resuspension occurs varies spatially with sediment grain size and in time with more weak unconsolidated sediment present following flow events. The predictions are also sensitive to the assumed friction coefficient associated with wave induced bed shear stress (f_w). Because of this substantial uncertainty related to the complex spatial and temporal variability of bed

1   properties the analysis has been presented primarily in a largely qualitative manner (Table 5C.D-9),
2   although the estimated frequency of resuspension events is also presented to provide transparent
3   context for the qualitative assessment (Table 5C.D-10).

4   **Table 5C.D-4. Locations of CIMIS Station Wind Data Records Used in the Wind Resuspension Analysis,**
5   **for Each ROA**

ROA	CIMIS Station (Station Number)	Data Period of Record
Cache Slough	Hastings Tract (122)	Mar 1995–Jun 2009
Cosumnes/Mokelumne	Bryte (155)	Dec 1998–active
South Delta	Manteca (70)	Nov 1997–active
Suisun Marsh	Suisun Valley (123)	Aug 1994–active
West Delta	Twitchell Island (140)	Oct 1997–active

6

7   **Table 5C.D-5. ROA Resuspension Frequency Categories**

Criteria	Resuspension Frequency Category
$\tau_{daily\,max} < \tau_{cr,weak}$ for > 80% of days	Rare or none
$\tau_{daily\,max} > \tau_{cr,weak}$ for > 20% of days	Sporadic
$\tau_{daily\,max} > \tau_{cr,strong}$ for > 20% of days	Common
$\tau_{daily\,max} > \tau_{cr,strong}$ for > 80% of days	Frequent

8

9   **Table 5C.D-6. Estimated Wind Wave Driven Resuspension in ROAs**

	ROA				
Process/Indicator	Cache Slough	Cosumnes/ Mokelumne	South Delta	Suisun Marsh	West Delta
Wind Speed	High	Moderate	Moderate	Moderate	High
Depth	Shallow to deep	Shallow	Mostly shallow	Moderate	Mostly shallow
Typical Resuspension Frequency	Sporadic to Common	Rare to Sporadic	Rare to Common	Rare to Sporadic	Rare to Common

10

1   **Table 5C.D-7. Summary of Percent of ROA Area in Each Resuspension Frequency Category**

ROA	Season	Resuspension Frequency Category (% of ROA Area)			
		Rare or None	Sporadic	Common	Frequent
Cache Slough	Summer	29.7	22.4	21.1	26.8
	Winter	26.4	19.7	53.3	0.6
Cosumnes/ Mokelumne	Summer	77.2	15.3	7.5	0.0
	Winter	65.8	20.2	14.0	0.0
South Delta	Summer	35.5	36.2	28.3	0.0
	Winter	8.9	51.8	39.3	0.0
Suisun Marsh	Summer	75.9	12.1	8.0	4.0
	Winter	80.5	10.7	8.8	0.0
West Delta	Summer	39.7	15.4	40.9	4.0
	Winter	26.8	21.4	51.8	0.0

2
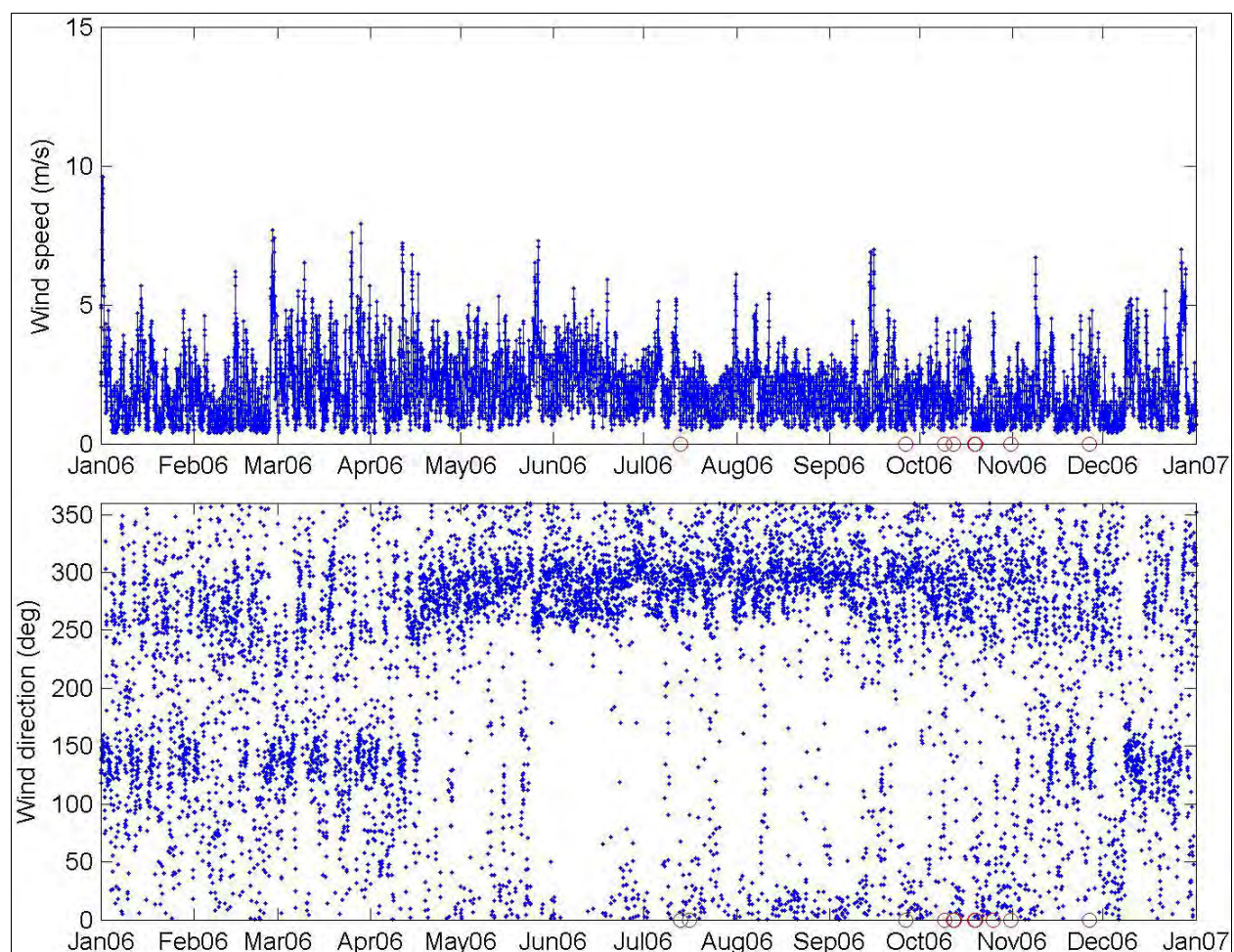
4   Missing or QC flagged data points are plotted as red circles on the x-axis.

5   **Figure 5C.D–27. Hourly Wind Speed and Direction Record for Manteca CIMIS Station (70) for 2006**
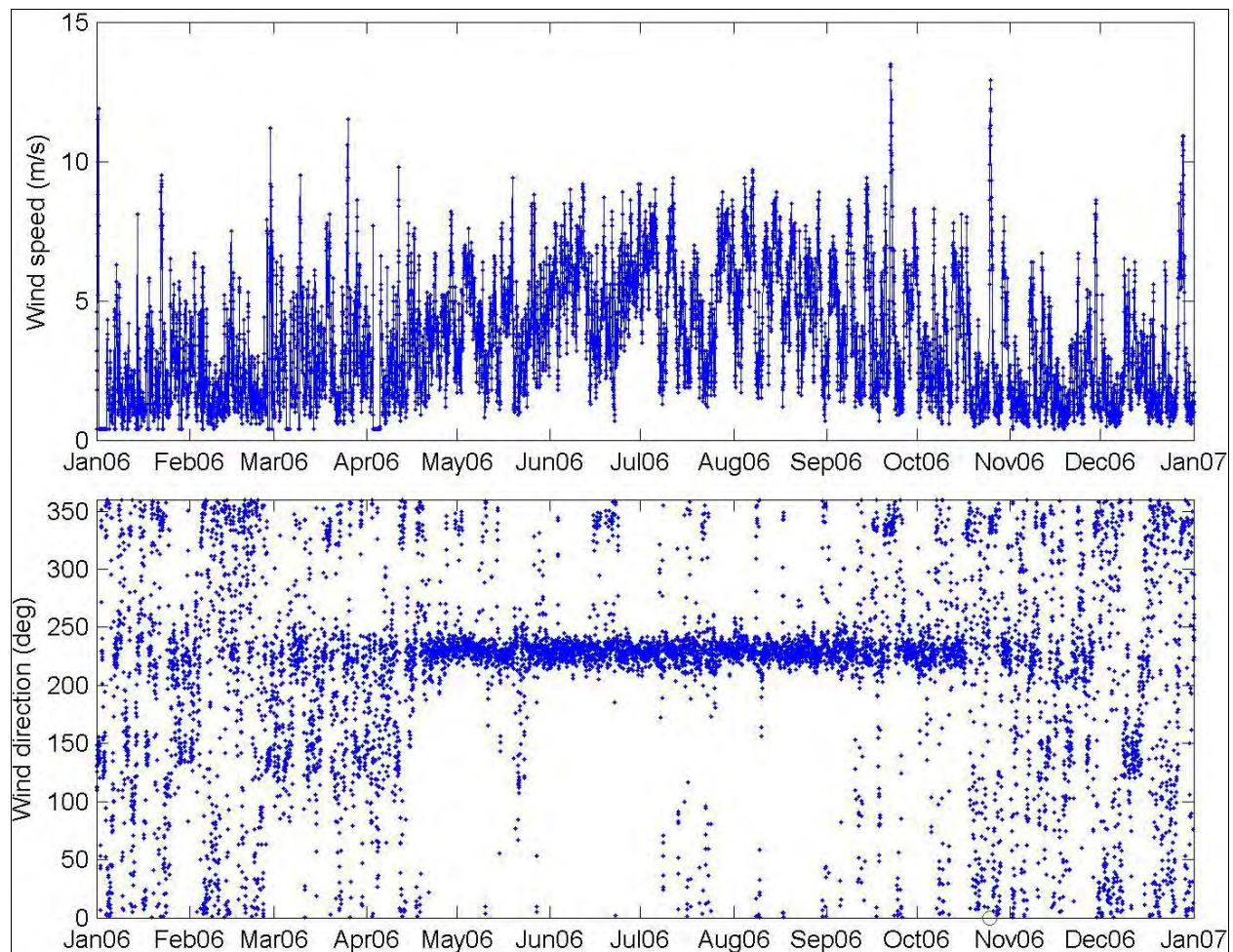
Missing or QC flagged data points are plotted as red circles on the x-axis.

Figure 5C.D–28. Hourly Wind Speed and Direction Record for Hastings Tract CIMIS Station (122) for 2006
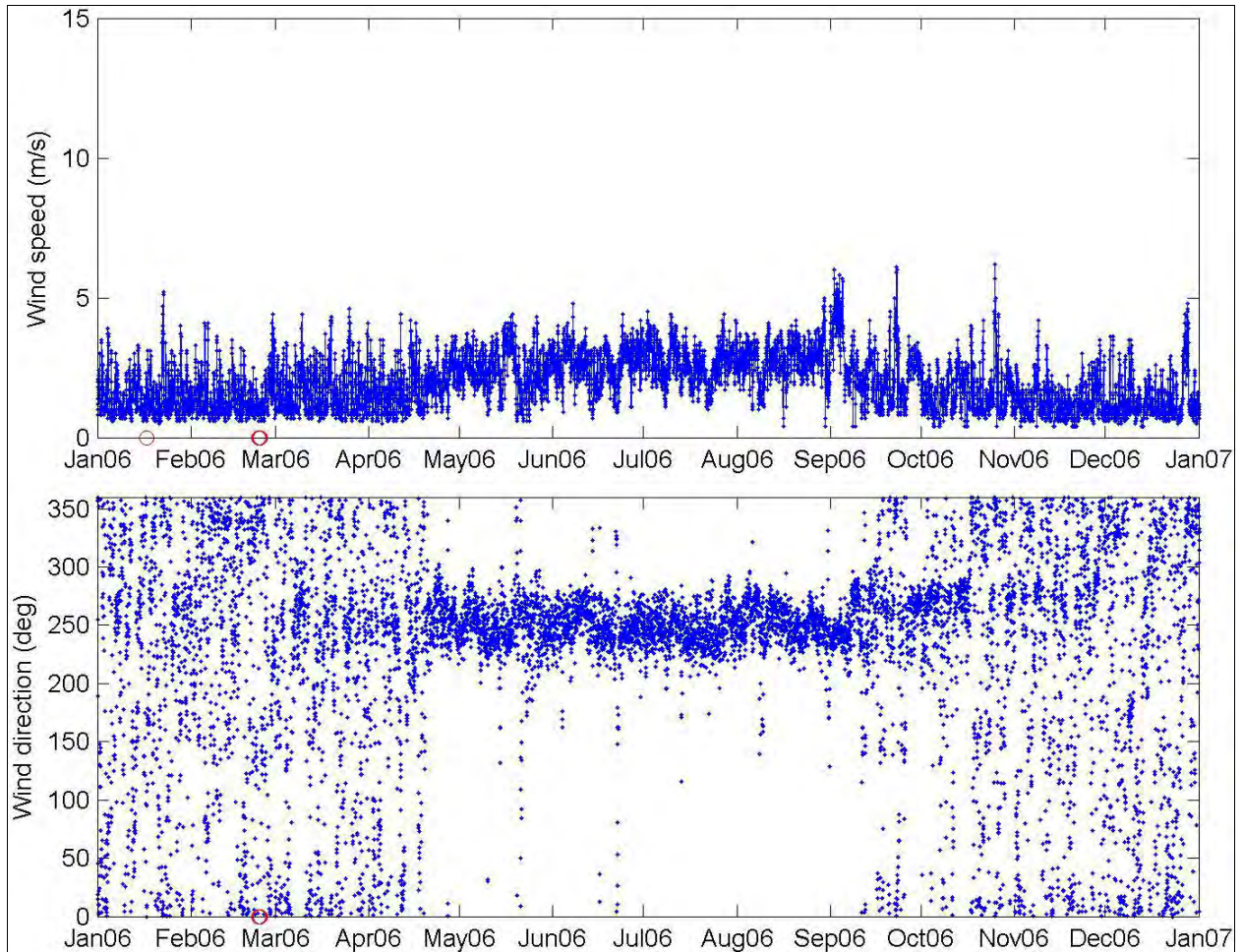
Missing or QC flagged data points are plotted as red circles on the x-axis.

Figure 5C.D–29. Hourly Wind Speed and Direction Record for Suisun Valley CIMIS Station (123) for 2006
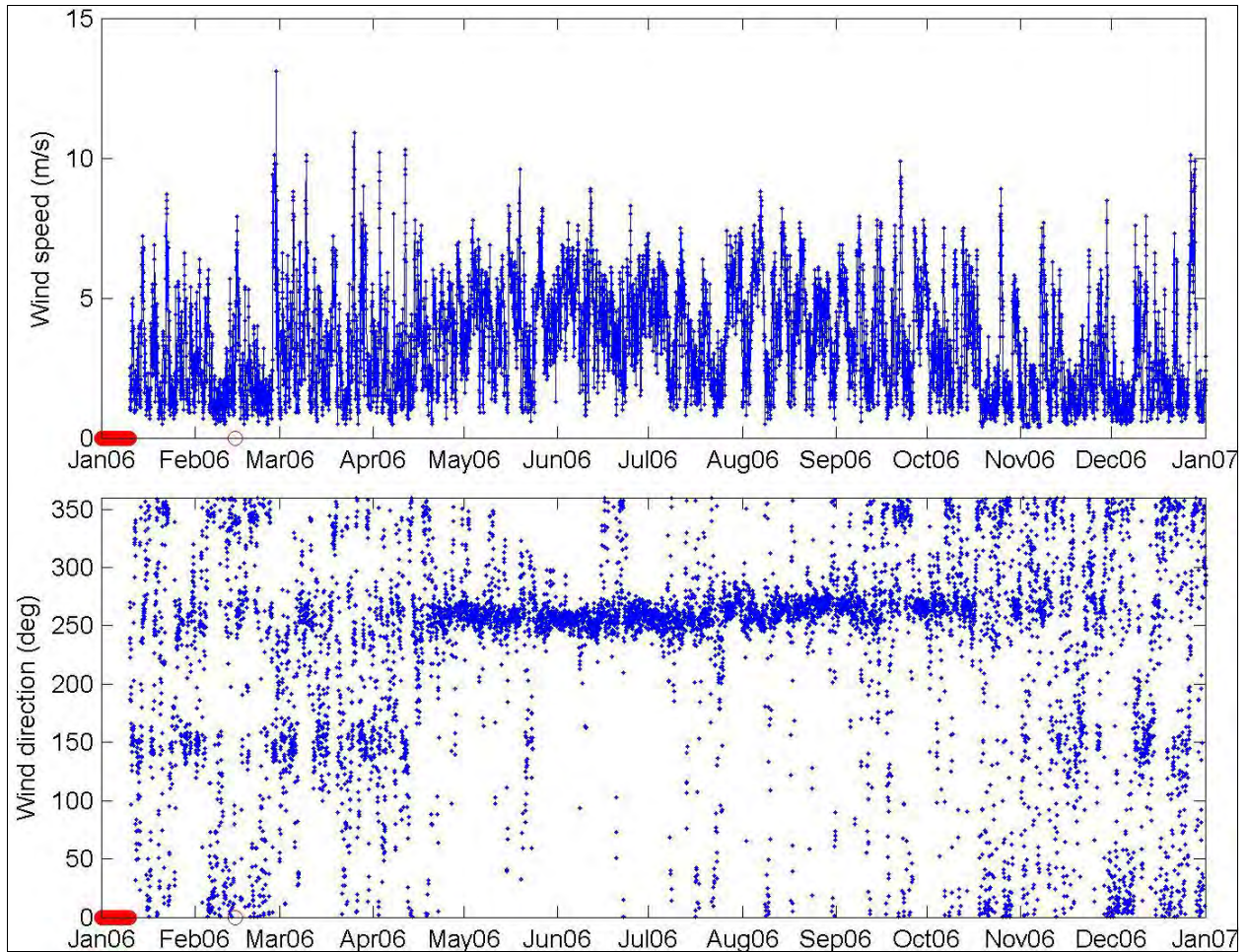
Missing or QC flagged data points are plotted as red circles on the x-axis.

Figure 5C.D–30. Hourly Wind Speed and Direction Record for Twitchell Island CIMIS Station (140) for 2006
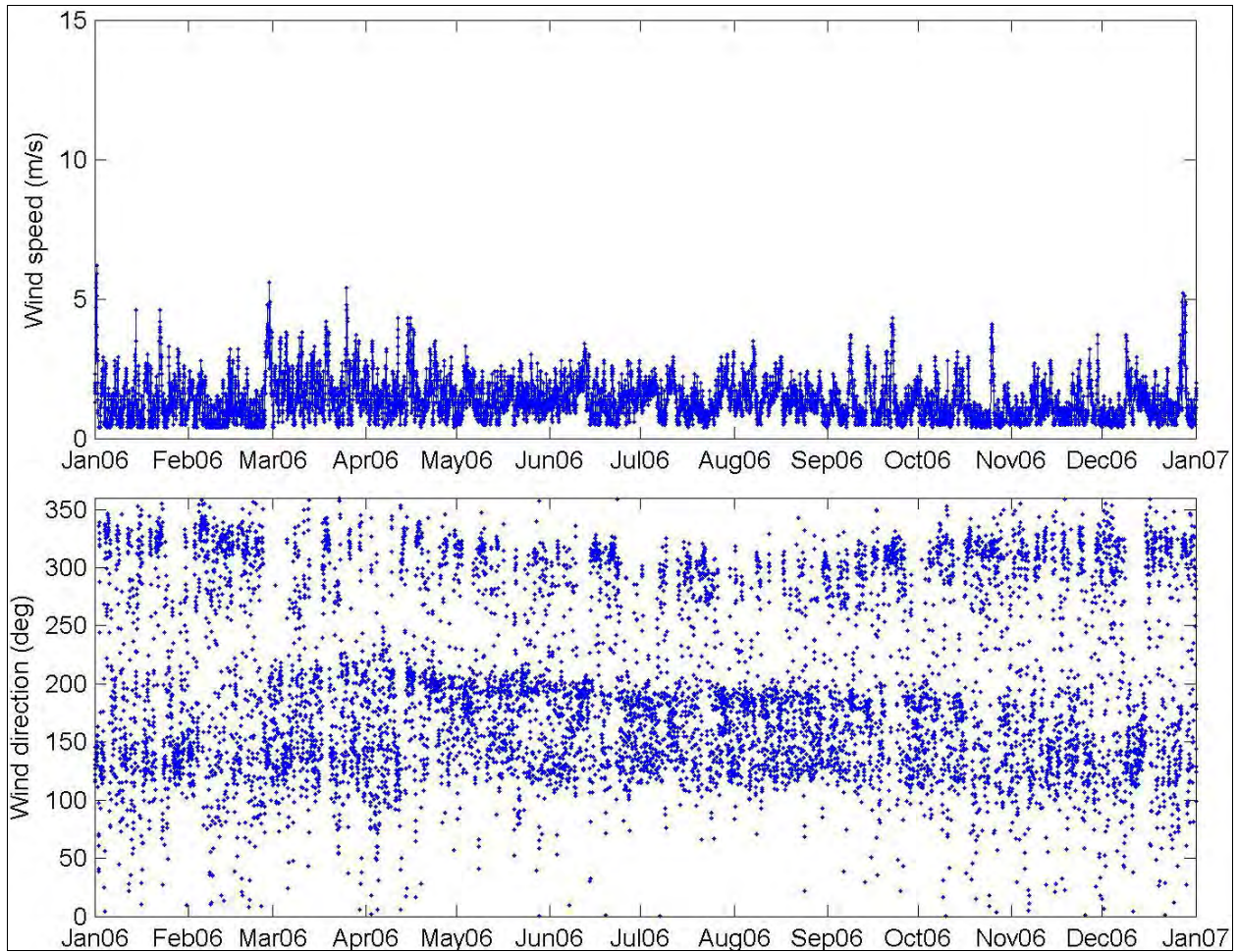
Missing or QC flagged data points are plotted as red circles on the x-axis.

Figure 5C.D–31. Hourly Wind Speed and Direction Record for Bryte CIMIS Station (155) for 2006
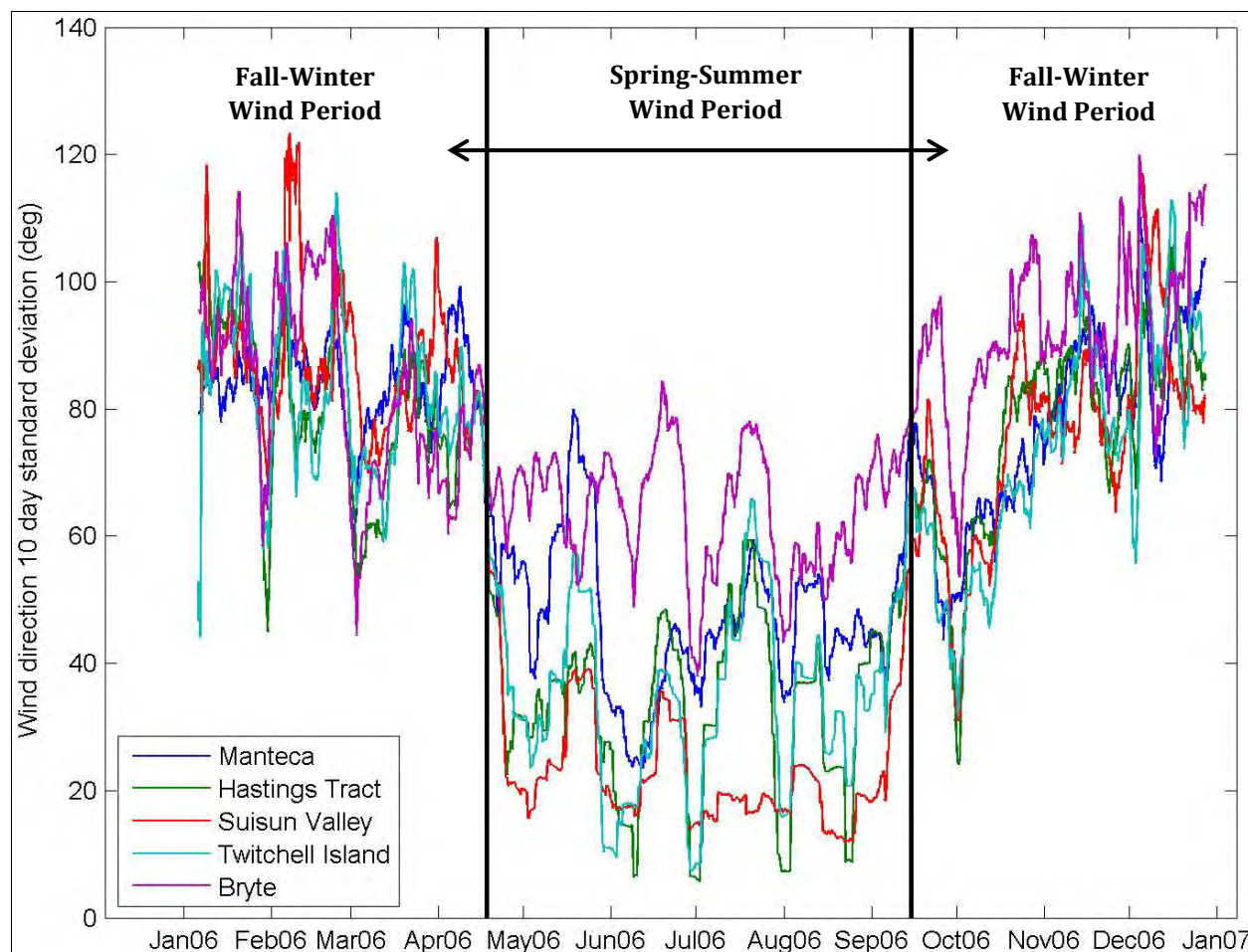
The separation of fall-winter and spring-summer periods in the resuspension analysis is based on seasonal differences in the consistency of the wind directions in the Plan Area.

Figure 5C.D–32. Ten Day Running Standard Deviation of the Wind Directions Shown for Selected Plan Area CIMIS Stations in 2006
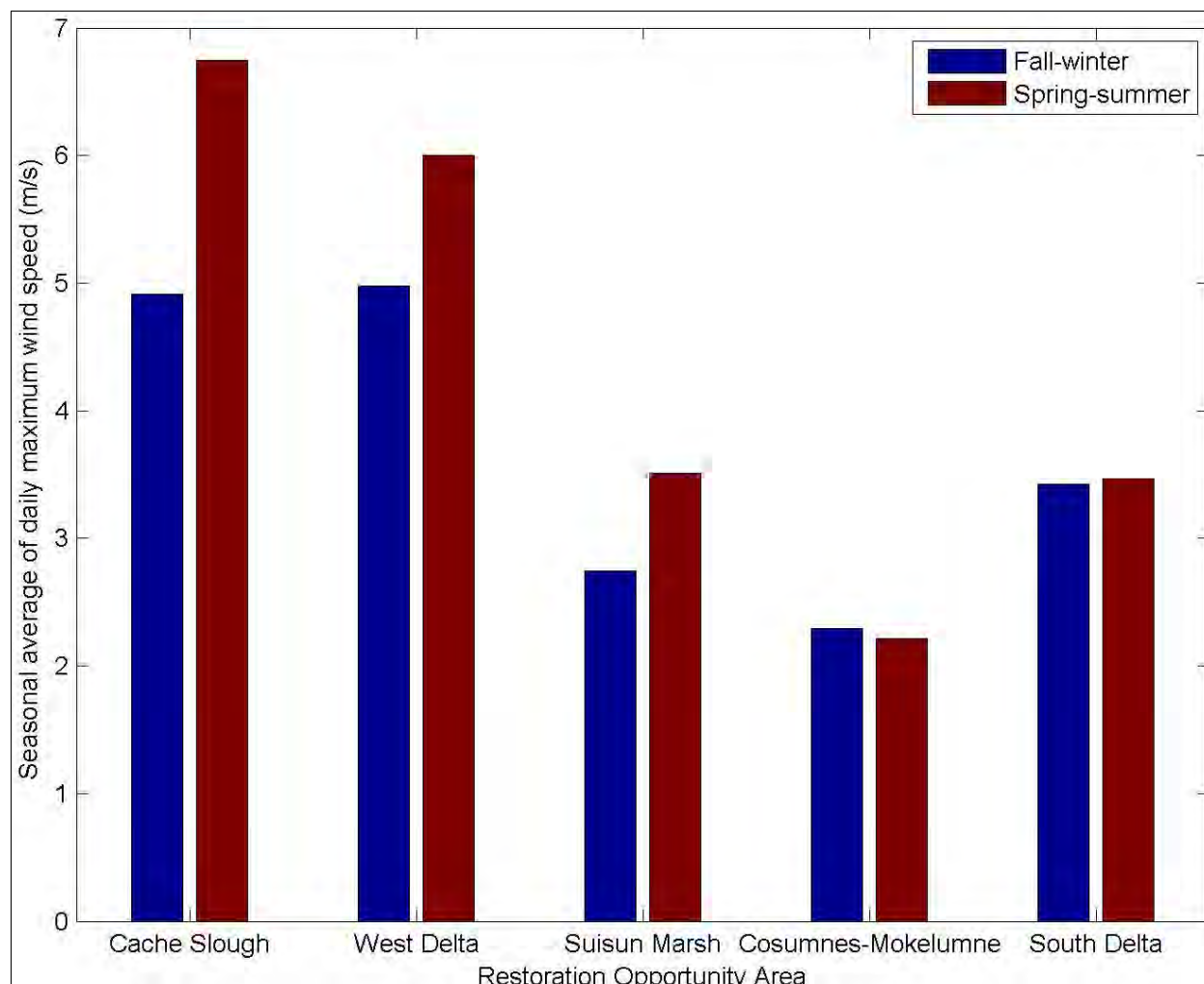
Figure 5C.D–33. Seasonal Averages of Maximum Daily Wind Speed at Each ROA, Based on 2006 Data
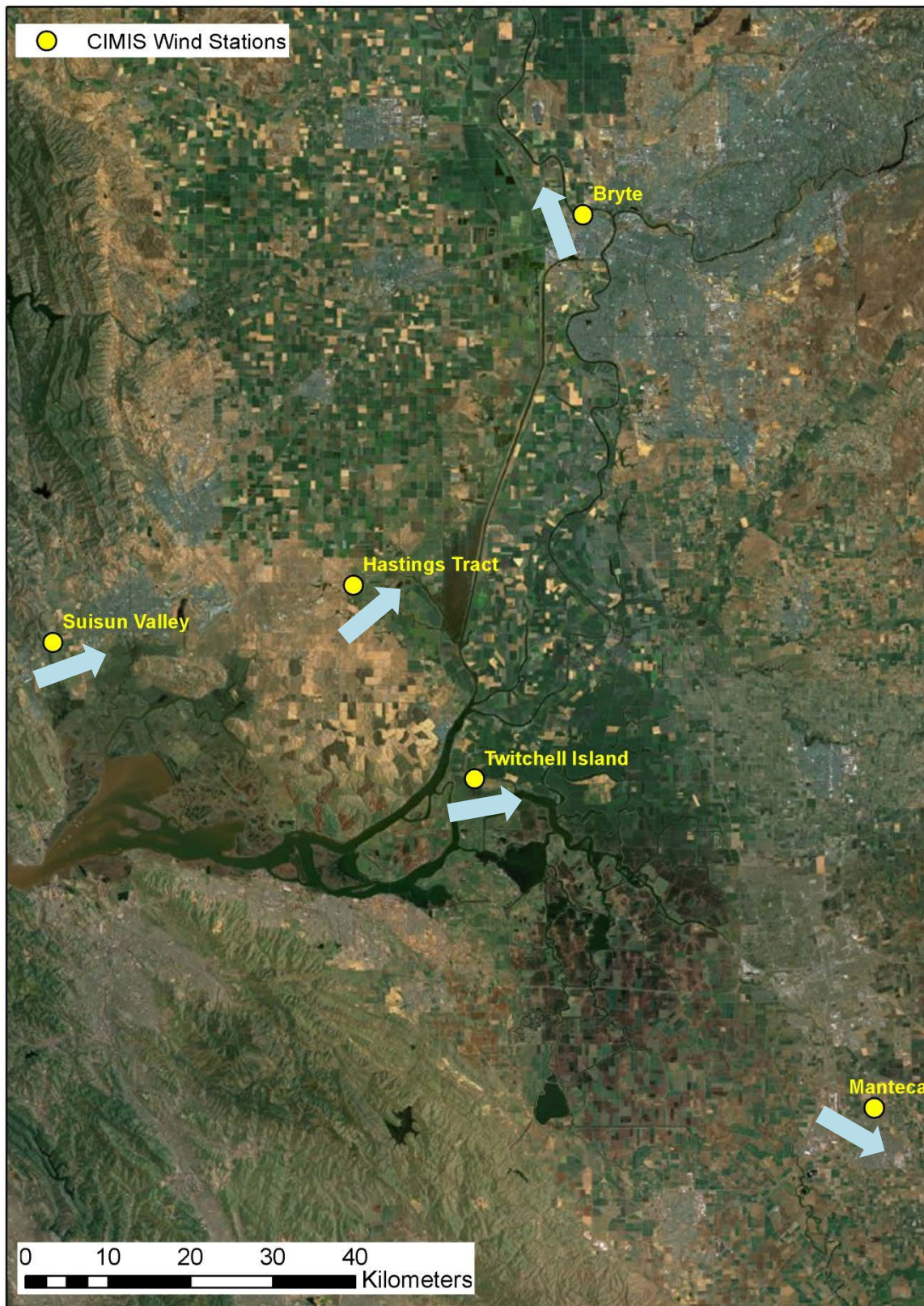
Figure 5C.D–34. Average 2006 Spring-Summer Seasonal Wind Directions for Selected CIMIS Stations in the Plan Area

5C.D.8 Combined Analysis of Factors Affecting Sediment Supply and Water Clarity in the Plan Area Subregions in the Late Long-Term Timeframe

Geomorphic changes resulting from patterns of erosion and deposition at the decadal time scale will ultimately determine the overall changes to water clarity in the Plan Area in each of the regions. In what follows, we assume that all local changes due to the breaching of levees as part of BDCP habitat restoration have stabilized (i.e., have come into partial equilibrium) and that full tidal exchange is available at each restoration site.

The assumption in what follows is that the depositional and erosional changes under consideration are due in large part to the availability of upstream sediment supply, and that the Plan Area, or at least portions of the Plan Area, remains depositional although the mass of sediment supply is unknown. Because the sediment supply is unknown (Wright and Schoellhamer 2004), the timeframe for any restoration area to reach a state of equilibrium or dynamic equilibrium (in a decadal sense) is also unknown.

Schoellhamer et al. (2007) proposed that the location of the restoration site in relation to sediment supply and other areas such as existing marsh or wetlands that are currently depositional should be considered. Because each of these areas is a sink for sediment, if the restoration site is upstream of the existing depositional area, it will receive sediment supplies formerly deposited in the existing site and the potential exists for the existing site to become erosional as sediment supply diminishes there.

This presents a complex picture for predicting changes to water clarity due to the large scale changes in ROAs proposed for the Plan Area in the LLT timeframe. In the section below, we hypothesize on changes that are likely to occur in each of the subregions given the conceptual models proposed in Schoellhamer et al. (2007) as well as the specific references identified in each section.

Brief summaries of tidal current, net flow, stratification, wind resuspension and SAV effects are also included. Zones with SAV are likely to be depositional for nearly all wind conditions. Where SAV is not present, resuspension of sediment caused by wind waves can increase turbidity in ROAs and slow net accretion of sediment.

The Cache Slough and Yolo Bypass Subregions are combined for this discussion.

5C.D.8.1 North Delta Subregion

Potential changes to turbidity in this region include episodic change due to seasonal shifts in outflow timing and volume due to climate change (such as earlier snowmelt). Changes to sediment supply in the Sacramento River are uncertain, as mentioned previously. There are no ROAs in this subregion. Sediment accretion may increase with sea level rise because the present channel geometry may be roughly in equilibrium with present flow rates (Simenstad et al. 2000). Under the ESO_LLT scenario, flows would be lower than under the EBC2_LLT scenario due to the proposed north Delta exports just downstream of Freeport while cross-sectional area will increase due to sea level rise.

1   Increased exports in the ESO_LLT scenario (see Section 5C.D.3, *Factors Affecting Sediment Supply*
2   *Because of BDCP Implementation of Dual Conveyance*, above) imply that the reduction of available
3   sediment load will result in decreased deposition of sediment in downstream ROAs.

5C.D.8.2   Cache Slough and Yolo Bypass Subregions

5   Because strong deposition is currently observed in the Yolo Bypass (Singer et al. 2008), these areas
6   will likely be depositional in the ESO_LLT scenario as increases in Yolo Bypass flows increase the
7   available sediment both in the Cache Slough and in the Yolo Bypass subregions. Some portions of the
8   Cache Slough ROA are near Mean Sea Level so are likely to rapidly become vegetated and trap and
9   accrete sediment effectively (Simenstad et al. 2000). As discussed in Appendix 5.F, *Biological*
10   *Stressors on Covered Fish* (Section 5F.4), it is possible for *Egeria* to become established in the Cache
11   Slough ROA, although the likelihood of this occurring is unknown and *CM13 Invasive Aquatic*
12   *Vegetation Control* is intended to limit colonization of ROAs by *Egeria* and other invasive aquatic
13   vegetation. Areas where wind resuspension may decrease water clarity in both the spring-summer
14   and fall-winter seasons are generally not potential *Egeria* habitat. There is likely to be a seasonal
15   decrease in water clarity in some portions of this ROA where vegetation has not become established.

16   Increased flows and sediment load passing through the Yolo Bypass may result in increased
17   turbidity and decreased water clarity in portions of the Sacramento River Deepwater Ship Channel.
18   It is possible that deposition in the Cache ROA will decrease deposition in downstream areas along
19   the Sacramento River and Suisun Bay, and thus slow the development of additional tidal marsh in
20   the Suisun Marsh, Suisun Bay and West Delta Subregions (McKee et al. 2006).

5C.D.8.3   West Delta Subregion

22   Less suspended sediment would be expected to traverse the West Delta subregion with the
23   deposition occurring in the upstream ROAs and the removal of sediment at the north Delta export
24   location. Some regions within the West Delta ROA along the Sacramento River and Threemile Slough
25   may be shallow enough for rapid establishment of a vegetated marsh plain which could lead to rapid
26   accretion of sediment and decreases in turbidity. Appendix 5.F, *Biological Stressors on Covered Fish*
27   (Section 5F.4) shows that potential *Egeria* habitat is widespread in this ROA. Areas where wind
28   resuspension may decrease water clarity in both the spring-summer and fall-winter seasons
29   generally coincide with the potential *Egeria* habitat. Wind resuspension would not be a factor if
30   *Egeria* became established. As described in Appendix 5.F, *CM13 Invasive Aquatic Vegetation Control*
31   is intended to limit colonization of ROAs by *Egeria* and other invasive aquatic vegetation. As also
32   noted in Appendix 5.F, the West Delta Subregion had several existing channels with a greater
33   number of modeled years below the *Egeria* establishment velocity threshold of 1.61 feet/second
34   under the ESO_LLT scenario compared to the EBC2_LLT scenario. It will be necessary to monitor
35   *Egeria* status and trends in these and other locations in order to assess the need for implementation
36   of *CM13 Invasive Aquatic Vegetation Control* outside the ROAs. Establishment of *Egeria*, were it to
37   occur, could reduce further sediment supply in comparison with the EBC2_LLT scenario.

38   Other factors trend toward decreasing water clarity on the Sacramento River downstream of Rio
39   Vista in the West Delta Subregion. Tidal flow on the lower Sacramento River (near Emmaton) was
40   modeled to be affected by the decrease in tidal range as a result of the Suisun Marsh restoration and
41   by the increase in tidal prism with the restoration upstream in Cache Slough. The result overall is a
42   small estimated increase in tidal flow of 2% for the ESO_LLT versus the EBC2_LLT with the RMA
43   model, while the DSM2 model indicated an 8% increase. Absent of other factors, higher tidal current

1 velocities would serve to slightly increase suspended sediment. Summer net outflow (Figure 5C.D–
2 26) was modeled to decrease and therefore EC would increase (Figure 5C.D–25) with an ESO_LLT
3 scenario, potentially increasing the exchange with higher turbidity sources downstream.

4 For the lower San Joaquin River, tidal velocities were modeled to be lower under the ESO_LLT
5 scenario relative to the EBC2_LLT scenario (Figure 5C.D–24), reducing the sediment resuspension
6 by tidal currents. Depending upon water-year type, late spring and early summer net outflows were
7 modeled to be slightly less (Figure 5C.D–26) and summer salinity intrusion slightly higher (Figure
8 5C.D–25) under the ESO_LLT relative to EBC2_LLT, indicating more exchange with higher turbidity
9 water from the west during the low flow period.

5C.D.8.4   Suisun Bay Subregion

11 Suisun Bay and the Suisun Marsh ROA are likely to experience reduced suspended sediment
12 concentrations and turbidity in the ESO_LLT scenario relative to the EBC2_LLT scenario due to
13 deposition in the upstream ROAs (in particular the Cache Slough and West Delta ROAs). A number of
14 other factors will complicate the predicted change in water clarity.

15 Deepening due to sea level rise makes the shallow areas of Suisun Bay more favorable to deposition
16 (Ganju and Schoellhamer 2010), although deposition is unlikely to keep pace with sea level rise.
17 Overall deposition in Suisun Bay will be dependent upon the sediment supply. This region is
18 expected to see a reduction in sediment supply due the combination of north Delta exports and
19 sediment deposition in upstream ROAs. Deposition in the Suisun Marsh ROA would further reduce
20 the sediment supply to Suisun Bay.

21 The Suisun Marsh and other ROAs increase the tidal prism and tidal currents in western Suisun Bay
22 (Figure 5C.D–24). The Suisun Marsh ROA sufficiently reduces the tidal range and therefore tidal flow
23 in eastern Suisun Bay, decreasing sediment resuspension from tidal currents and reducing the
24 expected low flow period suspended sediment concentration and increasing water clarity.

5C.D.8.5   Suisun Marsh Subregion

26 The ESO_LLT restoration increases tidal flow in Montezuma Slough, which could result in increased
27 suspension of channel sediments. Because the Suisun Marsh ROA is divided into several small
28 regions separated by channels and levees, fetch will be limited so wind wave resuspension may be
29 smaller than in larger open water regions. As discussed in Appendix 5.F, *Biological Stressors on*
30 *Covered Fish* (Section 5F.4), the potential for *Egeria* to become established is highly unlikely due to
31 the relatively high salinities in the region and the intent of *CM13 Invasive Aquatic Vegetation Control*
32 to limit colonization of ROAs by *Egeria* and other invasive aquatic vegetation.

33 This region has the potential for a reduction in sediment supply due to the combination of north
34 Delta exports and sediment deposition in upstream ROAs.

5C.D.8.6   East Delta Subregion

36 Sediment supply into the subregion from the Sacramento River occurs primarily when the DCC is
37 open. Generally the DCC is open for both the ESO_LLT and the EBC2_LLT from June into December
38 and closed January through May, with the gate opening also contingent upon the level of Sacramento
39 River flow (<25,000 cfs). Thus the DCC is typically closed during the winter and spring months when
40 the Sacramento River sediment load is highest.

1   Sediment supply from the Sacramento River into the subregion will be reduced under the ESO_LLT
2   scenario as flows through the DCC are significantly reduced due to added restoration area (Figure
3   5C.D–16). The DCC flow reductions result from a combination of decreased available Sacramento
4   River flow with the north Delta exports, decreased tidal range in the Sacramento River near
5   Georgiana Slough and the DCC and the connection of Miner Slough to the Sacramento Ship Channel
6   through the restoration of Prospect Island. Overall, DCC flow for the ESO_LLT scenario is 61% of the
7   EBC2_LLT flow.

8   The location of the ROAs downstream of the Mokelumne and Cosumnes Rivers means the potential
9   exists for deposition to occur from sediment supplied by these watersheds. However, these Rivers
10   have been estimated to be a very small percentage of the overall sediment supply in the Plan Area,
11   equivalent to only about 3.3% of the sediment discharge on the Sacramento River at Freeport
12   (Schoellhamer et al. 2007). As shown Appendix 5.F (Section 5F.4), the area of potential *Egeria*
13   habitat comprises a substantial portion of the ROA. Establishment of *Egeria* would increase the
14   likelihood of sediment deposition in this ROA, thus reducing the small percentage of sediment
15   supply available to downstream areas. As noted above and described in Appendix 5.F, *CM13 Invasive*
16   *Aquatic Vegetation Control* is intended to limit colonization of ROAs by *Egeria* and other invasive
17   aquatic vegetation. The likelihood of reduced water clarity due to wind resuspension is small in this
18   ROA.

5C.D.8.7   South Delta Subregion

20   Tidal flow in the south Delta subregion was modeled to be lower under the ESO_LLT scenario
21   compared to the EBC2_LLT scenario due to downstream restoration in Suisun Marsh, resulting in
22   decreased sediment resuspension from tidal currents. Previous modeling analyses (RMA 2010a)
23   showed that tidal flow in Middle River is reduced by downstream restoration. Tidal range is severely
24   diminished at RMID027 near the Union Island restoration area due to limited channel capacity in
25   Middle River. Sensitivity analyses (RMA 2012) show that increasing Middle River channel capacity
26   does restore some of the tidal range, although with the degree of dredging that was considered in
27   the ESO_LLT scenario, it is still less than half that of historical conditions. In contrast, sea level rise
28   increases tidal flow at all locations. There is a net decrease in tidal flow in Middle River resulting
29   from the combination of restoration and sea level rise. This is also the case in the lower San Joaquin.
30   However in the San Joaquin River above the mouth of Old River, in the Sacramento River, Suisun Bay
31   and in Montezuma Slough, there is a net increase in tidal flow resulting from the combination of
32   restoration and sea level rise (RMA 2010b).

33   Because this ROA consists of large open water areas, fetch length will be large leading to large wind
34   waves in deep regions. These waves will limit accretion rates and may periodically increase
35   turbidity locally during strong wind periods that resuspend previously deposited but
36   unconsolidated sediment. However, Appendix 5.F, *Biological Stressors on Covered Fish* (Section 5F.4),
37   shows that the area of potential *Egeria* habitat is substantial. Given the historical establishment of
38   *Egeria* in this area of the Delta, future establishment would be likely, in the absence of control
39   proposed under *CM13 Invasive Aquatic Vegetation Control*. Colonization by *Egeria* would diminish
40   the potential for wind wave resuspension and increase water clarity.

41   Less water is being diverted from San Joaquin River flows in the ESO_LLT alternatives as exports in
42   the south Delta diminish. The small amount of sediment supply not being exported is now available
43   for deposition in the south and central Delta. Although the future rate of sediment deposition from
44   either the Sacramento or San Joaquin Rivers is unclear, it is likely that depositional or erosional
45   changes would be small due to the changed export conditions.

5C.D.9   Summary of Potential BDCP Effects on Water Clarity

Table 5C.D-8 summarizes the effects on water clarity in the Plan Area under the ESO_LLT scenario due to the establishment of the ROAs to assess whether each subregion may become a depositional or an erosional environment. Table 5C.D-9 summarizes the specific effect of wind resuspension on water clarity within the ROAs, assuming control of *Egeria* proposed under *CM13 Invasive Aquatic Vegetation Control*. Table 5C.D-10 summarizes the specific effect of changes in net flow and tidal effects, including changes in salinity, on water clarity in each subregion under the ESO_LLT scenario.

Uncertainty in sediment supply in the future is high, and factors such as the timing of establishment of restoration within the ROAs and the potential use of options such as fill-in materials or wind breaks in the ROAs to reduce wind-driven resuspension preclude all but the most general analysis. The roles of benthic filter feeders, organic materials and other factors have not been considered. In addition, it should be noted that the critical shear stress of erosion has been observed to vary substantially with changes in benthic algae and macrofauna (Ysebaert et al. 2005), so their effects on water clarity could be substantial.

The Plan Area will remain regionally depositional in the LLT timeframe, in both the EBC2 and the ESO scenarios, although the location of the depositional regions will differ. The effects of sea level rise will depend on the balance between sediment supply from the watersheds and the rate of sea level rise, so it is unclear whether sediment supply will be sufficient to maintain the current extent of tidal marsh. The proposed North Delta exports in the ESO_LLT scenario will result in a reduction of sediment supply to downstream areas in comparison with the EBC2_LLT scenario. The initial effect of the ROAs in ESO_LLT is to decrease sediment supply downstream, but the longer term effects are uncertain as the ROAs reach a dynamic equilibrium after the Plan Area projects have been completed.

One possible scenario is that the deeper ROAs will eventually accrete enough sediment to evolve to depths where wind suspension may occur. However, this depends on sediment supply, the future trend of which is uncertain, and the magnitude of sea level rise. These forcing variables may also create conditions where sediment accretion is occurs in some, but not all of the deeper ROAs. An assumption of a static bed elevation was used in the wind wave analysis.

Under the ESO, the north Delta subregion will receive less sediment due to increased flows through the Yolo Bypass, but this may not be a large enough factor to differentiate these effects from the overall effects due to sea level rise and climate change alone in the EBC2_LLT scenario, leaving an uncertain overall effect. The Cache/Yolo subregions will become depositional with sediment that would otherwise be carried down the Sacramento River. While the ROAs have the potential to increase water clarity in existing open water areas such as Liberty Island at least initially, wind resuspension of unconsolidated sediment during the summer is likely to decrease water clarity in the region seasonally. These factors combine to produce a mixed overall effect on the Cache and Yolo subregions. The west Delta ROA will accrete sediment, which in combination with decreased supply due to sediment deposition in the Cache/Yolo region and reduction in sediment supply due to north Delta exports will result in a local increase in water clarity. The east Delta subregion is likely to experience increased water clarity due to decreased flow through Georgiana Slough (Figure 5C.D–15). The south Delta ROA consists of large open water areas that, barring establishment of SAV such as *Egeria,* will likely experience decreased water clarity due to wind resuspension in the summer.

1   The effect of the Suisun Marsh ROA, both locally and in combination with the effects resulting from
2   upstream ROAs, is complicated. Suisun Bay is currently erosional and the opening of ROAs upstream
3   is likely to increase this erosion (Schoellhamer et al. 2007) because of reduced sediment supply. As
4   mentioned in previous sections, if Suisun Bay continues to deepen and intertidal regions are lost,
5   wind waves will become less effective at suspending sediment, so erosion rates may slow. Parts of
6   the Suisun Marsh ROA located adjacent to Suisun Bay may exert a local decrease in water clarity
7   from seasonal resuspension due to wind. However, predicting the balance between the depositional
8   environment in the ROAs and increased regional erosion is very complicated, so the overall result
9   for water clarity is uncertain. The restored areas in the Suisun Marsh ROA will likely be depositional
10   due to local sediment supply, resulting in local increases in water clarity. The effects of wind
11   resuspension on decreasing water clarity will likely be limited to the larger ROAs in this region,
12   depending on wind direction.

13   Overall, it is probable that the future conversion of so much currently hydraulically-isolated land to
14   subtidal and marsh areas will remove sediment from upstream sources before it enters the western
15   Delta and Suisun areas. The cumulative effect of the ROAs will therefore be to decrease sediment
16   supply to seaward regions and increase water clarity in these regions. However, this effect does not
17   necessarily preclude decreases in local water clarity as a result of the ROAs. The creation of large
18   shallow open water areas makes it likely that turbidity inside and near several of the ROAs will
19   increase seasonally due to wind wave sediment resuspension. Suitable habitat exists for SAV such as
20   *Egeria,* which has the potential to dampen local turbidity increases, although *CM13 Invasive Aquatic*
21   *Vegetation Control* is intended to limit SAV colonization within the ROAs. As the water clarity
22   analyses presented above highlighted, many of the future changes to the Plan Area have
23   interdependent and complicated effects on sediment transport and water clarity. A dynamic, full
24   suspended sediment model of the Plan Area would be required to take into account the many
25   interacting factors that may influence water clarity and to reduce uncertainty regarding the
26   potential effects of BDCP on water clarity.

27   **Table 5C.D-8. Potential Regional Effects on Water Clarity in the ESO_LLT Scenario in Comparison to**
28   **the EBC2_LLT Scenario**

Subregion	Depositional or Erosional Change As a result of ROAs	Effect of D/E on Water Clarity in Subregion
North Delta	U	U
Cache/Yolo	D	M
West Delta	D	I
Suisun Bay	M	M
Suisun Marsh	D	I
East Delta	D	I
South Delta	D	I
Regional water clarity is influenced by the "D" Depositional or "E" Erosional characteristics within the region. Some regions are "M" mixed (some deposition and some erosion), "U" uncertainty is too high to estimate the characteristics; "I" increase in water clarity.		

29

1   **Table 5C.D-9. Potential Effect of Seasonal Winds on Water Clarity in the ROAs (Assuming Control**
2   **of SAV within the ROAs under *CM13 Invasive Aquatic Vegetation Control*) in the ESO_LLT Scenario**

ROA	Seasonal Wind Resuspension in the ROAs
Cache Slough	D
West Delta	D
Suisun Marsh	ME
Mok-Cosumnes	ME
South Delta	D
Seasonal winds influence water clarity depending on fetch, wind strength and water depth. Symbols are: "D" Decrease, "ME" Minor effect.	

3

4   **Table 5C.D-10. Estimated Regional Changes in Low Flow Season Water Clarity in Response to Tidal**
5   **Currents and Net Flow, and the Associated Change in Salinity Intrusion in the ESO_LLT Scenario in**
6   **Comparison to the EBC2_LLT Scenario**

Subregion	Low Flow Season Flow and Tidal Effects on Water Clarity
North Delta	ME
Cache/Yolo	D
West Delta	D
Suisun Bay	ME
Suisun Marsh	D
East Delta	ME
South Delta	ME
Symbols are: "ME" Minor effect, "D" Decrease in water clarity.	

7

5C.D.10 References Cited

5C.D.10.1 Literature Cited

Bricker, J.D. 2003. *Bed Drag Coefficient Variability under Wind Waves in a Tidal Estuary: Field Measurements and Numerical Modeling.* Ph.D. dissertation, Stanford University.

California Department of Boating and Waterways. 2001. "*Egeria densa* Control Program Final Environmental Impact Report." Available: <http://www.dbw.ca.gov/PDF/Egeria/EIR/Vol_1/Sec_1.pdf>.

Cappiela, K., C. Malzone, R. Smith, and B. Jaffe. 1999. *Sedimentation and Bathymetry Changes in Suisun Bay: 1867–1990.* USGS Open-File Report 99-563. Available: <http://geopubs.wr.usgs.gov/open-file/of99-563/>.

Cloern, J. E., N. Knowles, L. R. Brown, D. Cayan, M. D. Dettinger, T. L. Morgan, D. H. Schoellhamer, M. T. Stacey, M. van der Wegen, R. W. Wagner, and A. D. Jassby. 2011. *Projected Evolution of California's San Francisco Bay-Delta River System in a Century of Climate Change.* PLoS One 6(9).

Coastal Engineering Research Center. 1984. *Shore Protection Manual.* US Army Corps of Engineers, Waterways Experiment Station, Vicksburg, MS.

Dean, R. G., and R. A. Dalrymple. 2002. *Coastal Processes with Engineering Applications.* Cambridge University Press, Cambridge, UK.

Fagherazzi, S., C. Palermo, M. C. Rulli, L. Carniello, and A. Defina. 2007. Wind waves in shallow microtidal basins and the dynamic equilibrium of tidal flats. *Journal of Geophysical Research*, 112, F02024. [doi:10.1029/2006JF000572]

Ganju, N. K., and D. H. Schoellhamer. 2006. Annual sediment flux estimates in a tidal strait using surrogate measurements. *Estuarine Coastal and Shelf Science*, 69: 165–178.

Ganju, N. K., and D. H. Schoellhamer. 2007. Calibration of an Estuarine Sediment Transport Model to Sediment Fluxes as an Intermediate Step for Simulation of Geomorphic Evolution. *Continental Shelf Research*, 29: 148–158. doi:10.1016/j.csr.2007.09.005.

Ganju, N. K., and D. H. Schoellhamer. 2010. Decadal-timescale estuarine geomorphic change under future scenarios of climate and sediment supply. *Estuaries and coasts*, 33: 15–29.

Ganju, N. K, D. H. Schoellhamer, J. C. Waner, M. F. Barad, and S. G. Schladow. 2004. Tidal oscillation of sediment between a river and a bay: a conceptual model. *Estuarine and Coastal Shelf Science.* 60: 81–90.

Ganju, N. K., D. H. Schoellhamer, and B. A. Younis. 2006. "Development of a decadal-scale estuarine geomorphic model for Suisun Bay, California: Calibration, validation, and idealized time-stepping." Technical Completion Reports, University of California Water Resources Center, UC Berkeley. Available: <http://escholarship.org/uc/item/7cc2j5x6>.

Ganju, N. K., D. H. Schoellhamer, and B. E. Jafee. 2009. Hindcasting of decadal-timescale estuarine bathymetric change with a tidal-timescale model. *Journal of Geophysical Research*, 114, F04019. [doi:10.1029/2008JF001191]

Ganju, N. K., D. H. Schoellhamer, M. C. Murrell, J. W. Gartner, and S. A. Wright. 2007. Constancy of the relation between floc size and density in San Francisco Bay. pp. 75–91 in: J.P. Maa, L.H. Sanford, and D.H. Schoellhamer (Eds.), *Estuarine and Coastal Fine Sediment Dynamics*: *INTERCOH 2003*. Elsevier, Amsterdam, The Netherlands.

Hestir, E. L. 2010. *Trends in Estuarine Water Quality and Submerged Aquatic Vegetation Invasion*. Ph.D. dissertation. University of California, Berkeley.

Jones, N. L. and S. G. Monismith. 2008. Modeling the influence of wave enhanced turbulence in a shallow tide- and wind-driven water column. *Journal of Geophysical Research*, 113, C03009. [doi: 10.1029/2007JC004246]

Kimmerer, W. J. 2004. Open water processes on the San Francisco estuary: From physical forcing to biological responses. *San Francisco Estuary and Watershed Science*, 2(1): 1–142.

Kimmerer, W. J., Burau, J. R., and W. A. Bennet. 2002. Persistence of tidally-oriented vertical migration by zooplankton in a temperate estuary. *Estuaries*, 25(3): 359–371.

Kimmerer, W. J., A. E. Parker, U. E. Lidström, and E. J. Carpenter. 2012. Short-term and interannual variability in primary production in the low-salinity zone of the San Francisco Estuary. *Estuaries and Coasts*, 35(4): 913–929.

Madsen, O. S., and P. N. Wikramanayake. 1991. *Simple models for turbulent wave-current bottom boundary layer flow*. Contract Rep. DRP-91-1, U.S. Army Corps of Engineer Waterways Experiment Station, Vicksburg, MS, 150 pp.

McKee, L. J., N. K. Ganju, and D. H. Schoellhamer. 2006. Estimates of suspended sediment entering San Francisco Bay from the Sacramento and San Joaquin Delta, San Francisco Bay, California. *Journal of Hydrology*, 323: 335–352.

Nobriga, M. L., T. R. Sommer, F. Feyrer, and K. Fleming. 2008. Long-Term Trends in Summertime Habitat Suitability for Delta Smelt (*Hypomesus transpacificus*). San Francisco Estuary and Watershed Science 6(1).

Oltmann, R. N., and M. R. Simpson. 1997. "Measurement of tidal flows in the Sacramento-San Joaquin Delta, California." Poster. USGS San Francisco Bay and Delta Ecosystem Forum. U.S. Geological Survey, Sacramento, California, March 1997. Available: <http://sfbay.wr.usgs.gov/watershed/tidal_flow/images/miniposter.pdf>.

Reed, D. J. 2002. Understanding tidal marsh sedimentation in the Sacramento-San Joaquin Delta, California. *Journal of Coastal Research*, 36: 605–611.

Resource Management Associates, Inc. (RMA). 2010a. "Numerical Modeling in Support of Bay Delta Conservation Plan Technical Study #4 – Evaluation of Tidal Marsh Restoration Effects (Preliminary Results, March 2010 – For Internal Review Only)." Technical Report.

Resource Management Associates, Inc. (RMA). 2010b. "Numerical Modeling in Support of Bay Delta Conservation Plan Technical Study #4 – Evaluation of Tidal Marsh Restoration Effects (Effects Analysis, August 2010 – For Internal Review Only)." Technical Report.

Resource Management Associates, Inc. (RMA). 2010c. "Turbidity and Adult Delta Smelt Forecasting with RMA 2-D Models: December 2009–May 2010." Technical Report.

1   Resource Management Associates, Inc. (RMA). 2012. "Numerical Modeling in Support of Bay
2   Delta Conservation Plan –Tidal Marsh Assumptions Sensitivity Analysis." July 2012.

3   Schoellhamer, D.H. 2001. Influence of salinity, bottom topography, and tides on locations estuarine
4   turbidity maxima in northern San Francisco Bay. Pp. 343–357 in: W.H McAnally and A.J. Mehta
5   (Eds.), *Coastal and Estuarine Fine Sediment Transport Processes*, Elsevier, Amsterdam, The
6   Netherlands. Available: <http://ca.water.usgs.gov/abstract/sfbay/elsevier0102.pdf>.

7   Schoellhamer, D.H., S. Wright, J. Drexler, and M.Stacy. 2007. *Sacramento-San Joaquin Delta Regional
8   Ecosystem Restoration Implementation Plan, Ecosystem Conceptual Model: Sedimentation*. 35 pp.
9   Available:
10   <http://science.calwater.ca.gov/pdf/drerip/DRERIP_sediment_conceptual_model_final_111307.
11   pdf>.

12 Simenstad, C.J., J. Toft, H. Higgins, J. Cordell, M. Orr, P. Williams, L. Grimaldo, Z. Hymanson, and D.
13   Reed. 2000. *Sacramento/San Joaquin Delta breached levee wetland study (BREACH)*. Preliminary
14   report to CALFED. 51 pp. Available: <http://depts.washington.edu/calfed/breachii.htm>.

15 Singer, M.B., R. Aalto, and L.A. James. 2008. Status of the lower Sacramento Valley flood-control
16   system within the context of its natural geomorphic setting. *Natural Hazards Review* 9(3): 104–
17   115.

18 Sommer, T. Personal communication cited by P.B. Moyle and W.A. Bennett (2008).

19 SWAN team. 2009. *SWAN Scientific and Technical Documentation 40.72*. Delft University of
20   Technology, Delft, The Netherlands.

21 Wright, S.A. and D.H. Schoellhamer. 2004. Trends in the sediment yield of the Sacramento River,
22   California, 1957-2001. *San Francisco Estuary and Watershed Science*, 2(2): 1–14.

23 Wright, S.A. and D.H. Schoellhamer. 2005. Estimating sediment budgets at the interface between
24   rivers and estuaries with application to the Sacramento-San Joaquin River Delta. *Water
25   Resources Research*, 41(W09428).

26 Yarrow., M., V.H. Marin, M. Finlayson, A. Tironi, L.E. Delgado., and F. Fischer. 2009. The ecology of
27   *Egeria densa* Planchon (Liliopsida:Alismatales): A wetland ecosystem engineer?. *Revista Chilena
28   de Historia Natural*, 82: 299–313.

29 Ysebaert, T., M. Fettweis, P. Meire, and M. Sas. 2005. Benthic variability in intertidal soft-sediments
30   in the mesohaline part of the Shelde estuary. *Hydrobiologia*, 540: 197–216.

31 5C.D.10.2 Personal Communication

32 Miller, B. J. Consulting Engineer. October 5, 2011—emails to Marianne Guerin, Associate, Research
33   Management Associates, with Excel data analysis estimating entrainment.

cbec
eco engineering

Hydrology | Hydraulics | Geomorphology | Design | Field Services
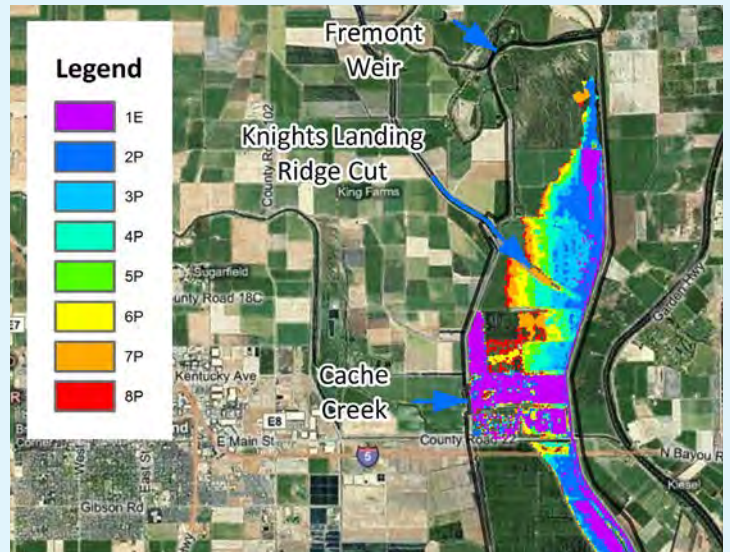
BDCP Effects Analysis:
2D Hydrodynamic Modeling of the
Fremont Weir Diversion Structure

Prepared for SAIC and the California
Department of Water Resources

November 2010

Project #: 10-1044
ID/IQ Subcontract Agreement #: P010058896

This report is intended solely for the use and benefit of SAIC and the California Department of Water Resources. No other person or entity shall be entitled to rely on the details contained herein without the express written consent of cbec, inc., eco engineering, 1255 Starboard Drive, Suite B, West Sacramento, CA 95691.

BDCP EFFECTS ANALYSIS: 2D HYDRODYNAMIC MODELING OF THE FREMONT WEIR DIVERSION STRUCTURE

TABLE OF CONTENTS

LIST OF FIGURES

LIST OF TABLES

1   INTRODUCTION

cbec, inc., eco engineering (cbec) applied a previously developed, but evolving, two-dimensional (2D) hydrodynamic model of the Yolo Bypass (Bypass Model) to predict inundation patterns and hydraulic conditions for a range of flow scenarios associated with the proposed diversion structure at Fremont Weir, as part of the habitat restoration components of the Bay Delta Conservation Project (BDCP) being undertaken by SAIC in cooperation with the California Department of Water Resources (DWR) and others. The Bypass Model was originally developed by cbec under contract with Metropolitan Water District (MWD) and extends from the Fremont Weir in the north to the Stair Step Channel at the northeast corner of Little Holland Tract in the south. Application of the Bypass Model to assess inundation patterns and hydraulic conditions resulting from the proposed diversion structure at Fremont Weir was made to inform a specific portion of the BDCP Effects Analysis. The inundation patterns and hydraulic conditions generated by the Bypass Model were provided to SAIC for their separate analyses to inform the Effects Analysis related to agriculture and habitat for juvenile salmon and splittail. The results of such analyses are not provided here. Rather, this report provides the following information:

- Overview of Bypass Model construction;
- Overview of Bypass Model calibration;
- Analysis of the proposed Fremont Weir diversion structure inundation; and
- Conclusions and recommendations.

2   MODEL CONSTRUCTION

2.1   MODEL OVERVIEW

An existing 2D model was developed for the Yolo Bypass in 2007 by the US Army Corps of Engineers, Sacramento District (USACE). However, this model (RMA2) is steady state and was developed for the purpose of assessing the flood flow capacity of the Bypass during peak flow events. It has subsequently been adopted by the Central Valley Flood Protection Board (CVFPB) for use by Encroachment Permit applicants undertaking any form of land use modification in the Yolo Bypass. For the BDCP, a model was needed that assessed more than just flood conveyance impacts in the Yolo Bypass, but also included information on the frequency, duration, depth, and area of inundation of lands during lower recurrence interval flows (e.g., 2-year flood down the Bypass when Fremont Weir begins to spill).   For such purposes, it is essential to use a 2D hydrodynamic model that can model hydrographs in addition to peak flows (i.e., quasi-steady conditions). The 2D hydrodynamic model used for the purpose of modeling the Yolo Bypass for this project was MIKE 21 Flexible Mesh (FM) (DHI, 2009), which has the following characteristics:

- 2D hydrodynamic (unsteady) model, meaning that it is able to model the secondary circulation of two-dimensional aspects of flow.
- Solves the fully dynamic Saint-Venant equations in 2 dimensions with the water depth defined in cell centers and a staggered velocity field defined with direction as the local grid based vector.
- Spatial domain is defined by a computational grid developed from topographic and bathymetric digital terrain models.
- Requires estimates of upstream boundary inflow, downstream boundary stage and roughness (Manning's n) at computational grid cell.
- Predicts water surface elevation, flow and average velocity at each computational grid cell.
- The accuracy of predicted parameters is dependent upon spatial density of computational grid cells. For areas with more complex flow structure, greater cell density is required.
- A flexible mesh version (used for this project) consisting of both triangular and quadrilateral cells, meaning that the mesh can be adjusted to the hydraulic shape of the situation being modeled. This provides great versatility in terms of being able to represent the hydraulics of the problem in question.
- 2D models such as MIKE 21 FM are typically used to model situations where it is important to understand the interaction between the channel and the floodplain. The physical connection between these two areas is represented much better in a 2D model.
- Floodplain flow can be approximated to 2D flow satisfactorily where the surface area of floodplain inundation is very large in comparison to the depth of floodplain flow. This is the case in the Yolo Bypass when inundated. The fundamental physics of fluid flow means that a 1D model does not represent the physics of this flow as well as a 2D model.
- 2D models are now able to model relatively large areas rapidly, and hence more cheaply since computational power has improved so dramatically in recent years.

2.2   DATA COLLECTION

As part of the Bypass Model development effort, an extensive data collection effort was undertaken, which is described in the following sections.

2.2.1   LiDAR

LiDAR data from 2005 was obtained from the Department of Water Resources (DWR). Figure 1 shows a shaded contour plot based on the 2005 LiDAR data for the Yolo Bypass. DWR LiDAR from 2007 also exists, but it only goes as far north as I80 and includes several data gaps due to ponded water returns. Since the overlap areas between the two datasets are very similar in elevation, the 2005 LiDAR was used solely for the Bypass Model.

2.2.2   Toe Drain and Tule Canal Bathymetry

Bathymetric surveys of the Toe Drain and Tule Canal were conducted by cbec in 2009 and 2010, respectively. The 2009 survey was contracted out to Environmental Data Solutions (EDS), who performed a Class 1 hydrographic survey of the Toe Drain in March and April 2009, referenced to NAVD88, and subject to standard QA/QC protocol. cbec performed the 2010 survey of the Tule Canal in January and February 2010, referenced to NAVD88, using an Ohmex SonarMite echosounder coupled to a Trimble R8 GNSS GPS receiver (survey-grade RTK GPS using the California Survey and Drafting Supply (CSDS) Virtual Survey Network (VSN)). These data were thoroughly checked for erroneous returns (e.g., shallow water, dense vegetation, etc.), which were removed from the final product. The overall extents of the bathymetric surveys were from approximately 1.75 miles south of the Fremont Weir to the confluence with Liberty Cut and Prospect Slough.

Based on the XYZ point file generated from the bathymetric surveys, a 3D surface for the Toe Drain and Tule Canal was created in GIS and combined with the 2005 LiDAR data for modeling purposes. Figure 2 shows excerpts of the point data and generated surface. It should be noted that the bathymetric surveys undertaken by cbec were augmented by data obtained from a 2002 DWR survey at Lisbon Weir. However, it is noted that additional rock was applied to the weir in 2003, and as such, it is likely that the 2002 survey elevations are lower than the present-day elevations of the rock weir.

Figure 3 shows a photograph of the bathymetric surveys being collected in the Tule Canal.

Figure 4 shows a longitudinal profile through the Tule Canal from Fremont Weir to Lisbon Weir. This profile shows an approximate thalweg profile (black line) as well as the water surface elevation (blue solid line) and the discharge (red dashed line) taken on February 19, 2010 (see Section 2.2.3).

2.2.3   Toe Drain and Tule Canal Flow and Stage

On February 19, 2010 and March 10, 2010, cbec conducted 3D velocity measurements in Tule Canal and the Toe Drain, respectively, using a SonTek 3.0 MHz Mini Acoustic Doppler Current Profiler (ADCP). The

resulting data were processed to provide estimates of flow passing down the channel. In addition, water surface elevation measurements (stage) were collected and referenced to NAVD88.

Flow and stage measurements were taken at 19 locations from the northerly extents of the Tule Canal to just downstream of Lisbon Weir near the DWR gage on February 19, 2010. Flow and stage measurements were taken at 4 locations from the Lisbon Weir near the DWR gage south towards Yolo Ranch on March 10, 2010. Figure 5 shows the locations of flow and stage measurements. Table 1 provides a summary of the flow and stage measurements taken on these two field deployments. The benefit of obtaining these measurements in February 2010 was that the flows in the Tule Canal were at a point where in most places they were just receding off of the floodplain, or just below the top of bank, thus providing a reasonable estimate of the flow capacity of the Tule Canal. In the simplest of terms, the Tule Canal can convey approximately 1000 cfs in the northerly extents prior to flows exceeding the top of bank and approximately 3000 cfs in the southerly extents just above Lisbon Weir prior to flows exceeding the top of bank.

Table 1. Toe Drain and Tule Canal flow and stage measurements

Location	Elevation (ft NAVD)	Measured Flow (cfs)
Measurements taken upstream of Lisbon Weir on February 19, 2010 (see Figure 5)		
ADCP1	17.3	N/A
ADCP2	17.5	151
ADCP3	17.1	920
ADCP4	16.6	1072
ADCP5	16.3	1344
ADCP6	15.9	1281
ADCP7	15.8	1443
ADCP8	15.4	1408
ADCP9	15.1	1539
ADCP10	14.7	1541
ADCP11	13.8	1644
ADCP12	11.7	2154
ADCP13	11.3	2307
ADCP14	11.2	2278
ADCP15	10.8	2526
ADCP16	10.5	2622
ADCP17	10.5	2692
ADCP18	10.0	2609
ADCP19	8.8	2805
Measurements taken downstream of Lisbon Weir on March 10, 2010 (see Figure 5)		
ADCP01S	4.3	1523
ADCP02S	4.4	1801
ADCP03S	5.1	1843
ADCP04S	5.8	1357

Flow measurements recorded in the Toe Drain and Tule Canal were approximately validated with flow measurements observed at Lisbon Weir as recorded on the California Data Exchange Center (CDEC) (http://cdec.water.ca.gov/cgi-progs/staMeta?station_id=LIS). Flow measurements taken by cbec in the region of Lisbon Weir were within 3.0% and 0.6% of those stated on CDEC at Lisbon Weir for the February and March measurements, respectively.

2.3 MODEL EXTENT AND BOUNDARIES

Figure 6 shows the extents of the Bypass Model. The modeling domain covers the complete Bypass from Fremont Weir to just north of the Stair Step where it connects into the Toe Drain at the northeast corner of Little Holland Tract. Figure 6 also shows the location of the flow boundaries to include:

- Fremont Weir
- Knights Landing Ridge Cut (KLRC)
- Cache Creek
- Sacramento Weir
- Willow Slough
- Putah Creek

For the purposes of modeling low flows in the Yolo Bypass, the Fremont Weir inflow was fixed at the northerly extent of the Tule Canal, approximately 1.75 miles south of the Fremont Weir.

For the purposes of the Bypass Model, a tidal boundary was implemented in the Toe Drain at the northeast corner of Little Holland Tract, in the vicinity of Yolo Ranch. As part of a separate effort, cbec installed a series of eight (8) water level recorders (including temperature and conductivity) in the slough system around Liberty Island and tied the elevations to NAVD88. These recorders were installed in 2008, and one of the recorders coincides with the downstream boundary of the Bypass Model. Based on the data obtained from these recorders, tidal datums for the Cache Slough Complex have been recalculated (unpublished).

2.4 MODEL BATHYMETRIC AND TOPOGRAPHIC MESH

MIKE 21FM uses a flexible mesh approach to discretize the model domain. The benefit of a flexible mesh approach is that the numerical cells can be "boundary fitted" to match the actual topographic and bathymetric terrain more realistically than other numerical mesh modeling schemes (such as orthogonal meshes). In addition, it is possible to vary the cell sizes proportional to the level of detail required. Figure 7 shows the overall coverage of the numerical mesh for the Bypass Model. Also shown is the mesh at a higher resolution. Areas of most importance for low-flow inundation modeling, such as the Toe Drain, Tule Canal, and the immediately adjacent floodplain, were discretized using a finer mesh. Areas of the Yolo Bypass where less detail was required, typically those floodplain areas that inundate less frequently, were discretized using a coarser mesh. Mesh cell sizes varied typically from 70 ft^2 to 3.5 acres.

2.5 MODEL ROUGHNESS

Model roughness, or Manning's n (in MIKE 21 Manning's M is actually used, where M=1/n), is used in numerical modeling to represent the relative roughness of vegetation in the channel or floodplain, and hence, is a numerical representation to the impedence of flow. The model roughness scheme utilized for this project was based on the roughness scheme developed by the USACE for the RMA2 model developed in 2007, and adopted by the CVFPB. Since the USACE calibrated and validated the RMA2 model to this roughness scheme, it is reasonable to use the same roughness scheme for this project. Based on the calibration (see Section 3), roughness for the Toe Drain and Tule Canal was set to a constant n-value of 0.02. Figure 8 shows the roughness grid used for the model.

3   MODEL CALIBRATION

The Toe Drain and Tule Canal portion of the Bypass Model was calibrated using flow and stage data as described in Section 2.2.3. Figure 9 shows the results of this calibration effort. The calibration effort should be considered preliminary and approximate; the results could be partially improved. However, for the preliminary purpose of calculating inundation at various low flow events, results of the calibration effort were considered satisfactory. In addition, no validation has been undertaken currently. The primary reason for this is that additional data (flow and stage) should be collected along the Toe Drain and Tule Canal for a separate event, which could be collected in an upcoming winter. It is not appropriate to perform calibration and validation using the same event.

It can be observed from Figure 9 that the difference between measured and simulated water surface elevation (or stage) (orange line) varied by approximately ± 0.3 meters (or approximately ± 1 foot).

The greatest differences between measured and simulated stage occur approximately immediately downstream of the I80 causeway and in the region on Knights Landing Ridge Cut. There are various reasons for these discrepancies of up to 0.3 meters (1 foot) which include:

- The flow structure at these locations is inherently complicated with high velocities and complex turbulent flow structures (note that the channel slope at both of these locations shows noticeably steeper slopes).
- Flows break out of the banks of the Tule Canal just upstream of these locations, and return back the channel just downstream of these locations. Therefore, there may be some discontinuities in volume through these reaches that is not accurately represented in the model (e.g., bathymetry or mesh does not accurately capture high ground, berms, or riprap control).
- There may be other phenomena occurring, such as vegetative roughness not being represented correctly in the model.

4   FREMONT WEIR DIVERSION STRUCTURE SCENARIOS

cbec used the Bypass Model to predict inundation patterns and hydraulic conditions (i.e., depths and velocities) for a range of flow scenarios associated with the proposed diversion structure at Fremont Weir. The inundation patterns and hydraulic conditions were provided to SAIC to inform their effects analysis related to agriculture and habitat for juvenile salmon and splittail.

4.1   INFLOWS

cbec collaborated with DWR to identify a range of flow scenarios that included west side tributaries inflows corresponding to a defined set of Fremont Weir notch flows. The 30-year flow record contained in the Yolo Bypass Management Strategy (J&S, 2001) was used to determine the relationship between daily flows in Knights Landing Ridge Cut (KLRC), Cache Creek, Willow Slough, and Putah Creek and daily flows in the Sacramento River at Verona (i.e., water years 1968 to 1998 with the exception of 1976 to 1998 for Knights Landing Ridge Cut). A hydraulic description of the Fremont Weir diversion structure (see Table 2) was used to determine the relationship between proposed restricted notch flows (up to 6000 cfs) and flows in the Sacramento River at Verona. Using these two sources of information, Table 3 was constructed by querying the west side tributary flows between December 1st and March 31st corresponding to a prescribed sampling flow range in the Sacramento River at Verona. Based on Table 2, the prescribed sampling flow range in the Sacramento River at Verona typically corresponded to the restricted notch flow ± 500 cfs. It was defined as such to generate sufficient data for averaging purposes. Deviations in the sampling flow range in Table 3 occur in the last row whereby a 2000 cfs flow range was defined to sample the west side tributary flows just before the Fremont Weir would spill (i.e., roughly 56000 cfs at Verona) under its present-day configuration. The sampling flow range was limited to the period between December 1st and March 31st to correspond to specific life histories for juvenile salmon and splittail.

A total of fifteen (15) flow scenarios were identified in Table 3 for simulation in the 2D hydrodynamic model. Eight (8) scenarios represent existing conditions (i.e., west side tributary inflows only) and seven (7) scenarios represent proposed conditions (i.e., west side tributary inflows plus restricted notch flows). Each set of flows were treated as constants over a 4-day simulation period, which was sufficient to achieve quasi-steady conditions.

KLRC flows entered the model domain at the Tule Canal rather than the west project levee due to inadequate topography in the channel connecting the KLRC to the Tule Canal. Cache Creek flows entered the model domain at the stilling basin weir at the west project levee. Willow Slough flows entered the model domain at the west project levee. Putah Creek flows entered the model domain at the Tule Canal rather than the west project levee due to inadequate topography in the creek.

Table 2. Summary hydraulic table for the new diversion structure[1,2]

Sacramento River Stage at Fremont Weir (feet, NAVD88)	Sacramento River Flow at Fremont Weir (cfs)	Sacramento River Flow at Verona (cfs)	Restricted Notch Flow (cfs)
17.5	14600	23100	0
18.6	17200	25700	100
19.2	17700	27200	250
19.8	18600	28600	500
20.7	20200	31000	1000
21.8	22200	34100	2000
22.7	24000	36500	3000
23.4	25300	38500	4000
23.9	26300	39900	5000
24.5	27700	41600	6000
24.9	28900	42700	6000
25.3	29900	43900	6000
25.7	31000	45100	6000
26.0	31900	46000	6000
---	---	56000	6000

[1] This table was reproduced from Table 4 in the Integration Team (2009) report

[2] 56000 cfs at Verona is the assumed flow condition just before Fremont Weir spills

Table 3. Average flow conditions from December through March for water years 1968 to 1998

Sacramento River Flow at Verona Sampling Range (cfs)		Restricted Notch Flow (cfs)	KLRC (cfs)	Cache Creek (cfs)	Willow Slough (cfs)	Putah Creek (cfs)	West Side Tribs Only[1] (Run ID; cfs)		West Side Tribs Plus Notch Flow[2] (Run ID; cfs)	
23100	28600	0	364	473	134	154	1E	1125	1E	1125
28600	32550	1000	735	965	179	291	2E	2170	2P	3170
32550	35300	2000	971	1079	213	383	3E	2647	3P	4647
35300	37500	3000	1047	1344	243	439	4E	3073	4P	6073
37500	39200	4000	998	1235	329	415	5E	2976	5P	6976
39200	40750	5000	1359	2227	353	403	6E	4343	6P	9343
40750	42150	6000 (A)	1654	1891	218	273	7E	4037	7P	10037
54000	56000	6000 (B)	1911	3190	428	760	8E	6289	8P	12289

[1] Existing conditions

[2] Proposed conditions

4.2 TIDAL BOUNDARY

For all flow scenarios identified in Table 3, the same tidal boundary was applied over a 4-day simulation period that started on 2/26/2010 at 12:00 and ended on 3/2/2010 at 12:00. The tidal boundary is shown by Figure 10 and includes measured water levels in the Stair Step Channel just off the Toe Drain at the northeast corner of Little Holland Tract. For reference, tidal datums calculated by cbec (unpublished) from various monitoring data in the Cache Slough Complex (as provided in Table 4) are also shown on Figure 10. As demonstrated by Figure 10, the tidal boundary includes fluvial influences as inflows from the west side tributaries are conveyed south past Lisbon Weir.

This particular simulation period was selected because the following set of conditions were met: observed flows were relatively constant (i.e., approximately 2400 cfs), the tidal fluctuations were fairly regular, and the high tides were consistent with the high tides that occurred in mid-February when flows were well in excess of 3000 cfs. The tide levels for this period were on average 6.2 feet (i.e., very close to MHHW) and ranged from 4.4 feet to 8.0 feet.

Table 4. Cache Slough Complex tidal datums (unpublished)

Tidal Datum	Elevation (feet, NAVD88) ± 0.15 feet
Mean Higher High Water (MHHW)	6.4
Mean High Water (MHW)	5.9
Mean Tide Level (MTL)	4.3
Mean Low Water (MLW)	2.7
Mean Lower Low Water (MLLW)	2.1

4.3 NOTCH SCENARIO RESULTS

Figure 11 and Figure 12 show inundation overlays for existing and project conditions for the range of flow scenarios, with Table 5 reporting the approximate inundation acreages. Referring back to Section 2.2.3, and in the simplest of terms, the Tule Canal can convey approximately 1000 cfs in the northerly extents prior to flows exceeding the top of bank and approximately 3000 cfs in the southerly extents just above Lisbon Weir prior to flows exceeding the top of bank. The existing conditions inundation extents (see Figure 11) reflect this for the most part, but deviations from capacity driven Tule Canal inundation are evident in Figure 11. In particular, Cache Creek and Willow Slough are treated as overland releases, and as such, inundation extending from the west project levee is expected even in the lower range of flow conditions.

Based on Table 5, Yolo Bypass inundation under existing conditions (i.e., west side tributary inflows only) ranges from 6377 acres at 1125 cfs up to 19244 acres at 6289 cfs. Under proposed conditions (i.e., west side tributary inflows plus restricted notch flows), the total inundation area goes up to 25136 acres at 12289 cfs at a flow condition where Fremont Weir is just about to spill. The data contained in Table 5 is also shown in another format by the graph in Figure 13, depicting the relationship between flow and

inundation area. Overall, Table 5 shows that the largest increase in proposed inundation above existing levels of inundation (i.e., 9553 acres) occurs at a notch flow of 4000 cfs with diminishing inundation returns at higher notch flows.

While it is possible that the southernmost 800 to 900 acres of inundation under scenario 1E might be overestimated due to the elevated tidal boundary, it is very likely (and known) that tide gates and flap gates on the Toe Drain for Yolo Ranch and Yolo Flyway Farms, and perhaps even the US Fish & Wildlife Service (FWS) easements directly north of Yolo Flyway Farms, are open in the wintertime to facilitate drainage of flood waters. Open tide gates and flap gates also allow floodwaters to backwater through the open structures and inundate the agricultural lands at this lower range of flow conditions. It is also known that wintertime activities on these properties in the southern end of the Yolo Bypass include water level management for waterfowl. Even though tide gates and flap gates were not explicitly modeled, and it would be difficult to do so without a survey of all possible locations in the Yolo Bypass, it would appear that inundation in the southern end of the Yolo Bypass is reasonably captured.

The influence of the tidal boundary, perhaps being slightly low for the higher flow scenarios, was also reviewed and was determined to have minimal impact on inundation. The tidal boundary as implemented in the model extends across the Toe Drain as well as across Yolo Ranch and the lower end of Mound Farms. The latter is a correct assumption because the tide gates on Yolo Ranch are open in the wintertime to facilitate drainage of floodwaters into Shag Slough and Liberty Cut. If the tidal boundary were slightly low, then water surface profiles in the Toe Drain resolve themselves in the first half-mile north of Little Holland Tract due to the limited capacity of the Toe Drain.

Detailed inundation acreages and hydraulic conditions are further provided in Table 6 through Table 9 to inform the effects analysis related to agriculture and habitat for juvenile salmon and splittail, as performed by SAIC.

Table 5. Fremont Weir notch scenario inundation results

Existing Run ID	Flow (cfs)	Inundation Area (acres)	Proposed Run ID	Flow (cfs)	Inundation Area (acres)	Area Increase (acres)
1E	1125	6377	---	---	---	---
2E	2170	8035	2P	3170	12671	4637
3E	2647	9733	3P	4647	17082	7349
4E	3073	11110	4P	6073	19310	8200
5E	2976	10863	5P	6976	20416	9553
6E	4343	15711	6P	9343	23027	7316
7E	4037	15621	7P	10037	23821	8199
8E	6289	19244	8P	12289	25136	5893

Table 6. Existing conditions inundation areas (in acres) by depth increments

Run ID	< 0.5 ft	0.5 - 1.0 ft	1.0 - 1.5 ft	1.5 - 2.0 ft	2.0 - 2.5 ft	2.5 - 3.0 ft	3.0 - 3.5 ft	3.5 - 4.0 ft	4.0 - 4.5 ft	4.5 - 5.0 ft	5.0 - 5.5 ft	5.5 - 6.0 ft	6.0 - 6.5 ft	> 6.5 ft
1E	3572	1517	487	192	146	51	42	36	22	27	16	14	17	239
2E	3573	2341	884	346	227	116	87	41	22	21	28	24	21	304
3E	3653	3065	1392	609	293	129	106	47	26	18	20	24	30	320
4E	3420	3473	2058	851	491	172	128	61	29	22	20	20	31	334
5E	3518	3414	1911	795	439	154	122	60	25	23	19	23	32	329
6E	3685	3737	2943	2281	1217	777	378	163	62	28	19	21	22	376
7E	3661	3728	3044	2264	1148	733	369	150	60	26	19	20	21	377
8E	3036	3618	3722	2986	2265	1450	833	456	308	97	27	18	20	408

Table 7. Proposed conditions inundation areas (in acres) by depth increments

Run ID	< 0.5 ft	0.5 - 1.0 ft	1.0 - 1.5 ft	1.5 - 2.0 ft	2.0 - 2.5 ft	2.5 - 3.0 ft	3.0 - 3.5 ft	3.5 - 4.0 ft	4.0 - 4.5 ft	4.5 - 5.0 ft	5.0 - 5.5 ft	5.5 - 6.0 ft	6.0 - 6.5 ft	> 6.5 ft
2P	3612	3618	2514	1233	682	300	153	79	38	22	22	21	25	355
3P	3452	4044	3161	2621	1562	887	488	293	79	38	21	24	21	392
4P	2851	3523	3817	3059	2399	1463	846	465	317	83	27	19	25	414
5P	2654	3194	3647	3445	2770	1924	1082	584	400	199	45	19	22	429
6P	2586	2964	3142	3438	3492	2784	1850	1049	577	409	223	42	19	453
7P	2577	2885	3077	3300	3507	3071	2143	1257	706	452	285	78	23	459
8P	2328	2855	2945	3109	3370	3424	2639	1802	971	573	389	220	39	470

Table 8. Existing conditions inundation areas (in acres) by velocity increments

Run ID	< 0.5 fps	0.5 - 1.0 fps	1.0 - 1.5 fps	1.5 - 2.0 fps	2.0 - 2.5 fps	> 2.5 fps
1E	5839	262	212	50	6	7
2E	7146	484	175	161	59	10
3E	8704	575	185	164	88	17
4E	9924	671	228	154	104	29
5E	9715	652	215	155	100	25
6E	13858	1140	388	145	88	92
7E	13840	1136	322	145	90	89
8E	16128	2274	445	196	85	115

Table 9. Proposed conditions inundation areas (in acres) by velocity increments

Run ID	< 0.5 fps	0.5 - 1.0 fps	1.0 - 1.5 fps	1.5 - 2.0 fps	2.0 - 2.5 fps	> 2.5 fps
2P	11272	867	221	148	116	48
3P	14789	1672	257	154	92	117
4P	15972	2606	319	179	98	136
5P	16380	3201	393	178	115	148
6P	16716	5024	781	209	129	167
7P	16673	5714	904	214	141	176
8P	16513	6768	1258	269	150	180

5   CONCLUSIONS AND RECOMMENDATIONS

The current Bypass Model described herein, and applied to inform the BDCP Effects Analysis on inundation patterns and hydraulic conditions resulting from the proposed diversion structure at Fremont Weir, has been constructed and calibrated to a preliminary level. However, there are several issues that should be addressed to further develop the modeling platform for future use:

- While the Toe Drain and Tule Canal are reasonably well represented in the Bypass Model, other major ditches, channels, and water control structures, of which there are many in the Yolo Bypass, are not represented in the Bypass Model. These features will be particularly important for assessing the ability of the floodplains of the Yolo Bypass to backwater on the rising limb and drain on the receding limb of the flood hydrograph. The ability of the floodplains of the Yolo Bypass to flood and drain is critical to assessing the potential impacts of more frequent floodplain inundation on current agricultural practices within the Yolo Bypass. We therefore recommend that the existing drainage features be identified, prioritized, surveyed, and documented regarding wintertime management activities (e.g., open or closed) and input into the Bypass Model.
- While the Toe Drain and Tule Canal are reasonably well represented in the Bypass Model, specific hydraulic controls in these channels should be accurately captured as they influence low flow stages and ultimate breakout conditions. Such features include Lisbon Weir, the temporary agricultural crossing, and riprap controls associated with bridges. Regarding Lisbon Weir, the 2002 DWR survey is outdated as additional rock as been added to the weir since 2003, which bolstered and likely raised the weir elevation.
- Additional efforts should be undertaken to update the roughness map for the Yolo Bypass, which is currently based on calibration and validation undertaken by the USACE for the RMA2 model of the Yolo Bypass based on 1997 conditions. This roughness map should be updated and refined for the areas of most interest.
- Validation of the Bypass Model should be undertaken, using a different dataset from that used for calibration. We recommend that the dataset for validation be collected during this upcoming winter.
- Additional calibration and validation data should be collected in the Yolo Bypass, with the focus for data collection being low flow hydrology, as well as high flow hydrology when the Yolo Bypass experiences significant flood events (such as that of 2006). Calibration of the Bypass Model was based on water surface elevations (stage) collected in February 2010 over a period of one day. This is a "snapshot" of the conditions on that day. For rigorous low flow capture of calibration data we recommend that a series of water level recorders be installed in the Toe Drain and Tule Canal from the northerly extents near Fremont Weir to the southerly extents near Liberty Island. We recommend that up to fifteen (15) recorders be installed over this reach, including key locations such as in the vicinity of the I80 crossing and Knights Landing Ridge Cut, where the current calibration identified the greatest discrepancies. These recorders could also provide valuable data if the Bypass experiences a significant flood event in future years. High flow calibration and validation of the Bypass Model will also be important for any future actions

in the Bypass as they relate to satisfying the requirements of the CVFPB and Encroachment Permits.

- Additional analysis of the simulated results should be undertaken to help ascertain opportunities and constraints as they relate to ecological enhancement and current agricultural practices in the Yolo Bypass. Modeling parameters that will be most beneficial to this analysis include:
  - o Flushing times – the average amount of time spent in the system by flows passing down the Bypass.
  - o Age – the time spent by a sample of flow, entering via a system boundary.
  - o Residence time – the time taken for a sample of flow to exit through a system boundary.

  In addition, the rate of recession of floodplain flows will also be important to identify potential impacts to current agricultural practices and effects on production of aquatic food web resources (this also relates to the need to represent the major channels, ditches and hydraulic control structures in the Bypass Model).

- A detailed sensitivity analysis should be undertaken using the Bypass Model. Currently, the Bypass Model has been used with a variable inflow boundary in the vicinity of the Fremont Weir at the northern extents of the model, and a tidal stage boundary at the southern extents of the model. However, numerous other inflow boundaries are incorporated into the model, as described in Section 2.4.2. The effects of inflows from tributaries such as Cache Creek and Putah Creek should be analyzed through a sensitivity analysis. In addition, other model parameters, such as model roughness and eddy viscosity should be analyzed for sensitivity. Finally, the sensitivity of the Bypass Model to a varying downstream tidal boundary should be identified. This will identify the potential impacts to floodplain inundation as a result of issues such as climate change or restoration efforts in the Cache Slough Complex affecting tidal datums in the southern extent of the model.

As applied to inform the BDCP effects analysis on inundation patterns and hydraulic conditions resulting from the proposed diversion structure at Fremont Weir, the Bypass Model indicated the following:

- A total of fifteen (15) flow scenarios representing existing (i.e., west side tributary inflows only) and proposed (i.e., west side tributary inflows plus restricted notch flows) conditions were generated from readily available information describing the relationship between daily flows in Knights Landing Ridge Cut, Cache Creek, Willow Slough, and Putah Creek and daily flows in the Sacramento River at Verona. Existing conditions inundation ranged from 6377 acres at 1125 cfs up to 19244 acres at 6289 cfs. The 6289 cfs west side tributary total inflow condition corresponds to Sacramento River flow conditions when the Fremont Weir is just about to spill. For the proposed conditions scenario with west-side tributary inflows at 6289 cfs and the 6000 cfs maximum released through the diversion structure (i.e., total flow = 12289 cfs) , inundation increases to 25136 acres. Overall, the largest increase in inundation surface area for the proposed conditions over existing conditions was 9553 acres and occured at a diversion release of 4000 cfs. For equivalent releases into the Bypass greater than 4000 cfs, the increments in inundation acreages diminished.

- The downstream tidal boundary estimate, which was the same for all flow scenarios, but most accurate for Toe Drain flows in the 2000 to 3000 cfs range (since the observed flows corresponding to this boundary were 2400 cfs), was determined to be reasonably accurate for all flow scenarios. The tidal fluctuations were regular, the high tides were consistent with the high tides that would occur for flows above 3000 cfs, and the average tide levels were very close to MHHW. Any discrepancies in the tidal boundary are thought to resolve themselves in the model within the first half-mile of the downstream boundary due to the limited capacity of the Toe Drain.

- It is recommended that the Effects Analysis consider further delineation of the inundation, depth, and velocity results by subreach or specific land holdings (e.g., Conway Ranch). There is considerable variability in the inundation extents, and thus hydraulic conditions, over the range of flows modeled. By further delineating the analysis, agricultural impacts and habitat benefits can be better understood at a scale finer than the entire Yolo Bypass.

6 REFERENCES

Integration Team. 2009 (Draft). Technical Study #2: Evaluation of North Delta Migration Corridors: Yolo Bypass. Prepared for Bay Delta Conservation Plan.

Jones & Stokes. 2001. A Framework for the Future: Yolo Bypass Management Strategy August. Sacramento, CA. Prepared for Yolo Basin Foundation.

USACE. 2007. Engineering Documentation Report: Yolo Bypass 2-D Hydraulic Model Development and Calibration. US Army Corps of Engineers, Sacramento District.
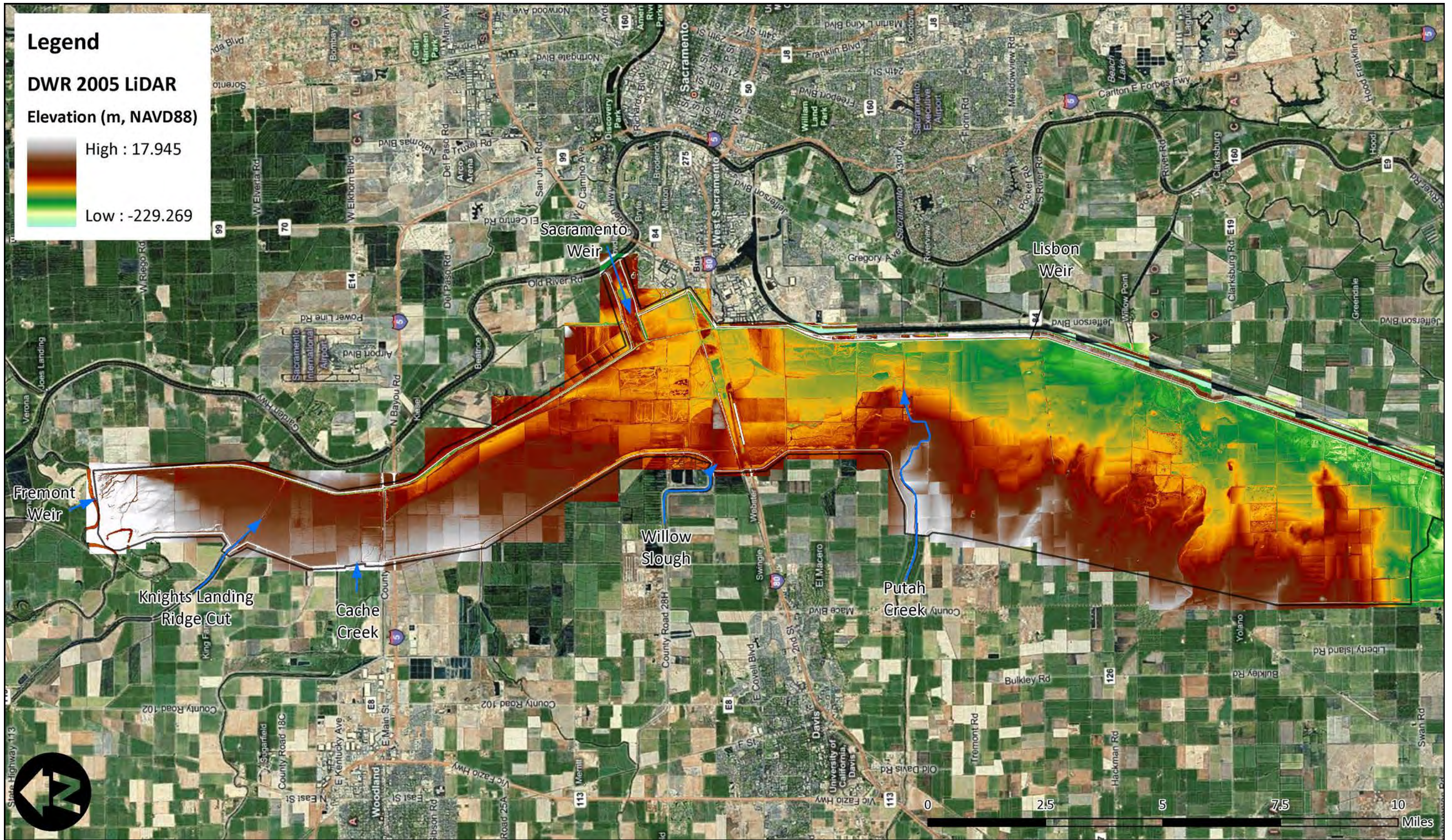
Legend

DWR 2005 LiDAR

Elevation (m, NAVD88)

High : 17.945

Low : -229.269

Sacramento Weir

Lisbon Weir

Fremont Weir

Knights Landing Ridge Cut

Cache Creek

Willow Slough

Putah Creek

N

0   2.5   5   7.5   10
Miles

Notes: background courtesy of Bing Maps

cbec
eco engineering

BDCP Effects Analysis – 2D Hydrodynamic Modeling
DWR 2005 LiDAR

| Project No. 10-1026 | Created By: CRC | **Figure 1** |

C:\Work\Projects\10-1026_BDCP_Modeling\Reporting\Figures\Fig1_2005_LiDAR.docx
11/8/2010
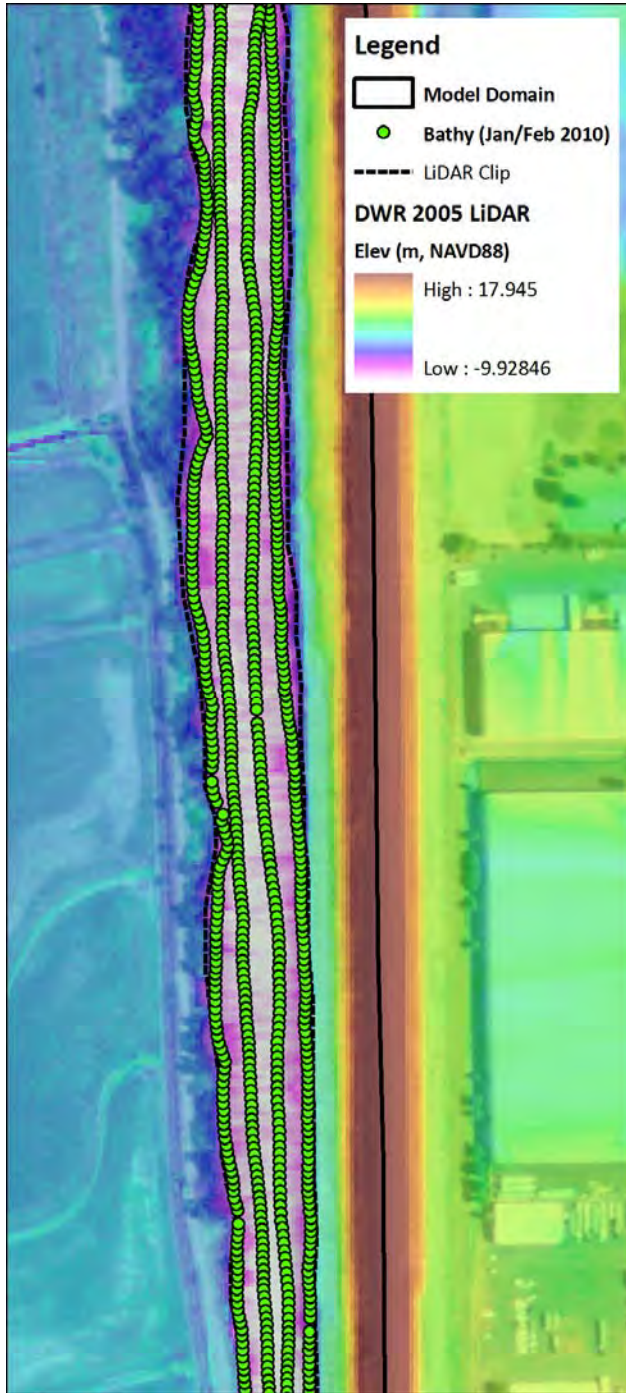
Below: bathymetric data DWR 2005
LiDAR in the region of Lisbon Weir

Source: cbec 2010

BDCP Effects Analysis – 2D Hydrodynamic Modeling

Tule Canal bathymetric data

Project No. 10-1026 | Created By: CRC | **Figure 2**

C:\Work\Projects\10-1026_BDCP_Modeling\Reporting\Figures\Fig2_Tule_Canal_Bathy.docx
11/7/2010

BDCP Effects Analysis – 2D Hydrodynamic Modeling

Tule Canal bathymetric survey

| Project No. 10-1026 | Created By: CRC | **Figure 3** |
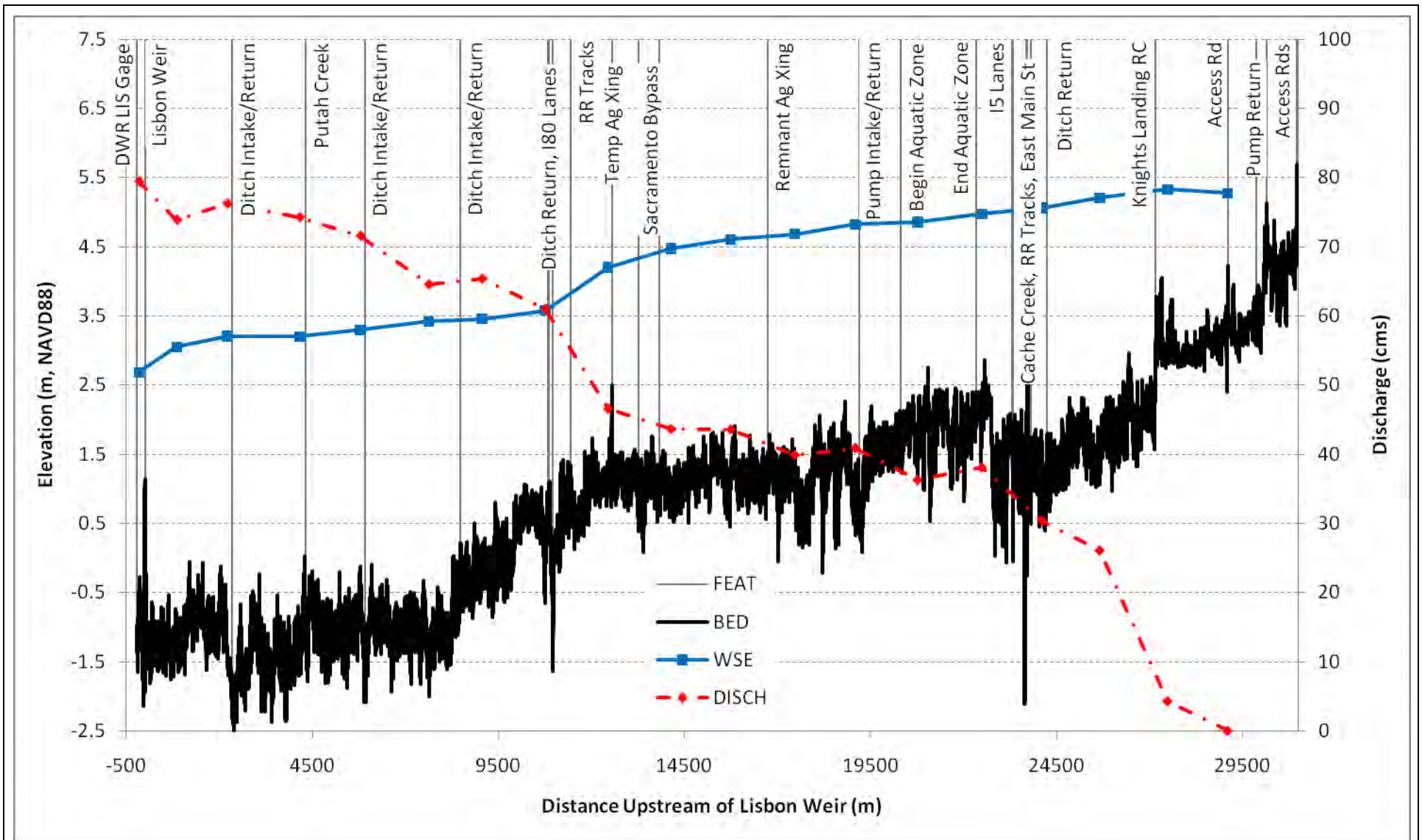
Tule Canal longitudinal profile and ACDP flow data

Source: cbec 2010

Notes: FEAT = feature of interest; BED = bed elevation profile; WSE = water surface elevation; and DISCH = discharge profile

BDCP Effects Analysis – 2D Hydrodynamic Modeling

Tule Canal longitudinal profile and ACDP flow data

Project No. 10-1026 | Created By: CRC | **Figure 4**

C:\Work\Projects\10-1044_BDCP_Modeling\Reporting\Figures\Fig4_Tule_Canal_Long_Profile.docx
11/17/2010

Legend
- Model Domain
- ▲ ADCP (Feb 2010)
- ▲ ADCP (Mar (2010))
- ● Bathy (Jan/Feb 2010)

ADCP01
ADCP02
ADCP03
ADCP04
ADCP05
ADCP06
ADCP07
ADCP08
ADCP09
ADCP10
ADCP11
ADCP12
ADCP13
ADCP14
ADCP15
ADCP16
ADCP17
ADCP04   ADCP19
ADCP03
ADCP02   ADCP01
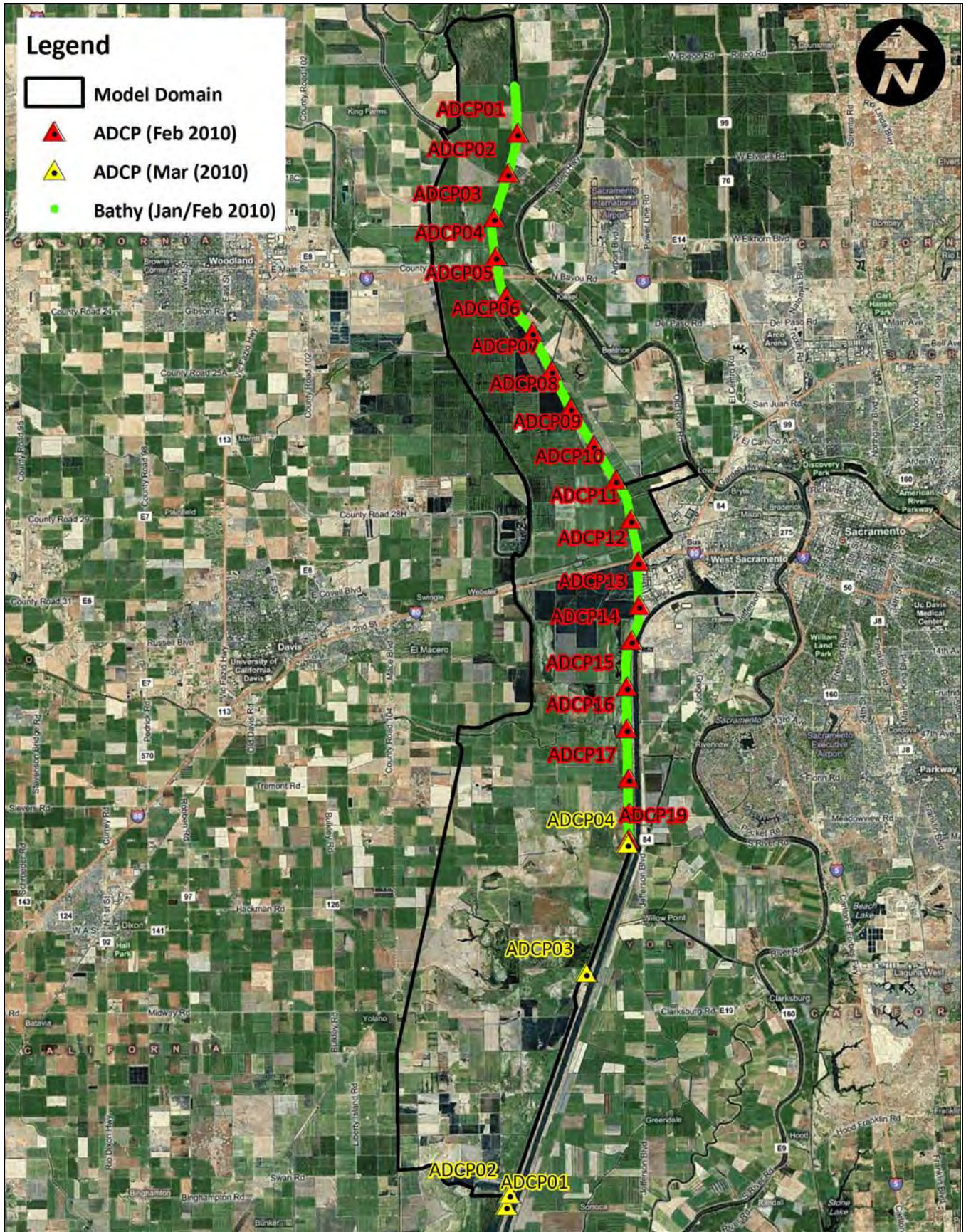
Source: cbec 2010

BDCP Effects Analysis – 2D Hydrodynamic Modeling

Flow and stage measurements

| Project No. 10-1026 | Created By: CRC | **Figure 5** |
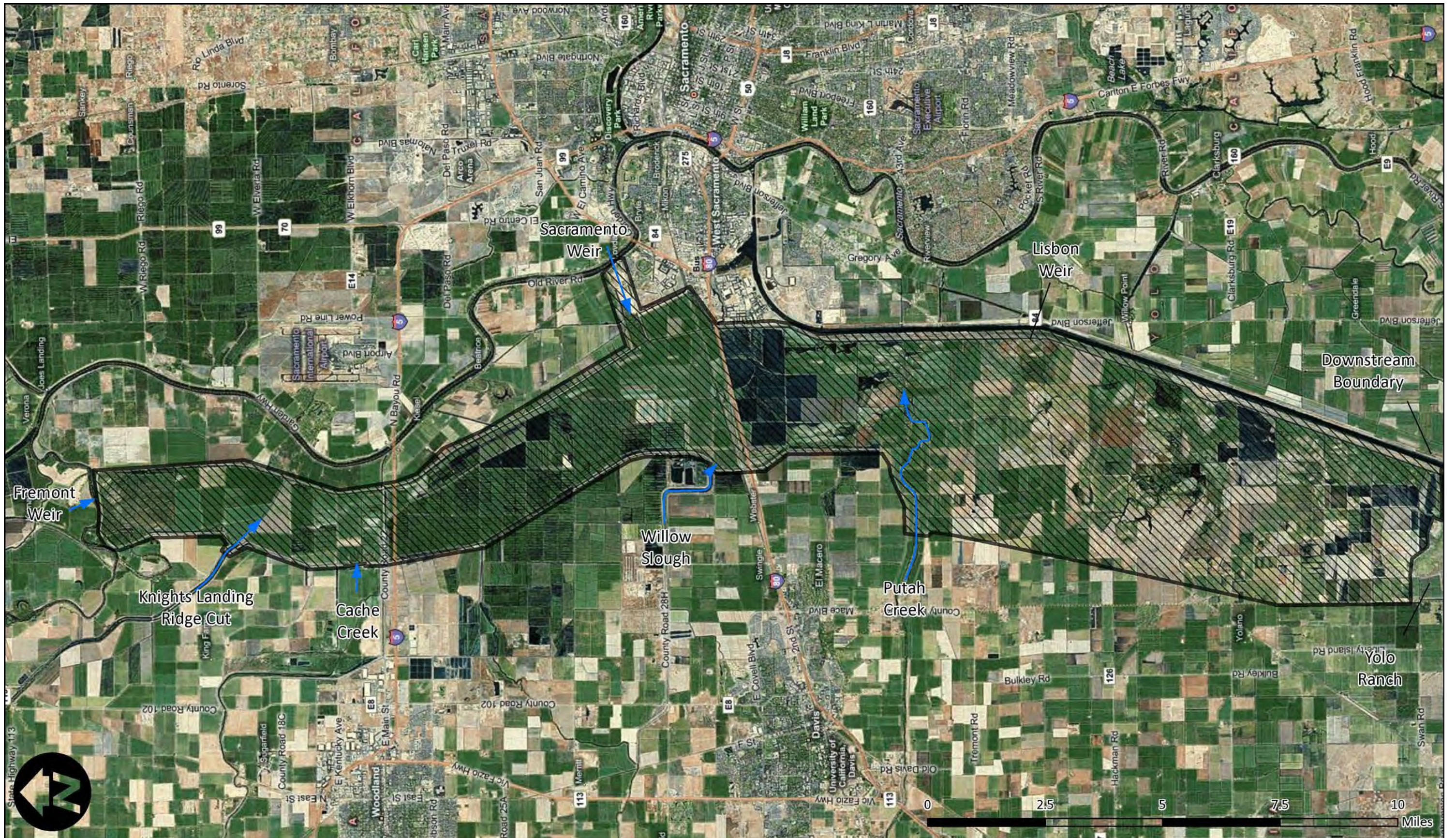
Labels on map: Sacramento Weir, Lisbon Weir, Downstream Boundary, Fremont Weir, Knights Landing Ridge Cut, Cache Creek, Willow Slough, Putah Creek, Yolo Ranch

cbec eco engineering

BDCP Effects Analysis – 2D Hydrodynamic Modeling

Bypass Model extents

| Project No. 10-1026 | Created By: CRC | **Figure 6** |

Toe Drain Model Domain

Bypass Model mesh

BDCP Effects Analysis – 2D Hydrodynamic Modeling

Bypass Model mesh

cbec
eco engineering

Project No. 10-1026 | Created By: CRC | **Figure 7**

Legend

Scale: 1 inch equals 7,500 feet

Project Levee

Agricultural Fields, n=0.030

Open Water, n=0.030

Wild Grassland, n=0.045

Maintained Levee Slope, n=0.050

Land use - Reeds and Rushes, n=0.050

Riparian Woodland, n=0.070

Mixed Grassland/Riparian, n=0.120

Bridge Crossing, n=0.070

Element Disabled

Yolo Bypass 2-Dimensional Hydraulic Model Development and Calibration

Plate 2

Source: USACE 2007

cbec
eco engineering

BDCP Effects Analysis – 2D Hydrodynamic Modeling

RMA2 calibrated Manning's n

| Project No. 10-1026 | Created By: CRC | **Figure 8** |
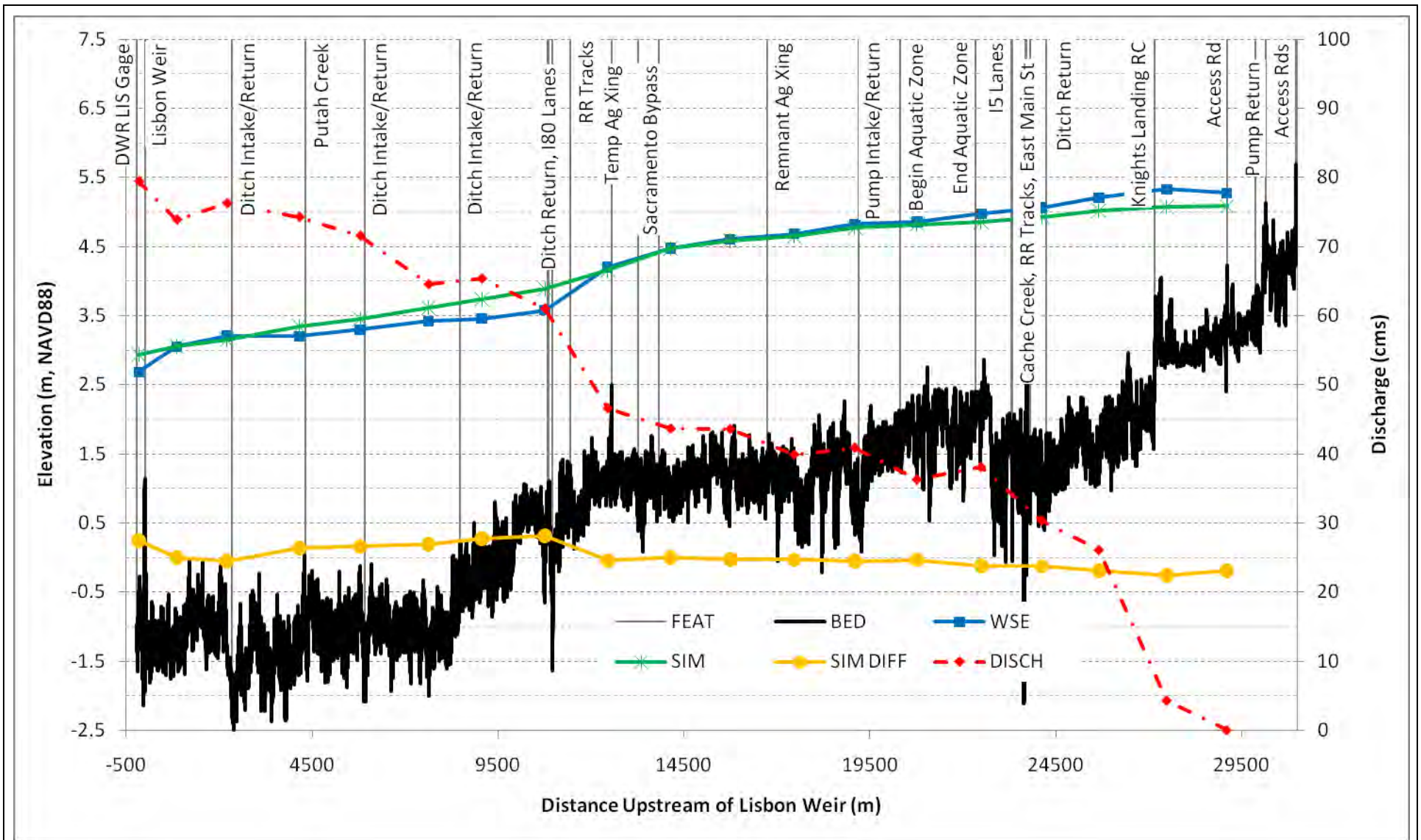
C:\Work\Projects\10-1026_BDCP_Modeling\Reporting\Figures\Fig8_RMA2_Rough.docx
11/7/2010

Source: cbec 2010
Notes: FEAT = feature of interest; BED = bed elevation profile; WSE = water surface elevation; DISCH = discharge profile; SIM = simulated results; and SIM DIFF = difference between simulated and measured results

BDCP Effects Analysis – 2D Hydrodynamic Modeling

Bypass Model calibration

Project No. 10-1026 | Created By: CRC | **Figure 9**

Figure 10. Tidal boundary conditions for inundation scenarios
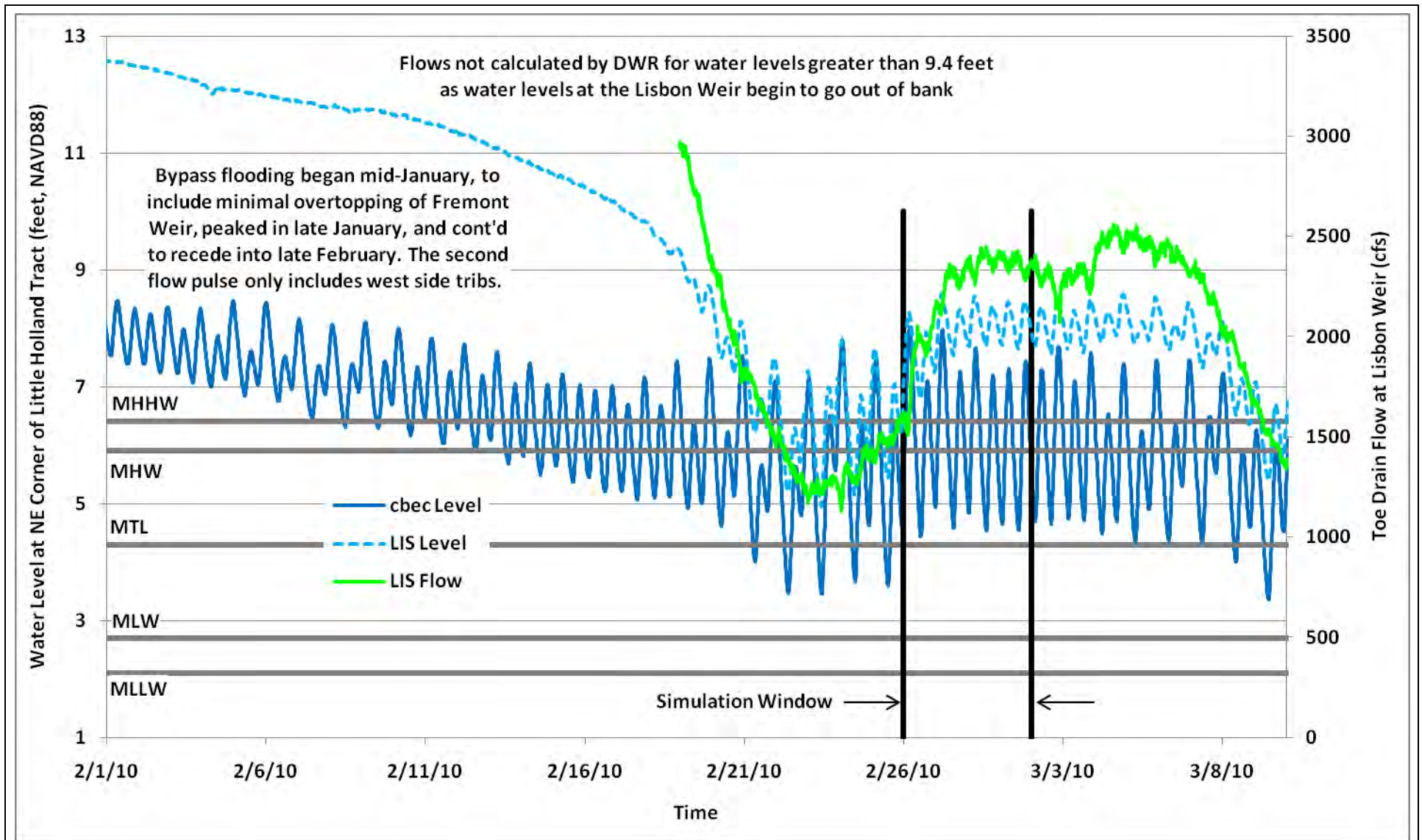
Notes: water level monitored by cbec in Stair Step at northeast corner of Little Holland Tract; discharge data provided by CDEC staff; tidal datums calculated by cbec from monitoring data (unpublished)

BDCP Effects Analysis – 2D Hydrodynamic Modeling

Tidal boundary conditions for inundation scenarios

| Project No. 10-1026 | Created By: CRC | **Figure 10** |

Legend

- 1E (magenta/purple)
- 2E (blue)
- 3E (cyan)
- 4E (teal)
- 5E (green)
- 6E (yellow)
- 7E (orange)
- 8E (red)

Sacramento Weir

Lisbon Weir

Fremont Weir

Knights Landing Ridge Cut

Cache Creek

Willow Slough

Putah Creek

Notes: background courtesy of Bing Maps

C:\Work\Projects\10-1026_BDCP_Modeling\Reporting\Figures\Fig11_Existing_Inun_Overlay.docx
11/8/2010

cbec eco engineering
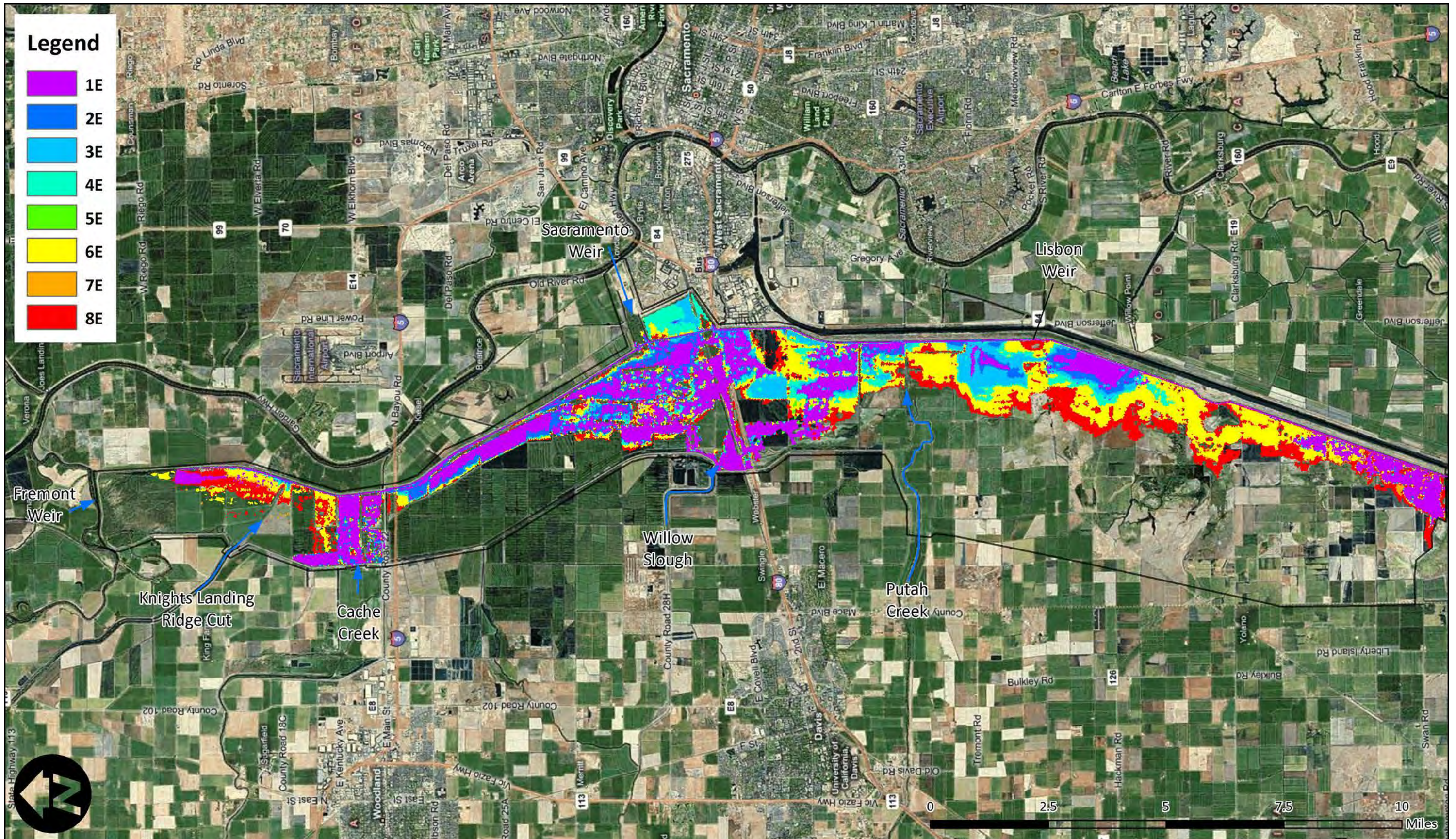
BDCP Effects Analysis – 2D Hydrodynamic Modeling

Existing conditions Yolo Bypass inundation

| Project No. 10-1026 | Created By: CRC | **Figure 11** |
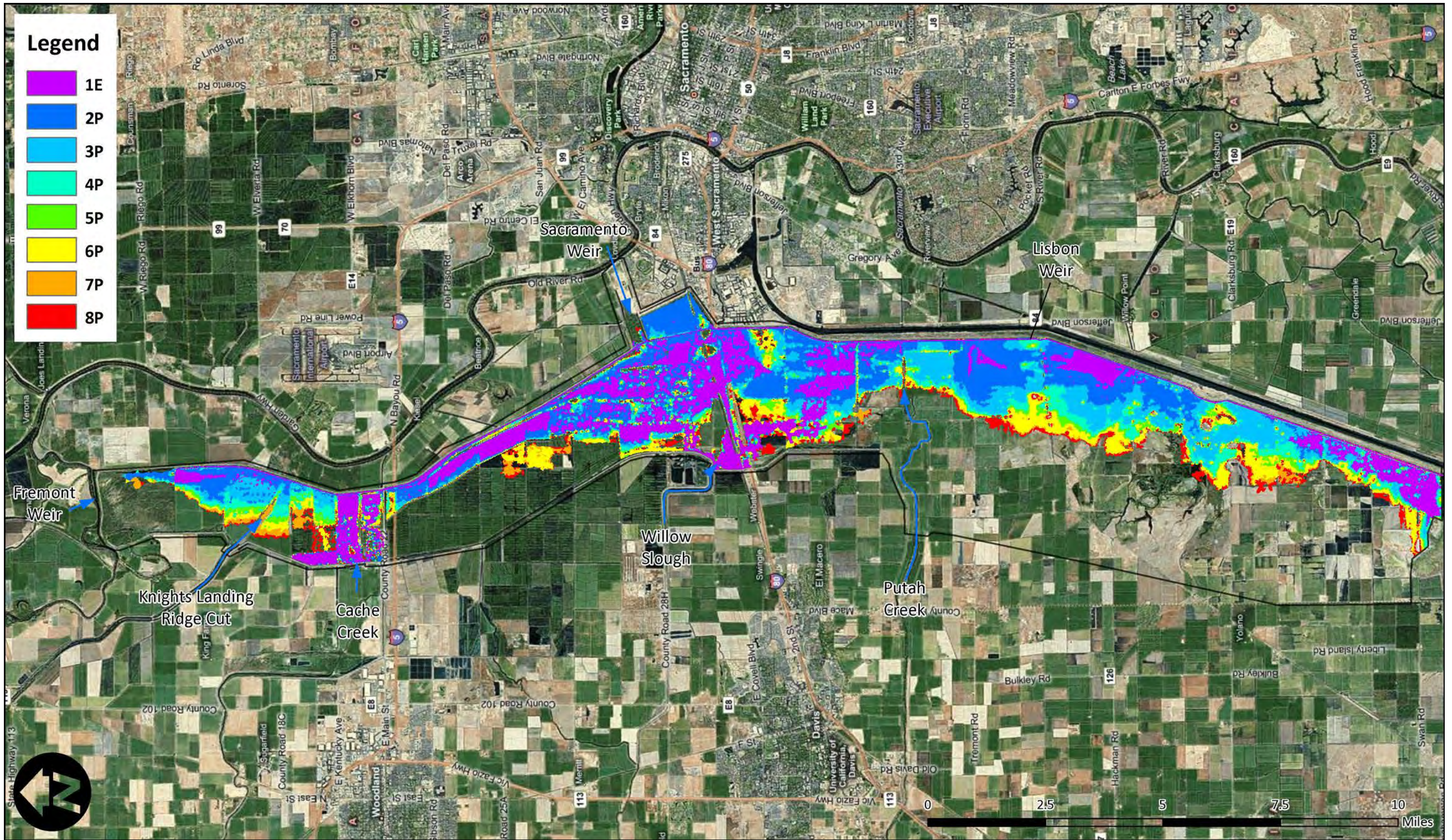
Legend
1E
2P
3P
4P
5P
6P
7P
8P

Sacramento Weir

Lisbon Weir

Fremont Weir

Knights Landing Ridge Cut

Cache Creek

Willow Slough

Putah Creek

BDCP Effects Analysis – 2D Hydrodynamic Modeling

Proposed conditions Yolo Bypass inundation

| Project No. 10-1026 | Created By: CRC | **Figure 12** |

cbec
eco engineering
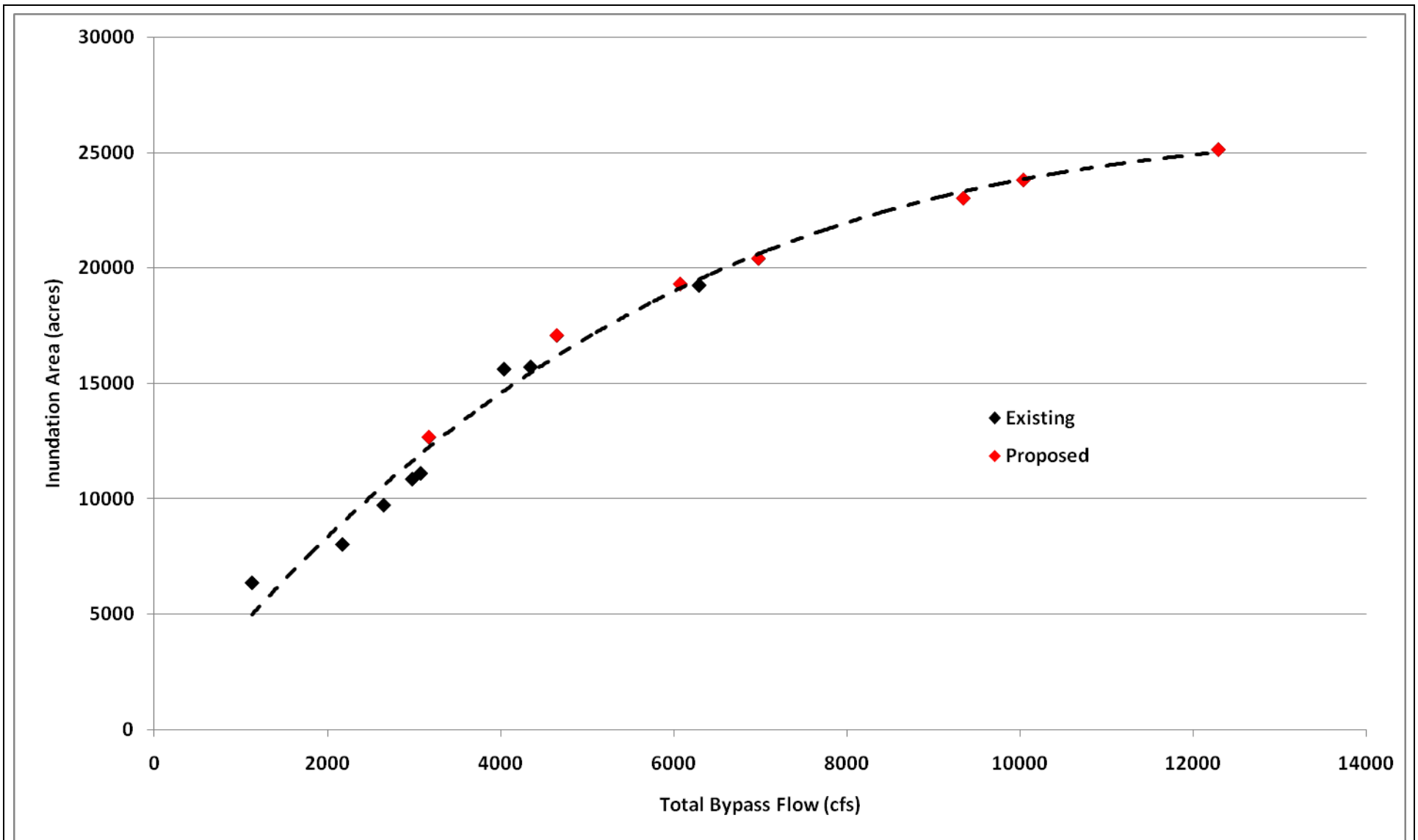
NUMERICAL MODELING IN SUPPORT OF

BAY DELTA CONSERVATION PLAN:

DSM2/QUAL NUTRIENT MODEL

MODELING NUTRIENTS AND TEMPERATURE

JANUARY 2011

RMA RESOURCE MANAGEMENT ASSOCIATES

• Table of Contents

TABLE OF FIGURES

TABLE OF TABLES

scenario. The right-hand columns simply show the sign of the differences calculated in the left-hand columns..**Error! Bookmark not defined.**

1. Executive Summary

The work discussed in this report covers three main topics – documentation on the calibration and validation of the DSM2/QUAL temperature and nutrient model, the application of the calibrated model to Bay-Delta Conservation Plan (BDCP) scenarios, and additional data and model analysis needed to increase confidence in nutrient model application to the changes in bathymetry envisaged for the Proposed Project scenarios. The latter discussion arises from unusual model results in scenarios implementing bathymetric changes assumed under the Proposed Project.

The DSM2/QUAL temperature and nutrient model was recalibrated for this project using historical data for the years 2000 – 2008. Revisions in the nutrient model implementation in previous versions of DSM2/QUAL, including changes to Delta bathymetry (Chilmakuri, 2009), a correction in the nutrient model solution algorithm methodology for the Algae constituent (a proxy for chlorophyll-a), and changes to calibration data for PO_4 necessitated a recalibration of the nutrient model initially calibrated in 2008 for the years 1990 – 2008 (Guerin, 2010). The major change to Delta bathymetry in the most recent calibration was the introduction of Liberty Island to the DSM2 grid of the Delta. Liberty Island flooded around 1997/8, and the new flooded area was introduced into the grid in 2010 as a DSM2 "reservoir" which is conceptualized as a single fully-mixed volume – this is the standard simplification for open water areas in DSM2 even though Liberty Island is tidally influenced and thus has fluctuating areas of "open water".

DSM2 was calibrated at multiple locations in the model domain for water temperature and for each of the nutrients included in the QUAL conceptual model for which there was data. Model calibration was followed by a validation step. Data availability, i.e., the spatial and temporal resolution of calibration data, limits the quality of the calibration. As a consequence, only monthly averaged model output and regionally averaged model output are presented in the analysis of the BDCP model scenarios. Although it is known that introduced species such as Asian clam, *Corbula amurensis*, have had a large impact on nutrients and algae especially in low outflow years, the DSM2 nutrient model had no mechanism for accounting for these benthic species. Thus, calibration results, particularly for algae, are clearly offset seasonally with respect to the data in locations where *Corbula* would likely be present.

Figures illustrating the calibration results and a categorical analysis of the calibration and validation results are included in the main document, while numerical statistical results of the calibration/validation process are included in an Appendix. The number of data points used to calculate model statistics is not large. Thus, although calibration/validation statistics were calculated for all relevant years and also split into wet and dry year types, the statistics may be represented by or dominated by a few measurements in some cases.

The boundary conditions for modeling water temperature – which include meteorological and water temperature boundary conditions – were available hourly. Temperature calibration statistics indicate the quality of the calibration was generally Very Good to Good particularly along the Sacramento River corridor. Modeled water temperature in the South Delta and the upstream section of the San Joaquin R. could be several Celsius degrees cooler than indicated by data in the summer. This offset is mainly due to the limitation in QUAL to a single meteorological region – previous results indicated that a minimum of two meteorological regions are required for modeling water temperature over the entire Delta (Guerin, 2010).

Detailed temperature calibration statistics for the period 2000 to 2008 are documented in an Appendix and discussed in the main report. Details on the temperature model calibration for the time span 1990 - 2008 are documented in (Guerin, 2010). No changes were made to the previous water temperature model parameterization, so any changes to the calibration results are due solely to changes in Delta bathymetry implemented in the revised grid.

Most nutrient model boundary conditions and calibration/validation data were developed from monthly grab samples. Measurements from different agencies (mainly from the Environmental Monitoring Program, EMP, and the USGS) were generally consistent giving confidence in the quality of data from these sources. Organic-P measurements are a notable exception, as there were no in-Delta organic-P measurements, and measurements at the boundary were limited to a few grab samples over 3 – 4 years at a couple of inflow boundaries. PO_4 measurements, although limited, had some in-Delta spatial and temporal availability. There was no data available in the publically accessible databases for macroalgae or for sediment interactions, such as sediment mineral sources or sinks for nutrients.

The calibration statistics for most nutrient model constituents ranged from Satisfactory to Very Good at most locations of interest to the BDCP studies, which focused on the Sacramento R. downstream of Rio Vista, the lower San Joaquin R. and Suisun Bay.

Two important areas in the model, Suisun Marsh and the Cache Slough/Liberty Island area, had little or no data for setting boundary conditions for the nutrient model. Results for nutrients in Suisun Marsh are therefore speculative. After the model calibration was complete, data from a 2004 -2005 project in Liberty Island was obtained. Comparison between model and data indicates that the boundary conditions for inflow to Liberty Island need to be changed, and perhaps some of the parameters conceptualizing benthic interactions and algal growth may also need to be changed.

This combination of factors, especially the limited spatial and temporal availability of calibration and boundary conditions data, combine to limit the interpretation of nutrient model results for all constituents(except temperature) to monthly averages, and to further limit exclude the use of organic-P model output entirely. The relatively complete set of boundary conditions and uniformly good quality of the calibration/validation results for modeled water temperature

indicate that the temperature sub-model is more robust than the nutrient model. Diurnal fluctuations are captured as assessed in calibration datasets with hourly data.

The BDCP scenarios, covering modeled years 1976 – 1991, represent proposed or predicted changes to Delta bathymetry, to Delta operations (such as exports and the volume and timing of reservoir releases), to meteorological conditions due to climate change, and to stage height at the tidal boundary (at Martinez) due to sea level rise. Differences in model output between the scenarios and an Existing Biological Condition (EBC), the current condition case, therefore reflect changes due to these conditions alone. Changes in nutrient concentrations at the inflow boundaries due to upstream effects from climate change, changes in runoff, changes in reservoir usage, changes in effluent volume due to population changes or any of a number of possibly influential parameters were not considered. Changes in nutrient concentration were considered only at the upstream portion of the model on the Sacramento R. through variation on Sacramento Regional effluent concentrations, and then only for nitrogen-constituents (N-constituents).

Boundary conditions representing current-day (2000 – 2005) conditions in the Delta were synthesized for the QUAL nutrient and temperature model from data. A single set of nutrient concentrations and effluent boundary conditions were developed and applied to all of the scenarios. With the exception of the addition of effluent inflow from wastewater treatment plants discharging into the Delta, hydrodynamic conditions for each of the BDCP model scenarios were used without alteration. Effluent inflow and nutrient concentrations were synthesized from existing effluent data, and the resulting boundary conditions the boundary conditions were applied to all of the scenarios. Three main analysis regions were used for comparison of the scenarios – several representative model output locations were selected and averaged to represent results in each region. For the EBC scenarios, four additional regions were used to summarize the changes from the EBC simulations in future years.

Meteorological and water temperature boundary conditions were developed independently from the boundary conditions for constituents in the nutrient model. Projected daily average temperatures for the two future climate change conditions were used as a basis for formulating meteorological boundary conditions. The new meteorological time series was developed by closely matching average air temperature under climate change conditions with historical air temperature at approximately the same annual date (+/- 2 days), creating a correspondence between these historical dates with the model dates. Existing hourly meteorological data from the historical dates was then used to build the model time series for meteorological and water temperature boundary conditions.

Boundary conditions for nutrients representing current-day, 2000 – 2005, conditions in the Delta were synthesized using existing nutrient data for river and effluent inflow boundaries for each modeled year (1976 – 1991), creating a correspondence between each model year with one historical year. Sacramento or San Joaquin Water Year Types for 2000 – 2005 were used as a general guide for creating this correspondence, and historical Sacramento or San Joaquin R.

3

nutrient concentration boundary conditions (respectively) were applied for each year 1975 – 1991 (i.e., boundary conditions were applied on an annual year basis, not by water year). Model year 1975 was used as a "spin-up" year for the nutrient model concentrations. Sacramento Regional Wastewater Treatment Plant (SRWTP) effluent flows were scaled, using this year-correspondence, to assure the percentage of effluent flow in Sacramento R. inflow remained below the historical 2000 -2005 daily maximum (~ 4.5%). All other effluent flows were applied without scaling using the same annual year selection as the Sacramento R. boundary years.

Model results for the scenarios comparing EBC simulations (a current condition case, and two future conditions) reflect changes without the Proposed Project. Differences among these scenarios are attributable to changes in inflow, meteorology and sea level rise. The differences between these simulations are modest. The modest changes in modeled water temperature mainly reflect changes in meteorological boundary conditions. Changes in water temperature appear to be a very minor factor contributing to changes in reaction rates in the modeled constituents. Changes in the quantity and timing of inflow also contributed to changes in nutrient levels.

Increases in the amount of open water area, conceptualized as 'reservoirs' in DSM2, simulated in the Proposed Project scenarios were the major factor contributing to the large changes in constituent concentrations in comparison with the EBC (no-project) simulations. The results of these scenarios indicate that the current model parameterization for open water areas is most probably incorrect.

Large increases in PO_4 concentration were seen in the Proposed Project scenarios – these increases were not expected and indicated that these simulations should not be accepted as reasonable. In addition to the large increases in PO_4, large changes in Algal growth and NO_3 were seen in these simulations. The conclusion was that model parameterization in the new open water areas was responsible, and the suspicion was that one benthic parameter was causing the high PO_4 values.

Due to these unexpected results, a simple sensitivity analysis was performed to verify that the suspect parameter, which simulates benthic release of PO_4, was causing the problem. Removing this source of PO_4 does lead to more reasonable PO_4 concentration in a Proposed Project model. However, agricultural sources of nutrients in the model ("DICU" sources) are also a potential source of high nutrient levels particularly on the San Joaquin R. and possibly also in the south Delta.

As documented in the original DSM2 nutrient model calibration report (Guerin, 2010), there is clearly the need for special studies investigating: the effect of introducing Liberty Island into the DSM2 nutrient model; and, the concentration of DICU nutrient inflow. Although the DSM2 nutrient model calibration is reasonable (given the resolution of calibration data), these two areas are sources of high uncertainty that have surfaced as problems in extending the nutrient model to include the large open water areas called for in the Proposed Project.

Several steps (special studies) can be taken to investigate and potentially correct the current DSM2 nutrient model parameterization of reservoirs and the influence of DICU concentrations:

1. Obtain nutrient data from special studies carried out by DWR and by the USGS to recalibrate the parameterization of Liberty Island, and other open water areas such as Mildred Island. Such studies have been completed, but the data is not available on publically accessible databases.

2. Investigate the conceptualization of areas such as Liberty Island as "reservoirs" in DSM2. It is possible that the magnitude and timing of reactions in these reservoirs have a large influence on nutrient dynamics in surrounding channels in DSM2, and that this conceptualization may be inadequate for use in Proposed Project scenarios. This could be accomplished by modeling Liberty Island in the RMA two-dimensional water quality model, which has the ability to model nutrients, using DSM2 nutrient model output to supply boundary conditions downstream of Liberty Island.

3. Identify local experts on sediment/water column interactions in the Delta to obtain information on the likely interactions.

4. Review the currently available information on agricultural sources of nutrients that form the basis for the DICU concentrations – such data has been compiled by DWR.

Background

Restoration of tidal marsh has been proposed by the Bay-Delta Conservation Plan process (BDCP) for various regions of the Delta, denoted Restoration Opportunity Areas (ROAs), to improve habitat diversity and food availability for covered species. Preliminary simulations have been performed to assess the impacts of operations, sea level rise, climate change and tidal marsh restoration on nutrient levels and temperature using the DSM2/QUAL temperature and nutrient model (nutrient model). Hydrodynamic and meteorological boundary conditions for each simulation reflect changes in salinity intrusion and stage due to sea level rise, changes in meteorological conditions due to climate change, and changes in Delta flows due to modified Delta operations.

Six "Standard" simulations were originally developed based on two alternatives, "Existing Biological Condition" (EBC) and "Proposed Project" (PP) each with three time step scenarios in the tidal marsh restoration process: current condition with no restoration, no sea level rise and current climate conditions (Base); Early Long-term (ELT) with 25,000 acres of restoration, 15 cm of sea level rise and altered meteorological conditions simulating climate change, and Late Long-Term (LLT) with 65,000 acres of restoration, 45 cm of sea level rise and additional altered meteorological conditions simulating additional changes in the climate. With the exception of

metrological and water temperature boundary conditions, all of the nutrient model boundary conditions are identical for these six scenarios. However, flow and stage boundaries vary between the scenarios.

Only five of these simulations were analyzed – the PP alternative under current-day conditions was not included in the final analysis. In addition, two scenarios with modified nitrogen constituent (N-constituent) levels near the Sacramento inflow boundary were developed and analyzed for each of the alternative/time step scenarios, for a total of ten additional nutrient model simulations. The "Reduced Sacramento NH3" (Remove NH3) scenario removed ammonia, denoted herein by NH_3, in effluent inflow near the Sacramento boundary, and the "Altered NH3/NO3 Levels" scenario decreased NH_3 and increased NO_3 by a proportion of that decrease in effluent inflow to the Delta. Details on the methodology used to implement these changes are documented in subsequent sections.

This progress report documents progress to date on calibration of the DSM2/QUAL nutrient, a sensitivity analysis of selected changes to reservoir parameterization and delta island consumptive use (DICU) inflow concentrations, model as well as preliminary results for each of the twenty nutrient model simulations. RMA has completed a calibration and validation of the DSM2/QUAL nutrient and temperature model, as well as numerical modeling exercises and preliminary analysis of nutrient model results for the Standard simulations and for the two modified N-constituent models under the three time step scenarios. Model output has also been provided to SAIC for incorporation in food web and fisheries analyses.

DSM2/QUAL Nutrient Model

The Delta Simulation Model-2,[1] or DSM2, is a one-dimensional model that was used in this project to model nutrient dynamics in the Delta under a range of changes to Delta bathymetry due to the restoration of tidal marsh area, as well as changes due to Delta operations, sea level rise and climate change.

DSM2 is a suite of models developed by California's Department of Water Resources (DWR). The hydrodynamic and water quality modules, HYDRO and QUAL, respectively, have been developed by DWR to model historical conditions in the Delta – this implementation is called the "Historical Model"- as well as hypothetical scenarios.

Objectives

---

[1] http://baydeltaoffice.water.ca.gov/modeling/deltamodeling/models/dsm2/dsm2.cfm

The main objectives of the work discussed in this document were to: (1) calibrate DSM2/QUAL to simulate temperature and nutrient interactions; (2) document model parameterization and boundary conditions that need further analysis; and, (3) provide information to assist development of food web and fisheries conservation measures in the BDCP process and to assess the anticipated changes to nutrient levels (NH_3, NO_3, NO_2, organic-N, algae/chlorophyll-a, and PO_4), dissolved oxygen (DO) and temperature due to the introduction of tidal marsh, sea level rise, climate change and Delta operations.

2. DSM2 Model Description

DSM2 – General information

DSM2 is a one-dimensional (1-D) hydrodynamic and water quality simulation model used to represent conditions in the Sacramento-San Joaquin Delta. The model was developed by the Department of Water Resources (DWR) and is frequently used to model impacts associated with projects in the Delta, such as changes in exports, diversions, or channel geometries associated with dredging in Delta channels. It is considered the official Delta water quality model, and as such it has been used extensively to model hydrodynamics and salinity as well as Dissolved Organic Carbon (DOC). Salinity is modeled as electrical conductivity (EC), which is assumed to behave as a conservative constituent.

The simplification of the Delta to a one-dimensional (1-D) model domain means that DSM2 can simulate the entire Delta region rapidly in comparison with higher dimensional models. Although many channels in the Delta are modeled well in 1-D, the loss of spatial detail in areas that are clearly multi-dimensional limit DSM2's accuracy in those areas.

DSM2 contains three separate modules, a hydrodynamic module (HYDRO), a water quality module (QUAL), and a particle tracking module (PTM). HYDRO was developed from the USGS FOURPT model (USGS, 1997). DWR adapted the model to the Delta, accounting for such features as operable gates, open water areas, and export pumps. The water quality module, QUAL, is based on the Branched Lagrangian Transport Model (Jobson, 1997), also developed by the USGS. QUAL uses the hydrodynamics simulated in HYDRO as the basis for its transport calculations. The capability to simulate nutrient dynamics and primary production in QUAL was developed by Rajbhandari (1995). The third module in the DSM2 suite is PTM, which simulates the fate and transport of neutrally buoyant particles. PTM also uses hydrodynamic results from HYDRO to track the fate of particles released at user-defined points in space and in time.

Detailed descriptions of the mathematical formulation implemented in the hydrodynamic module, DSM2-HYDRO and for salinity in the water quality module, DSM2-QUAL, the data required for simulation, calibration of HYDRO and QUAL, and past applications of the DSM2 Historical model are documented in a series of reports available at:

Documentation on the calibration and validation of the HYDRO module and the QUAL module for salinity used in the current implementation of DSM2 is available at that website. The calibration of DSM2 has generally focused on hydrodynamics and the transport of salinity, modeled as electrical conductivity (EC), and of dissolved organic carbon (DOC). The current calibration of HYDRO in DSM2 Version 8 for these constituents is assumed to be sufficient for our purposes.

Recently (Guerin, 2010), the temperature and nutrient models in QUAL Version 6 were calibrated in the Delta to model the transport of nutrients and water temperature as an extension of the base Historical Model implementation from 1990 - 2008. This recent calibration and the data collected to support the nutrient model calibration served as the basis for the work described in this document.

With the introduction of a new bathymetry in the DSM2 model grid of the delta to incorporate the flooding of Liberty Island (in the Cache Slough area) due to a levee break in 1997, a recalibration of the hydrodynamics in HYDRO for this bathymetry change (Chilmakuri, 2009), and a new version for the DSM2 suite of models, Version 8[2], that corrected an error in the formulation of the algae constituent dynamics in the nutrient model, a recalibration of the nutrient model was required.

The Version 6 nutrient model calibration (Guerin, 2010) required the collection and synthesis of a large quantity of data needed to set the model boundary conditions over the modeled time span, 1990 – 2008, and to calibrate and validate the model calculations for each of the eleven constituents conceptualized in QUAL. The description of the data used in that project, and subsequently for recalibration of the QUAL nutrient model in this project, is covered in detail in (Guerin, 2010).

Base Model

Figure 2-1 shows the changes to the network of the DSM2 model (Chilmakuri, 2009) used for the EBC-Base hydrodynamic and DSM2/QUAL simulations in this study. The major changes are the inclusion of the Liberty Island open water area (this is modeled as a "reservoir" in DSM2 terminology) and an extension and refinement in the grid at the northern boundary of the model.   Figure 2-2 shows the earlier DSM2 Version 6 grid with channels, nodes and open water areas other than Liberty Island.

---

[2] http://baydeltaoffice.water.ca.gov/modeling/deltamodeling/models/dsm2/dsm2.cfm
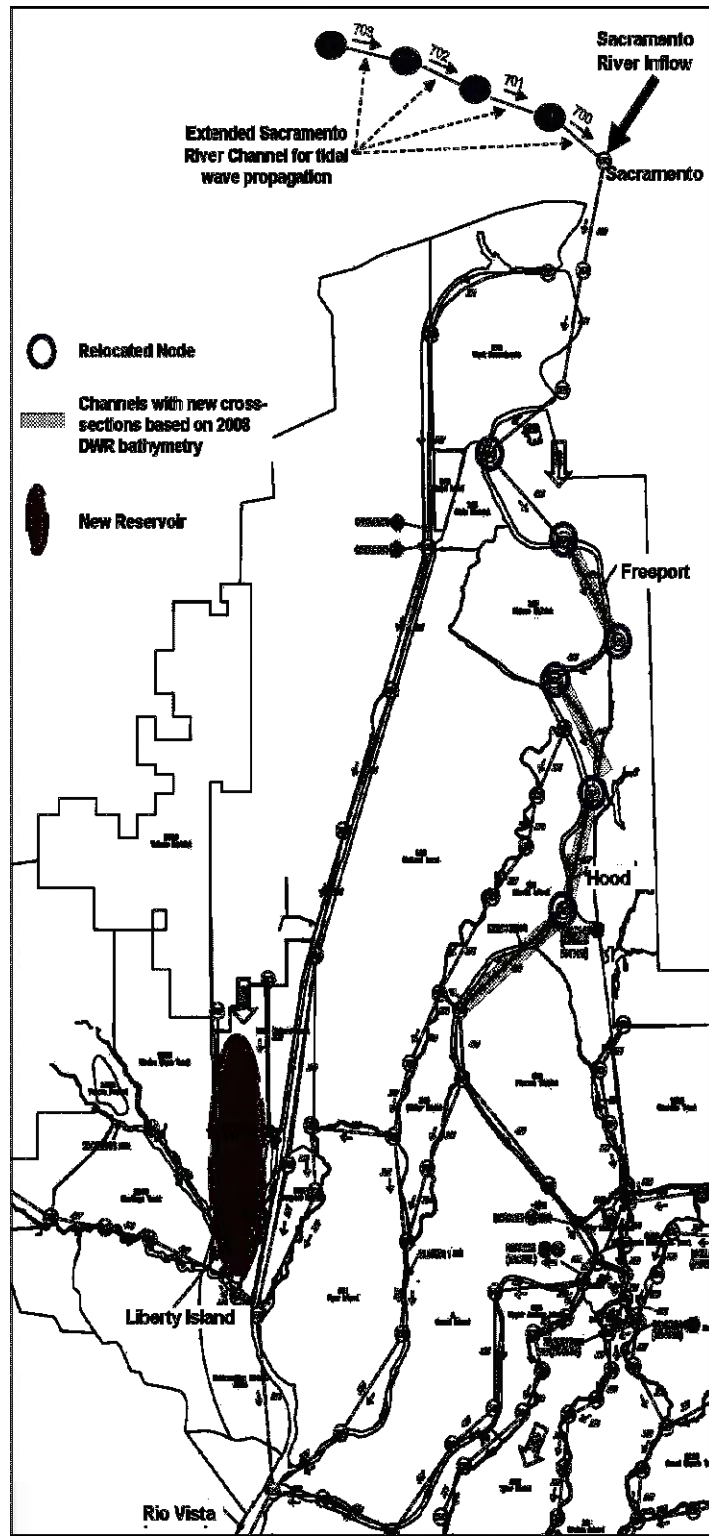
Figure 2-1 Changes implemented in the DSM2 V.8 model grid showing the new Liberty Island "reservoir" location, and changes to the grid and modes along the upstream portion of the Sacramento River.

1. Franks Tract
2. Bethel island
3. Mildred Island
4. Discovery Bay
5. Clifton Court Forebay
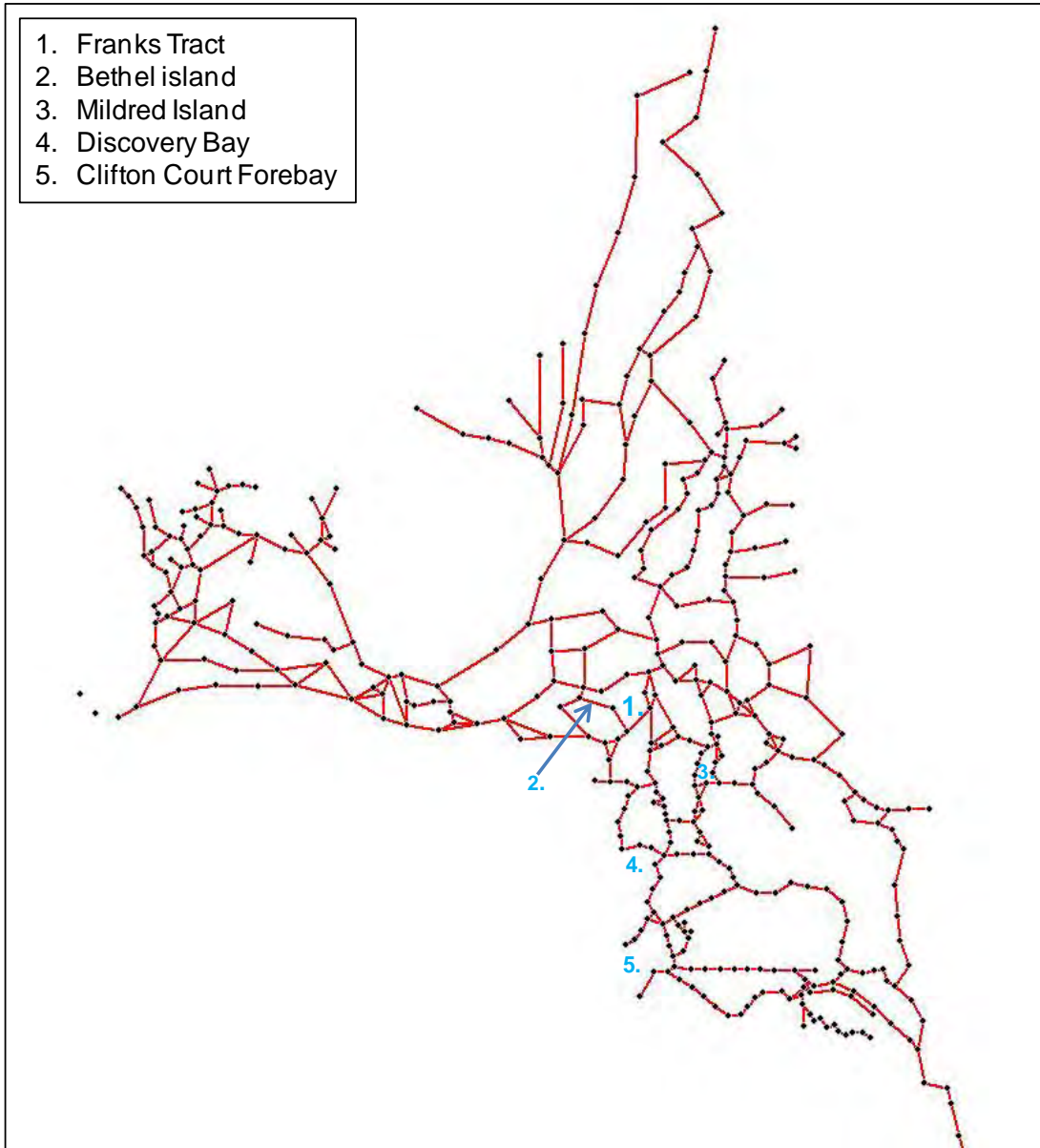
Figure 2-2 DSM2 Version 6 model grid showing channels (red), reservoirs (blue numbers), and nodes (black).

ELT Model

The restoration acreage goal for the Early Long-term (ELT) restorations scenario is 25,000 acres. The modeled ELT restoration scenario consists of 12,900 acres in the Cache Slough ROA, 8,130 acres in Suisun Marsh, 3,990 acres in the West Delta ROA, and 2,900 acres in the Mokelumne-

Cosumnes ROA. There is no restoration in the East Delta ROA or South Delta ROA for the ELT case.

LLT Model

The restoration acreage goal for the Late Long-term (LLT) restorations scenario is 65,000 acres. The modeled LLT restoration scenario consists of 20,330 acres in the Cache Slough ROA, 14,390 acres in Suisun Marsh, 4,240 acres in the West Delta ROA, 3,290 acres in the Mokelumne-Cosumnes ROA, 2,160 acres in the East Delta ROA and 22,480 acres in the South Delta ROA. All ELT areas are included in the LLT grid. There is additional restoration in the East Delta ROA and South Delta ROA for the LLT case.

3. Description of the QUAL nutrient model

The implementation of the DSM2 modules HYDRO and QUAL discussed in this report extends the standard configuration of the "Historical Model" by including effluent inflow from most of the wastewater treatment plants (WWTPs) with outfalls within DSM2's model domain in the Delta. Although the volume of many of these effluent inflows is small in comparison with other inflows to the Delta, they are important sources of the nutrients modeled in QUAL.

Previous nutrient models using DSM2/QUAL

Previous uses of QUAL to simulate nutrient dynamics in the Delta focused on dissolved oxygen (DO). Rajbhandari (2000, 2001, 2003, 2004, and 2005) used QUAL to model DO dynamics on the San Joaquin River, addressing concerns about low DO in the vicinity of Stockton. Subsequently, the application and area of DO calibration was extended to the San Joaquin Deep Water Ship Channel. The final application focusing on DO extended model development to a wider region of the Delta to support technical studies for the In-Delta Storage Project Feasibility Study. This model study assessed the potential impact of the project on temperature and DO levels using CALSIM II (Rajbhandari, 2004)) output for the hydrological conditions in the 16-year scenarios (1975 – 1991). This type of study is an example of a Planning Study in which DSM2 is used to quantify the effects a modification in the Delta water regime, such as construction of a new gate, may have on hydrodynamics and water quality. Many DSM2 Planning models currently cover the period from 1922 to 2003 using CALSIM II simulated hydrology.

HYDRO flow and stage boundaries

Boundaries that define the movement of water into and out of the Delta, and thus also the movement of nutrients, consist of inflow boundaries, outflow boundaries and a stage boundary set at Martinez. In Figure 3-1, the main inflow boundaries are denoted by blue stars. These boundaries are found at the each of the major rivers (Sacramento, San Joaquin, Calaveras, Mokelumne and Cosumnes), and at the Yolo Bypass and the Lisbon Toe Drain (in the Yolo region). The Yolo boundary only has inflow during periods of high Sacramento River inflow which can occur late fall through early spring. Flows at the Lisbon Toe Drain near Liberty Island on the north western edge of the Delta, used in the Version 6 implementation of the nutrient model and the Version 8 calibration discussed herein, are incorporated in the Yolo flow boundary for each of the BDCP scenarios discussed in this document.

Figure 3-2 shows the approximate location of effluent inflow boundaries discussed in this report. The volume of effluent water is small in comparison with other inflow contributions except in periods of very low inflow.

The effects of evaporation, precipitation, and channel depletions and additions ascribed to agricultural influences are modeled using the Delta Island Consumptive Use (DICU) model[3]. This model is used to set boundary conditions at 258 locations throughout the Delta – these locations are subdivided into 142 regions. DICU flow boundary conditions vary monthly by region and are set by Water Year Type. The uncertainty in the estimates of DICU inflow, outflow and constituent concentrations is high. During periods of low inflow, errors in volumes ascribed to DICU boundaries may dominate model results.

QUAL's Conceptual Model for Nutrient Dynamics

Figure 3-3 is a conceptualization of the interactions between the main constituents used to model nutrient dynamics in the QUAL mass transport model. This figure is an adaptation of figures shown in (Rajbhandari, 2003). Each box (or oval) in the blue region (water) symbolizes one of the nine equations for non-conservative constituents in the transport model. There are equations for: dissolved oxygen (DO); nitrate (NO_3); nitrite (NO_2); ammonia (NH_3); organic-N; carbonaceous biochemical oxygen demand (CBOD); orthophosphate (PO_4), denoted dissolved-P in the Figure; organic-P; and, algae. Chlorophyll a (Chl-a) measurements are used to calculate the biomass of algae in the model. Salinity is modeled as a conservative constituent - it is not included in Figure 3-3.

Arrows in Figure 3-3 indicate a relationship, modeled as a temperature-dependent reaction rate, between two variables or for adding or removing mass into or out of the model calculation for a given constituent, respectively. Water temperature influences the dynamics of the constituent interactions as a factor in the rate of reactions - an increase in water temperature results in a change, generally an increase, in reaction rates. Conversely, modeled DO saturation decreases with increased temperature. Water temperature is not influenced by any reaction modeled in QUAL.

Although each of the constituents occurs in an ionized form in aqueous solutions, charges on the constituents are not used in the model or in this report except where specifically indicated. In reality, each constituent occurs in a suite of sub-species in solution with variable charge and potentially associated with many other aqueous species. As this level of interaction is not explicitly accounted for QUAL, no single charge can be legitimately assigned.

---

[3] http://www.iep.ca.gov/dsm2pwt/reports/DSM2FinalReport_v07-19-02.pdf,
http://baydeltaoffice.water.ca.gov/modeling/deltamodeling/models/dicu/DICU_Dec2000.pdf

An important distinction needs to be made between term "ammonia" and the concentrations of each of the chemical species NH_3 and NH_4^+. NH_3 occurs naturally as a gas that is dissolved in the aqueous phase, but the gas is also ionized to NH_4^+, *i.e.* ammonium, in a pH-dependent reaction in solution. At neutral pH (pH = 7.0), the majority of the "ammonia" in solution occurs in its ionized form as NH_4^+. For example, at a water temperature of 25°C the equilibrium reaction constant, $\log_K$, for the aqueous association reaction yields that approximately 50% of the "ammonia" occurs as NH_4^+ at pH 9.5. The amount of NH_4^+ increases with decreasing pH, so that at pH 8.5 only about 9% of the ammonia is present in its unionized (NH_3) form. In most of the Delta, the pH is typically less than pH 8.5 except for episodic, localized increases.

Because QUAL does not explicitly model pH and cannot distinguish between the unionized and ionized forms, the term "ammonia" is used in this report to indicate the total concentration[4] of $[NH_3] + [NH_4^+]$. A simplifying assumption in interpreting model results is that the majority of the "ammonia" concentration reported in calculations is occurring in the ionized "ammonium" form. Measured data collected for setting boundary conditions and as calibration/validation data is generally reported by the collecting agency as "ammonia", and is actually reporting the total $[NH_3] + [NH_4^+]$.

The conceptual model and the equation describing the dynamics for each constituent is discussed in greater detail in (Guerin, 2010).

---

[4] Unlike the convention in aqueous chemistry, square brackets are used to symbolize the concentration of an aqueous species (not the activity) in solution. The units of concentration are understood to be the units in the model unless specifically stated otherwise.
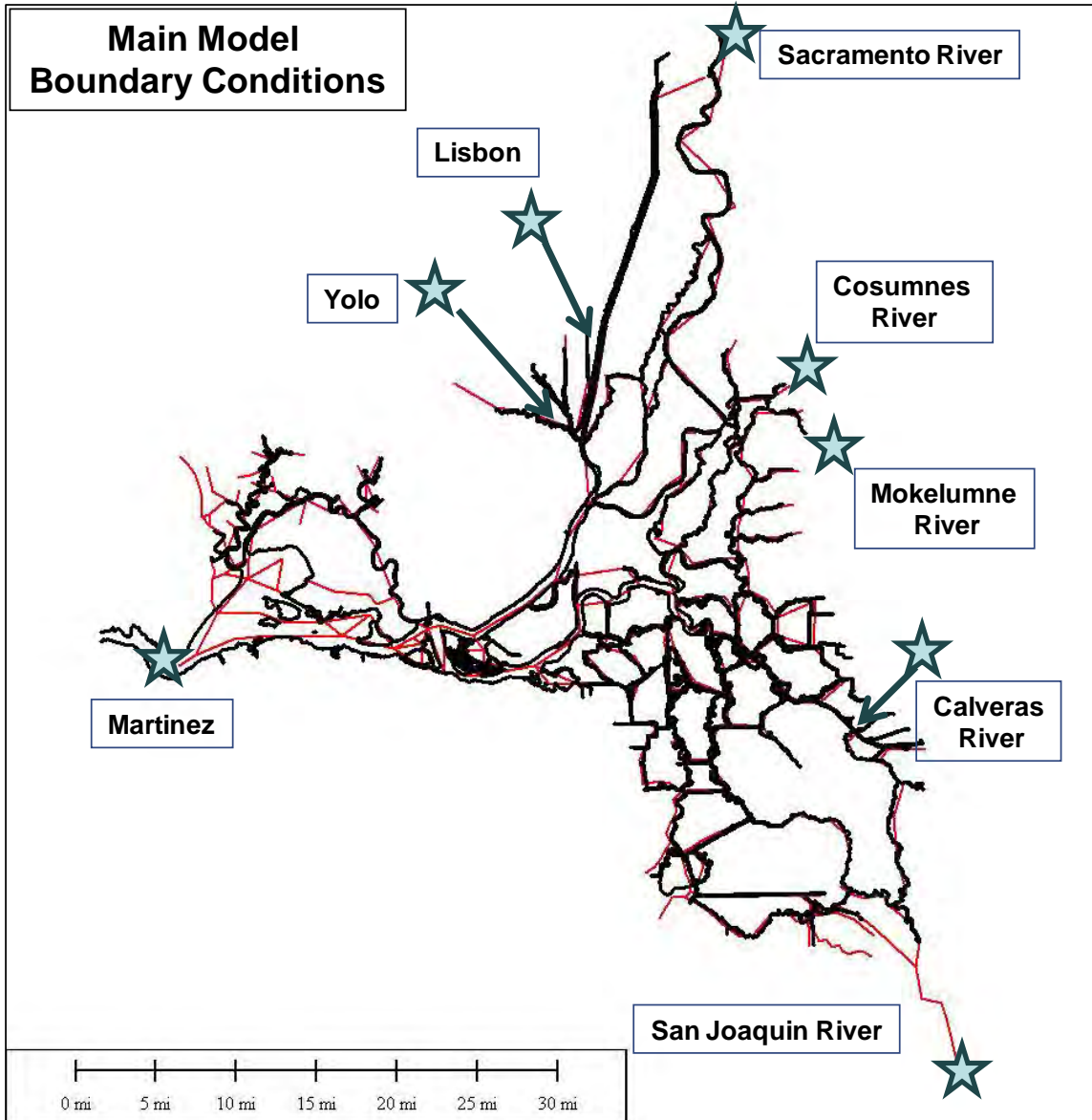
Figure 3-1 Approximate location of the model inflow (or outflow) boundaries (blue stars). The stage boundary is at Martinez.
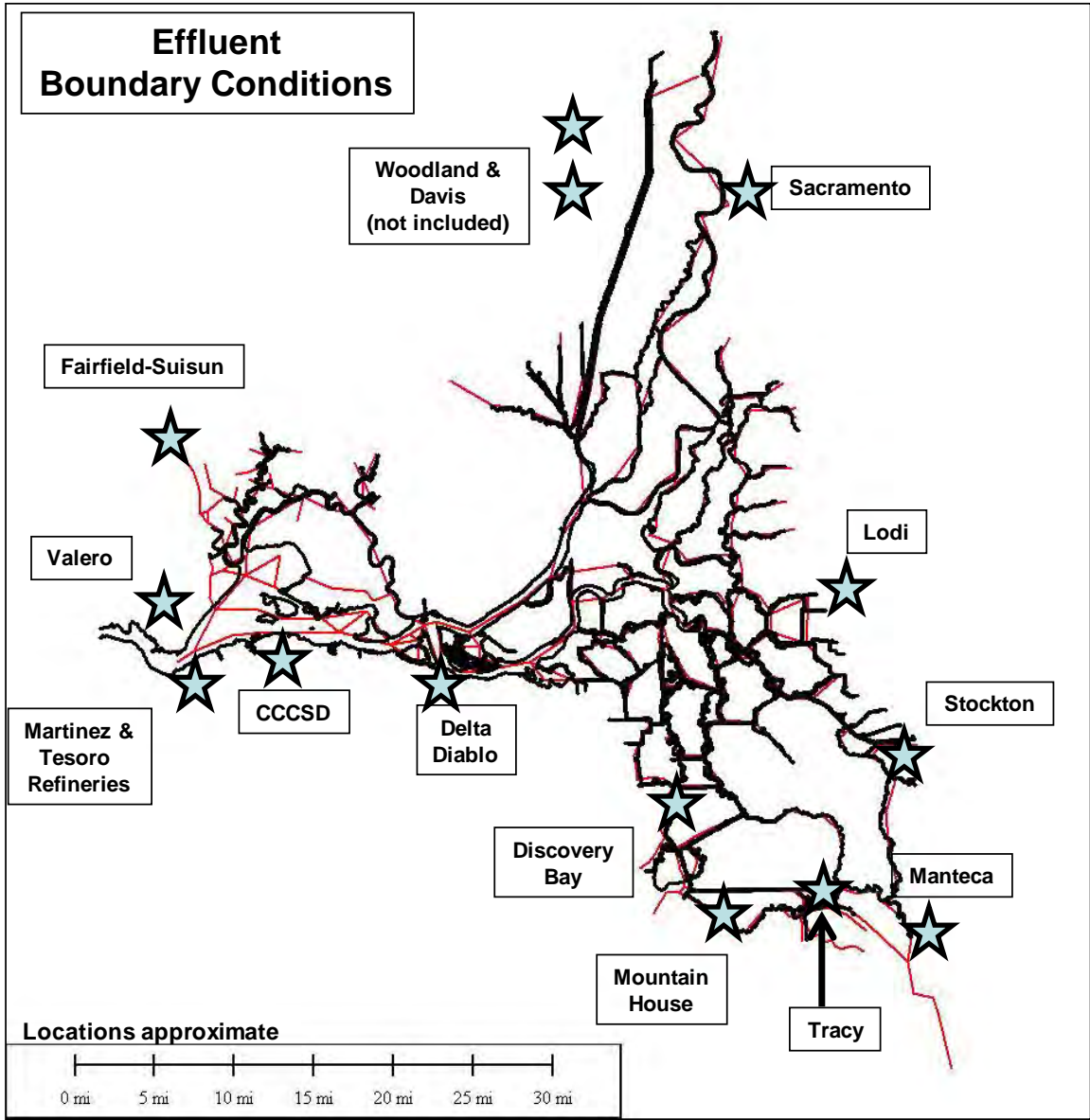
Figure 3-2 Approximate location of effluent boundary conditions for waste water treatment plants considered in this report.
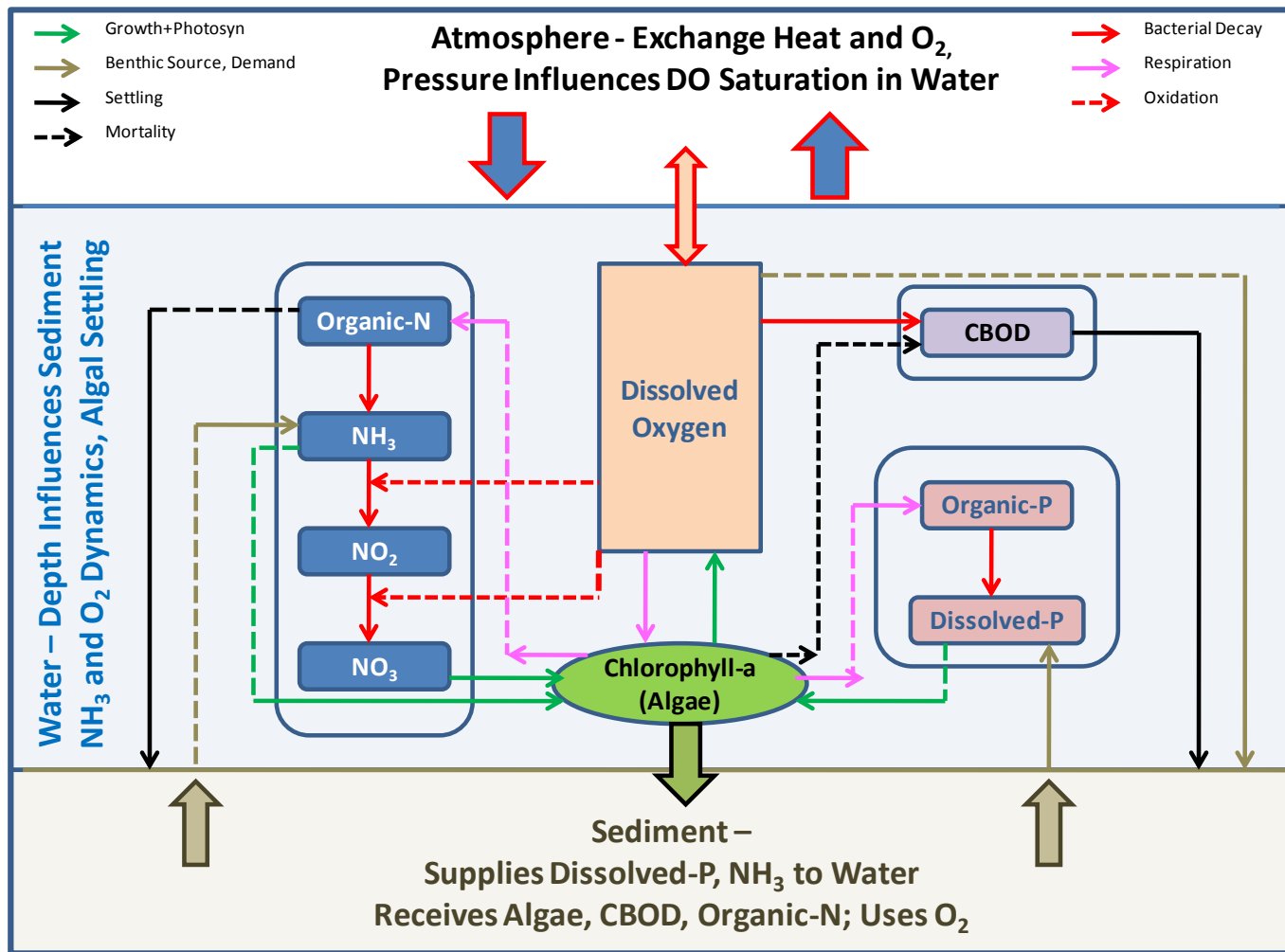
Figure 3-3 The interactions between main nutrient model constituents, and external influences (an adaptation from original DWR references). Water temperature (blue region) influences reaction rates, denoted by arrows.

4. Nutrient Model Calibration

Background

Data acquisition to support the nutrient and temperature model calibration is discussed in the Appendix, Section 8. Discussion on the sources and quality of this data is covered in great detail in (Guerin, 2010).

Both graphical and statistical model evaluation techniques were used in the analysis of calibration and validation results. Because nutrient data was only available on a monthly basis and the number of values available was limited, only two types of hydrologic conditions[5] were considered is assessing the quality of the calibration. The Wet type is composed of Wet and Above Average Water Year types, while the Dry type is composed of Critically Dry and Dry Water Year types:

	Calibration Years	**Validation Years**
DRY	2001, 2002	2007, 2008
WET	2000, 2003	2005, 2006

Water temperature calibration and validation statistics were calculated on an annual basis by Wet or Dry Water Year Type at each available location. Nutrient calibration results were grouped for the calculation of calibration statistics for the entire calibration/validation period (all years, i.e., 2000 – 2003 plus 2005 – 2008). These years were also subdivided into calibration and validation ranges, shown in table inserted into the text above, and grouped into Dry Years and Wet Years.

Several statistics were calculated, but only three statistical measures are recorded and discussed herein – Nash-Sutcliffe Efficiency (NSE), RMSE-Standard deviation Ratio (RSR), and Percent Bias (PBIAS). These statistics give an overall view of the quality of the calibration – the statistical measures are discussed in THE NEXT Section. At each location where calibration data was available, model statistics were calculated and ranked categorically as Very Good, Good, Satisfactory or Unsatisfactory using ranges of the statistics to perform the rankings. Ranges for model calibration performance ratings for the NSE, RSR and PBIAS statistics are discussed in (Moriasi *et.al.*, 2007). Different statistical ranges were used for temperature calibration and validation than for the nutrient model, as the data availability and quality was very different between the two.

---

[5] See: http://cdec.water.ca.gov/cgi-progs/iodir/wsihist for a discussion of water year type.

Definition of the statistical measures

The following methodology and statistics adapted from (Moriasi et al., 2007) were used:

Mean Residual – The mean of the residual values gives an indication of the magnitude of model under-prediction (positive residuals) or over-prediction in a region. The optimal value is zero, which occurs in the unlikely situation that the model is a perfect fit for the data.

Standard Deviation of Residual – The standard deviation of the residual values gives an indication of the variability in model under-prediction and over-prediction in a region.

Residual Histogram – The histogram documents the shape of the residual distribution. Along with the mean and standard deviation, this gives a first-order view of the goodness of model fit. The ideal histogram would have an approximately normal shape centered at zero with a small spread. Histograms were prepared using annual calculations at each location.

MSE – The Mean Squared Error is a standard statistic that measures the quality of the prediction. The optimal value is zero:

$$MSE = \left| \frac{\sum_{i=1}^{n}\left(Y_i^{Obs} - Y_i^{Sim}\right)^2}{n} \right| \quad (A3)$$

RMSE – The Root Mean Squared Error is a standard statistic used to indicate the accuracy of the simulation. It is the square root of the MSE. The optimal value is zero.

NSE – The Nash-Sutcliffe Efficiency is a normalized statistic that measures the relative magnitude of the residual variance compared to the data variance. NSE indicates how well the measured vs. modeled data fit the 1:1 line (Moriasi et al., 2007). A value of 1 of optimal, values between 0 and 1 are acceptable, and negative values indicate that the data mean is a better predictor of the data than the model:

$$NSE = 1 - \left| \frac{\sum_{i=1}^{n}\left(Y_i^{Obs} - Y_i^{Sim}\right)^2}{\sum_{i=1}^{n}\left(Y_i^{Obs} - Y_i^{Mean}\right)^2} \right| \quad (A4)$$

PBIAS – Percent bias measures the average tendency of the simulated data to be larger or smaller than the measured data. A value of 0 of optimal – a positive value indicates underestimation bias and a negative value indicate overestimation bias:

$$PBIAS = \left| \frac{\sum_{i=1}^{n}\left(Y_i^{Obs} - Y_i^{Sim}\right)*100}{\sum_{i=1}^{n}\left(Y_i^{Obs}\right)} \right| \quad \text{(A5)}$$

RSR – The RMSE-observation standard deviation ratio is a statistic that normalizes the RMSE using the standard deviation of the observations. Because it is normalized, it can be used to compare errors among various constituents (Moriasi et al., 2007). A value of 0 is optimal:

$$RSR = \frac{\left[\sqrt{\sum_{i=1}^{n}\left(Y_i^{Obs} - Y_i^{Sim}\right)^2}\right]}{\left[\sqrt{\sum_{i=1}^{n}\left(Y_i^{Obs} - Y_i^{Mean}\right)^2}\right]} \quad \text{(A6)}$$

Calibration data

Figure 4-1 shows the location of temperature data for the 1990 – 2008 period – only a portion of these sites were available for the 2000 – 2008 period covered in the current calibration. Figure 8-8through Figure 8-17 in the Appendix illustrate some aspects of data availability and data quality. Table 8-4 and Table 8-5 in the Appendix give details on the availability of effluent data.

Parameterization

Rate coefficients in Delta channels were set regionally for groups of channels – reservoir coefficients are defined for each individual reservoir. Regional parameterization was changed from the DSM2/QUAL nutrient model calibration from 2009 primarily by changing organic-N and organic-P settling and decay rates. Organic-N and organic-P settling and decay rates were each set in each channel at a constant value Delta-wide.

Reservoir parameterization was changed from the original DSM2/QUAL nutrient model calibration from 2009 by changing organic-N and organic-P settling and decay rates. These rates were set to the same values for all reservoirs at the same values set Delta-wide for the channels.

Calibration/validation statistics and residual analysis

Two methods were used for calculating and assessing residual statistics. Residuals for water temperature were calculated as the difference (data – model) between the measured data and the modeled result on the same time scale, hourly or daily averages.

The methodology for assessing the calibration of nutrients and DO required further development. Because nutrient model boundary conditions for each month are generally composed of grab samples taken on a (approximately) monthly basis, data for different nutrients are generally sampled at different times on different days, and calibration data is also composed of grab samples, comparing average monthly model output values (the appropriate time scale given the boundary condition time scale) with an instantaneous data measurement did not make sense.

Instead, calibration data measurements were compared with modeled monthly maximum and minimum values – this is denoted the modeled monthly nutrient "envelope". If the calibration data fell within the envelope (i.e., was less than the maximum and greater than the minimum), the residual was calculated as zero. Otherwise, the residual was calculated as the difference between the data value and the nearest envelope value. So, for example, if the data was lower than the modeled monthly minimum, the residual (data – model minimum) would be negative.

Conceptually, the nutrient calibration is thus interpreted to be accurate if the data falls within the model envelope (residual is zero). Calculations of residual statistics use these zero values and the positive and negative residual values for data points that fall outside the envelope.

Model bias, i.e., the underestimation or overestimation of data by the model, was calculated but should be interpreted with the following provisos: when data was listed as "Below Detection limit", a value of (detection limit)/2 was ascribed to that datum, and, the number of data points used to calculate model statistics is quite small. Thus, although calibration or validation statistics were calculated for all relevant years and also split into wet and dry year types, the quality of the statistics may be dominated by a few measurements.

Water temperature statistics

Ranges for model calibration performance ratings for the NSE, RSR and PBIAS statistics are given in (Moriasi et.al., 2007). Following those general guide lines, temperature calibration is viewed as "Very Good" for the NSE statistic if NSE is greater than 0.75. Similarly, a PBIAS value less than +/-(10 – 25) and a RSR value less than 0.50 are "Very Good". Under each of these three criteria,

both the calibration and the validation of water temperature is "Very Good" at each location for both the Dry and Wet Water Year types.

Residual Analysis of the Nutrient Model

The same statistics used in the temperature calibration were calculated in the calibration and validation of the nutrients. In addition, residuals were assessed by plotting residual histograms. The majority of the calibration data were from EMP locations, although a few constituents were available from other agencies. Under these criteria, there was no BOD/CBOD data available for calibration and validation over the selected time span. BOD measurements were lacking except in a short reach along the San Joaquin River, and these were limited in the temporal frame. There were essentially no measurements for organic-P and the measurements for nitrite and nitrate individually were sparse.

Only RSR, PBIAS and NSE were used to evaluate the results as discussed in (Moriasi et al., 2007). The recommendations in that paper were followed with one modification. Unlike the ranges used in Moriasi (2007), NSE was ruled unsatisfactory only when negative, so the satisfactory range was essentially extended to all positive values. Thus, the following categories were used to evaluate the quality of the nutrient constituent calibration:

Table 4-1 Categories used to rate the quality of the nutrient calibration/validation.

Performance Rating	RSR	NSE	PBIAS (%)
Very Good	$0.00 \leq RSR \leq 0.50$	$0.75 < NSE \leq 1.00$	PBIAS < +/- 25
Good	$0.50 < RSR \leq 0.60$	$0.65 < NSE \leq 0.75$	+/- 25 ≤ PBIAS < +/- 40
Satisfactory	$0.60 < RSR \leq 0.70$	$0.00 \leq NSE \leq 0.65$	+/- 40 ≤ PBIAS < +/- 70
Unsatisfactory	RSR > 0.7	NSE < 0.0	PBIAS ≥ +/- 70

Although the PBIAS ranges are specific to N- and P-nutrients, the ranges for RSR and NSE are not constituent-specific in the general performance ratings presented in (Moriasi et al, 2007). PBIAS ranges for constituents tend to be more lenient than those listed for streamflow or sediment transport. Thus, we can expect that the ratings for RSR and NSE are quite strict when applied to constituent calibration/validation statistics. To accommodate this observation somewhat, the NSE range for "Satisfactory" was extended to all positive values. The range for RSR was not altered.

Temperature and Nutrient Calibration/Validation Results

Detailed calibration results and statistics for modeled temperature and nutrients are given in Appendix, Section 9 and in Appendix III, Section 10, respectively.

Selected plots documenting the quality model calibration are shown in Figure 4-3 through Figure 4-13. Plots illustrating the nutrient calibration focus on two locations well away from model boundaries to illustrate the fate of nutrients. Potato Point is along the San Joaquin R. but with influences from Sacramento R. water flowing through the Mokelumne R. and Georgiana Slough, and PO-649 shows influences from Sacramento R. water and also from the complicated mixtures of water near the confluence of the Sacramento and San Joaquin Rivers. These locations are indicated in Figure 4-2.

At these two locations, the model calibrations for algae and NH_3 are shown in Figure 4-3 and Figure 4-4 respectively. The results for NO_3+NO_2, Figure 4-5, show opposite bias at the two locations. Figure 4-6 shows the results for organic-N are biased slightly negative (model results are somewhat high) – this is partly because the measured value was at the detection limit of the water quality analysis methodology. Such values were replaced by (Detection limit)/2 for the purposes of statistical analysis of the calibration/validation. This replacement means that a bias has been introduced to the statistics, but the replacement was assumed to be a reasonable assumption and the consequences for the calibration statistics can be traced to these assumptions.

Figure 4-7 shows the calibration of DO at two different in-Delta locations – in this case the measurement data and model output is hourly. Data trends and magnitudes are followed closely by the model. Figure 4-8 shows that the results for PO_4 are acceptable to Potato Pt,, but peaks and lows appear to be shifted in time at Pt. Sacramento.

Figure 4-9 through Figure 4-13 show the results for the calibration of water temperature - this portion of the model did not require recalibration. As discussed in (Guerin, 2010), the temperature model calibration results are generally Very Good. The main draw-back in the DSM2/QUAL temperature model is that meteorological boundary conditions are applied globally over the model domain, but model results indicate that a minimum of two temperature regions are required to improve results. The current model results are very good along the Sacramento River corridor where the calibration was focused. In the Central and South Delta, modeled water temperatures in the summer months can be several degrees Celsius cooler than indicated by the data, as illustrated at ROLD024 (Figure 4-13). However, the model temperature trends are correct and diurnal variation is reasonable.

Figure 4-14 through Figure 4-17 depict a summary of model bias at the calibration locations for each of the constituents. There are no striking patterns to model bias either regionally or by constituent.

Liberty Island Analysis

In the original nutrient model calibration, details found in (Guerin, 2010), the DSM2 grid did not include Liberty Island which flooded in 1997/8. In 2010, Liberty Island was included in the DSM2 grid (Chilmakuri, 2010). In DSM2, areas such as Liberty Island are set as open water "reservoirs", even though they are actually tidally influenced with changes in flooded area as the tidal cycle progresses. These reservoirs are thus conceptualized as fully mixed tank reactors. This simplification will be less valid as the area of the "reservoir" increases and the actual reactions due to tidal wetting and drying depart from the simple tank calculation.

At the time that Liberty Island was included in the DSM2 grid, a calibration exercise was performed, although at that time there was no data available to check the parameterization of the new area or to set inflow boundary concentrations influencing the region, the Yolo Bypass inflow. Boundary conditions and model parameterization in the area in and Liberty Island were based on calibration targets at Rio Vista and downstream.

Unexpected results in the Proposed Project scenarios raised questions about the conceptualization, boundary conditions and parameterization in the new "open water" areas proposed for this project. Specifically, PO_4 levels were too high in proposed project scenarios. On request for use in BDCP, data was supplied from DWR to use in checking the Historical nutrient model in Liberty Island. The comparison of that data, supplied by P. Lehman (DWR), with model results is covered in this section. The data was collected for a project that is discussed in (Lehman *et al.,* 2010). The reader is referred to that document for details about data collection and analysis methods (in the Methods section of the Lehman paper).

In brief, data was collected monthly from February 2004 to July 2005 from 4 locations within Liberty Island (See Figure 1 in the Lehman paper). Data from water samples that were analyzed included several modeled constituents, NH_3, NO_3, chlorophyll-a and PO_4 (called Soluble-P in the Lehman data). On each sample date, data for these constituents from the four locations (labeled north, south, east and west in Figure 1 in Lehman's paper) were averaged for comparison with model output. These comparisons are shown in Figure 4-18 through Figure 4-21.

The comparisons show that the modeled constituents NH_3 and Organic-N in Liberty Island compare well with Lehman's data, Figure 4-18 and Figure 4-19 respectively, while modeled NO_3 and PO_4 (Soluble-P in Lehman's terminology) are too low by approximately a factor of two in comparison with data. The largest difference occurs in the magnitude of Algae where the DSM2 concentration of Algae is nearly an order of magnitude greater than Lehman's data. Lehman's

chlorophyll-a was converted to Algae using the conversion factor between chlorophyll-a and algae assumed in the DSM2 nutrient modeling (conversion is 67 g algae (dry weight)/mg chl-a).

The Algal growth rate used in the Liberty Island parameterization was somewhat higher than the rates used for the other reservoirs and the same as rates used in many of the model channels. For example in other reservoirs, growths rates varied from $7 - 30\%$ in comparison with the Liberty Island rate. The Liberty Island growth rate was about 30% higher than the growth rate used in Franks Tract, but only 7% higher than rates used in Mildred and Bethel Islands.

The final data/model comparison is between DIN:DIP ratios, where DIN=NH_3+NO_3+NO_2 and DIP=PO_4. Figure 4-20 shows the comparison between Lehman's calculated ratios and DSM2 Liberty Island calculated Monthly MAX and MIN ratios. For comparison, Figure 4-21 shows the results of DIN:DIP calculations for four locations in the DSM2 Historical model. On average, Lehman's data ratios are higher than the DSM2 calculated values in Liberty Island, and higher than any of the other four DSM2 locations. Note that the DSM2 calculated ratios are approximately the same as P. Glibert's DIN:DIP ratios (personal communication).

As a final comparison, model output from three of the "open water" areas conceptualized as reservoirs in DSM2 are presented in Figure 4-22 through Figure 4-25. Liberty Island concentrations for Algae, DO, NO_3, NO_2, PO_4 Organic-N, BOD and NH_3 are compared with Mildred Island and Franks Tract. Several differences are apparent – Liberty Island concentrations for all constituents except NO_2 and DO are noticeable higher or lower than for the other two reservoirs. However, these reservoirs are physically close to each other, and in the Central Delta far from boundaries, while Liberty Island is just downstream of the Yolo boundary. In addition, The Cache Slough/Yolo area receives significant tidal excursion which includes Sacramento R. nutrient loads.

The results presented in this section comparing DSM2 Historical nutrient model output for Liberty Island with the Lehman data for comparable nutrients indicate that some changes to Yolo inflow boundary concentrations should be made and that the growth rate for Algae should be decreased. In addition, a volumetric fingerprinting analysis of Liberty Island water sources along with nutrient concentrations arriving from Sacramento R. sources should be undertaken to help constraint these parameters.

A more extensive analysis should also be undertaken to help define potential pitfalls with the conceptualization of Liberty Island as a fully mixed reservoir in DSM2. This analysis could include implementation of a nutrient model in a 2-D setting, such as the RMA11 nutrient model and also a brief literature review. Since Liberty Island is essentially at the model boundary (*e.g.*, in comparison with Franks Tract) once the Yolo Bypass stops flowing, it could be that this simplification is causing problems with the parameterization of the "bed" of the reservoir. In particular, DSM2 parameters conceptualizing benthic releases of NH_3, PO_4 and benthic demand on DO may be overestimating Liberty Island interactions once the Yolo flows become very low. In DSM2 reservoirs such as Franks Tract and Mildred Island, benthic releases/interactions are

mixed with Delta waters flowing through the Islands at each time step. In Liberty Island on the other hand, these mixing processes are muted due to its location near the model boundary. Finally, DICU contributes a source of nutrients that be overestimated – resolving this question would require gathering additional information on agricultural sources of nutrient loads to this area in the DSM2 model domain.

Figure 4-1 Locations of temperature data regular time series. Data quality and length of record was variable.
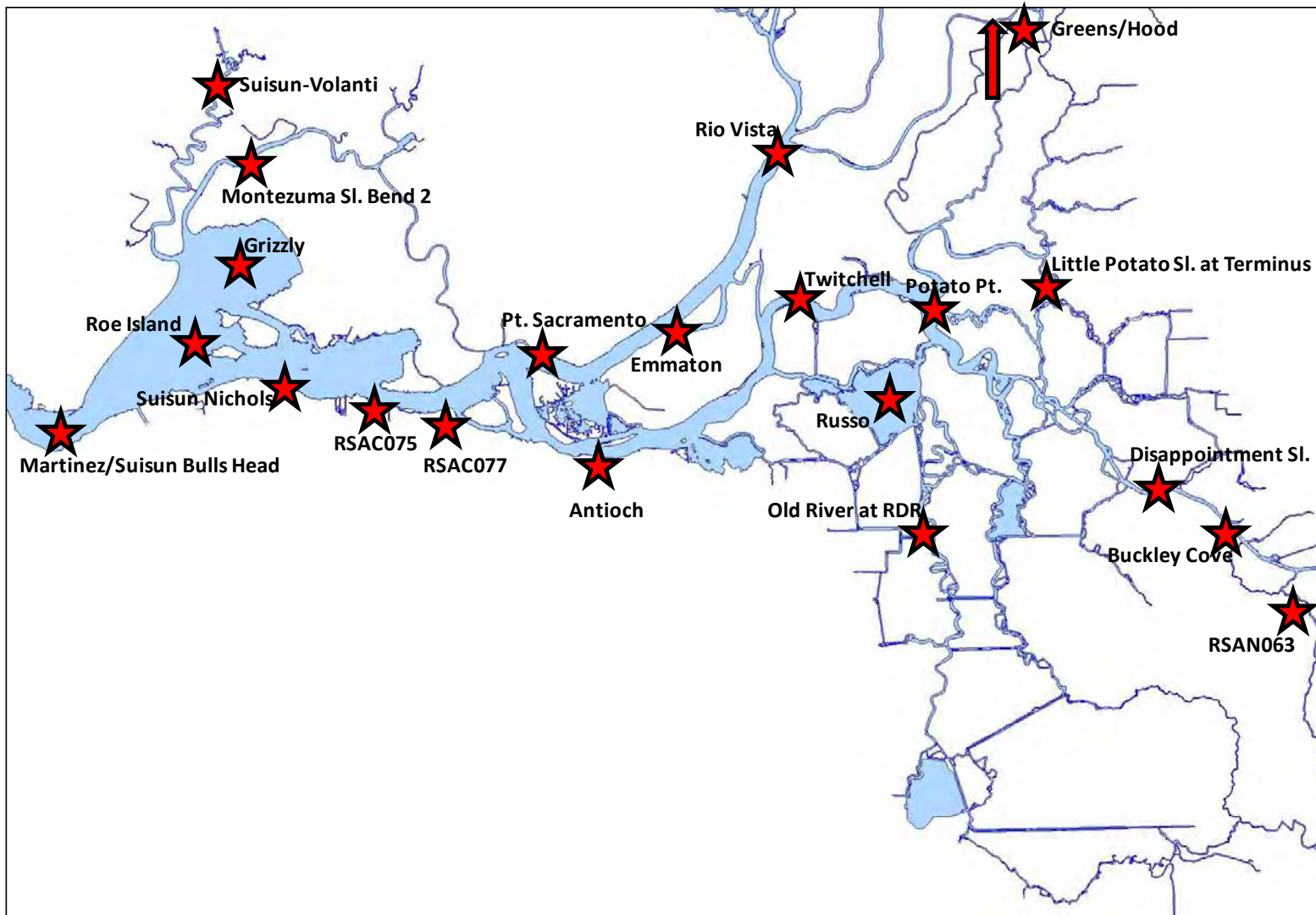
Figure 4-2 Location of nutrient data time series used in model calibration and validation. Model constituents vary by location.
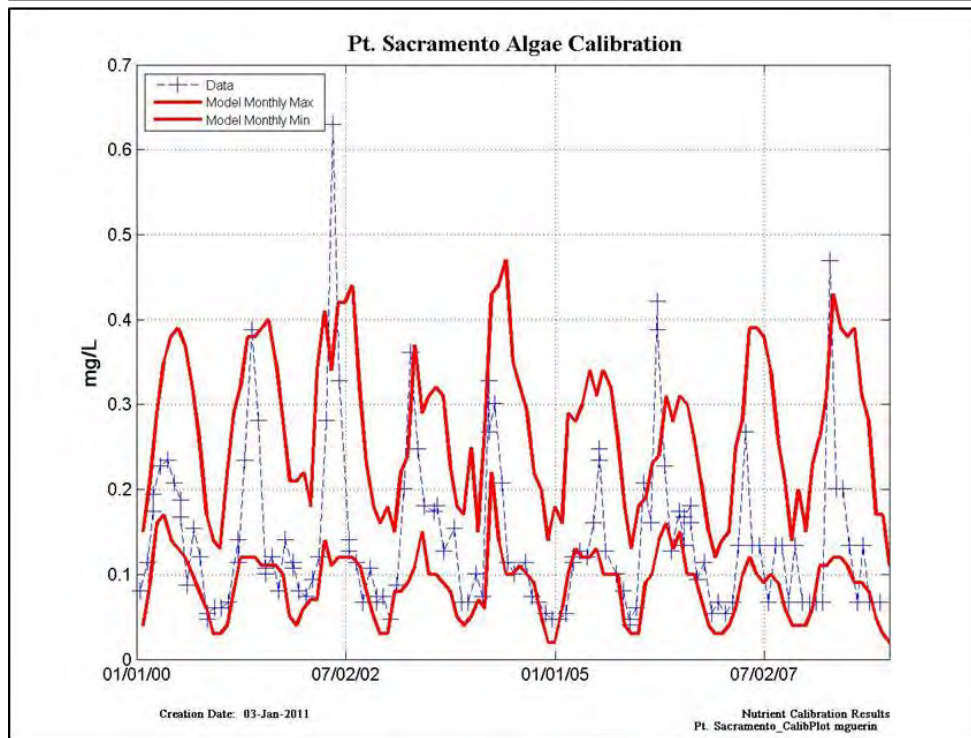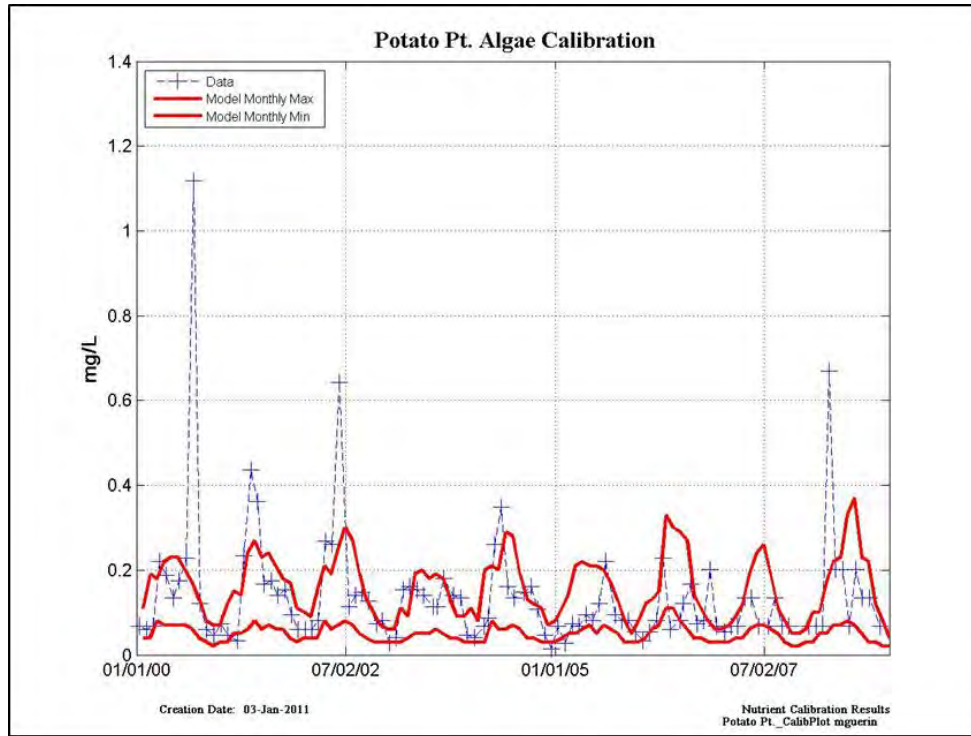
Figure 4-3 Calibration results for algae at Potato Pt. and at Pt. Sacramento. Blue symbols are data, red lines are the modeled monthly maximum and minimum from 15-minute model output.
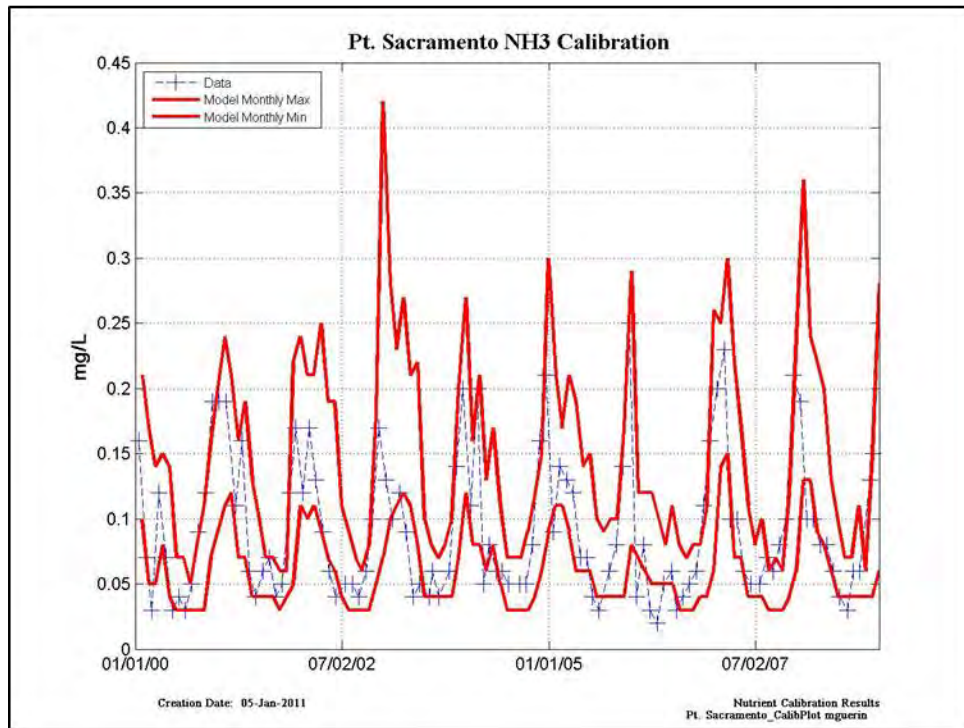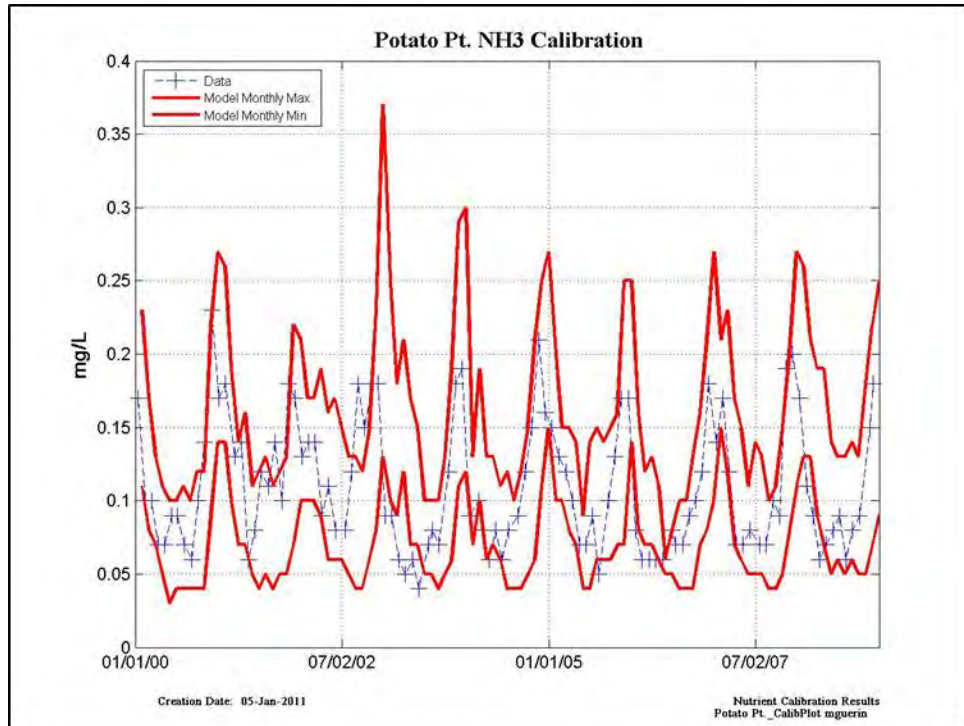
Figure 4-4 Calibration results for ammonia at Potato Pt. and at Pt. Sacramento. Blue symbols are data, red lines are the modeled monthly maximum and minimum from 15-minute model output.

30
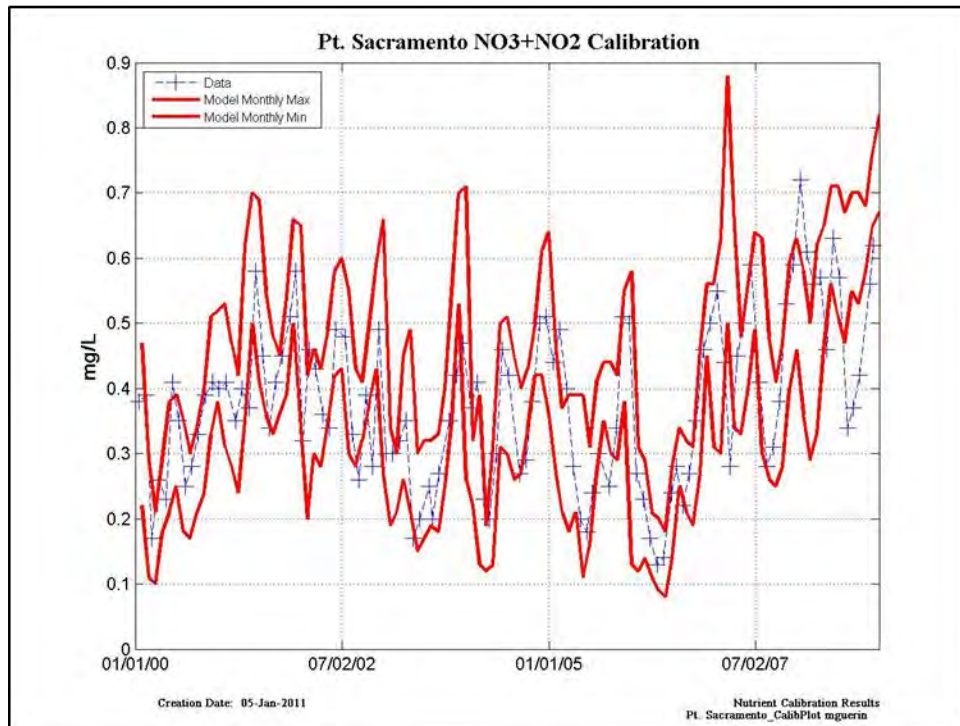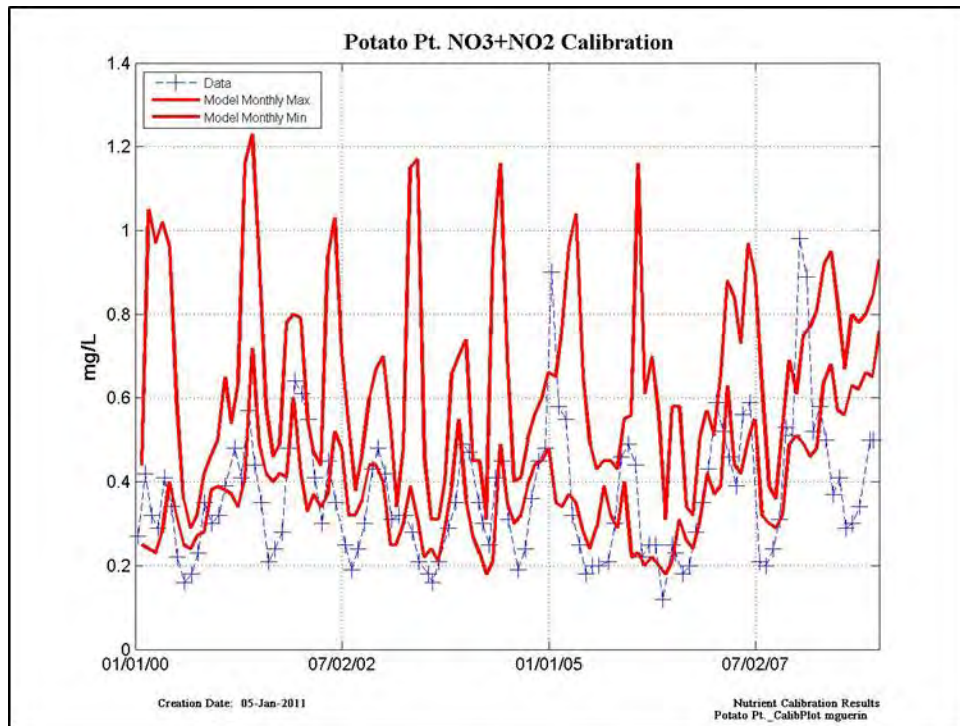
Figure 4-5 Calibration results for NO3+NO2 at Potato Pt. and at Pt. Sacramento. Blue symbols are data, red lines are the modeled monthly maximum and minimum from 15-minute model output.

31
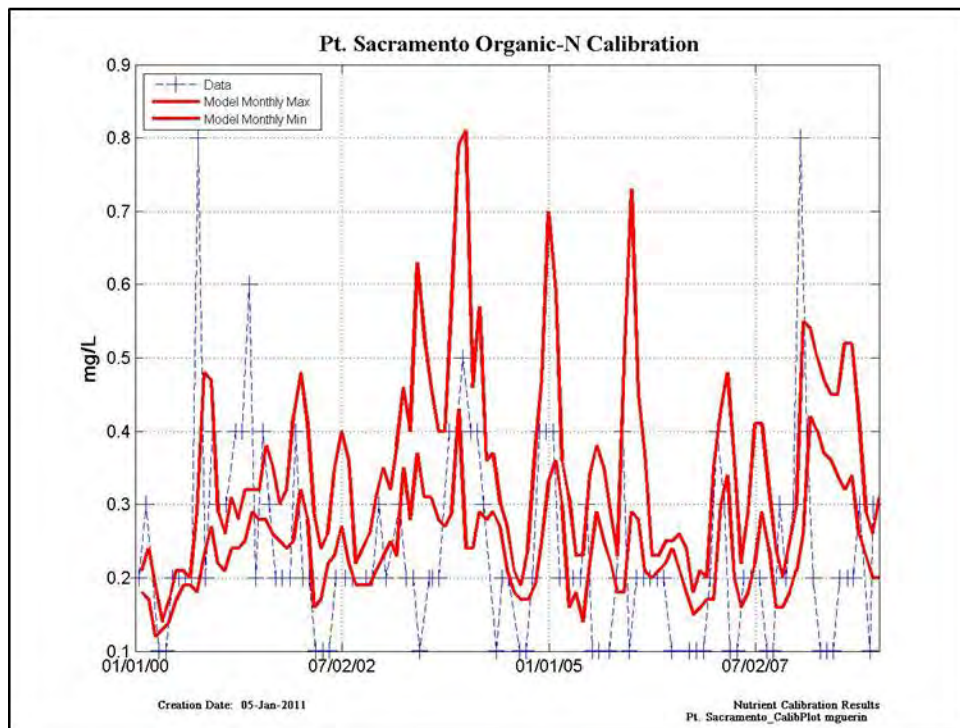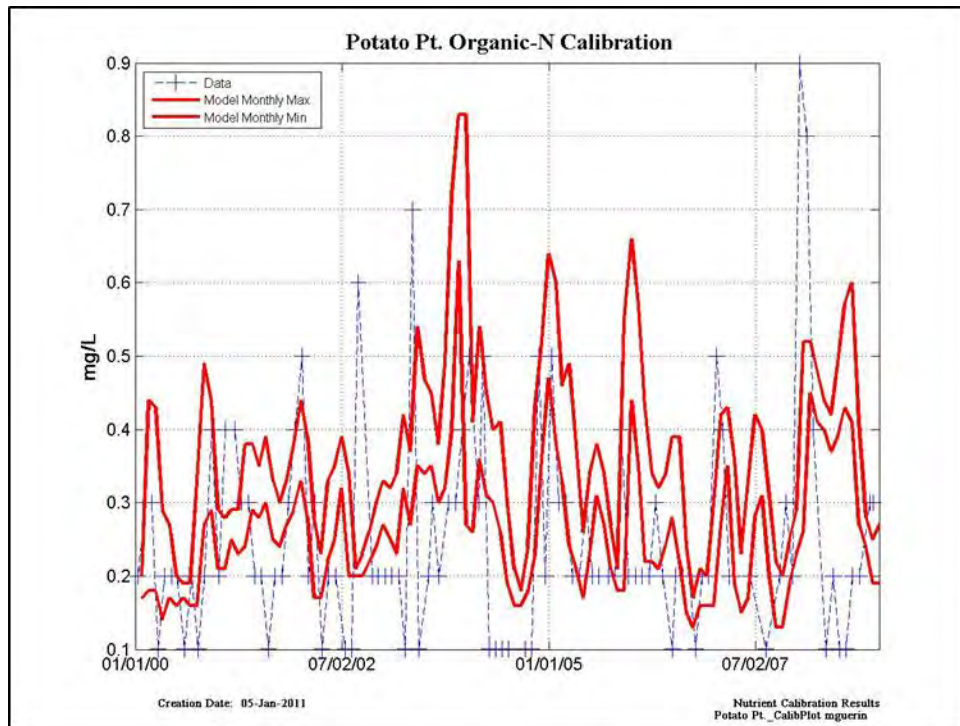
Figure 4-6 Calibration results for Organic-N at Potato Pt. and at Pt. Sacramento. Blue symbols are data, red lines are the modeled monthly maximum and minimum from 15-minute model output.
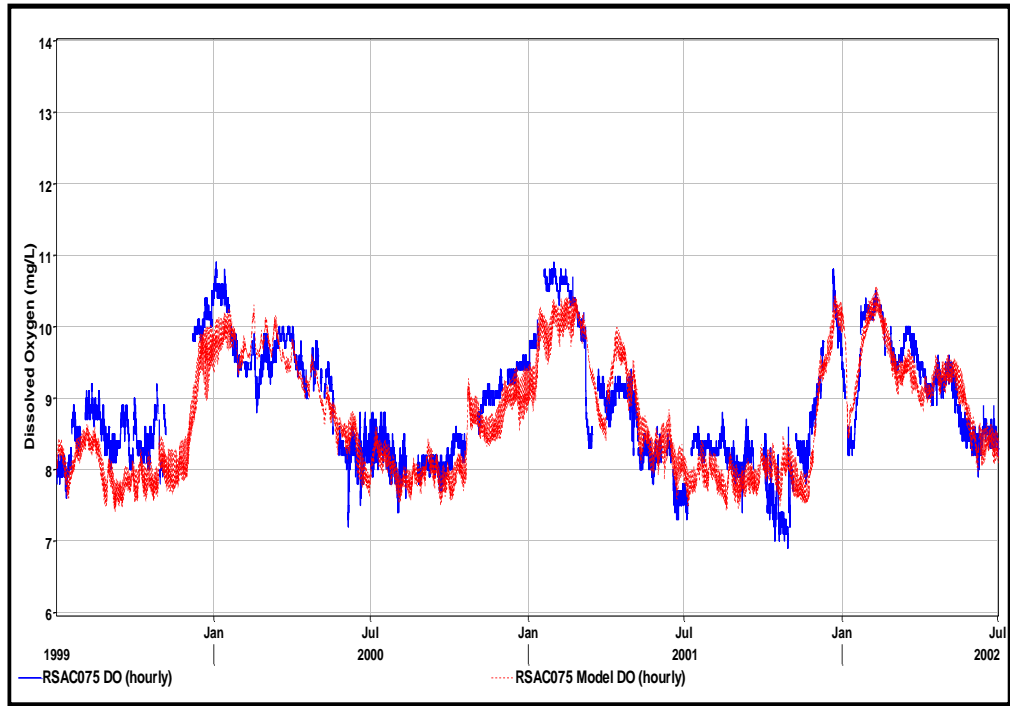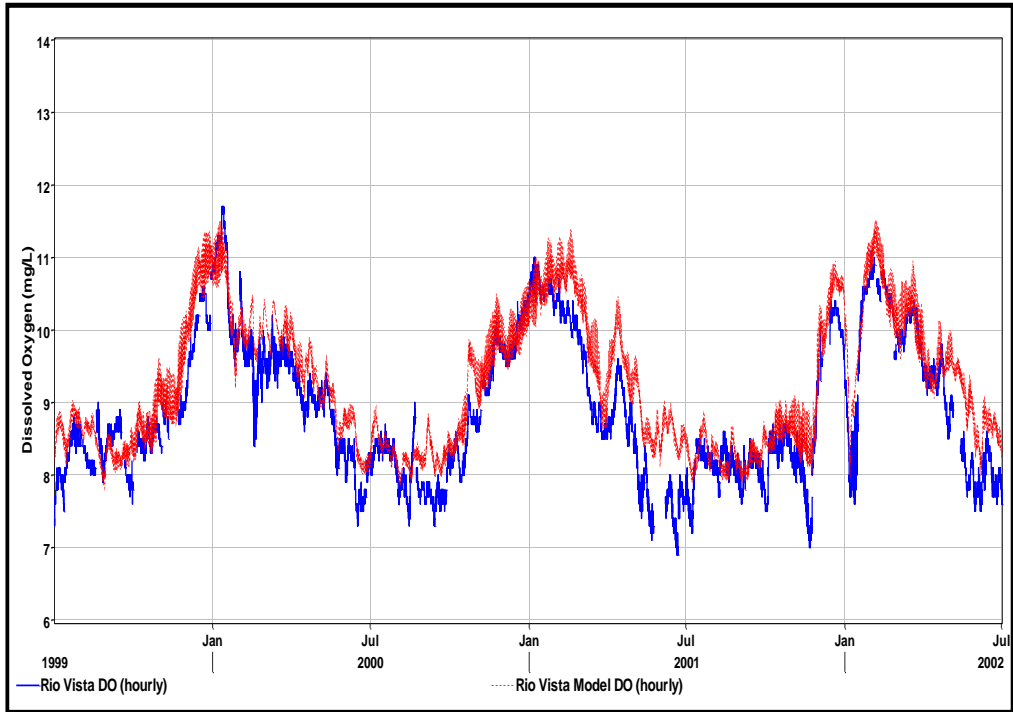
Figure 4-7 Hourly calibration results for DO at RIO Vista and at RSAC075. Blue lines are data, red lines are the modeled hourly results averaged from 15-minute model output.

33
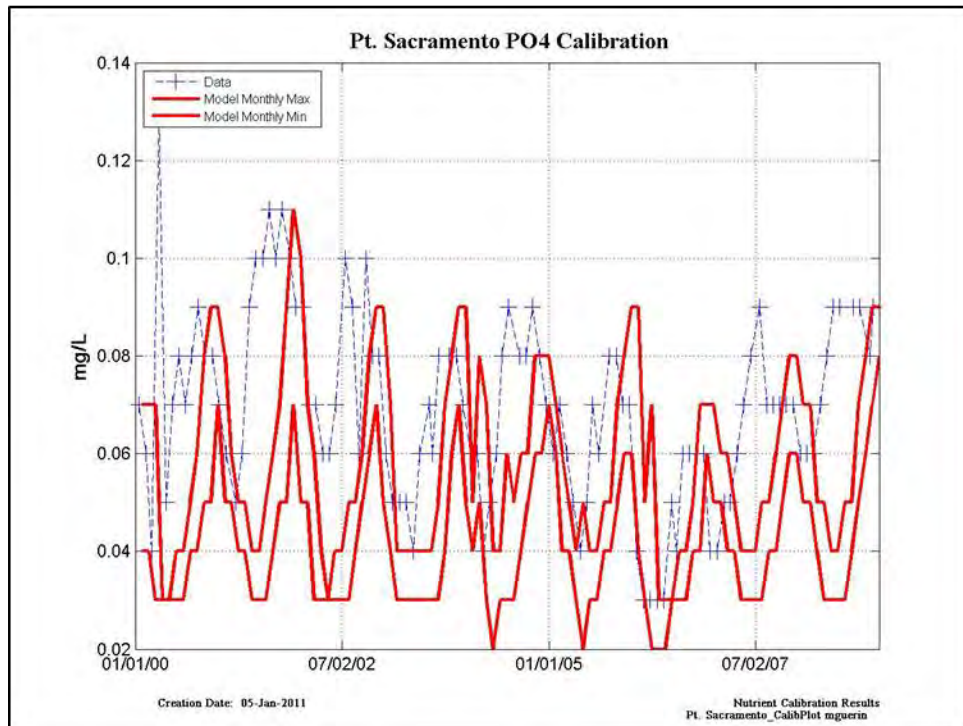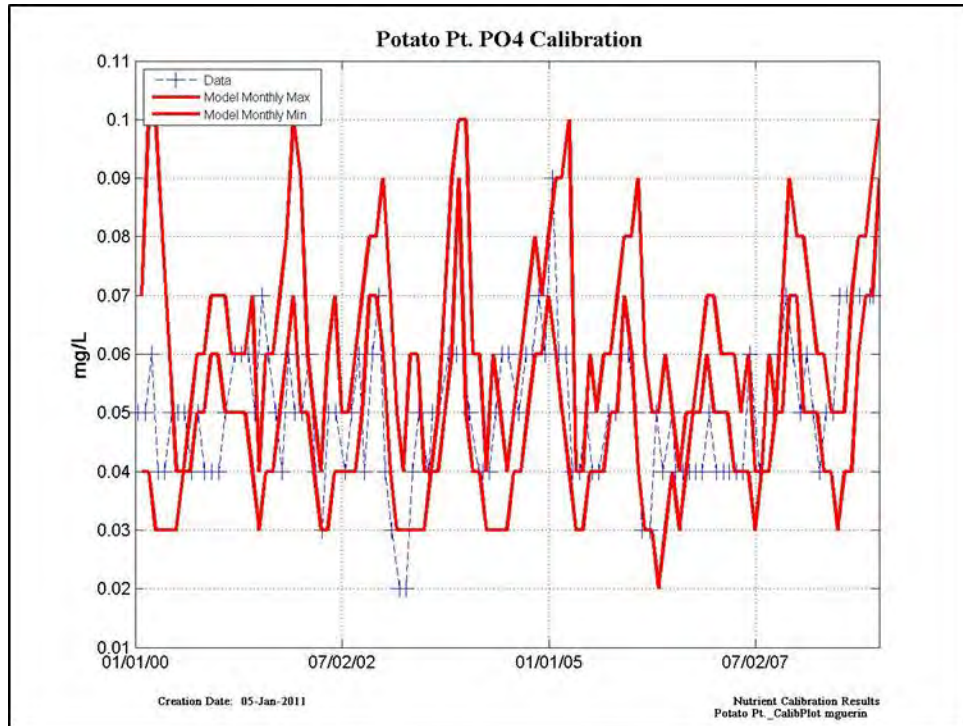
Figure 4-8 Calibration results for PO₄ at Potato Pt. and at Pt. Sacramento. Blue symbols are data, red lines are the modeled monthly maximum and minimum from 15-minute model output
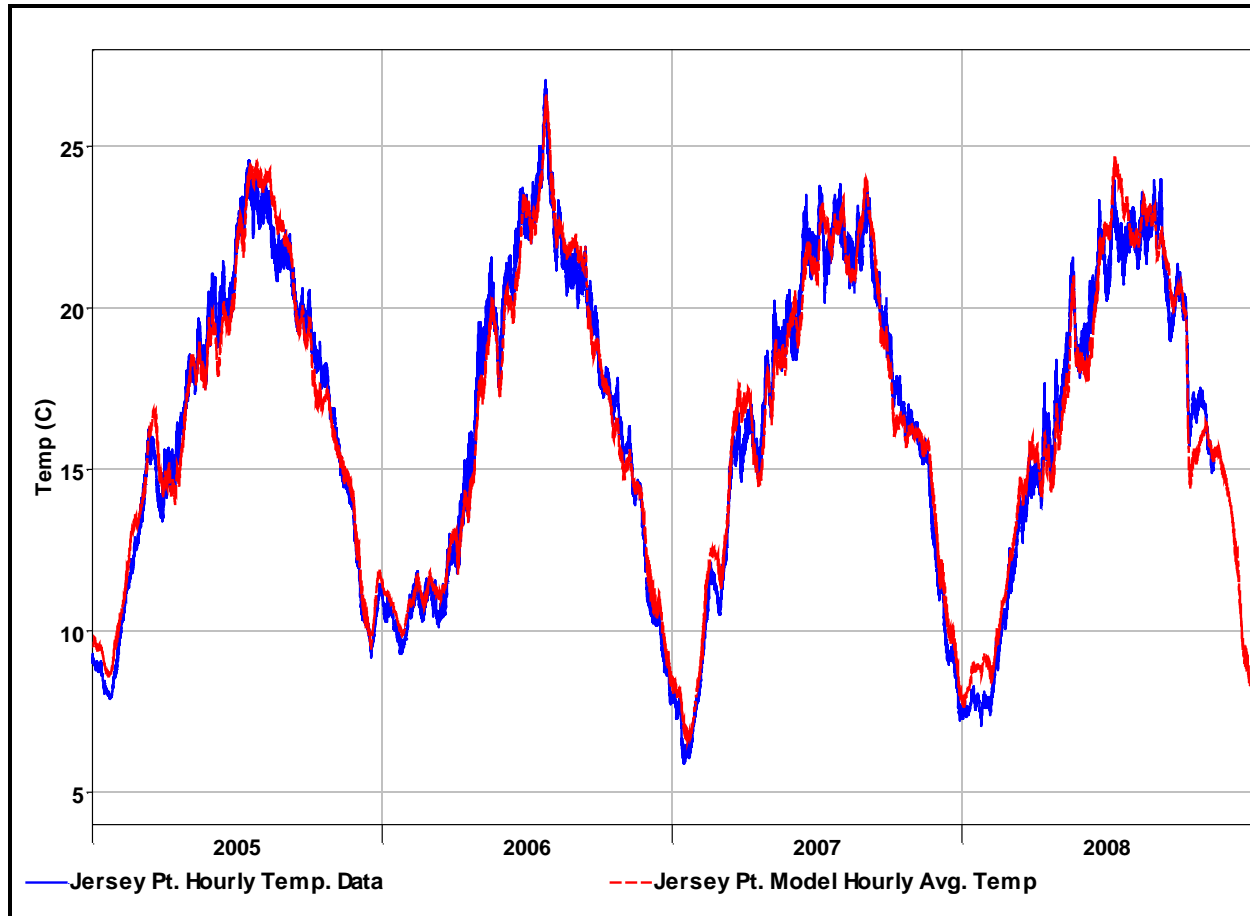
Figure 4-9 Hourly calibration results for water temperature at Jersey Point. Blue line is hourly data, red line is the modeled hourly result averaged from 15-minute model output.
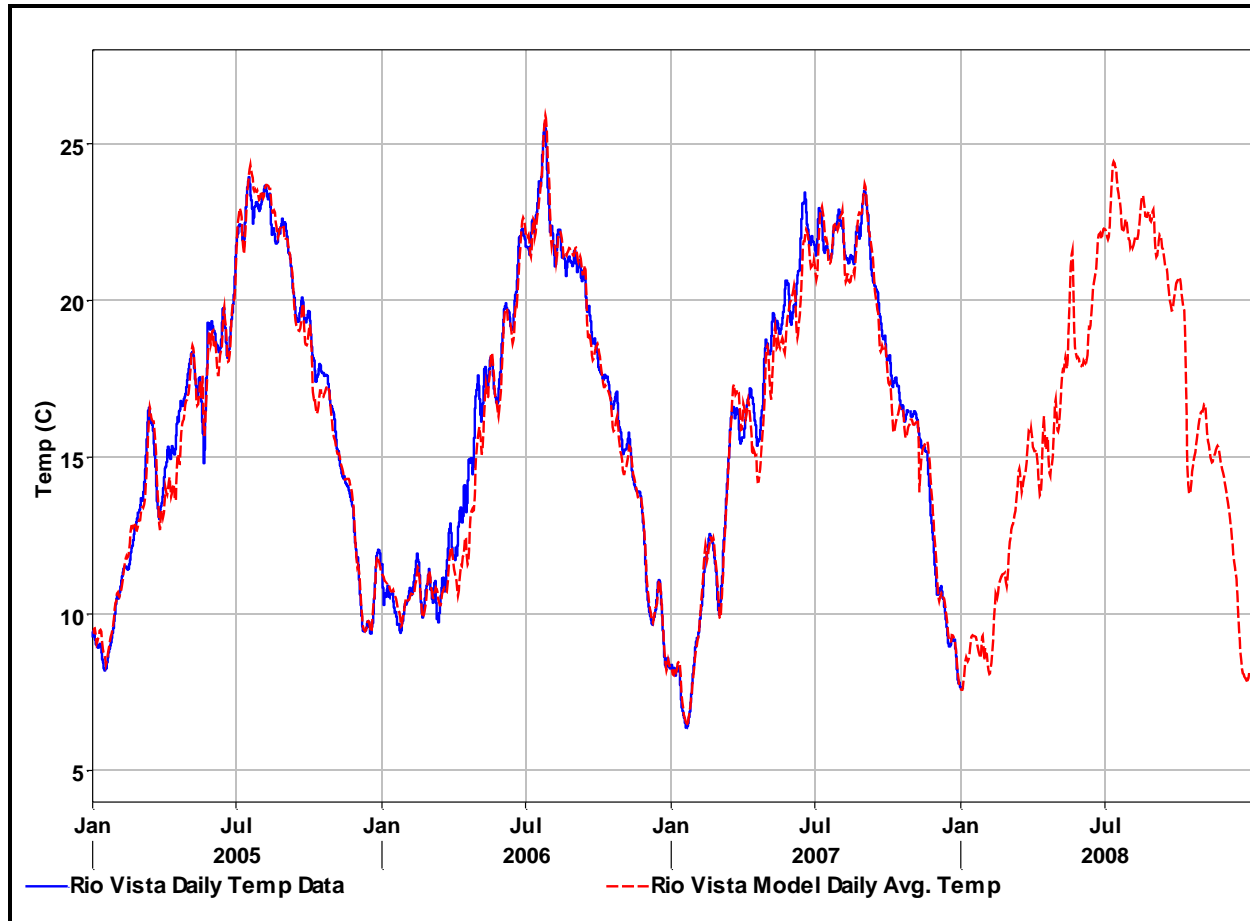
Figure 4-10 Daily calibration results for water temperature at Rio Vista. Blue line is daily data, red line is the modeled daily result averaged from 15-minute model output.
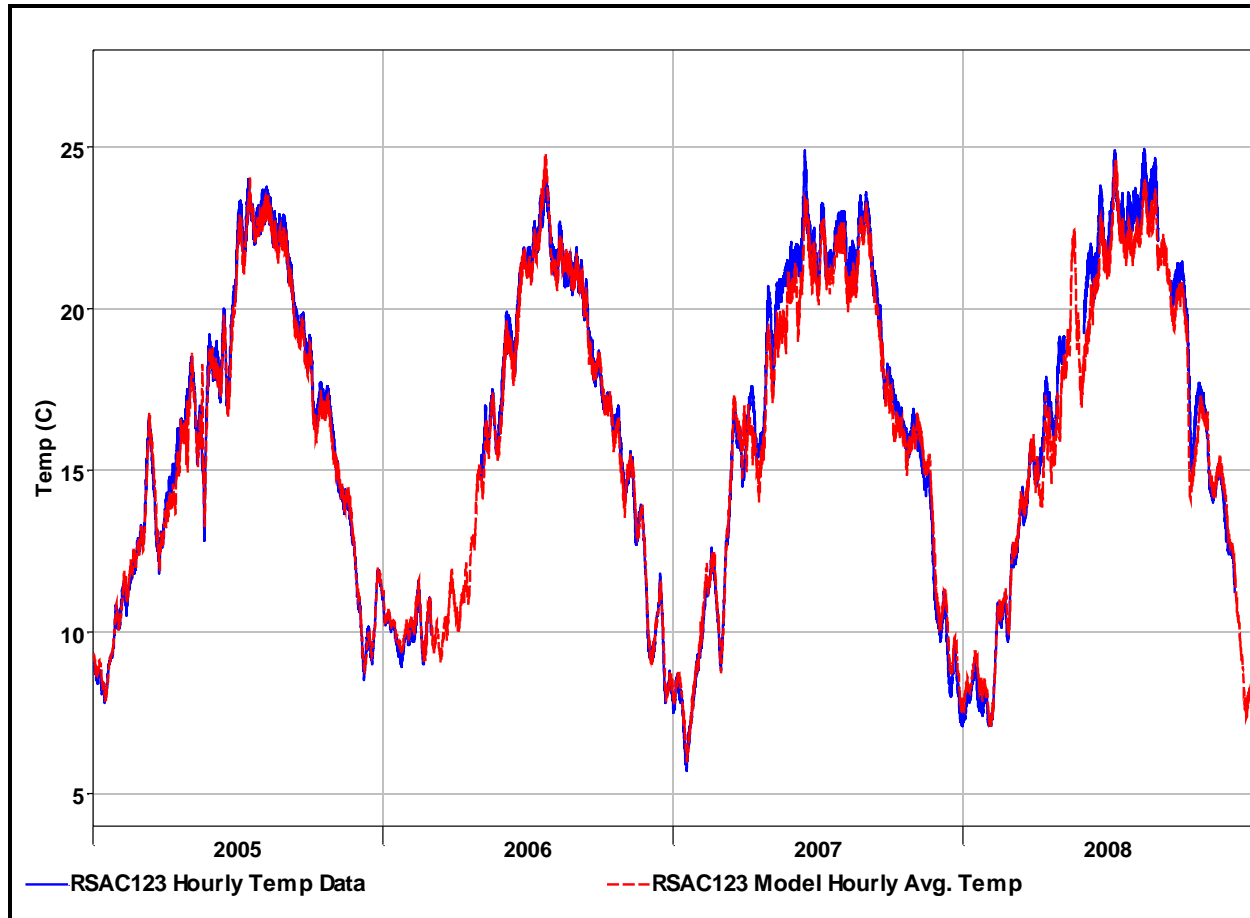
Figure 4-11 Hourly calibration results for water temperature at RSAC123. Blue line is hourly data, red line is the modeled hourly result averaged from 15-minute model output.
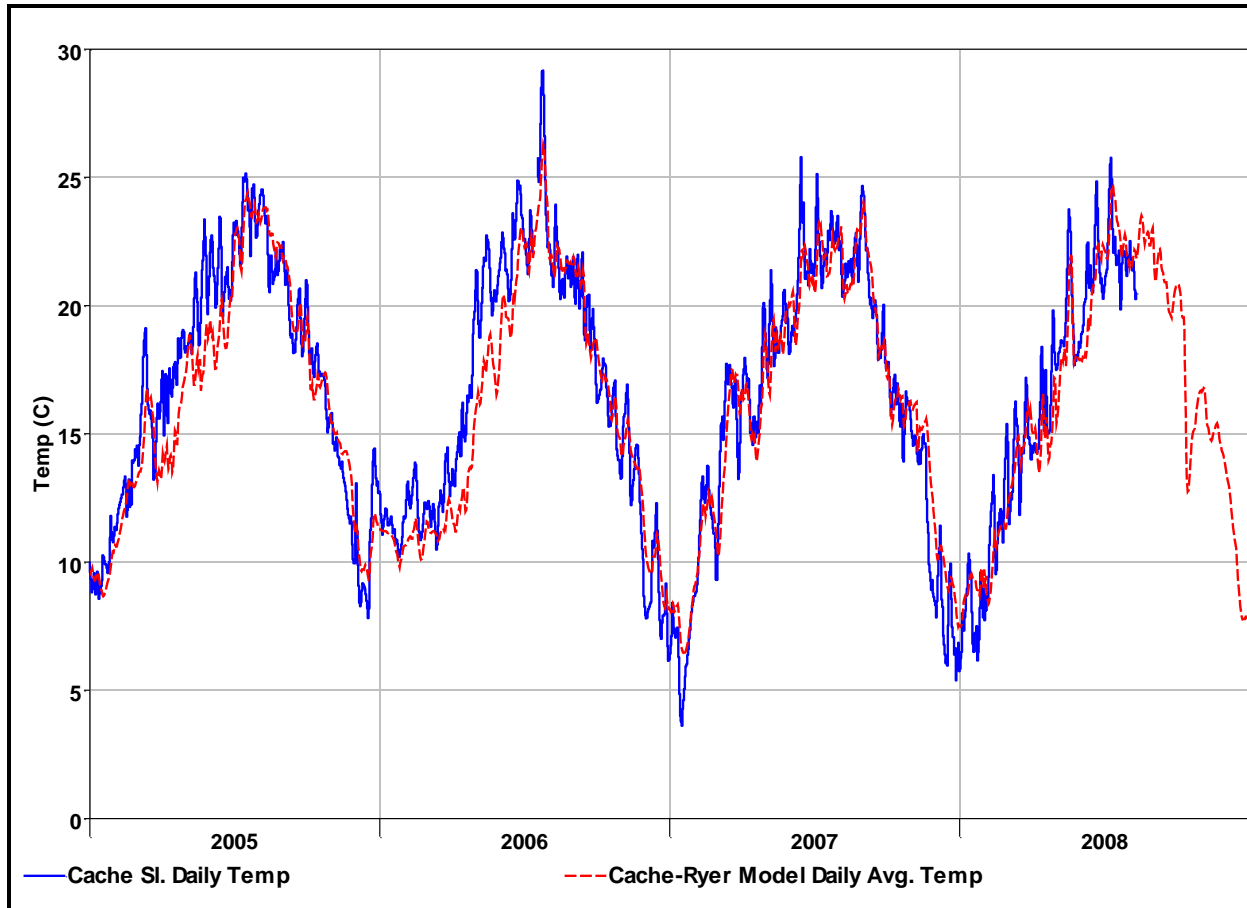
Figure 4-12 Hourly calibration results for water temperature at locations in the Cache Slough area. Blue line is daily data, red line is the modeled daily result averaged from 15-minute model output.
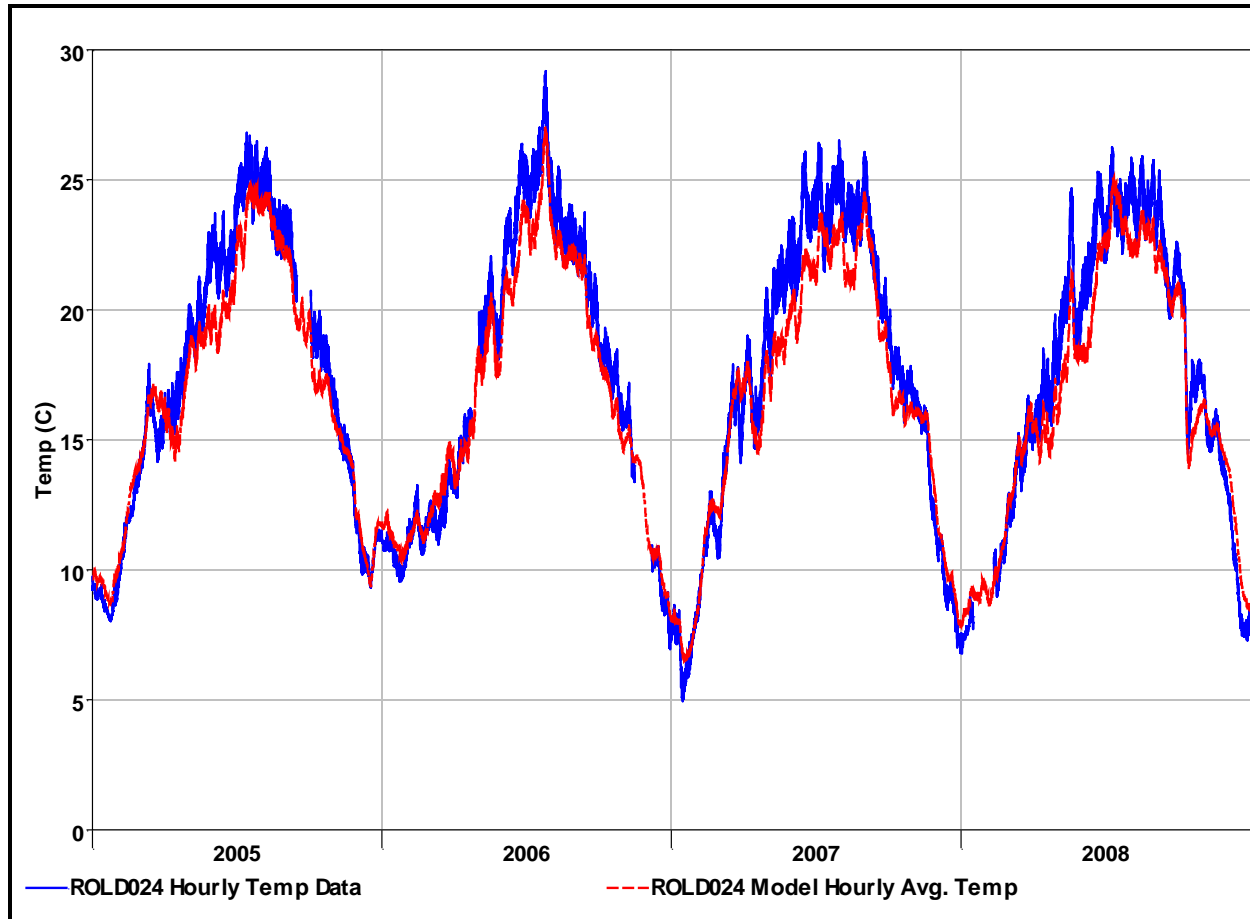
Figure 4-13 Hourly calibration results for water temperature at ROLD024. Blue line is hourly data, red line is the modeled hourly result averaged from 15-minute model output.
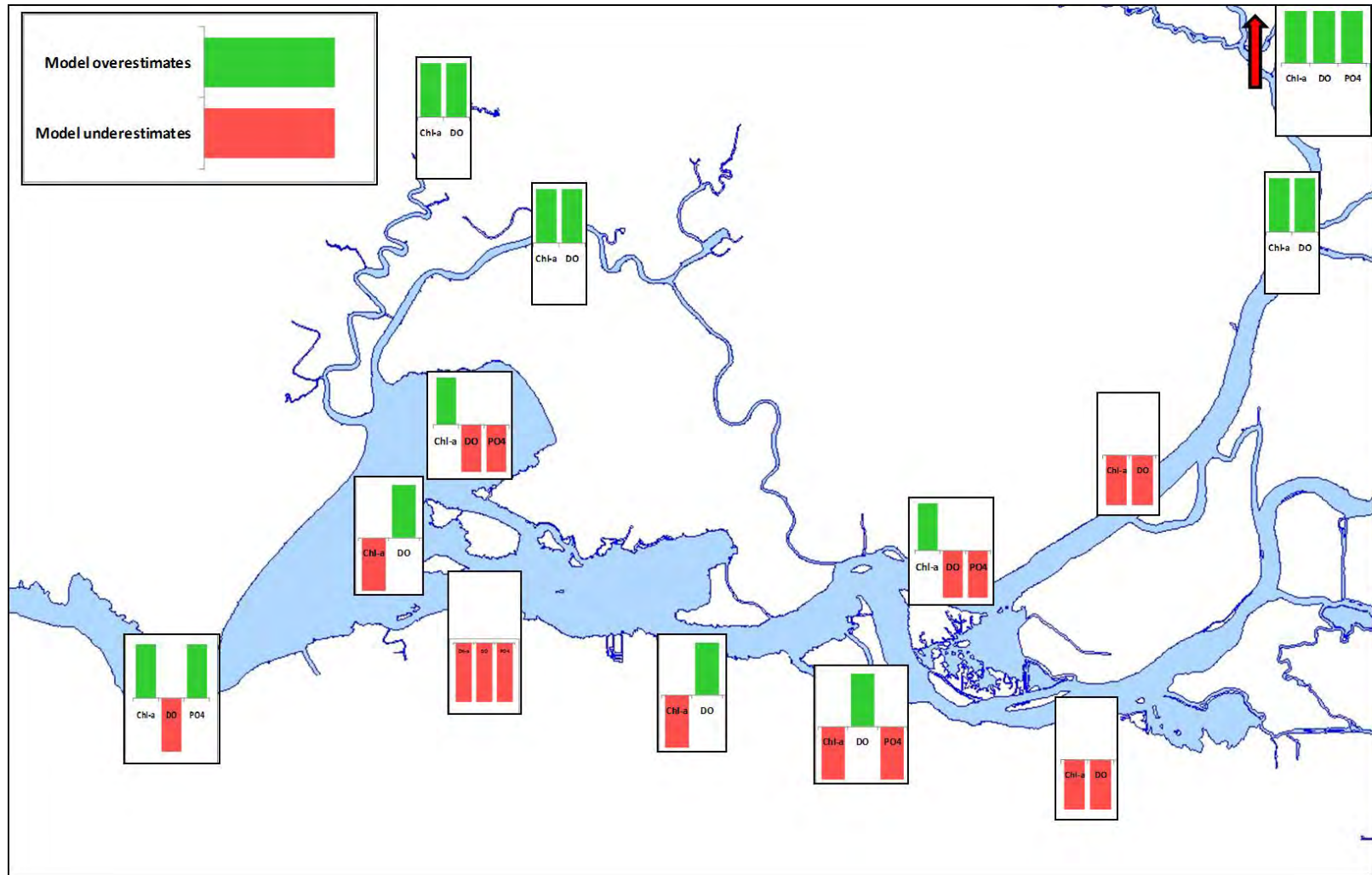
Figure 4-14 Categorical residual bias analysis of the nutrient model calibration for chl-a (converted to Algae in DSM2), DO and PO4. The arrow indicates Greenes/Hood results.
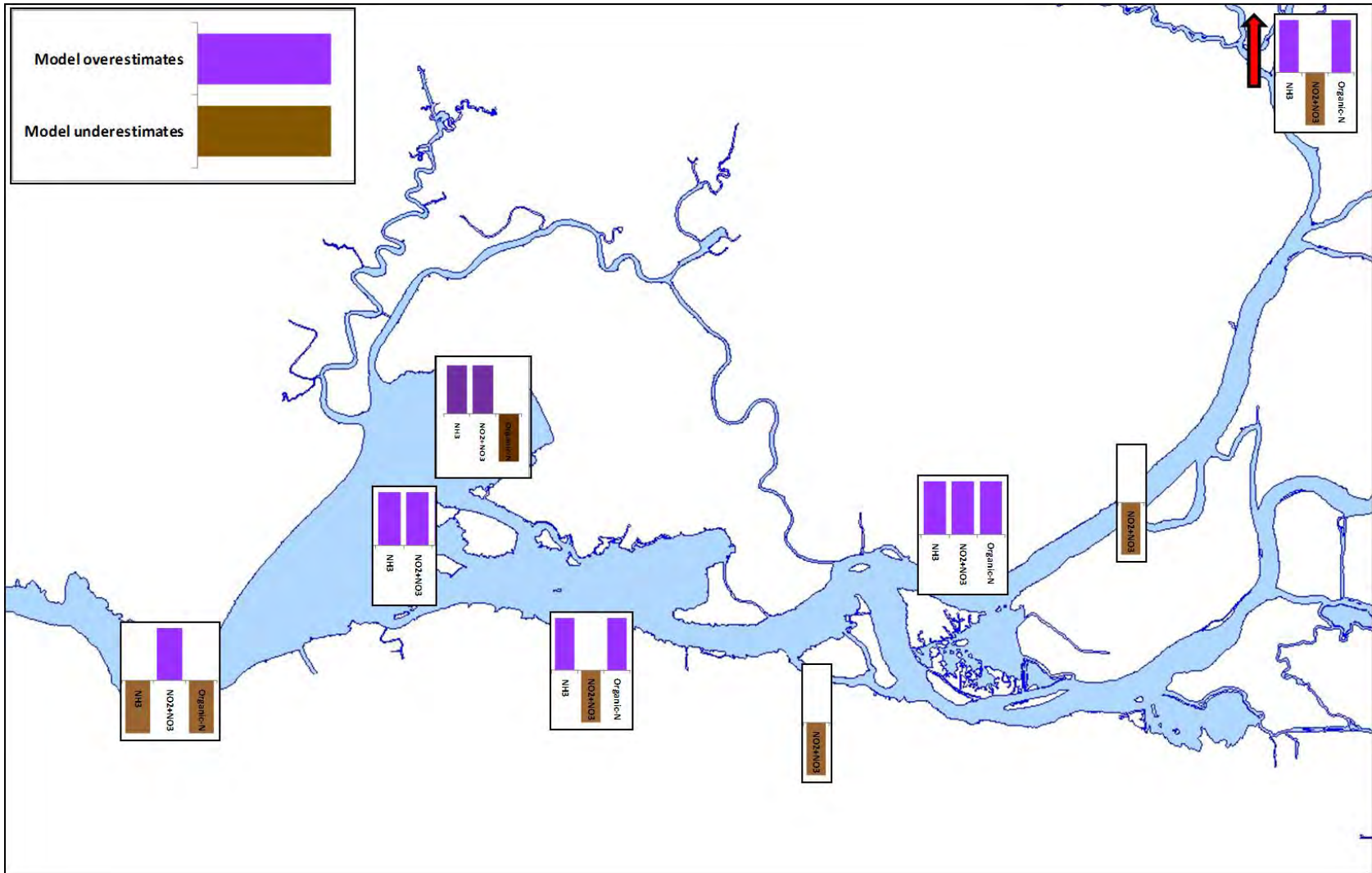
Figure 4-15 Categorical residual bias analysis of the nutrient model calibration for NH$_3$, NO$_2$+NO$_3$, and Organic-N. The arrow indicates Hood results .
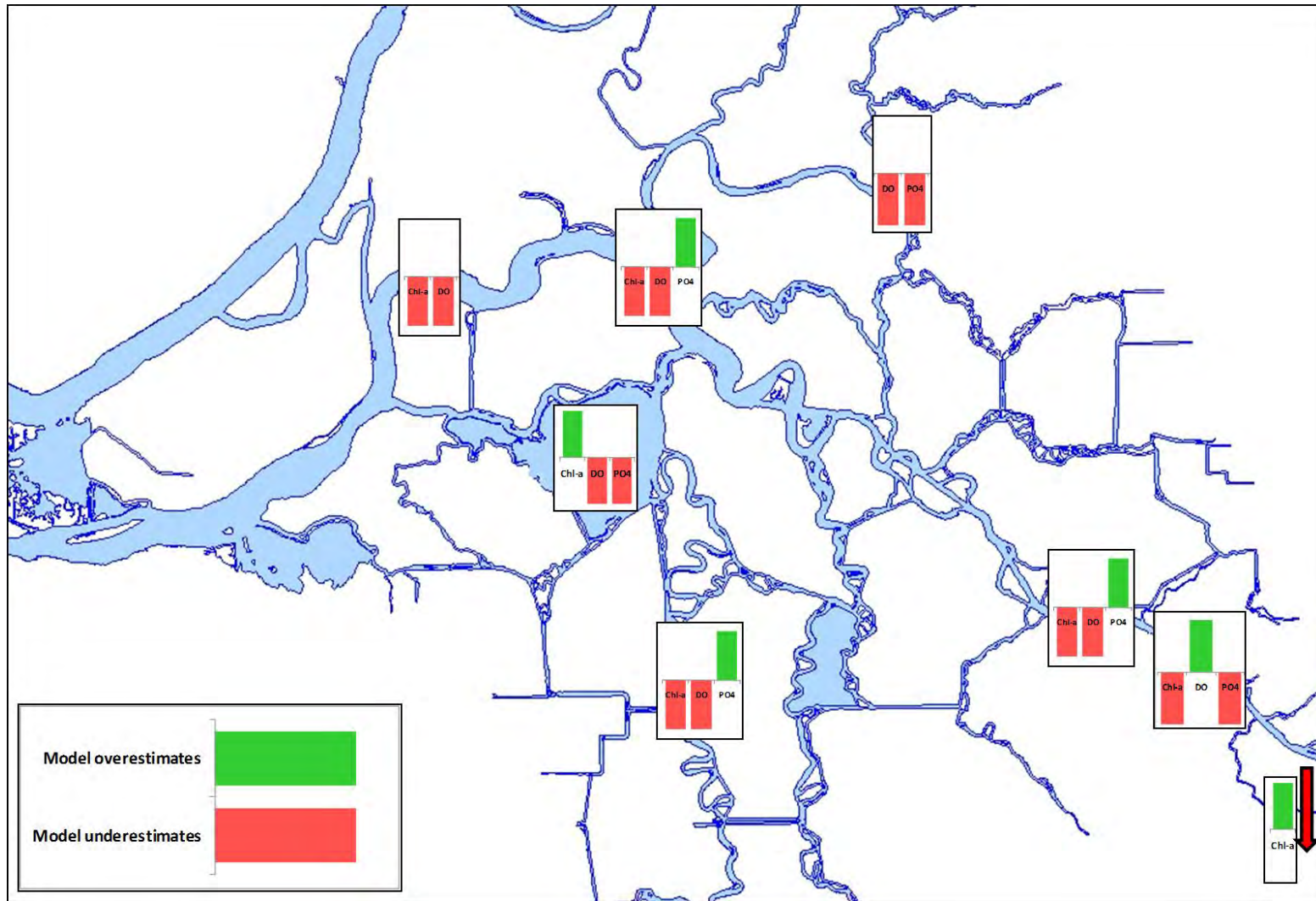
Figure 4-16 Categorical residual bias analysis of the nutrient model calibration for chl-a (converted to Algae in DSM2), DO and PO4. The arrow indicates RSAN063 results.
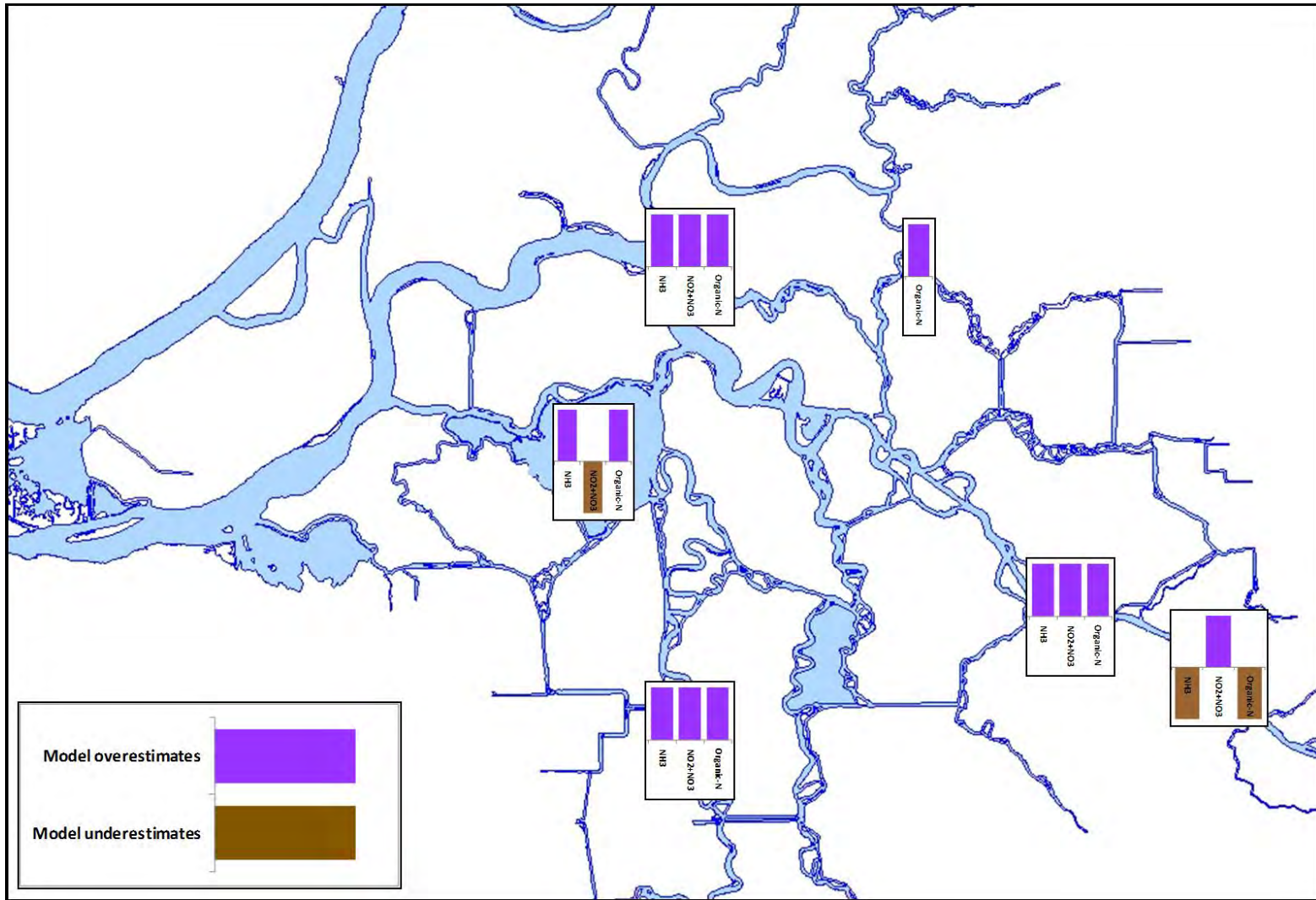
Figure 4-17 Categorical residual bias analysis of the nutrient model calibration for NH3, NO2+NO3, and Organic-N.
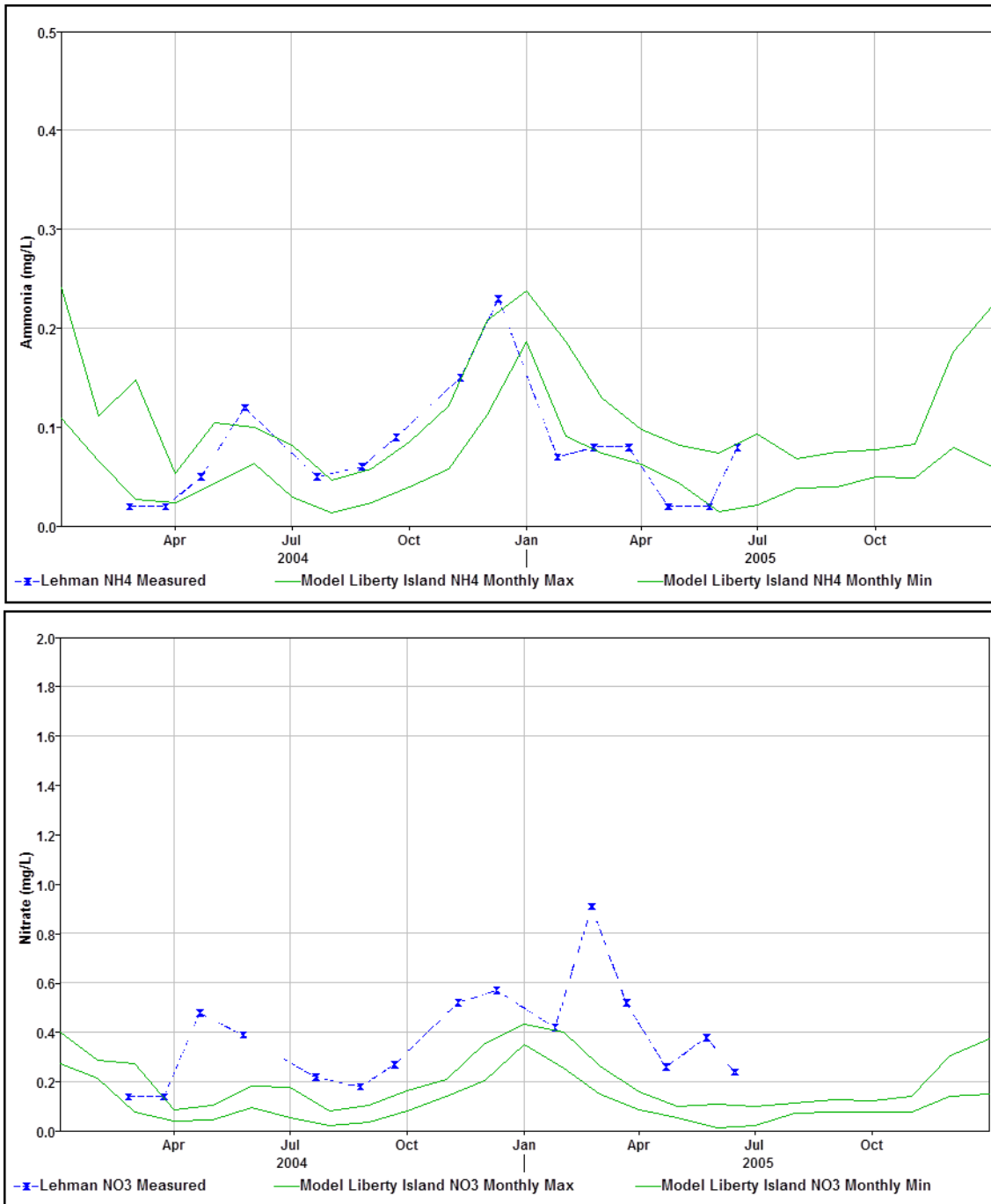
Figure 4-18 Comparison of data averaged from four locations in Liberty Island (Lehman et al., 2010) with DSM2 Historical nutrient model output for NH$_3$ and NO$_3$+NO$_2$. Model output is represented as the monthly MAX and MIN of the original 15-minute model output.
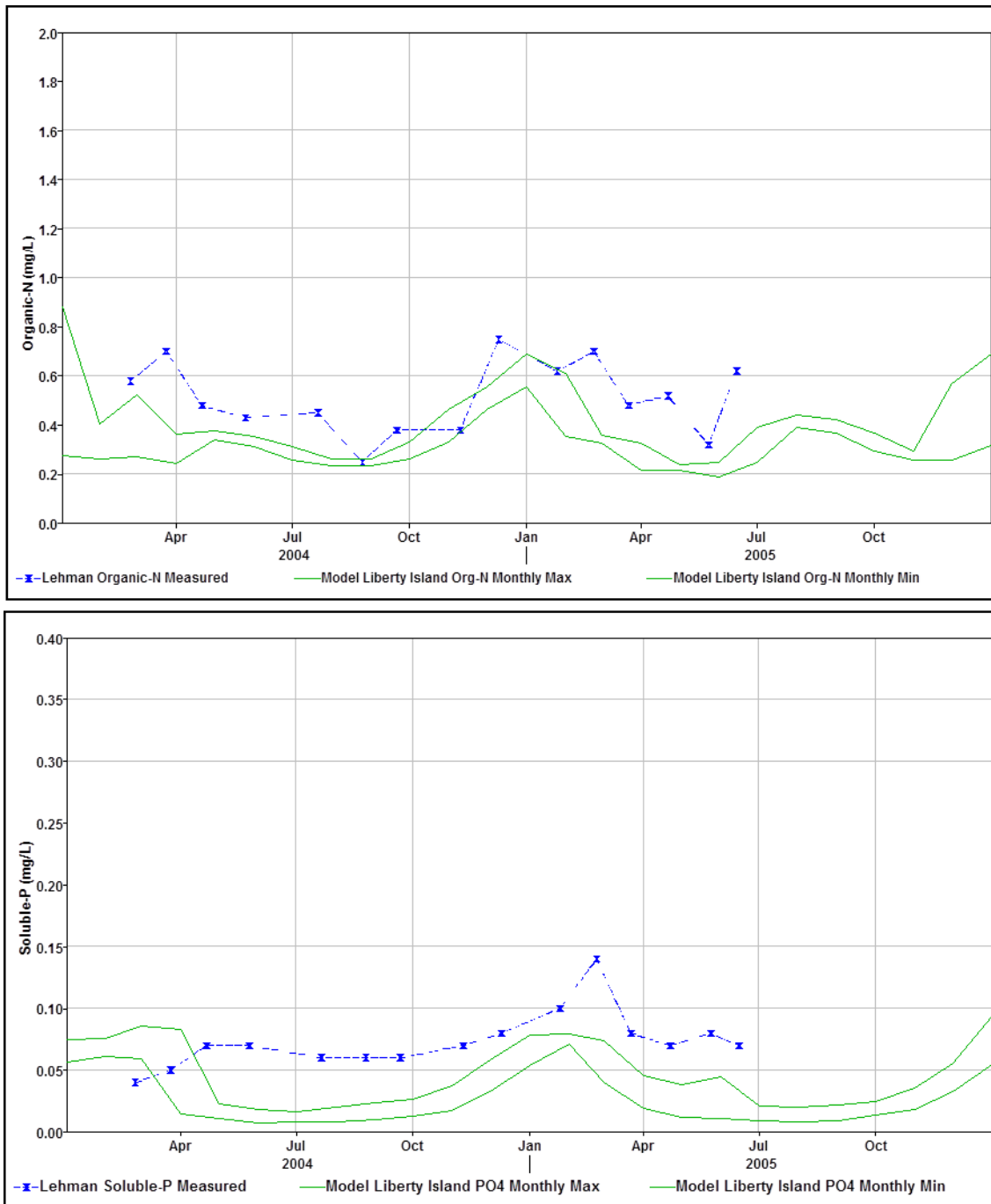
Figure 4-19 Comparison of data averaged from four locations in Liberty Island (Lehman et al., 2010) with DSM2 Historical nutrient model output for Organic-N and PO₄. Model output is represented as the monthly MAX and MIN of the original 15-minute model output.

45
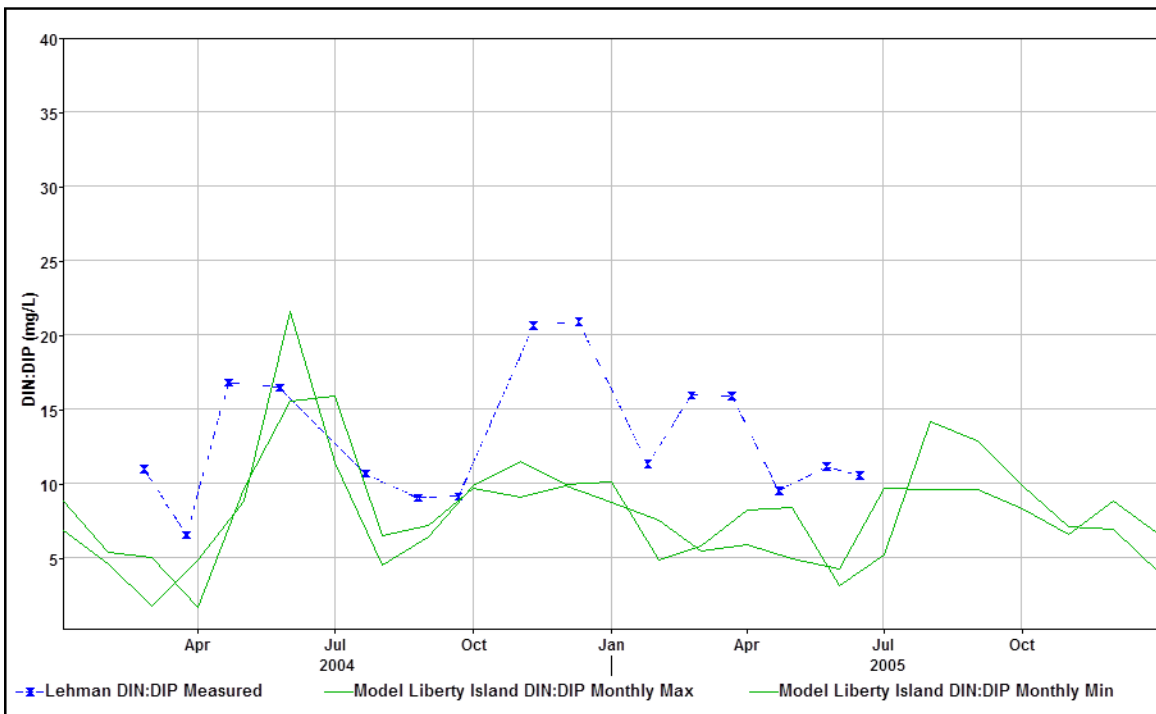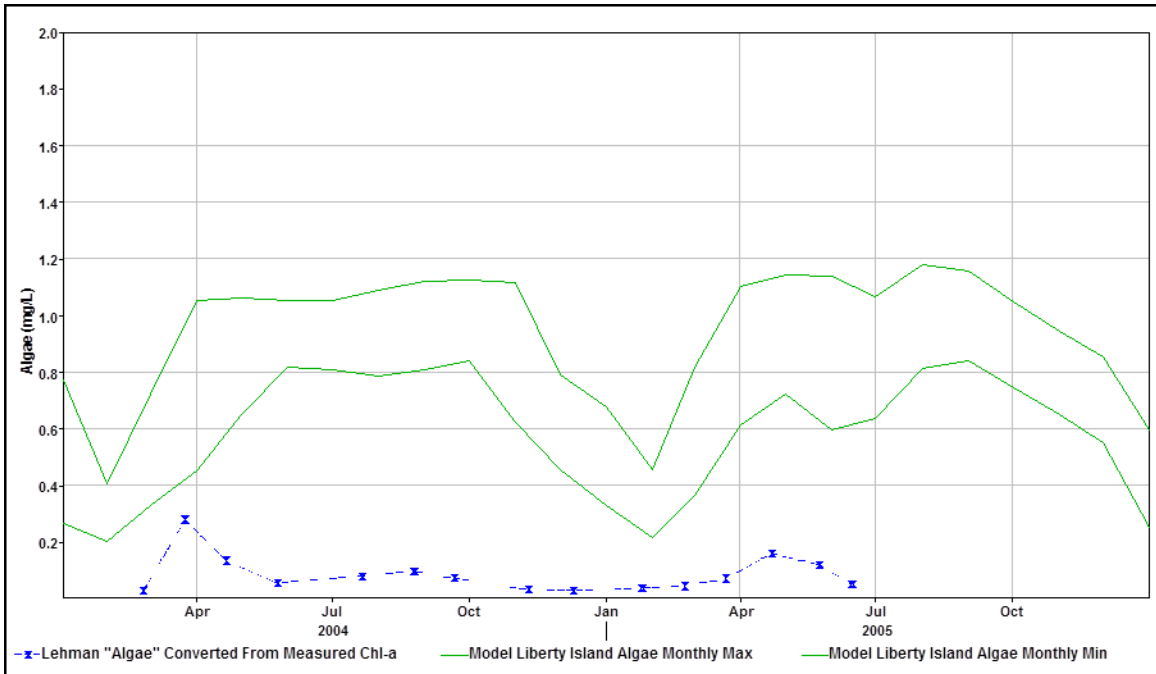
Figure 4-20 Comparison of data averaged from four locations in Liberty Island (Lehman et al., 2010) with DSM2 Historical nutrient model output for Algae (calculated using a conversion 67 g algae (dry weight)/mg chl-a) and DIN:DIP, where DIN=NO$_3$+NO$_2$+NH$_3$, and DIP=PO$_4$. Model output is represented as the monthly MAX and MIN of the original 15-minute model output.
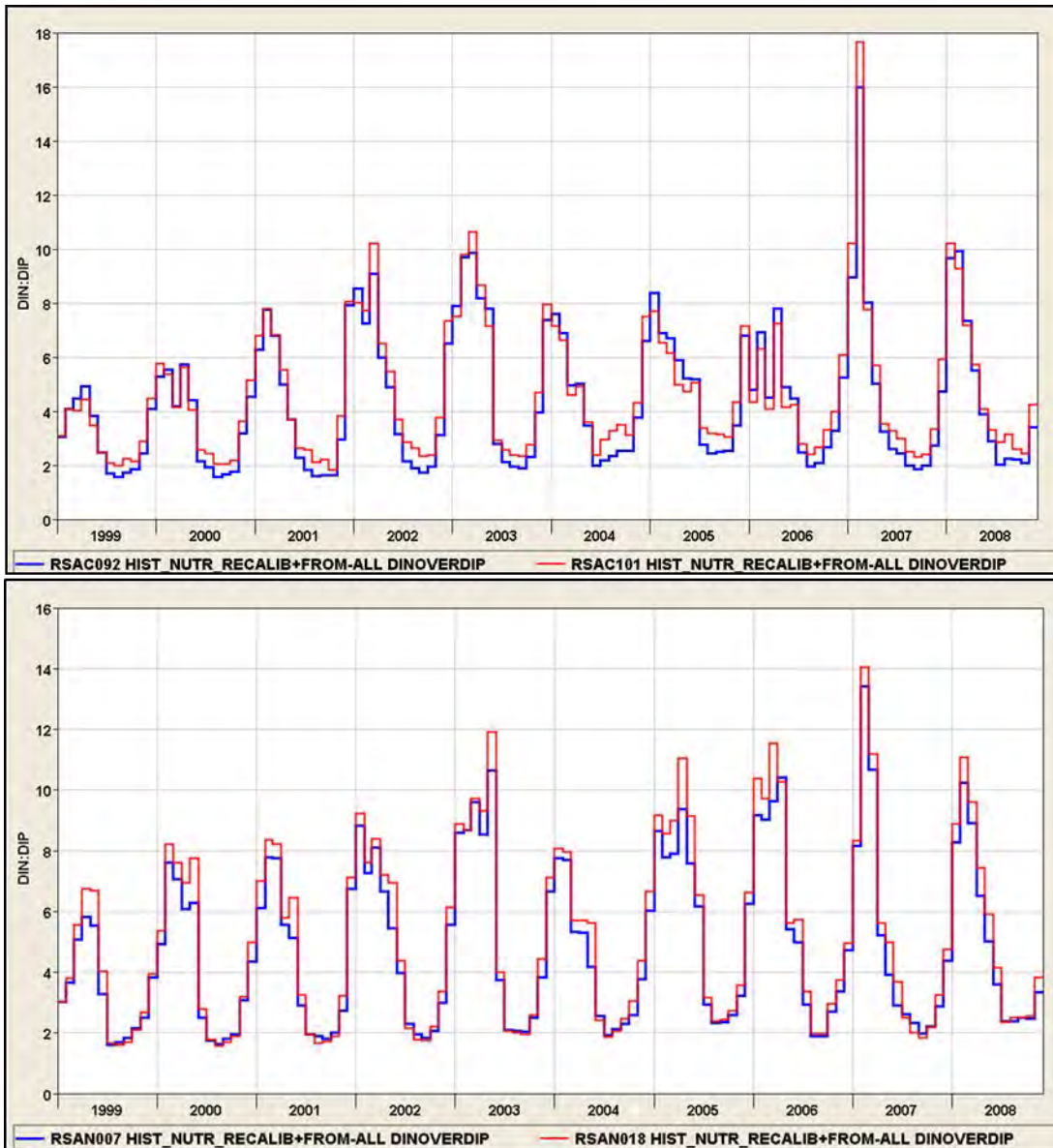
Figure 4-21 DSM2 Historical nutrient model results DIN:DIP, where DIN=NO$_3$+NO$_2$+NH$_3$, and DIP=PO$_4$. Model output is calculated as the monthly average of the original 15-minute model output.
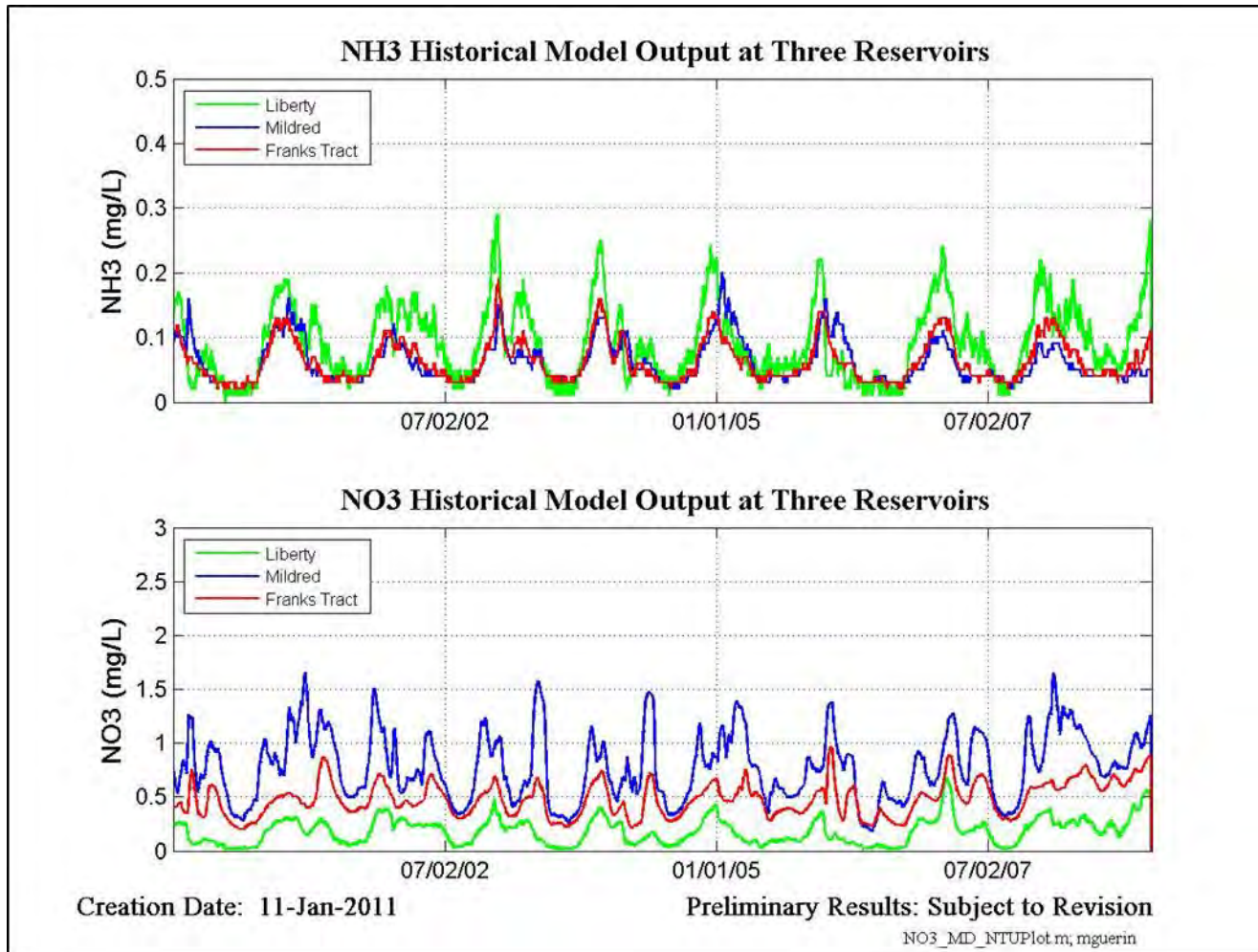
Figure 4-22 Comparison of 15-minute model output for NH₃ and NO₃ from the DSM2 Historical nutrient model at three DSM2 "reservoirs".
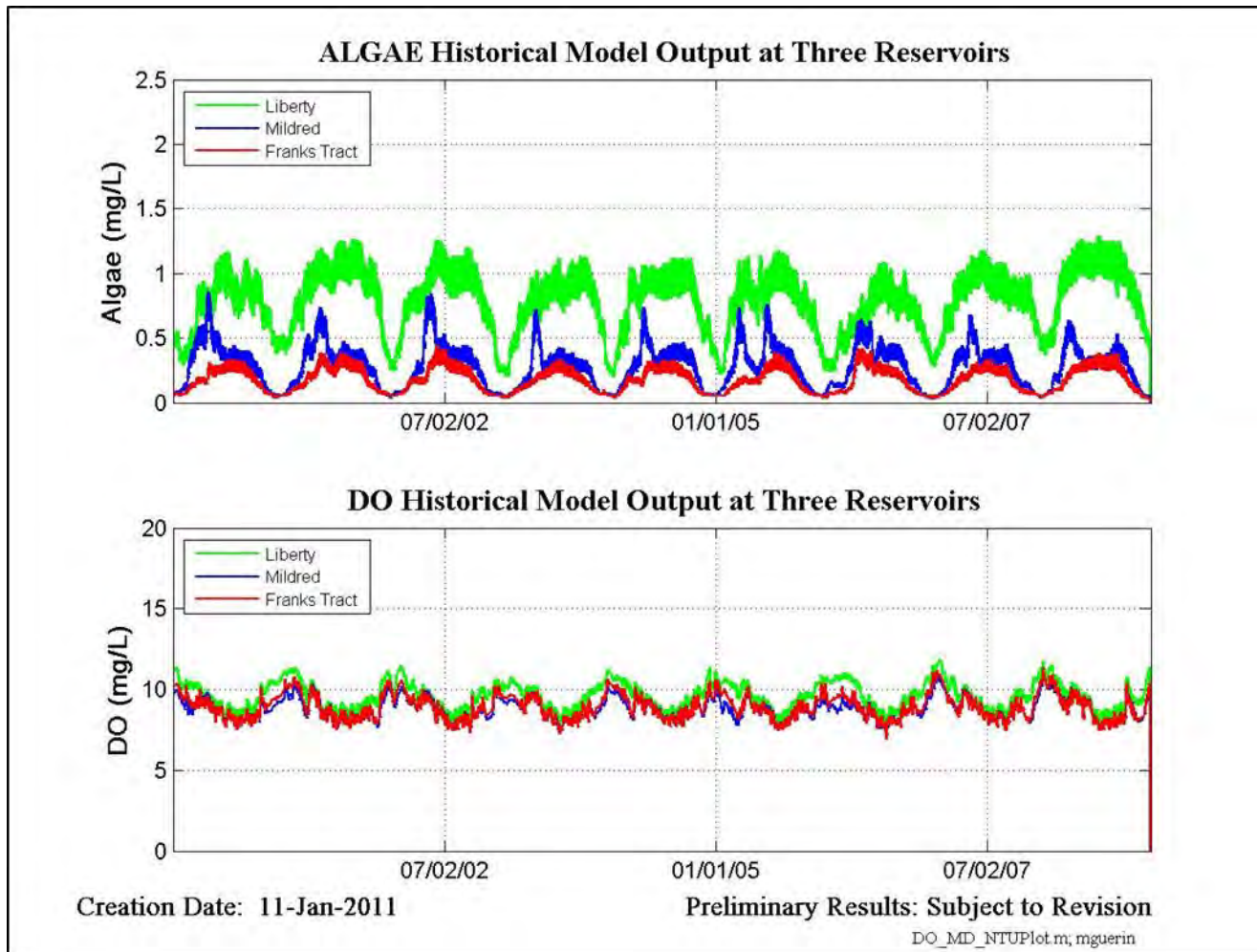
Figure 4-23 Comparison of 15-minute model output for Algae and DO from the DSM2 Historical nutrient model at three DSM2 "reservoirs".

49
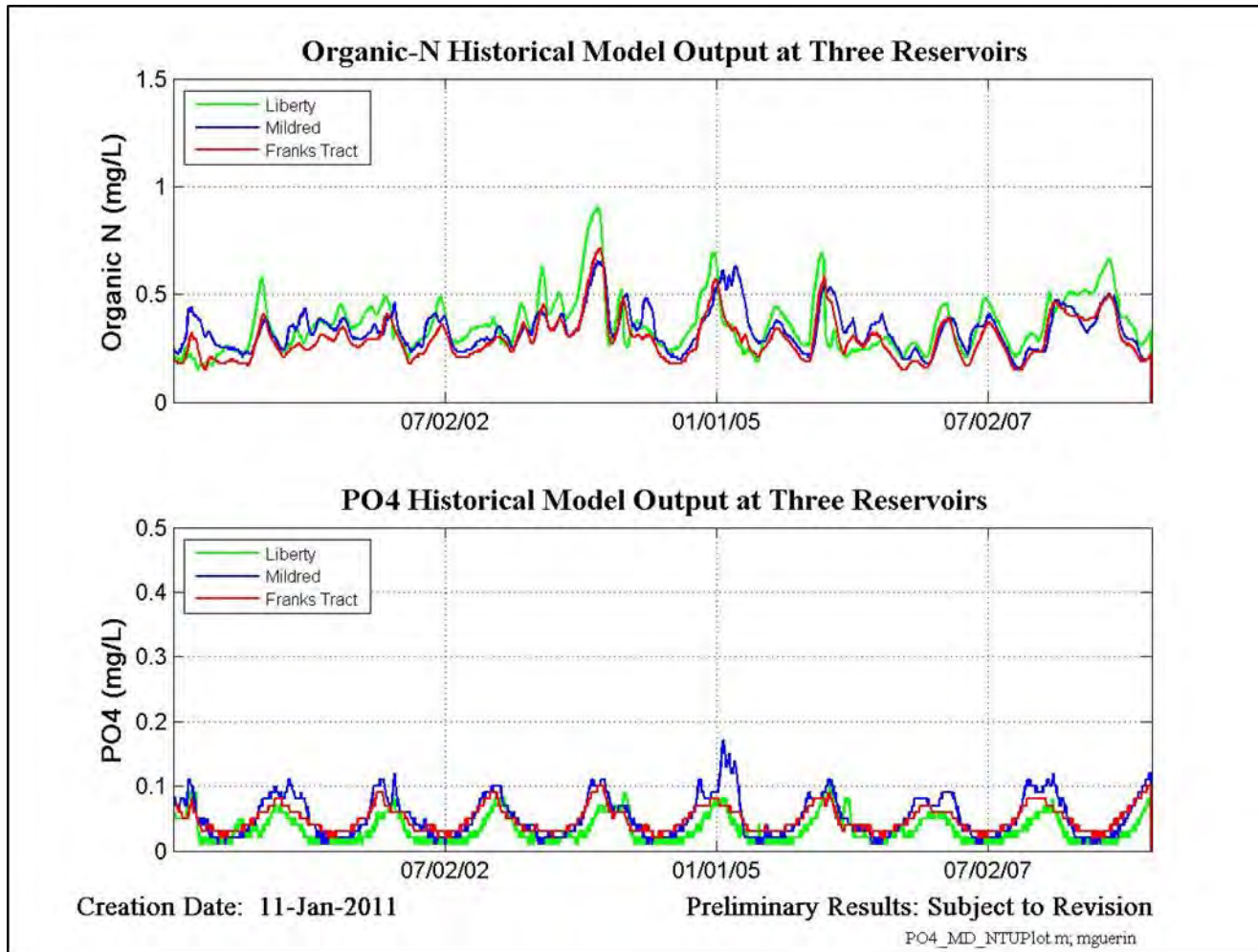
Figure 4-24 Comparison of 15-minute model output for Organic-N and PO$_4$ from the DSM2 Historical nutrient model at three DSM2 "reservoirs".
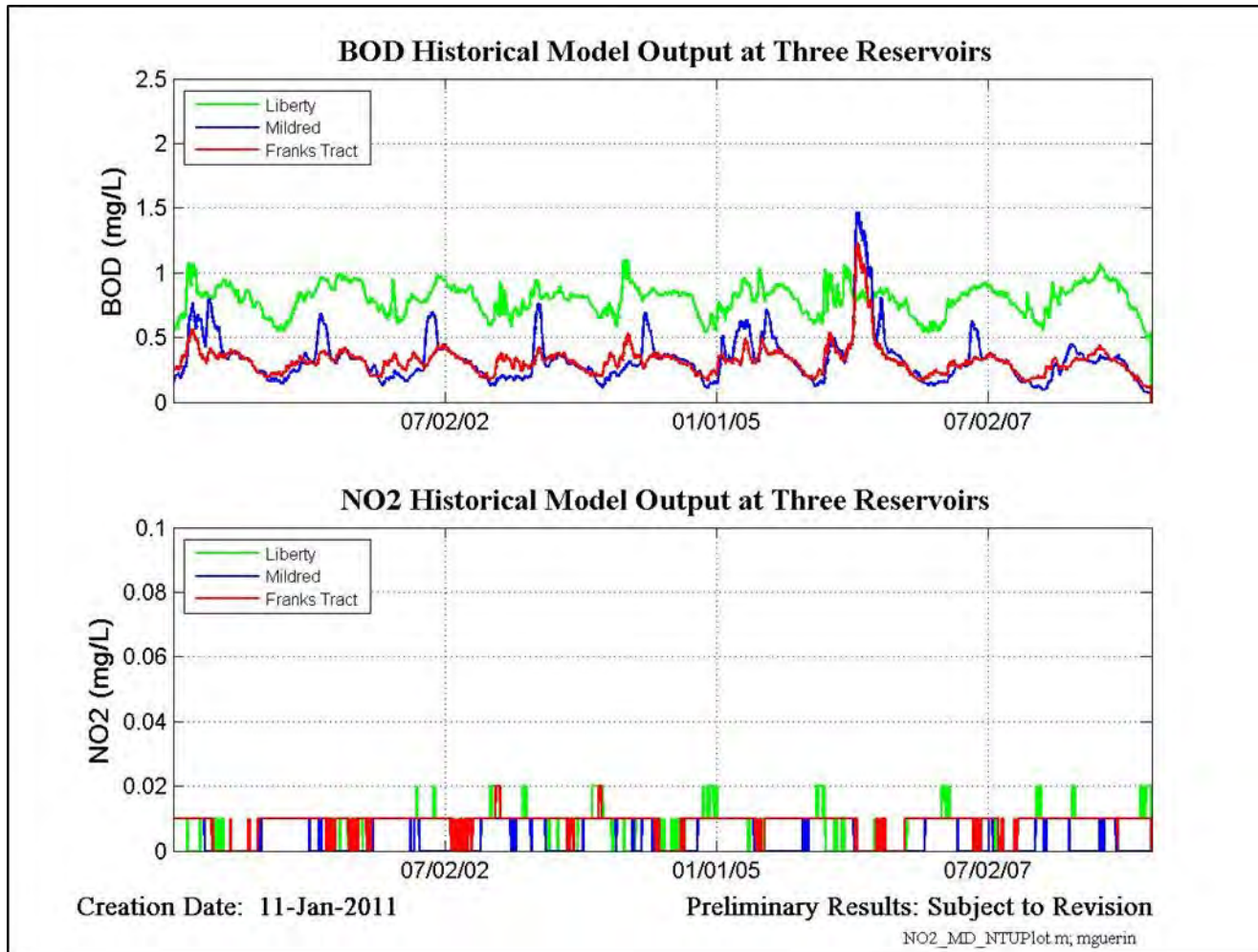
Figure 4-25 Comparison of 15-minute model output for BOD and NO₂ from the DSM2 Historical nutrient model at three DSM2 "reservoirs".

5. Simulations

There are three subsections of simulations discussed – the five main simulations for the alternatives, scenarios changing N-constituent concentrations at the Sacramento R., and a sensitivity analysis to investigate unexpectedly high values of PO_4 in the simulations.

Simulations were performed for two alternatives, EBC and PP, and for three different time periods: Present, "Early Long Term" (ELT) and "Late Long Term" (LLT).   The resulting combinations are as follows:

- EBC (Present)
- EBC-ELT
- EBC-LLT
- PP-ELT
- PP-LLT

Each simulation was run for the entire analysis period, 1976 – 1991, as described below.

In addition, for each of these five simulations, two scenarios were developed changing N-constituent concentration in the Sacramento R. by changing Sacramento Regional Wastewater Treatment Plant (WTP) effluent concentrations. In one scenario, all of the NH3 was removed from the effluent and in the other scenario, the NH_3 concentration was reduced by 50%, and the NO_3 concentration of N-atoms was increased proportionately (*i.e.,* working through molar units moles/L instead of weight units of, mg/L).

Finally, because of unexpectedly high values for PO_4 in proposed project scenarios, a sensitivity analysis was performed to see the effect of changing one calibration parameter, benthic release of PO_4 from reservoirs, and the additional effect of removing DICU concentrations as an in-Delta set of boundary conditions.

Analysis Period

The analysis period January 1976 – December 1991 was used for the purpose of nutrient and temperature analysis. The year 1975 was modeled solely as a spin-up year for the nutrient model.

Boundary Conditions for the Five Main Scenarios

Boundary conditions for nutrients and temperature are specified at all inflow locations and at the tidal boundary which is set at Martinez, the western boundary of the model. The locations of the model boundaries are shown in Figure 3-1. Nutrient concentration boundary conditions, including effluent boundaries, were identical for the five standard models. In contrast, the

boundary conditions for meteorological parameters representing climate change varied between the three time periods, Present, ELT and LLT - the details are covered in Section 0.

Boundary conditions representing current-day (2000 – 2005) conditions in the Delta were synthesized for the QUAL nutrient and temperature model scenario - a single set of nutrient concentrations and effluent boundary conditions were developed and applied to each of the scenarios.

Hydrodynamic and EC boundary conditions

Hydrodynamic and EC boundary conditions for all simulations were provided by CH2MHill for DSM2 model input and output. Effluent inflow boundaries were added to the HYDRO – this is covered in the section on setting effluent boundary conditions. With the exception of effluent inflow, hydrodynamic conditions for each of the BDCP model scenarios were used without alteration. The same effluent inflow conditions were used for each scenario.

EC boundary conditions are set at all inflow boundaries. Table 5-1 gives the EC boundary conditions supplied by CH2MHill. Boundaries are either set as a constant, or as a time series (for the San Joaquin R), or by month and location for DICU.

Table 5-1 EC boundary conditions.

Boundary Location	Value (μmhos cm^{-1})
Sacramento River	175
Yolo Bypass	175
San Joaquin River	Time Series
Cosumnes River	150
Mokelumne River	150
Calaveras River	150
DICU	Monthly Time Series

Synthesis of nutrient and temperature boundary conditions

Nutrient and DO concentrations on the inflow boundaries were set using historical data 2000 – 2005 – boundary conditions from a historical year were selected to represent each modeled year. The historical year to use for nutrient concentration boundary condition during a given model year, 1975 – 1991, was selected using a similar water year type as a general guide for either the San Joaquin River or the Sacramento River. The Sacramento R., Yolo Bypass, Mokelumne R., Cosumnes R and Martinez boundaries used the same matching of model year to Sacramento R. historical year, using the Sacramento Water Year Type as a guide. The San Joaquin R. and Calaveras R. nutrient boundaries were set using the same matching of historical year to model year using the San Joaquin Water Year Type as a guide. Table 5-2 and Table 5-3 show the annual correspondence established between current conditions (Column 2) and the modeled year (Column 1).

Effluent inflow and nutrient boundary concentrations were synthesized from existing effluent data in a similar manner, using the year correspondence shown in Table 5-2. Sacramento Regional Wastewater Treatment Plant (SRWTP) effluent flows were scaled, using this year-correspondence, to assure the daily percentage of effluent flow in Sacramento R. inflow remained below the historical 2000 -2005 maximum (~ 4.5%, see Figure 5-1). Daily effluent flows for Stockton WWTP daily effluent remained below ~ 6.2 % of San Joaquin R. inflow, the historical maximum percentage.

All other effluent flows were applied without scaling using the same annual year selection as the Sacramento R. These effluent inflow boundary values were considered relatively small, so inflow values were used directly (i.e., no scaling). Concentrations of nutrients, water temperature and DO were not changed from the values recorded in the historical time series for these effluent locations.

Synthesis of meteorological and water temperature boundary conditions

Meteorological and water temperature boundary conditions were developed separately from the boundary conditions for constituents in the nutrient model. Three sets of synthetic meteorology were generated using historical data, for present day and two future climate change conditions. Meteorological boundary conditions include air temperature, wet bulb temperature, atmospheric pressure, wind speed and cloud cover.

Projected daily average temperatures for the two climate change conditions were used as a basis for meteorological boundary condition development by closely matching average air temperature under climate change with historical air temperature at approximately the same annual date (+/- 2 days) using existing meteorological data[6]. For a given model day for one of the climactic conditions, the projected average daily temperature is compared with average

---

[6] This methodology was adapted from a method developed by Don Smith (president of RMA) for creating meteorological boundary conditions from historical data.

temperatures within +/-two days for all available historical years. The closest temperature is chosen from the list, the selected day and year is recorded, and the set of meteorological conditions from the chosen historical day and year is then used for that model day.

Three sets of boundary conditions for water temperature were also generated using historical data by using the same dates used in matching the projected air temperatures. The historical water temperature at the Sacramento R., Martinez and the San Joaquin R. from that day is then mapped into the boundary conditions for water temperature - these are the only three time series used in setting all boundary water temperatures.

A similar strategy (using the dates selected by matching air temperatures) was attempted for the DO boundary time series, but the resulting time series of data did not look reasonable, so DO was instead developed using the methodology for synthesizing boundary conditions for the nutrients.

DICU nutrient boundary conditions

DICU flows incorporate channel depletions, infiltration, evaporation, and precipitation, as well as Delta island agricultural use (DWR, 1995). DICU values, which are applied on a monthly average basis, estimate monthly diversions (incorporate agricultural use, evaporation and precipitation), drains (agricultural returns), seeps (channel depletions). These flows are distributed to multiple elements throughout the Delta.

Results for the Five Main Scenarios

The nutrient model was used to compare predicted nutrients and temperature for Existing Biological Condition (EBC) and Proposed Project (PP) scenarios of Current conditions (EBC), Early Long Term (ELT) conditions with a Sea Level Rise of 15 cm (SLR 15) and Late Long Term (LLT) conditions with a Sea Level Rise of 45 cm (SLR 45). All plots of model results are shown as monthly-averages of 15-minute model output.

Model results at representative locations in three main regions were combined to supply monthly-averaged, regionally averaged model output for the fisheries and food web analyses. The regions and the approximate locations of data points selected within these regions are shown in Figure 5-2 and Figure 5-3. The areas denoted "West to Martinez" and "Suisun Marsh" in Figure 5-2 are not considered calibrated – the area near Martinez is too close to the boundary, and there were too few calibration data points in Suisun Marsh.

Four additional averaging regions were developed for analysis – Central Delta, South Delta, East Delta and Cache/Yolo – of selected model comparisons within this document only. These areas and the approximate location of the model output points are shown in Figure 5-4 to Figure 5-7.

Figures illustrating the difference among five model scenarios are shown for each of the three main regions and each constituent below. Plots for each region are shown on the same scale to allow for direct comparison between regions. Only seven of the modeled years are shown for ease of comparison.

In addition, model results between scenarios were compared as percent differences averaged by month over the modeled time span. However, as described in the Executive Summary, the model results for the Proposed Project scenarios have results that are suspect – PO_4 concentrations are too high. Therefore, only limited comparison is made for the Proposed Project scenarios.

Discussion of scenario results

Due to the uncertainties in the initial model calibration and the nature of the boundary conditions (monthly grab samples), all model results are presented as monthly averages. Comparisons between model scenarios are presented in Tables as percent differences. Calculations of (monthly) percent difference are averaged over the locations within each region (*e.g.,* Suisun Region or East Delta region), and then averaged by month for each region over the modeled time span. These types of averages – a single number representing the combined results for each of the twelve months - are called "Average Monthly" calculations.

The major factors potentially affecting the differences in nutrient results between scenarios include: hydrodynamic boundary conditions; seal level rise; climate change; and bathymetry changes in the Delta. The changes in hydrodynamic boundary conditions considered here are inflow changes at the Sacramento and San Joaquin Rivers, inflow at the Yolo Bypass, and changes in export regime between the North Delta (on the Sacramento R.) and the South Delta (SWP+CVP exports). Total Exports consists of the sum of North Delta and South Delta Exports.

The changes in bathymetry, discussed in Section 2, consist of the introduction of tidal marsh into the Delta in the ELT and LLT scenarios. These areas are mostly introduced as "reservoirs" in DSM2 (there is an exception in the S. Delta where the open water is conceptualized as channels). Reservoirs are essentially open water areas, and calculations are made for the reservoir as a single fully-mixed volume at each computational step.

Two types of comparisons are made: between the EBC scenario and the EBC-ELT and EBC-LLT scenarios, calculated, for example as (EBC-LLT – EBC)/EBC, and between the PP scenarios at ELT and at LLT, calculated, for example, as (PP-LLT – PP-ELT)/PP-ELT. Comparisons with the EBC

scenario and EBC-ELT or EBC-LLT tend to capture effects due to climate change (*i.e.,* changes in meteorology) and sea level rise.

The constituents each have percent difference calculations made for all three of the main regions for the EBC scenario comparisons and for the four secondary regions – for the PP scenarios, comparisons are only made for the three primary regions.

Average changes in inflow and export boundary conditions

The most significant difference between the scenarios in Sacramento R. inflow is seen in the EBC scenario (Figure 5-29). At the Yolo Bypass (Figure 5-29), both of the PP scenarios and the EBC SLR 45 scenario, with much higher average flows February through April. On the San Joaquin River (Figure 5-30), the story is similar – higher average flows are seen on the San Joaquin January – May for both of the PP scenarios and the EBC SLR 45 scenario.

The PP scenario, we see the introduction of North Delta Exports (Figure 5-31) and a decrease in S. Delta Exports on average for all months except April – June. Total Exports are higher on average for both PP scenarios (Figure 5-30) January – June. The PP-LLT scenario actually sees a decrease in total exports July – December.

Average changes in water temperature

Table 5-4 and Table 5-5 present the percent difference monthly average comparisons for the ELT scenario comparisons for water temperature. In the ELT time frame (Table 5-4), changes due to climate change generally results in higher water temperature. Adding in the PP, average water temperature decreases slightly in areas of the Delta affected by Yolo and Sacramento R. water in part due to higher Winter/Spring flows on the Yolo and the moderation of the open water areas in the Cache Slough region. In the S. Delta, water temperature also decreases slightly June - October, possibly due to the lower S. Delta exports during that time.

In the LLT time frame (Table 5-5), water temperature increases in the Cache/Yolo area both due to the climate changes (increases in air temperature) and due to the large open water areas with increased residence time. With the introduction of the PP, water temperature decreases slightly in the lower San Joaquin through to Suisun - this appears to be due to the effects of lower S. Delta exports. Large open water areas in the South Delta result in somewhat warmer water temperatures.

Average changes in NH_3, NO_2+NO_3, Organic-N and PO_4

In comparing the EBC, EBC-ELT and EBC-LLT scenarios (Table 5-6 through Table 5-9), we see the changes due to future conditions (ELT and LLT) are not large in comparison with present conditions. The general trend is for Algal growth to increase in the future (shown as increases in Chl-a), and for PO_4 to decrease. The changes are greater for the LLT scenario than for the ELT scenario, as expected. The NO_3+NO_2 differences are also negative, indicating that the increased Algal growth is supported by PO_4 and by NO_3 rather than NH_3. Model parameterization was set so that algal growth had no preference between N-constituents – so a higher concentration of NO_3 will results in preferred usage of this N-constituent over NH_3. In addition, lower flow rates on the Sacramento R in the future (see Figure 5-29, upper plot), as well as changes in the seasonality of flow, means that Sacramento Regional effluent inflow, which is high in ammonia, could increase the downstream concentrations of NH_3 – this also influences the Lower San Joaquin Region. The lower Algal growth for the Lower San Joaquin Region shown in Table 5-6 (EBC-ELT) may be due to decreases in Sacramento R. inflow in the ELT time frame – less flow will come through the eastside of the Delta into the lower San Joaquin R. Increases in algal growth in the Sacramento and Suisun regions, in comparison, may reflect a shift of flow through the Yolo Bypass, instead of past Freeport on the Sacramento R.

Results for PO_4 for all the scenarios are included here for the record, but they should not be viewed with any confidence for the PP scenarios due to problems in setting parameters in the new and enlarged DSM2 "reservoirs". As shown in Figure 5-26 through Figure 5-28 and in Table 5-6 and Table 5-8, PO_4 decreases in the future without the PP as it is utilized by increased Algal growth due to changed meteorological conditions, while it increases everywhere with the PP scenarios - this result is not sensible.

Tables for differences between the PP-ELT and PP-LLT scenarios, Table 5-10 and Table 5-11 respectively, are included for completeness, but not discussed as the results are not viewed as reliable.

Scenarios Changing Sacramento Regional WTP N-Constituents

Only selected results for constituents NH_3 and NO_3+NO_2 are included in this section, Figure 5-32 through Figure 5-37 – a complete set of Scenario results is available in Appendix V, Section 12, along with percent difference Tables (calculated as (Scenario – EBC-ELT)/EBC-ELT, for example). The Proposed Project results should be ignored when examining the model output.

Tabular results show that removing NH_3 in Sacramento Regional WTP effluent results in a decrease in Algal growth (indicated in Tables as a decrease in Chl-a). The decrease was greater in the LLT scenario comparison. Increasing NO_3 in the effluent and concurrently decreasing NH3 also results in a decrease in Algal growth, a decrease in the utilization of PO_4 and an increase (obviously) in NO_3+NO_2 concentrations.

Sensitivity Analysis

A small sensitivity analysis was performed to examine the consequences of changing two of the potential sources of excess PO_4 in Proposed Project scenarios. Several results are shown in this section, Figure 5-38, Figure 5-39 and Figure 5-40. A full set of model results is found in Appendix VI, Section 13 . (Also see the Appendix VI for plots for the LLT scenarios). Each plot in this section shows model results for the PP-ELT scenario (dark blue), the PP-ELT scenario with benthic sources of PO_4 removed from all reservoirs (green) in the DSM2 model domain, the PP-ELT scenario with benthic sources of PO_4 removed from all reservoirs and all DICU sources of nutrients turned off (red), and the EBC-ELT scenario (light blue) for comparison.

Removing the benthic source of PO_4 from the PP-ELT scenario, Figure 5-39, in reservoirs reduces PO_4 to levels that are comparable, or below, the levels found in the EBC-ELT scenario. Similar results are seen for modeled Algae in Figure 5-38 – removing this source reduces Algal growth significantly. The amount of reduction in PO_4 and Algae depends on the region, as shown in the Figures.

This result shows that the benthic source of PO_4 in reservoirs forms a significant contribution to modeled PO_4, and that variation in this release not only will affect the level of PO4 modeled in the Delta, but also affect algal growth and therefore the utilization and production of the other nutrients.

Further removing all sources of DICU reduces the level of each nutrient and Algal growth further. This is another means of controlling in-Delta sources of PO_4.
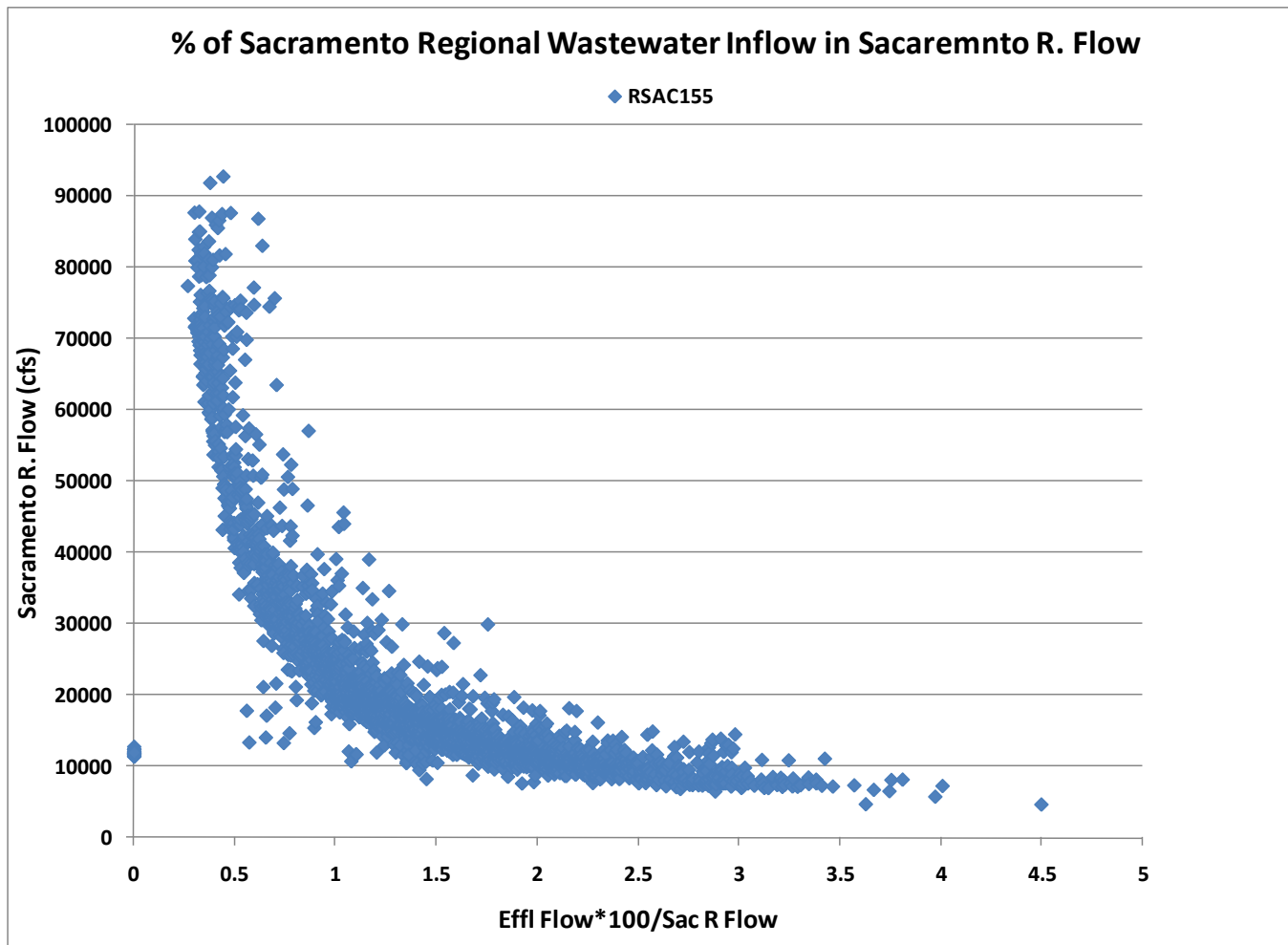
Figure 5-1 Maximum percentage of Sacramento Regional Wastewater inflow in Sacramento R. inflow was typically less than 4 %.

Table 5-2 Correspondence between the BDCP scenario model year (Column 1) and the Historical Year (Column 3) used to apply nutrient BC for the Sacramento R. and all Effluent BC, and the factor used to scale SRWTP effluent inflow (Column 4).

Model year	Sac WY Type	Historical BC Year	Factor*SRWTP Flow
1975	W	2000	1.0
1976	C	2004	1/1.4
1977	C	2002	1/1.6
1978	AN	2000	1.15
1979	BN	2004	1.0
1980	AN	2000	1.0
1981	D	2001	1.0
1982	W	2000	1.7
1983	W	2001	1.5
1984	W	2002	1.2
1985	D	2001	1.0
1986	W	2000	1.0
1987	D	2001	1/1.1
1988	C	2002	1/1.5
1989	D	2004	1/1.25
1990	C	2001	1/2.1
1991	C	2000	1/2

Table 5-3 Correspondence between the BDCP scenario model year (Column 1) and the Historical Year (Column 3) used to apply nutrient BC for the San Joaquin R.

Model year	SJR WY Type	Historical BC Year
1975	W	2005
1976	C	2001
1977	C	2001
1978	W	2005
1979	AN	2000
1980	W	2005
1981	D	2002
1982	W	2005
1983	W	2005
1984	AN	2000
1985	D	2002
1986	W	2005
1987	C	2001
1988	C	2001
1989	C	2001
1990	C	2001
1991	C	2001
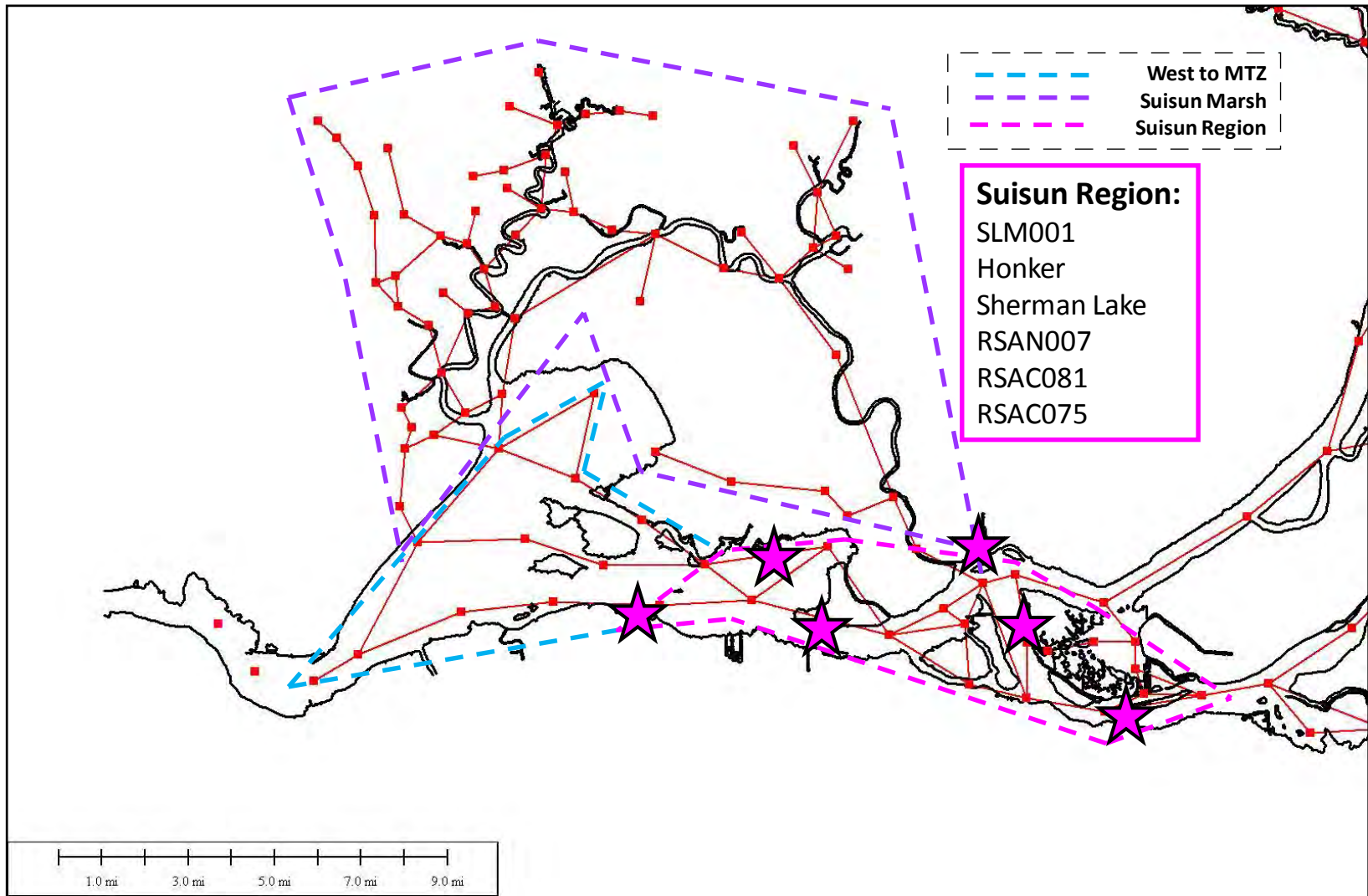
Figure 5-2 Suisun analysis region shown in pink – locations are approximate. Calibration results are also shown at location names indicated by stars.
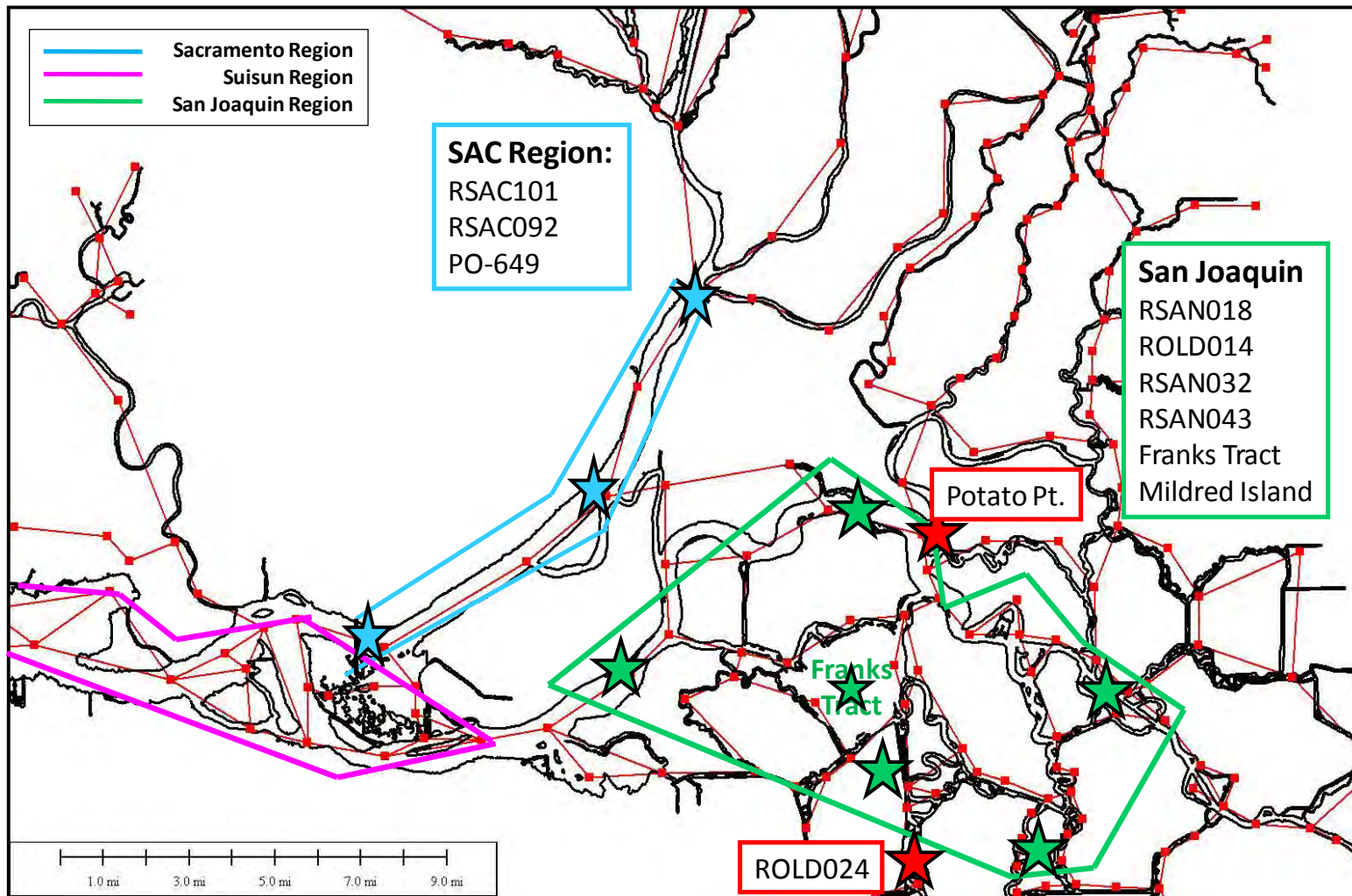
Figure 5-3 Sacramento Region (blue) and San Joaquin Region – locations are approximate. Calibration results are also shown at location names indicated by stars – red stars indicate two additional locations for calibration results (not included in regional averages).

Figure 5-4 Three locations averaged to represent the results for the Central Delta Region.
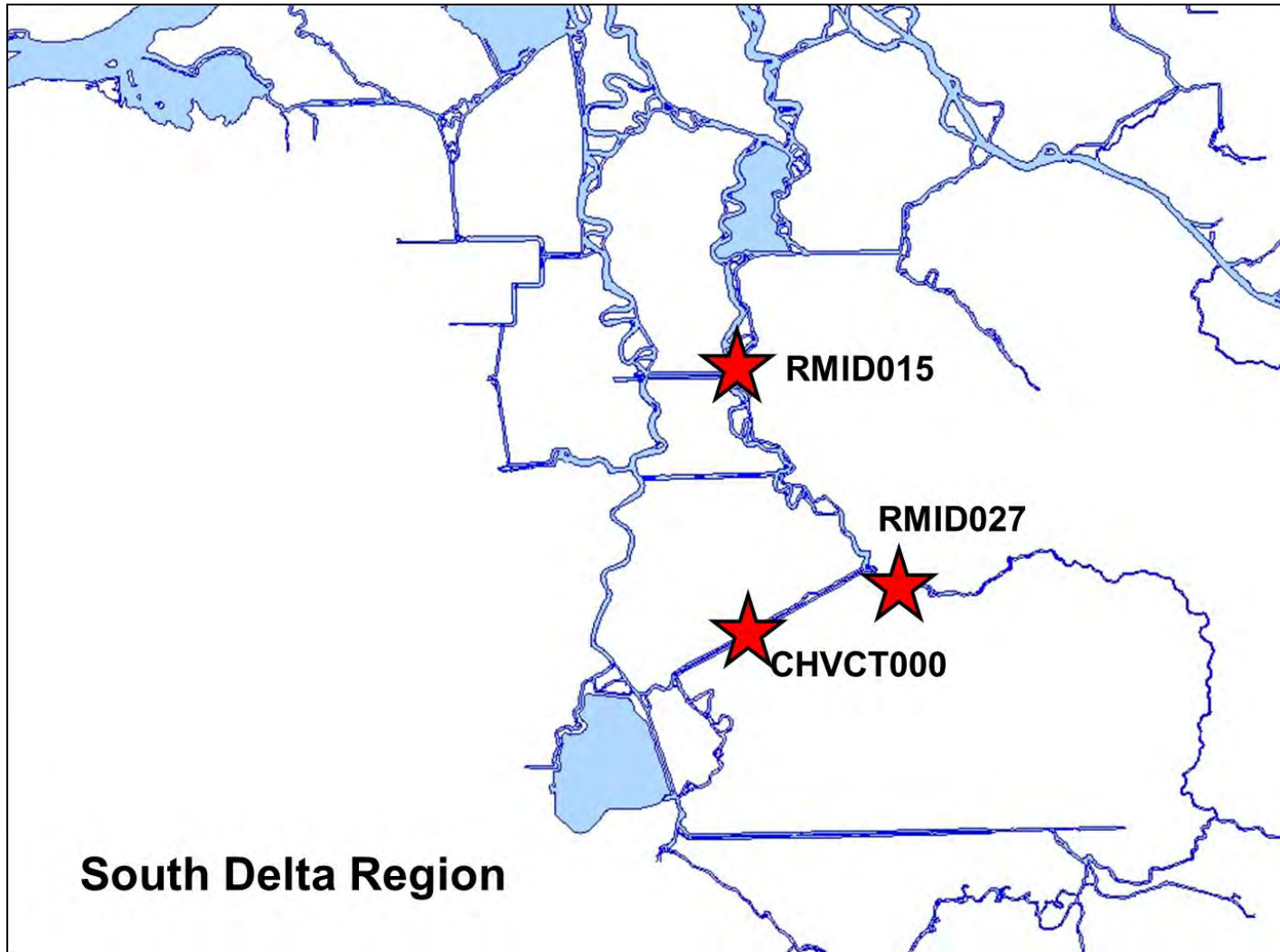
Figure 5-5 Three locations averaged to represent the results for the South Delta Region.
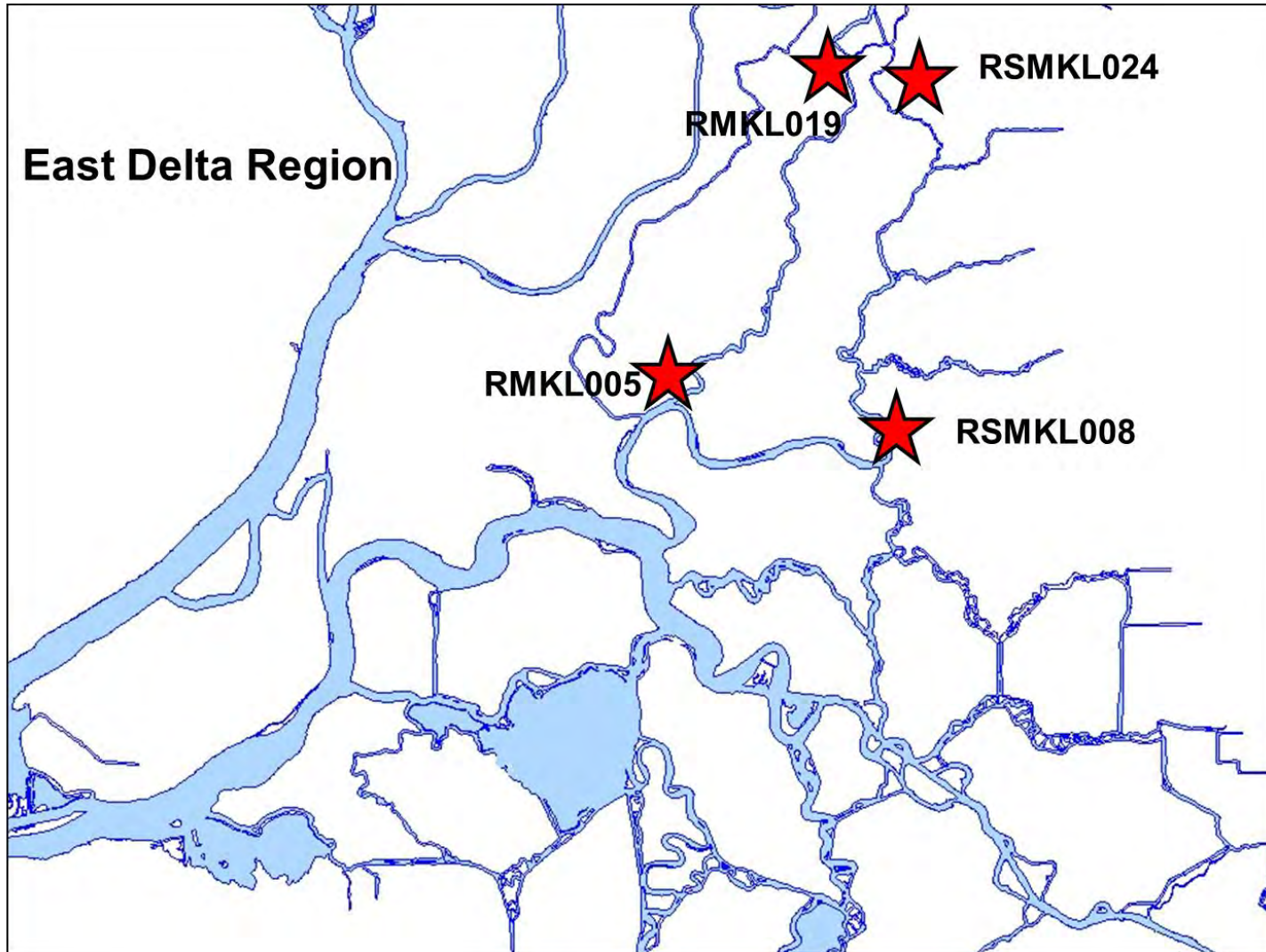
Figure 5-6 Four locations averaged to represent the results for the East Delta Region.
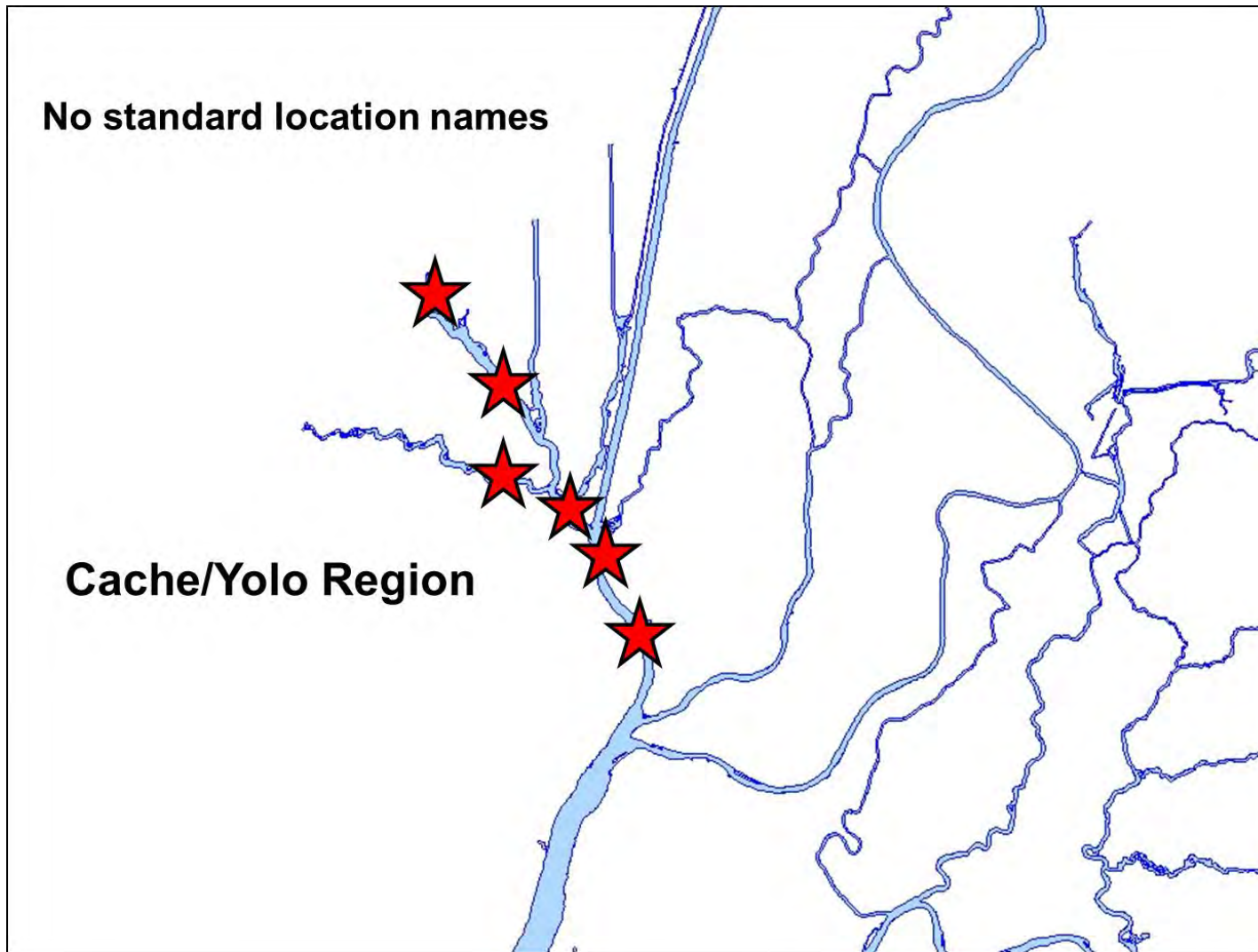
Figure 5-7 Six locations averaged to represent the results for the Cache/Yolo Region.
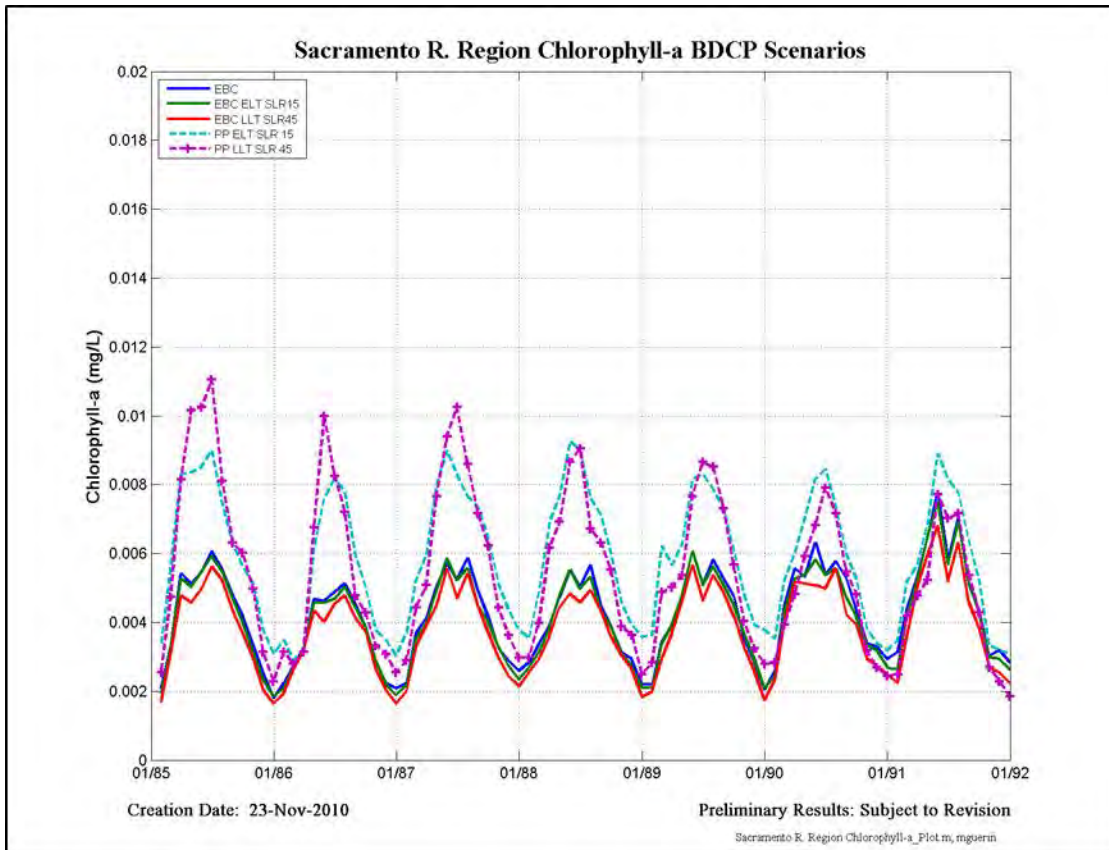
Figure 5-8 Chl-a results in the Sacramento Region.
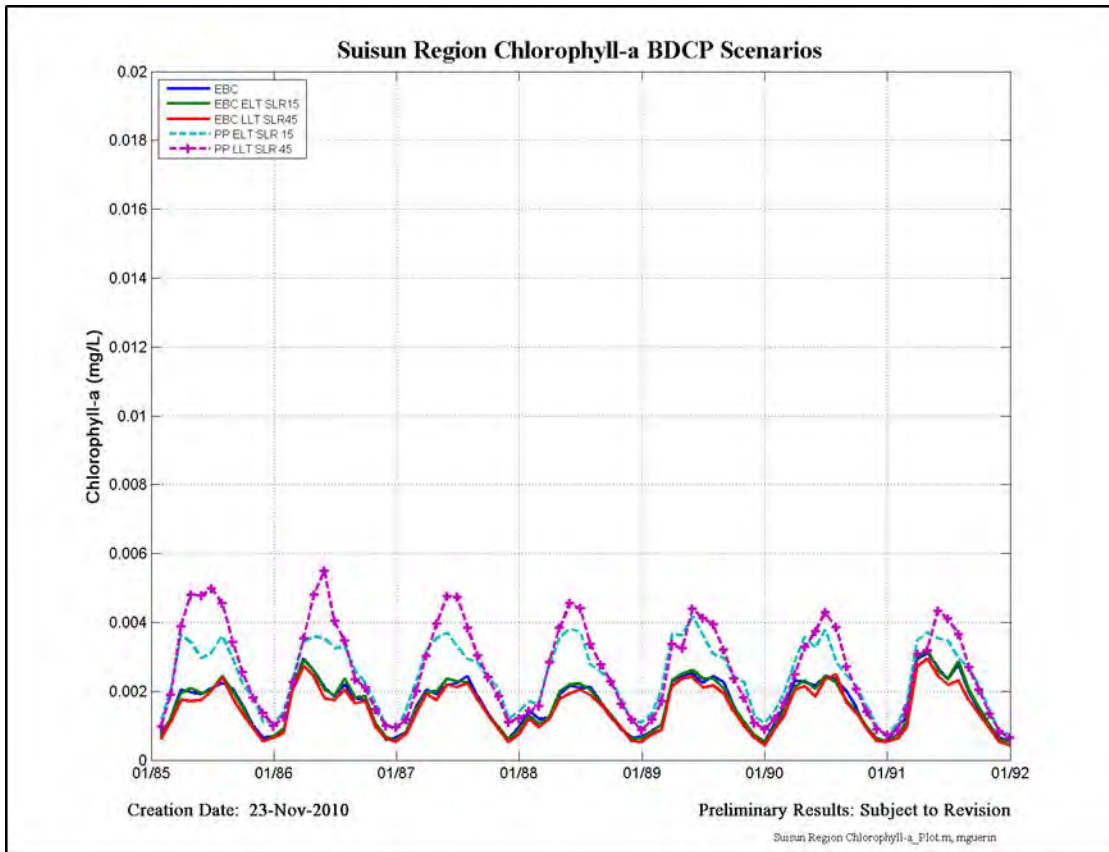
Figure 5-9 Chl-a results in the Suisun Region.
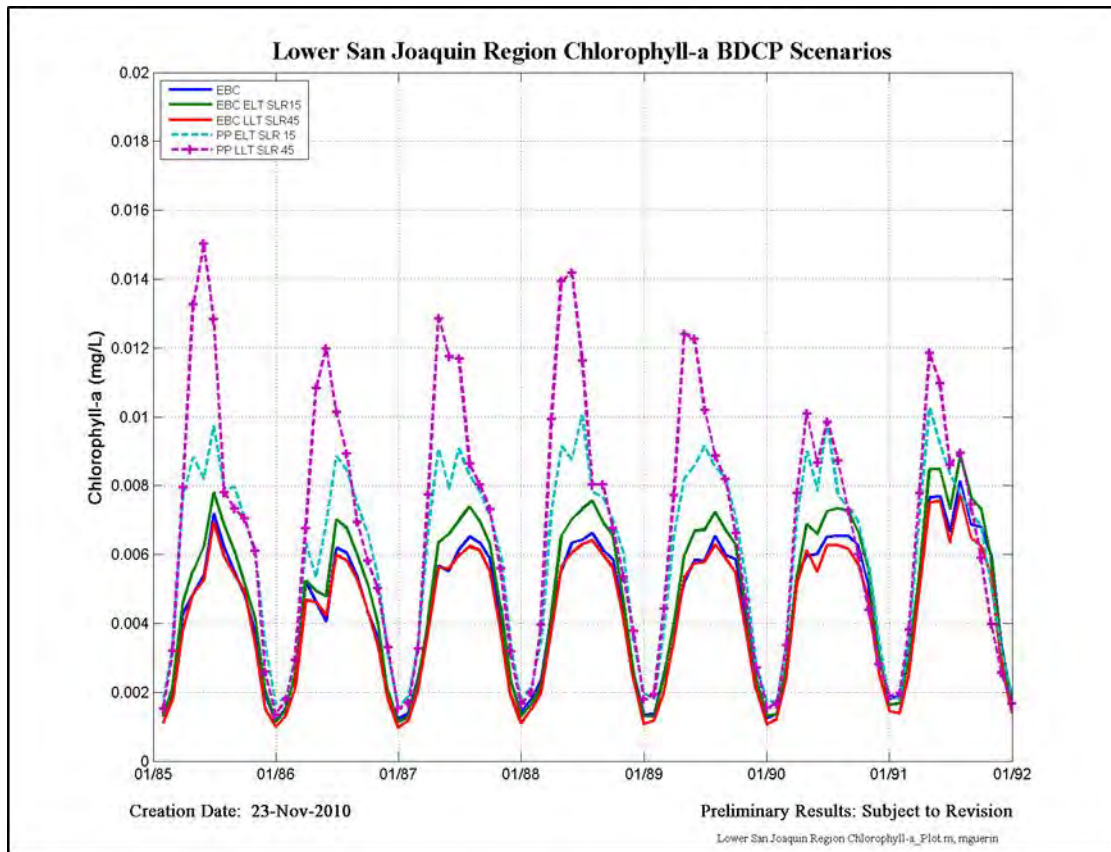
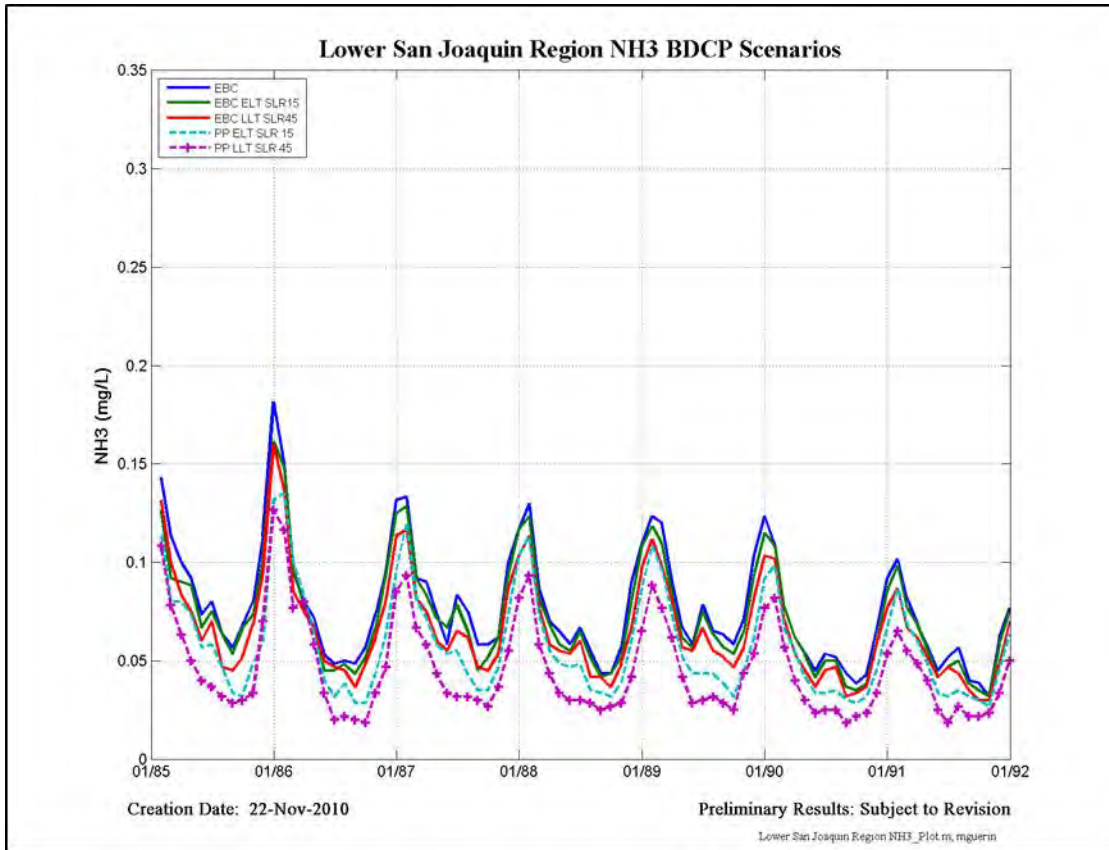**Figure 5-10 Chl-a results in the San Joaquin Region.**
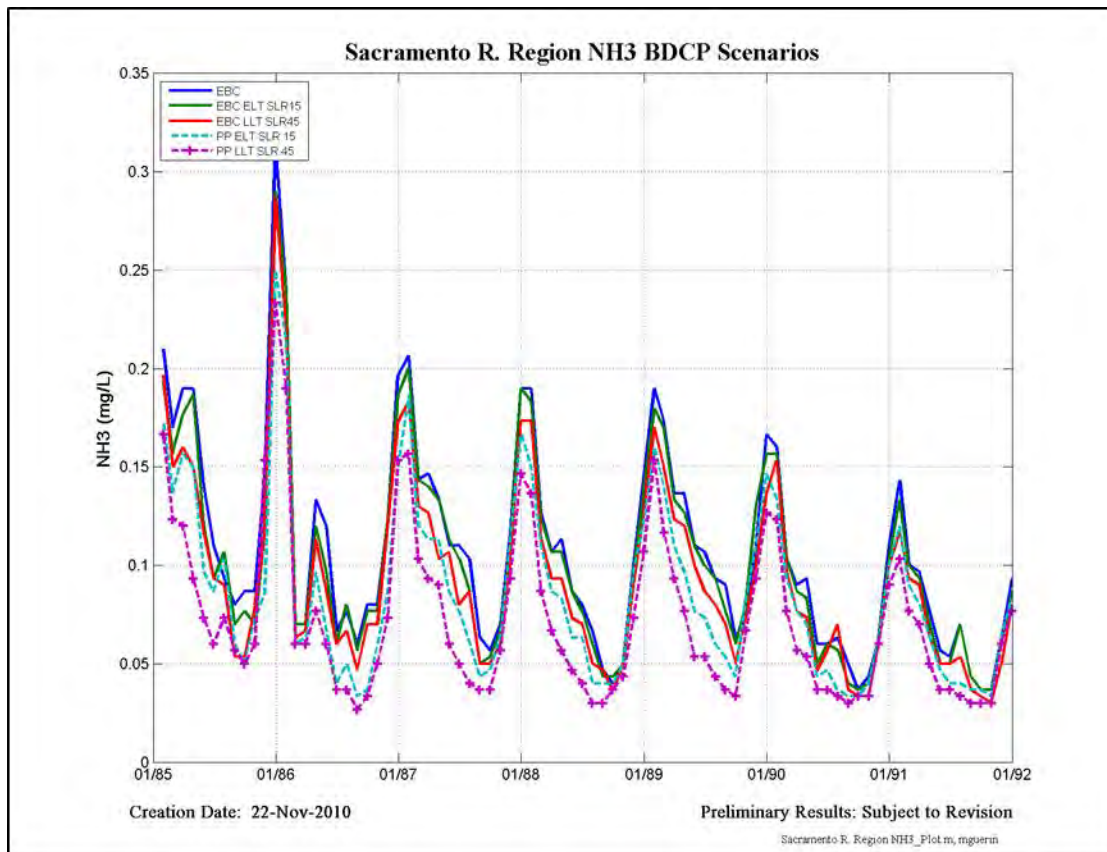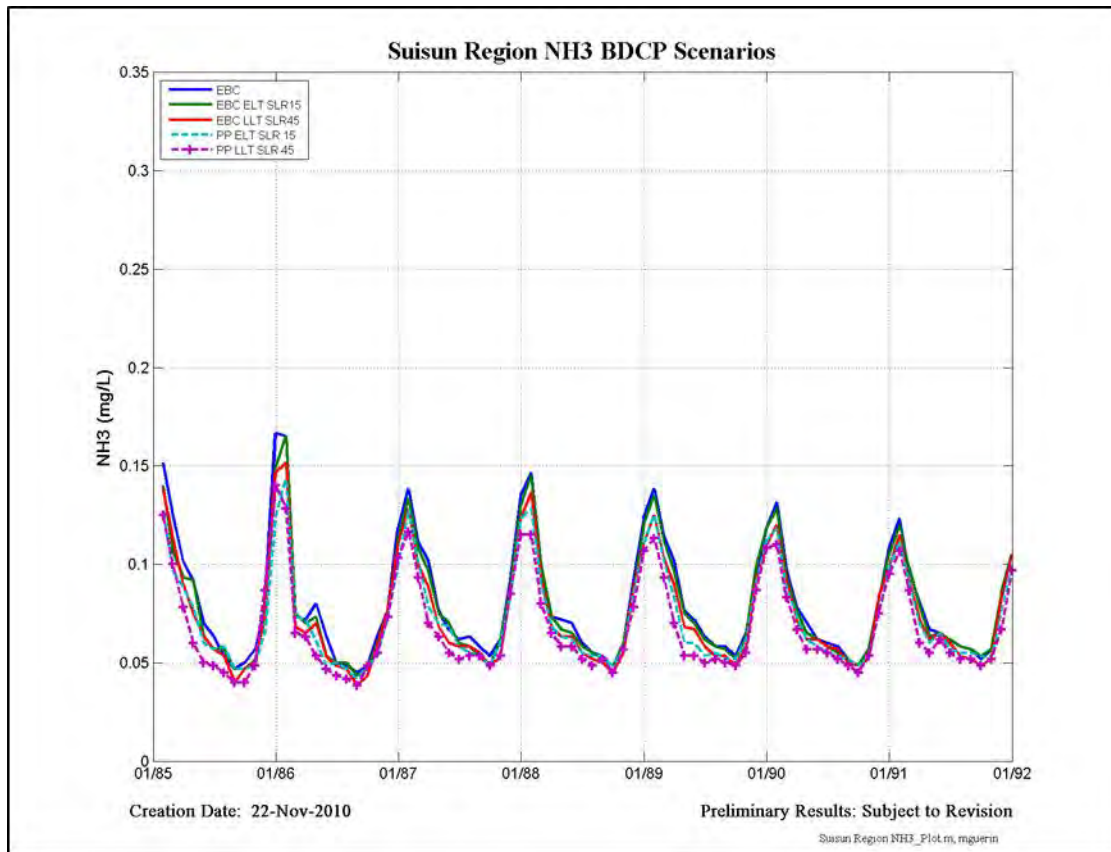
Figure 5-11 NH$_3$ results in the Sacramento Region.

Figure 5-12 NH$_3$ results in the San Joaquin Region.
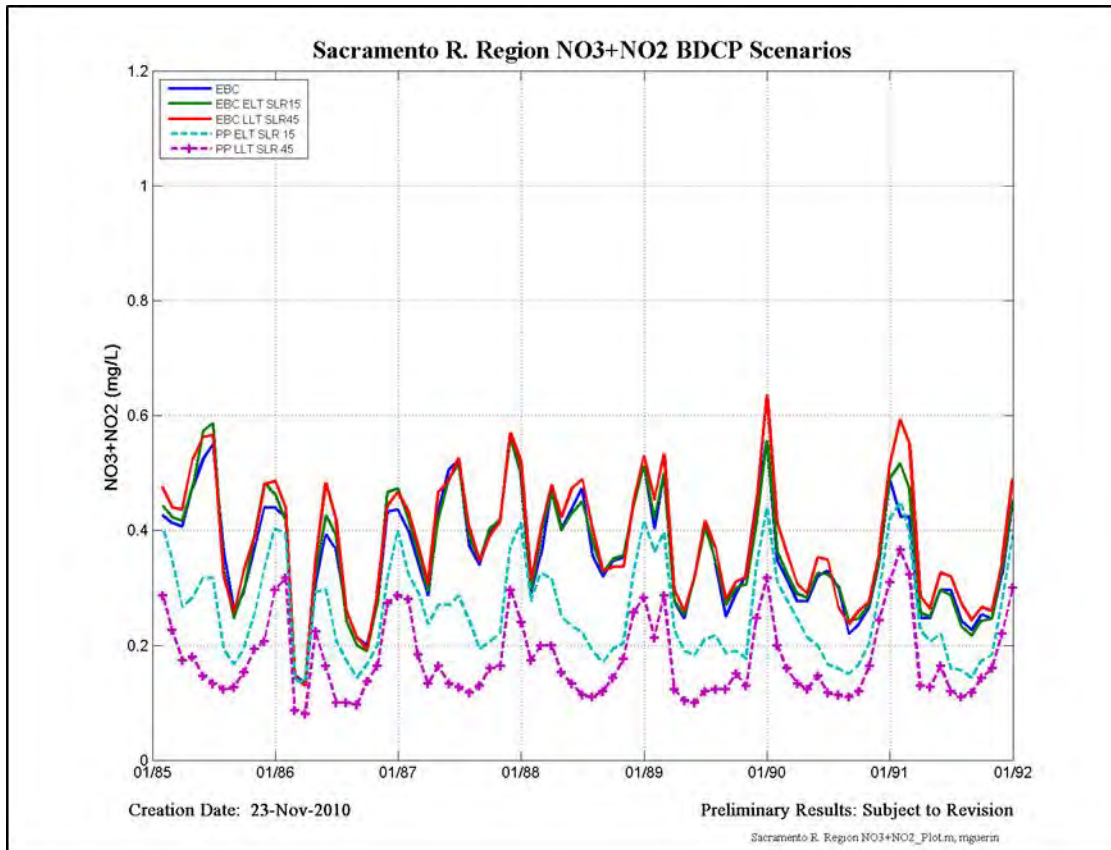
Figure 5-13 NH$_3$ results in the Suisun Region.
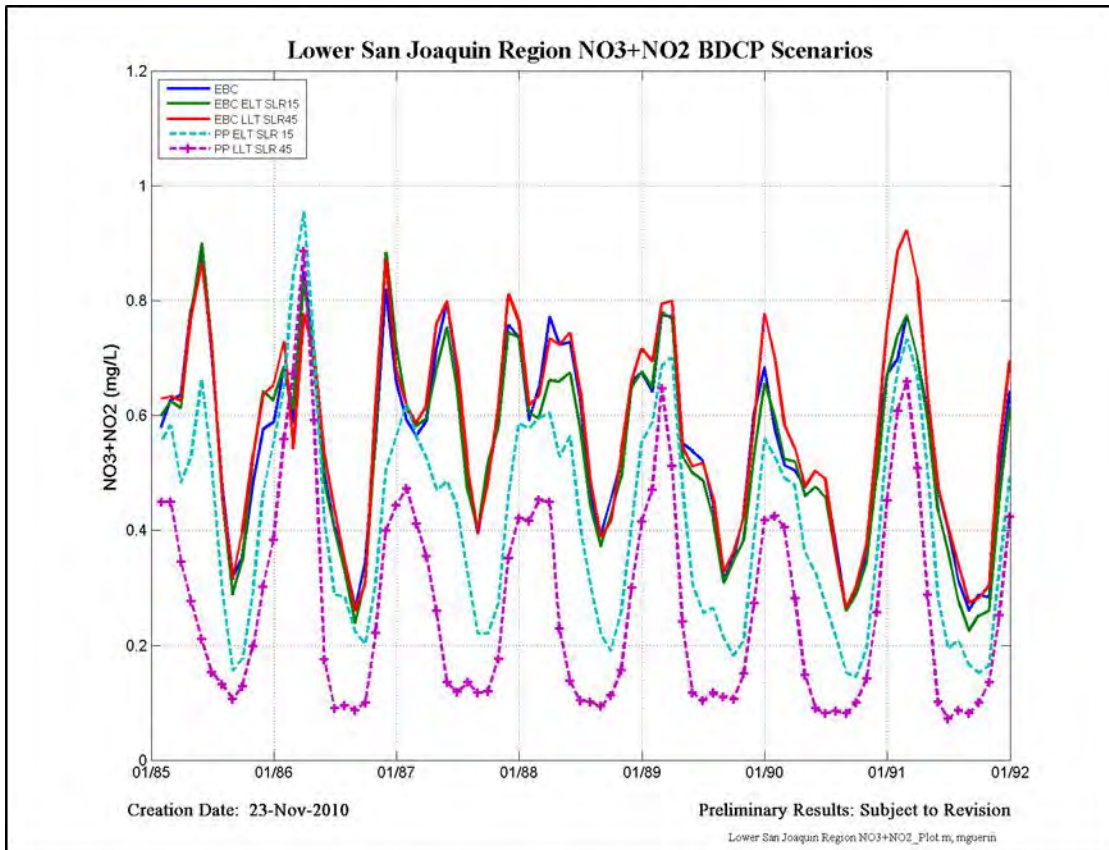
Figure 5-14 NO₂+NO₃ results in the Sacramento Region.

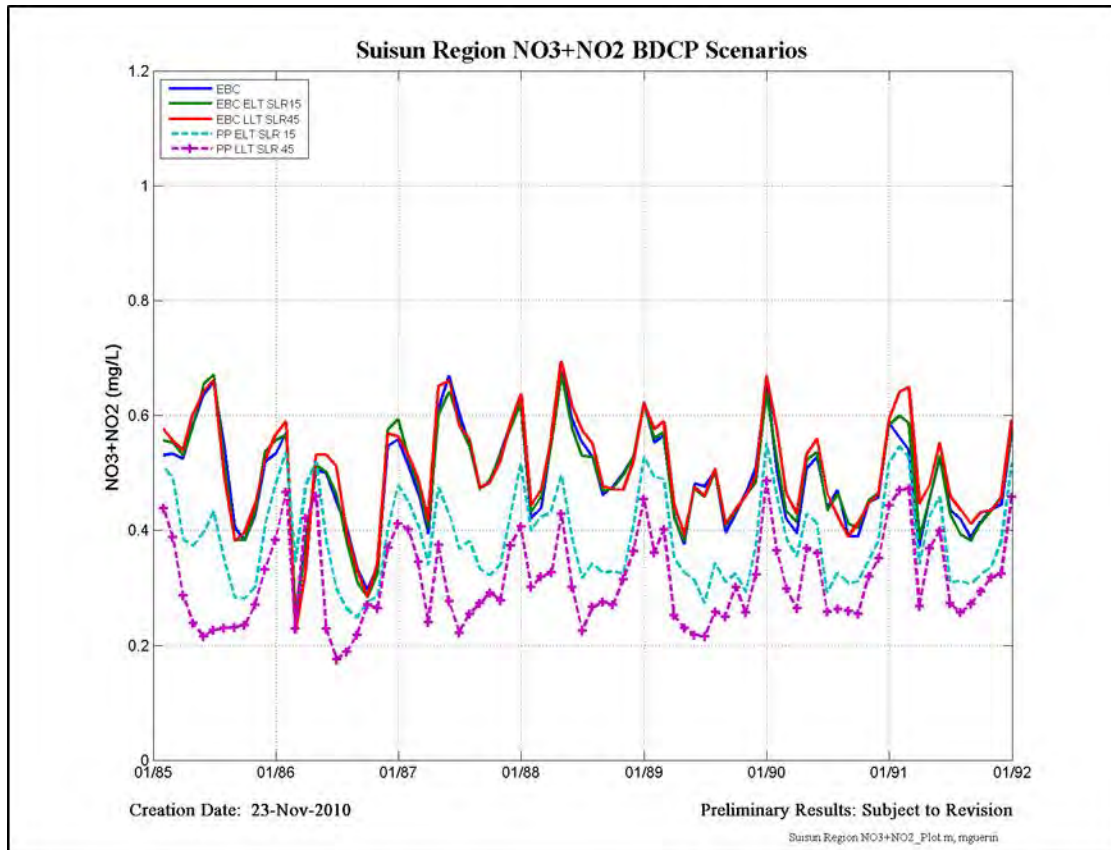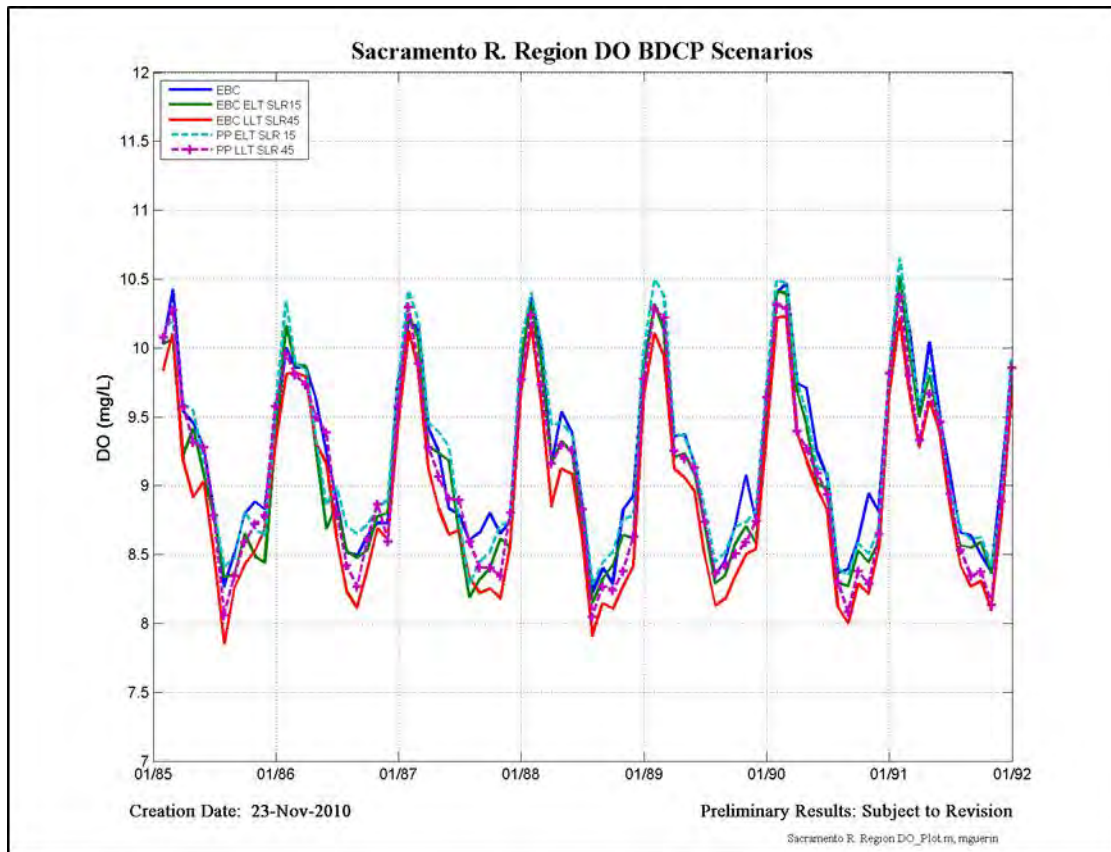**Figure 5-15 NO$_2$+NO$_3$ results in the San Joaquin Region.**

Figure 5-16 NO₂+NO₃ results in the Suisun Region.

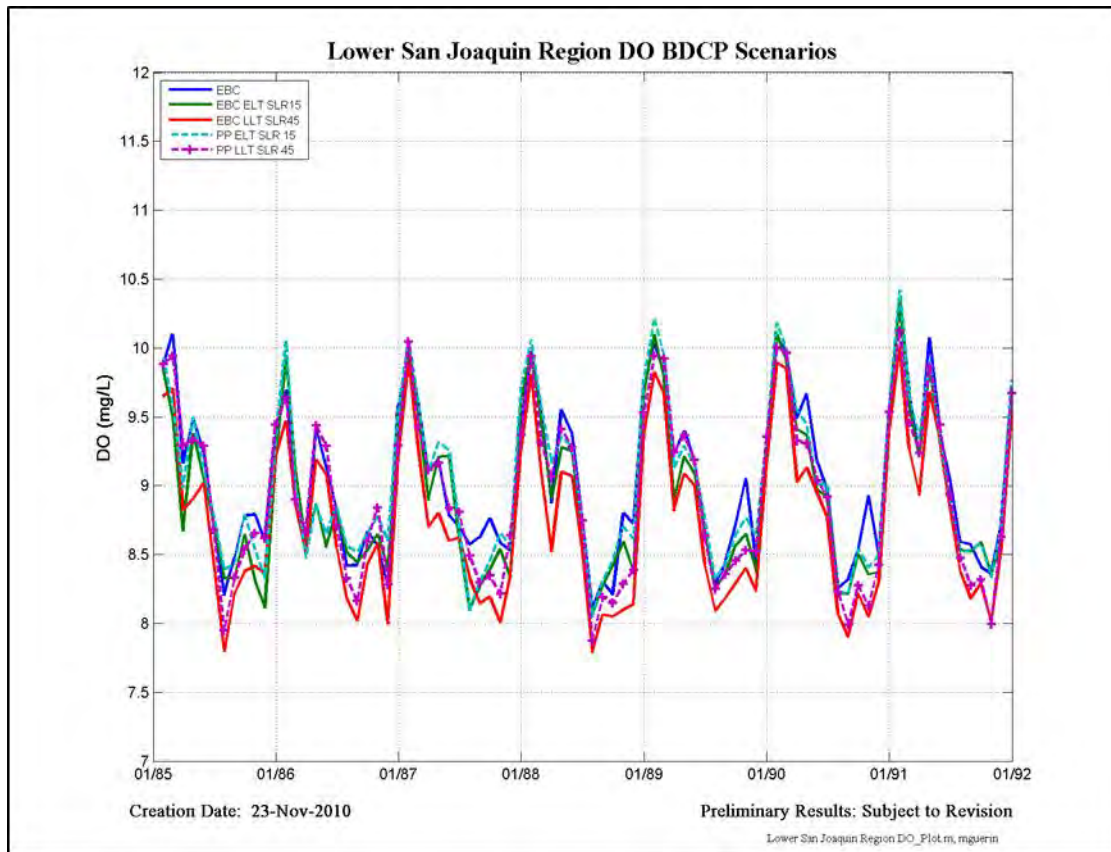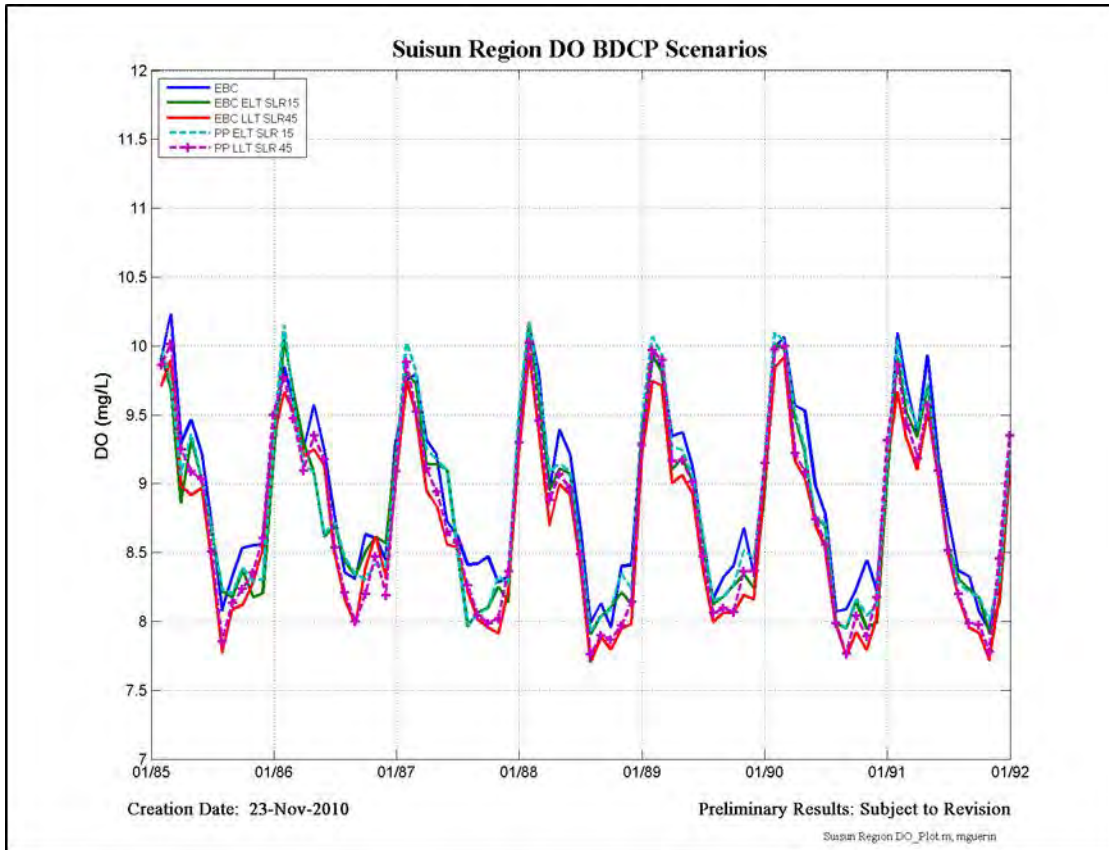**Figure 5-17 DO results in the Sacramento Region.**

Figure 5-18 DO results in the San Joaquin Region.
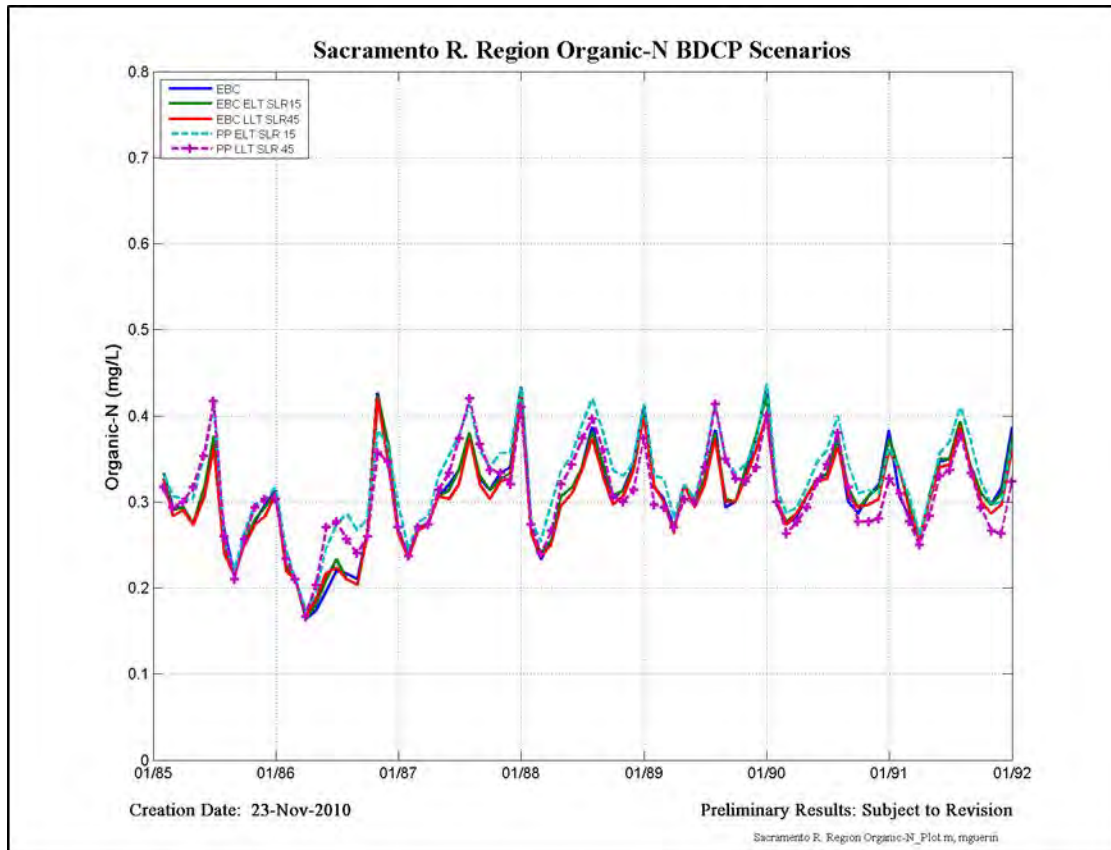
Figure 5-19 DO results in the Suisun Region.

Figure 5-20 Organic-N results in the Sacramento Region.

Figure 5-21 Organic-N results in the San Joaquin Region.

Figure 5-22 Organic-N results in the Suisun Region.

Figure 5-23 Water Temperature results in the Sacramento Region.
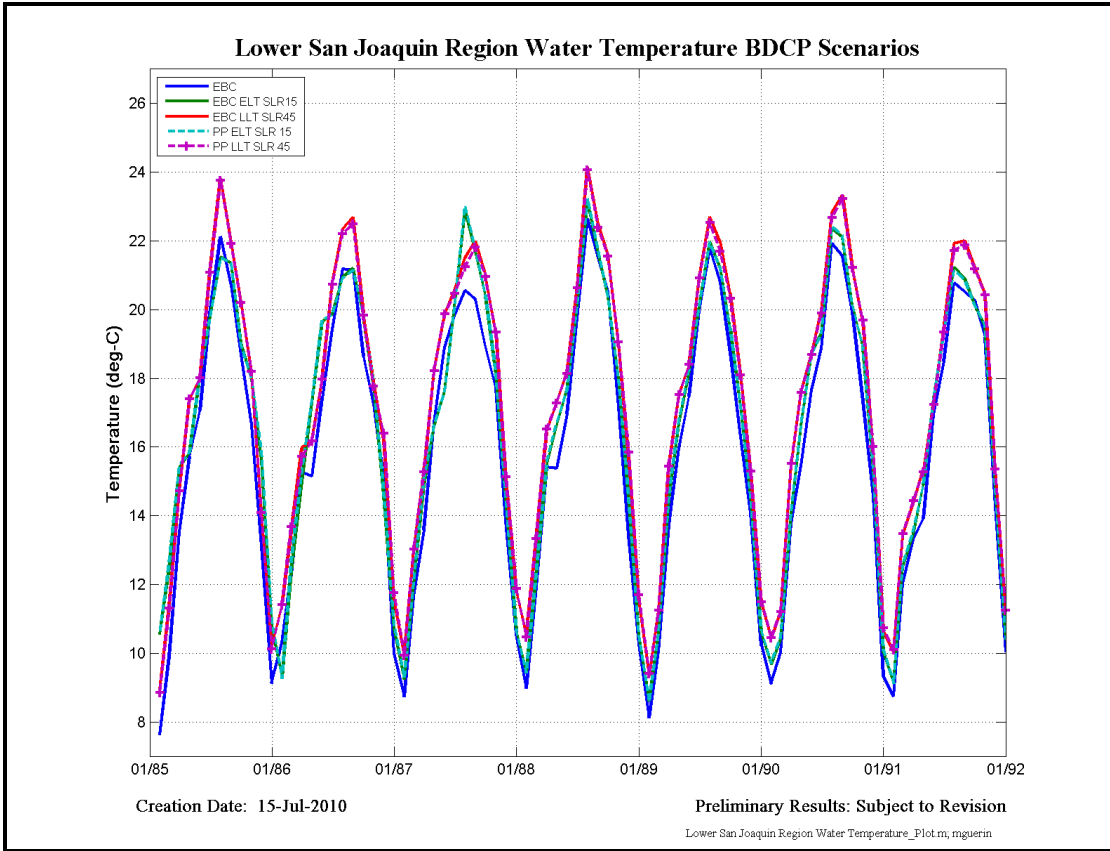
Figure 5-24 Water Temperature results in the San Joaquin Region.
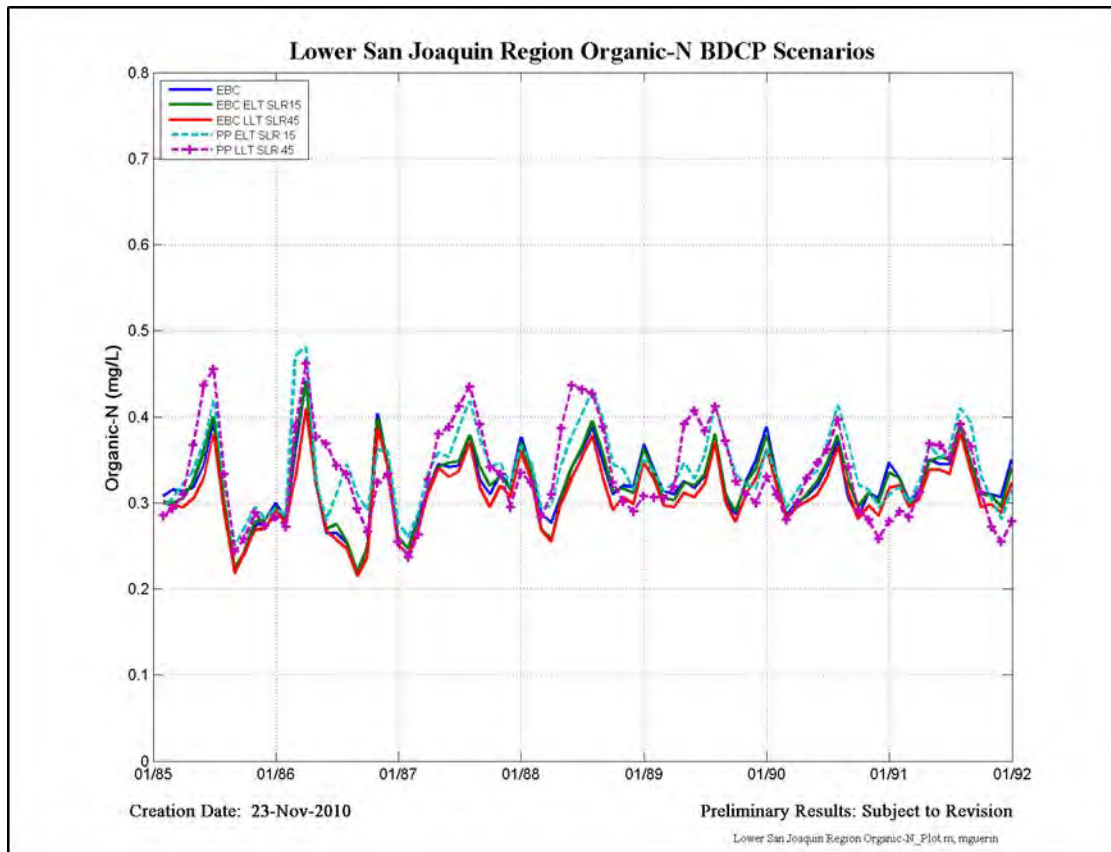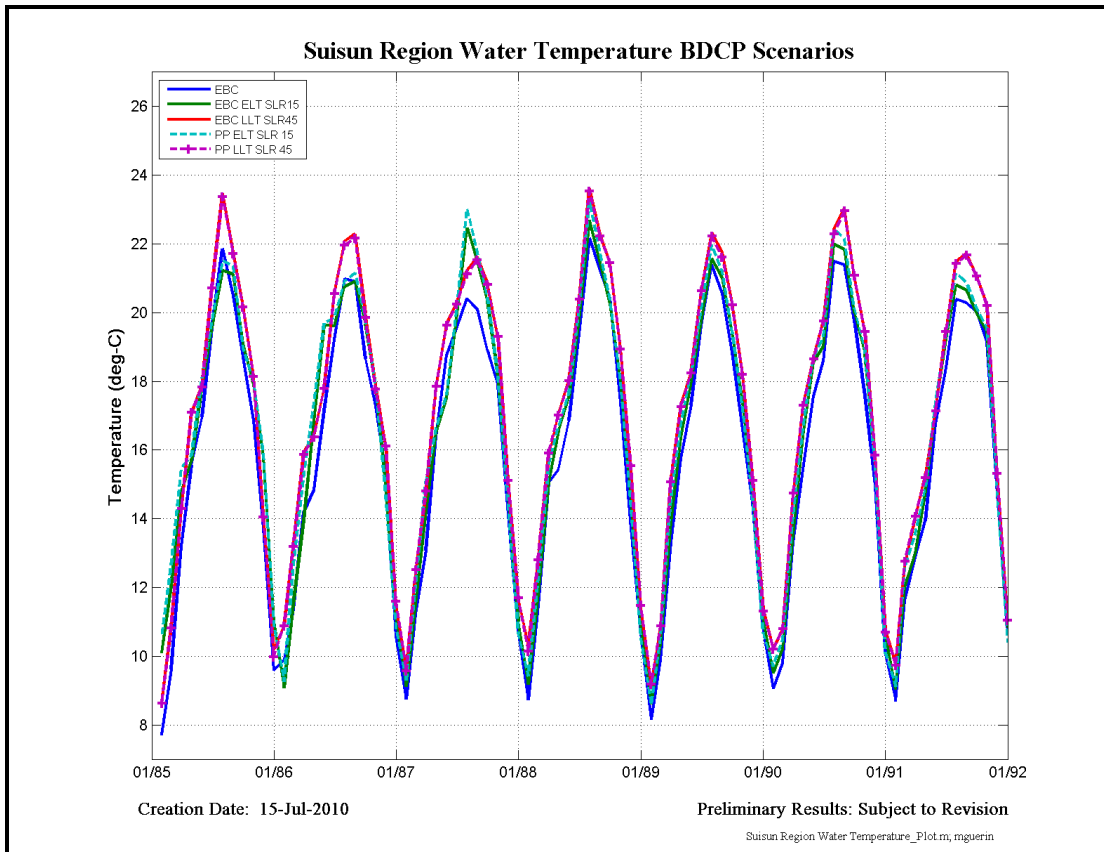
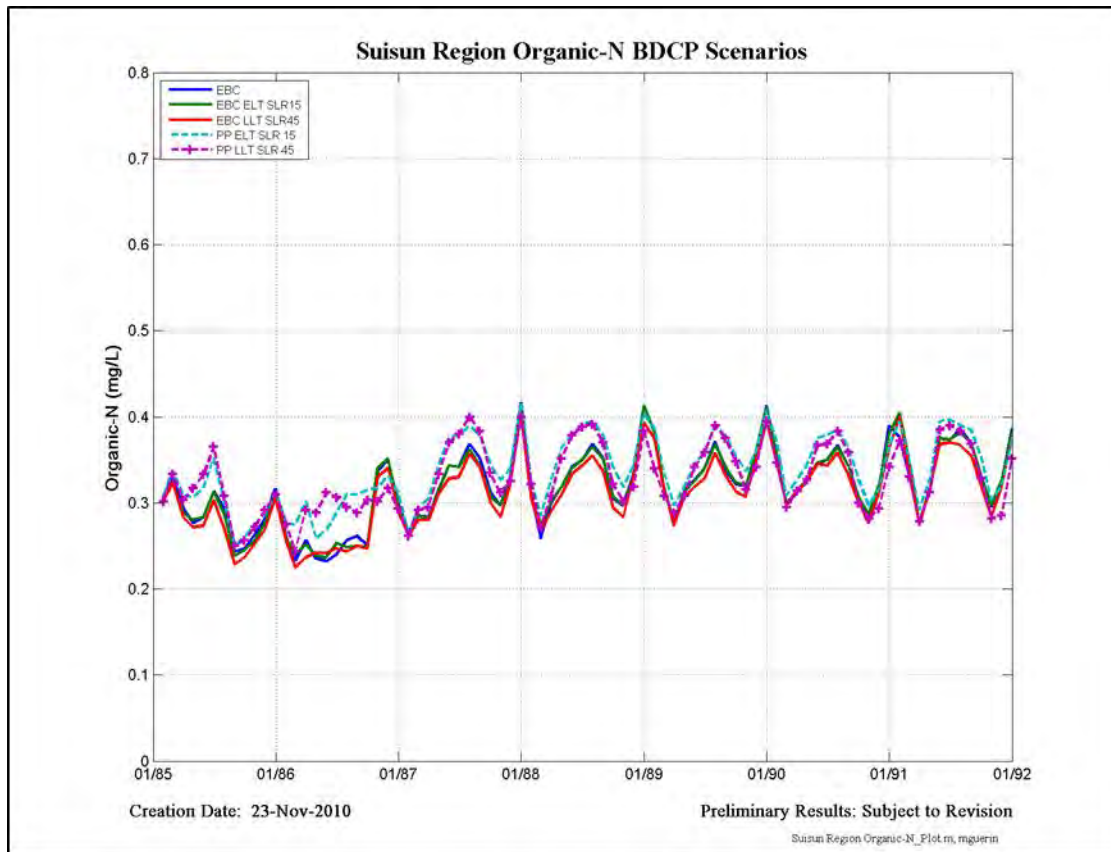**Figure 5-25 Water Temperature results in the Suisun Region.**
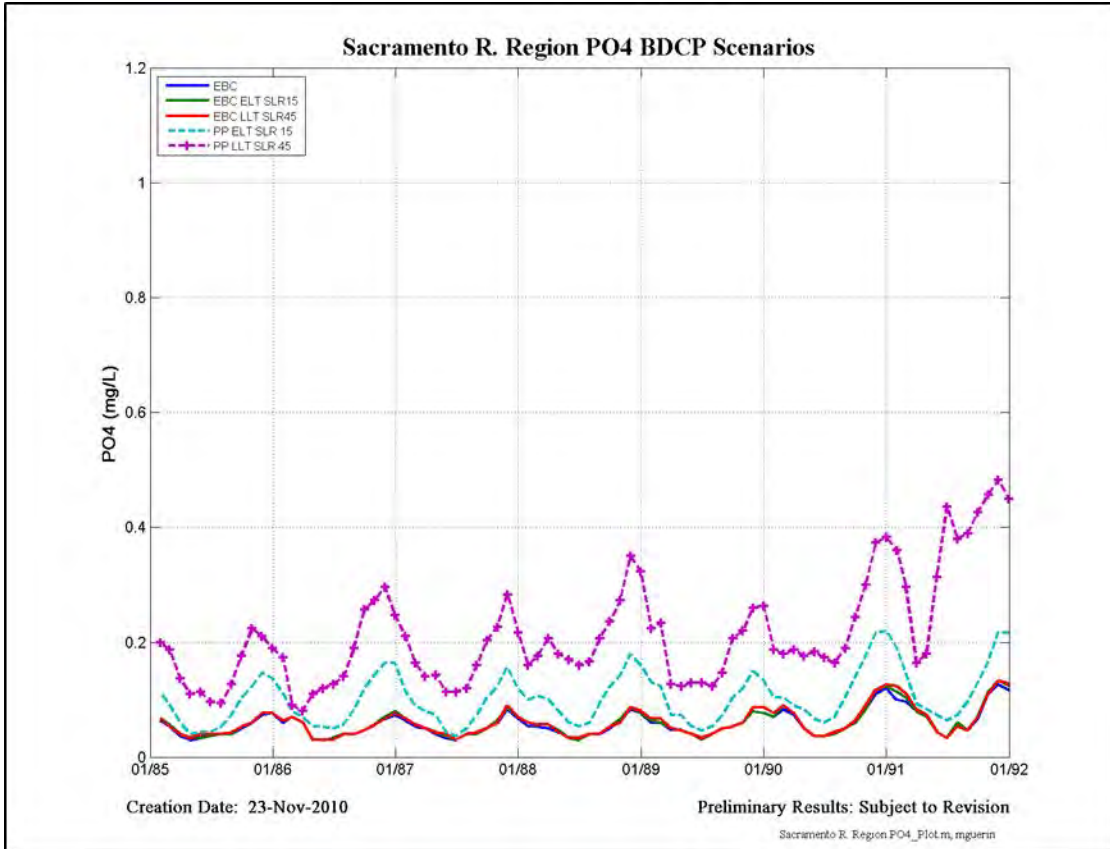
Figure 5-26 PO$_4$ results in the Sacramento Region.

Figure 5-27 PO$_4$ results in the San Joaquin Region.
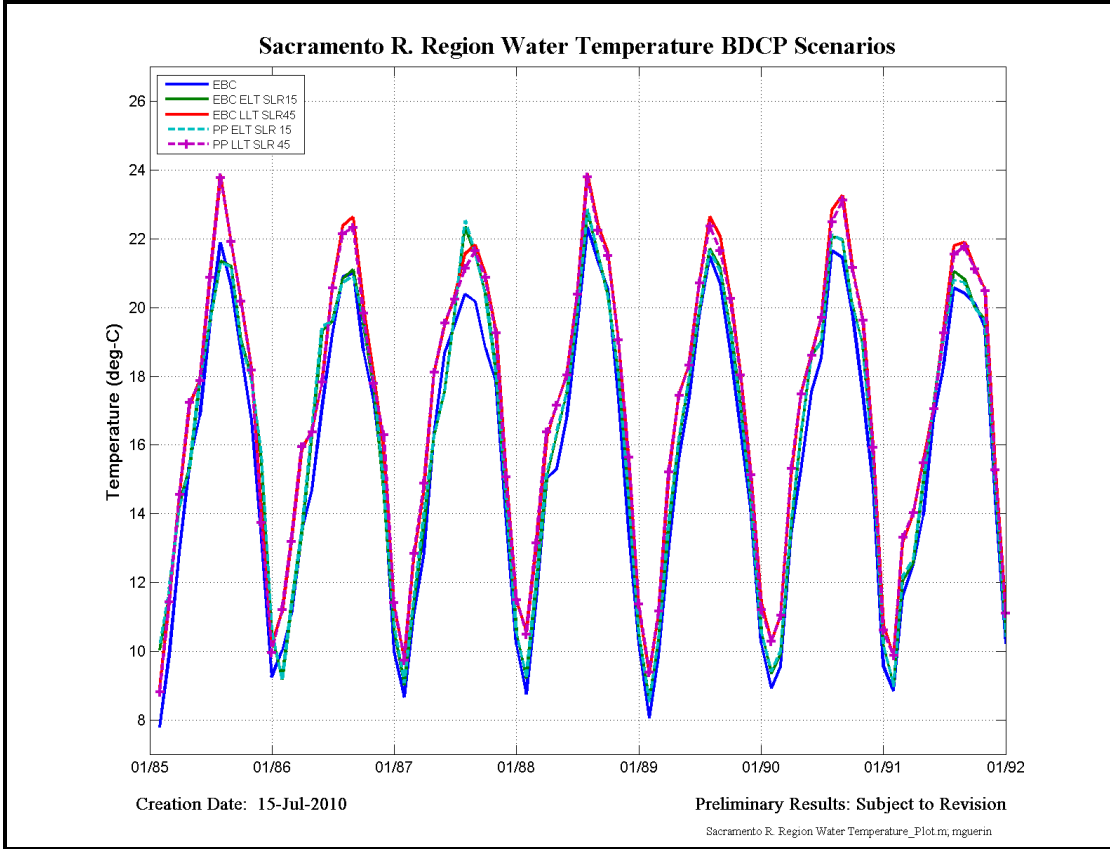
Figure 5-28 PO$_4$ results in the Suisun Region.

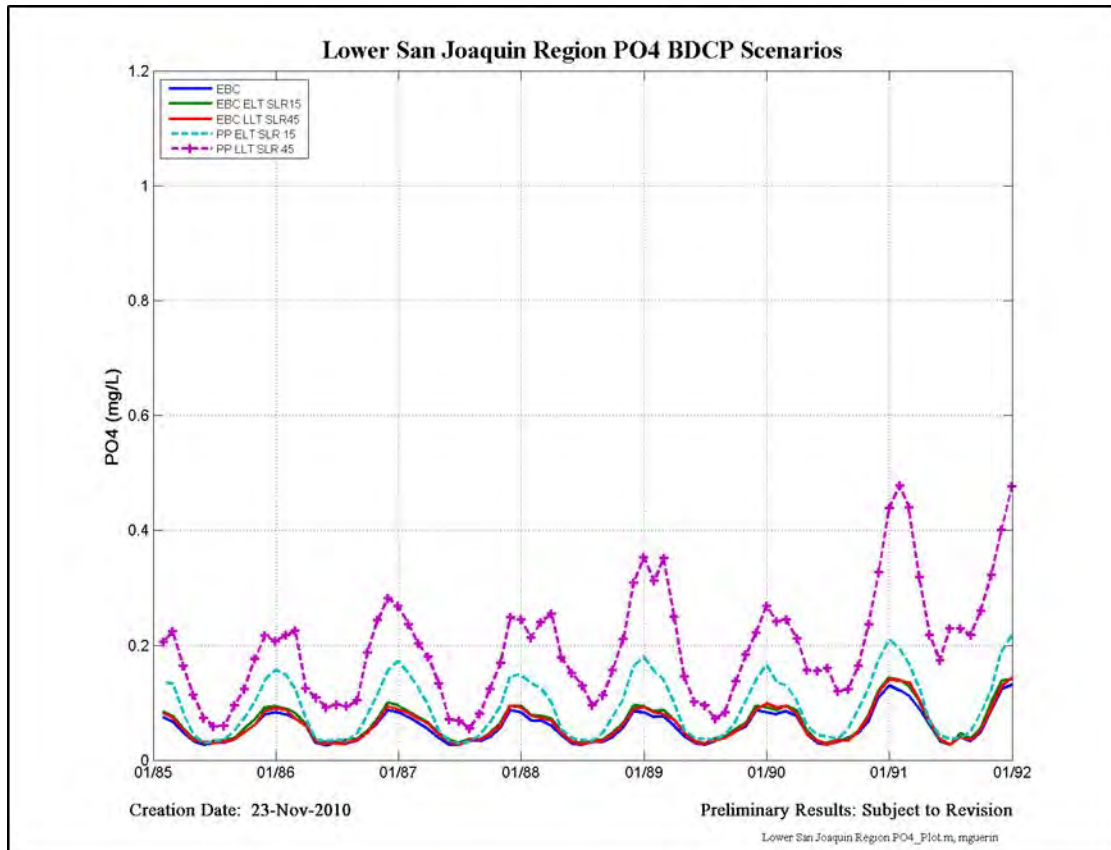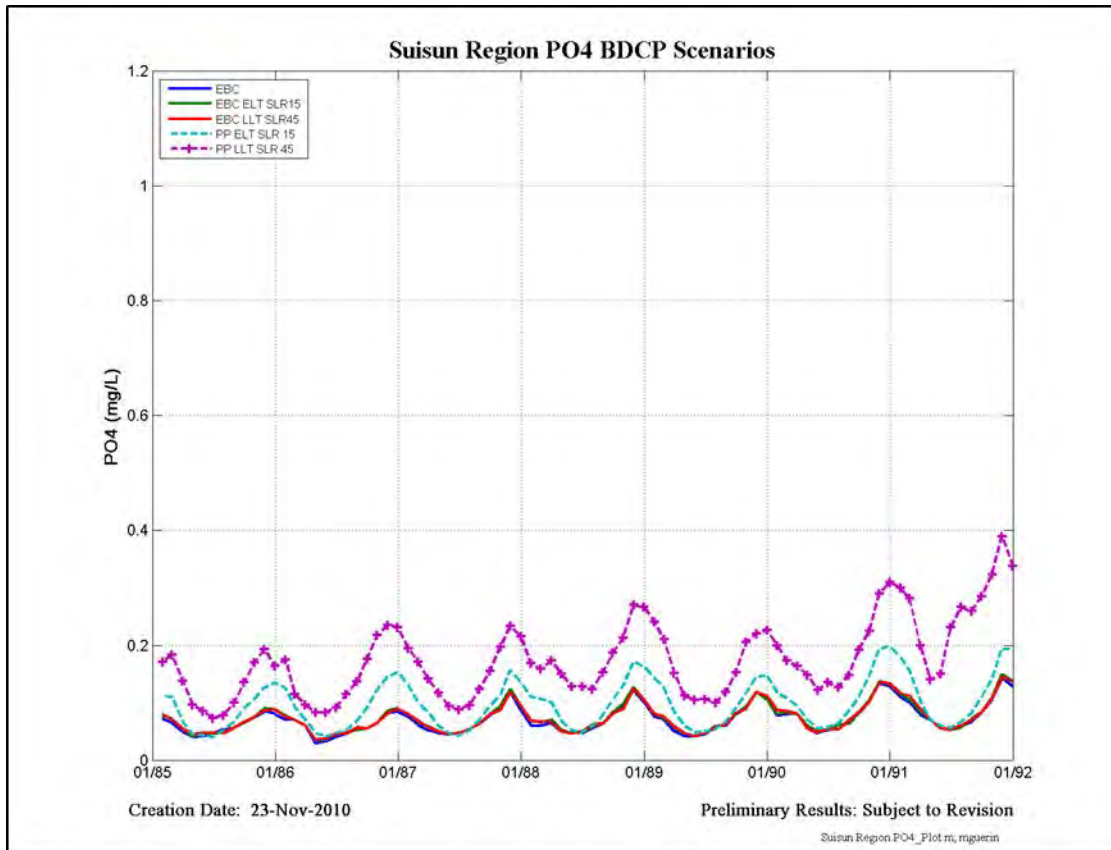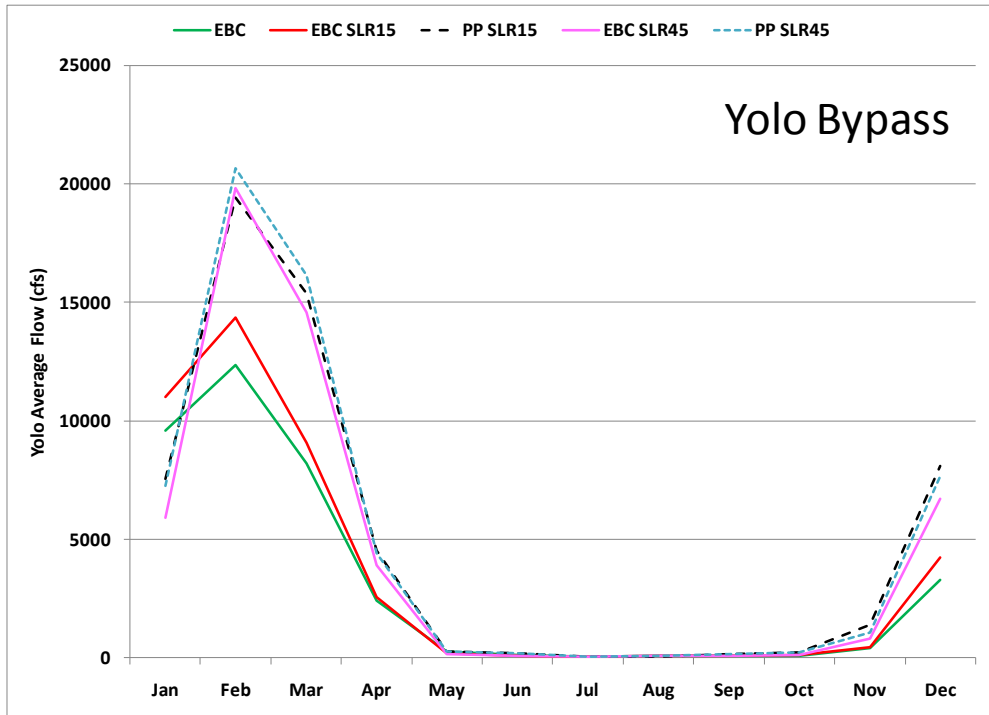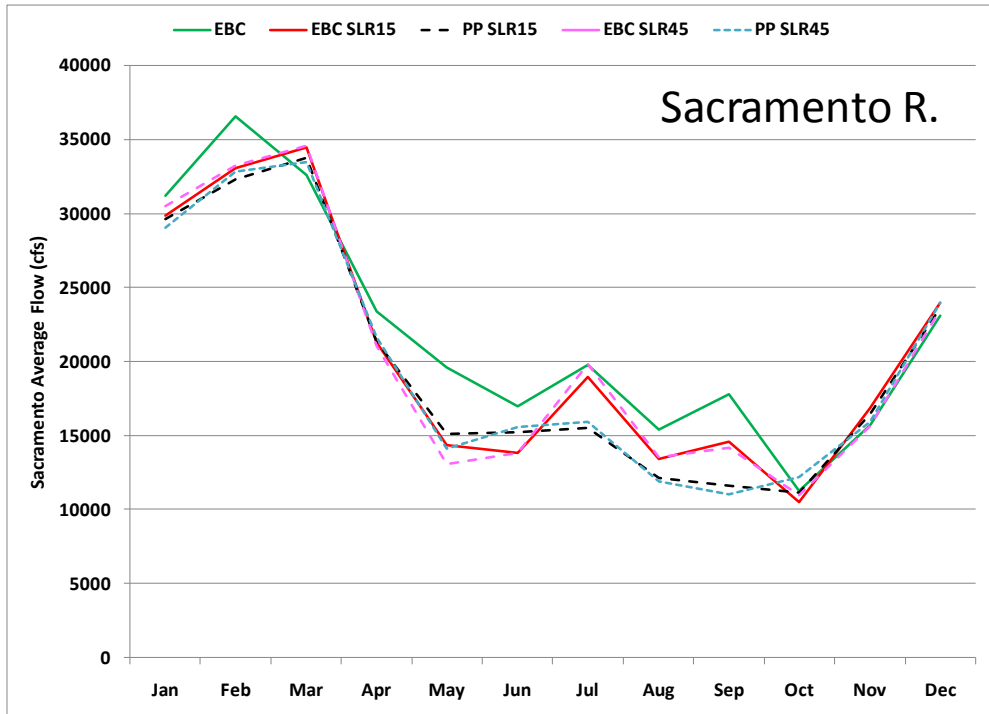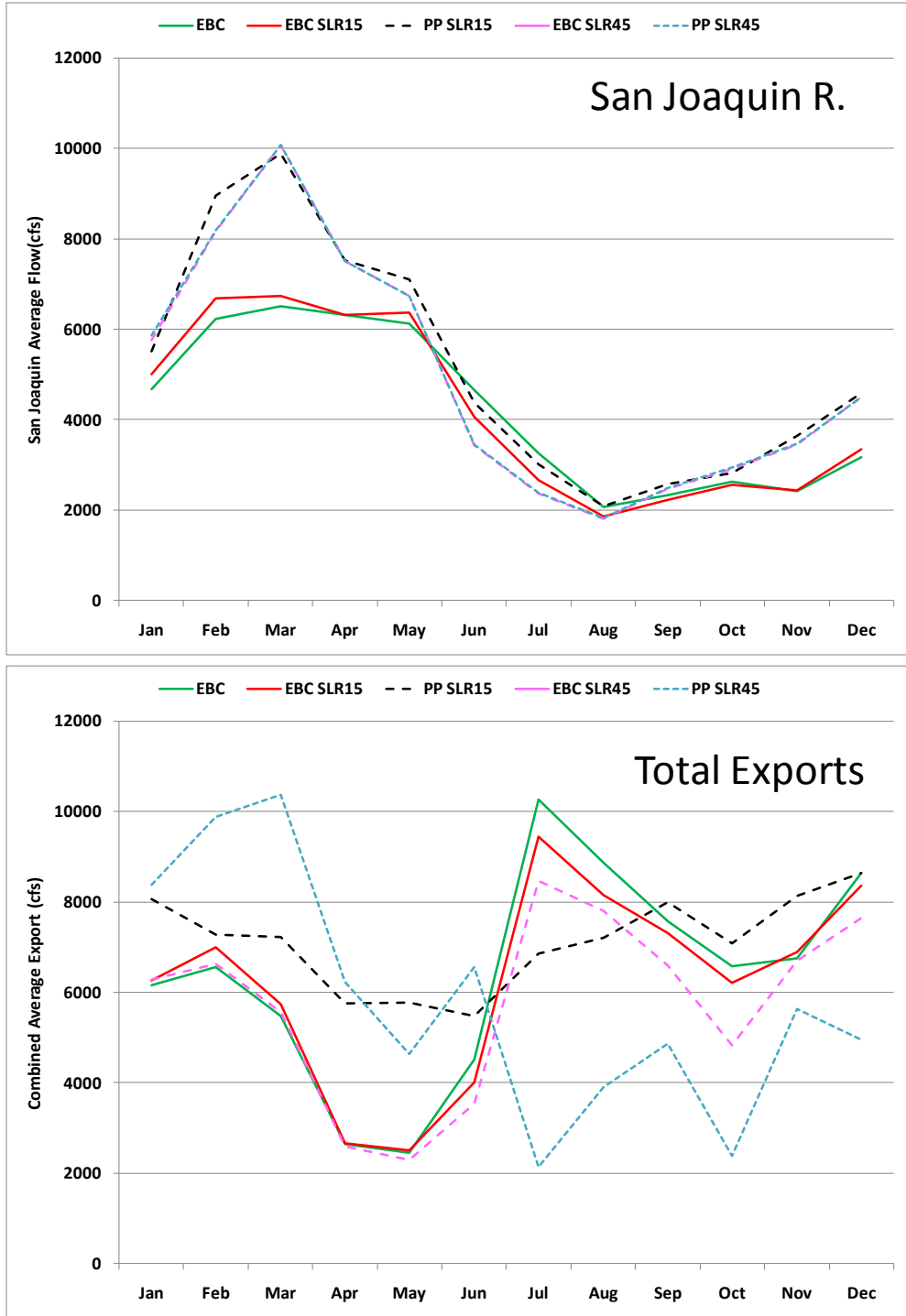**Figure 5-29 Average monthly inflow at the Sacramento R. and the Yolo Bypass.**

Figure 5-30 Average monthly inflow at the San Joaquin R. and Total Exports (North Delta + South Delta).
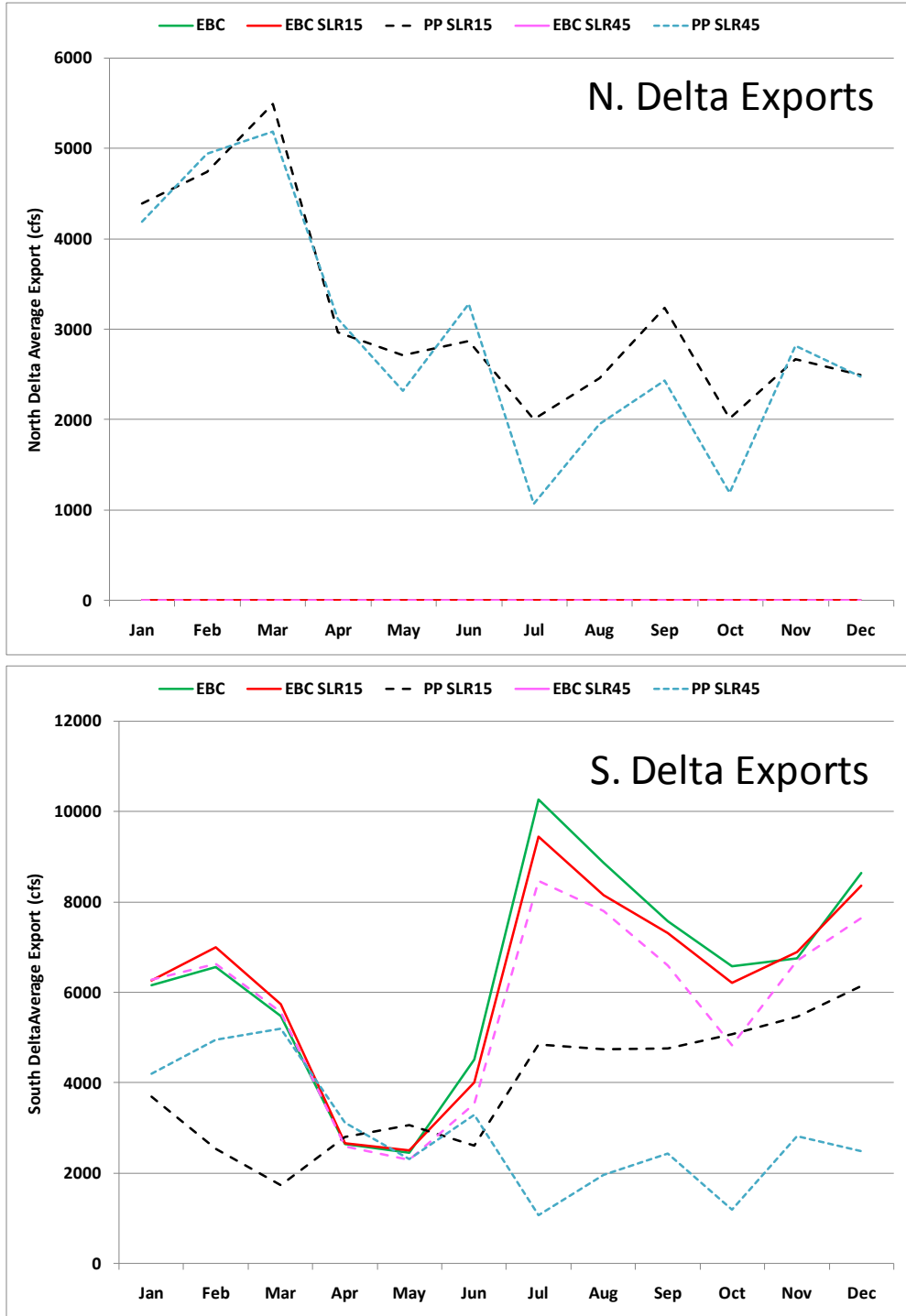
Figure 5-31 Average monthly exports at the North Delta and at the South Delta.

Table 5-4 Average Monthly percent difference in water temperature in the seven regions between the EBC-ELT and the EBC scenarios, and between the PP-ELT and EBC-ELTscenarios. The right-hand columns simply show the sign of the differences calculated in the left-hand columns.

EBC/SLR15-EBC	Cache/ Yolo	SAC Region	Suisun Region	SJR Region	South Delta	Central Delta	East Delta	Cache/ Yolo	SAC Region	Suisun Region	SJR Region	South Delta	Central Delta	East Delta
Jan	5.0	3.9	4.1	4.9	4.7	4.8	3.0	+	+	+	+	+	+	+
Feb	4.1	4.0	4.0	4.2	4.1	4.0	3.1	+	+	+	+	+	+	+
Mar	3.2	3.1	3.1	3.3	3.7	3.3	2.9	+	+	+	+	+	+	+
Apr	4.3	4.0	4.3	4.5	4.4	4.4	3.1	+	+	+	+	+	+	+
May	3.8	3.8	3.9	3.8	3.3	3.7	3.1	+	+	+	+	+	+	+
Jun	2.6	2.5	2.4	2.5	2.3	2.4	2.4	+	+	+	+	+	+	+
Jul	2.7	2.6	2.5	2.5	2.3	2.3	1.9	+	+	+	+	+	+	+
Aug	2.4	2.4	2.4	2.4	2.5	2.3	1.7	+	+	+	+	+	+	+
Sep	1.9	1.8	1.9	1.9	2.0	1.8	1.4	+	+	+	+	+	+	+
Oct	3.8	3.4	3.1	3.7	4.0	3.7	2.3	+	+	+	+	+	+	+
Nov	3.6	3.7	3.2	3.7	4.1	3.6	2.6	+	+	+	+	+	+	+
Dec	4.5	4.0	3.3	4.3	4.7	4.2	2.8	+	+	+	+	+	+	+

PP- EBC (SLR 15)	Cache/ Yolo	SAC region	Suisun Region	SJR Region	South Delta	Central Delta	East Delta	Cache/ Yolo	SAC Region	Suisun Region	SJR Region	South Delta	Central Delta	East Delta
Jan	-0.9	0.4	0.5	0.6	0.2	0.6	-0.8	-	+	+	+	+	+	-
Feb	-0.7	0.9	1.1	1.1	0.5	1.1	1.7	-	+	+	+	+	+	+
Mar	-0.7	1.0	1.2	1.2	-0.1	1.1	2.8	-	+	+	+	-	+	+
Apr	-0.3	0.2	0.2	0.3	0.0	0.3	0.5	-	+	+	+	-	+	+
May	-0.3	0.0	-0.1	0.0	0.0	0.0	-0.2	-	-	-	+	+	-	-
Jun	-0.4	-0.1	-0.1	-0.1	-0.2	-0.1	0.0	-	-	-	-	-	-	-
Jul	-0.4	0.0	-0.1	0.1	-0.1	0.1	0.9	-	-	-	+	-	+	+
Aug	-0.6	-0.2	-0.1	0.0	-0.1	0.1	-0.1	-	-	-	+	-	+	-
Sep	-0.5	-0.1	0.0	0.0	-0.1	0.0	-0.1	-	-	-	-	-	+	-
Oct	-0.6	0.1	0.1	0.2	0.0	0.3	0.7	-	+	+	+	-	+	+
Nov	-0.8	0.1	0.2	0.3	0.3	0.5	0.7	-	+	+	+	+	+	+
Dec	-1.3	0.1	0.3	0.4	0.4	0.7	0.0	-	+	+	+	+	+	+

Table 5-5 Average Monthly percent difference in water temperature in the seven regions between the EBC-LLT and the EBC scenarios, and between the PP-LLT and EBC-LLT scenarios. The right-hand columns simply show the sign of the differences calculated in the left-hand columns.

EBC/SLR45 - EBC	Cache/ Yolo	SAC Region	Suisun Region	SJR Region	South Delta	Central Delta	East Delta	Cache/ Yolo	SAC Region	Suisun Region	SJR Region	South Delta	Central Delta	East Delta
Jan	14.5	14.6	12.3	13.0	9.6	12.2	13.0	+	+	+	+	+	+	+
Feb	12.8	15.3	11.7	10.4	5.4	9.2	14.8	+	+	+	+	+	+	+
Mar	11.2	13.7	10.2	8.5	3.7	7.2	14.1	+	+	+	+	+	+	+
Apr	9.3	10.1	8.6	8.1	5.8	7.4	9.9	+	+	+	+	+	+	+
May	5.4	5.5	5.6	5.4	4.3	5.1	5.2	+	+	+	+	+	+	+
Jun	5.6	5.5	5.3	5.1	4.1	4.8	6.2	+	+	+	+	+	+	+
Jul	6.2	6.6	5.3	5.3	3.8	5.2	9.2	+	+	+	+	+	+	+
Aug	6.6	6.8	6.3	6.4	5.6	6.5	8.0	+	+	+	+	+	+	+
Sep	7.0	6.8	6.4	6.7	6.1	6.6	7.2	+	+	+	+	+	+	+
Oct	8.6	8.2	7.3	8.5	8.0	8.4	8.0	+	+	+	+	+	+	+
Nov	7.9	7.4	5.7	8.3	8.9	8.2	5.9	+	+	+	+	+	+	+
Dec	11.6	10.0	7.0	11.3	11.4	11.1	9.1	+	+	+	+	+	+	+

PP- EBC (SLR 45)	Cache/ Yolo	SAC region	Suisun Region	SJR Region	South Delta	Central Delta	East Delta	Cache/ Yolo	SAC Region	Suisun Region	SJR Region	South Delta	Central Delta	East Delta
Jan	13.4	-0.1	0.1	0.0	10.0	12.1	10.8	+	-	+	-	+	+	+
Feb	12.1	0.6	0.3	0.0	5.0	8.8	14.3	+	+	+	+	+	+	+
Mar	10.7	0.8	0.3	-0.1	2.8	6.7	15.2	+	+	+	-	+	+	+
Apr	9.2	-0.2	-0.2	-0.2	5.3	7.2	9.1	+	-	-	-	+	+	+
May	5.4	0.0	-0.1	-0.1	3.6	4.9	4.7	+	+	-	-	+	+	+
Jun	5.5	-0.2	-0.2	-0.3	3.1	4.3	5.5	+	-	-	-	+	+	+
Jul	5.6	-1.0	-0.4	-0.6	3.1	4.4	7.3	+	-	-	-	+	+	+
Aug	6.1	-0.8	-0.4	-0.6	4.9	5.8	6.2	+	-	-	-	+	+	+
Sep	6.7	-0.4	-0.3	-0.2	5.6	6.4	6.6	+	-	-	-	+	+	+
Oct	8.3	-0.4	-0.1	0.0	8.2	8.5	8.2	+	-	-	-	+	+	+
Nov	7.6	0.2	0.3	0.6	9.6	9.2	7.8	+	+	+	+	+	+	+
Dec	11.0	-0.1	0.2	0.6	12.3	12.2	9.7	+	-	+	+	+	+	+

Table 5-6 Average Monthly percent difference in the three main regions between the EBC-ELT and the EBC scenarios. The right-hand columns simply show the sign of the differences calculated in the left-hand columns. Positive values indicate an increase in the constituent in the EBC-ELT scenario.

SAC Region	CHL-a	NH3	PO4	ORG-N	NO3+NO2	CHL-a	NH3	PO4	ORG-N	NO3+NO2
Jan	4.4	2.9	-4.8	0.2	-2.1	+	+	-	+	-
Feb	2.6	2.7	-4.6	0.1	-1.0	+	+	-	+	-
Mar	2.2	3.5	-4.5	-0.1	-2.1	+	+	-	-	-
Apr	0.9	5.5	-2.6	-0.6	-1.2	+	+	-	-	-
May	-0.5	6.0	-4.0	-1.6	-2.2	-	+	-	-	-
Jun	0.1	7.2	-2.2	-1.4	-1.9	+	+	-	-	-
Jul	2.7	4.2	-2.4	0.5	-0.2	+	+	-	+	-
Aug	3.3	10.5	-0.5	-1.4	-0.9	+	+	-	-	-
Sep	2.3	4.3	-0.4	-0.4	-1.0	+	+	-	-	-
Oct	2.1	4.3	-2.3	0.2	-1.7	+	+	-	+	-
Nov	3.1	1.2	-3.3	0.0	-2.9	+	+	-	+	-
Dec	2.8	4.7	-3.5	1.1	-0.9	+	+	-	+	-

SJR Region	CHL-a	NH3	PO4	ORG-N	NO3+NO2	CHL-a	NH3	PO4	ORG-N	NO3+NO2
Jan	4.1	4.0	-9.9	0.5	-1.9	+	+	-	+	-
Feb	1.3	4.9	-10.8	1.2	-0.5	+	+	-	+	-
Mar	-3.8	4.0	-14.4	0.9	0.3	-	+	-	+	+
Apr	-11.8	4.4	-14.4	-0.5	2.2	-	+	-	-	+
May	-15.2	6.1	-15.7	-1.5	3.9	-	+	-	-	+
Jun	-13.6	5.4	-10.2	-1.3	4.4	-	+	-	-	+
Jul	-10.5	5.7	-13.4	0.2	7.9	-	+	-	+	+
Aug	-12.4	8.9	-7.4	-2.1	5.8	-	+	-	-	+
Sep	-10.1	4.9	-11.0	-1.7	4.0	-	+	-	-	+
Oct	-7.6	6.8	-13.1	-0.6	1.1	-	+	-	-	+
Nov	-2.6	6.4	-9.8	1.0	-0.1	-	+	-	+	-
Dec	2.0	4.6	-9.7	1.3	-0.9	+	+	-	+	-

Suisun Region	CHL-a	NH3	PO4	ORG-N	NO3+NO2	CHL-a	NH3	PO4	ORG-N	NO3+NO2
Jan	4.0	2.7	-4.3	0.1	-1.7	+	+	-	+	-
Feb	2.5	3.4	-4.9	-0.4	-1.6	+	+	-	-	-
Mar	1.6	3.7	-6.6	0.2	-1.1	+	+	-	+	-
Apr	-2.4	4.4	-5.9	-0.4	-0.3	-	+	-	-	-
May	-2.6	5.2	-1.9	-0.7	0.3	-	+	-	-	+
Jun	-2.0	4.8	-1.8	-1.5	0.8	-	+	-	-	+
Jul	0.9	2.8	0.3	0.9	2.4	+	+	+	+	+
Aug	2.9	2.8	-2.7	0.2	0.6	+	+	-	+	+
Sep	0.3	2.0	-1.8	-0.3	0.1	+	+	-	-	+
Oct	-0.8	2.6	-2.4	0.7	-0.1	-	+	-	+	-
Nov	0.7	1.6	-3.5	0.2	-1.9	+	+	-	+	-
Dec	1.5	3.3	-3.1	0.8	-1.0	+	+	-	+	-

Table 5-7 Average Monthly percent difference in constituents in the four secondary regions between the EBC-ELT and the EBC scenarios. The right-hand columns simply show the sign of the differences calculated in the left-hand column. Positive values indicate an increase in the constituent in the EBC-ELT scenario.

Cache-Yolo	CHL-a	NH3	PO4	ORG-N	NO3+NO2	CHL-a	NH3	PO4	ORG-N	NO3+NO2
Jan	3.3	2.7	-3.7	0.7	-2.4	+	+	-	+	-
Feb	2.3	2.8	-3.2	0.8	-1.8	+	+	-	+	-
Mar	1.7	2.0	-2.2	0.3	-1.6	+	+	-	+	-
Apr	1.2	3.9	-0.9	-0.8	0.3	+	+	-	-	+
May	0.4	4.4	-0.7	-1.3	0.1	+	+	-	-	+
Jun	0.9	4.3	2.8	-1.2	-3.5	+	+	+	-	-
Jul	1.8	3.5	-0.5	-0.6	-2.3	+	+	-	-	-
Aug	1.6	5.7	-0.3	-1.3	-3.0	+	+	-	-	-
Sep	1.8	3.0	-1.4	-0.9	-3.9	+	+	-	-	-
Oct	1.8	2.9	-3.9	-0.2	-1.9	+	+	-	-	-
Nov	3.6	2.0	-4.7	0.0	-2.3	+	+	-	+	-
Dec	1.6	3.9	-3.2	0.7	-1.5	+	+	-	+	-

E Delta	CHL-a	NH3	PO4	ORG-N	NO3+NO2	CHL-a	NH3	PO4	ORG-N	NO3+NO2
Jan	2.1	1.1	-1.5	-0.1	-2.0	+	+	-	-	-
Feb	1.9	1.8	-0.3	0.2	-0.8	+	+	-	+	-
Mar	0.0	0.4	-0.5	-0.8	-1.9	-	+	-	-	-
Apr	-1.2	0.9	0.5	-1.3	-3.3	-	+	+	-	-
May	-1.0	2.2	0.0	-1.1	-3.3	-	+	+	-	-
Jun	-4.1	0.7	0.3	-1.4	-6.1	-	+	+	-	-
Jul	-2.3	-0.4	-0.5	0.1	-4.6	-	-	-	+	-
Aug	-5.7	0.0	-0.4	-2.6	-9.1	-	+	-	-	-
Sep	-4.0	-4.1	-1.9	-2.7	-8.0	-	-	-	-	-
Oct	-1.7	-1.3	-0.4	-2.2	-7.8	-	-	-	-	-
Nov	2.3	3.9	0.2	0.4	-1.9	+	+	+	+	-
Dec	3.4	1.3	-1.2	0.4	-1.0	+	+	-	+	-

Central Delta	CHL-a	NH3	PO4	ORG-N	NO3+NO2	CHL-a	NH3	PO4	ORG-N	NO3+NO2
Jan	4.5	3.3	-6.3	0.9	-1.6	+	+	-	+	-
Feb	1.2	4.1	-6.8	1.2	-0.1	+	+	-	+	-
Mar	-2.5	3.4	-7.6	0.6	-0.2	-	+	-	+	-
Apr	-5.0	4.3	-6.5	-0.1	0.9	-	+	-	-	+
May	-6.4	4.8	-6.0	-0.4	1.9	-	+	-	-	+
Jun	-6.7	4.7	-0.7	-0.3	2.6	-	+	-	-	+
Jul	-2.7	5.0	-2.4	0.7	6.0	-	+	-	+	+
Aug	-5.2	6.9	-3.1	-1.6	2.9	-	+	-	-	+
Sep	-5.3	4.5	-5.2	-1.4	2.1	-	+	-	-	+
Oct	-4.7	5.1	-8.1	-0.9	-1.3	-	+	-	-	-
Nov	-2.1	5.6	-6.3	0.8	0.0	-	+	-	+	-
Dec	2.0	4.7	-6.9	1.0	-1.1	+	+	-	+	-

S Delta	CHL-a	NH3	PO4	ORG-N	NO3+NO2	CHL-a	NH3	PO4	ORG-N	NO3+NO2
Jan	7.6	5.7	-4.2	2.4	-0.9	+	+	-	+	-
Feb	6.0	5.4	-3.8	2.2	0.2	+	+	-	+	+
Mar	0.7	5.0	-7.5	1.9	1.2	+	+	-	+	+
Apr	-4.7	4.1	-1.3	0.0	2.3	-	+	-	-	+
May	-2.8	2.1	-0.8	0.0	4.2	-	+	-	-	+
Jun	-7.4	1.7	5.8	-2.4	7.4	-	+	+	-	+
Jul	-7.1	3.4	1.5	-1.1	7.6	-	+	+	-	+
Aug	-6.4	6.0	1.0	0.0	8.3	-	+	+	-	+
Sep	-6.6	4.0	-3.7	-0.7	2.3	-	+	-	-	+
Oct	-5.4	6.8	-4.3	-0.2	1.9	-	+	-	-	+
Nov	0.9	6.3	-4.9	1.2	0.7	+	+	-	+	+
Dec	5.4	8.3	-6.6	1.5	-0.1	+	+	-	+	-

Table 5-8 Average Monthly percent difference in the three main regions between the EBC-LLT and the EBC scenarios. The right-hand columns simply show the sign of the differences calculated in the left-hand columns. Positive values indicate an increase in the constituent in the EBC-LLT scenario.

SAC Region	CHL-a	NH3	PO4	ORG-N	NO3+NO2	CHL-a	NH3	PO4	ORG-N	NO3+NO2
Jan	10.3	8.0	-5.8	1.4	-6.9	+	+	-	+	-
Feb	10.0	10.6	-7.9	1.1	-5.6	+	+	-	+	-
Mar	6.5	11.3	-6.5	0.0	-7.3	+	+	-	+	-
Apr	6.8	14.2	-2.4	-0.4	-7.1	+	+	-	-	-
May	7.7	13.2	-4.3	-1.6	-11.0	+	+	-	-	-
Jun	6.6	13.2	-3.4	0.3	-7.9	+	+	-	+	-
Jul	8.3	11.6	-2.9	3.5	-0.6	+	+	-	+	-
Aug	9.7	22.0	-3.1	1.2	-3.6	+	+	-	+	-
Sep	9.6	16.8	-0.8	1.7	-5.7	+	+	-	+	-
Oct	9.0	9.3	-3.2	2.9	-5.3	+	+	-	+	-
Nov	11.7	9.0	-4.7	2.7	-7.6	+	+	-	+	-
Dec	12.1	9.6	-5.5	2.5	-7.1	+	+	-	+	-

SJR Region	CHL-a	NH3	PO4	ORG-N	NO3+NO2	CHL-a	NH3	PO4	ORG-N	NO3+NO2
Jan	14.0	10.6	-7.8	2.5	-7.0	+	+	-	+	-
Feb	14.7	11.7	-7.4	4.0	-2.7	+	+	-	+	-
Mar	5.3	11.3	-11.0	2.6	-4.0	+	+	-	+	-
Apr	-0.5	11.7	-8.5	1.6	-1.8	-	+	-	+	-
May	-1.1	11.6	-8.2	1.3	-1.2	-	+	-	+	-
Jun	2.7	10.2	-0.4	2.7	-0.7	+	+	-	+	-
Jul	5.2	18.2	-4.1	4.5	3.9	+	+	-	+	+
Aug	2.9	19.9	-1.3	2.5	0.7	+	+	-	+	+
Sep	3.4	17.4	-4.6	2.7	-1.5	+	+	-	+	-
Oct	7.0	15.2	-7.0	3.6	-6.4	+	+	-	+	-
Nov	11.1	15.0	-6.1	4.1	-5.3	+	+	-	+	-
Dec	16.9	11.4	-8.1	4.0	-6.4	+	+	-	+	-

Suisun Region	CHL-a	NH3	PO4	ORG-N	NO3+NO2	CHL-a	NH3	PO4	ORG-N	NO3+NO2
Jan	10.8	7.4	-4.8	2.0	-4.3	+	+	-	+	-
Feb	12.1	9.2	-5.2	2.0	-2.3	+	+	-	+	-
Mar	8.0	10.6	-7.4	1.2	-4.3	+	+	-	+	-
Apr	6.4	10.9	-6.0	0.3	-3.9	+	+	-	+	-
May	7.7	10.6	-2.3	0.3	-3.8	+	+	-	+	-
Jun	5.5	8.8	-1.7	0.5	-4.0	+	+	-	+	-
Jul	6.1	8.2	0.6	5.0	3.8	+	+	+	+	+
Aug	9.1	10.1	-4.4	3.3	1.1	+	+	-	+	+
Sep	8.8	8.4	-2.9	2.7	-1.8	+	+	-	+	-
Oct	6.4	9.8	-1.0	4.6	-1.8	+	+	-	+	-
Nov	10.1	4.5	-2.4	2.3	-4.0	+	+	-	+	-
Dec	11.9	7.3	-4.0	2.7	-3.3	+	+	-	+	-

Table 5-9 Average Monthly percent difference in constituents in the four secondary regions between the EBC-LLT and the EBC scenarios. The right-hand columns simply show the sign of the differences calculated in the left-hand columns. Positive values indicate an increase in the constituent in the EBC-LLT scenario.

Cache-Yolo	CHL-a	NH3	PO4	ORG-N	NO3+NO2	CHL-a	NH3	PO4	ORG-N	NO3+NO2
Jan	10.7	6.5	-8.2	76.8	-7.0	+	+	-	+	-
Feb	9.3	6.9	-12.4	80.9	-7.3	+	+	-	+	-
Mar	4.3	7.4	-6.3	86.8	-3.9	+	+	-	+	-
Apr	4.8	9.9	-4.6	90.2	-1.9	+	+	-	+	-
May	4.1	7.1	-5.1	93.1	-5.8	+	+	-	+	-
Jun	5.0	9.0	-1.0	94.0	-7.4	+	+	-	+	-
Jul	5.7	11.8	-2.6	93.6	-4.7	+	+	-	+	-
Aug	6.0	14.6	-7.0	91.0	-5.5	+	+	-	+	-
Sep	6.2	11.7	-8.7	89.1	-6.0	+	+	-	+	-
Oct	7.3	6.4	-11.3	87.7	-4.1	+	+	-	+	-
Nov	9.0	5.9	-9.9	83.6	-5.8	+	+	-	+	-
Dec	10.0	5.3	-10.2	79.1	-8.3	+	+	-	+	-

E Delta	CHL-a	NH3	PO4	ORG-N	NO3+NO2	CHL-a	NH3	PO4	ORG-N	NO3+NO2
Jan	8.4	4.7	-2.5	80.3	-3.7	+	+	-	+	-
Feb	6.4	5.0	-2.0	85.8	-3.3	+	+	-	+	-
Mar	2.3	5.4	-0.5	85.8	-3.7	+	+	-	+	-
Apr	1.4	5.6	0.0	86.2	-8.0	+	+	+	+	-
May	1.1	2.9	-3.0	89.6	-11.0	+	+	-	+	-
Jun	-1.1	4.1	-1.7	85.3	-9.0	-	+	-	+	-
Jul	-5.9	12.3	2.7	82.2	-12.9	-	+	+	+	-
Aug	-5.7	8.1	-1.5	75.2	-16.1	-	+	-	+	-
Sep	-4.2	4.4	-2.1	76.2	-17.8	-	+	-	+	-
Oct	3.8	6.2	-0.5	80.4	-8.8	+	+	-	+	-
Nov	5.3	4.7	-1.9	78.7	-9.4	+	+	-	+	-
Dec	8.1	1.3	-3.6	80.8	-7.0	+	+	-	+	-

Central Delta	CHL-a	NH3	PO4	ORG-N	NO3+NO2	CHL-a	NH3	PO4	ORG-N	NO3+NO2
Jan	13.4	9.5	-4.8	74.7	-6.5	+	+	-	+	-
Feb	12.9	10.2	-3.7	76.5	-2.8	+	+	-	+	-
Mar	5.3	9.2	-5.1	81.5	-4.5	+	+	-	+	-
Apr	5.0	9.6	-2.0	87.1	-1.7	+	+	-	+	-
May	4.0	7.1	-2.2	90.0	-2.0	+	+	-	+	-
Jun	5.8	6.8	3.8	91.1	-1.4	+	+	+	+	-
Jul	9.1	16.3	2.3	90.7	2.3	+	+	+	+	+
Aug	5.9	17.3	1.0	87.5	-1.6	+	+	+	+	-
Sep	4.8	16.6	0.4	83.5	-4.4	+	+	+	+	-
Oct	10.0	14.7	-6.6	81.1	-14.1	+	+	-	+	-
Nov	10.9	13.6	-3.5	73.5	-5.9	+	+	-	+	-
Dec	14.6	10.7	-5.2	73.0	-7.5	+	+	-	+	-

S Delta	CHL-a	NH3	PO4	ORG-N	NO3+NO2	CHL-a	NH3	PO4	ORG-N	NO3+NO2
Jan	16.9	13.3	-6.2	71.8	-4.4	+	+	-	+	-
Feb	14.9	11.8	-3.6	73.1	-0.6	+	+	-	+	-
Mar	7.2	9.3	-10.0	78.9	-0.9	+	+	-	+	-
Apr	1.0	7.1	-6.5	88.6	1.0	+	+	-	+	+
May	4.9	5.1	-2.7	91.2	3.7	+	+	-	+	+
Jun	1.3	3.1	5.9	90.7	7.9	+	+	+	+	+
Jul	3.4	7.4	2.1	90.4	9.0	+	+	+	+	+
Aug	5.5	14.3	-0.7	87.5	12.3	+	+	-	+	+
Sep	2.1	15.5	-4.1	82.3	5.1	+	+	-	+	+
Oct	-0.6	18.8	-3.1	72.8	0.4	-	+	-	+	+
Nov	11.7	17.2	-4.2	62.4	-1.9	+	+	-	+	-
Dec	15.9	15.8	-8.8	63.5	-6.3	+	+	-	+	-

Table 5-10 Average Monthly percent difference in the three main regions between the PP-ELT and the EBC-ELT scenarios. The right-hand columns simply show the sign of the differences calculated in the left-hand columns. Positive values indicate a higher value in the constituent in the PP-EBC scenario.

SAC Region	CHL-a	NH3	PO4	ORG-N	NO3+NO2	CHL-a	NH3	PO4	ORG-N	NO3+NO2
Jan	-43.9	10.4	-57.3	-3.4	9.1	-	+	-	-	+
Feb	-36.4	12.6	-52.9	-4.1	6.5	-	+	-	-	+
Mar	-32.7	15.7	-45.0	-8.1	9.4	-	+	-	-	+
Apr	-41.4	18.7	-53.9	-8.8	21.2	-	+	-	-	+
May	-47.3	23.2	-44.4	-11.0	33.2	-	+	-	-	+
Jun	-54.8	23.8	-40.6	-11.3	42.6	-	+	-	-	+
Jul	-40.9	31.9	-41.4	-14.0	36.7	-	+	-	-	+
Aug	-45.2	28.2	-89.6	-15.6	35.8	-	+	-	-	+
Sep	-42.2	32.1	-108.8	-8.3	27.6	-	+	-	-	+
Oct	-43.9	16.3	-115.0	0.4	21.5	-	+	-	+	+
Nov	-47.1	17.5	-91.0	0.1	15.2	-	+	-	+	+
Dec	-49.3	10.8	-68.0	-1.6	11.6	-	+	-	-	+

SJR Region	CHL-a	NH3	PO4	ORG-N	NO3+NO2	CHL-a	NH3	PO4	ORG-N	NO3+NO2
Jan	-24.8	6.6	-54.7	-6.5	-4.7	-	+	-	-	-
Feb	-35.5	4.1	-50.8	-12.7	-15.0	-	+	-	-	-
Mar	-44.7	8.3	-25.8	-14.0	-5.5	-	+	-	-	-
Apr	-33.8	13.0	-11.3	-6.4	12.2	-	+	-	-	+
May	-29.4	15.8	-8.7	-3.3	21.2	-	+	-	-	+
Jun	-25.3	29.2	-8.6	-7.7	29.5	-	+	-	-	+
Jul	-13.4	29.1	4.5	-14.5	23.8	-	+	+	-	+
Aug	-17.4	32.6	-20.8	-21.1	27.2	-	+	-	-	+
Sep	-21.3	36.3	-34.0	-15.8	31.8	-	+	-	-	+
Oct	-36.4	31.5	-46.4	-0.3	21.5	-	+	-	-	+
Nov	-45.7	28.2	-53.2	2.5	16.6	-	+	-	+	+
Dec	-36.9	15.9	-60.7	-0.1	6.7	-	+	-	-	+

Suisun Region	CHL-a	NH3	PO4	ORG-N	NO3+NO2	CHL-a	NH3	PO4	ORG-N	NO3+NO2
Jan	-44.3	7.7	-52.1	-5.4	-0.2	-	+	-	-	-
Feb	-44.0	6.0	-49.7	-9.1	-11.7	-	+	-	-	-
Mar	-52.7	9.3	-38.0	-15.5	-6.6	-	+	-	-	-
Apr	-52.0	12.6	-21.2	-12.9	11.0	-	+	-	-	+
May	-51.2	9.6	-10.2	-11.0	25.5	-	+	-	-	+
Jun	-51.0	6.9	-1.0	-11.3	32.2	-	+	-	-	+
Jul	-33.9	6.5	-4.2	-10.6	28.7	-	+	-	-	+
Aug	-45.6	3.2	-17.8	-12.3	24.8	-	+	-	-	+
Sep	-46.8	6.7	-36.3	-13.0	21.4	-	+	-	-	+
Oct	-82.7	10.0	-47.0	-2.0	16.0	-	+	-	-	+
Nov	-67.1	12.4	-46.9	0.9	9.1	-	+	-	+	+
Dec	-54.2	10.7	-46.9	-0.4	5.2	-	+	-	-	+

Table 5-11 Average Monthly percent difference in the three main regions between the PP-LLT and the EBC-LLT scenarios. The right-hand columns simply show the sign of the differences calculated in the left-hand columns. Positive values indicate a higher value in the constituent in the EBC-LLT scenario.

SAC Region	CHL-a	NH3	PO4	ORG-N	NO3+NO2	CHL-a	NH3	PO4	ORG-N	NO3+NO2
Jan	-26.2	14.4	-157.1	-0.6	39.3	-	+	-	-	+
Feb	-26.1	16.4	-147.9	-0.1	43.2	-	+	-	-	+
Mar	-28.7	23.9	-157.4	-4.1	46.1	-	+	-	-	+
Apr	-55.4	30.3	-209.5	-7.2	54.1	-	+	-	-	+
May	-81.5	38.9	-263.5	-12.9	64.5	-	+	-	-	+
Jun	-82.6	41.0	-296.5	-13.5	71.9	-	+	-	-	+
Jul	-55.2	43.8	-231.6	-14.3	64.9	-	+	-	-	+
Aug	-43.8	36.2	-308.3	-14.3	59.3	-	+	-	-	+
Sep	-44.2	32.0	-324.8	-5.4	48.6	-	+	-	-	+
Oct	-39.5	16.3	-294.7	4.6	46.0	-	+	-	+	+
Nov	-38.3	18.1	-234.9	3.9	37.3	-	+	-	+	+
Dec	-32.0	14.1	-176.3	3.0	41.6	-	+	-	+	+

SJR Region	CHL-a	NH3	PO4	ORG-N	NO3+NO2	CHL-a	NH3	PO4	ORG-N	NO3+NO2
Jan	-37.4	15.0	-187.3	-2.9	12.7	-	+	-	-	+
Feb	-67.1	13.1	-213.1	-9.3	1.1	-	+	-	-	+
Mar	-95.2	16.6	-194.7	-14.4	16.5	-	+	-	-	+
Apr	-130.9	25.4	-217.5	-18.4	46.6	-	+	-	-	+
May	-133.4	35.9	-213.0	-23.6	67.2	-	+	-	-	+
Jun	-77.8	50.2	-227.0	-20.7	74.5	-	+	-	-	+
Jul	-45.8	41.3	-147.4	-20.5	71.0	-	+	-	-	+
Aug	-37.9	45.3	-176.9	-26.0	68.9	-	+	-	-	+
Sep	-39.9	47.0	-207.6	-17.8	66.7	-	+	-	-	+
Oct	-64.3	38.1	-211.3	0.3	56.1	-	+	-	+	+
Nov	-65.8	37.9	-192.7	5.5	39.7	-	+	-	+	+
Dec	-48.2	23.4	-179.5	4.6	27.5	-	+	-	+	+

Suisun Region	CHL-a	NH3	PO4	ORG-N	NO3+NO2	CHL-a	NH3	PO4	ORG-N	NO3+NO2
Jan	-32.4	11.5	-135.5	-4.7	16.4	-	+	-	-	+
Feb	-45.4	8.6	-141.6	-7.5	7.9	-	+	-	-	+
Mar	-69.8	13.4	-141.7	-14.8	11.9	-	+	-	-	+
Apr	-100.2	18.0	-138.1	-16.4	32.0	-	+	-	-	+
May	-131.4	16.3	-122.5	-18.1	51.0	-	+	-	-	+
Jun	-112.7	13.7	-110.1	-17.2	58.2	-	+	-	-	+
Jul	-77.2	8.4	-109.3	-15.1	51.0	-	+	-	-	+
Aug	-65.8	1.0	-115.3	-13.7	40.0	-	+	-	-	+
Sep	-57.1	5.4	-145.2	-12.8	33.6	-	+	-	-	+
Oct	-88.0	5.2	-161.4	-1.1	33.7	-	+	-	-	+
Nov	-81.5	11.5	-137.7	2.5	23.8	-	+	-	+	+
Dec	-56.3	9.9	-118.5	1.4	19.7	-	+	-	+	+
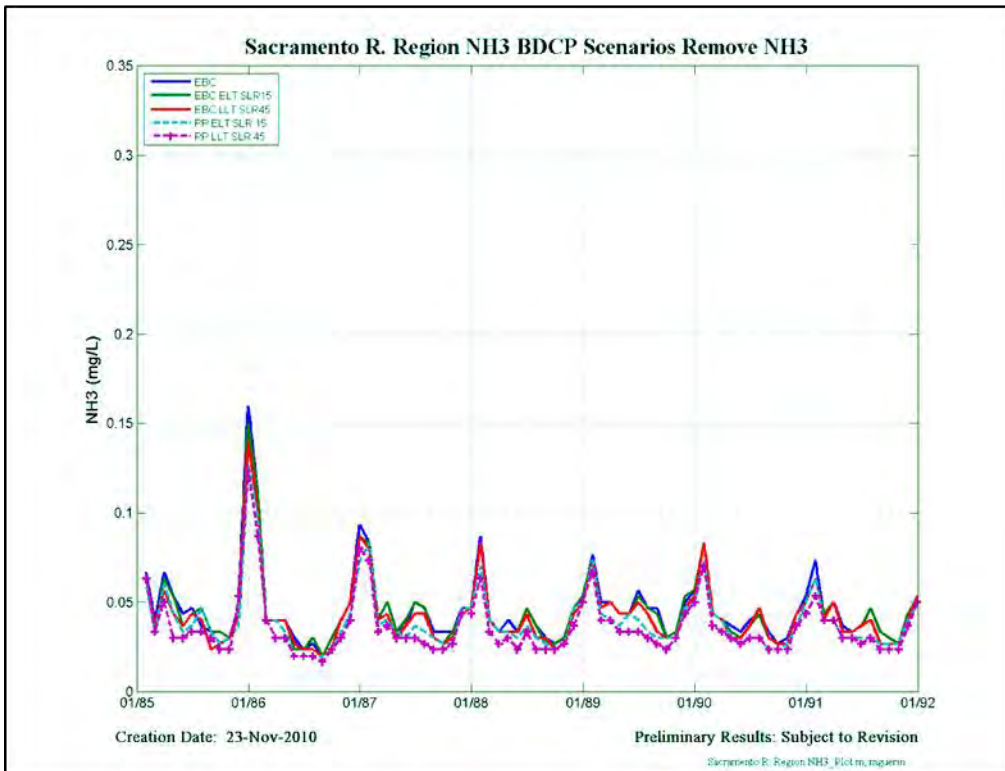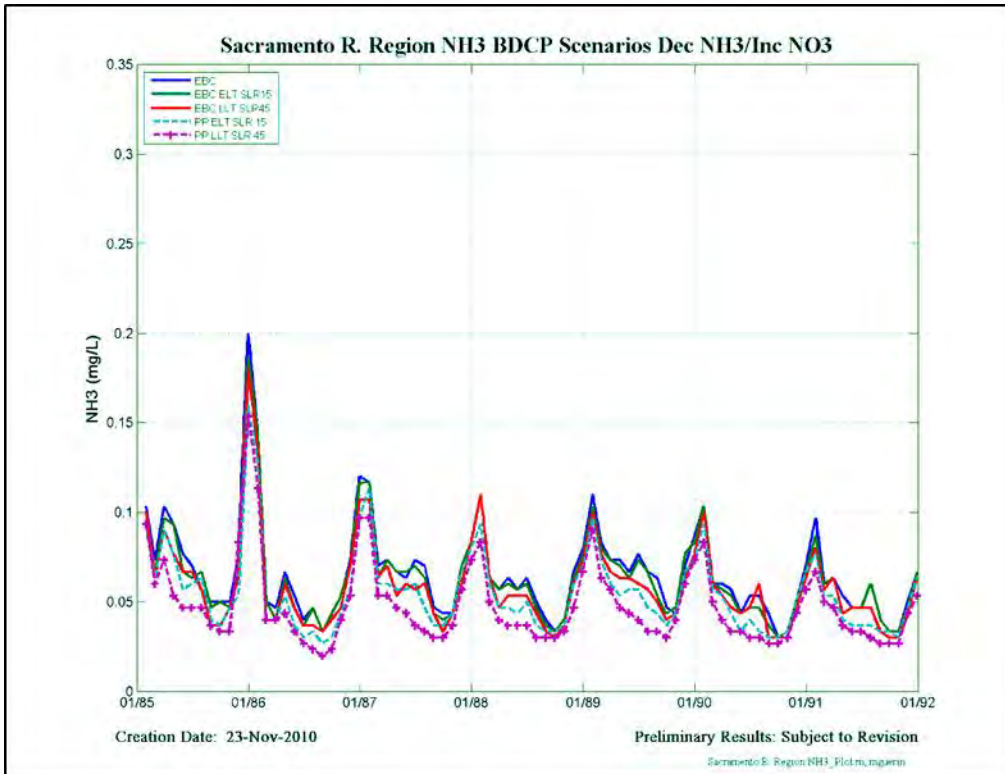
Figure 5-32 Scenarios changing Sacramento N-concentrations – Sacramento Region model output for NH₃.
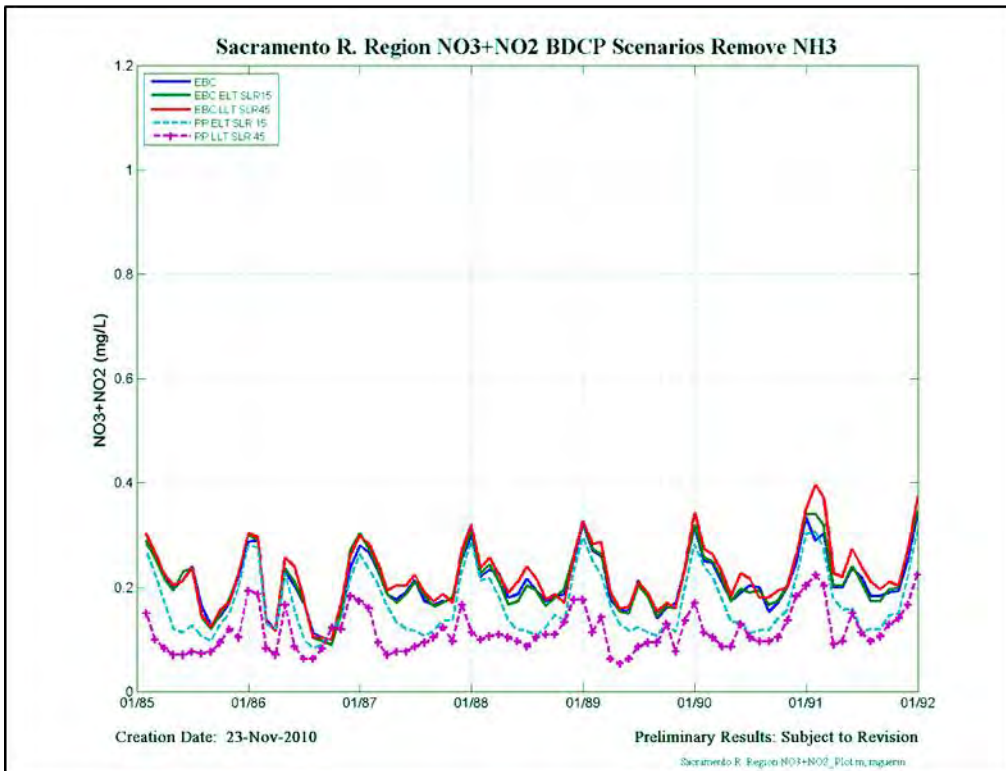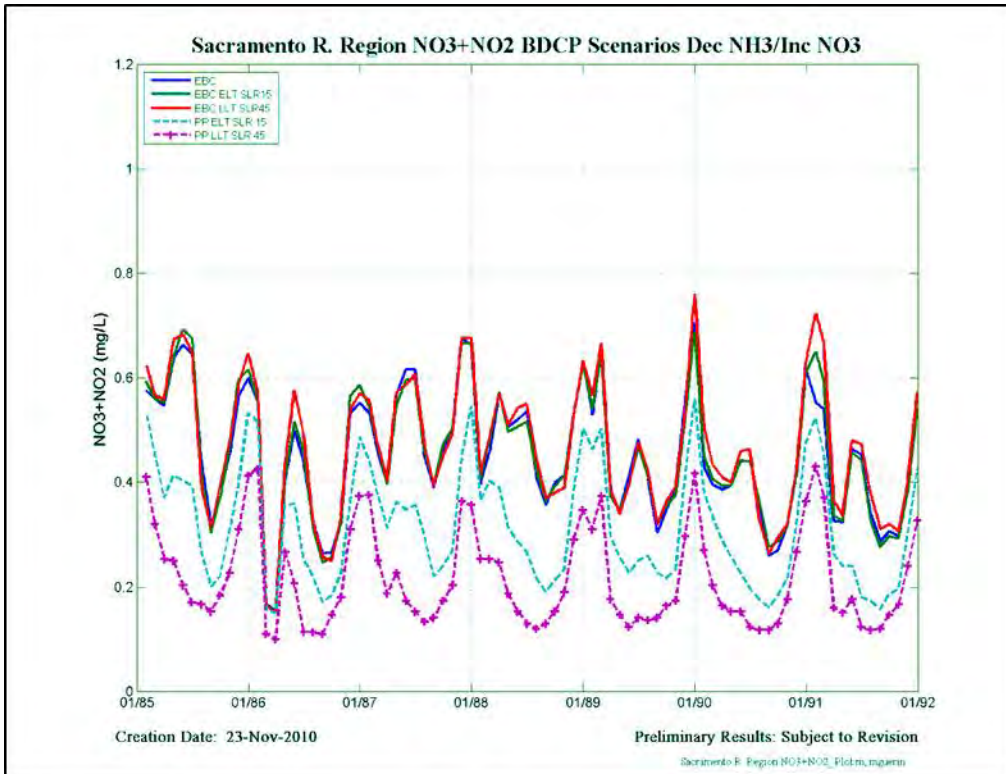
Figure 5-33 Scenarios changing Sacramento N-concentrations – Sacramento Region model output for NO$_3$+NO$_2$.
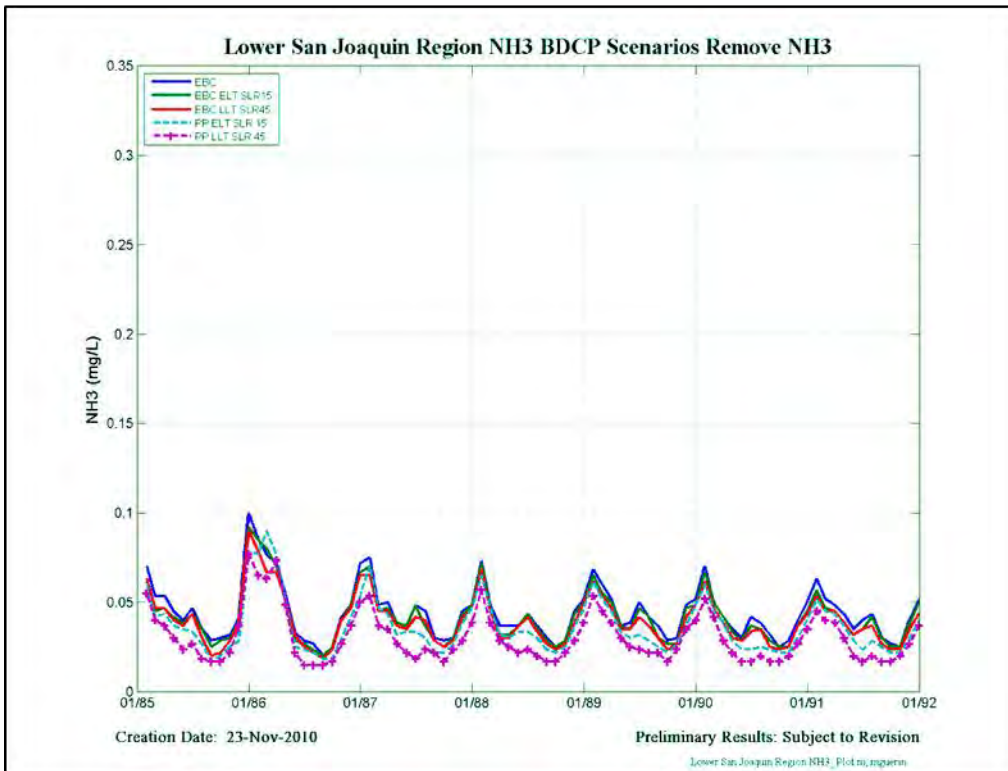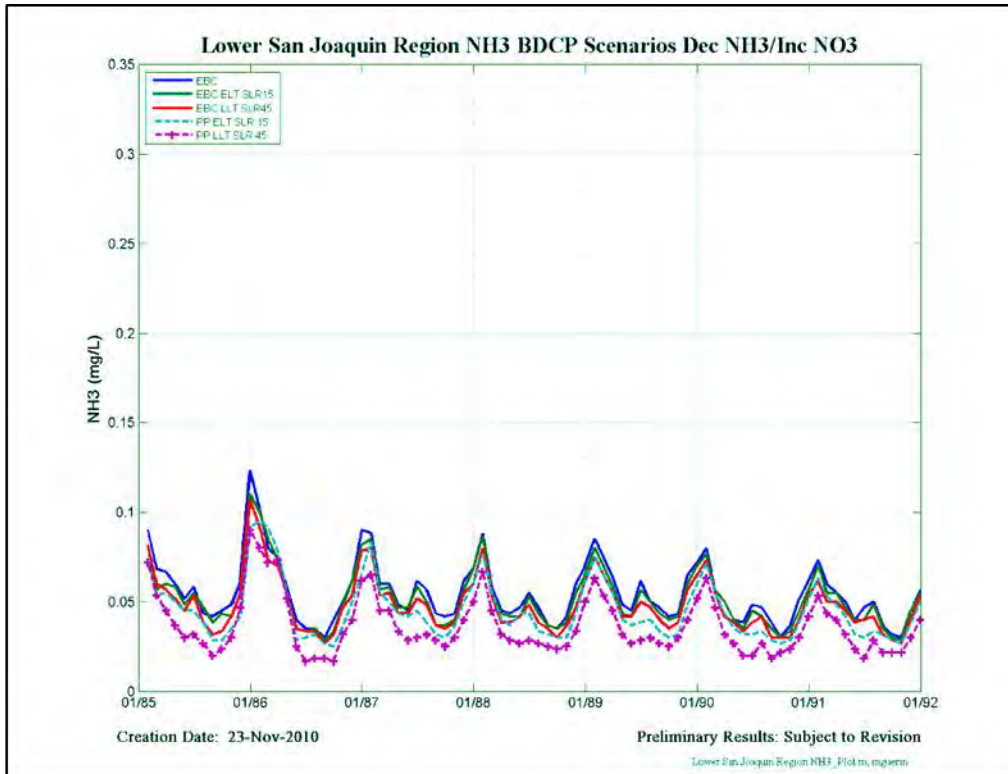
Figure 5-34 Scenarios changing Sacramento N-concentrations – Lower San Joaquin Region model output for NH₃.
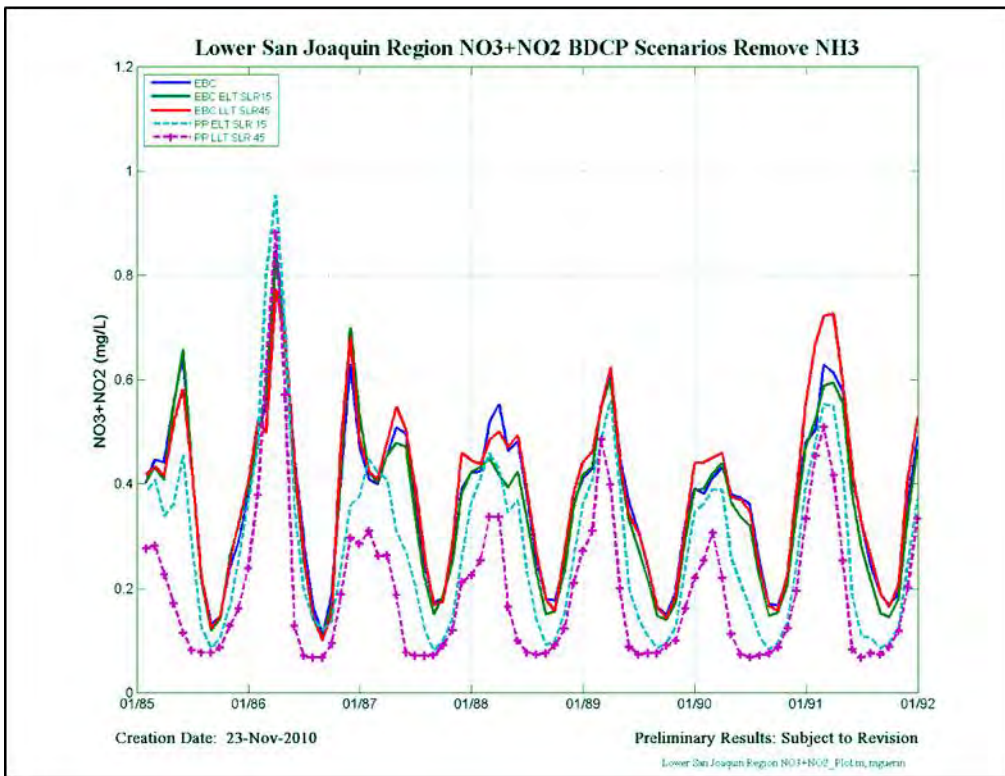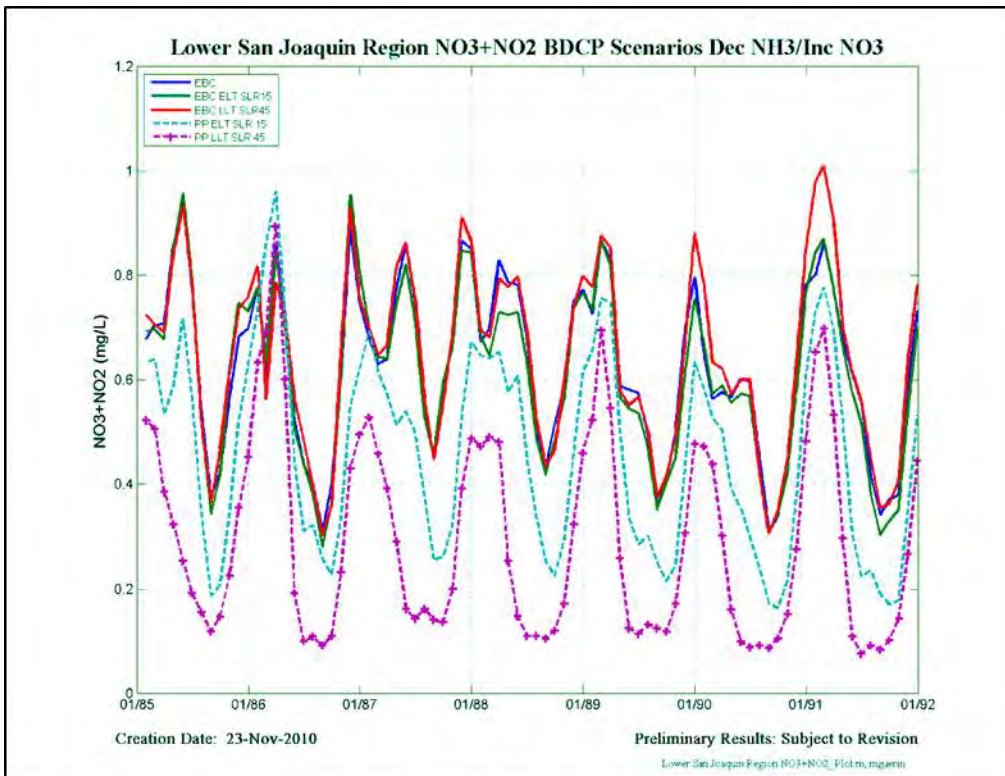
Figure 5-35 Scenarios changing Sacramento N-concentrations – Lower San Joaquin Region model output for NO$_3$+NO$_2$.
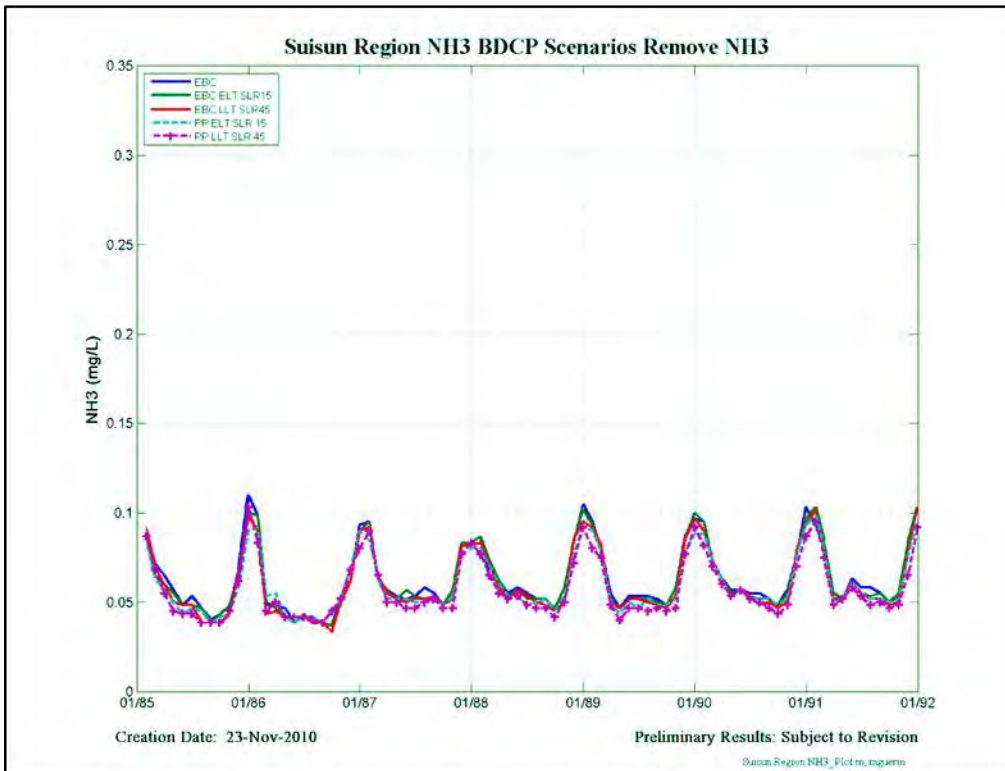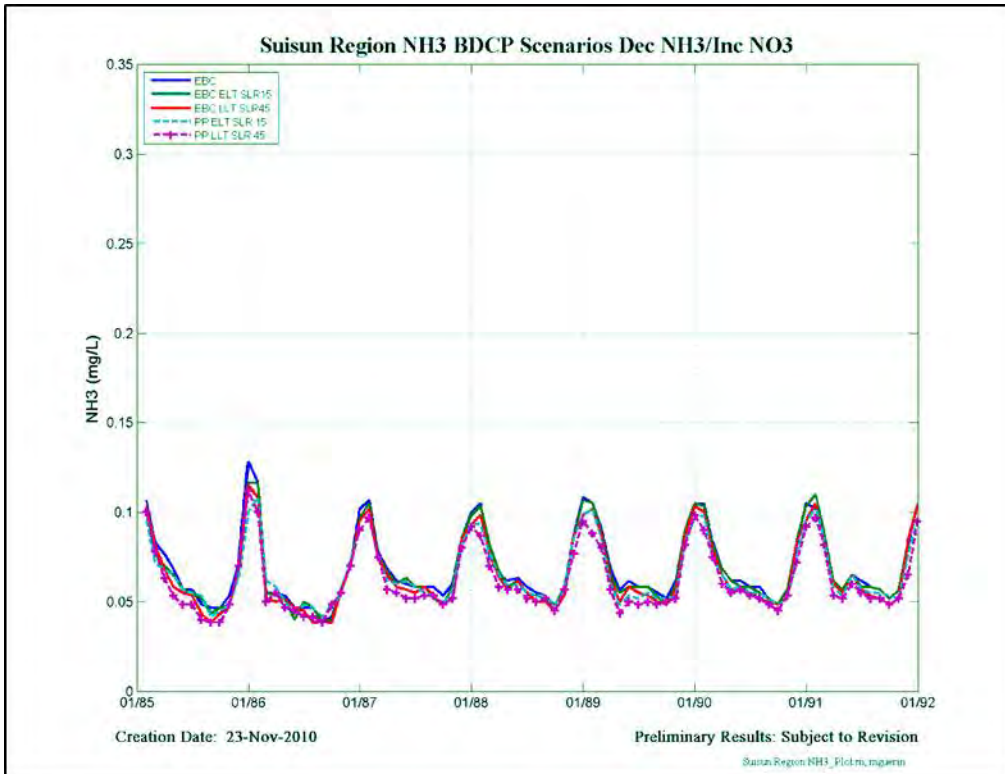
Figure 5-36 Scenarios changing Sacramento N-concentrations – Suisun Region model output for NH₃.
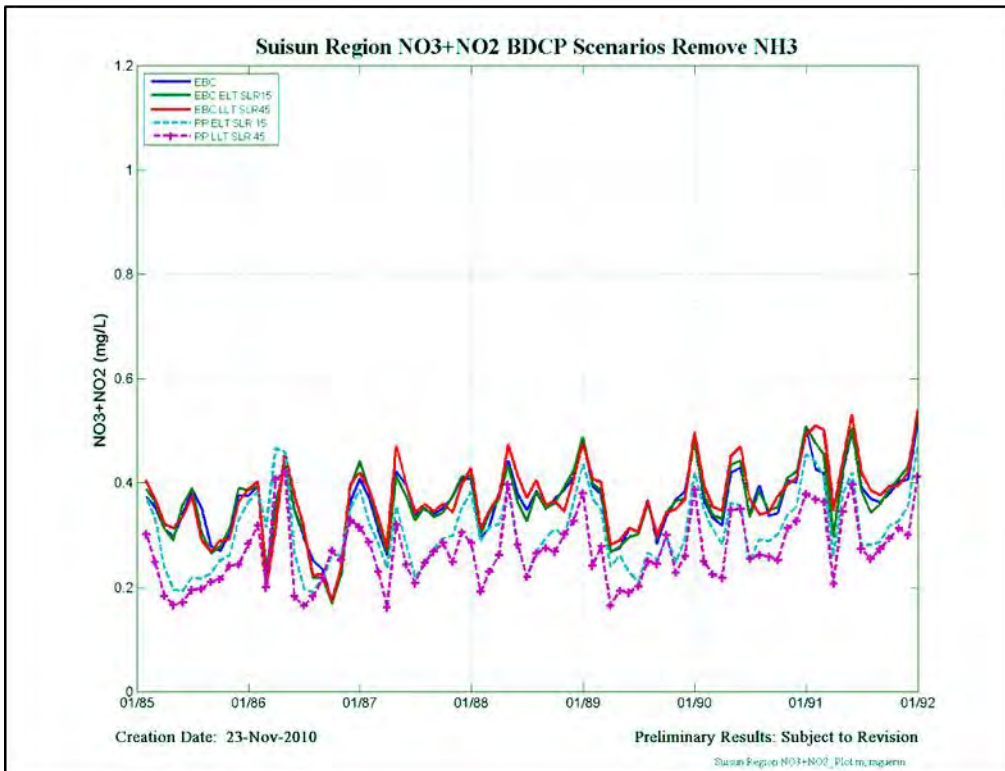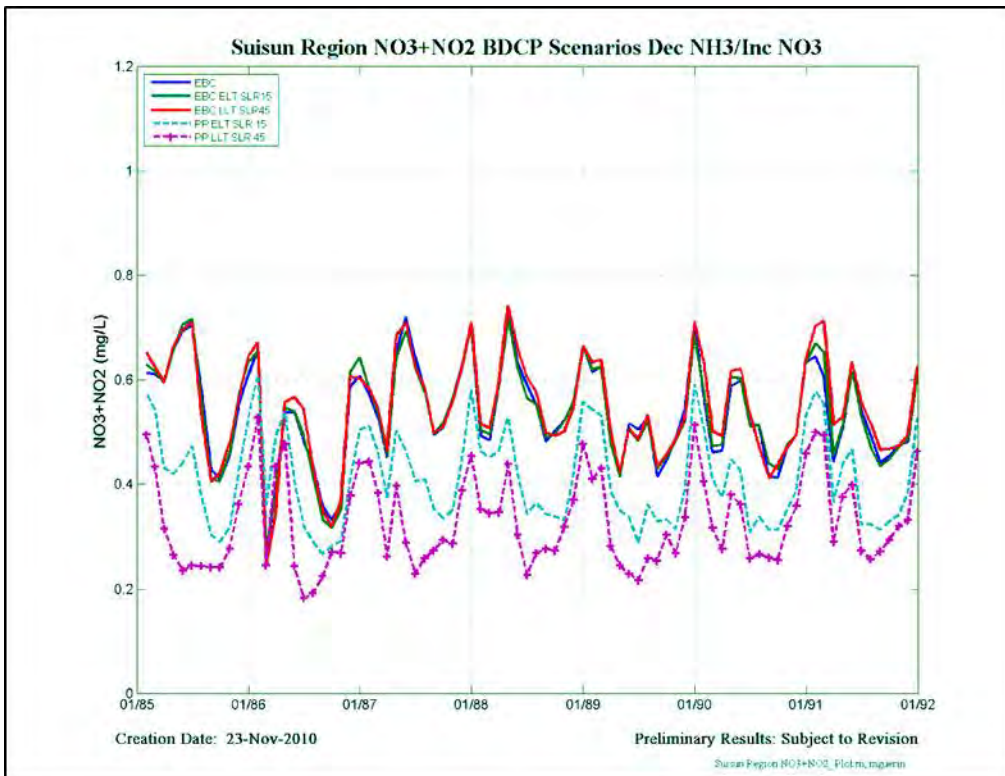
Figure 5-37 Scenarios changing Sacramento N-concentrations – Suisun Region model output for NO$_3$+NO$_2$.
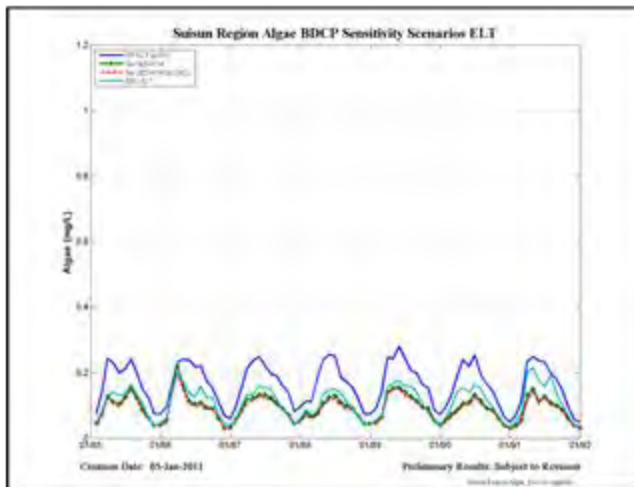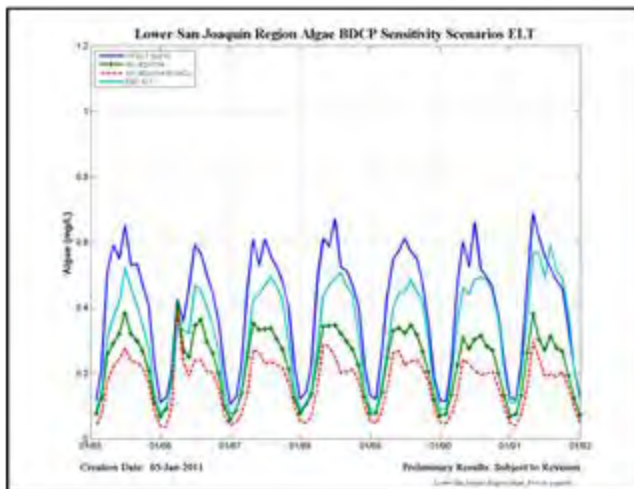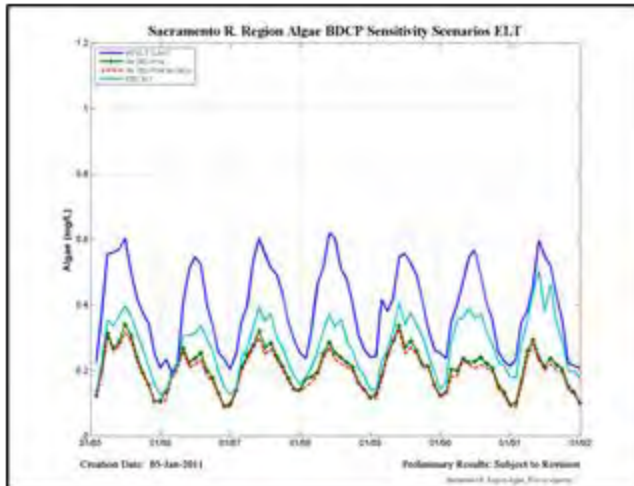
Figure 5-38 Sensitivity of the modeled constituent Algae to PO$_4$ reservoir sediment release with and without all-nutrient DICU contributions for the three defined regions in the ELT time frame.

107
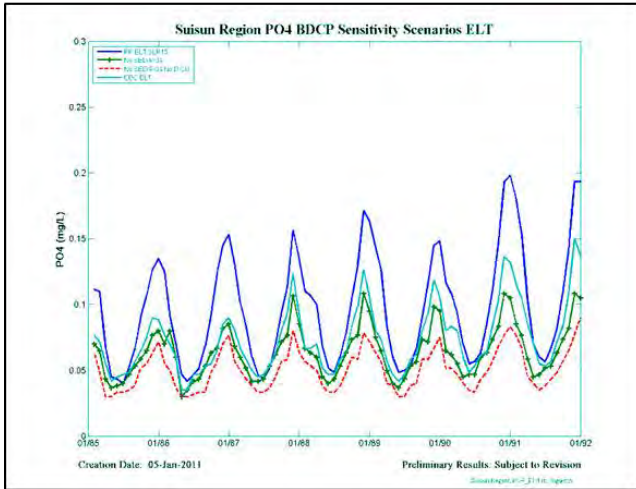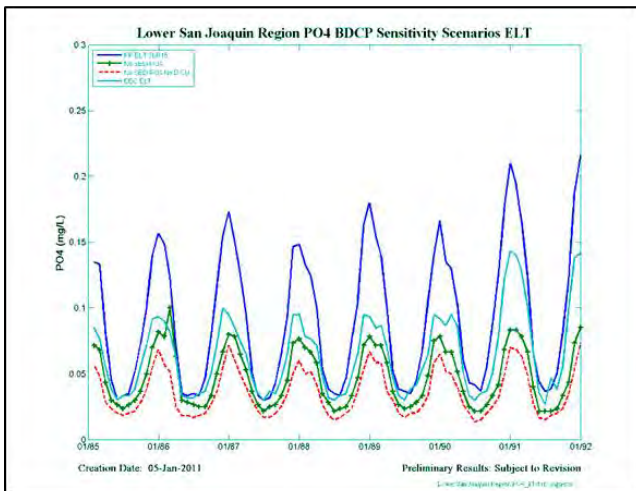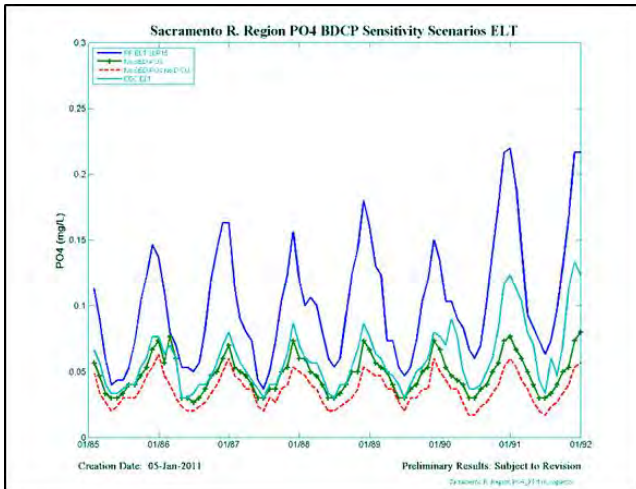
Figure 5-39 Sensitivity of the modeled constituent PO$_4$ to PO$_4$ reservoir sediment release with and without all-nutrient DICU contributions for the three defined regions in the ELT time frame.
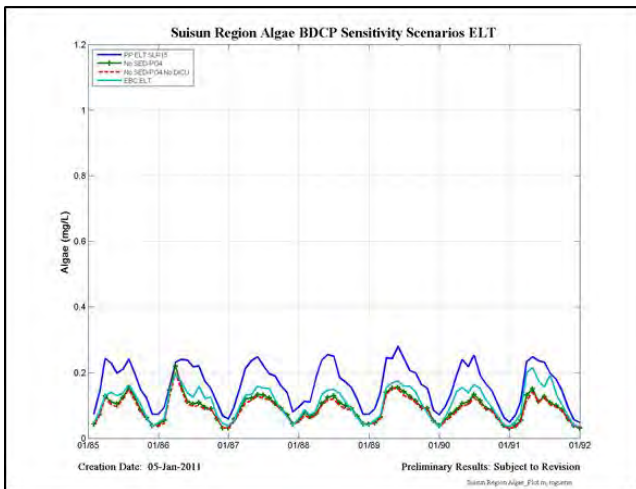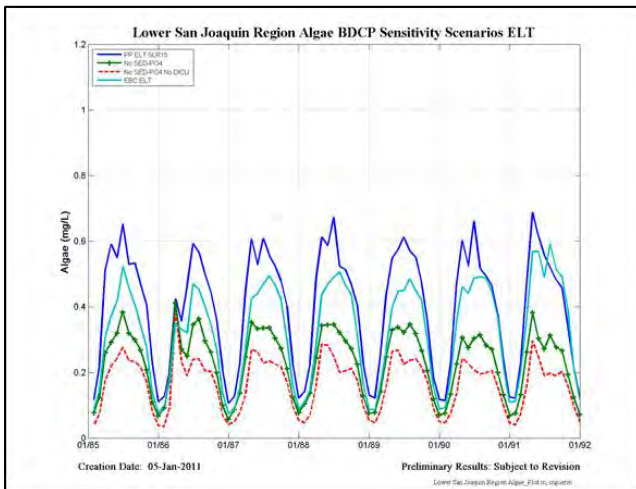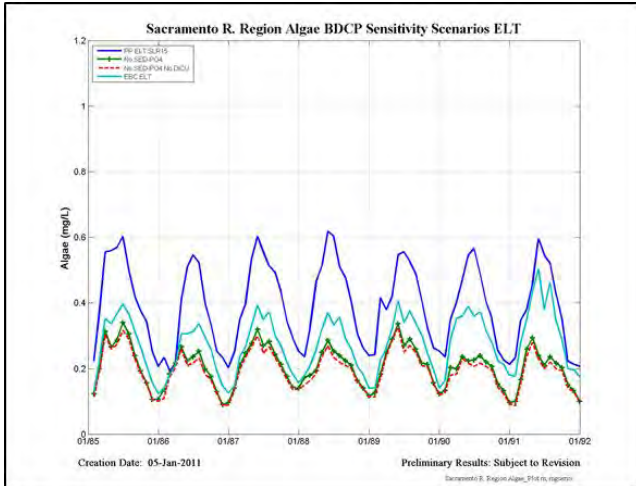
Figure 5-40 Sensitivity of the modeled constituent Algae to PO₄ reservoir sediment release with and without all-nutrient DICU contributions for the three defined regions in the ELT time frame.

6. Summary and Recommendations

Summary

The DSM2/QUAL temperature and nutrient model was calibrated and validated for the years 2000 - 2008. Calibration and validation results are similar when viewed over all years (wet and dry), and also similar for wet and dry year types separately. Temperature calibration could be improved with the introduction of additional meteorological regions in DSM2 – the single meteorological region led to an underestimation of water temperature in the S. Delta and along the upper San Joaquin R. Water. Temperature calibration and validation results were otherwise ranked Very Good as assessed by categorical calibration statistics.

The calibration results for nutrient constituents varied by the region and the constituent. Generally, results for N-constituents were Satisfactory to Very Good throughout the Delta, although some constituents (e.g., Algae along the Sacramento) were biased in some regions. The recent calibration significantly improved the statistics for PO_4.

Some locations generally showed poor calibration and validation, such as Old River at RDR, while others, such as Pt. Sacramento were generally very good to satisfactory for each of the constituents. Calibration for DO was very good, not surprising given that data for boundary conditions was available on an hourly basis. For NH3 and NO3, calibration data in-Delta was generally quite good and the calibration results reflect the quality and quantity of this data.

All model results for the BDCP scenarios were averaged to monthly values. Seven regions were established in the Delta for the averaging of model output – 15-minute model output was averaged to monthly values and then individual time series were averaged by region. Model results were assessed by plotting and by calculating percent differences between scenarios. The percent difference tables were expressed as Monthly Averages – i.e., the model results for each region were averaged over the entire model time frame to produce a single value for each month expressing the percent difference between two scenarios.

Differences in the EBC scenarios appear to be driven largely by changes due to climate (i.e., in meteorological boundary conditions), the changes in boundary flows. Changes in water temperature were generally small. Changes in nutrients were generally greater in the EBC-LLT scenario in comparison with the EBC-ELT scenario.

Due to the lack of confidence in the representation of the "reservoirs" in DSM2 in the Proposed Project scenarios, results for those scenarios are only briefly mentioned. Instead, suggestions on how to address and improve the representation are given in the next section.

Recommendations

The changes in bathymetry for the Proposed Project, discussed in Section 2, consist of the introduction of tidal marsh into the Delta in the ELT and LLT scenarios. These areas are mostly introduced as "reservoirs" in DSM2 (there is an exception in the S. Delta where the open water is conceptualized as channels). Reservoirs are essentially open water areas, and calculations are made as a single fully-mixed volume at each computational step.

The results presented in this document comparing DSM2 Historical nutrient model output for Liberty Island with the Lehman data for comparable nutrients indicate that some changes to Yolo inflow boundary concentrations should be made and that the growth rate for Algae should be decreased. In addition, a volumetric fingerprinting analysis of Liberty Island water sources along with nutrient concentrations arriving from Sacramento R. sources should be undertaken to help constraint these parameters.

A more extensive analysis should also be undertaken to help define potential pitfalls with the conceptualization of Liberty Island as a fully mixed reservoir. This analysis could include implementation of a nutrient model in a 2-D setting, such as the RMA11 nutrient model and also a literature review. Since Liberty Island is essentially at the model boundary (*e.g.*, in comparison with Franks Tract) once the Yolo Bypass stops flowing, it could be that this simplification is causing problems with the parameterization of the "bed" of the reservoir. In particular, DSM2 parameters conceptualizing benthic releases of NH_3, PO_4 and benthic demand on DO may be overestimating Liberty Island interactions once the Yolo flows become very low. In DSM2 reservoirs such as Franks Tract and Mildred Island, benthic releases/interactions are mixed with Delta waters flowing through the Islands at each time step. In Liberty Island on the other hand, these mixing processes are muted due to its location near the model boundary. Finally, DICU contributes a source of nutrients that be overestimated – resolving this question would require gathering additional information on agricultural sources of nutrient loads to this area in the DSM2 model domain.

7. References

Brown, L. C., and T. O. Barnwell, Jr. *The Enhanced Stream Water Quality Models QUAL2E andQUAL2E-UNCAS: Documentation and User Manual.* EPA-600/3-87/007. U.S. Environmental Protection Agency, Athens, GA. 1987.

Chapra, S., G. Pelletier, H. Tao. QUAL2K: A modeling framework for simulating river and stream water quality. Model Documentation. 2008.

Chilmakuri,C. 2009. Overview of Recent DSM2 Recalibration for BDCP. http://baydeltaoffice.water.ca.gov/modeling/deltamodeling/DSM2UsersGroup/DSM2_Recalibration_102709.pdf

DWR, 2007a. California Department of Water Resources, Delta-Suisun Marsh Office, 2007, LiDAR Survey of the Sacramento-San Joaquin Delta.

DWR, 2007b. California Department of Water Resources, Technical memorandum: Hydrodynamic and Water Quality Modeling for Franks Tract Project Alternatives, October, 2007.

DWR, 2004. California Department of Water Resources, "Methodology for Flow and Salinity Estimates in the Sacramento-San Joaquin Delta and Suisun Marsh, Twenty-fifth Annual Progress Report to the State Water Resources Control Board", October 2004.

DWR, Suisun Marsh Branch, 2004. Unpublished data in preparation.

DWR, 2002. California Department of Water Resources, "Methodology for Flow and Salinity Estimates in the Sacramento-San Joaquin Delta and Suisun Marsh, Twenty-third Annual Progress Report to the State Water Resources Control Board", June 2002.

DWR, 1995. California Department of Water Resources, "Estimation of Delta Island Diversions and Return Flows", February 1995.

Guerin, 2010 (Final document in preparation). Modeling the Fate and Transport of Ammonia Using DSM2 QUAL. Resource Management Associates.

Jobson,1997 (USGS). http://baydeltaoffice.water.ca.gov/modeling/deltamodeling/models/misc/BLTMenhancementsUSGSWRI97_4050.pdf

Lehman, P.W., S. Mayr, L. Mecum, C. Enright. (2010) The freshwater tidal wetland Liberty Island, CA was both a source and sink on inorganic and organic material to the San Francisco Estuary. Aquat. Ecol. 44:359-372.

Moriasi, D.N., J.G. Arnold, M.W. Van Liew, R.L. Bingner, R.D. Harmel, T.L. Vieth (2007) Model evaluation guidelines for systematic quantification of accuracy in watershed simulations. Transactions of the ASABE, Vol. 50(3), 885 – 900.

Rajbhandari, H. DWR 2005 Annual Progress Report, Chap 4: Sensitivity of DSM2 Temperature Simulations to Time Step Size. 2005.

Rajbhandari, H. DWR 2004 Annual Progress Report, Chap 4: Modeling Dissolved Oxygen and Temperature in DSM2 Planning Studies. 2004.

Rajbhandari, H. DWR 2003 Annual Progress Report, Chap 3: Extending DSM2-QUAL Calibration of Dissolved Oxygen. 2003.

Rajbhandari, H. DWR 2001 Annual Progress Report, Chap 6: Dissolved Oxygen and Temperature Modeling Using DSM2. 2001.

Rajbhandari, H. DWR 2000 Annual Progress Report, Chap 9: Dissolved Oxygen Modeling Using DSM2-QUAL. 2000.

Rajbhandari, H. DWR 1995 Annual Progress Report, Chap 3: Water Quality. 1995b.

Rajbhandari, H. Dynamic simulation of water quality in surface water sytems utilizing a Langrangian reference frame. Ph.D. Dissertation. University of California, Davis. 1995a.

USGS,1997.
http://baydeltaoffice.water.ca.gov/modeling/deltamodeling/models/misc/FourPointUSGSWRI97_4016.pdf

8. Appendix I

Nutrient Model formulation

The ten equations that comprise the nine non-conservative constituents in the nutrient model plus temperature are discussed individually below. The equation for salinity, the conservative constituent, is not discussed.

Each mass balance equation represents the mass per unit volume of water (mg L^{-1}). The transport of the constituent due to advection is not shown due to the assumption of a Lagrangian reference frame that moves through the domain at the mean velocity of the water - additional information can be found in (Rajbhandari, 1995a and 1995b).

There are 47 adjustable parameters that are used in the equations, illustrated in Table 8-2 and continued in Table 8-3. Some of the symbols appearing in the Tables do not appear explicitly in the equations. Parameters that appear in the equations that are not listed in the Tables are defined at their initial appearance in the text. There are sixteen temperature coefficients for reaction rates shown in Table 8-3. Temperature coefficients are defined by the relationships $k(T) = k(20)\Theta^{(T-20)}$, where $k(T)$ is the reaction rate day^{-1} at temperature T in °C and Θ is the user-defined temperature coefficient for the reaction shown in the Table. The values used for these coefficients were set at standard literature values.

Table 8-1Definitions for variables appearing in equations 1 – 10.

Variable Symbol	Modeled Constituent
O	DO
L	CBOD
NH_3	Total ammonia as N
NO_2	Nitrite as N
NO_3	Nitrate as N
A	Phytoplankton biomass
N-org	Organic nitrogen
P-org	Organic phosphorus
PO_4	Orthophosphate as P
T	Temperature

Temperature

The formulation for the transport of temperature in the model, equation (1) was adapted from the QUAL2E model (Brown and Barnwell, 1987), with several changes documented in (Rajbhandari, 1995b). Water temperature influences the interactions between the modeled constituents as discussed in the overview to this Section.

The net transfer of energy, Q_n, across the air-water interface is formulated as a function of net short wave radiation flux, net long wave atmospheric radiation flux, water surface back radiation flux, evaporative heat flux and sensible heat flux. The expressions accounting for this energy transfer are functions of the meteorological inputs (not shown). In the equation, p is the density of water, C is the specific heat of water and d is the hydraulic depth of the water. E_x is the longitudinal dispersion coefficient.

$$\frac{\partial [T]}{\partial t} = \frac{\partial}{\partial \xi}\left[E_x\, \frac{\partial T}{\partial \xi}\right] + Q_n\Big/ pcd \quad \textbf{(1)}$$

Dissolved Oxygen (DO)

DO concentration is a critical indicator of the general health of an aquatic ecosystem (Rajbhandari, 1995a; Cole and Wells, 2008). Equation (2) specifies the rate of change in DO concentration due to sources (reaeration and photosynthesis), sinks (CBOD, oxidation of NH_3 and NO_2, algal respiration and benthic demand) and dispersion. The expressions used to model DO saturation and reaeration are discussed in detail in (Rajbhandari, 1995a).

Benthic oxygen demand represents a generic expression encompassing several processes in the sediment that remove oxygen from the water column, including the decay of organic matter and utilization of dissolved oxygen by benthic species (such as clams) and macrophytes.

$$\frac{\partial [O]}{\partial t} = \frac{\partial}{\partial \xi}\left[E_x \frac{\partial [O]}{\partial \xi}\right] - (k_1 + k_3)L + k_2(O_s - [O]) - \alpha_5 k_n[NH_3] - \alpha_6 k_{ni}[NO_2] + \alpha_3 \mu[A] - \alpha_4 \rho[A] - K_4\big/d \tag{2}$$

Diffusion   CBOD   Reaeration   Ammonia ox.   Nitrite ox.   Photosynthesis Respiration Benthic

Carbonaceous Biochemical Oxygen Demand (CBOD)

Carbonaceous biochemical oxygen demand refers to the potential for microorganisms to consume oxygen as they utilize organic-carbon substrates. A related measurement is nitrogenous BOD (NBOD) – this refers to the oxygen consumed by nitrifying bacteria as they consume organic and inorganic materials that contain a reduced form of nitrogen. Collectively, CBOD+NBOD is called BOD, and tests that measure any of the three forms occur over a number of days, typically five or twenty days. For the purposes of this project, we utilized CBOD$_5$, a five-day test for CBOD.

Equation 3 accounts for the sources and sinks of CBOD due to the death of algae or oxidation, respectively.

$$\frac{\partial [L]}{\partial t} = \frac{\partial}{\partial \xi}\left[E_x \frac{\partial [L]}{\partial \xi}\right] - (k_1 + k_3)L + \sigma_6[A] \tag{3}$$

Algae (Phytoplankton)

Equation 4 accounts for the biomass of algae in the model. Algae utilize chlorophyll pigments to convert solar radiation to energy, and chlorophyll a (a particular form of pigment) measurements are typically used as an indicator of algal biomass. A conversion factor is used to convert chlorophyll a concentrations to algal biomass. For this project, we used a conversion factor of 67 g algae (dry weight)/mg chl-a (Clesceri et al., 1999), although there are many different algal species (Cole and Wells, 2008) with variable characteristics including growth rates, preferred nutrient sources, and levels of chlorophyll per unit of mass.

$$\frac{\partial [A]}{\partial t} = \frac{\partial}{\partial \xi}\left[E_x \frac{\partial [A]}{\partial \xi}\right] + (\mu - \rho)[A] - \sigma_1 [A]/d - \sigma_6 [A] \quad \text{(4)}$$

Algal growth is a function of the difference between the respiration rate, ρ, and the growth rate, μ, of this generic algal population. The growth in algal biomass is assumed to be limited by availability of light, F_L, inorganic nitrogen, N, as the sum of the concentrations of NH_3 and NO_3, and inorganic phosphorus, P, as expressed in the following equation (4a):

$$\mu = \mu_{MAX}\, F_L\, Min\left(\frac{N}{K_N + N}, \frac{P}{K_P + P} \right) \quad \text{(4a)}$$

where K_N and K_P are the half-saturation constants of nitrogen and phosphorus, respectively. F_L is further expressed as a Monod equation as a function of light intensity at a given depth (Rajbhandari, 1995a). As shown is subsequent sections, the generic algal biomass is assumed to be composed of a set ratio of N:P concentrations, although this ratio can vary between different algal species.

Organic nitrogen (Org-N)

Organic nitrogen dynamics are represented by equation 5:

$$\frac{\partial [N-org]}{\partial t} = \frac{\partial}{\partial \xi}\left[E_x \frac{\partial [N-org]}{\partial \xi}\right] - \alpha_1 \rho [A] - k_{N-org}[N-org] - \sigma_4 [N-org] \quad \text{(5)}$$

The only source of nitrogen due to nutrient dynamics occurs as a result of algal respiration as a fraction of the algal biomass assumed to be nitrogen. Org-N is lost from the system as it decays and settles.

Because organic-N measurements are frequently unavailable, Total Kjeldahl Nitrogen (TKN) can be used to calculate organic-N if ammonia measurements are also available, as TKN = organic-N + ammonia.

Ammonia (NH$_3$)

Ammonia nitrogen dynamics are represented by equation 6:

$$\frac{\partial [NH_3]}{\partial t} = \frac{\partial}{\partial \xi}\left[E_x \frac{\partial [NH_3]}{\partial \xi}\right] - f\alpha_1 \mu [A] + k_{N-org}[N-org] - k_n [NH_3] + \sigma_3/d \quad \text{(6)}$$

Although ammonia concentration is represented in this equation by the formula NH_3, in fact the concentration of ammonia is assumed implicitly to be the total of aqueous NH_3 (g) and NH_4^+, as discussed previously. NH_3 is a nutrient source for algae, as is NO_3, and the preferential consumption of these two sources of nitrogen is given by a preference factor, $0.0 \leq p \leq 1.0$, in the following expression:

$$f = \frac{p[NH_3]}{p[NH_3] + (1-p)[NO_3]} \quad \text{(6a)}$$

where the square brackets indicate modeled concentration.

Nitrite (NO_2)

In equation 6, NH_3 is seen to decay at a set rate – in equation 7 we see that that the NH_3 has decayed into NO_2:

$$\frac{\partial[NO_2]}{\partial t} = \frac{\partial}{\partial \xi}\left[E_x \frac{\partial[NO_2]}{\partial \xi}\right] - k_{ni}[NO_2] + k_n[NH_3] \quad \text{(7)}$$

Nitrate (NO_3)

Nitrate dynamics are given by equation 8. Here we see that NO_2 has decayed into NO_3:

$$\frac{\partial[NO_3]}{\partial t} = \frac{\partial}{\partial \xi}\left[E_x \frac{\partial[NO_3]}{\partial \xi}\right] - (1-f)\alpha_1 \mu[A] + k_{ni}[NO_2] \quad \text{(8)}$$

Nitrate is consumed by algae, where the rate is assumed to be governed by the preference of algae for NH_3 or NO_3.

Organic Phosphorus (Org-P)

Equation 9 shows the sources and sinks for org-P in the nutrient dynamics:

$$\frac{\partial[P-org]}{\partial t} = \frac{\partial}{\partial \xi}\left[E_x \frac{\partial[P-org]}{\partial \xi}\right] + \alpha_2 \rho[A] - k_{P-org}[P-org] - \sigma_5[P-org] \quad \text{(9)}$$

Dissolved Phosphorus (PO_4)

The final equation represents the sources and sinks of inorganic phosphorus, which is assumed to the concentration of ortho-phosphate, PO_4:

$$\frac{\partial[PO_4]}{\partial t} = \frac{\partial}{\partial \xi}\left[E_x \frac{\partial[PO_4]}{\partial \xi}\right] - \alpha_2 \mu[A] + k_{P-org}[PO_4] + \sigma_2/d \quad \textbf{(10)}$$

Reaction Rates and Parameters

There are 16 Regional Reaction Rate parameters (in Table 8-2 and Table 8-3)that can that can be varied by channel in the grid as well as in each open water body (reservoir). There are 31 Global Reaction Parameters that are set for the entire model domain. The sixteen temperature coefficients for reaction rates (Table 8-2) are set globally. The values listed in the "Calibrated Values" column give the ranges set in the model.

Table 8-2 Adjustable parameters used in the model equations.

Symbols	Description	Lit. Range Min/Max	Calibrated Values	Units	Source
k_{ni}	Nitrite decay rate at the ambient temperature	0.2-2.0	2.0	day^{-1}	Rajbhandari (1995)
$k_n + k_{ni}$	Ammonia decay rate + Nitrite decay rate at the ambient temperature	0.001-1.3	-	day^{-1}	Bowie et al. (1985)
k_{n-org}	Rate constant for hydrolysis of organic nitrogen to ammonia nitrogen at the ambient temperature	0.02-0.4	0.1	day^{-1}	Rajbhandari (1995)
σ_4	Organic nitrogen settling rate at the ambient temperature	0.001-0.1	0.0 - 0.01	day^{-1}	Rajbhandari (1995)
k_{p-org}	Organic phosphorus decay rate at the ambient temperature	0.01-0.7	0.05 - 0.1	day^{-1}	Rajbhandari (1995)
σ_5	Organic phosphorus settling rate at the ambient temperature	0.001-0.1	0.0 – 0.9	day^{-1}	Rajbhandari (1995)
σ_2	Benthic release rate for orthophosphate at the ambient temperature (mass transfer rate of PO_4 in the sediment)	1.0 0.0816 0.057–21.0	0.0 - 0.1	mg m^{-2} day^{-1} m day^{-1} mg m^{-2} day^{-1}	Rajbhandari (1995) Sanford and Crawford(2000) Cole & Wells (2008)
σ_3	Benthic release rate for ammonia-N at the ambient temperature (mass transfer rate of NH_3 in the sediment)	4.0 0.06-0.1464	0.0-0.14	mg m^{-2} day^{-1} m day^{-1}	Rajbhandari (1995) Sanford and Crawford(2000) Cole & Wells (2008)
k_4	Benthic oxygen demand	30 – 300 0.3 – 5.8	30 - 300	g m^{-2} day^{-1} g m^{-2} day^{-1}	Rajbhandari (1995) Chapra (1997)
Temperature Coefficients for Reaction Rates					
$\theta(1)$	BOD decay	1.047 1.02	1.047		Wilson et al. (1998) Cole & Wells (2008)
$\theta(2)$	BOD settling	1.024	1.024		Wilson et al. (1998)
$\theta(3)$	DO Reaeration	1.024	1.024		Wilson et al. (1998); Chapra (1997)
$\theta(4)$	DO SOD	1.060 1.04-1.13	1.06		Wilson et al. (1998) Cole & Wells (2008)
$\theta(5)$	Organic-N decay	1.047	1.047		Wilson et al. (1998)
$\theta(6)$	Organic-N settling	1.024	1.024		Wilson et al. (1998)
$\theta(7)$	Ammonia-N decay	1.083	1.083		Wilson et al. (1998)
$\theta(8)$	Ammonia-N benthic source	1.074	1.074		Wilson et al. (1998)
$\theta(9)$	Nitrite-N decay	1.047	1.047		Wilson et al. (1998)
$\theta(10)$	Organic-P decay	1.047	1.047		Wilson et al. (1998)
$\theta(11)$	Organic-P settling	1.024	1.024		Wilson et al. (1998)
$\theta(12)$	Dissolved-P benthic source	1.074	1.074		Wilson et al. (1998)
$\theta(13)$	Algae growth	1.047	1.047		Wilson et al. (1998)
$\theta(14)$	Algae respiration	1.047	1.047		Wilson et al. (1998)
$\theta(15)$	Algae settling	1.024	1.024		Wilson et al. (1998)
$\theta(16)$	Algae death	1.047	1.047		Wilson et al. (1998)
θ_{rxn}^{T-20}	the non-dimensional temperature multipliers of reaction	1.045-1.08			Bowie et al. (1985)

Table 8-3 More adjustable parameters used in the model equations.

Symbols	Description	Lit. Range Min/Max	Calibrated Value	Units	Source
Global Reaction Parameters					
α_5	Amount of oxygen consumed in conversion of ammonia to nitrite	3.0-4.0	3.0	-	Rajbhandari (1995)
α_6	Amount of oxygen consumed in conversion of nitrite to nitrate	1.0-1.14	1.14	-	Rajbhandari (1995)
P	Preference factor for ammonia nitrogen	0-1.0	0.5	-	Rajbhandari (1995)
α_7					
α_1	Fraction of algal biomass, which is nitrogen	0.07-0.09 0.02-0.11	0.09	-	Rajbhandari (1995) Cole & Wells (2008)
α_2	Fraction of algal biomass, which is phosphorus	0.01-0.02 0.001-0.03	0.012	-	Rajbhandari (1995) Cole & Wells (2008)
α_3	Amount of oxygen produced per unit of algal photosynthesis	1.4-4.8	1.60	-	Rajbhandari (1995)
α_4	Amount of oxygen consumed per unit of algal respired	1.6-2.3	2.0	-	Rajbhandari (1995)
K_L					
K_N	Half saturation constant for nitrogen	0.01-0.3 0.01–4.3	0.05	mg L^{-1}	Rajbhandari (1995) Cole & Wells (2008)
K_P	Half saturation constant for phosphorus	0.001-0.05 0.001-1.5	0.035	mg L^{-1}	Rajbhandari (1995) Cole & Wells (2008)
λ_0	Non-algal portion of the light extinction coefficient	0.116	0.26	ft^{-1}	Rajbhandari (1995)
λ_1	Linear algal self shading coefficient	0.002-0.02	0.003	ft^{-1} (μg-Chla L^{-1})$^{-1}$	Rajbhandari (1995)
λ_2	Nonlinear algal self shading coefficient	0.0165	0.0165	ft^{-1} (μg-Chla L^{-1})$^{-2/3}$	Rajbhandari (1995)
λ_3	Algal mortality contribution to BOD	1.0	1.0	day^{-1}	Rajbhandari (2002)
Regional Reaction Rates					
k_1		0.01 – 0.06 ?			Cole & Wells (2008)
k_3	Rate of loss of CBOD due to settling at the ambient temperature	-0.36-0.36	0.1	day^{-1}	Rajbhandari (1995)
N_{TBSA}					
ρ	Phytoplankton respiration rate at the ambient temperature	0.05-0.5 0.01-0.04	0.15	day^{-1}	Rajbhandari (1995) Cole & Wells (2008)
σ_1	Phytoplankton settling rate at the ambient temperature	0.5-6.0 0.06-33.0	0.2 – 1.5	ft day^{-1}	Rajbhandari (1995) Cole & Wells (2008)
σ_{21}	Phytoplankton death rate at the ambient temperature	0.2 0.03-0.3	0.11 – 0.7	ft day^{-1}	Rajbhandari (2002) Cole & Wells (2008)
k_n	Ammonia decay rate at the ambient temperature Ammonium decay rate	0.1-1.0 0.001 – 0.95	0.05 - 0.20	day^{-1}	Rajbhandari (1995) Cole & Wells (2008)

Data availability and quality

Data was needed to set concentrations for each of the eleven constituents at each river boundary illustrated in Figure 3-1 at each effluent boundary shown in Figure 3-2, and at the 258 DICU boundaries for the modeled time period, 2000 – 2008. In addition, data was needed in the interior of the Delta for calibration and validation of the model.

No data were available to constrain modeled nutrient concentrations or to set boundary conditions in the Yolo/Cache region. Only a few measurements were available in Suisun Marsh.

Data quality was mixed, depending on the constituent. Data for each constituent was assessed visually (by plotting) to check for unreasonable values (*e.g.,* negative numbers) and in comparison with data at nearby locations. When problems with data quality clearly occurred (*e.g.,* all nearby stations had significantly different magnitudes), suspect data were deleted from the time series. Measurements identified as occurring at the detection limit were set at the detection limit, and non-detects in an analysis (i.e., for concentrations below the instrumental detection limit) were set at half the detection limit. Note that this introduces a bias in the data that can skew both model results and calibration/validation statistics.

Continuous time series data (15-minute or hourly) tended to suffer from large gaps in measurement. For example, temperature data at some locations would decrease in magnitude and suddenly jump in value. Continuous time series of temperature and DO data were available at or near the main model boundaries on the Sacramento River, the San Joaquin River and at Martinez at well as at several other locations. There were frequently large gaps in the data during the modeled period for each of these data types.

The quality of grab sample data used for setting nutrient boundary conditions was good, although it was generally only available at approximately monthly or bi-monthly intervals. However, data gathered by different agencies could have different ranges of values.

Figure 8-2 shows a comparison of Environmental Monitoring Program (EMP) and USGS measurements at Rio Vista and Point Sacramento. The original measurement of chlorophyll a was converted to algal biomass as described in Appendix I, Section 8. Both agencies performed these measurements at irregular intervals, approximately monthly. The measurements are within the same range of magnitude in most months, but could also vary by factors of 2 – 5, particularly when a peak occurred. The general pattern was similar.

Figure 8-3 shows similar comparison for DO data at the same locations. The measurements generally track very closely, both in magnitude and pattern. Figure 8-4 shows NO_3+NO_2 measurements – again they track fairly closely in magnitude when taken at similar times.

USGS measurements for PO_4 are currently under review, and not available for comparison.

Figure 8-5 through Figure 8-6 show interagency comparison at similar locations on the lower Sacramento River below the confluence – comparing Martinez and Suisun at Bulls Head and Chipps and Pittsburg. As with the direct location comparisons, algae (Figure 8-6), DO (Figure 8-6), and NO_3+NO_2 (Figure 8-5) track closely in magnitude and pattern.

Meteorological data

Figure 8-7 shows the locations of the Stockton NOAA and CIMIS meteorological measurement data reviewed for the 2009 calibration. NOAA Stockton meteorological measurements were used for the entire period except for wind. CIMIS Brentwood wind speed measurements were use as they were available for the entire time period of the initial DSM2/QUAL calibration, 1990 - 2008 (see (Guerin, 2009) for details).

Water temperature data

Water temperature data were generally available as regular time series at hourly intervals, or occasionally at 15-minute intervals. Much of the temperature data were obtained from the DWR Water Data library, or from the IEP and CDEC databases. The data were of mixed quality, although data quality and availability generally improved after 2000. Figure 4-1 shows the locations where water temperature data were available in the Delta.

DO data

DO is the only constituent other than temperature for which continuous time series were available, and they were downloaded from the IEP and CDEC data bases. Continuous DO data were generally sparse and noisy with large data gaps. DO measurements in the interior of the Delta were available as regular time series at five locations (Rio Vista, RSAC075, RSAN007, RSAN058 and RSAN061) and as irregular time series from the USGS and BDAT databases and from the Stockton WWTP receiving water data.

Some USGS measurements were used to help constrain boundary conditions, but they were mainly used in model calibration and validation.

DICU data

DICU nutrient data, with the exception of PO$_4$, were set as constant values in the previous DO-models (Rajbhandari 1995a, 2000, 2001, 2003). PO$_4$ was set at 0.005, down from 0.4 ppm in the V6 nutrient model calibration.

Chlorophyll-a/Algae

Algae utilize chlorophyll pigments to convert solar radiation to energy, and chlorophyll a (a particular form of pigment) measurements are typically used as an indicator of algal biomass. A conversion factor is used to convert chlorophyll a concentrations to algal biomass. We used a conversion factor of 67 g algae/mg chl-a (Clesceri et al., 1999), although there are many different algal species (Cole and Wells, 2008) with variable characteristics including growth rates, preferred nutrient sources, and levels of chlorophyll per unit of mass.

Chl-a measurements derived from continuous measurement equipment as fluorescence was deemed to be of insufficient quality to use in setting model boundary conditions or as calibration data. Grab sample measurements from a variety of sources, predominantly EMP and USGS, were used exclusively for calculating algae concentrations from chl-a values.

Effluent data

Data were obtained for the effluent flow and nutrient composition from 17 WWTPs. The approximate location of the outfalls is shown in Figure 3-2. The time periods and availability of constituents is shown in Table 8-4 and in Table 8-5. Data for Vacaville, Davis and Woodland was gathered but is not yet implemented. Because they are located outside of the model domain, estimation of flow containing their effluent into the Yolo/Cache area needs the support of additional flow data. Benicia effluent data does not need to be considered as the outfall is downstream of the model boundary at Martinez.
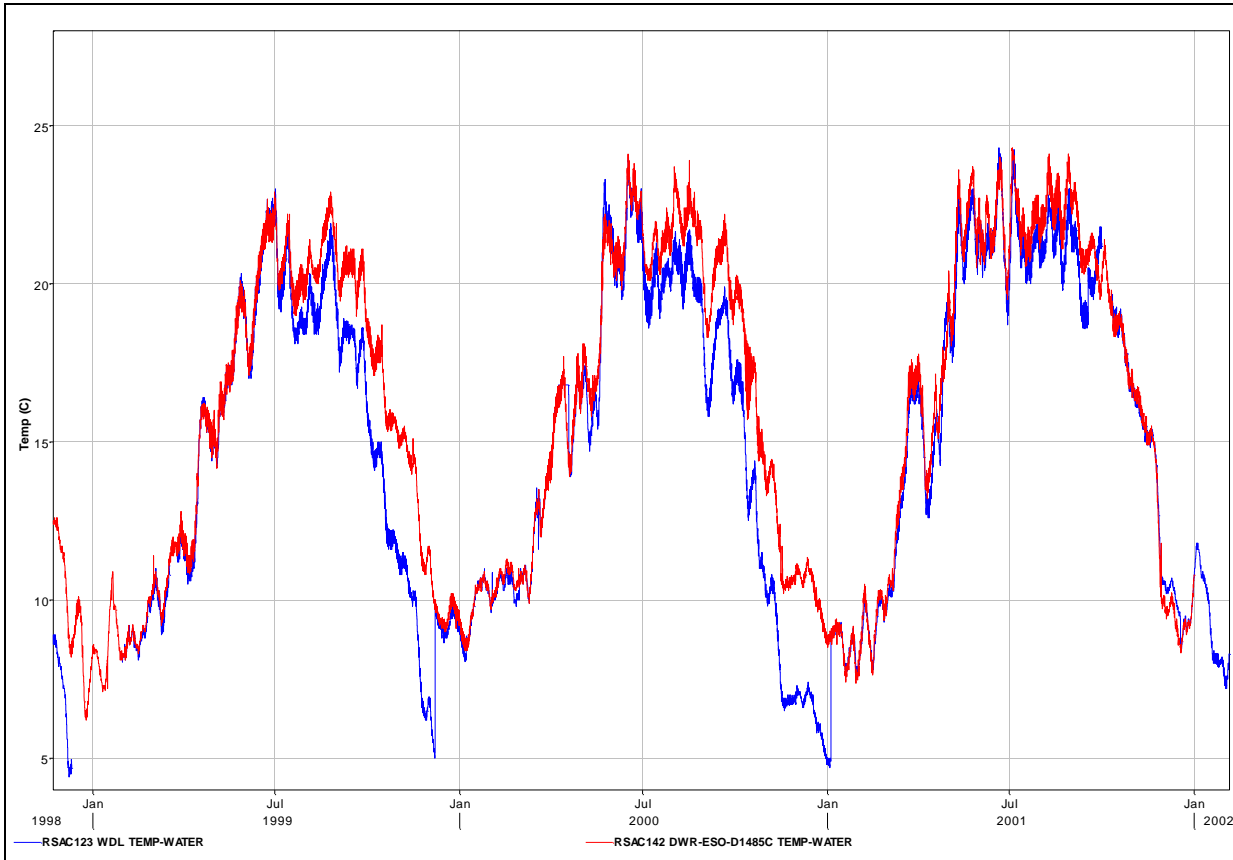
Figure 8-1 Suspect data were identified at RSAC123 (blue line) by large jumps in value at low temperatures in comparison with water temperature data at RSAC142 (red line).
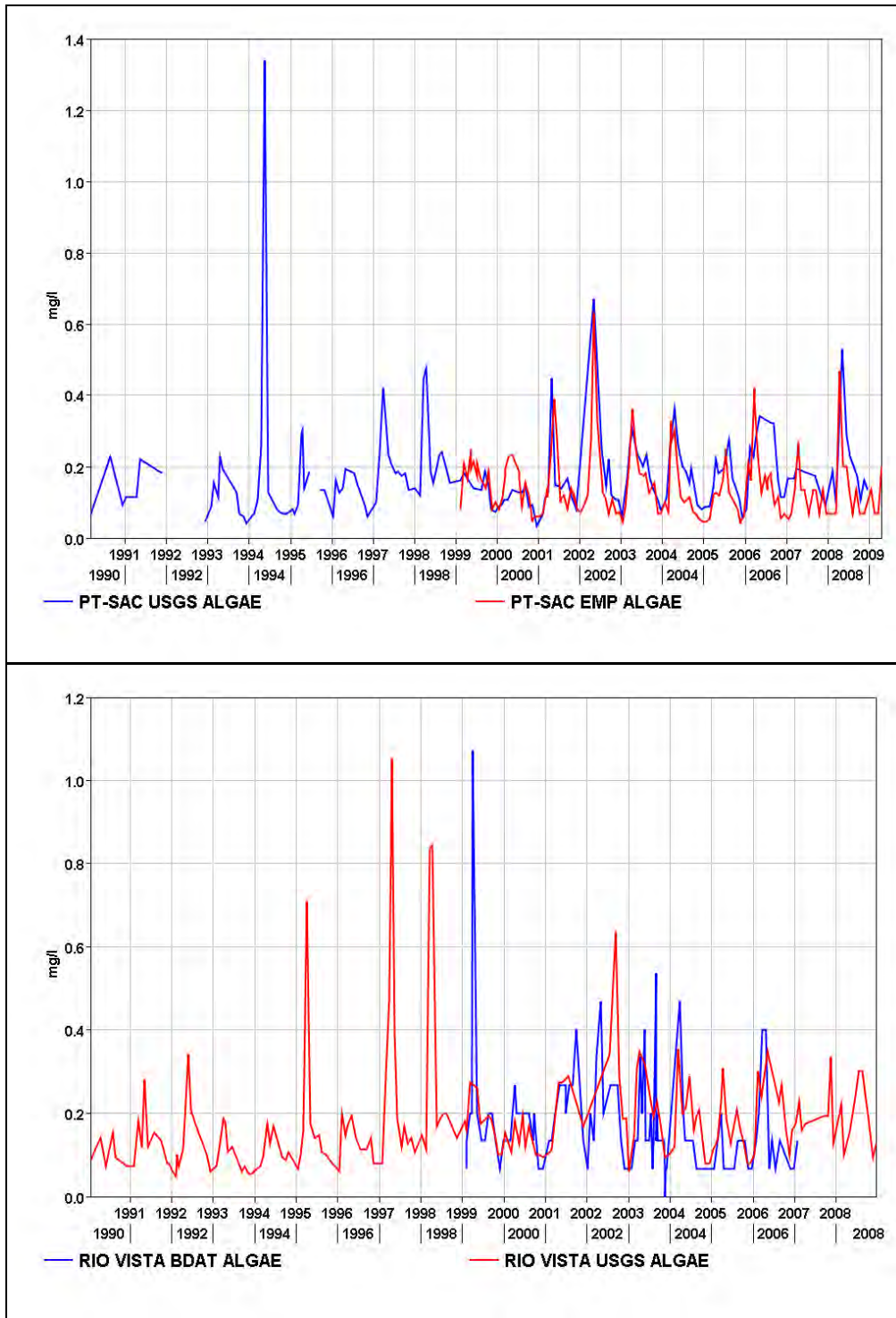
Figure 8-2 Comparison of EMP and USGS measurements at Point Sacramento (upper) Rio Vista (lower) – chlorophyll a measurements were converted to biomass of algae.
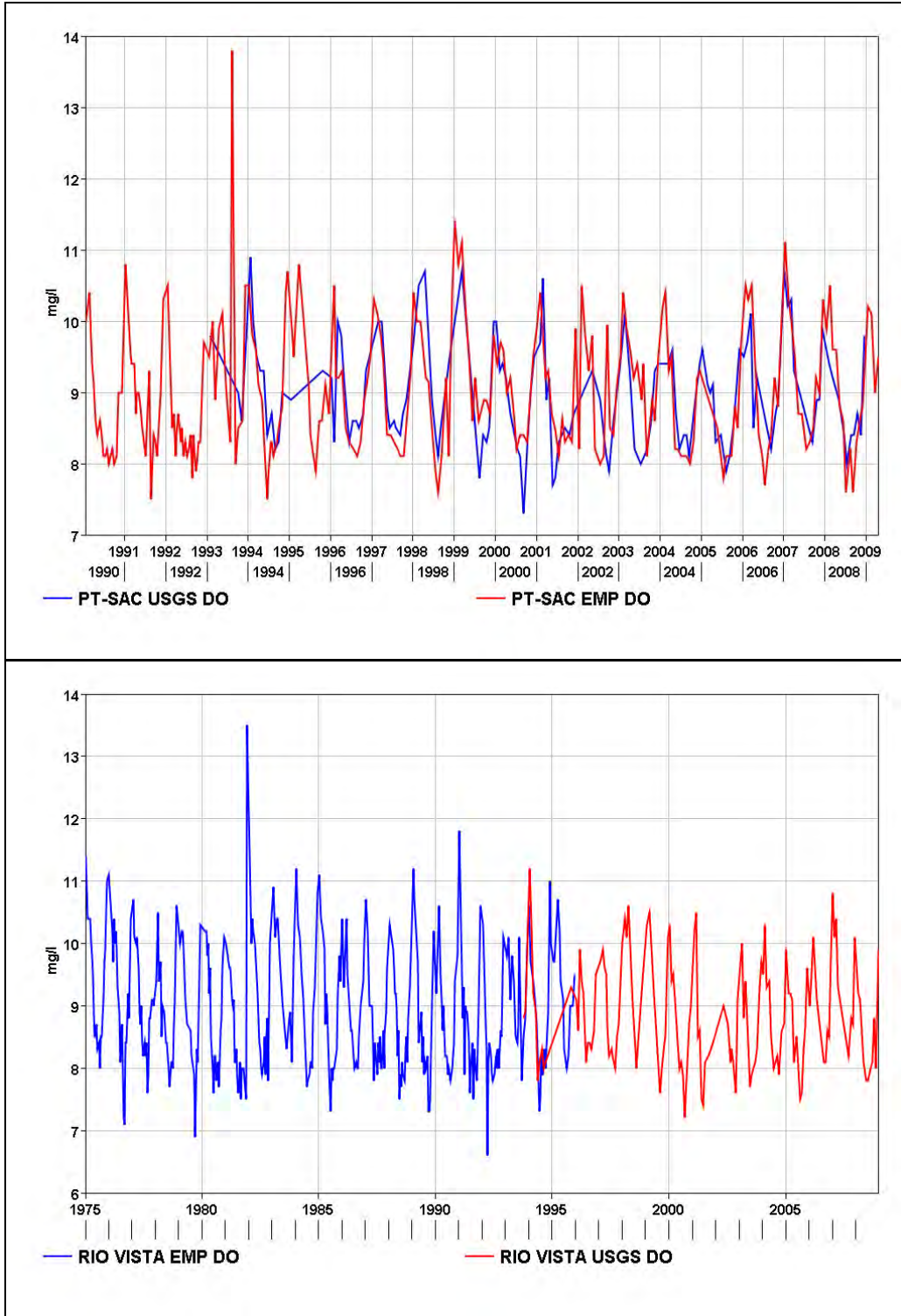
Figure 8-3 Comparison of EMP and USGS DO measurements at Point Sacramento (upper) Rio Vista (lower).
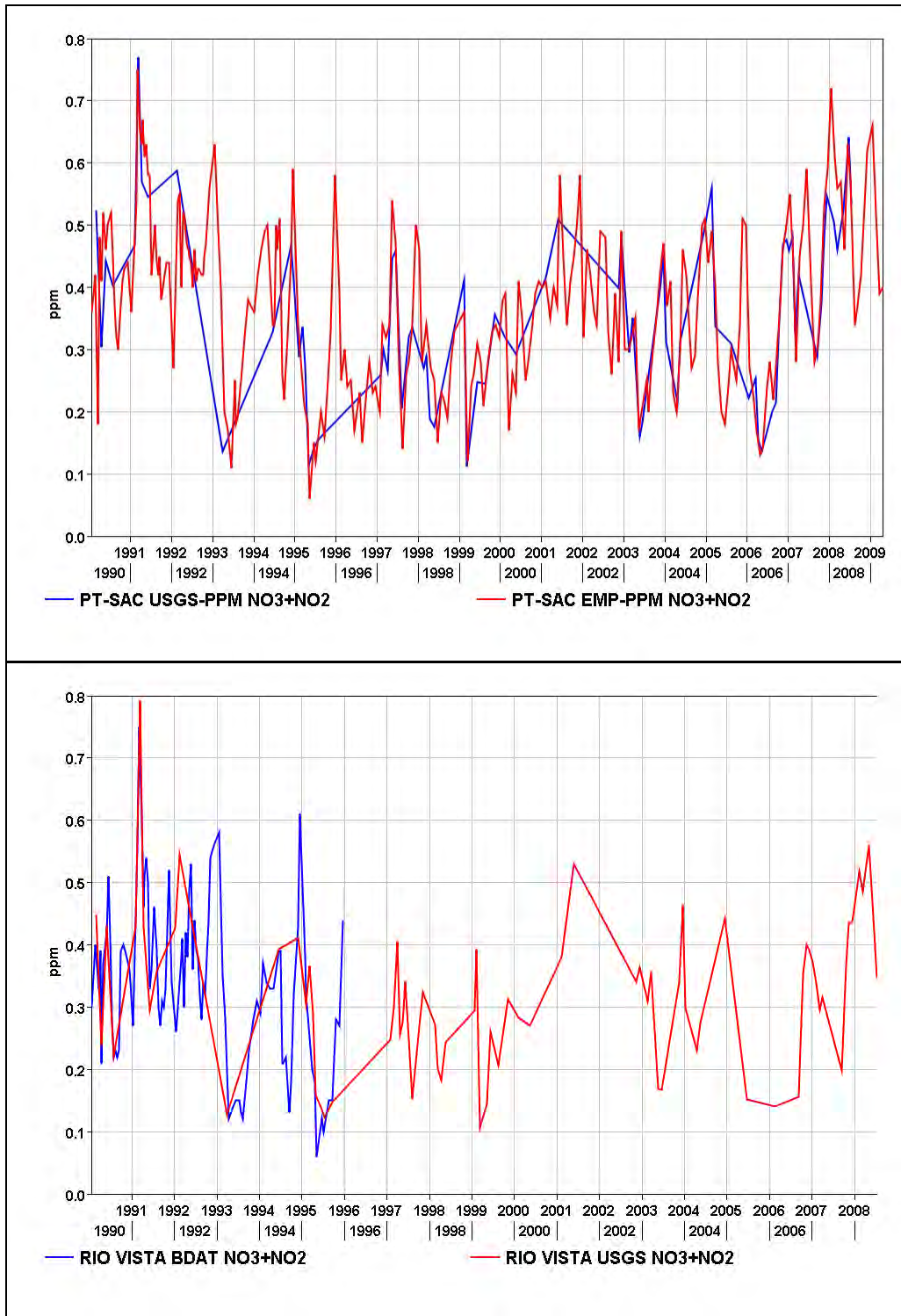
Figure 8-4 Comparison of EMP and USGS Nitrate+Nitrite measurements at Point Sacramento (upper) Rio Vista (lower).
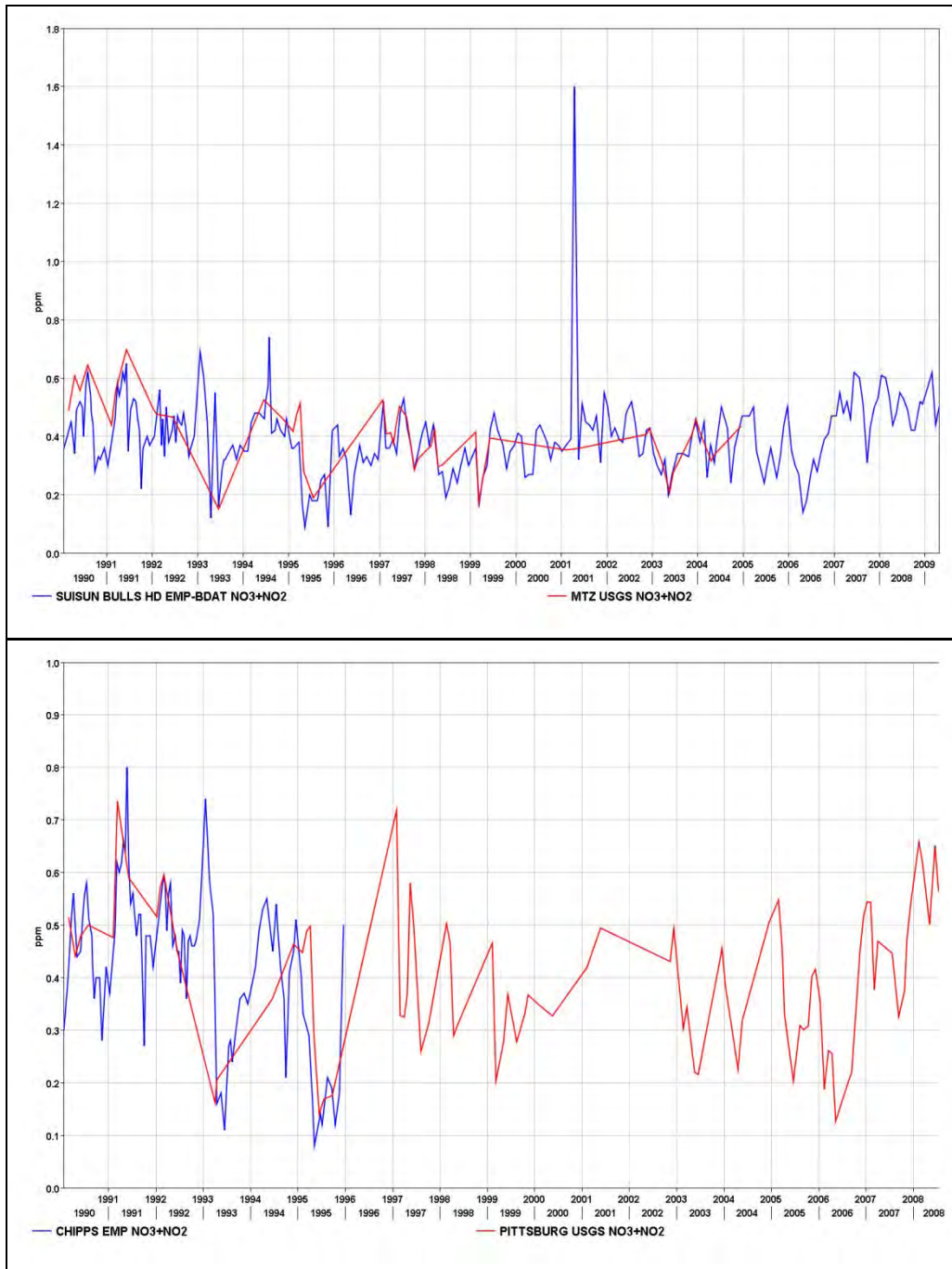
Figure 8-5 Comparison of EMP and USGS Nitrate+Nitrite (NO$_3$+NO$_2$) measurements near Martinez (upper) and near Chipps and Pittsburg (lower).
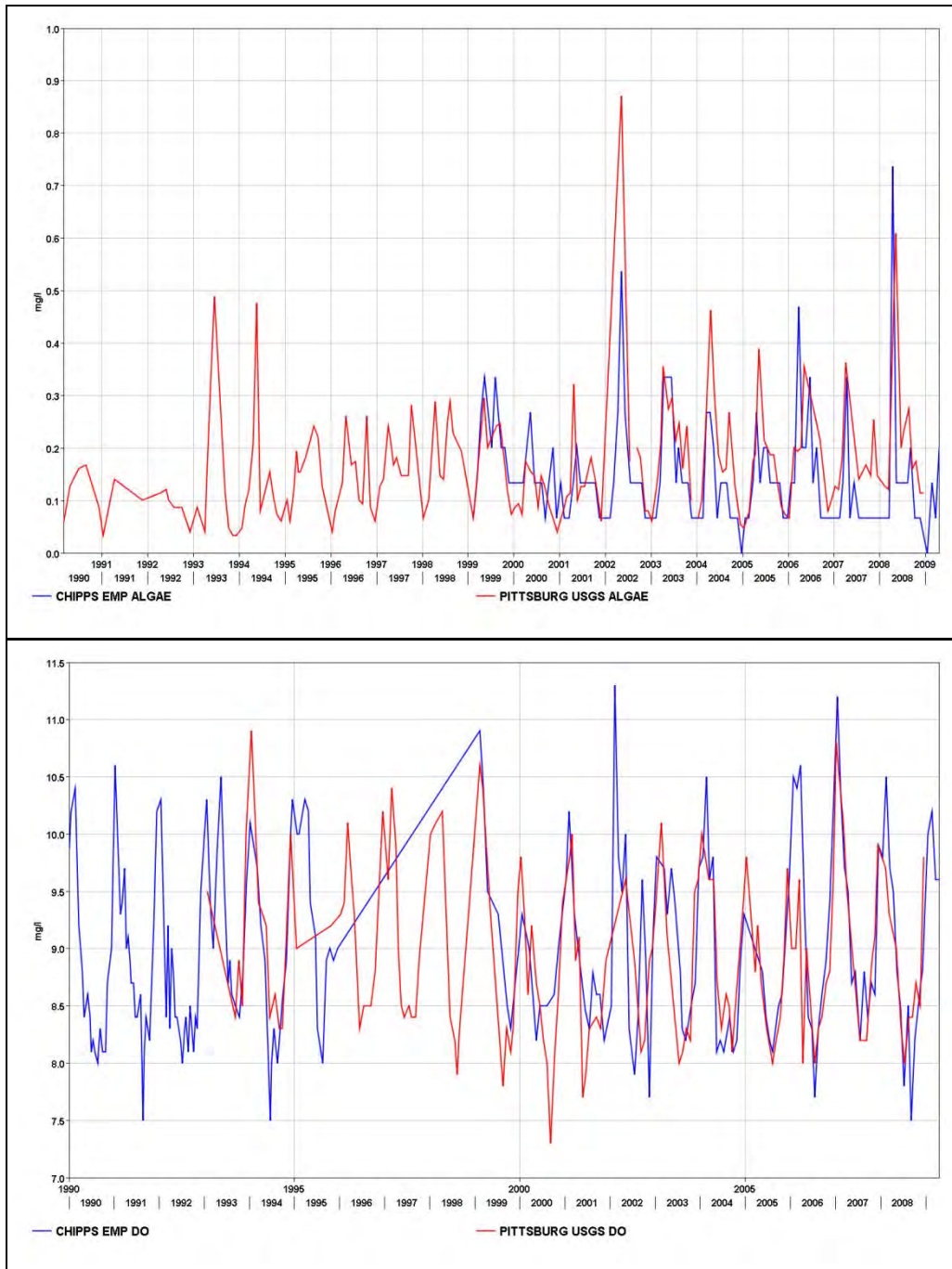
Figure 8-6 Comparison of EMP and USGS algae (upper) and DO (lower) measurements near Chipps and Pittsburg .
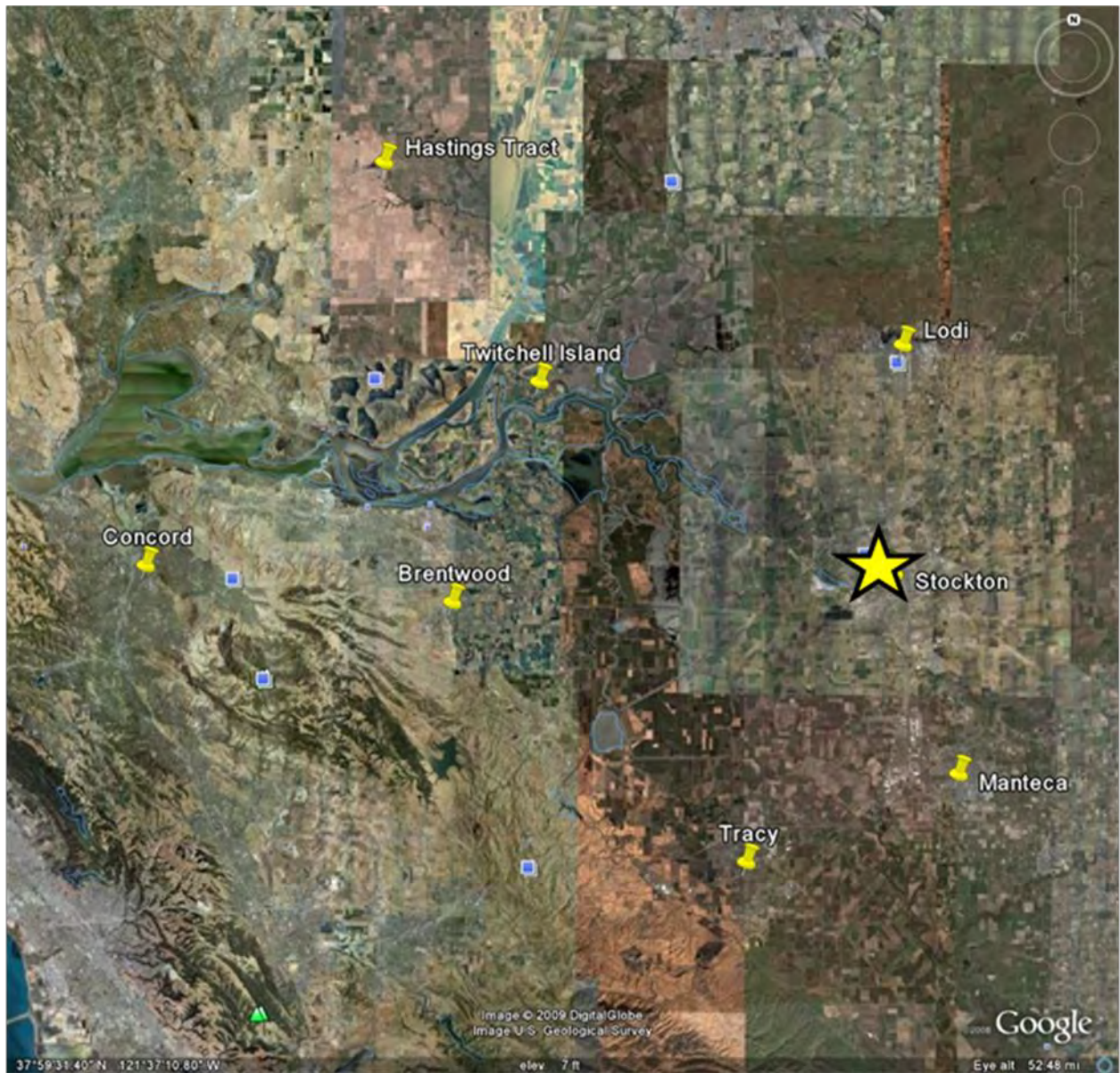
Figure 8-7 Meteorological measurements from NOAA at the Stockton airport (yellow star), and CIMIS measurements, indicated by yellow Google Earth push-pins

Table 8-4Availability of measurements for seven WWTPs in the DSM2 model domain

Location	Stockton	Sac Regional	CCCSD	Delta Diablo	Tracy	Manteca	Lodi	Fairfield-Suisun
	Tertiary since September 20'06	Secondary	Secondary	Secondary	Tertiary since July 2007	Tertiary since 06-08/03	Tertiary	Advanced secondary
Flow	mid-1992 - 2008	1990 - 2008	2000 - 2008	2004 - 2008	07/98 to 2008	04/04 to 08/08	05/00 - 07/06	2004 - 2008
Temp	1996 -2008, missing 2001, 2002	1998 - 2008	2000 - 2008	no data	07/98 to 2008	04/04 to 08/08	02/05 - 07/06	2004 - 2008
NH3	mid-1992 - 2008	1990 - 2008	2000 - 2008	03/04 to 2008	07/98 to 2008	05/04 to 08/08	05/00 - 07/06	03/04 to 2008
NO3	mid-1992 - 2008	1990 - 2008, missing short periods	2000 - 2008	no data	07/2007 to 2008	07/06 to 08/08	no data	10/07 to 2008
NO2	mid-1992 - 2008	2002 - 2008, missing segments	2000 - 2008	no data	07/2007 to 2008	07/06 to 08/08	no data	no data
Org-N	mid-1992 - 2008	1990 -2008, missing segments	2000 - 2008	no data	07/2007 to 2008	no data	no data	10/07 to 2008
BOD5	mid-1992 - 2008	1998 - 2008		no data	07/98 to 2008	04/04 to 08/08	05/00 - 07/06	2004 - 2008
CBOD	mid-1992 - 2008		2000 - 2008	no data				
PO4	mid-1992 - 2008	1998 - mid-08, missing segments	2000 - 2008	no data	no data	no data	no data	10/2007 to 2008
Org-P	no data	no data	no data	no data	no data	no data	no data	no data
DO	mid-1999 - 2008	no data	2000 - 2008	no data	no data	no data	02/05 - 05/06	no data
Chl-a	no data	no data	no data	no data	no data	no data	no data	no data
EC	mid-1992 - 2008	2004 - 2008	no data	no data	07/98 to 2008	09/05 to 08/08	05/00 - 07/06	no data
pH	mid-1993 - 2008	2000 - 2008	no data	no data	07/98 to 2008	04/04 to 08/08	02/05 - 07/06	2004 to 05/07

Table 8-5 Availability of measurements from the other WWTP's with effluent reaching the Delta. Vacaville, Davis and Woodland were not considered in this model. Benicia outfall is downstream of the model boundary.

Location	MTZ Refinery (Biological treatment)	Tesoro Refinery (Various treatments)	Valero (Ben) Refinery (Various treatments)	Benicia	Davis Secondary	Woodland Secondary	Vacaville	Disc. Bay Secondary	Mtn House Secondary (?) Mo Avg 05/04 - 06
Flow	2006 - 2008	2006 - 2008	2006 - 2008	2006 - 2008	2001 to 10-05	1996 - 2008	01/05 to 2008	2004 - 2007	Yes
Temp	no data	no data	no data	no data	2001 to 10-05	1996 - 2008	no data	2004 - 2007	Yes
NH3	2006 - 2008	2006 - 2008	2006 - 2008	few points	2001 to 10-05	1996 - 2008	no data	2004 - 2007	Yes
NO3	no data	no data	no data	no data		1996 - 2008	12/04 - 11/07	2004 - 2007	Yes
NO2	no data	no data	no data	no data	no data	no data	12/04 - 11/07	no data	Yes
Org-N	no data	no data	no data	no data	no data	no data	no data	no data	No
BOD5	no data	no data	no data	no data	2001 to 10-05	1996 - 2008	no data	2004 - 2007	No
CBOD	no data	no data	no data	no data			no data		No
PO4	no data	no data	no data	no data	no data	1996 - 2008	(TOT-P)	no data	Tot-P
Org-P	no data	no data	no data	no data	no data	no data	no data	no data	No
DO	no data	no data	no data	no data	no data	no data	no data	2004 - 2007	No
Chl-a	no data	no data	no data	no data	no data	no data	no data	no data	No
EC	no data	no data	no data	no data	2001 to 10-05	1996 - 2008	12/04 - 11/07	2004 - 2007	Yes
pH	no data	no data	no data	no data	2001 to 10-05	1996 - 2008	12/04 - 11/07	2004 - 2007	Yes

Setting NH₃ and NO₃ at the Sacramento R. boundary

Data to set the NH_3 boundary condition (BC) on the Sacramento River was obtained from a variety of sources, including Sac Regional receiving water measurements, MWQI and a dataset from R. Dahlgren at UC Davis. The ammonia data are sparse, generally range from 0.01 mg/L to a maximum of about 1.3 mg/L, and are quite variable between measurement agencies as shown in Figure 8-8.

Figure 8-9 shows a comparison of Sac Regional receiving water measurements near Freeport and the boundary condition for ammonia set using merged BDAT data from Greenes Landing and Hood, but reduced by a factor 0.4. Although the ranges of the data values shown Figure 8-8 are comparable for the different agencies, particularly at maximum values, these data suggest that the ammonia boundary condition shown in Figure 8-9 at the Sacramento River boundary is frequently high. Note that the detection level of ammonia for the Sac Regional receiving water dataset varies, although it was frequently quoted as 0.1 mg/L. For the purposes of comparisons in plotting, the plotted value was set at (detection limit)/2 on dates where a measurement was taken but below the specified limit.

Several strategies were used to develop a revised Sacramento R. ammonia BC. Several of these strategies are illustrated in figures, below. A straight-forward mass balance approach[7] is shown in Figure 8-10 in comparison with the boundary condition (blue) set at (Greens/Hood ammonia)*(0.4). The boundary concentration values calculated using this simple mass balance approach are frequently negative – negative values have been suppressed in the figure. A variation on this approach was used for the calculation shown in Figure 8-11 to avoid negative values – the Sac Regional receiving water data is shown for comparison (red line). In this case, scaling factors were applied in the calculation to lower the effluent ammonia concentration and the overall concentration at the Sac R. boundary.

The effect of the Sacramento flow magnitude was also investigated - some results are shown in Figure 8-12 and in Figure 8-13 in comparison with Sac Regional receiving water data (Figure 8-12, green) and with the UC Davis data (Figure 8-13, green). In the "low flow" case, the boundary value was set at 0.015 mg/L below 10,000 cfs Sacramento R. flow, and otherwise at 0.015 mg/L plus an additional factor of 15% of the scaled mass-balance ammonia calculation. In the "high flow" case, above 60,000 cfs Sacramento R. flow, the value was calculated at 0.015 mg/L plus 15% of the mass balance ammonia and at 0.015 mg/L otherwise. In both of these cases, the components in the mass balance calculation were altered by constant scaling factors to improve the fit.

---

[7] (Final Concentration*Final Volume) = (Concentration at BC)*(Volume BC) + (Concentration Effl * Volume Effl); then solve for concentration at BC.

None of the calculations give a clear-cut best fit for the measured ammonia near Freeport, so the high flow case was selected to test as a boundary condition in the nutrient model as it captured some of the variability in the UC Davis dataset.

Figure 8-14 and Figure 8-15 illustrate results for modeled ammonia concentration at three locations downstream of the Sacramento R. boundary. Figure 8-14 (upper plot) is a comparison of two models with results at RSAC139 (Greens Landing) – the models were run with different Sacramento R. ammonia BC's. The blue lines are the modeled monthly MAX and MIN envelope for the calculated "high flow" case, denoted the V12 model run. The red lines are the MAX and MIN envelope of the V11 model run with the Sac R. BC set at (Greens/Hood ammonia)*(0.4). Figure 8-14 (lower) shows the V12 results at RSAC139 (Greens Landing) for both the Greens and Hood EMP data over a longer time span. Figure 8-15shows the V12 ("high flow") Max and Min envelope model results for ammonia at Point Sacramento (upper) and at Potato Point (lower) in comparison with data (green symbols).

Although Figure 8-12 shows that the difference in values between these two boundary conditions ranged between no difference and a factor of four increase (with the Greens/Hood*0.4 values generally higher than the calculated high flow case), there is much less difference in the modeled envelopes between the two models (Figure 8-14, upper). The two model runs would be deemed nearly equivalent in terms of the calibration. This result is generally consistent with the Sac R. ammonia BC sensitivity runs (+/- 20% in BC value) for an earlier set of boundary conditions, where the differences were also not large.

The situation for the Sacramento River nitrate boundary condition was simple in comparison with the ammonia BC. Figure 8-16 and Figure 8-17 show comparisons between different nitrate datasets near Freeport and with the nitrate BC set using the EMP data at Greens/Hood reduced by a factor of 0.825, respectively. The variability in the datasets is small (Figure 8-16), and the nitrate BC was set at a value that is consistent with the data (Figure 8-17).

The conclusions from this analysis are mixed. Because the data for ammonia near the model boundary are quite variable, and only partially consistent between data-gathering agencies, this leads to a high level of uncertainty in the setting of the ammonia boundary condition for the Sacramento R. The final four plots illustrate the implications of this observation.

An additional simulation was run with a constant Sacramento R. ammonia BC – the concentration was set at 0.05 mg/L which is the (higher) Sac Regional detection limit for ammonia*0.5. Note that Freeport (RSAC155) is below the model boundary for Sacramento inflow. Figure 8-15 shows a comparison between the V12 model run ("high flow"), the constant concentration boundary condition and the UC Davis measured ammonia concentration near Freeport. The modeled ammonia for the constant concentration run has changed from the constant boundary value due to algal growth and decay of ammonia from the parameterization

for this region. The V12 model boundary condition was selected because it had some resemblance to the UC Davis data at Freeport, and this resemblance is maintained at Freeport, while the constant concentration boundary has too little variability in comparison with the UC Davis data.

Figure 8-19 shows a comparison of the same two models, constant concentration boundary and V12 ("high flow"), plotted with the Sac Regional receiving water data near Freeport. In this case, neither model appears to yield a suitable representation of the data, as the variability in the data is much greater than the models produced, although the V12 "high flow" model does catch some of the dips in the receiving water measurements.

Figure 8-20 shows that at Greens Landing, RSAC139, the choice of the constant concentration boundary or the calculated "high flow" mass balance approach is immaterial – they are nearly identical. The final comparison, Figure 8-20, is comparison of EMP ammonia data measured at Greens landing with three model runs - constant concentration (green dash), V12 "high flow" (red), and V10 with the Sacramento boundary set at (Greens/Hood ammonia)*(0.4) (blue dash) – showing that each of the three Sacramento R. ammonia BC settings gives a good representation of this sparse calibration dataset, although all but the V10 model run tend to be low in comparison with the Greens Landing data.

The final observation from the data analysis was that negative values produced during of the mixing model calculations for BC NH_3 were apparently related to the ratio:

Flow ratio = (Total Sac flow)/ Sacramento R. inflow)

as shown In Figure 8-10, where the value

Total Sac flow = Sacramento R. BC inflow + Sac Regional effluent flow.

Following this observation, the final mixing model formula for the Sacramento NH_3 BC was set as:

(Total Sac flow)*(NH_3 Grns/Hood) – (Sac Reg Effl flow)*(Effl NH_3)*0.8 / (Total Sac flow)*(Flow ratio)

Any remaining negative values in this time series were then set to 0.025 mg/L, and the factor of 0.8 was used to account for reactions between the outfall and the measurement point at Greenes/Hood.
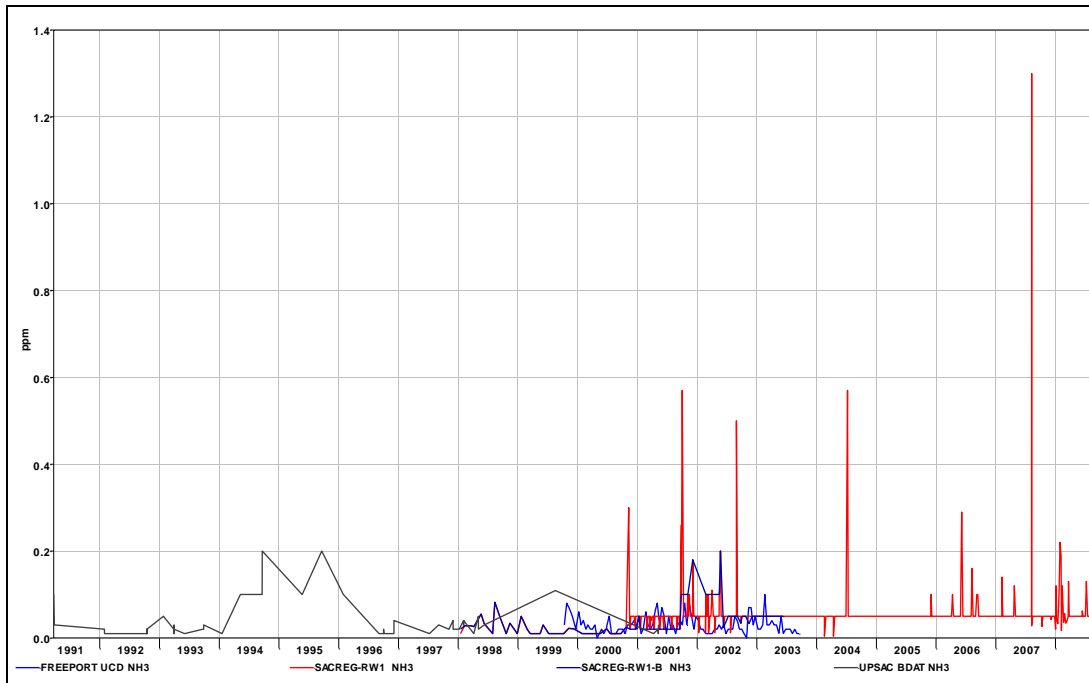
Figure 8-8 Ammonia concentration data above Freeport from three sources, UC Davis (blue), BDAT (black) and Sac Regional receiving waters monitoring (two data sets, red and dark blue).
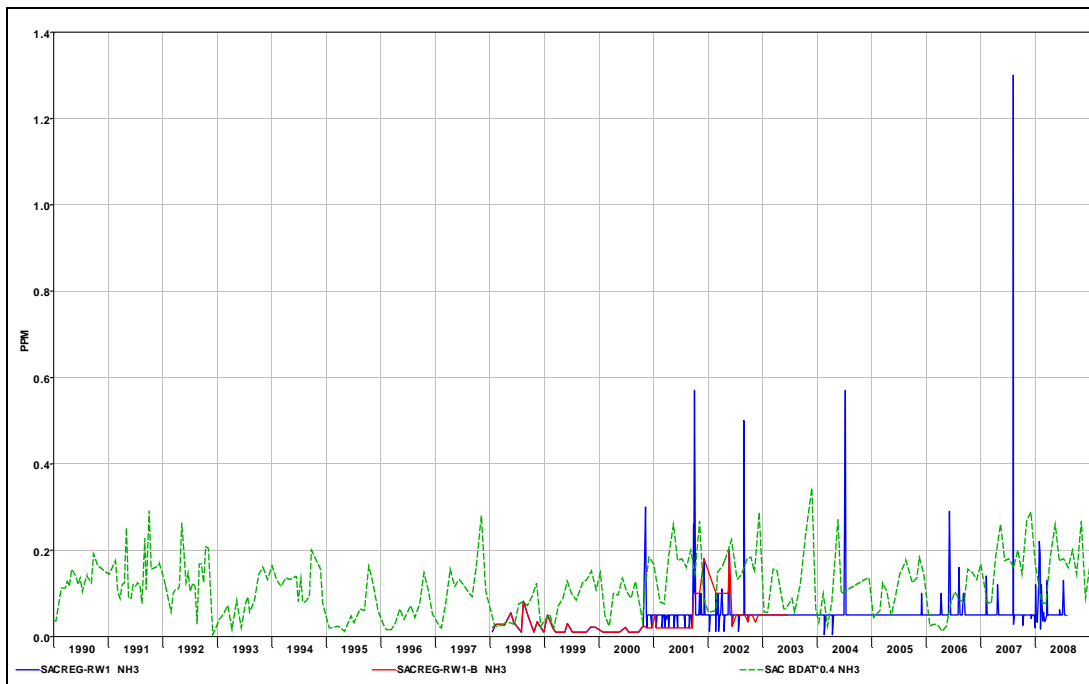
Figure 8-9 NH$_3$ concentration from Sac Regional receiving water measurements (blue and red) in comparison with NH$_3$ boundary condition set at BDAT Greens/Hood ammonia*0.4.
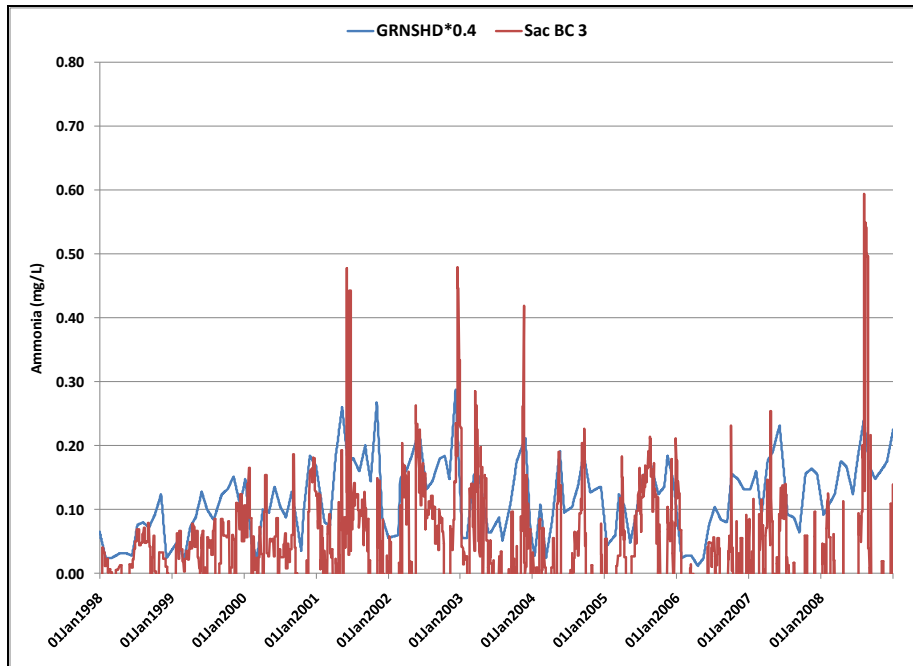
Figure 8-10 Sacramento R. NH₃ boundary condition (red) calculated using a mass balance approach in comparison with previous boundary condition (blue).
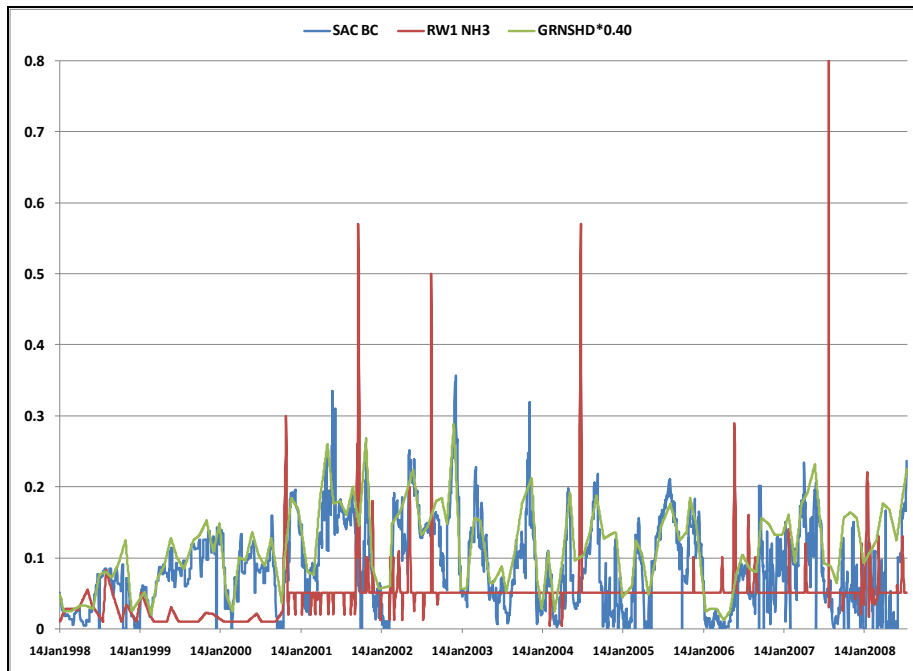
Figure 8-11 Sacramento R. NH₃ boundary (blue) calculated using a revised mass balance approach in comparison with Sac Regional receiving water NH₃ data (red) and previous boundary condition (green).
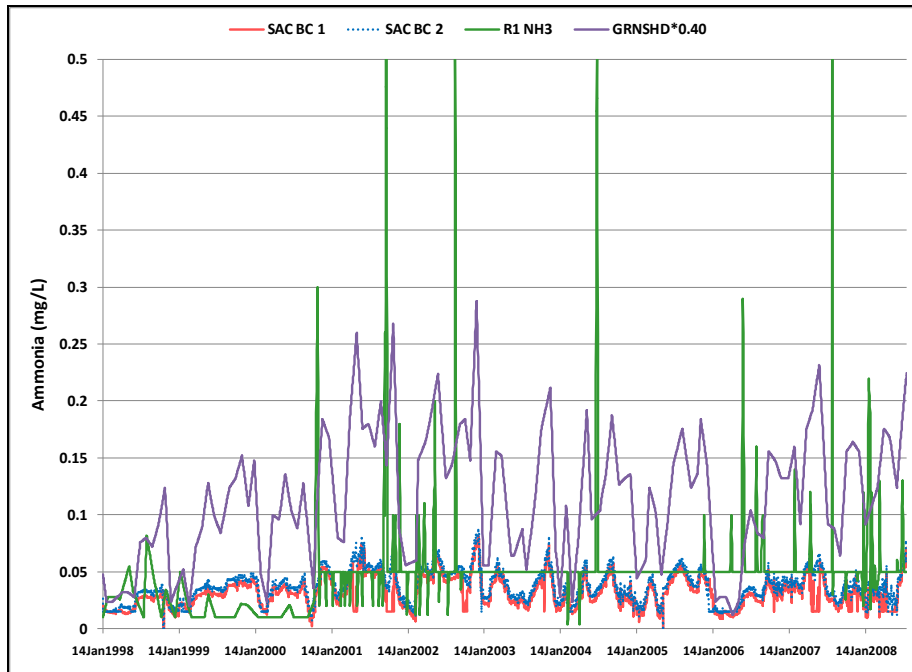
Figure 8-12 Two calculated NH₃ boundary conditions: low flow (red) and high flow (blue) constraint with a minimum value compared with Sac Regional receiving water NH₃ (green) and previous BC (purple).
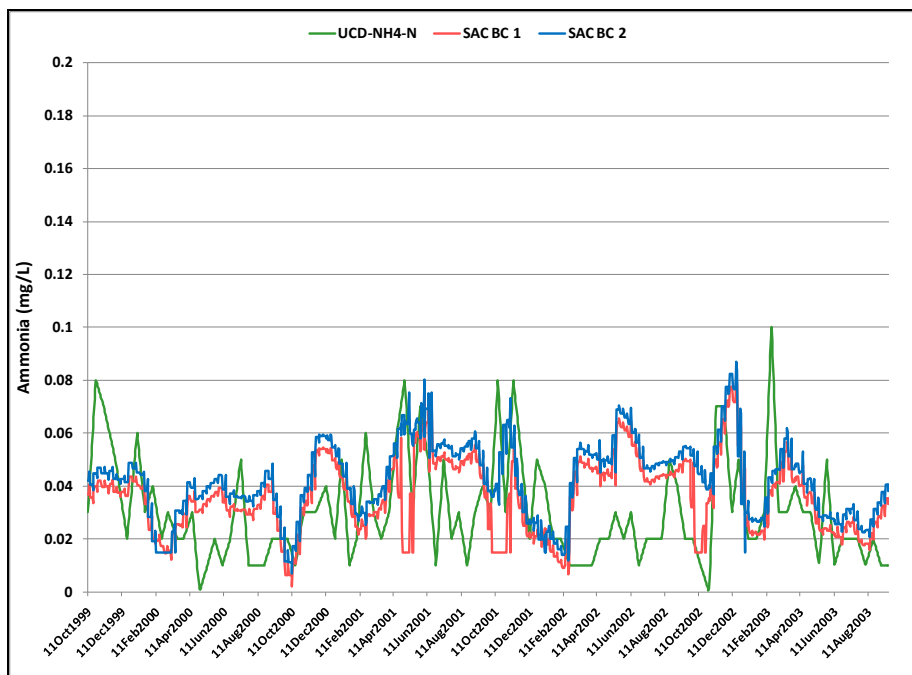
Figure 8-13 The same two calculated boundary conditions as in Figure 8-12, in comparison with UC Davis Freeport measured ammonia (green)
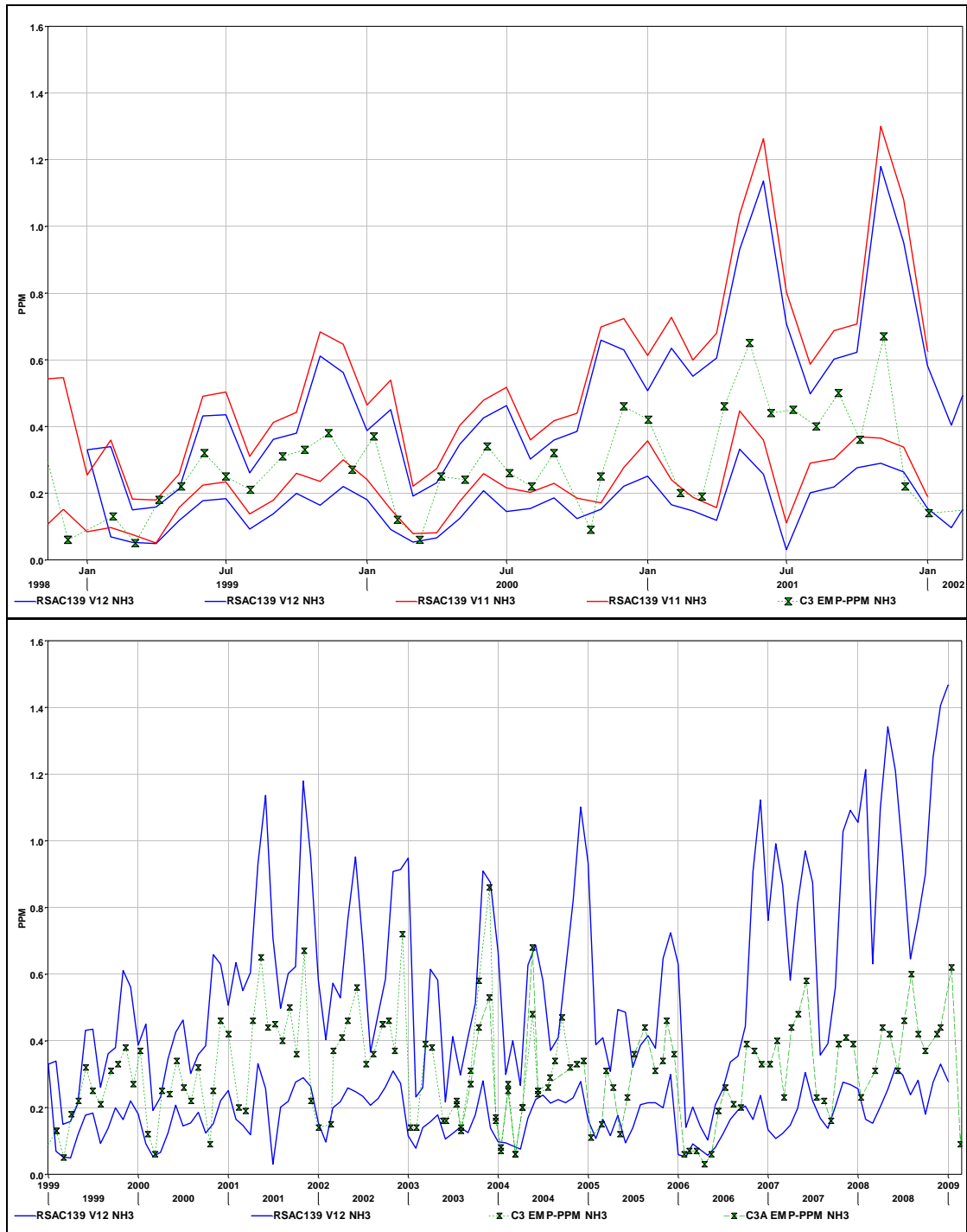
Figure 8-14 Modeled (blue) and measured (green symbol) ammonia at Greens Landing (RSAC139). Upper: Model V12 Sac R. BC with high flow constraint; V11 (red) with a GRNSHOOD*0.4 BC. Lower: V12 model output at Greenes Landing vs. Greenes (C3) and Hood (C3A) ammonia data.
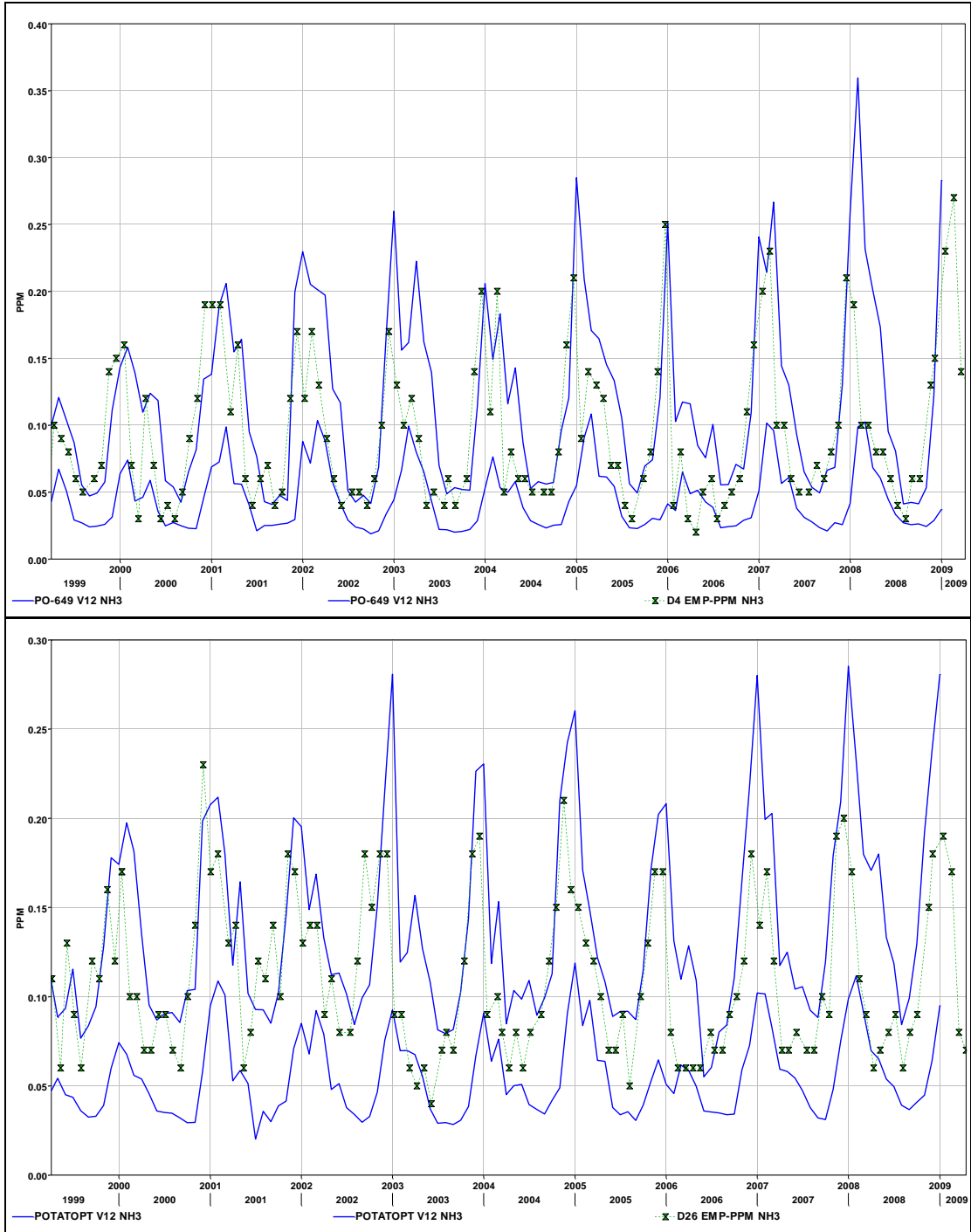
Figure 8-15 V12 model (calculated ammonia BC w/high flow constraint) at downstream locations, Point Sacramento (upper, PO-649) and at Potato Point (lower, D26).

142
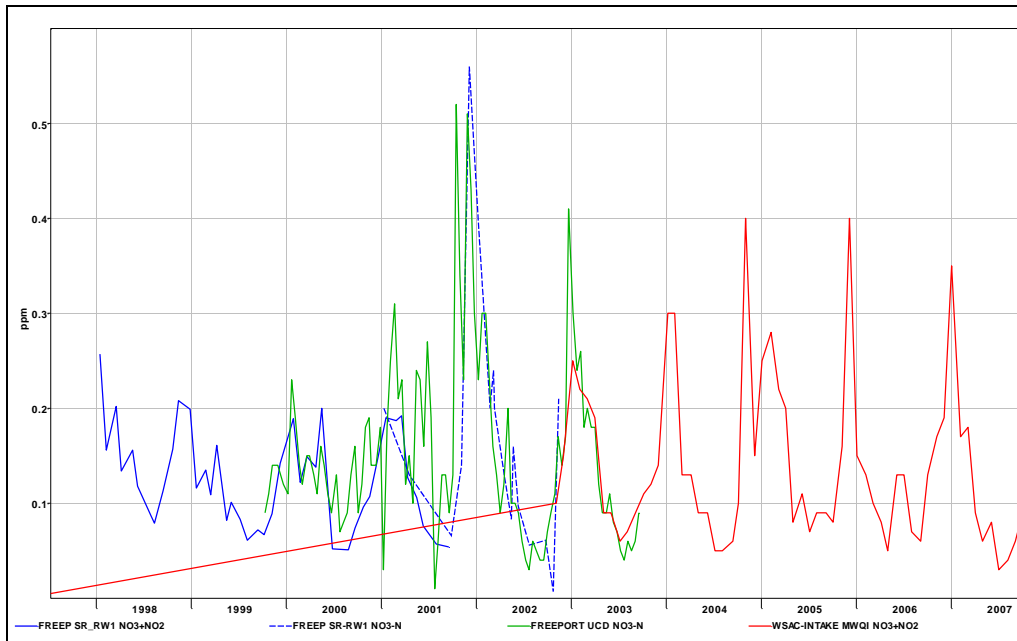
Figure 8-16 Four nitrate concentrations at or near Freeport – UC Davis data (green), BDAT data (red) and two Sac Regional receiving water datasets (blue, solid and dashed).
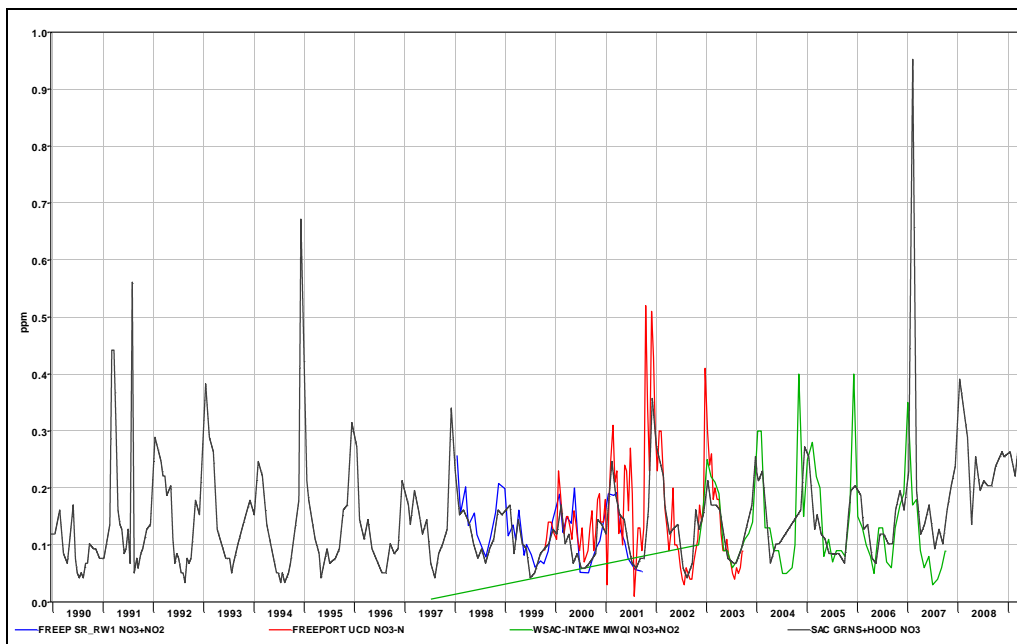
Figure 8-17 Nitrate data at or near Freeport *vs.* Sacramento R. BC: (black) BC set using EMP (Greens/Hood nitrate)*(0.825) vs. UC Davis data (green), Sac Regional receiving water data (blue) and MWQI monitoring data (green).
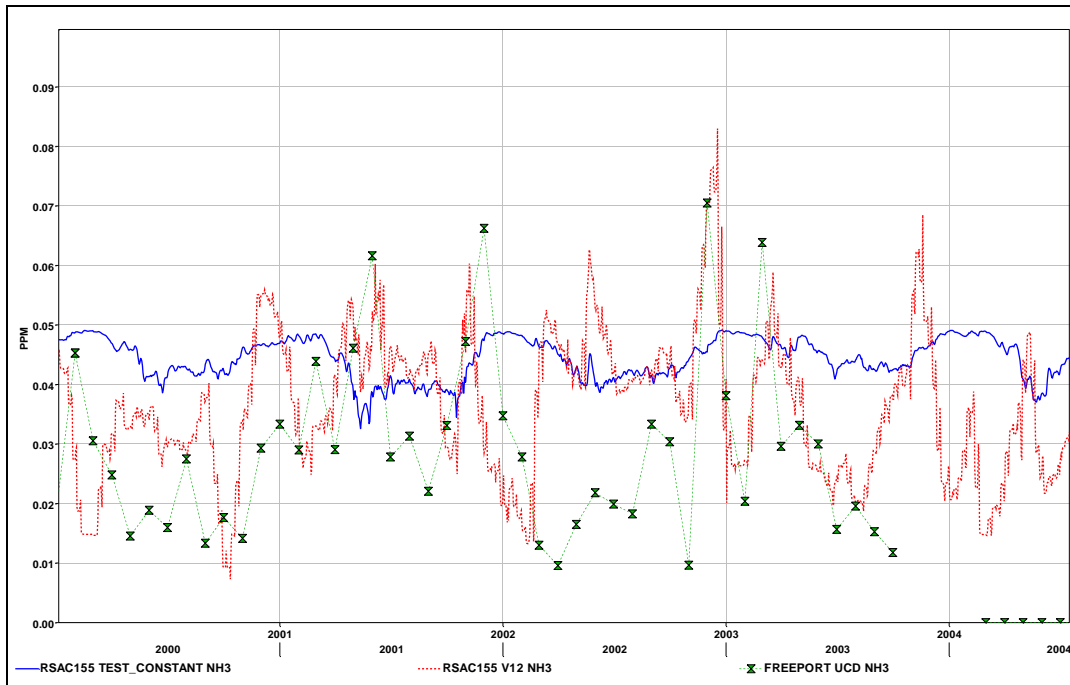
Figure 8-18 Modeled ammonia with constant concentration boundary (blue), "high flow" V12 boundary (red dash) vs. UC Davis ammonia data near Freeport (green symbols).
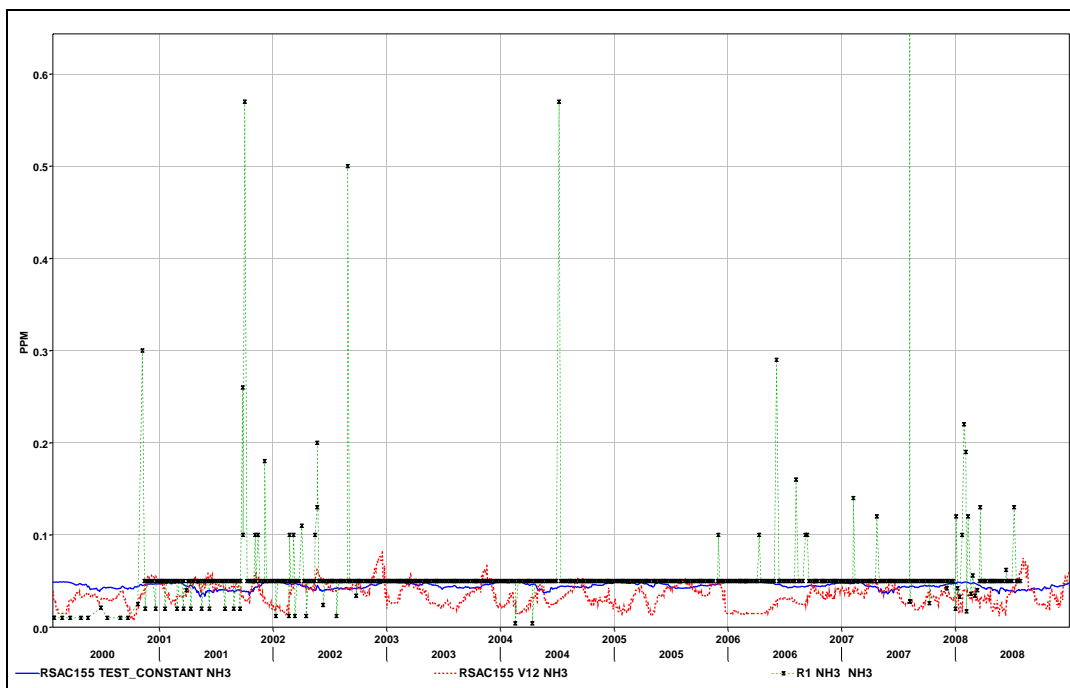
Figure 8-19 Modeled ammonia with the constant concentration boundary (blue) and. the "high flow" V12 boundary (red dash) vs. Sac Regional receiving water ammonia near Freeport (green symbols).

144
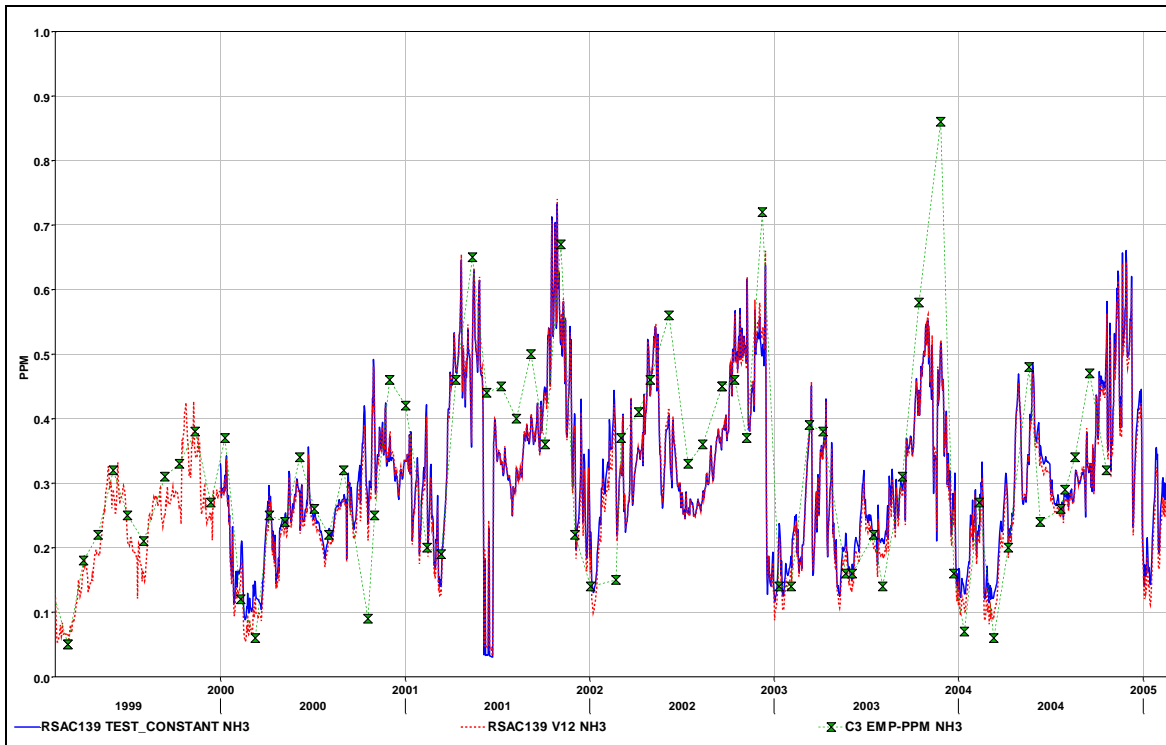
Figure 8-20 Modeled ammonia using the constant concentration boundary (blue) and the "high flow" V12 boundary (red dash) vs. EMP ammonia calibration data near Greens Landing (green symbols).

9. Appendix II - Temperature Calibration/validation results

Calibration results
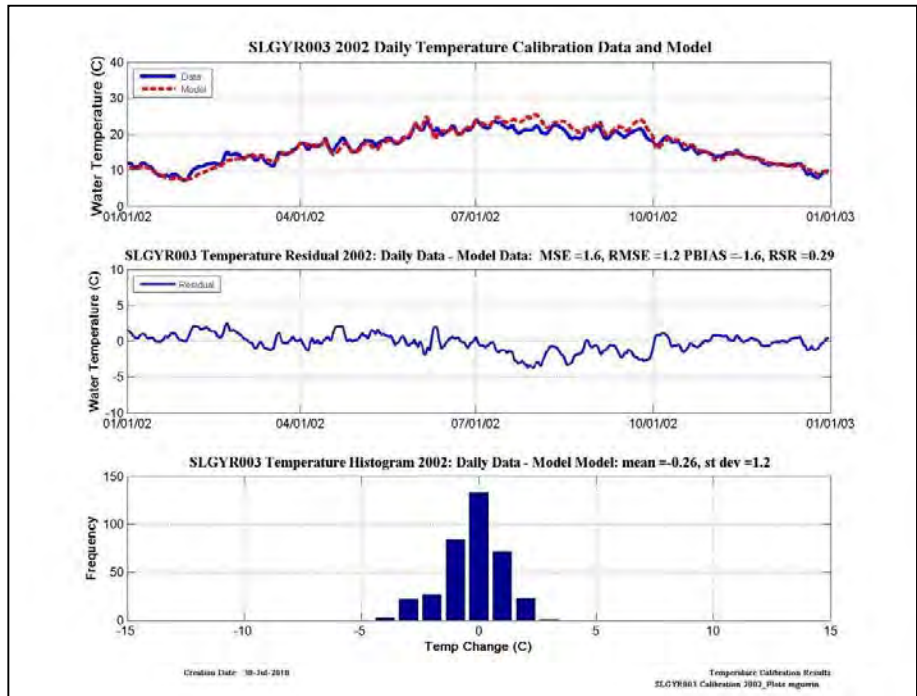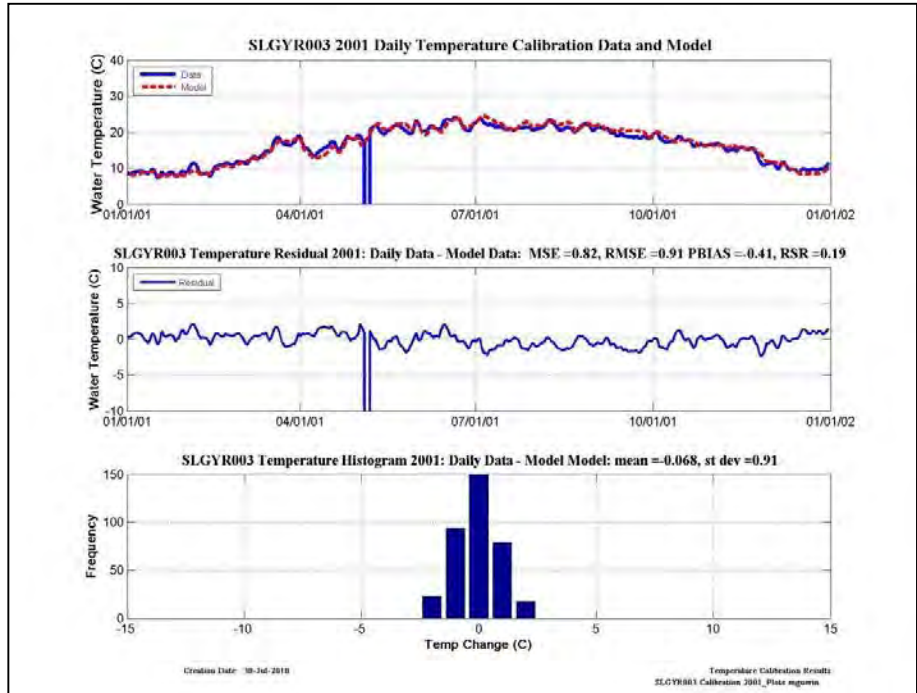
Dry-Calibration	NSE	PBIAS	Bias	RSR
2001	VG	VG	Overestimate	VG
2002	VG	VG	Overestimate	VG

Figure 9-1 Dry year temperature calibration plots, residual plots, histograms and categorical statistics at SLGYR003.
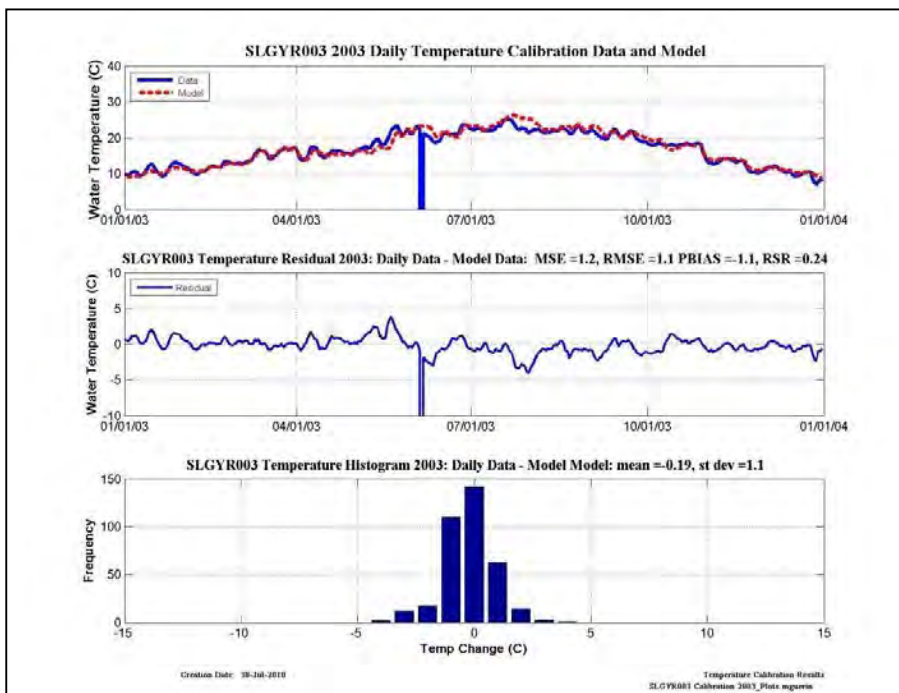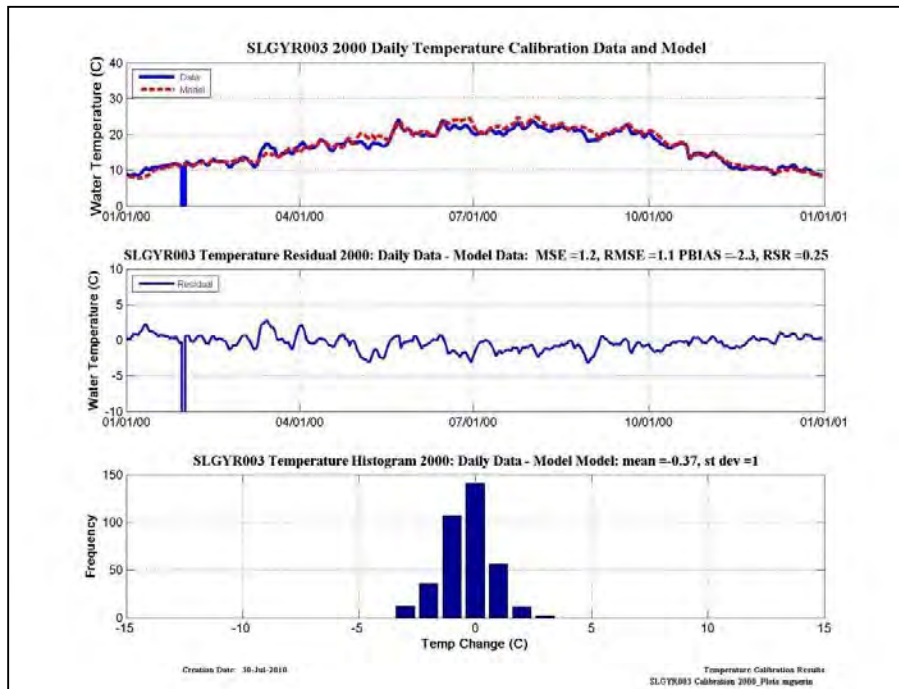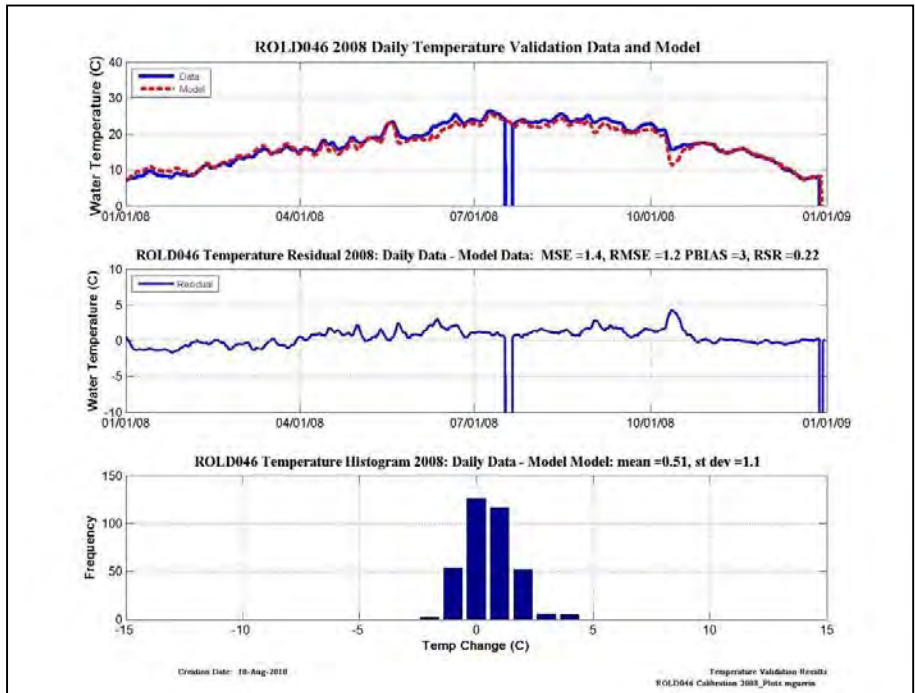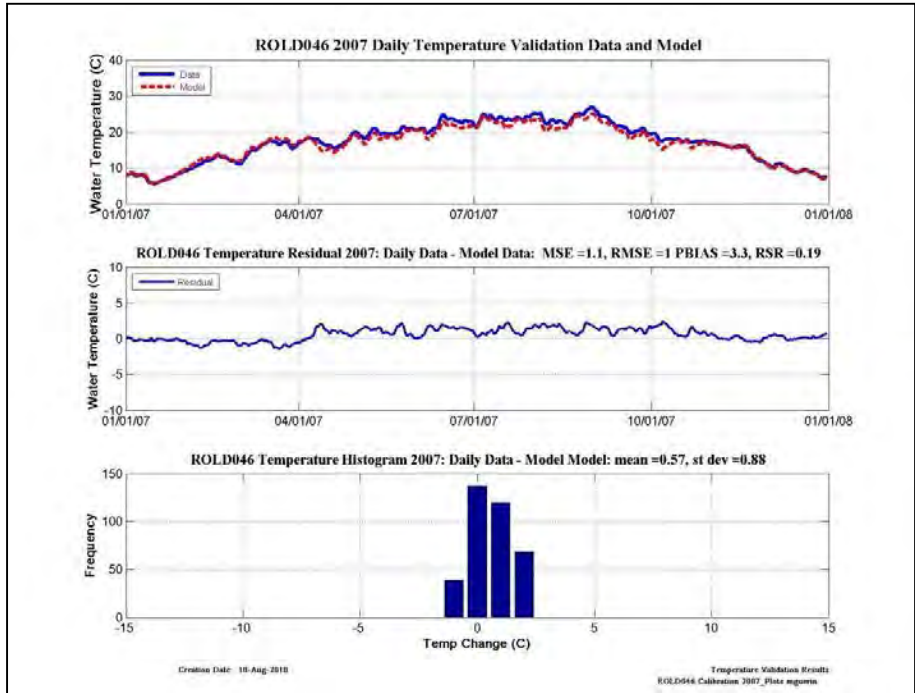
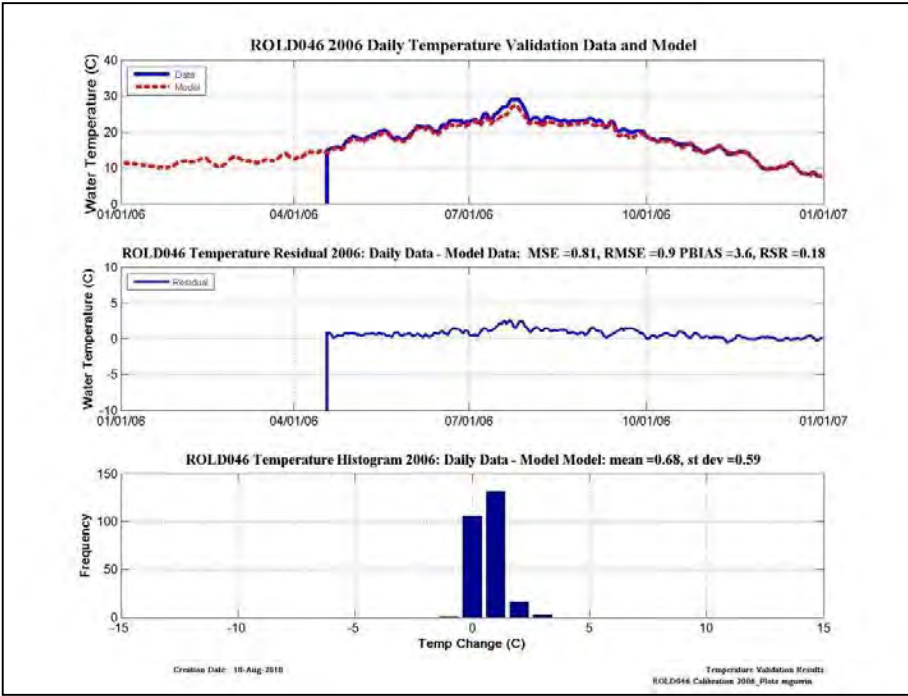| Wet-Calibration	NSE	PBIAS	Bias	RSR
2000	VG	VG	Overestimate	VG
2003	VG	VG	Overestimate	VG

Figure 9-2 Wet year temperature calibration plots, residual plots, histograms and categorical statistics at SLGYR003.
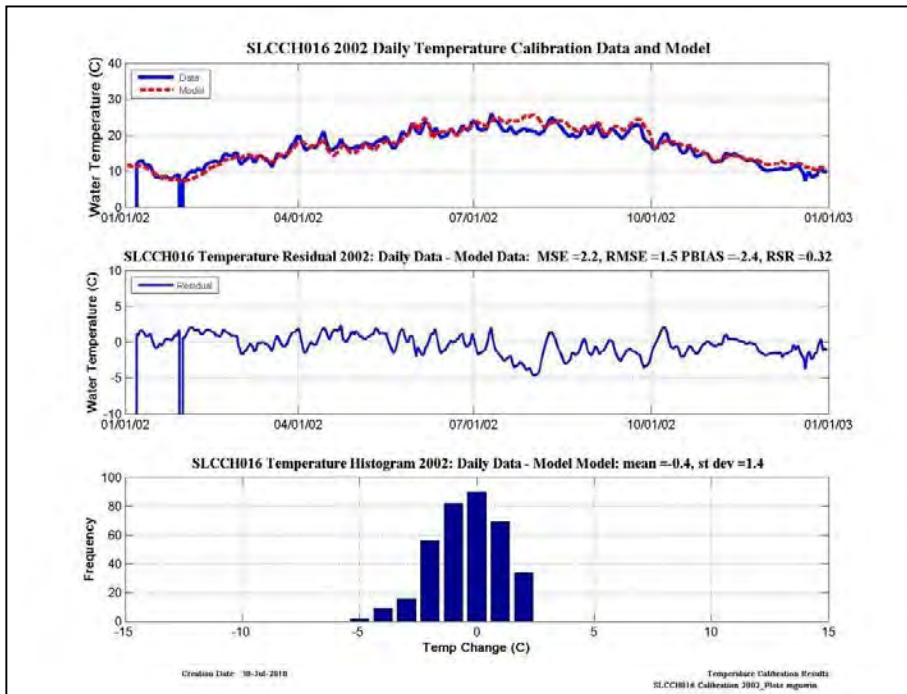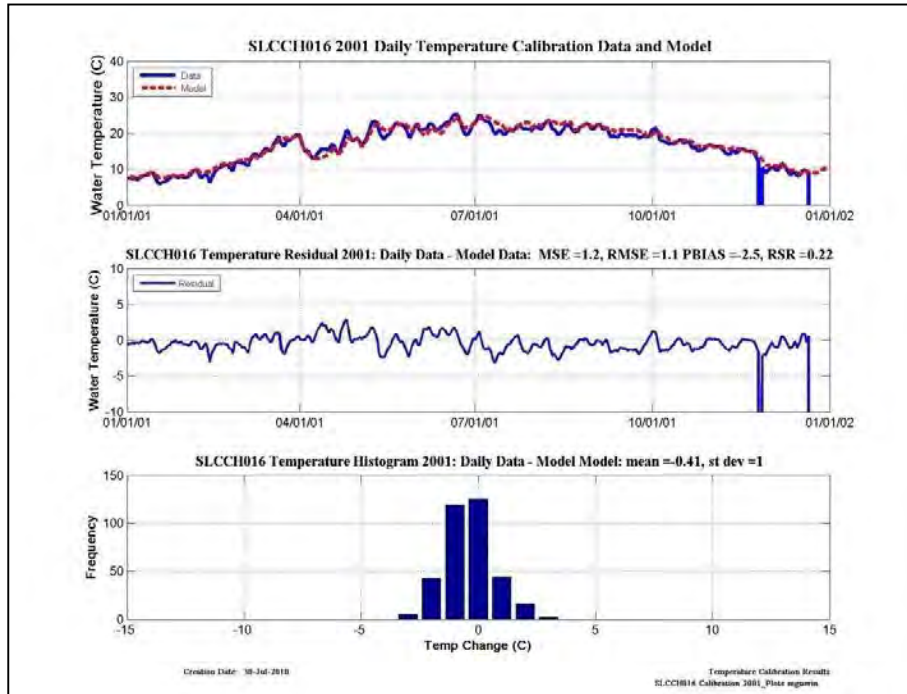
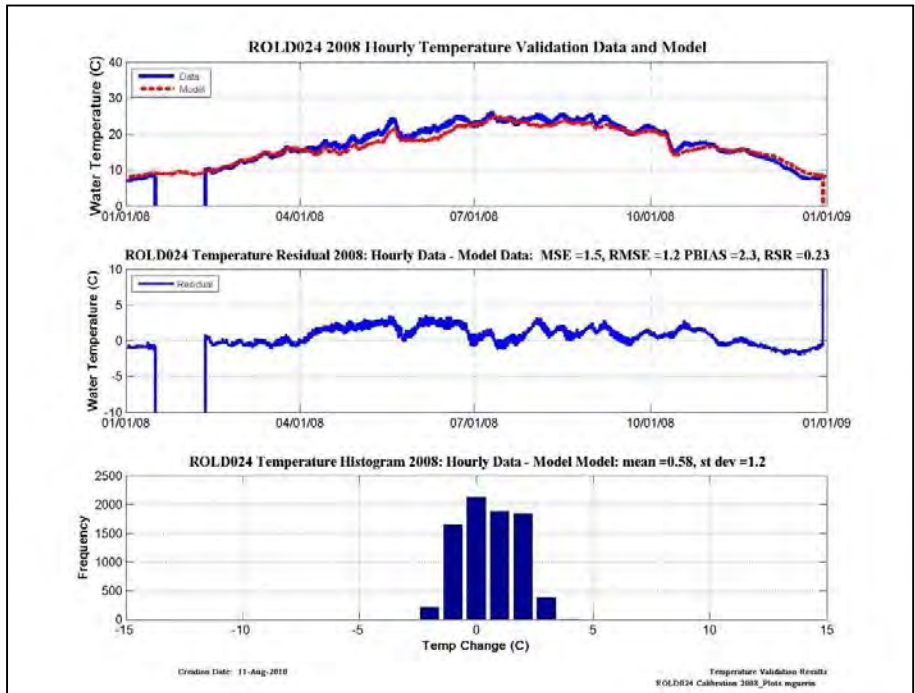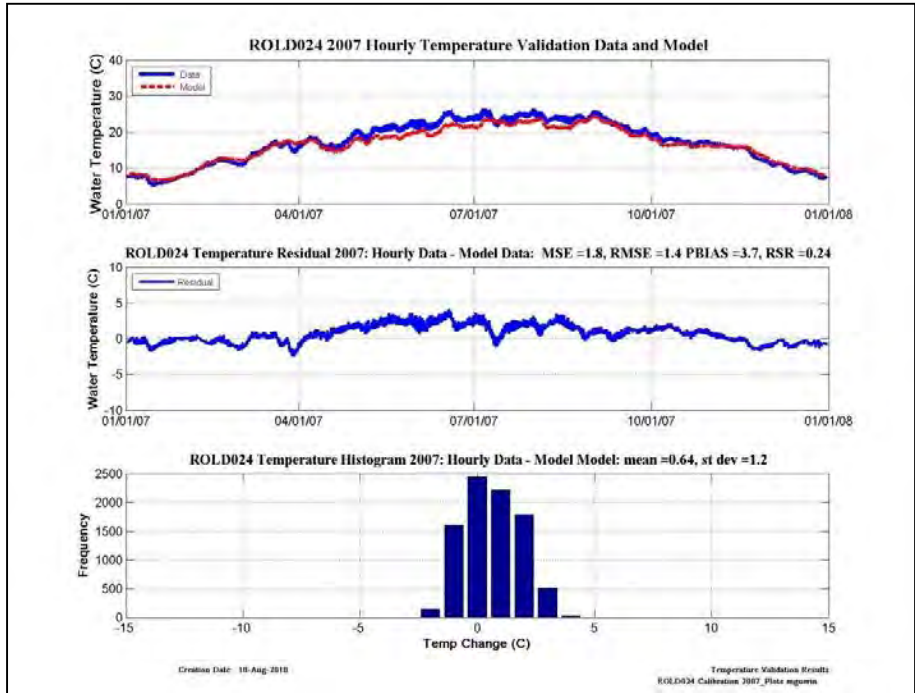| Dry-Calibration	NSE	PBIAS	Bias	RSR
2001	VG	VG	Overestimate	VG
2002	VG	VG	Overestimate	VG

Figure 9-3 Dry year temperature calibration plots, residual plots, histograms and categorical statistics at SLCCH016.
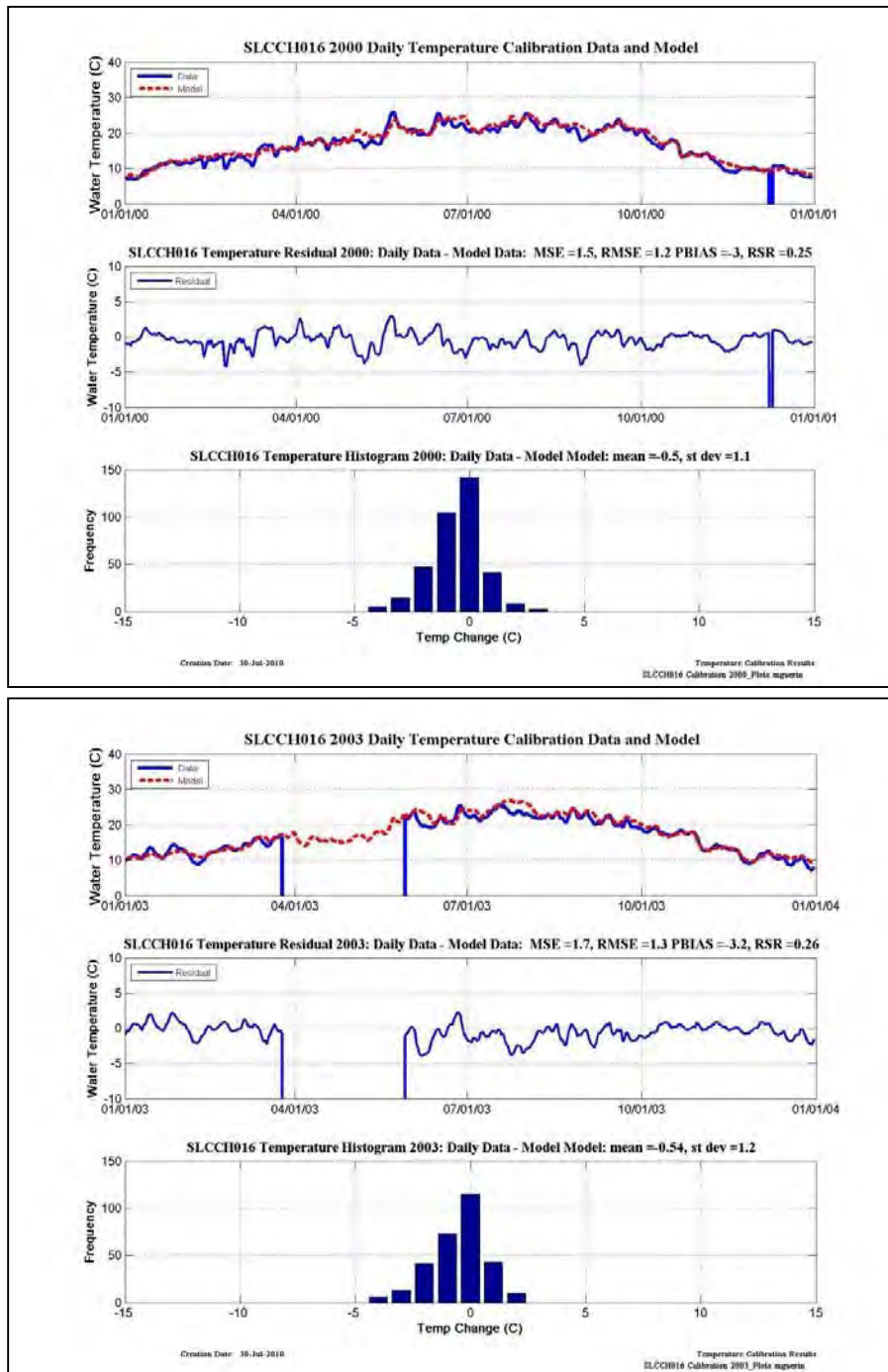
Wet-Calibration	NSE	PBIAS	Bias	RSR
2000	VG	VG	Overestimate	VG
2003	VG	VG	Overestimate	VG

Figure 9-4 Wet year temperature calibration plots, residual plots, histograms and categorical statistics at SLCCH016.
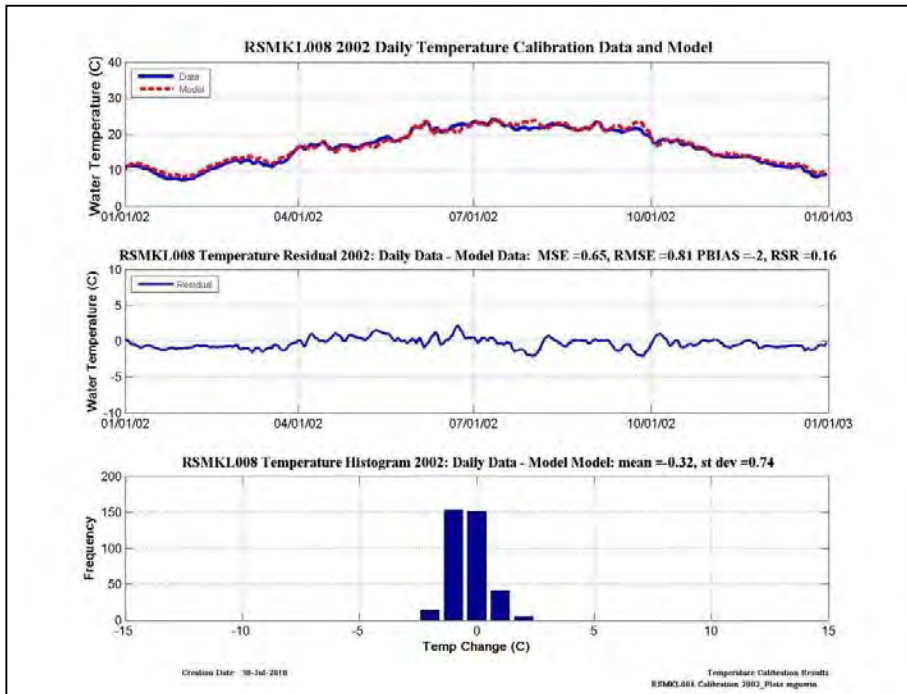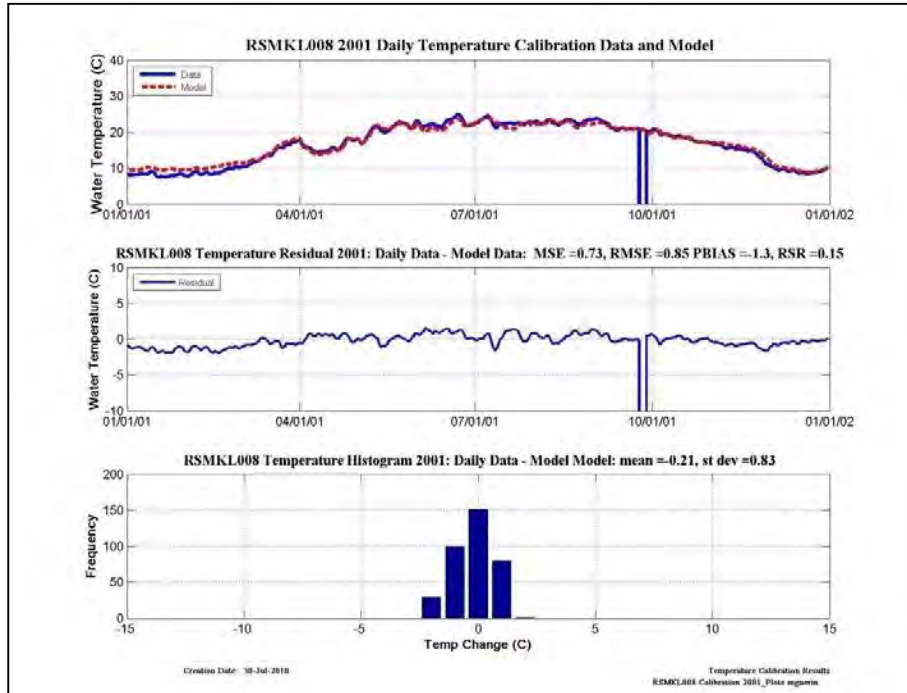
Dry-Calibration	NSE	PBIAS	Bias	RSR
2001	VG	VG	Overestimate	VG
2002	VG	VG	Overestimate	VG

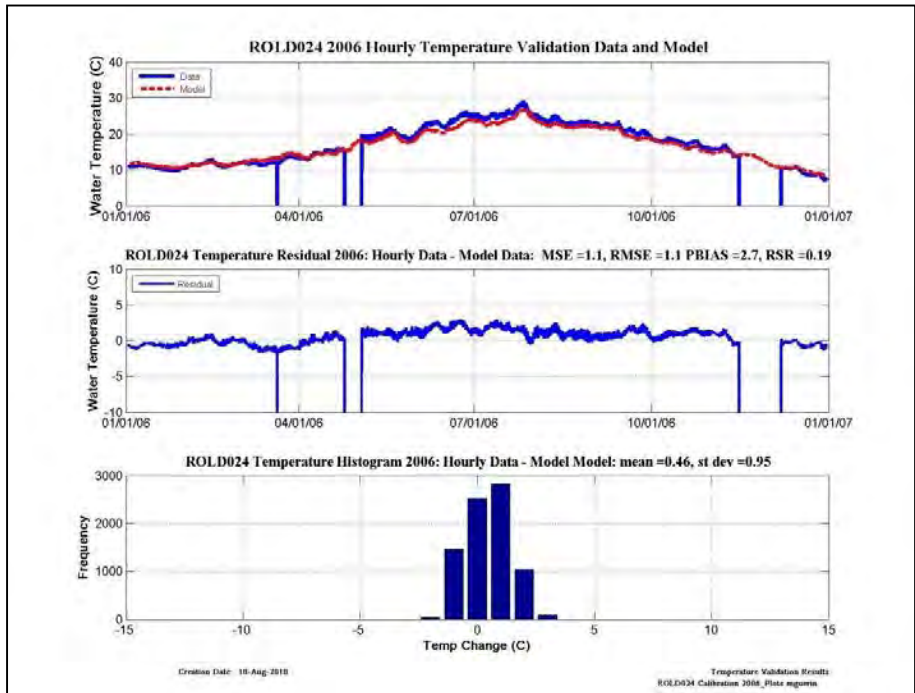**Figure 9-5 Dry year temperature calibration plots, residual plots, histograms and categorical statistics at RSMKL008.**
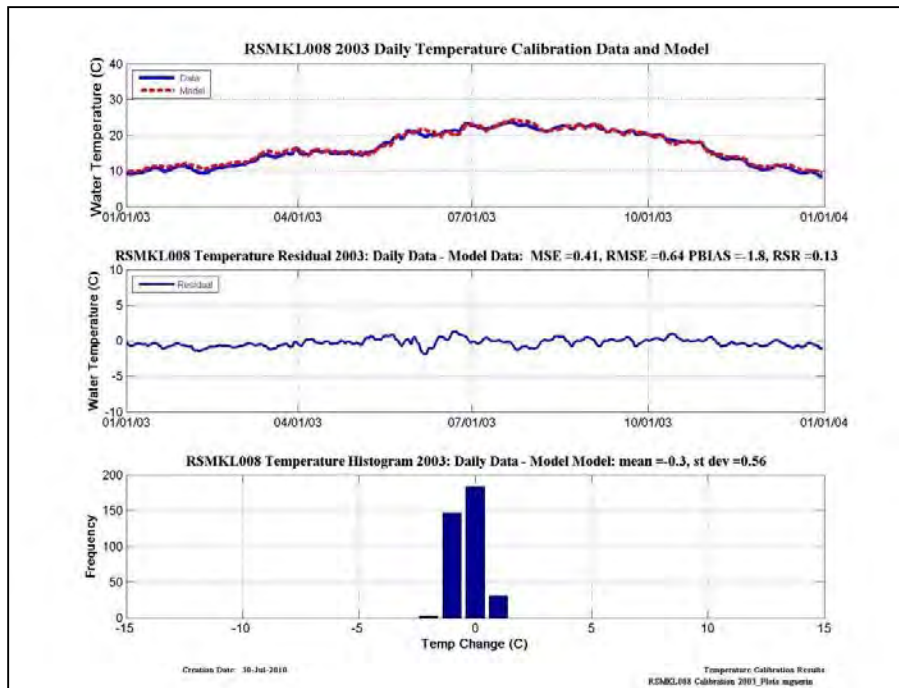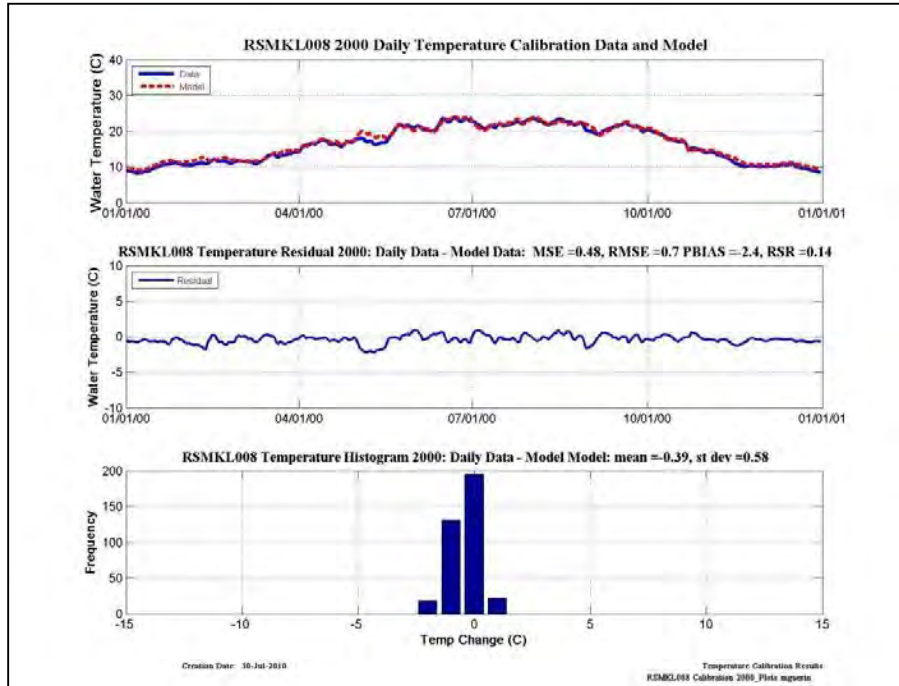
Wet-Calibration	NSE	PBIAS	Bias	RSR
2000	VG	VG	Overestimate	VG
2003	VG	VG	Overestimate	VG

Figure 9-6 Wet year temperature calibration plots, residual plots, histograms and categorical statistics at RSMKL008.
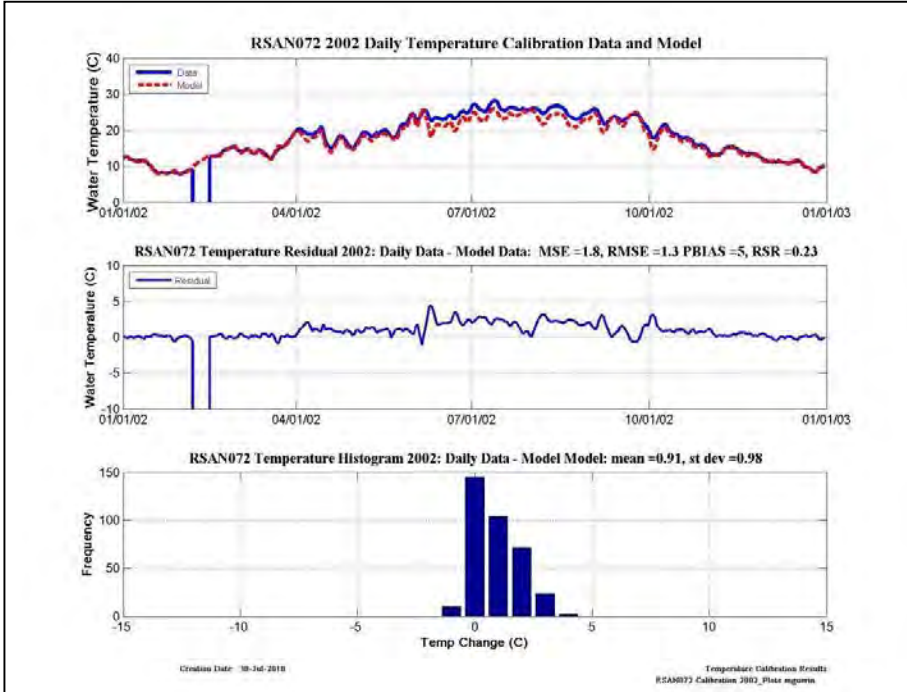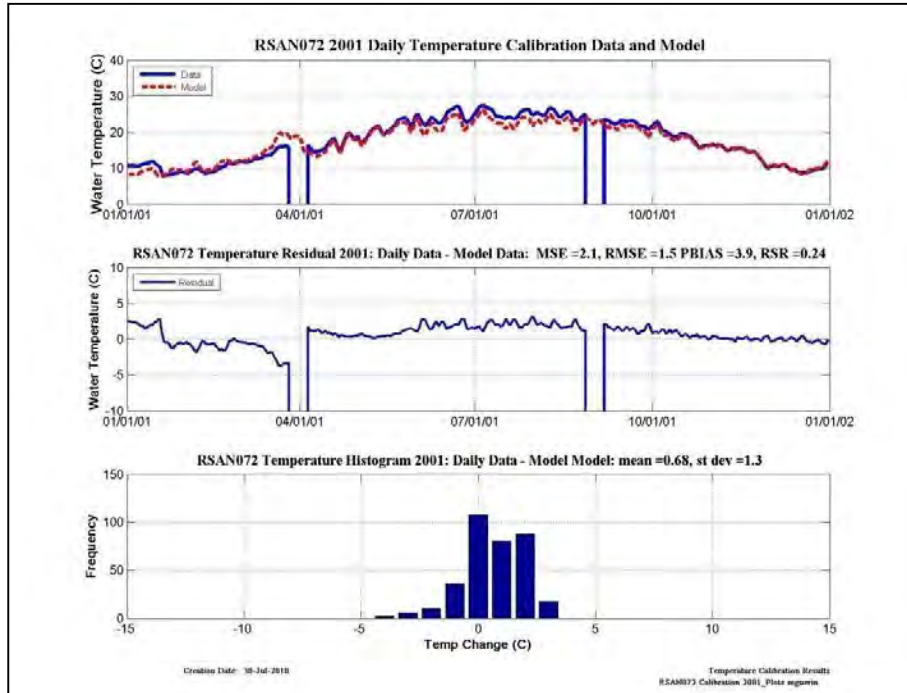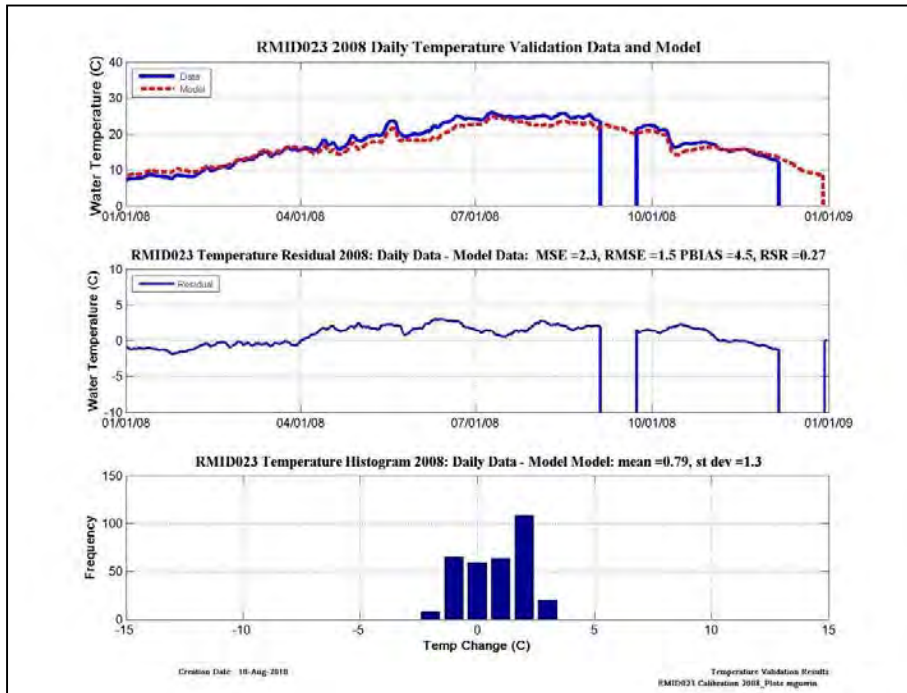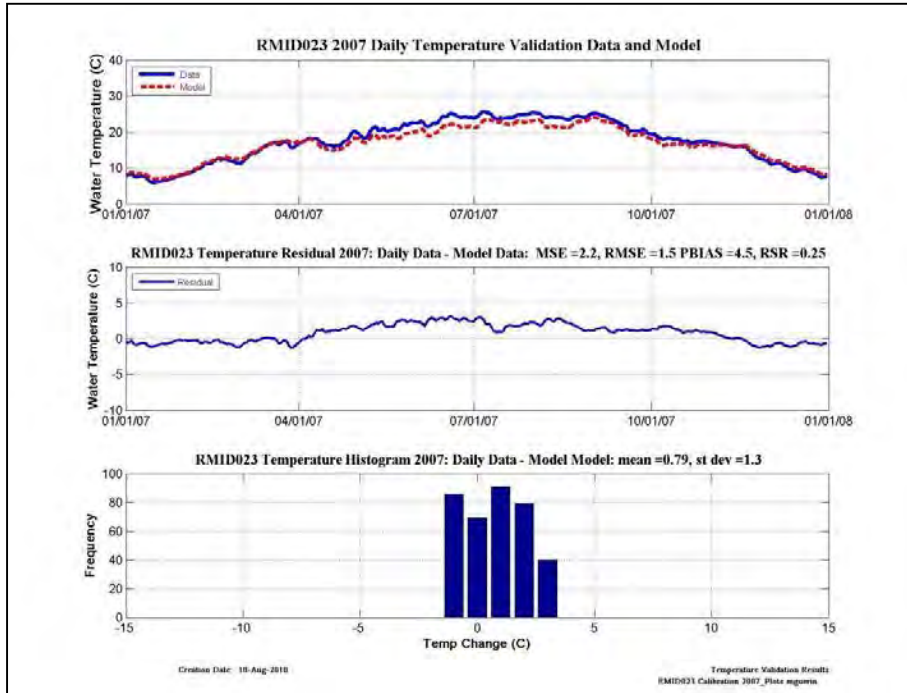
Dry-Calibration	NSE	PBIAS	Bias	RSR
2001	VG	VG	Underestimate	VG
2002	VG	VG	Underestimate	VG

Figure 9-7 Dry year temperature calibration plots, residual plots, histograms and categorical statistics at RSAN072.
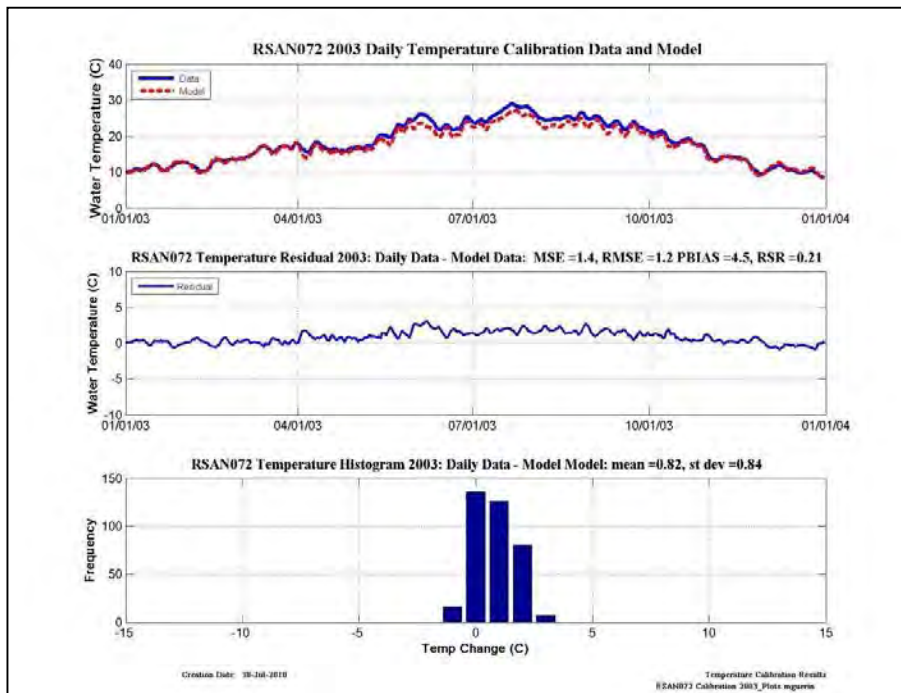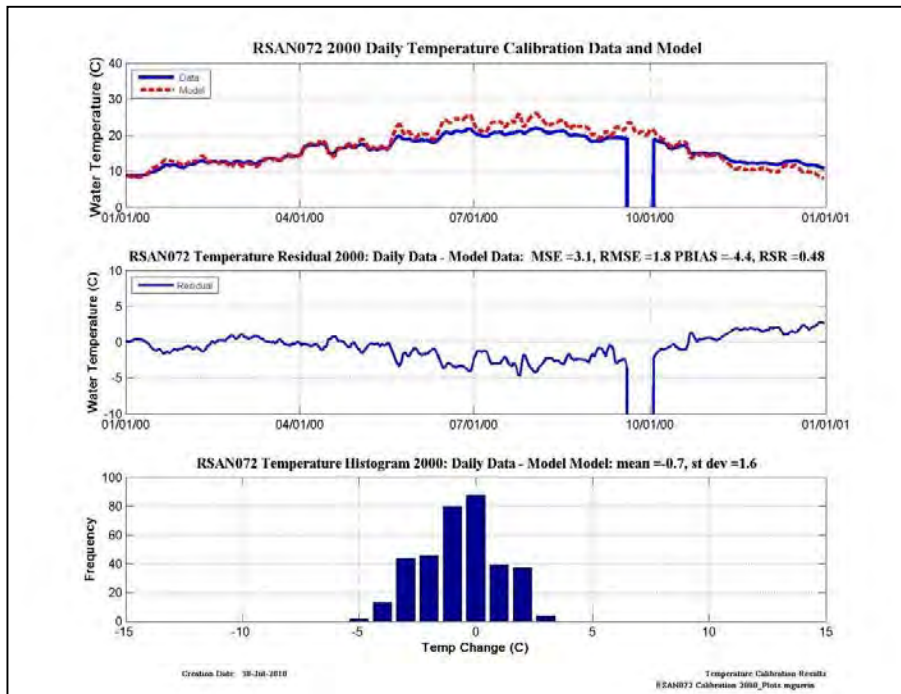
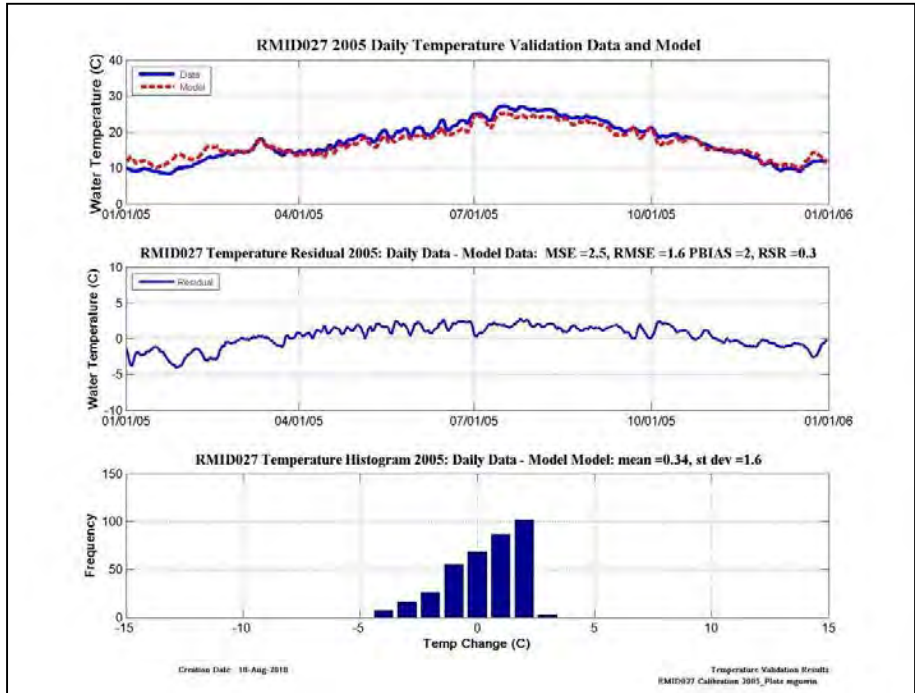| Wet-Calibration	NSE	PBIAS	Bias	RSR
2000	VG	VG	Underestimate	VG
2003	VG	VG	Underestimate	VG

Figure 9-8 Wet year temperature calibration plots, residual plots, histograms and categorical statistics at RSAN072.
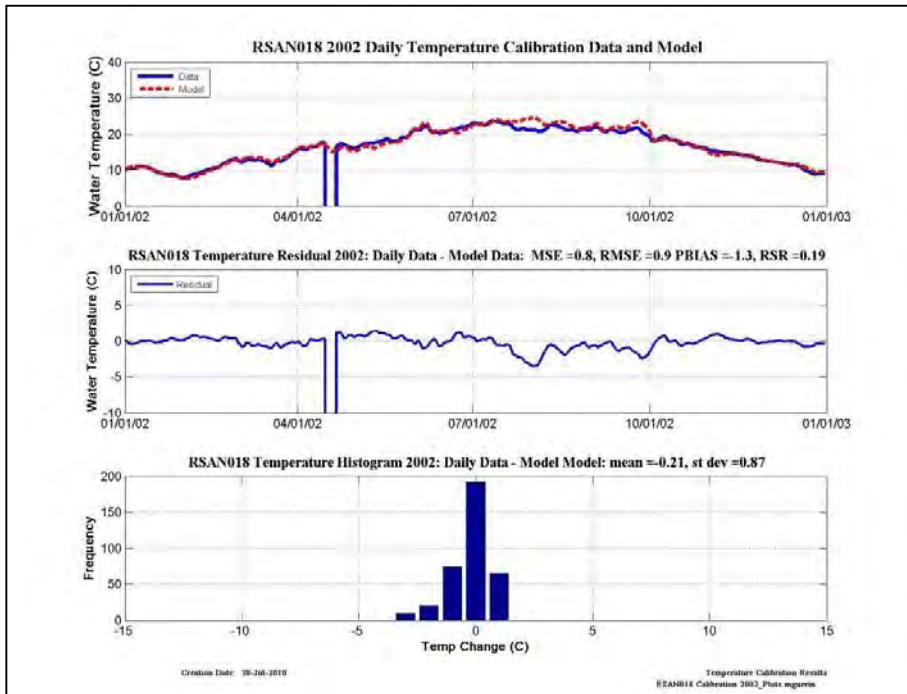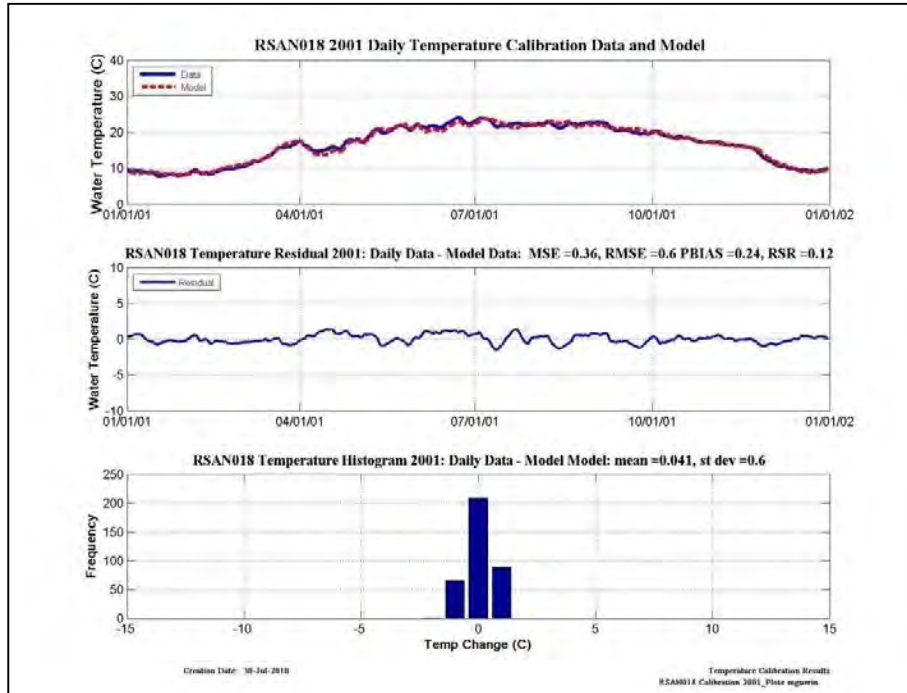
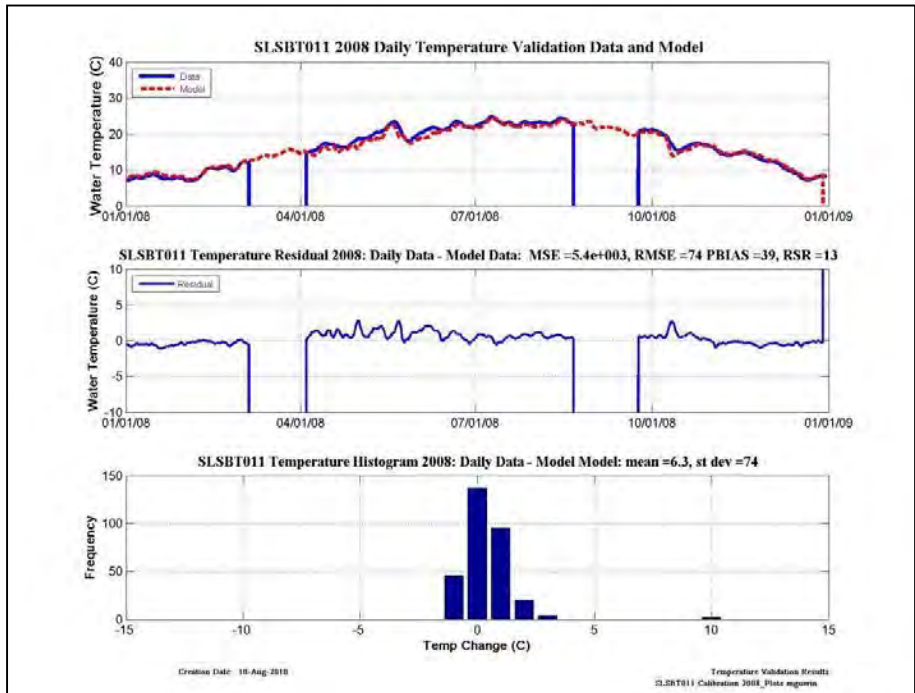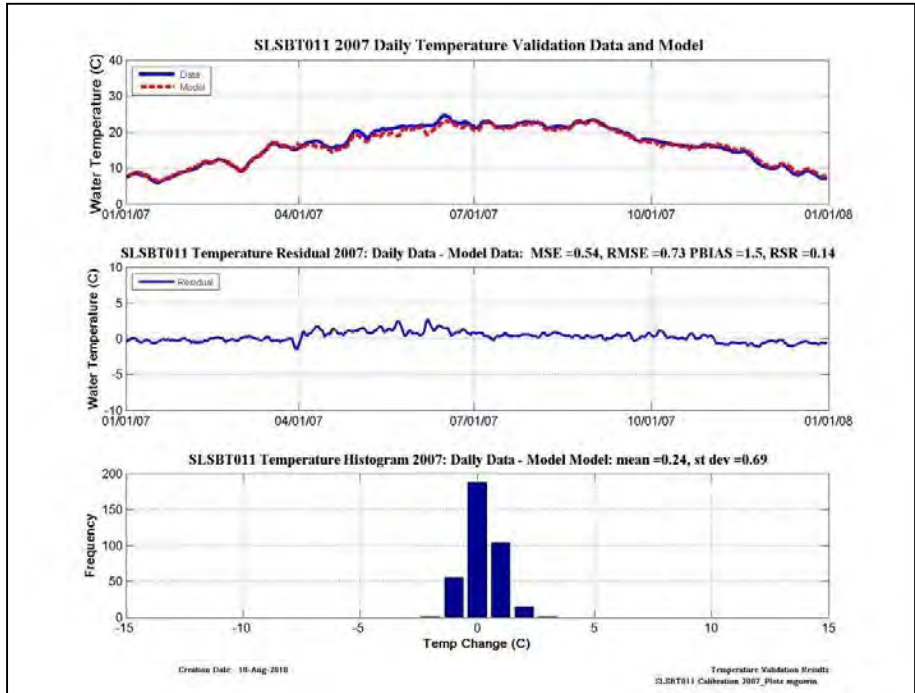| Dry-Calibration	NSE	PBIAS	Bias	RSR
2001	VG	VG	Underestimate	VG
2002	VG	VG	Overestimate	VG

Figure 9-9 Dry year temperature calibration plots, residual plots, histograms and categorical statistics at RSAN018.
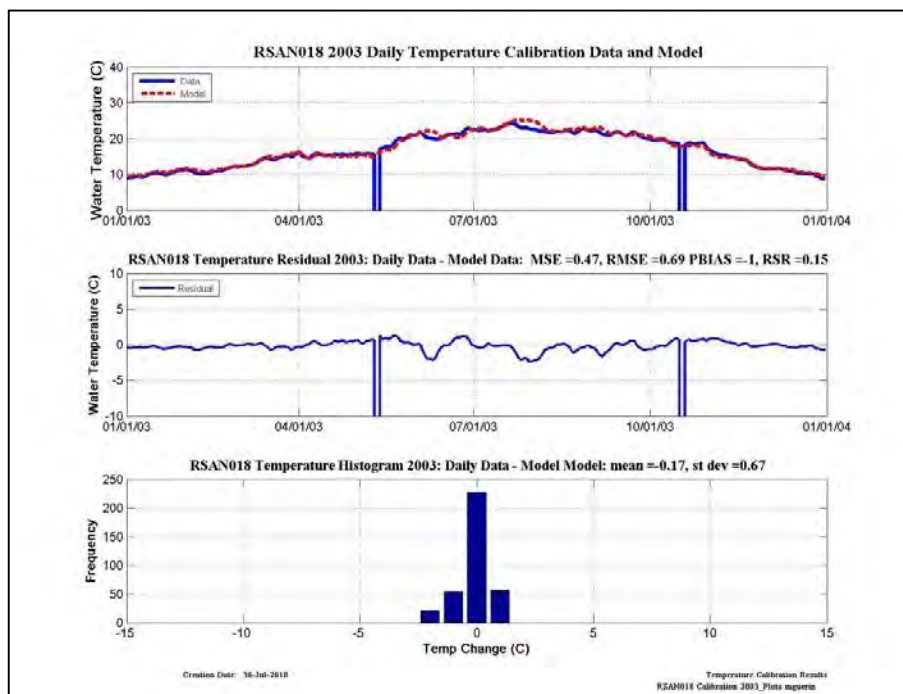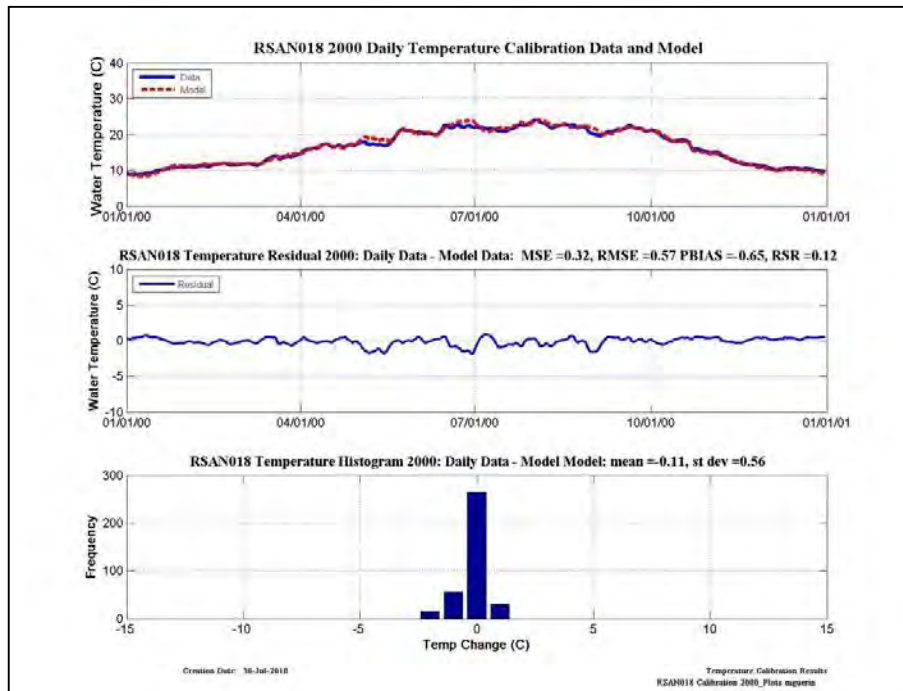
Wet-Calibration	NSE	PBIAS	Bias	RSR
2000	VG	VG	Underestimate	VG
2003	VG	VG	Underestimate	VG

Figure 9-10 Wet year temperature calibration plots, residual plots, histograms and categorical statistics at RSAN018.
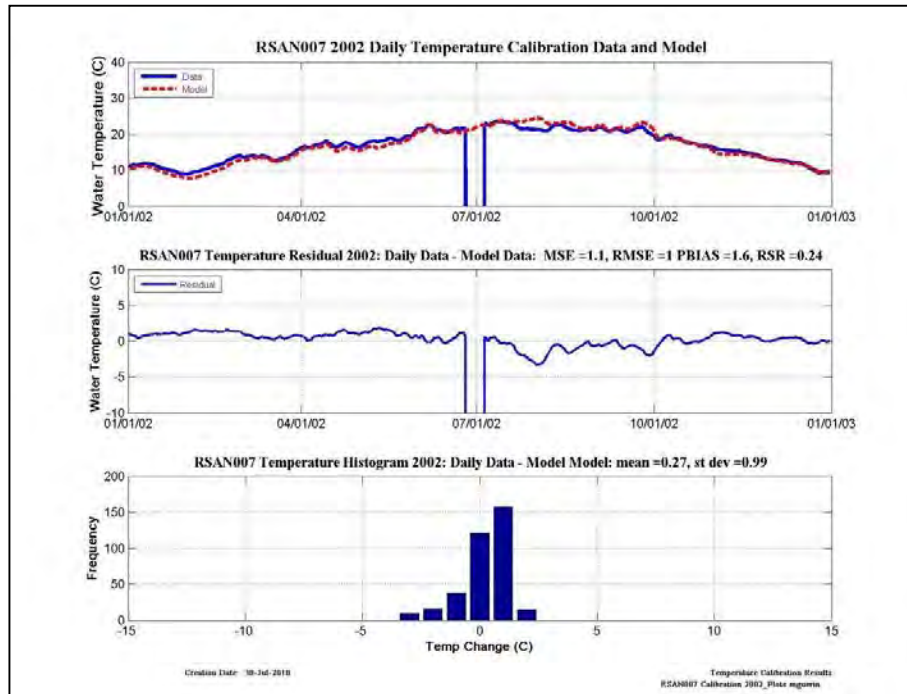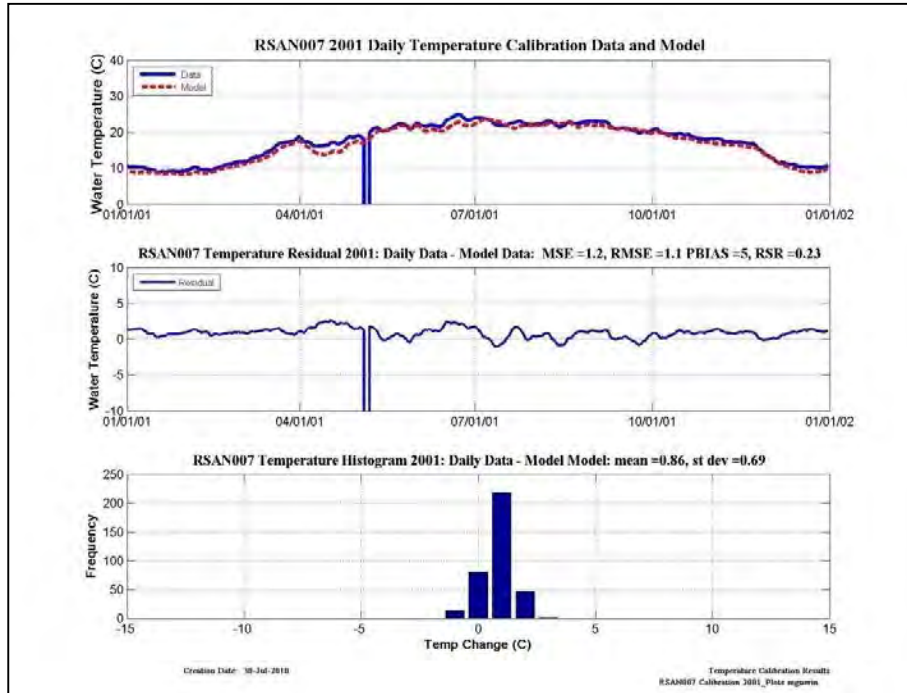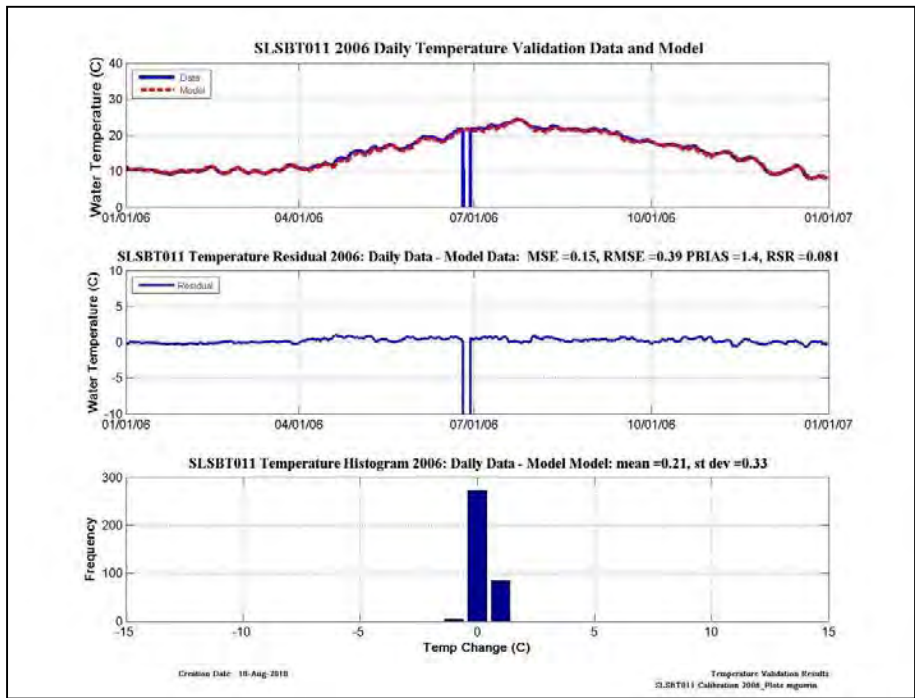
Dry-Calibration	NSE	PBIAS	Bias	RSR
2001	VG	VG	Underestimate	VG
2002	VG	VG	Underestimate	VG

Figure 9-11 Dry year temperature calibration plots, residual plots, histograms and categorical statistics at RSAN007.
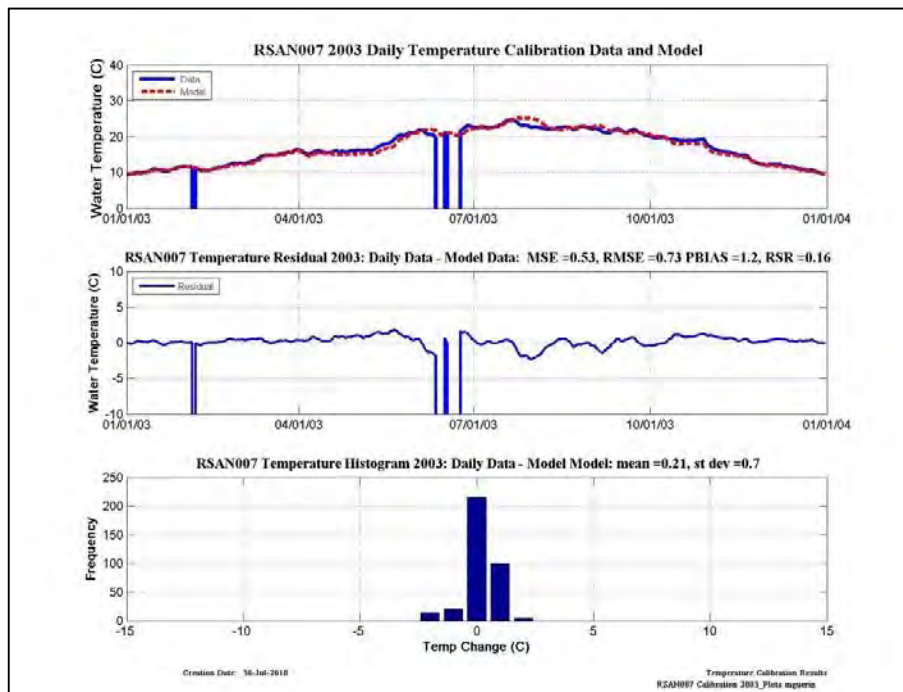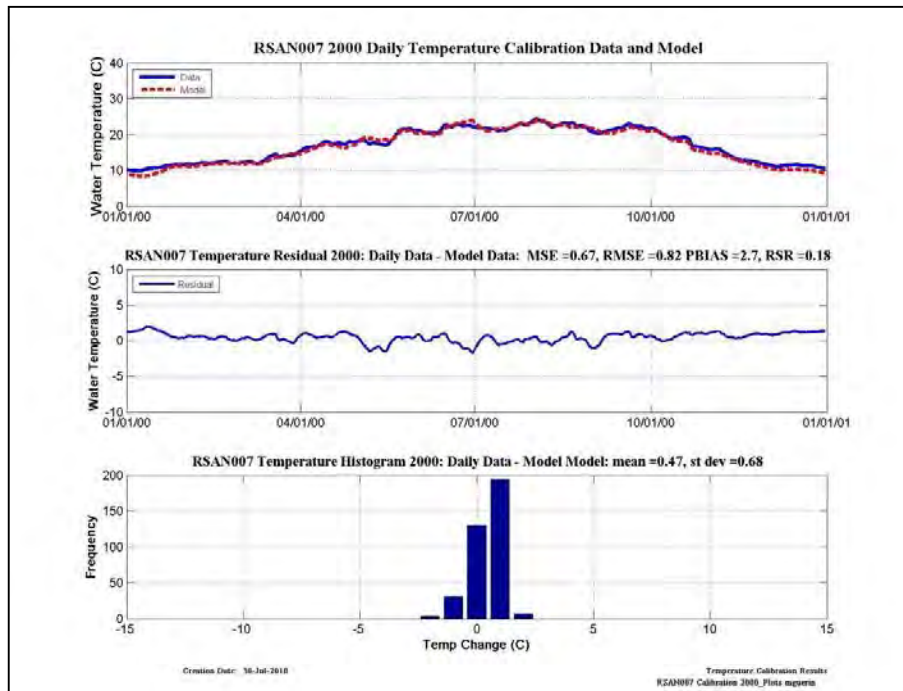
Wet-Calibration	NSE	PBIAS	Bias	RSR
2000	VG	VG	Underestimate	VG
2003	VG	VG	Underestimate	VG

Figure 9-12 Wet year temperature calibration plots, residual plots, histograms and categorical statistics at RSAN007.
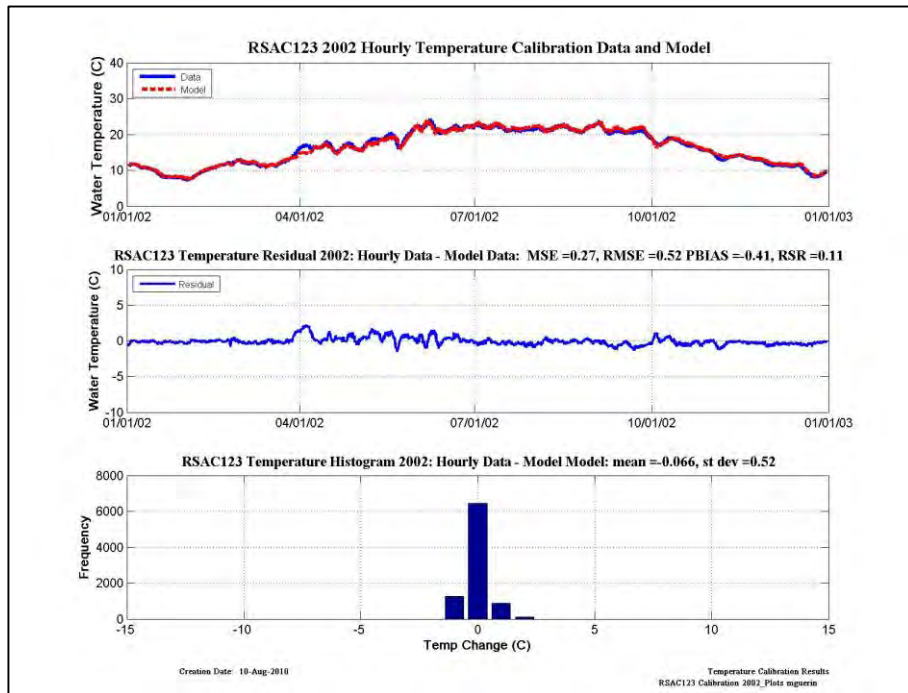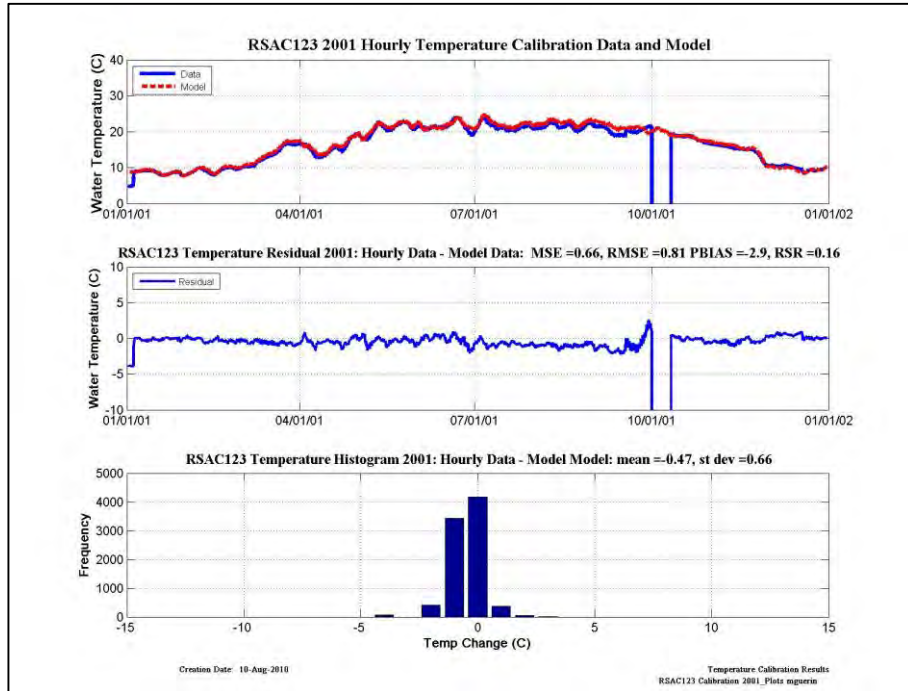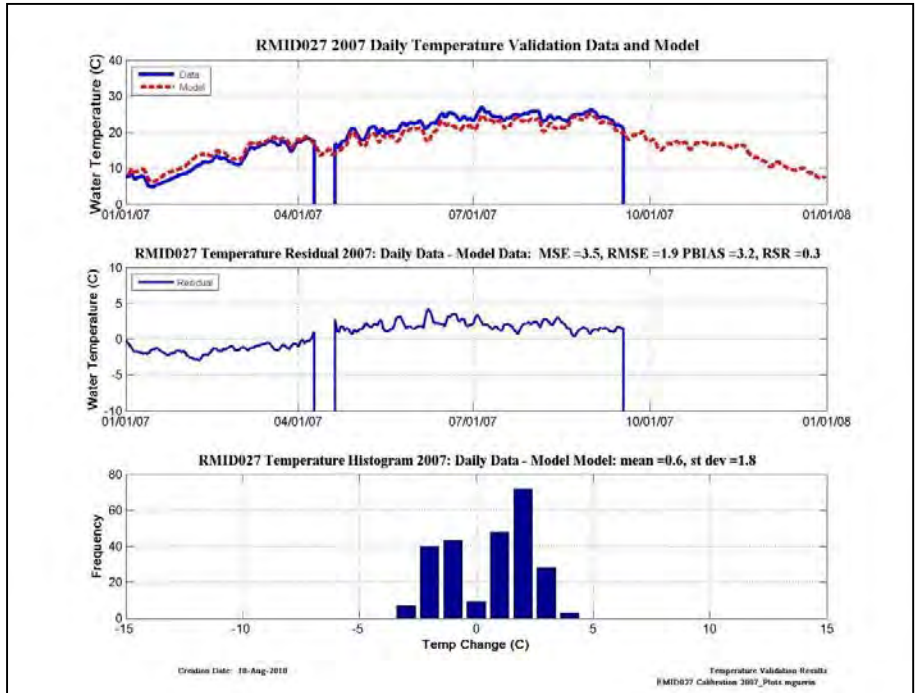
Dry-Calibration	NSE	PBIAS	Bias	RSR
2001	VG	VG	Overestimate	VG
2002	VG	VG	Overestimate	VG

Figure 9-13 Dry year temperature calibration plots, residual plots, histograms and categorical statistics at RSAC123.
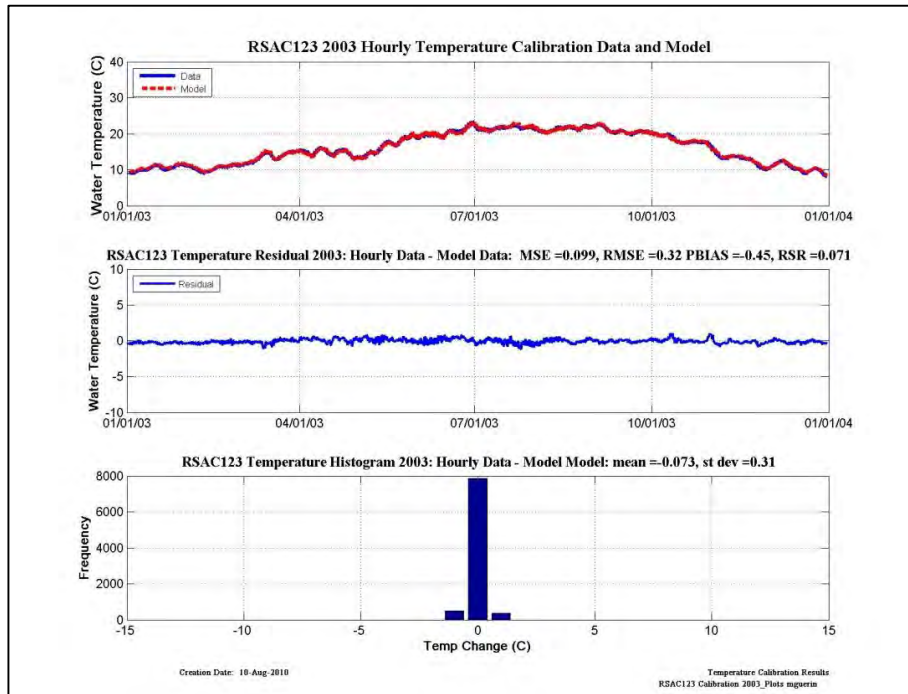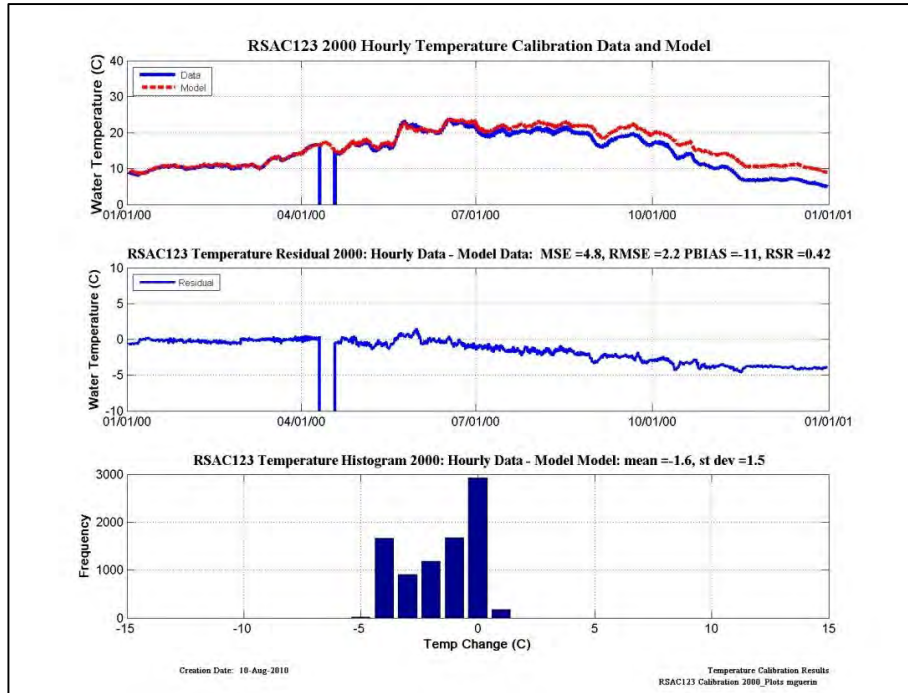
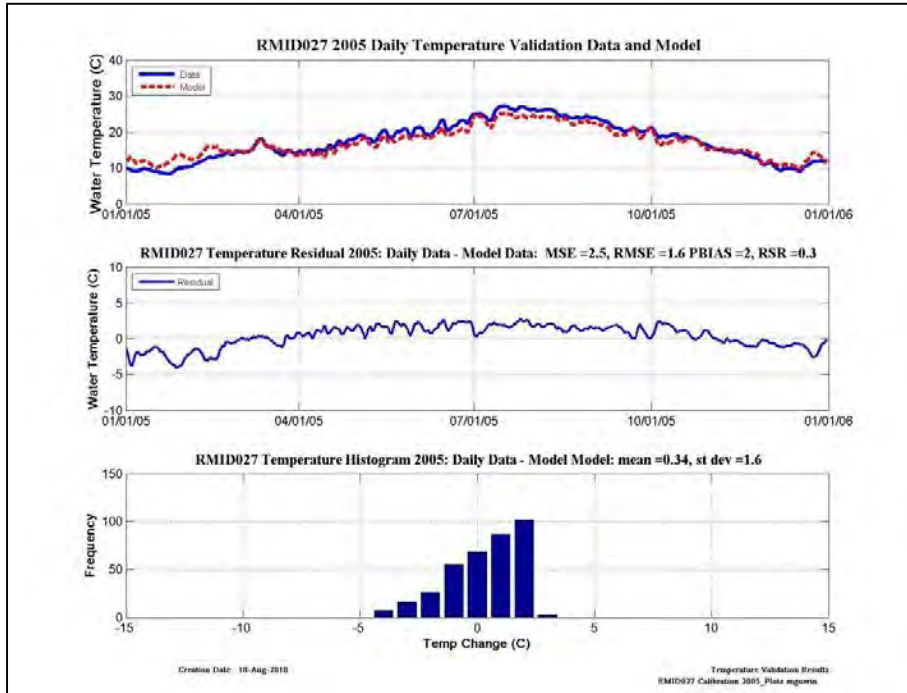| Wet-Calibration	NSE	PBIAS	Bias	RSR
2001	VG	VG	Overestimate	VG
2002	VG	VG	Overestimate	VG

Figure 9-14 Wet year temperature calibration plots, residual plots, histograms and categorical statistics at RSAC123.
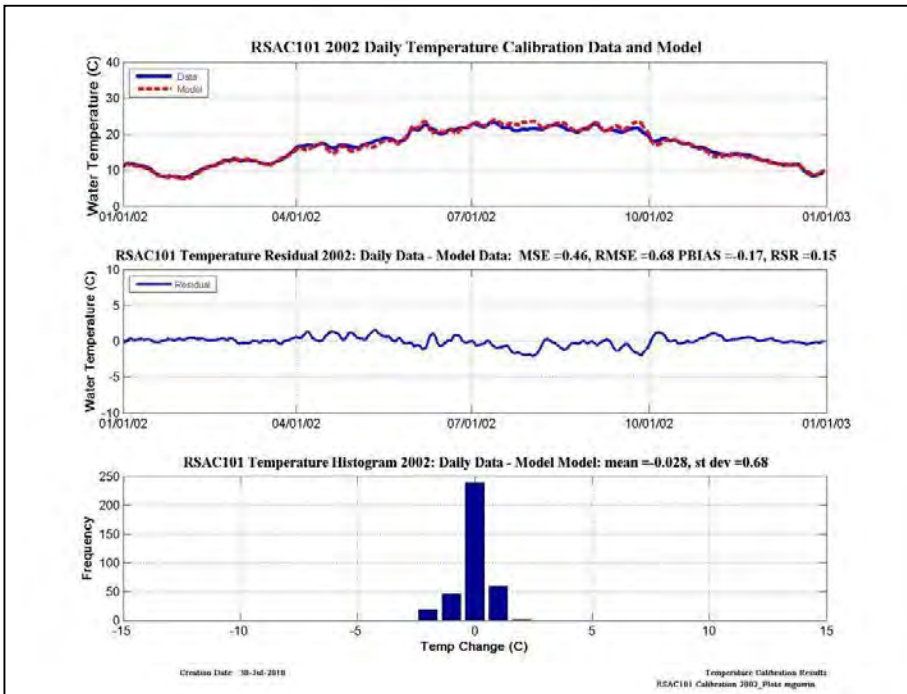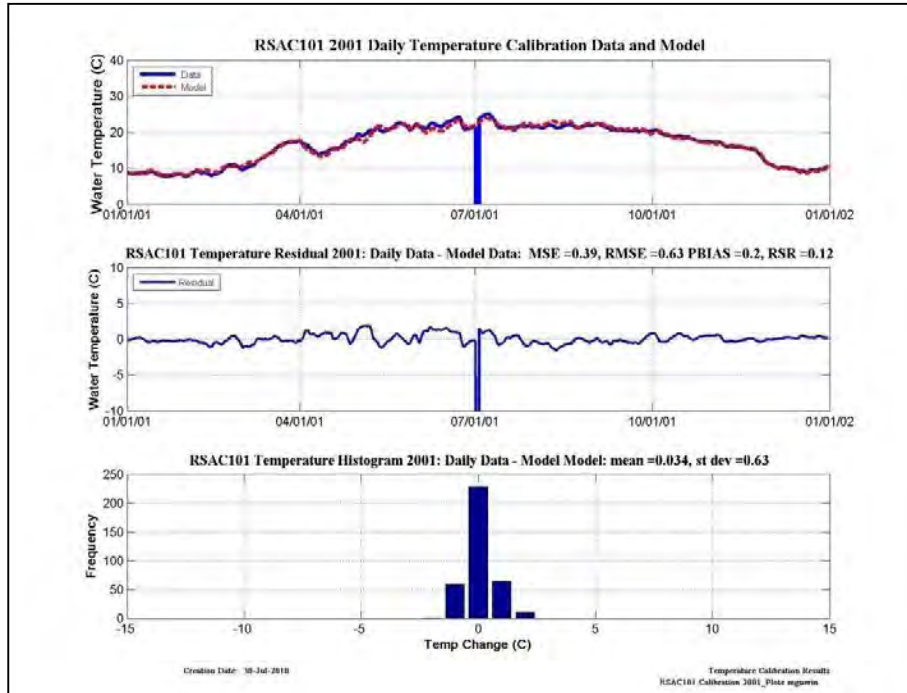
Dry-Calibration	NSE	PBIAS	Bias	RSR
2001	VG	VG	Underestimate	VG
2002	VG	VG	Overestimate	VG

Figure 9-15 Dry year temperature calibration plots, residual plots, histograms and categorical statistics at RSAC101.
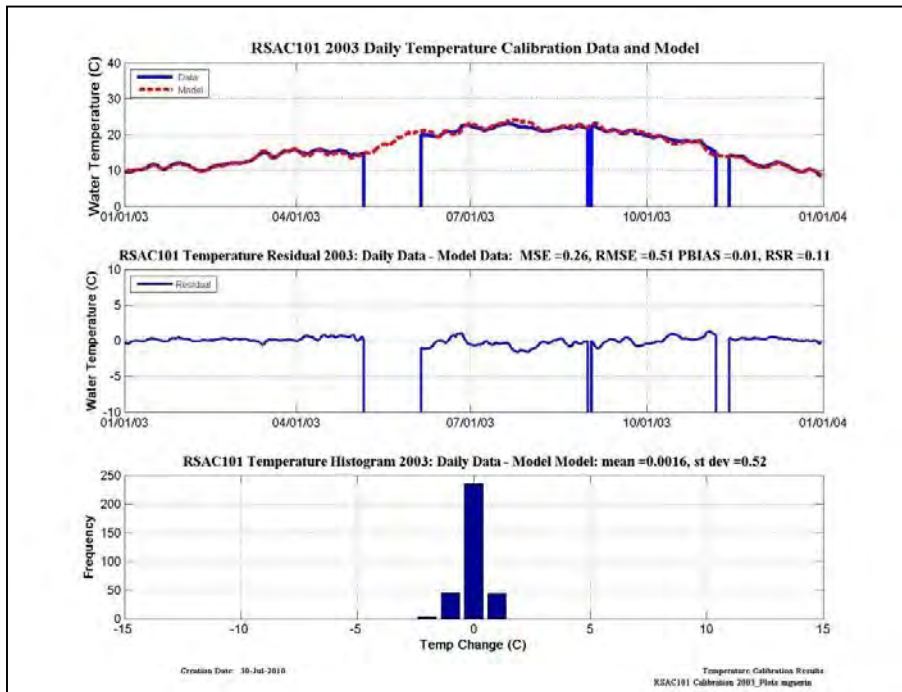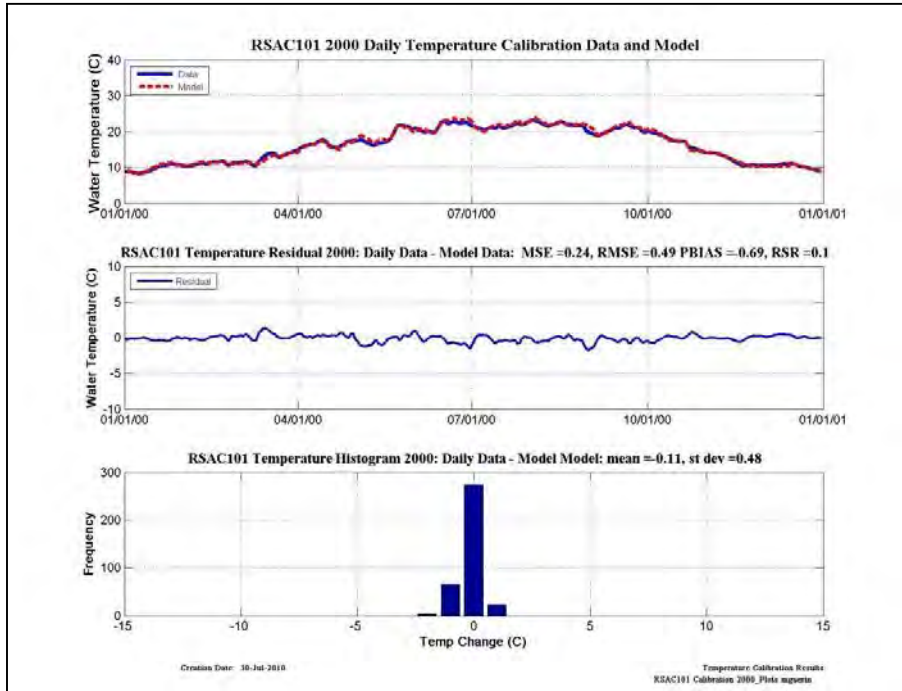
Wet-Calibration	NSE	PBIAS	Bias	RSR
2000	VG	VG	Underestimate	VG
2003	VG	VG	Overestimate	VG

Figure 9-16 Wet year temperature calibration plots, residual plots, histograms and categorical statistics at RSAC101.
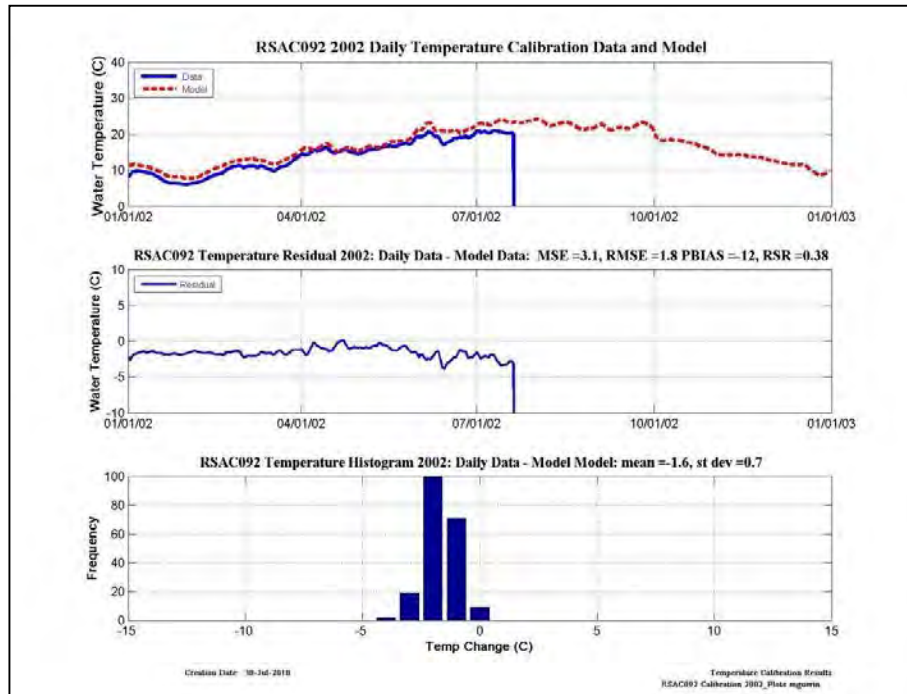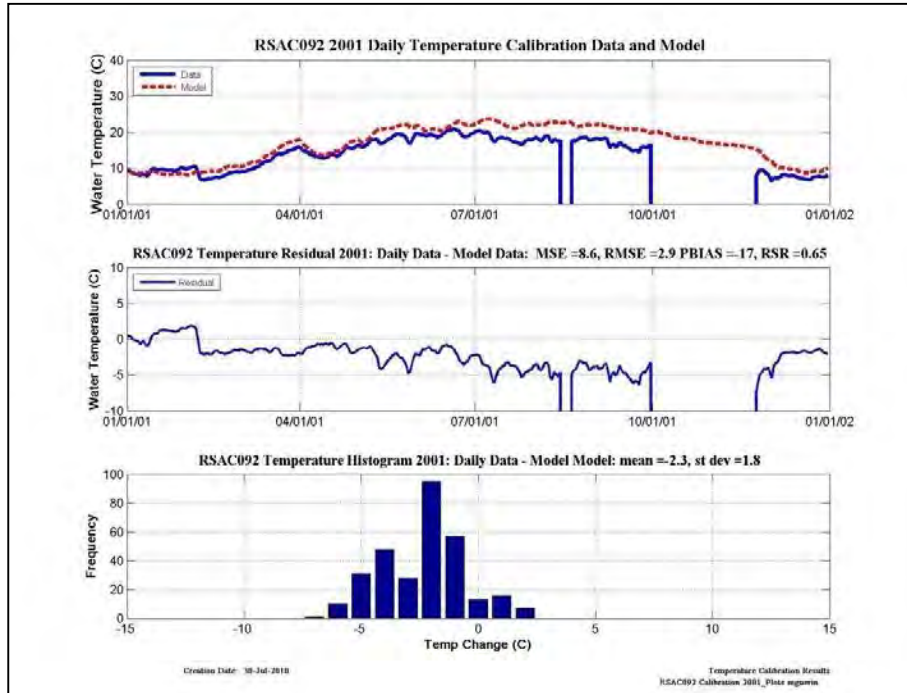
Dry-Calibration	NSE	PBIAS	Bias	RSR
2001	VG	VG	Overestimate	S
2002	VG	VG	Overestimate	VG

Figure 9-17 Dry year temperature calibration plots, residual plots, histograms and categorical statistics at RSAC092.
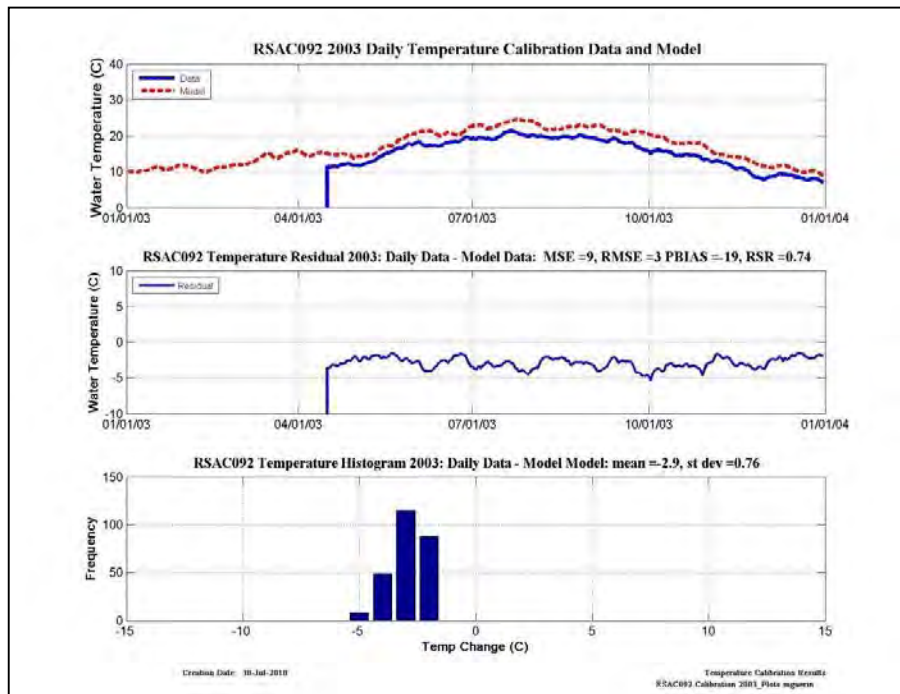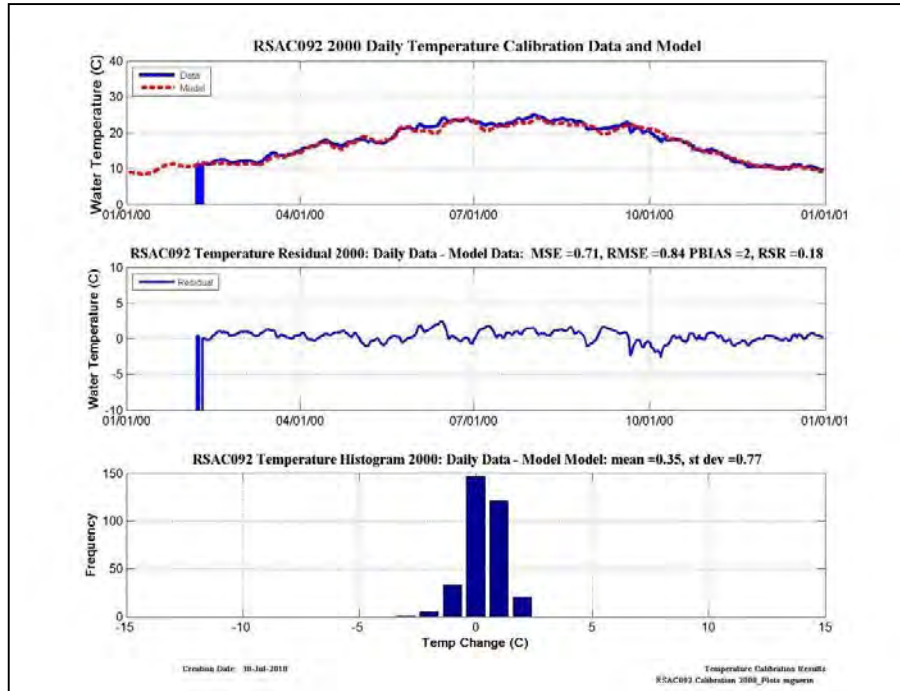
Wet-Calibration	NSE	PBIAS	Bias	RSR
2000	VG	VG	Underestimate	VG
2003	VG	VG	Overestimate	VG

Figure 9-18 Wet year temperature calibration plots, residual plots, histograms and categorical statistics at RSAC092.
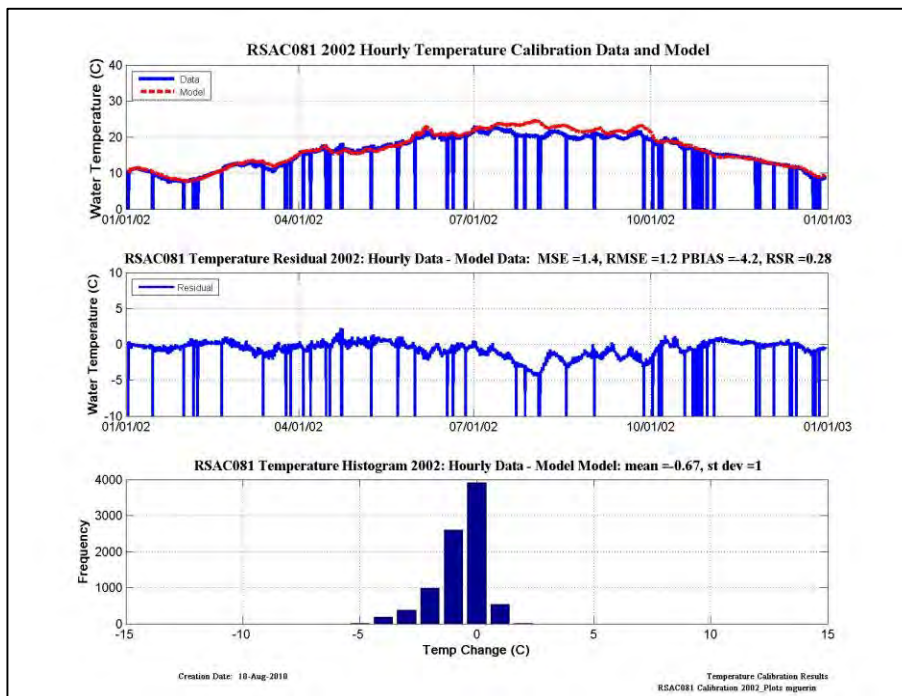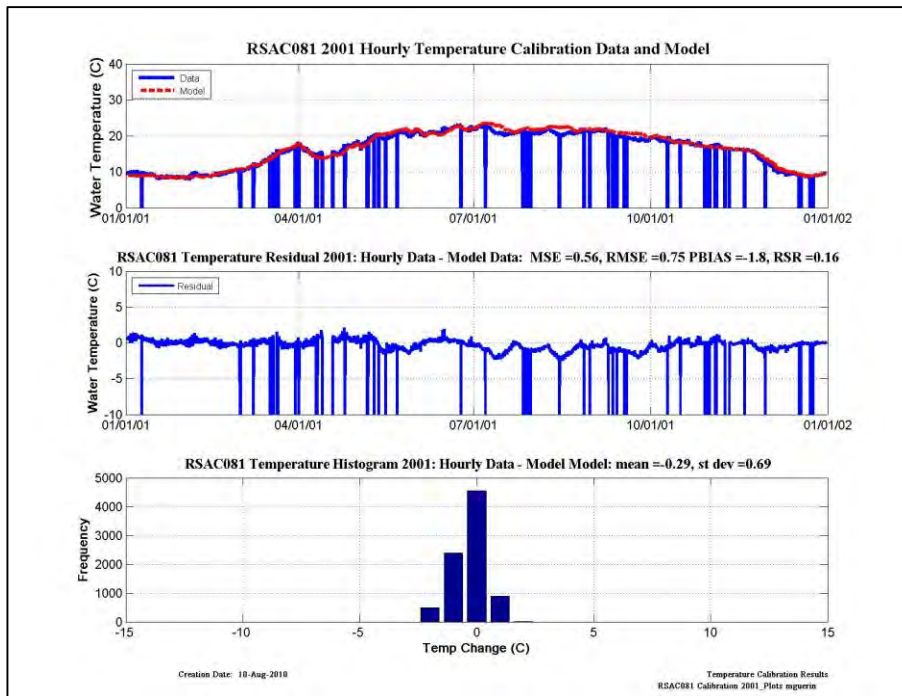
Dry-Calibration	NSE	PBIAS	Bias	RSR
2001	VG	VG	Overestimate	VG
2002	VG	VG	Overestimate	VG

Figure 9-19 Dry year temperature calibration plots, residual plots, histograms and categorical statistics at RSAC081.
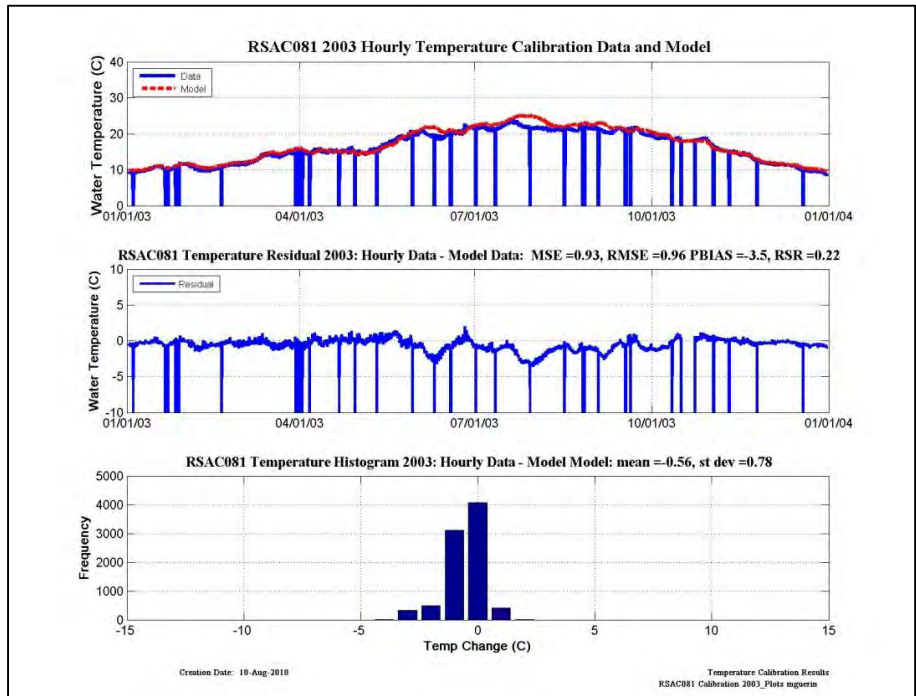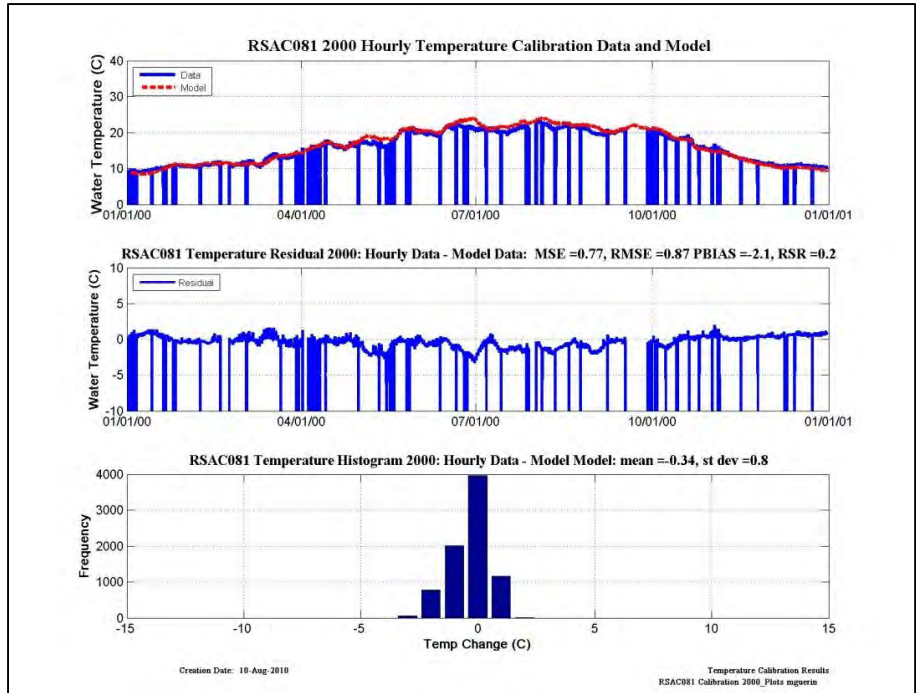
Wet-Calibration	NSE	PBIAS	Bias	RSR
2001	VG	VG	Overestimate	VG
2002	VG	VG	Overestimate	VG

Figure 9-20 Wet year temperature calibration plots, residual plots, histograms and categorical statistics at RSAC081.
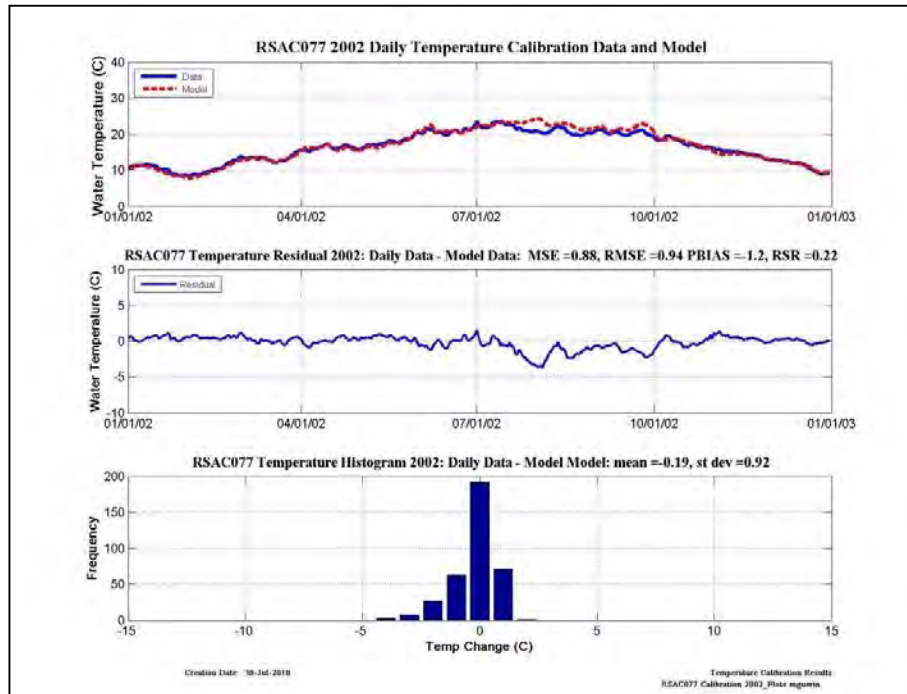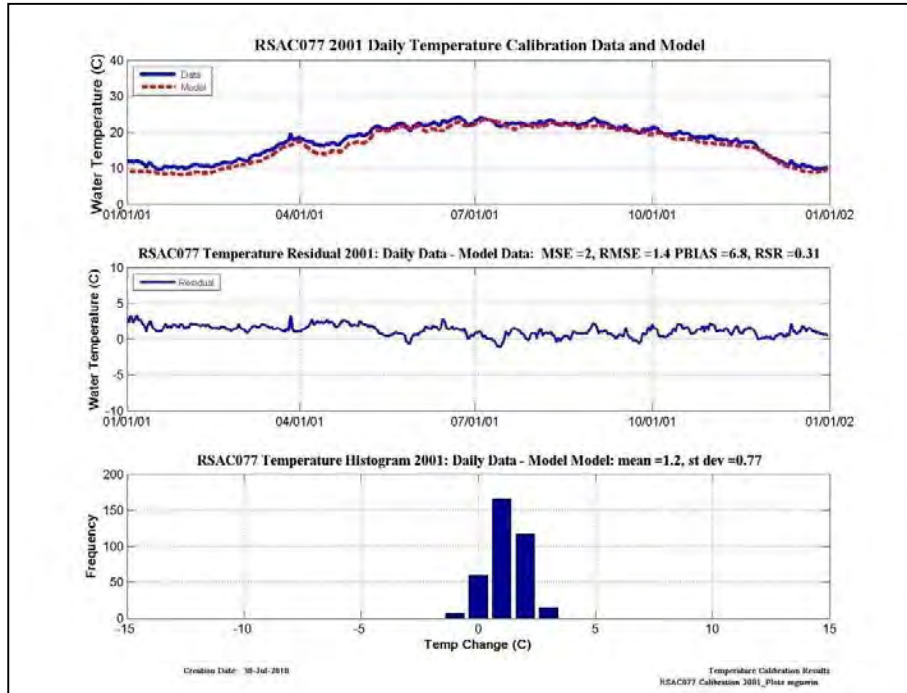
Dry-Calibration	NSE	PBIAS	Bias	RSR
2001	VG	VG	Underestimate	VG
2002	VG	VG	Overestimate	VG

Figure 9-21 Dry year temperature calibration plots, residual plots, histograms and categorical statistics at RSAC077.
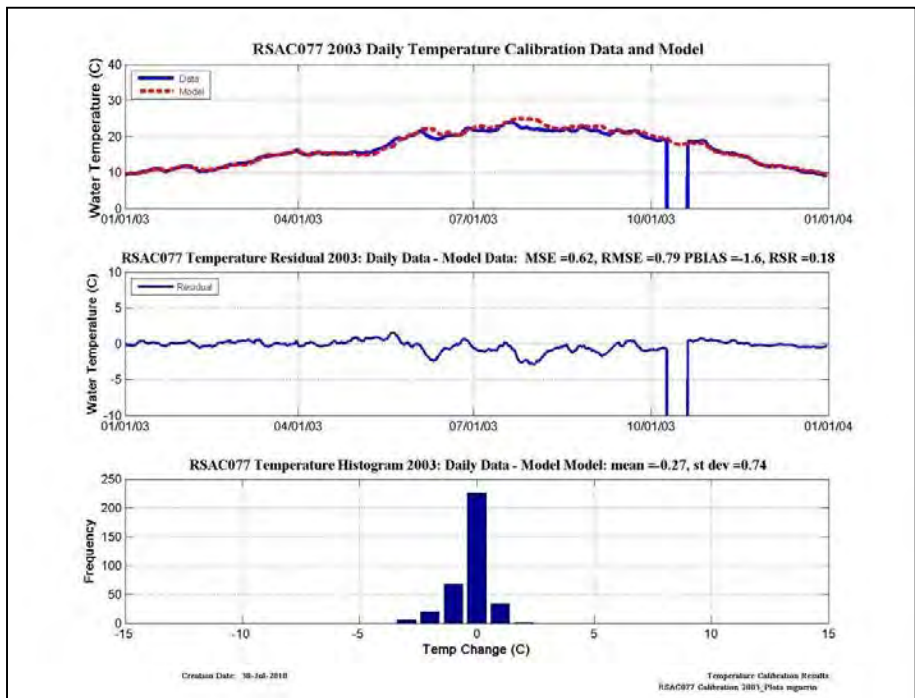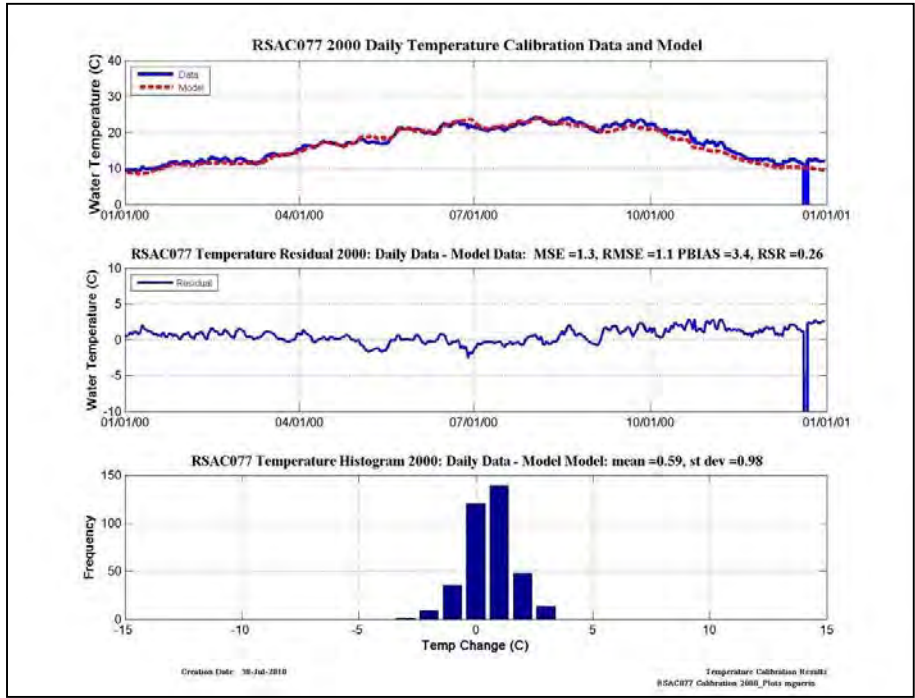
Wet-Calibration	NSE	PBIAS	Bias	RSR
2000	VG	VG	Underestimate	VG
2003	VG	VG	Overestimate	VG

Figure 9-22 Wet year temperature calibration plots, residual plots, histograms and categorical statistics at RSAC077.
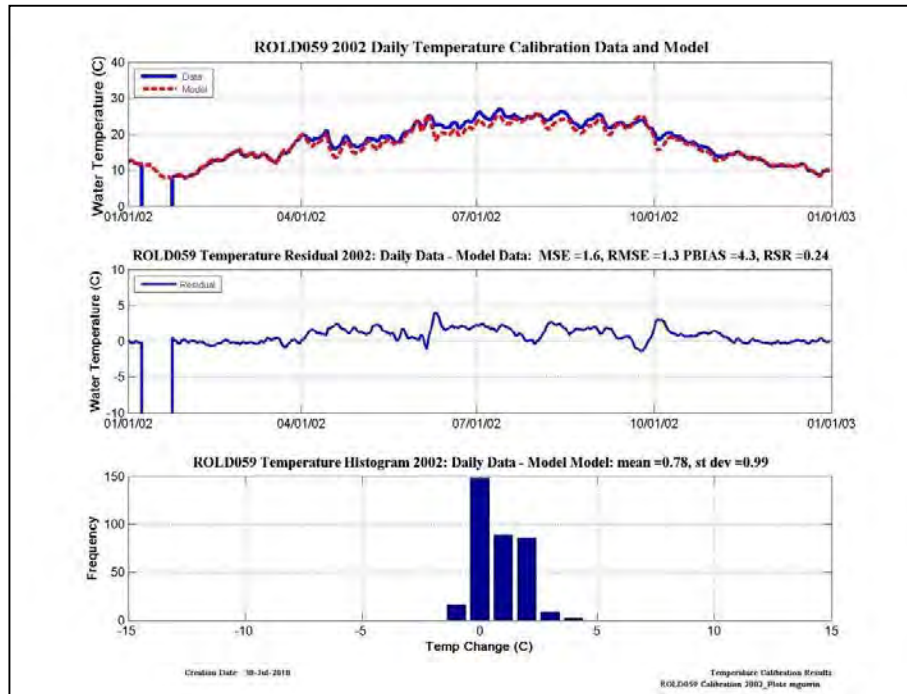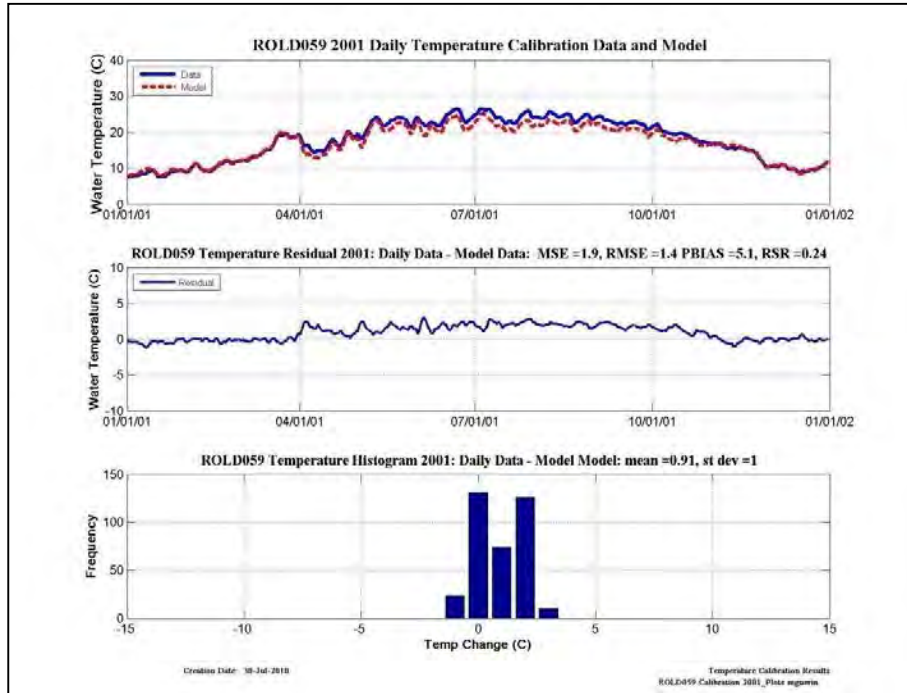
Dry-Calibration	NSE	PBIAS	Bias	RSR
2001	VG	VG	Underestimate	VG
2002	VG	VG	Underestimate	VG

Figure 9-23 Dry year temperature calibration plots, residual plots, histograms and categorical statistics at ROLD059.

169
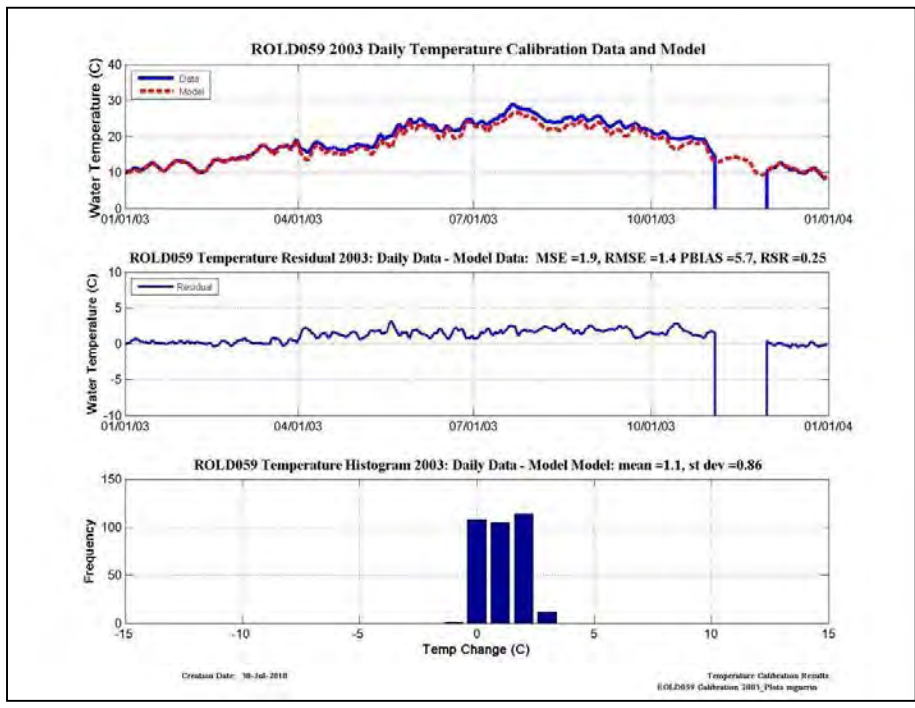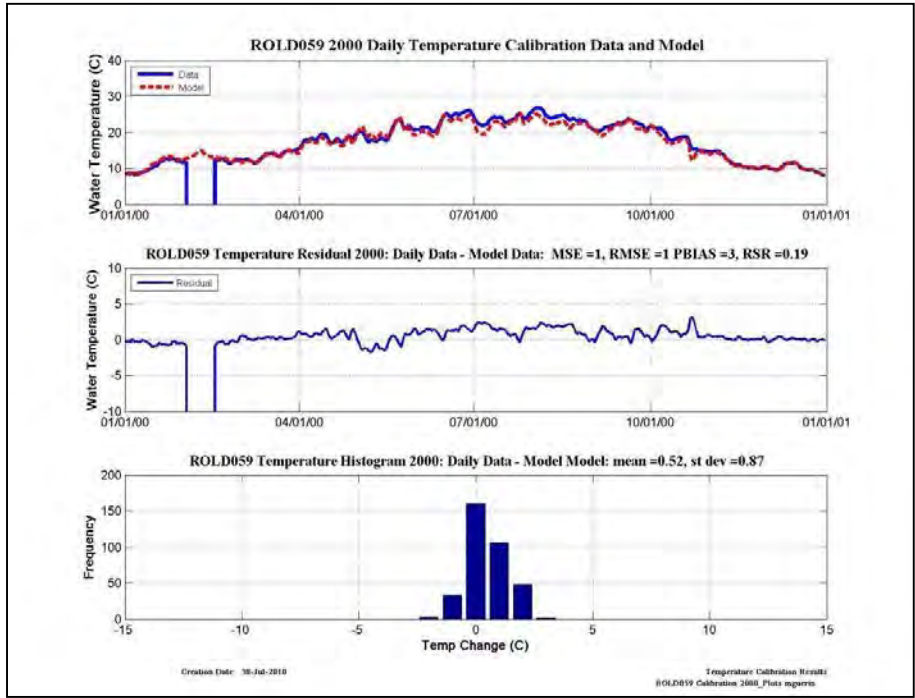
Wet-Calibration	NSE	PBIAS	Bias	RSR
2000	VG	VG	Underestimate	VG
2003	VG	VG	Underestimate	VG

Figure 9-24 Wet year temperature calibration plots, residual plots, histograms and categorical statistics at ROLD059.
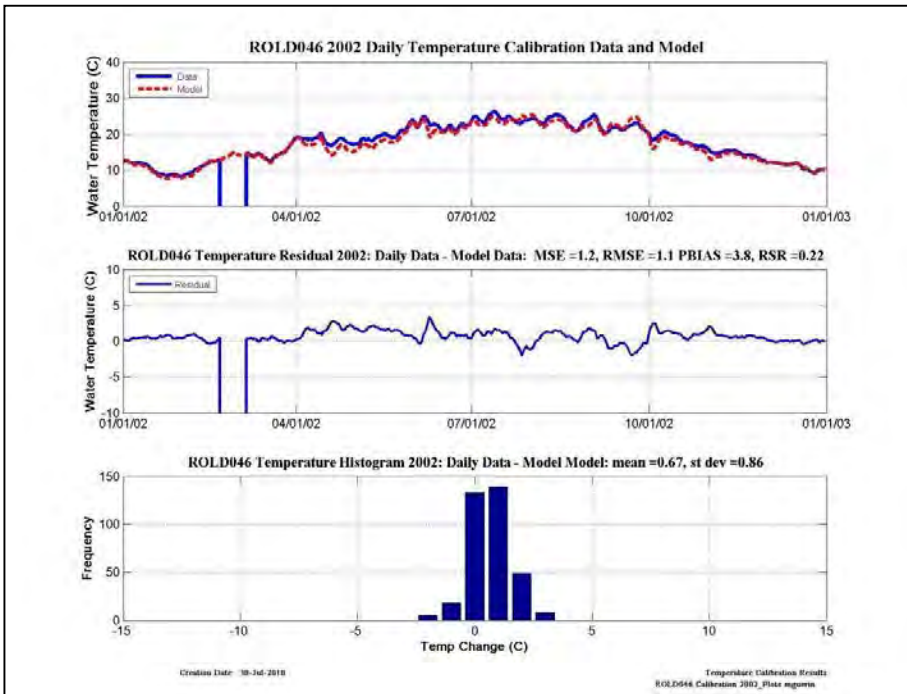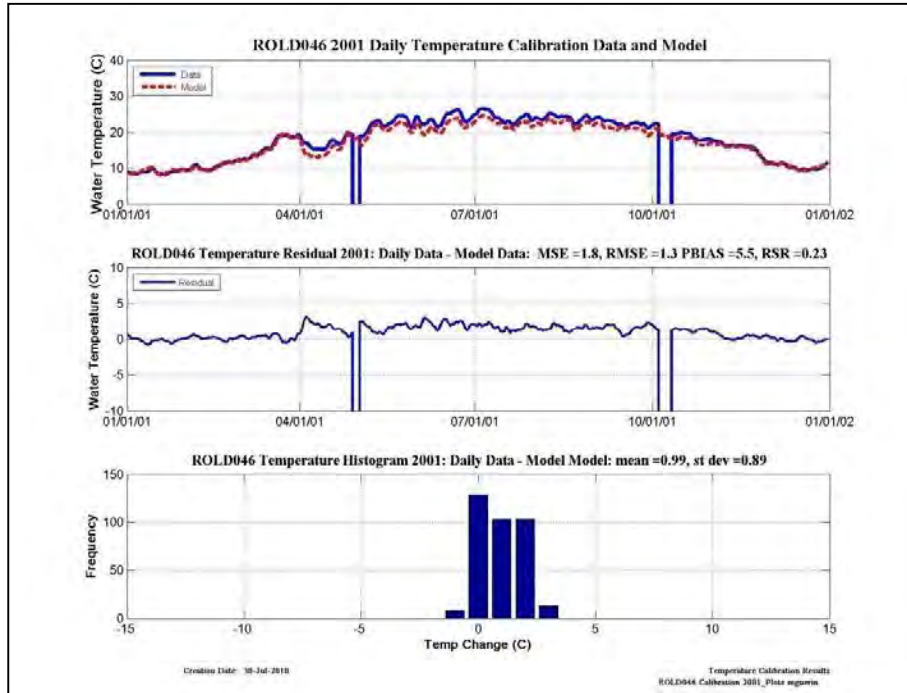
Dry-Calibration	NSE	PBIAS	Bias	RSR
2001	VG	VG	Underestimate	VG
2002	VG	VG	Underestimate	VG

Figure 9-25 Dry year temperature calibration plots, residual plots, histograms and categorical statistics at ROLD046.
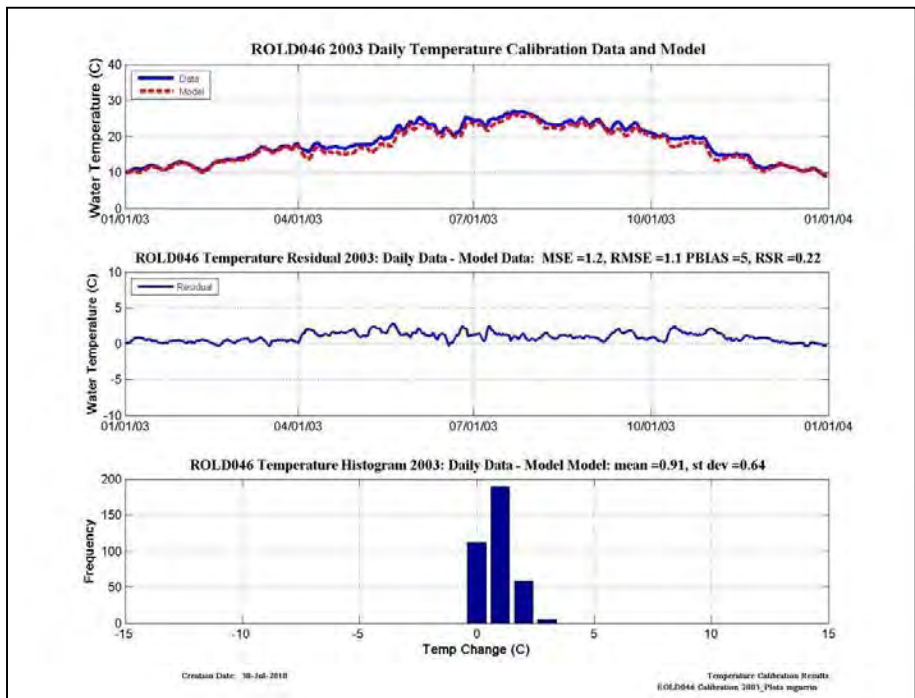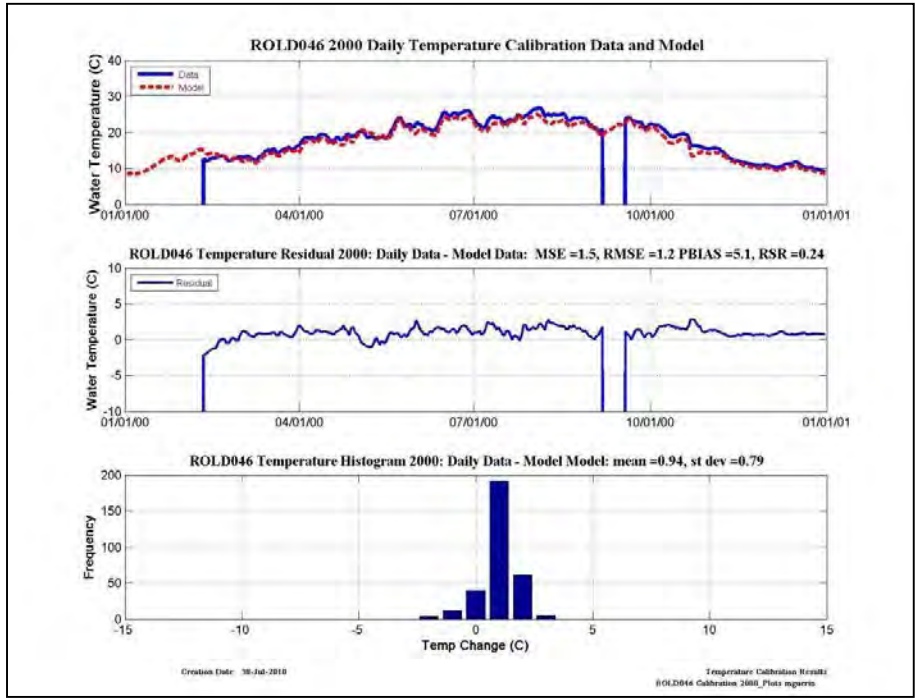
Wet-Calibration	NSE	PBIAS	Bias	RSR
2000	VG	VG	Underestimate	VG
2003	VG	VG	Underestimate	VG

Figure 9-26 Wet year temperature calibration plots, residual plots, histograms and categorical statistics at ROLD046.
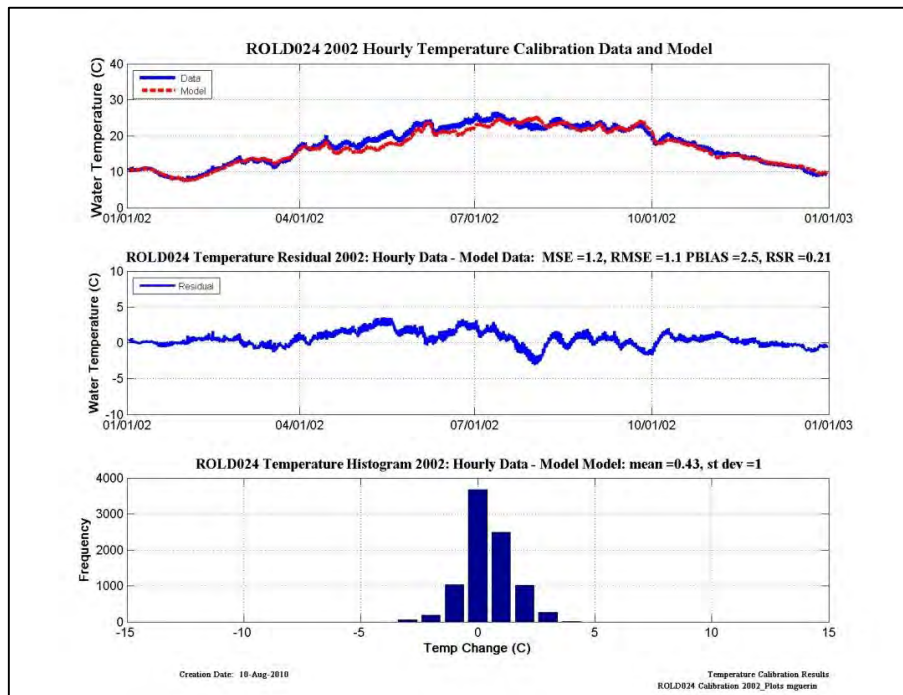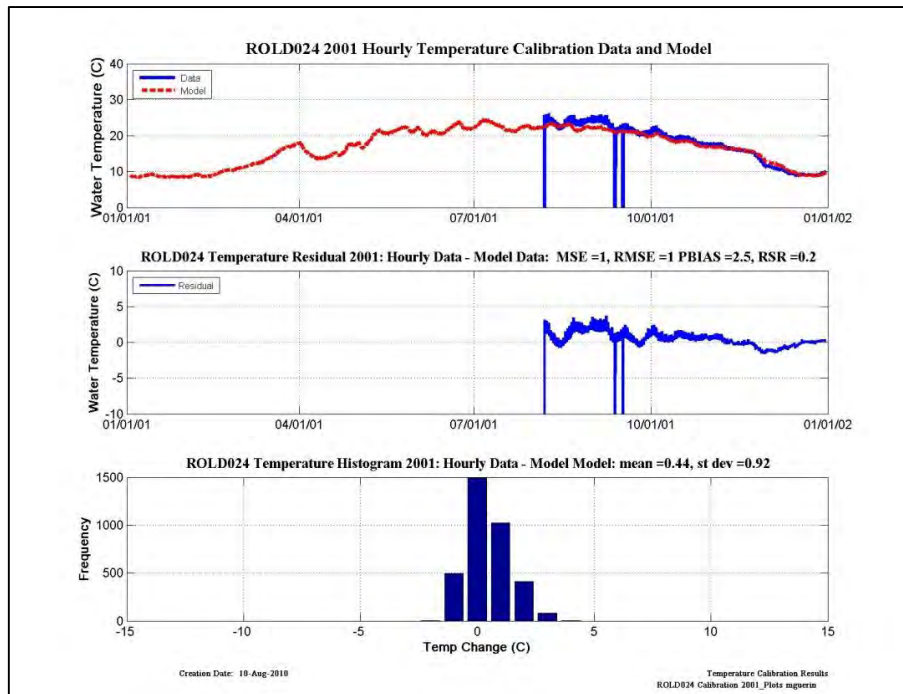
Dry-Calibration	NSE	PBIAS	Bias	RSR
2001	VG	VG	Underestimate	VG
2002	VG	VG	Underestimate	VG

Figure 9-27 Dry year temperature calibration plots, residual plots, histograms and categorical statistics at ROLD024.

No Data Available for
ROLD024 during 2000

ROLD024 2003 Hourly Temperature Calibration Data and Model

ROLD024 Temperature Residual 2003: Hourly Data - Model Data: MSE =0.95, RMSE =0.97 PBIAS =2.8, RSR =0.19

ROLD024 Temperature Histogram 2003: Hourly Data - Model Model: mean =0.49, st dev =0.84
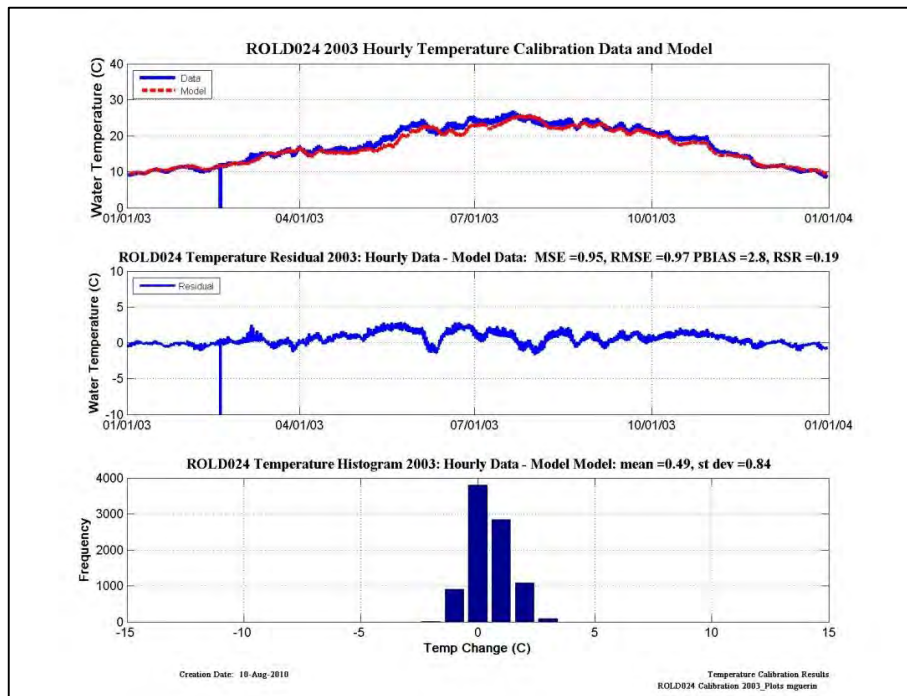
Wet-Calibration	NSE	PBIAS	Bias	RSR
2001				
2002	VG	VG	Underestimate	VG

Figure 9-28 Wet year temperature calibration plots, residual plots, histograms and categorical statistics at ROLD024.
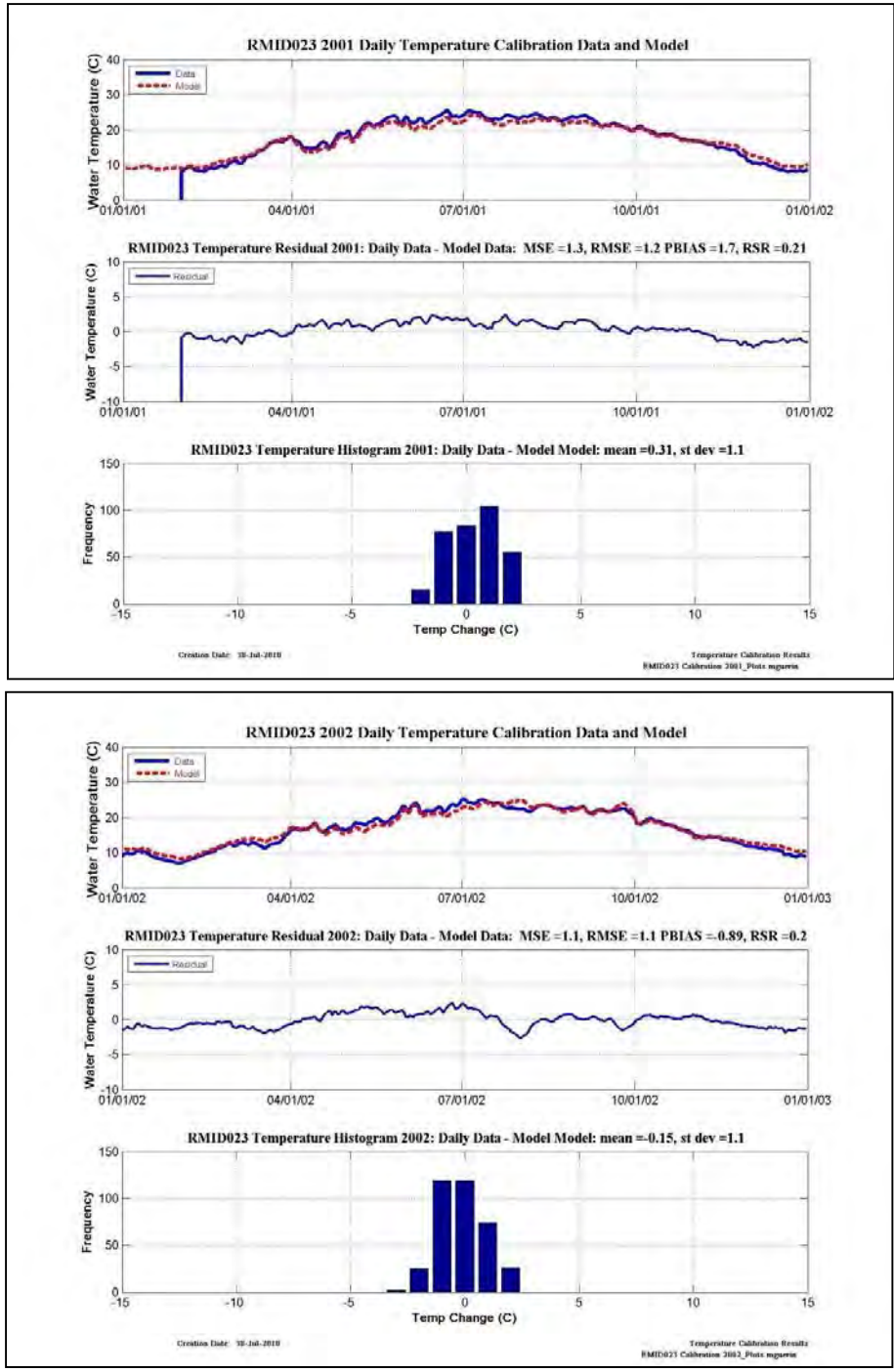
Dry-Calibration	NSE	PBIAS	Bias	RSR
2001	VG	VG	Underestimate	U
2002	VG	VG	Underestimate	VG

Figure 9-29 Dry year temperature calibration plots, residual plots, histograms and categorical statistics at RMID023.
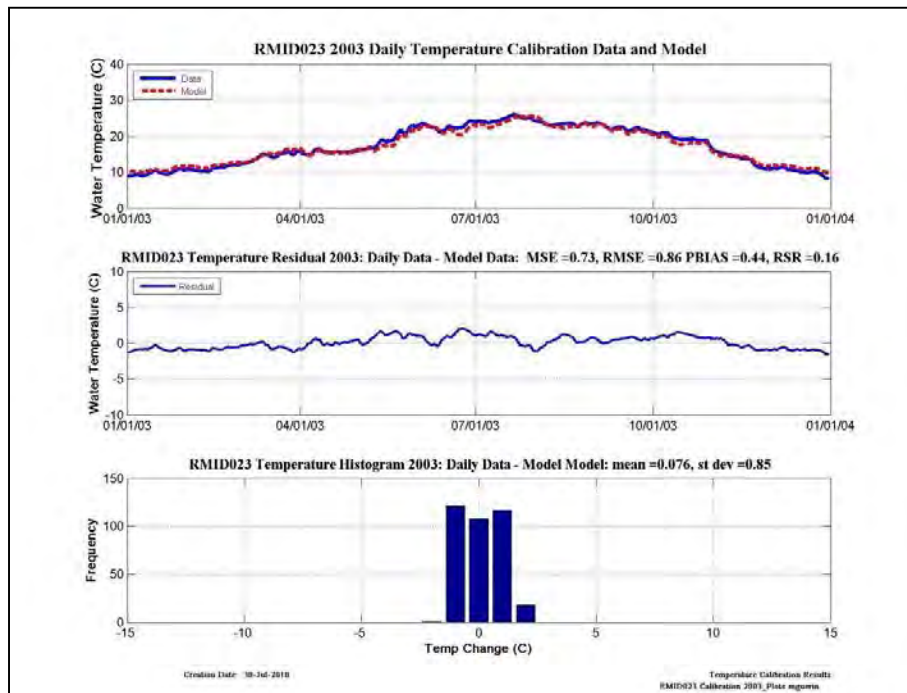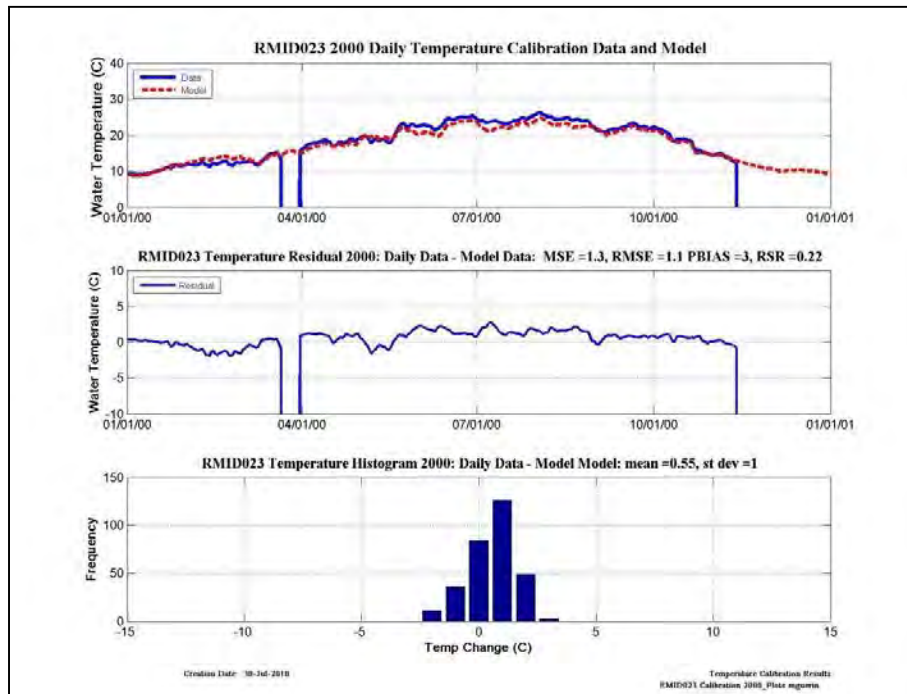
Wet-Calibration	NSE	PBIAS	Bias	RSR
2000	VG	VG	Underestimate	U
2003	VG	VG	Underestimate	VG

Figure 9-30 Wet year temperature calibration plots, residual plots, histograms and categorical statistics at RMID023.
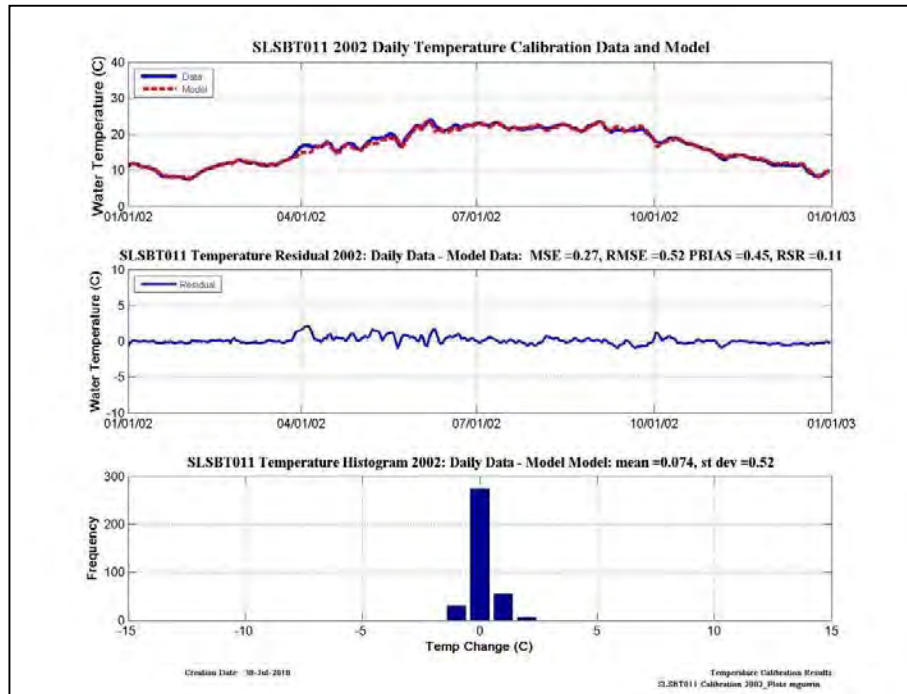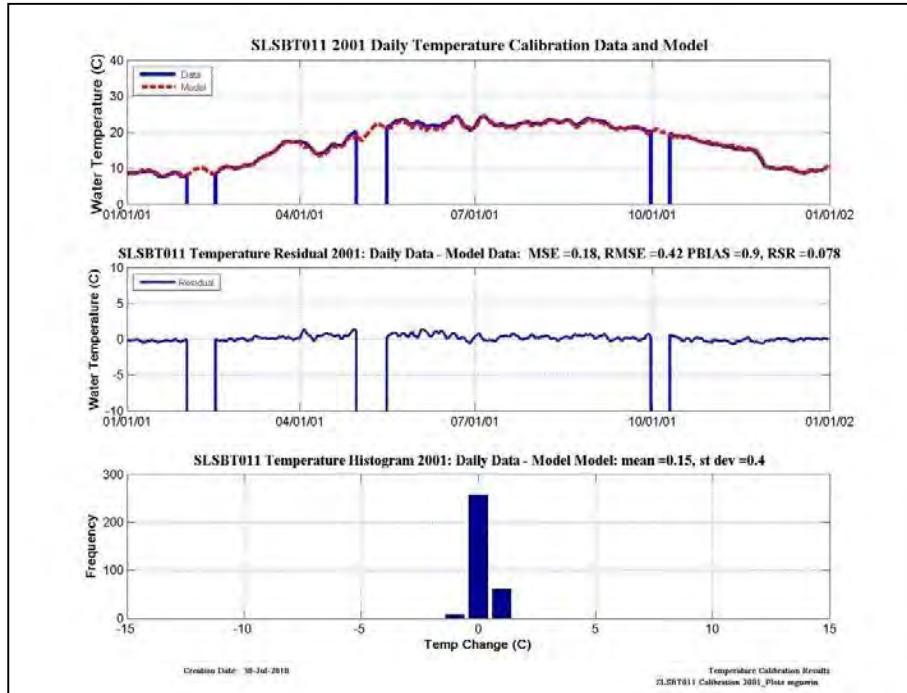
Dry-Calibration	NSE	PBIAS	Bias	RSR
2001	VG	VG	Underestimate	VG
2002	VG	VG	Underestimate	VG

Figure 9-31 Dry year temperature calibration plots, residual plots, histograms and categorical statistics at SLSBT011.
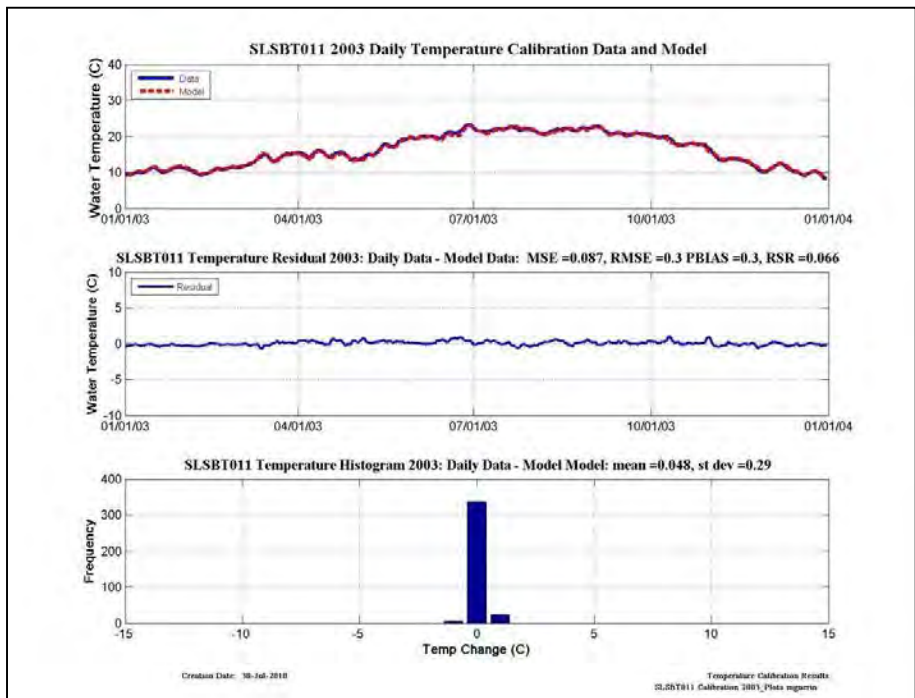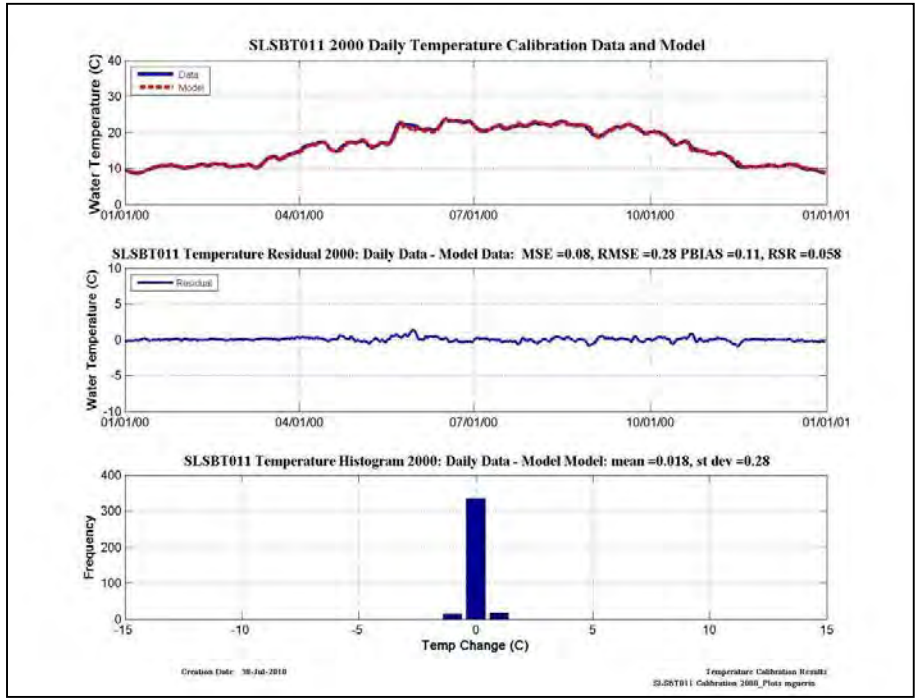
Wet-Calibration	NSE	PBIAS	Bias	RSR
2000	VG	VG	Underestimate	VG
2003	VG	VG	Underestimate	VG

Figure 9-32 Wet year temperature calibration plots, residual plots, histograms and categorical statistics at SLSBT011.

Validation results
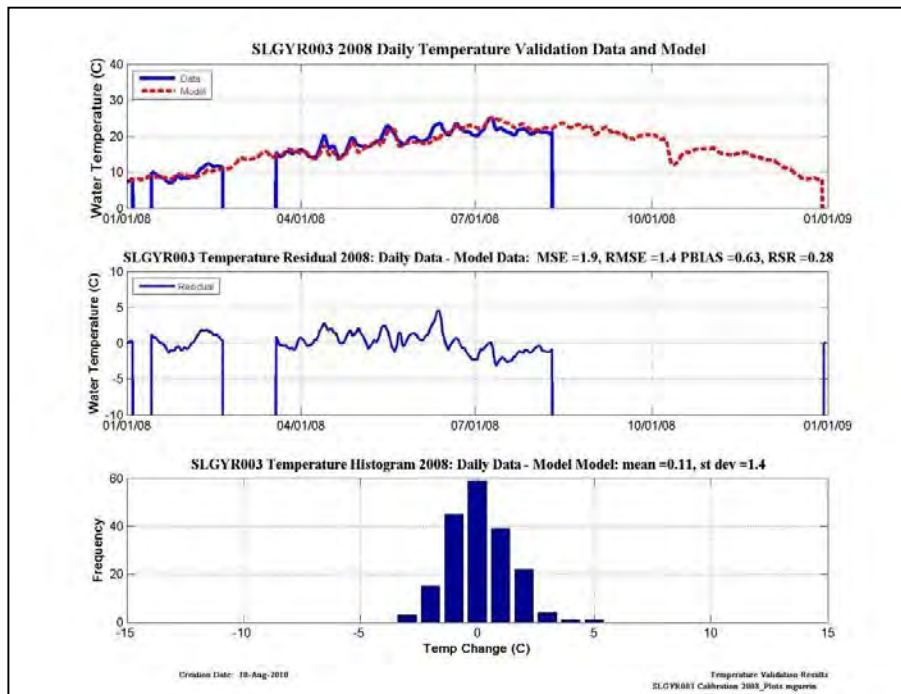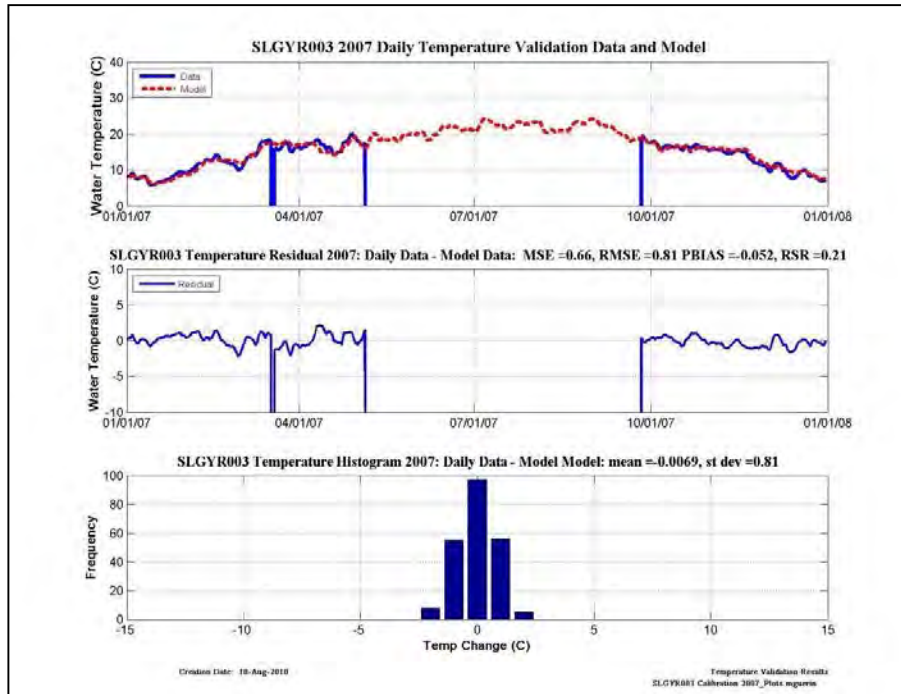
Dry-Validation	NSE	PBIAS	Bias	RSR
2007	VG	VG	Overestimate	VG
2008	VG	VG	Underestimate	VG

Figure 9-33 Dry year temperature validation plots, residual plots, histograms and categorical statistics at SLGYR003.
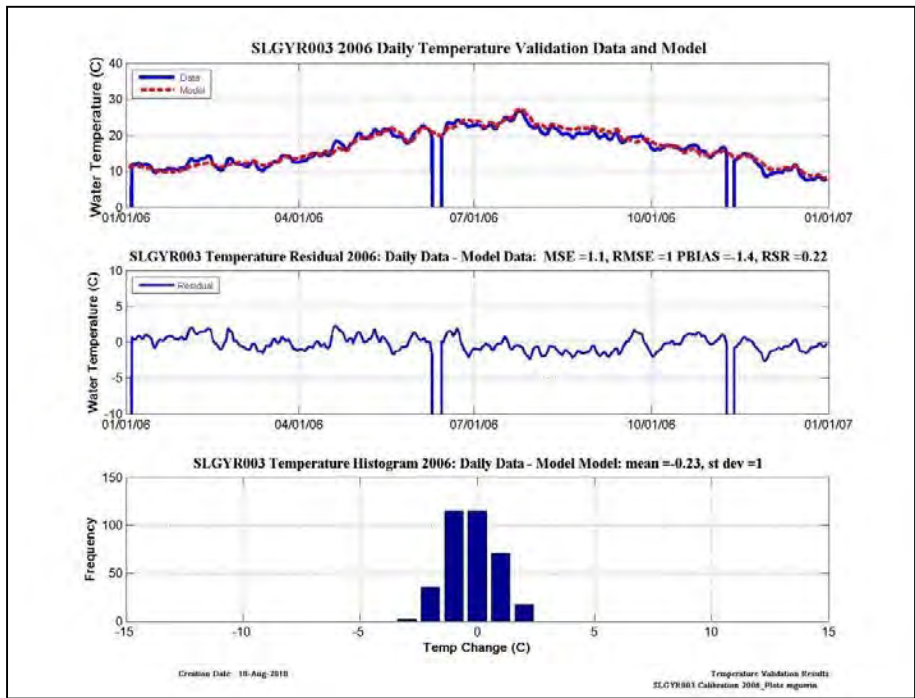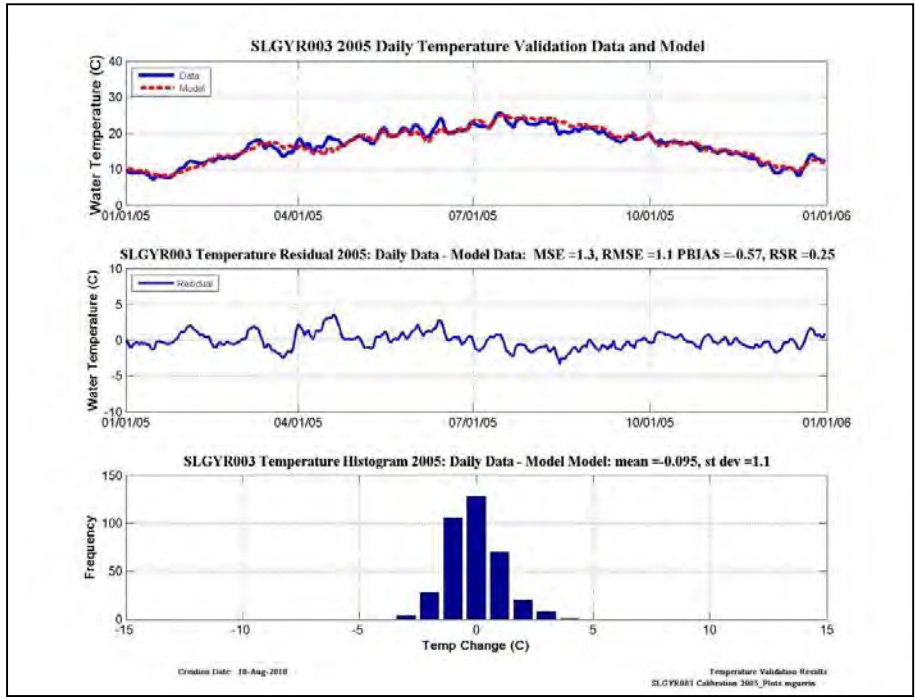
Wet-Validation	NSE	PBIAS	Bias	RSR
2005	VG	VG	Overestimate	VG
2006	VG	VG	Overestimate	VG

Figure 9-34 Wet year temperature validation plots, residual plots, histograms and categorical statistics at SLGYR003.
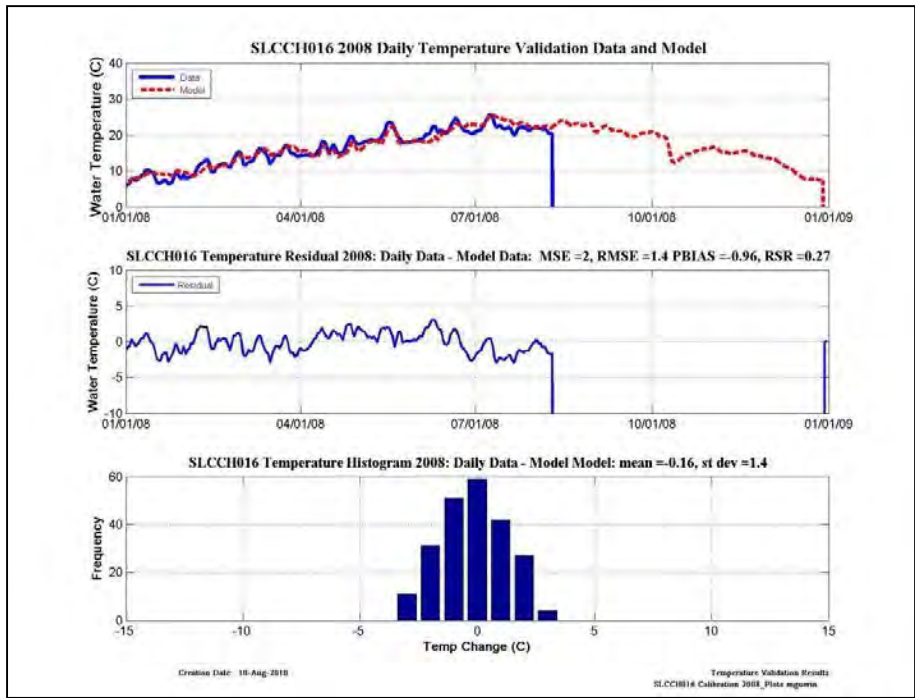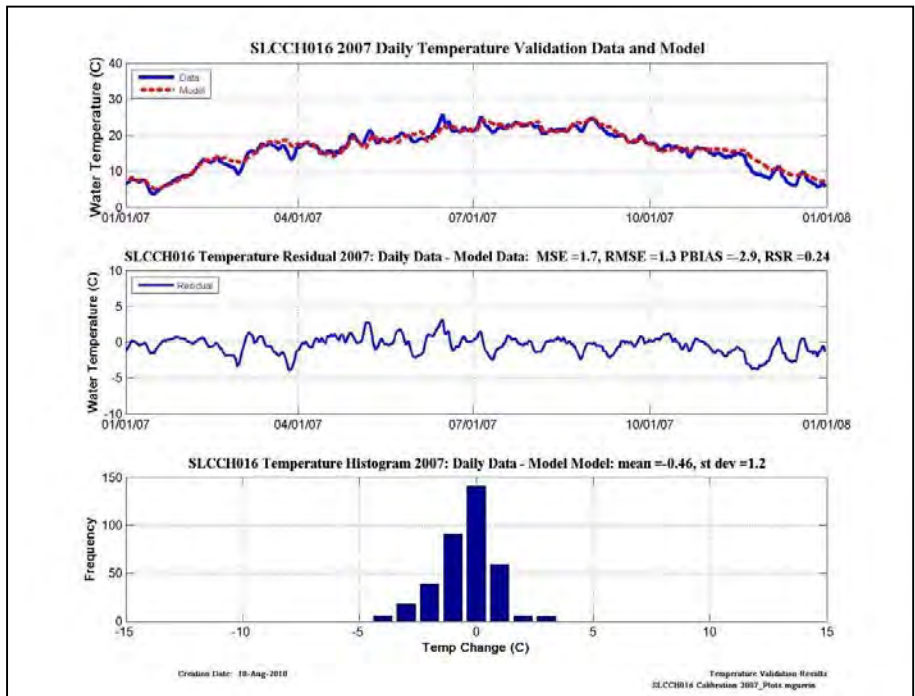
Dry-Validation	NSE	PBIAS	Bias	RSR
2007	VG	VG	Overestimate	VG
2008	VG	VG	Overestimate	VG

Figure 9-35 Dry year temperature validation plots, residual plots, histograms and categorical statistics at SLCCH016.
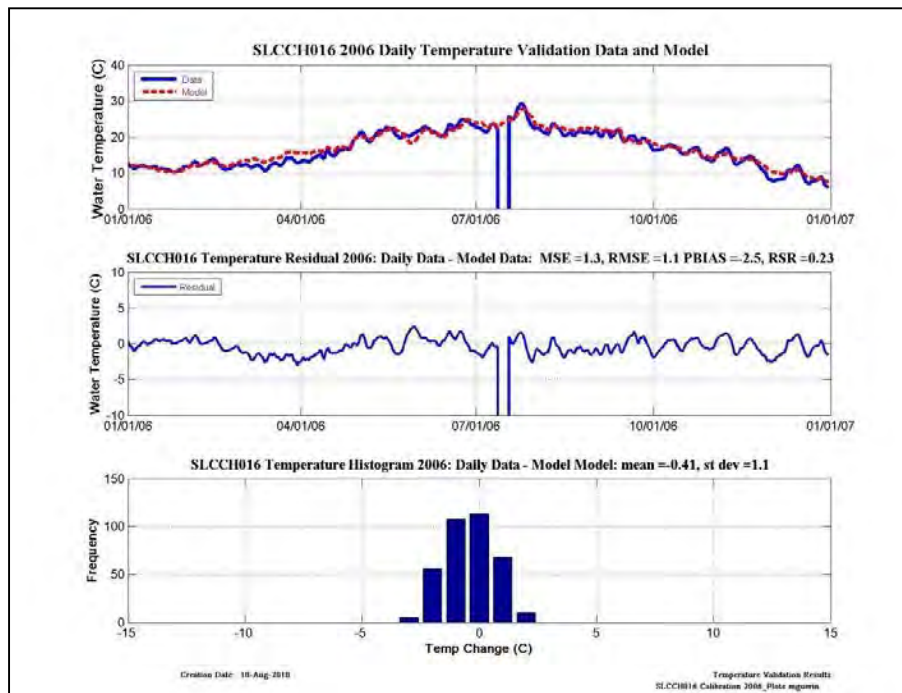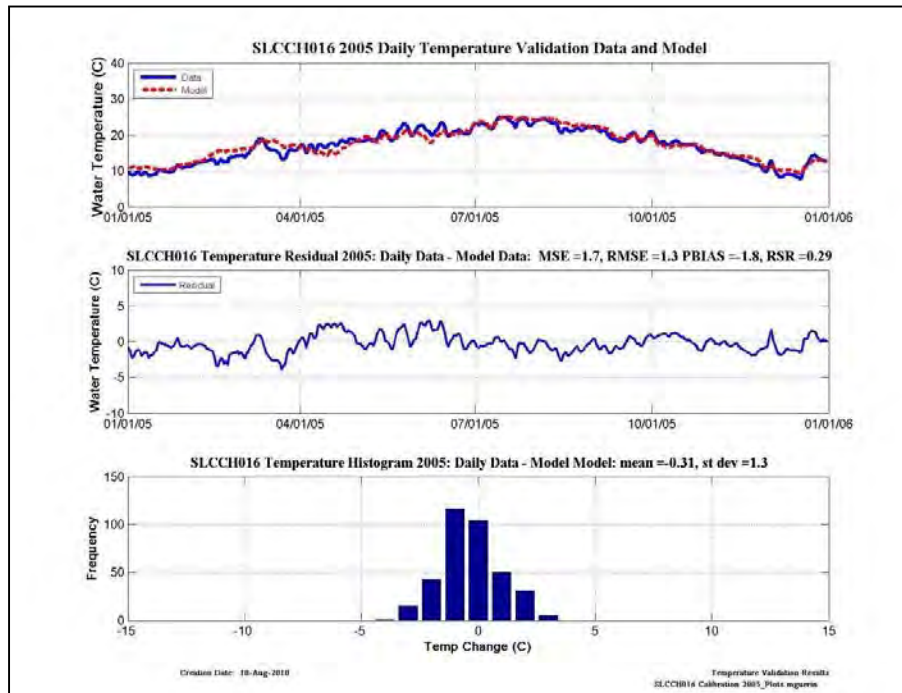
Wet-Validation	NSE	PBIAS	Bias	RSR
2005	VG	VG	Overestimate	VG
2006	VG	VG	Overestimate	VG

Figure 9-36 Wet year temperature validation plots, residual plots, histograms and categorical statistics at SLCCH016.
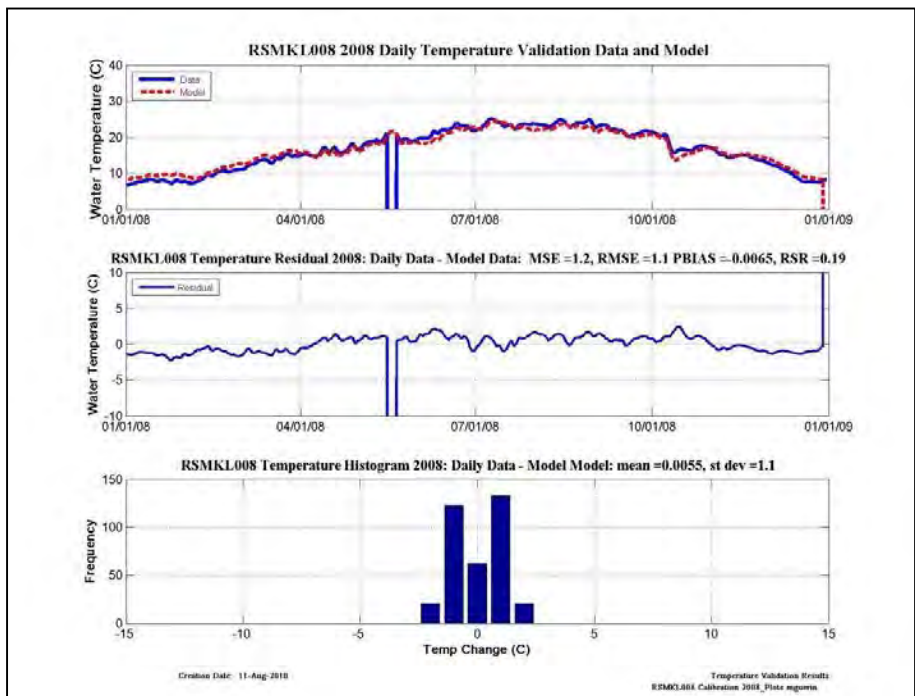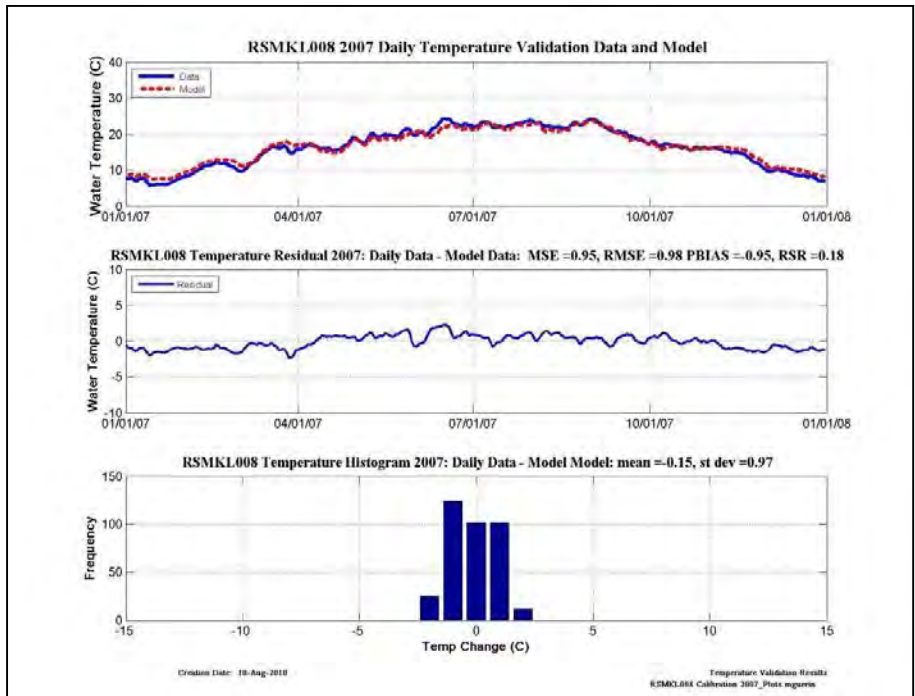
Dry-Validation	NSE	PBIAS	Bias	RSR
2007	VG	VG	Overestimate	VG
2008	VG	VG	Overestimate	VG

Figure 9-37 Dry year temperature validation plots, residual plots, histograms and categorical statistics at RSMKL008.
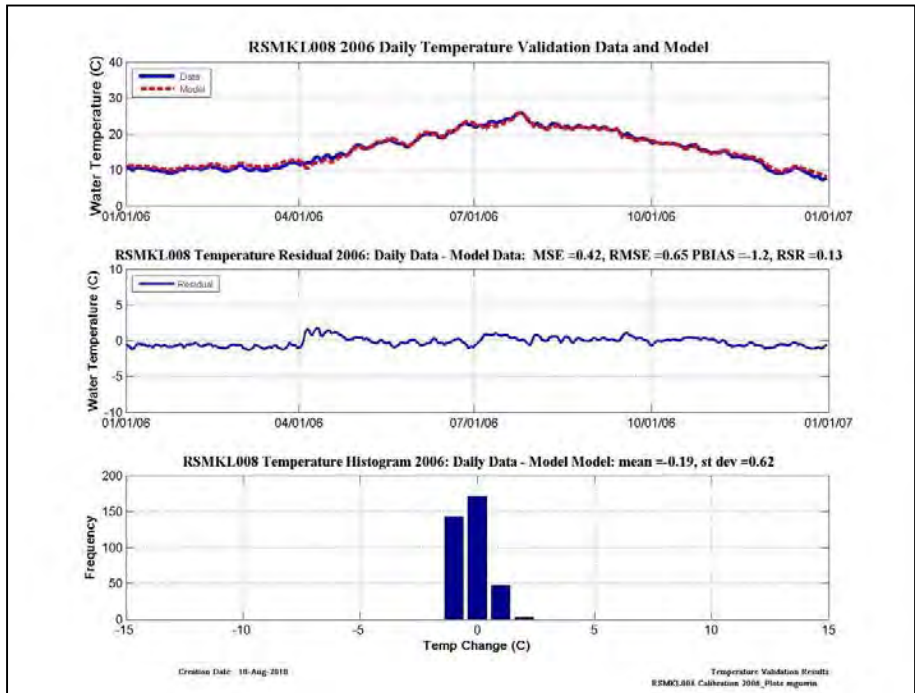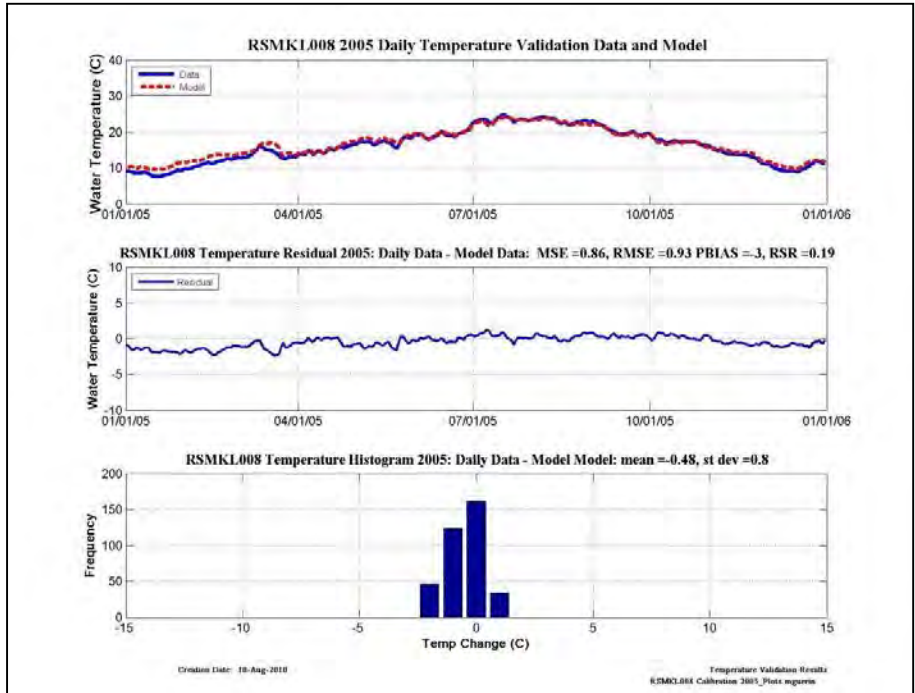
Wet-Validation	NSE	PBIAS	Bias	RSR
2005	VG	VG	Overestimate	VG
2006	VG	VG	Overestimate	VG

Figure 9-38 Wet year temperature validation plots, residual plots, histograms and categorical statistics at RSMKL008.
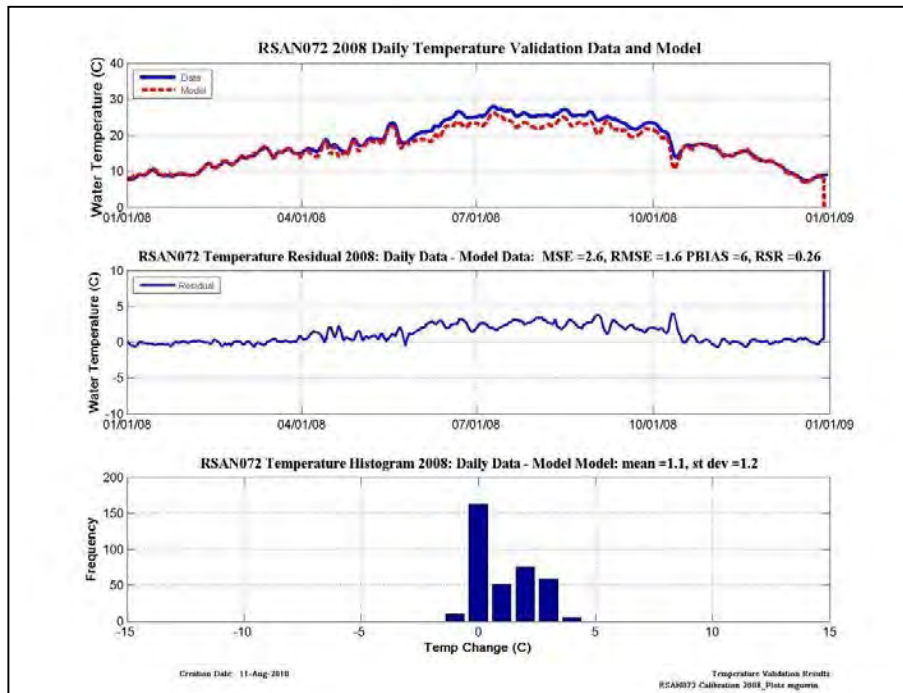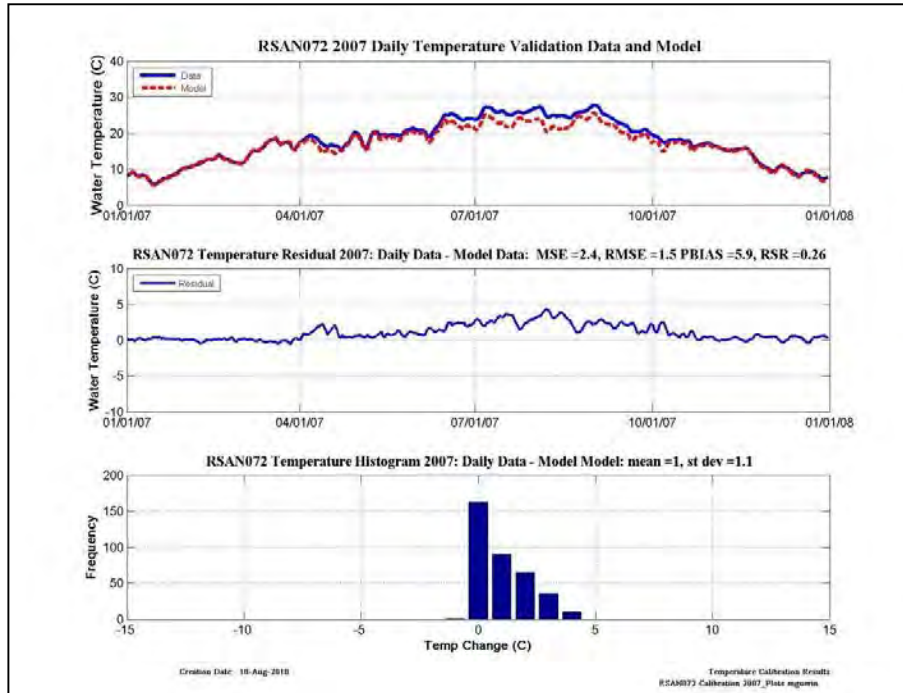
Dry-Validation	NSE	PBIAS	Bias	RSR
2007	VG	VG	Underestimate	VG
2008	VG	VG	Underestimate	VG

Figure 9-39 Dry year temperature validation plots, residual plots, histograms and categorical statistics at RSAN072.
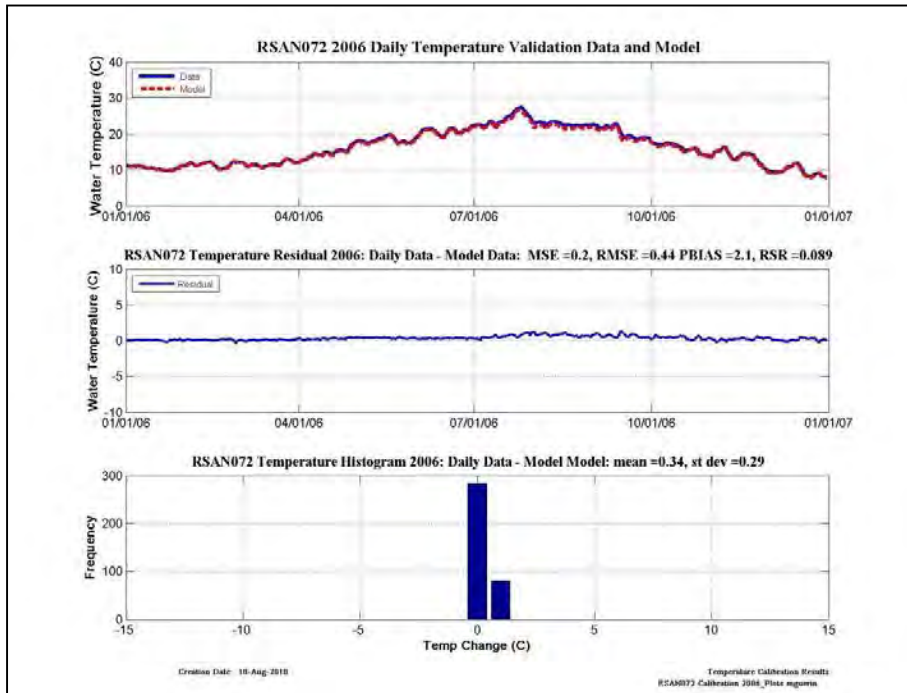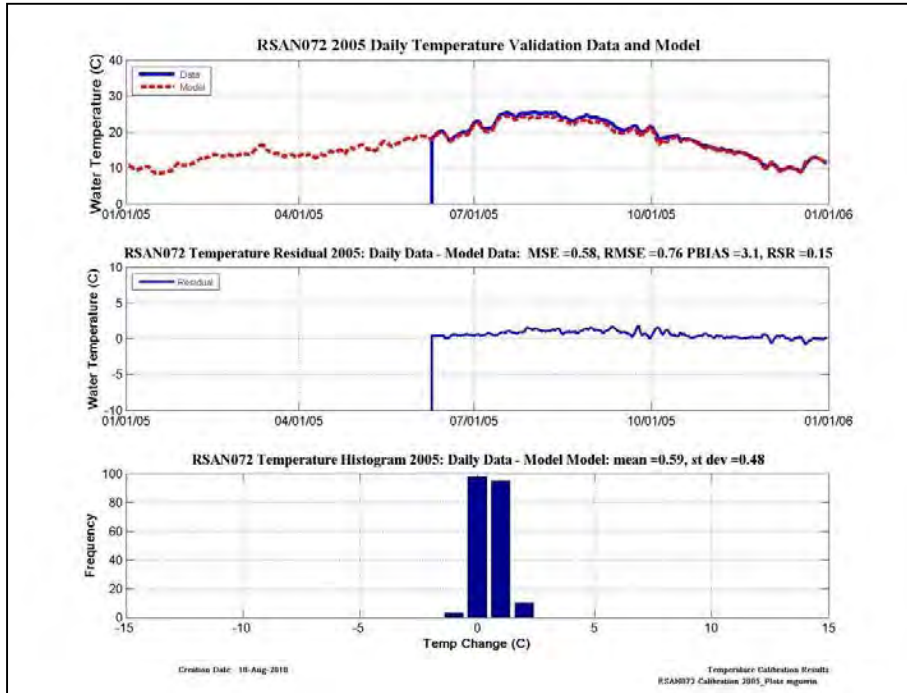
Wet-Validation	NSE	PBIAS	Bias	RSR
2005	VG	VG	Underestimate	VG
2006	VG	VG	Underestimate	VG

Figure 9-40 Wet year temperature validation plots, residual plots, histograms and categorical statistics at RSAN072.

187
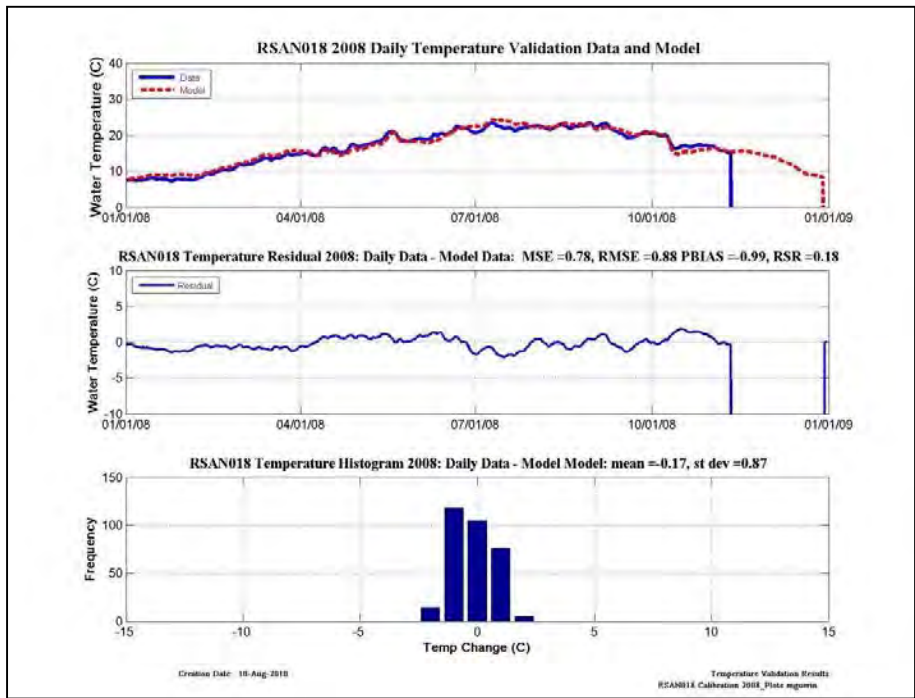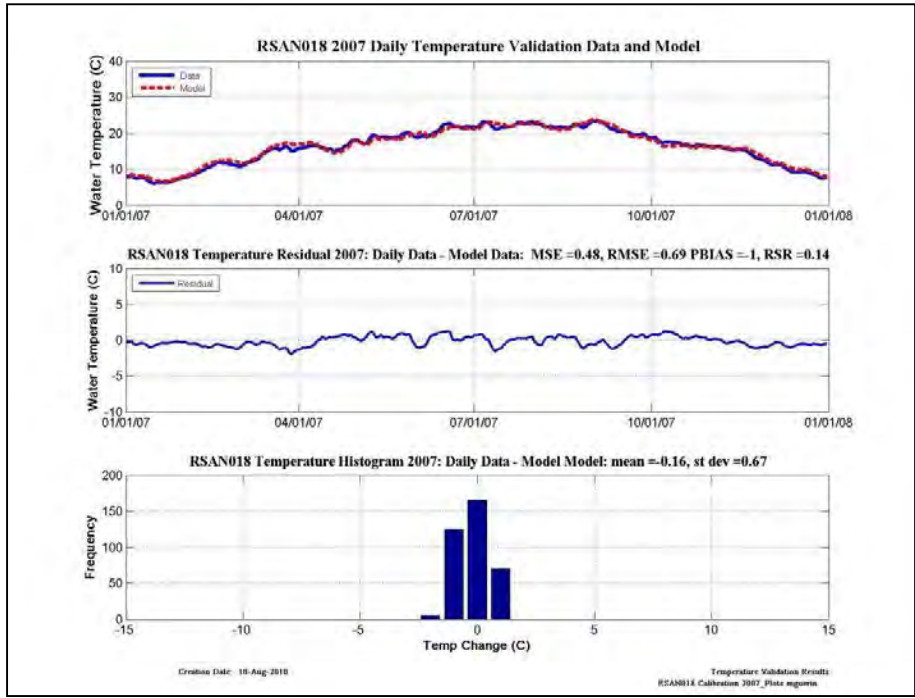
Dry-Validation	NSE	PBIAS	Bias	RSR
2007	VG	VG	Overestimate	VG
2008	VG	VG	Overestimate	VG

Figure 9-41 Dry year temperature validation plots, residual plots, histograms and categorical statistics at RSAN 018.
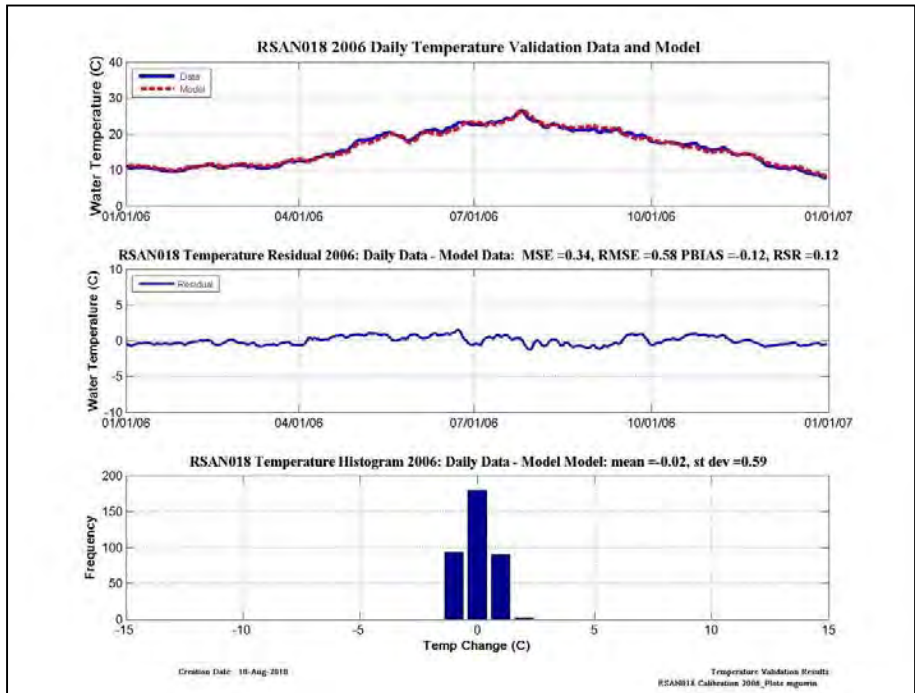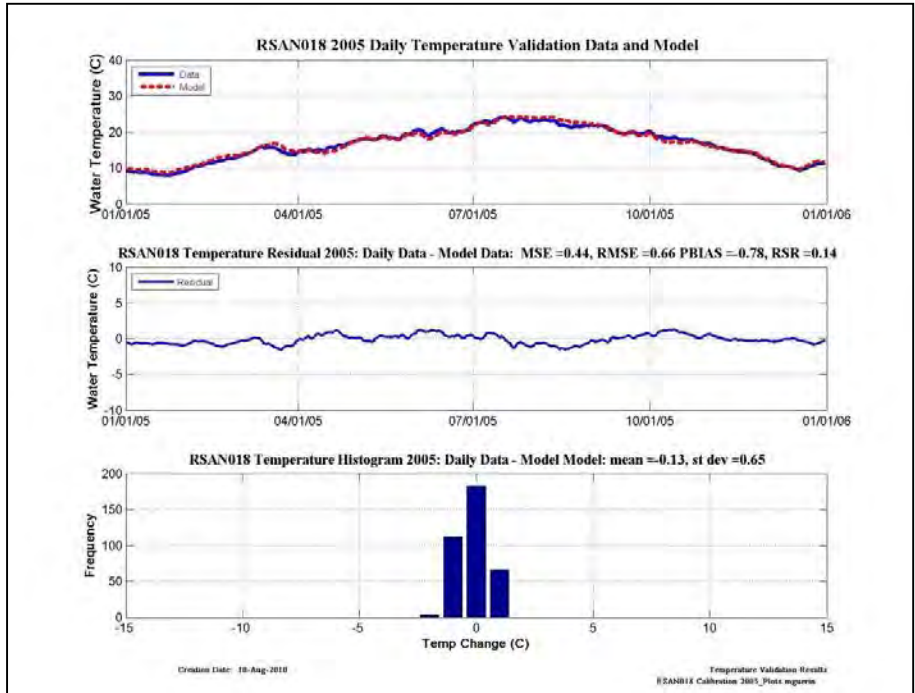
Wet-Validation	NSE	PBIAS	Bias	RSR
2005	VG	VG	Overestimate	VG
2006	VG	VG	Overestimate	VG

Figure 9-42 Wet year temperature validation plots, residual plots, histograms and categorical statistics at RSAN018.
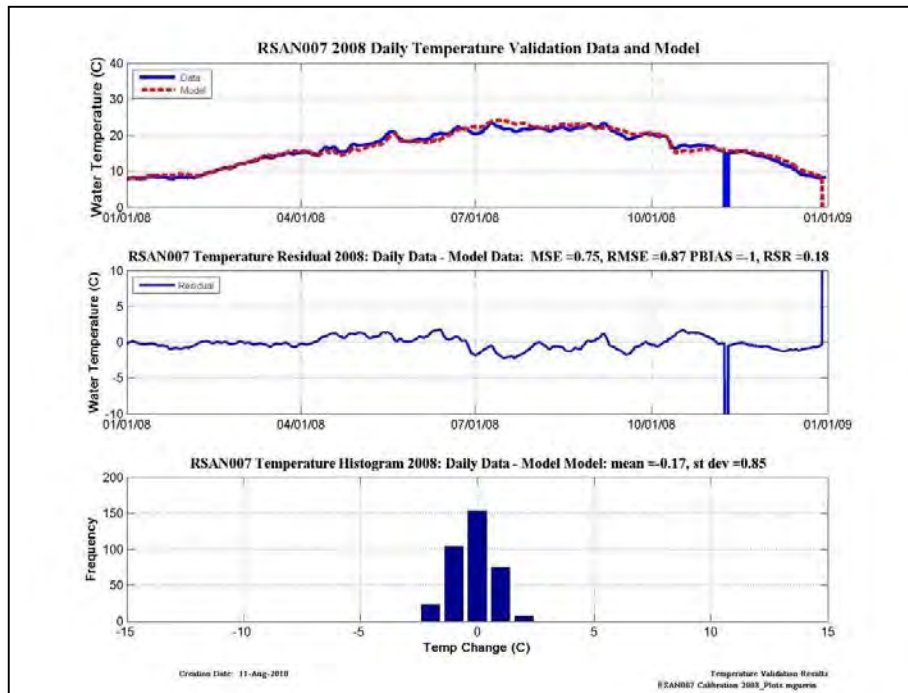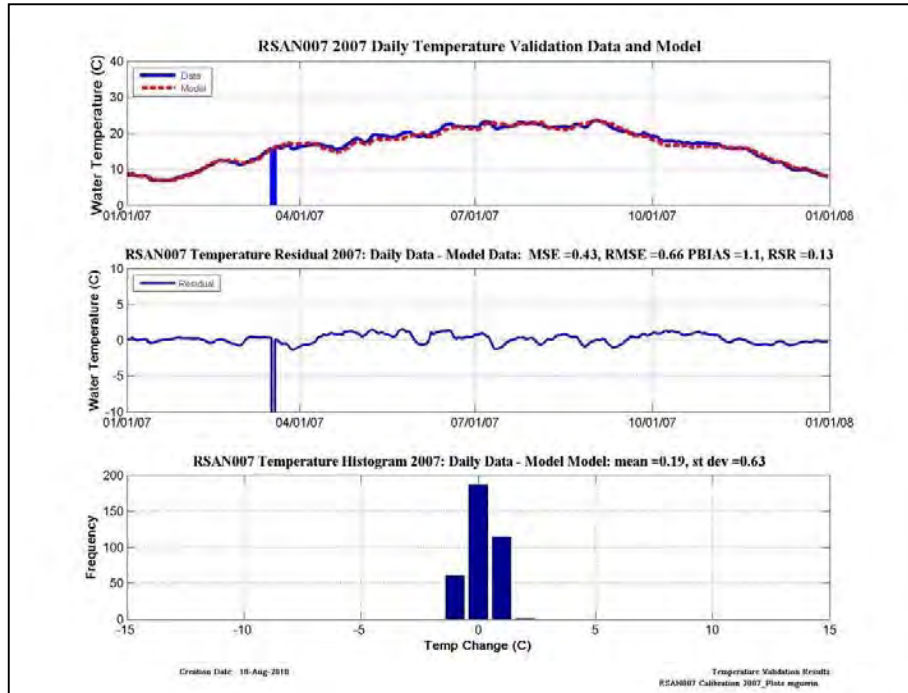
Dry-Validation	NSE	PBIAS	Bias	RSR
2007	VG	VG	Underestimate	VG
2008	VG	VG	Underestimate	VG

Figure 9-43 Dry year temperature validation plots, residual plots, histograms and categorical statistics at RSAN007.
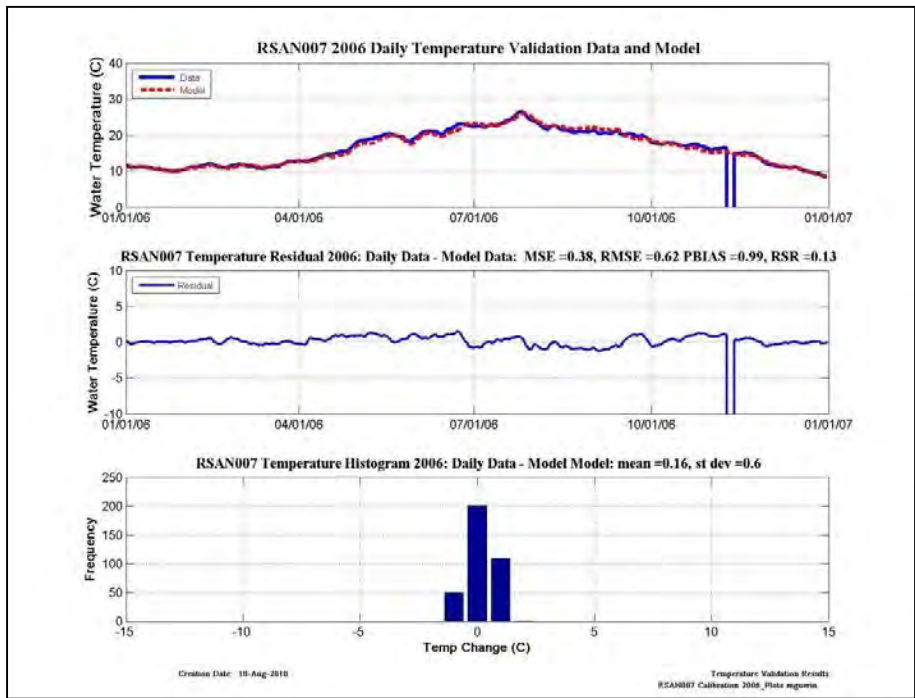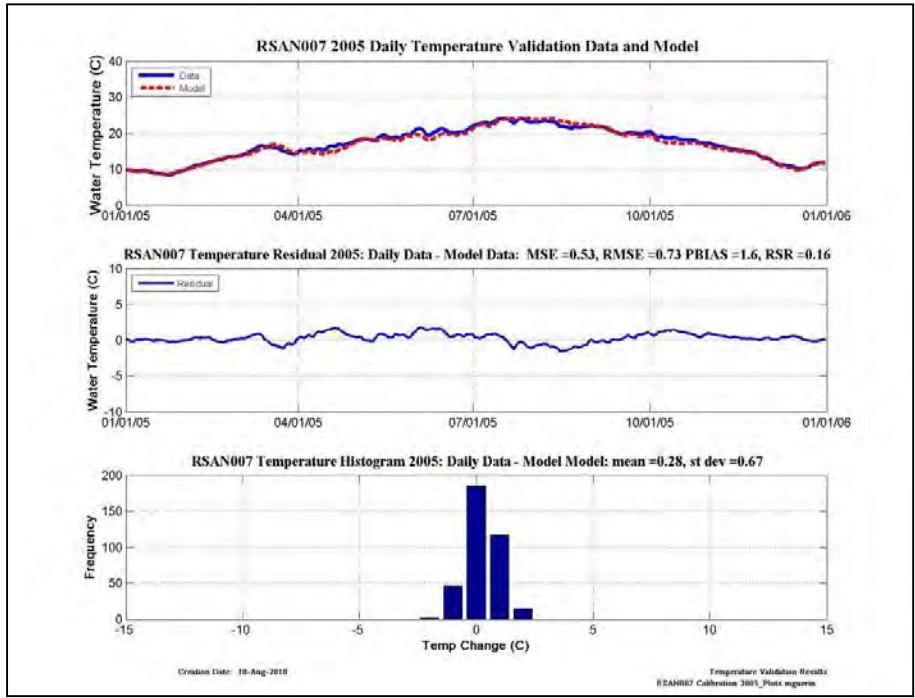
Wet-Validation	NSE	PBIAS	Bias	RSR
2005	VG	VG	Underestimate	VG
2006	VG	VG	Underestimate	VG

Figure 9-44 Wet year temperature validation plots, residual plots, histograms and categorical statistics at RSAN007
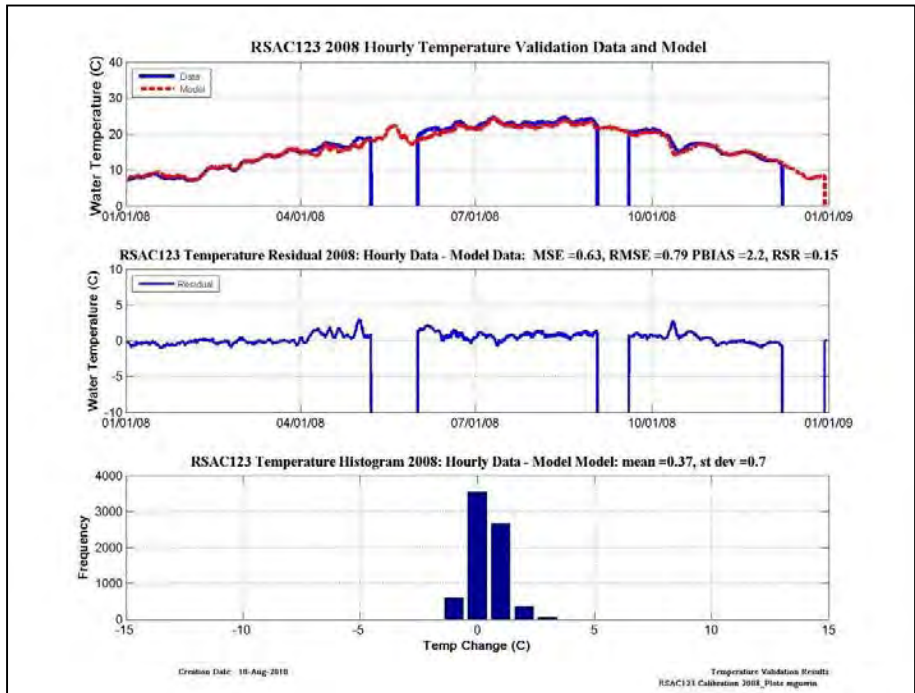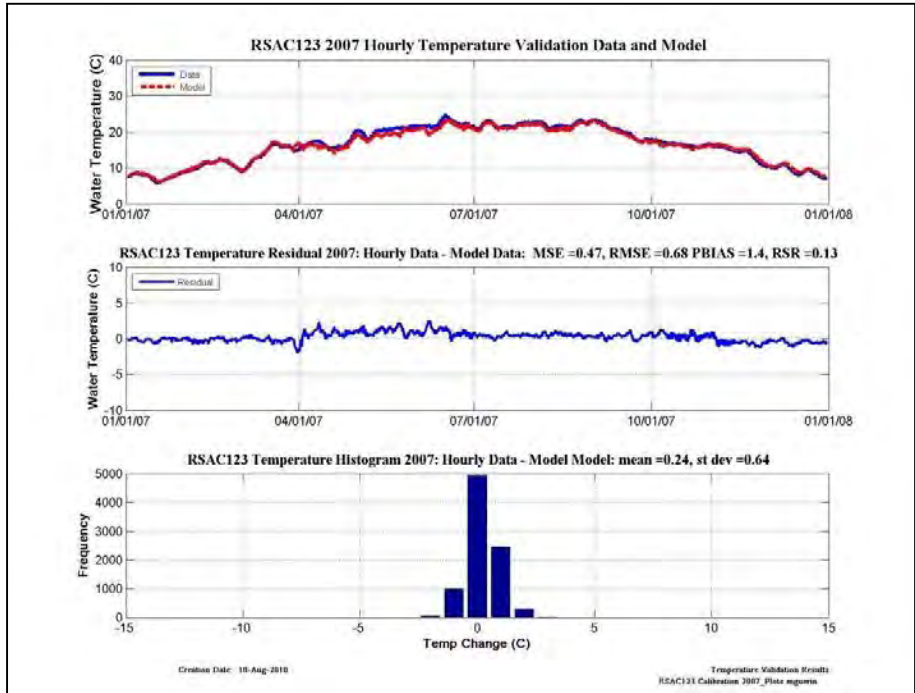
Dry-Validation	NSE	PBIAS	Bias	RSR
2007	VG	VG	Underestimate	VG
2008	VG	VG	Underestimate	VG

Figure 9-45 Dry year temperature validation plots, residual plots, histograms and categorical statistics at RSAC123.
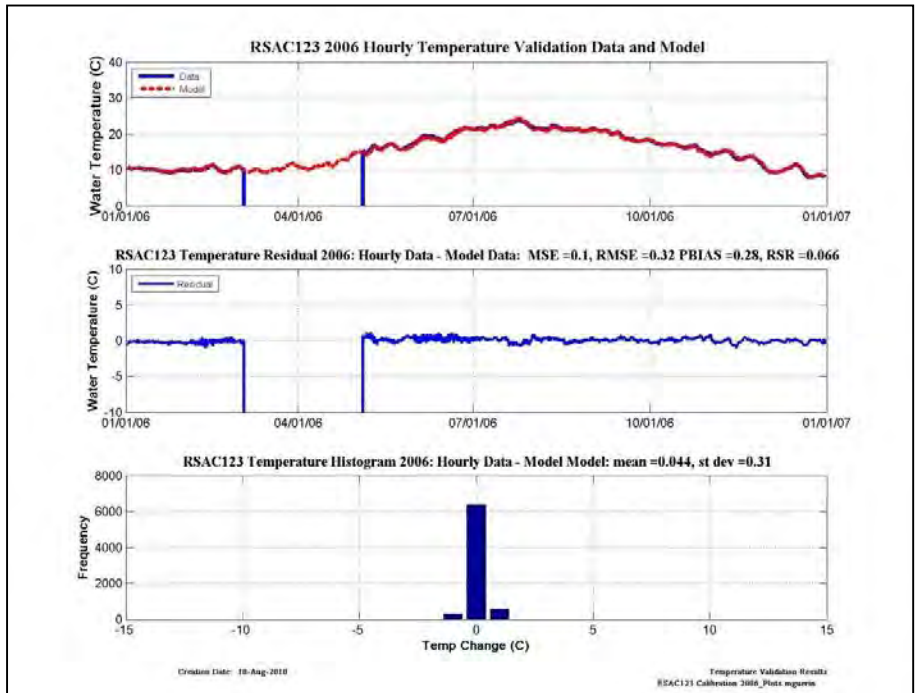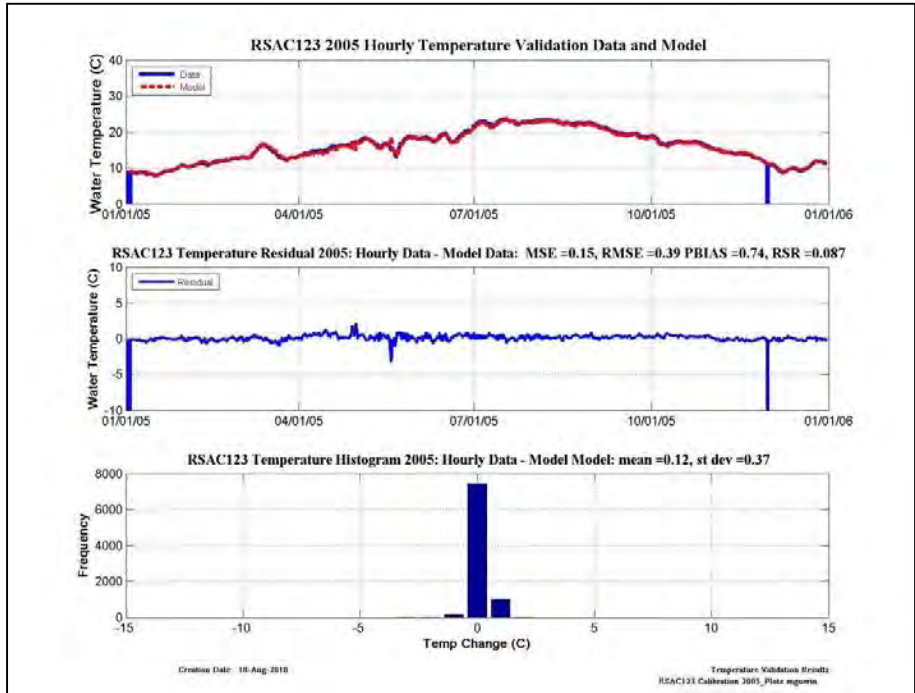
Wet-Validation	NSE	PBIAS	Bias	RSR
2005	VG	VG	Underestimate	VG
2006	VG	VG	Underestimate	VG

Figure 9-46 Wet year temperature validation plots, residual plots, histograms and categorical statistics at RSAC123.
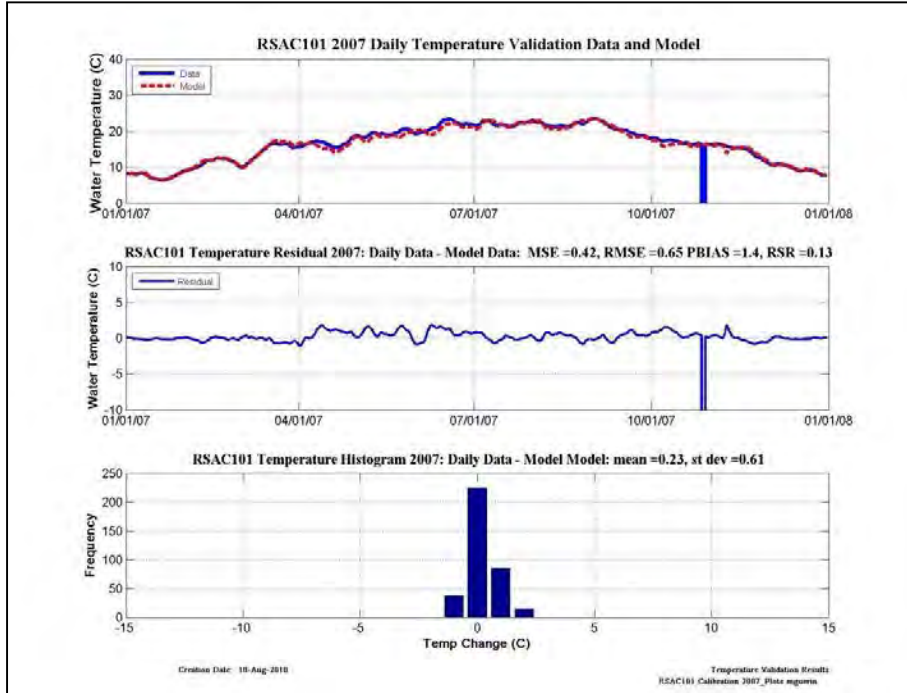
Dry-Validation	NSE	PBIAS	Bias	RSR
2007	VG	VG	Underestimate	VG
2008				

Figure 9-47 Dry year temperature validation plots, residual plots, histograms and categorical statistics at RSAC101.
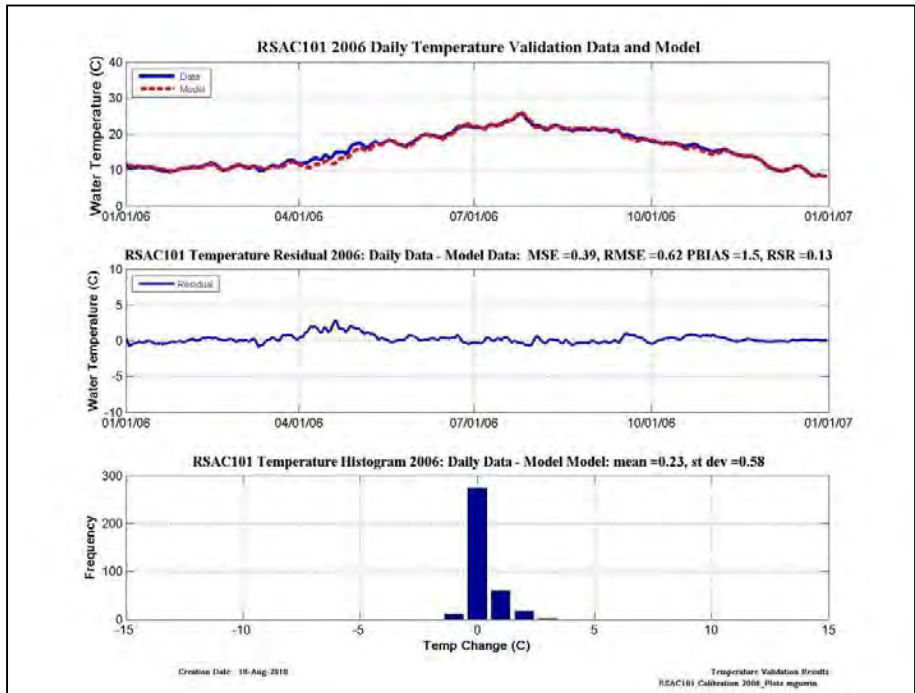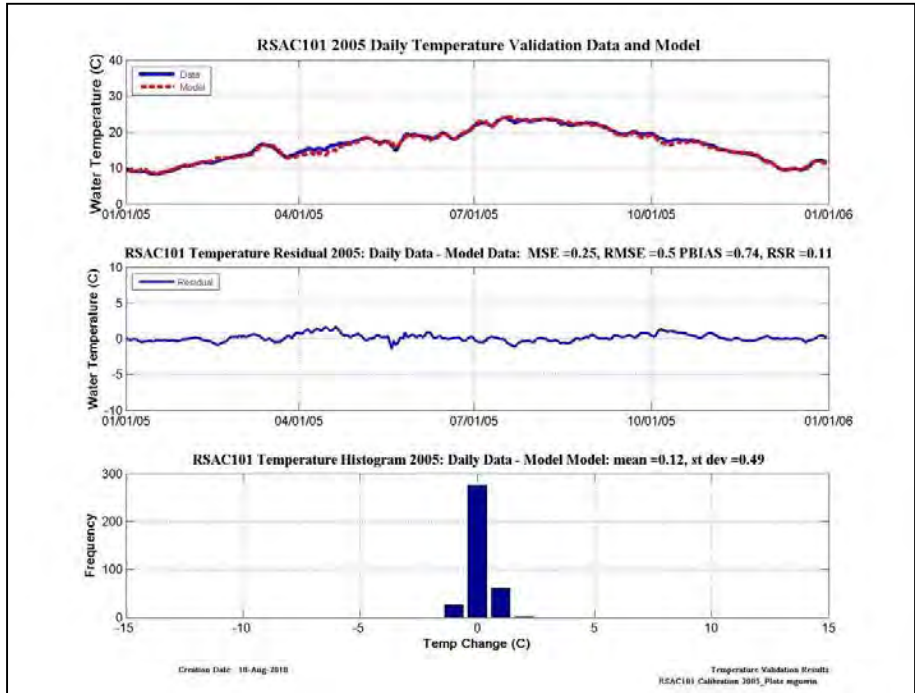
Wet-Validation	NSE	PBIAS	Bias	RSR
2005	VG	VG	Underestimate	VG
2006	VG	VG	Underestimate	VG

Figure 9-48 Wet year temperature validation plots, residual plots, histograms and categorical statistics at RSAC101.
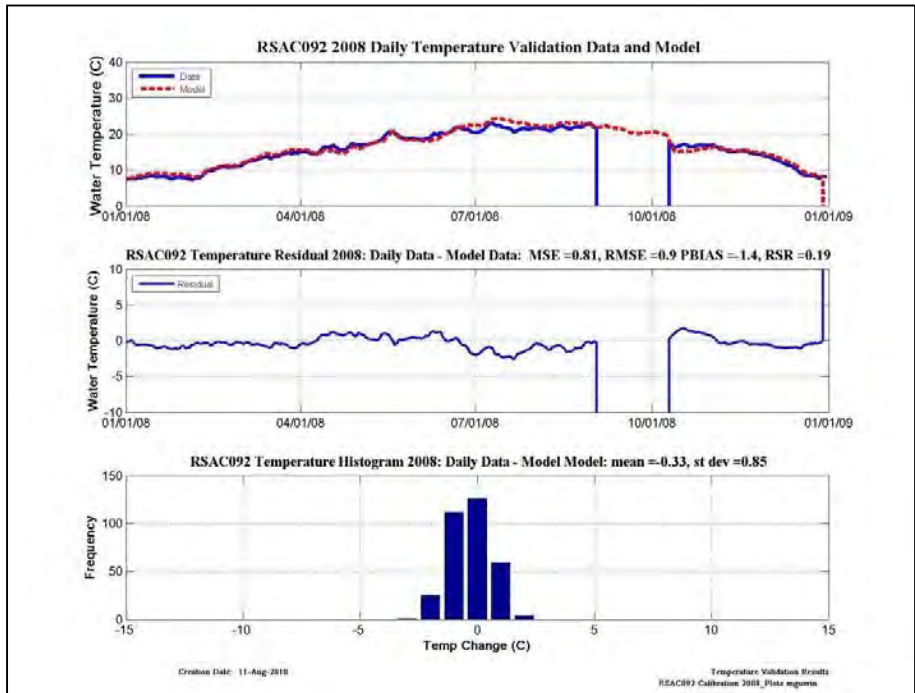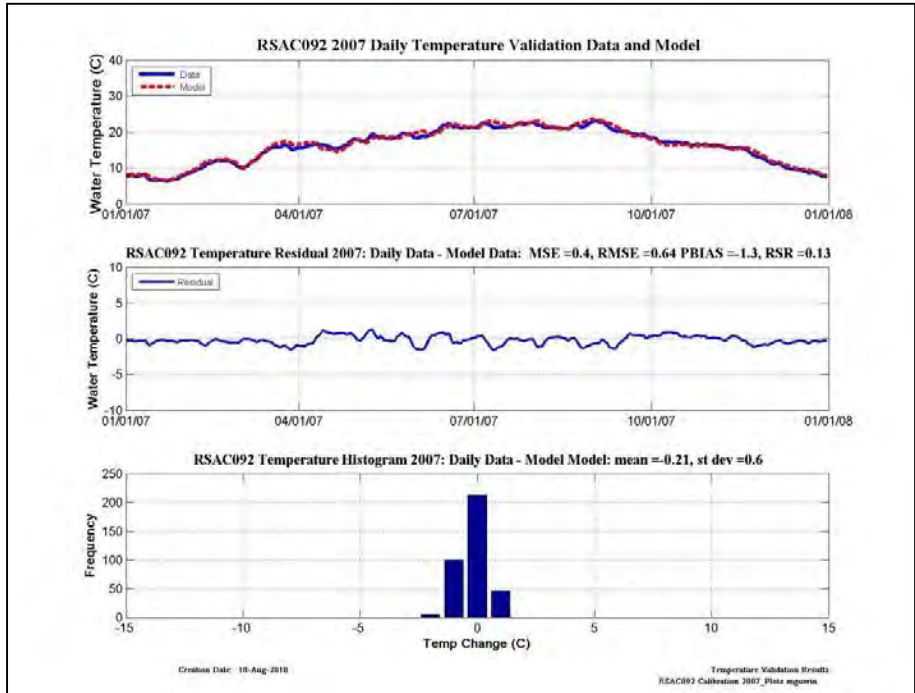
Dry-Validation	NSE	PBIAS	Bias	RSR
2007	VG	VG	Overestimate	VG
2008	VG	VG	Overestimate	VG

Figure 9-49 Dry year temperature validation plots, residual plots, histograms and categorical statistics at RSAC092.
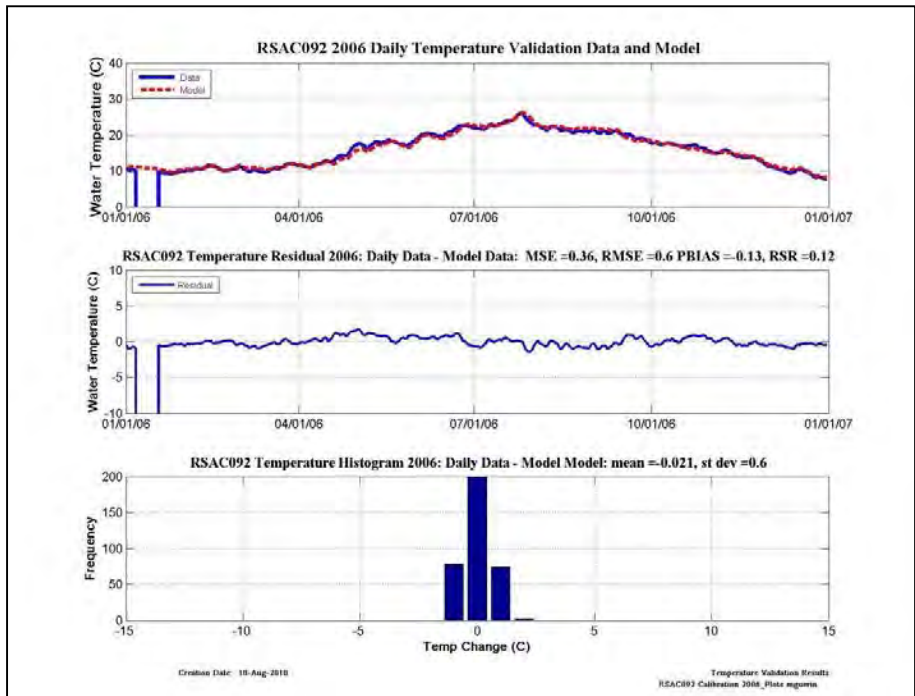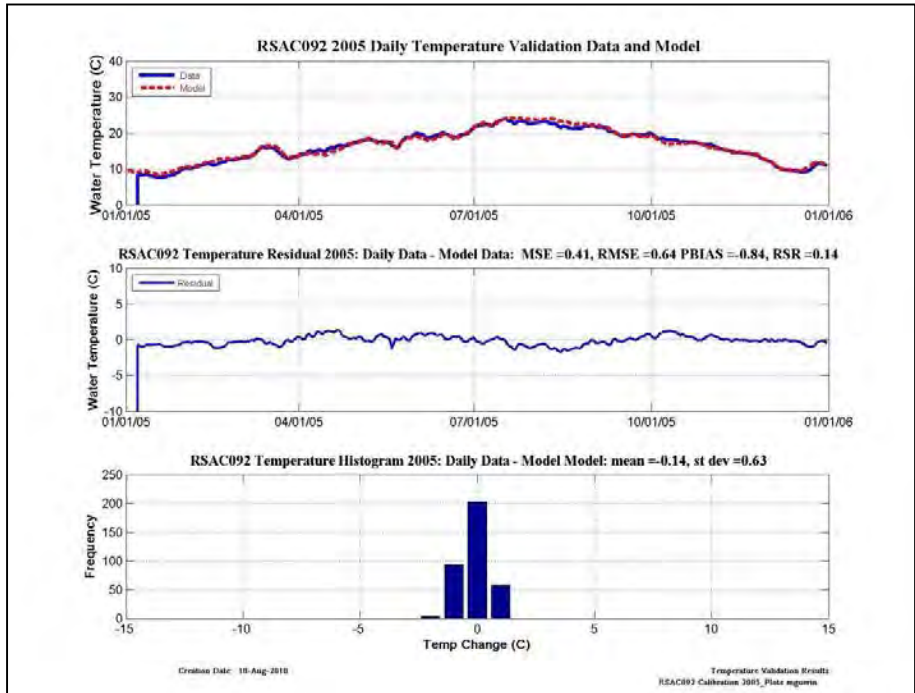
Wet-Validation	NSE	PBIAS	Bias	RSR
2005	VG	VG	Overestimate	VG
2006	VG	VG	Overestimate	VG

Figure 9-50 Wet year temperature validation plots, residual plots, histograms and categorical statistics at RSAC092.

197
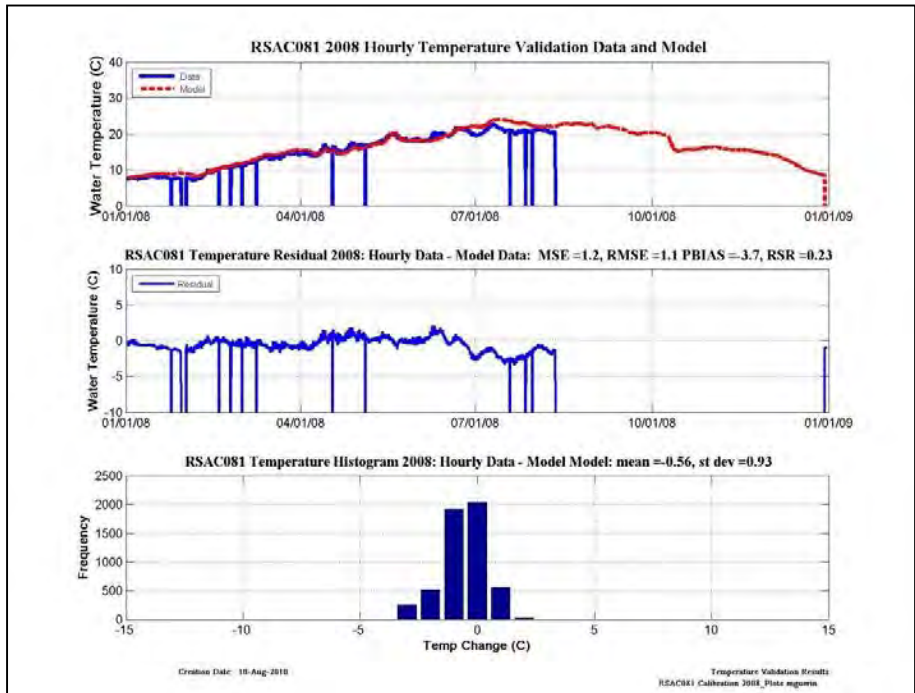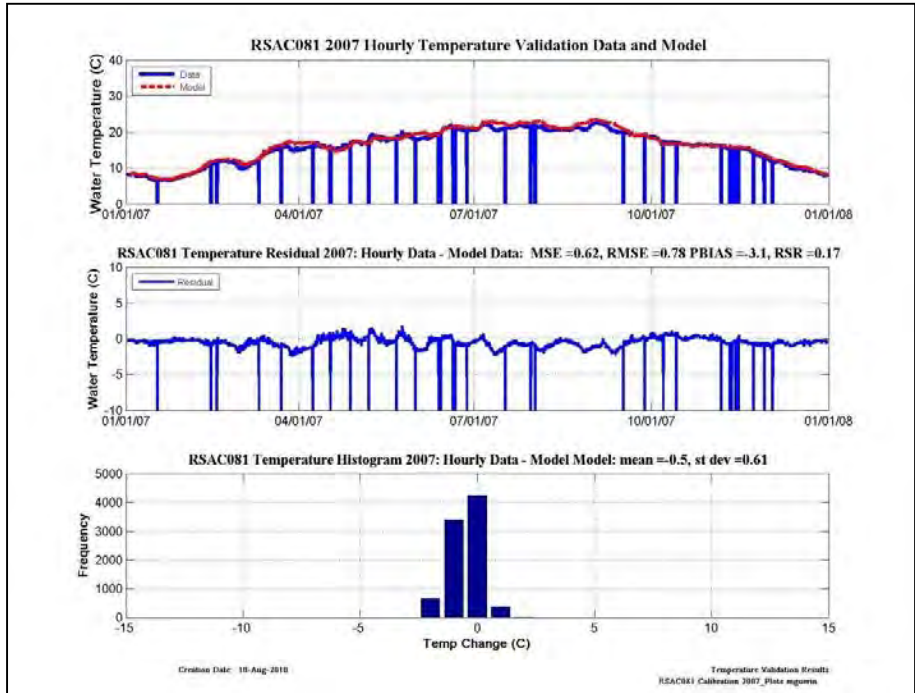
Dry-Validation	NSE	PBIAS	Bias	RSR
2007	VG	VG	Overestimate	VG
2008	VG	VG	Overestimate	VG

Figure 9-51 Dry year temperature validation plots, residual plots, histograms and categorical statistics at RSAC081.
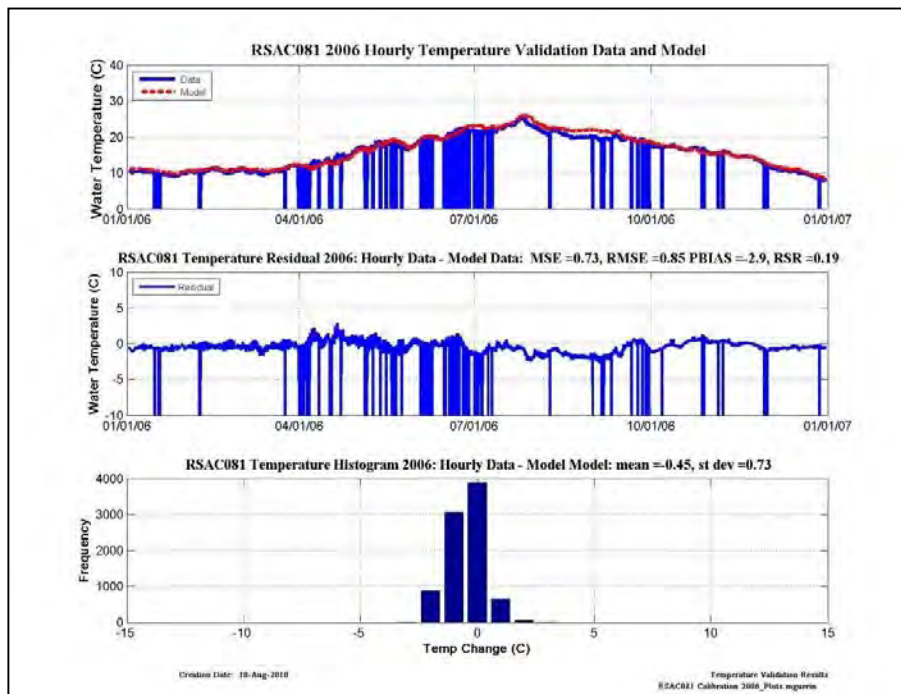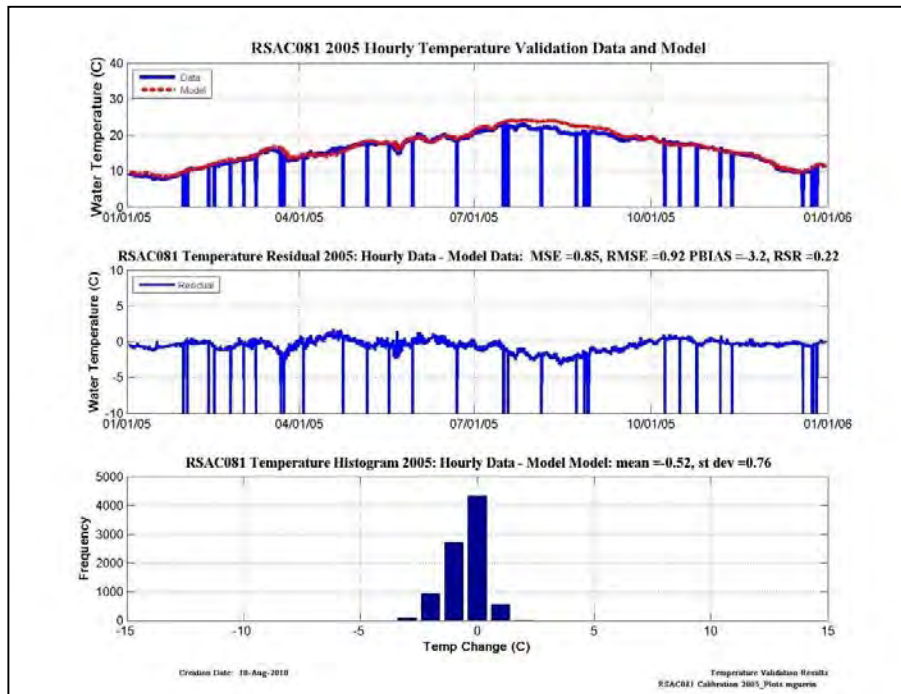
Wet-Validation	NSE	PBIAS	Bias	RSR
2005	VG	VG	Overestimate	VG
2006	VG	VG	Overestimate	VG

Figure 9-52 Wet year temperature validation plots, residual plots, histograms and categorical statistics at RSAC081.
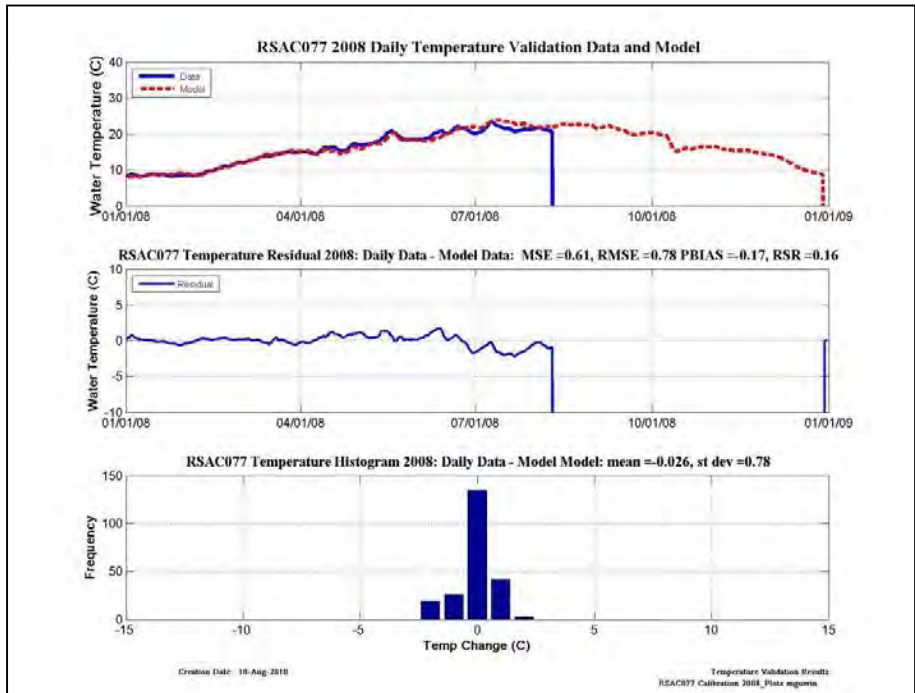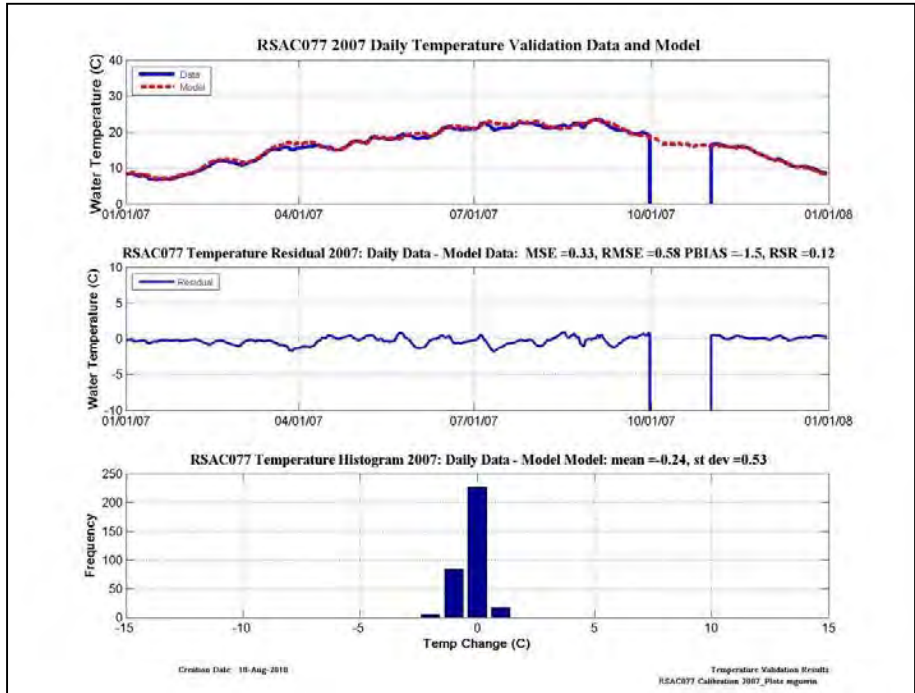
Dry-Validation	NSE	PBIAS	Bias	RSR
2007	VG	VG	Overestimate	VG
2008	VG	VG	Overestimate	VG

Figure 9-53 Dry year temperature validation plots, residual plots, histograms and categorical statistics at RSAC077.
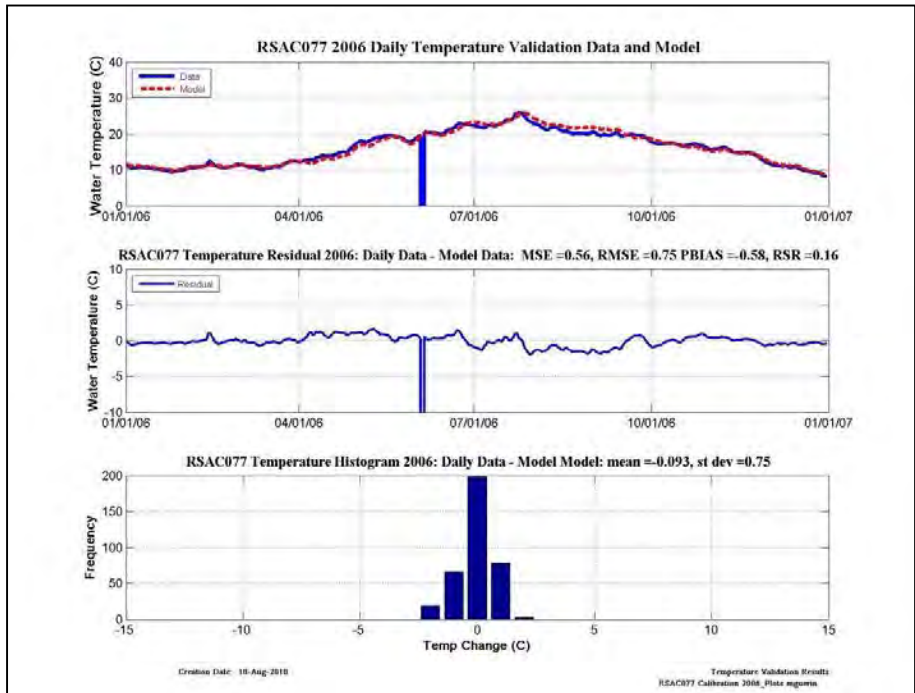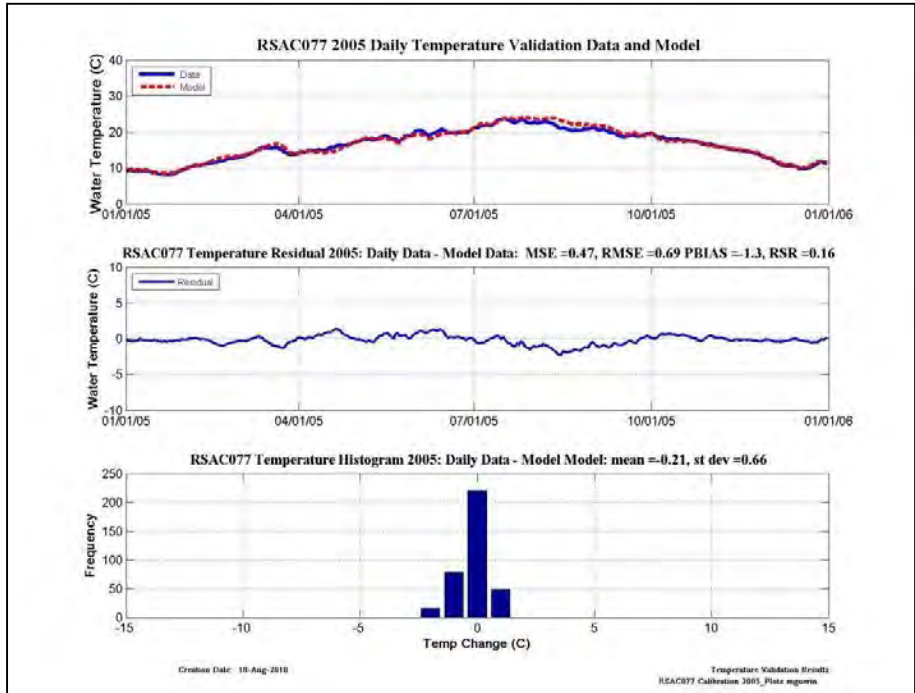
Wet-Validation	NSE	PBIAS	Bias	RSR
2005	VG	VG	Overestimate	VG
2006	VG	VG	Overestimate	VG

Figure 9-54 Wet year temperature validation plots, residual plots, histograms and categorical statistics at RSAC077.
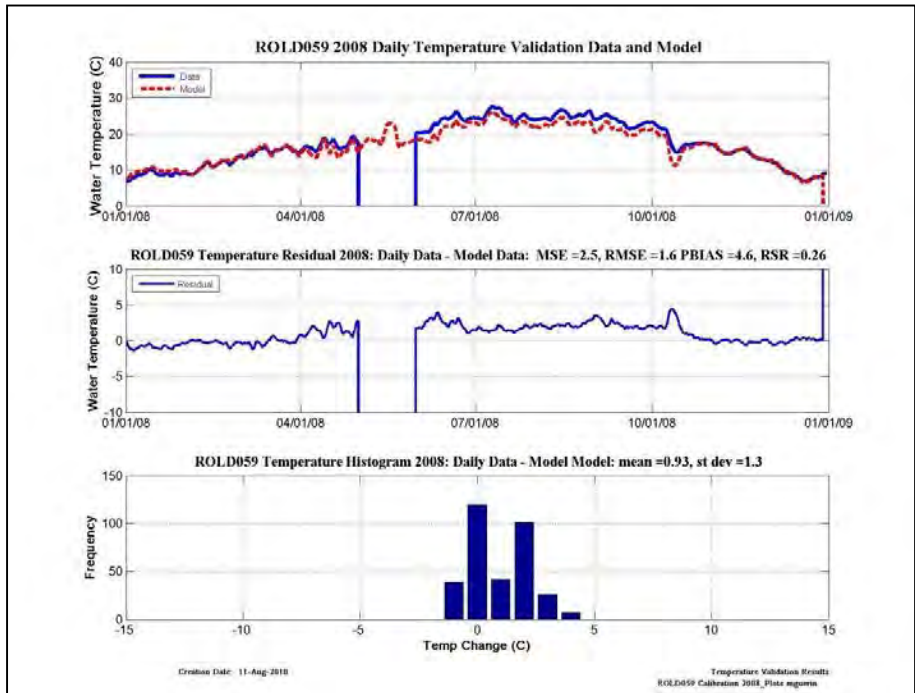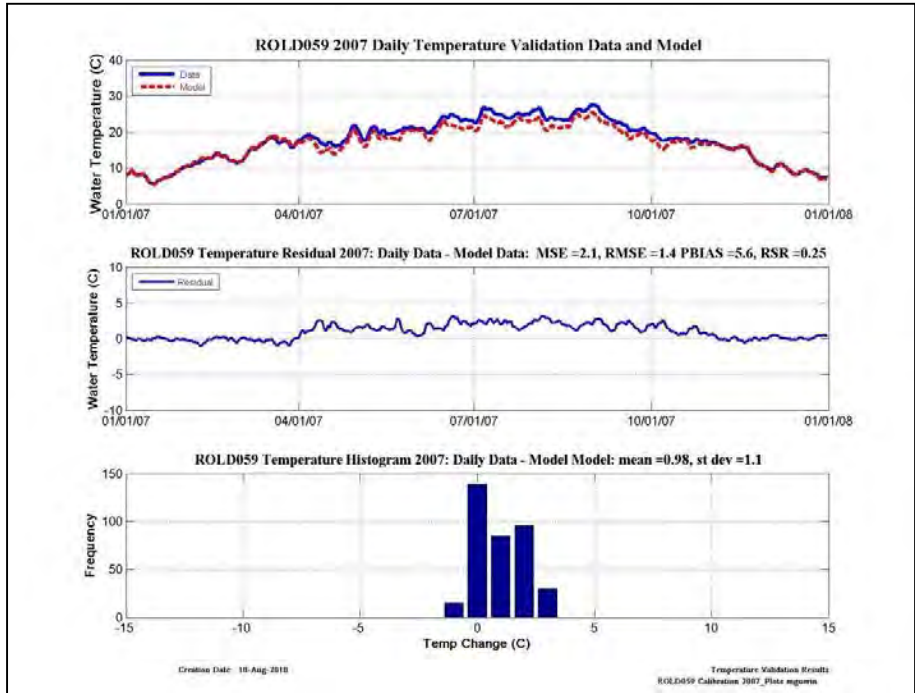
Dry-Validation	NSE	PBIAS	Bias	RSR
2007	VG	VG	Underestimate	VG
2008	VG	VG	Underestimate	VG

Figure 9-55 Dry year temperature validation plots, residual plots, histograms and categorical statistics at ROLD059.
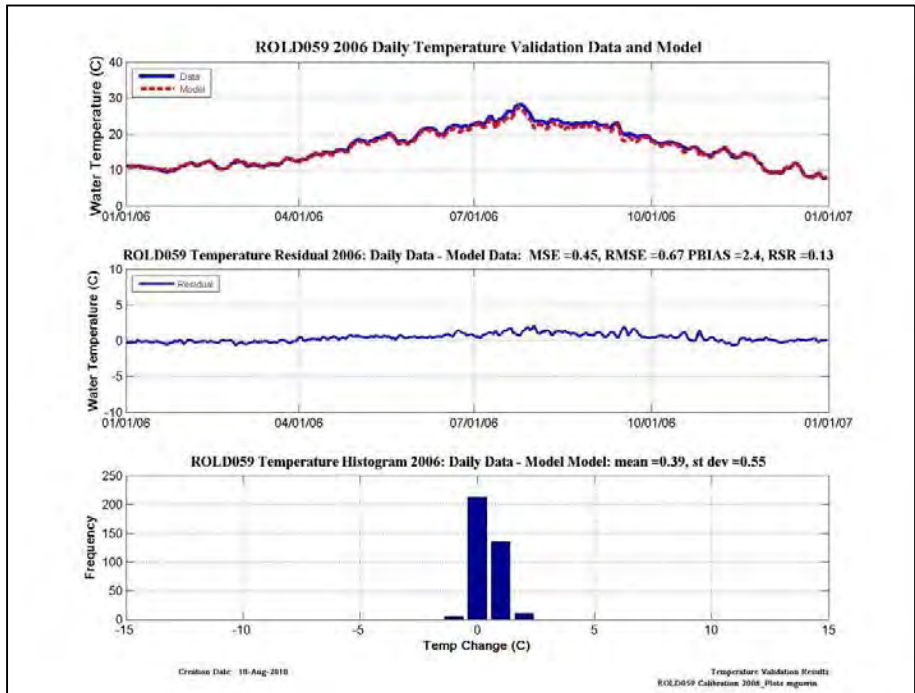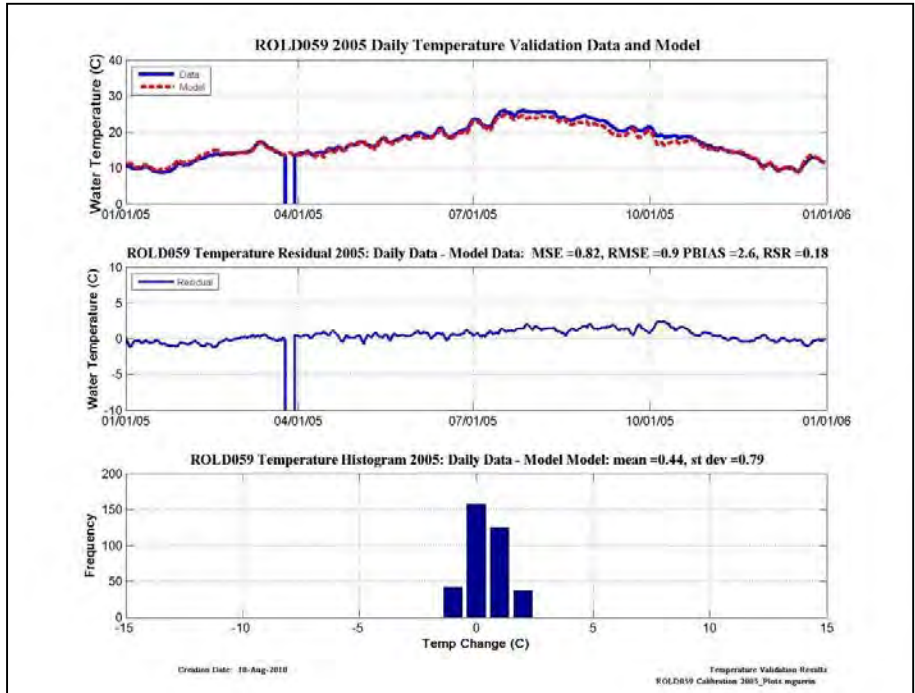
Wet-Validation	NSE	PBIAS	Bias	RSR
2005	VG	VG	Underestimate	VG
2006	VG	VG	Underestimate	VG

Figure 9-56 Wet year temperature validation plots, residual plots, histograms and categorical statistics at ROLD059.

Dry-Validation	NSE	PBIAS	Bias	RSR
2007	VG	VG	Underestimate	VG
2008	VG	VG	Underestimate	VG

Figure 9-57 Dry year temperature validation plots, residual plots, histograms and categorical statistics at ROLD046.

Figure 9-58 Wet year temperature validation plots, residual plots, histograms and categorical statistics at ROLD046.

Wet-Validation	NSE	PBIAS	Bias	RSR
2005				
2006	VG	VG	Underestimate	VG

Dry-Validation	NSE	PBIAS	Bias	RSR
2007	VG	VG	Underestimate	VG
2008	VG	VG	Underestimate	VG

Figure 9-59 Dry year temperature validation plots, residual plots, histograms and categorical statistics at ROLD024.
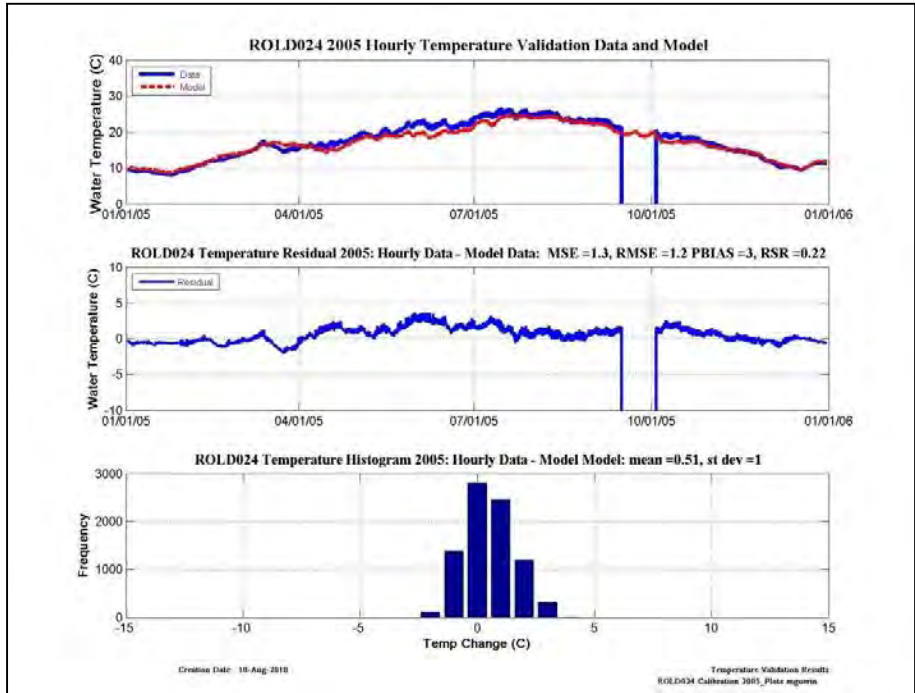
Wet-Validation	NSE	PBIAS	Bias	RSR
2005	VG	VG	Underestimate	VG
2006	VG	VG	Underestimate	VG

Figure 9-60 Wet year temperature validation plots, residual plots, histograms and categorical statistics at ROLD024.

Dry-Validation	NSE	PBIAS	Bias	RSR
2007	VG	VG	Underestimate	U
2008	VG	VG	Underestimate	U

Figure 9-61 Dry year temperature validation plots, residual plots, histograms and categorical statistics at RMID023.
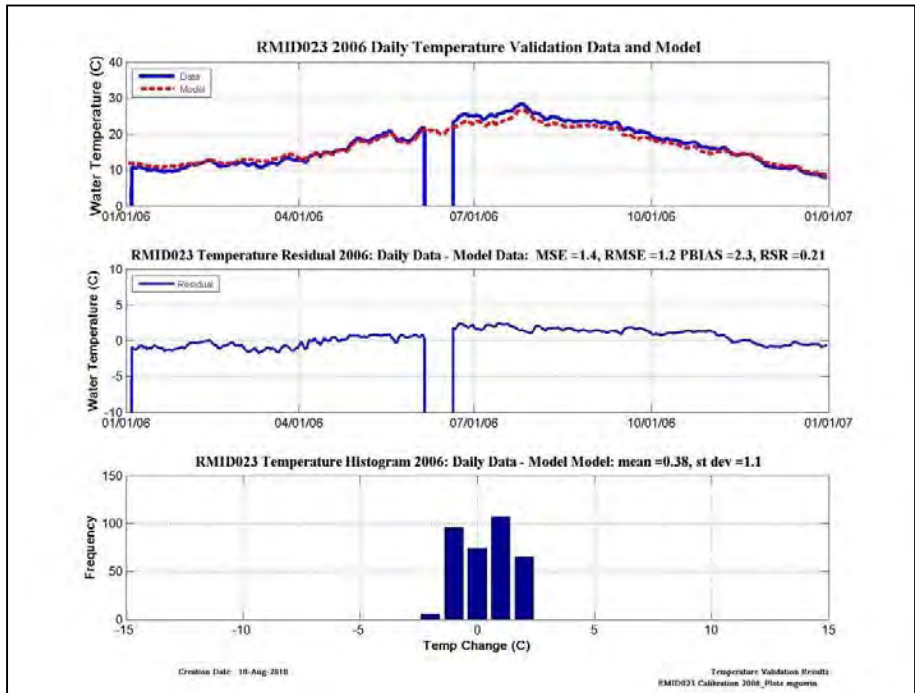
Wet-Validation	NSE	PBIAS	Bias	RSR
2005	VG	VG	Underestimate	U
2006	VG	VG	Underestimate	U

Figure 9-62 Wet year temperature validation plots, residual plots, histograms and categorical statistics at RMID023.

Dry-Validation	NSE	PBIAS	Bias	RSR
2007	VG	VG	Underestimate	VG
2008	VG	VG	Underestimate	VG

Figure 9-63 Dry year temperature validation plots, residual plots, histograms and categorical statistics at SLSBT011.
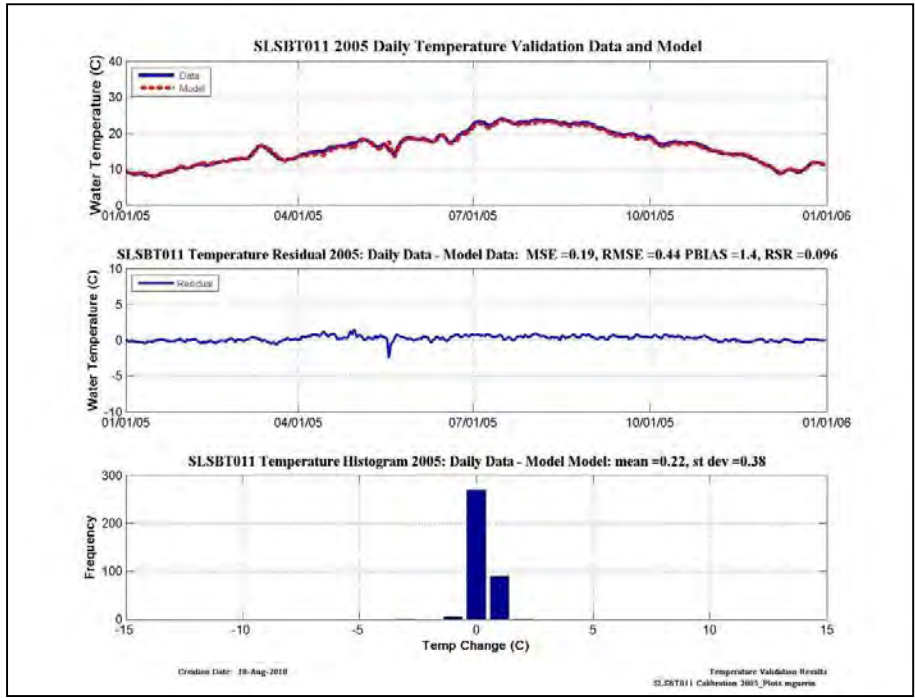
Wet-Validation	NSE	PBIAS	Bias	RSR
2005	VG	VG	Underestimate	VG
2006	VG	VG	Underestimate	VG

Figure 9-64 Wet year temperature validation plots, residual plots, histograms and categorical statistics at SLSBT011.

Dry-Validation	NSE	PBIAS	Bias	RSR
2007	VG	VG	Underestimate	VG
2008				

Figure 9-65 Dry year temperature validation plots, residual plots, histograms and categorical statistics at RMID027.
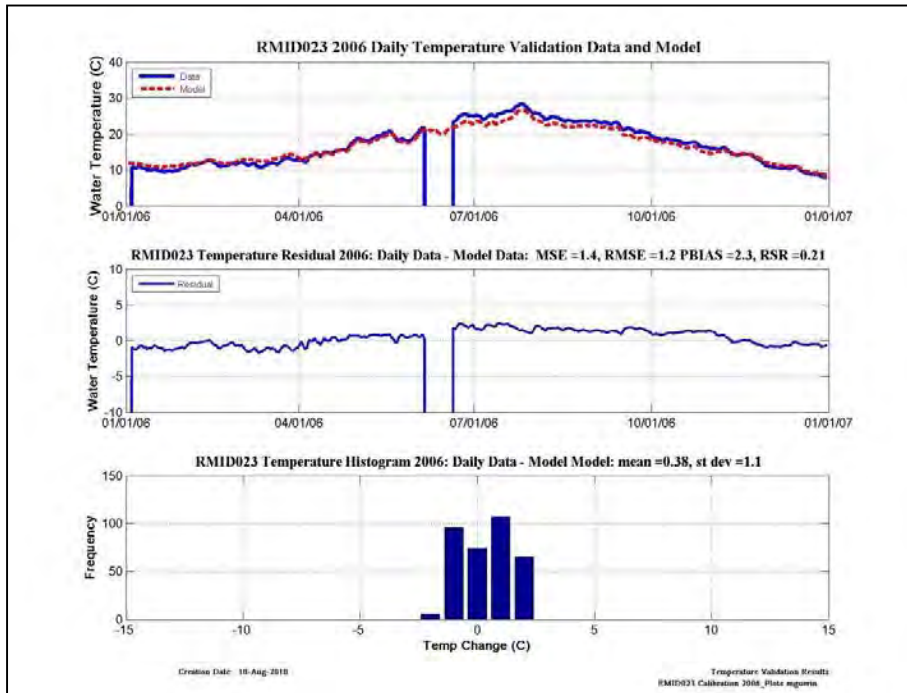
Wet-Validation	NSE	PBIAS	Bias	RSR
2005	VG	VG	Underestimate	U
2006	VG	VG	Underestimate	U

Figure 9-66 Wet year temperature validation plots, residual plots, histograms and categorical statistics at RMID023.

10.　　Appendix III - Calibration Figures and Statistics

Algae
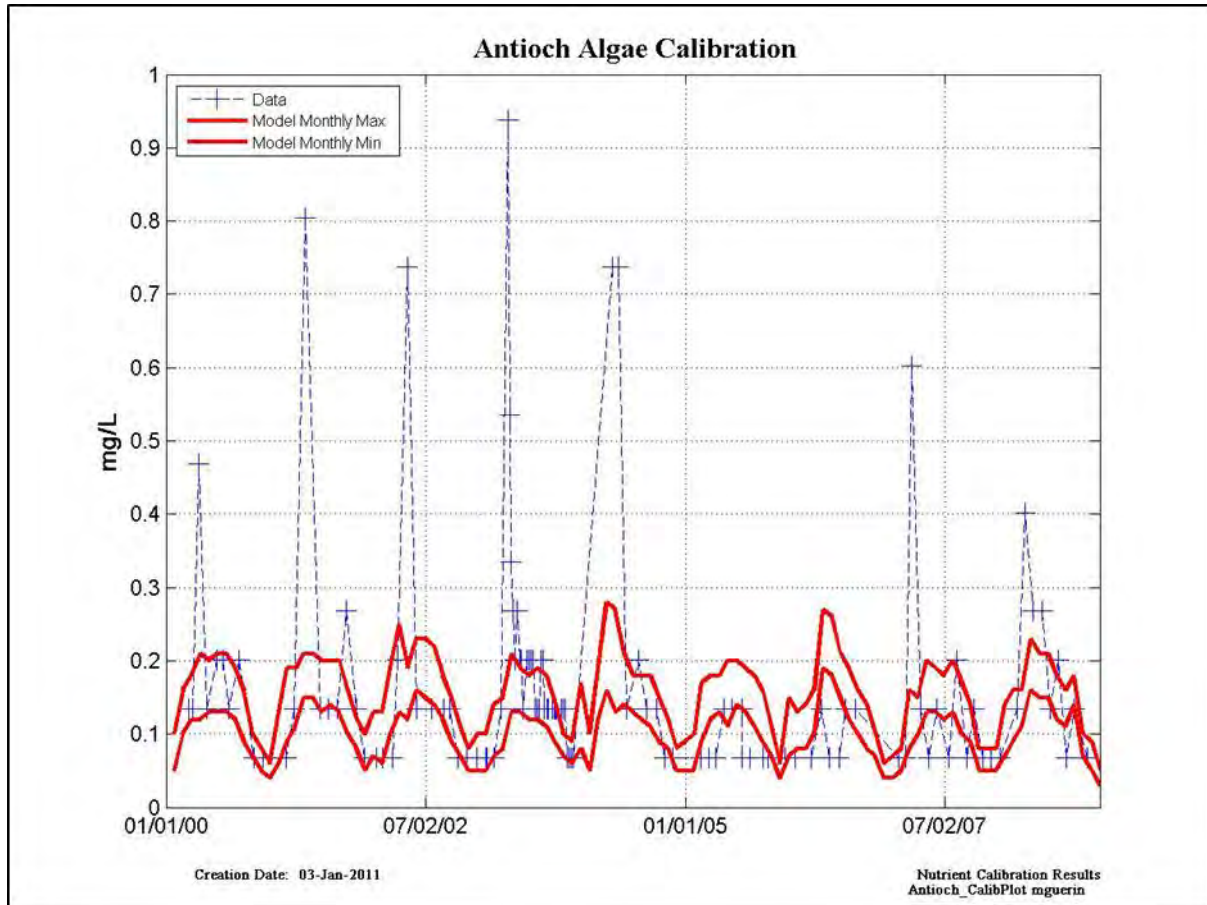
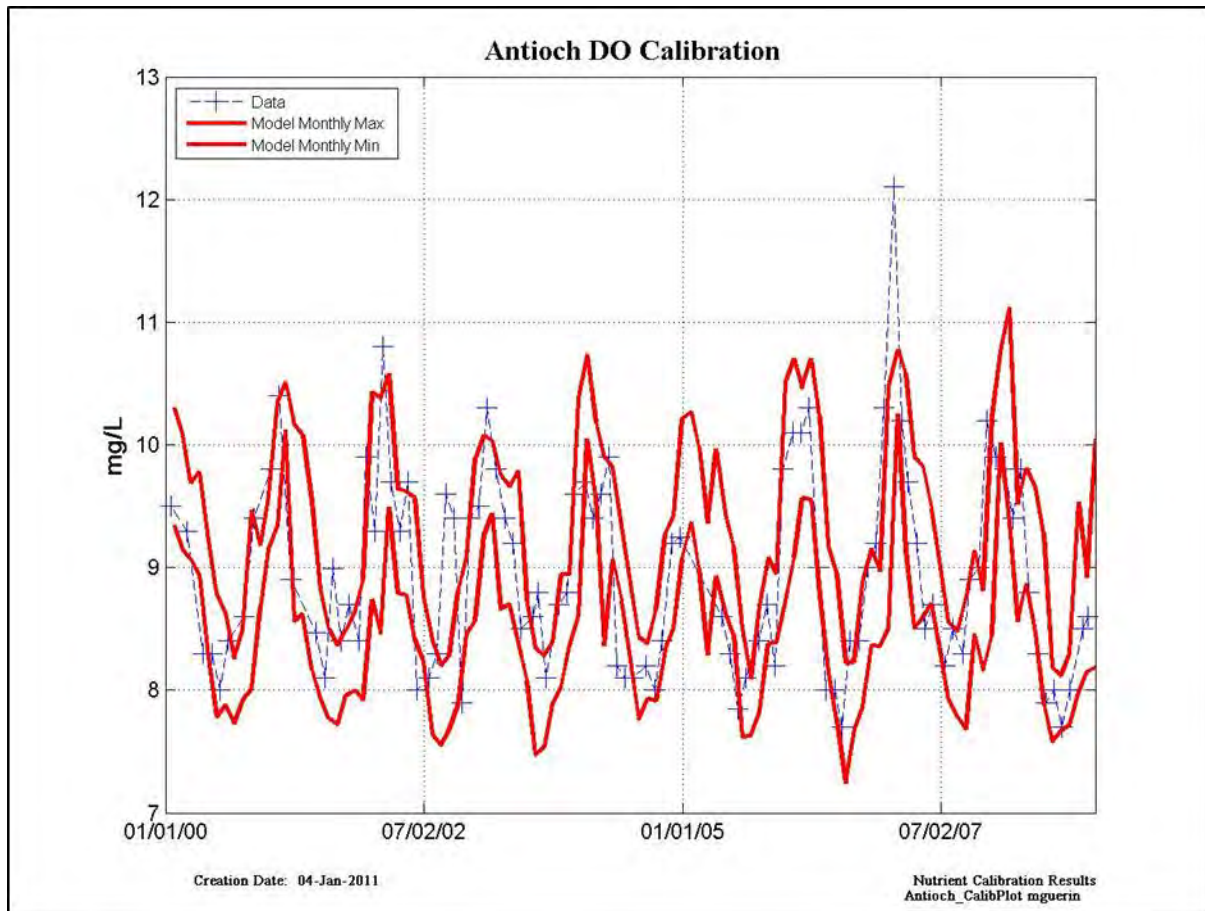**Figure 10-1 Modeled algae (see text for conversion to Chl-a) calibration results at Antioch – data points are located at blue symbols, monthly modeled maximum and minimum are denoted by solid red lines.**

Table 10-1 Model calibration/validation statistics at Antioch for algae (see text for conversion to Chl-a) for the entire modeled period ("All"); Calibration for Dry Years (2001, 2002) and Wet Years (2000, 2003); and Validation for Dry Years (2007, 2008) and Wet Years (2005, 2006).

	NSE	PBIAS	Bias	RSR
ALL	S	VG	Underestimate	U
Dry WY Calibration	S	G	Underestimate	U
Wet WY Calibration	S	VG	Underestimate	U
Dry WY Validation	S	VG	Underestimate	U
Wet WY Validation	U	G	Overestimate	U
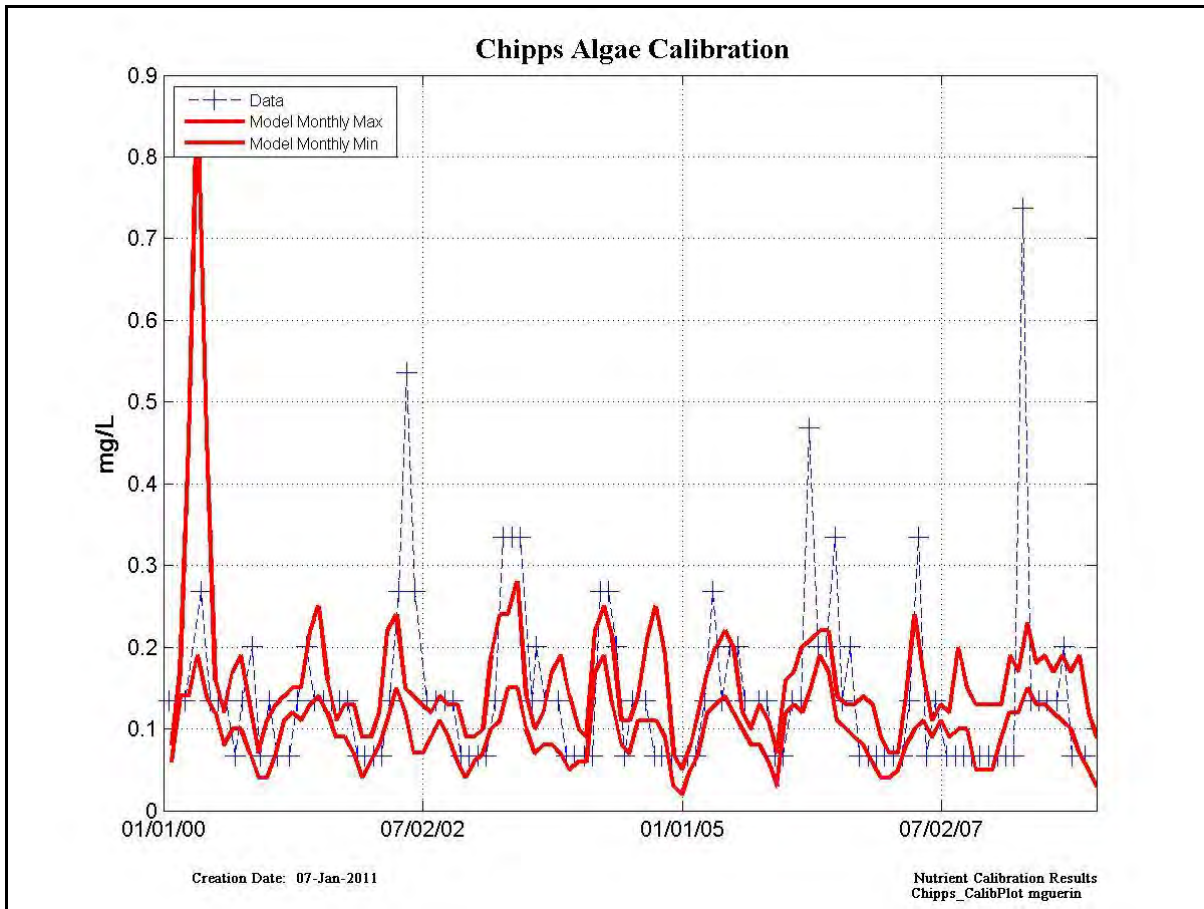
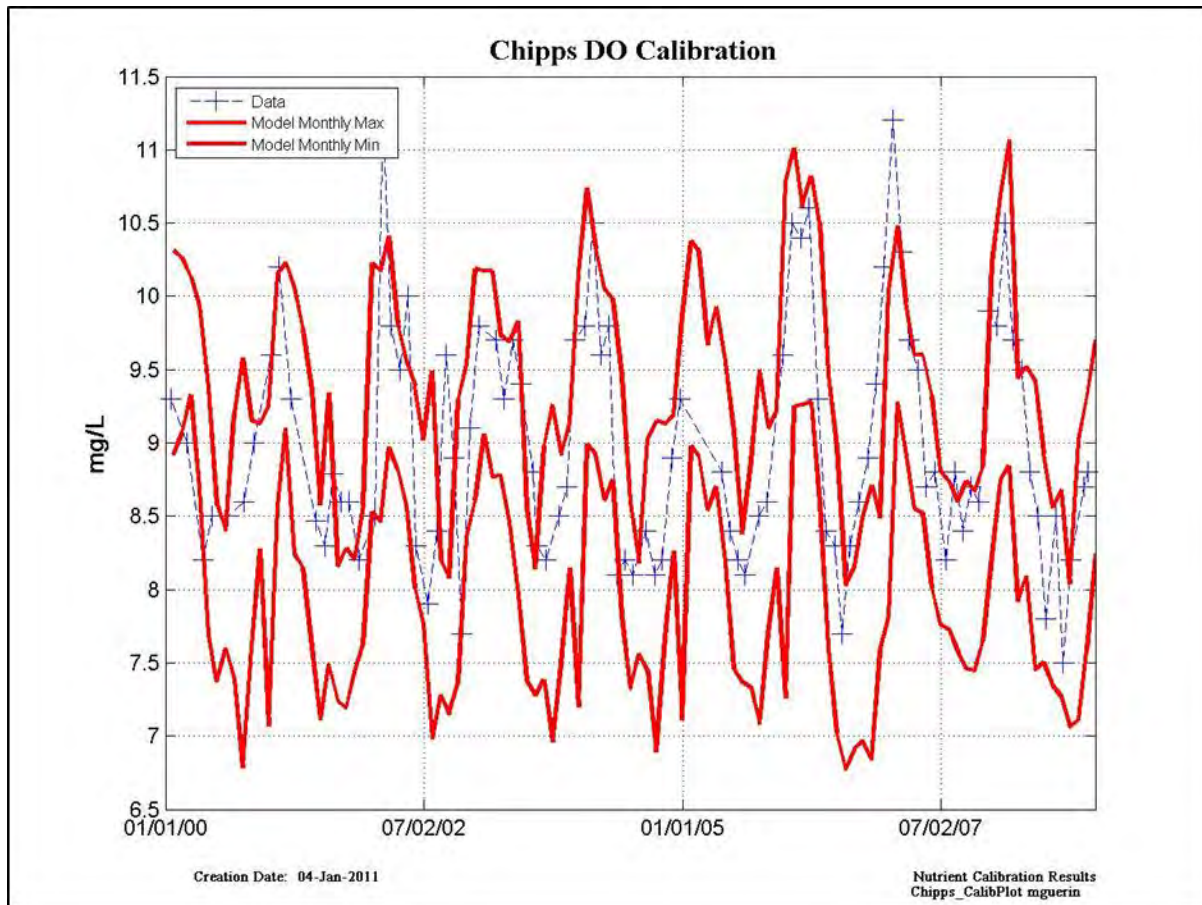**Figure 10-2 Modeled algae (see text for conversion to Chl-a) calibration results at Chipps – data points are located at blue symbols, monthly modeled maximum and minimum are denoted by solid red lines.**

Table 10-2 Model calibration/validation statistics at Chipps for algae (see text for conversion to Chl-a) for the entire modeled period ("All"); Calibration for Dry Years (2001, 2002) and Wet Years (2000, 2003); and Validation for Dry Years (2007, 2008) and Wet Years (2005, 2006).

	NSE	PBIAS	Bias	RSR
ALL	S	VG	Underestimate	U
Dry WY Calibration	S	VG	Underestimate	U
Wet WY Calibration	G	VG	Underestimate	S
Dry WY Validation	S	VG	Underestimate	U
Wet WY Validation	S	VG	Underestimate	U

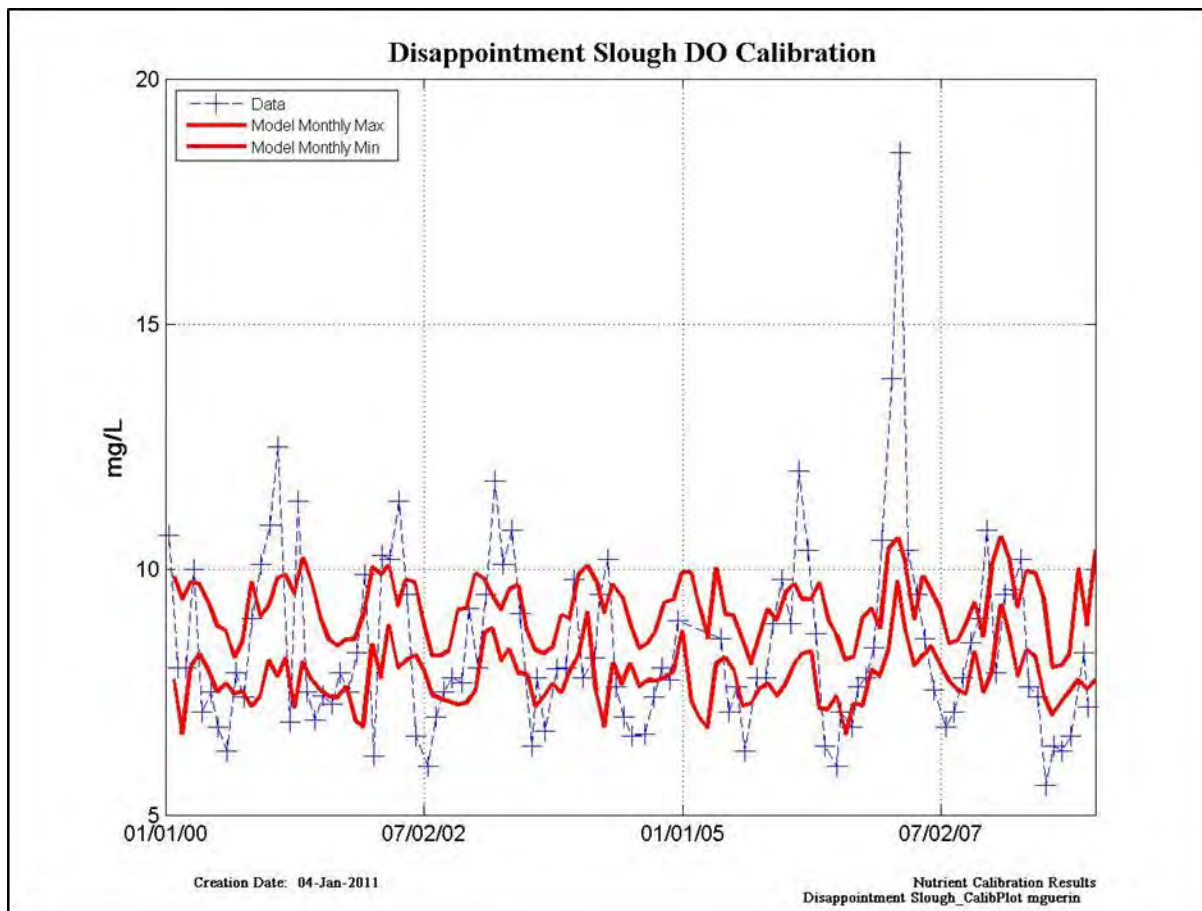**Figure 10-3 Modeled algae (see text for conversion to Chl-a) calibration results at Disappointment Sl. – data points are located at blue symbols, monthly modeled maximum and minimum are denoted by solid red lines.**

Table 10-3 Model calibration/validation statistics at Disappointment Sl. for algae (see text for conversion to Chl-a) for the entire modeled period ("All"); Calibration for Dry Years (2001, 2002) and Wet Years (2000, 2003); and Validation for Dry Years (2007, 2008) and Wet Years (2005, 2006).

	NSE	PBIAS	Bias	RSR
ALL	S	G	Underestimate	U
Dry WY Calibration	S	S	Underestimate	U
Wet WY Calibration	G	VG	Underestimate	G
Dry WY Validation	S	S	Underestimate	U
Wet WY Validation	G	VG	Underestimate	G

216
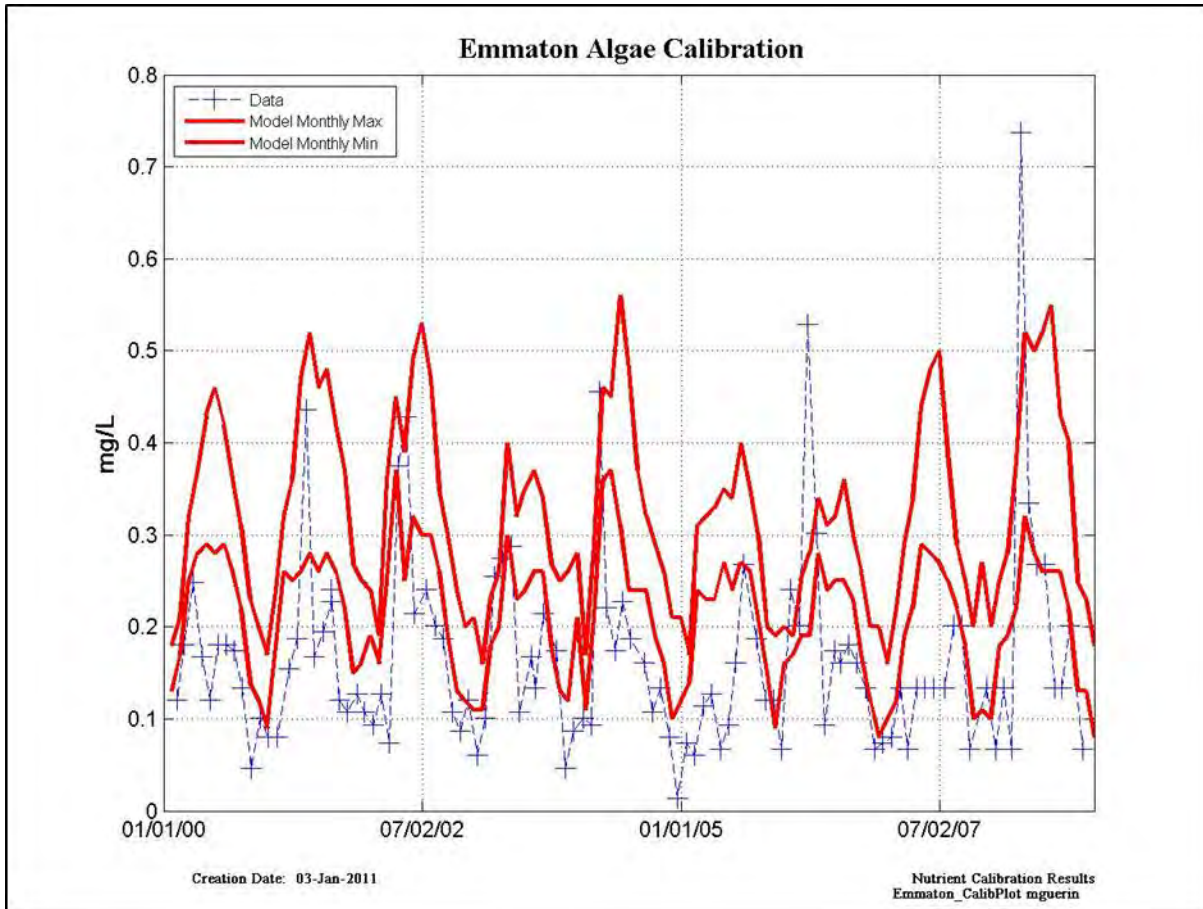
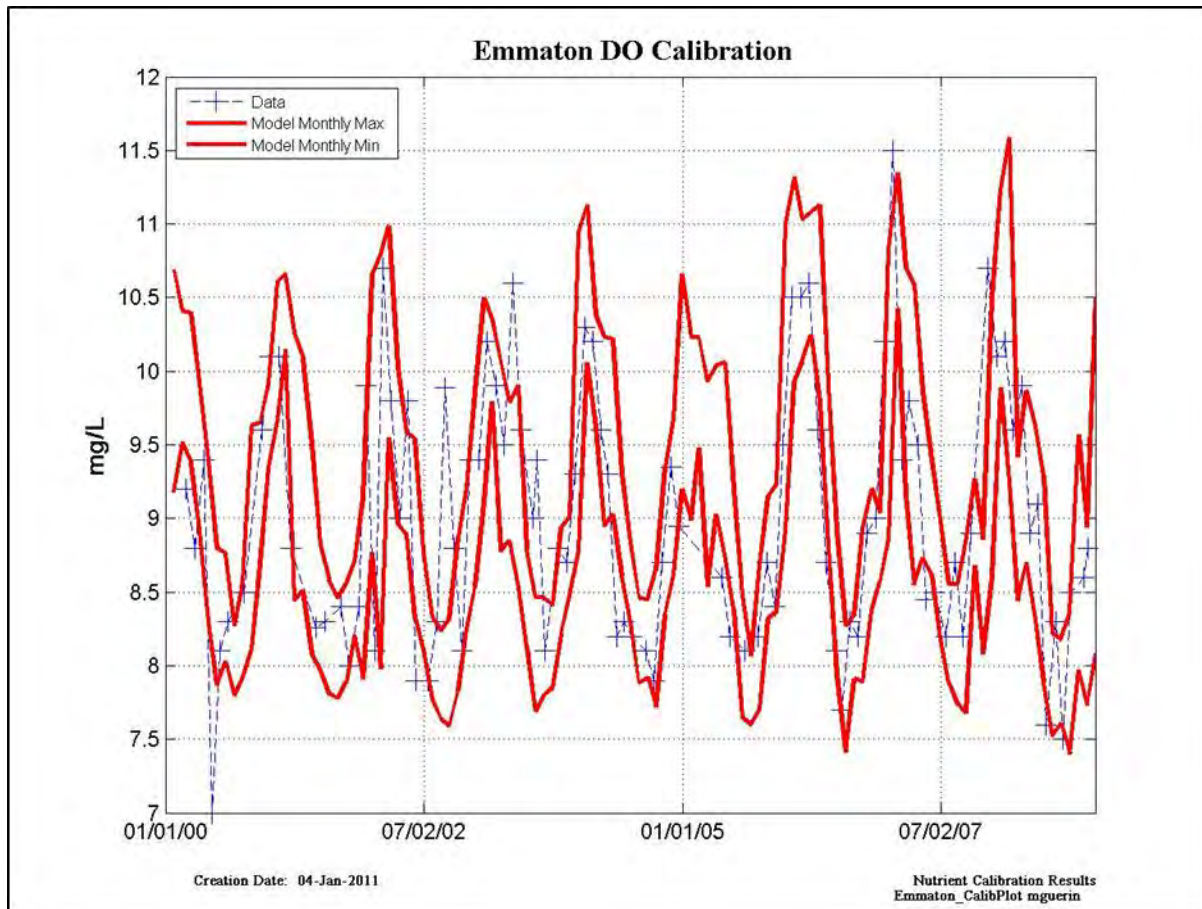**Figure 10-4 Modeled algae (see text for conversion to Chl-a) calibration results at Emmaton – data points are located at blue symbols, monthly modeled maximum and minimum are denoted by solid red lines.**

Table 10-4 Model calibration/validation statistics at Emmaton for algae (see text for conversion to Chl-a) for the entire modeled period ("All"); Calibration for Dry Years (2001, 2002) and Wet Years (2000, 2003); and Validation for Dry Years (2007, 2008) and Wet Years (2005, 2006).

	NSE	PBIAS	Bias	RSR
ALL	S	G	Overestimate	U
Dry WY Calibration	S	G	Overestimate	U
Wet WY Calibration	S	S	Overestimate	U
Dry WY Validation	G	G	Overestimate	S
Wet WY Validation	S	G	Overestimate	U

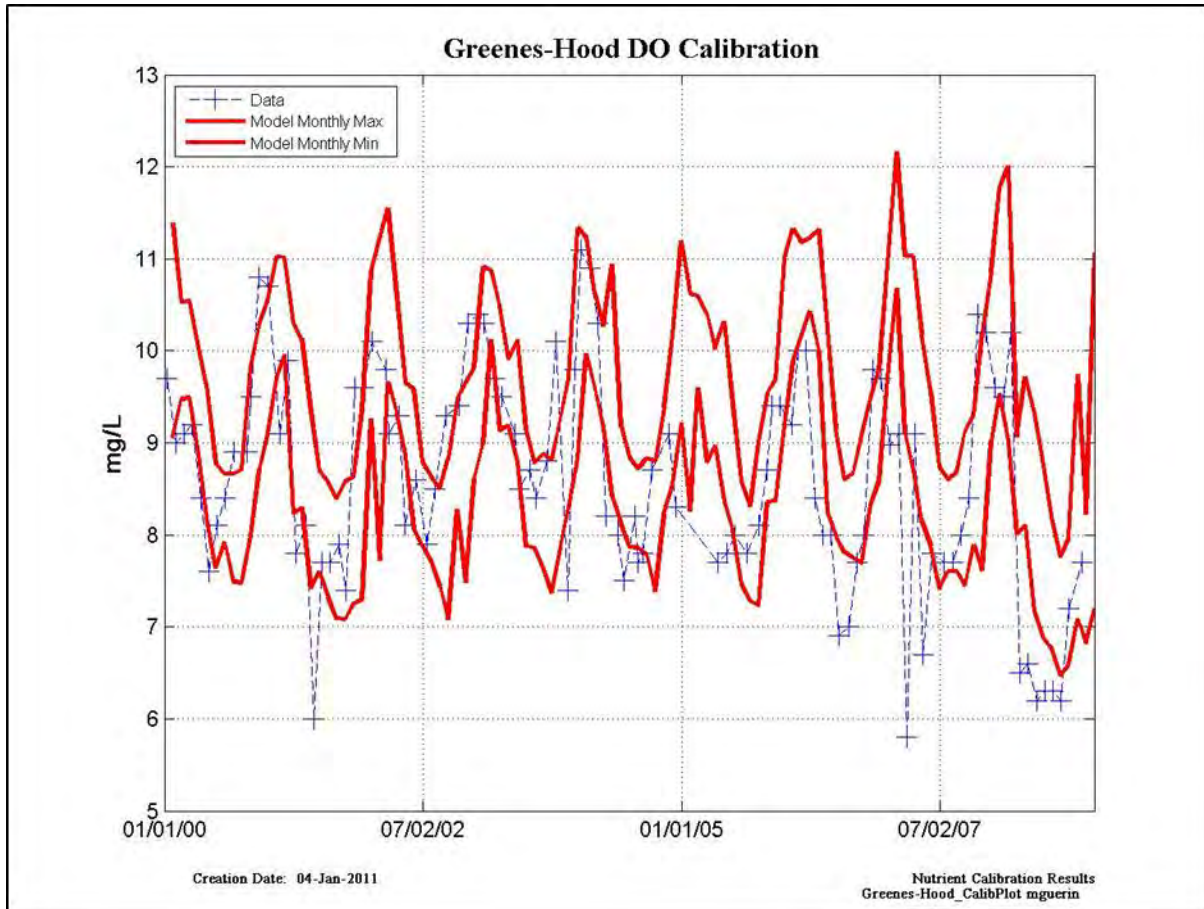**Figure 10-5 Modeled algae (see text for conversion to Chl-a) calibration results at Green-Hood – data points are located at blue symbols, monthly modeled maximum and minimum are denoted by solid red lines.**

Table 10-5 Model calibration/validation statistics at Green-Hood for algae (see text for conversion to Chl-a) for the entire modeled period ("All"); Calibration for Dry Years (2001, 2002) and Wet Years (2000, 2003); and Validation for Dry Years (2007, 2008) and Wet Years (2005, 2006).

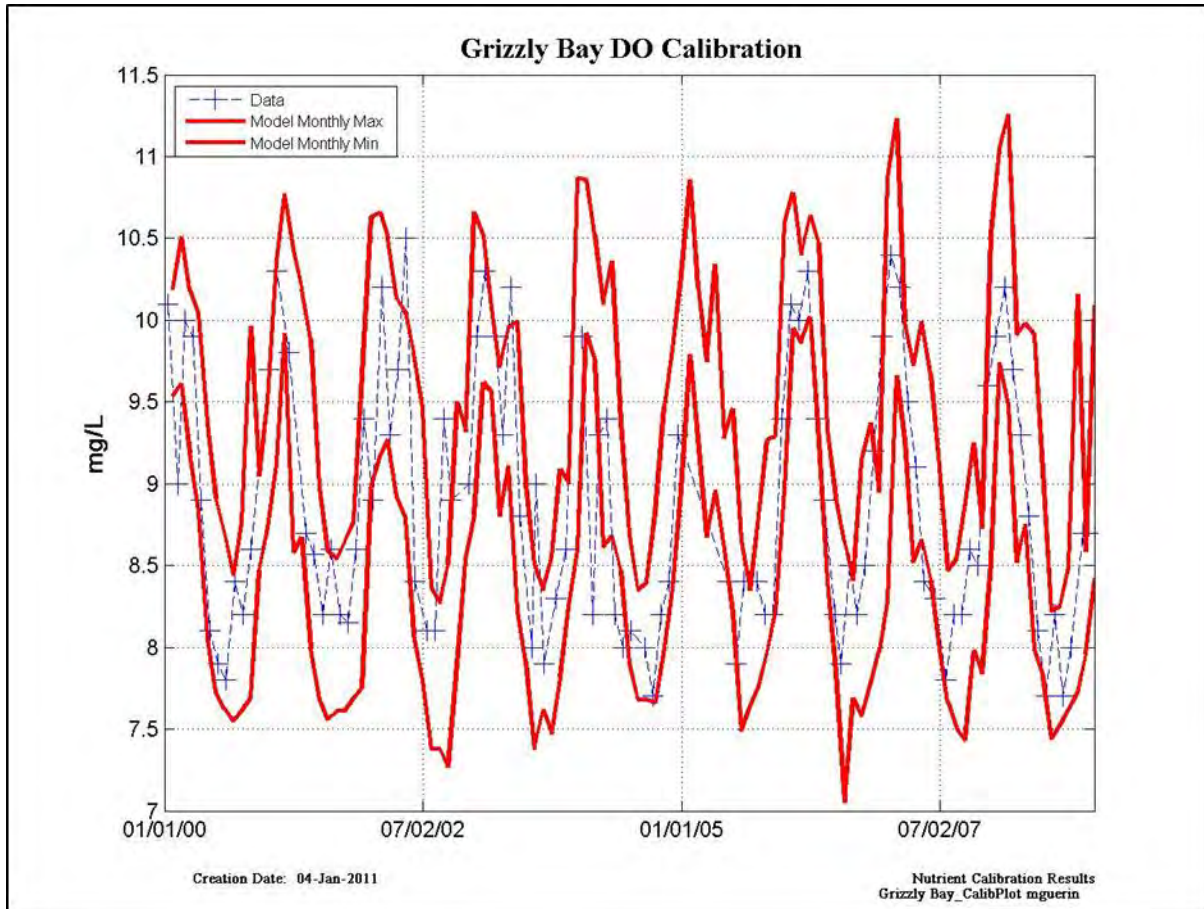|	NSE	PBIAS	Bias	RSR
ALL	VG	VG	Overestimate	VG
Dry WY Calibration	S	VG	Overestimate	U
Wet WY Calibration	VG	VG	Overestimate	VG
Dry WY Validation	VG	VG	Overestimate	VG
Wet WY Validation	VG	VG	Overestimate	VG

Figure 10-6 Modeled algae (see text for conversion to Chl-a) calibration results at Grizzly – data points are located at blue symbols, monthly modeled maximum and minimum are denoted by solid red lines.

Table 10-6 Model calibration/validation statistics at Grizzly for algae (see text for conversion to Chl-a) for the entire modeled period ("All"); Calibration for Dry Years (2001, 2002) and Wet Years (2000, 2003); and Validation for Dry Years (2007, 2008) and Wet Years (2005, 2006).

	NSE	PBIAS	Bias	RSR
ALL	S	VG	Overestimate	U
Dry WY Calibration	S	G	Overestimate	U
Wet WY Calibration	S	VG	Underestimate	U
Dry WY Validation	S	G	Overestimate	U
Wet WY Validation	S	VG	Overestimate	G

Figure 10-7 Modeled algae (see text for conversion to Chl-a) calibration results at Mallard Slough – data points are located at blue symbols, monthly modeled maximum and minimum are denoted by solid red lines.

Table 10-7 Model calibration/validation statistics at Mallard Sl. for algae (see text for conversion to Chl-a) for the entire modeled period ("All"); Calibration for Dry Years (2001, 2002) and Wet Years (2000, 2003); and Validation for Dry Years (2007, 2008) and Wet Years (2005, 2006).

	NSE	PBIAS	Bias	RSR
ALL	S	VG	Underestimate	U
Dry WY Calibration	S	VG	Underestimate	U
Wet WY Calibration	S	G	Underestimate	U
Dry WY Validation	U	G	Overestimate	U
Wet WY Validation	S	VG	No Bias	VG

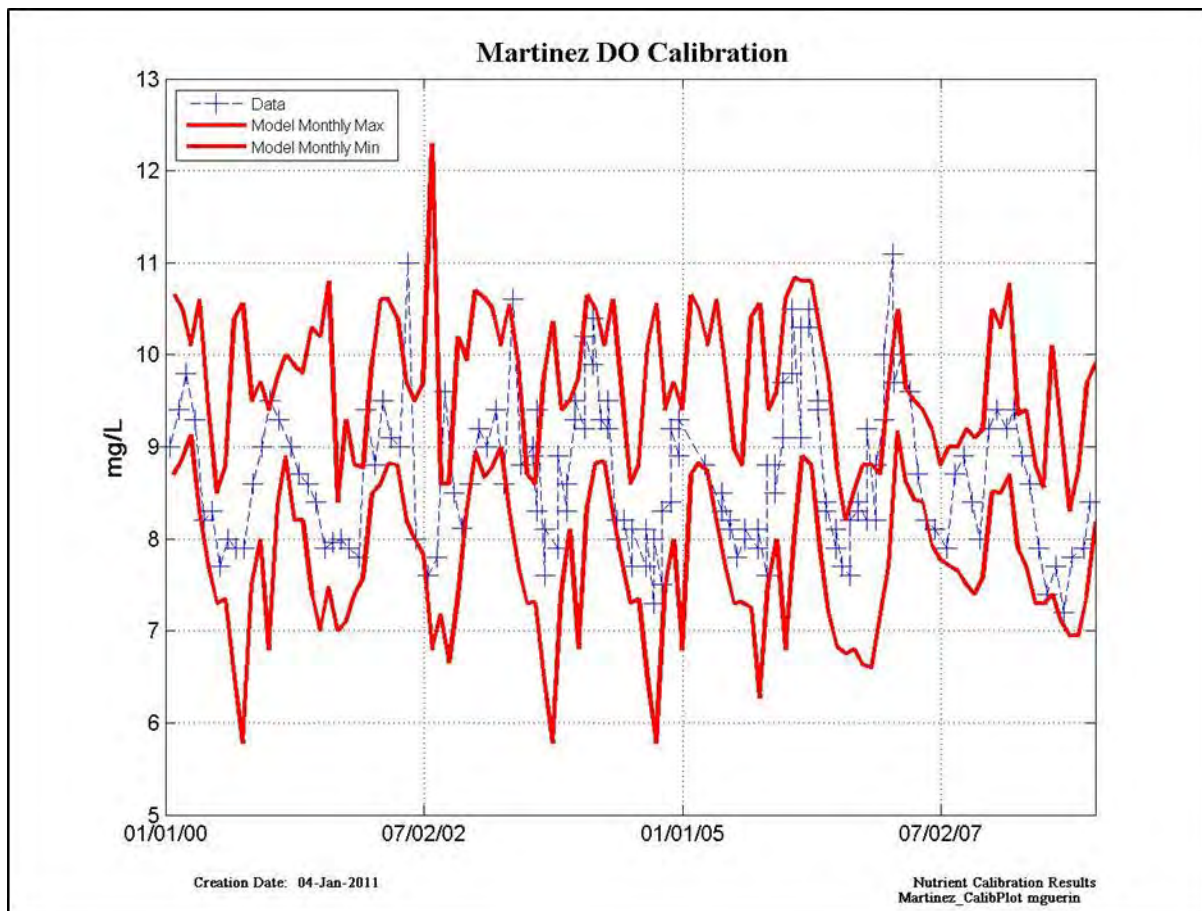**Figure 10-8 Modeled algae (see text for conversion to Chl-a) calibration results at Martinez – data points are located at blue symbols, monthly modeled maximum and minimum are denoted by solid red lines.**

Table 10-8 Model calibration/validation statistics at Martinez for algae (see text for conversion to Chl-a) for the entire modeled period ("All"); Calibration for Dry Years (2001, 2002) and Wet Years (2000, 2003); and Validation for Dry Years (2007, 2008) and Wet Years (2005, 2006).

	NSE	PBIAS	Bias	RSR
ALL	VG	VG	Underestimate	VG
Dry WY Calibration	VG	VG	Underestimate	VG
Wet WY Calibration	VG	VG	Underestimate	VG
Dry WY Validation	VG	VG	Underestimate	VG
Wet WY Validation	VG	VG	Underestimate	VG

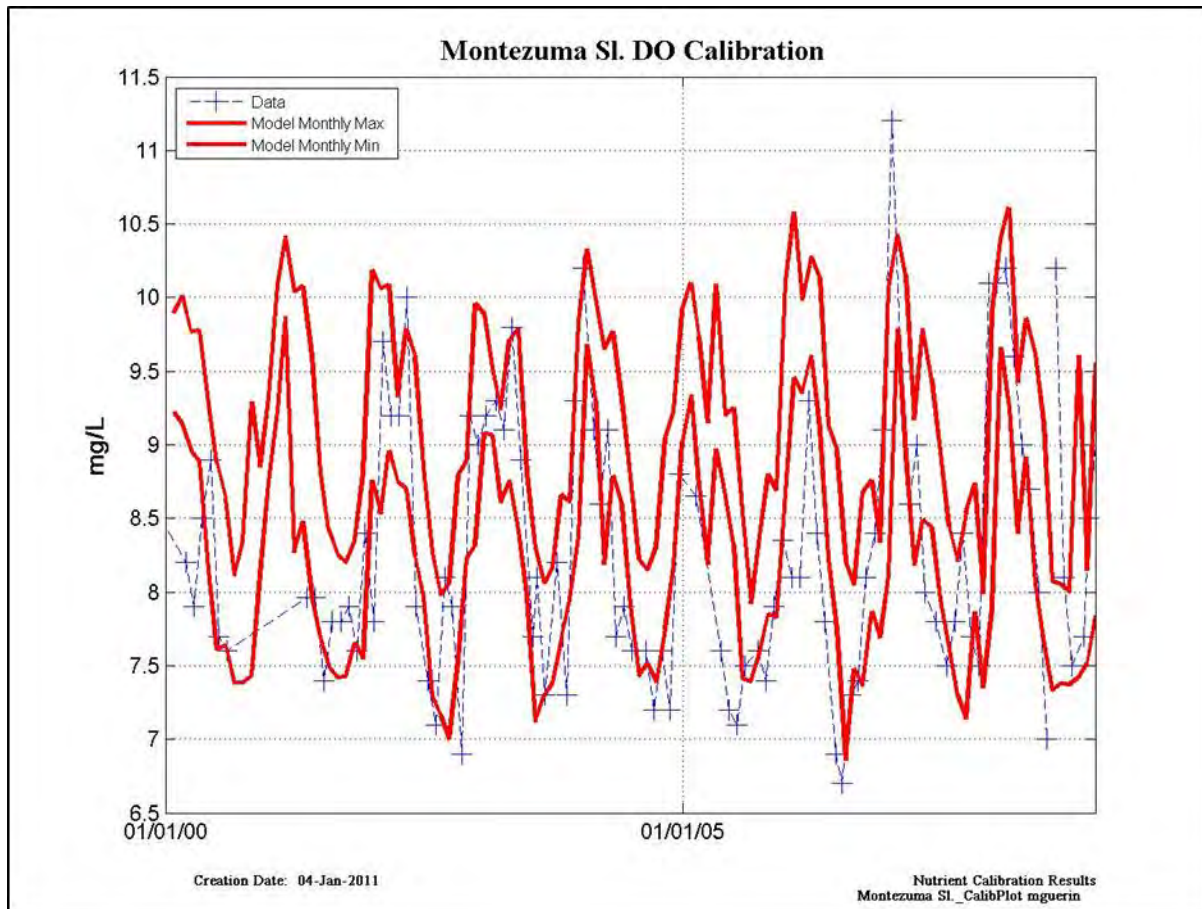**Figure 10-9 Modeled algae (see text for conversion to Chl-a) calibration results at Montezuma Sl. Bend 2 – data points are located at blue symbols, monthly modeled maximum and minimum are denoted by solid red lines.**

Table 10-9 Model calibration/validation statistics at Montezuma Sl. for algae (see text for conversion to Chl-a) for the entire modeled period ("All"); Calibration for Dry Years (2001, 2002) and Wet Years (2000, 2003); and Validation for Dry Years (2007, 2008) and Wet Years (2005, 2006).

	NSE	PBIAS	Bias	RSR
ALL	U	S	Overestimate	U
Dry WY Calibration	U	S	Overestimate	U
Wet WY Calibration	U	S	Overestimate	U
Dry WY Validation	S	G	Overestimate	U
Wet WY Validation	U	S	Overestimate	U
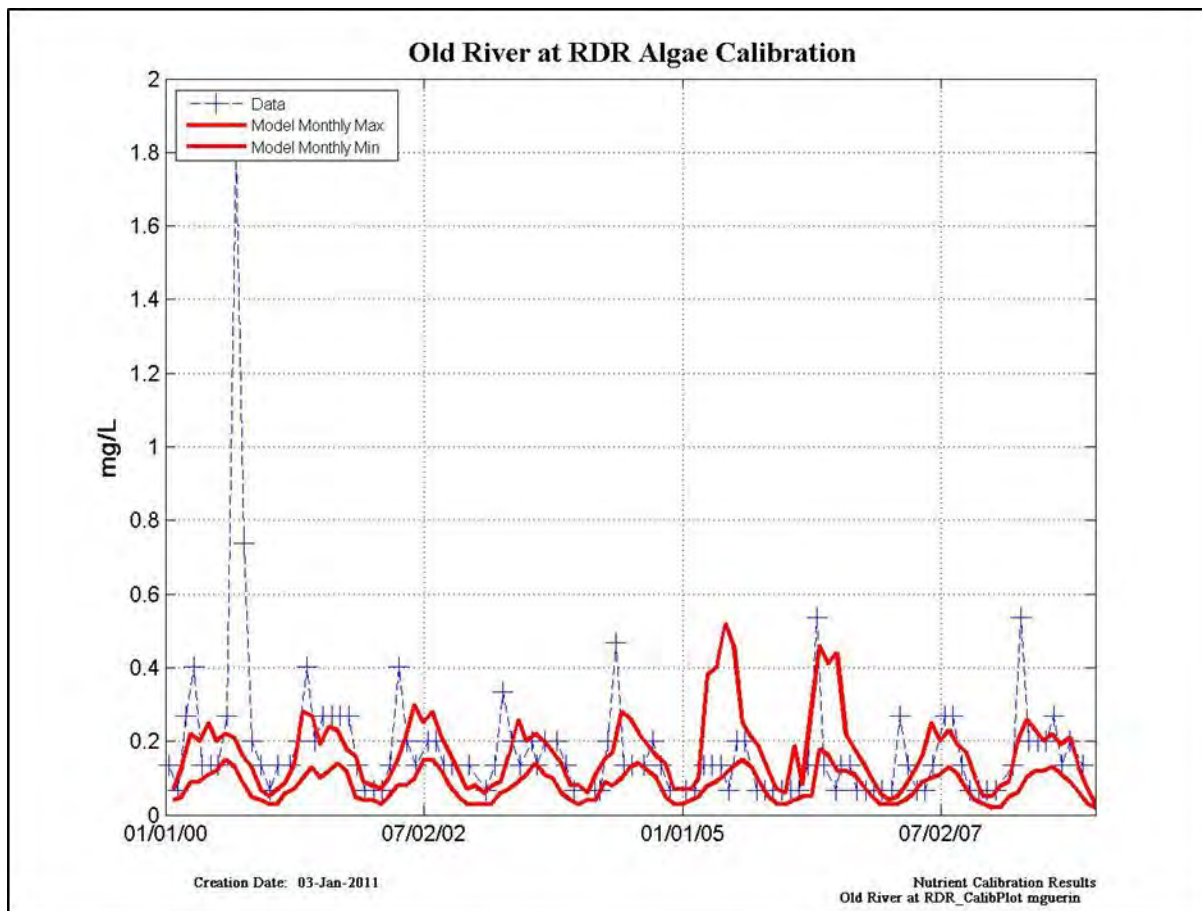
Figure 10-10 Modeled algae (see text for conversion to Chl-a) calibration results at Old R. at RDR – data points are located at blue symbols, monthly modeled maximum and minimum are denoted by solid red lines.

Table 10-10 Model calibration/validation statistics at Old R. at RDR for algae (see text for conversion to Chl-a) for the entire modeled period ("All"); Calibration for Dry Years (2001, 2002) and Wet Years (2000, 2003); and Validation for Dry Years (2007, 2008) and Wet Years (2005, 2006).

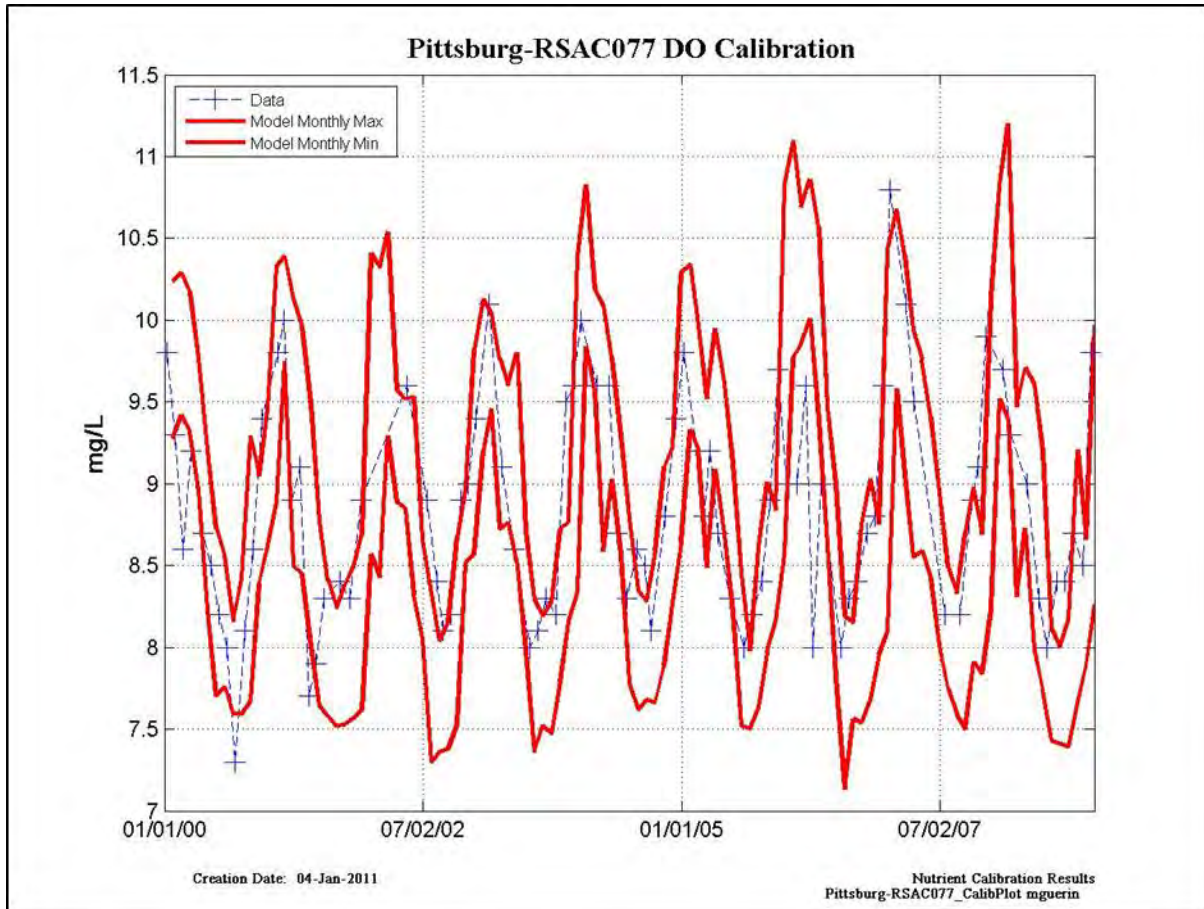|	NSE	PBIAS	Bias	RSR
ALL	S	G	Underestimate	U
Dry WY Calibration	G	VG	Underestimate	S
Wet WY Calibration	S	S	Underestimate	U
Dry WY Validation	S	VG	Underestimate	U
Wet WY Validation	VG	VG	Overestimate	VG

223

Figure 10-11 Modeled algae (see text for conversion to Chl-a) calibration results at Pittsburg – data points are located at blue symbols, monthly modeled maximum and minimum are denoted by solid red lines.

Table 10-11 Model calibration/validation statistics at Pittsburg for algae (see text for conversion to Chl-a) for the entire modeled period ("All"); Calibration for Dry Years (2001, 2002) and Wet Years (2000, 2003); and Validation for Dry Years (2007, 2008) and Wet Years (2005, 2006)

	NSE	PBIAS	Bias	RSR
ALL	S	G	Underestimate	U
Dry WY Calibration	S	G	Underestimate	U
Wet WY Calibration	S	VG	Underestimate	U
Dry WY Validation	S	G	Underestimate	U
Wet WY Validation	S	VG	Underestimate	U
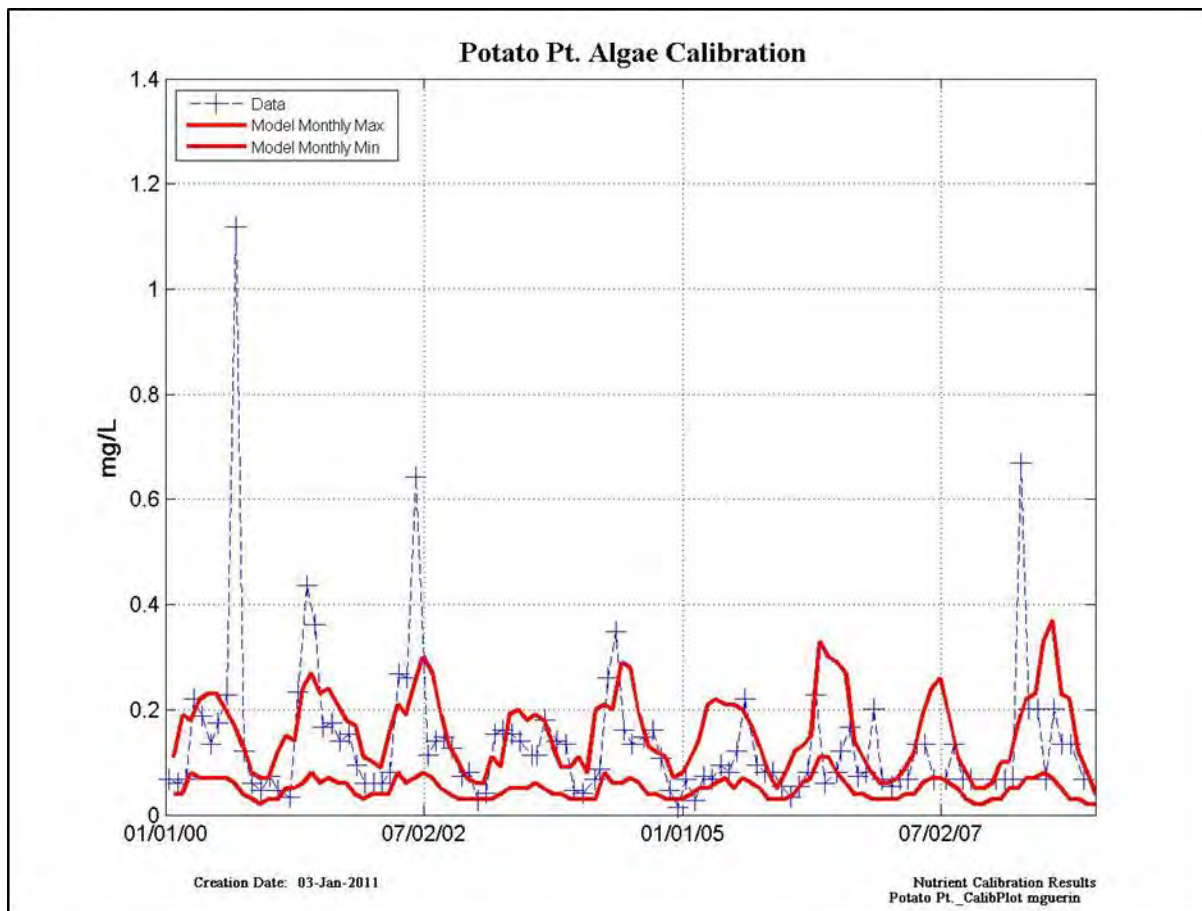
Figure 10-12 Modeled algae (see text for conversion to Chl-a) calibration results at Potato Pt. – data points are located at blue symbols, monthly modeled maximum and minimum are denoted by solid red lines.

Table 10-12 Model calibration/validation statistics at Potato Pt. for algae (see text for conversion to Chl-a) for the entire modeled period ("All"); Calibration for Dry Years (2001, 2002) and Wet Years (2000, 2003); and Validation for Dry Years (2007, 2008) and Wet Years (2005, 2006).

	NSE	PBIAS	Bias	RSR
ALL	S	VG	Underestimate	U
Dry WY Calibration	G	VG	Underestimate	G
Wet WY Calibration	S	G	Underestimate	U
Dry WY Validation	S	VG	Underestimate	U
Wet WY Validation	S	VG	Underestimate	S

Figure 10-13 Modeled algae (see text for conversion to Chl-a) calibration results at Pt. Sacramento – data points are located at blue symbols, monthly modeled maximum and minimum are denoted by solid red lines.

Table 10-13 Model calibration/validation statistics at Pt. Sacramento for algae (see text for conversion to Chl-a) for the entire modeled period ("All"); Calibration for Dry Years (2001, 2002) and Wet Years (2000, 2003); and Validation for Dry Years (2007, 2008) and Wet Years (2005, 2006).

	NSE	PBIAS	Bias	RSR
ALL	VG	VG	Underestimate	VG
Dry WY Calibration	VG	VG	Underestimate	VG
Wet WY Calibration	VG	VG	Overestimate	VG
Dry WY Validation	VG	VG	Overestimate	VG
Wet WY Validation	VG	VG	Underestimate	VG

Figure 10-14 Modeled algae (see text for conversion to Chl-a) calibration results at Rio Vista – data points are located at blue symbols, monthly modeled maximum and minimum are denoted by solid red lines.
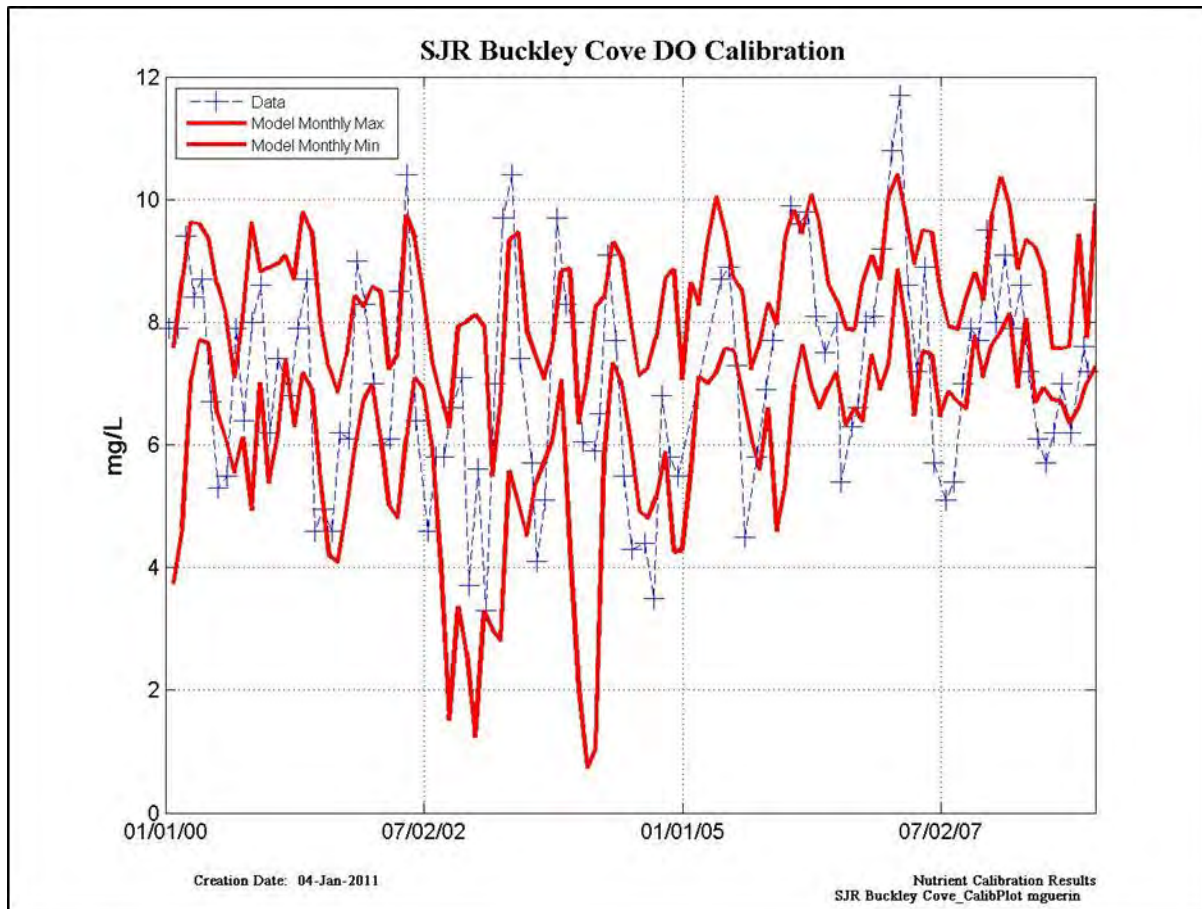
Table 10-14 Model calibration/validation statistics at Rio Vista for algae (see text for conversion to Chl-a) for the entire modeled period ("All"); Calibration for Dry Years (2001, 2002) and Wet Years (2000, 2003); and Validation for Dry Years (2007, 2008) and Wet Years (2005, 2006).

	NSE	PBIAS	Bias	RSR
ALL	S	S	Overestimate	U
Dry WY Calibration	S	S	Overestimate	U
Wet WY Calibration	S	S	Overestimate	U
Dry WY Validation	S	S	Overestimate	U
Wet WY Validation	S	VG	No Bias	VG
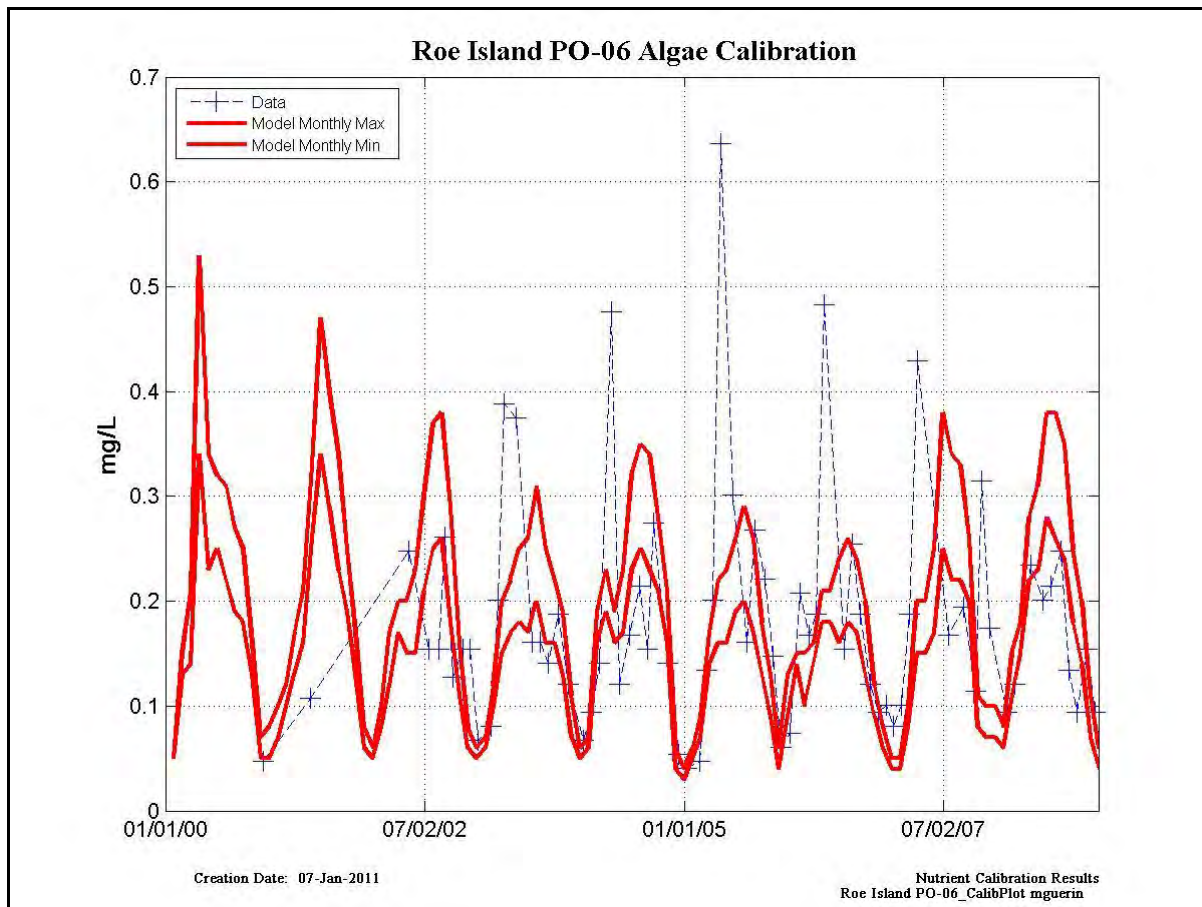
Figure 10-15 Modeled algae (see text for conversion to Chl-a) calibration results at Roe Island – data points are located at blue symbols, monthly modeled maximum and minimum are denoted by solid red lines.

Table 10-15 Model calibration/validation statistics at Roe Island for algae (see text for conversion to Chl-a) for the entire modeled period ("All"); Calibration for Dry Years (2001, 2002) and Wet Years (2000, 2003); and Validation for Dry Years (2007, 2008) and Wet Years (2005, 2006).

	NSE	PBIAS	Bias	RSR
ALL	S	VG	Underestimate	U
Dry WY Calibration	U	VG	Overestimate	U
Wet WY Calibration	G	VG	Underestimate	G
Dry WY Validation	S	VG	Underestimate	U
Wet WY Validation	S	VG	Underestimate	U

Figure 10-16 Modeled algae (see text for conversion to Chl-a) calibration results at Russo – data points are located at blue symbols, monthly modeled maximum and minimum are denoted by solid red lines.

Table 10-16 (INSUFFICIENT DATA)
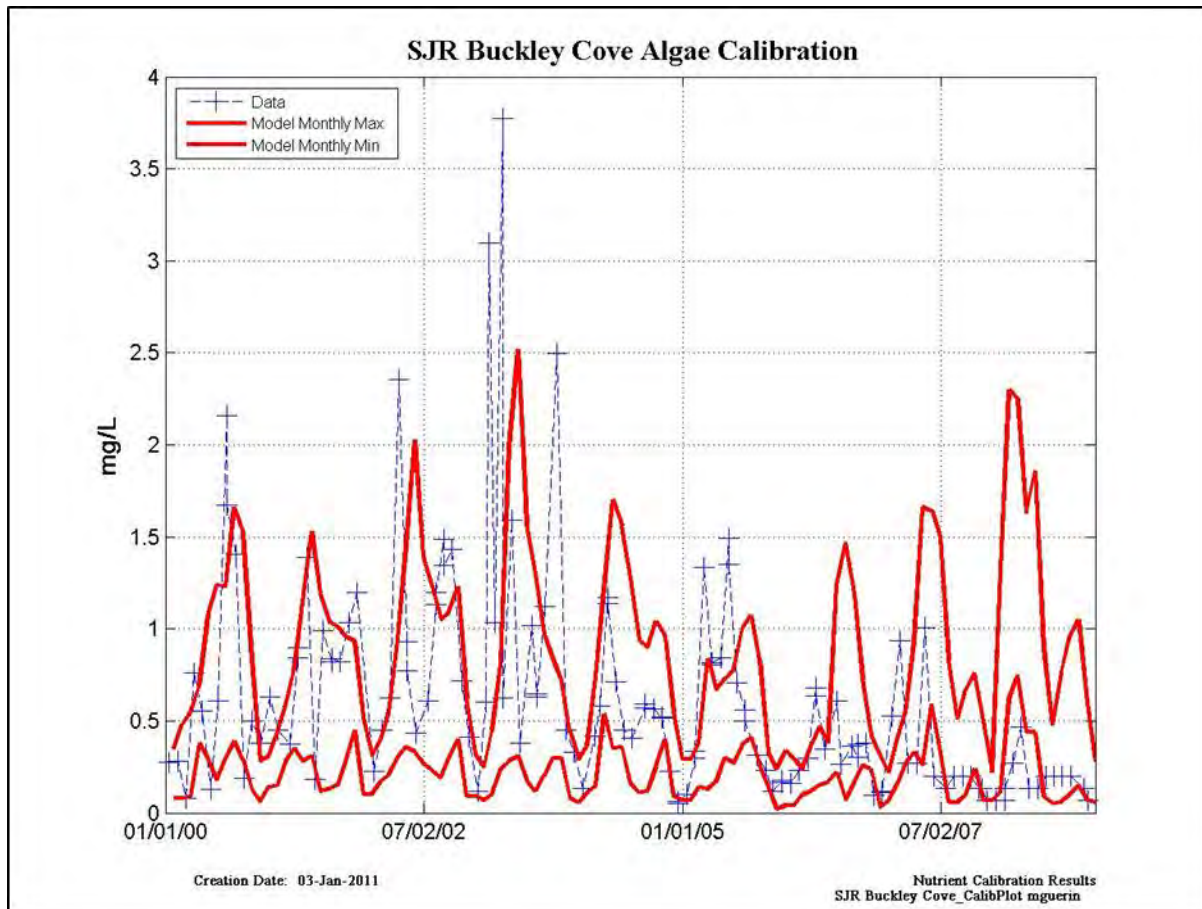
Figure 10-17 Modeled algae (see text for conversion to Chl-a) calibration results at Buckley Cove on the San Joaquin R. – data points are located at blue symbols, monthly modeled maximum and minimum are denoted by solid red lines.

Table 10-17 Model calibration/validation statistics at Buckley Cove for algae (see text for conversion to Chl-a) for the entire modeled period ("All"); Calibration for Dry Years (2001, 2002) and Wet Years (2000, 2003); and Validation for Dry Years (2007, 2008) and Wet Years (2005, 2006).

	NSE	PBIAS	Bias	RSR
ALL	S	VG	Underestimate	S
Dry WY Calibration	VG	VG	Underestimate	G
Wet WY Calibration	S	G	Underestimate	U
Dry WY Validation	S	VG	Overestimate	U
Wet WY Validation	VG	VG	Underestimate	G

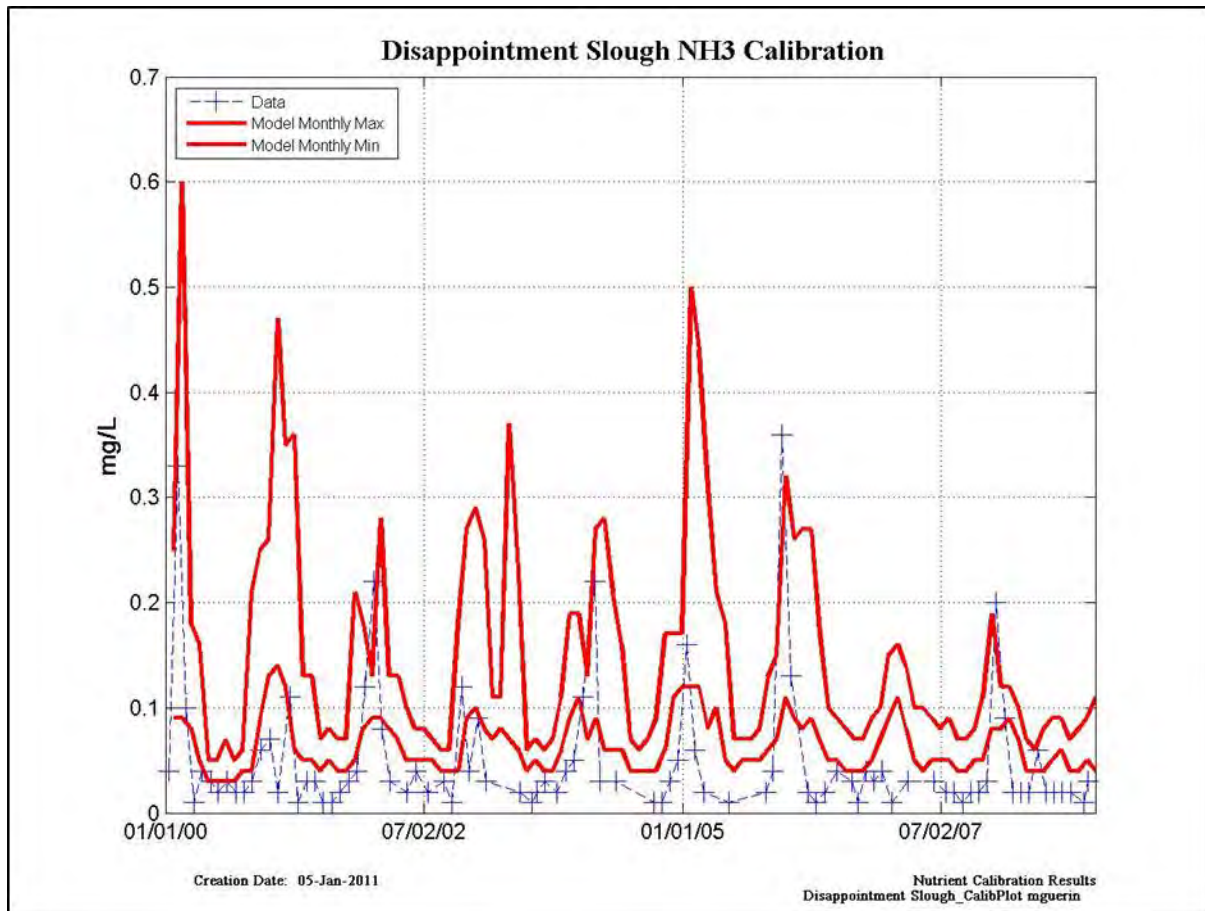**Figure 10-18 Modeled algae (see text for conversion to Chl-a) calibration results at Stockton – data points are located at blue symbols, monthly modeled maximum and minimum are denoted by solid red lines.**

Table 10-18 Model calibration/validation statistics at Stockton for algae (see text for conversion to Chl-a) for the entire modeled period ("All"); Calibration for Dry Years (2001, 2002) and Wet Years (2000, 2003); and Validation for Dry Years (2007, 2008) and Wet Years (2005, 2006).

|	NSE	PBIAS	Bias	RSR
ALL	U	S	Overestimate	U
Dry WY Calibration	U	S	Overestimate	U
Wet WY Calibration	U	S	Overestimate	U
Dry WY Validation	U	S	Overestimate	U
Wet WY Validation	S	VG	No Bias	VG
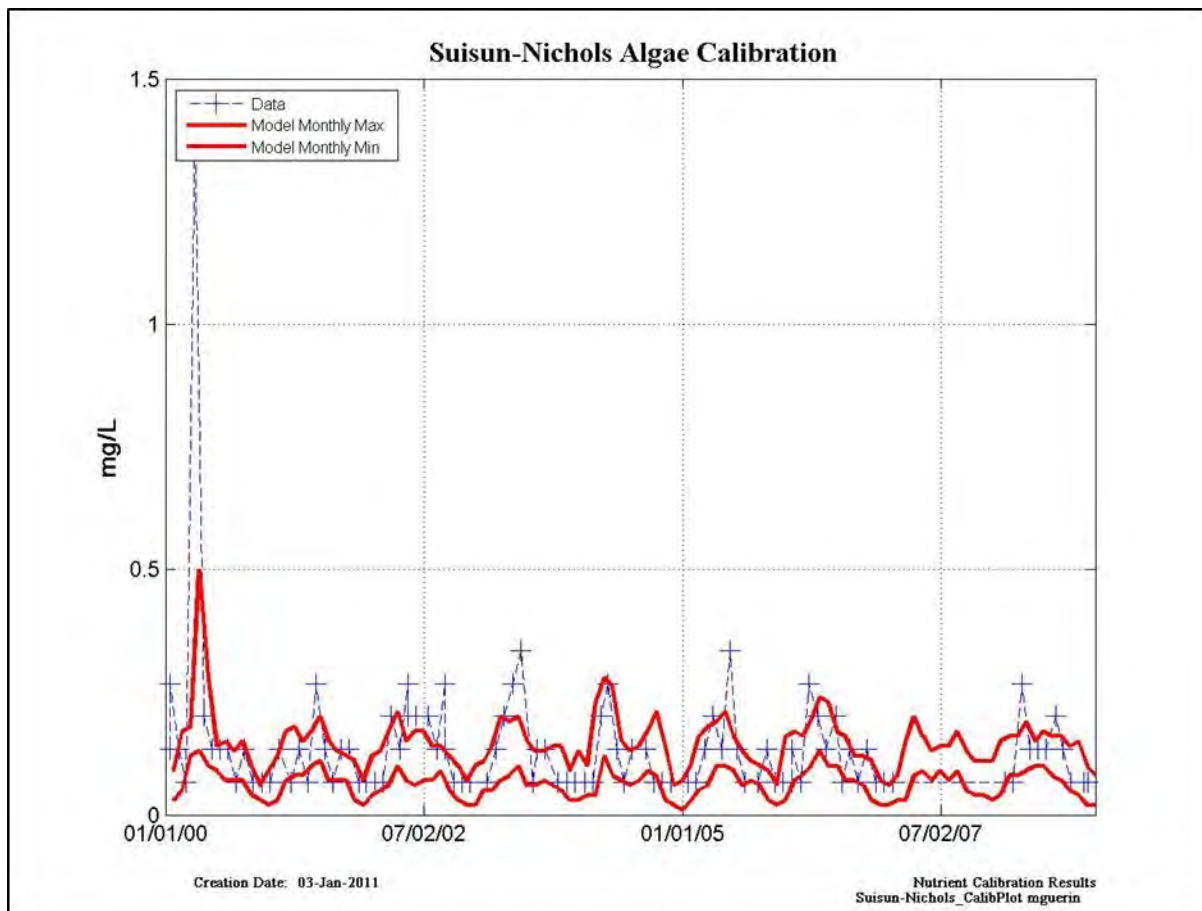
Figure 10-19 Modeled algae (see text for conversion to Chl-a) calibration results at Suisun Nichols – data points are located at blue symbols, monthly modeled maximum and minimum are denoted by solid red lines.

Table 10-19 Model calibration/validation statistics at Suisun Nichols for algae (see text for conversion to Chl-a) for the entire modeled period ("All"); Calibration for Dry Years (2001, 2002) and Wet Years (2000, 2003); and Validation for Dry Years (2007, 2008) and Wet Years (2005, 2006).

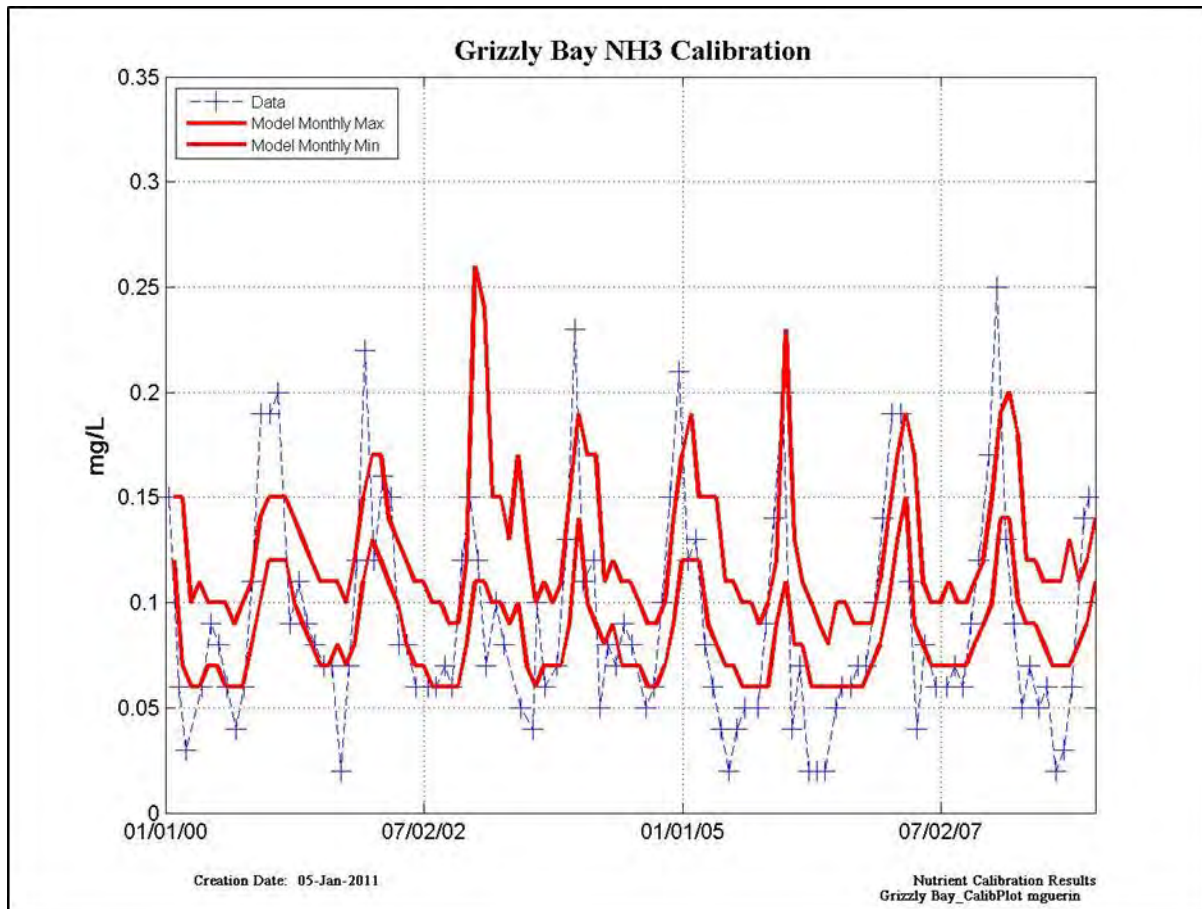|	NSE	PBIAS	Bias	RSR
ALL	S	VG	Underestimate	S
Dry WY Calibration	G	VG	Underestimate	G
Wet WY Calibration	S	G	Underestimate	U
Dry WY Validation	VG	VG	Underestimate	VG
Wet WY Validation	G	VG	Underestimate	G

Figure 10-20 Modeled algae (see text for conversion to Chl-a) calibration results at Suisun Volanti – data points are located at blue symbols, monthly modeled maximum and minimum are denoted by solid red lines.

Table 10-20 Model calibration/validation statistics at Suisun Volanti for algae (see text for conversion to Chl-a) for the entire modeled period ("All"); Calibration for Dry Years (2001, 2002) and Wet Years (2000, 2003); and Validation for Dry Years (2007, 2008) and Wet Years (2005, 2006).

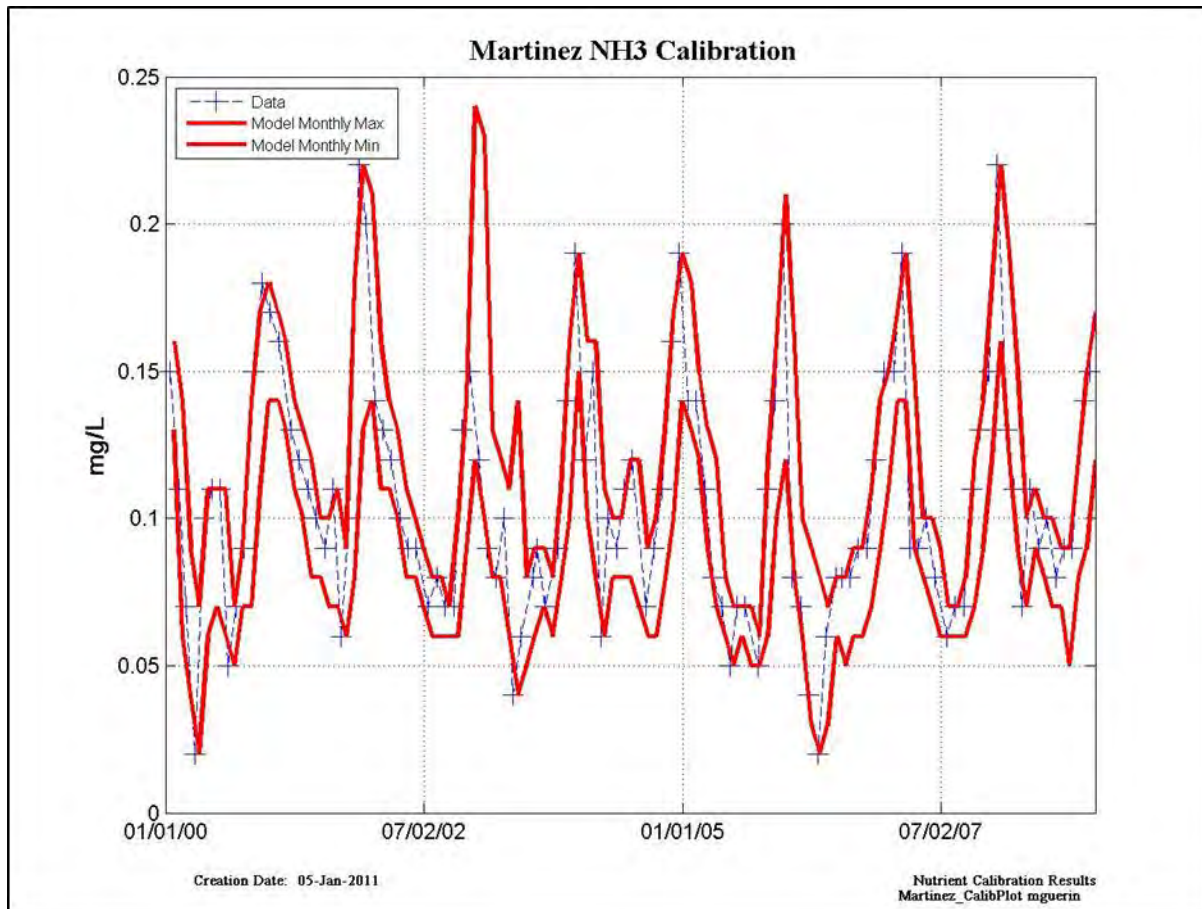|	NSE	PBIAS	Bias	RSR
ALL	U	S	Overestimate	U
Dry WY Calibration	U	S	Overestimate	U
Wet WY Calibration	U	S	Overestimate	U
Dry WY Validation	U	S	Overestimate	U
Wet WY Validation	U	S	Overestimate	U
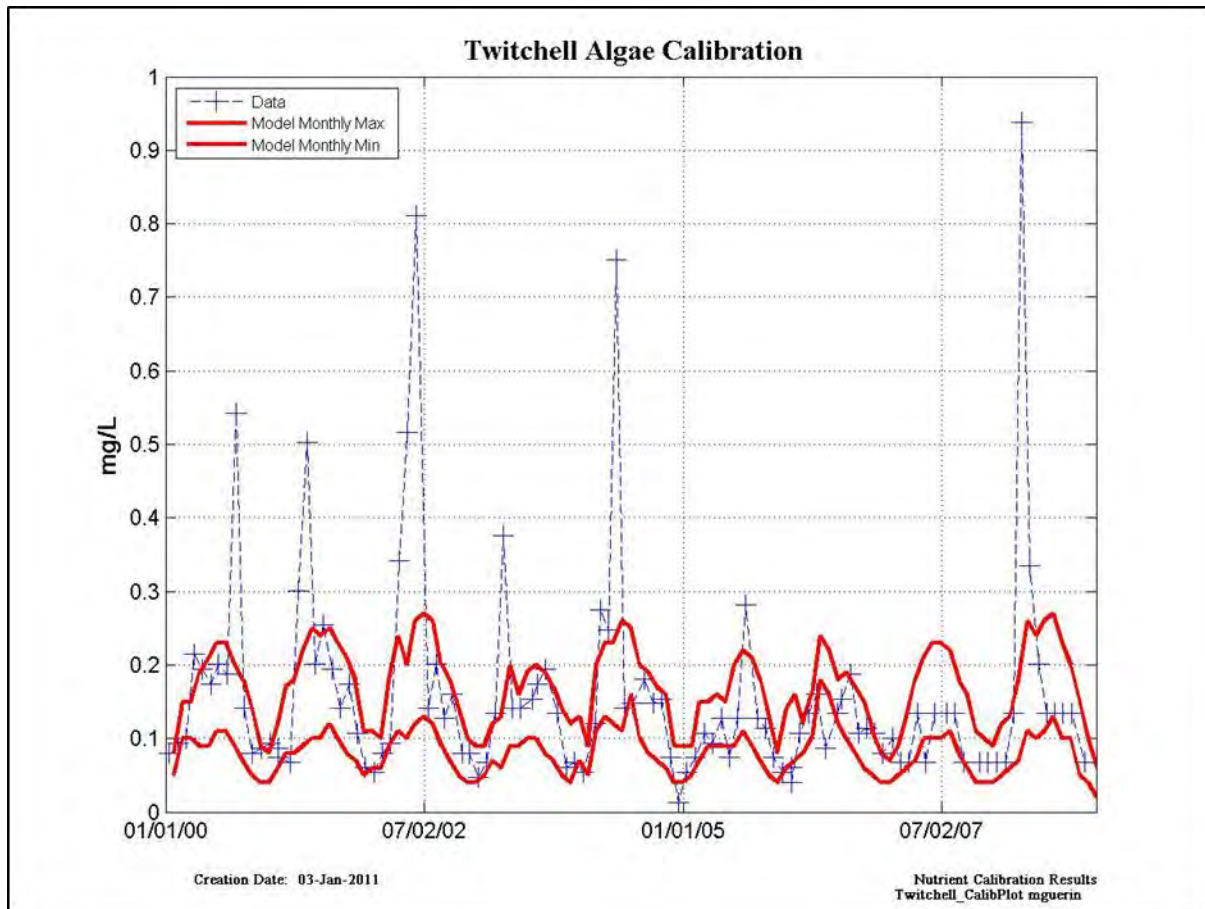
Figure 10-21 Modeled algae (see text for conversion to Chl-a) calibration results at Twitchell – data points are located at blue symbols, monthly modeled maximum and minimum are denoted by solid red lines.

Table 10-21 Model calibration/validation statistics at Twitchell for algae (see text for conversion to Chl-a) for the entire modeled period ("All"); Calibration for Dry Years (2001, 2002) and Wet Years (2000, 2003); and Validation for Dry Years (2007, 2008) and Wet Years (2005, 2006).

	NSE	PBIAS	Bias	RSR
ALL	S	VG	Underestimate	U
Dry WY Calibration	S	VG	Underestimate	U
Wet WY Calibration	S	VG	Underestimate	U
Dry WY Validation	S	VG	Underestimate	U
Wet WY Validation	VG	VG	Overestimate	VG

Dissolved Oxygen

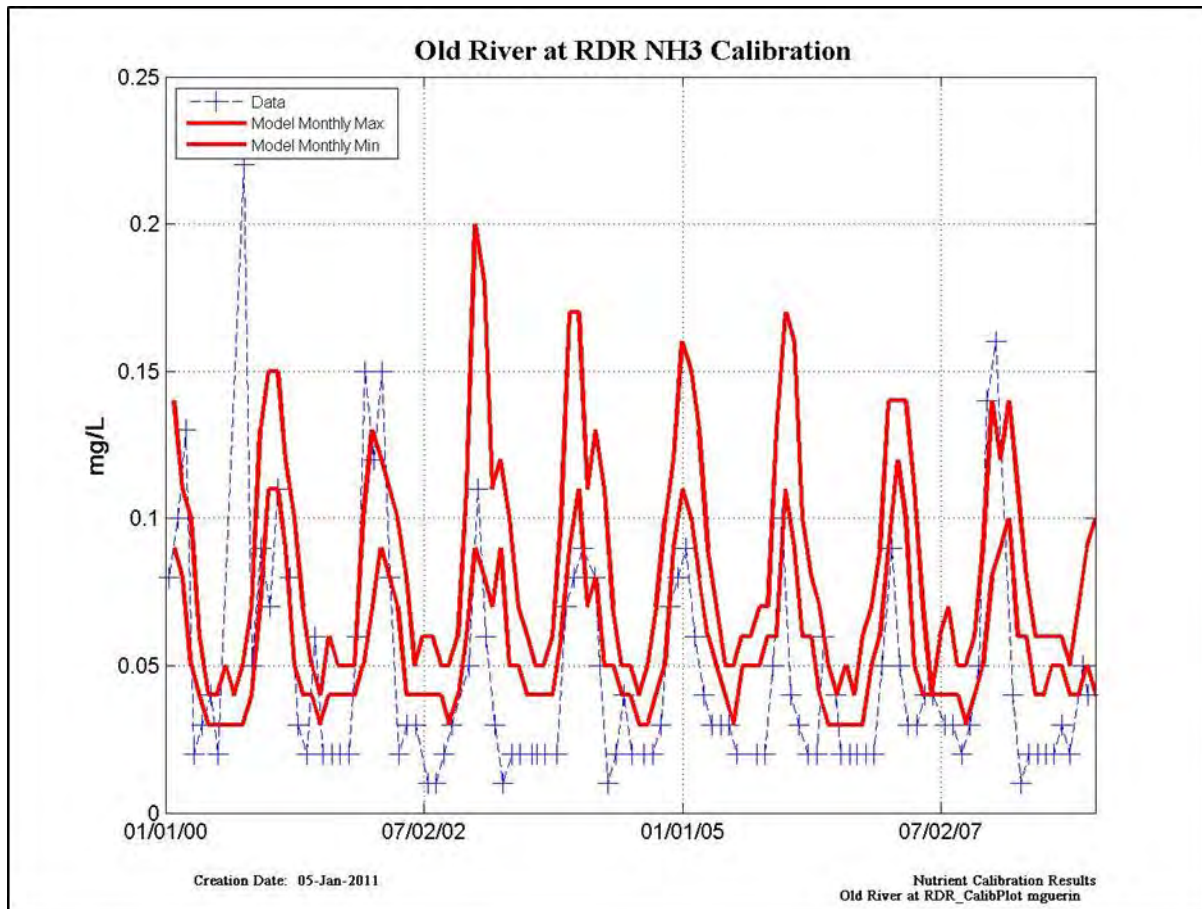**Figure 10-22 Modeled dissolved oxygen calibration results at Antioch – data points are located at blue symbols, monthly modeled maximum and minimum are denoted by solid red lines.**

Table 10-22 Model calibration/validation statistics at Antioch for dissolved oxygen for the entire modeled period ("All"); Calibration for Dry Years (2001, 2002) and Wet Years (2000, 2003); and Validation for Dry Years (2007, 2008) and Wet Years (2005, 2006).

	NSE	PBIAS	Bias	RSR
ALL	VG	VG	Underestimate	VG
Dry WY Calibration	VG	VG	Underestimate	VG
Wet WY Calibration	VG	VG	Underestimate	VG
Dry WY Validation	VG	VG	Underestimate	VG
Wet WY Validation	VG	VG	Overestimate	VG

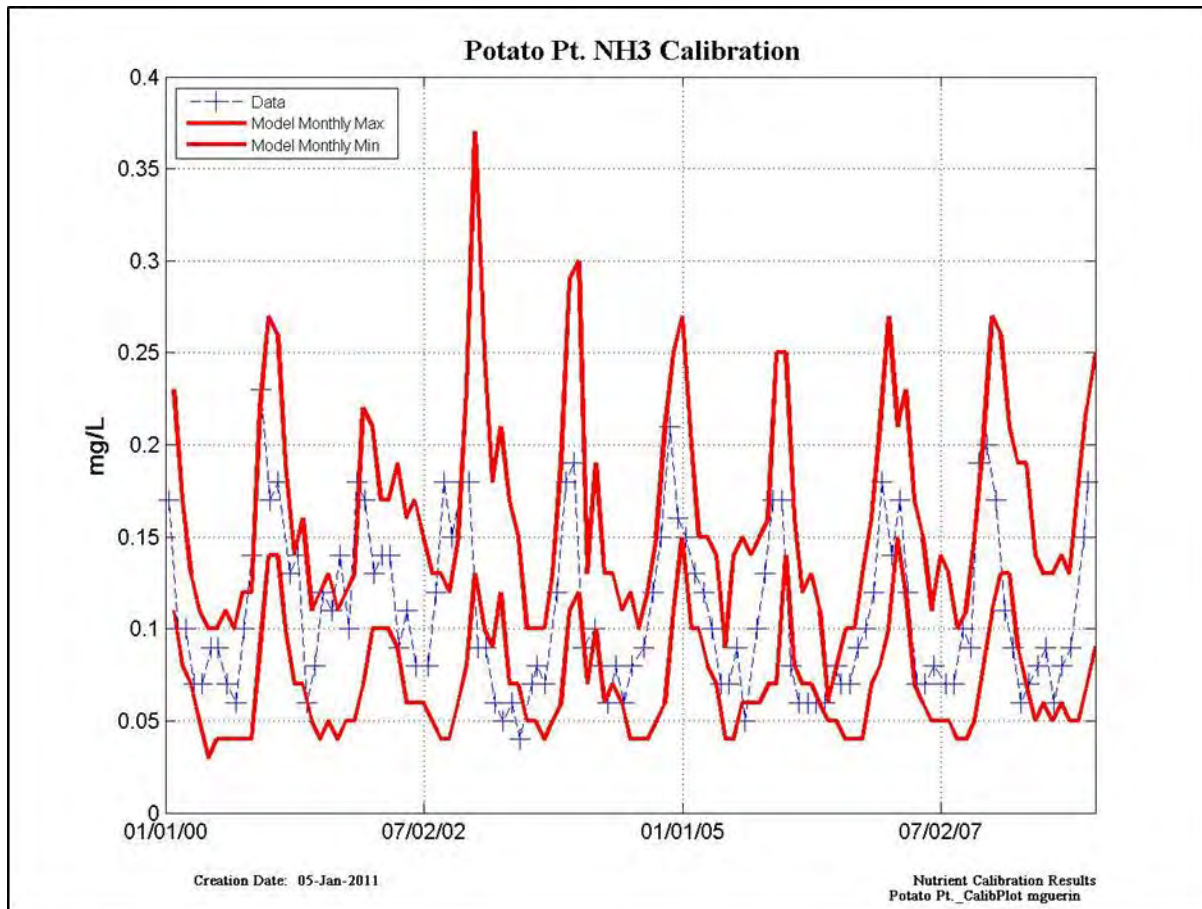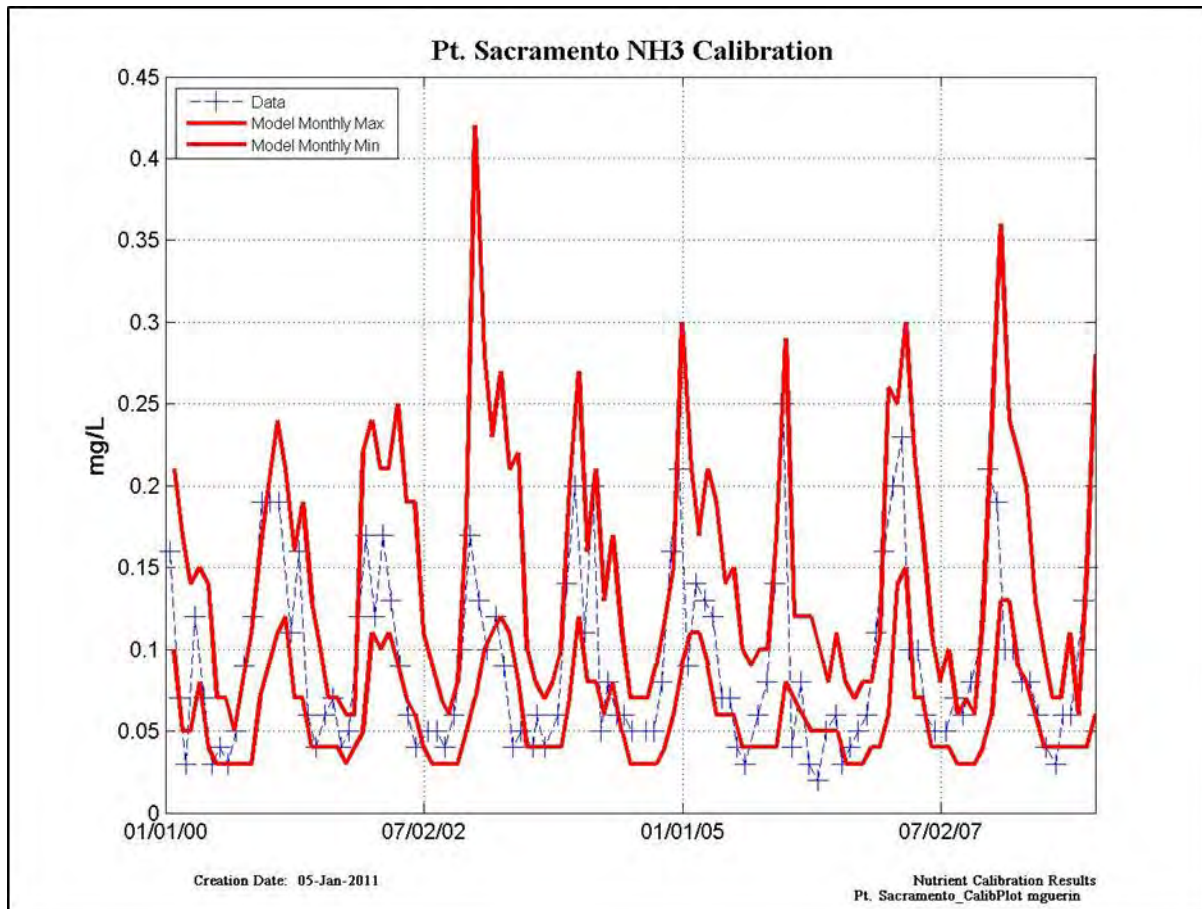**Figure 10-23 Modeled dissolved oxygen calibration results at Chipps – data points are located at blue symbols, monthly modeled maximum and minimum are denoted by solid red lines.**

Table 10-23 Model calibration/validation statistics at Chipps for dissolved oxygen for the entire modeled period ("All"); Calibration for Dry Years (2001, 2002) and Wet Years (2000, 2003); and Validation for Dry Years (2007, 2008) and Wet Years (2005, 2006).

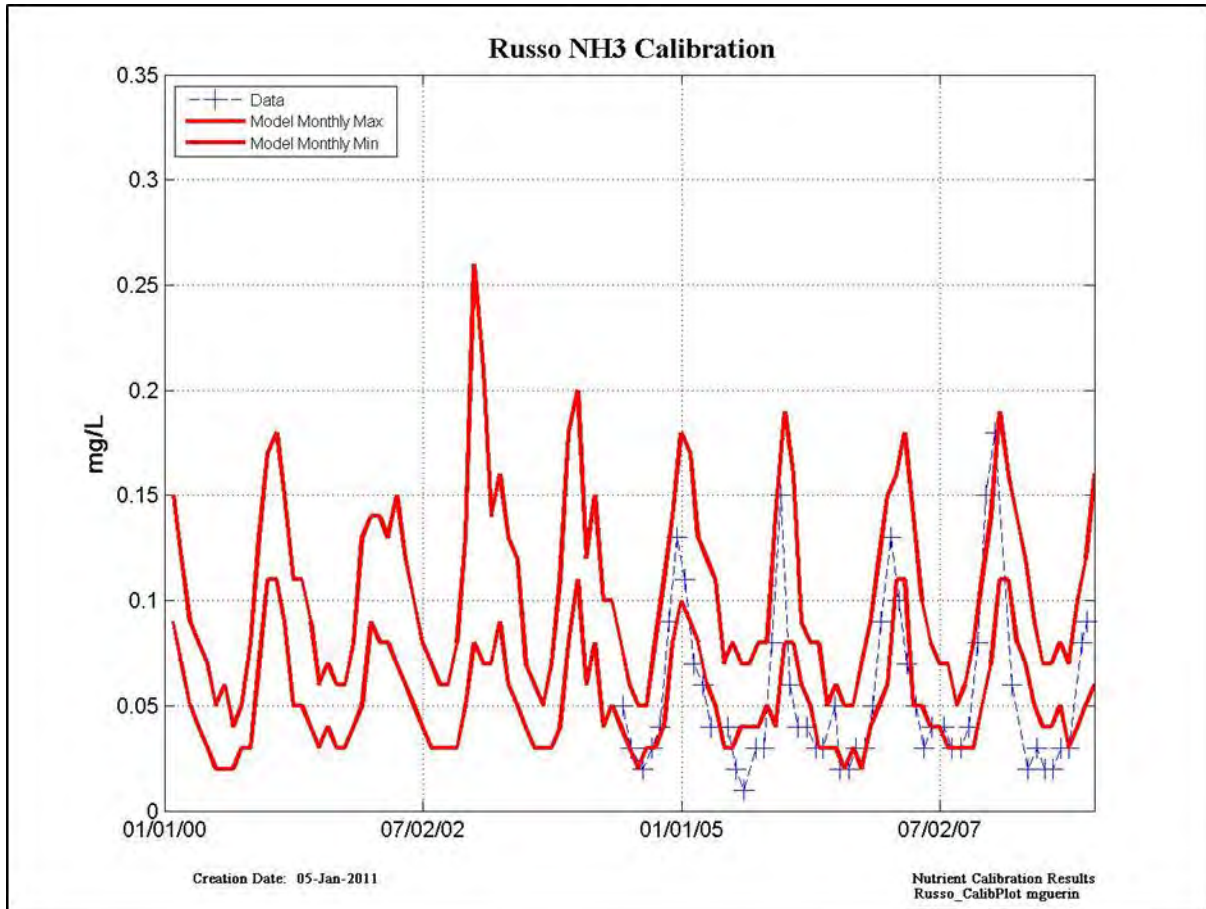|	NSE	PBIAS	Bias	RSR
ALL	VG	VG	Underestimate	VG
Dry WY Calibration	VG	VG	Underestimate	G
Wet WY Calibration	VG	VG	Underestimate	VG
Dry WY Validation	VG	VG	Underestimate	VG
Wet WY Validation	VG	VG	Underestimate	VG

Figure 10-24 Modeled dissolved oxygen calibration results at Disappointment Sl. – data points are located at blue symbols, monthly modeled maximum and minimum are denoted by solid red lines.

Table 10-24 Model calibration/validation statistics at Disappointment Sl. for dissolved oxygen for the entire modeled period ("All"); Calibration for Dry Years (2001, 2002) and Wet Years (2000, 2003); and Validation for Dry Years (2007, 2008) and Wet Years (2005, 2006).

	NSE	PBIAS	Bias	RSR
ALL	S	VG	Underestimate	S
Dry WY Calibration	G	VG	Underestimate	VG
Wet WY Calibration	G	VG	Underestimate	G
Dry WY Validation	S	VG	Underestimate	U
Wet WY Validation	G	VG	Overestimate	G

Figure 10-25 Modeled dissolved oxygen calibration results at Emmaton – data points are located at blue symbols, monthly modeled maximum and minimum are denoted by solid red lines.

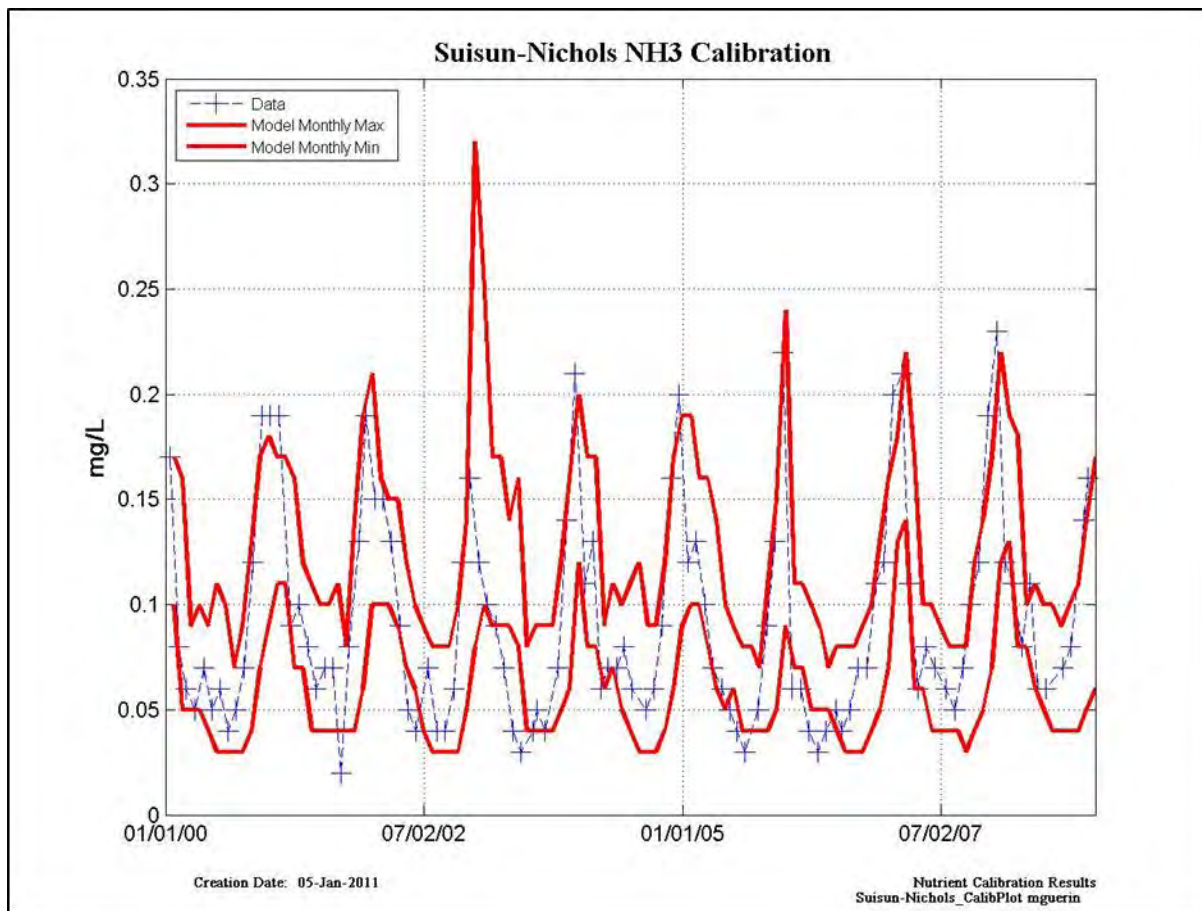**Table 10-25 Model calibration/validation statistics at Antioch for dissolved oxygen for the entire modeled period ("All"); Calibration for Dry Years (2001, 2002) and Wet Years (2000, 2003); and Validation for Dry Years (2007, 2008) and Wet Years (2005, 2006).**

	NSE	PBIAS	Bias	RSR
ALL	VG	VG	Underestimate	VG
Dry WY Calibration	VG	VG	Underestimate	VG
Wet WY Calibration	G	VG	Underestimate	G
Dry WY Validation	VG	VG	Underestimate	VG
Wet WY Validation	VG	VG	Overestimate	VG

238

Figure 10-26 Modeled dissolved oxygen calibration results at Green-Hood – data points are located at blue symbols, monthly modeled maximum and minimum are denoted by solid red lines.

Table 10-26 Model calibration/validation statistics at Green-Hood for dissolved oxygen for the entire modeled period ("All"); Calibration for Dry Years (2001, 2002) and Wet Years (2000, 2003); and Validation for Dry Years (2007, 2008) and Wet Years (2005, 2006).

|	NSE	PBIAS	Bias	RSR
ALL	VG	VG	Overestimate	VG
Dry WY Calibration	VG	VG	Overestimate	VG
Wet WY Calibration	VG	VG	Overestimate	VG
Dry WY Validation	G	VG	Overestimate	G
Wet WY Validation	VG	VG	Overestimate	G

Figure 10-27 Modeled dissolved oxygen calibration results at Grizzly – data points are located at blue symbols, monthly modeled maximum and minimum are denoted by solid red lines.

Table 10-27 Model calibration/validation statistics at Grizzly for dissolved oxygen for the entire modeled period ("All"); Calibration for Dry Years (2001, 2002) and Wet Years (2000, 2003); and Validation for Dry Years (2007, 2008) and Wet Years (2005, 2006).

	NSE	PBIAS	Bias	RSR
ALL	VG	VG	Underestimate	VG
Dry WY Calibration	VG	VG	Underestimate	VG
Wet WY Calibration	VG	VG	Underestimate	VG
Dry WY Validation	VG	VG	Underestimate	VG
Wet WY Validation	VG	VG	Underestimate	VG

Figure 10-28 Modeled dissolved oxygen calibration results at Little Potato Sl. at Terminous – data points are located at blue symbols, monthly modeled maximum and minimum are denoted by solid red lines.

Table 10-28 Model calibration/validation statistics at Little Potato Sl. at Terminous for dissolved oxygen for the entire modeled period ("All"); Calibration for Dry Years (2001, 2002) and Wet Years (2000, 2003); and Validation for Dry Years (2007, 2008) and Wet Years (2005, 2006).

	NSE	PBIAS	Bias	RSR
ALL	G	VG	Overestimate	G
Dry WY Calibration	G	VG	Overestimate	G
Wet WY Calibration	VG	VG	Overestimate	VG
Dry WY Validation	VG	VG	Overestimate	VG
Wet WY Validation	S	VG	No Bias	VG

241

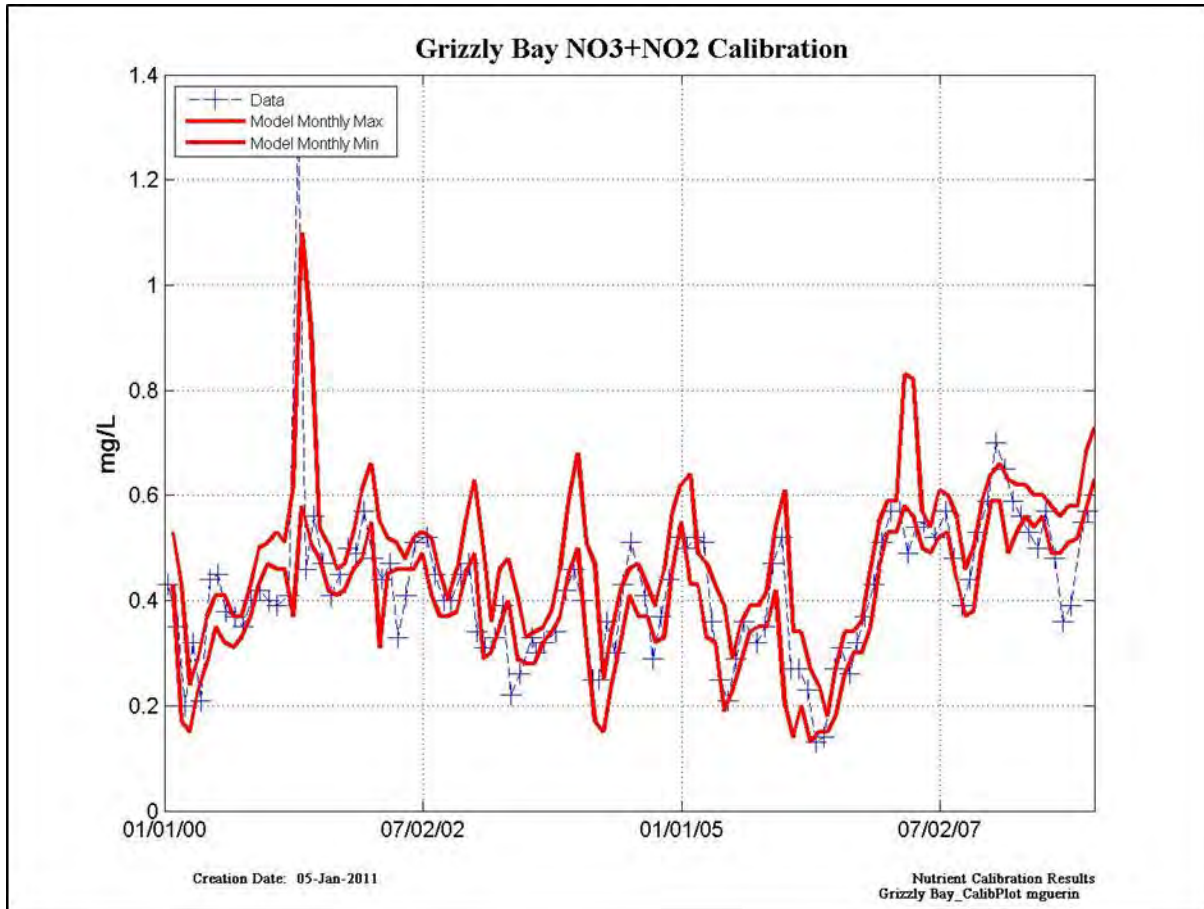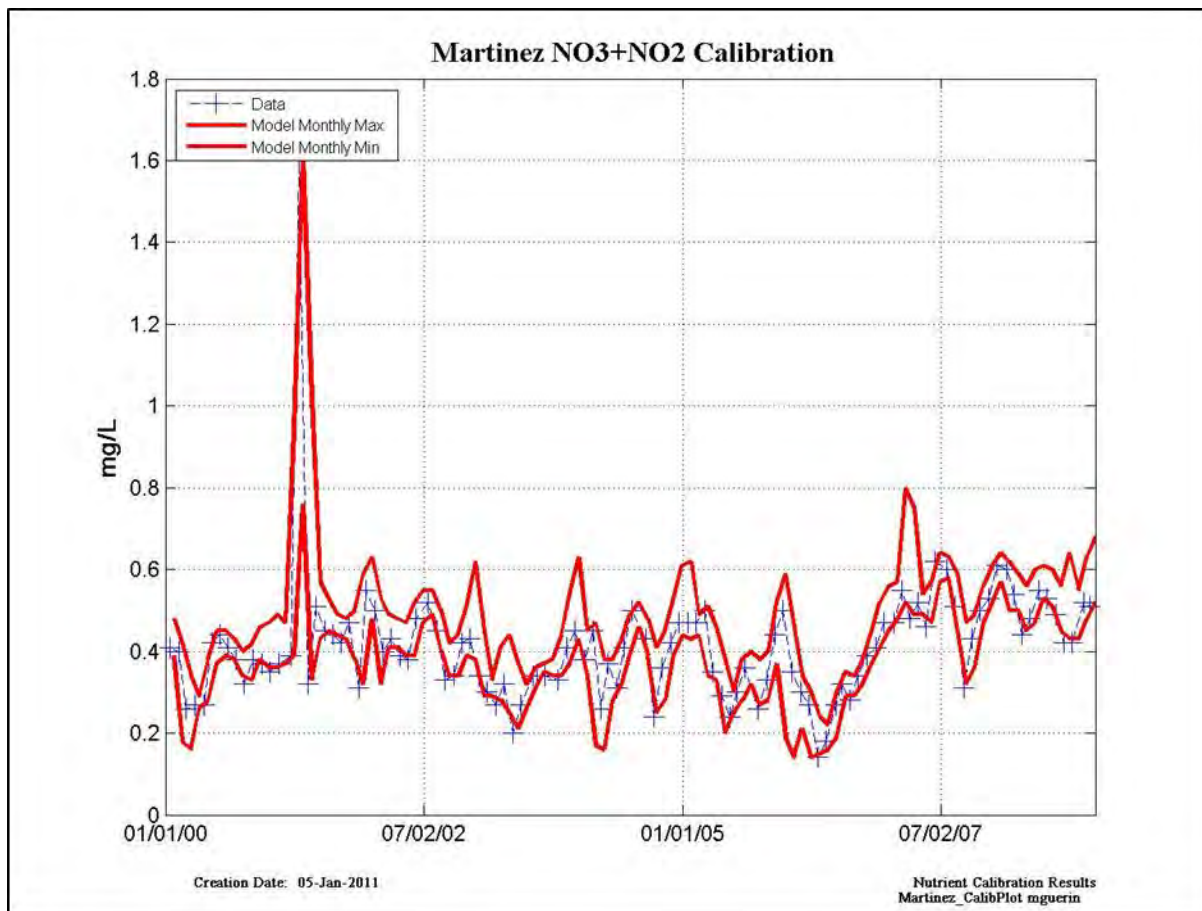**Figure 10-29 Modeled dissolved oxygen calibration results at Martinez – data points are located at blue symbols, monthly modeled maximum and minimum are denoted by solid red lines.**

Table 10-29 Model calibration/validation statistics at Martinez for dissolved oxygen for the entire modeled period ("All"); Calibration for Dry Years (2001, 2002) and Wet Years (2000, 2003); and Validation for Dry Years (2007, 2008) and Wet Years (2005, 2006).

	NSE	PBIAS	Bias	RSR
ALL	VG	VG	Underestimate	VG
Dry WY Calibration	VG	VG	Underestimate	VG
Wet WY Calibration	VG	VG	Underestimate	VG
Dry WY Validation	VG	VG	Underestimate	VG
Wet WY Validation	VG	VG	Underestimate	VG

Figure 10-30 Modeled dissolved oxygen calibration results at Montezuma Sl. Bend 2 – data points are located at blue symbols, monthly modeled maximum and minimum are denoted by solid red lines.

Table 10-30 Model calibration/validation statistics at Montezuma Sl. Bend 2 for dissolved oxygen for the entire modeled period ("All"); Calibration for Dry Years (2001, 2002) and Wet Years (2000, 2003); and Validation for Dry Years (2007, 2008) and Wet Years (2005, 2006).

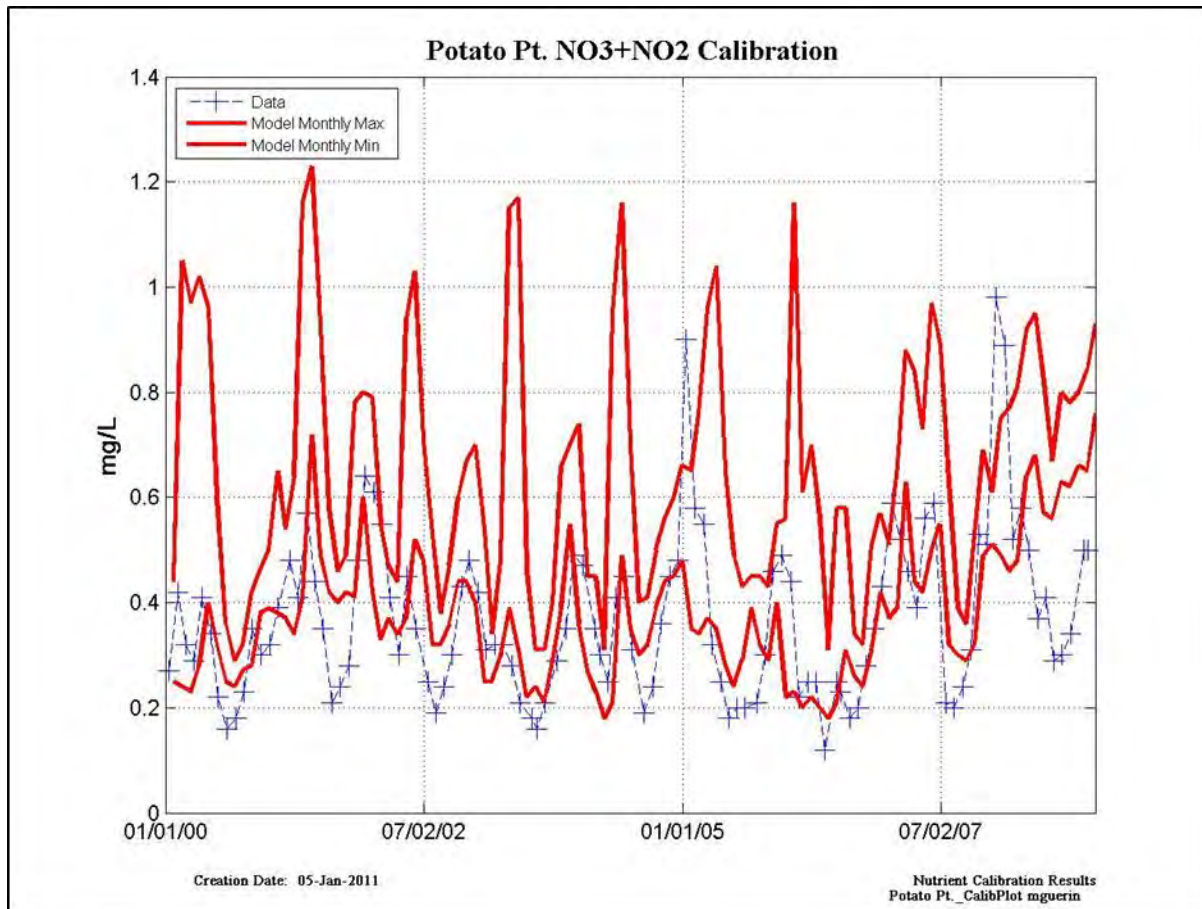|	NSE	PBIAS	Bias	RSR
ALL	VG	VG	Overestimate	VG
Dry WY Calibration	VG	VG	Overestimate	VG
Wet WY Calibration	VG	VG	Overestimate	VG
Dry WY Validation	VG	VG	Underestimate	VG
Wet WY Validation	S	VG	Overestimate	U

243

Figure 10-31 Modeled dissolved oxygen calibration results at Old R. at RDR – data points are located at blue symbols, monthly modeled maximum and minimum are denoted by solid red lines.

Table 10-31 Model calibration/validation statistics at Old R. at RDR for dissolved oxygen for the entire modeled period ("All"); Calibration for Dry Years (2001, 2002) and Wet Years (2000, 2003); and Validation for Dry Years (2007, 2008) and Wet Years (2005, 2006).

	NSE	PBIAS	Bias	RSR
ALL	VG	VG	Underestimate	VG
Dry WY Calibration	VG	VG	Underestimate	VG
Wet WY Calibration	VG	VG	Underestimate	G
Dry WY Validation	VG	VG	Underestimate	VG
Wet WY Validation	VG	VG	Underestimate	VG

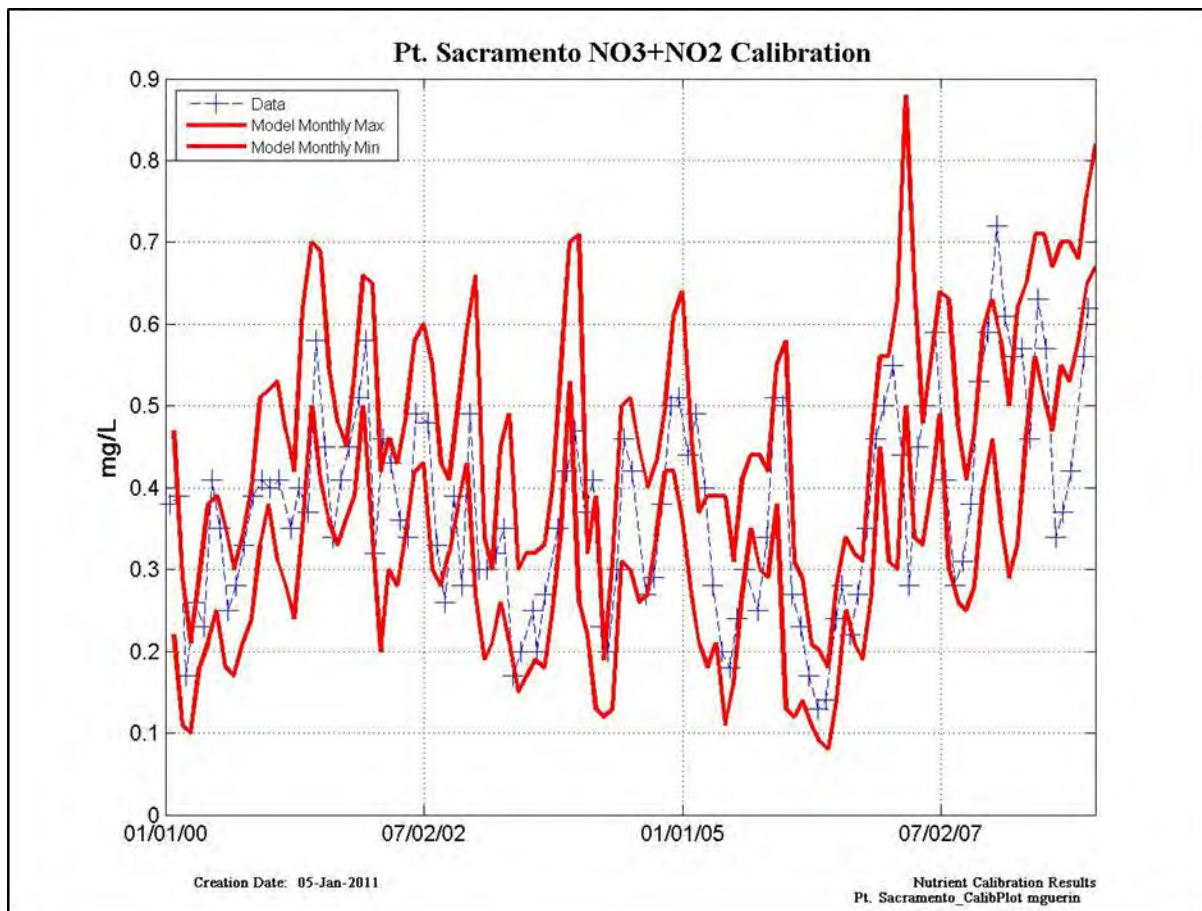**Figure 10-32 Modeled dissolved oxygen calibration results at Potato Pt. – data points are located at blue symbols, monthly modeled maximum and minimum are denoted by solid red lines.**

Table 10-32 Model calibration/validation statistics at Potato Pt. for dissolved oxygen for the entire modeled period ("All"); Calibration for Dry Years (2001, 2002) and Wet Years (2000, 2003); and Validation for Dry Years (2007, 2008) and Wet Years (2005, 2006).

	NSE	PBIAS	Bias	RSR
ALL	VG	VG	Underestimate	VG
Dry WY Calibration	VG	VG	Underestimate	VG
Wet WY Calibration	VG	VG	Underestimate	VG
Dry WY Validation	VG	VG	Underestimate	VG
Wet WY Validation	VG	VG	Underestimate	VG

245

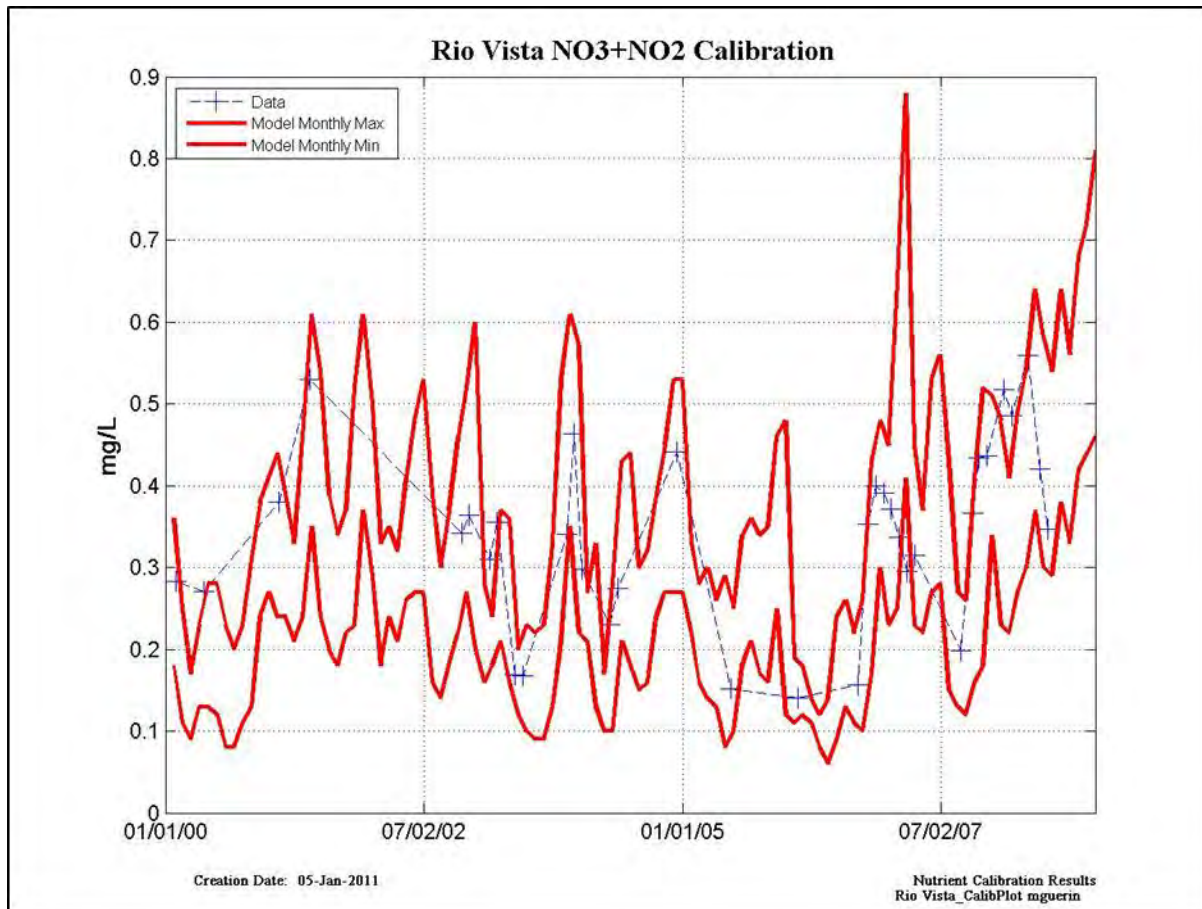**Figure 10-33 Modeled dissolved oxygen calibration results at Pittsburg – data points are located at blue symbols, monthly modeled maximum and minimum are denoted by solid red lines.**

Table 10-33 Model calibration/validation statistics at Pittsburg for dissolved oxygen for the entire modeled period ("All"); Calibration for Dry Years (2001, 2002) and Wet Years (2000, 2003); and Validation for Dry Years (2007, 2008) and Wet Years (2005, 2006).

|	NSE	PBIAS	Bias	RSR
ALL	VG	VG	Overestimate	VG
Dry WY Calibration	VG	VG	Underestimate	VG
Wet WY Calibration	VG	VG	Overestimate	VG
Dry WY Validation	VG	VG	Underestimate	VG
Wet WY Validation	S	VG	Overestimate	U

Figure 10-34 Modeled dissolved oxygen calibration results at Pt. Sacramento – data points are located at blue symbols, monthly modeled maximum and minimum are denoted by solid red lines.

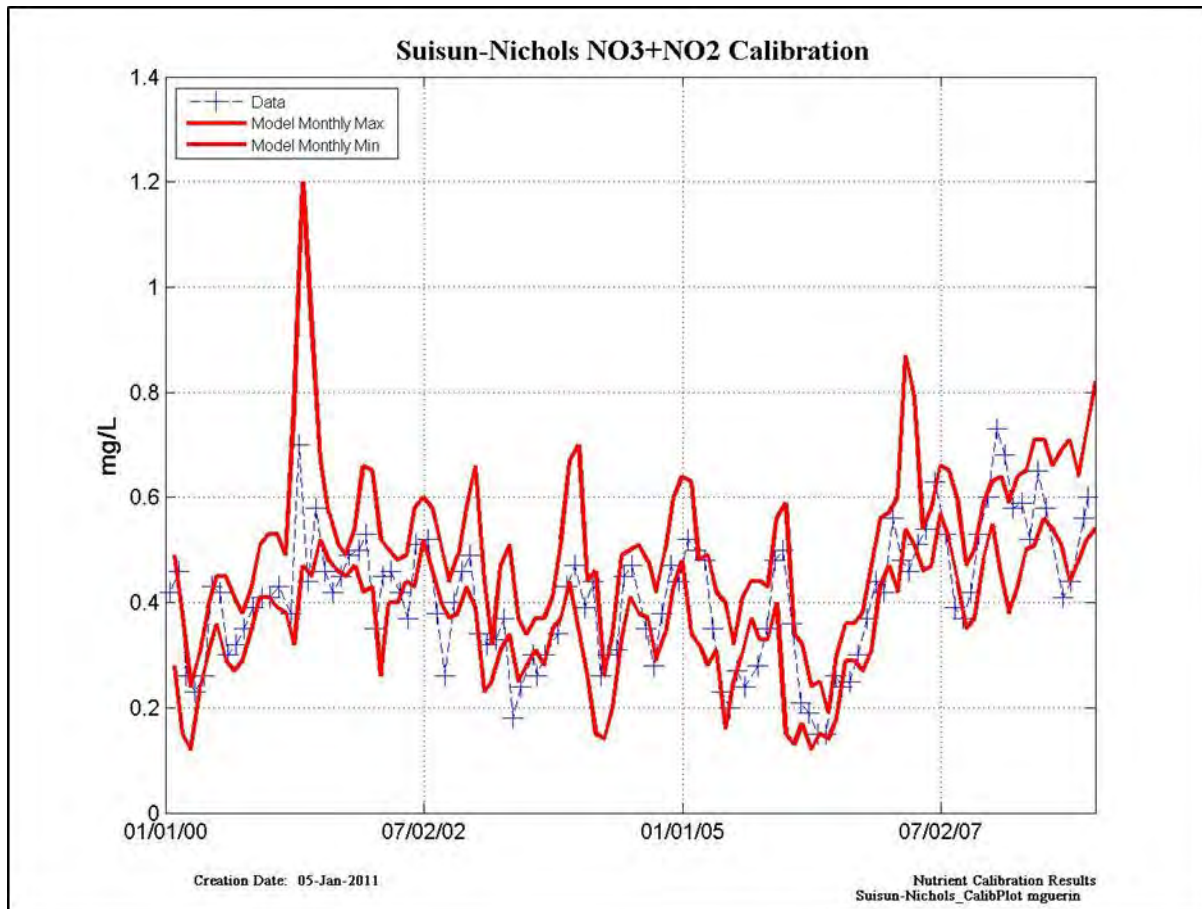**Table 10-34 Model calibration/validation statistics at Pt. Sacramento for dissolved oxygen for the entire modeled period ("All"); Calibration for Dry Years (2001, 2002) and Wet Years (2000, 2003); and Validation for Dry Years (2007, 2008) and Wet Years (2005, 2006).**

	NSE	PBIAS	Bias	RSR
ALL	VG	VG	Underestimate	VG
Dry WY Calibration	VG	VG	Underestimate	VG
Wet WY Calibration	VG	VG	Underestimate	VG
Dry WY Validation	VG	VG	Underestimate	VG
Wet WY Validation	VG	VG	Overestimate	VG

Figure 10-35 Modeled dissolved oxygen calibration results at Rio Vista – data points are located at blue symbols, monthly modeled maximum and minimum are denoted by solid red lines.

Table 10-35 Model calibration/validation statistics at Rio Vista for dissolved oxygen for the entire modeled period ("All"); Calibration for Dry Years (2001, 2002) and Wet Years (2000, 2003); and Validation for Dry Years (2007, 2008) and Wet Years (2005, 2006).

|	NSE	PBIAS	Bias	RSR
ALL	VG	VG	Overestimate	VG
Dry WY Calibration	VG	VG	Overestimate	VG
Wet WY Calibration	VG	VG	Overestimate	VG
Dry WY Validation	VG	VG	Overestimate	VG
Wet WY Validation	VG	VG	Overestimate	VG

Figure 10-36 Modeled dissolved oxygen calibration results at Roe Island – data points are located at blue symbols, monthly modeled maximum and minimum are denoted by solid red lines.

Table 10-36 Model calibration/validation statistics at Roe Island for dissolved oxygen for the entire modeled period ("All"); Calibration for Dry Years (2001, 2002) and Wet Years (2000, 2003); and Validation for Dry Years (2007, 2008) and Wet Years (2005, 2006).

|	NSE	PBIAS	Bias	RSR
ALL	VG	VG	Overestimate	VG
Dry WY Calibration	VG	VG	Underestimate	VG
Wet WY Calibration	VG	VG	Overestimate	VG
Dry WY Validation	VG	VG	Underestimate	VG
Wet WY Validation	G	VG	Overestimate	G

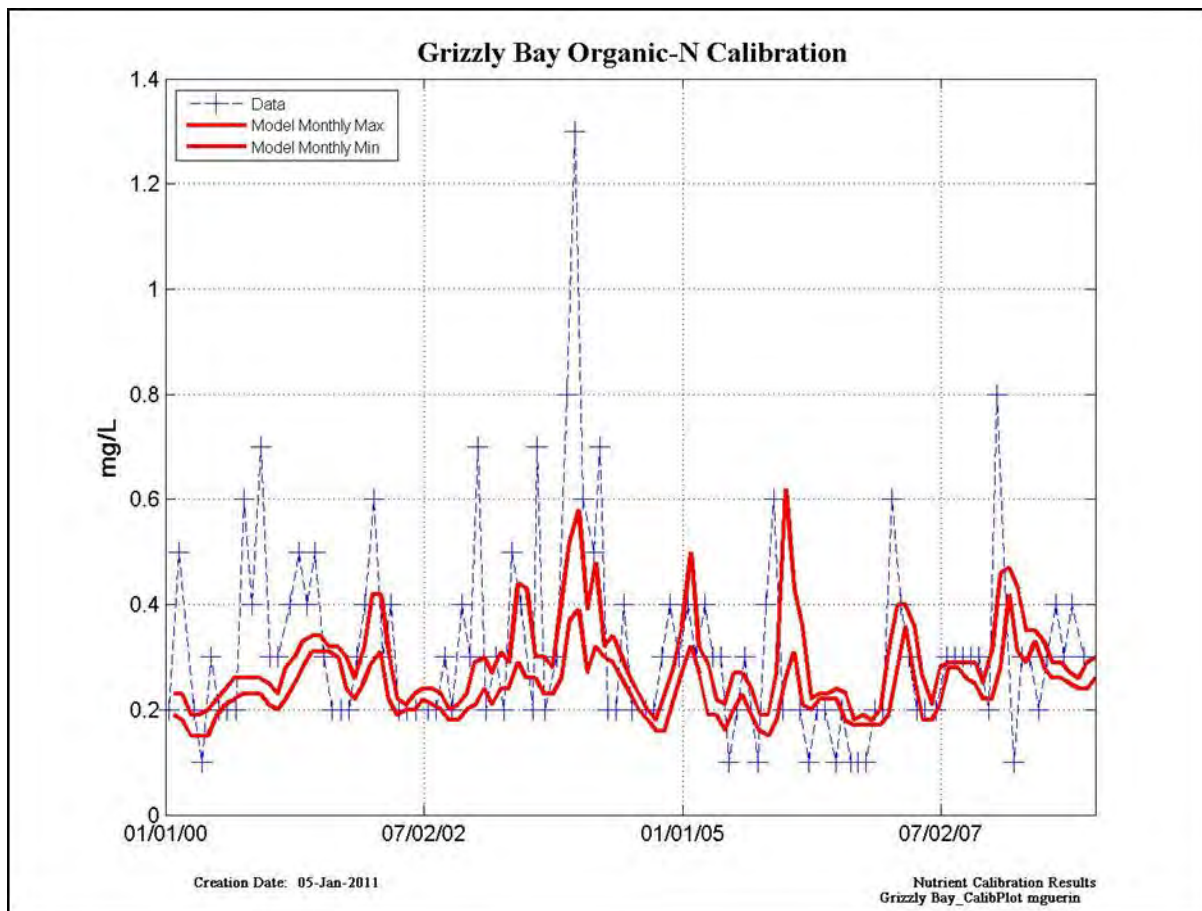**Figure 10-37 Modeled dissolved oxygen calibration results at Russo – data points are located at blue symbols, monthly modeled maximum and minimum are denoted by solid red lines.**

Table 10-37 (INSUFFICIENT DATA)

Figure 10-38 Modeled dissolved oxygen calibration results at Buckley Cove on the San Joaquin R. – data points are located at blue symbols, monthly modeled maximum and minimum are denoted by solid red lines.

Table 10-38 Model calibration/validation statistics at Buckley Cove for dissolved oxygen for the entire modeled period ("All"); Calibration for Dry Years (2001, 2002) and Wet Years (2000, 2003); and Validation for Dry Years (2007, 2008) and Wet Years (2005, 2006).

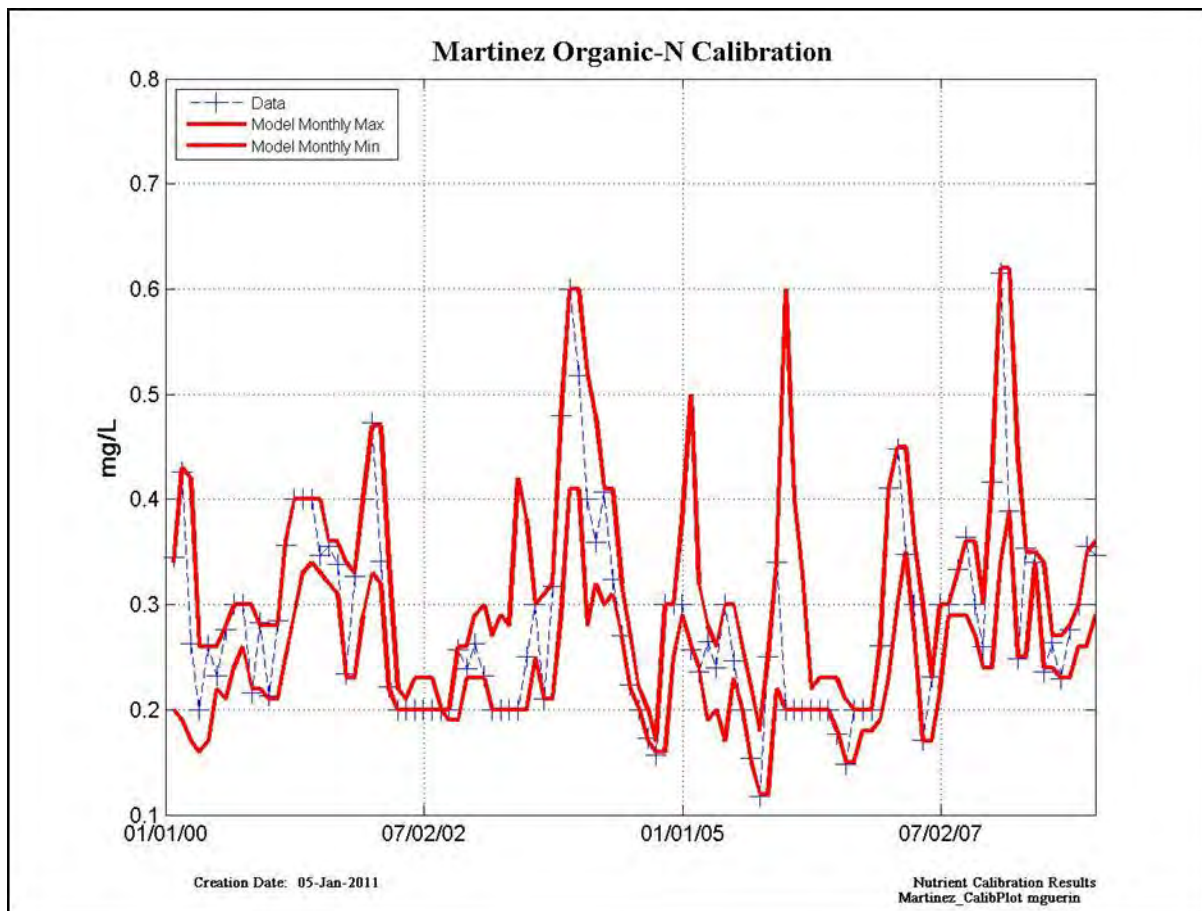|	NSE	PBIAS	Bias	RSR
ALL	VG	VG	Overestimate	VG
Dry WY Calibration	VG	VG	Overestimate	VG
Wet WY Calibration	VG	VG	Underestimate	VG
Dry WY Validation	VG	VG	Overestimate	VG
Wet WY Validation	VG	VG	Overestimate	VG

Figure 10-39 Modeled dissolved oxygen calibration results at Suisun Nichols – data points are located at blue symbols, monthly modeled maximum and minimum are denoted by solid red lines.

Table 10-39 Model calibration/validation statistics at Suisun Nichols for dissolved oxygen for the entire modeled period ("All"); Calibration for Dry Years (2001, 2002) and Wet Years (2000, 2003); and Validation for Dry Years (2007, 2008) and Wet Years (2005, 2006).

	NSE	PBIAS	Bias	RSR
ALL	VG	VG	Underestimate	VG
Dry WY Calibration	G	VG	Underestimate	G
Wet WY Calibration	G	VG	Underestimate	G
Dry WY Validation	VG	VG	Underestimate	VG
Wet WY Validation	VG	VG	Underestimate	VG

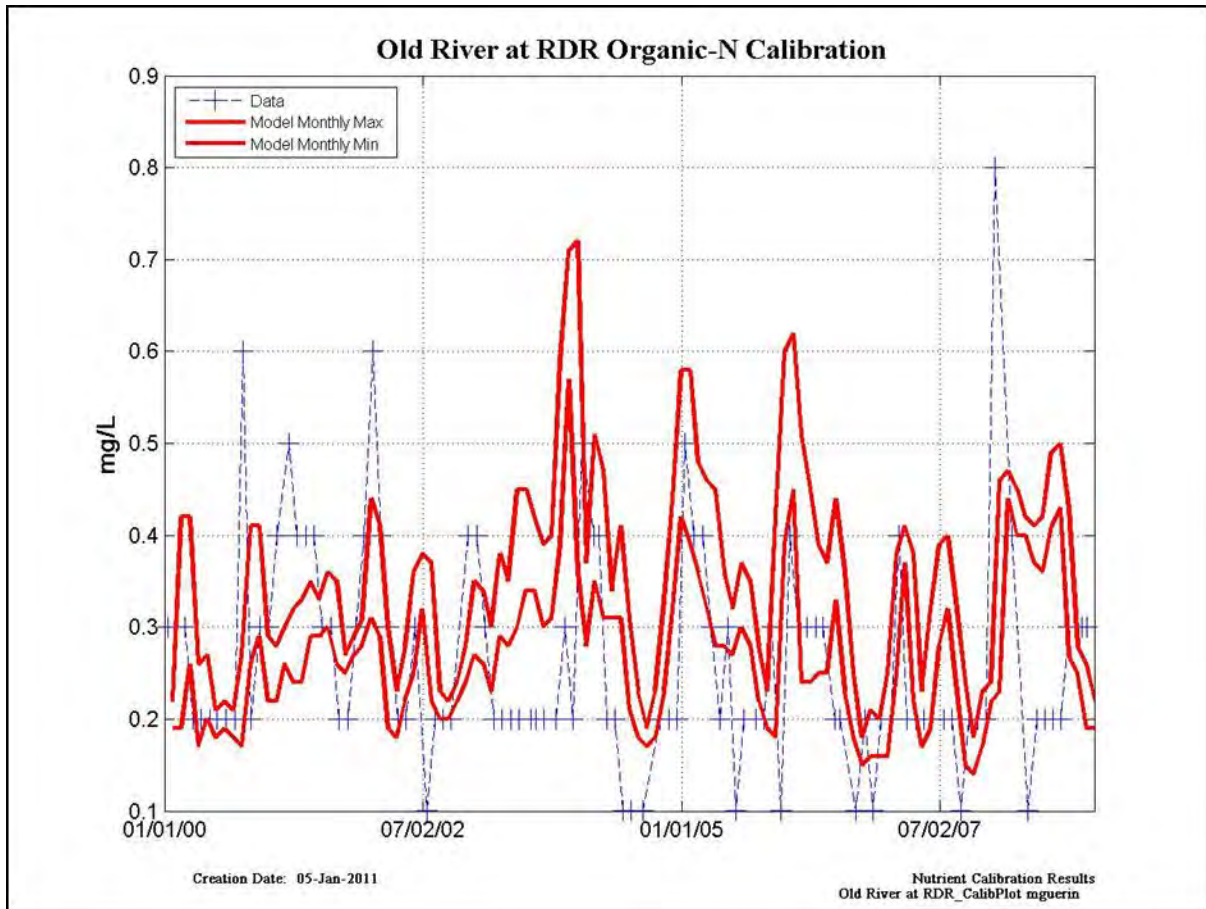**Figure 10-40 Modeled dissolved oxygen calibration results at Suisun Volanti – data points are located at blue symbols, monthly modeled maximum and minimum are denoted by solid red lines.**

Table 10-40 Model calibration/validation statistics at Suisun Volanti for dissolved oxygen for the entire modeled period ("All"); Calibration for Dry Years (2001, 2002) and Wet Years (2000, 2003); and Validation for Dry Years (2007, 2008) and Wet Years (2005, 2006).

	NSE	PBIAS	Bias	RSR
ALL	VG	VG	Overestimate	G
Dry WY Calibration	S	VG	Overestimate	S
Wet WY Calibration	G	VG	Overestimate	G
Dry WY Validation	VG	VG	Overestimate	VG
Wet WY Validation	S	VG	Overestimate	U

253

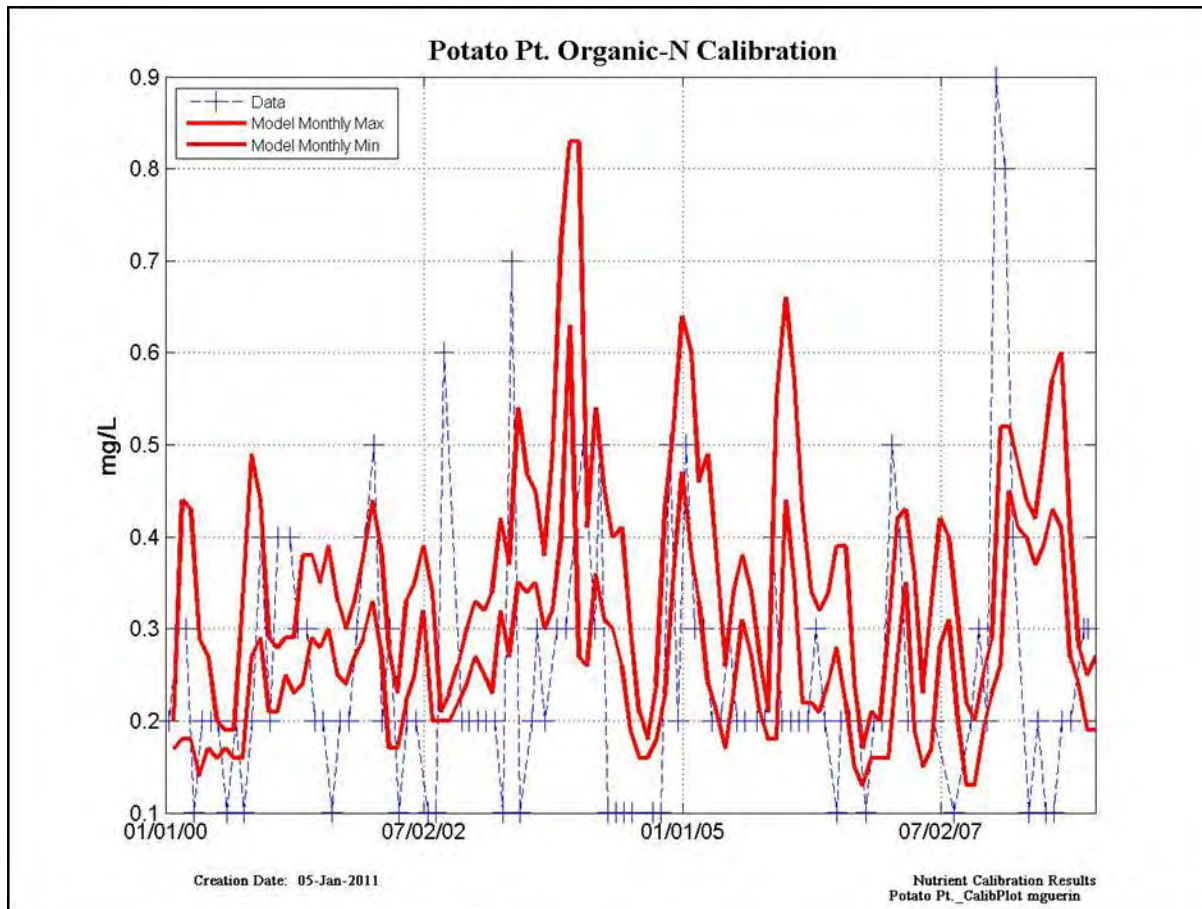**Figure 10-41 Modeled dissolved oxygen calibration results at Twitchell – data points are located at blue symbols, monthly modeled maximum and minimum are denoted by solid red lines.**

Table 10-41 Model calibration/validation statistics at Twitchell for dissolved oxygen for the entire modeled period ("All"); Calibration for Dry Years (2001, 2002) and Wet Years (2000, 2003); and Validation for Dry Years (2007, 2008) and Wet Years (2005, 2006).

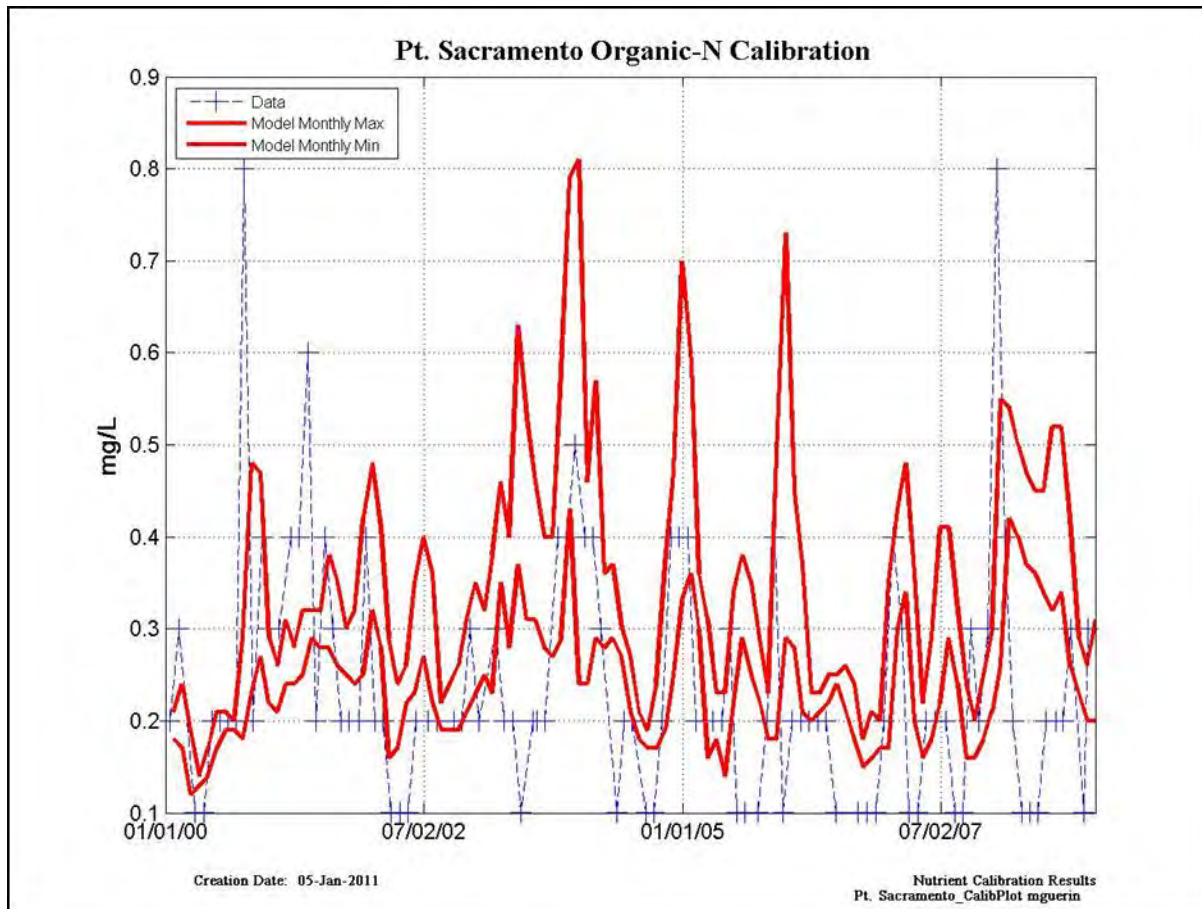|	NSE	PBIAS	Bias	RSR
ALL	VG	VG	Underestimate	VG
Dry WY Calibration	VG	VG	Underestimate	VG
Wet WY Calibration	VG	VG	Underestimate	G
Dry WY Validation	VG	VG	Underestimate	VG
Wet WY Validation	VG	VG	Underestimate	VG

NH3

Figure 10-42 NH$_3$ calibration results at Disappointment Sl. – data points are located at blue symbols, monthly modeled maximum and minimum are denoted by solid red lines.

Table 10-42 Model calibration/validation statistics at Disappointment Sl. for NH$_3$ for the entire modeled period ("All"); Calibration for Dry Years (2001, 2002) and Wet Years (2000, 2003); and Validation for Dry Years (2007, 2008) and Wet Years (2005, 2006).

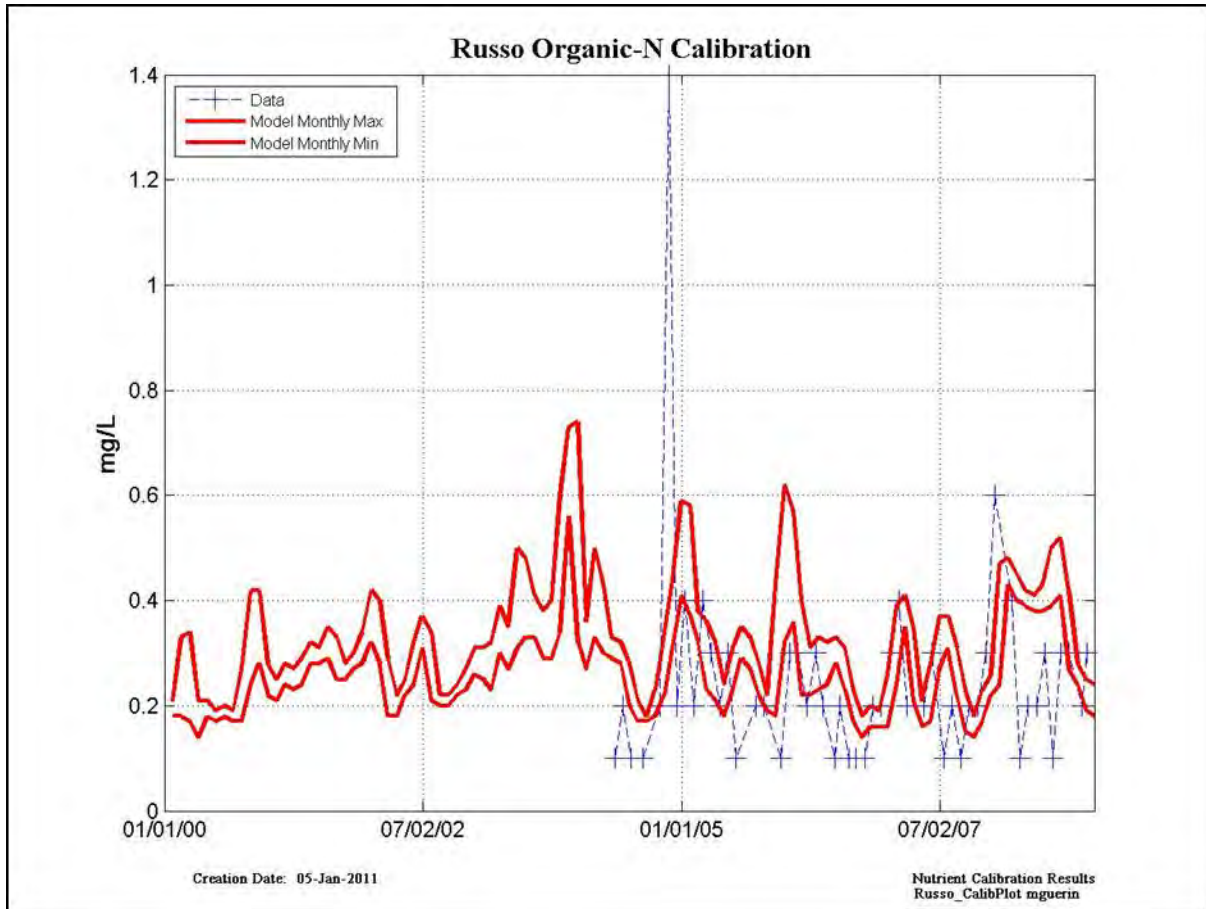|	NSE	PBIAS	Bias	RSR
ALL	VG	S	Overestimate	S
Dry WY Calibration	VG	S	Overestimate	U
Wet WY Calibration	VG	S	Overestimate	G
Dry WY Validation	S	S	Overestimate	U
Wet WY Validation	VG	S	Overestimate	VG
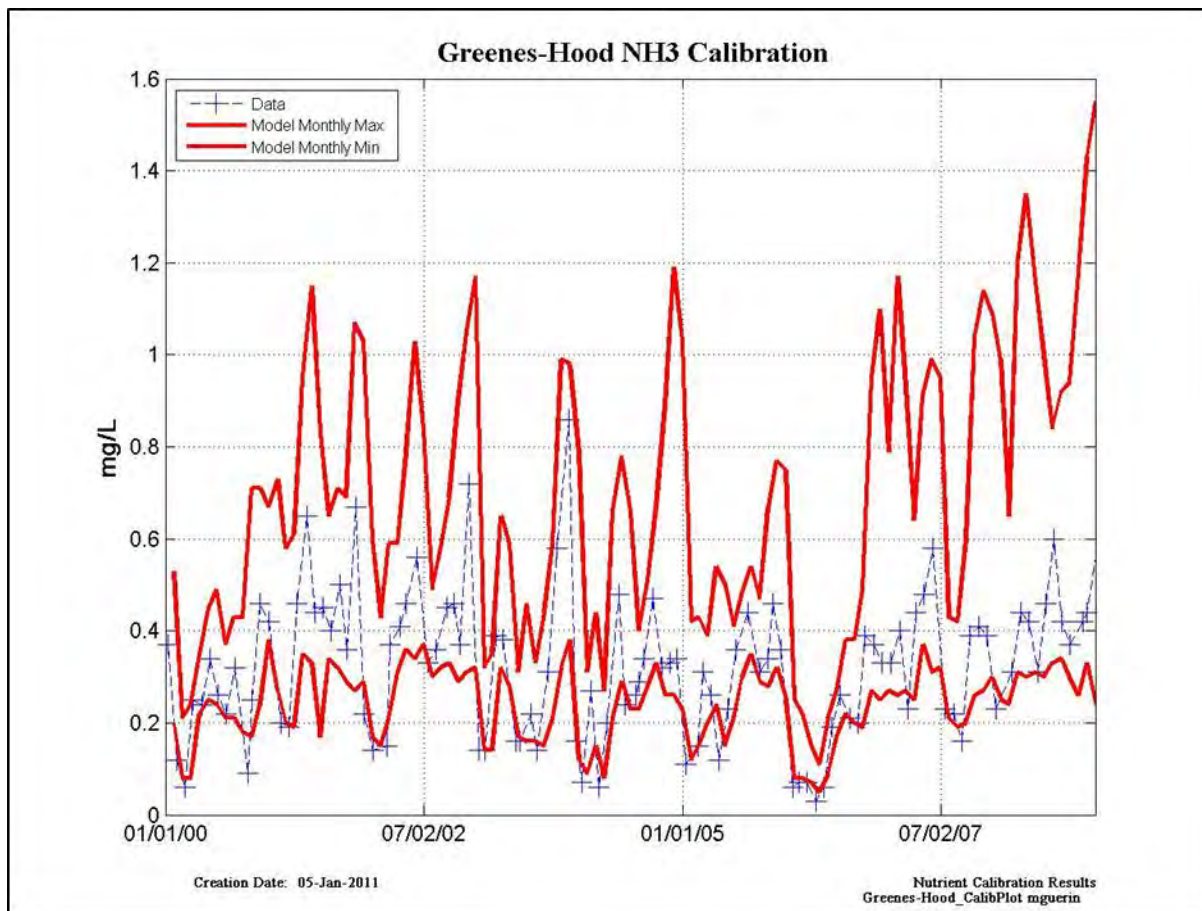
Figure 10-43 NH$_3$ calibration results at Greens-Hood – data points are located at blue symbols, monthly modeled maximum and minimum are denoted by solid red lines.

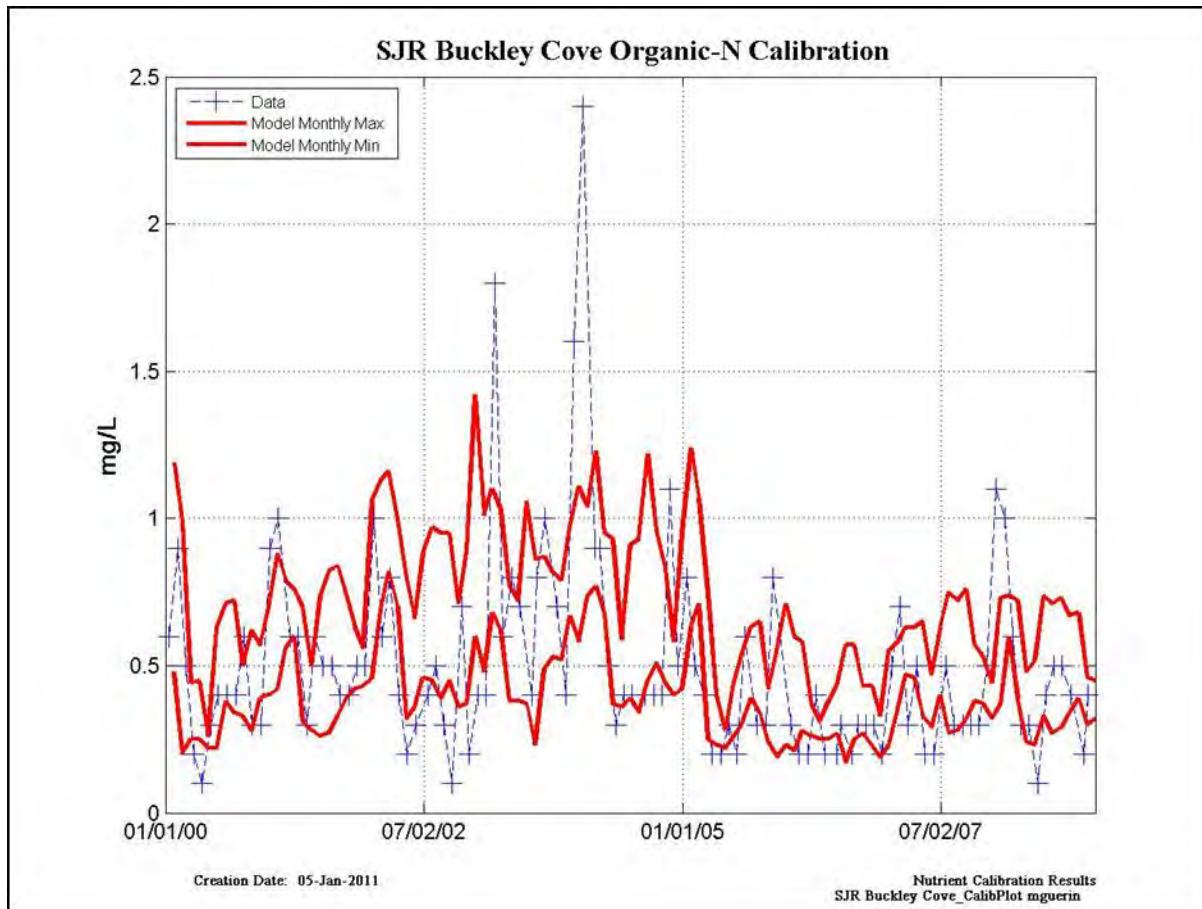**Table 10-43 Model calibration/validation statistics at Greens-Hood for NH$_3$ for the entire modeled period ("All"); Calibration for Dry Years (2001, 2002) and Wet Years (2000, 2003); and Validation for Dry Years (2007, 2008) and Wet Years (2005, 2006).**

	NSE	PBIAS	Bias	RSR
ALL	VG	VG	Overestimate	VG
Dry WY Calibration	VG	VG	Overestimate	VG
Wet WY Calibration	VG	VG	Overestimate	VG
Dry WY Validation	VG	VG	Overestimate	VG
Wet WY Validation	VG	VG	Overestimate	VG

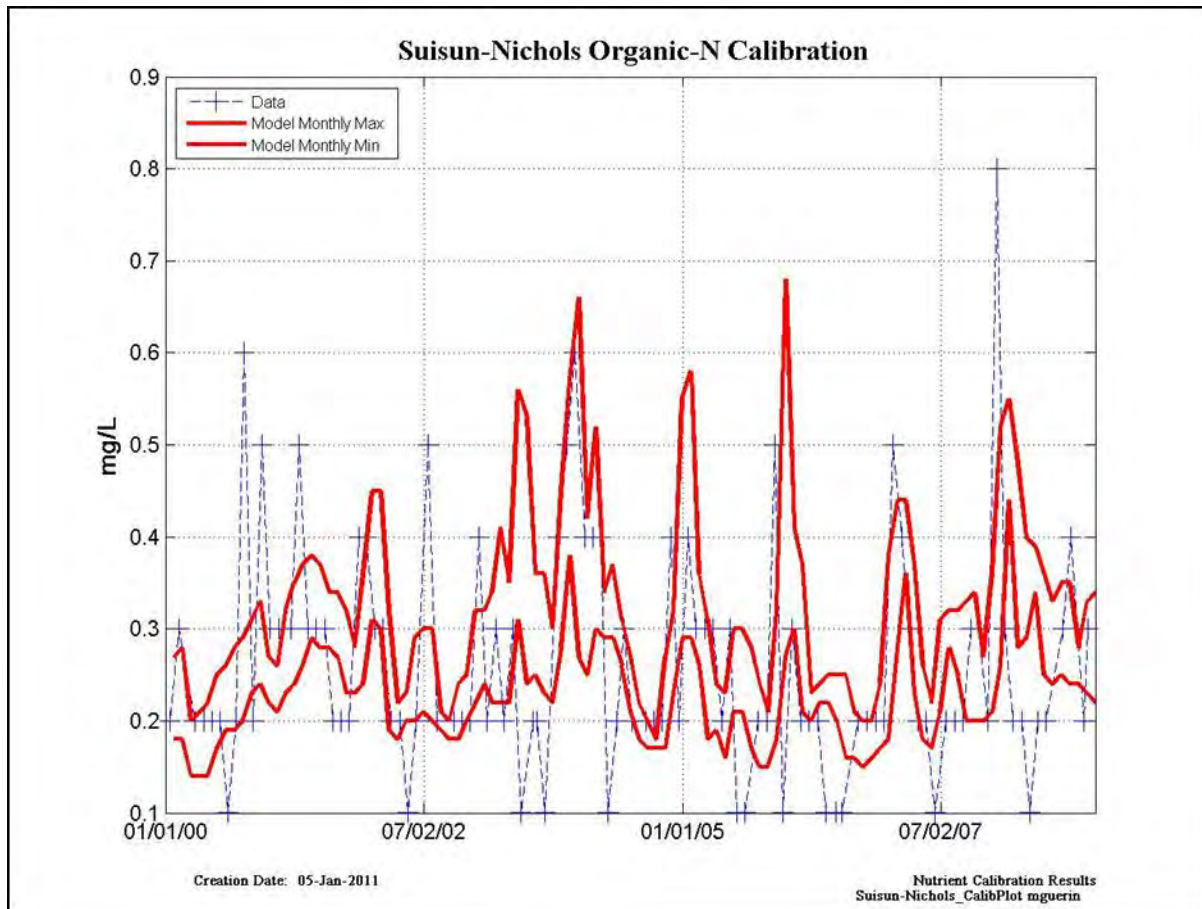**Figure 10-44 NH$_3$ calibration results at Grizzly – data points are located at blue symbols, monthly modeled maximum and minimum are denoted by solid red lines.**

Table 10-44 Model calibration/validation statistics at Grizzly for NH$_3$ for the entire modeled period ("All"); Calibration for Dry Years (2001, 2002) and Wet Years (2000, 2003); and Validation for Dry Years (2007, 2008) and Wet Years (2005, 2006).

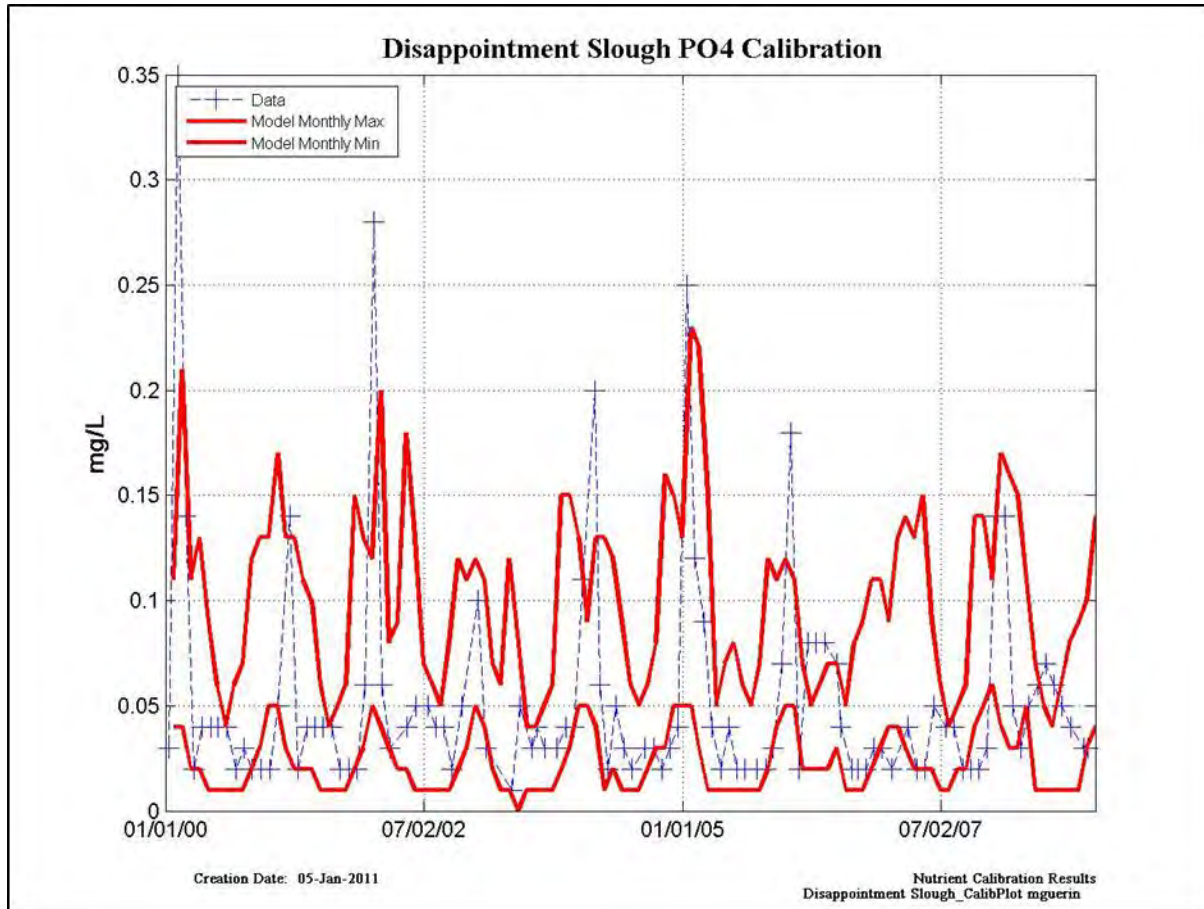|	NSE	PBIAS	Bias	RSR
ALL	VG	VG	Overestimate	VG
Dry WY Calibration	VG	VG	Underestimate	VG
Wet WY Calibration	VG	VG	Overestimate	VG
Dry WY Validation	VG	VG	Overestimate	VG
Wet WY Validation	VG	VG	Overestimate	VG

Figure 10-45 NH$_3$ calibration results at Martinez – data points are located at blue symbols, monthly modeled maximum and minimum are denoted by solid red lines.

Table 10-45 Model calibration/validation statistics at Martinez for NH$_3$ for the entire modeled period ("All"); Calibration for Dry Years (2001, 2002) and Wet Years (2000, 2003); and Validation for Dry Years (2007, 2008) and Wet Years (2005, 2006).

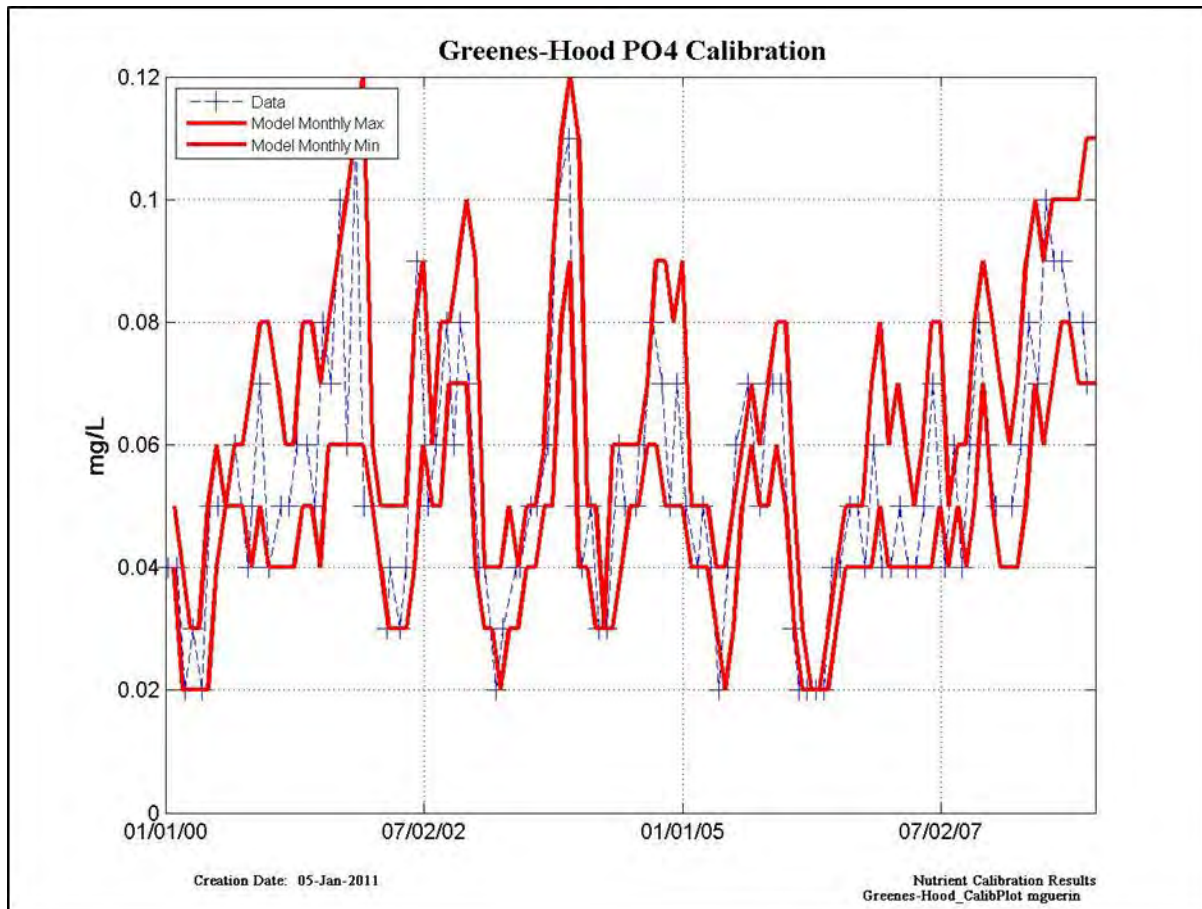|	NSE	PBIAS	Bias	RSR
ALL	VG	VG	Underestimate	VG
Dry WY Calibration	VG	VG	Underestimate	VG
Wet WY Calibration	VG	VG	Underestimate	VG
Dry WY Validation	VG	VG	Underestimate	VG
Wet WY Validation	VG	VG	Underestimate	VG

Figure 10-46 NH$_3$ calibration results at Old R. at RDR – data points are located at blue symbols, monthly modeled maximum and minimum are denoted by solid red lines.

Table 10-46 Model calibration/validation statistics at Old R. at RDR for NH$_3$ for the entire modeled period ("All"); Calibration for Dry Years (2001, 2002) and Wet Years (2000, 2003); and Validation for Dry Years (2007, 2008) and Wet Years (2005, 2006).

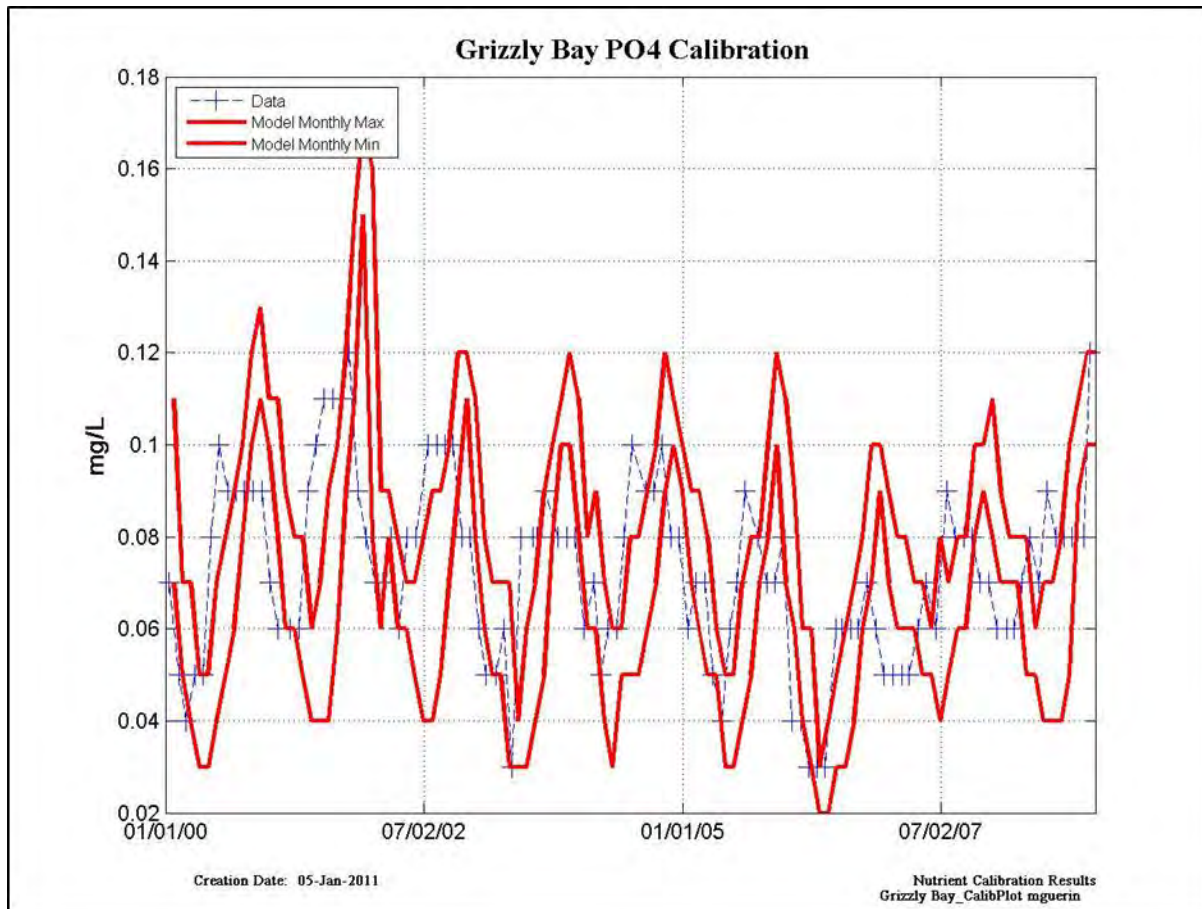|	NSE	PBIAS	Bias	RSR
ALL	S	G	Overestimate	U
Dry WY Calibration	VG	VG	Overestimate	VG
Wet WY Calibration	S	VG	Overestimate	U
Dry WY Validation	G	G	Overestimate	S
Wet WY Validation	S	S	Overestimate	U

Figure 10-47 NH$_3$ calibration results at Potato Pt. – data points are located at blue symbols, monthly modeled maximum and minimum are denoted by solid red lines.

Table 10-47 Model calibration/validation statistics at Potato Pt. for NH$_3$ for the entire modeled period ("All"); Calibration for Dry Years (2001, 2002) and Wet Years (2000, 2003); and Validation for Dry Years (2007, 2008) and Wet Years (2005, 2006).

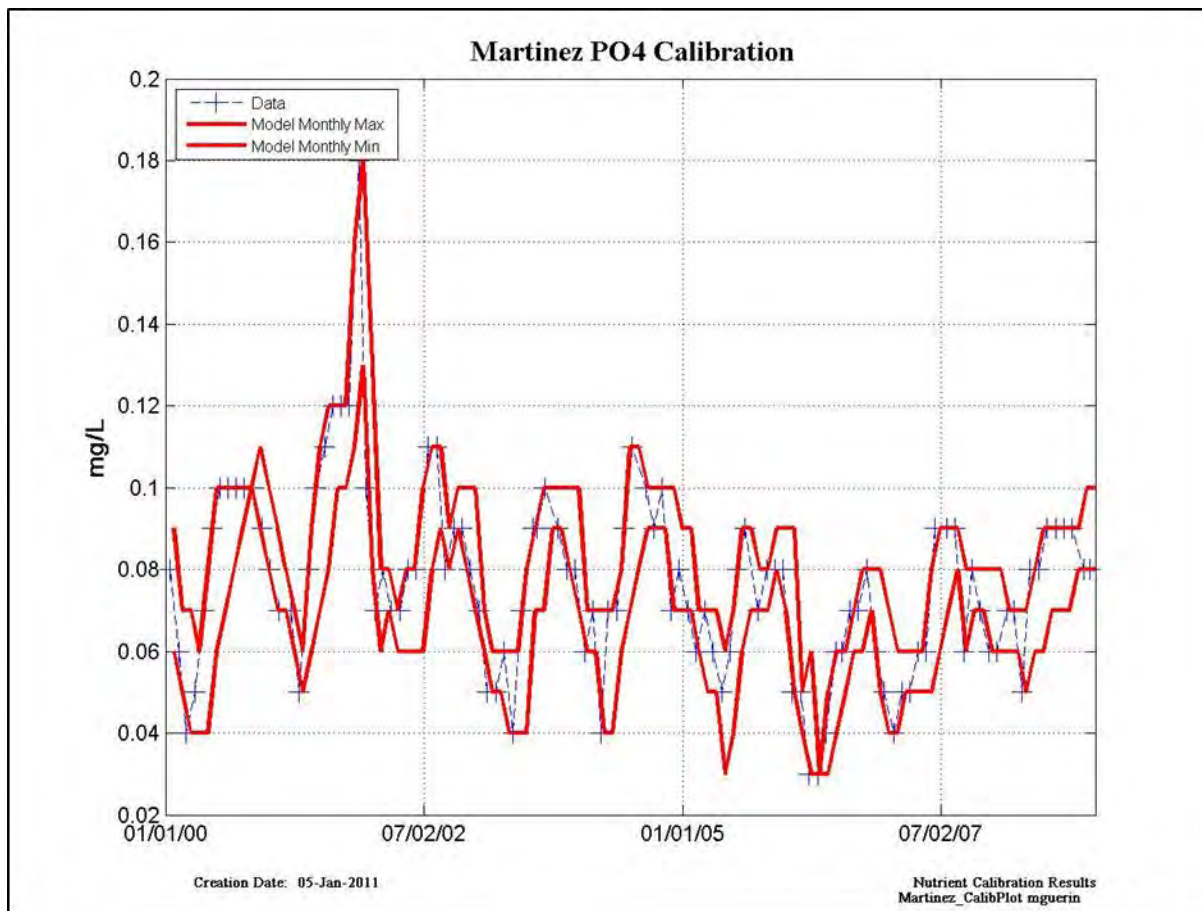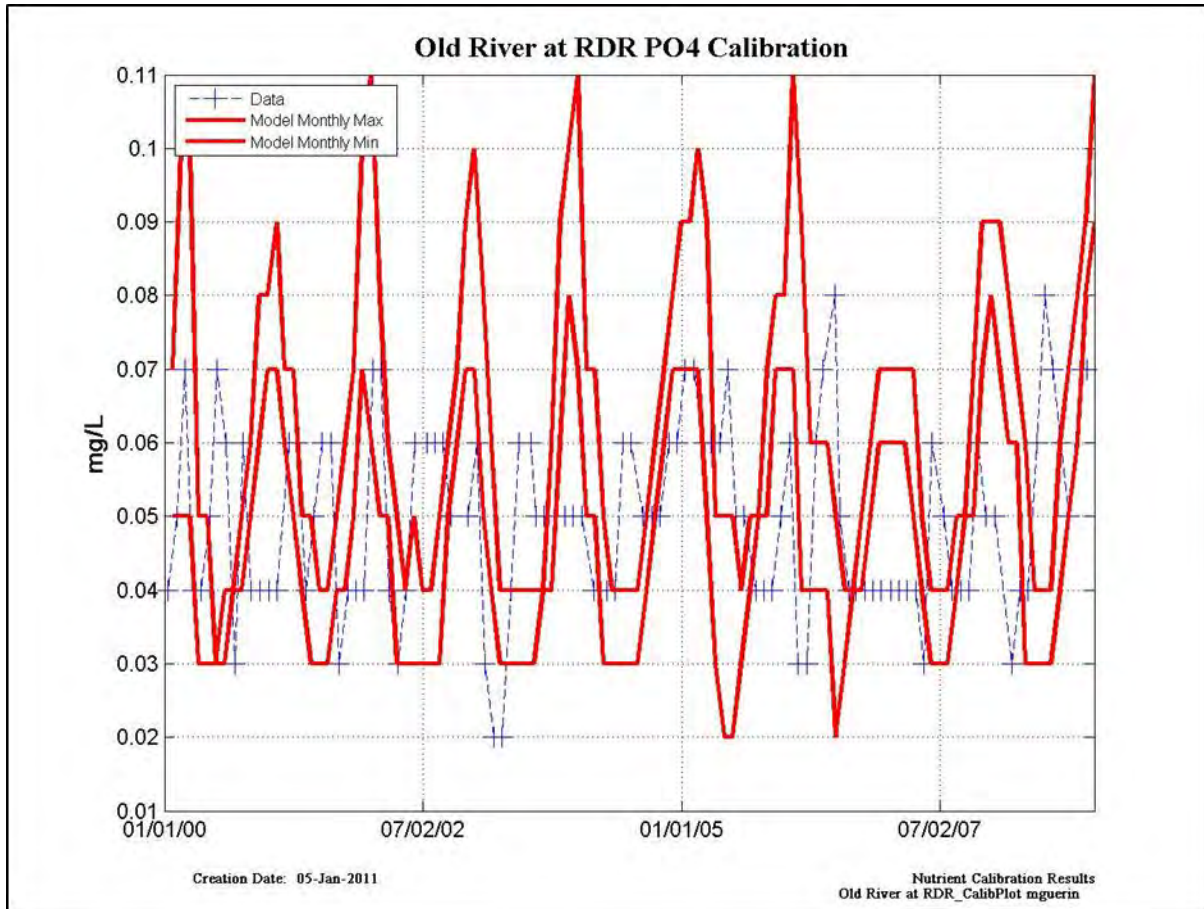|	NSE	PBIAS	Bias	RSR
ALL	VG	VG	Overestimate	VG
Dry WY Calibration	VG	VG	Underestimate	VG
Wet WY Calibration	VG	VG	Overestimate	VG
Dry WY Validation	VG	VG	Overestimate	VG
Wet WY Validation	VG	VG	Overestimate	VG

Figure 10-48 NH$_3$ calibration results at Pt. Sacramento – data points are located at blue symbols, monthly modeled maximum and minimum are denoted by solid red lines.

Table 10-48 Model calibration/validation statistics at Pt. Sacramento for NH$_3$ for the entire modeled period ("All"); Calibration for Dry Years (2001, 2002) and Wet Years (2000, 2003); and Validation for Dry Years (2007, 2008) and Wet Years (2005, 2006).

	NSE	PBIAS	Bias	RSR
ALL	VG	VG	Overestimate	VG
Dry WY Calibration	VG	VG	Overestimate	VG
Wet WY Calibration	VG	VG	Overestimate	VG
Dry WY Validation	VG	VG	Overestimate	VG
Wet WY Validation	VG	VG	Overestimate	VG

Figure 10-49 NH$_3$ calibration results at Russo – data points are located at blue symbols, monthly modeled maximum and minimum are denoted by solid red lines.
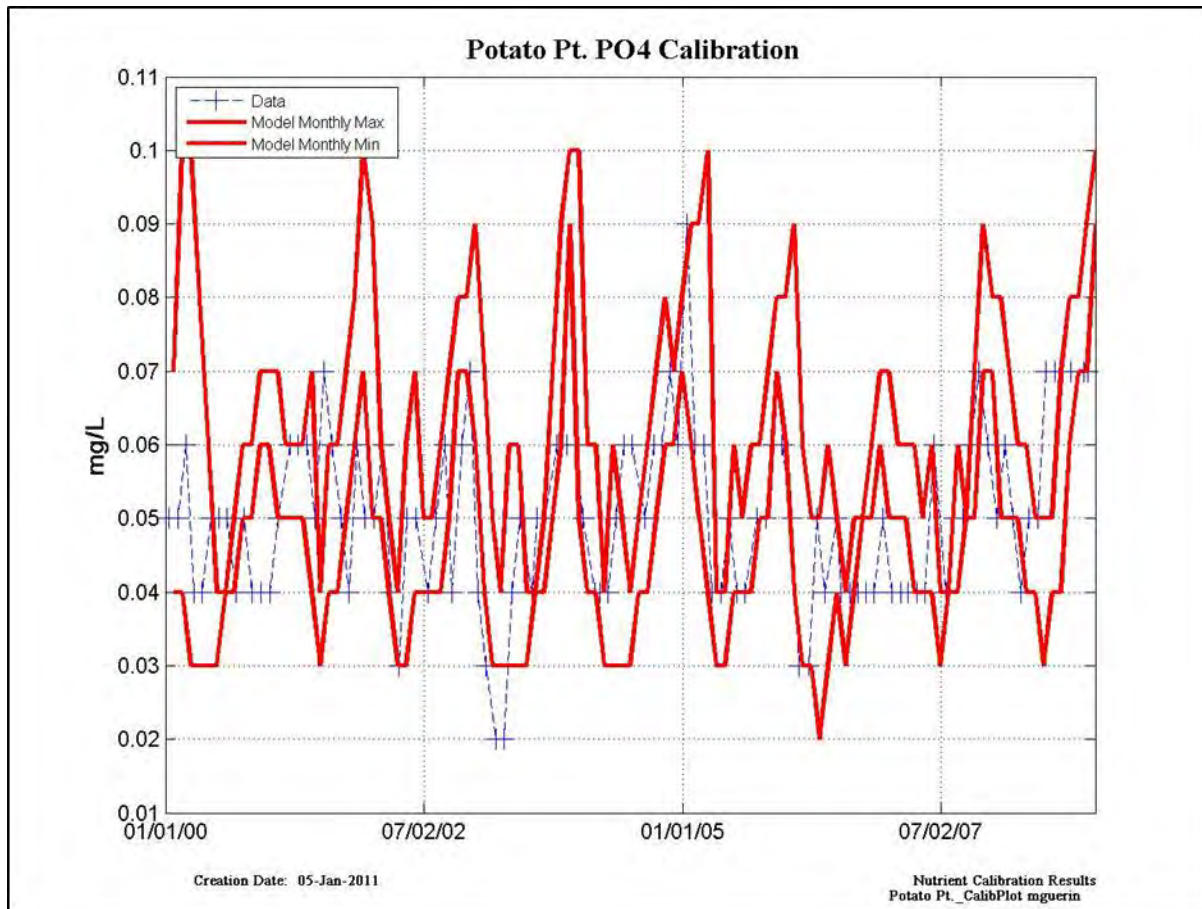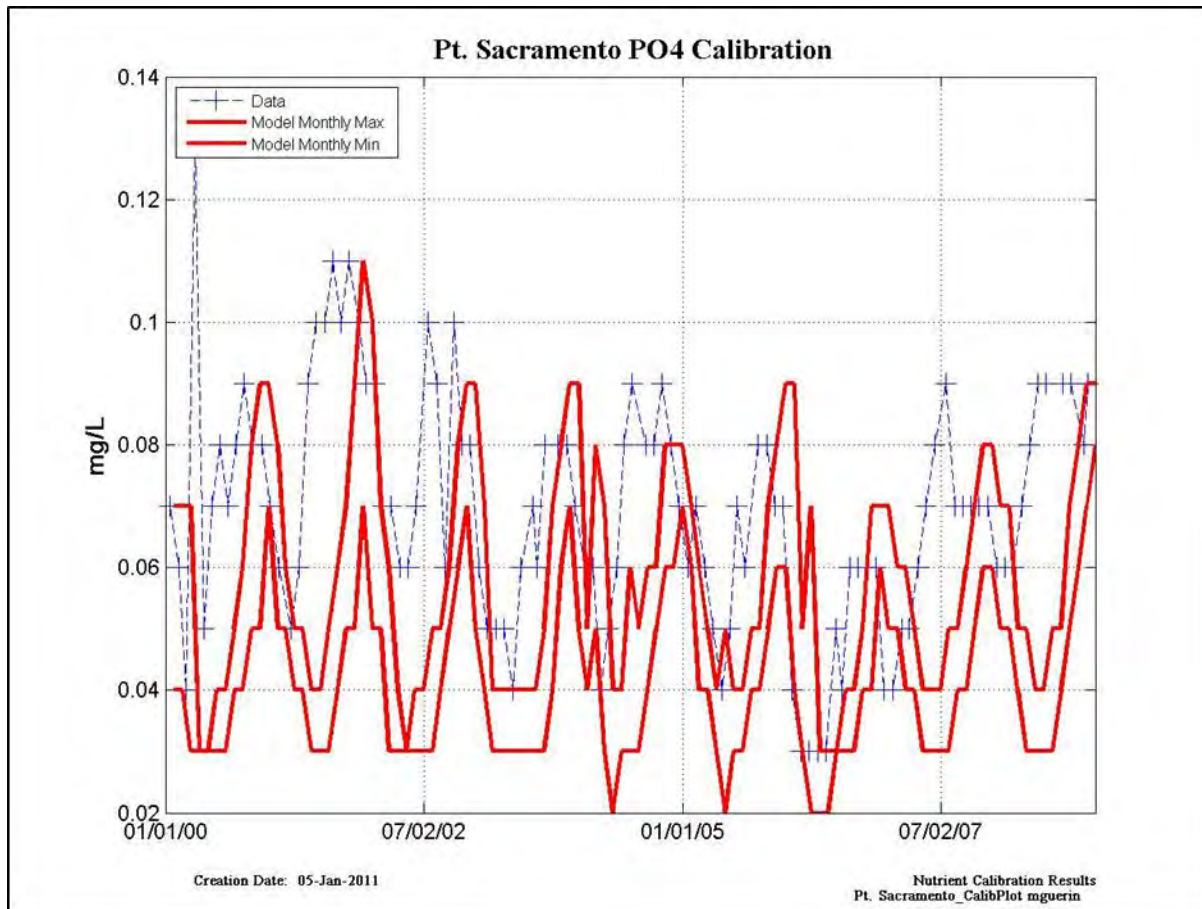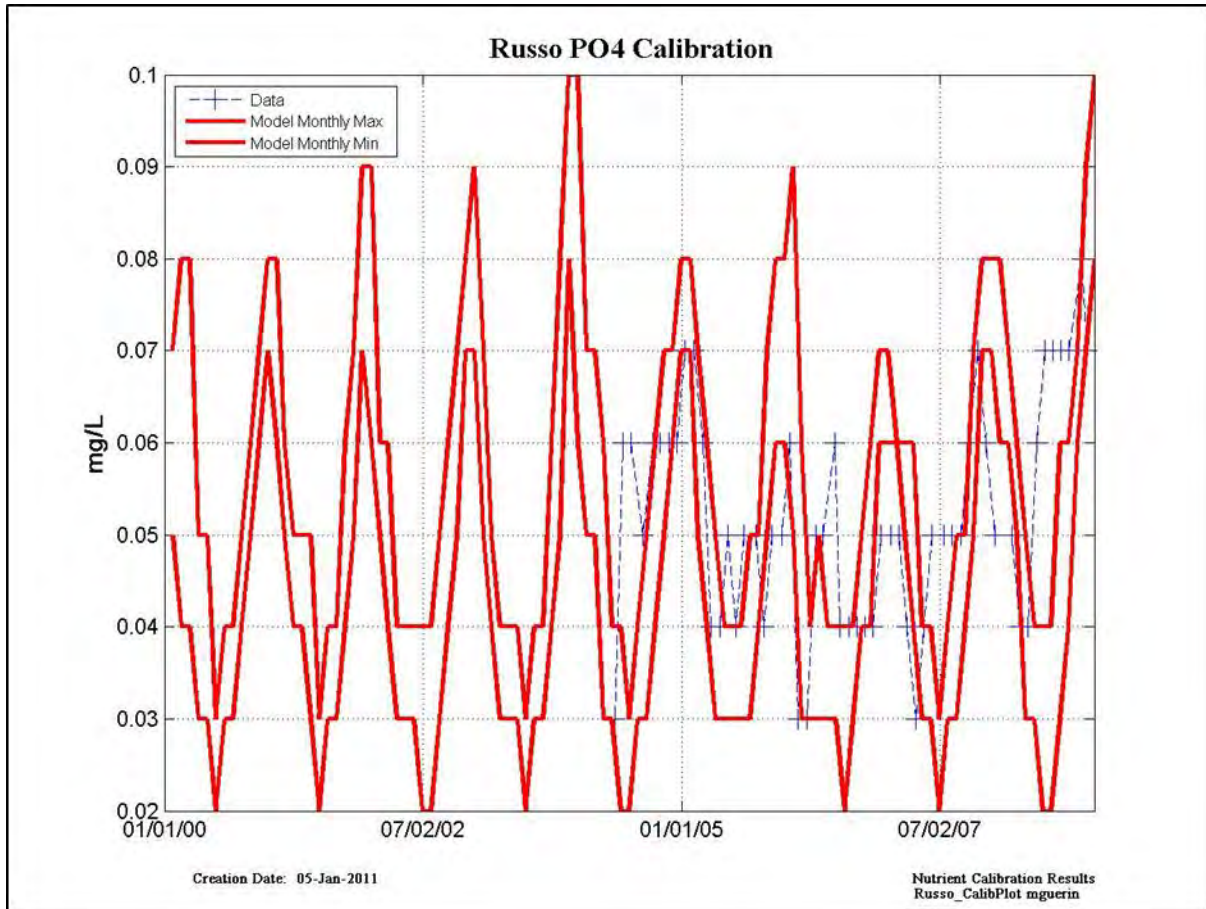
Table 10-49 (INSUFFICIENT DATA)

Figure 10-50 NH$_3$ calibration results at Suisun Nichols – data points are located at blue symbols, monthly modeled maximum and minimum are denoted by solid red lines.

Table 10-50 Model calibration/validation statistics at Suisun Nichols for NH$_3$ for the entire modeled period ("All"); Calibration for Dry Years (2001, 2002) and Wet Years (2000, 2003); and Validation for Dry Years (2007, 2008) and Wet Years (2005, 2006).

	NSE	PBIAS	Bias	RSR
ALL	VG	VG	Overestimate	VG
Dry WY Calibration	VG	VG	Underestimate	VG
Wet WY Calibration	VG	VG	Overestimate	VG
Dry WY Validation	VG	VG	Underestimate	VG
Wet WY Validation	VG	VG	Overestimate	VG

Figure 10-51 Modeled NH$_3$ calibration results at Buckley Cove on the San Joaquin R. – data points are located at blue symbols, monthly modeled maximum and minimum are denoted by solid red lines.

Table 10-51 Model calibration/validation statistics at Buckley Cove for NH$_3$ for the entire modeled period ("All"); Calibration for Dry Years (2001, 2002) and Wet Years (2000, 2003); and Validation for Dry Years (2007, 2008) and Wet Years (2005, 2006).

	NSE	PBIAS	Bias	RSR
ALL	VG	VG	Underestimate	VG
Dry WY Calibration	VG	VG	Underestimate	VG
Wet WY Calibration	VG	VG	Overestimate	VG
Dry WY Validation	VG	VG	Underestimate	VG
Wet WY Validation	VG	VG	Underestimate	VG

NO3+NO2
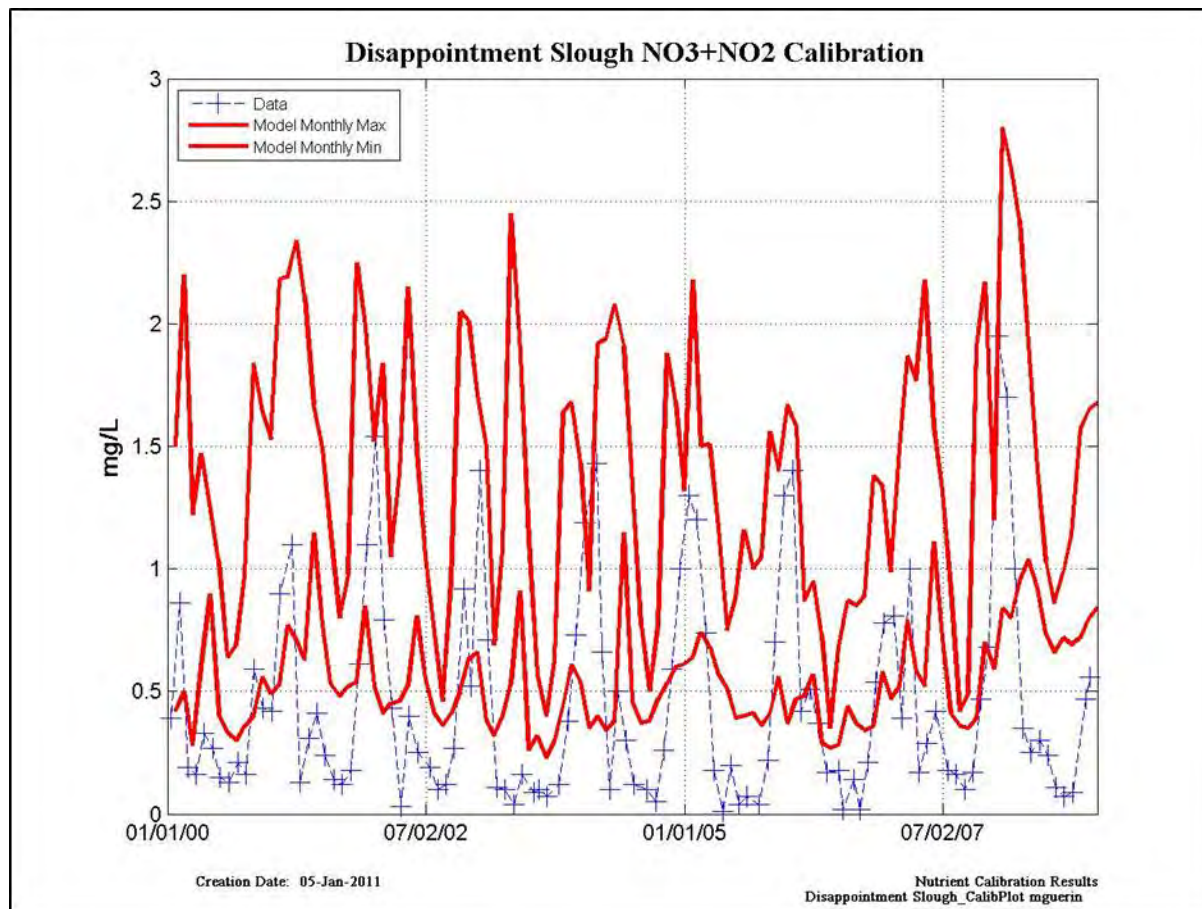
Figure 10-52 NO$_3$ + NO$_2$ calibration results at Disappointment Sl. – data points are located at blue symbols, monthly modeled maximum and minimum are denoted by solid red lines.
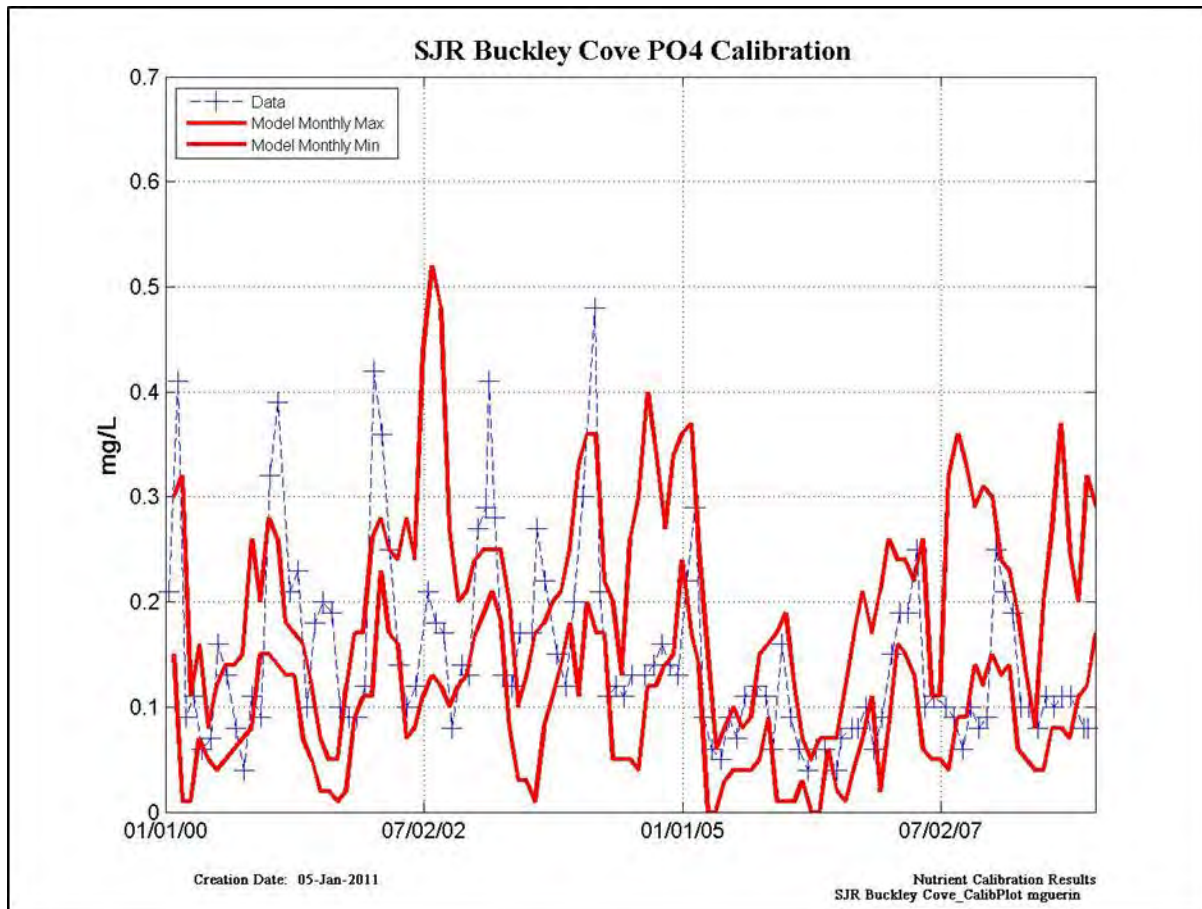

Table 10-52 Model calibration/validation statistics at Disappointment Sl. for NO$_3$ + NO$_2$ for the entire modeled period ("All"); Calibration for Dry Years (2001, 2002) and Wet Years (2000, 2003); and Validation for Dry Years (2007, 2008) and Wet Years (2005, 2006).

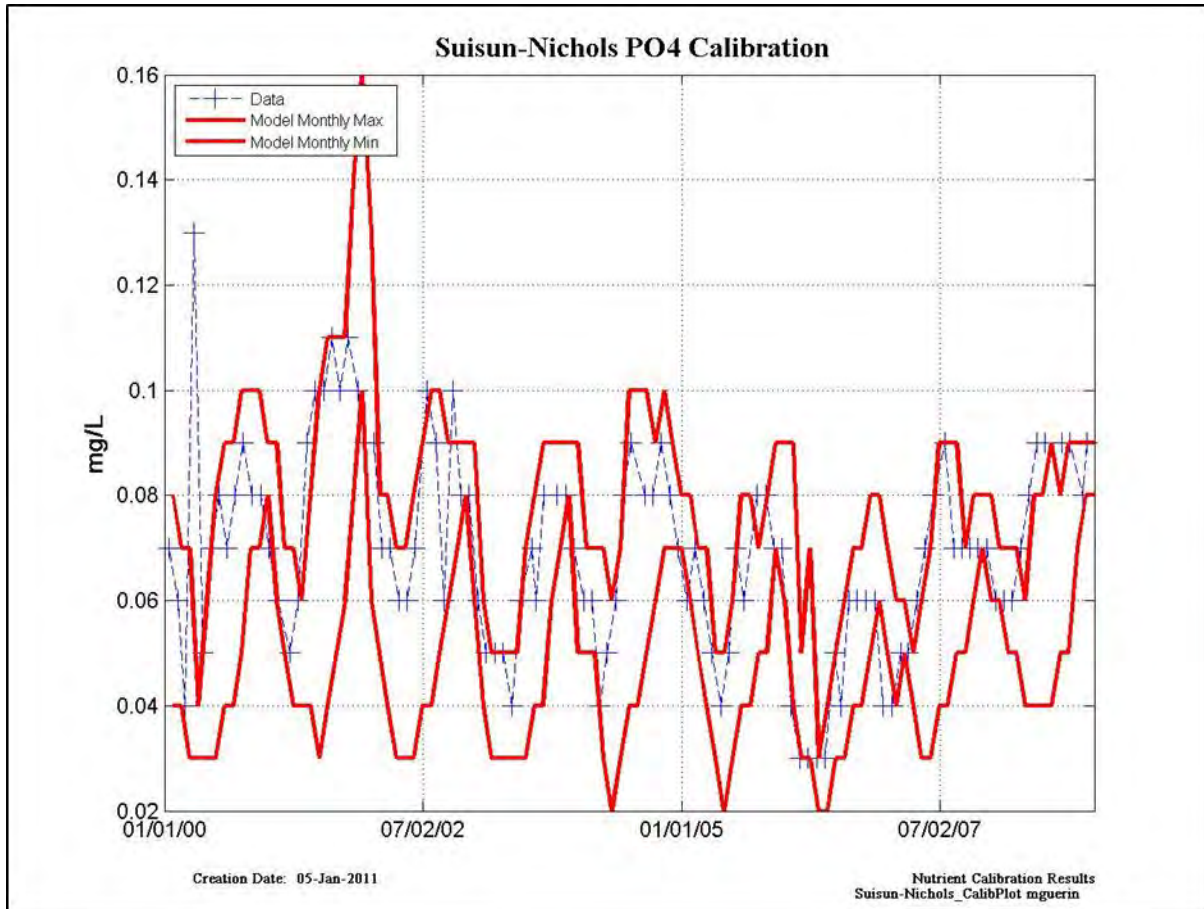|	NSE	PBIAS	Bias	RSR
ALL	G	S	Overestimate	U
Dry WY Calibration	G	S	Overestimate	U
Wet WY Calibration	S	S	Overestimate	U
Dry WY Validation	G	S	Overestimate	U
Wet WY Validation	VG	G	Overestimate	VG
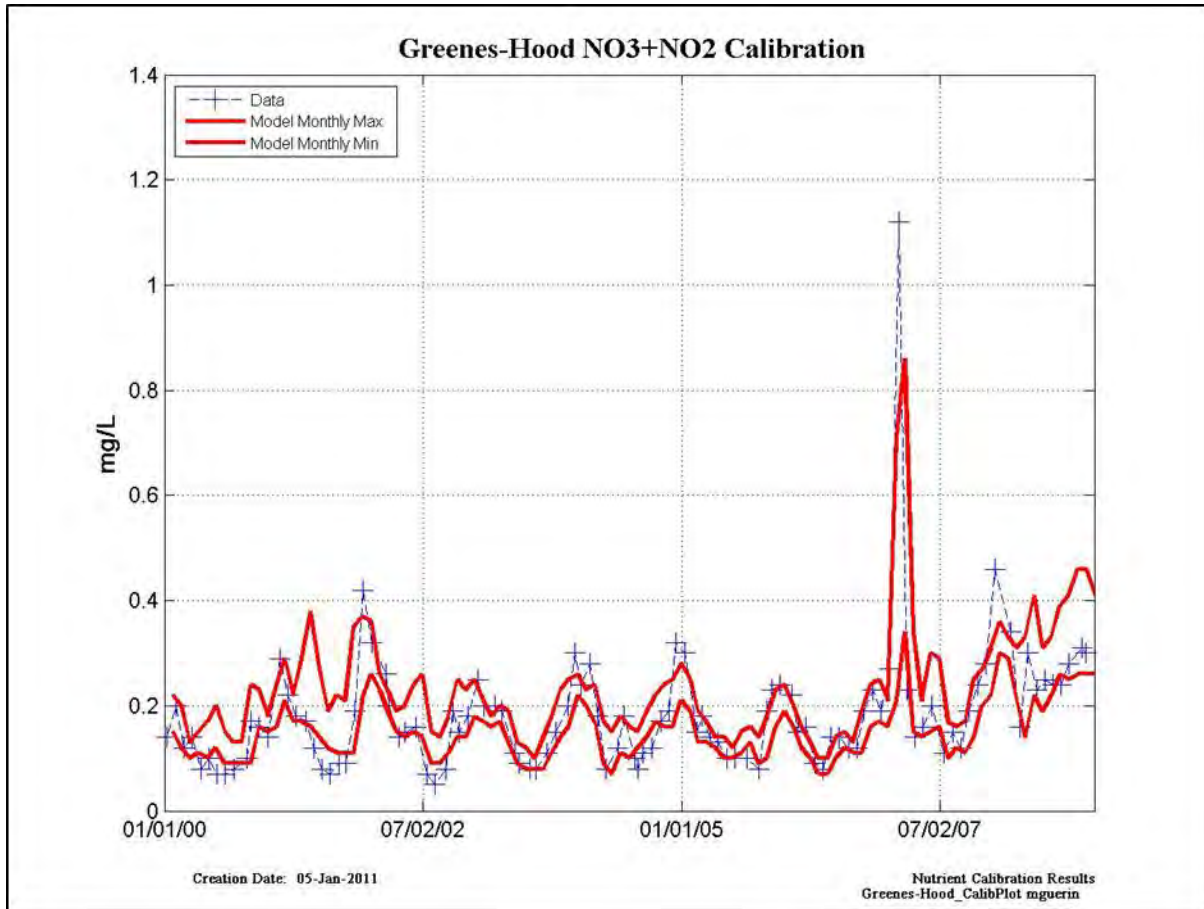
Figure 10-53 NO$_3$ + NO$_2$ calibration results at Greens-Hood – data points are located at blue symbols, monthly modeled maximum and minimum are denoted by solid red lines.

Table 10-53 Model calibration/validation statistics at Greens-Hood for NO$_3$ + NO$_2$ for the entire modeled period ("All"); Calibration for Dry Years (2001, 2002) and Wet Years (2000, 2003); and Validation for Dry Years (2007, 2008) and Wet Years (2005, 2006).

	NSE	PBIAS	Bias	RSR
ALL	VG	VG	Underestimate	VG
Dry WY Calibration	VG	VG	Overestimate	VG
Wet WY Calibration	VG	VG	Underestimate	VG
Dry WY Validation	VG	VG	Underestimate	VG
Wet WY Validation	VG	VG	Underestimate	VG

Figure 10-54 NO$_3$ + NO$_2$ calibration results at Grizzly Bay – data points are located at blue symbols, monthly modeled maximum and minimum are denoted by solid red lines.

Table 10-54 Model calibration/validation statistics at Grizzly Bay for NO$_3$ + NO$_2$ for the entire modeled period ("All"); Calibration for Dry Years (2001, 2002) and Wet Years (2000, 2003); and Validation for Dry Years (2007, 2008) and Wet Years (2005, 2006).

	NSE	PBIAS	Bias	RSR
ALL	VG	VG	Overestimate	VG
Dry WY Calibration	VG	VG	Overestimate	VG
Wet WY Calibration	VG	VG	Overestimate	VG
Dry WY Validation	G	VG	Overestimate	S
Wet WY Validation	VG	VG	Overestimate	VG

Figure 10-55 NO$_3$ + NO$_2$ calibration results at Martinez – data points are located at blue symbols, monthly modeled maximum and minimum are denoted by solid red lines.

Table 10-55 Model calibration/validation statistics at Martinez for NO$_3$ + NO$_2$ for the entire modeled period ("All"); Calibration for Dry Years (2001, 2002) and Wet Years (2000, 2003); and Validation for Dry Years (2007, 2008) and Wet Years (2005, 2006).

	NSE	PBIAS	Bias	RSR
ALL	VG	VG	Overestimate	VG
Dry WY Calibration	VG	VG	Overestimate	VG
Wet WY Calibration	VG	VG	Overestimate	VG
Dry WY Validation	VG	VG	Overestimate	VG
Wet WY Validation	VG	VG	Overestimate	VG

268

Figure 10-56 NO₃ + NO₂ calibration results at Old R. at RDR – data points are located at blue symbols, monthly modeled maximum and minimum are denoted by solid red lines.

Table 10-56 Model calibration/validation statistics at Old R. at RDR for NO₃ + NO₂ for the entire modeled period ("All"); Calibration for Dry Years (2001, 2002) and Wet Years (2000, 2003); and Validation for Dry Years (2007, 2008) and Wet Years (2005, 2006).

	NSE	PBIAS	Bias	RSR
ALL	S	VG	Overestimate	U
Dry WY Calibration	S	VG	Overestimate	U
Wet WY Calibration	S	VG	Overestimate	U
Dry WY Validation	S	G	Overestimate	U
Wet WY Validation	VG	VG	Overestimate	G

269

Figure 10-57 NO$_3$ + NO$_2$ calibration results at Potato Pt. – data points are located at blue symbols, monthly modeled maximum and minimum are denoted by solid red lines.

Table 10-57 Model calibration/validation statistics at Potato Pt. for NO$_3$ + NO$_2$ for the entire modeled period ("All"); Calibration for Dry Years (2001, 2002) and Wet Years (2000, 2003); and Validation for Dry Years (2007, 2008) and Wet Years (2005, 2006).

	NSE	PBIAS	Bias	RSR
ALL	G	VG	Overestimate	S
Dry WY Calibration	G	VG	Overestimate	U
Wet WY Calibration	G	VG	Overestimate	U
Dry WY Validation	S	VG	Overestimate	U
Wet WY Validation	VG	VG	Overestimate	VG

Figure 10-58 NO$_3$ + NO$_2$ calibration results at Pt. Sacramento – data points are located at blue symbols, monthly modeled maximum and minimum are denoted by solid red lines.

Table 10-58 Model calibration/validation statistics at Pt. Sacramento for NO$_3$ + NO$_2$ for the entire modeled period ("All"); Calibration for Dry Years (2001, 2002) and Wet Years (2000, 2003); and Validation for Dry Years (2007, 2008) and Wet Years (2005, 2006).

	NSE	PBIAS	Bias	RSR
ALL	VG	VG	Overestimate	VG
Dry WY Calibration	G	VG	Overestimate	G
Wet WY Calibration	VG	VG	Underestimate	VG
Dry WY Validation	S	VG	Overestimate	S
Wet WY Validation	VG	VG	Underestimate	VG

271

Figure 10-59 NO$_3$ + NO$_2$ calibration results at Rio Vista – data points are located at blue symbols, monthly modeled maximum and minimum are denoted by solid red lines.

Table 10-59 Model calibration/validation statistics at Rio Vista for NO$_3$ + NO$_2$ for the entire modeled period ("All"); Calibration for Dry Years (2001, 2002) and Wet Years (2000, 2003); and Validation for Dry Years (2007, 2008) and Wet Years (2005, 2006).

	NSE	PBIAS	Bias	RSR
ALL	VG	VG	Underestimate	VG
Dry WY Calibration	VG	VG	No Bias	VG
Wet WY Calibration	VG	VG	Underestimate	VG
Dry WY Validation	VG	VG	Underestimate	VG
Wet WY Validation	VG	VG	No Bias	VG
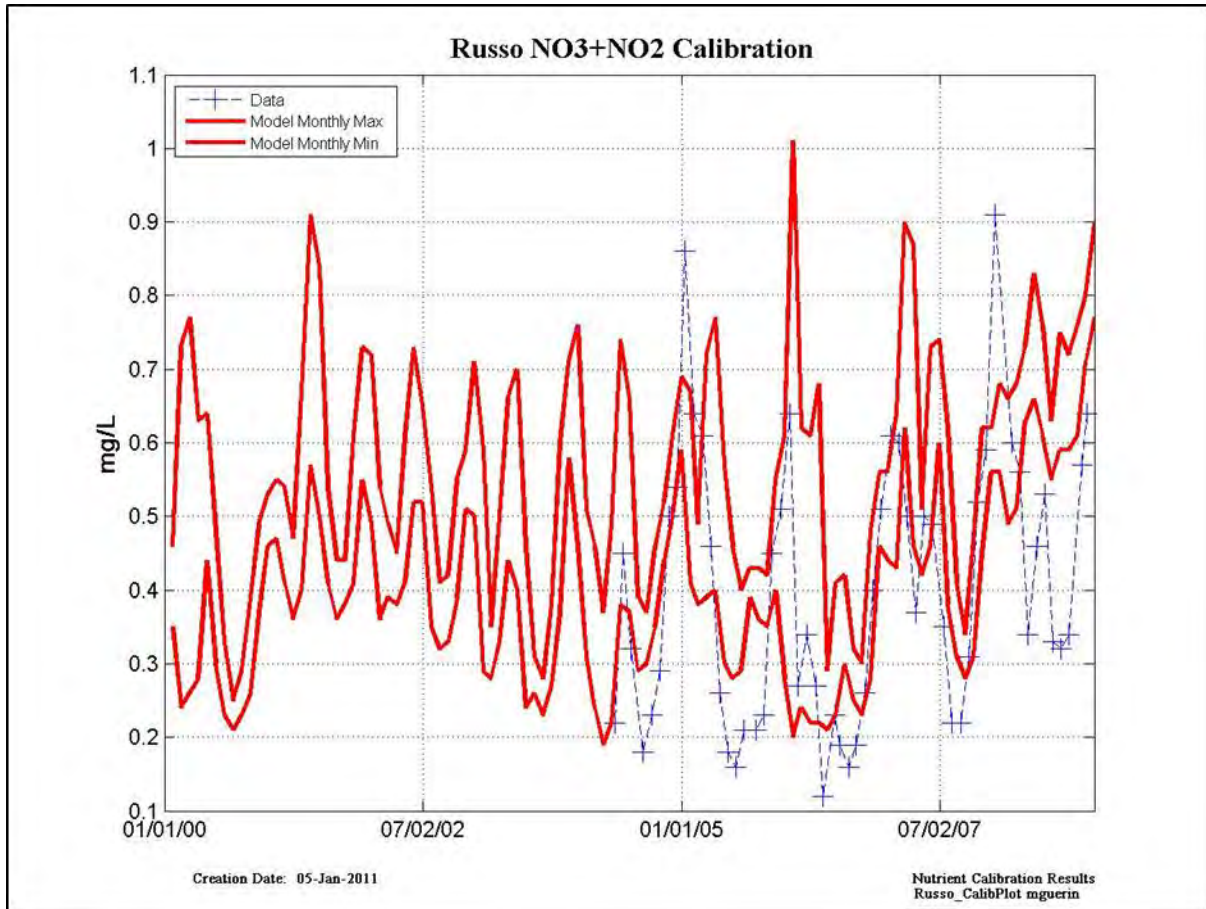
Figure 10-60 NO$_3$ + NO$_2$ calibration results at Russo – data points are located at blue symbols, monthly modeled maximum and minimum are denoted by solid red lines.

Table 10-60 (INSUFFICIENT DATA)

273

Figure 10-61 NO$_3$ + NO$_2$ calibration results at Suisun Nichols – data points are located at blue symbols, monthly modeled maximum and minimum are denoted by solid red lines.

Table 10-61 Model calibration/validation statistics at Suisun Nichols for NO$_3$ + NO$_2$ for the entire modeled period ("All"); Calibration for Dry Years (2001, 2002) and Wet Years (2000, 2003); and Validation for Dry Years (2007, 2008) and Wet Years (2005, 2006).

	NSE	PBIAS	Bias	RSR
ALL	VG	VG	Overestimate	VG
Dry WY Calibration	VG	VG	Overestimate	VG
Wet WY Calibration	VG	VG	Overestimate	VG
Dry WY Validation	VG	VG	Overestimate	VG
Wet WY Validation	VG	VG	Overestimate	VG

Figure 10-62 $NO_3 + NO_2$ calibration results at Buckley Cove on the San Joaquin r. – data points are located at blue symbols, monthly modeled maximum and minimum are denoted by solid red lines.

Table 10-62 Model calibration/validation statistics at Buckley Cove for $NO_3 + NO_2$ for the entire modeled period ("All"); Calibration for Dry Years (2001, 2002) and Wet Years (2000, 2003); and Validation for Dry Years (2007, 2008) and Wet Years (2005, 2006).

	NSE	PBIAS	Bias	RSR
ALL	VG	VG	Overestimate	VG
Dry WY Calibration	VG	VG	Overestimate	VG
Wet WY Calibration	VG	VG	Overestimate	VG
Dry WY Validation	VG	VG	Overestimate	VG
Wet WY Validation	VG	VG	Underestimate	VG

E. Organic-N
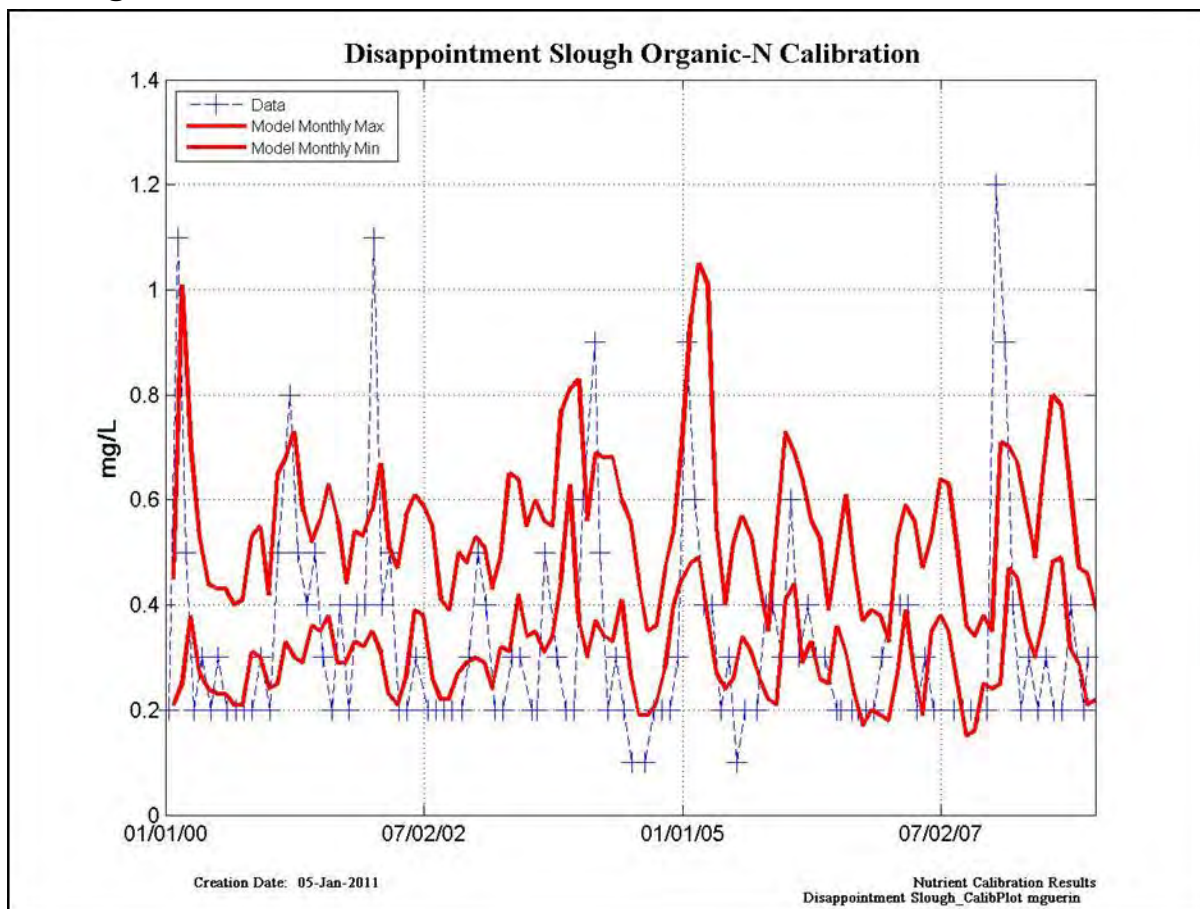
Figure 10-63 Organic-N calibration results at Disappointment Sl. – data points are located at blue symbols, monthly modeled maximum and minimum are denoted by solid red lines.

Table 10-63 Model calibration/validation statistics at Disappointment Sl. for Organic-N for the entire modeled period ("All"); Calibration for Dry Years (2001, 2002) and Wet Years (2000, 2003); and Validation for Dry Years (2007, 2008) and Wet Years (2005, 2006).

	NSE	PBIAS	Bias	RSR
ALL	G	VG	Overestimate	G
Dry WY Calibration	G	VG	Overestimate	G
Wet WY Calibration	G	VG	Overestimate	S
Dry WY Validation	S	VG	Overestimate	S
Wet WY Validation	VG	VG	Overestimate	VG
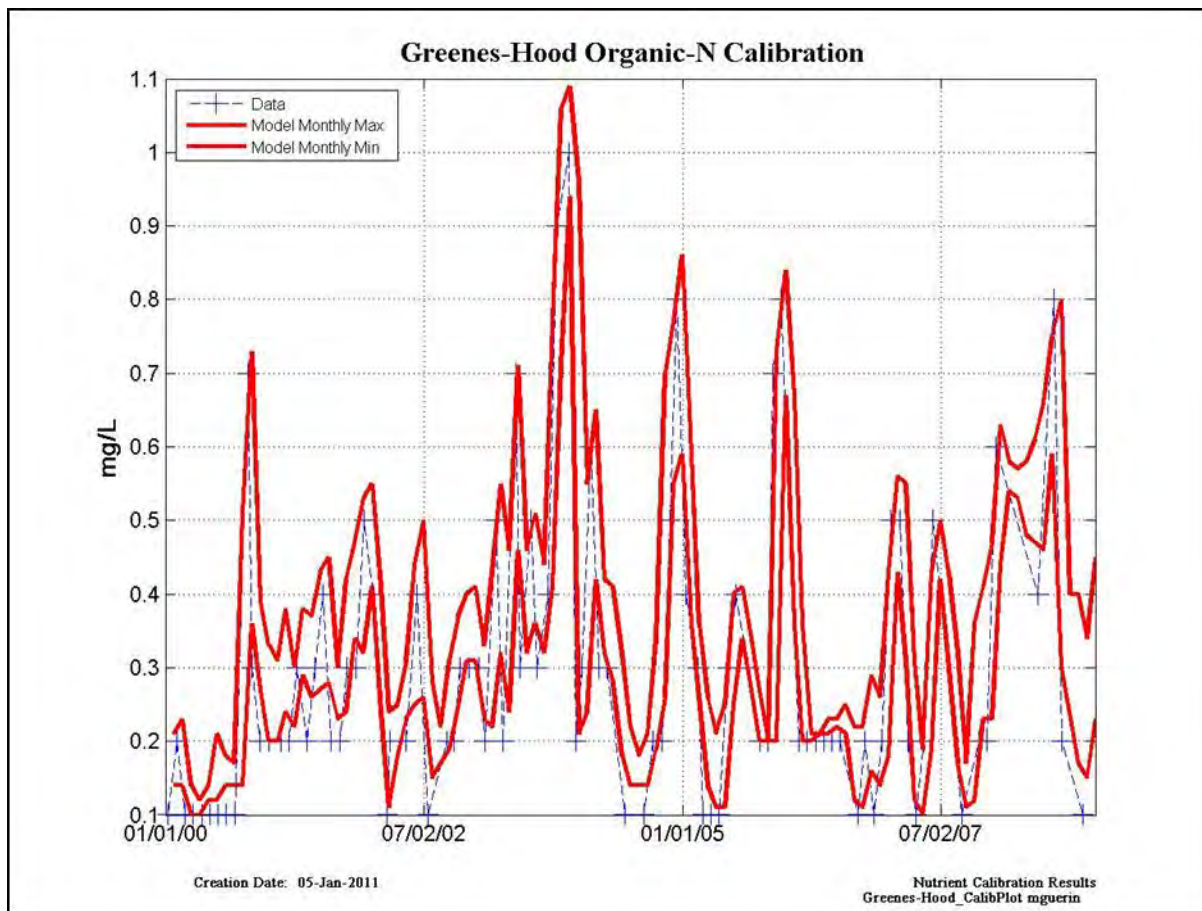
Figure 10-64 Organic-N calibration results at Greens-Hood – data points are located at blue symbols, monthly modeled maximum and minimum are denoted by solid red lines.

Table 10-64 Model calibration/validation statistics at Greens-Hood for Organic-N for the entire modeled period ("All"); Calibration for Dry Years (2001, 2002) and Wet Years (2000, 2003); and Validation for Dry Years (2007, 2008) and Wet Years (2005, 2006).

	NSE	PBIAS	Bias	RSR
ALL	VG	VG	Overestimate	VG
Dry WY Calibration	VG	VG	Overestimate	VG
Wet WY Calibration	VG	VG	Overestimate	VG
Dry WY Validation	VG	VG	Overestimate	VG
Wet WY Validation	VG	VG	Overestimate	VG

277

Figure 10-65 Organic-N calibration results at Grizzly Bay – data points are located at blue symbols, monthly modeled maximum and minimum are denoted by solid red lines.

Table 10-65 Model calibration/validation statistics at Grizzly Bay for Organic-N for the entire modeled period ("All"); Calibration for Dry Years (2001, 2002) and Wet Years (2000, 2003); and Validation for Dry Years (2007, 2008) and Wet Years (2005, 2006).

	NSE	PBIAS	Bias	RSR
ALL	S	VG	Underestimate	U
Dry WY Calibration	S	VG	Underestimate	U
Wet WY Calibration	S	G	Underestimate	U
Dry WY Validation	S	VG	Underestimate	U
Wet WY Validation	S	VG	Underestimate	U

Figure 10-66 Organic-N calibration results at Martinez – data points are located at blue symbols, monthly modeled maximum and minimum are denoted by solid red lines.

Table 10-66 Model calibration/validation statistics at Martinez for Organic-N for the entire modeled period ("All"); Calibration for Dry Years (2001, 2002) and Wet Years (2000, 2003); and Validation for Dry Years (2007, 2008) and Wet Years (2005, 2006).

	NSE	PBIAS	Bias	RSR
ALL	VG	VG	Underestimate	VG
Dry WY Calibration	VG	VG	Underestimate	VG
Wet WY Calibration	VG	VG	Underestimate	VG
Dry WY Validation	VG	VG	Underestimate	VG
Wet WY Validation	VG	VG	Overestimate	VG

Figure 10-67 Organic-N calibration results at Old R. at RDR – data points are located at blue symbols, monthly modeled maximum and minimum are denoted by solid red lines.

Table 10-67 Model calibration/validation statistics at Old R. at RDR for Organic-N for the entire modeled period ("All"); Calibration for Dry Years (2001, 2002) and Wet Years (2000, 2003); and Validation for Dry Years (2007, 2008) and Wet Years (2005, 2006).

	NSE	PBIAS	Bias	RSR
ALL	S	VG	Overestimate	U
Dry WY Calibration	S	VG	Underestimate	S
Wet WY Calibration	U	VG	Overestimate	U
Dry WY Validation	S	VG	Overestimate	U
Wet WY Validation	S	VG	Overestimate	U

280

Figure 10-68 Organic-N calibration results at Potato Pt. – data points are located at blue symbols, monthly modeled maximum and minimum are denoted by solid red lines.

Table 10-68 Model calibration/validation statistics at Potato Pt. for Organic-N for the entire modeled period ("All"); Calibration for Dry Years (2001, 2002) and Wet Years (2000, 2003); and Validation for Dry Years (2007, 2008) and Wet Years (2005, 2006).

	NSE	PBIAS	Bias	RSR
ALL	S	VG	Overestimate	U
Dry WY Calibration	S	VG	Overestimate	U
Wet WY Calibration	S	VG	Overestimate	U
Dry WY Validation	S	VG	Overestimate	U
Wet WY Validation	S	VG	Overestimate	U

Figure 10-69 Organic-N calibration results at Pt. Sacramento – data points are located at blue symbols, monthly modeled maximum and minimum are denoted by solid red lines.

Table 10-69 Model calibration/validation statistics at Pt. Sacramento for Organic-N for the entire modeled period ("All"); Calibration for Dry Years (2001, 2002) and Wet Years (2000, 2003); and Validation for Dry Years (2007, 2008) and Wet Years (2005, 2006).

	NSE	PBIAS	Bias	RSR
ALL	S	VG	Overestimate	U
Dry WY Calibration	S	VG	Overestimate	U
Wet WY Calibration	S	VG	Overestimate	S
Dry WY Validation	S	G	Overestimate	U
Wet WY Validation	S	G	Overestimate	U

Figure 10-70 Organic-N calibration results at Russo – data points are located at blue symbols, monthly modeled maximum and minimum are denoted by solid red lines.

Table 10-70 (INSUFFICIENT DATA)

Figure 10-71 Organic-N calibration results at Buckley Cove on the San Joaquin R. – data points are located at blue symbols, monthly modeled maximum and minimum are denoted by solid red lines.

Table 10-71 Model calibration/validation statistics at Buckley Cove for the entire modeled period ("All"); Calibration for Dry Years (2001, 2002) and Wet Years (2000, 2003); and Validation for Dry Years (2007, 2008) and Wet Years (2005, 2006).

	NSE	PBIAS	Bias	RSR
ALL	G	VG	Underestimate	G
Dry WY Calibration	G	VG	Overestimate	G
Wet WY Calibration	G	VG	Underestimate	G
Dry WY Validation	G	VG	Overestimate	G
Wet WY Validation	VG	VG	Overestimate	VG

Figure 10-72 Organic-N calibration results at Suisun Nichols – data points are located at blue symbols, monthly modeled maximum and minimum are denoted by solid red lines.

Table 10-72 Model calibration/validation statistics at Suisun Nichols for Organic-N for the entire modeled period ("All"); Calibration for Dry Years (2001, 2002) and Wet Years (2000, 2003); and Validation for Dry Years (2007, 2008) and Wet Years (2005, 2006).

	NSE	PBIAS	Bias	RSR
ALL	S	VG	Overestimate	S
Dry WY Calibration	G	VG	Underestimate	G
Wet WY Calibration	S	VG	Underestimate	S
Dry WY Validation	S	VG	Overestimate	S
Wet WY Validation	S	VG	Overestimate	S

PO4

Figure 10-73 Modeled PO₄ calibration results at Disappointment Sl. – data points are located at blue symbols, monthly modeled maximum and minimum are denoted by solid red lines.

Table 10-73 Model calibration/validation statistics at Disappointment Sl. for PO₄ for the entire modeled period ("All"); Calibration for Dry Years (2001, 2002) and Wet Years (2000, 2003); and Validation for Dry Years (2007, 2008) and Wet Years (2005, 2006).

	NSE	PBIAS	Bias	RSR
ALL	VG	VG	Underestimate	VG
Dry WY Calibration	VG	VG	Underestimate	VG
Wet WY Calibration	VG	VG	Underestimate	VG
Dry WY Validation	VG	VG	Overestimate	VG
Wet WY Validation	VG	VG	Underestimate	VG

Figure 10-74 Modeled PO₄ calibration results at Greens-Hood – data points are located at blue symbols, monthly modeled maximum and minimum are denoted by solid red lines.

Table 10-74 Model calibration/validation statistics at Greens-Hood for PO₄ for the entire modeled period ("All"); Calibration for Dry Years (2001, 2002) and Wet Years (2000, 2003); and Validation for Dry Years (2007, 2008) and Wet Years (2005, 2006).

	NSE	PBIAS	Bias	RSR
ALL	VG	VG	Overestimate	VG
Dry WY Calibration	VG	VG	Overestimate	VG
Wet WY Calibration	VG	VG	Overestimate	VG
Dry WY Validation	VG	VG	Overestimate	VG
Wet WY Validation	VG	VG	Overestimate	VG

287

Figure 10-75 Modeled PO₄ calibration results at Grizzly – data points are located at blue symbols, monthly modeled maximum and minimum are denoted by solid red lines.

Table 10-75 Model calibration/validation statistics at Grizzly for PO₄ for the entire modeled period ("All"); Calibration for Dry Years (2001, 2002) and Wet Years (2000, 2003); and Validation for Dry Years (2007, 2008) and Wet Years (2005, 2006).

	NSE	PBIAS	Bias	RSR
ALL	S	VG	Overestimate	S
Dry WY Calibration	S	VG	Underestimate	U
Wet WY Calibration	G	VG	Overestimate	G
Dry WY Validation	S	VG	Overestimate	S
Wet WY Validation	S	VG	Overestimate	S

Figure 10-76 Modeled PO₄ calibration results at Martinez – data points are located at blue symbols, monthly modeled maximum and minimum are denoted by solid red lines.

Table 10-76 Model calibration/validation statistics at Martinez for PO₄ for the entire modeled period ("All"); Calibration for Dry Years (2001, 2002) and Wet Years (2000, 2003); and Validation for Dry Years (2007, 2008) and Wet Years (2005, 2006).

	NSE	PBIAS	Bias	RSR
ALL	VG	VG	Underestimate	VG
Dry WY Calibration	VG	VG	Underestimate	VG
Wet WY Calibration	VG	VG	Underestimate	VG
Dry WY Validation	VG	VG	Underestimate	VG
Wet WY Validation	VG	VG	Underestimate	VG

Figure 10-77 Modeled PO₄ calibration results at Old R. at RDR – data points are located at blue symbols, monthly modeled maximum and minimum are denoted by solid red lines.

Table 10-77 Model calibration/validation statistics at Old R. at RDR for PO₄ for the entire modeled period ("All"); Calibration for Dry Years (2001, 2002) and Wet Years (2000, 2003); and Validation for Dry Years (2007, 2008) and Wet Years (2005, 2006).

	NSE	PBIAS	Bias	RSR
ALL	U	VG	Overestimate	U
Dry WY Calibration	U	VG	Overestimate	U
Wet WY Calibration	U	VG	Overestimate	U
Dry WY Validation	U	VG	Overestimate	U
Wet WY Validation	S	VG	Overestimate	U

Figure 10-78 Modeled PO₄ calibration results at Potato Pt. – data points are located at blue symbols, monthly modeled maximum and minimum are denoted by solid red lines.

Table 10-78 Model calibration/validation statistics at Potato Pt. for PO₄ for the entire modeled period ("All"); Calibration for Dry Years (2001, 2002) and Wet Years (2000, 2003); and Validation for Dry Years (2007, 2008) and Wet Years (2005, 2006).

	NSE	PBIAS	Bias	RSR
ALL	S	VG	Overestimate	S
Dry WY Calibration	S	VG	Overestimate	U
Wet WY Calibration	S	VG	Overestimate	U
Dry WY Validation	S	VG	Overestimate	S
Wet WY Validation	VG	VG	Overestimate	VG

Figure 10-79 Modeled PO$_4$ calibration results at Pt. Sacramento – data points are located at blue symbols, monthly modeled maximum and minimum are denoted by solid red lines.

Table 10-79 Model calibration/validation statistics at Pt. Sacramento for PO$_4$ for the entire modeled period ("All"); Calibration for Dry Years (2001, 2002) and Wet Years (2000, 2003); and Validation for Dry Years (2007, 2008) and Wet Years (2005, 2006).

	NSE	PBIAS	Bias	RSR
ALL	S	VG	Underestimate	U
Dry WY Calibration	U	G	Underestimate	U
Wet WY Calibration	U	VG	Underestimate	U
Dry WY Validation	U	VG	Underestimate	U
Wet WY Validation	S	VG	Underestimate	U

Figure 10-80 Modeled PO$_4$ calibration results at Russo – data points are located at blue symbols, monthly modeled maximum and minimum are denoted by solid red lines.

Table 10-80 (INSUFFICIENT DATA)

Figure 10-81 Modeled PO₄ calibration results at Buckley Cove on the San Joaquin R. – data points are located at blue symbols, monthly modeled maximum and minimum are denoted by solid red lines.

Table 10-81 Model calibration/validation statistics AT Buckley Cove for PO₄ for the entire modeled period ("All"); Calibration for Dry Years (2001, 2002) and Wet Years (2000, 2003); and Validation for Dry Years (2007, 2008) and Wet Years (2005, 2006).

	NSE	PBIAS	Bias	RSR
ALL	G	VG	Underestimate	G
Dry WY Calibration	S	VG	Underestimate	U
Wet WY Calibration	VG	VG	Underestimate	VG
Dry WY Validation	VG	VG	Overestimate	VG
Wet WY Validation	VG	VG	Underestimate	VG

294

Figure 10-82 Modeled PO$_4$ calibration results at Suisun Nichols – data points are located at blue symbols, monthly modeled maximum and minimum are denoted by solid red lines.

Table 10-82 Model calibration/validation statistics at Suisun Nichols for PO$_4$ for the entire modeled period ("All"); Calibration for Dry Years (2001, 2002) and Wet Years (2000, 2003); and Validation for Dry Years (2007, 2008) and Wet Years (2005, 2006).

	NSE	PBIAS	Bias	RSR
ALL	VG	VG	Underestimate	VG
Dry WY Calibration	VG	VG	Underestimate	VG
Wet WY Calibration	S	VG	Underestimate	U
Dry WY Validation	VG	VG	Underestimate	VG
Wet WY Validation	VG	VG	Overestimate	VG

11. Appendix IV - Calibration Statistics by Constituent and Location
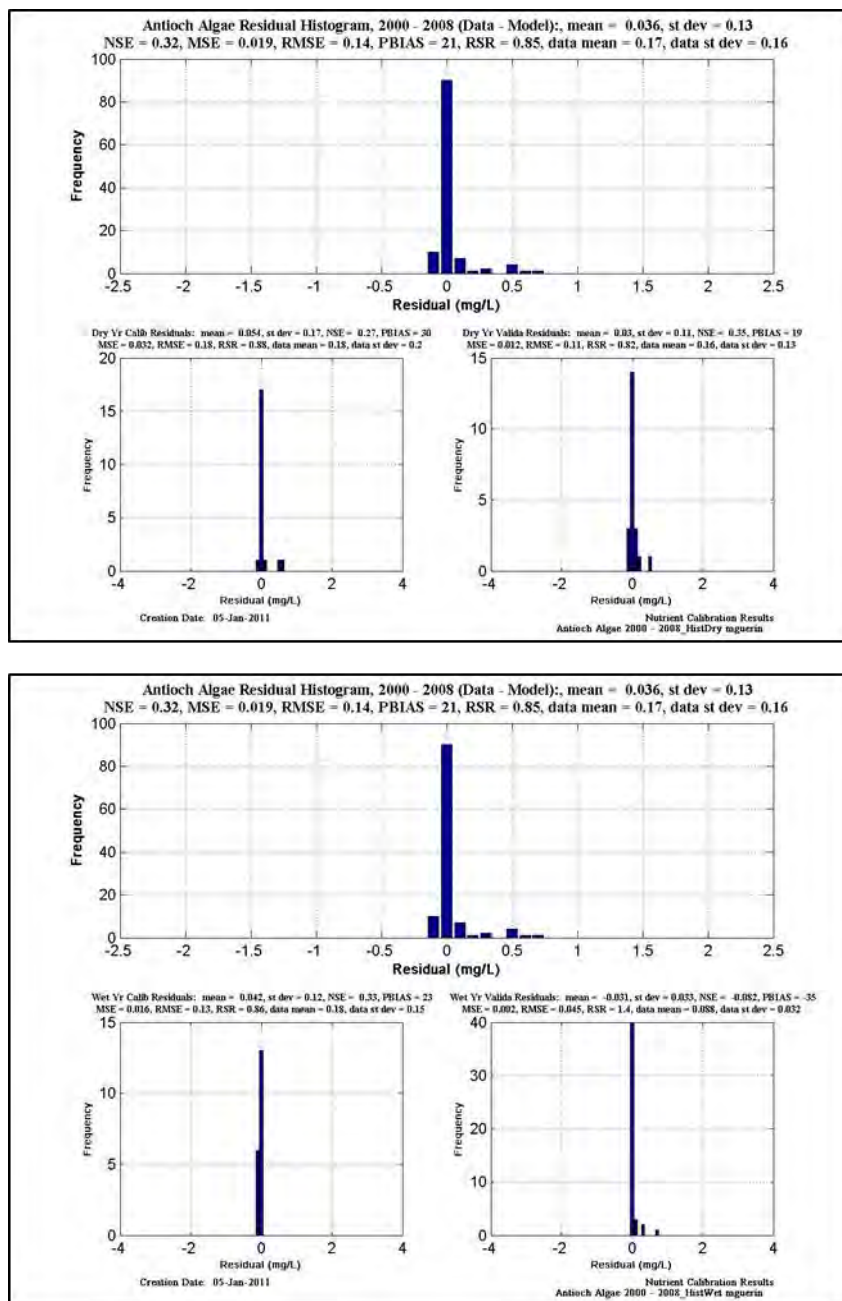
Figure 11-1Calibration/validation statistics for Algae at Antioch. Upper figure is calibration & validation statistics for dry years; lower figure is calibration & validation statistics for wet years.
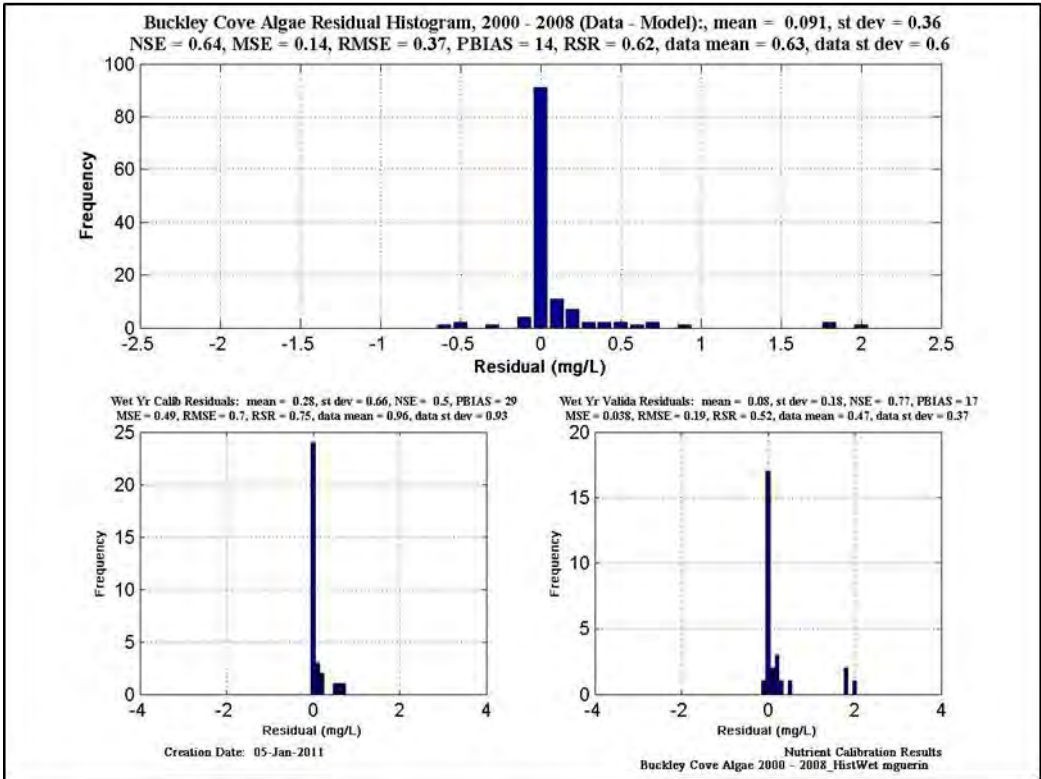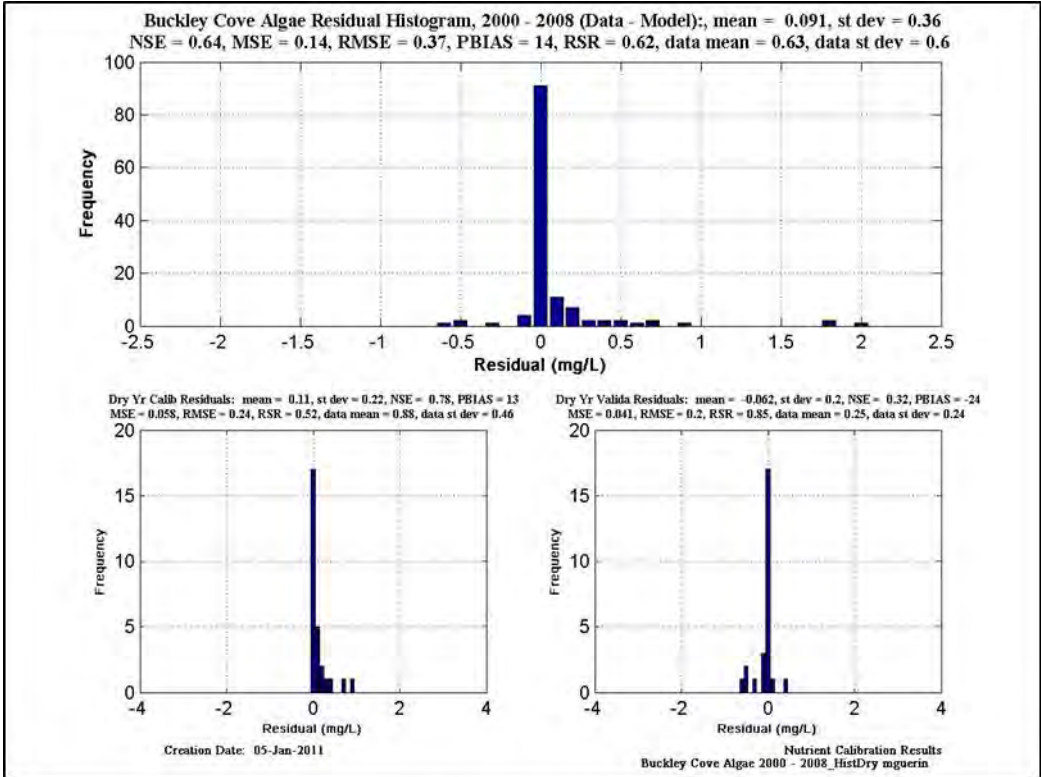
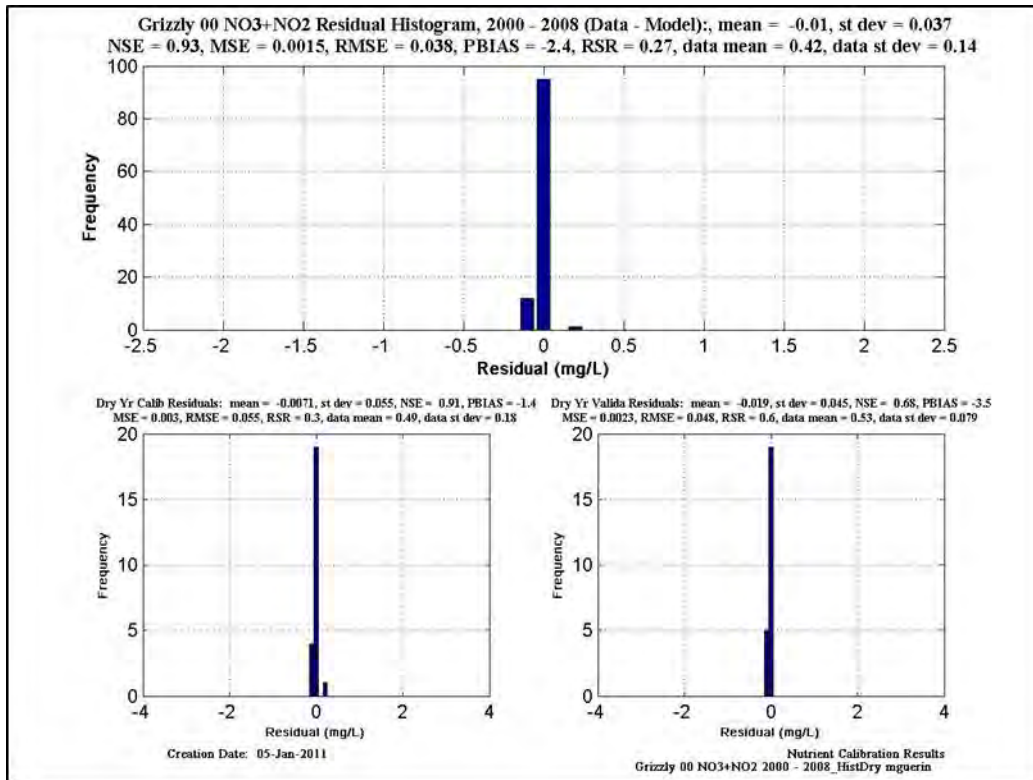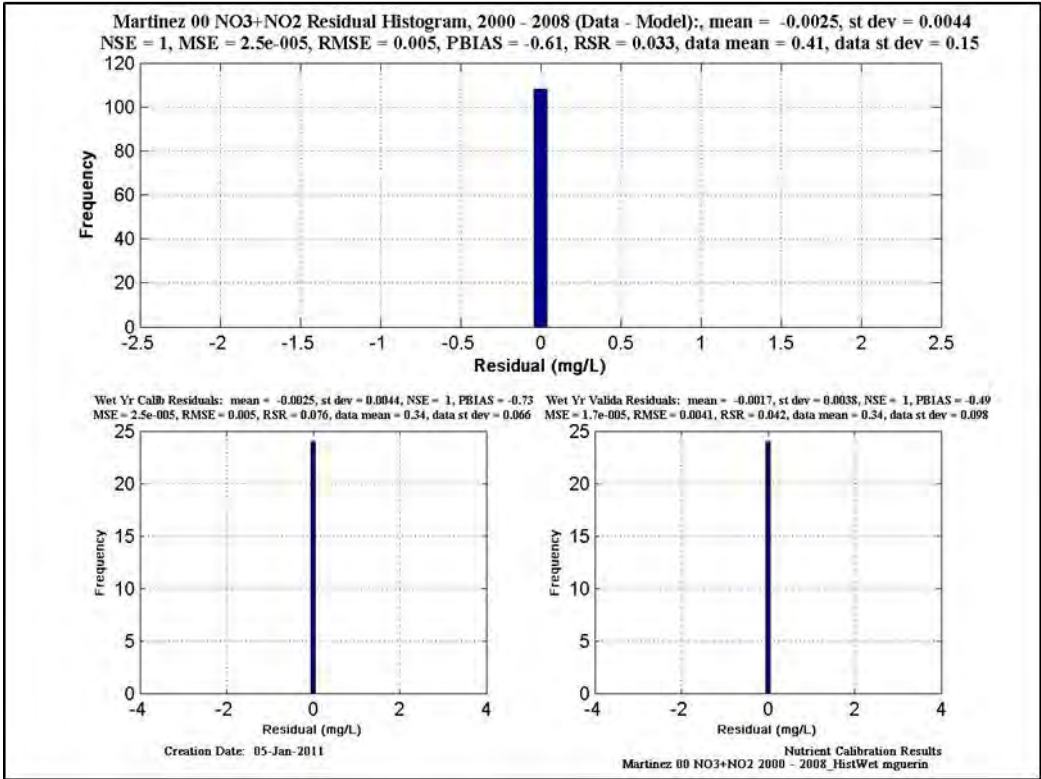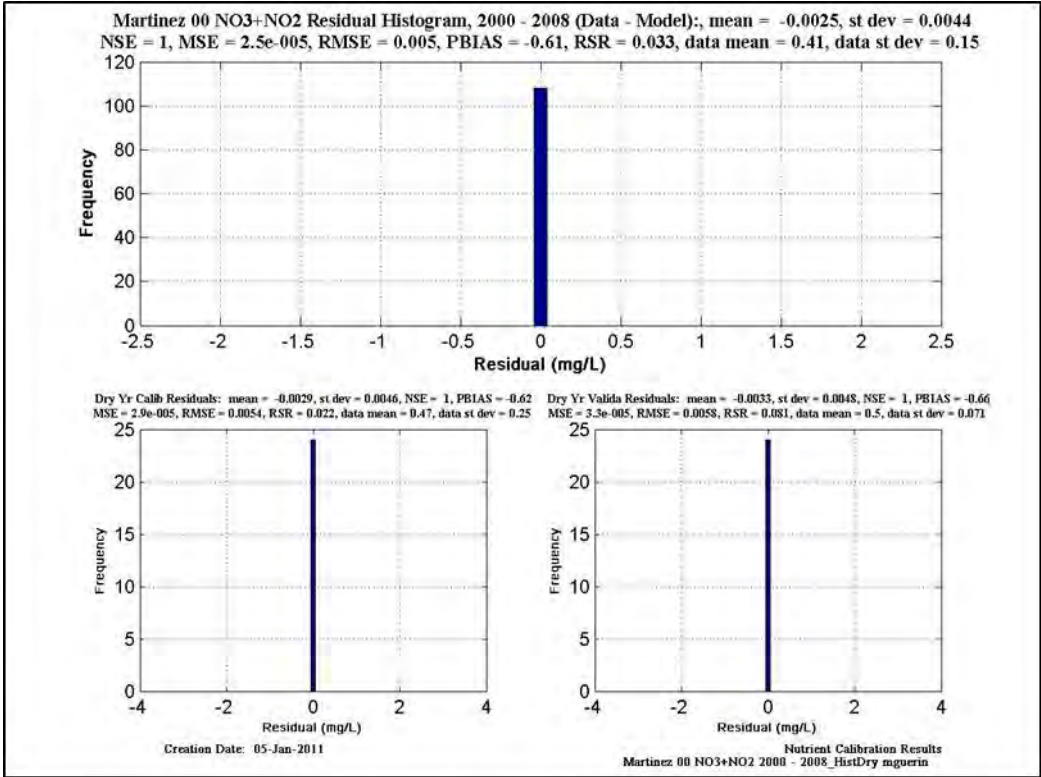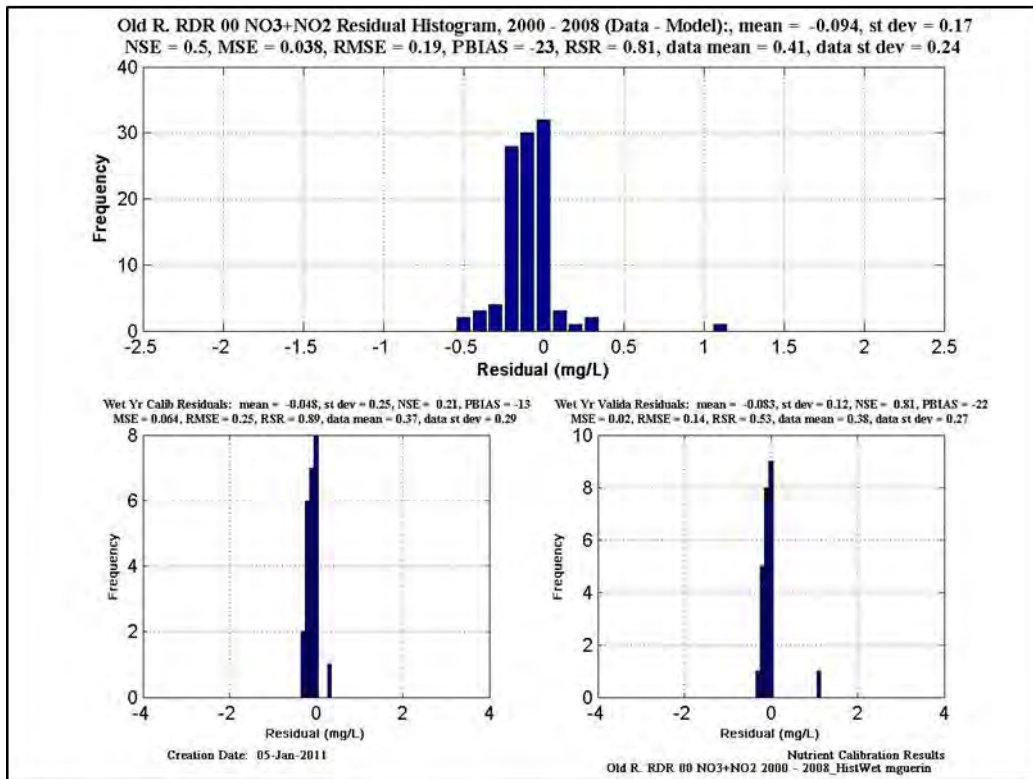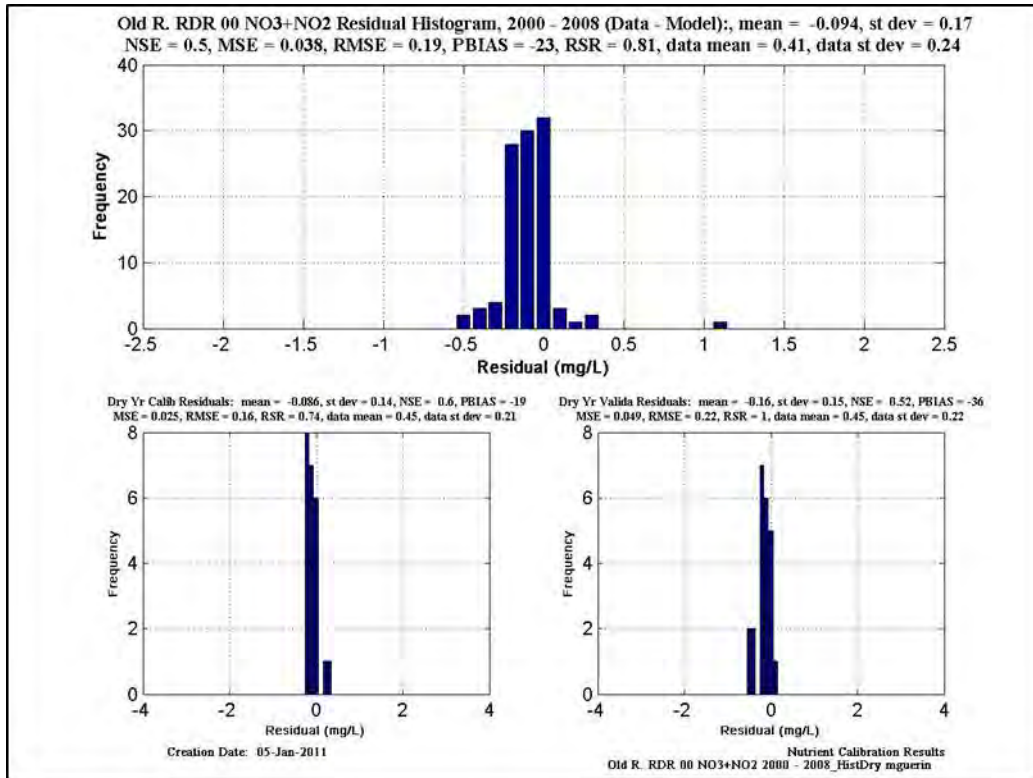**Figure 11-2 Calibration/validation statistics for Algae at Buckley Cove. Upper figure is calibration & validation statistics for dry years; lower figure is calibration & validation statistics for wet years.**
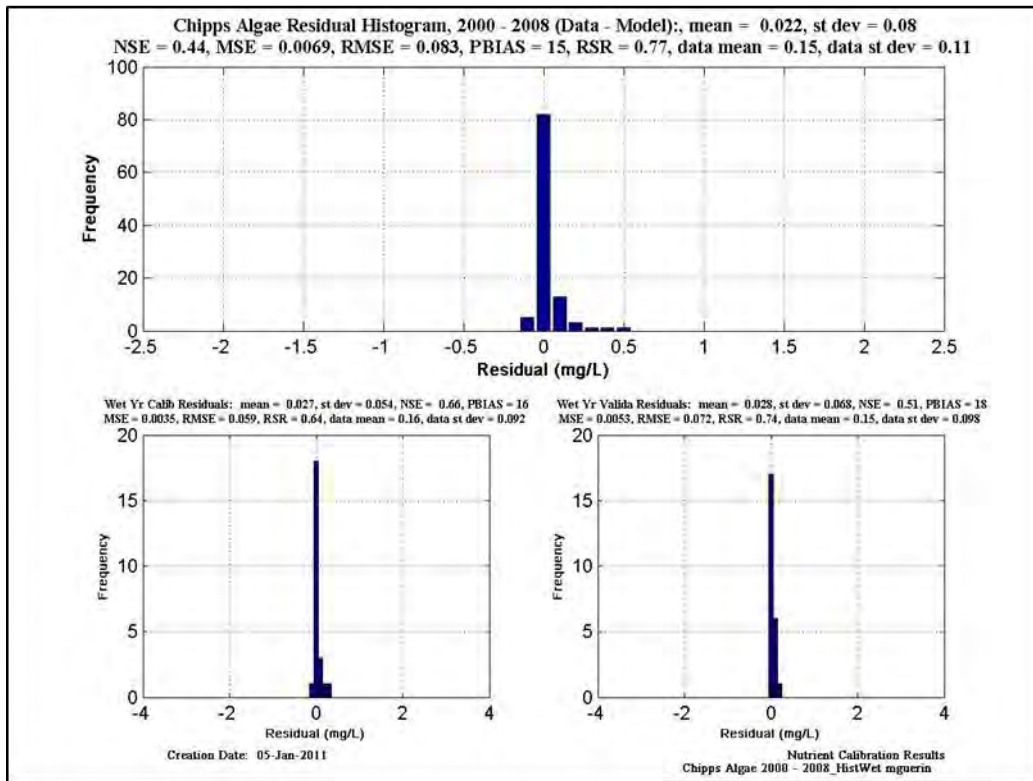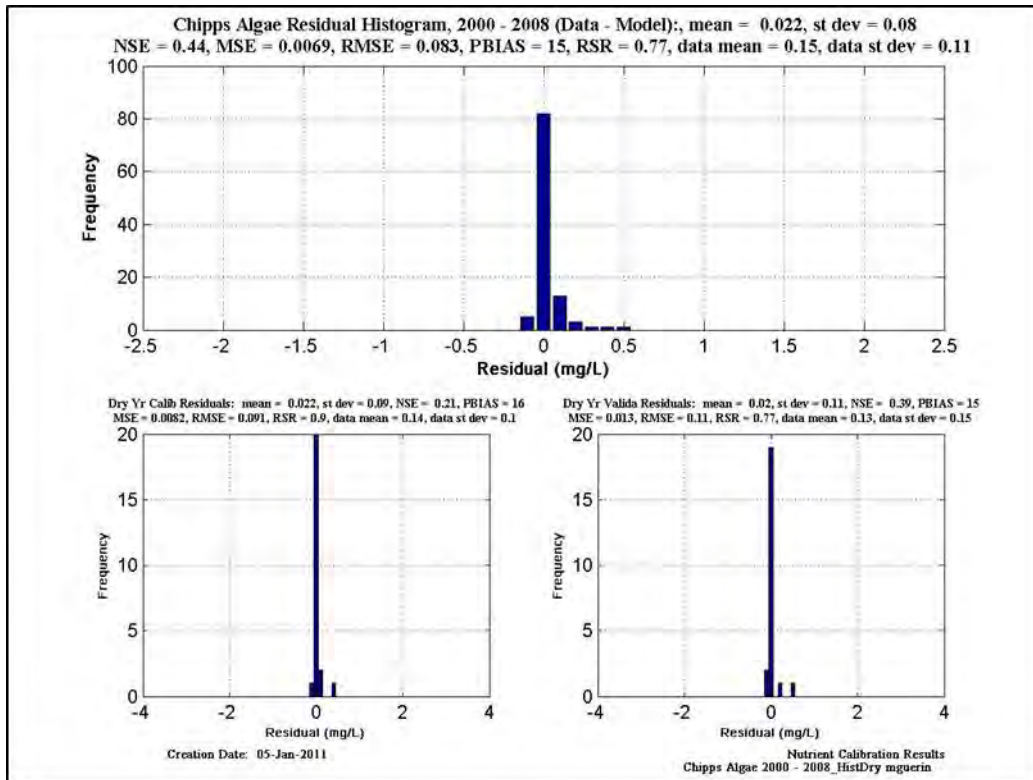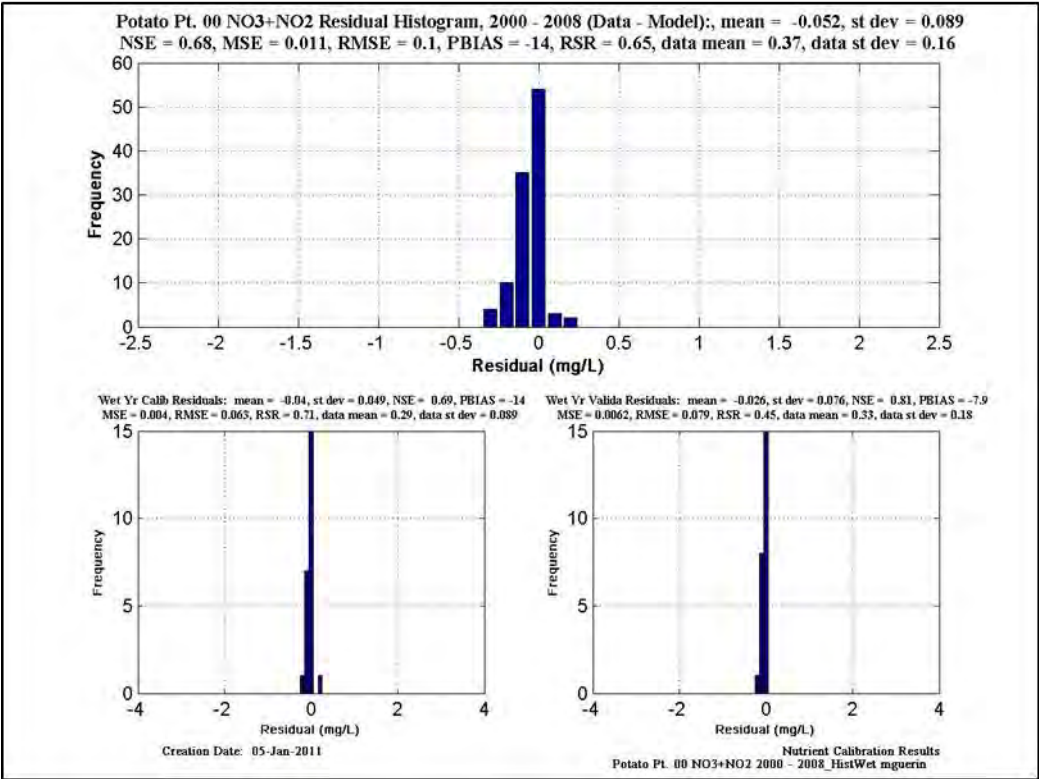
Figure 11-3 Calibration/validation statistics for Algae at Chipps. Upper figure is calibration & validation statistics for dry years; lower figure is calibration & validation statistics for wet years.
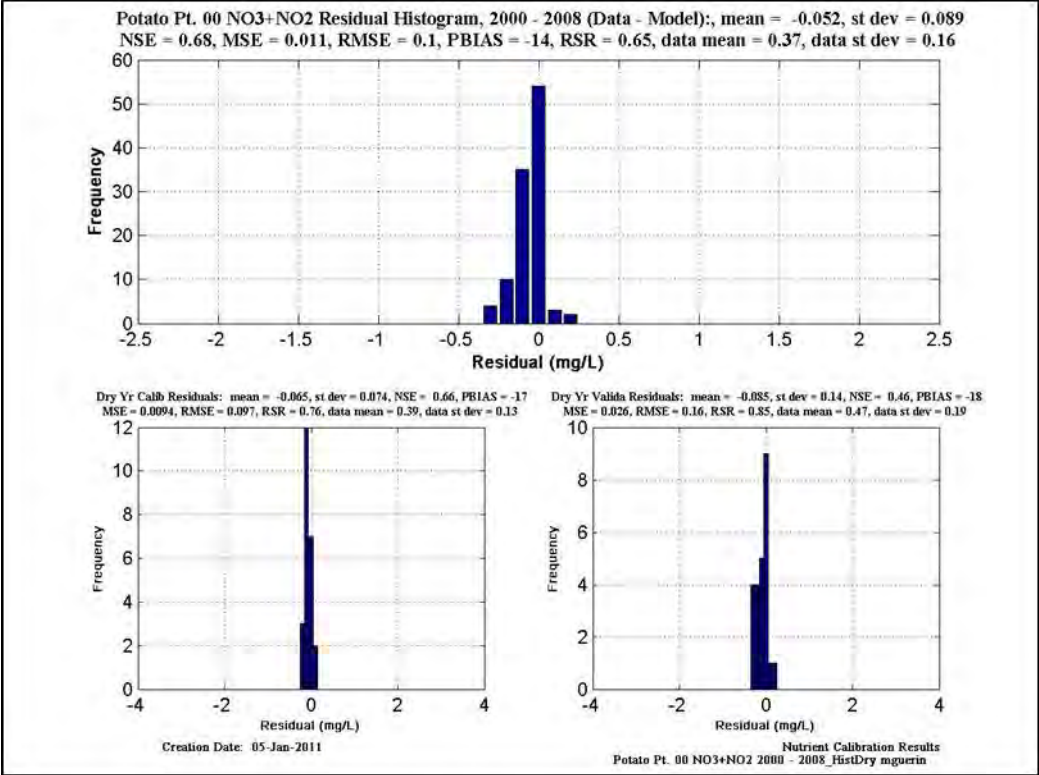
298
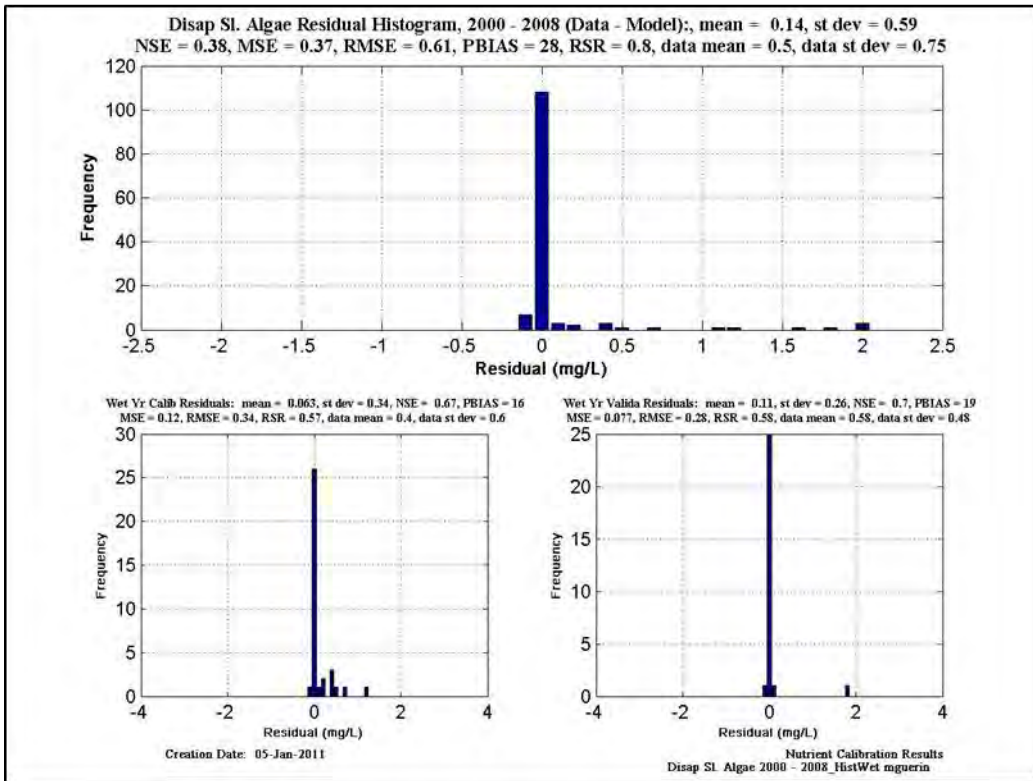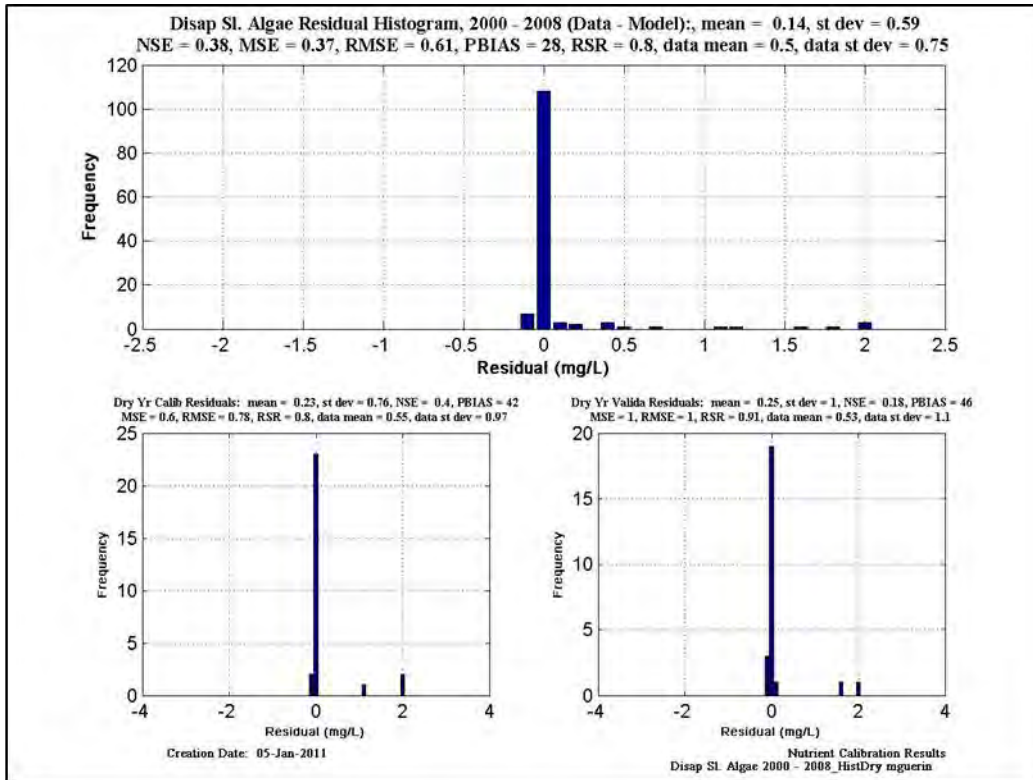
Figure 11-4 Calibration/validation statistics for Algae at Disappointment Sl. Upper figure is calibration & validation statistics for dry years; lower figure is calibration & validation statistics for wet years.
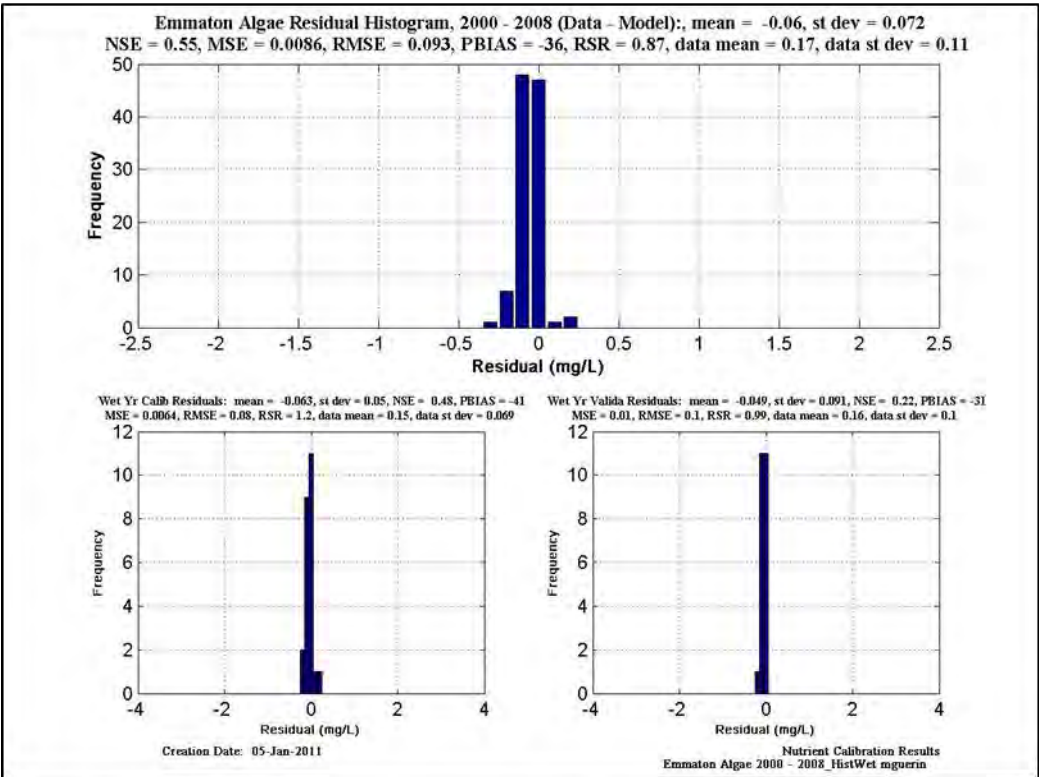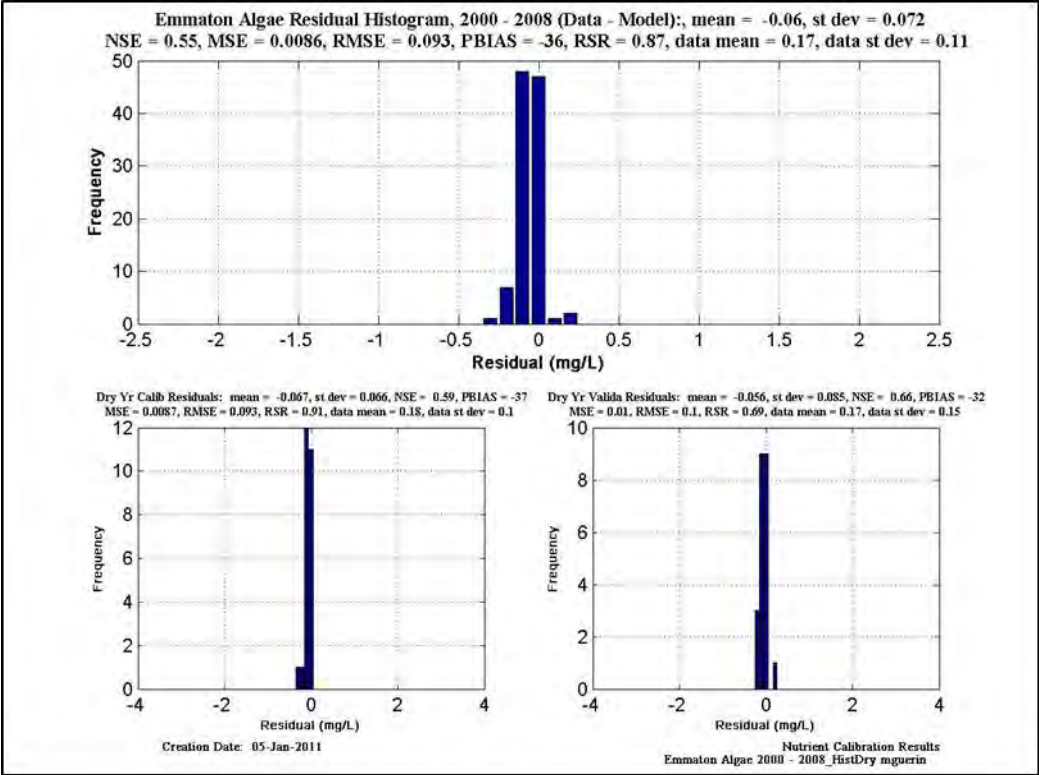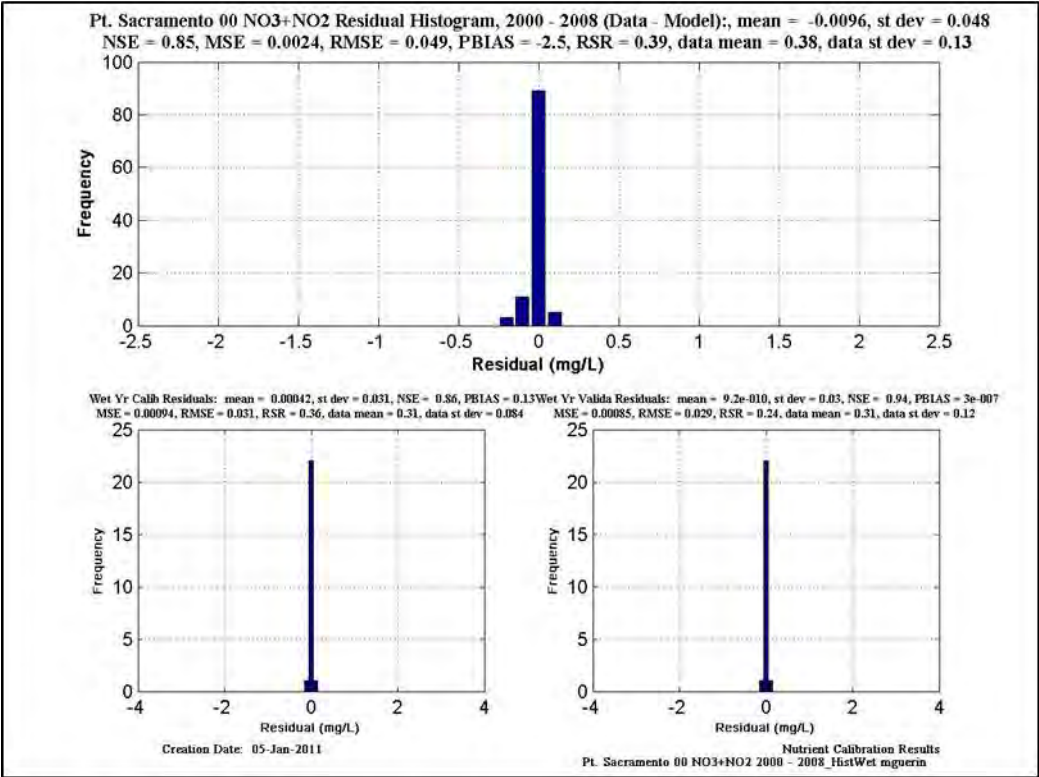
Figure 11-5 Calibration/validation statistics for Algae at Emmaton. Upper figure is calibration & validation statistics for dry years; lower figure is calibration & validation statistics for wet years.
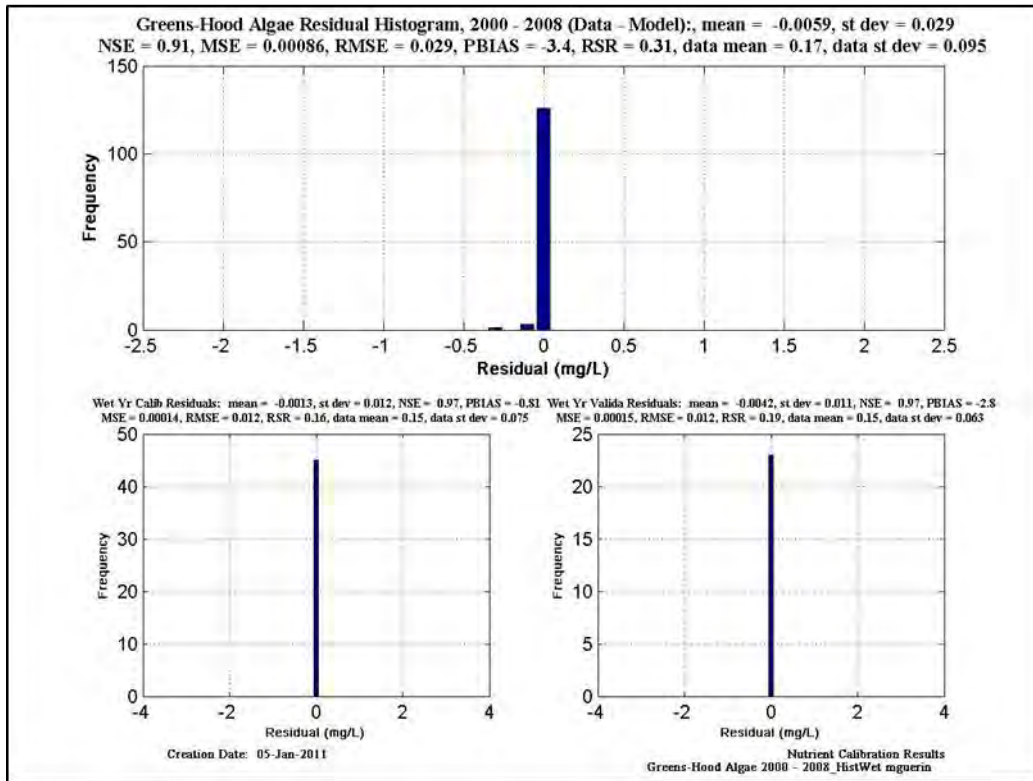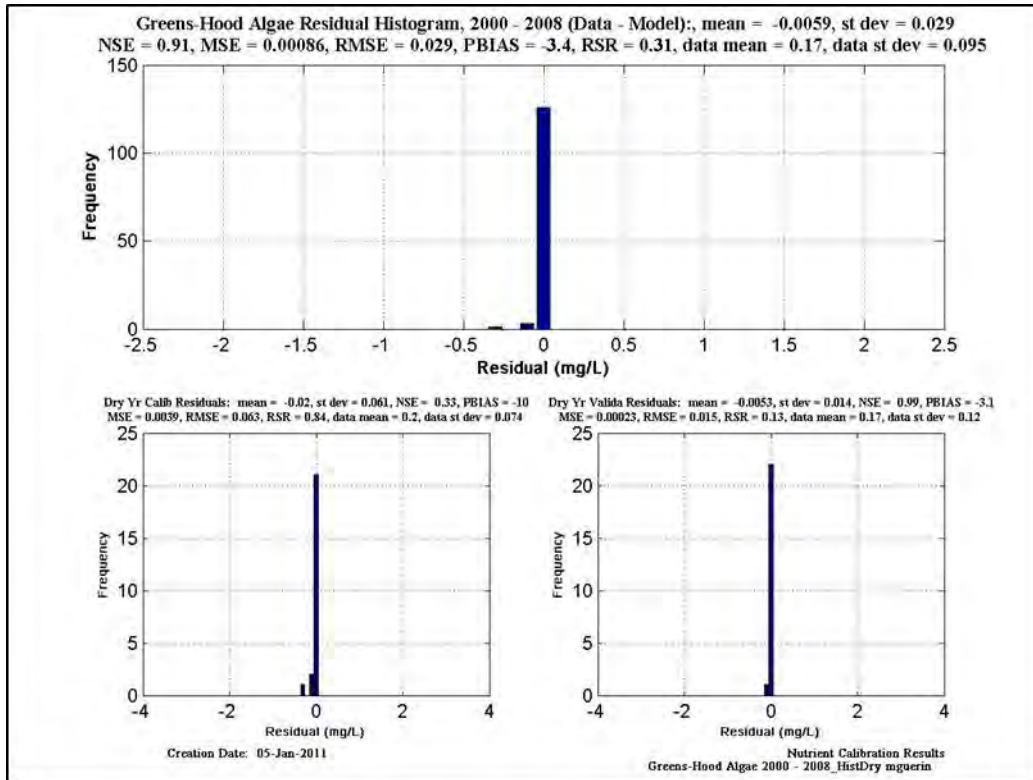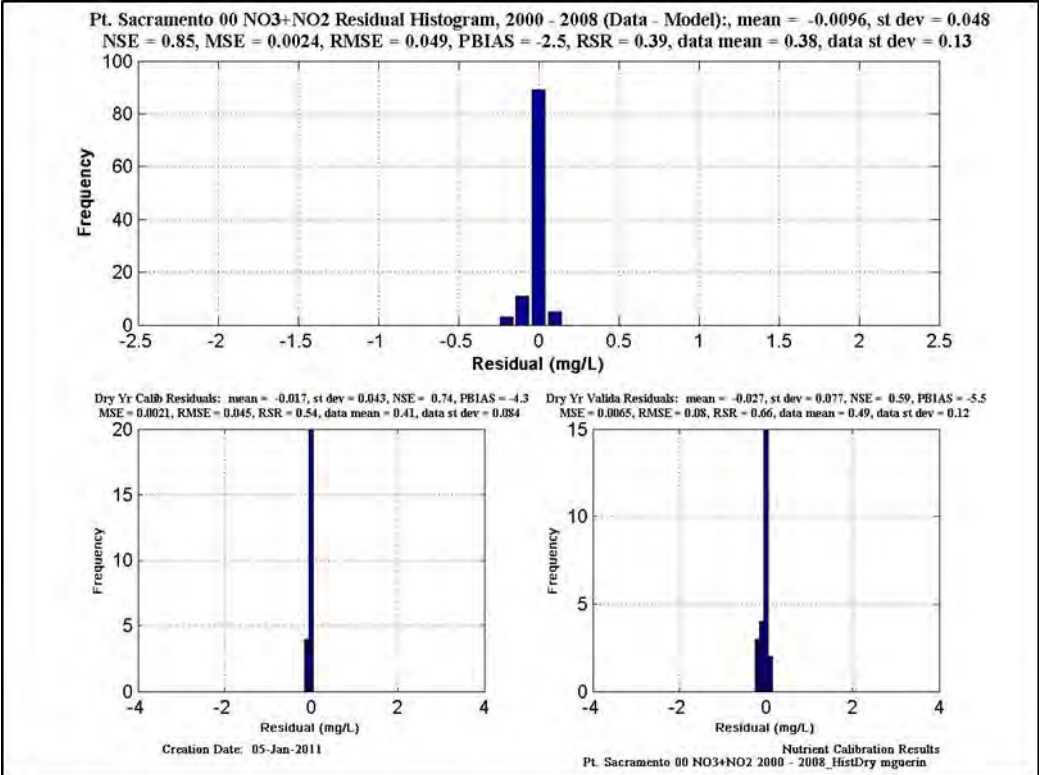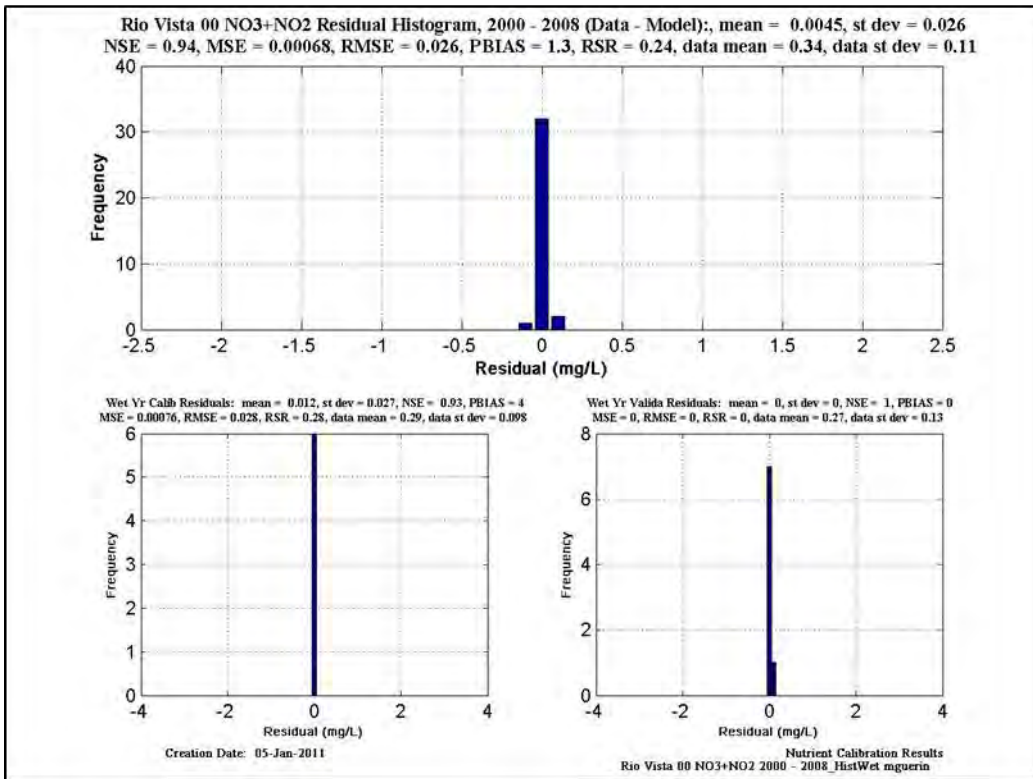
Figure 11-6 Calibration/validation statistics for Algae at Greens-Hood. Upper figure is calibration & validation statistics for dry years; lower figure is calibration & validation statistics for wet years.
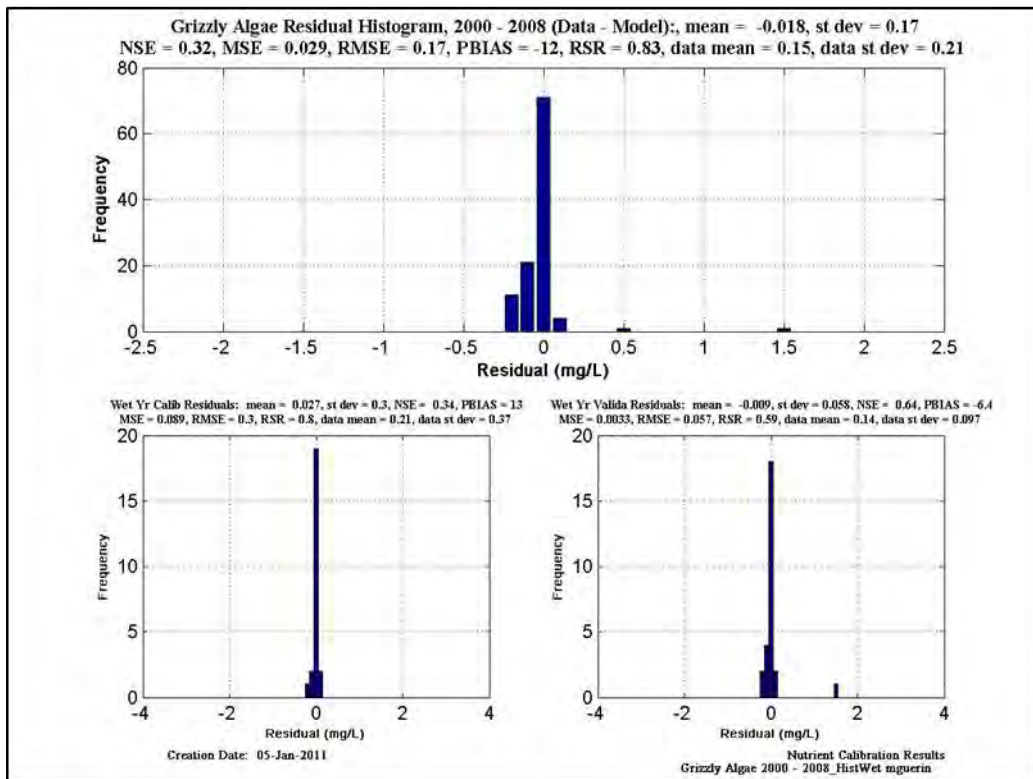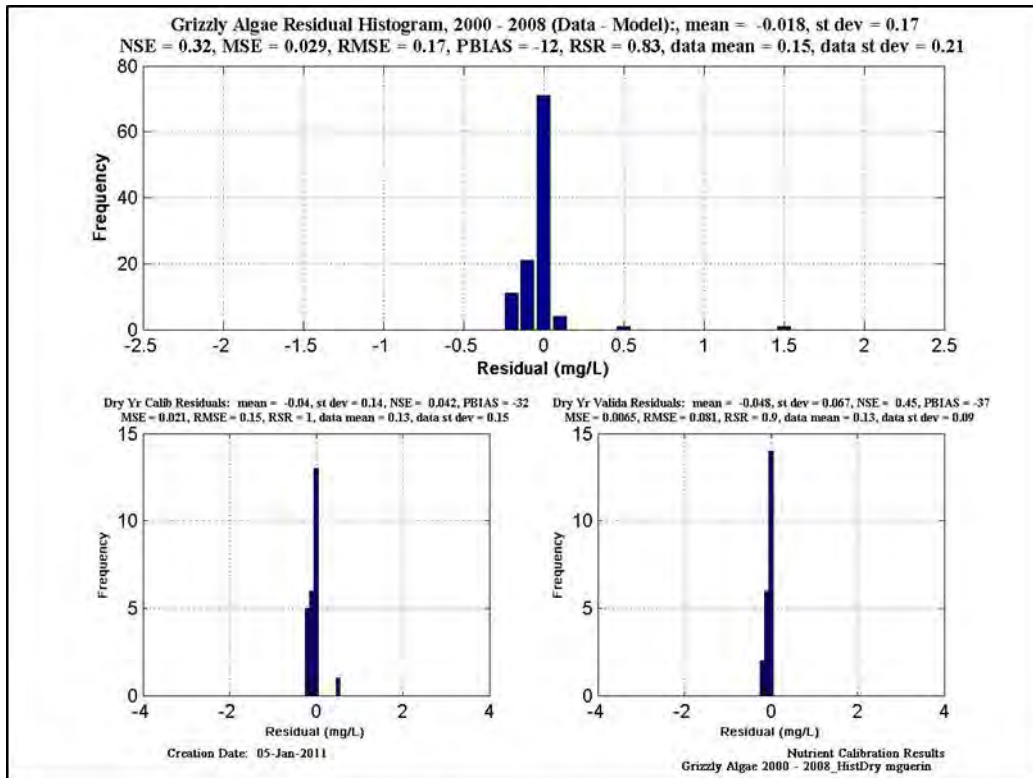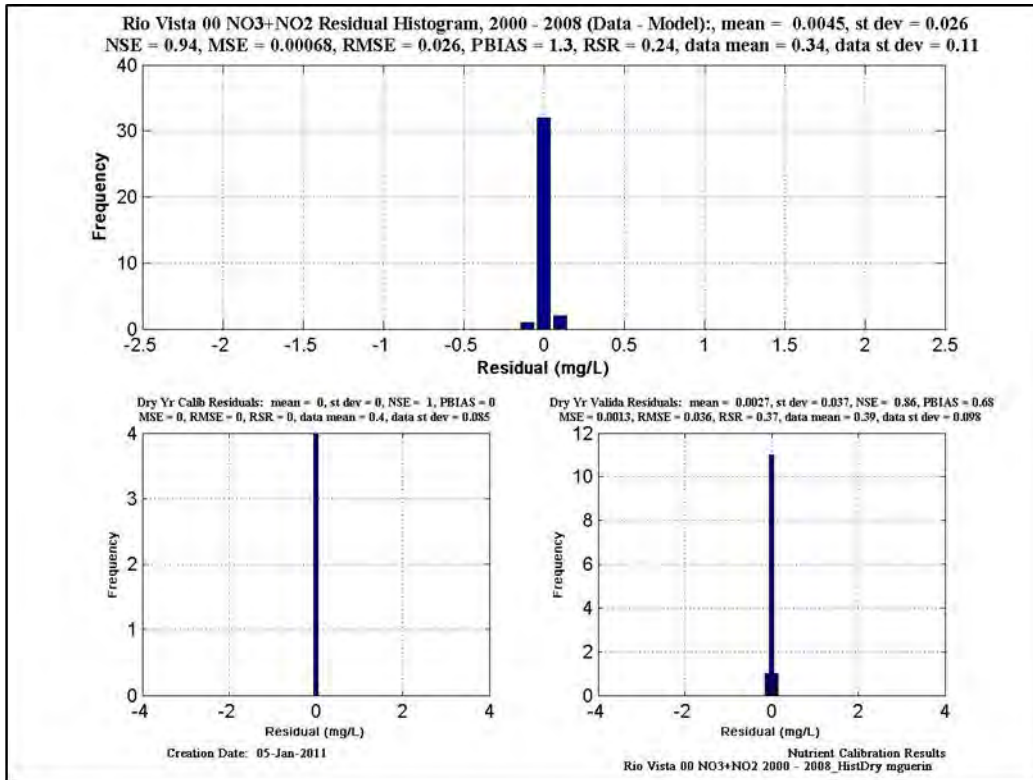
Figure 11-7 Calibration/validation statistics for Algae at Grizzly. Upper figure is calibration & validation statistics for dry years; lower figure is calibration & validation statistics for wet years.
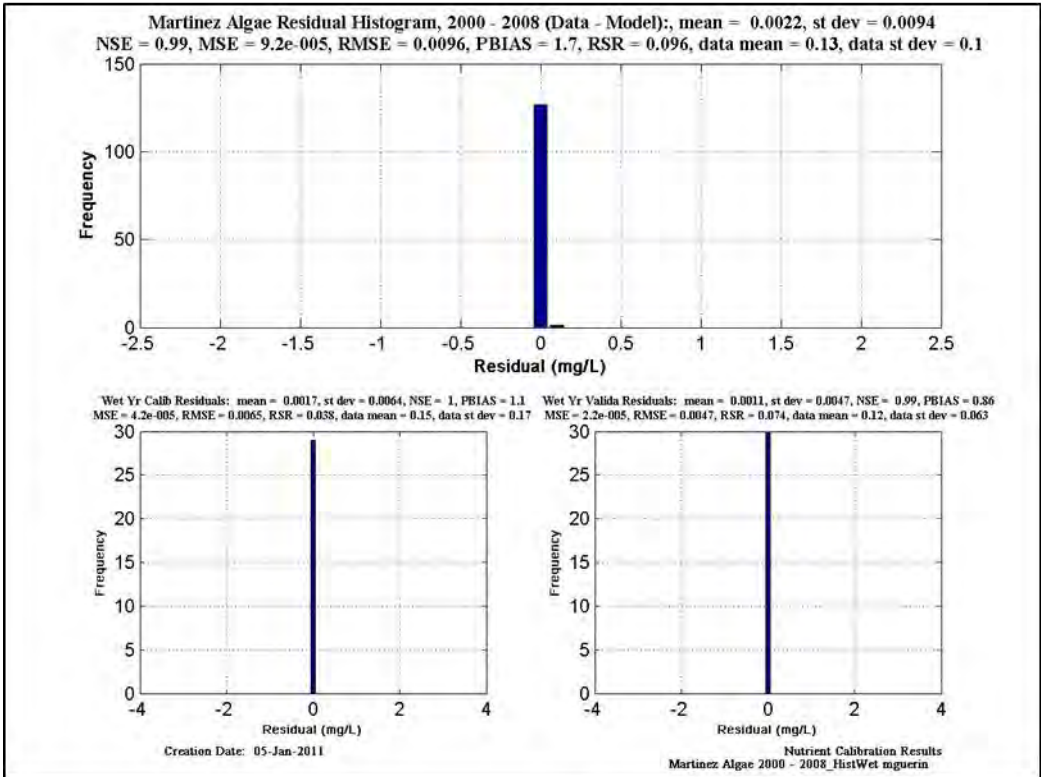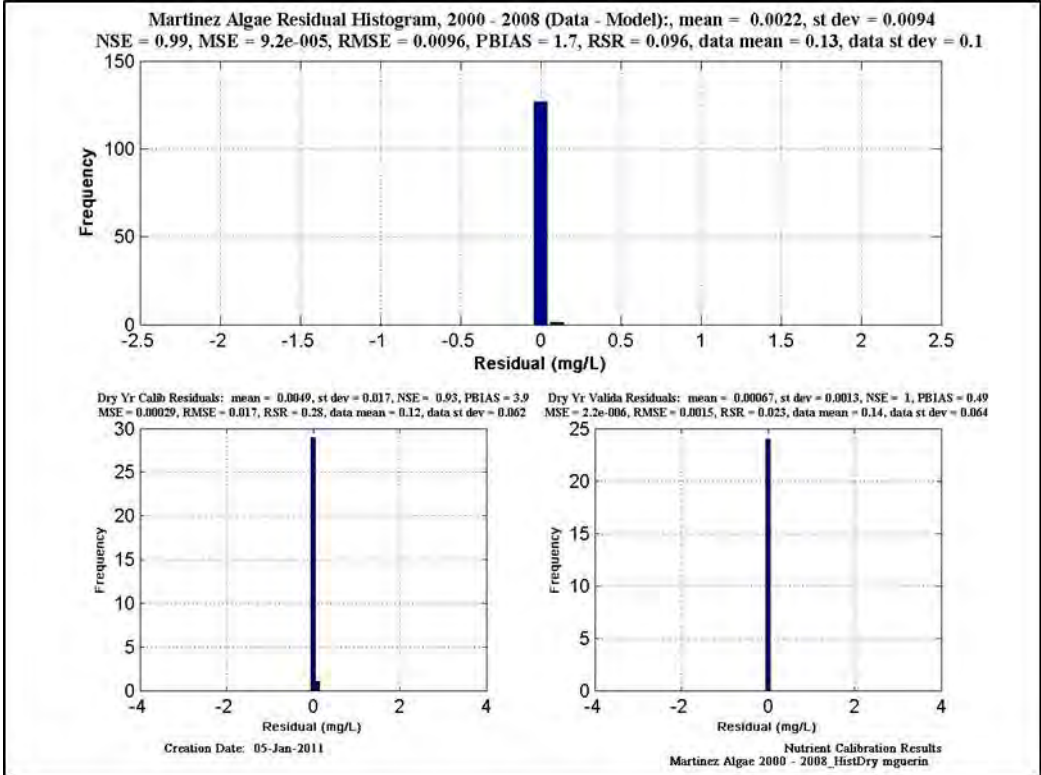
Figure 11-8 Calibration/validation statistics for Algae at Martinez. Upper figure is calibration & validation statistics for dry years; lower figure is calibration & validation statistics for wet years.
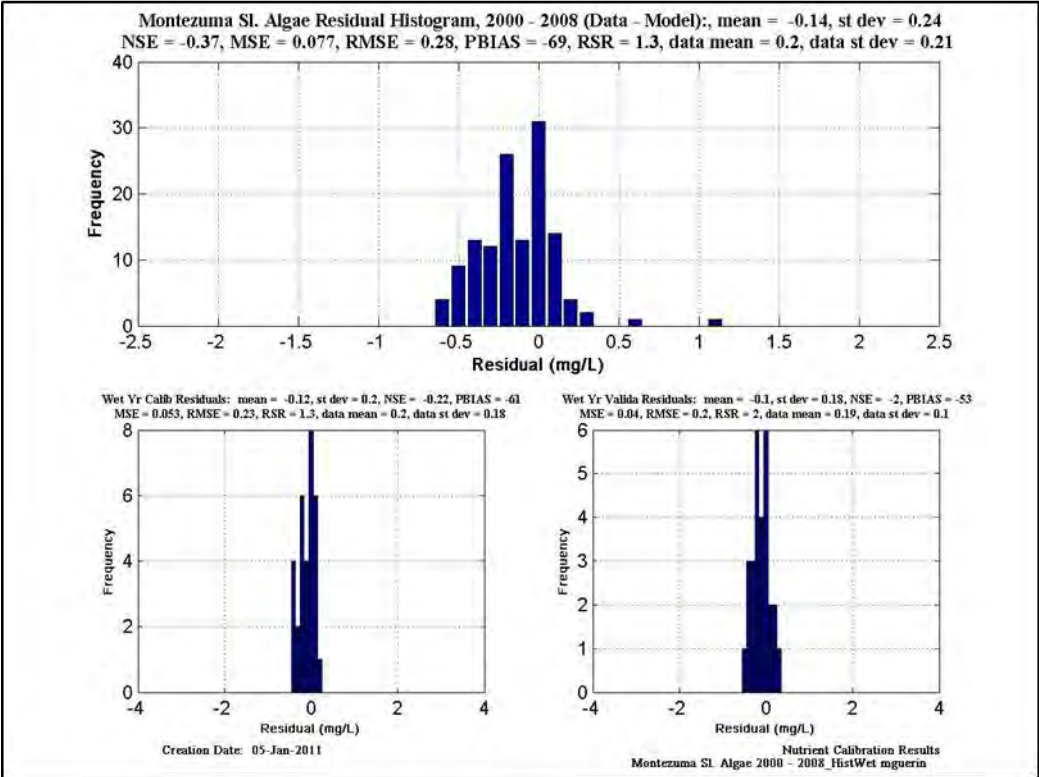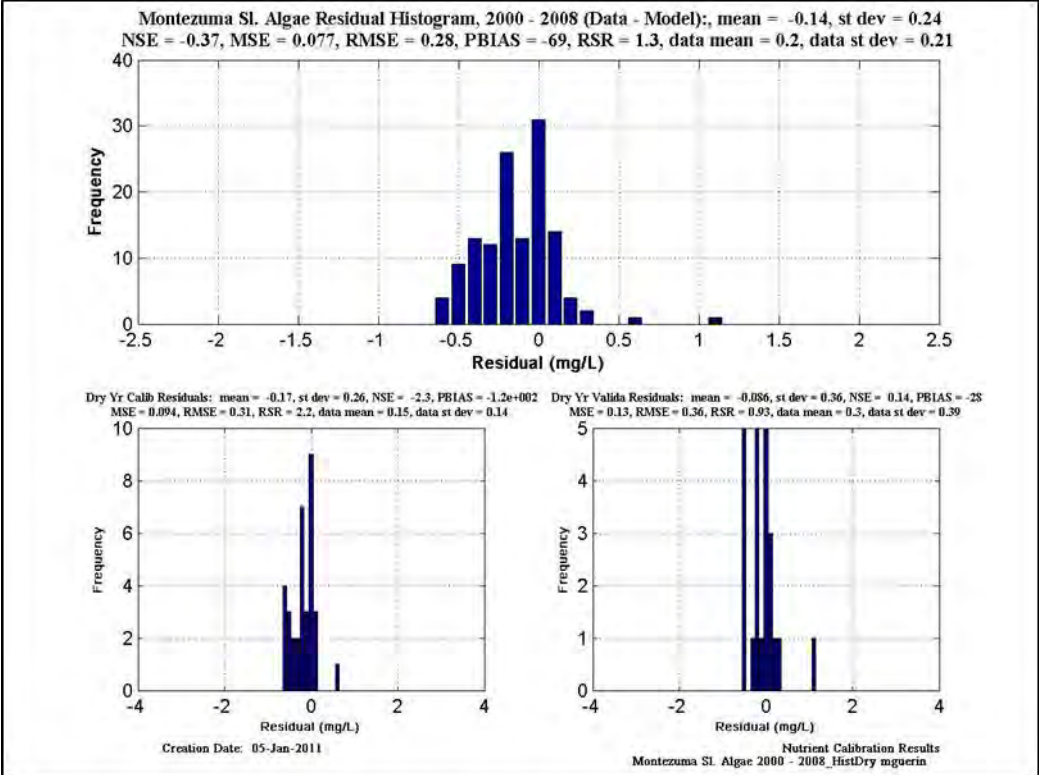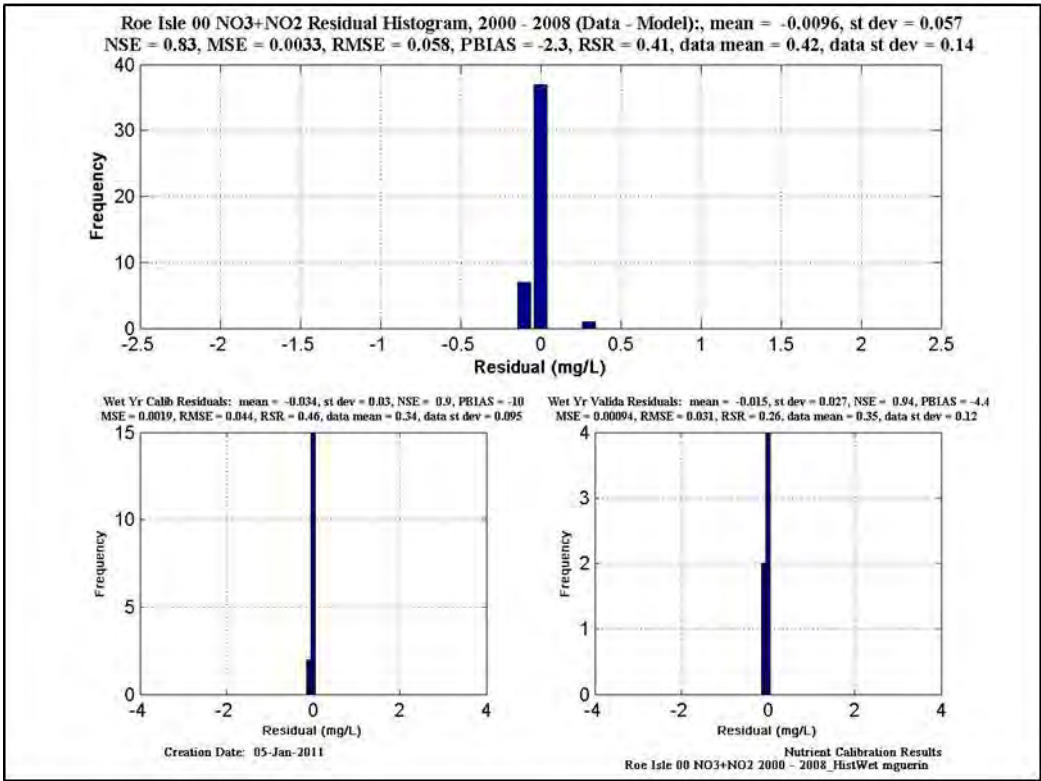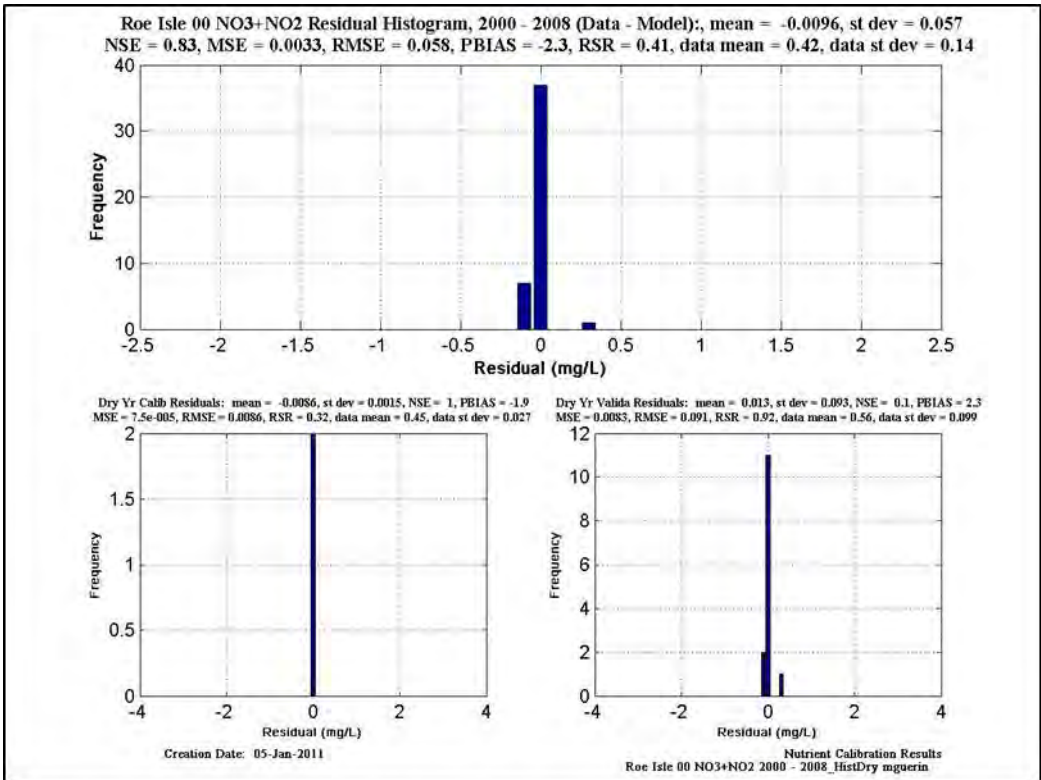
Figure 11-9 Calibration/validation statistics for Algae at Montezuma Sl. Upper figure is calibration & validation statistics for dry years; lower figure is calibration & validation statistics for wet years.
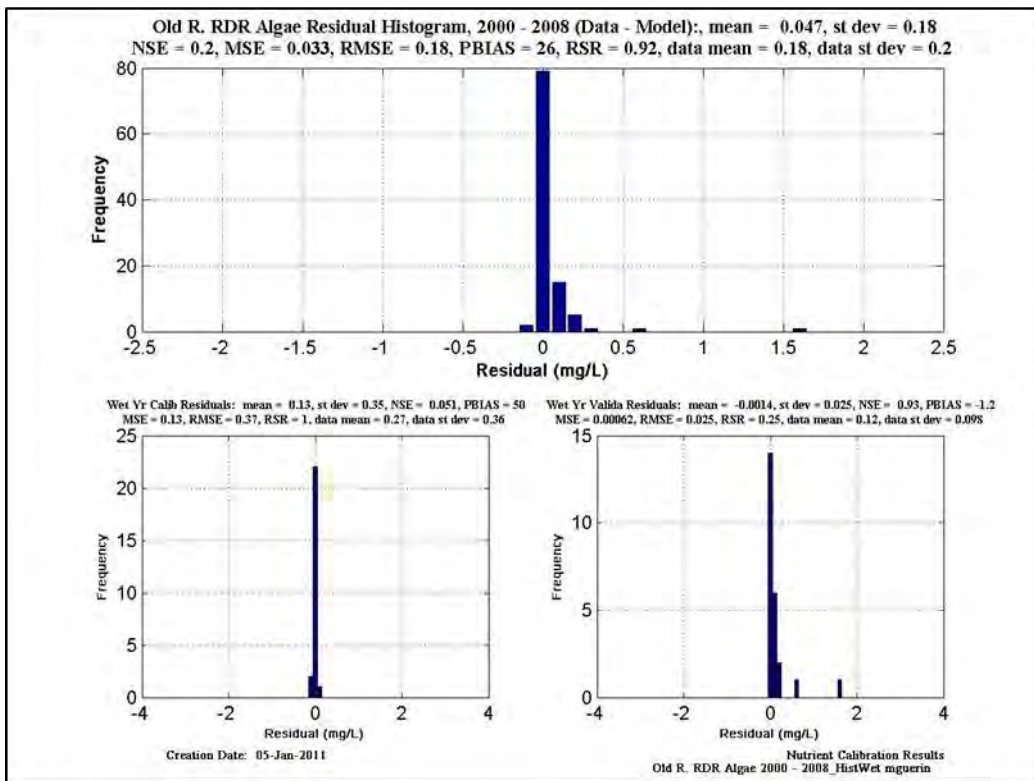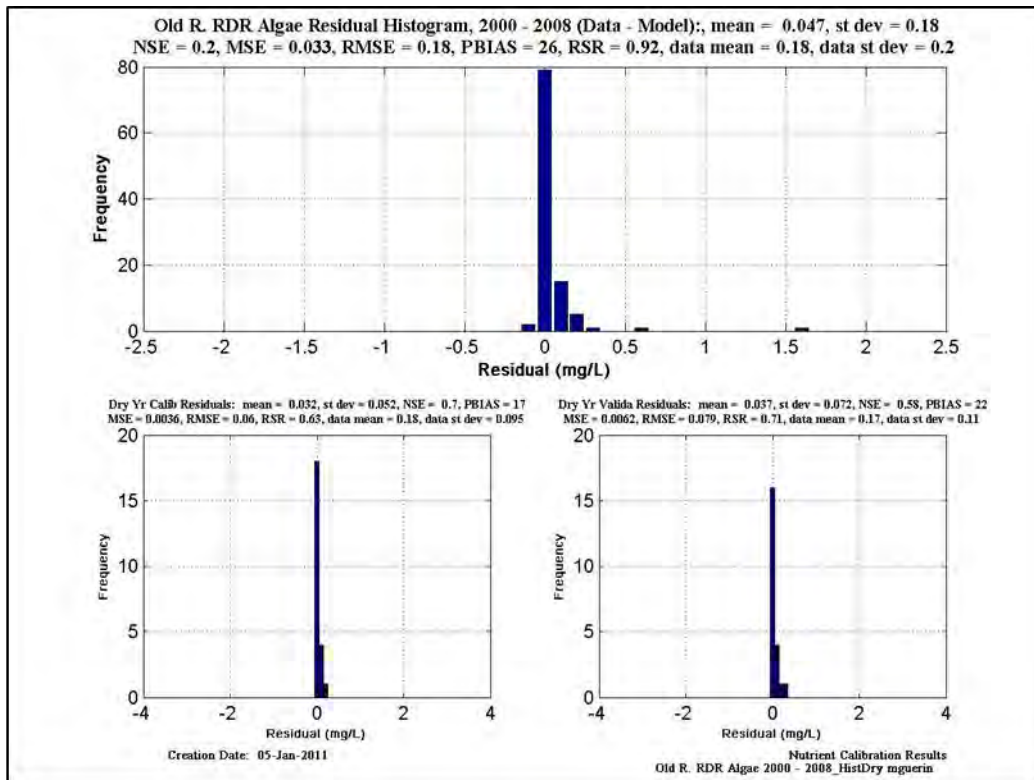
Figure 11-10 Calibration/validation statistics for Algae at Old R. RDR. Upper figure is calibration & validation statistics for dry years; lower figure is calibration & validation statistics for wet years.
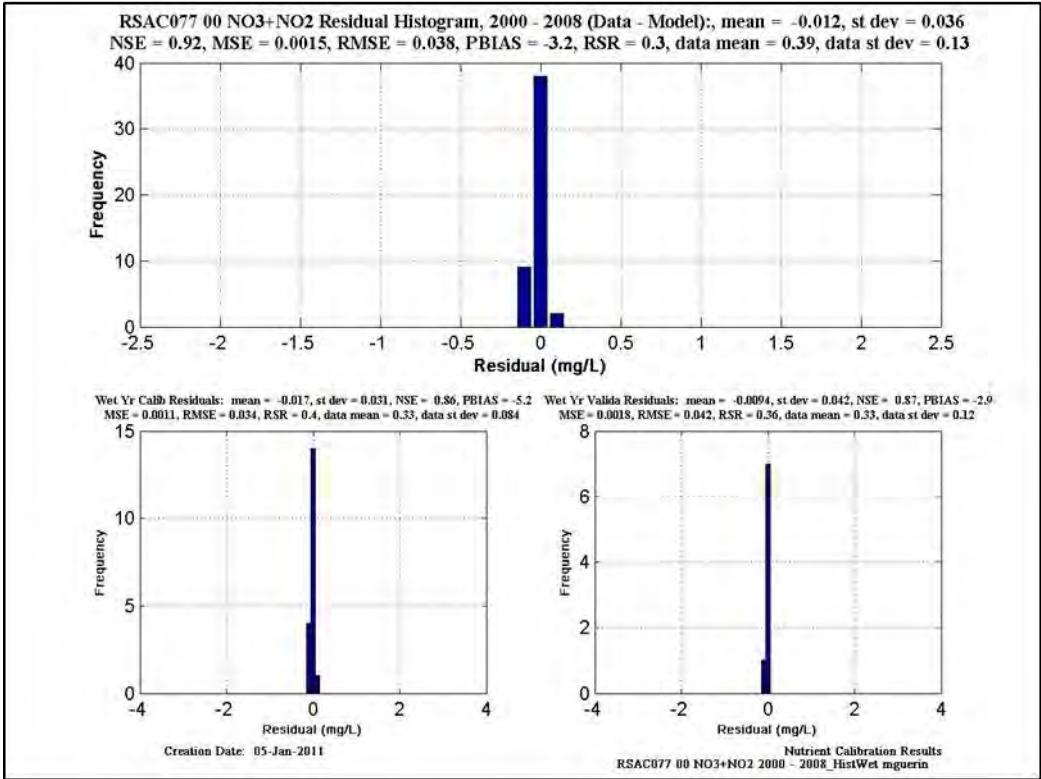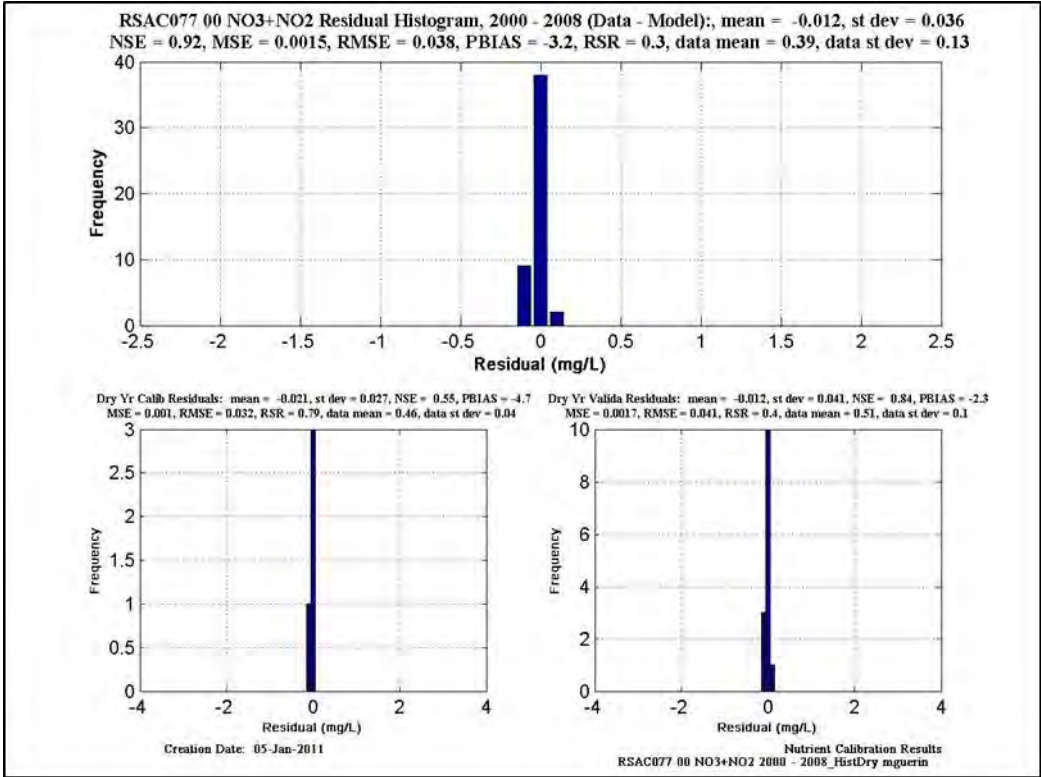
305
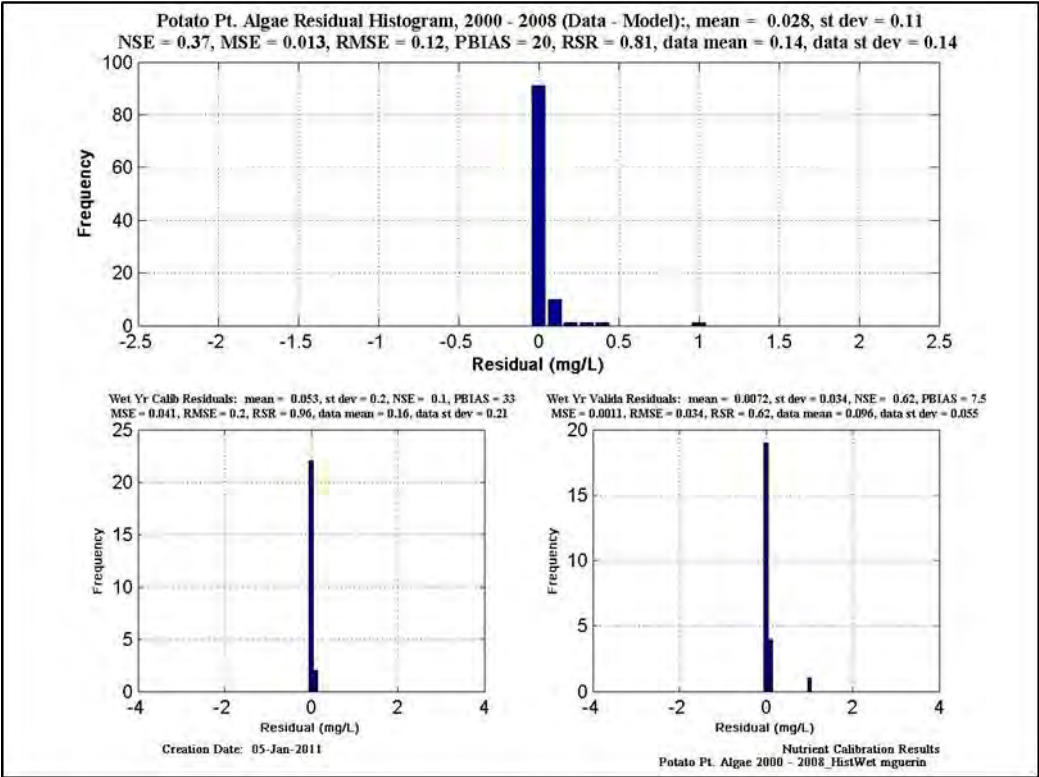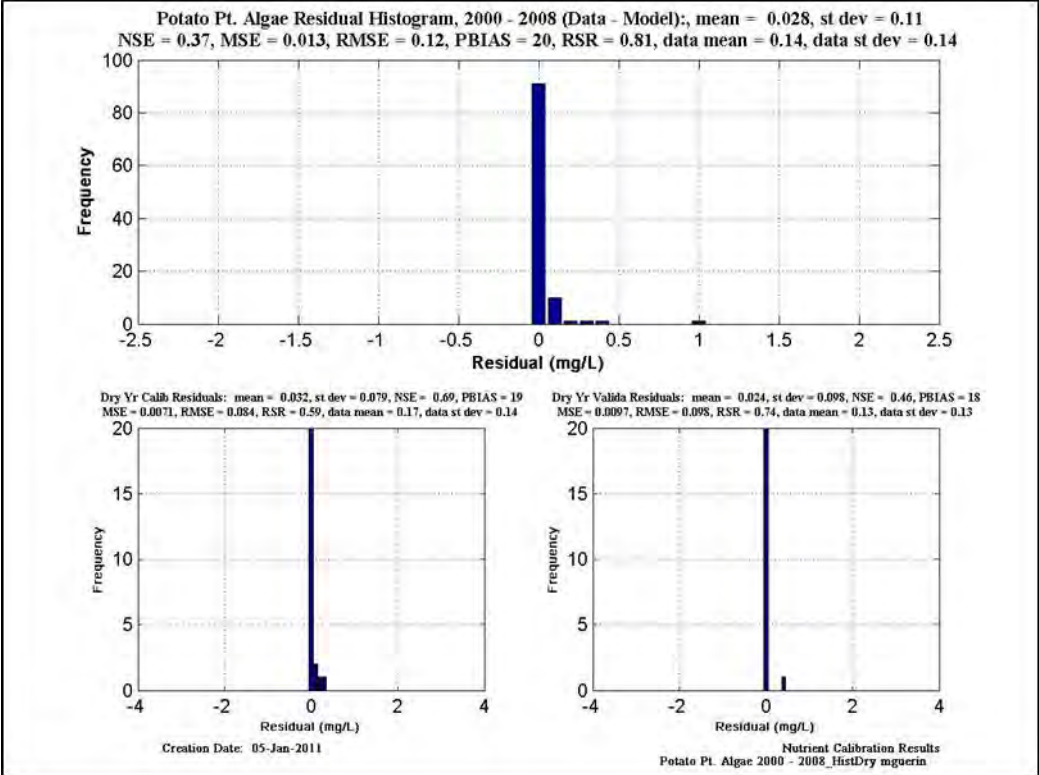
Figure 11-11 Calibration/validation statistics for Algae at Potato Pt. Upper figure is calibration & validation statistics for dry years; lower figure is calibration & validation statistics for wet years.
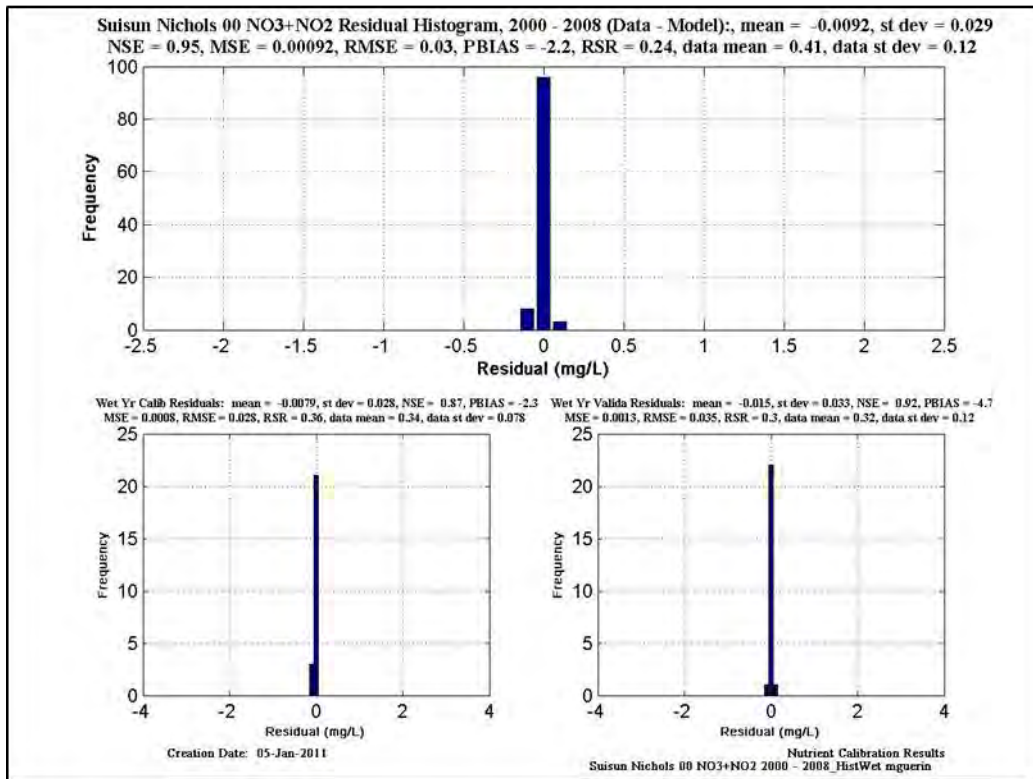
306
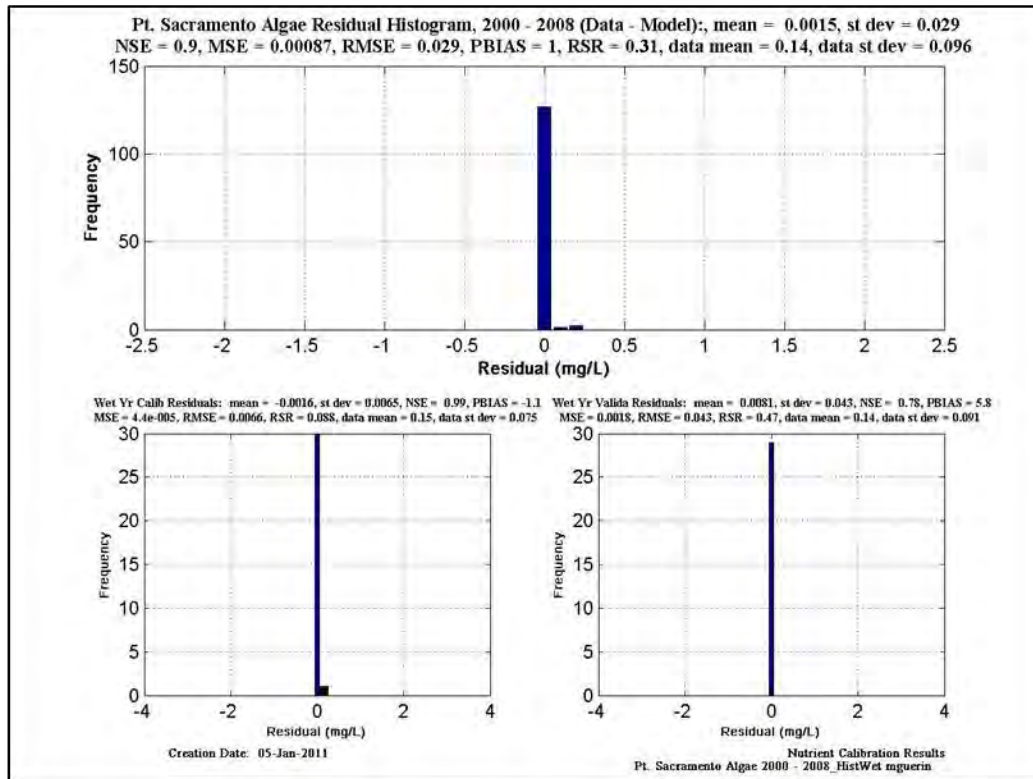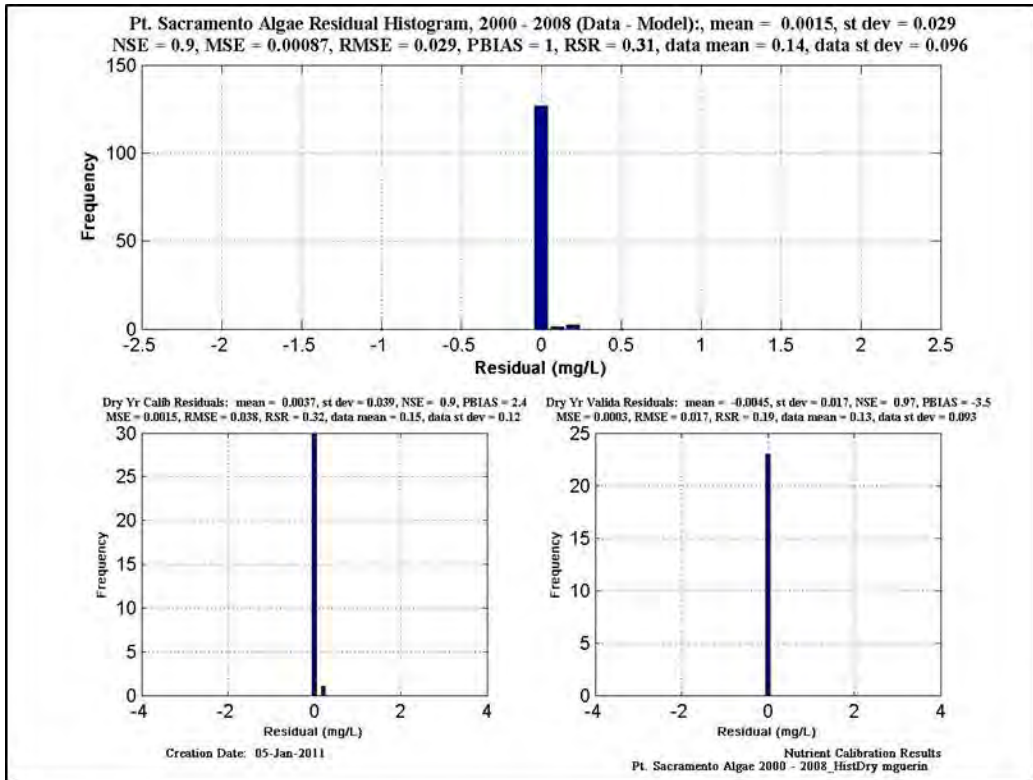
Figure 11-12 Calibration/validation statistics for Algae at Pt. Sacramento. Upper figure is calibration & validation statistics for dry years; lower figure is calibration & validation statistics for wet years.

307
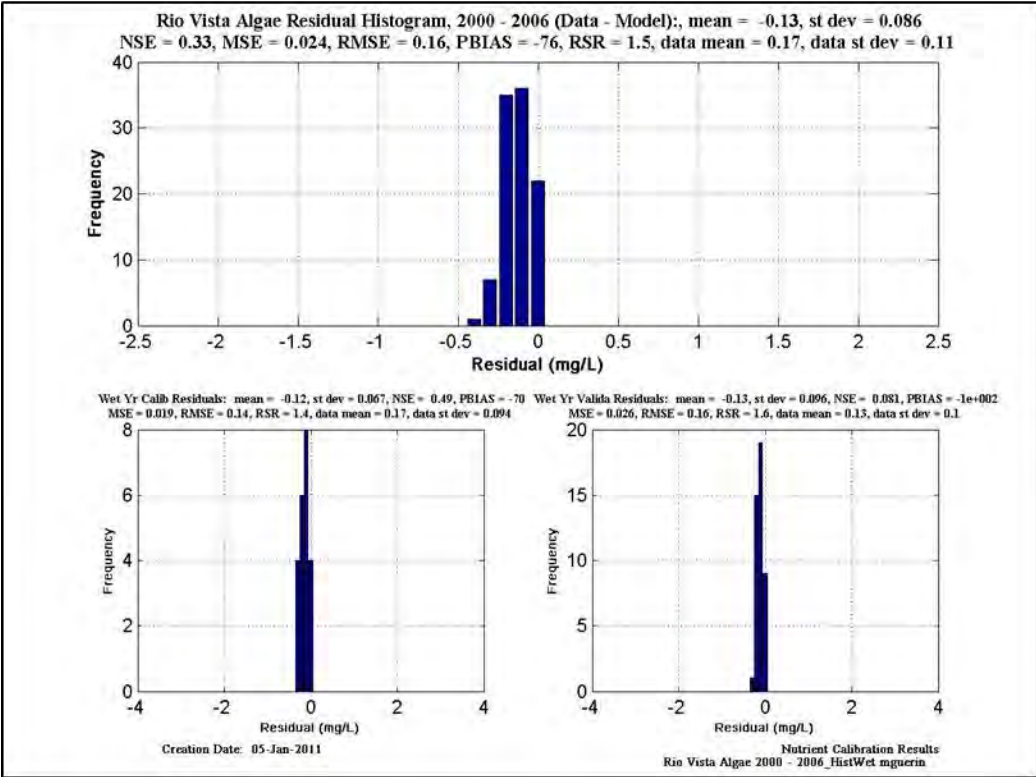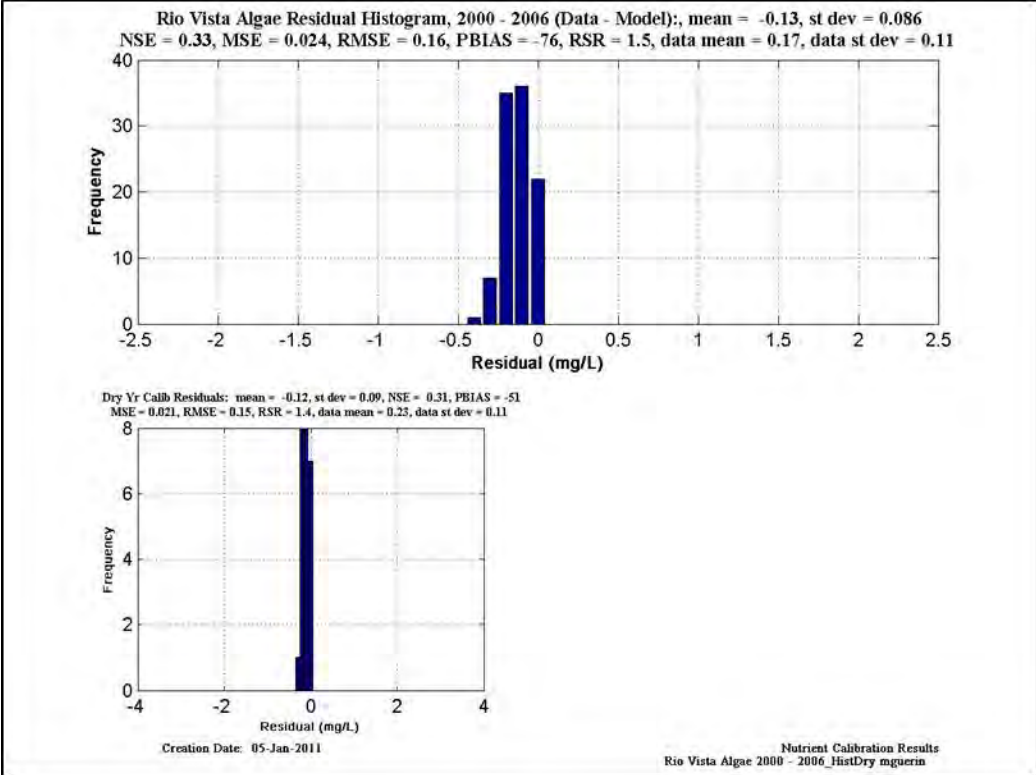
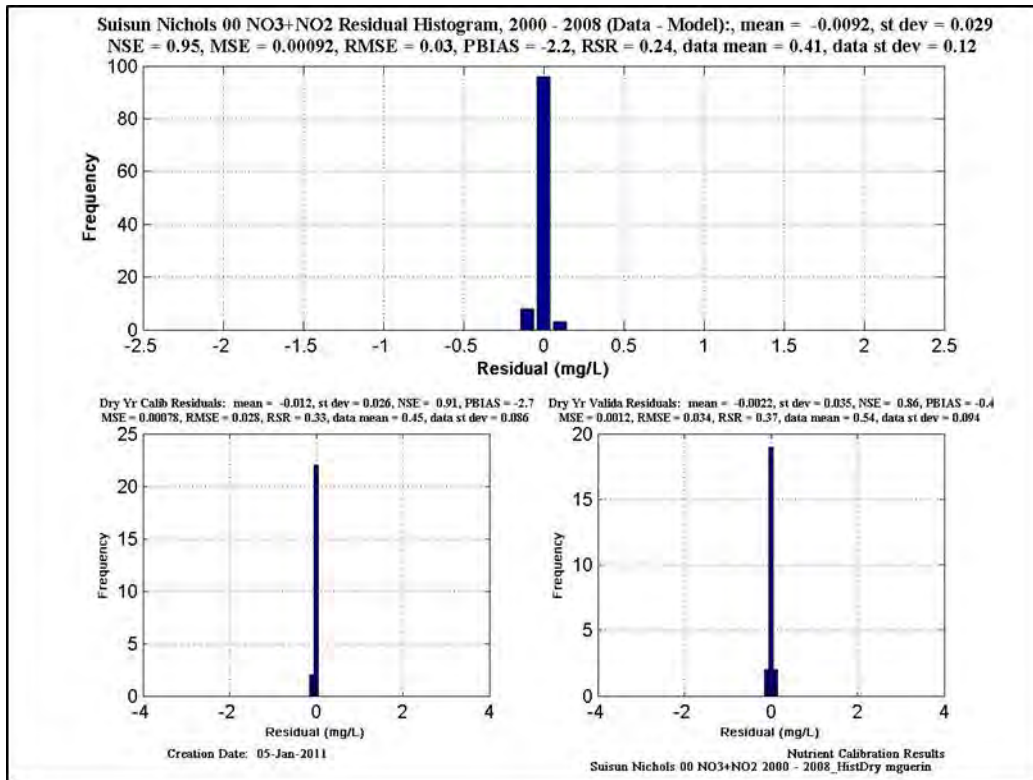**Figure 11-13 Calibration/validation statistics for Algae at Rio Vista. Upper figure is calibration & validation statistics for dry years; lower figure is calibration & validation statistics for wet years.**
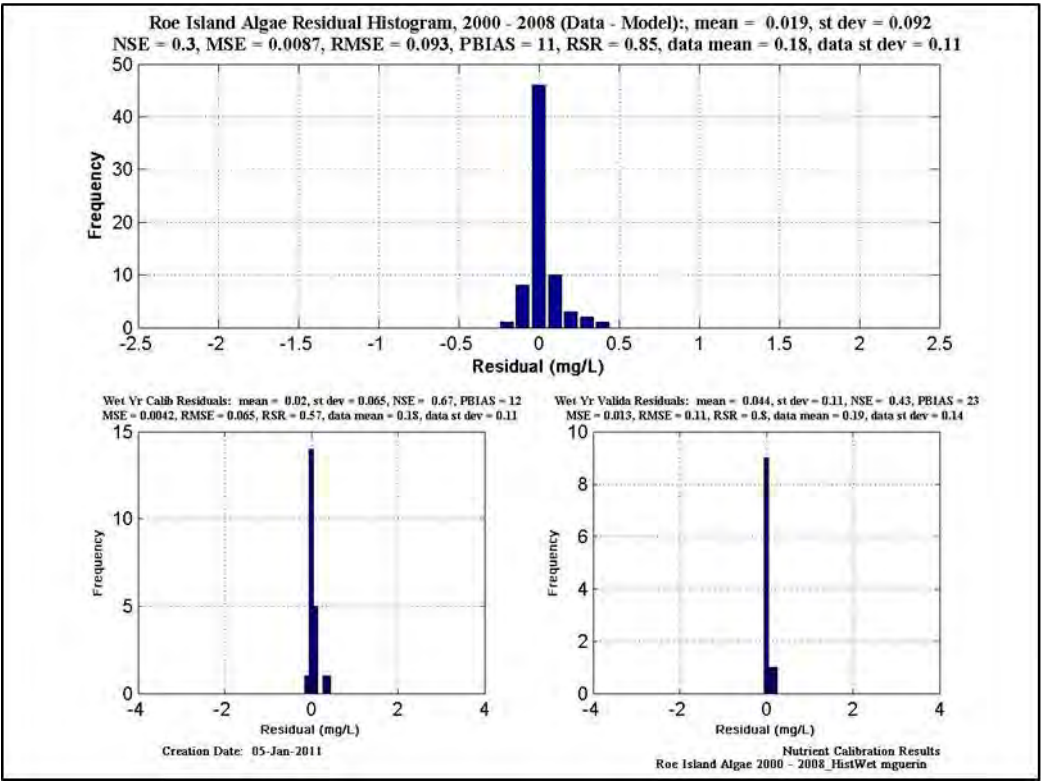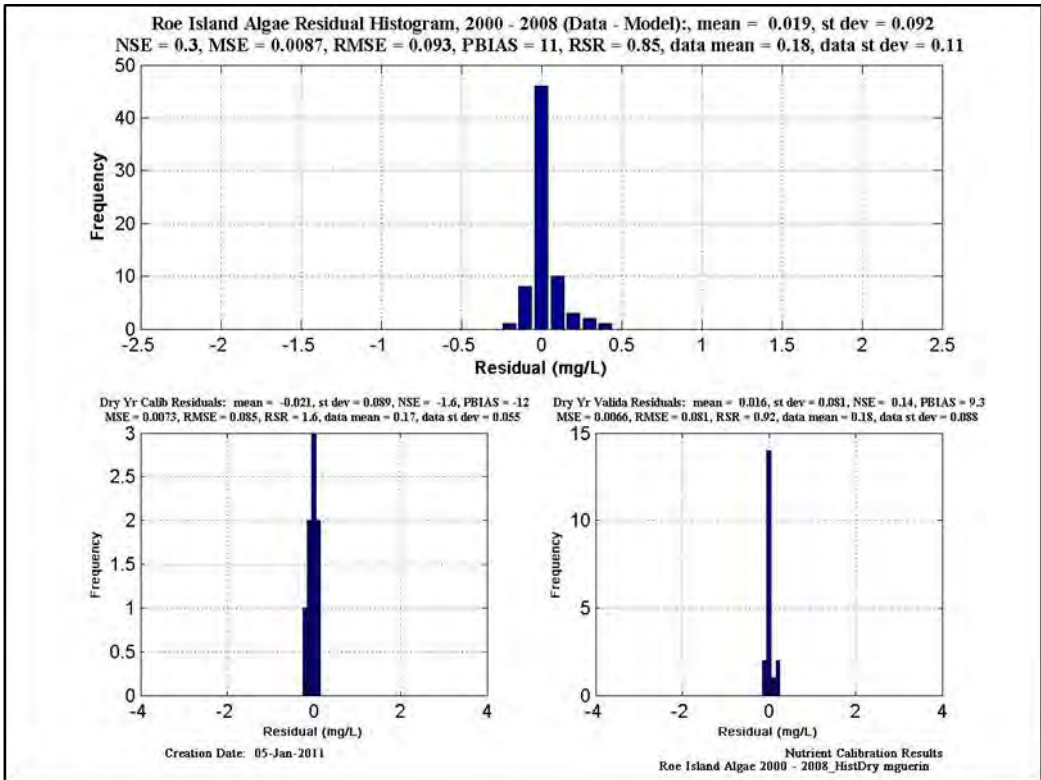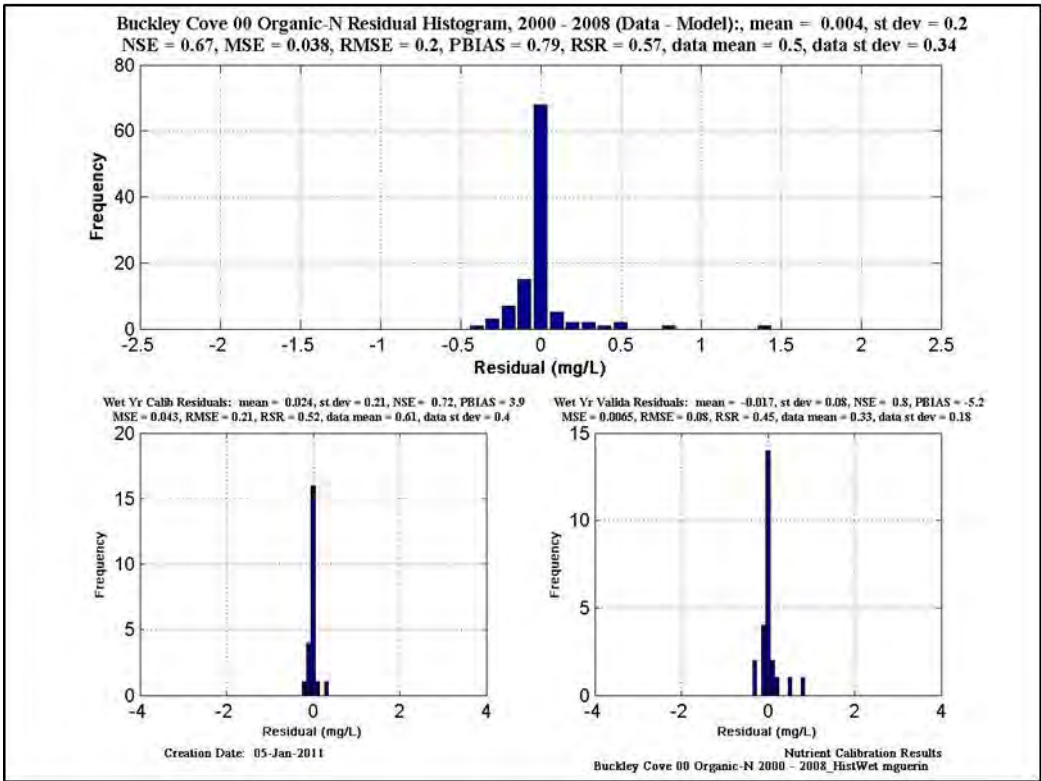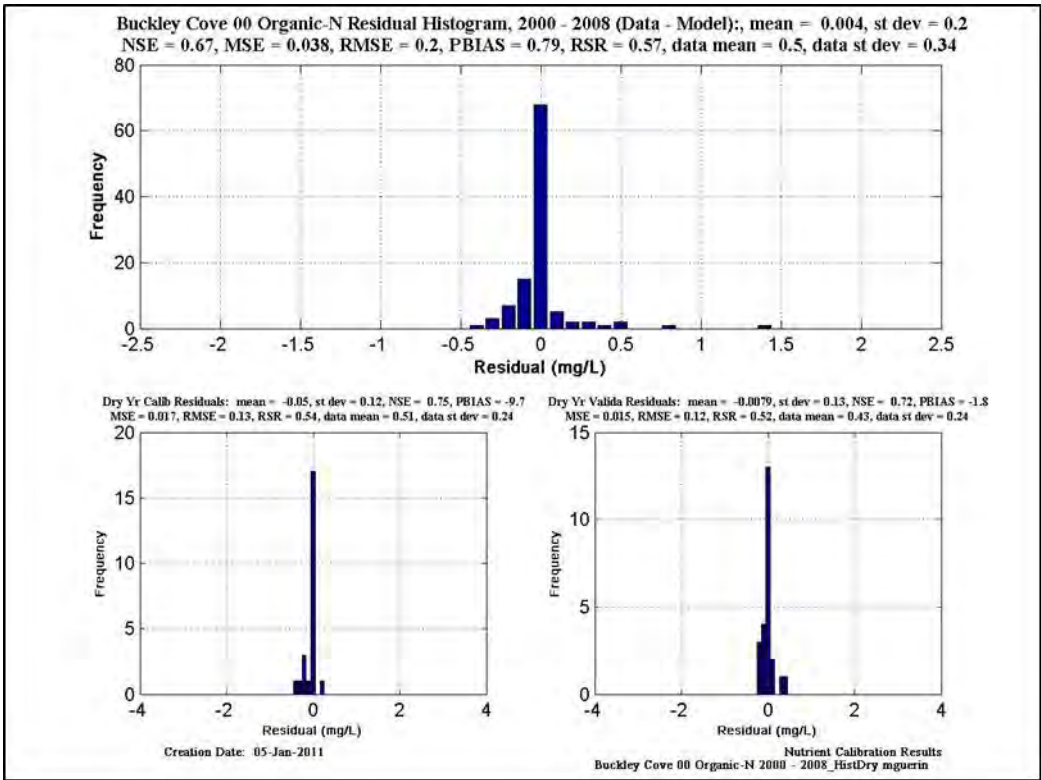
Figure 11-14 Calibration/validation statistics for Algae at Roe Island. Upper figure is calibration & validation statistics for dry years; lower figure is calibration & validation statistics for wet years.
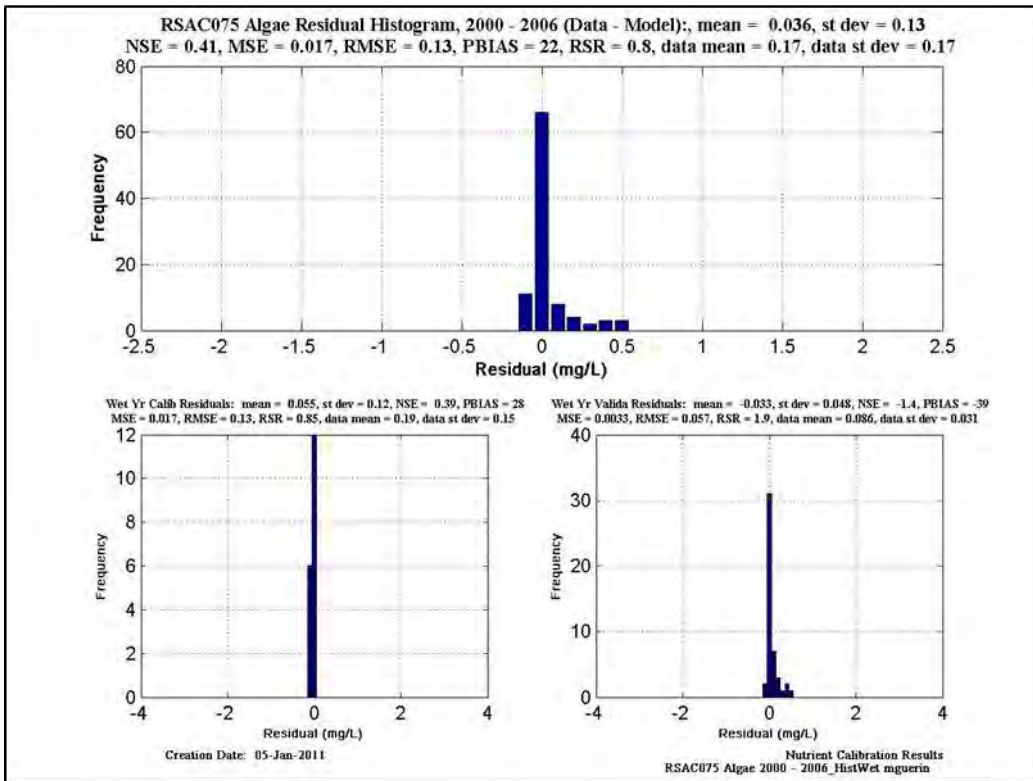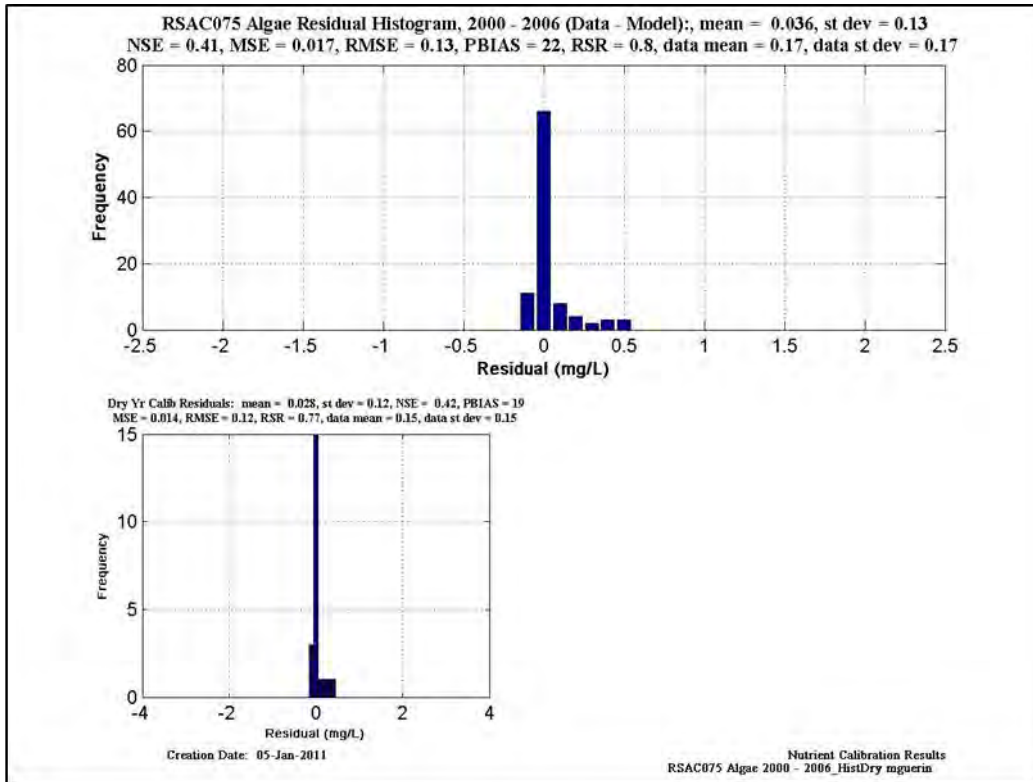
Figure 11-15 Calibration/validation statistics for Algae at RSAC075. Upper figure is calibration & validation statistics for dry years; lower figure is calibration & validation statistics for wet years.
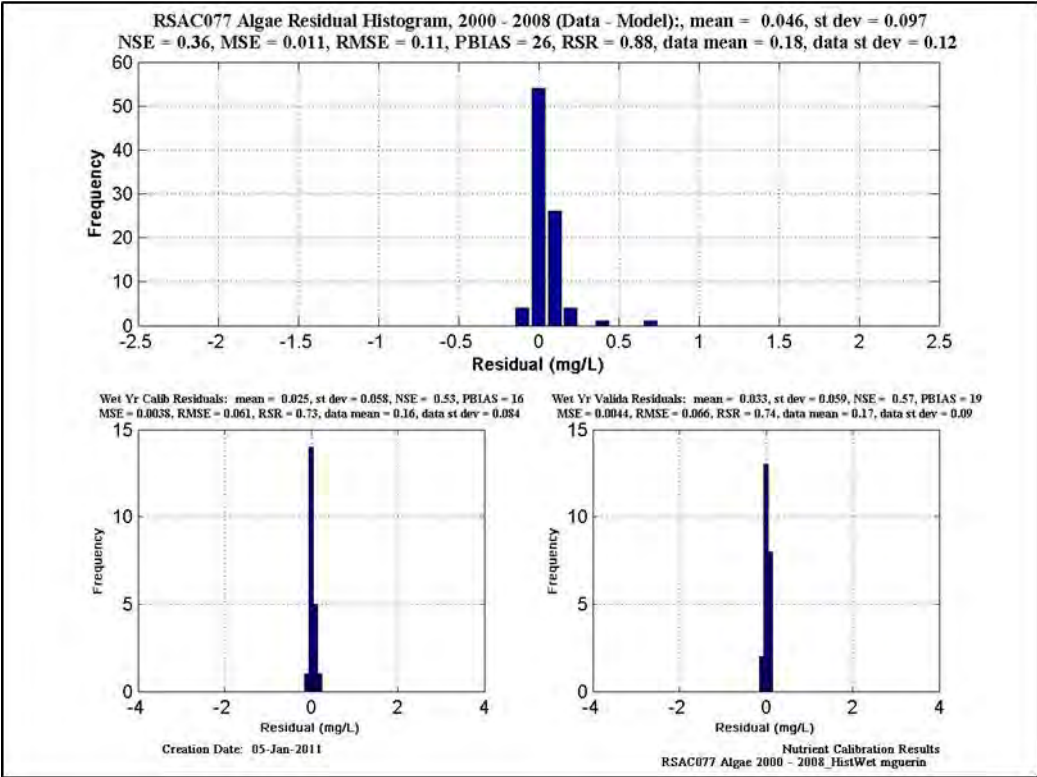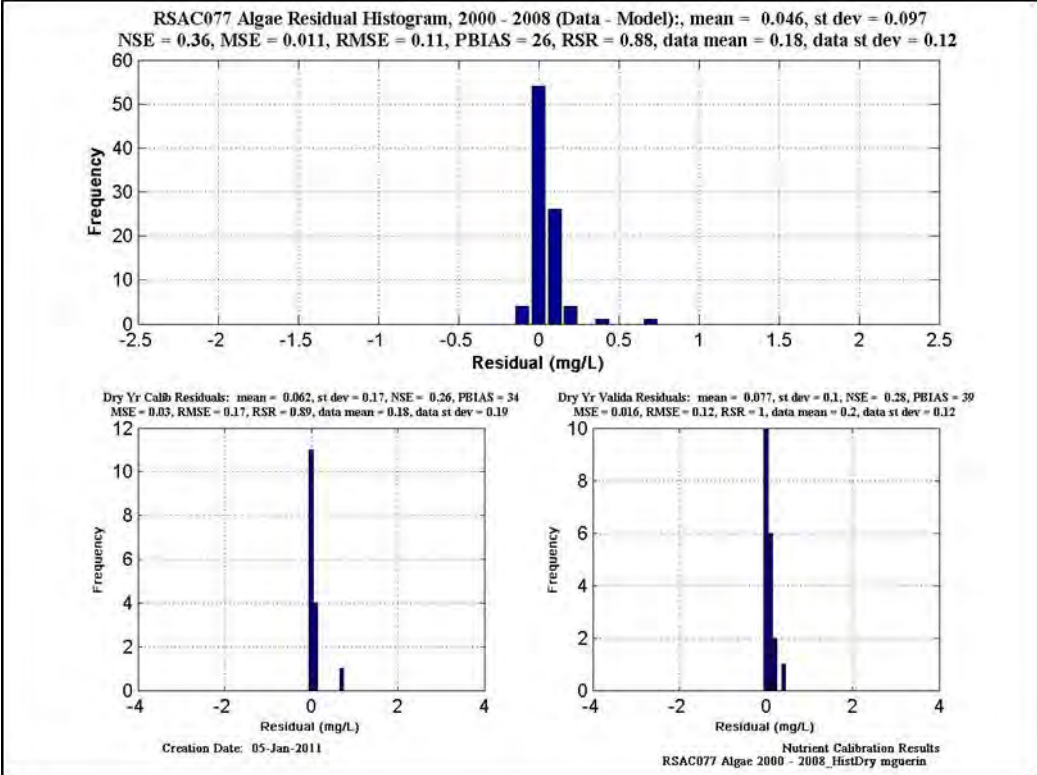
Figure 11-16 Calibration/validation statistics for Algae at RSAC077. Upper figure is calibration & validation statistics for dry years; lower figure is calibration & validation statistics for wet years.
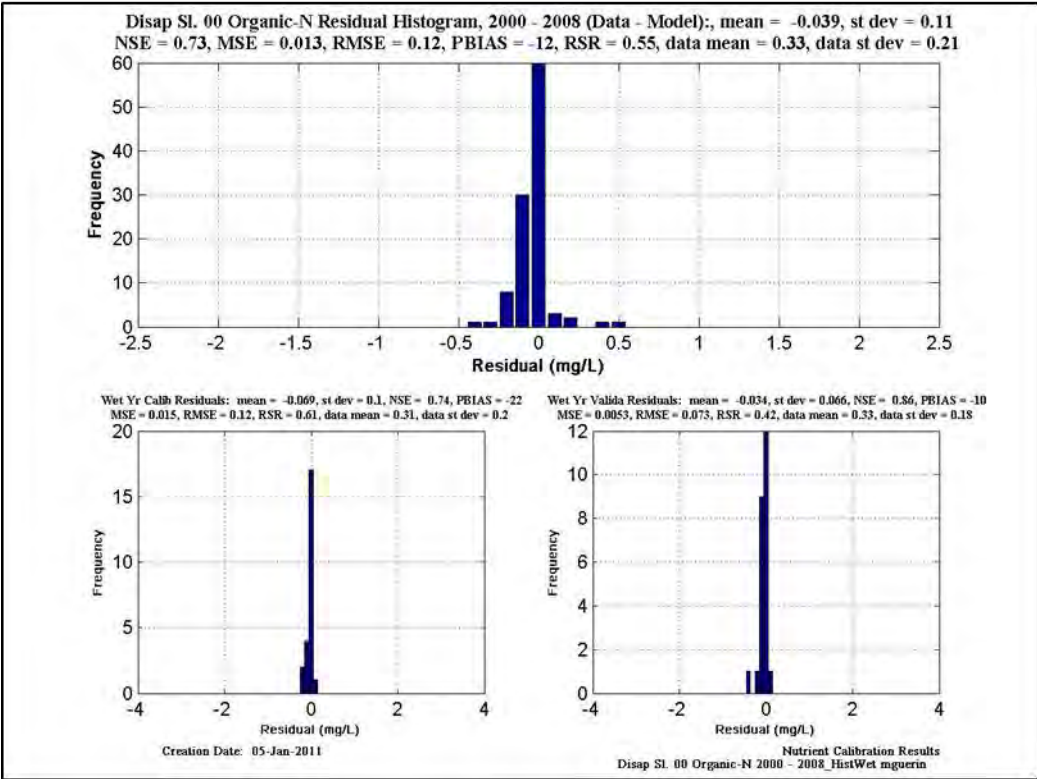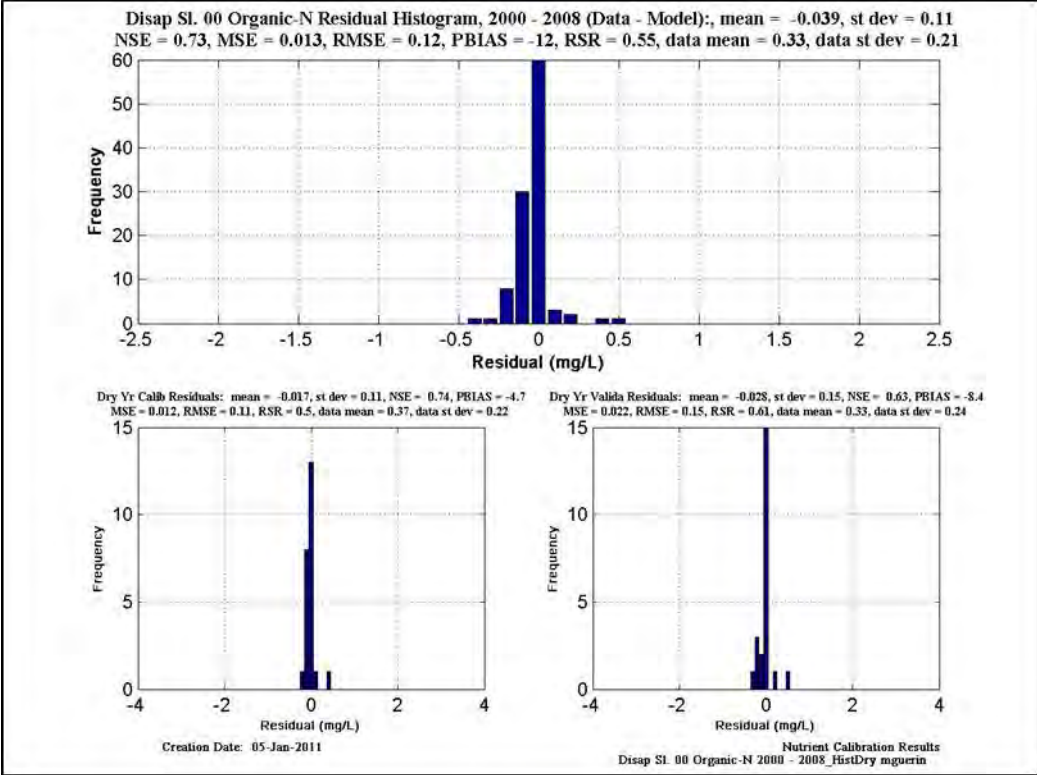
311
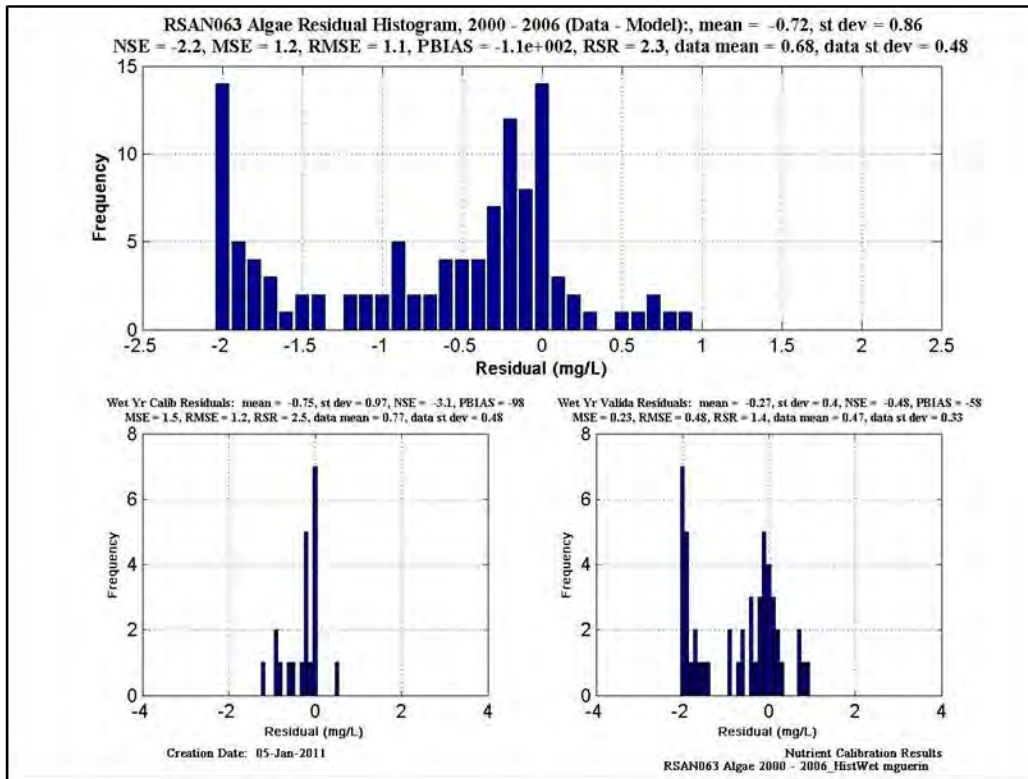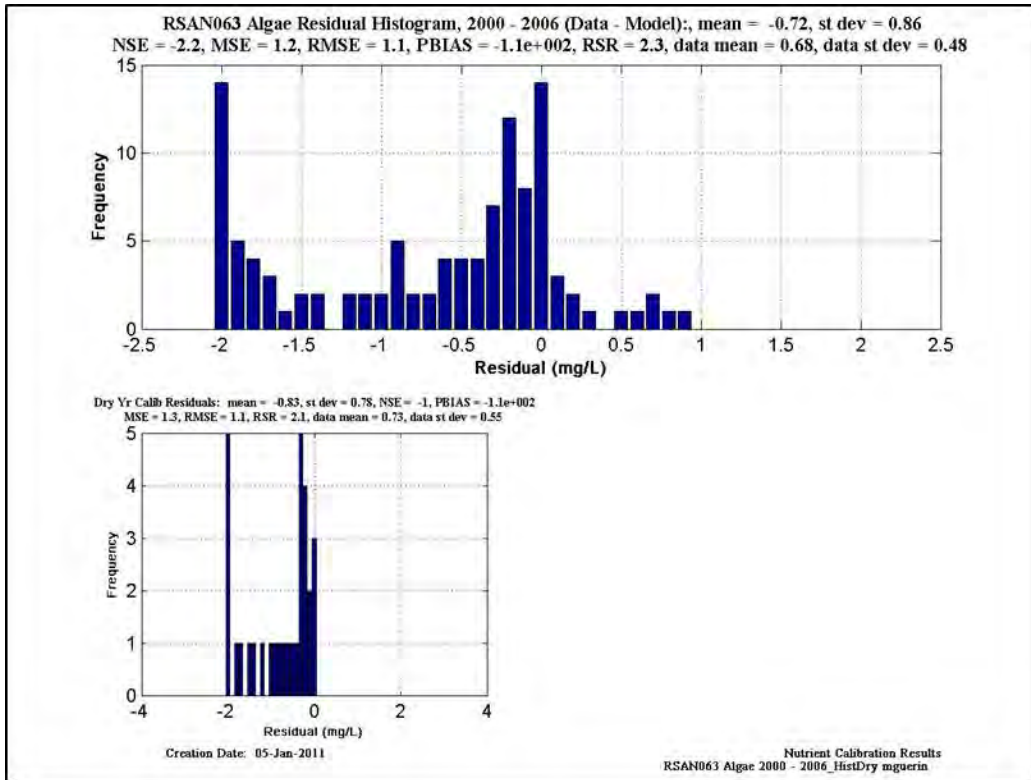
Figure 11-17 Calibration/validation statistics for Algae at RSAN063. Upper figure is calibration & validation statistics for dry years; lower figure is calibration & validation statistics for wet years.
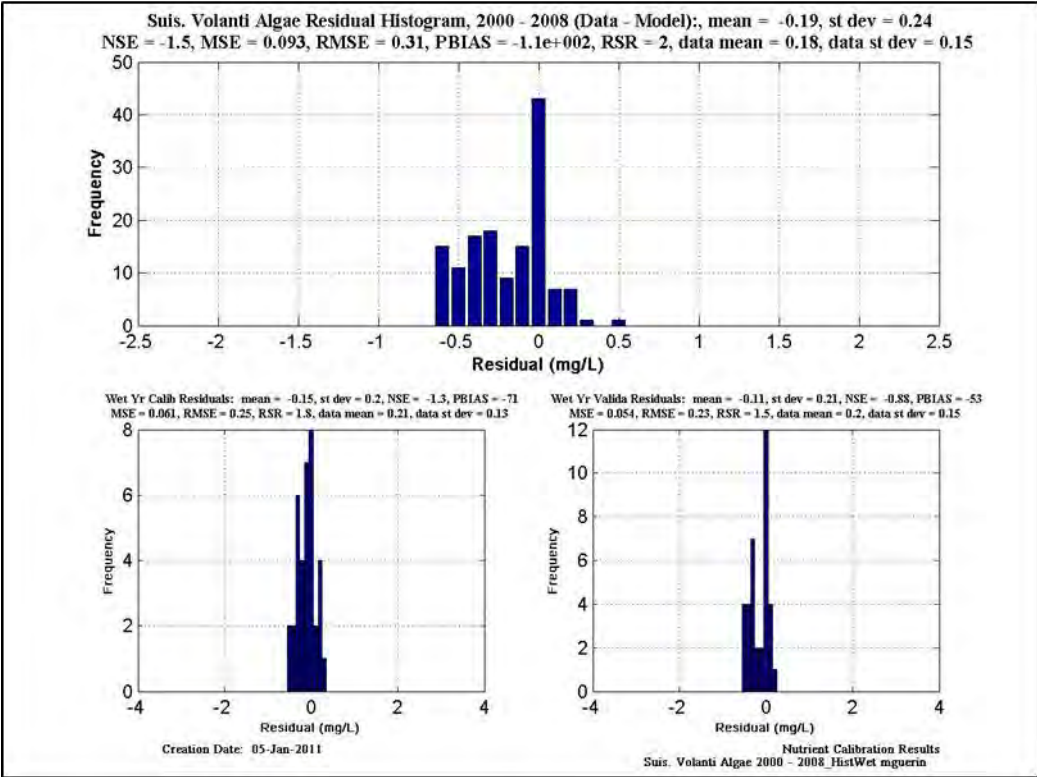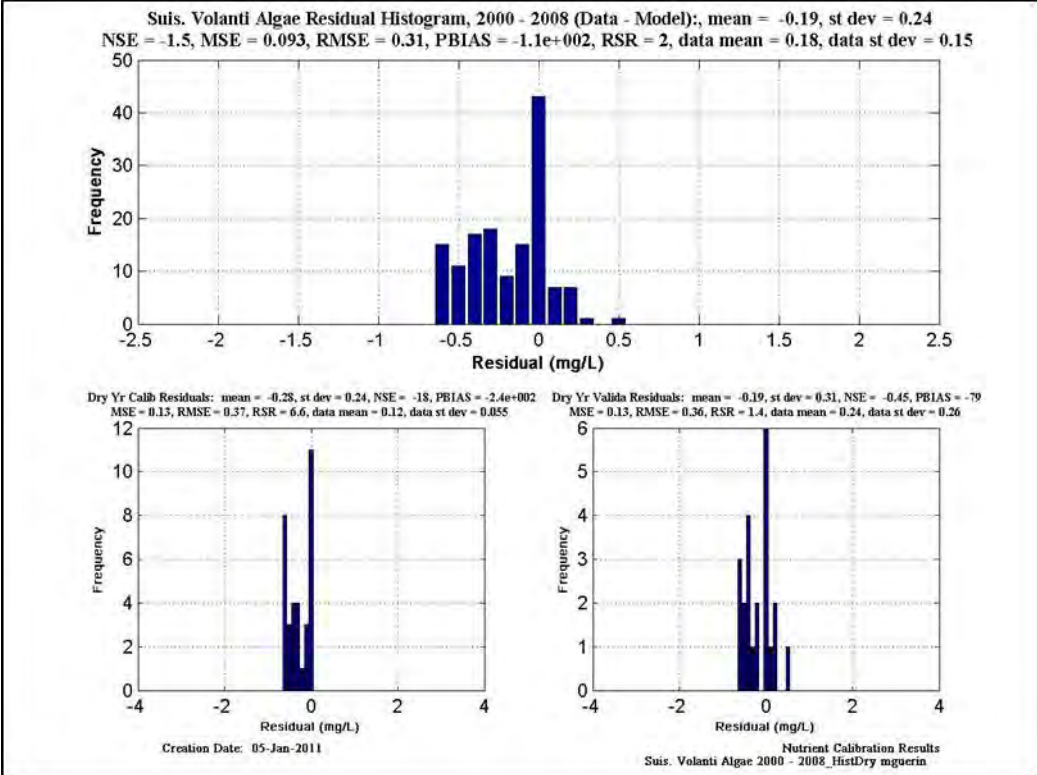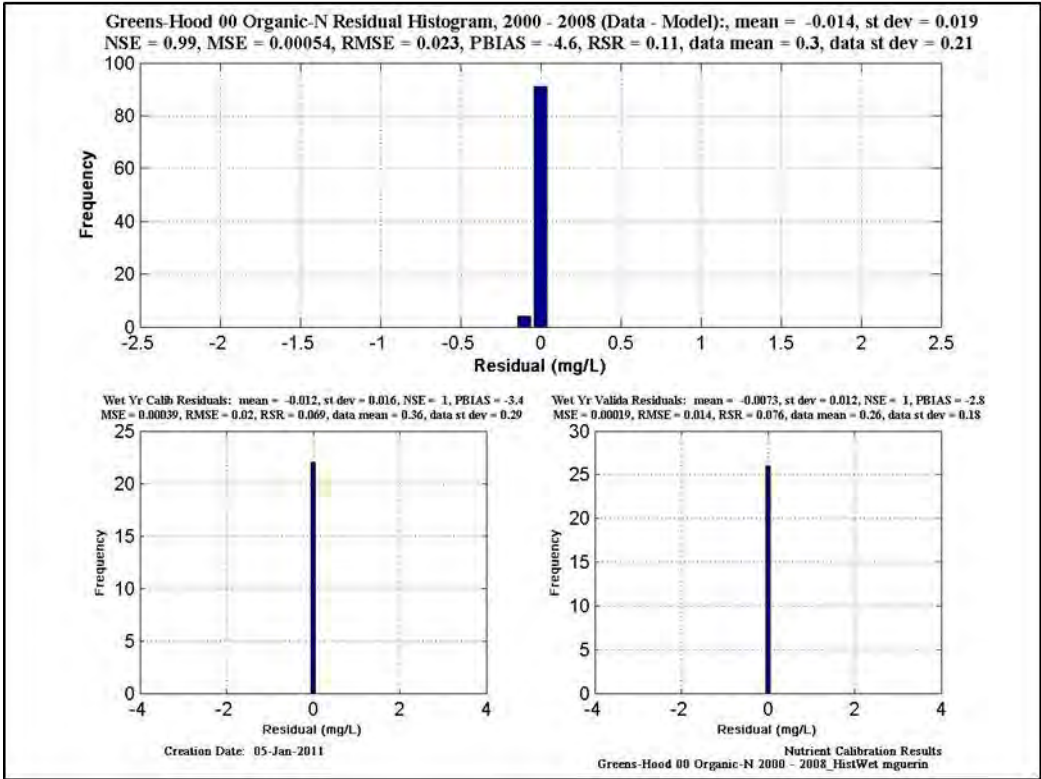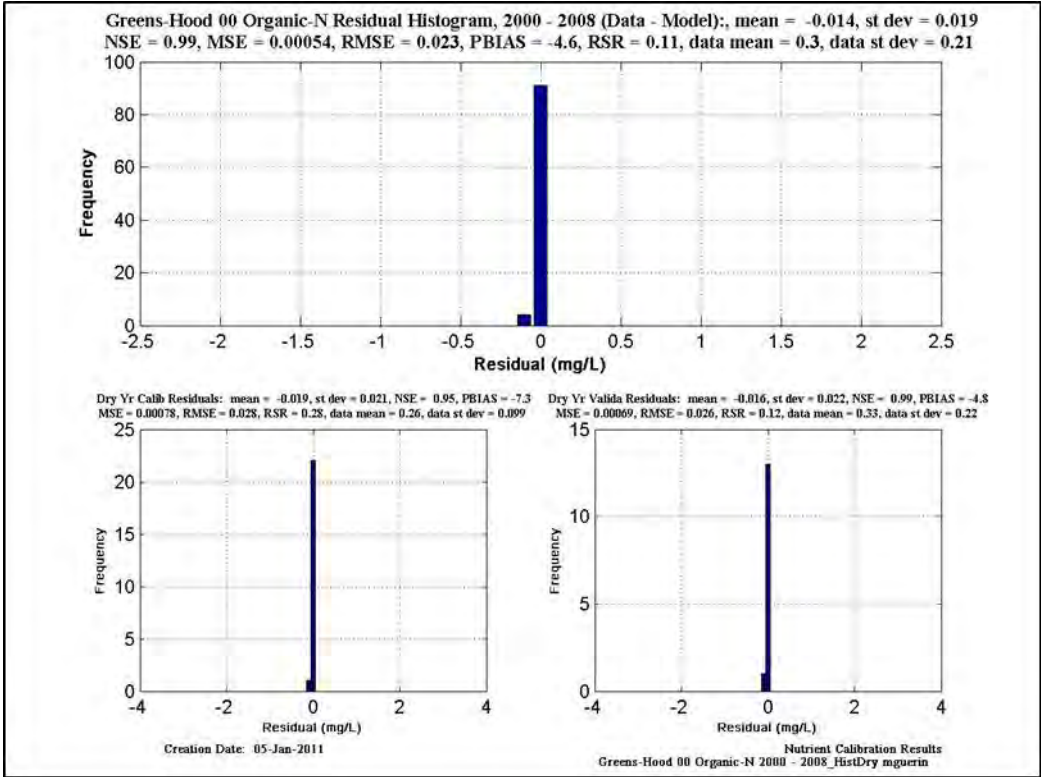
Figure 11-18 Calibration/validation statistics for Algae at Suisun Volanti. Upper figure is calibration & validation statistics for dry years; lower figure is calibration & validation statistics for wet years.
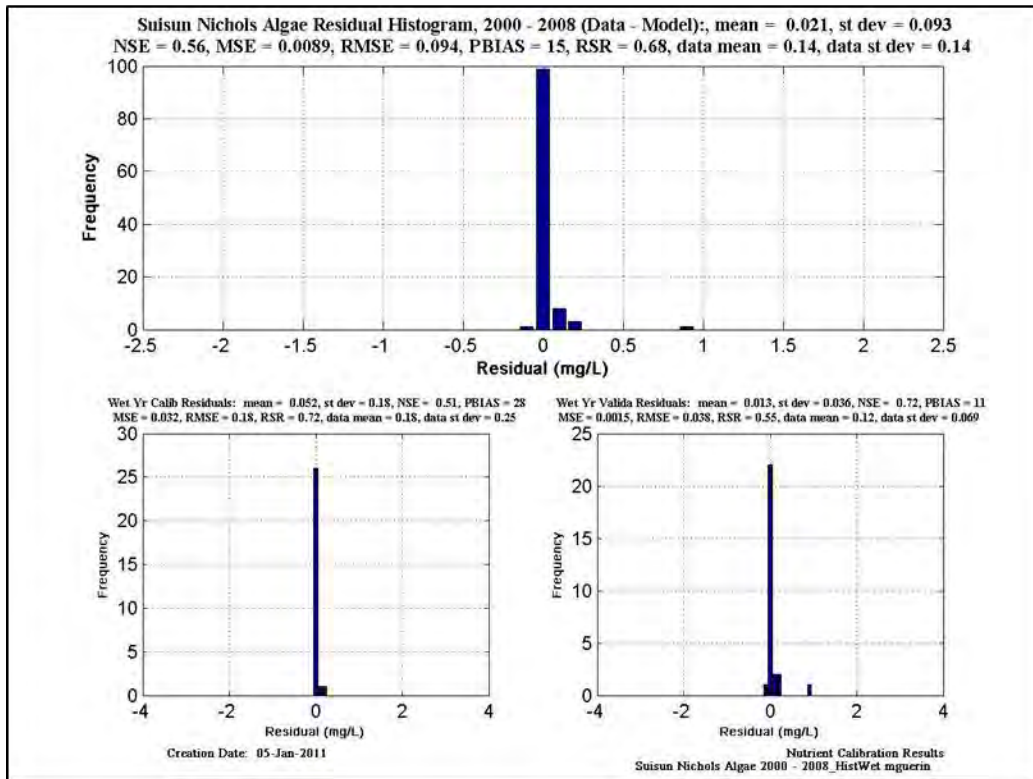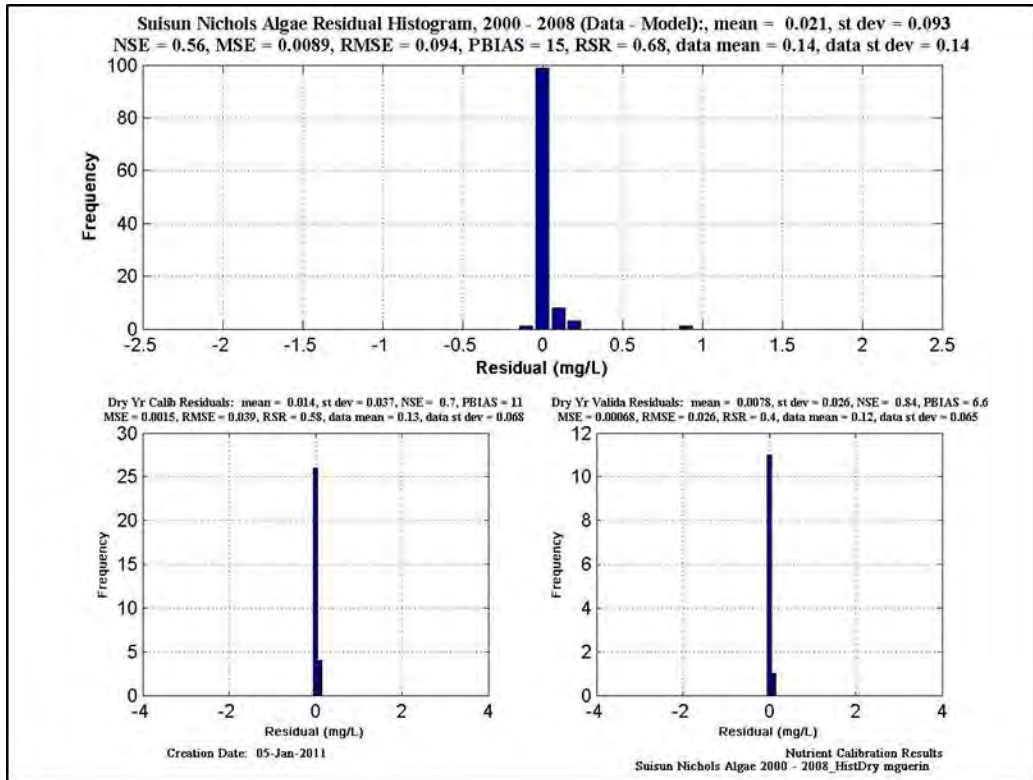
Figure 11-19 Calibration/validation statistics for Algae at Antioch. Upper figure is calibration & validation statistics for dry years; lower figure is calibration & validation statistics for wet years.
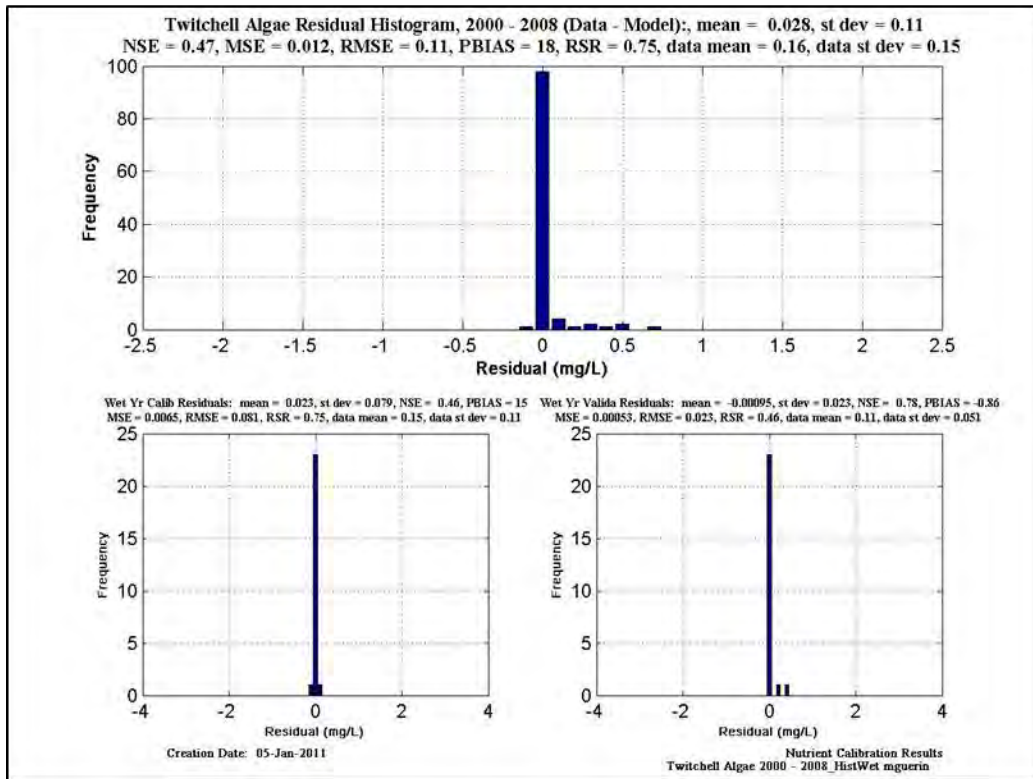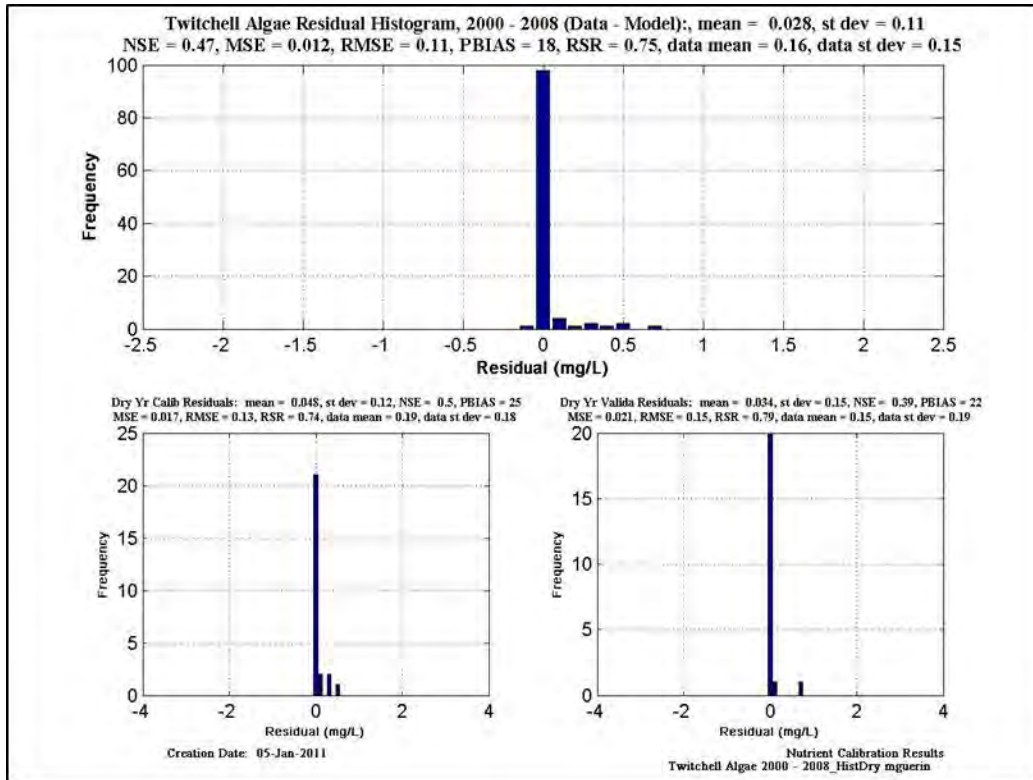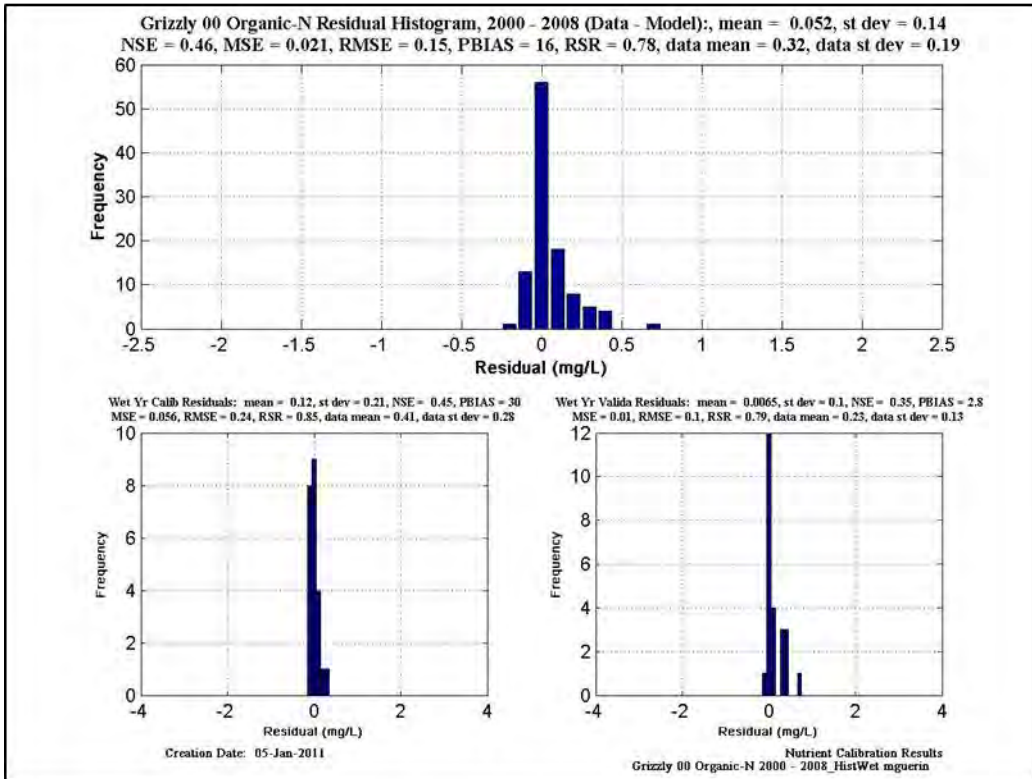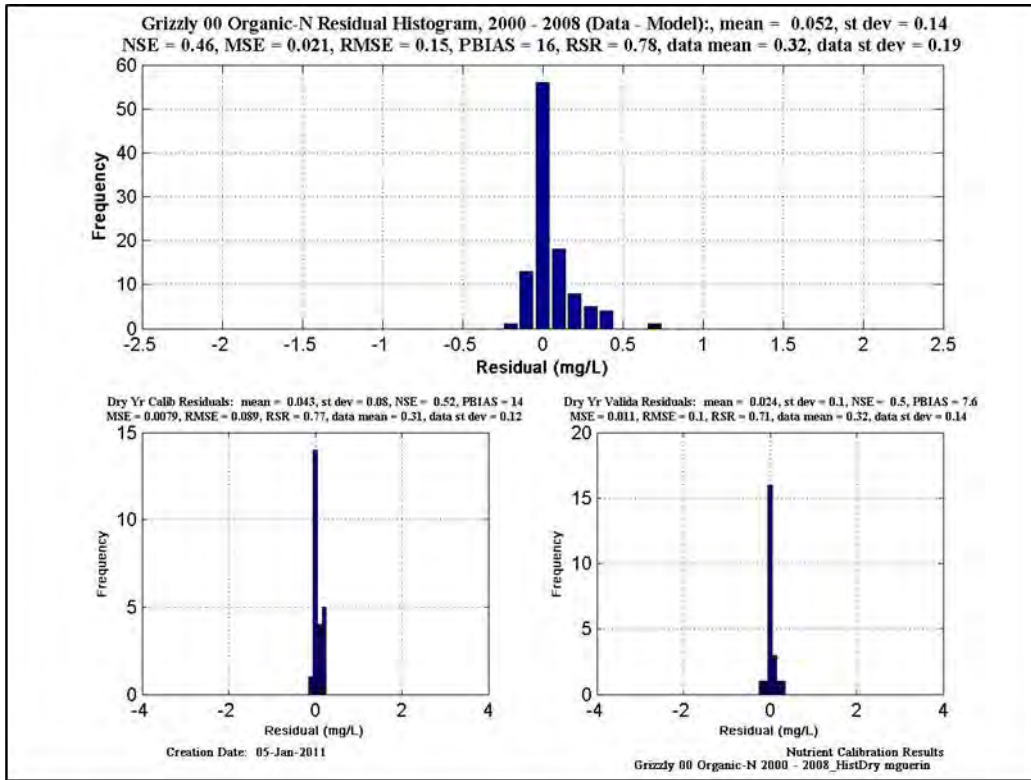
Figure 11-20 Calibration/validation statistics for Algae at Twitchell. Upper figure is calibration & validation statistics for dry years; lower figure is calibration & validation statistics for wet years.
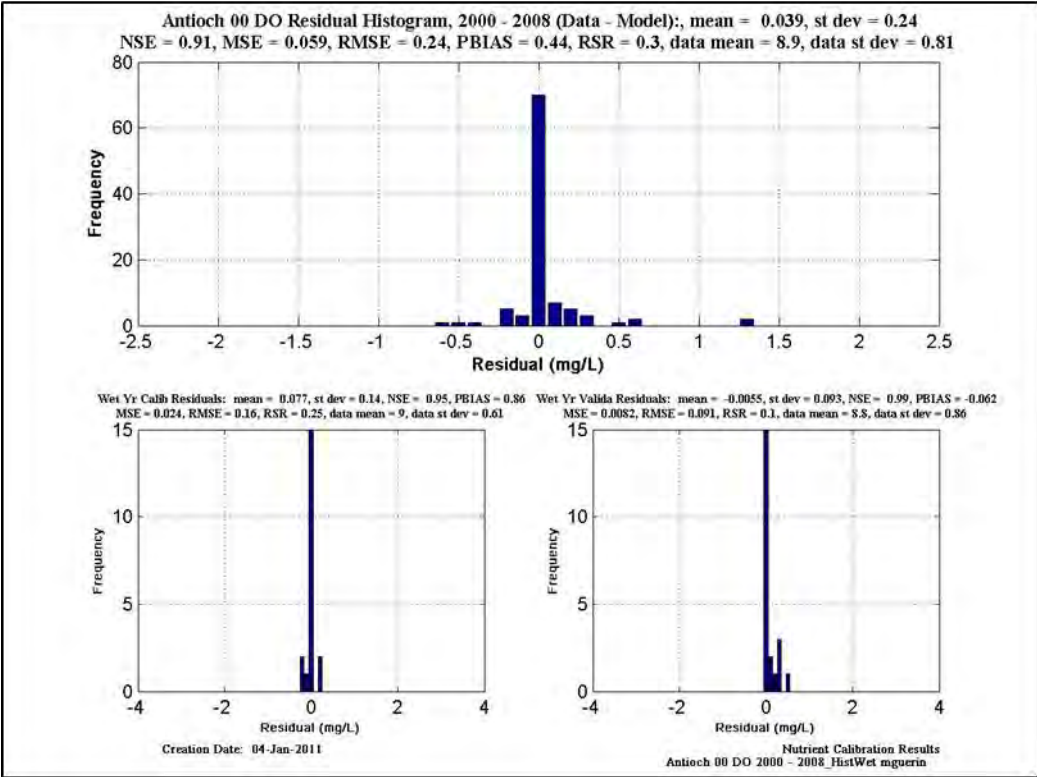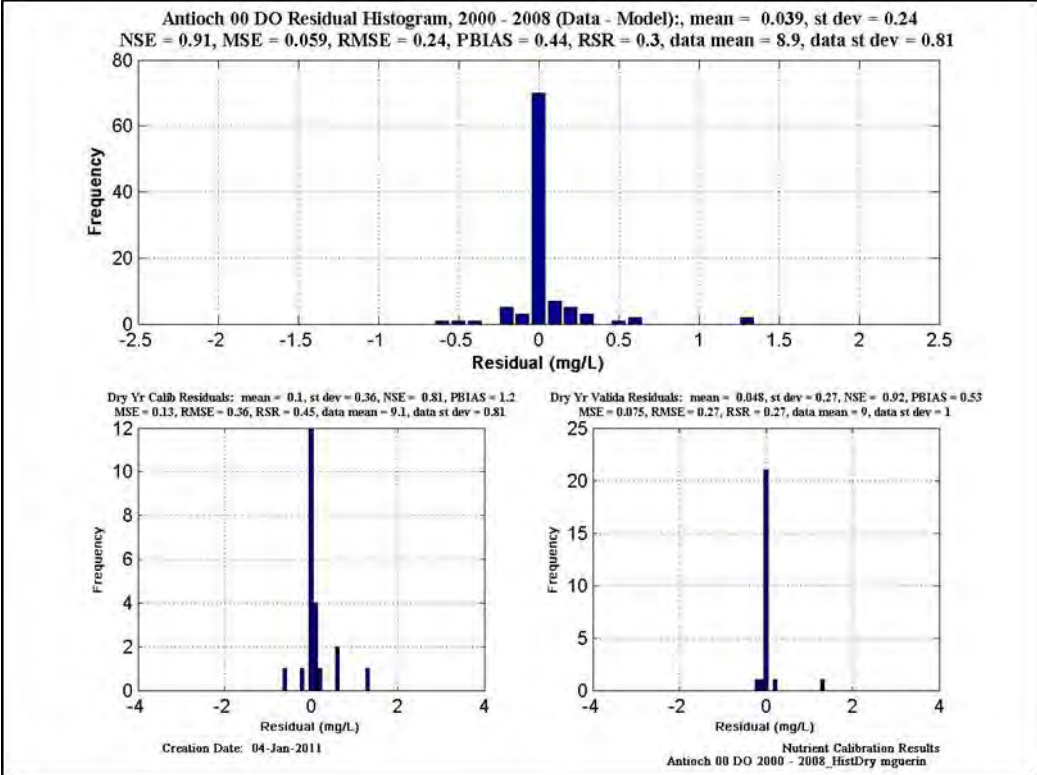
Figure 11-21 Calibration/validation statistics for DO at Antioch. Upper figure is calibration & validation statistics for dry years; lower figure is calibration & validation statistics for wet years.
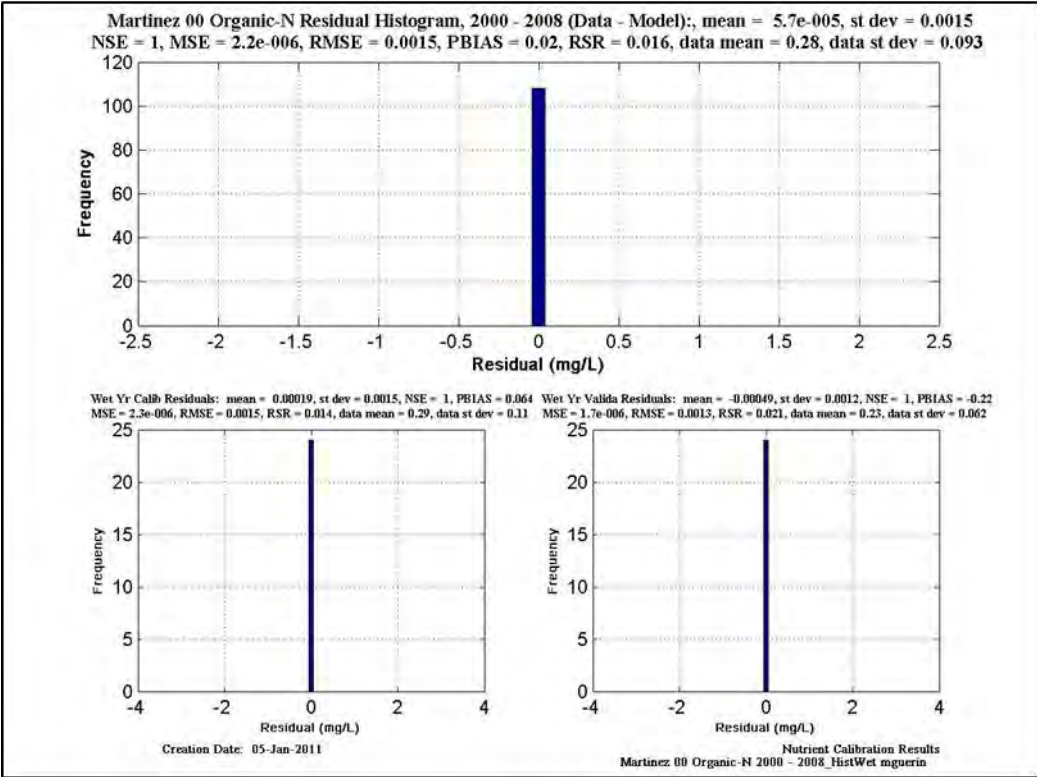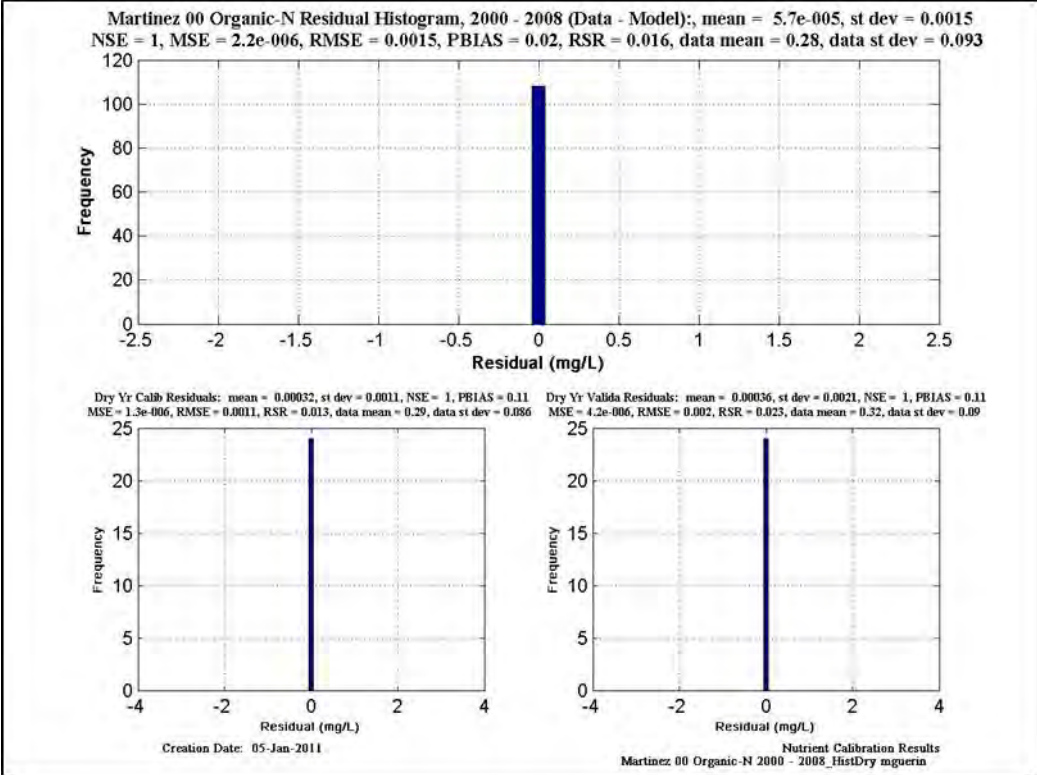
316
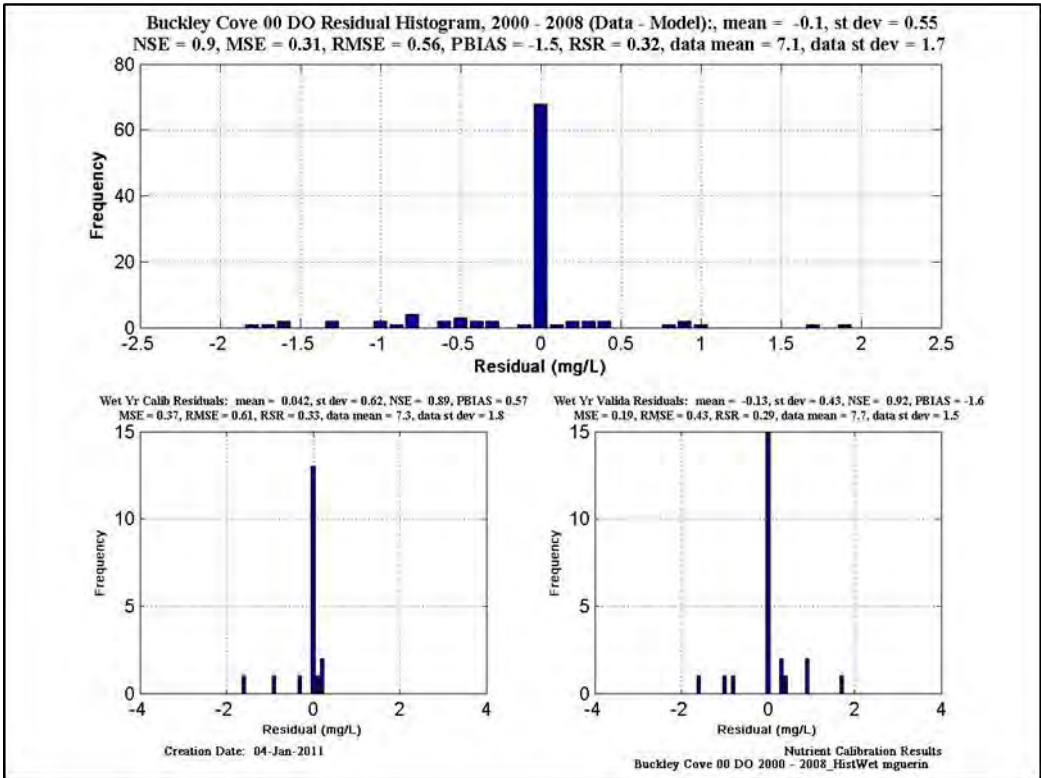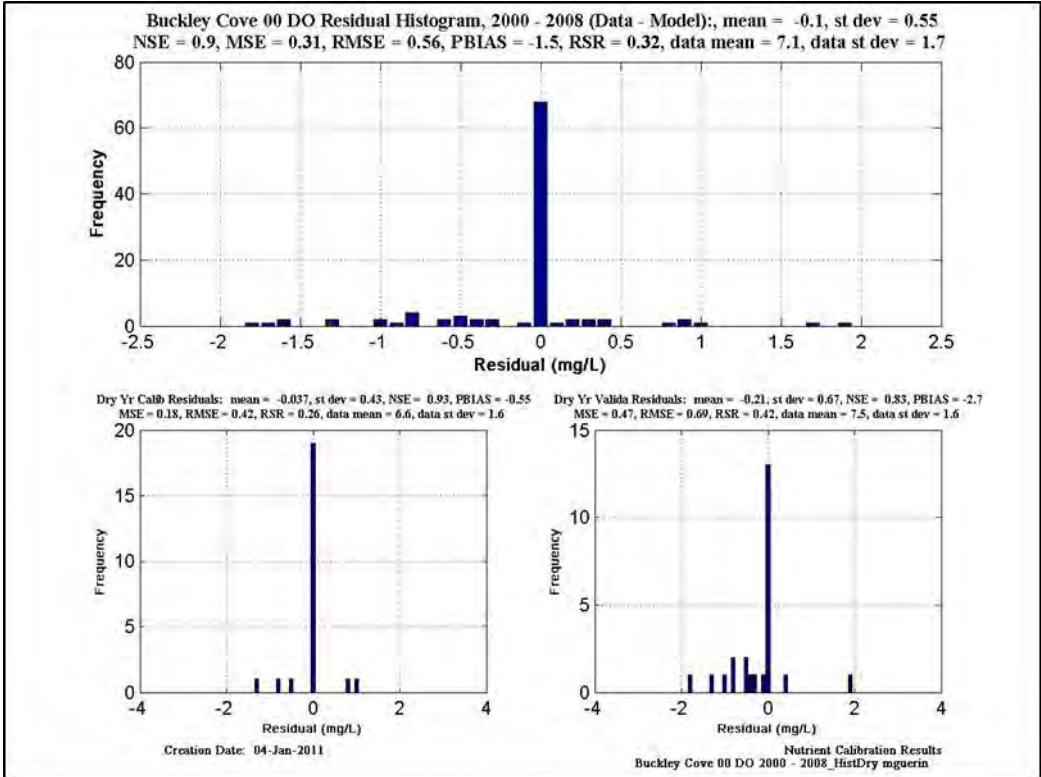
Figure 11-22 Calibration/validation statistics for DO at Buckley Cove. Upper figure is calibration & validation statistics for dry years; lower figure is calibration & validation statistics for wet years.

317
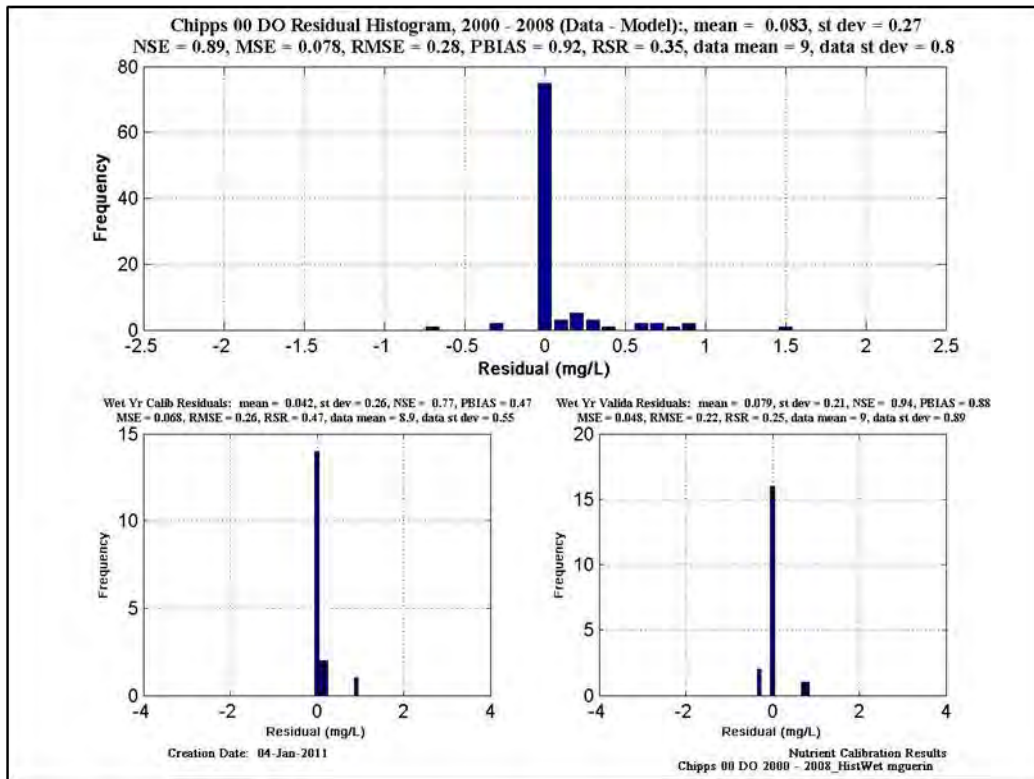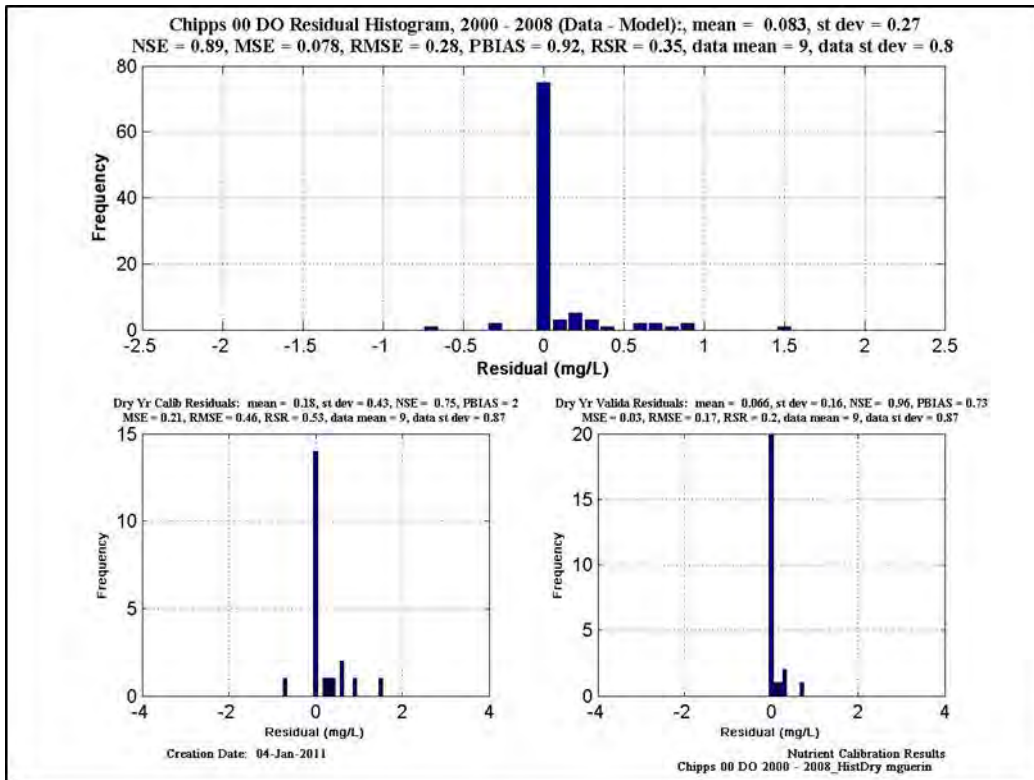
Figure 11-23 Calibration/validation statistics for DO at Chipps. Upper figure is calibration & validation statistics for dry years; lower figure is calibration & validation statistics for wet years.
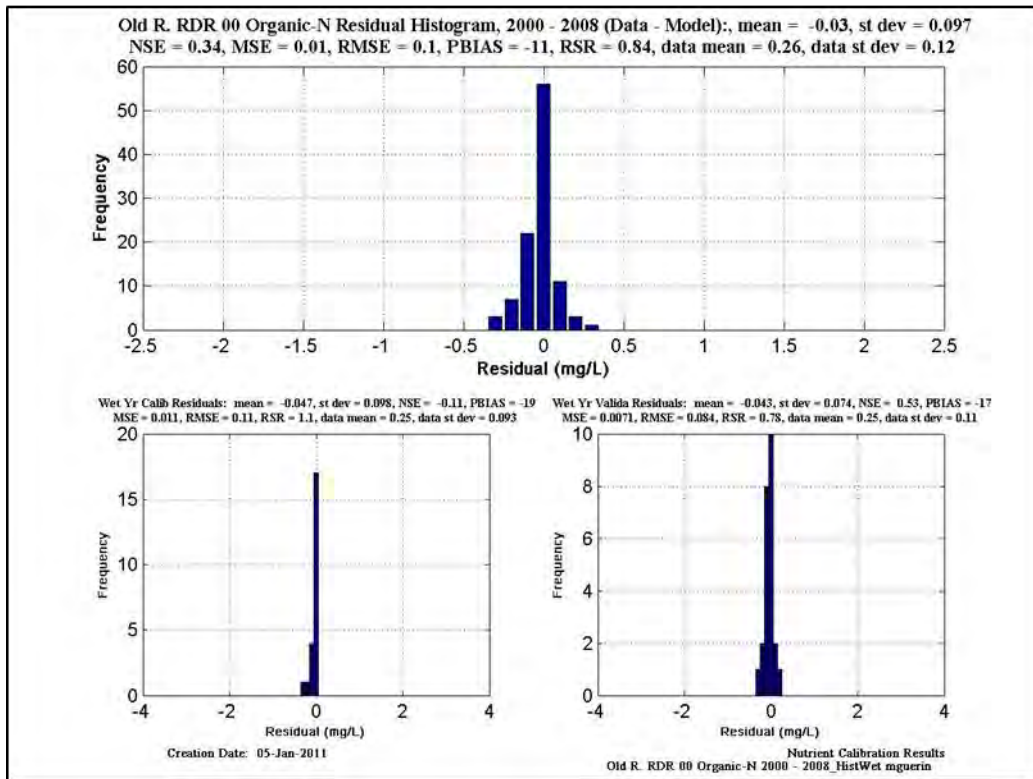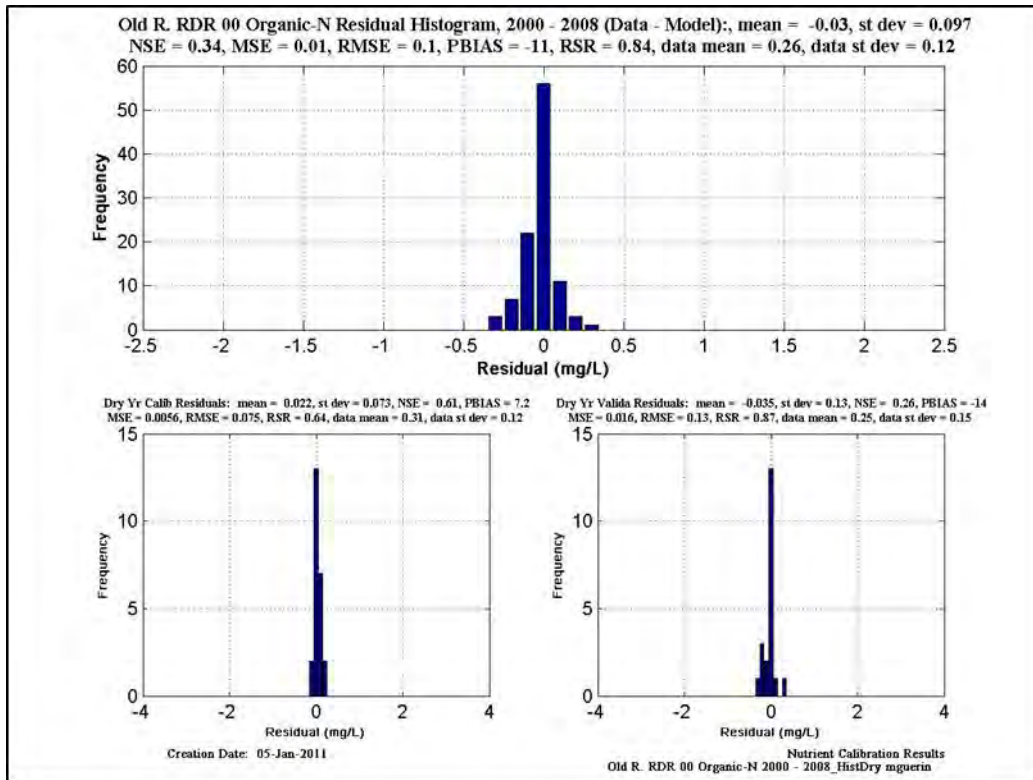
318
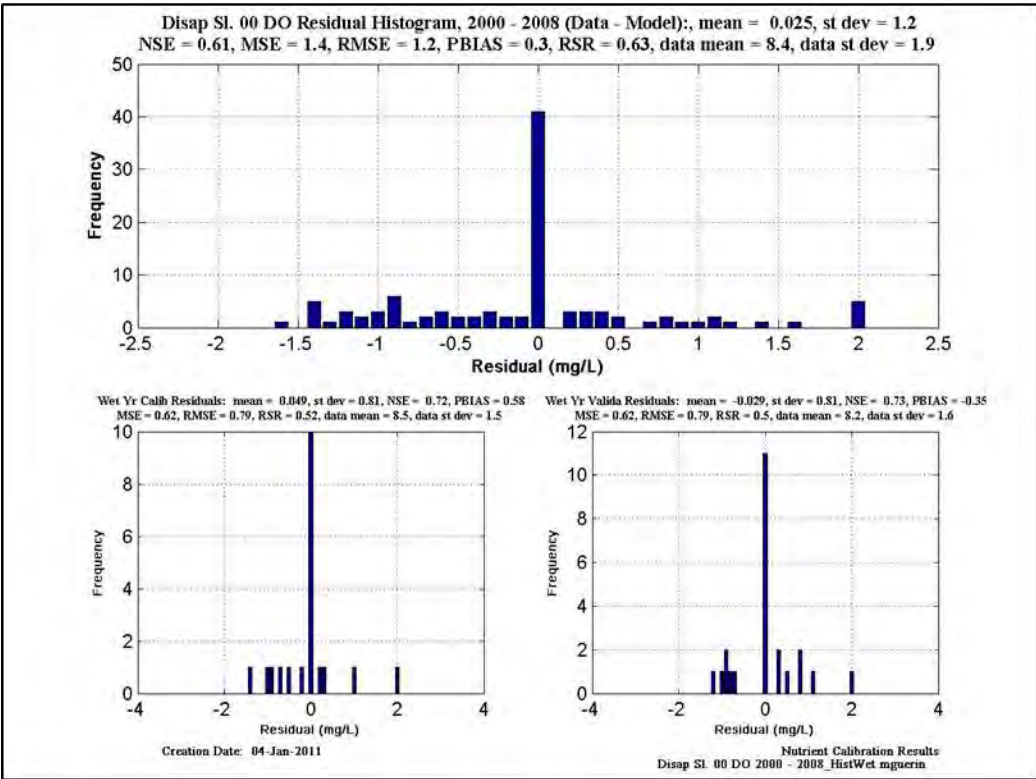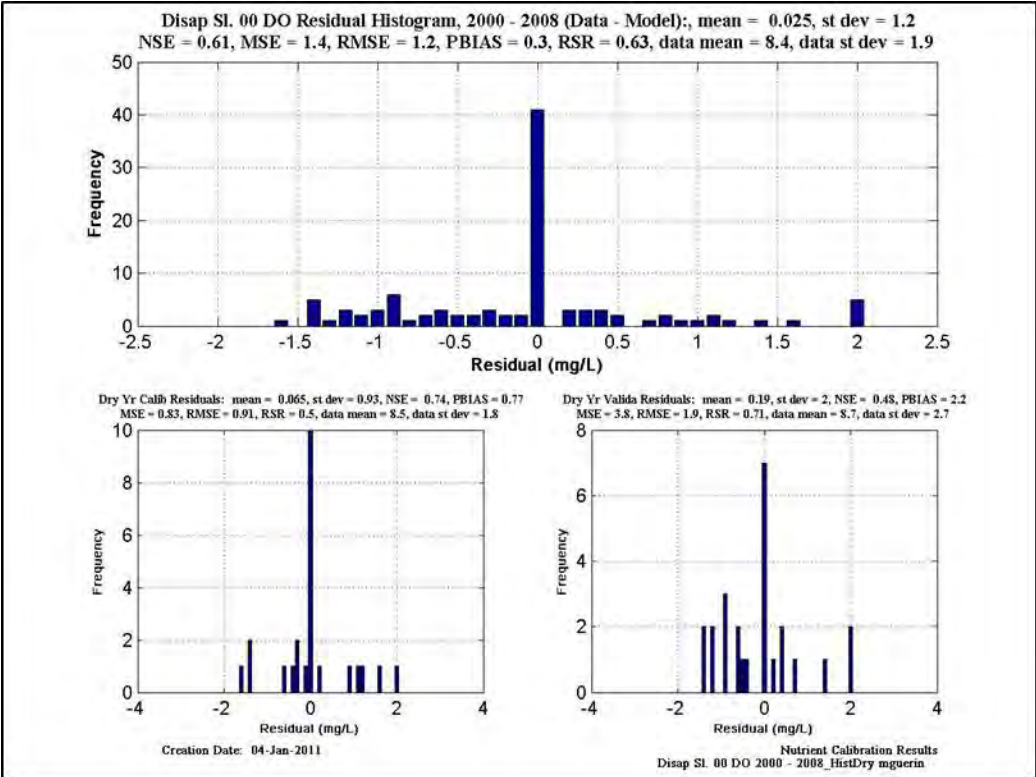
Figure 11-24 Calibration/validation statistics for DO at Disappointment Sl. Upper figure is calibration & validation statistics for dry years; lower figure is calibration & validation statistics for wet years.

319
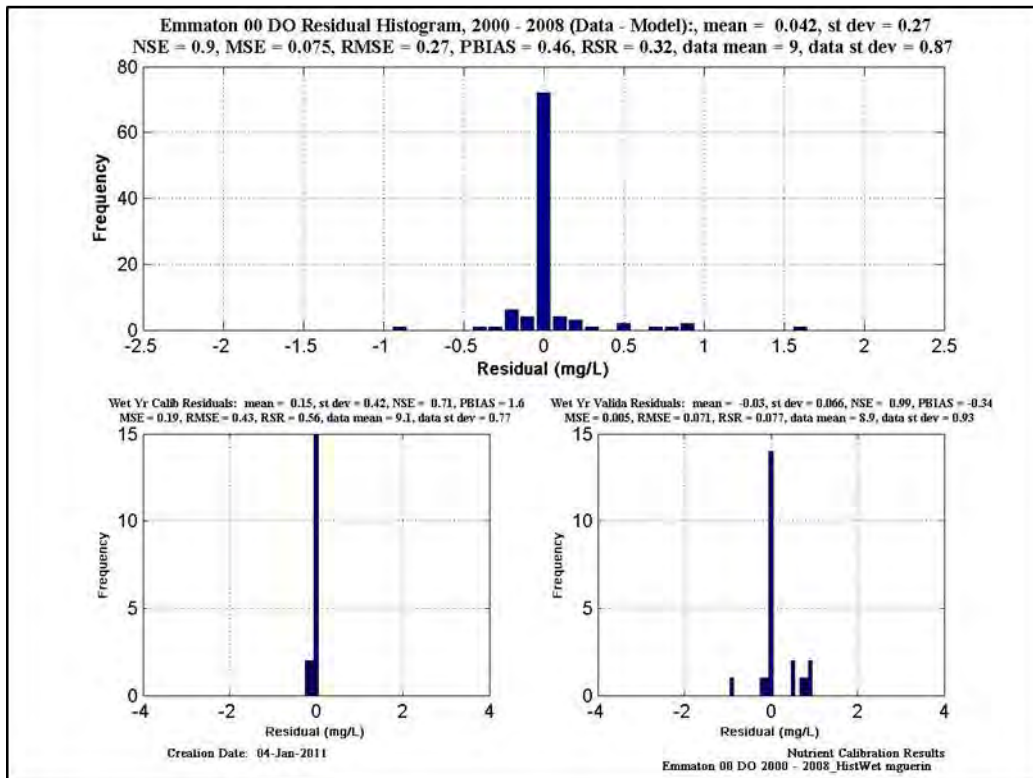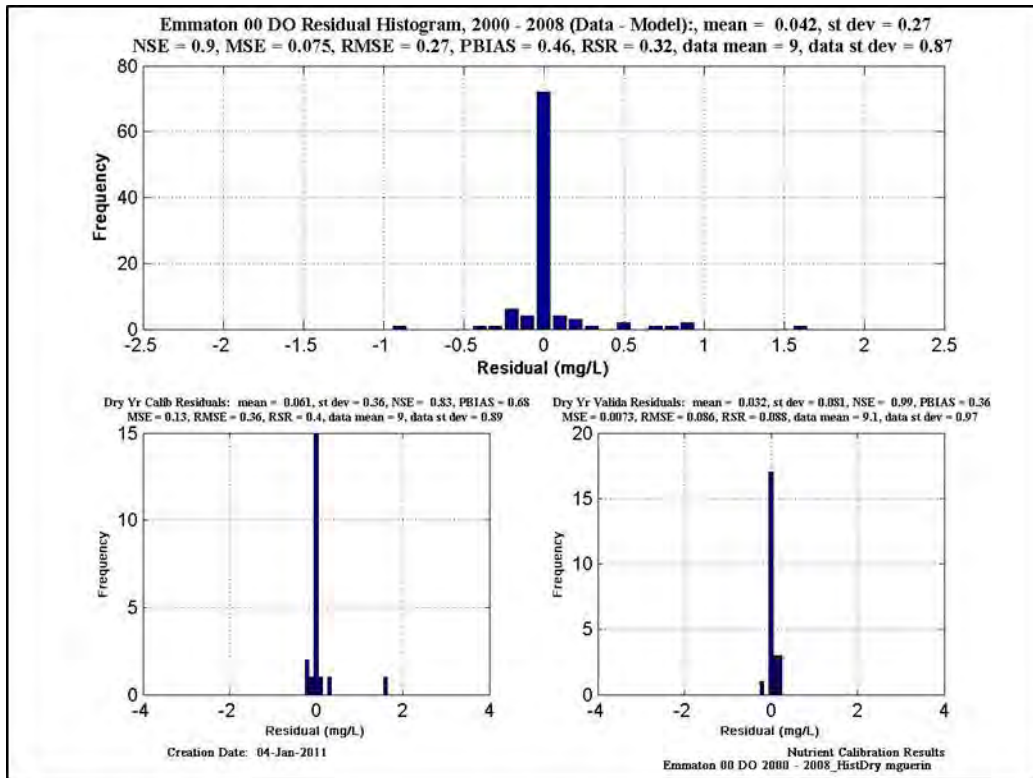
Figure 11-25 Calibration/validation statistics for DO at Emmaton. Upper figure is calibration & validation statistics for dry years; lower figure is calibration & validation statistics for wet years.
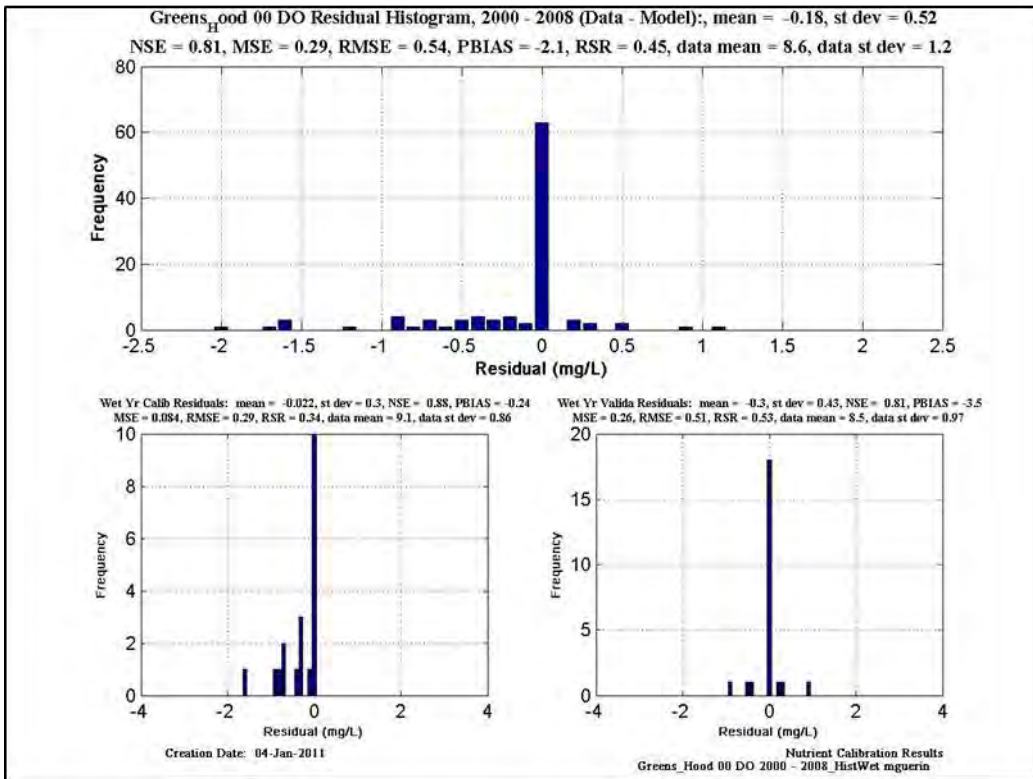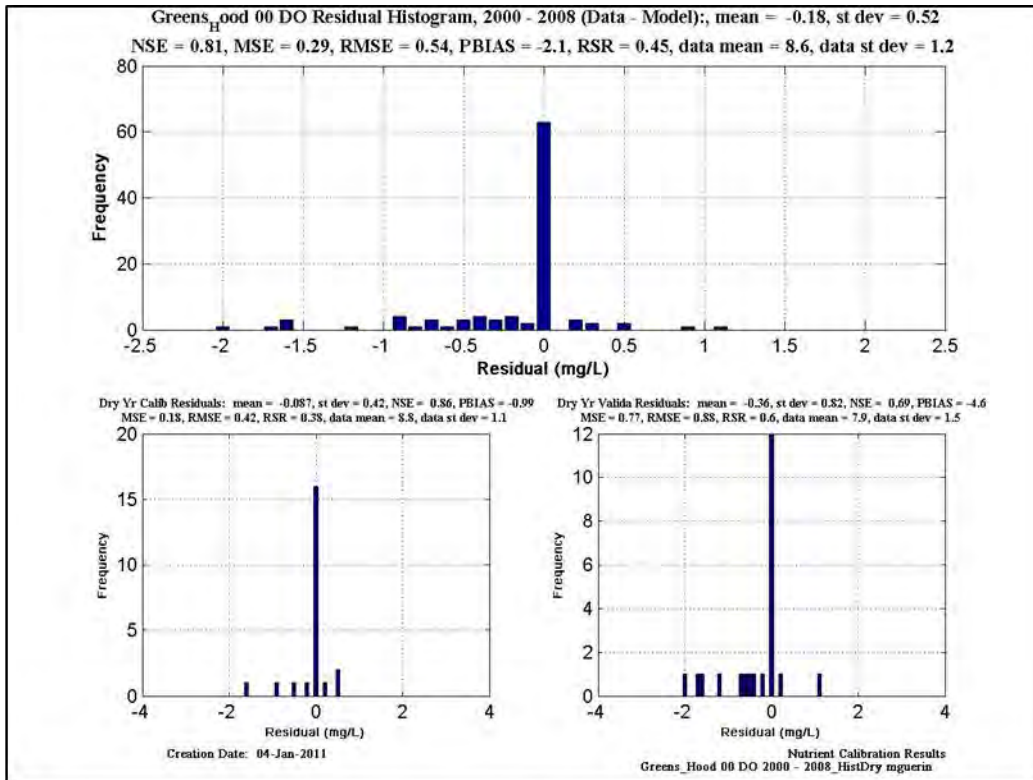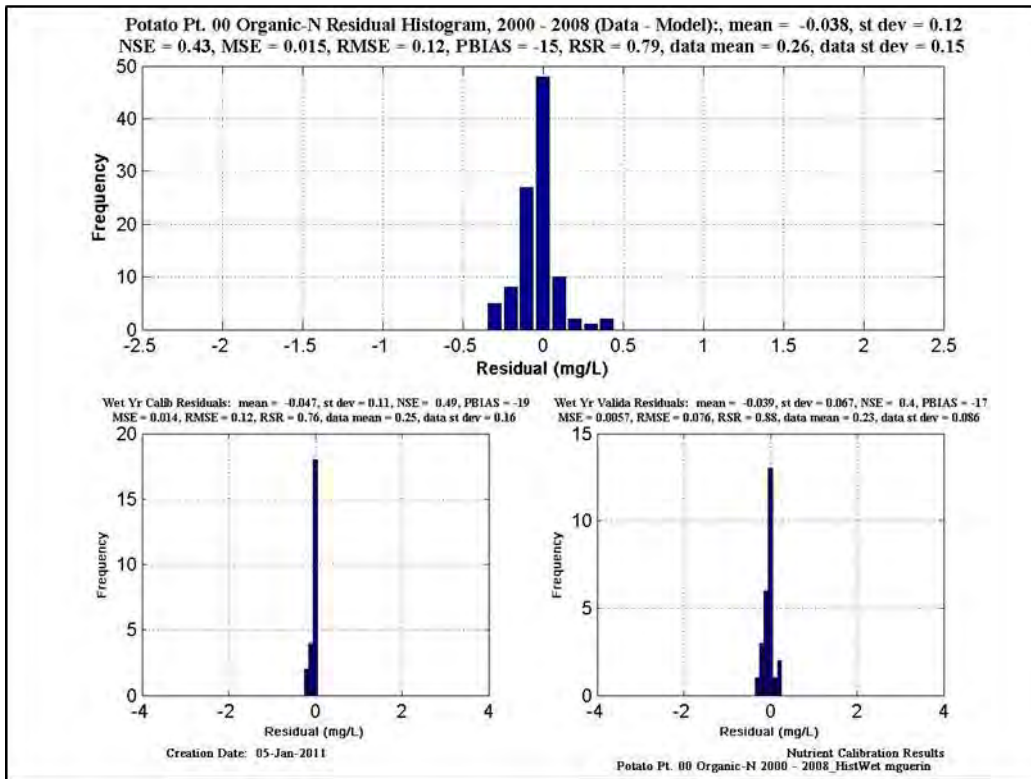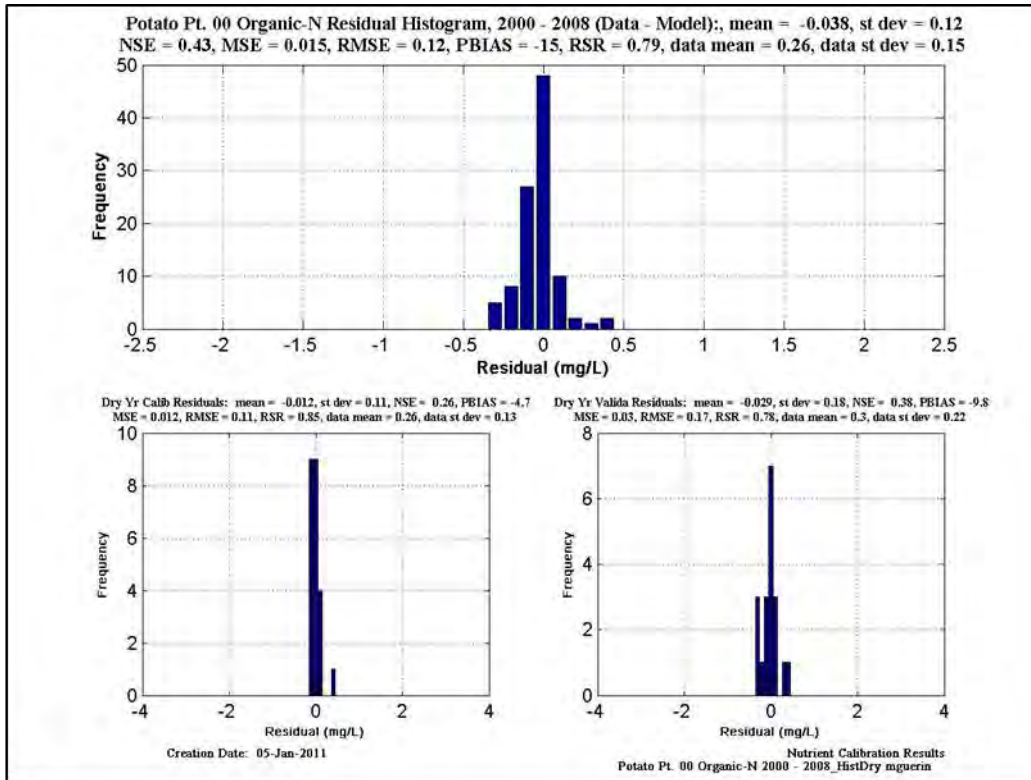
Figure 11-26 Calibration/validation statistics for DO at Greens Hood. Upper figure is calibration & validation statistics for dry years; lower figure is calibration & validation statistics for wet years.
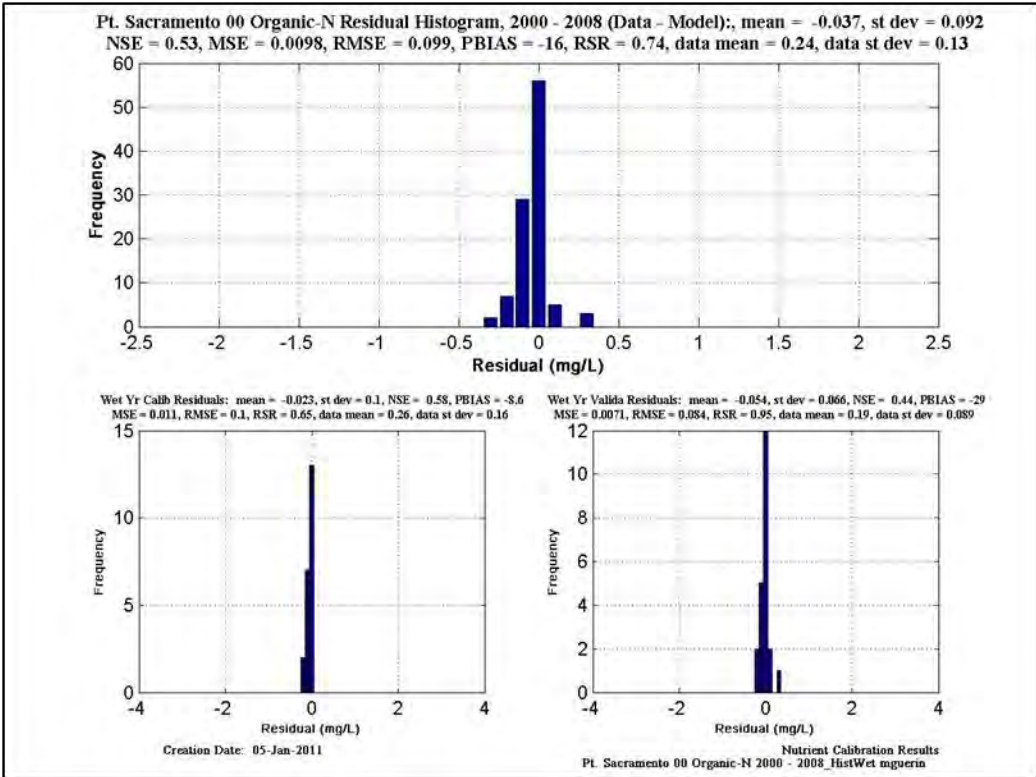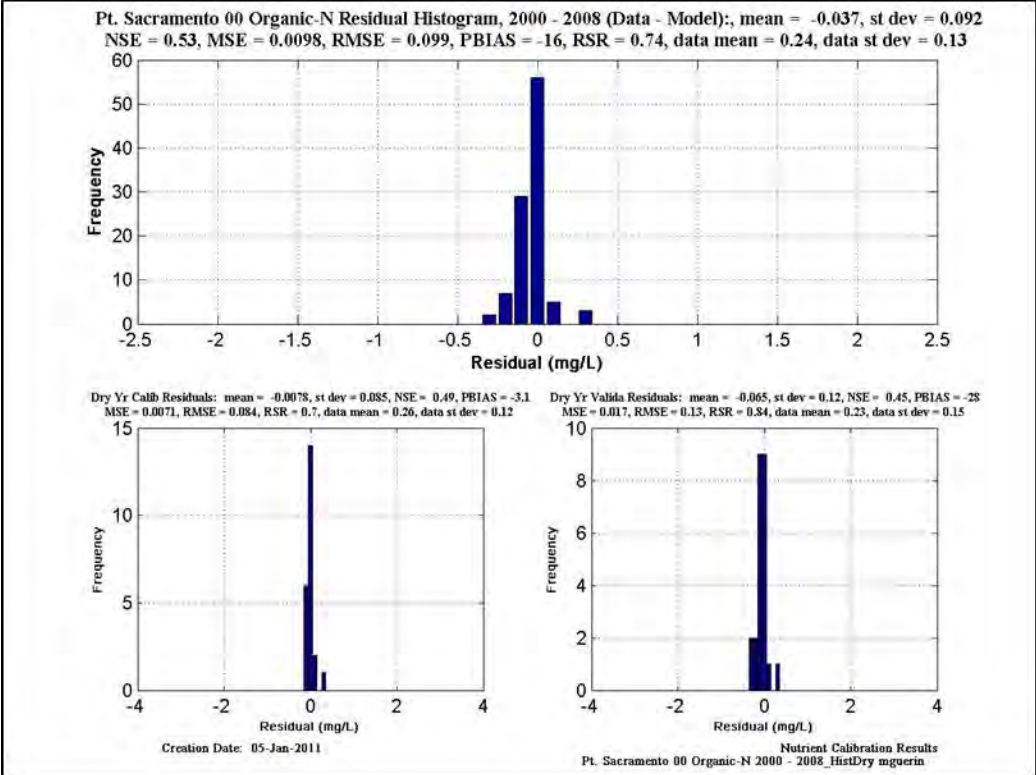
321
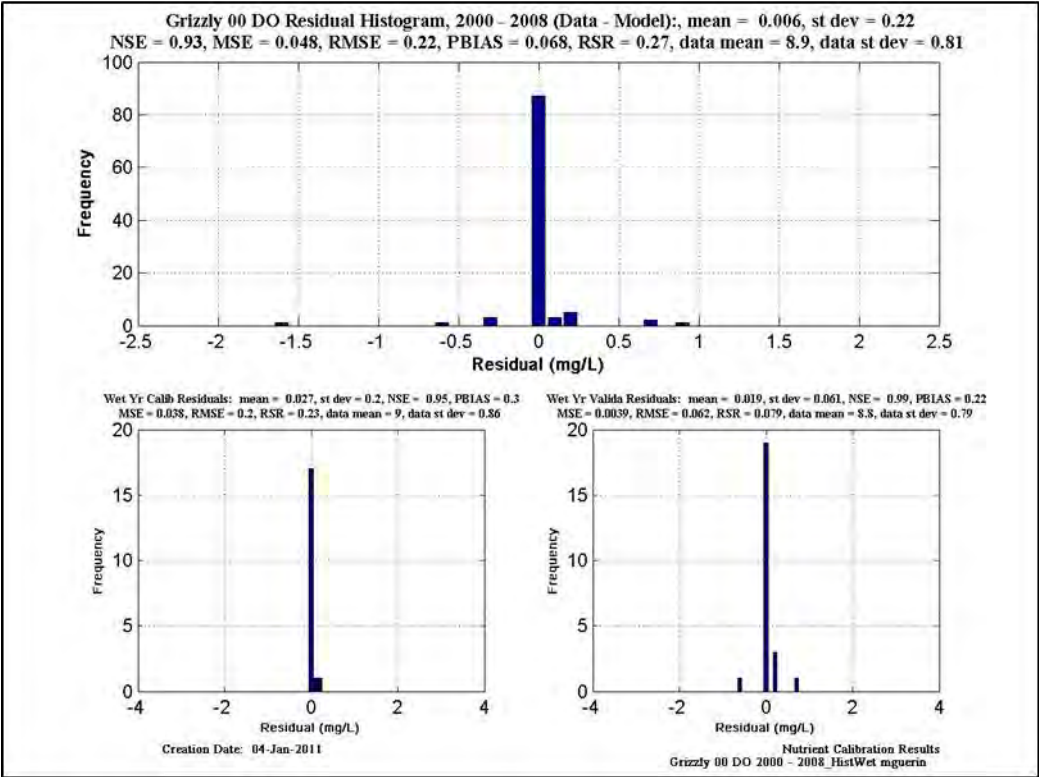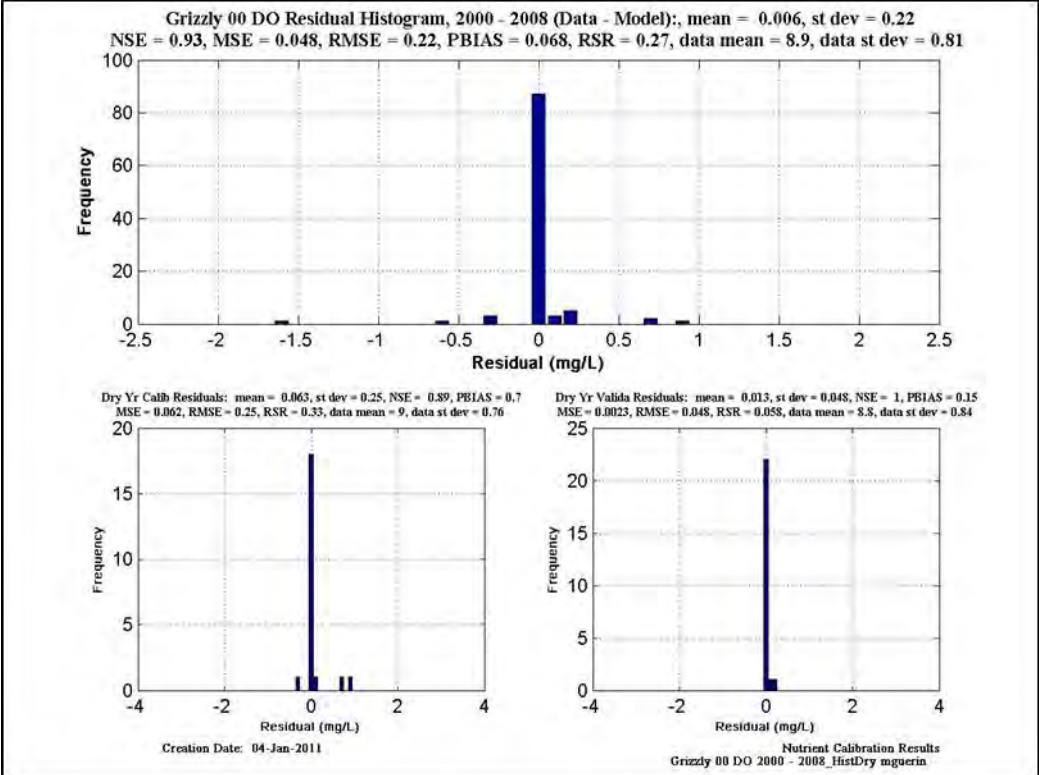
Figure 11-27 Calibration/validation statistics for DO at Grizzly. Upper figure is calibration & validation statistics for dry years; lower figure is calibration & validation statistics for wet years.
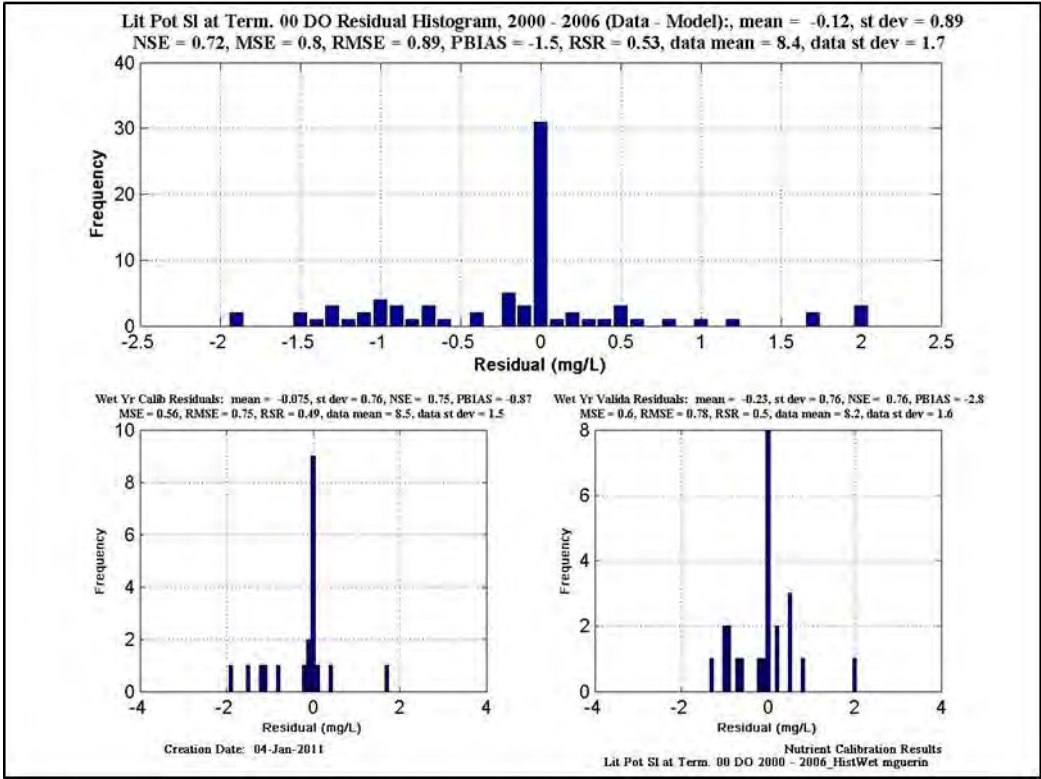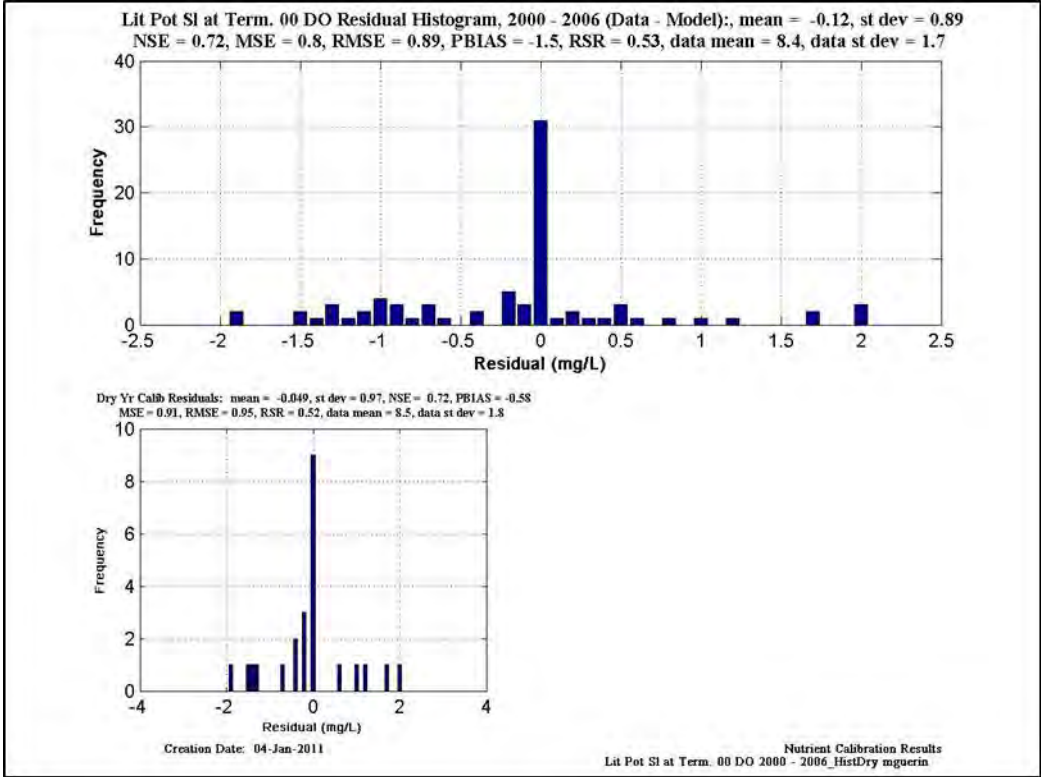
Figure 11-28 Calibration/validation statistics for DO at Lit Pot Sl. Upper figure is calibration & validation statistics for dry years; lower figure is calibration & validation statistics for wet years.
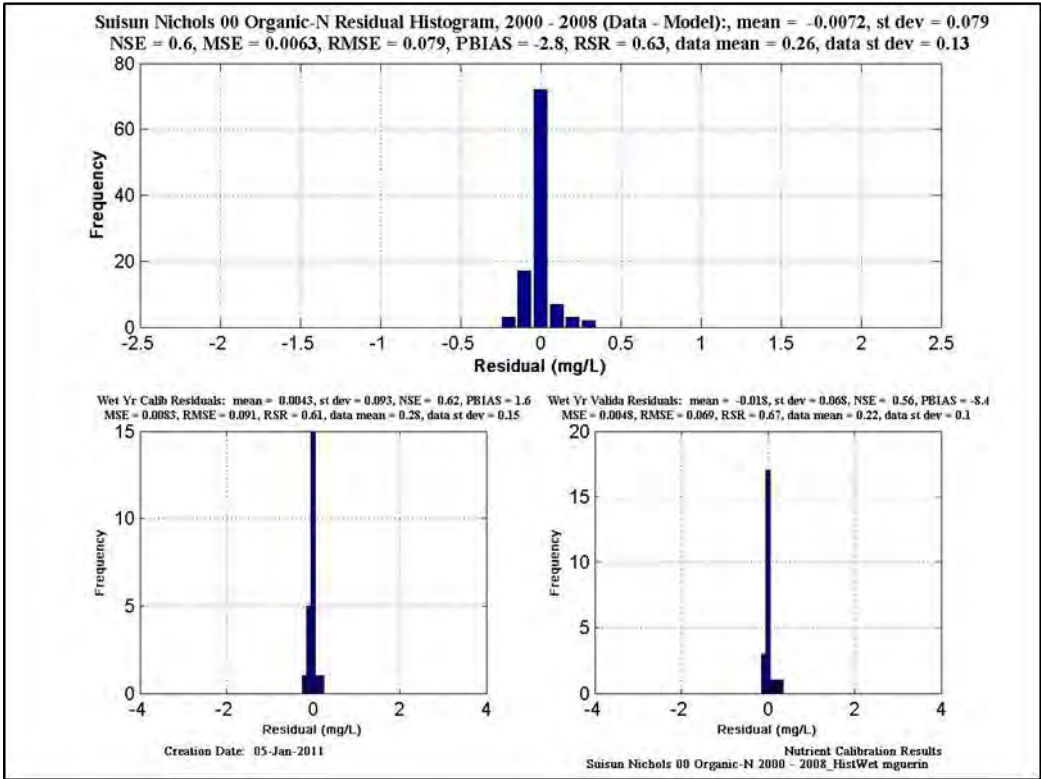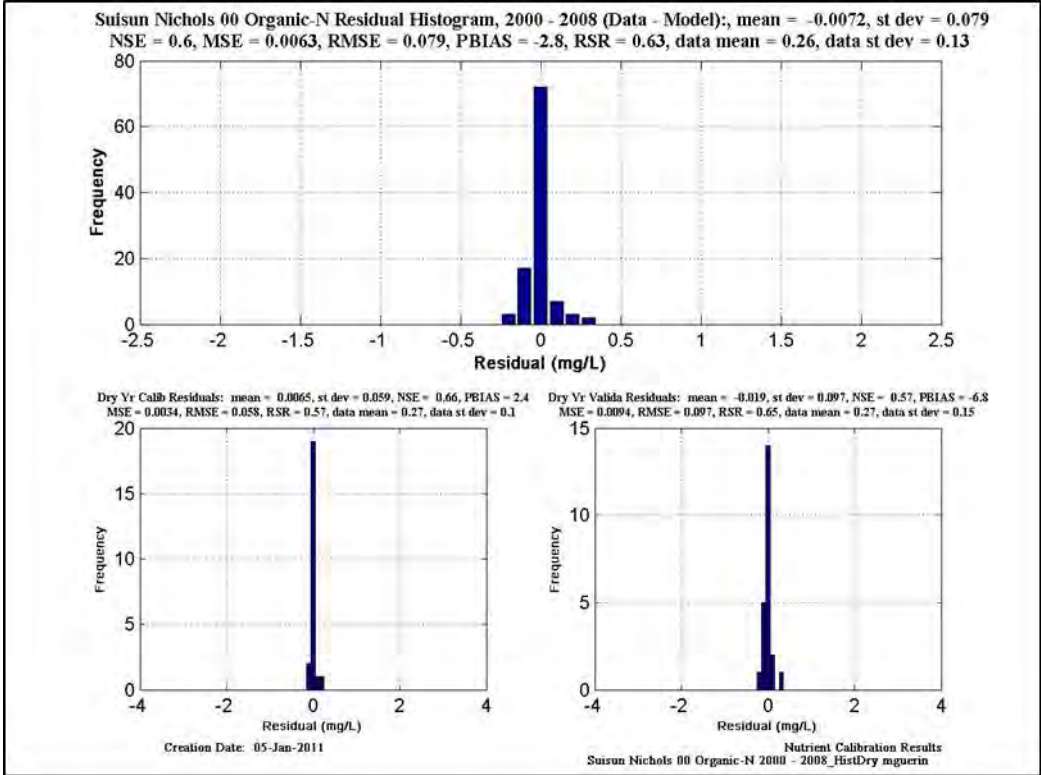
323
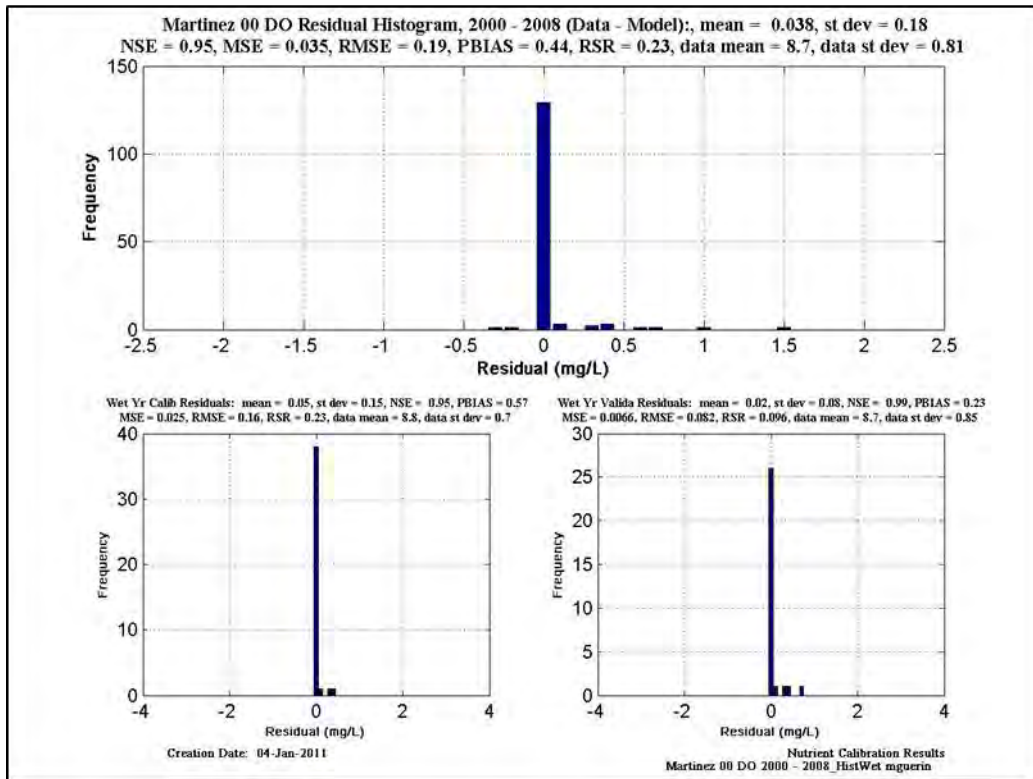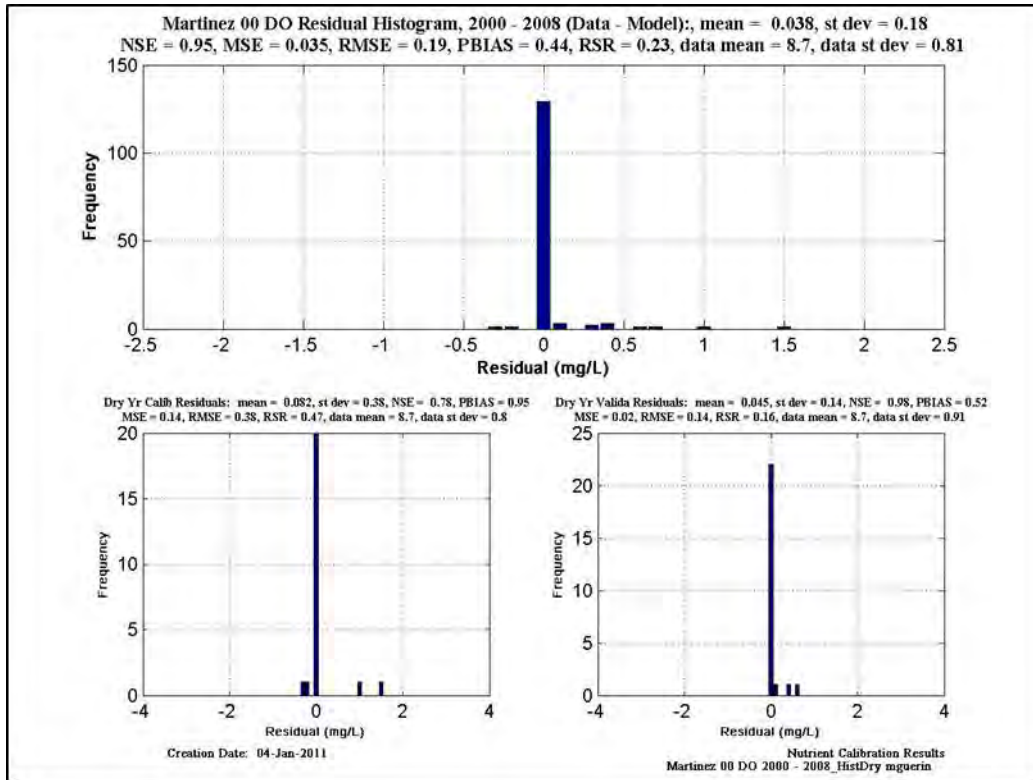
Figure 11-29 Calibration/validation statistics for DO at Martinez. Upper figure is calibration & validation statistics for dry years; lower figure is calibration & validation statistics for wet years.
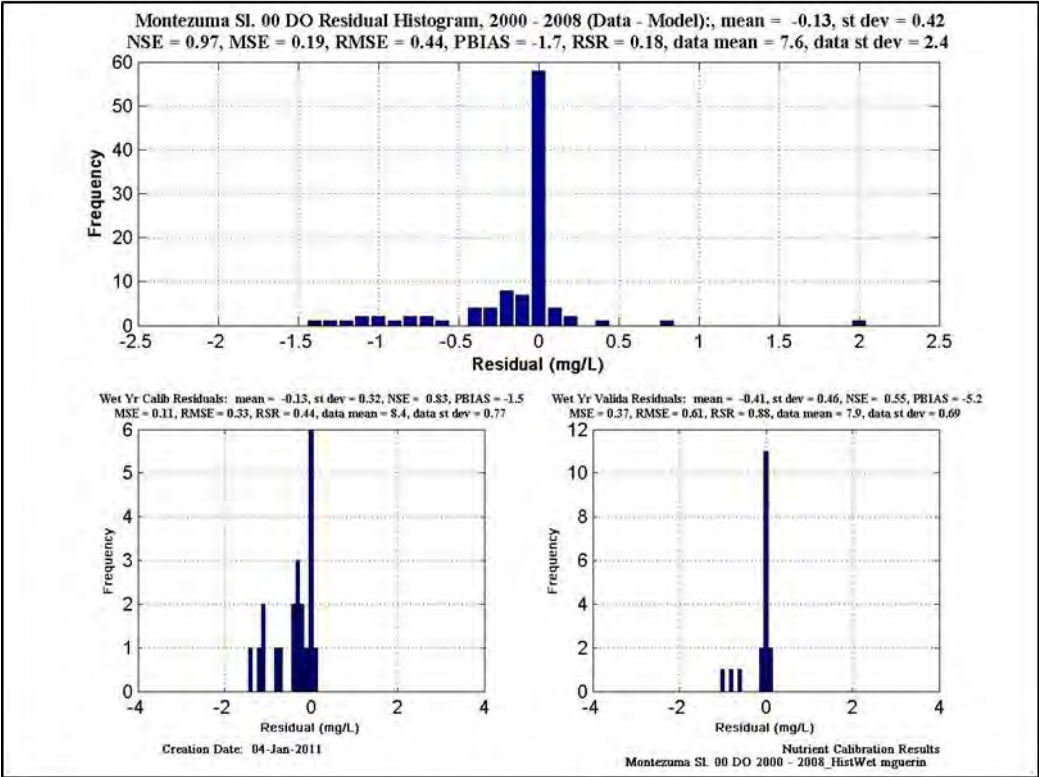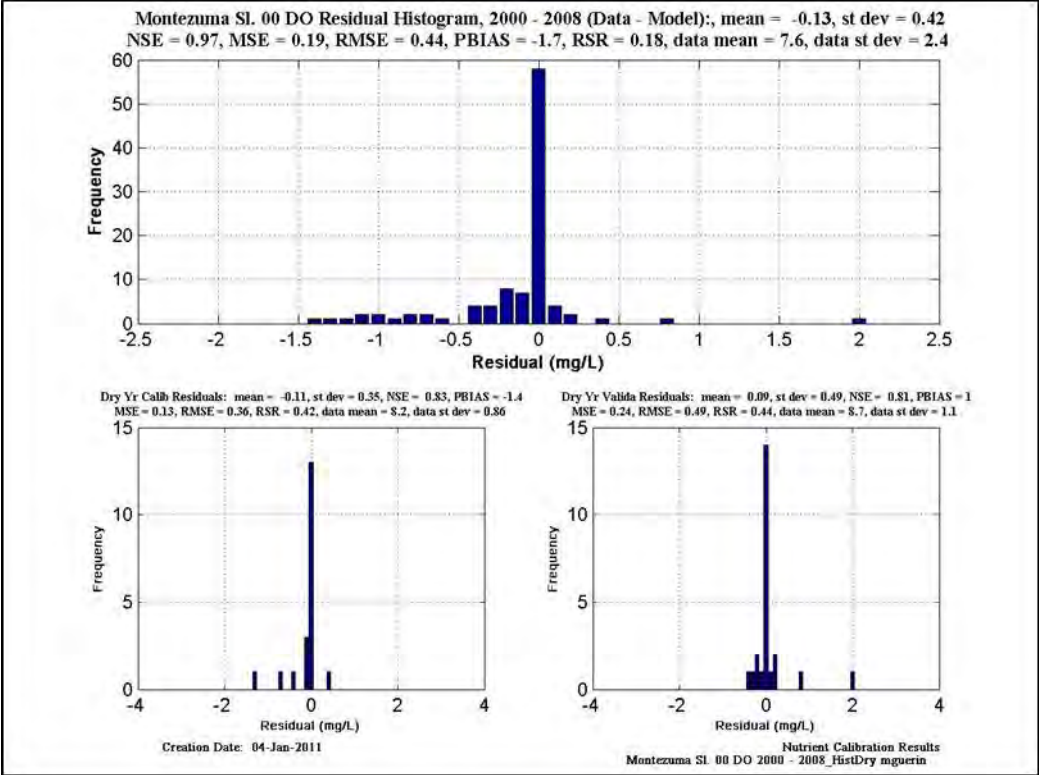
Figure 11-30 Calibration/validation statistics for DO at Montezuma. Upper figure is calibration & validation statistics for dry years; lower figure is calibration & validation statistics for wet years.
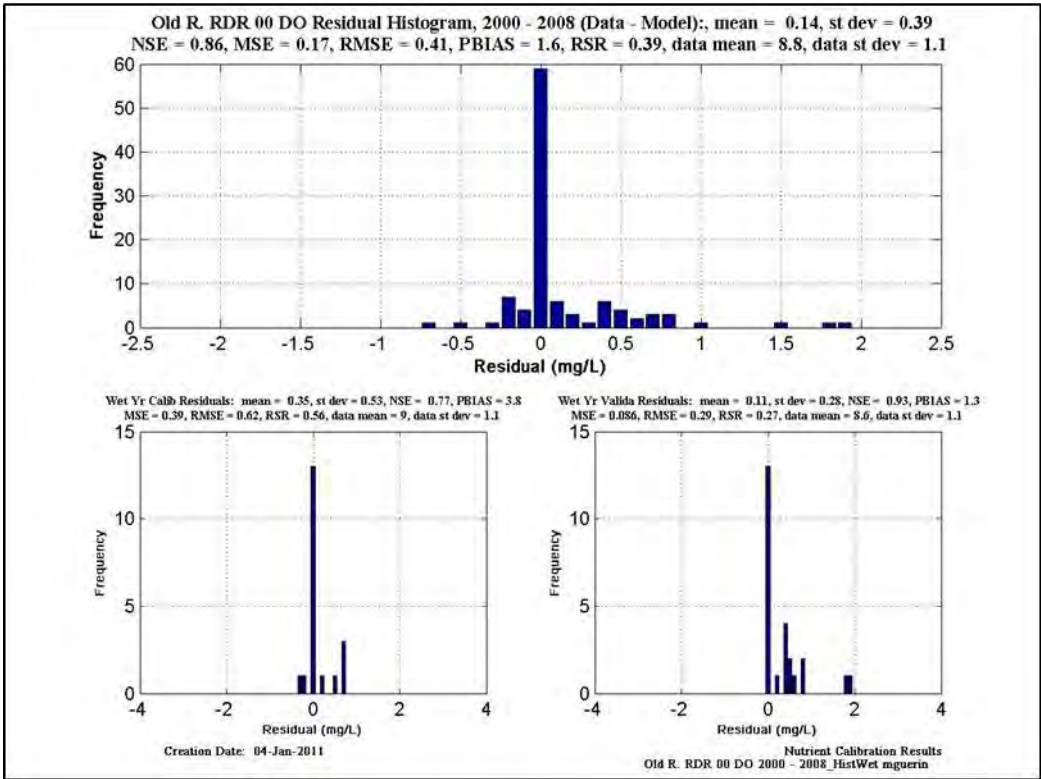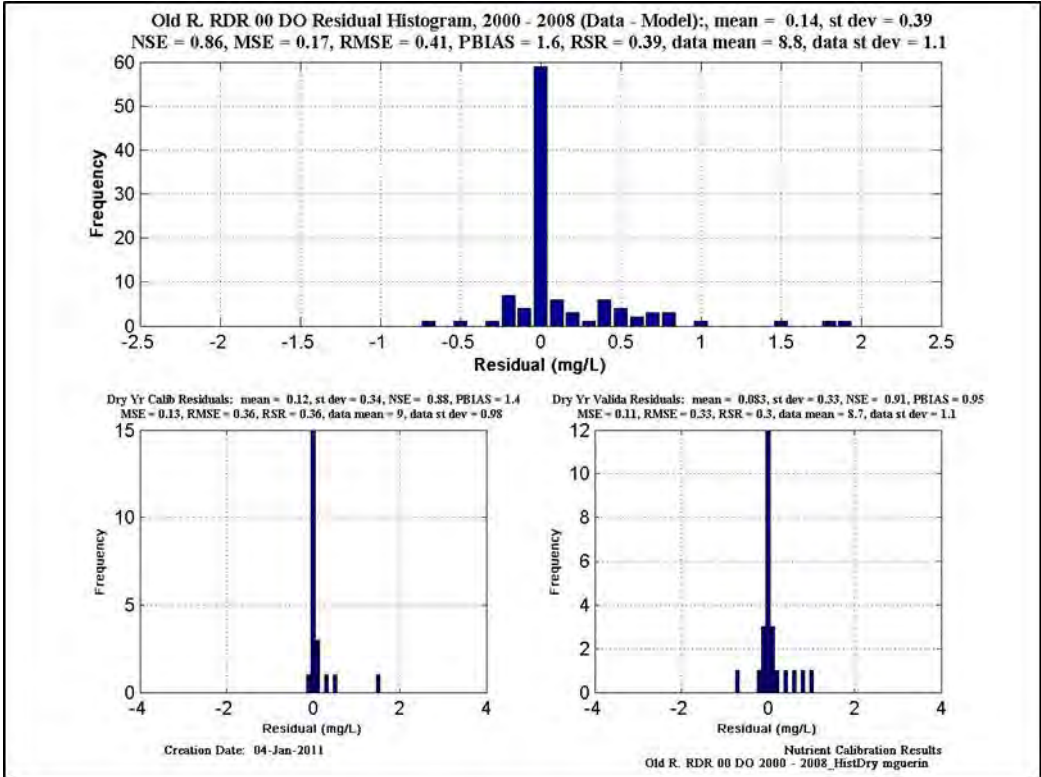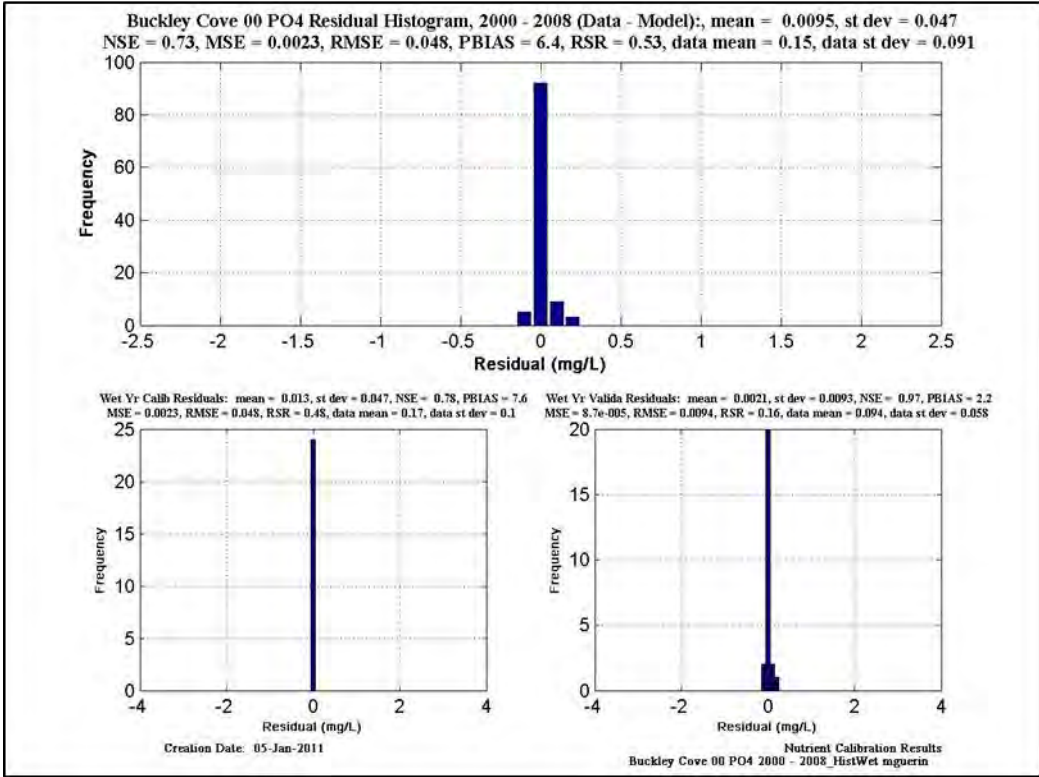
Figure 11-31 Calibration/validation statistics for DO at Old R. RDR. Upper figure is calibration & validation statistics for dry years; lower figure is calibration & validation statistics for wet years.
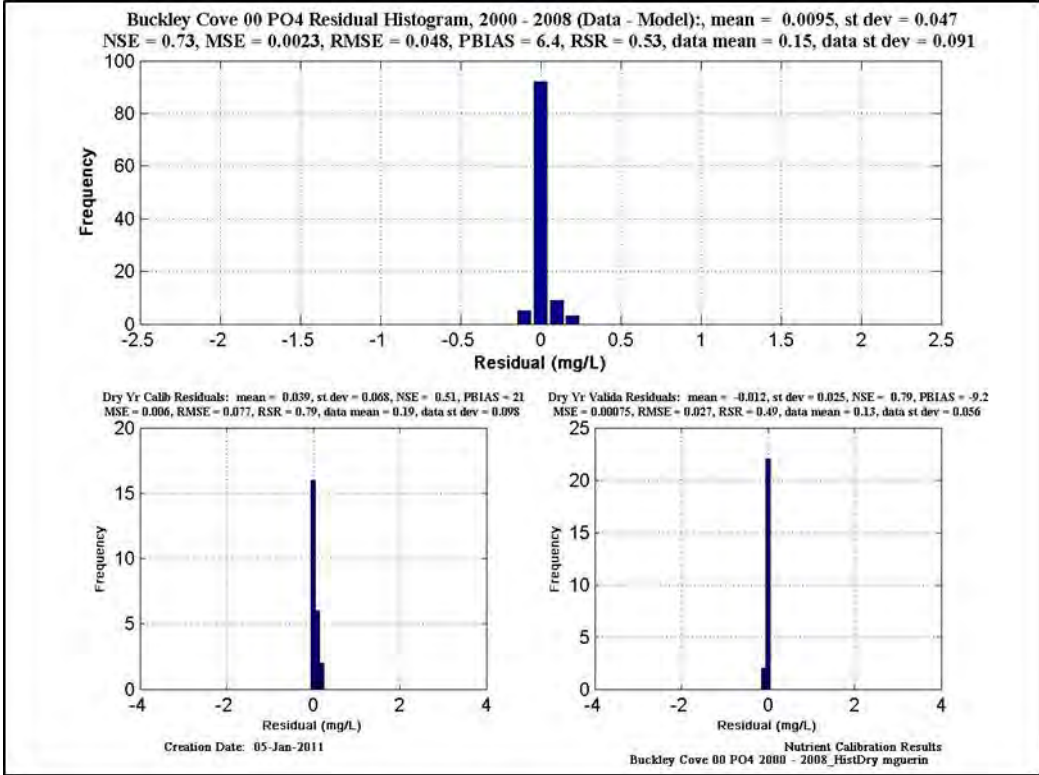
326
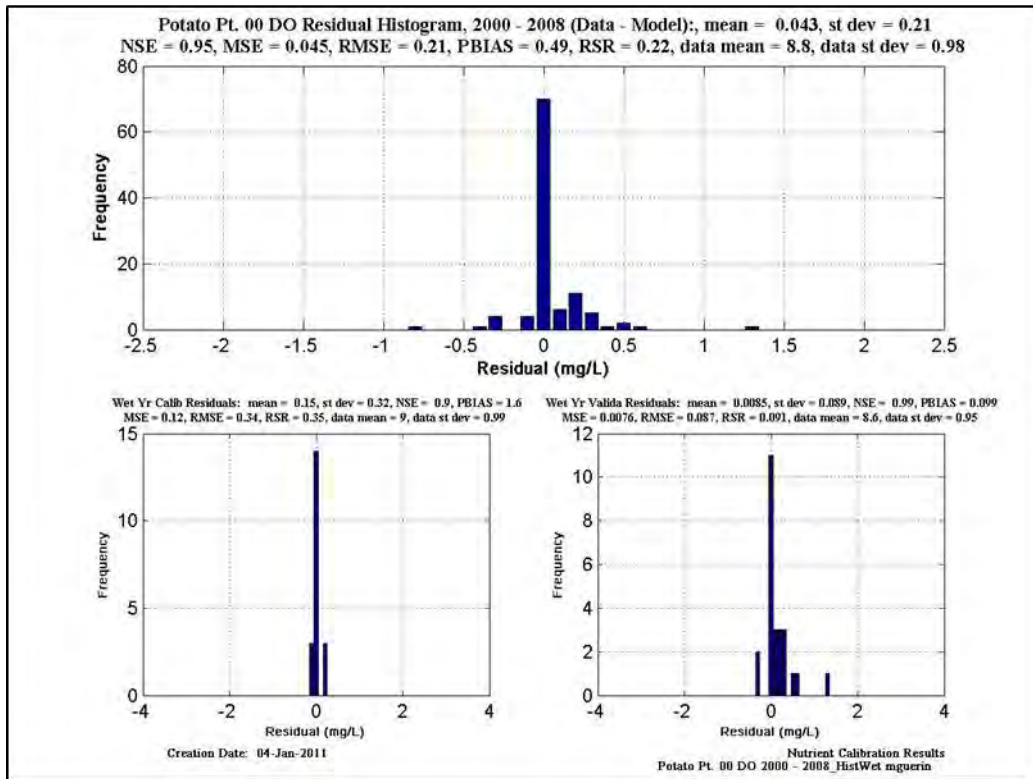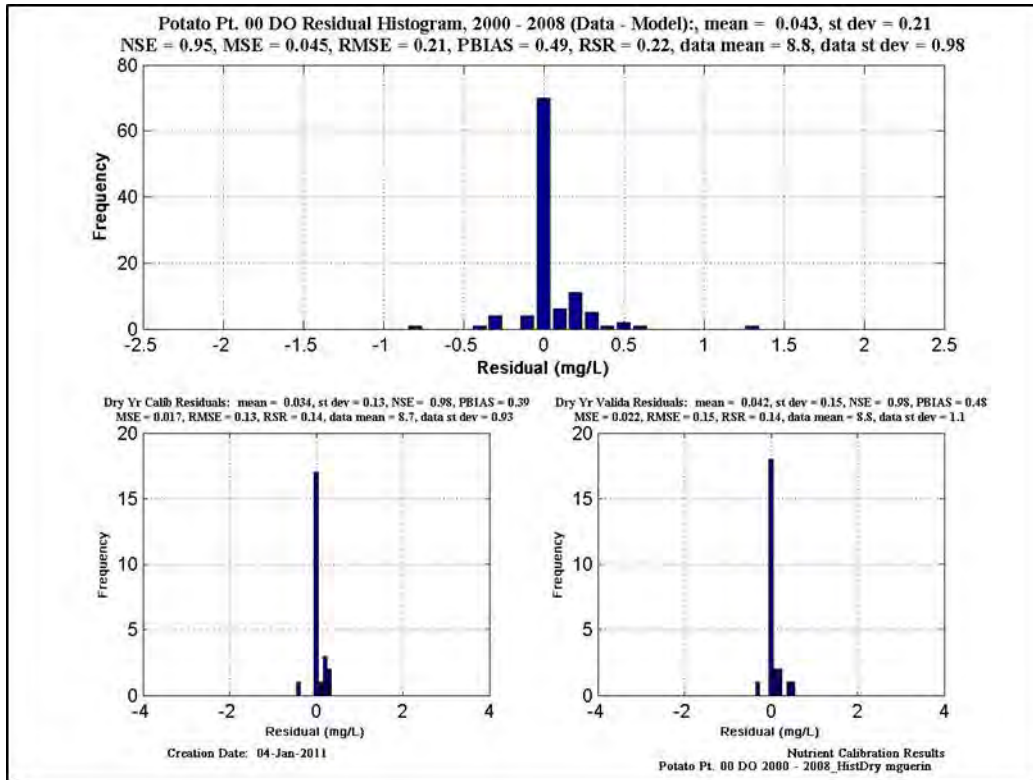
Figure 11-32 Calibration/validation statistics for DO at Potato Pt. Upper figure is calibration & validation statistics for dry years; lower figure is calibration & validation statistics for wet years.
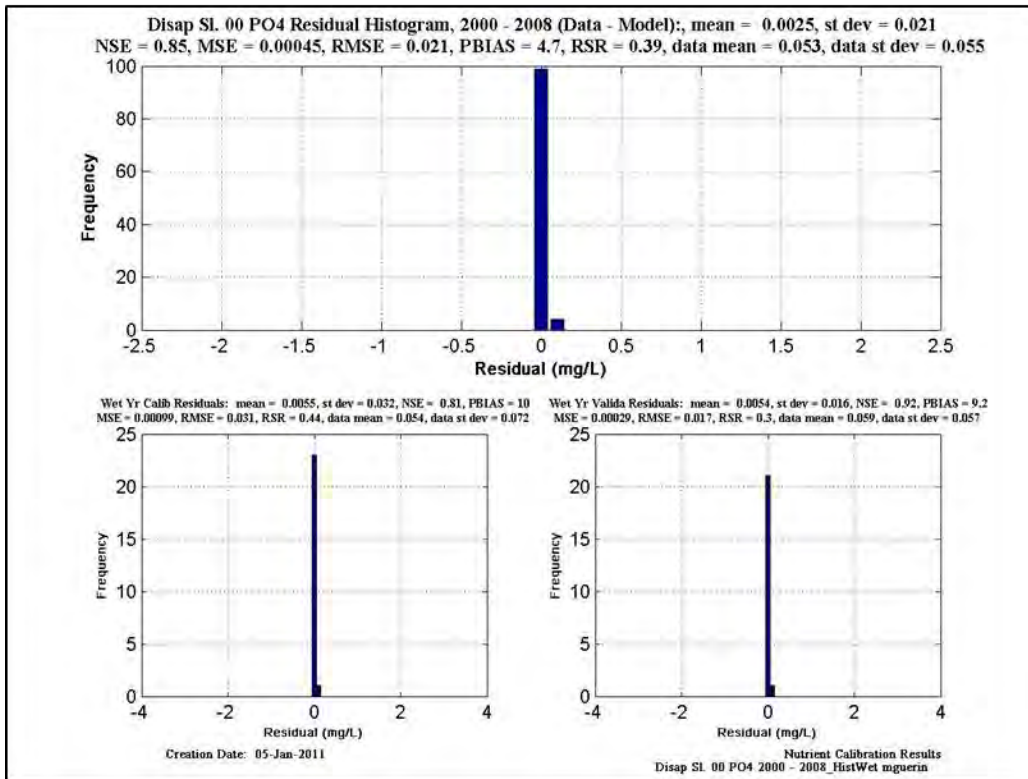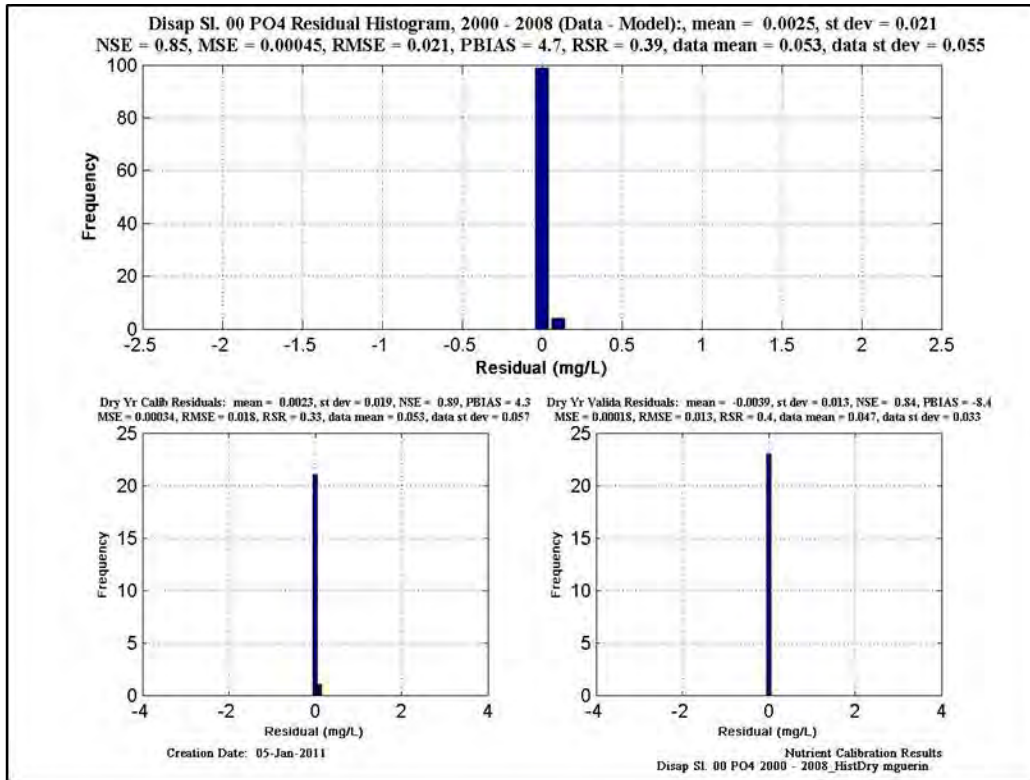
327
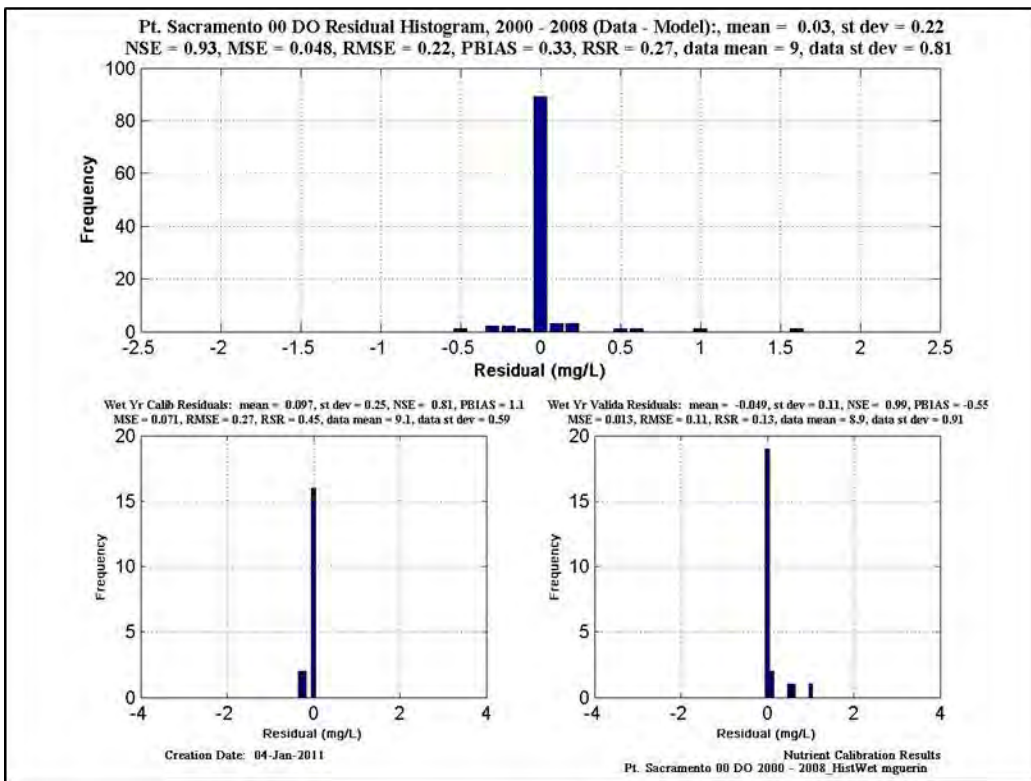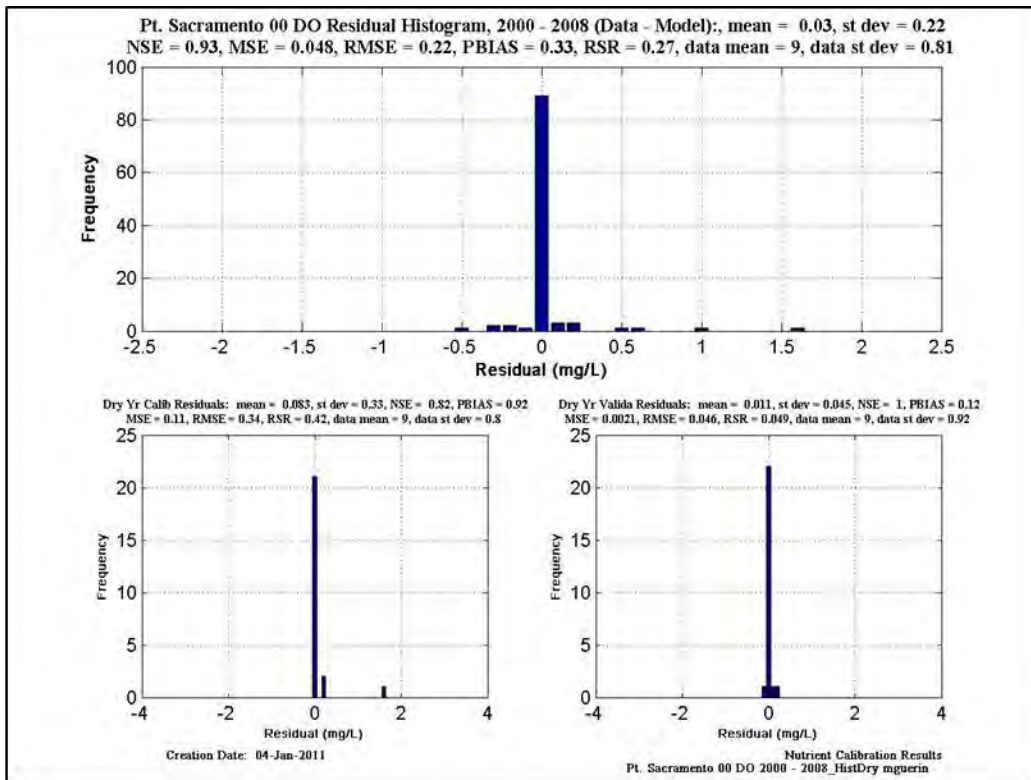
Figure 11-33 Calibration/validation statistics for DO at Pt. Sacramento. Upper figure is calibration & validation statistics for dry years; lower figure is calibration & validation statistics for wet years.
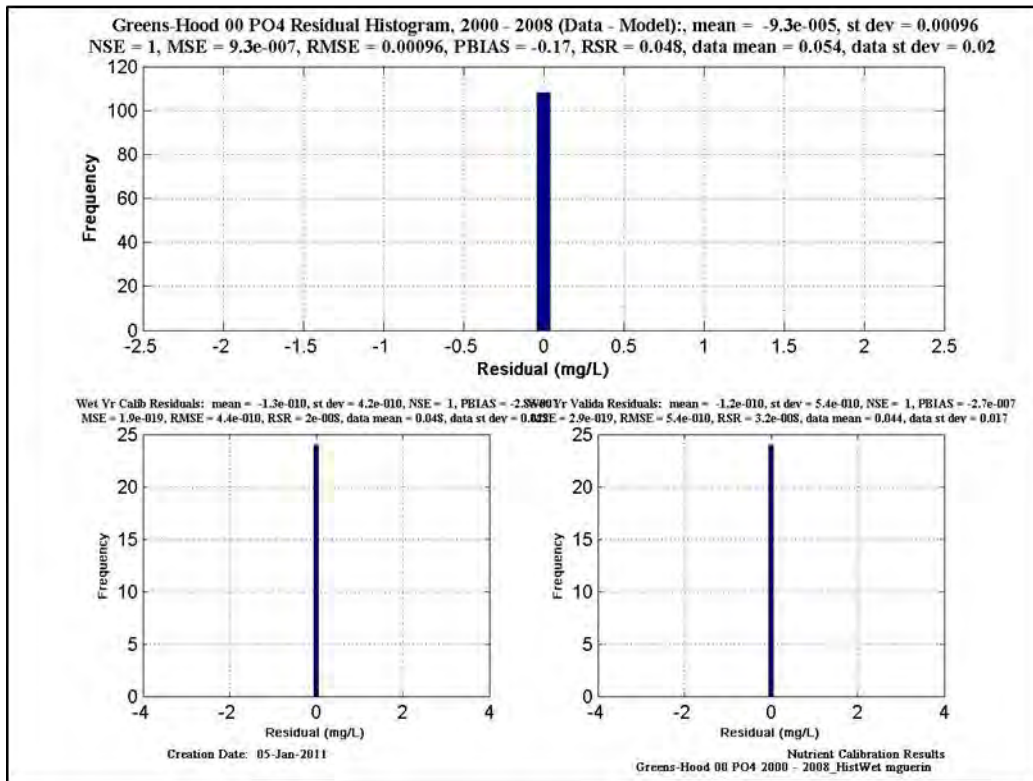
328
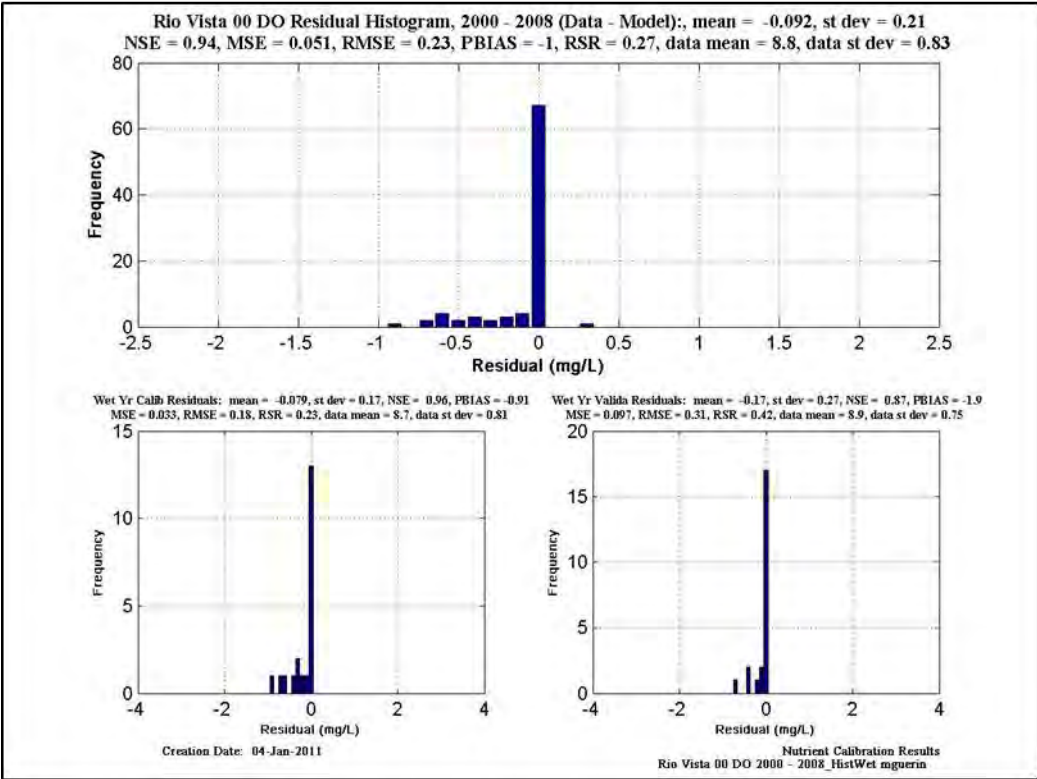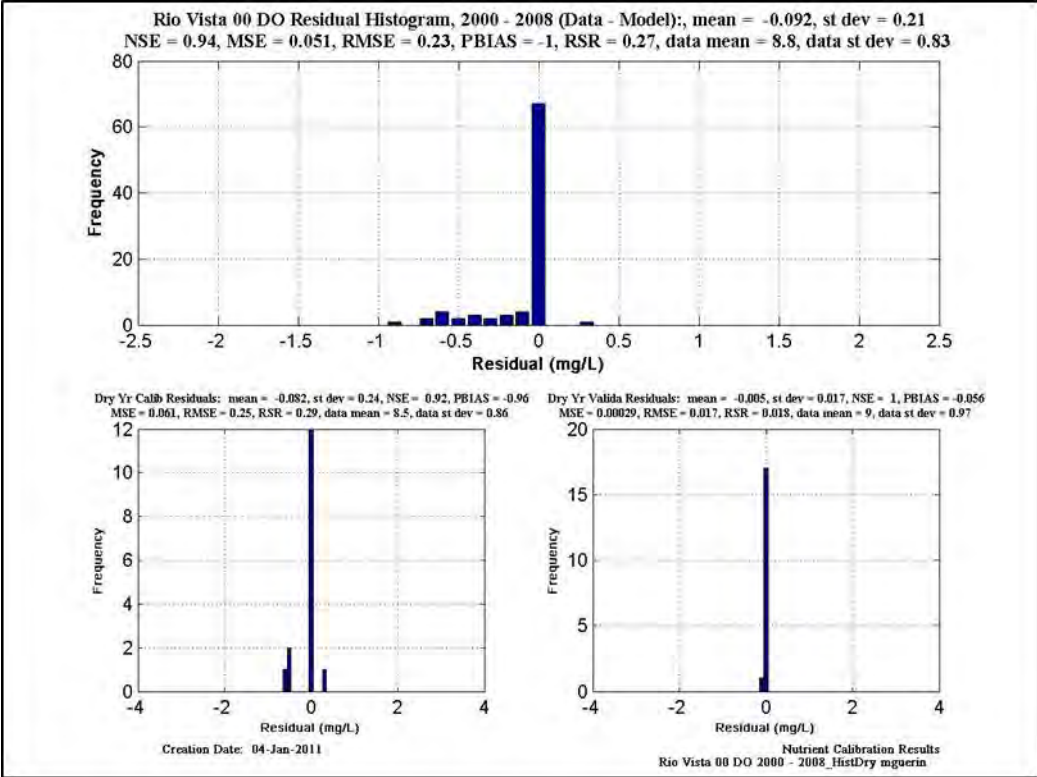
Figure 11-34 Calibration/validation statistics for DO at Rio Vista. Upper figure is calibration & validation statistics for dry years; lower figure is calibration & validation statistics for wet years.
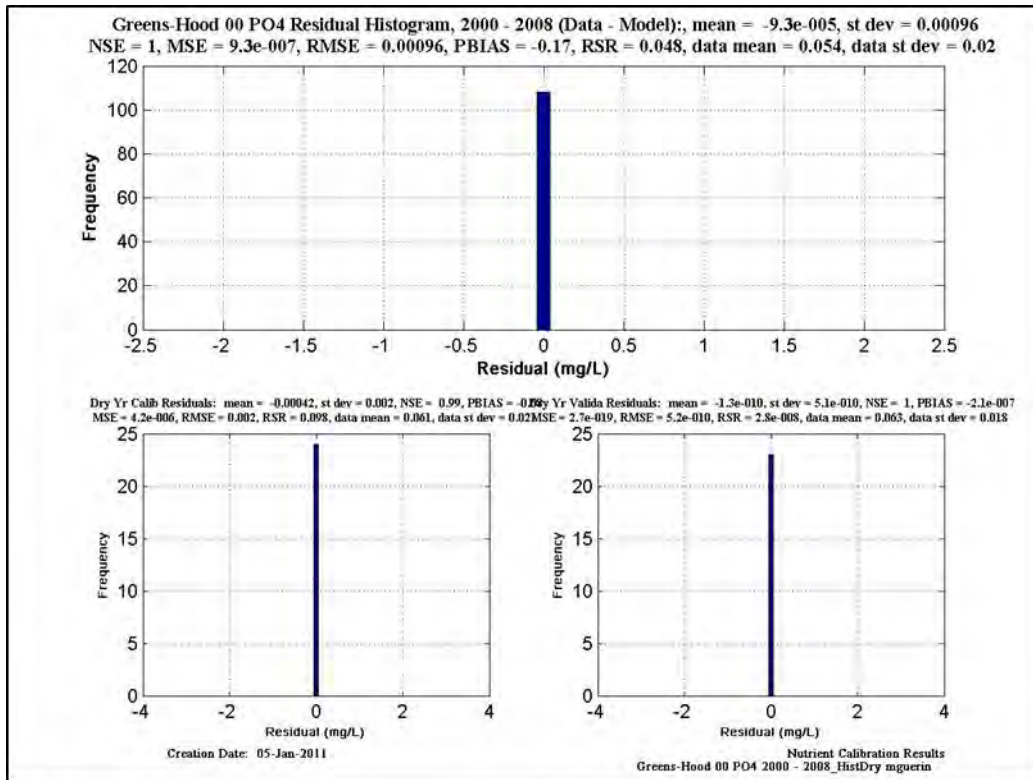
329
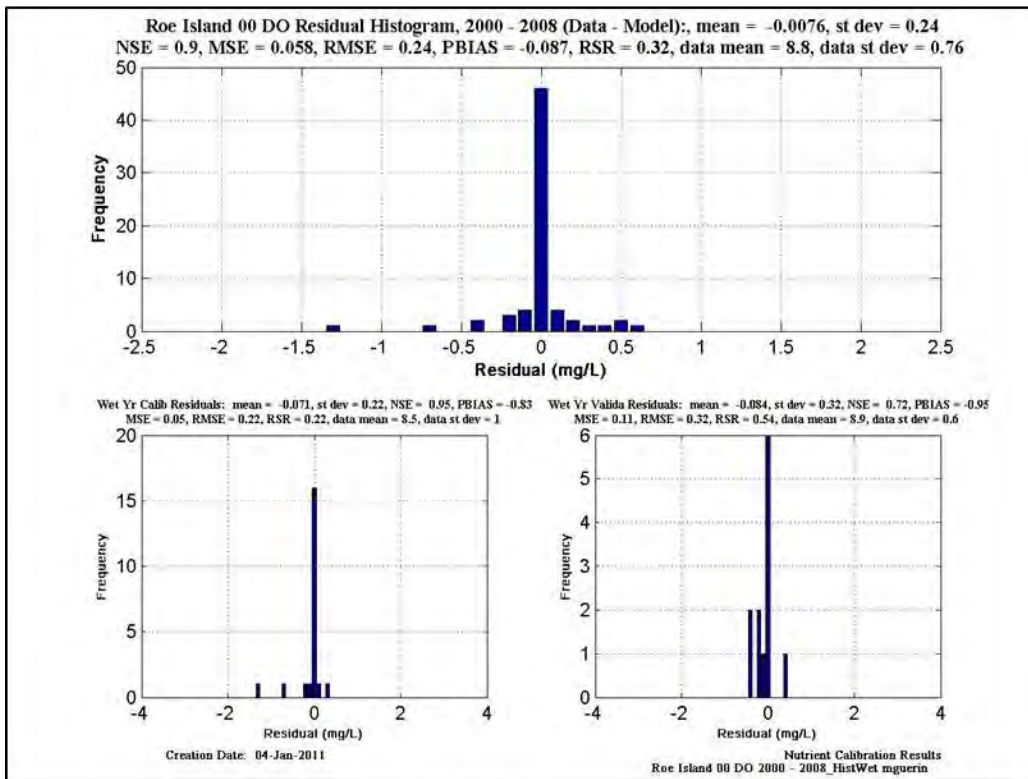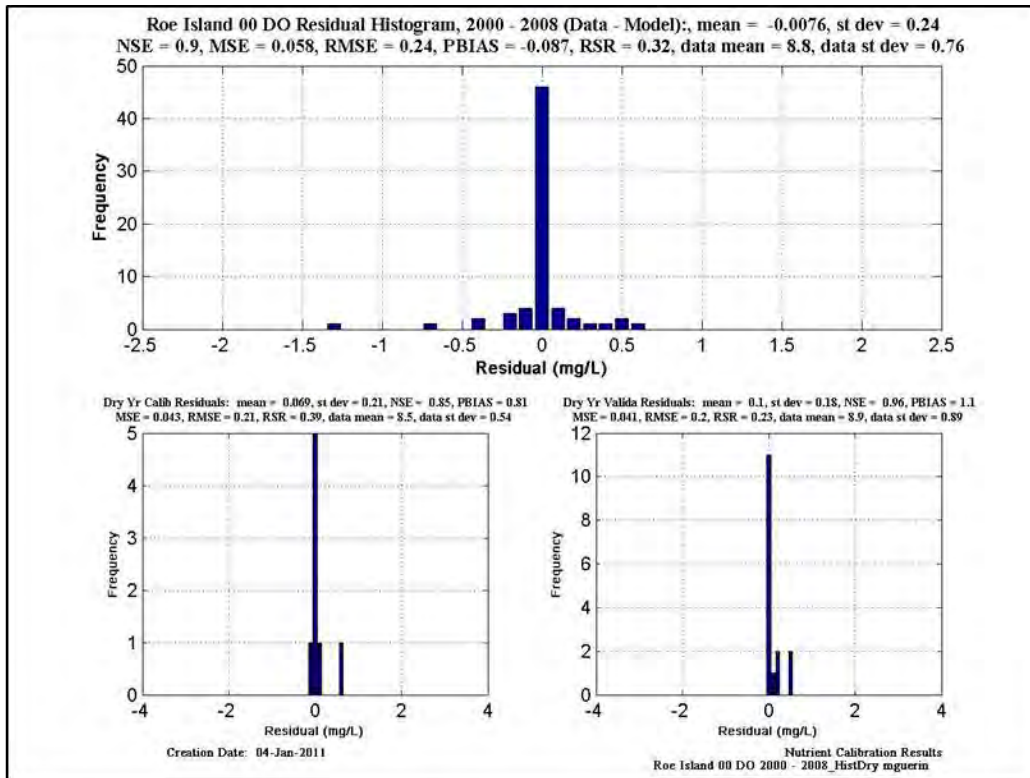
Figure 11-35 Calibration/validation statistics for DO at Roe Island. Upper figure is calibration & validation statistics for dry years; lower figure is calibration & validation statistics for wet years.
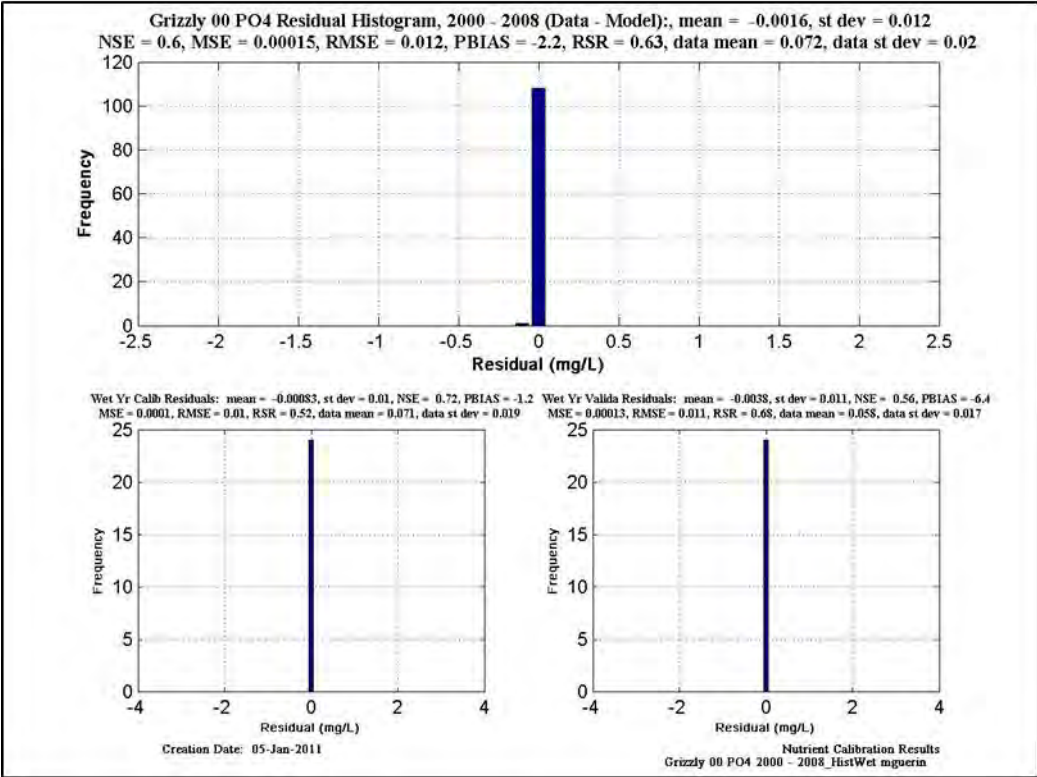
330
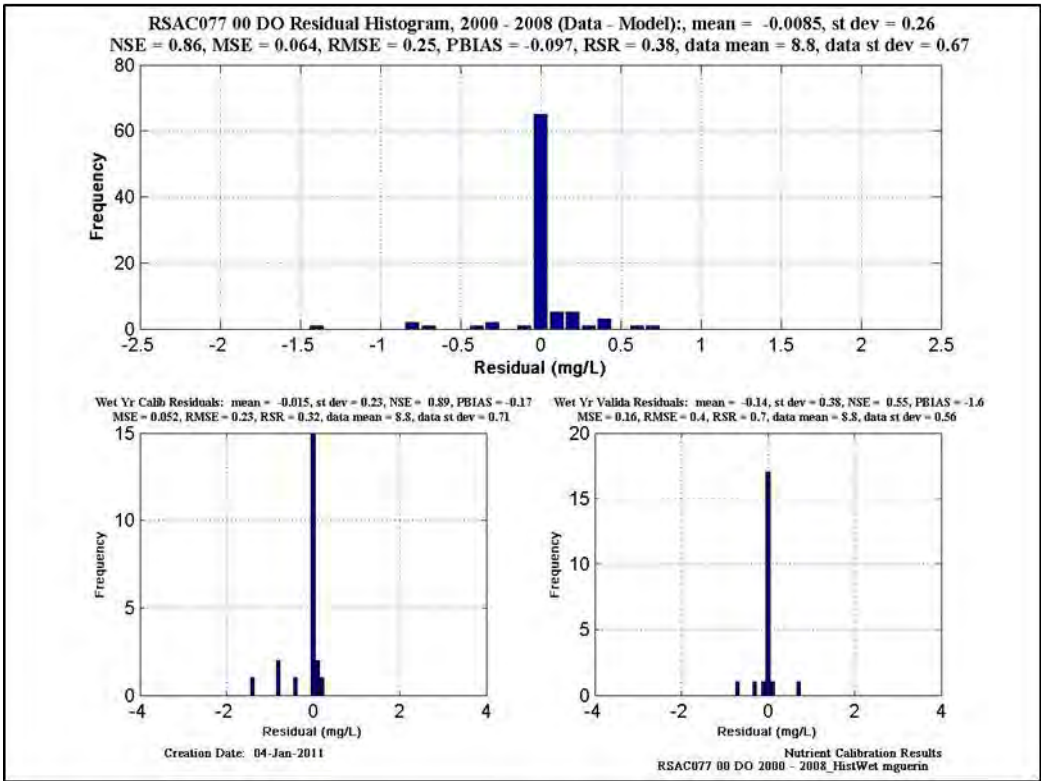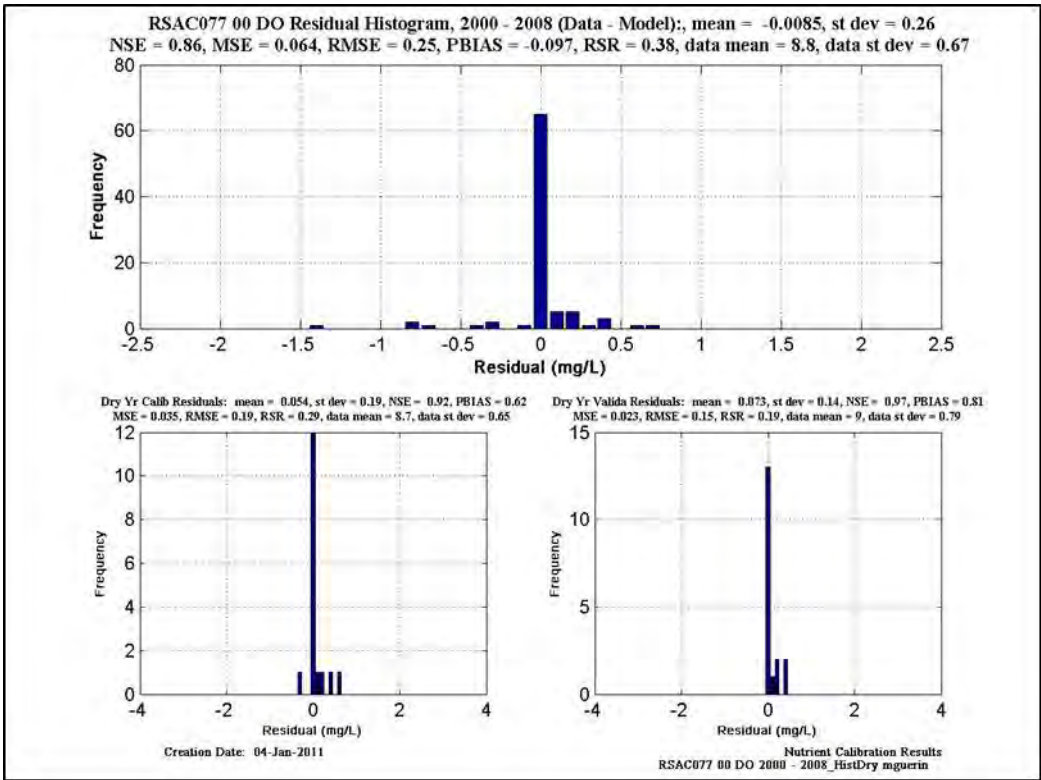
Figure 11-36 Calibration/validation statistics for DO at RSAC077. Upper figure is calibration & validation statistics for dry years; lower figure is calibration & validation statistics for wet years.
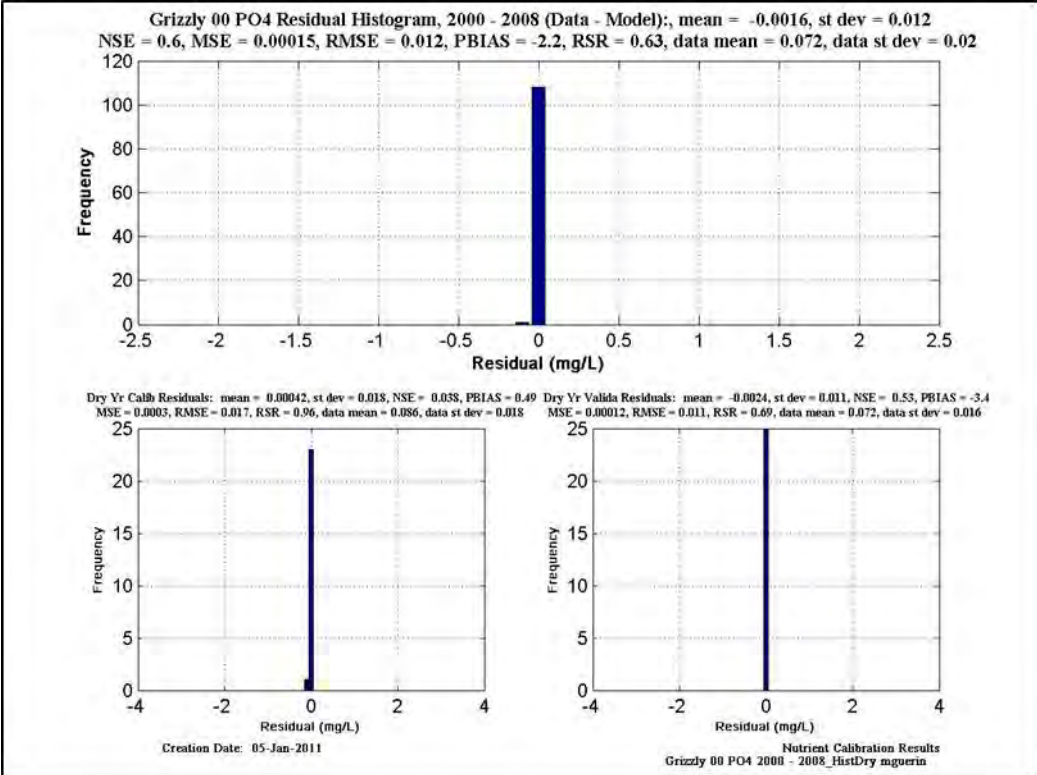
331
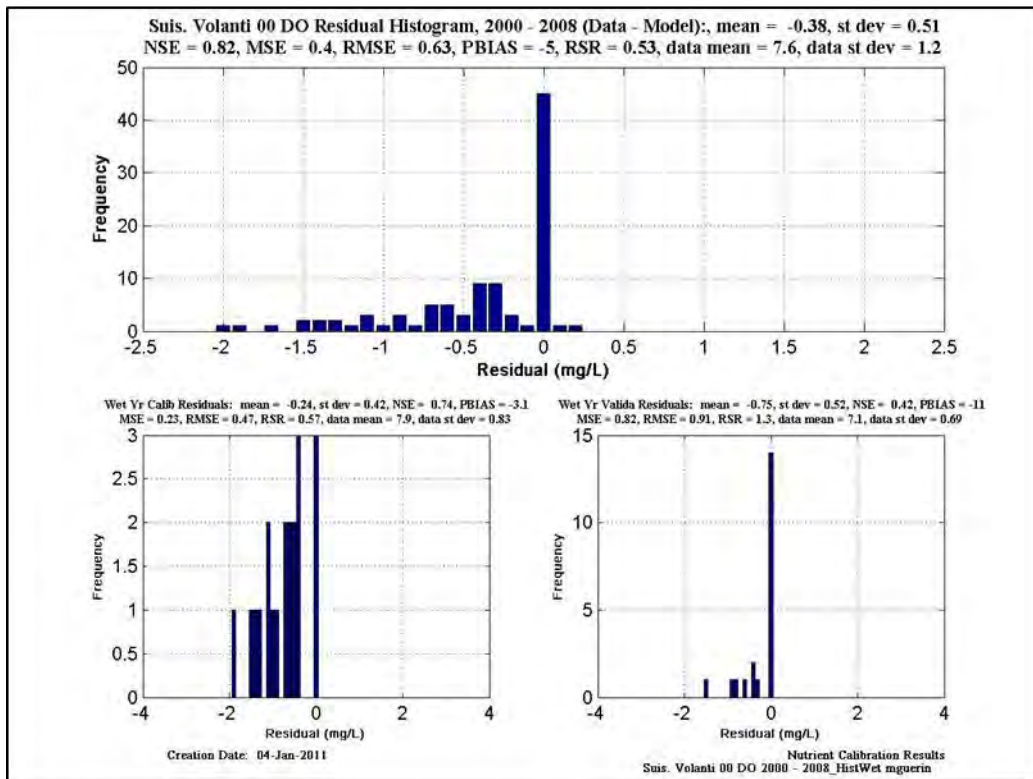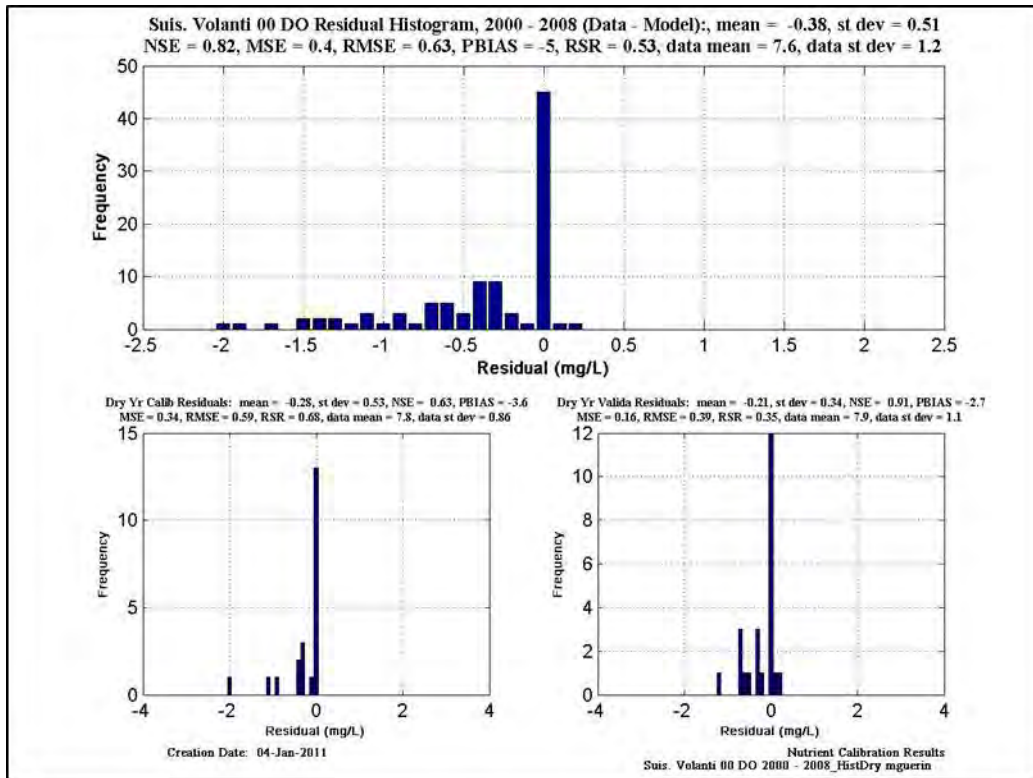
Figure 11-37 Calibration/validation statistics for DO at Suisun Volanti. Upper figure is calibration & validation statistics for dry years; lower figure is calibration & validation statistics for wet years.
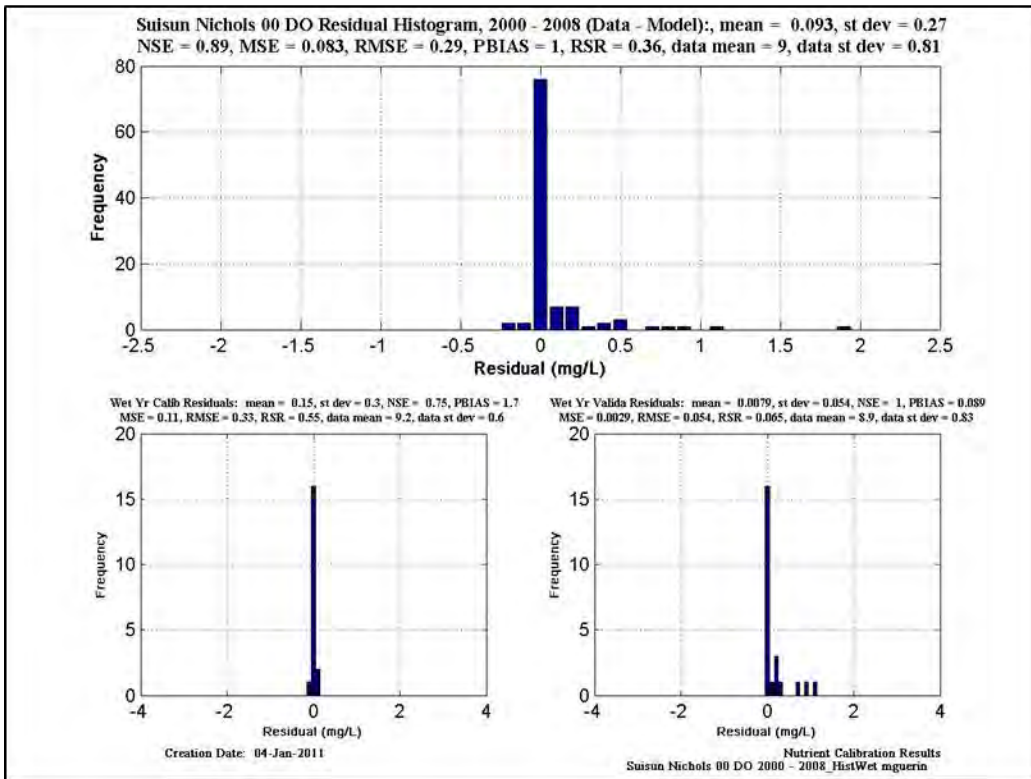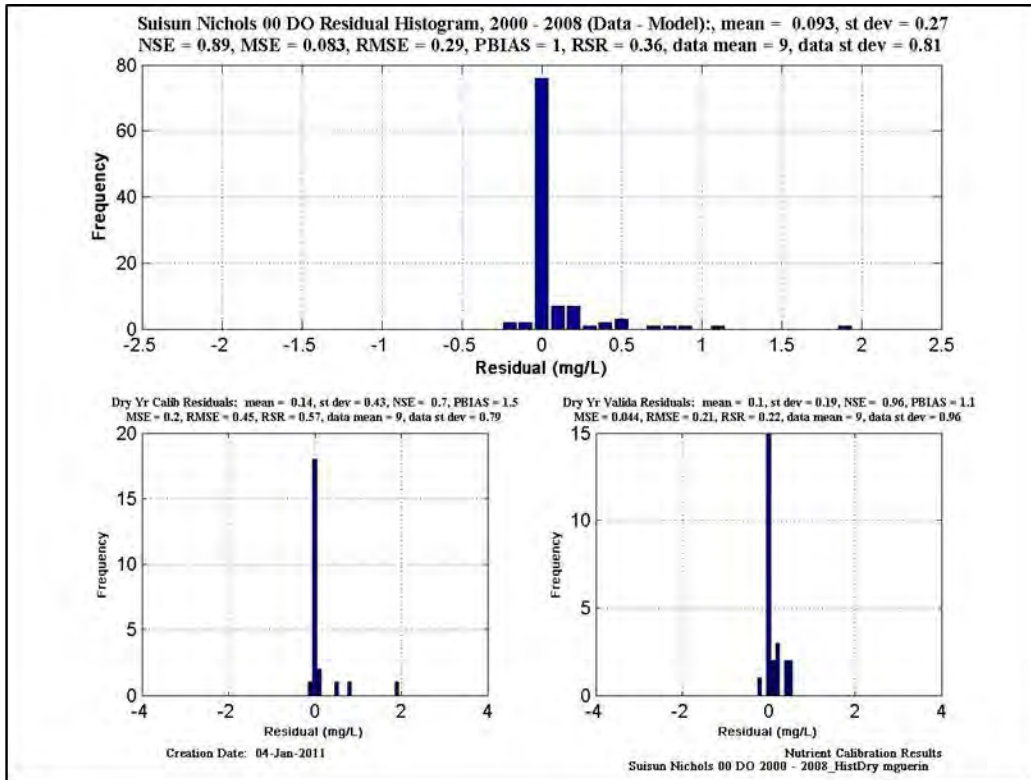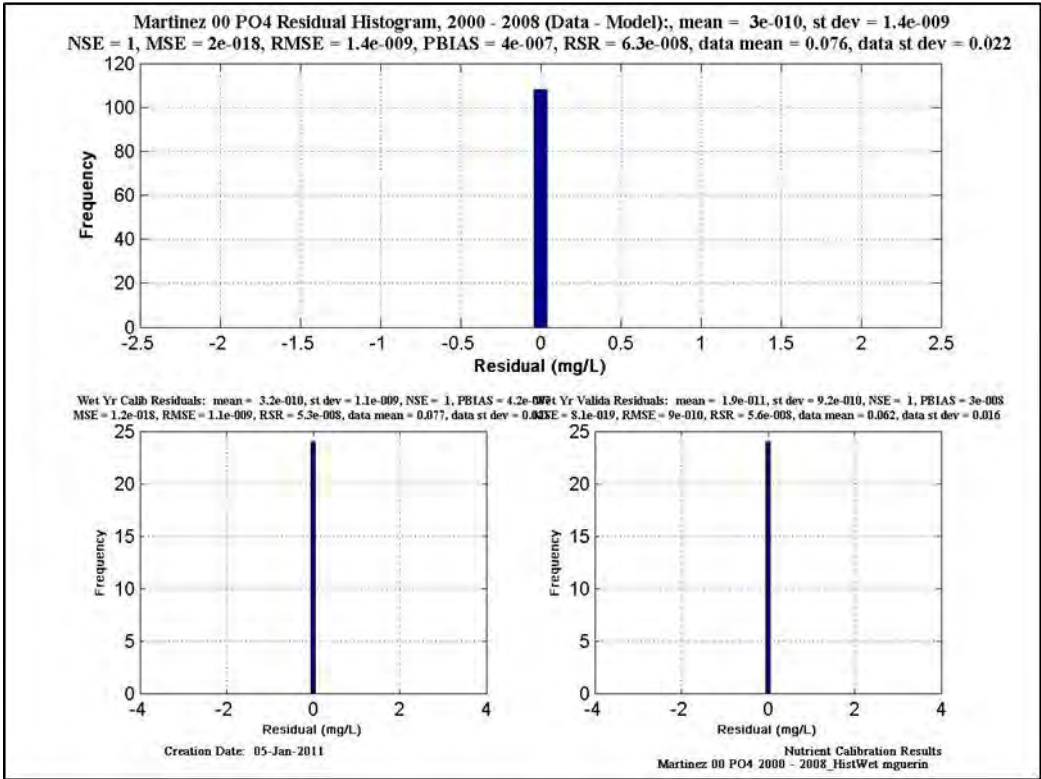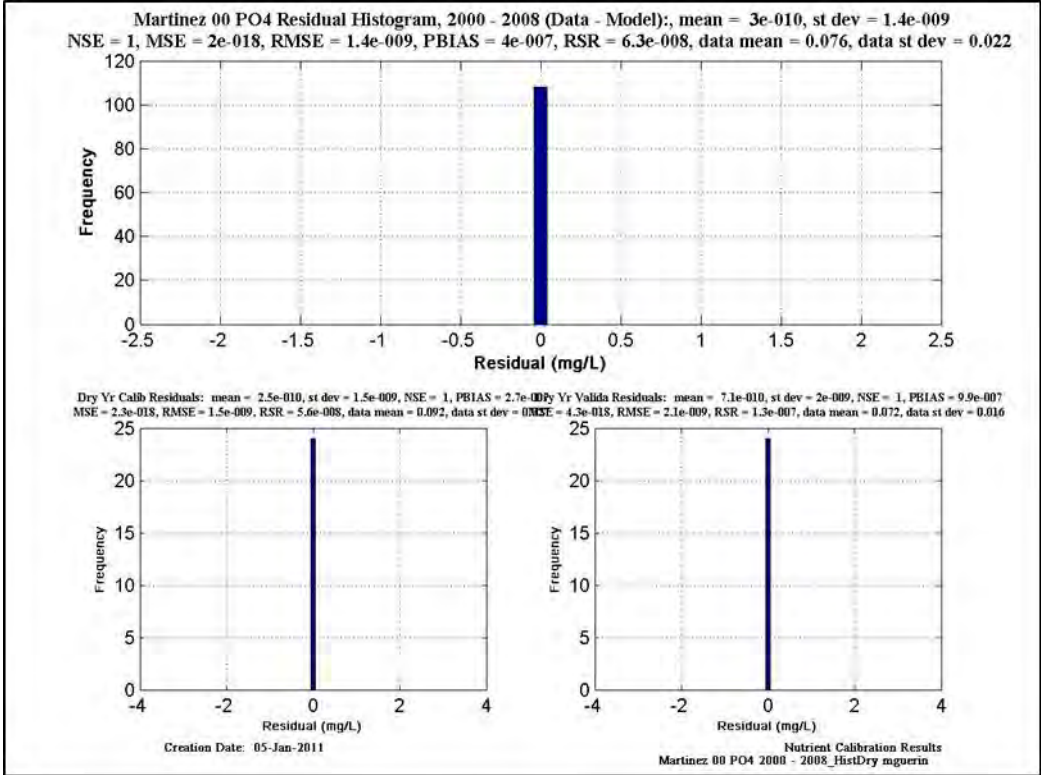
Figure 11-38 Calibration/validation statistics for DO at Suisun Nichols. Upper figure is calibration & validation statistics for dry years; lower figure is calibration & validation statistics for wet years.

333
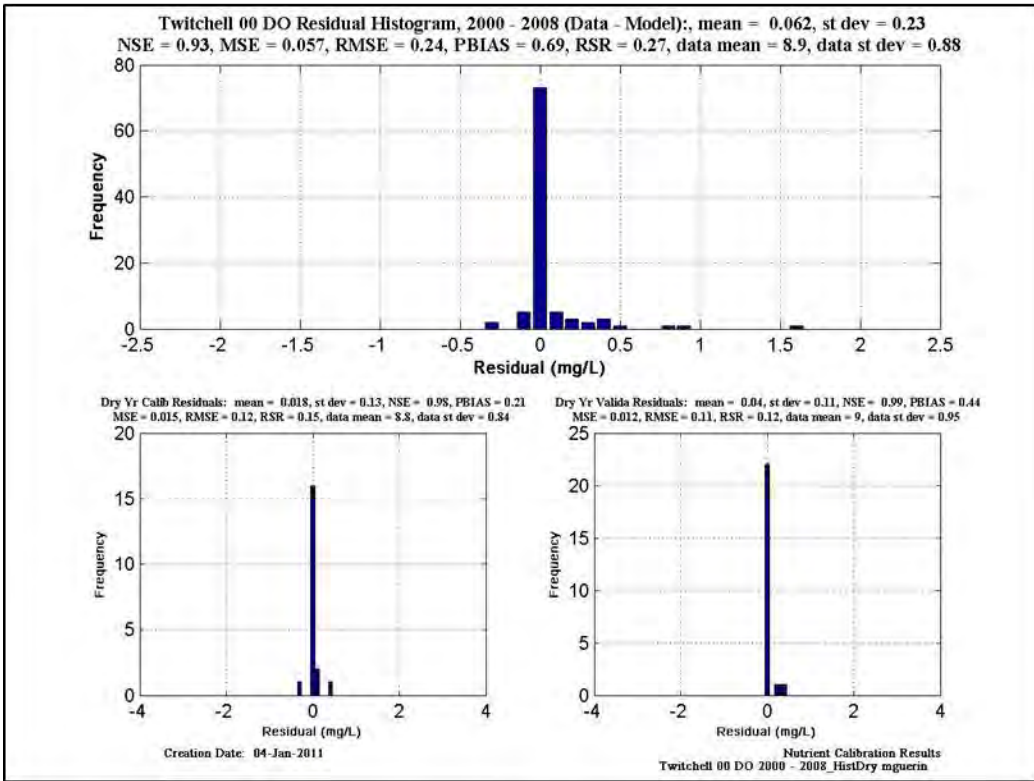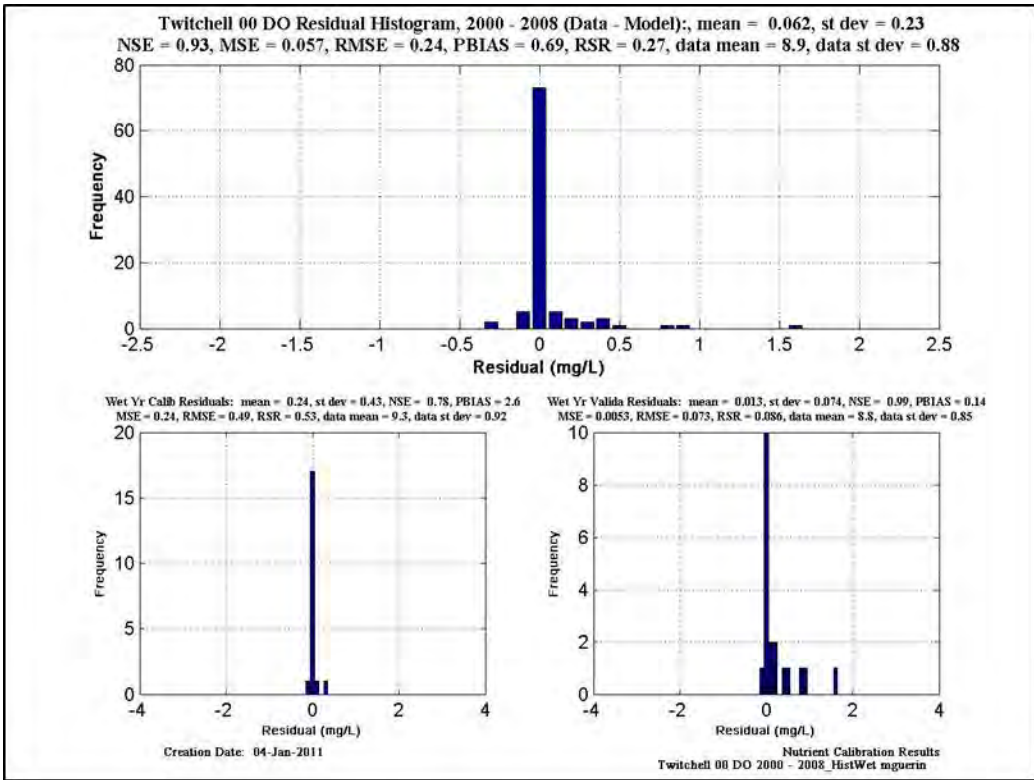
Figure 11-39 Calibration/validation statistics for DO at Twitchell. Upper figure is calibration & validation statistics for dry years; lower figure is calibration & validation statistics for wet years.
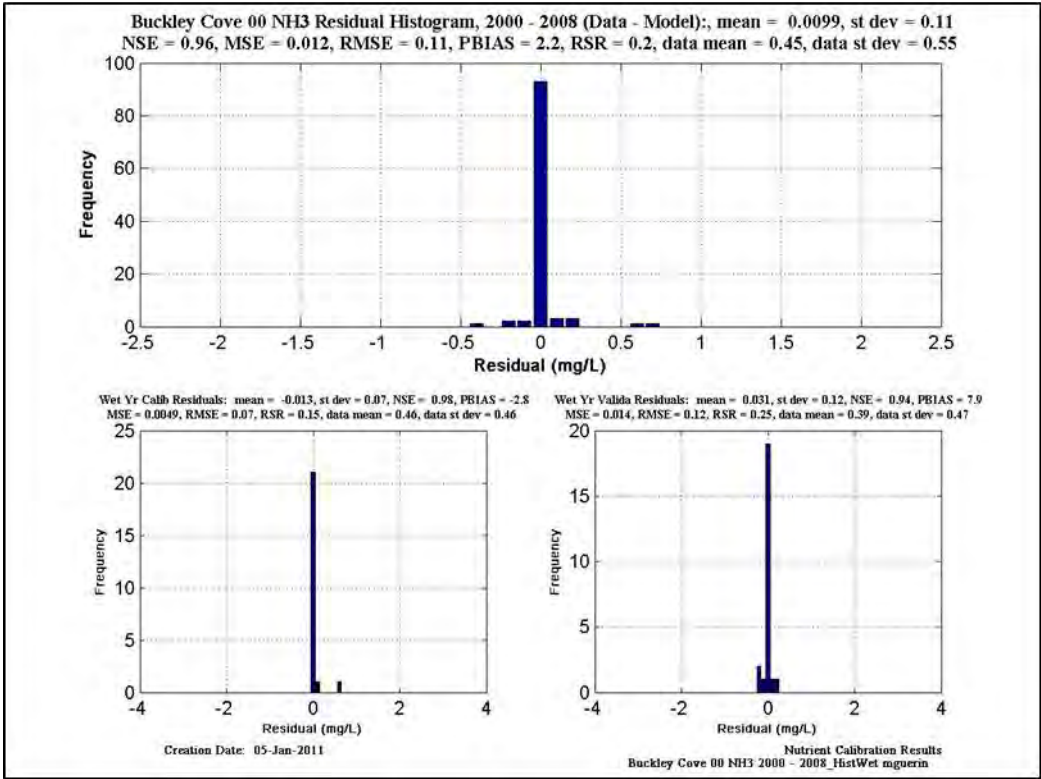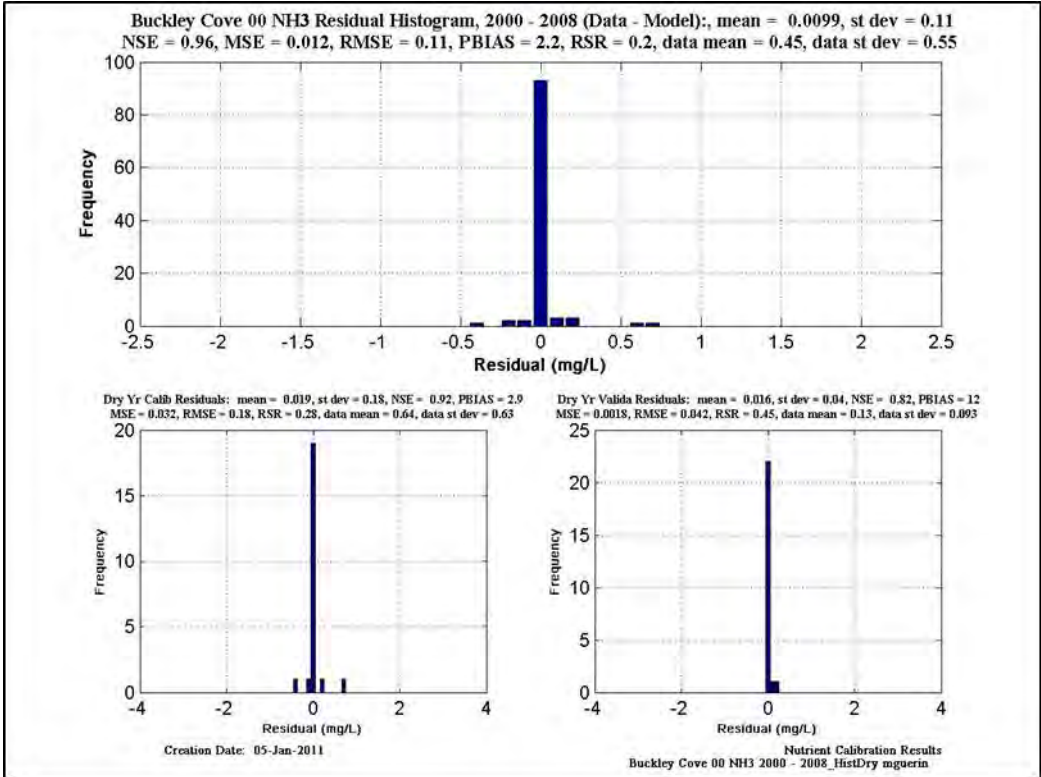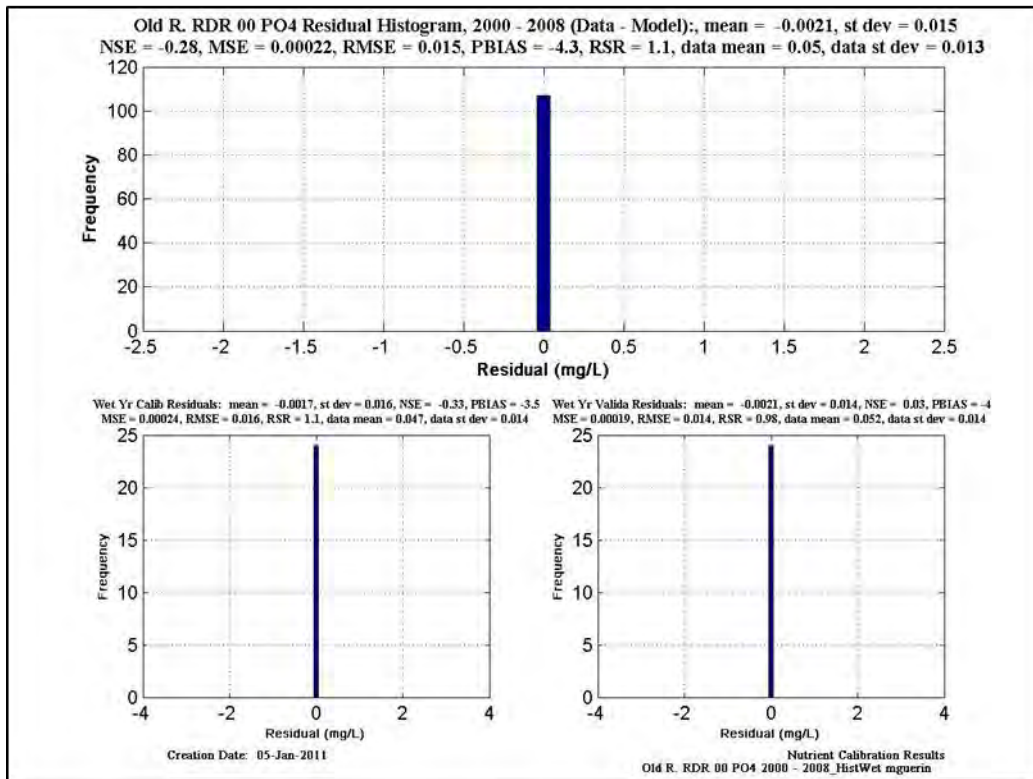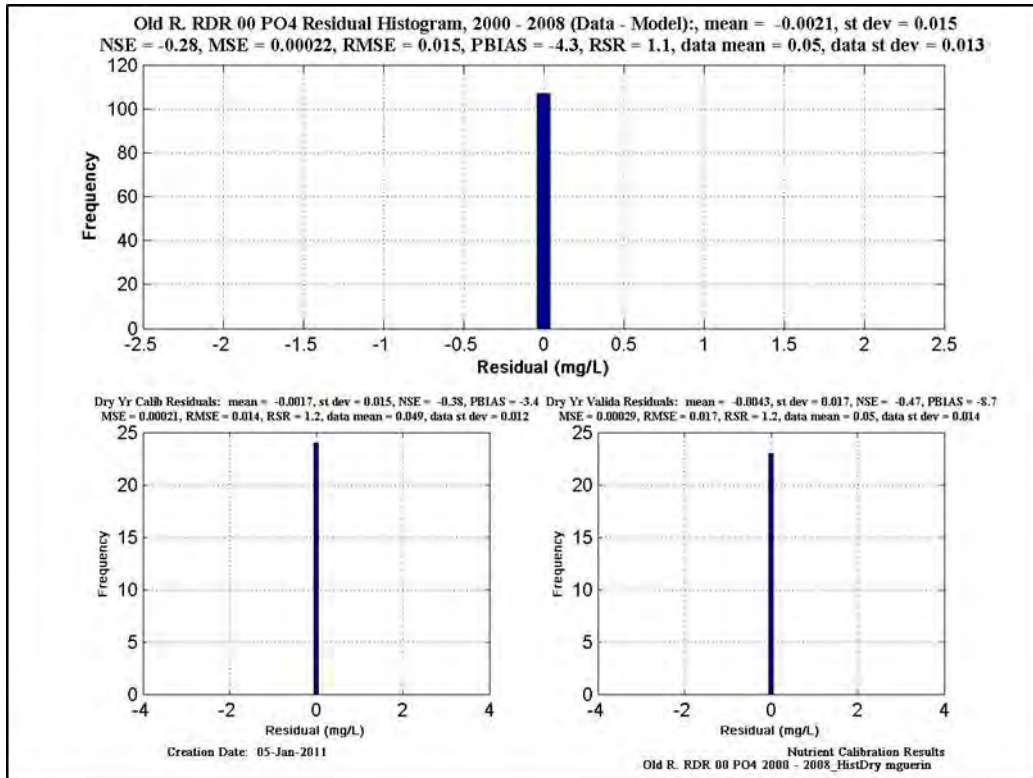
Figure 11-40 Calibration/validation statistics for NH3 at Buckley Cove. Upper figure is calibration & validation statistics for dry years; lower figure is calibration & validation statistics for wet years.

335
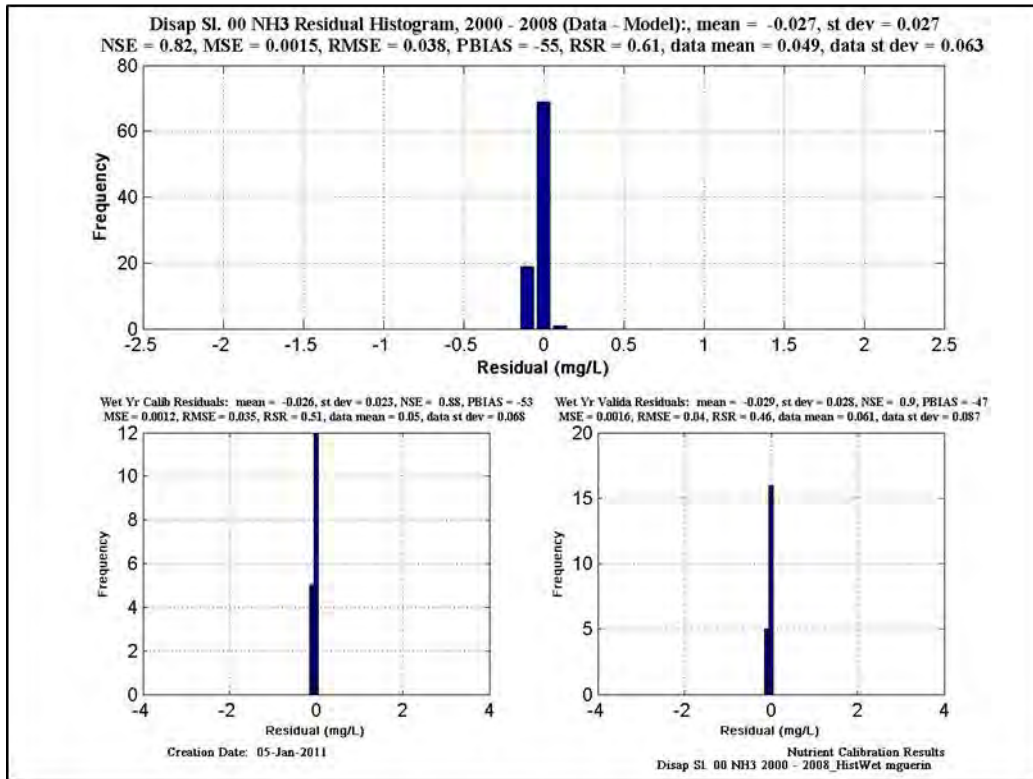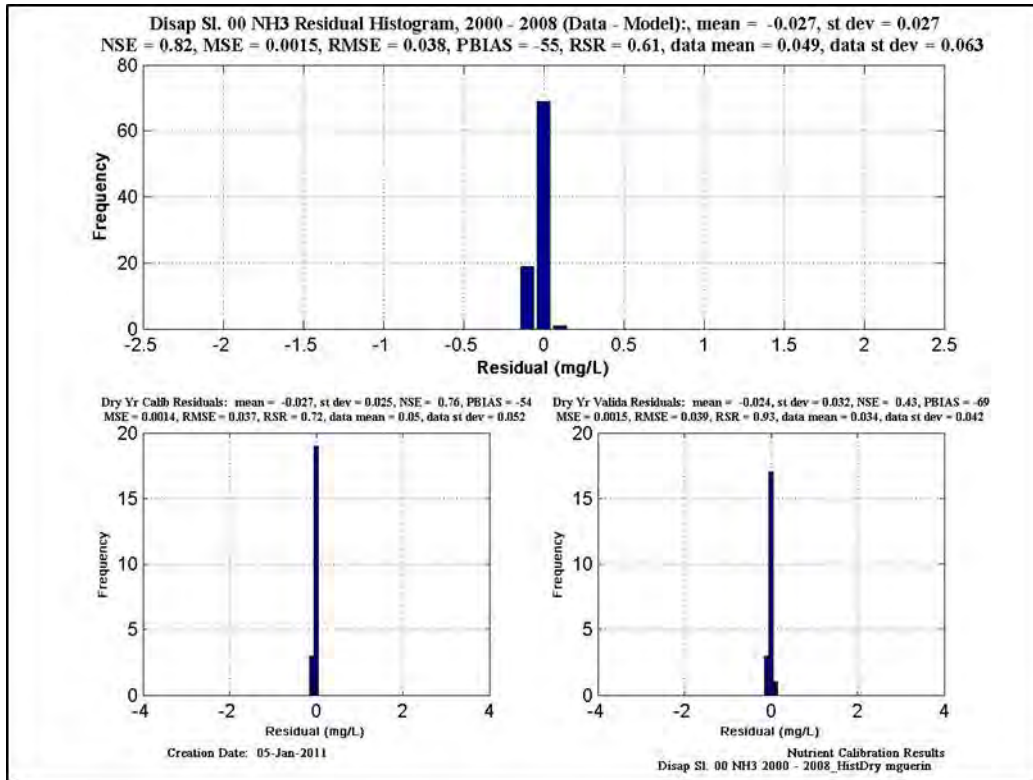
Figure 11-41 Calibration/validation statistics for NH3 at Disappointment Sl. Upper figure is calibration & validation statistics for dry years; lower figure is calibration & validation statistics for wet years.

336
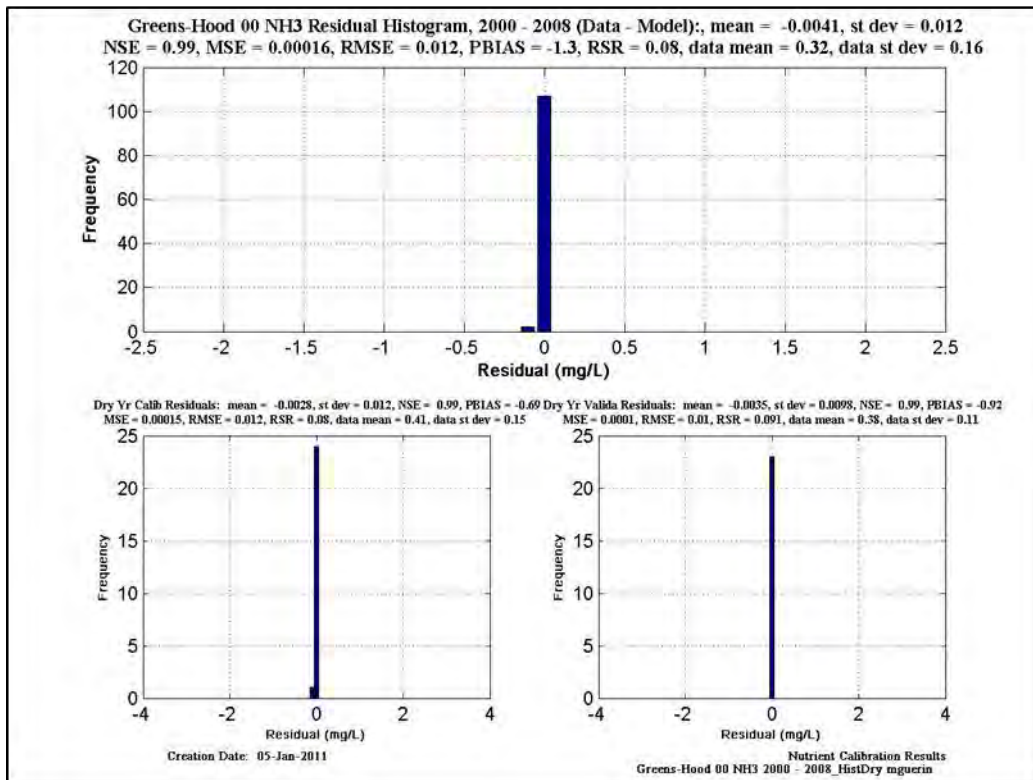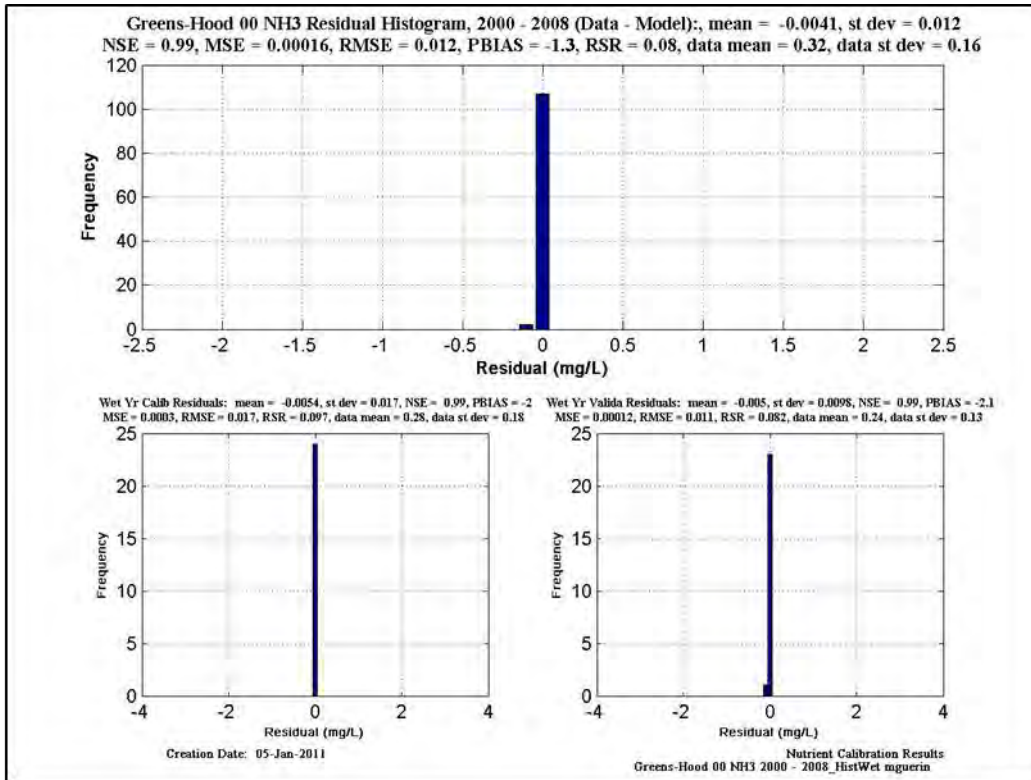
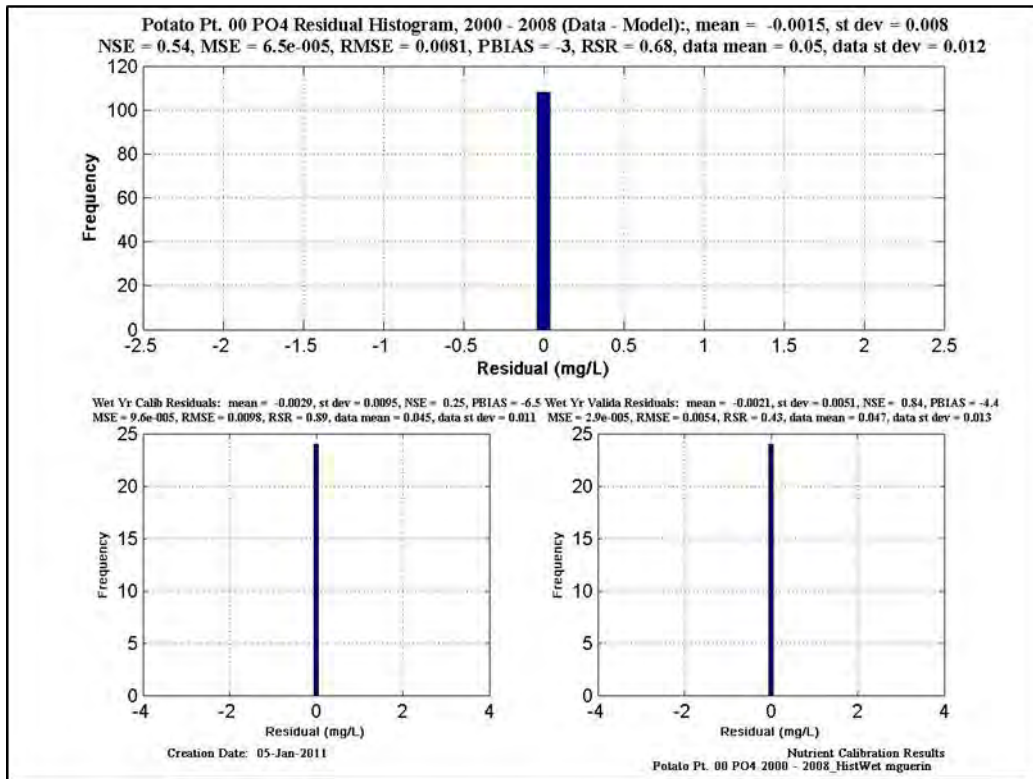**Figure 11-42 Calibration/validation statistics for NH3 at Greens-Hood. Upper figure is calibration & validation statistics for dry years; lower figure is calibration & validation statistics for wet years.**
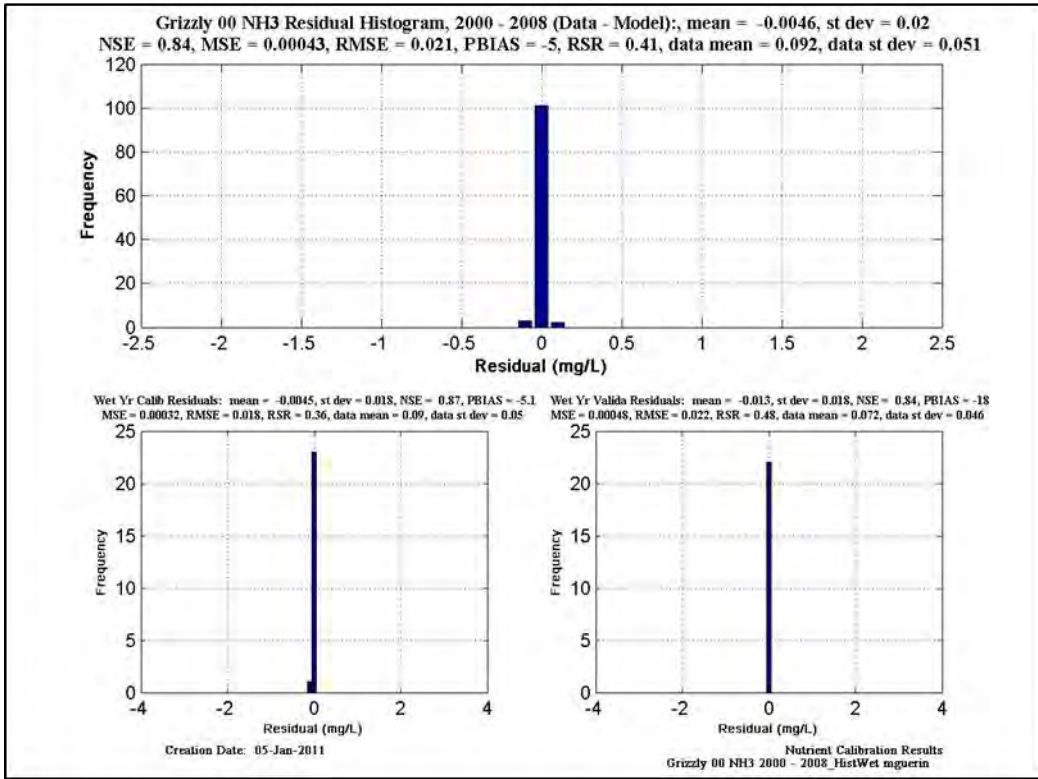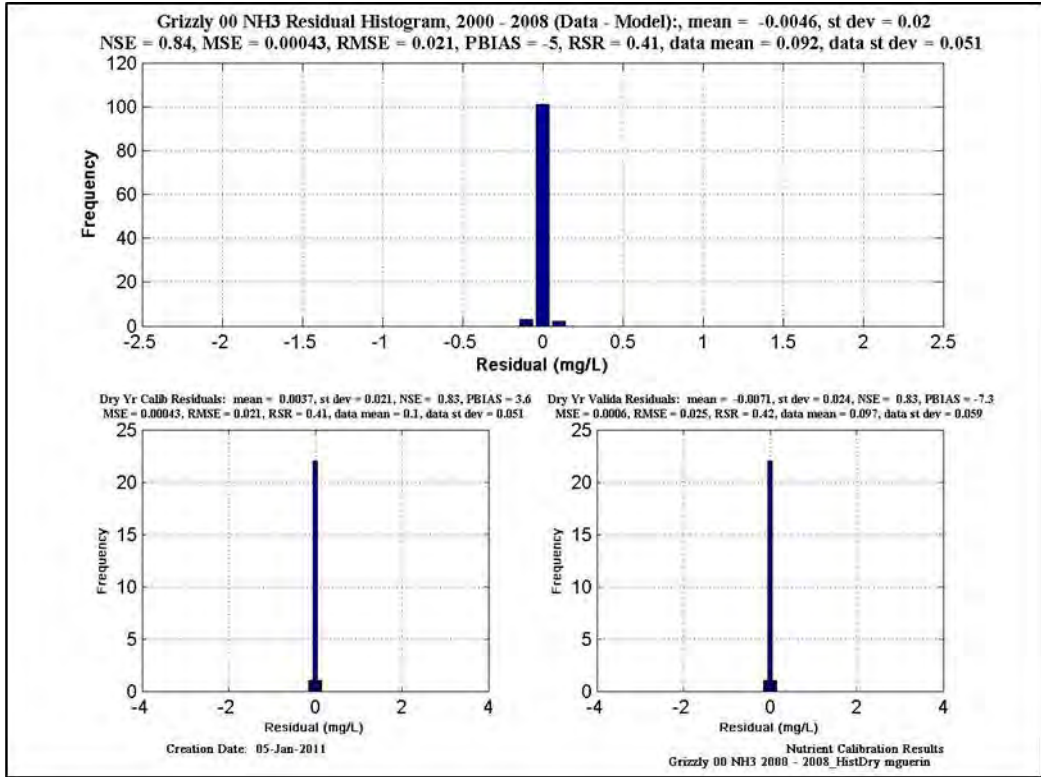
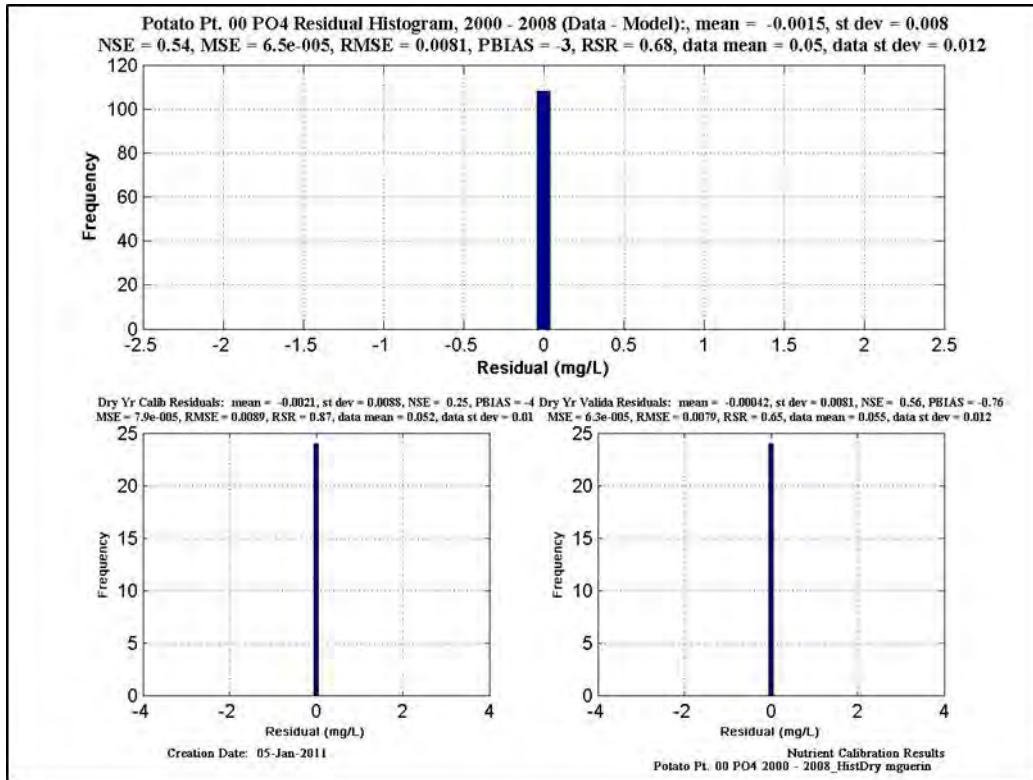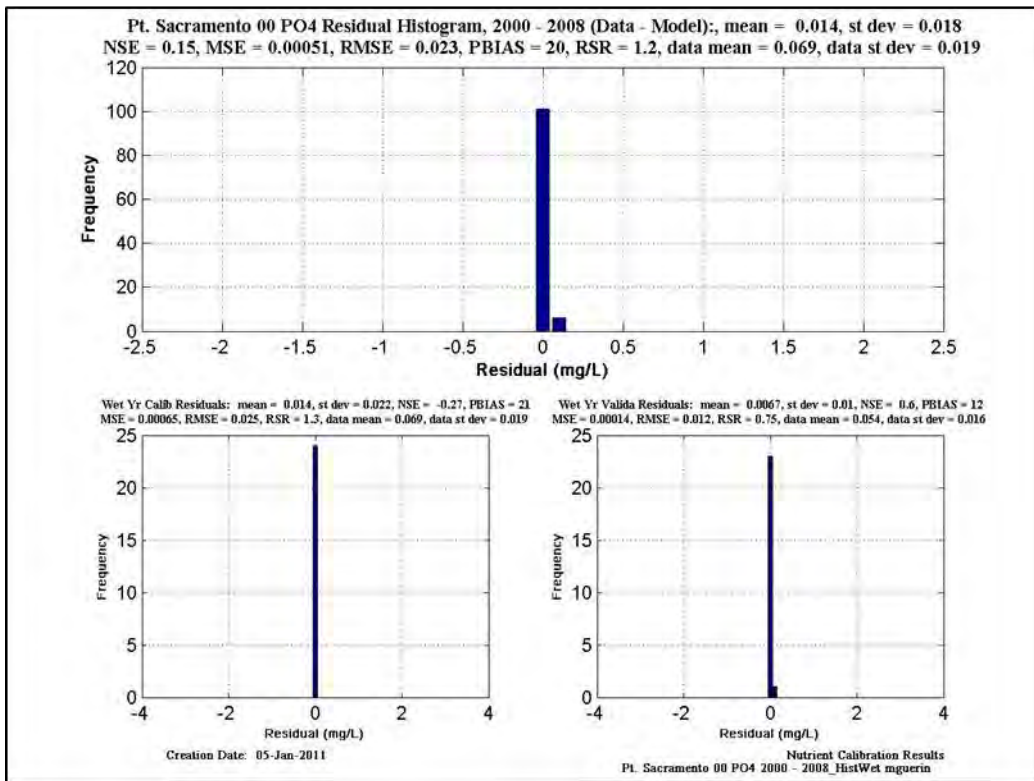**Figure 11-43 Calibration/validation statistics for NH3 at Grizzly. Upper figure is calibration & validation statistics for dry years; lower figure is calibration & validation statistics for wet years.**
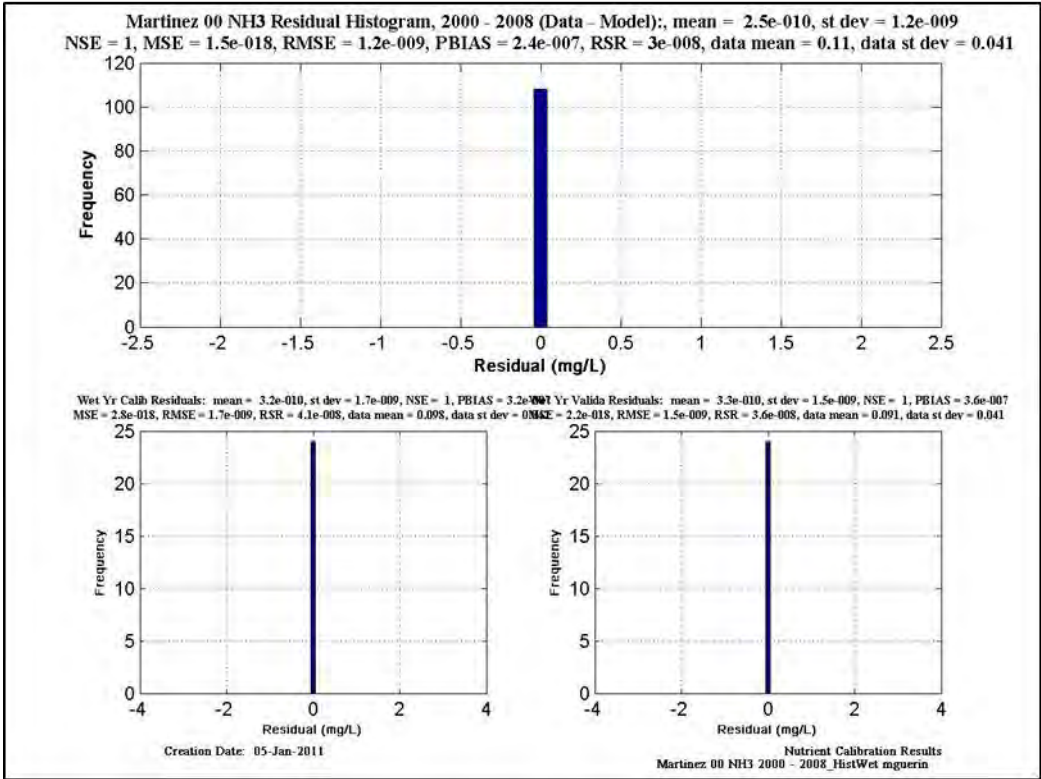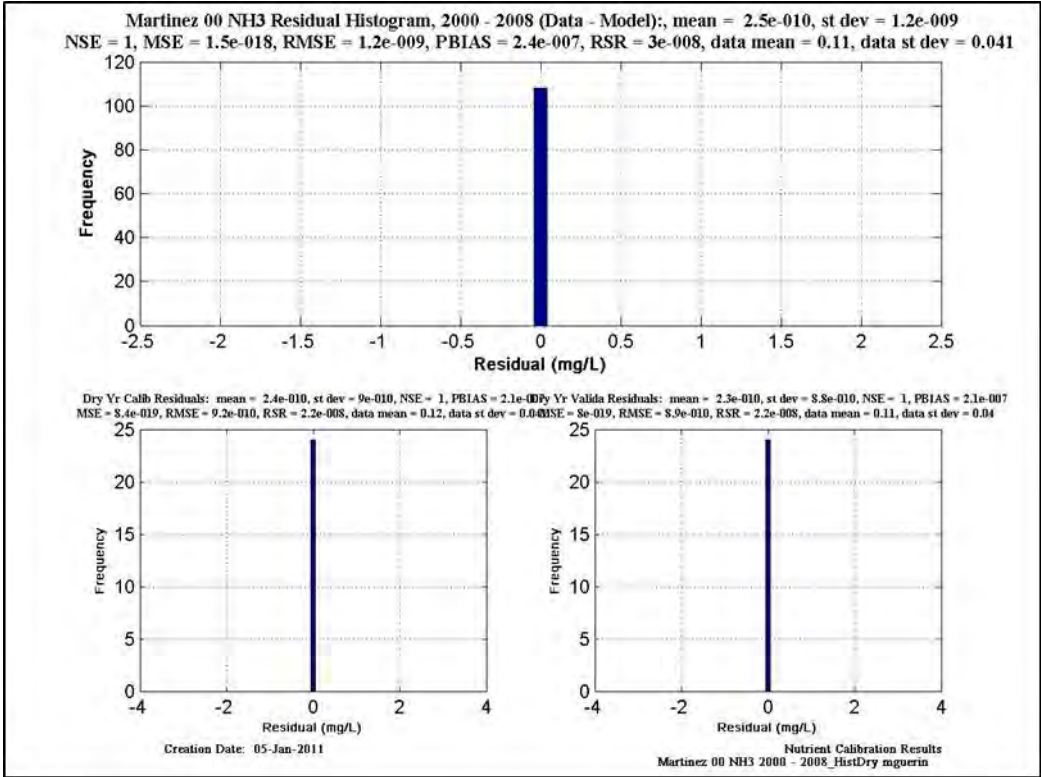
Figure 11-44 Calibration/validation statistics for NH3 at Martinez. Upper figure is calibration & validation statistics for dry years; lower figure is calibration & validation statistics for wet years.
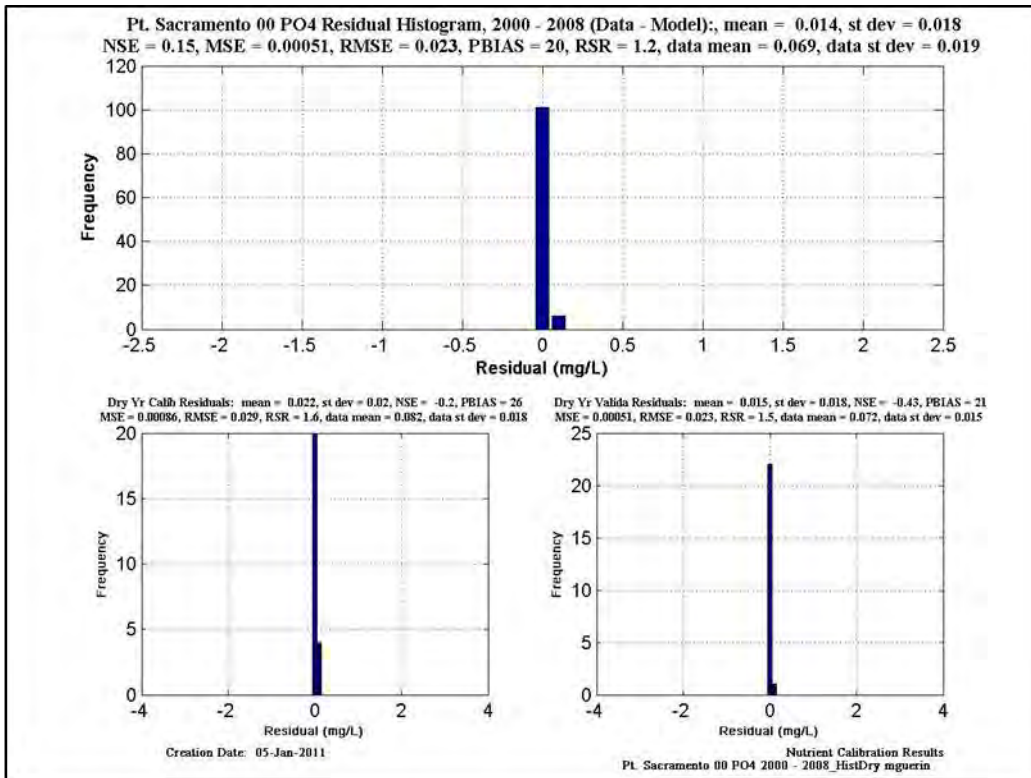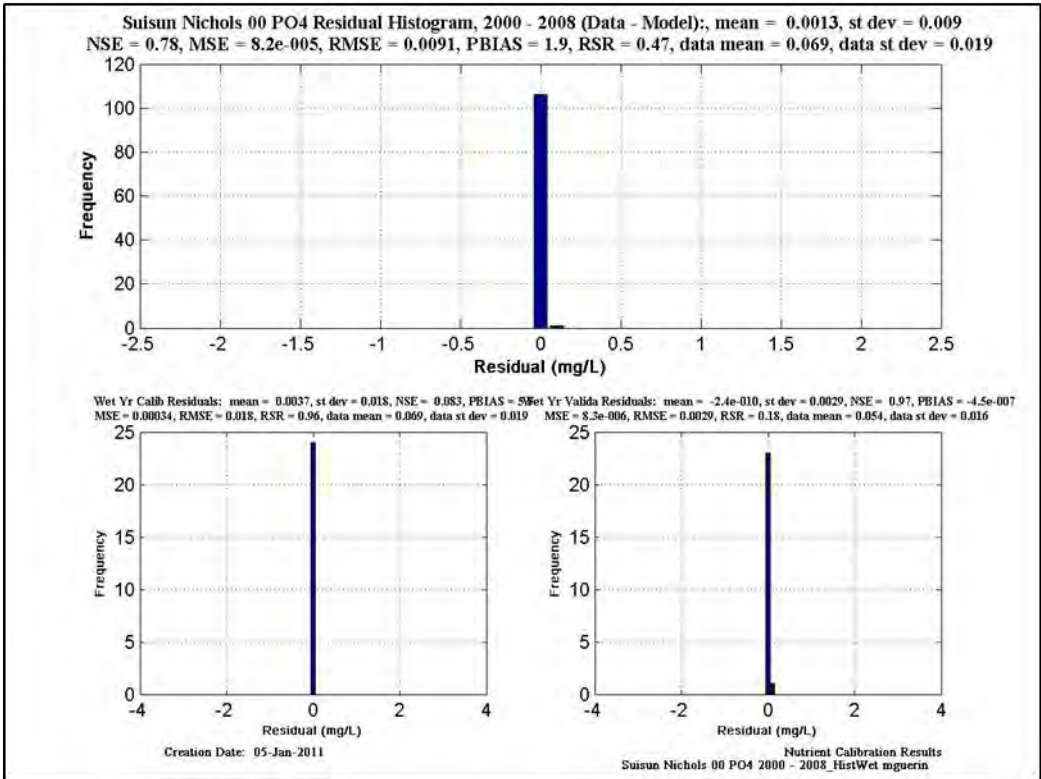
339
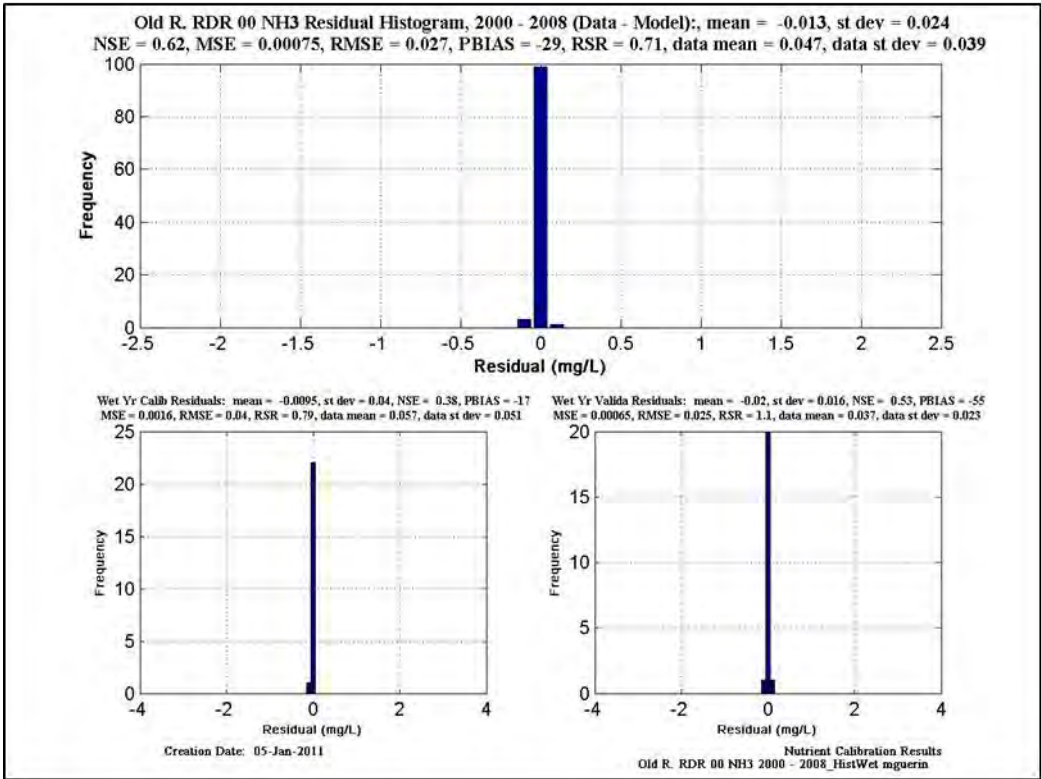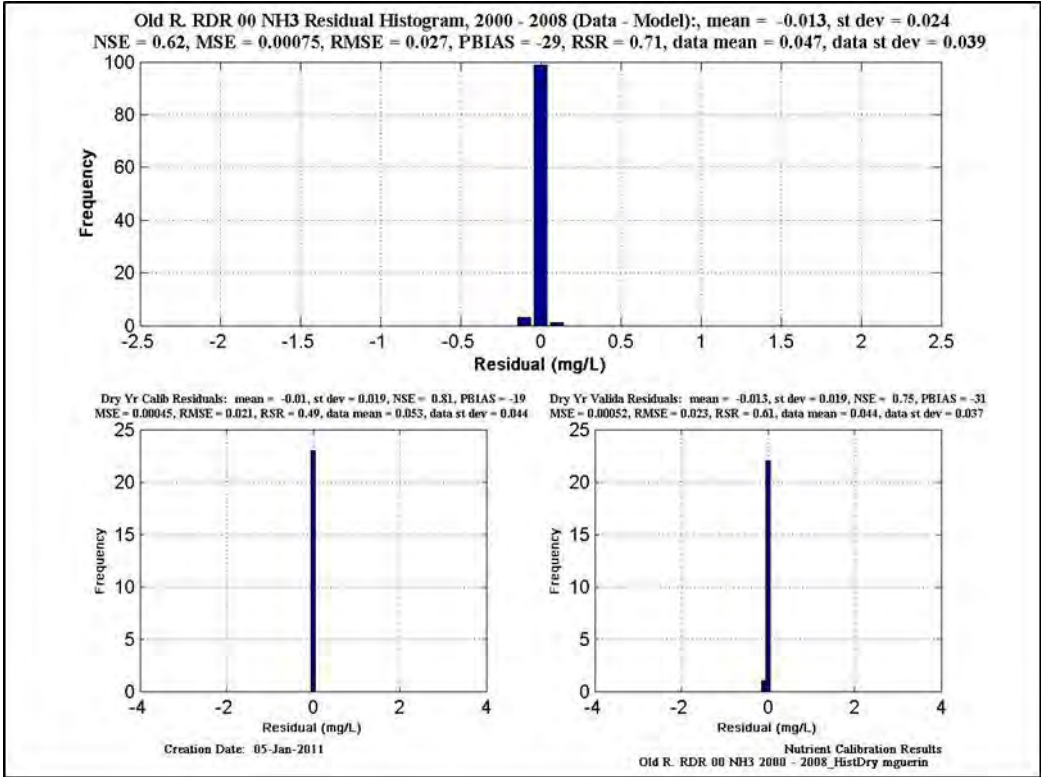
Figure 11-45 Calibration/validation statistics for NH3 at Buckley Cove. Upper figure is calibration & validation statistics for dry years; lower figure is calibration & validation statistics for wet years.
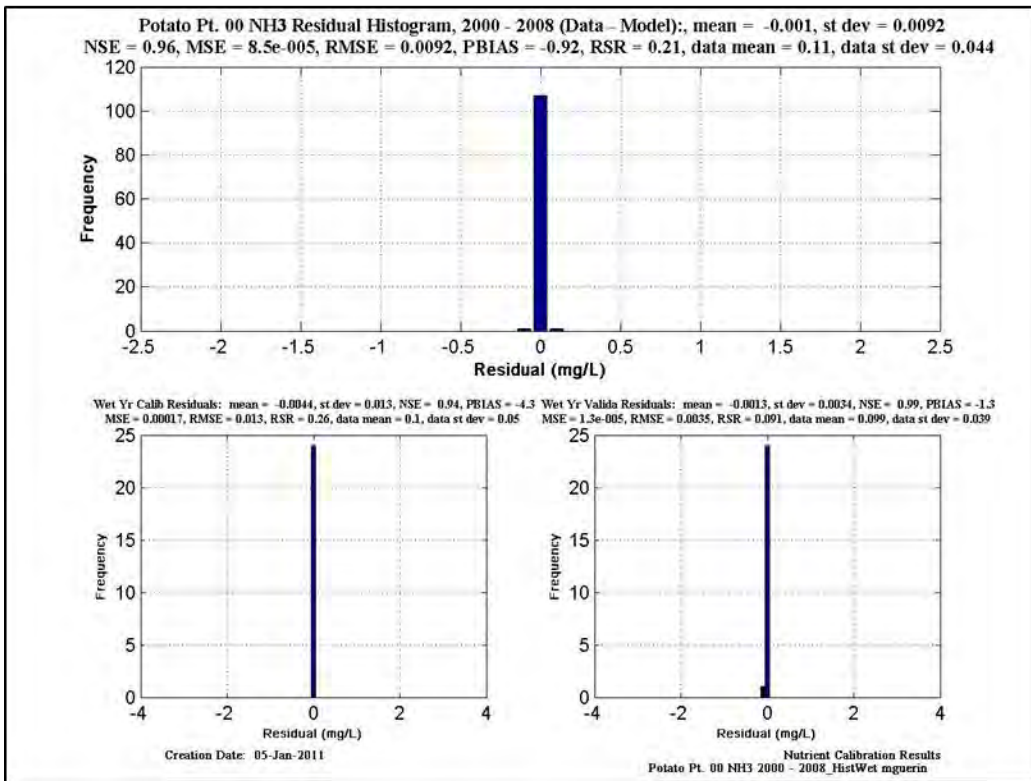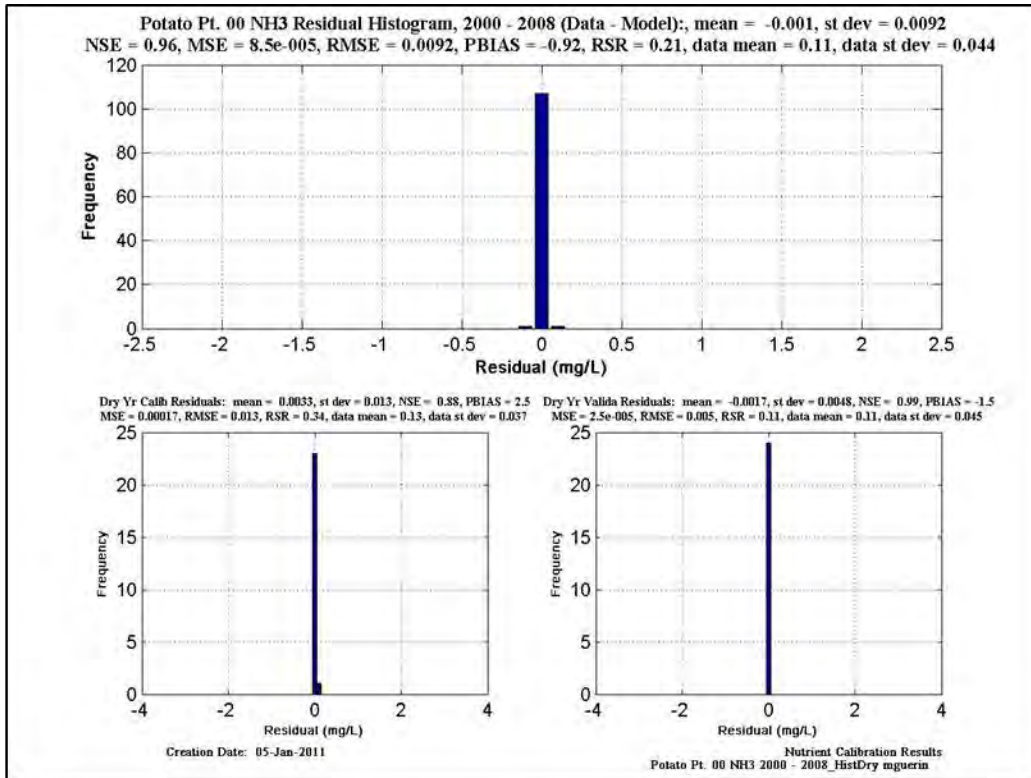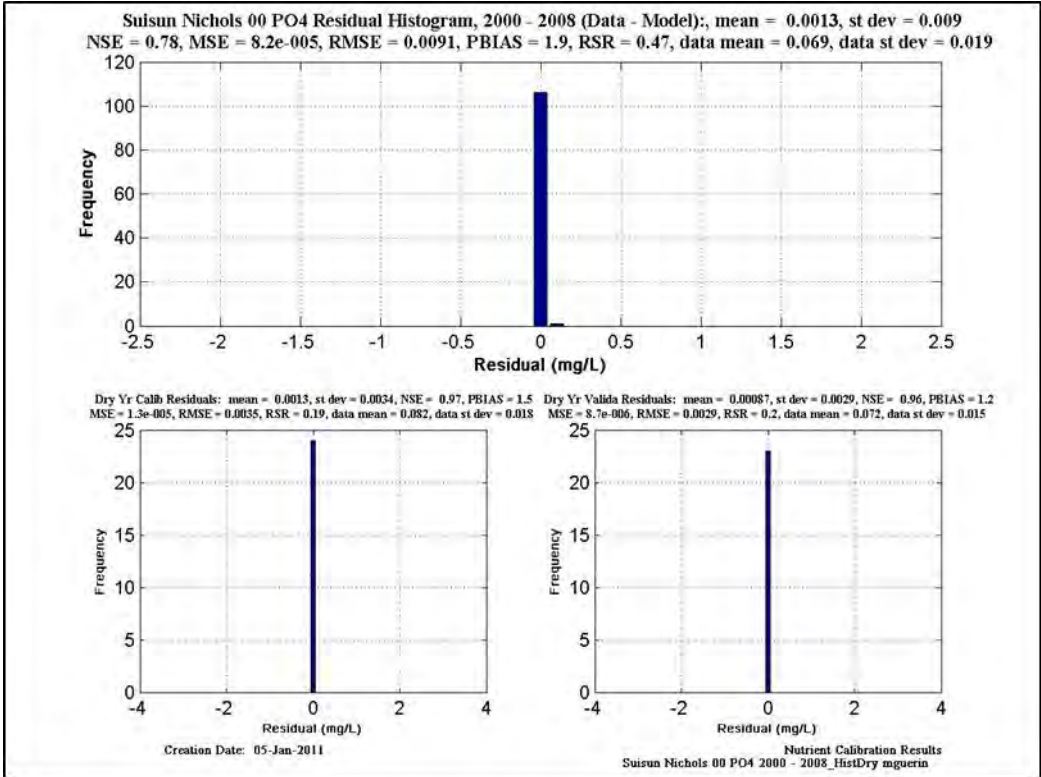
Figure 11-46 Calibration/validation statistics for NH3 at Potato Pt. Upper figure is calibration & validation statistics for dry years; lower figure is calibration & validation statistics for wet years.

341
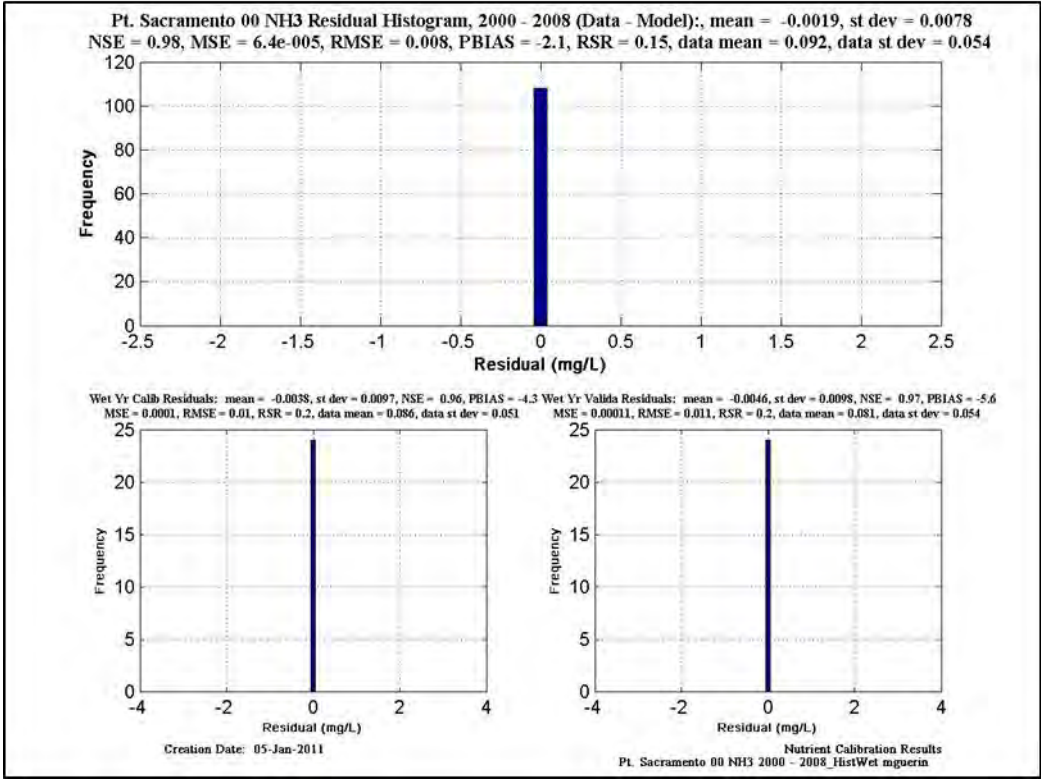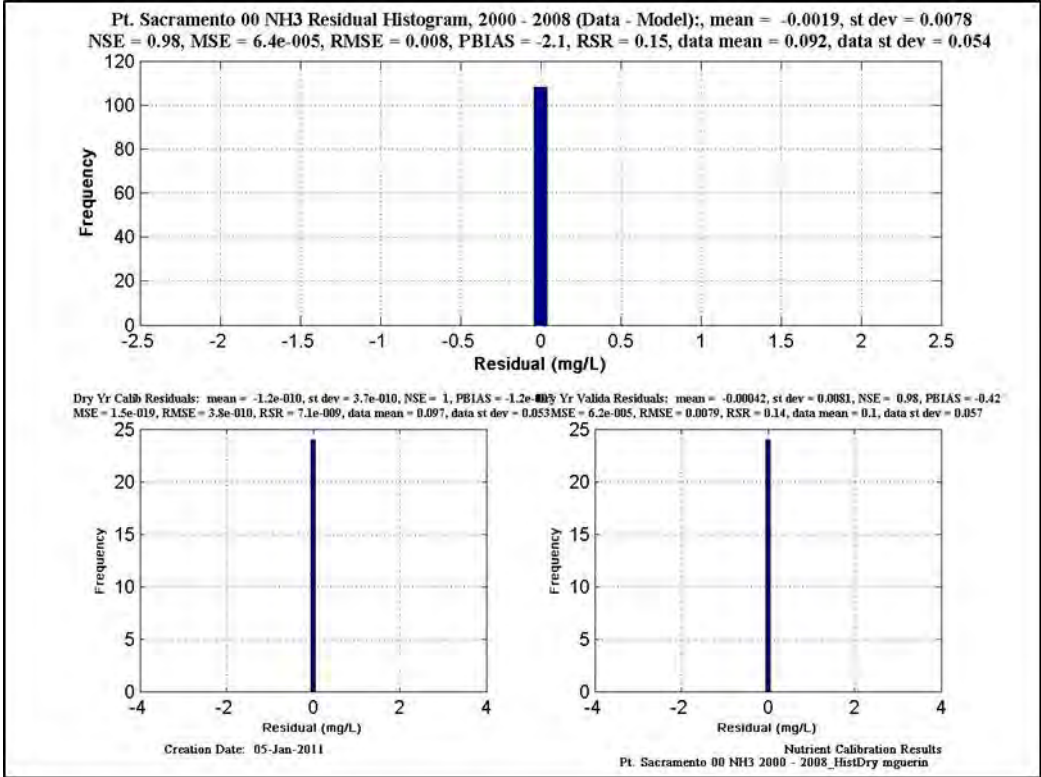
Figure 11-47 Calibration/validation statistics for NH3 at Pt. Sacramento. Upper figure is calibration & validation statistics for dry years; lower figure is calibration & validation statistics for wet years.
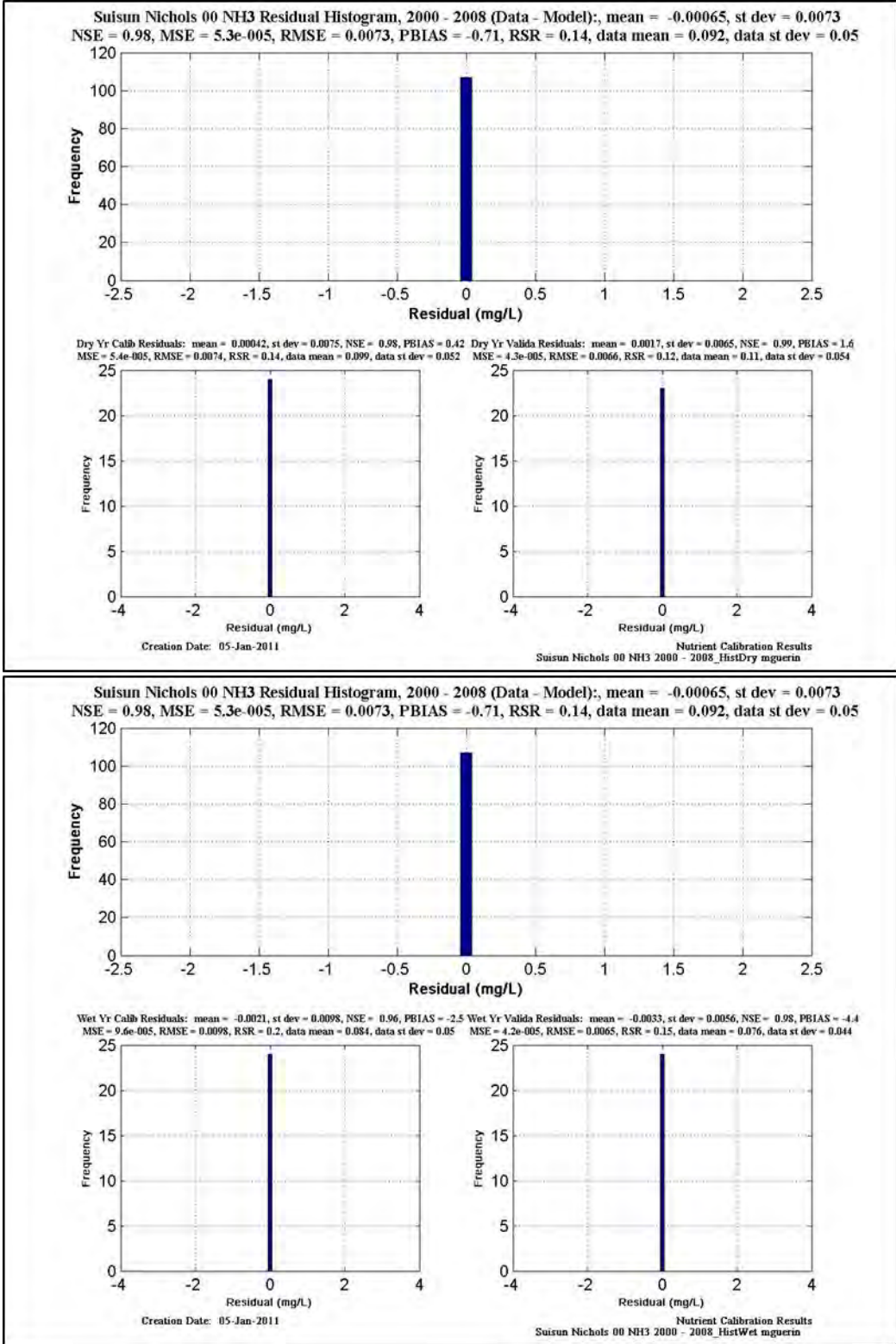
Figure 11-48 Calibration/validation statistics for NH3 at Suisun Nichols. Upper figure is calibration & validation statistics for dry years; lower figure is calibration & validation statistics for wet years.

343
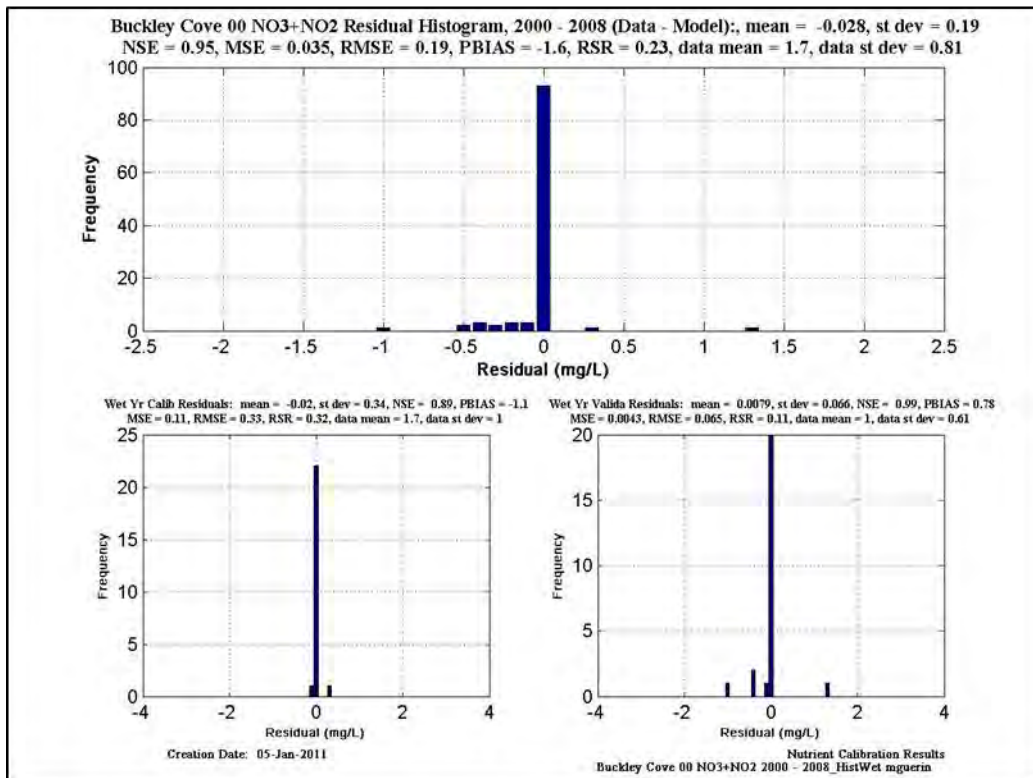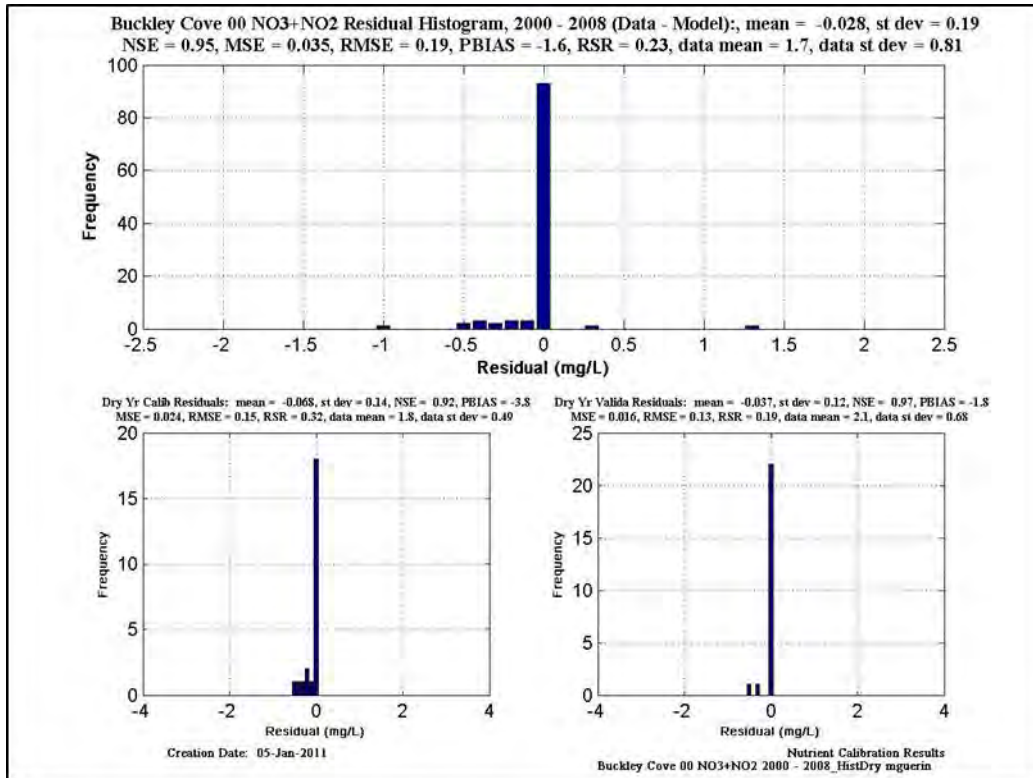
Figure 11-49 Calibration/validation statistics for NO3+NO3 at Buckley Cove. Upper figure is calibration & validation statistics for dry years; lower figure is calibration & validation statistics for wet years.
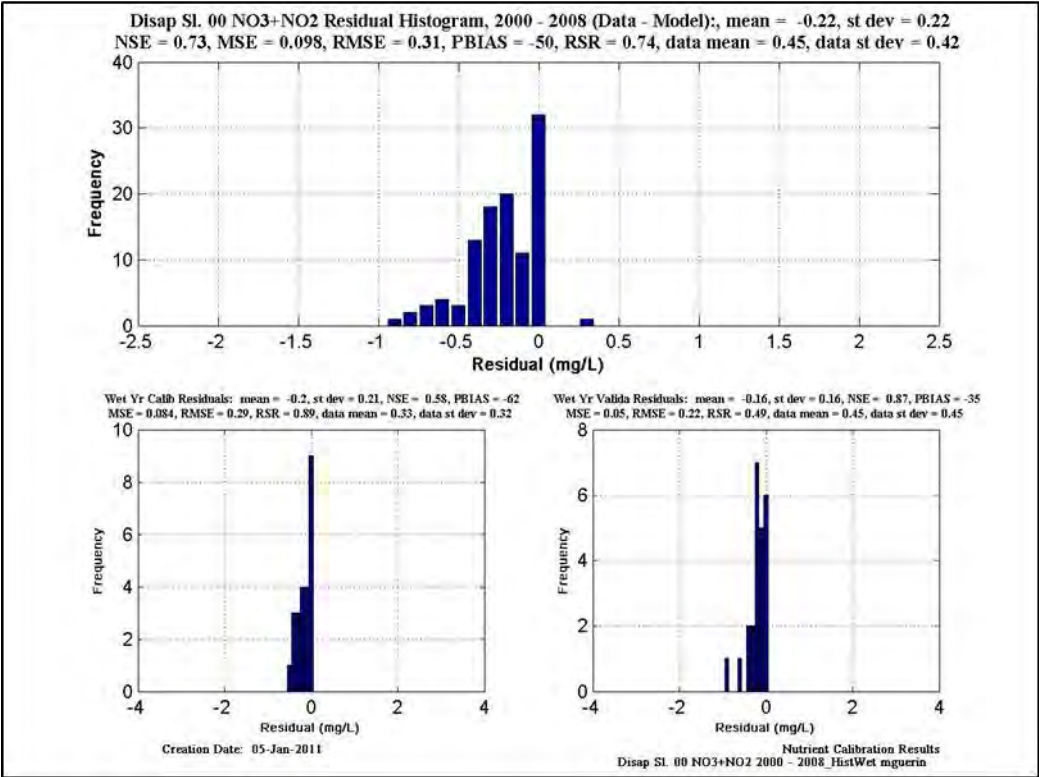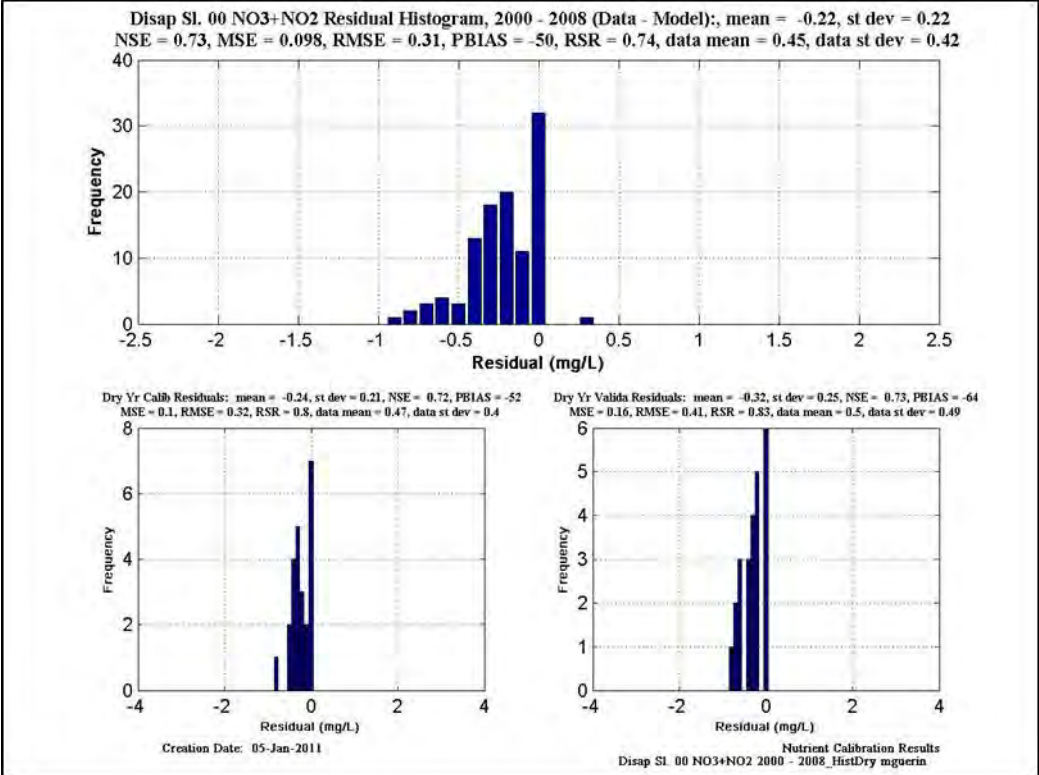
Figure 11-50 Calibration/validation statistics for NO3+NO3 at Disappointment Sl. Upper figure is calibration & validation statistics for dry years; lower figure is calibration & validation statistics for wet years.

345
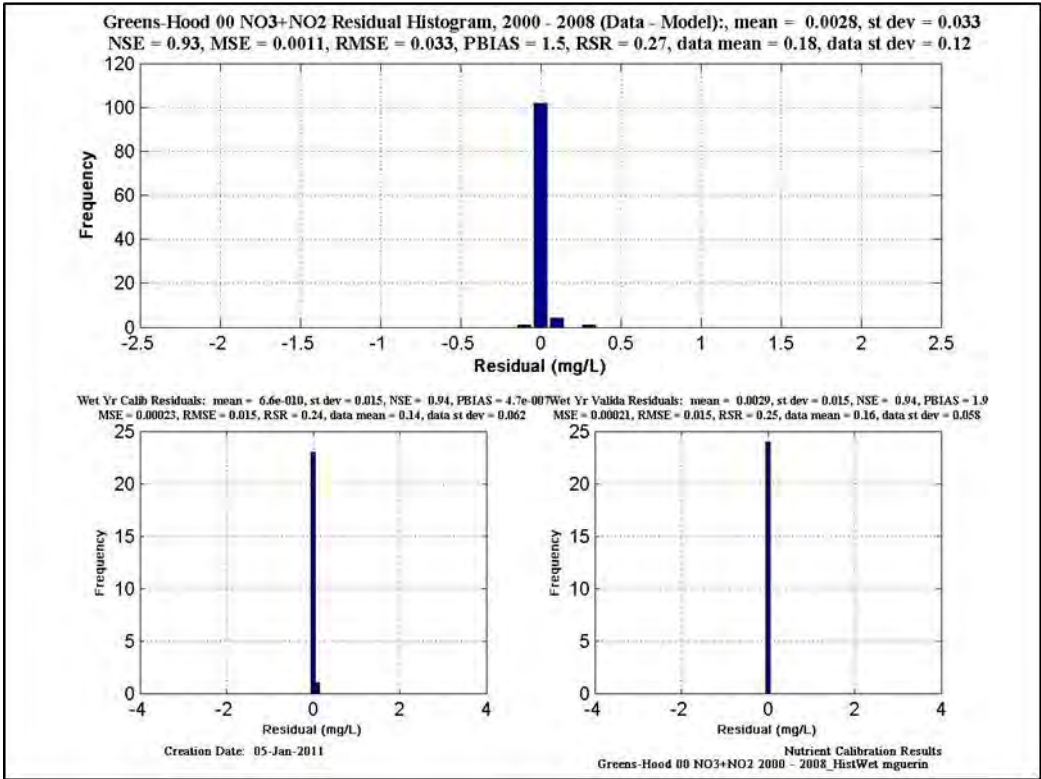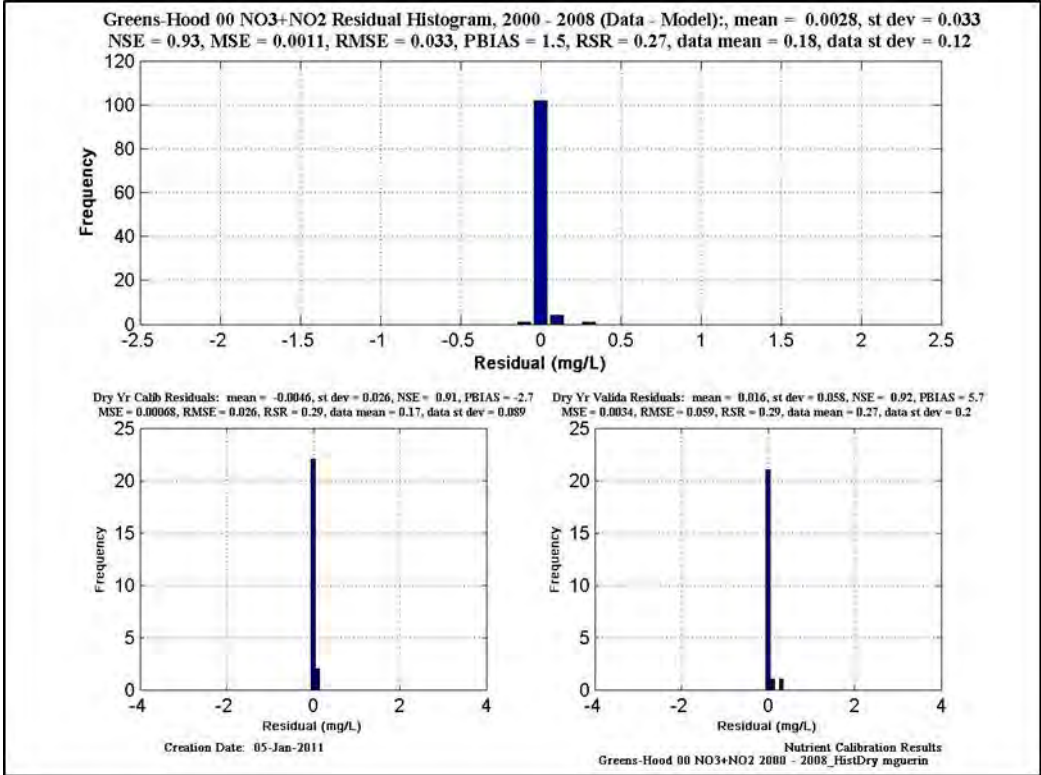
Figure 11-51 Calibration/validation statistics for NO3+NO3 at Greens-Hood. Upper figure is calibration & validation statistics for dry years; lower figure is calibration & validation statistics for wet years.
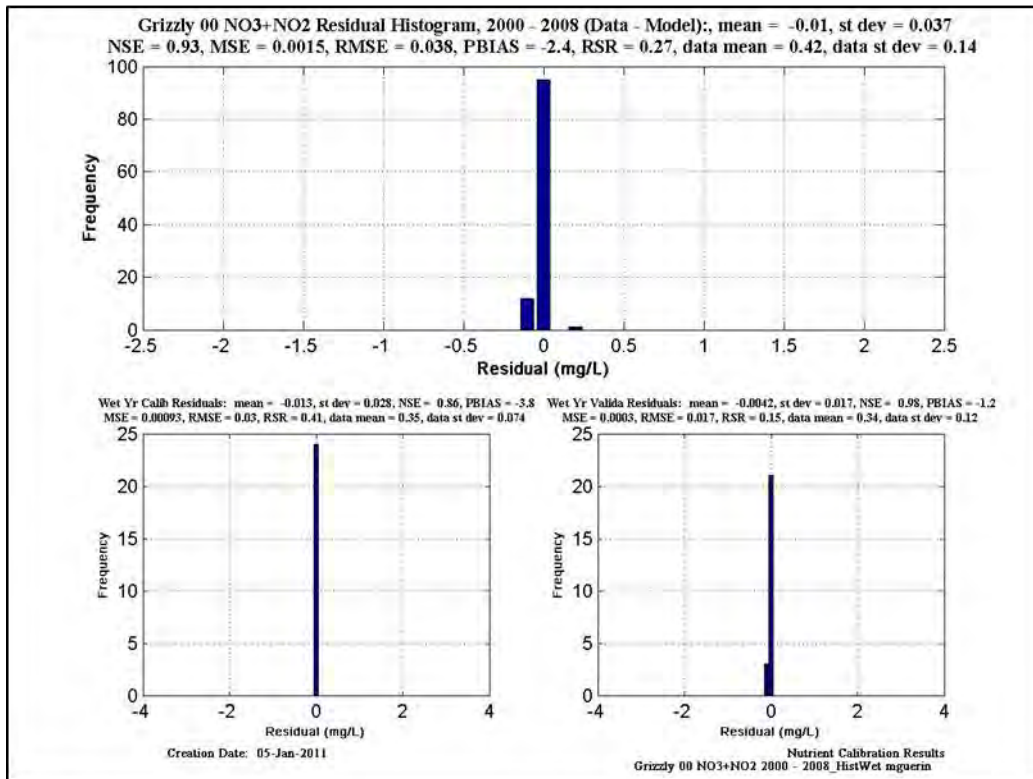
Figure 11-52 Calibration/validation statistics for NO3+NO3 at Grizzly. Upper figure is calibration & validation statistics for dry years; lower figure is calibration & validation statistics for wet years.

347

Figure 11-53 Calibration/validation statistics for NO3+NO3 at Martinez. Upper figure is calibration & validation statistics for dry years; lower figure is calibration & validation statistics for wet years.

348

Figure 11-54 Calibration/validation statistics for NO3+NO3 at Old R. RDR. Upper figure is calibration & validation statistics for dry years; lower figure is calibration & validation statistics for wet years.

Figure 11-55 Calibration/validation statistics for NO3+NO3 at Potato Pt. Upper figure is calibration & validation statistics for dry years; lower figure is calibration & validation statistics for wet years.

Figure 11-56 Calibration/validation statistics for NO3+NO3 at Pt. Sacramento. Upper figure is calibration & validation statistics for dry years; lower figure is calibration & validation statistics for wet years.

351

Figure 11-57 Calibration/validation statistics for NO3+NO3 at Rio Vista. Upper figure is calibration & validation statistics for dry years; lower figure is calibration & validation statistics for wet years.

Figure 11-58 Calibration/validation statistics for NO3+NO3 at Roe Isle. Upper figure is calibration & validation statistics for dry years; lower figure is calibration & validation statistics for wet years.

353

Figure 11-59 Calibration/validation statistics for NO3+NO3 at RSAC077. Upper figure is calibration & validation statistics for dry years; lower figure is calibration & validation statistics for wet years.

Figure 11-60 Calibration/validation statistics for NO3+NO3 at Suisun Nichols. Upper figure is calibration & validation statistics for dry years; lower figure is calibration & validation statistics for wet years.

Figure 11-61 Calibration/validation statistics for Organic N at Buckley Cove. Upper figure is calibration & validation statistics for dry years; lower figure is calibration & validation statistics for wet years.

Figure 11-62 Calibration/validation statistics for Organic N at Disappointment Sl. Upper figure is calibration & validation statistics for dry years; lower figure is calibration & validation statistics for wet years.

Figure 11-63 Calibration/validation statistics for Organic N at Greens-Hood. Upper figure is calibration & validation statistics for dry years; lower figure is calibration & validation statistics for wet years.

Figure 11-64 Calibration/validation statistics for Organic N at Grizzly. Upper figure is calibration & validation statistics for dry years; lower figure is calibration & validation statistics for wet years.

359

Figure 11-65 Calibration/validation statistics for Organic N at Martinez. Upper figure is calibration & validation statistics for dry years; lower figure is calibration & validation statistics for wet years.

360

Figure 11-66 Calibration/validation statistics for Organic N at Old R. RDR. Upper figure is calibration & validation statistics for dry years; lower figure is calibration & validation statistics for wet years.

Figure 11-67 Calibration/validation statistics for Organic N at Potato Pt. Upper figure is calibration & validation statistics for dry years; lower figure is calibration & validation statistics for wet years.

Figure 11-68 Calibration/validation statistics for Organic N at Pt. Sacramento. Upper figure is calibration & validation statistics for dry years; lower figure is calibration & validation statistics for wet years.

Figure 11-69 Calibration/validation statistics for Organic N at Suisun Nichols. Upper figure is calibration & validation statistics for dry years; lower figure is calibration & validation statistics for wet years.

Figure 11-70 Calibration/validation statistics for PO4 at Buckley Cove. Upper figure is calibration & validation statistics for dry years; lower figure is calibration & validation statistics for wet years.

Figure 11-71 Calibration/validation statistics for PO4 at Disappointment Sl. Upper figure is calibration & validation statistics for dry years; lower figure is calibration & validation statistics for wet years.

Figure 11-72 Calibration/validation statistics for PO4 at Greens-Hood. Upper figure is calibration & validation statistics for dry years; lower figure is calibration & validation statistics for wet years.

Figure 11-73 Calibration/validation statistics for PO4 at Grizzly. Upper figure is calibration & validation statistics for dry years; lower figure is calibration & validation statistics for wet years.

Figure 11-74 Calibration/validation statistics for PO4 at Martinez. Upper figure is calibration & validation statistics for dry years; lower figure is calibration & validation statistics for wet years.

369

Figure 11-75 Calibration/validation statistics for PO4 at Old R. RDR. Upper figure is calibration & validation statistics for dry years; lower figure is calibration & validation statistics for wet years.

Figure 11-76 Calibration/validation statistics for PO4 at Potato Pt. Upper figure is calibration & validation statistics for dry years; lower figure is calibration & validation statistics for wet years.

371

Figure 11-77 Calibration/validation statistics for PO4 at Pt. Sacramento. Upper figure is calibration & validation statistics for dry years; lower figure is calibration & validation statistics for wet years.

372

Figure 11-78 Calibration/validation statistics for PO4 at Suisun Nichols. Upper figure is calibration & validation statistics for dry years; lower figure is calibration & validation statistics for wet years.

12.   Appendix V - Scenario Figures

Two scenarios were developed – in both the concentration of N-constituents in Sacramento Regional WTP was altered.

Algae Model Output
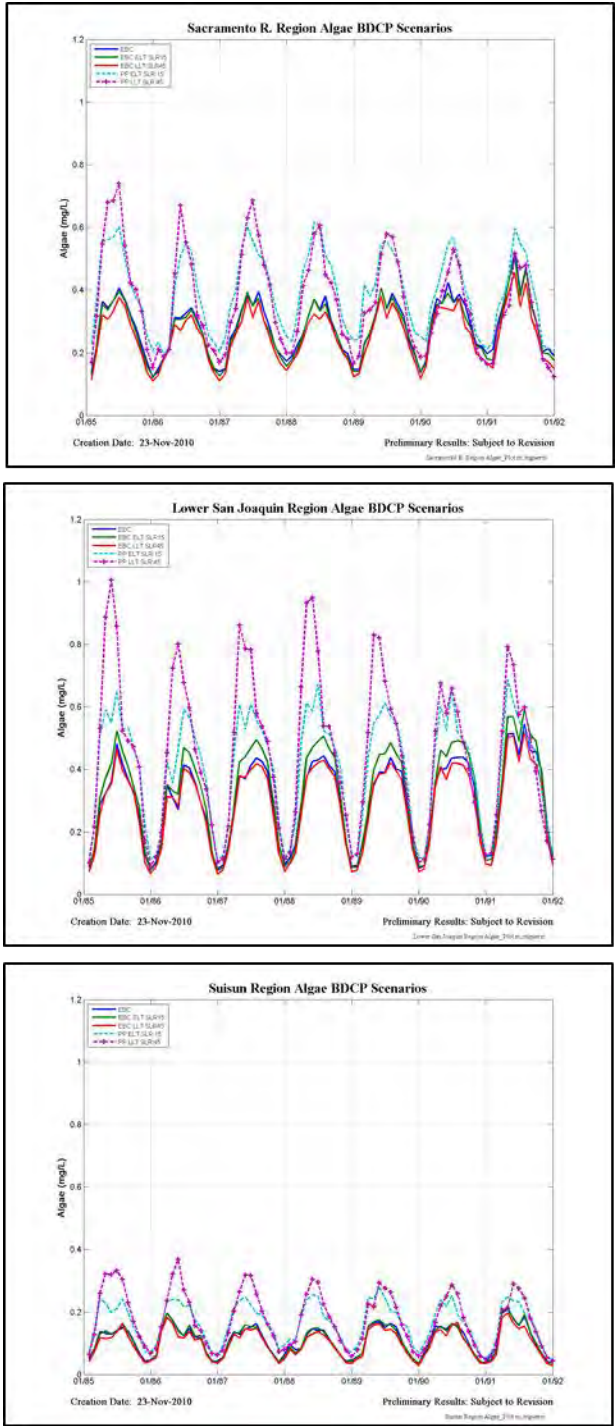
Figure 12-1Algae model output for the original five scenarios for each of the three analysis regions.
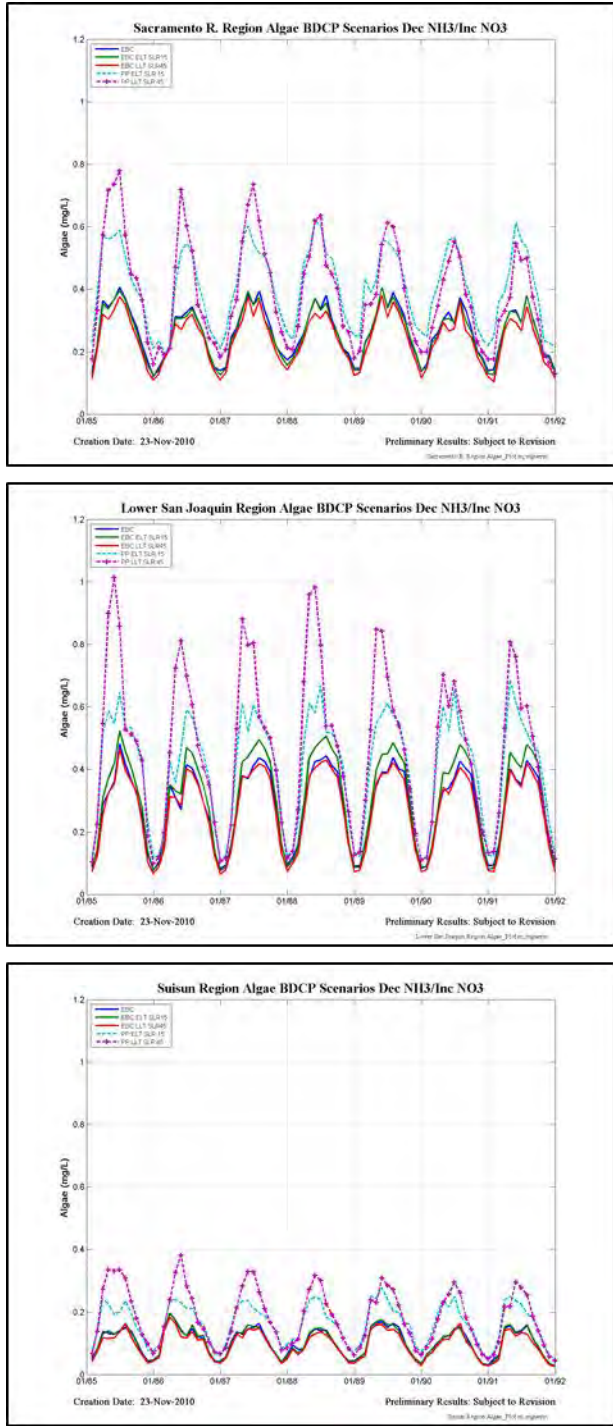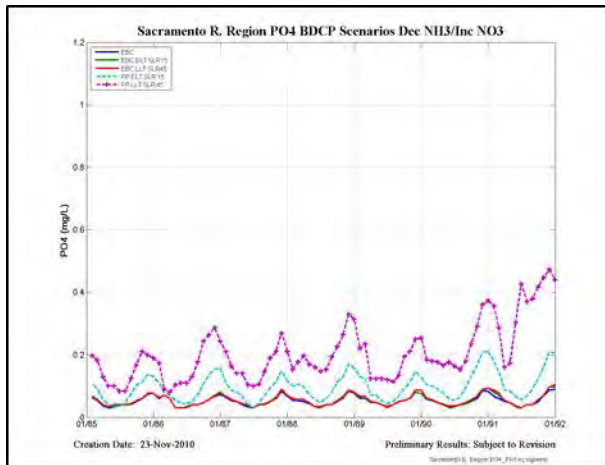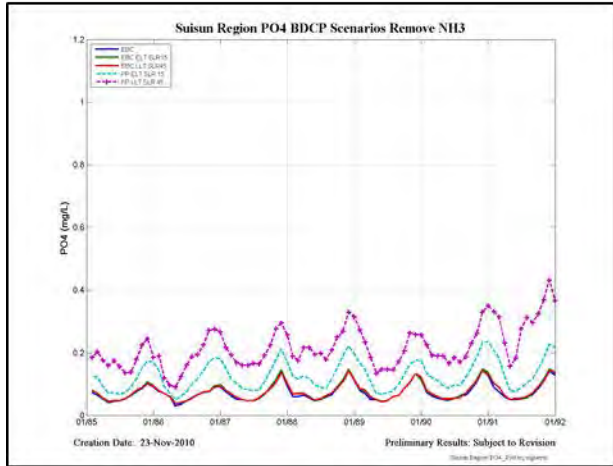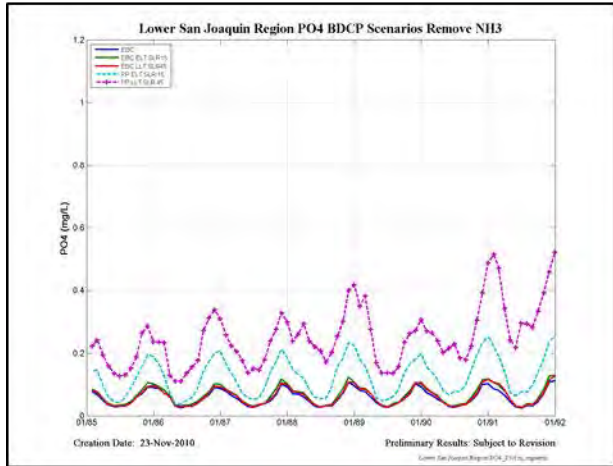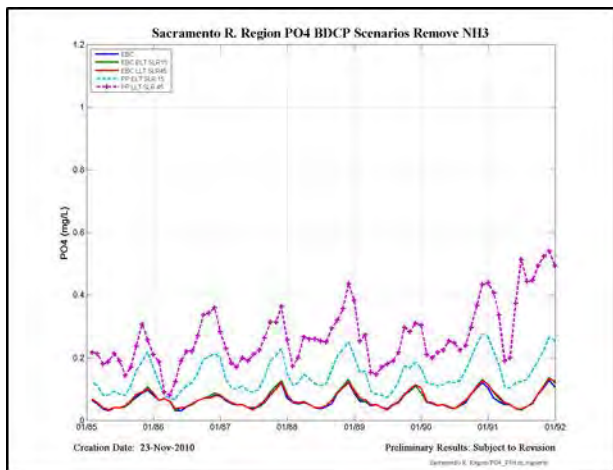
Figure 12-2 Algae model output for the five scenarios changing N-constituent concentrations (decreasing NH$_3$ and increasing NO$_3$) in Sacramento Regional WTP effluent for each of the three analysis regions.
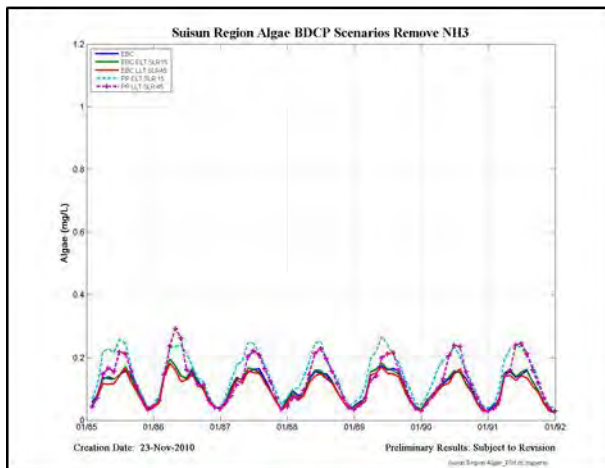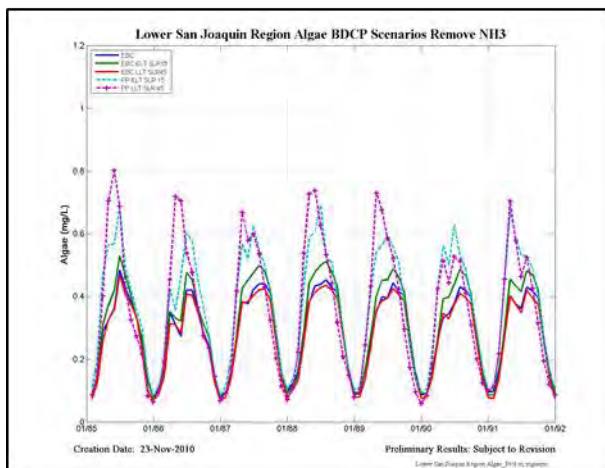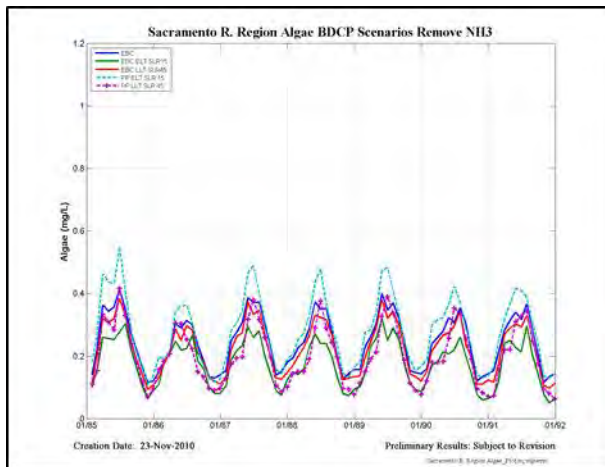
Figure 12-3 Algae model output for the five scenarios removing NH₃ from Sacramento Regional WTP effluent for each of the three analysis regions.

DO model output
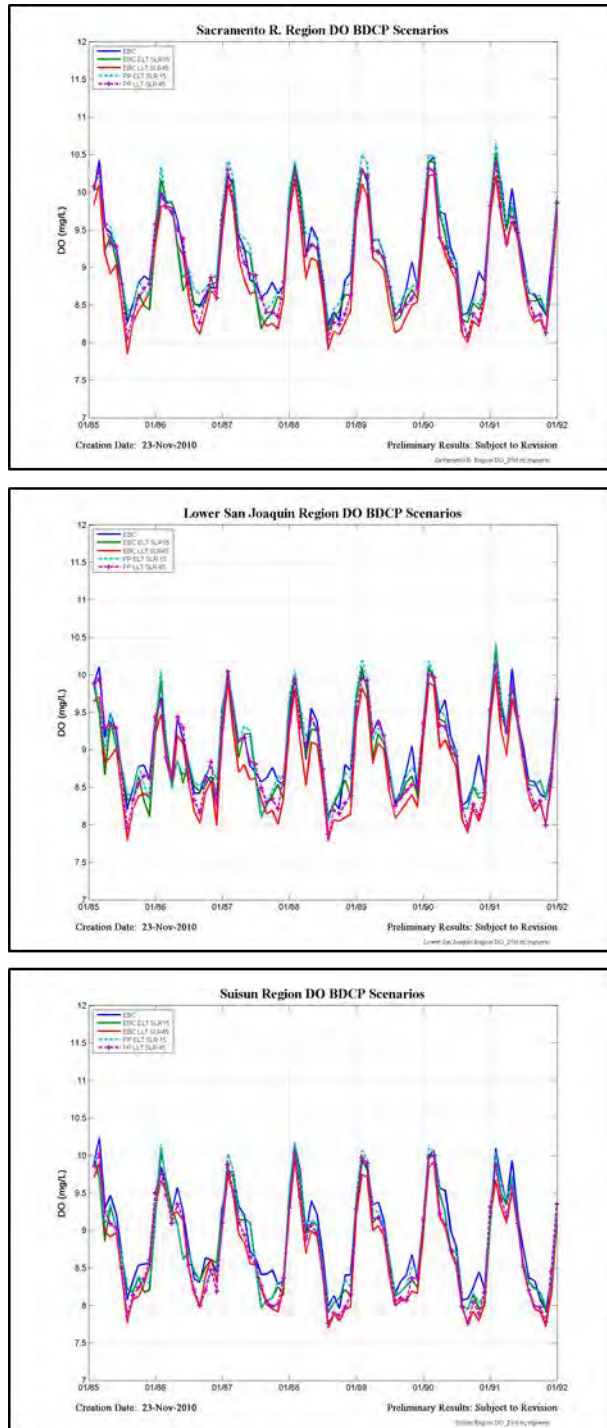
Figure 12-4 DO model output for the original five scenarios for each of the three analysis regions.
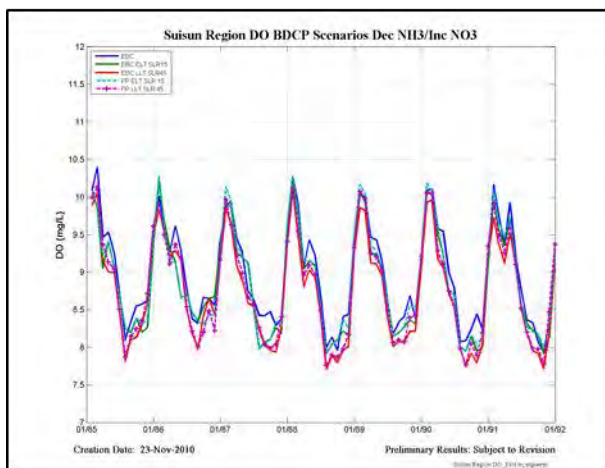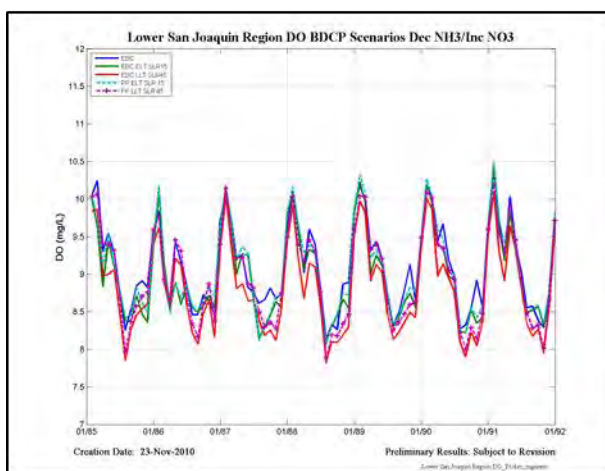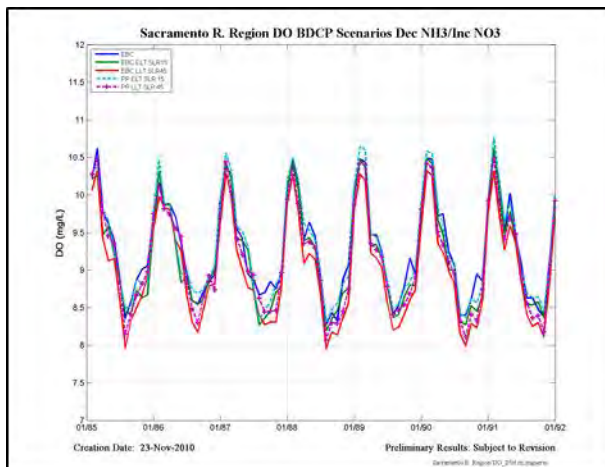
Figure 12-5 DO model output for the five scenarios changing N-constituent concentrations (decreasing NH$_3$ and increasing NO$_3$) in Sacramento Regional WTP effluent for each of the three analysis regions.
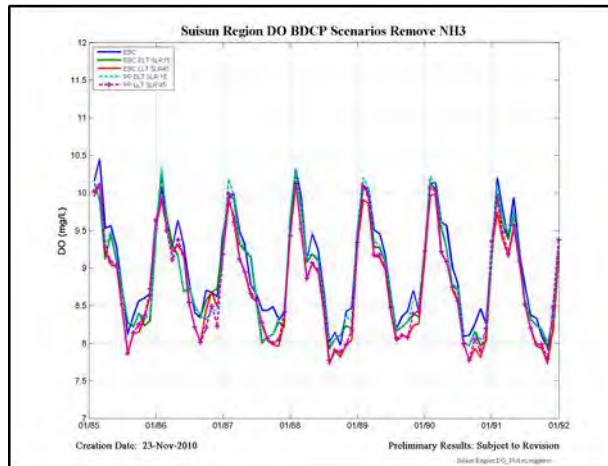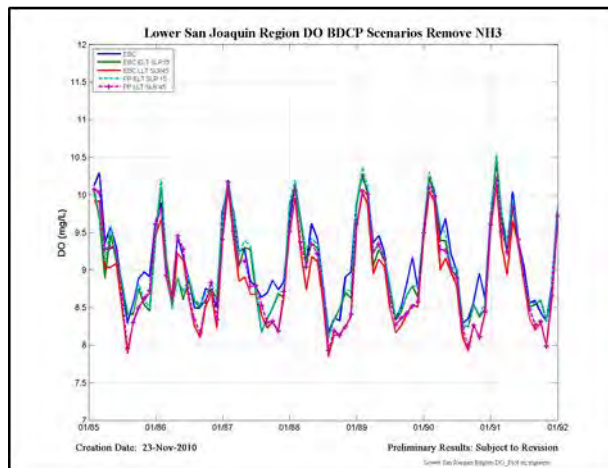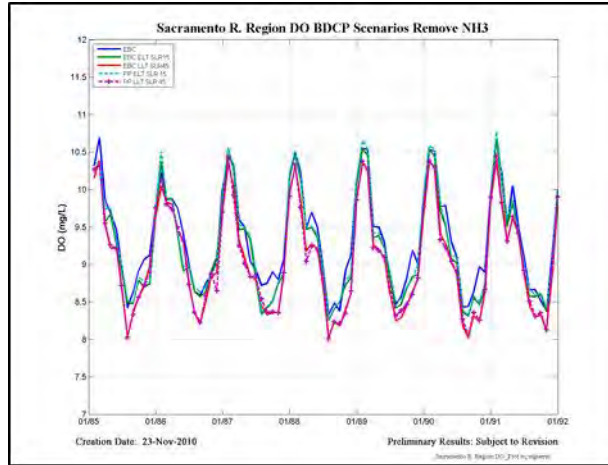
Figure 12-6 DO model output for the five scenarios removing NH₃ from Sacramento Regional WTP effluent for each of the three analysis regions.

NH₃ model output
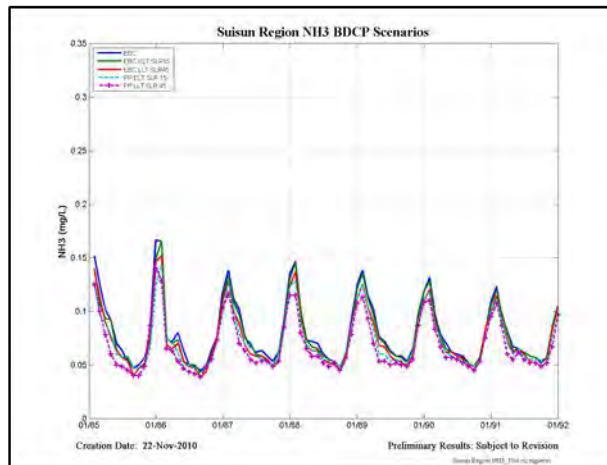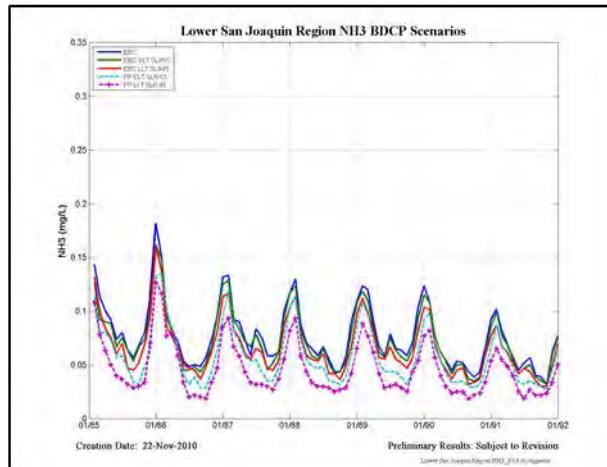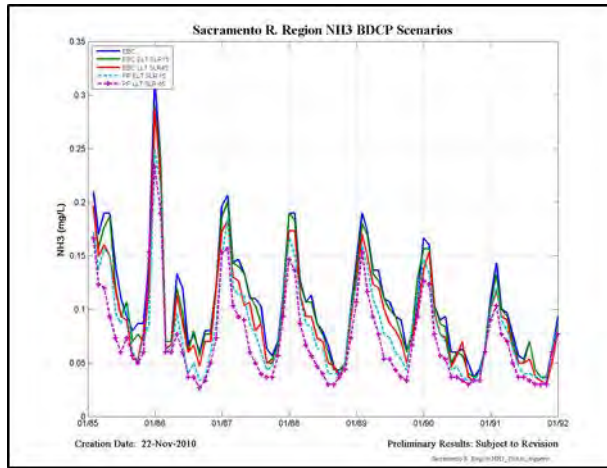
Figure 12-7 NH3 model output for the original five scenarios for each of the three analysis regions.
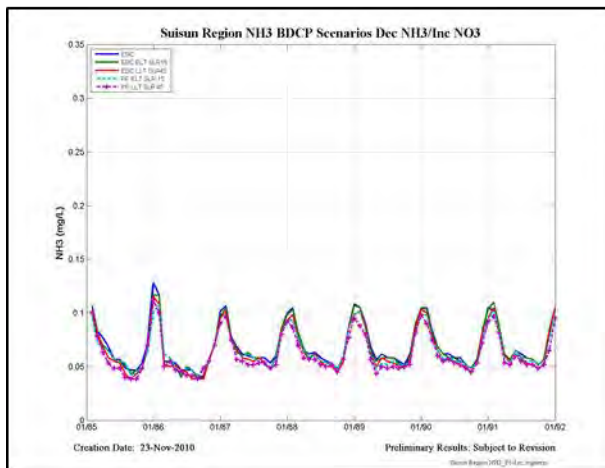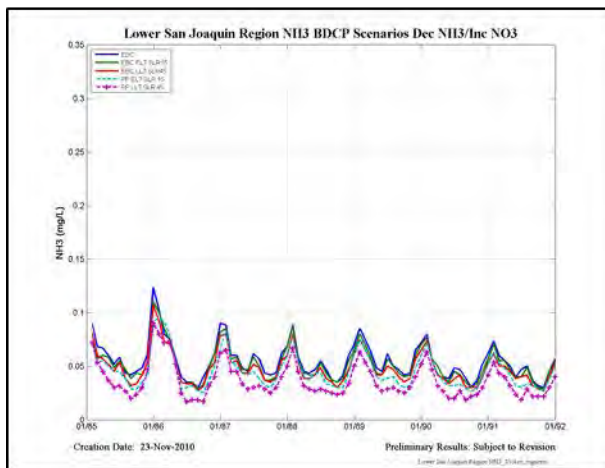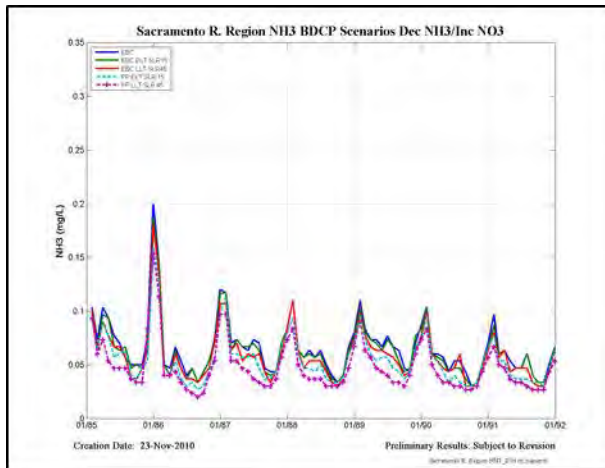
Figure 12-8 NH3 model output for the five scenarios changing N-constituent concentrations (decreasing NH$_3$ and increasing NO$_3$) in Sacramento Regional WTP effluent for each of the three analysis regions.

382
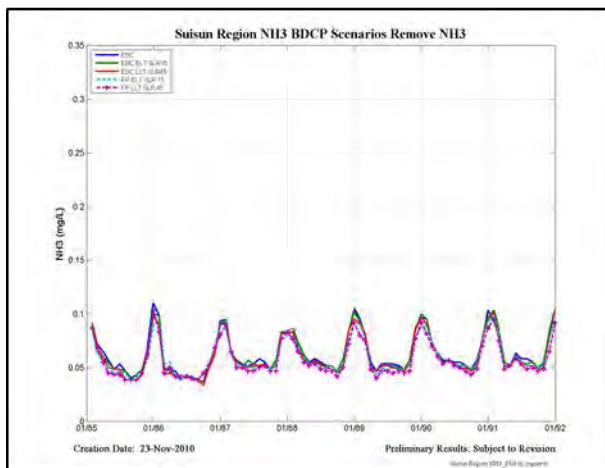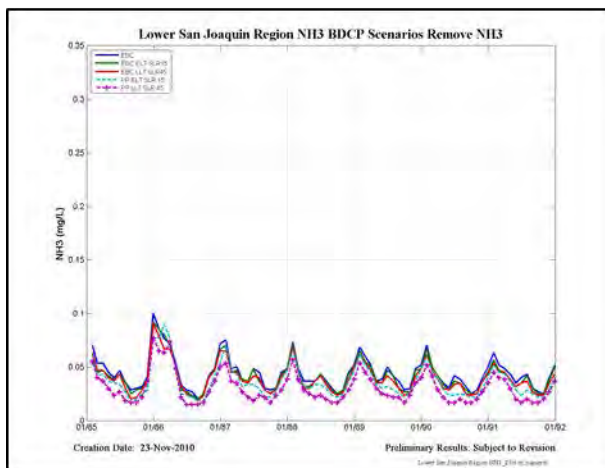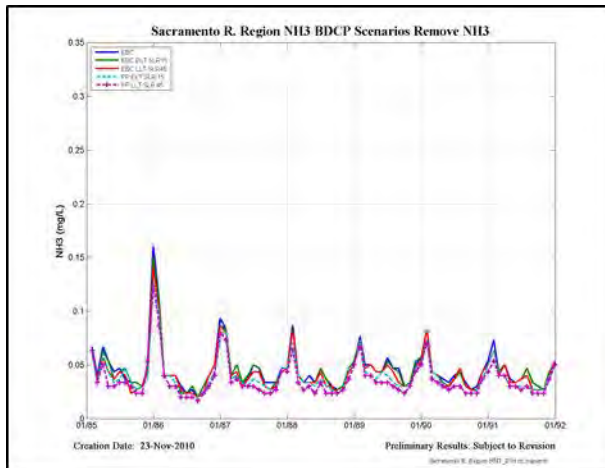
Figure 12-9 NH3 model output for the five scenarios removing NH₃ from Sacramento Regional WTP effluent for each of the three analysis regions.

NO$_3$+NO$_2$ model output
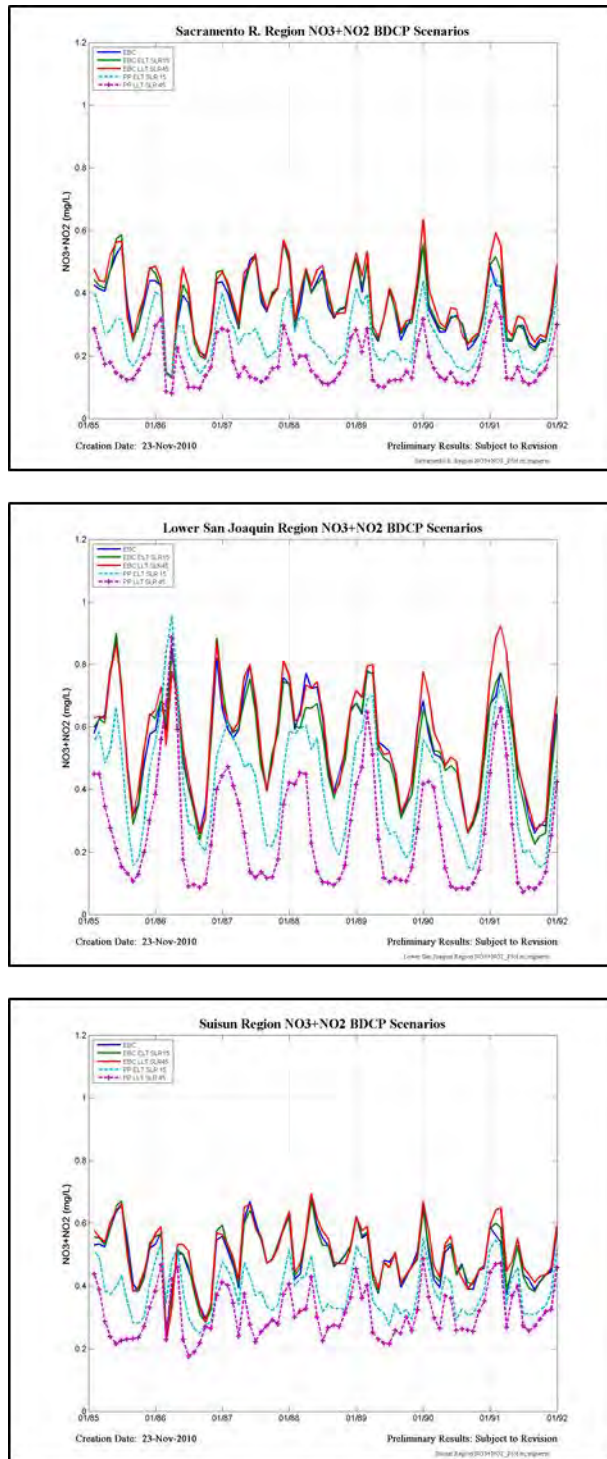
Figure 12-10 NO3+NO2 model output for the original five scenarios for each of the three analysis regions.
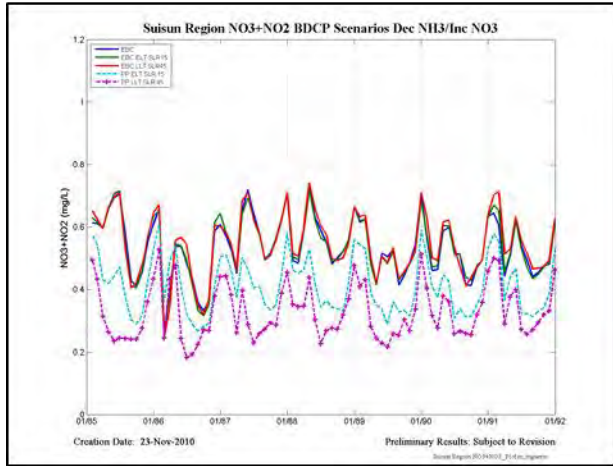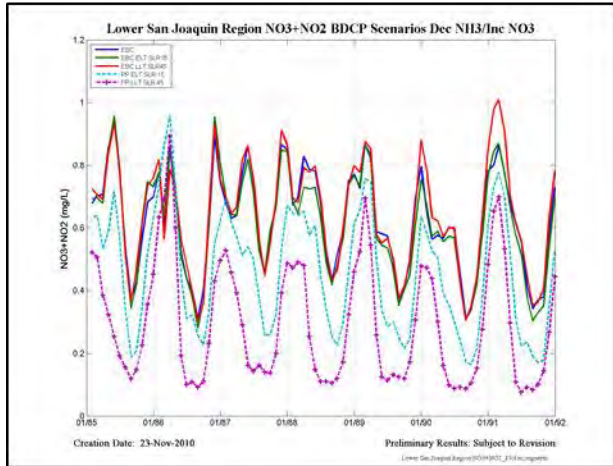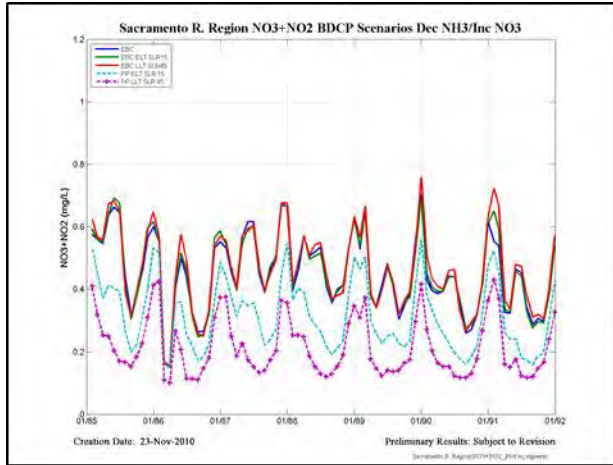
Figure 12-11 NO3+NO2 output for the five scenarios changing N-constituent concentrations (decreasing NH$_3$ and increasing NO$_3$) in Sacramento Regional WTP effluent for each of the three analysis regions.
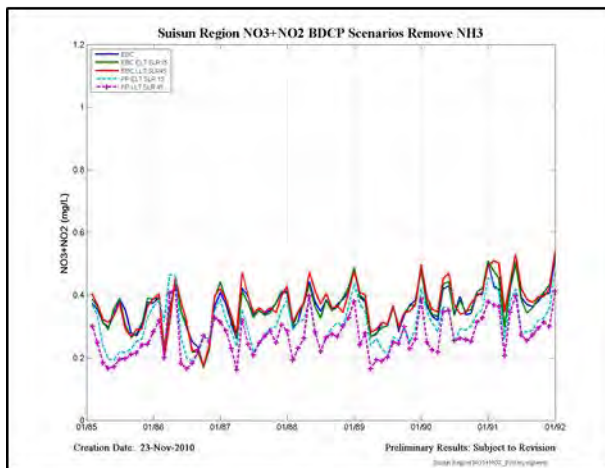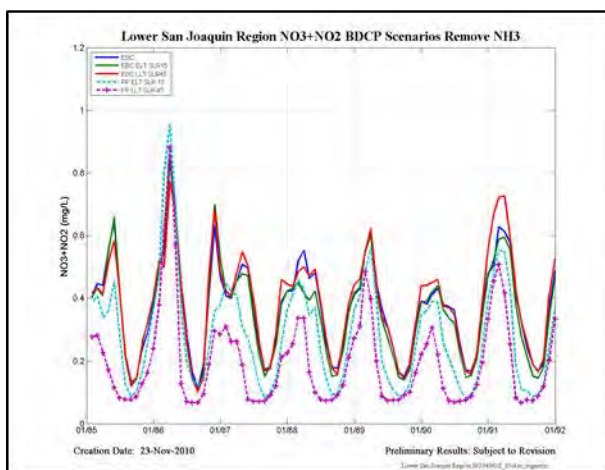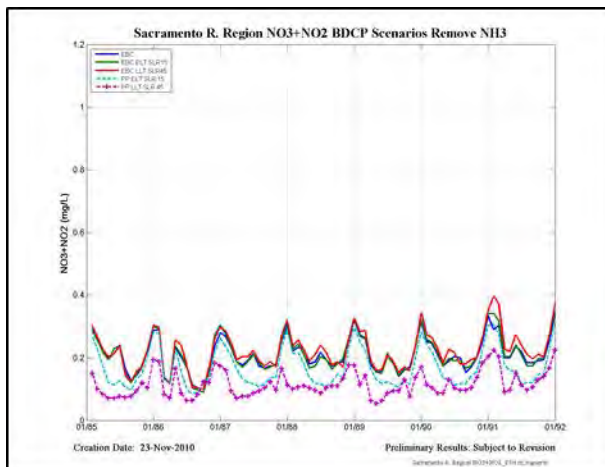
Figure 12-12 NO3+NO2 model output for the five scenarios removing NH$_3$ from Sacramento Regional WTP effluent for each of the three analysis regions.
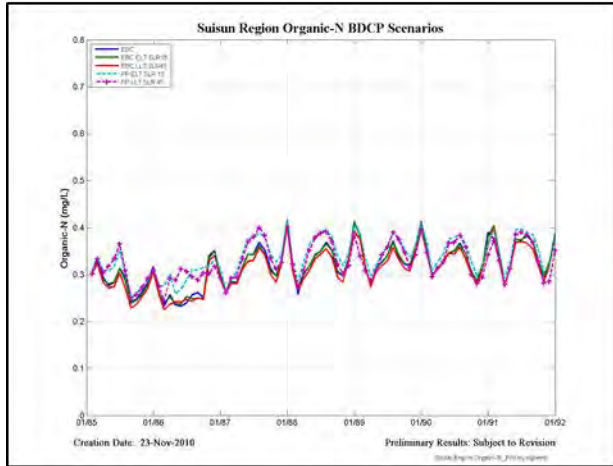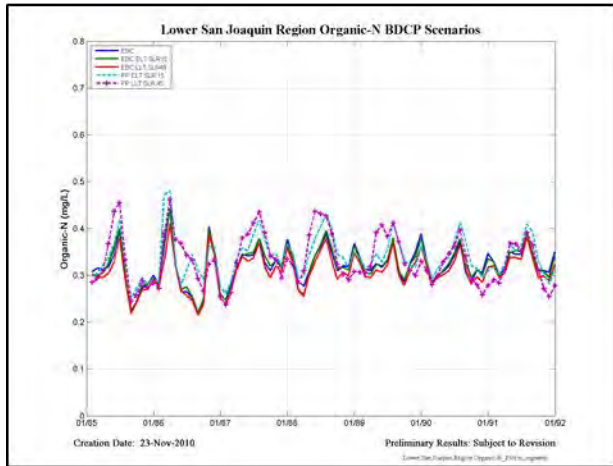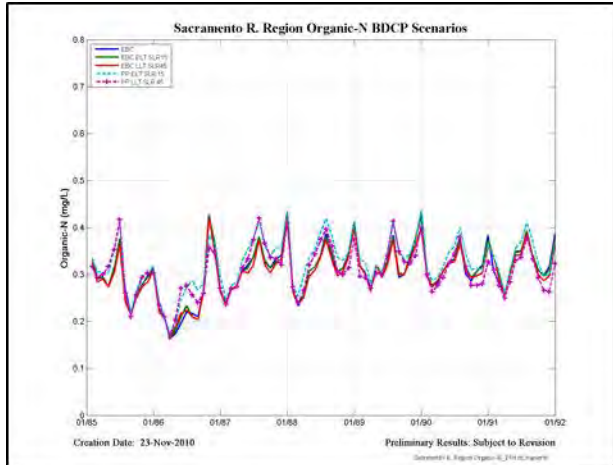
Figure 12-13 Organic N model output for the original five scenarios for each of the three analysis regions.
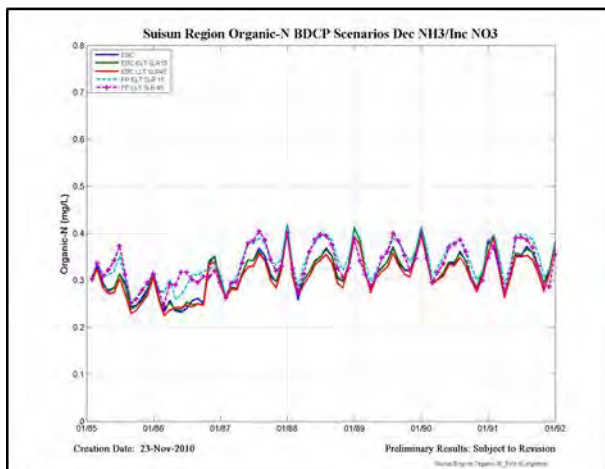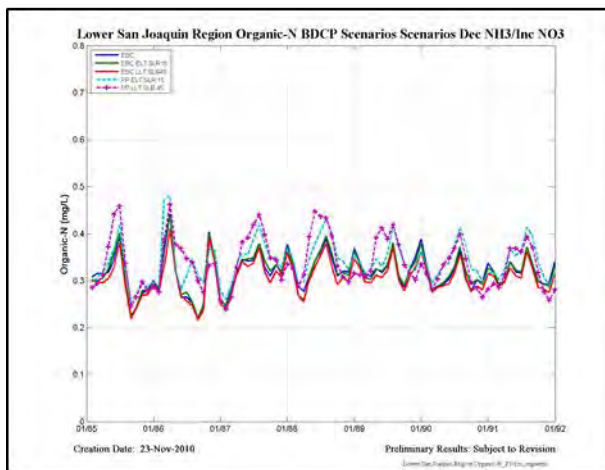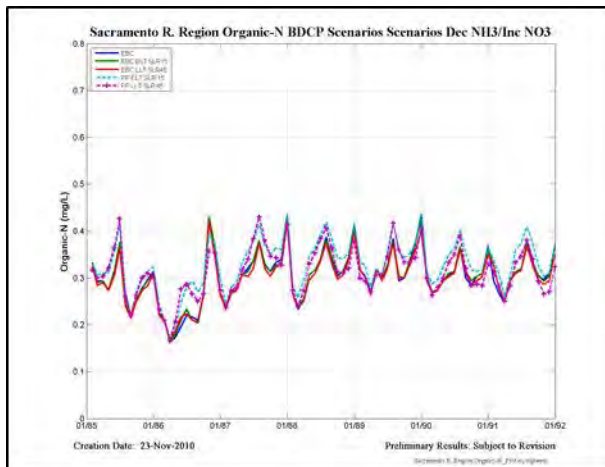
Figure 12-14 Organic N model output for the five scenarios changing N-constituent concentrations (decreasing NH$_3$ and increasing NO$_3$) in Sacramento Regional WTP effluent for each of the three analysis regions.
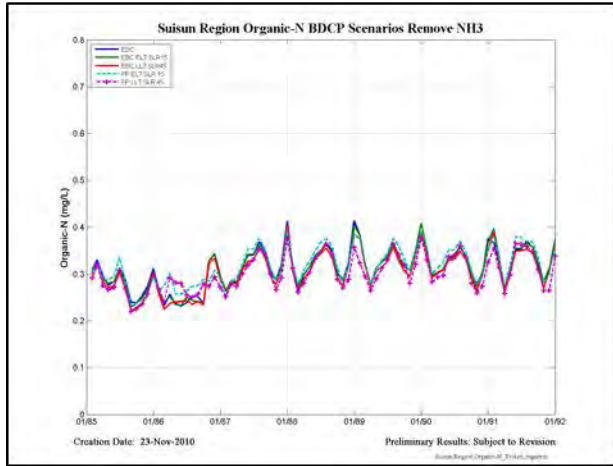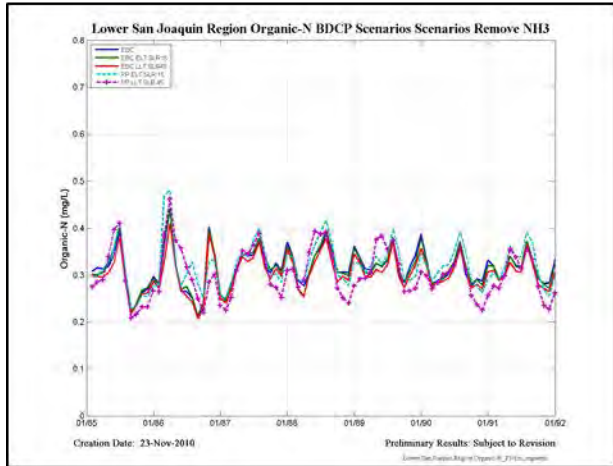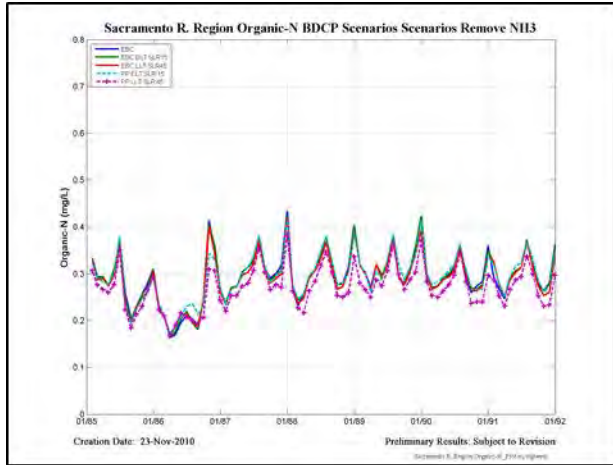
Figure 12-15 Organic N model output for the five scenarios removing NH₃ from Sacramento Regional WTP effluent for each of the three analysis regions.
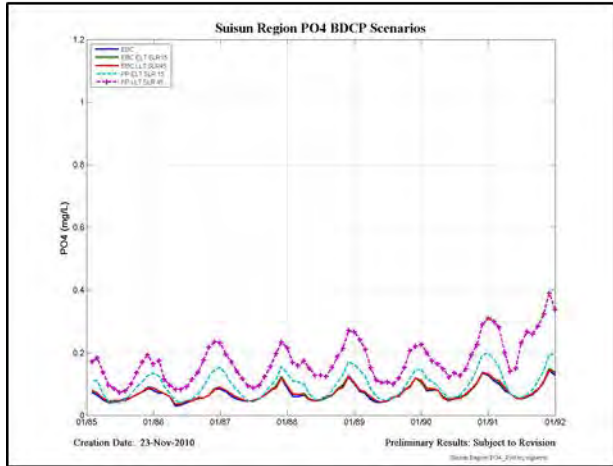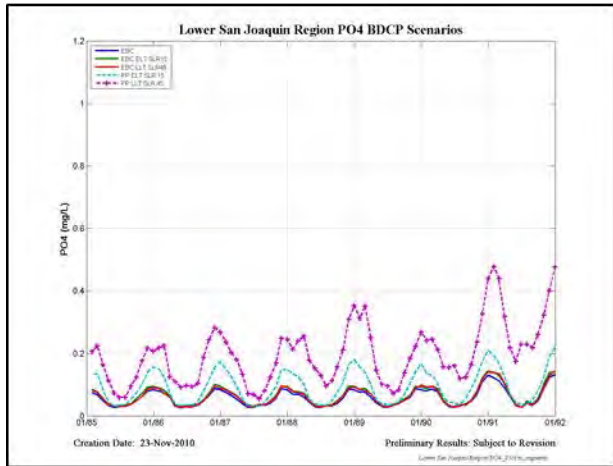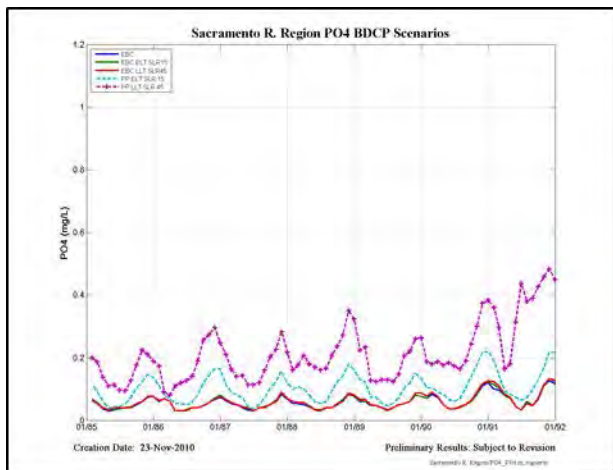
Figure 12-16 PO4 model output for the original five scenarios for each of the three analysis regions.
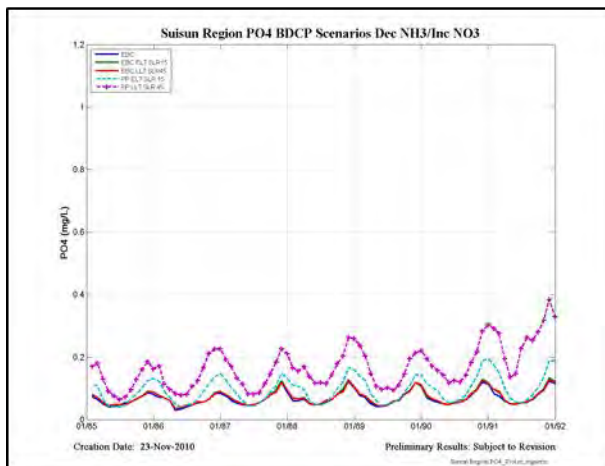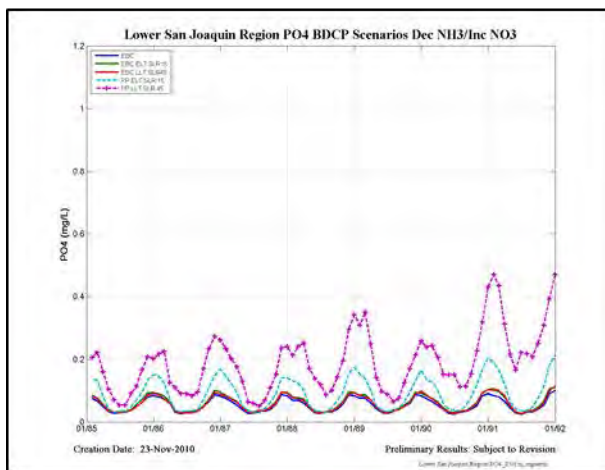
Figure 12-17 PO4 model output for the five scenarios changing N-constituent concentrations (decreasing NH$_3$ and increasing NO$_3$) in Sacramento Regional WTP effluent for each of the three analysis regions.

Figure 12-18 PO4 model output for the five scenarios removing NH₃ from Sacramento Regional WTP effluent for each of the three analysis regions.

Scenario Percent Difference Tables

Table 12-1 Average Monthly percent difference in the three main regions between the EBC-ELT scenario decreasing NH$_3$ and increasing NO$_3$ in Sac Regional effluent and the EBC-ELT scenario. The right-hand columns simply show the sign of the differences calculated in the left-hand columns.

SAC Region	CHL-a	NH3	PO4	ORG-N	NO3+NO2	CHL-a	NH3	PO4	ORG-N	NO3+NO2
Jan	-2.3	-38.8	-3.0	-0.2	30.0	-	-	-	-	+
Feb	-2.8	-48.1	-4.3	-0.5	27.8	-	-	-	-	+
Mar	-2.9	-44.0	-4.5	-0.5	32.1	-	-	-	-	+
Apr	-2.5	-45.5	-2.9	-0.5	35.1	-	-	-	-	+
May	-3.5	-41.0	-2.1	-1.0	29.9	-	-	-	-	+
Jun	-2.6	-32.2	-1.2	-0.9	23.0	-	-	-	-	+
Jul	-1.4	-33.4	-2.1	-0.4	22.2	-	-	-	-	+
Aug	-1.1	-29.5	-1.7	-0.2	20.6	-	-	-	-	+
Sep	-1.1	-33.3	-2.2	-0.1	26.3	-	-	-	-	+
Oct	-1.3	-33.3	-3.6	0.0	24.2	-	-	-	-	+
Nov	-1.7	-39.7	-3.1	-0.3	28.1	-	-	-	-	+
Dec	-3.3	-36.2	-2.9	-0.3	29.0	-	-	-	-	+

SJR Region	CHL-a	NH3	PO4	ORG-N	NO3+NO2	CHL-a	NH3	PO4	ORG-N	NO3+NO2
Jan	-1.8	-26.8	-2.1	-0.2	10.7	-	-	-	-	+
Feb	-2.6	-27.0	-2.9	-0.2	7.7	-	-	-	-	+
Mar	-2.8	-23.9	-3.1	-0.4	7.3	-	-	-	-	+
Apr	-2.2	-26.2	-2.2	-0.5	8.1	-	-	-	-	+
May	-2.3	-23.3	-0.9	-0.9	8.9	-	-	-	-	+
Jun	-1.9	-24.5	-0.8	-0.9	12.5	-	-	-	-	+
Jul	-1.3	-23.8	-1.1	-0.4	15.0	-	-	-	-	+
Aug	-1.1	-25.6	-0.8	-0.3	17.5	-	-	-	-	+
Sep	-1.3	-29.0	-1.4	-0.3	17.7	-	-	-	-	+
Oct	-2.8	-31.2	-3.7	-0.4	16.0	-	-	-	-	+
Nov	-2.8	-34.2	-3.0	-0.4	13.6	-	-	-	-	+
Dec	-3.1	-30.4	-3.1	-0.3	13.0	-	-	-	-	+

Suisun Region	CHL-a	NH3	PO4	ORG-N	NO3+NO2	CHL-a	NH3	PO4	ORG-N	NO3+NO2
Jan	-1.3	-23.1	-1.6	-0.2	12.1	-	-	-	-	+
Feb	-2.4	-25.7	-2.5	-0.2	10.9	-	-	-	-	+
Mar	-3.4	-25.7	-3.4	-0.5	11.8	-	-	-	-	+
Apr	-2.9	-24.3	-2.8	-0.4	11.1	-	-	-	-	+
May	-2.1	-17.0	-1.0	-0.4	9.3	-	-	-	-	+
Jun	-1.4	-8.0	0.0	-0.5	9.0	-	-	-	-	+
Jul	-1.2	-6.5	-0.4	-0.4	8.1	-	-	-	-	+
Aug	-1.1	-4.8	-0.4	-0.2	6.9	-	-	-	-	+
Sep	-1.1	-8.5	-0.3	-0.1	8.4	-	-	-	-	+
Oct	-1.9	-6.5	-0.9	-0.1	7.9	-	-	-	-	+
Nov	-2.1	-12.9	-1.2	-0.1	9.4	-	-	-	-	+
Dec	-2.3	-15.5	-1.3	-0.1	10.6	-	-	-	-	+

13. Appendix VI - Sensitivity Analysis Figures

ELT time frame
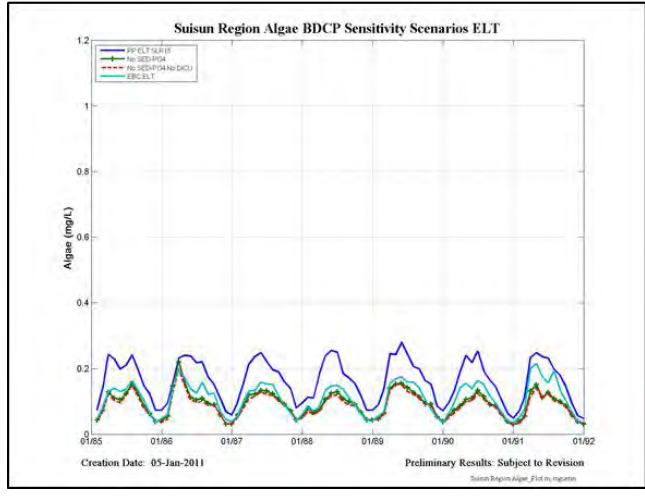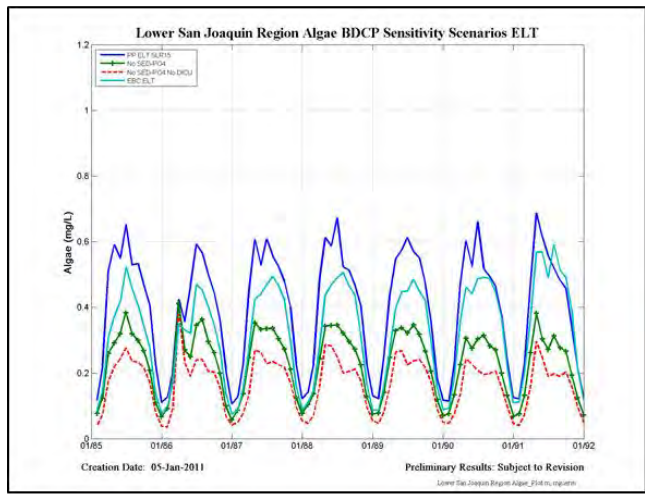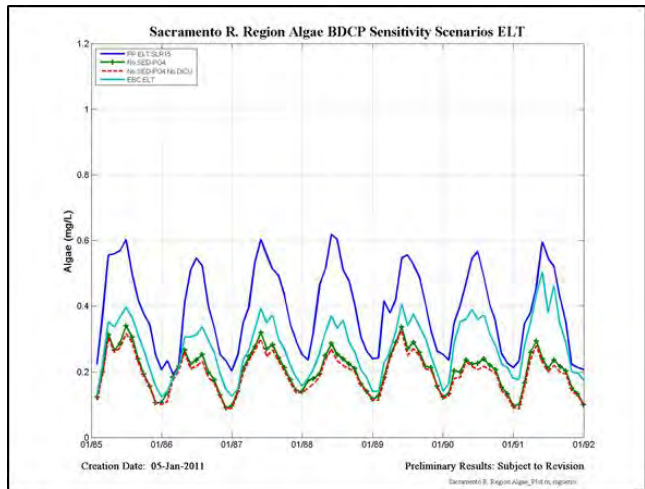
Figure 13-1 Sensitivity of the modeled constituent Algae to PO$_4$ reservoir sediment release with and without all-nutrient DICU contributions for the three defined regions in the ELT time frame.
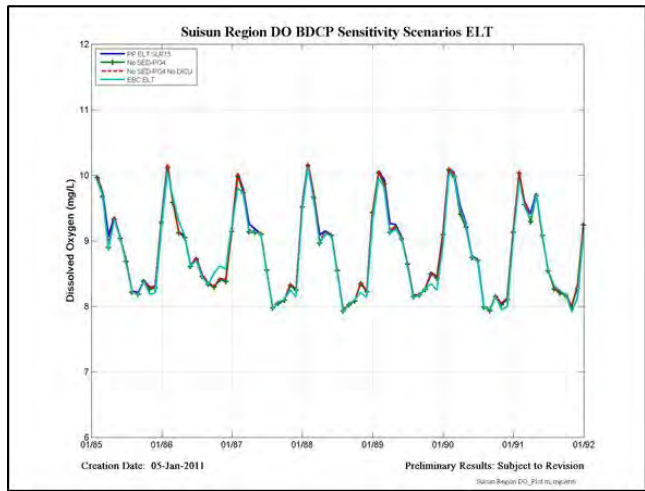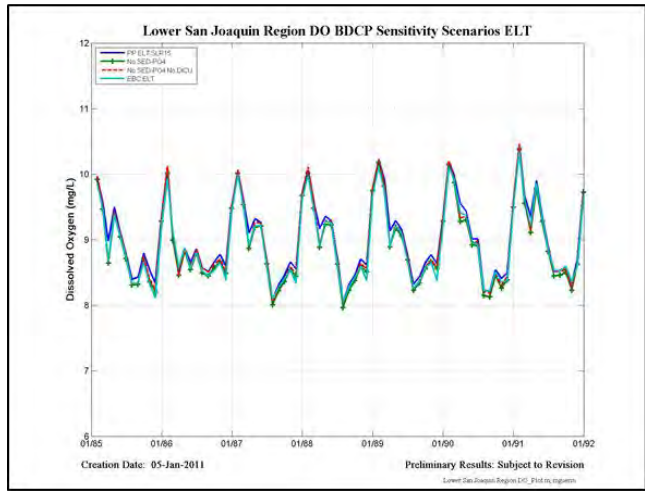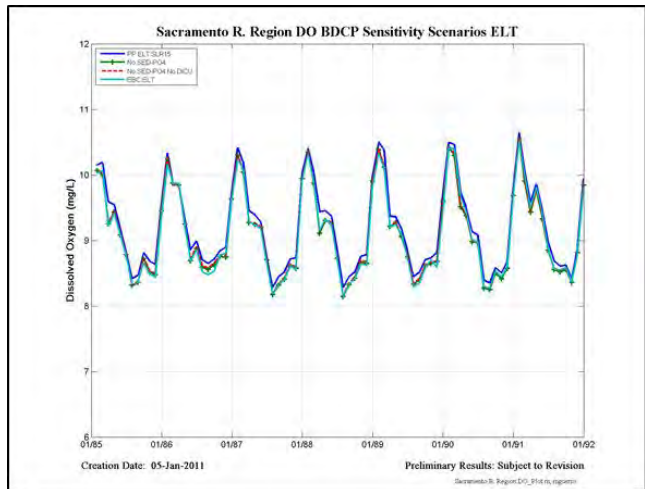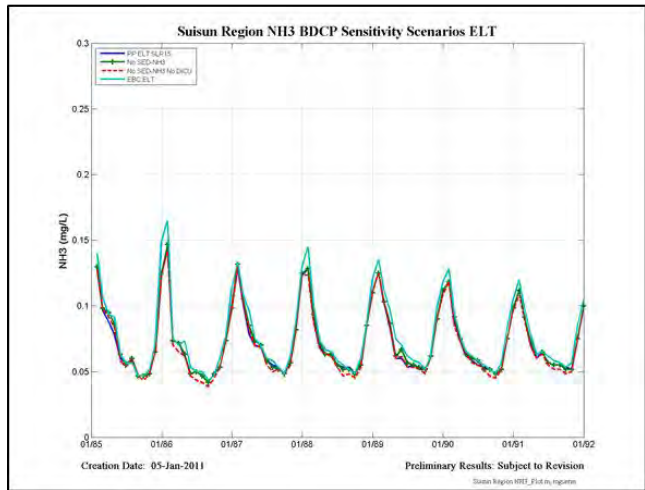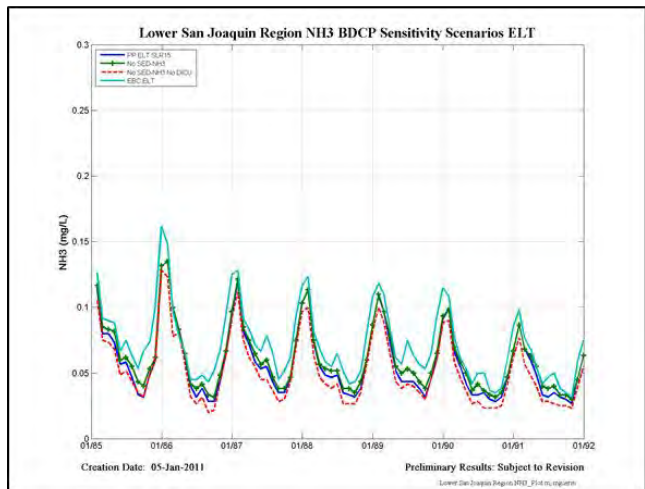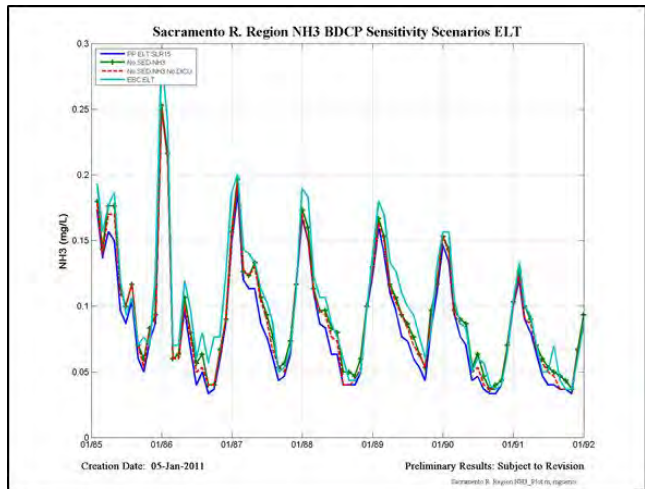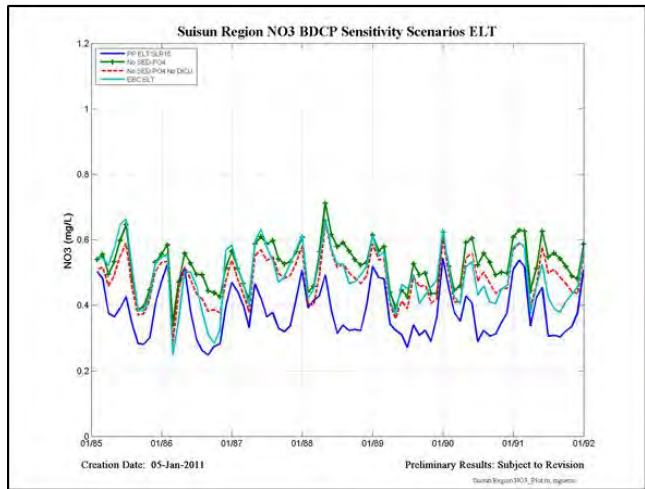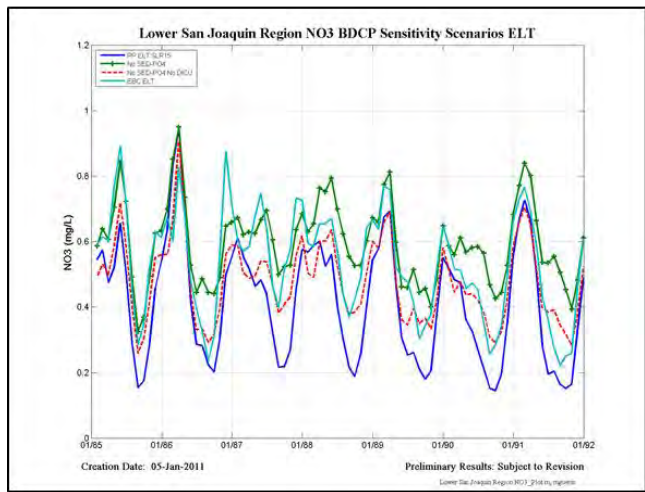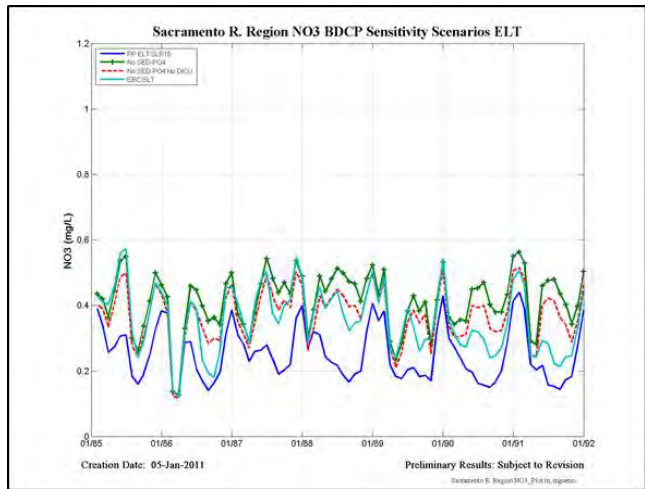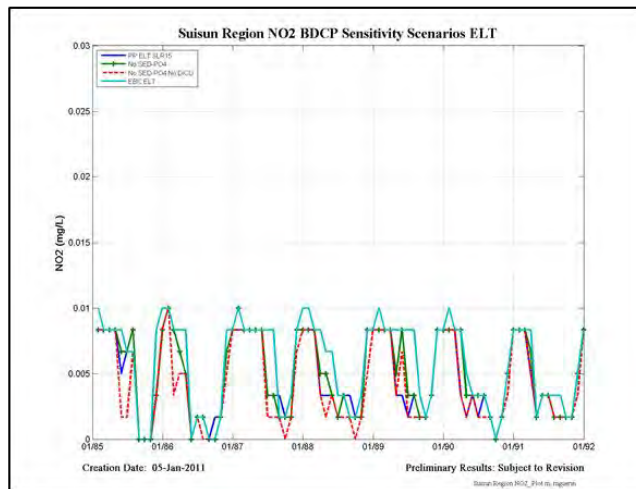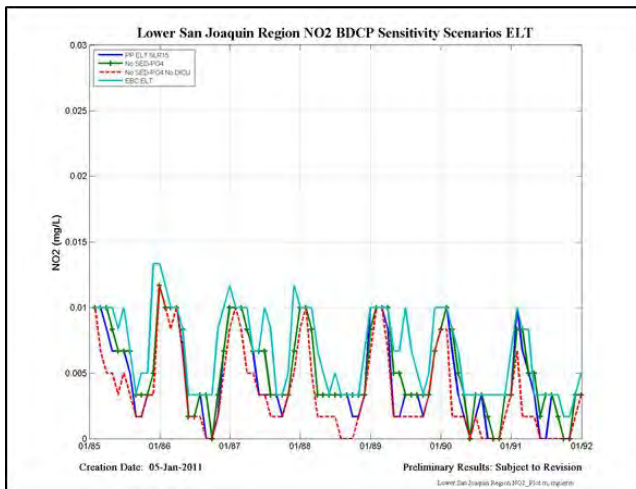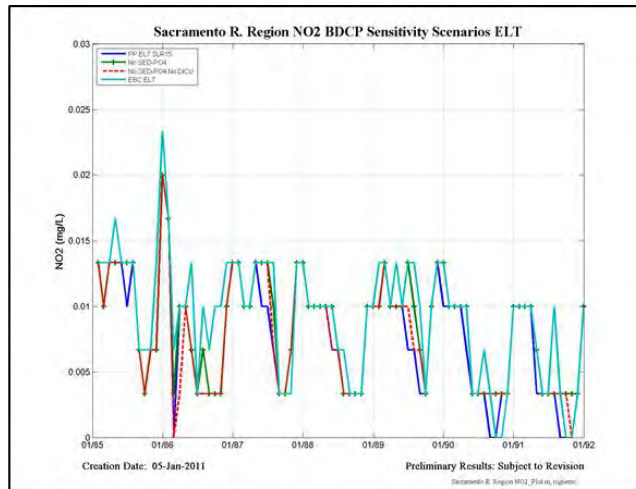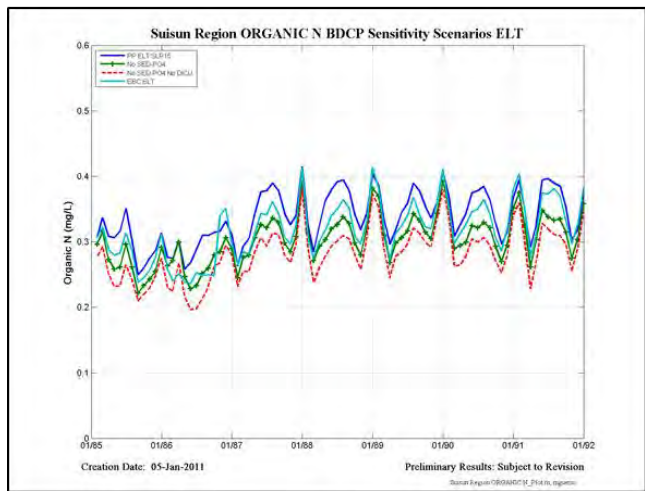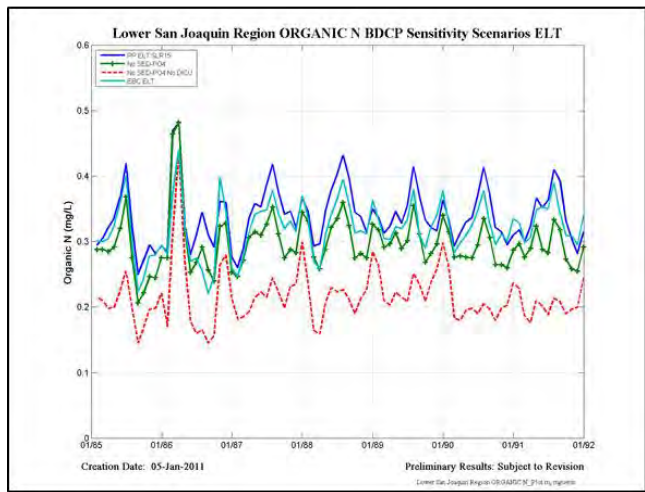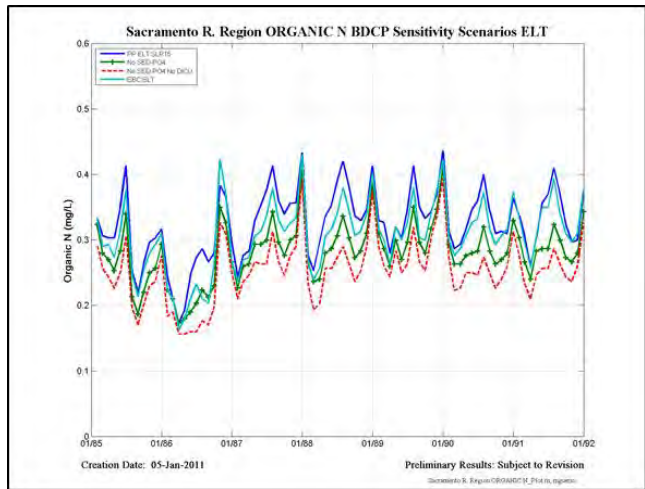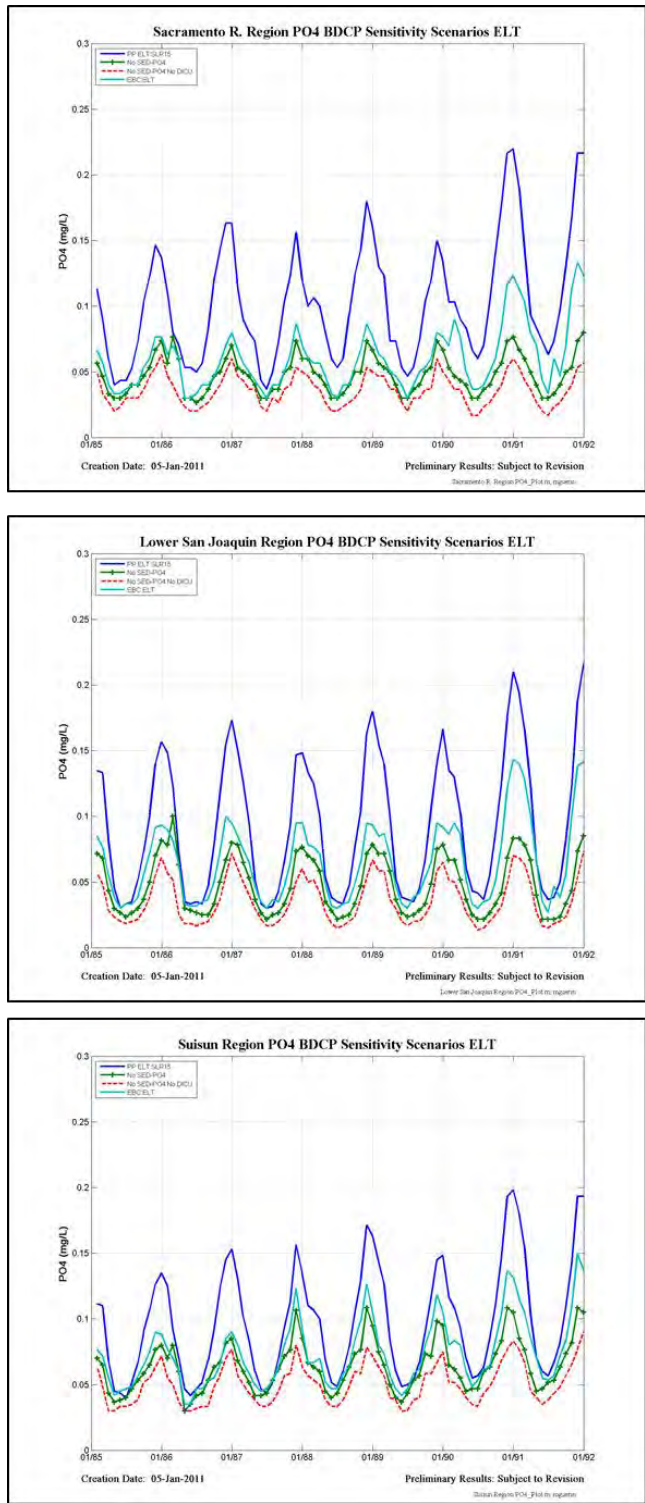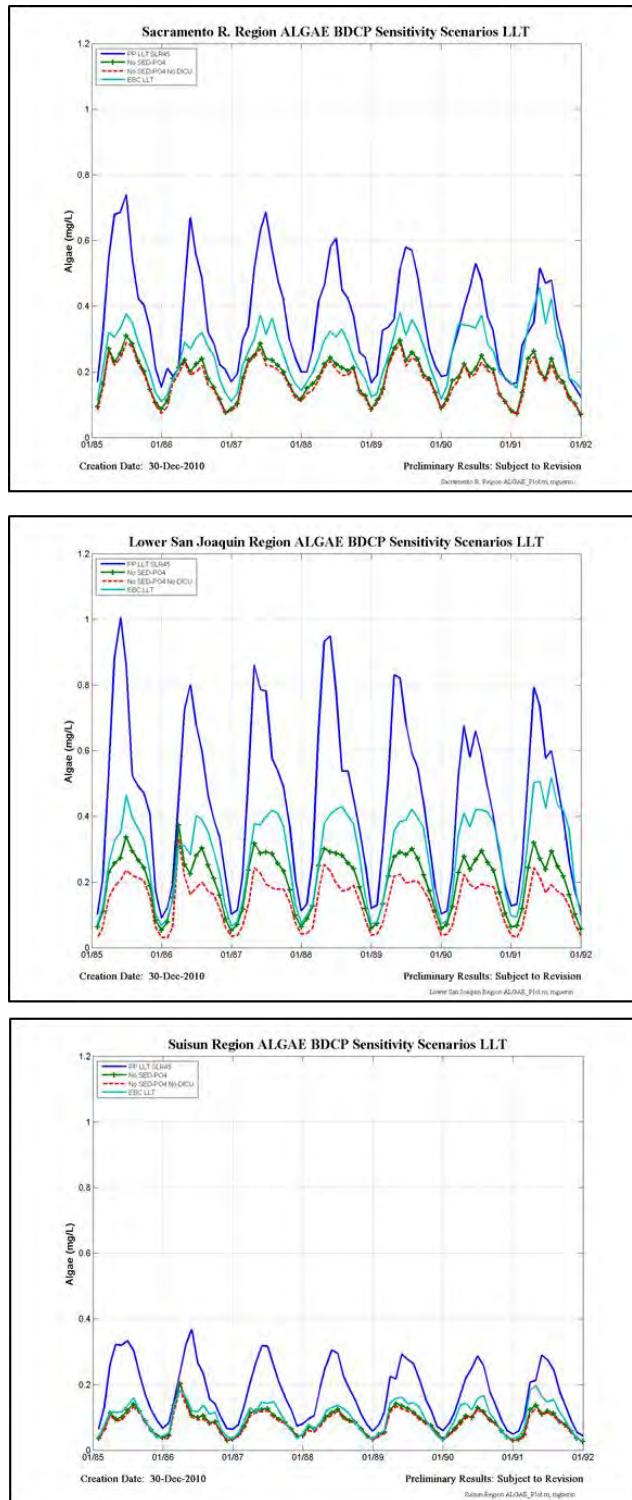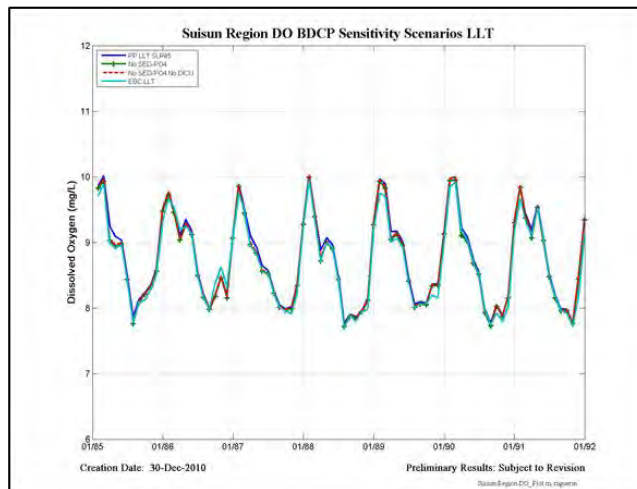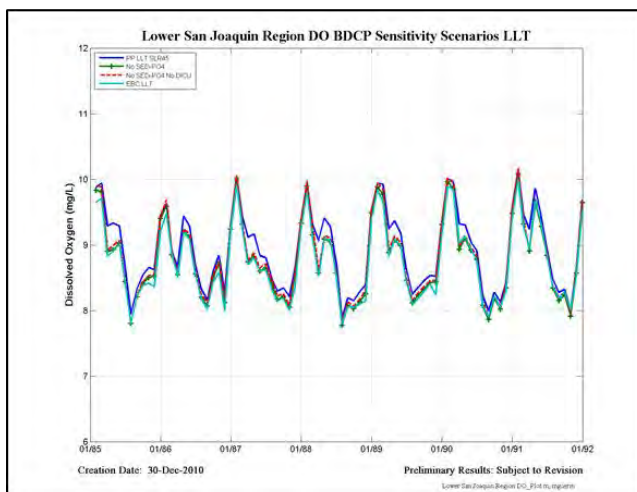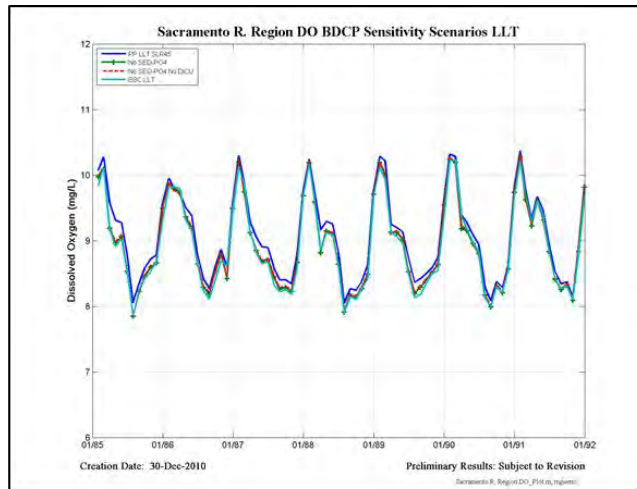
Figure 13-2 Sensitivity of the modeled constituent Dissolved Oxygen to PO₄ reservoir sediment release with and without all-nutrient DICU contributions for the three defined regions in the ELT time frame.
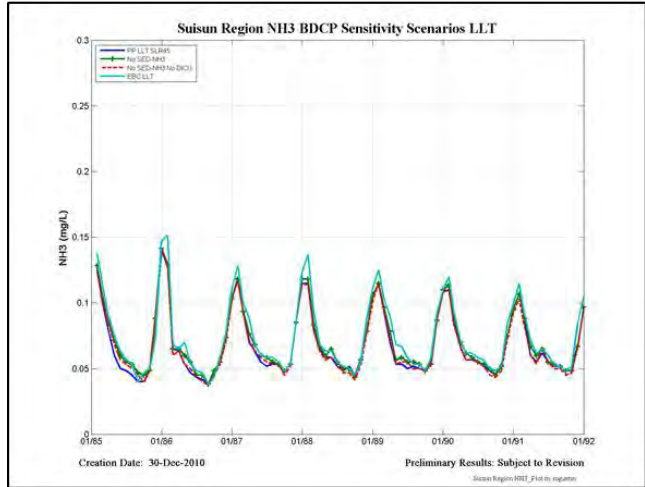
Figure 13-3 Sensitivity of the modeled constituent NH3 to PO$_4$ reservoir sediment release with and without all-nutrient DICU contributions for the three defined regions in the ELT time frame.

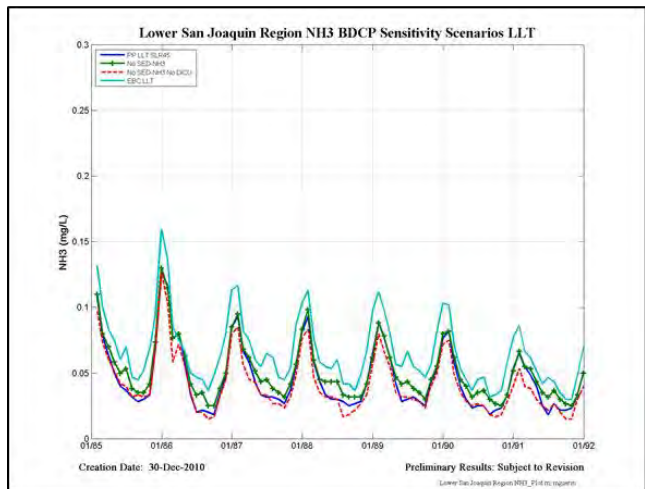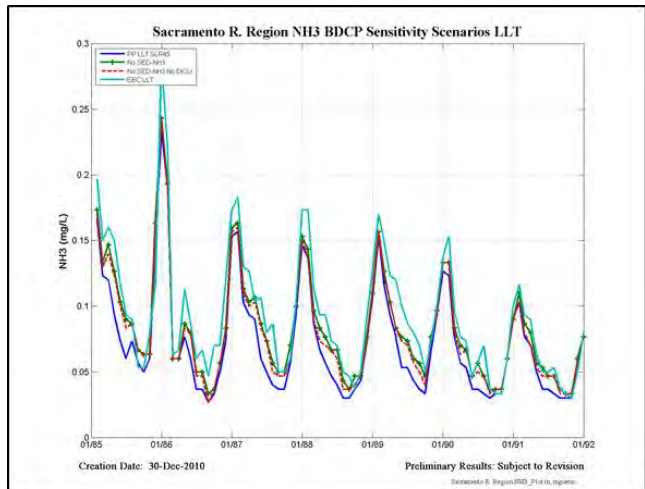**Figure 13-4 Sensitivity of the modeled constituent NO3 to PO₄ reservoir sediment release with and without all-nutrient DICU contributions for the three defined regions in the ELT time frame.**
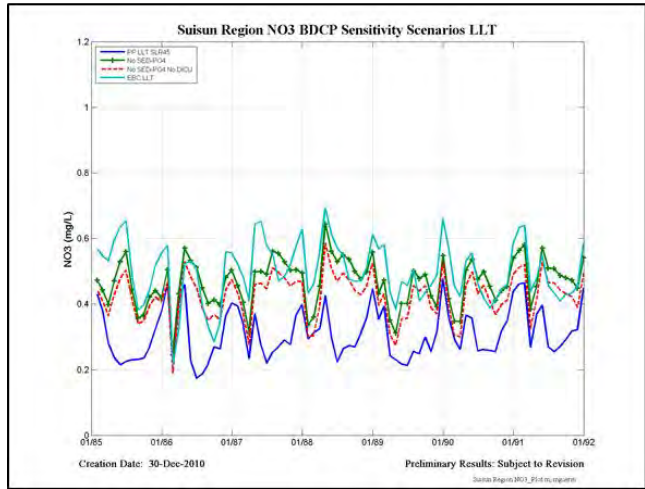
Figure 13-5 Sensitivity of the modeled constituent NO2 to PO₄ reservoir sediment release with and without all-nutrient DICU contributions for the three defined regions in the ELT time frame.

Figure 13-6 Sensitivity of the modeled constituent Organic N to PO$_4$ reservoir sediment release with and without all-nutrient DICU contributions for the three defined regions in the ELT time frame.
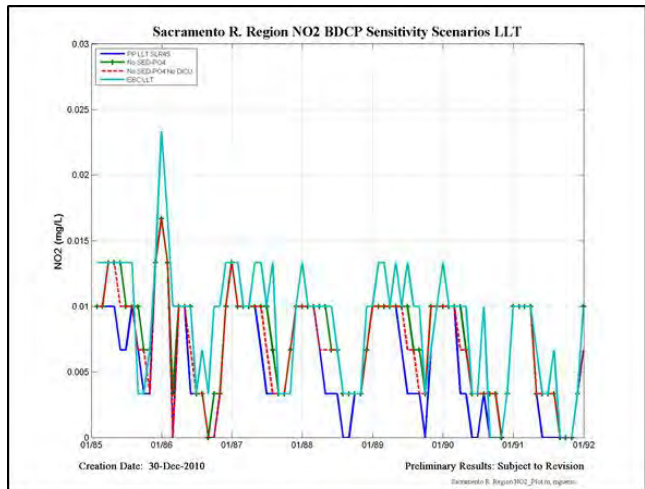
Figure 13-7 Sensitivity of the modeled constituent PO4 to PO$_4$ reservoir sediment release with and without all-nutrient DICU contributions for the three defined regions in the ELT time frame.
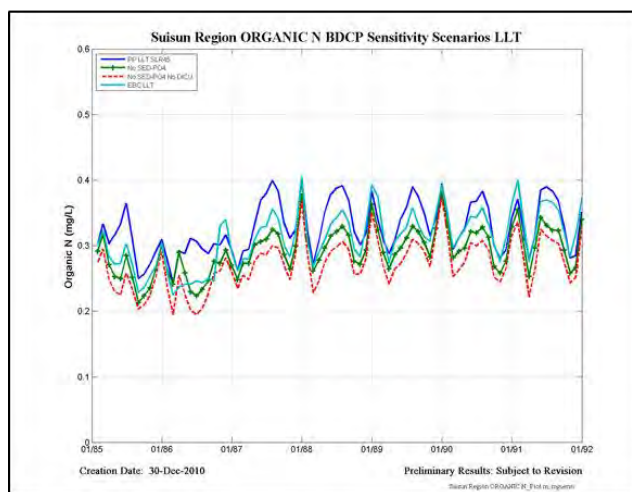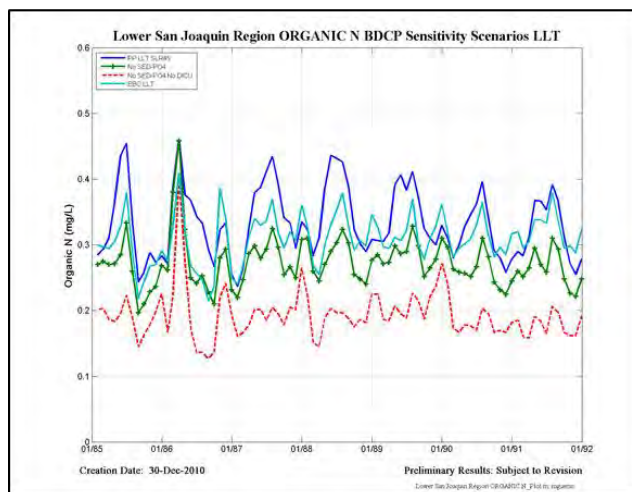
LLT time frame

Figure 13-8 Sensitivity of the modeled constituent Algae to PO$_4$ reservoir sediment release with and without all-nutrient DICU contributions for the three defined regions in the LLT time frame.

402

Figure 13-9 Sensitivity of the modeled constituent Dissolved Oxygen to PO$_4$ reservoir sediment release with and without all-nutrient DICU contributions for the three defined regions in the LLT time frame.
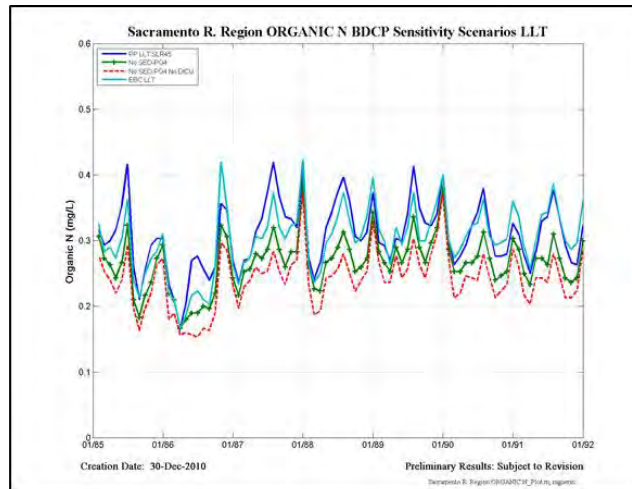
Figure 13-10 Sensitivity of the modeled constituent NH3 to PO$_4$ reservoir sediment release with and without all-nutrient DICU contributions for the three defined regions in the LLT time frame.
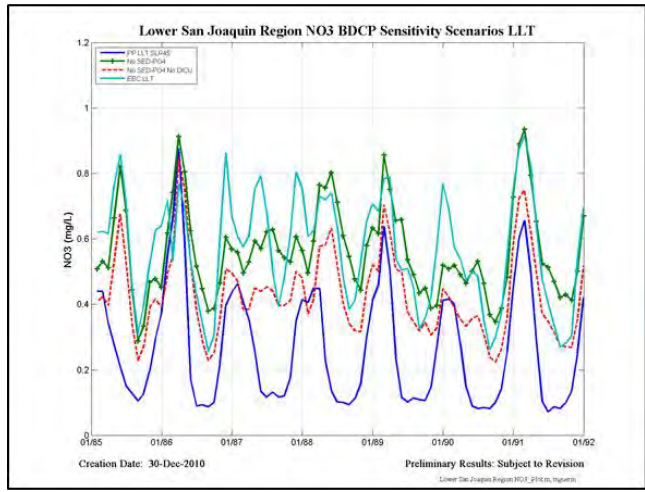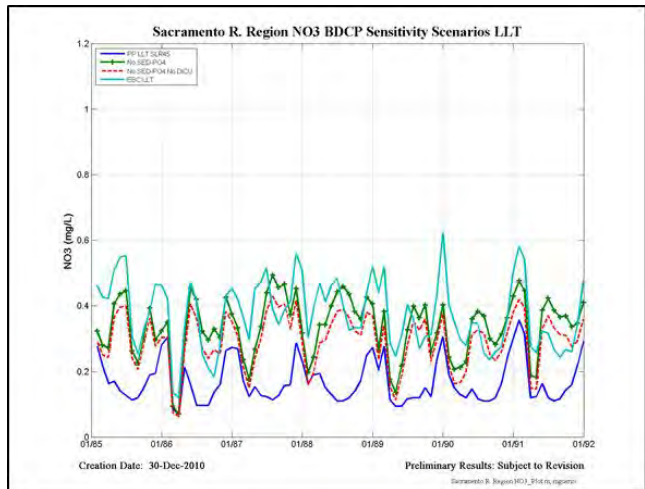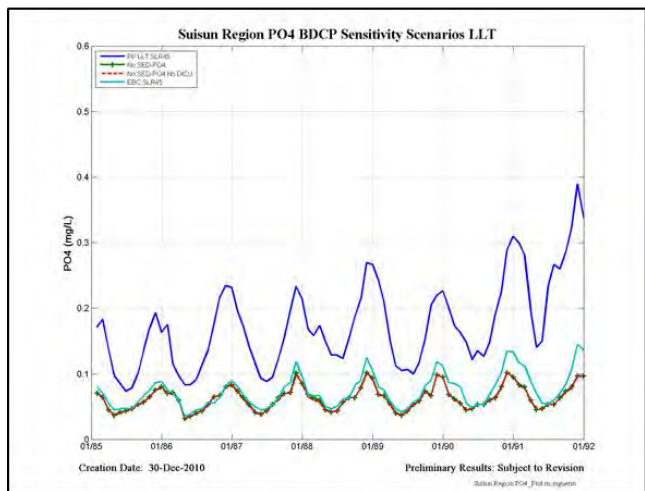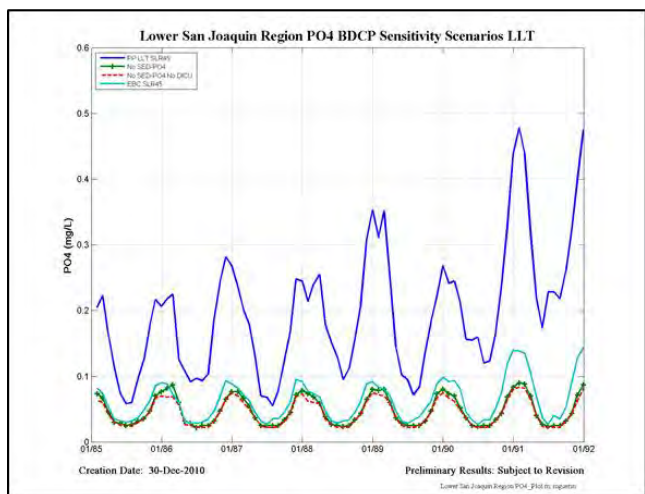
Figure 13-11 Sensitivity of the modeled constituent NO3 to PO$_4$ reservoir sediment release with and without all-nutrient DICU contributions for the three defined regions in the LLT time frame.
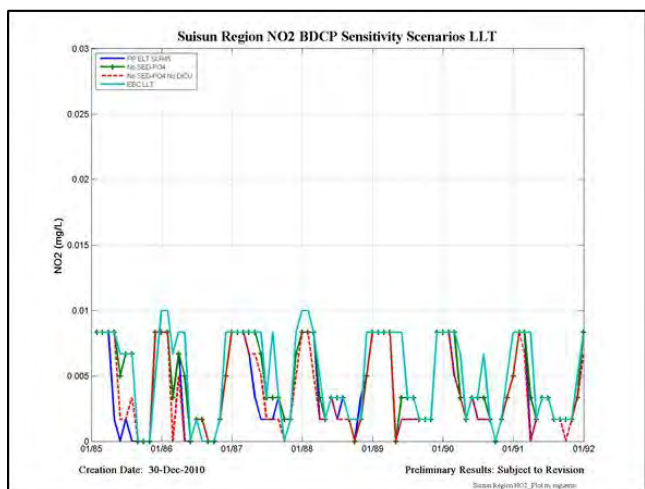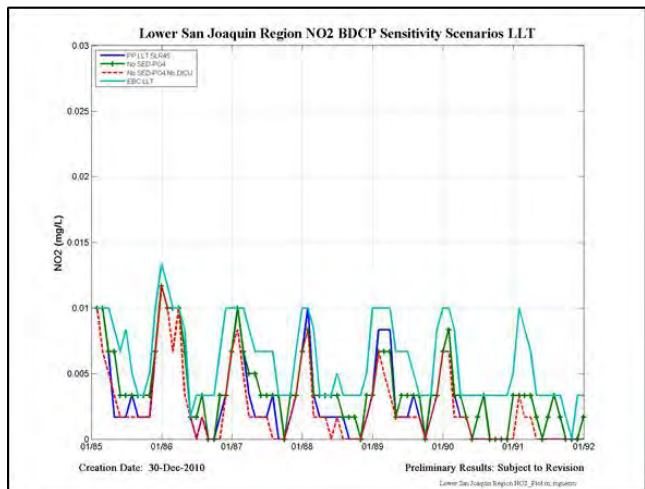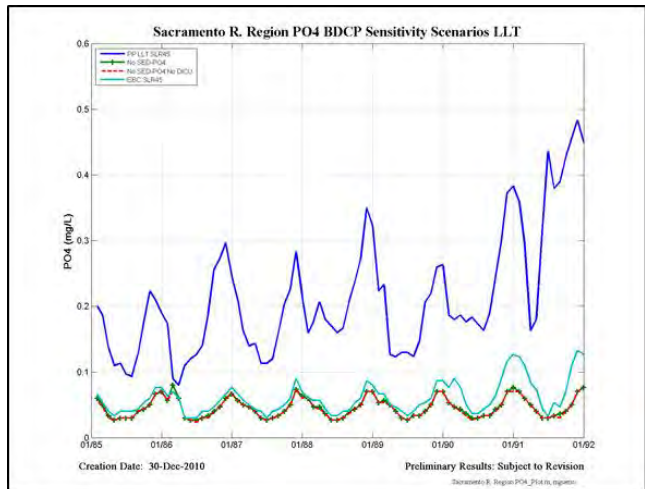
Figure 13-12 Sensitivity of the modeled constituent NO2 to PO$_4$ reservoir sediment release with and without all-nutrient DICU contributions for the three defined regions in the LLT time frame.

Figure 13-13 Sensitivity of the modeled constituent Organic N to PO$_4$ reservoir sediment release with and without all-nutrient DICU contributions for the three defined regions in the LLT time frame.

Figure 13-14 Sensitivity of the modeled constituent PO4 to PO$_4$ reservoir sediment release with and without all-nutrient DICU contributions for the three defined regions in the LLT time frame.